UNIVERSITAT POLITÈCNICA DE VALÈNCIA

DOCTORADO EN INGENIERÍA Y PRODUCCIÓN INDUSTRIAL

TESIS DOCTORAL

Desarrollo y optimización de nuevos materiales poliméricos, mezclas y compuestos de alto rendimiento medioambiental a partir de poliésteres y poliamidas procedentes de recursos renovables de interés en el sector envase y embalaje

Autor

Luis Jesús Quiles Carrillo

Dirigida por:

Dr. Rafael Antonio Balart Gimeno
Dr. Sergio Torres Giner

Mayo de 2020

UNIVERSITAT POLITÈCNICA DE VALÈNCIA

DOCTORADO EN INGENIERÍA Y PRODUCCIÓN INDUSTRIAL

TESIS DOCTORAL

Desarrollo y optimización de nuevos materiales poliméricos, mezclas y compuestos de alto rendimiento medioambiental a partir de poliésteres y poliamidas procedentes de recursos renovables de interés en el sector envase y embalaje

Luis Jesús Quiles Carrillo

El Dr. Rafael Antonio Balart Gimeno, Catedrático de Universidad del Departamento de Ingeniería Mecánica y de Materiales de la Universitat Politècnica de València y el Dr. Sergio Torres Giner, investigador en el Instituto de Agroquímica y Tecnología de Alimentos(IATA) perteneciente al Consejo Superior de Investigaciones Científicas(CSIC), en calidad de directores de la Tesis Doctoral (modalidad Doctorado Internacional) presentada por D. Luis Jesús Quiles Carrillo, con el título "**Desarrollo y optimización de nuevos materiales poliméricos, mezclas y compuestos de alto rendimiento medioambiental a partir de poliésteres y poliamidas procedentes de recursos renovables de interés en el sector envase y embalaje**".

CERTIFICAN

Que la presente memoria, "**Desarrollo y optimización de nuevos materiales poliméricos, mezclas y compuestos de alto rendimiento medioambiental a partir de poliésteres y poliamidas procedentes de recursos renovables de interés en el sector envase y embalaje**", para aspirar al grado de Doctor por la Universitat Politècnica de València reúne las condiciones adecuadas para constituir la tesis doctoral de D. Luis Jesús Quiles Carrillo (modalidad Doctorado Internacional).

Asimismo, certifican que la citada tesis doctoral se ha realizado en el Instituto de Tecnología de Materiales de la Universitat Politècnica de València y en el Dipartimento di Ingegneria Civile ed Ambientale de la Universidad de Perugia (Italia).

Y para que conste a los efectos oportunos, firman la presente en Alcoy a 11 de marzo de 2020.

Fdo. Dr. Rafael Balart Gimeno   Fdo. Dr. Sergio Torres Giner

A mi familia

"El miedo es natural en el prudente, y el saberlo vencer es ser valiente"

Alonso de Ercilla y Zúñiga

AGRADECIMIENTOS

En primer lugar, quiero agradecer enormemente a la persona que me dió la oportunidad de poder empezar mi carrera investigadora, "mi padrino investigador" y director Rafael Balart. Muchas gracias Rafa por todo tu tiempo y paciencia, gracias por contagiarme tu energía y espíritu de trabajo, por apostar y confiar en mí sin conocerme de nada y por haberme enseñado tantas cosas, sin pedir nada a cambio. En segundo lugar, quiero darle las gracias a mi codirector, Sergio Torres, por mostrarme siempre cómo mejorar y depositar tanta confianza en mí. Muchas gracias a los dos por haberme guiado e inculcado el "gusanillo" de la investigación. Gracias por hacer de mí un mejor investigador, sois y sereis mis referentes. ¡MUCHAS GRACIAS!

Al Instituto de Tecnología de Materiales (ITM) y al campus de Alcoy de la Universitat Politècnica de València, donde se llevó a cabo el presente trabajo.

A los catedráticos David García Sanoguera, Juan López Martínez y Lourdes Sánchez Nácher quiero agradecerles todos los consejos y la ayuda que me han brindado durante mi camino. En especial a Lourdes y a David, por contar conmigo como uno más de esta familia y depositar tanta confianza en mí.

A los profesores Octavio Fenollar, Teodomiro Boronat, Emilio Rayón y Néstor Montañés quiero agradecerles todo el tiempo que han invertido en ayudarme y explicarme durante estos años. En especial quiero agradecer a Néstor el haber compartido conmigo su limitado tiempo y haber tenido tanta paciencia para enseñarme y ayudarme en todo momento, ¡gracias por todo!

A los técnicos de laboratorio Matías, Javi y Rafa por su ayuda con todos aquellos problemas que han ido surgiendo durante mi tesis. En especial a Matías y Javi, por aguantarme durante tanto tiempo y ayudarme en todo momento de una manera desinteresada.

A mis compañeros de laboratorio: Alfredo, Dani, Diego, Mado, Pelayo, Juan, Harrison, Cris, Miguel y Sandra, muchas gracias por haber compartido conmigo estos laboratorios tan especiales y por haberme ayudado en todo momento.

Al profesor Luigi Torre de la Universidad de Perugia, por permitirme realizar mi investigación en sus instalaciones, y a Débora, Francesca, Silvia, Marco, Iván, Franco, Roberto, Mauricio y Genni, por ayudarme en todo momento y compartir conmigo tantos momentos en el pranzo. En especial a Franco Dominicci, porque ha sido mi familia, profesor y amigo durante mis meses de estancia. Gracias por haberme hecho sentir como en casa, grazie mille!!

RESUMEN

"Desarrollo y optimización de nuevos materiales poliméricos, mezclas y compuestos de alto rendimiento medioambiental a partir de poliésteres y poliamidas procedentes de recursos renovables de interés en el sector envase y embalaje"

El principal objetivo de la presente tesis doctoral se ha centrado en la obtención, desarrollo y caracterización de nuevas formulaciones de alto rendimiento medioambiental a partir de la utilización de poliésteres y poliamidas de origen renovable para el sector del envase y embalaje. A lo largo de todo el proceso de investigación, se han abordado y evaluado diferentes frentes de mejora con el objetivo de mejorar al máximo las propiedades de estos materiales desde un punto de vista altamente eficiente para el medio ambiente. Para este cometido, se han analizado desde diferentes tipos de mezclas binarias y ternarias, hasta la incorporación de cargas y refuerzos naturales, incorporación de aditivos y utilización de plastificantes capaces de solventar problemas de fragilidad y adhesión ligados a ciertos poliésteres como el PLA.

En la primera fase de la tesis se han analizado y estudiado la miscibilidad y propiedades mecánicas, térmicas y morfológicas de mezclas ternarias y binarias basadas en poliéster como el PHBH o el PLA como elementos principales. Se ha utilizado la extrusión reactiva (REX) consiguiendo resultados muy positivos con la incorporación de materiales como el PCL, TPS y PBAT a los poliésteres anteriormente comentados. Se ha mejorado la miscibilidad entre los distintos componentes, a partir de elementos como el ESAO o agentes compatibilizadores como PE-g-MA, PE-*co*-GMA y DCP, y sobretodo, MLO como compatibilizante natural, para desarrollar plásticos totalmente renovables con ductilidad y tenacidad mejoradas para su aplicación en el sector envase y embalaje. Dentro de las mezclas binarias, la combinación del PLA con un polietileno de origen renovable ha resultado ser una solución prometedora dentro del sector del envase y embalaje.

Por otro lado, para mejorar los problemas de tenacidad y el coste del PLA, se han evaluado y analizado la incorporación de aditivos y cargas naturales. La utilización de aceites naturales derivados de la soja, linaza y cáñamo han mejorado en gran medida la ductilidad del PLA. Además, estos aceites se han combinado con cargas derivadas de la cáscara de almendra y la piel de naranja en proporciones de hasta un 30%, consiguiendo un buen equilibrio de propiedades mecánicas y obteniendo WPCs capaces de ser altamente eficientes y rentables en algunas aplicaciones de envasado.

En la búsqueda de polímeros respetuosos por el medio ambiente, se han evaluado las propiedades de diferentes poliamidas de base biológica, y se ha seleccionado la PA1010 como candidata perfecta, gracias a sus excelentes propiedades y a su origen 100% renovable. En este contexto, se ha estudiado la viabilidad de incorporar fibras naturales como refuerzo, con unos resultados muy prometedores para las fibras de pizarra, consiguiendo mejoras de resistencia máxima de más del doble con elementos totalmente naturales. Hay que resaltar que la combinación de la PA1010 y el PLA con diferentes agentes naturales como el ELO y el MLO para la fabricación de films, han dado como resultado una notable mejora en las propiedades mecánicas, y sobre todo, una mejora en el efecto barrera al oxígeno.

En la última fase de la tesis, se ha optimizado la extracción de elementos antioxidantes como el ácido gálico a partir de residuos agroalimentarios. La incorporación de este elemento en el PLA ha dado como resultado la fabricación de films para envases activos, favoreciendo en gran medida su aplicación en el sector del envasado de alimentos. Además, se ha corroborado el efecto que posee este tipo de antioxidante natural en la preservación de films de bio-HDPE frente a agentes externos como la temperatura y la radiación UV. Por último, se ha conseguido mejorar en gran medida la ventana de procesamiento y las propiedades mecánicas y térmicas de las mezclas de biopolímeros de PA1010 y bio-HDPE.

RESUM

"Desenvolupament i optimització de nous materials polimèrics, mescles i compostos d'alt rendiment mediambiental a partir de polièsters i poliamides procedents de recursos renovables d'interés en el sector envase i embalatge"

El principal objectiu de la present tesi doctoral s'ha centrat en l'obtenció, desenvolupament i caracterització de noves formulacions d'alt rendiment mediambiental a partir de la utilització de polièsters i poliamides d'origen renovable per al sector de l'envàs i embalatge. Al llarg de tot el procés d'investigació, s'han abordat i avaluat diferents fronts de millora amb l'objectiu de millorar al màxim les propietats d'aquests materials des d'un punt de vista altament eficient per al medi ambient. Amb aquest objectiu, s'han analitzat des de diferents tipus de mescles binàries i ternàries, fins a la incorporació de càrregues i reforços naturals, incorporació d'additius i utilització de plastificants capaços de solventar problemes de fragilitat i adhesió lligats a certs polièsters com el PLA.

En la primera fase de la tesi s'han analitzat i estudiat la miscibilitat i propietats mecàniques, tèrmiques i morfològiques de mescles ternàries i binàries basades en polièster com el PHBH o el PLA com a elements principals. S'ha utilitzat l'extrusió reactiva (REX) aconseguint resultats molt positius amb la incorporació de materials com el PCL, TPS i PBAT als polièsters anteriorment comentats. Per a la millora de la miscibilitat entre els diferents components, s'han utilitzat elements com el ESAO o agents compatibilitzants com a PE-g-MA., PE-co-GMA i DCP, i sobretot, MLO com compatibilitzant natural, per a desenvolupar plàstics totalment compostables amb ductilitat i tenacitat millorades per a la seua aplicació en el sector envase i embalatge. Dins de les mescles binàries, la combinació del PLA amb un polietilé d'origen renovable ha resultat ser una solució prometedora dins del sector de l'envàs i l'embalatge.

D'altra banda, per a millorar els problemes de tenacitat i el cost del PLA, s'han avaluat i analitzat la incorporació d'additius i càrregues naturals. La utilització d'olis naturals derivats de la soja, llinosa i cànem han millorat en gran manera la ductilitat del PLA. A més, aquests olis s'han combinat amb càrregues derivades de la corfa d'ametla i la pell de taronja en proporcions de fins a un 30%, aconseguint un bon equilibri de propietats mecàniques i obtenint WPCs capaços de ser altament eficients i rendibles en algunes aplicacions d'envasament.

Dins de la cerca de polímers respectuosos pel medi ambient, s'han avaluat les propietats de diferents poliamides de base biològica, i s'ha seleccionat la PA1010 com a candidata perfecta gràcies a les seues excel·lents propietats i al seu origen 100% renovable. En aquest context, s'ha estudiat la viabilitat d'incorporar fibres naturals com a reforç, amb uns resultats molt prometedors per a les fibres de pissarra, aconseguint uns resultats de resistència màxima de més del doble amb elements totalment naturals. Hi ha que ressaltar que la combinació de la PA1010 amb el PLA amb diferents agents naturals com el ELO i el MLO per a la fabricació de films atorga una millora notable per a la fabricació de films, gràcies a la seua notable millora en les propietats mecàniques i dúctils, i sobretot, la millora en l'efecte barrera a l'oxigen.

En l'última fase de la tesi, s'ha optimitzat l'extracció d'elements antioxidants com l'àcid gàl·lic a partir de residus agroalimentaris. La incorporació d'aquest element en el PLA ha donat com a resultat la fabricació de films i envasos actius, afavorint en gran manera la seua aplicació en el sector de l'envasament d'aliments. A més, s'ha avaluat l'efecte que posseeix aquest tipus d'antioxidant natural en la preservació de films de bio-HDPE enfront d'agents externs com la temperatura i la radiació UV. Finalment, s'ha aconseguit millorar en gran manera la finestra de processament i les propietats mecàniques i tèrmiques de les mescles de biopolímers com PA1010 i bio-HDPE.

ABSTRACT

"Development and optimisation of new high environmental performance polymeric materials, blends and compounds from polyesters and polyamides from renewable resources of interest to the packaging sector"

The main objective of this doctoral thesis has been focused on obtaining, developing and characterizing new formulations with high environmental performance from the use of polyesters and polyamides of renewable origin for the packaging sector. Throughout the research process, different improvement fronts have been addressed and evaluated with the aim of improving the properties of these materials to the maximum from a highly efficient point of view for the environment. For this purpose, different types of binary and ternary mixtures have been analysed, as well as the incorporation of natural fillers and reinforcements, the incorporation of additives and the use of plasticisers capable of solving problems of fragility and adhesion linked to certain polyesters such as PLA.

In the first phase of the thesis, the miscibility and mechanical, thermal and morphological properties of ternary and binary mixtures based on polyester such as PHBH or PLA as main elements have been analysed and studied. Reactive extrusion (REX) has been used, obtaining very positive results with the incorporation of materials such as PCL, TPS and PBAT to the previously mentioned polyesters. Miscibility between the different components has been improved, using elements such as ESAO or compatibilizing agents such as PE-g-MA, PE-co-GMA and DCP, and above all, MLO as a natural compatibilizer, to develop totally renewable plastics with improved ductility and tenacity for application in the packaging sector. Within binary mixtures, the combination of PLA with a polyethylene of renewable origin has proved to be a promising solution within the packaging sector.

On the other hand, to improve the toughness problems and the cost of PLA, the incorporation of additives and natural fillers has been evaluated and analysed. The use of natural oils derived from soya, flax and hemp has greatly improved the ductility of PLA. In addition, these oils have been combined with fillers derived from almond shells and orange peel in proportions of up to 30%, achieving a good balance of mechanical properties and obtaining WPCs capable of being highly efficient and cost-effective in some packaging applications.

In the search for environmentally friendly polymers, the properties of different bio-based polyamides have been evaluated, and PA1010 has been selected as a perfect candidate thanks to its excellent properties and 100% renewable origin. In this context, the viability of incorporating natural fibres as reinforcement has been studied, with very promising results for slate fibres, achieving maximum resistance improvements of more than double with totally natural elements. It should be noted that the combination of PA1010 and PLA with different natural agents such as ELO and MLO for the manufacture of films, have resulted in a significant improvement in mechanical properties, and above all, an improvement in the oxygen barrier effect.

In the last phase of the thesis, the extraction of antioxidant elements such as gallic acid from food waste has been optimized. The incorporation of this element in PLA has resulted in the manufacture of films for active packaging, greatly favoring its

application in the food packaging sector. In addition, the effect of this type of natural antioxidant on the preservation of bio-HDPE films against external agents such as temperature and UV radiation has been corroborated. Finally, the processing window and the mechanical and thermal properties of PA1010 and bio-HDPE biopolymer blends have been greatly improved.

TABLA DE CONTENIDOS

LISTADO DE ARTÍCULOS

La presente tesis doctoral se ha estructurado y realizado a partir de un compendio de los siguientes artículos:

I. Melt grafting of sepiolite nanoclay onto poly(3-hydroxybutyrate-co-4-hydroxybutyrate) by reactive extrusion with multi-functional epoxy-based styrene-acrylic oligomer.

II. Ductility and Toughness Improvement of Injection-Molded Compostable Pieces of Polylactide by Melt Blending with Poly(e-caprolactone) and Thermoplastic Starch.

III. In Situ Compatibilization of Biopolymer Ternary Blends by Reactive Extrusion with Low-Functionality Epoxy-Based Styrene Acrylic Oligomer.

IV. A comparative study on the effect of different reactive compatibilizers on injection-molded pieces of bio-based high-density polyethylene/polylactide blends.

V. Enhancement of the mechanical and thermal properties of injection-molded polylactide parts by the addition of acrylated epoxidized soybean oil.

VI. Reactive toughening of injection-molded polylactide pieces using maleinized hemp seed oil

VII. On the use of acrylated epoxidized soybean oil as a reactive compatibilizer in injection-molded compostable pieces consisting of polylactide filled with orange peel flour.

VIII. Effect of different compatibilizers on injection-molded green composite pieces based on polylactide filled with almond shell flour.

IX. Compatibilization of highly sustainable polylactide/almond shell flour composites by reactive extrusion with maleinized linseed oil.

X. Evaluation of the engineering performance of different bio-based aliphatic homopolyamide tubes prepared by profile extrusion.

XI. Injection-molded parts of fully bio-based polyamide 1010 strengthened by waste derived slate fibers pre-treated with glycidyl- and amino-silane coupling agents.

XII. Development of high-performance polyamide 1010/coconut fibers composites by reactive extrusion with natural and petrochemical derived compatibilizers.

XIII. A comparative study on the reactive compatibilization of melt-processed polyamide 1010/polylactide blends by multi-functionalized additives derived from linseed oil and petroleum.

XIV. Optimization of microwave-assisted extraction of phenolic compounds with antioxidant activity from carob pods.

XV. Bioactive Multilayer Polylactide Films with Controlled Release Capacity of Gallic Acid Accomplished by Incorporating Electrospun Nanostructured Coatings and Interlayers.

XVI. On the use of gallic acid as a natural antioxidant and ultraviolet light stabilizer in cast-extruded bio-based high-density polyethylene films.

XVII. Enhancement of the processing window and performance of polyamide 1010/bio-based high-density polyethylene blends by melt mixing with natural additives.

ECUACIONES

$$X_C = \left[\frac{\Delta H_m - \Delta H_{CC}}{\Delta H_m^0 \cdot (w)}\right] \cdot 100$$

X_c = Grado de cristalinidad
ΔH_m = Entalpía de fusión
ΔH_{CC} = Entalpía de cristalización en frio
ΔH_m^0 = Entalpía de fusión para un polímero 100% cristalino
w = Fracción de peso del polímero

$$\delta = \frac{\rho \cdot \sum G}{M_n}$$

δ = Parámetro de solubilidad
ρ = Densidad del polímero
M_n = Peso molecular por unidad repetitiva
$\sum G$ = Constante de atracción molar

$$Weight\ loss(\%) = \left(\frac{W_0 - W_t}{W_0}\right) \cdot 100$$

W_t = Peso de la muestra después de un tiempo de enterramiento
W_0 = Peso seco inicial de la muestra

$$\frac{W_t}{W_S} = \frac{4}{d}\left(\frac{D\,t}{\pi}\right)^{\frac{1}{2}}$$

$\frac{W_t}{W_S}$ = Representación lineal para calcular el coefcidiente de difusión
d = Espesor inicial de la muestra
D = Coeficiente de difusión

$$D = 0.0625\,\pi\,d^2\theta^2$$

D = Coeficiente de difusión
θ = Pendiente de la recta
d = Espesor inicial de la muestra

$$D_c = D\left(1 + \frac{d}{h} + \frac{d}{w}\right)^{-2}$$

D_c = Coeficiente de corrección del coeficiente de difusión según geometría de la muestra
h = Longitud total
w = Ancho muestra
d = Espesor muestra

$$\Delta E_{ab}* = \sqrt{\Delta L^{*2} + \Delta a^{*2} + \Delta b^{*2}}$$

$\Delta E_{ab}*$ = Valores de cambio en la intensidad del color
ΔL^* = Diferencia de luminosidad entre dos muestras
Δa^* = Diferencia en las coordenadas de a^*
Δb^* = Diferencia en las coordenadas de b^*

$$Y = \beta_0 + \sum \beta_i X_i + \sum \beta_{ii} X_i^2 + \sum \sum \beta_{ij} X_i X_j$$	**Y** = Respuesta prevista **X** = Variables del sistema **i** = Variables de diseño **j** = Variables de diseño **β₀** = Constante **βᵢ** = Coeficiente lineal **βᵢᵢ** = Coeficiente cuadrático **βᵢⱼ** = Coeficiente de interacción de las variables i y j
$$Extraction\ yield(\%) = \frac{W_{ext}}{W_0} \cdot 100$$	**Wₑₓₜ** = Masa del extracto seco **W₀** = Masa seca utilizada para la extracción
$$I(\%) = \frac{A_0 - A_1}{A_0} \cdot 100$$	**I(%)** = Porcentaje de DPPH **A₀** = Absorción del control **A₁** = Absorción del extracto después de 30 minutos

ABREVIATURAS

AA	Ácido acrílico
ABS	Poli(acrilonitrilo-butadieno-estireno)
ABTS	2,2'azinobis(3-ethylbenzthiazoline)-6-ácido sulfúrico
AC	Carbodiimida aromática
AEHO	Aceite de semillas de cáñamo acrilado y epoxidado
AESO	Aceite de soja epoxidado acrilado
ASF	Harina de cáscara de almendra
A-SF	Fibra de pizarra tratada con amino-silano
ATBC	Acetil tri-n-butil citrato
B2MTH	Sebo dimetil bencil hidrogenado de amonio cuaternario
BBD	Diseño de Box-Behnken
BF	Fibra de basalto
BHET	Bis(2-hidroxietil) tereftalato
Bio-HDPE	Polietileno de alta densidad de base biológica
Bio-PAs	Poliamidas de base biológica
BPMS	Paraloid BPMS- 260
BRs	Gomas de polibutadieno
CF	Fibra de carbono
CFs	Fibras de coco
CLTE	Coeficiente de expansión térmica lineal
CN	Nitrato de celulosa
CNCs	Nanocristales de celulosa
CO	Aceite de ricino
CTAB	Bromuro de metilo-trimetilo de amonio
D	Diámetro
DCM	Diclorometano
DCP	Peróxido de dicumilo
DHM	Dihidromiricetina
DIAMIN T	Sebo N-hidrogenado-1,3-diaminopropano
DMDA	1,10-decametilendiamina
DMF	N,N-dimetilformamida
DMTA	Análisis térmico mecánico dinámico
DPPH	2,2-difenil-1-picrilhidrazilo
DSC	Calorimetria diferencial de barrido
DTG	Derivada termogravimétrica
DTPS	Almidón termoplástico seco
EE$_W$	Peso equivalente de epoxi
EFAE	Ésteres de ácidos grasos epoxidados
E$_{flexural}$	Módulo de flexión
EG	Etilén glicol
EHDP	Procesamiento electrohidrodinámico
EHO	Aceite de semillas de cáñamo epoxidado

EHT	Tensión extra alta
ELO	Aceite de linaza epoxidado
EPO	Aceite de palma epoxidado
ESAO	Oligómero de estireno acrílico a base de epoxi
ESBO/ESO	Aceite de soja epoxidado
E$_{tensile}$	Módulo de tensión
EVA	Etileno acetato de vinilo
EVOH	Poly(ethylene-co-vinyl alcohol)
EVOs	Aceites vegetales epoxidados
FDA	Administración de Alimentos y Medicamentos
FESEM	Microscopía electrónica de barrido de emisión de campo
FRAP	Reducción ferrítica de polvo antioxidante
FTIR	Infrarrojo con transformación de Fourier
G″	Módulo de pérdidas
G′	Módulo de almacenamiento
GA	Ácido gálico
GFRP	Plásticos reforzados con fibra de vidrio
GMA	Metacrilato de glicidílico
G-SF	Fibra de pizarra tratada con glicidil-silano
GTE	Extracto de té verde
HDPE	Polietileno de alta densidad
HDT	Temperatura de deflexión por calor
HF	Fibra de cáñamo
HIPS	Poliestireno de alto impacto
HMDA	1,6-hexametilendiamina
HO	Aceite de la semilla de cáñamo
HPLC	Cromatografía líquida de alta eficacia
HSF	Harina de cáscara de avellana
HV	3-hidroxivalerato
KOH	Hidróxido de potasio
L	Longitud
LA	Ácido láctico
LCP	Adaptador de baja viscosidad
LDPE	Polietileno de baja densidad
LLDPE	Polietileno lineal de baja densidad
LP	Permeabilidad del limoneno
LPR	Tasa de permeación del limoneno
LSD	Diferencia menos significativa de Fisher
MAE	Extracción asistida por microondas
MAH	Anhídrido maleico
MCSO	Aceite de semilla de algodón maleinizado
MFI	Índice de flujo de fusión
MFR	Tasa de flujo de fusión
MHO	Aceite de semillas de cáñamo maleinizado
MLO	Aceite de linaza maleinizado

MMT	Montmorillonita
MSO	Aceite de soja maleinizado
MTO	Aceite de tung maleinizado
MVOs	Aceites vegetales maleinizados
M$_W$	Peso molecular
MWCNTs	Nanotubos de carbono de múltiples paredes
NaOH	Hidróxido de sodio
NFRP	Polímero con un refuerzo de fibra natural
OIT	Tiempo de inducción de la oxidación
OLAs	Oligómero de ácido láctico
OOT	Temperatura de oxidación inicial
OP	Permeabilidad del oxígeno
OPF	Harina de cáscara de naranja
OTMS	Octil trimetoxi silano
OTR	Tasa de transmisión de oxígeno
PA1010	Poliamida 1010
PA1012	Poliamida 1012
PA11	Poliamida 11
PA6	Poliamida 6
PA610	Poliamida 610
PA66	Poliamida 6,6
PAI	Poliamida imida
PAs	Poliamidas
PBA	Polibutilén adipato
PBAT	Poli(butilén adipato-*co*-tereftalato)
PBS	Polibutilén succinato
PBSA	Poly(butileno succinato-*co*-adipato)
PBT	Polibutilén tereftalato
PC	Policarbonato
PCL	Policaprolactona
PDLA	Poli($_D$-lactide)
PDLLA	Poli($_{DL}$-lactide)
PE	Polietileno
PE-co-AA	Ácido poli(etileno-co-acrílico)
PE-*co*-GMA	Poli(metacrilato de etileno-co-glicidil)
PEEK	Poliéter éter cetona
PEEKK	Poliéter éter cetona cetona
PEF	Polietilén Furanoato
PEF	Furanato de polietileno
PEG	Poli(etilenglicol)
PE-*g*-MA	Anhídrido maleico de polietileno
PE-*g*-PEO	Poli(etileno-injerto-óxido de etileno)
PEI	Poliéter imida
PEK	Poliéter cetona
PEKEKK	Poliéter éter cetona éter cetona cetona

PEMA	Poli(etil metacrilato)
PES	Poliéter sulfona
PET	Polietilén tereftalato
PF	Resina de fenol-formaldehído
PGA	Ácido poliglicólico
PHA$_{MC}$	Polihidroxialcanoatos de cadena media
PHAs	Polihidroxialcanoatos
PHA$_{SC}$	Polihidroxialcanoatos de cadena corta
PHB	Poli(3-hidroxibutirato)
PHBH	Poli(3-hidroxibutirato-*co*-3-hidroxihexanoato)
PHBV	Poli(3-hidroxibutirato-*co*-3-hidroxivalerato)
PHEMA	Poli(2- hidroxietil metacrilato)
phr	Partes por cada cien de resina
PI	Poliimida
PLA	Ácido poliláctico
PLLA	Poli($_L$-lactide)
PMMA	Polimetil metacrilato
POE-*co*-GMA	Poli(etileno octano-co-glicidil metacrilato)
PP	Polipropileno
PPC	Poli(carbonato de propileno)
PPG	Poli(propilenglicol)
PP-*g*-MA	Polipropileno-*grafted*-maleico anídrido
PS	Poliestireno
PS-GMA	Copolímero aleatorio de poliestireno-glicidil-metacrilato
PTFE	Politetrafluoroetileno
PTMS	Propiltrimetoxi silano
PTT	Politrimetilén tereftalato
PVC	Policloruro de vinilo
REX	Extrusión reactiva
RH	Humedad relativa
ROP	Polimerización con apertura del anillo
RSM	Metodología de la superficie de respuesta
SAN	Poli(estireno-co-acrilonitrilo)
SEM	Microscopio electrónico de barrido
SFE	Extracción de fluido supercrítico
SFs	Fibras de pizarra
SO	Aceite de soja
T$_{5\%}$	Temperatura al 5% de pérdida de peso
TA	Ácido tereftálico
tan δ	Factor de amortiguación dinámico
T$_{deg}$	Temperatura de máxima degradación
TEC	Citrato de trietilo
TEM	Microscopía electrónica de transmisión
T$_g$	Temperatura de transición vítrea
TGA	Análisis termogravimétrico

T$_m$	Temperaturas de fusión
TMA	Análisis termomecánico
T$_{onset}$	Temperatura de inicio de la degradación térmica
TPC	Fenóles totales
TPS	Almidón termoplástico
TT-SF	Fibra de pizarra tratada térmicamente
UAE	Extracción asistida por ultrasonido
UF	Urea-formaldehído
UV	Ultravioleta
VN	Número de viscosidad
VST	Temperatura de reblandecimiento Vicat
VTES	Vinilo triethoxy silano
WD	Distancia de trabajo
WPC	Compuestos de madera y plástico
WVP	Permeabilidad del vapor de agua
WVPR	Tasa de permeación del vapor de agua
X$_c$	Grado de cristalinidad
XOs	Xilo-oligosacáridos
XRF	Fluorescencia de rayos X
3-APTS	3-aminopropil triethoxyl silane
3MTH	Sebo trimetil hidrogenado de amonio cuaternario
4HB	4-hidroxibutirato
ΔH$_c$	Entalpía de cristalización
ΔH$_{cc}$	Entalpía de cristalización en frio
ΔH$_m$	Entalpía de fusión
ε$_b$	Elongación en la rotura
σ$_{flexural}$	Resistencia a la flexión
σ$_{max}$	Máxima resistencia a la tracción
σ$_y$	Resistencia a la tracción en el límite de elasticidad

INTRODUCCIÓN

INTRODUCCIÓN

I.1. Clasificación de polímeros.

Actualmente, los polímeros o plásticos, son materiales fundamentales en nuestra cultura y vida cotidiana, ya que los tenemos presentes en todo tipo de elementos como ropa, envases, dispositivos electrónicos, vehículos, sector médico, deportes, juguetes, etc. No obstante, su historia es relativamente corta, ya que no fue hasta principios del siglo XX cuando se empezaron a utilizar e introducir de manera más visible en la industria y en los productos cotidianos.

Desde el punto de vista de la ingeniería de materiales, los polímeros siguen siendo materiales relativamente jóvenes, ya que no fue hasta 1833 cuando el químico sueco Jöns Jacob Berzelius, describió aquellos compuestos, que tenían la misma fórmula empírica, pero con diferentes pesos moleculares, como polímeros. A raíz de esta definición, compuestos naturales como el caucho y la celulosa empezaron a ser denominados de esta manera y, realmente, son polímeros que existen en la naturaleza desde hace millones de años, al igual que los filamentos altamente resistentes de las arañas, los gusanos de seda o el algodón.

Desde mitad del siglo XIX y principios del siglo XX, continuas investigaciones y pruebas, empezaron a dar como fruto la creación de nuevos polímeros tales como el policloruro de vinilo (PVC) o el nitrato de celulosa (CN), arrancando así una gran innovación industrial en la industria de los materiales poliméricos. Con el auge del petróleo a principios del siglo XX, empiezan a aparecer nuevos y mejorados polímeros tales como la baquelita o resina de fenol-formaldehído (PF), o el poliestireno (PS), con unos costes muy reducidos y con un gran abanico de posibles aplicaciones.

Hasta hace relativamente pocos años, el gran número de ventajas que suponía la utilización de los polímeros derivados del petróleo, tales como la baja densidad, las buenas propiedades mecánicas y térmicas, su facilidad de procesado y, en especial, el bajo coste, habían situado a estos materiales como líderes en producción y consumo. Durante las últimas décadas el empleo de materiales plásticos se ha extendido a prácticamente la totalidad de los sectores industriales. Si bien es cierto que los materiales plásticos se emplean en aplicaciones de ingeniería con una vida en servicio importante, también es cierto que el sector del envase y embalaje es el mayor consumidor de material plástico. En muchas ocasiones, se emplean en productos con un ciclo de vida corto y/o de un solo uso. Por ello, los residuos de estos materiales han tenido un rápido crecimiento en las últimas décadas [1]. Por poner en contexto las cantidades, en los últimos años, alrededor de un 6% del petróleo producido mundialmente se ha destinado íntegramente a la fabricación de polímeros, dato que ha generado preocupaciones medioambientales [2]. En general, los polímeros derivados del petróleo, no son biodegradables y acaban generando enormes volúmenes de residuos de los cuales, solo una mínima cantidad se somete a procesos de reciclaje.

Este enorme volumen de residuos plásticos, está generando una importante contaminación oceánica, además de problemas a todo tipo de especies tanto animales como vegetales, así como la generación de gases de efecto invernadero, entre otros. Debido a estos factores, en las últimas décadas ha crecido de manera significativa una gran conciencia social ligada a minimizar la huella de carbono, reducir al máximo el

uso de recursos fósiles, mejorar el reciclado y revalorizar ciertos residuos con el objetivo de solventar dichos problemas. Este aumento en el pensamiento colectivo sobre los problemas medioambientales, ha generado en las organizaciones e industrias un impulso para el desarrollo de nuevos materiales con un bajo impacto ambiental. Tal y como se ha descrito anteriormente, el sector del envase y embalaje es uno de los que contribuye en mayor extensión a la problemática de la ingente generación de residuos. Además de la conciencia social, la legislación no es ajena a esta problemática y, recientemente, se han aprobado directivas en distintos países para la total eliminación de plásticos en aplicaciones de un solo uso. A nivel europeo, en 2019 se aprobó una directiva dirigida a la reducción del impacto medioambiental de algunos plásticos, así como el desarrollo de economías circulares para potenciar la sostenibilidad del sector del plástico[3].

Hasta ahora se ha empleado el término plástico/polímero de forma genérica, que incluye en su definición todos los tipos de polímeros: lineales o termoplásticos, reticulares o termoestables y entrecruzados/vulcanizados o elastómeros. Los aspectos medioambientales relacionados con la generación masiva de residuos, están íntimamente ligados al empleo de polímeros lineales o termoplásticos en aplicaciones de un solo uso o de ciclos de vida cortos (sector envase y embalaje, productos desechables, higiene, etc.). Es por ello que el sector de polímeros termoplásticos es el que ha suscitado un mayor interés en el desarrollo de nuevos materiales de alto rendimiento medioambiental.

El problema se ha abordado desde dos puntos de vista. Una de las aproximaciones se basa en el origen, ya que la mayoría de los polímeros se obtienen como derivados de la industria del petróleo con su consiguiente efecto negativo sobre la huella de carbono y emisiones de CO_2. En este sentido, se han llevado a cabo muchas investigaciones dirigidas al empleo de materias renovables para la obtención de polímeros con aplicación industrial. Incluso se ha dado un paso adelante en tanto en cuanto, muchas de estas fuentes renovables consisten en residuos industriales o del sector agrario, con lo cual, su utilización para la síntesis de polímeros, no solo pretende resolver la fuerte dependencia de los combustibles fósiles, sino que, además, contribuye positivamente a la generación de economías circulares que favorecen el desarrollo sostenible y optimización de los recursos disponibles [4-6]. El otro planteamiento se centra en el final del Ciclo de Vida ya que la mayoría de los plásticos de origen petroquímico no presentan biodegradabilidad y ello conlleva a la acumulación de residuos plásticos. Con este planteamiento, se han desarrollado polímeros que al final de su Ciclo de Vida acaben desapareciendo en determinadas condiciones. Se trata de los polímeros biodegradables o, más correctamente, biocompostables; polímeros que son capaces de descomponerse en condiciones de compost. En este contexto, la **Figura I.1** muestra, según estas aproximaciones medioambientales (origen o final de Ciclo de Vida), la clasificación de los polímeros.

Biodegradables

POLIÉSTERES
ALIFÁTICOS
PCL, PLA, PDO, PBS, PBSA
POLIÉSTERES
AROMÁTICOS
PBAT
OTROS
Polialcohol vinílico (PVA)

PLA
POLISACÁRIDOS
Almidón, Celulosa, Pectina
quitina/quitosano, etc
POLIDROXIALCANOATOS
PHB, PHBV, etc
PROTEINAS
Gluten, queratina, caseína
proteína de soja, ovoalbúmina, etc

Origen Petroquímico ← → **Origen Renovable**

DE USO COMÚN
PE, PP, PS, PVC, PET
TÉCNICOS
PA, PC, PBT, POM
ALTAS PRESTACIONES
PEK, PEEK, PI

Bio polietilén tereftalato (BioPET)
Bio polipropileno (BioPP)
Bio policarbonato (BioPC)
Bio poliuretano (BioPUR)
Bio poliamida (Bio PA)
Bio polietileno(BioPE)

No Biodegradables

Figura I.1. Clasificación de polímeros termoplásticos según su origen y capacidad de biodegradación.

Se puede apreciar una gran cantidad de materiales provenientes de recursos renovables e incluso materiales de origen petroquímico con capacidad para ser desintegrados en condiciones de compost. Este factor es muy positivo para la industria, ya que le proporciona un gran abanico de materiales de alto rendimiento medioambiental. A continuación, se describen las particularidades de los polímeros enmarcados en cada uno de los cuadrantes de la figura anterior.

I.1.1. Polímeros de origen petroquímico no biodegradables.

Desde principios del siglo XX, numerosas empresas e investigadores han trabajado con el petróleo como fuente principal para la obtención de polímeros. Gracias a los bajos costes y las excelentes propiedades obtenidas, se han ido generando una amplia gama de polímeros, según su aplicación, prestaciones o necesidades. Además, debido a que no se tenía puesta una mirada al futuro, ni tampoco idea de los problemas que estos materiales podían ocasionar al medio ambiente, no se concebían ni diseñaban para ser biodegradables, sino únicamente para cumplir su función, más o menos técnica, de la manera más eficaz y rentable posible. Dentro del grupo de polímeros de origen petroquímico y no biodegradables es posible realizar una clasificación en función de su tecnicidad.

I.1.1.1 Plásticos de uso común.

Este grupo incluye polímeros como el polietileno (PE), polipropileno (PP) poliestireno (PS) o policloruro de vinilo (PVC). Se trata de materiales que, generalmente, ofrecen un coste bajo ya que hay una gran oferta; además son relativamente fáciles de procesar y ofrecen una relación propiedades/coste muy favorable. Muchos de estos polímeros se obtienen mediante procesos de poliadición, una de las técnicas más empleadas y optimizadas en la obtención de polímeros termoplásticos, la cual no genera subproductos y consigue reducir al máximo el coste final [7].

Numerosas aplicaciones y sectores a lo largo de estos años han respaldado la gran utilización que se le ha dado a este tipo de polímeros. Normalmente el uso que se le concede a este tipo de materiales es trivial, no suponiendo usos de altas prestaciones o situaciones en las cuales se puedan ver comprometidos. Para ver realmente la gran implantación que han tenido este tipo de materiales, sectores como el envase y embalaje [8, 9], automoción [10, 11], juguetes [12], agricultura [13] o medicina [14, 15] han sido unos de los que mayor implantación de este tipo de materiales han generado en sus filas. Algunas de las estructuras químicas de este tipo de polímeros se pueden ver en la **Figura I.2**.

polietileno - PE   polipropileno - PP   policloruro de vinilo - PVC

poliestireno - PS   poli(estireno-*co*-acrilonitrilo) - SAN

polietilén tereftalato - PET   poli(acrilonitrilo-butadieno-estireno) - ABS
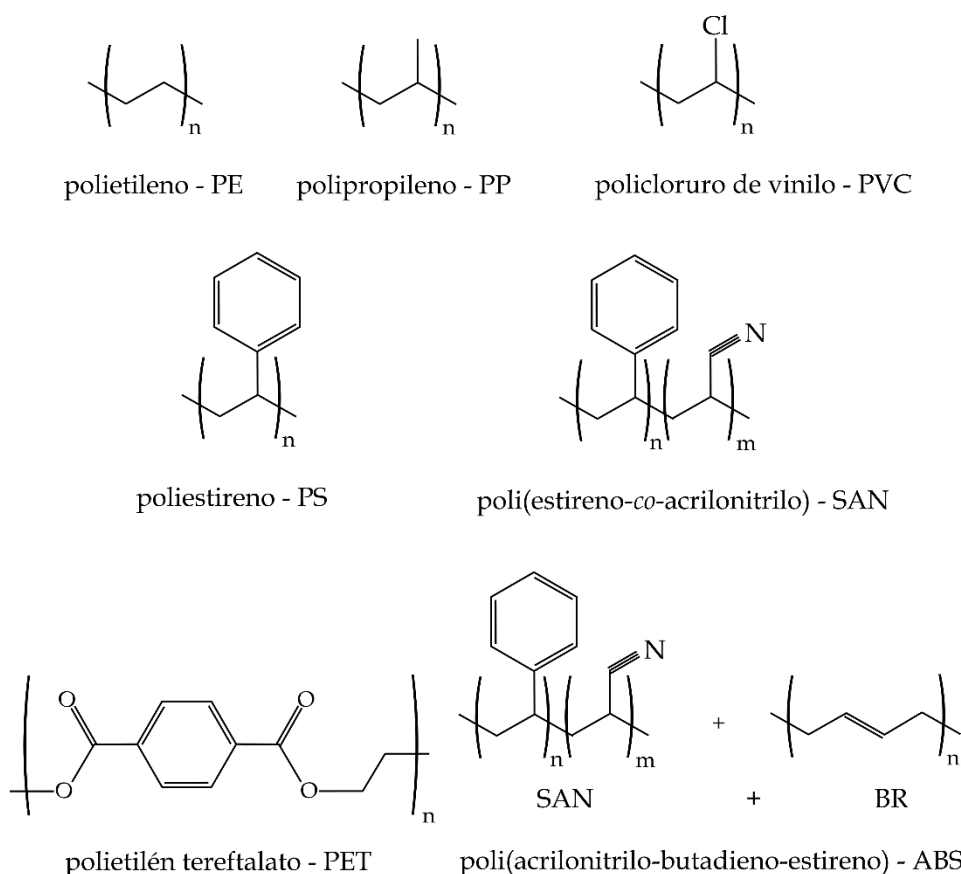
Figura I.2 Estructura de la unidad momonérica de diferentes polímeros de uso común o "commodities".

En particular, estos polímeros se han empleado de forma masiva en el sector envase y embalaje, y en aplicaciones desechables (higiene, alimentación, sector médico, etc.) debido a su coste relativamente bajo, fácil procesabilidad y, sobre todo, a su buen rendimiento mecánico y su alta capacidad de barrera tanto al O_2, CO_2, así como a compuestos aromáticos. No obstante, uno de los problemas más importantes de estos materiales, además de su origen petroquímico y su no biodegradabilidad, es la dificultad que se tiene en muchos casos para ser reciclados. Ello se debe a problemas de contaminación por contacto directo con alimentos u otras substancias que hacen inviable económicamente su reciclado [16, 17], o bien por las dificultades de separación de los residuos ya que, como se aprecia en la **Figura I.2**, se trata de polímeros con estructuras diferentes que, en muchas ocasiones, presentan alta incompatibilidad [18]. Es precisamente la problemática del reciclado ligada a este grupo de polímeros, la que ha puesto de manifiesto la ingente acumulación de residuos plásticos sin capacidad de someterse a procesos de reciclaje. La gran "*isla de plástico*" del Pacífico con un peso de al menos 79.000 toneladas y una extensión de 1,6 millones de km^2, es una de las evidencias más claras de la problemática generada por la acumulación de residuos plásticos [19]. Todo ello ha potenciado la conciencia social y medioambiental, situando la biodegradabilidad, no solo como un requisito funcional que deben tener los polímeros, sino también como un atributo medioambiental muy importante a la hora de reducir al máximo los residuos que se generan/acumulan.

I.1.1.2 Plásticos técnicos o de ingeniería.

Dentro de los polímeros derivados del petróleo y no biodegradables, los plásticos técnicos o de ingeniería tienen una gran relevancia en aplicaciones donde las prestaciones y propiedades son prioritarias, debido a que el correcto funcionamiento o estabilidad del sistema al que pertenecen es muy relevante. Algunos de los más utilizados en la industria son el polibutilén tereftalato (PBT), las poliamidas (PAs) o el policarbonato (PC), entre otros.

Este tipo de materiales se utilizan principalmente para aplicaciones con requisitos concretos y exigentes como la automoción o líneas de suministro de alta presión, donde los requerimientos técnicos de cada elemento son exigentes [20]. Otra aplicación de estos materiales, es la sustitución del vidrio por plásticos como el PC o el polimetil metacrilato (PMMA). Esto se debe a su estructura (**Figura I.3**), que es fundamentalmente amorfa, lo que le permite dejar pasar la luz visible. Además, las excelentes propiedades mecánicas y térmicas que poseen tanto el PC como el PMMA, permiten su uso en sectores tecnológicos para substituir elementos de vidrio en faros de automóvil o vidrios de seguridad, generando un menor peso final, una mayor libertad de diseño y una mayor seguridad derivada de la de rotura generada por este tipo de polímeros técnicos [21].

Merece la pena destacar que este tipo de polímeros suelen tener un Ciclo de Vida largo ya que sus aplicaciones son tecnológicas y, generalmente, al tener un coste elevado, se diseñan para un servicio prolongado. Es por ello que este grupo de polímeros, si bien tiene un impacto medioambiental, en tanto en cuanto son derivados

del petróleo, la acumulación al final del Ciclo de Vida no genera grandes volúmenes. Además, debido a su elevado coste, suele ser habitual su reciclaje.

policarbonato - PC   polióxido de metileno - POM   polimetil metacrilato - PMMA

polibutilén tereftalato) - PBT   poliamida 66 - PA66
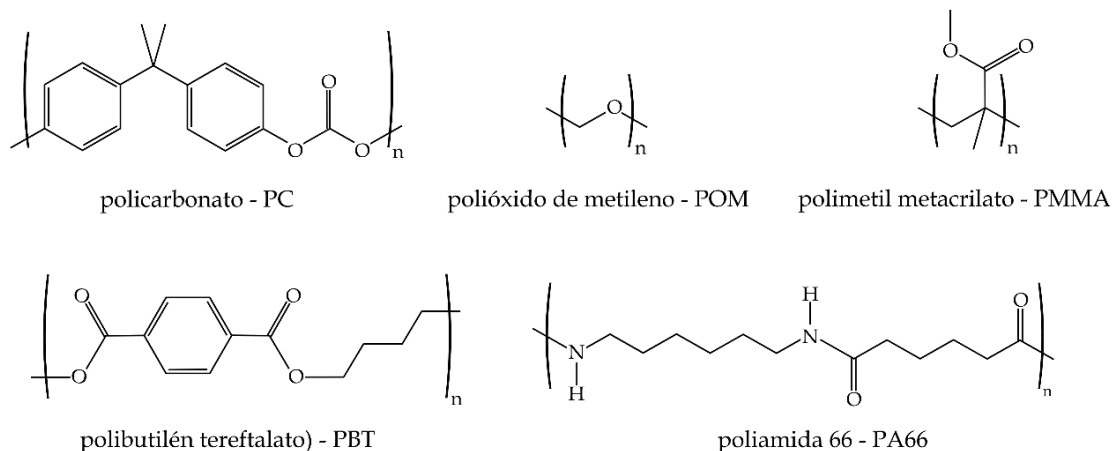
Figura I.3. Estructura de la unidad monomérica de diversos polímeros técnicos o de ingeniería.

I.1.1.3 Plásticos de altas prestaciones.

Por último, materiales como la poliéter éter cetona (PEEK), la poliéter imida (PEI) o la poliéter sulfona (PES) se consideran polímeros/plásticos de altas prestaciones. Este tipo de polímeros están especialmente diseñados para aplicaciones muy concretas en sectores tales como la industria eléctrica, nuclear o aeroespacial, donde se requiere de manera obligatoria que las propiedades mecánicas, térmicas y resistencia química alcancen sinergia y soporten una serie de condiciones extremas con el menor daño/deterioro posible [22-24].

Se trata de materiales de alto coste, cuyos procesos de fabricación son costosos y requieren, en la mayoría de casos, maquinaria especial para su transformación. Muchos de estos polímeros se encuentran reforzados con fibras y, evidentemente, su Ciclo de Vida es muy prolongado. Por ello, al igual que los plásticos técnicos, los plásticos de altas prestaciones, a pesar de su origen petroquímico, no suponen un gran problema medioambiental al final del Ciclo de Vida. En la **Figura I.4** se muestra la estructura de diversos polímeros de altas prestaciones donde se puede apreciar la complejidad de la unidad monomérica de muchos de ellos.

poliéter cetona - PEK

poliéter éter cetona - PEEK

poliéter éter cetona cetona - PEEKK

poliéter sulfona - PES

poliéter éter cetona éter cetona cetona - PEKEKK

poliéter imida - PEI

poliamida imida - PAI
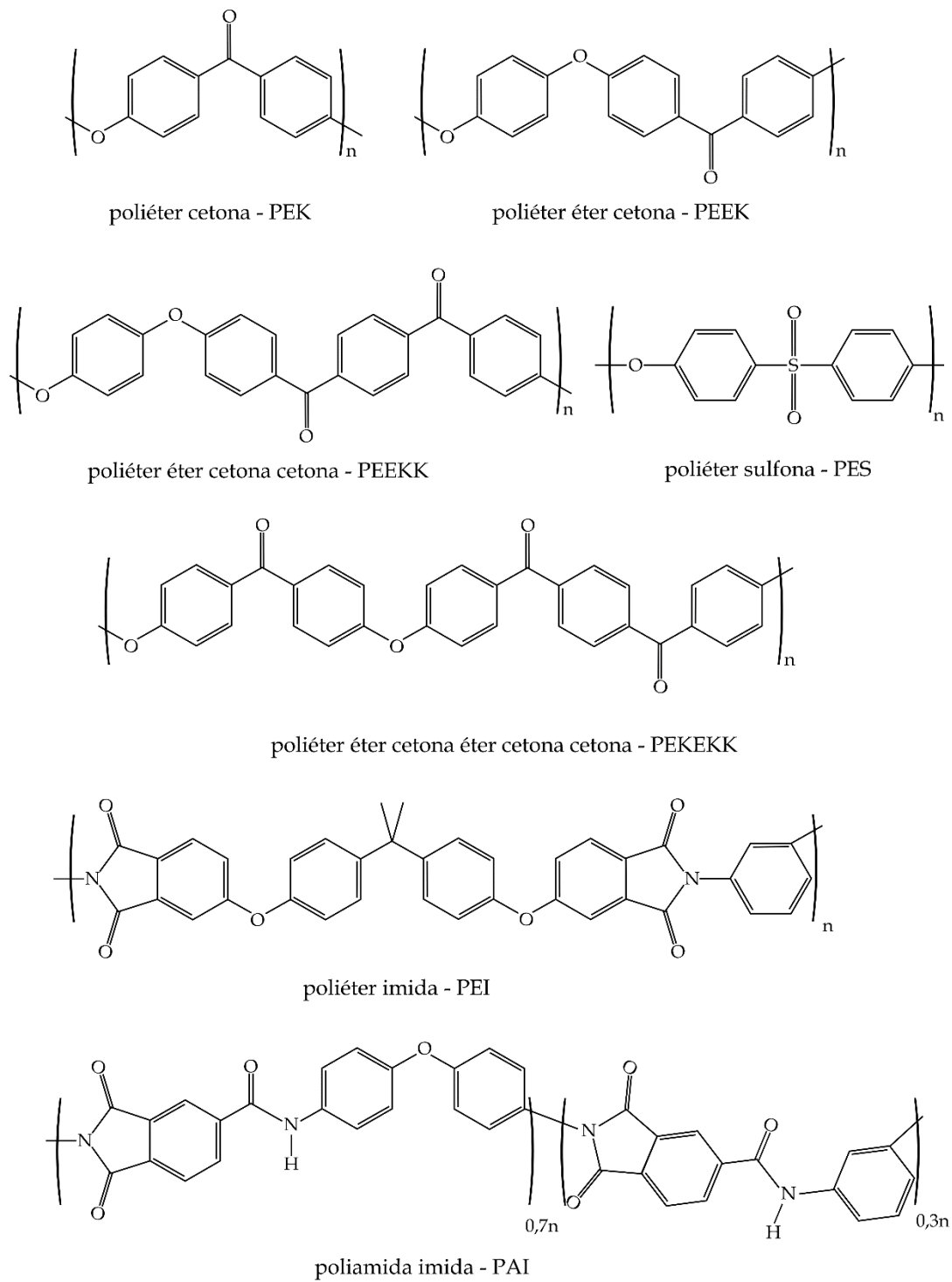
Figura I.4. Estructura de la unidad monomérica de diversos polímeros de altas prestaciones.

I.1.2. Polímeros de origen petroquímico biodegradables.

Como consecuencia del esfuerzo llevado a cabo en las investigaciones de las últimas décadas, se ha conseguido obtener una serie de materiales capaces de degradarse (desintegrarse en condiciones de compost), de manera mucho más rápida y sencilla, aunque sigan procediendo de recursos petroquímicos. Este tipo de materiales reducen de manera muy significativa el impacto medioambiental que se genera con su deshecho al final del Ciclo de Vida, aunque su origen no sea renovable.

Entre los polímeros con origen petroquímico y capacidad de biodegradación es posible encontrar muchos poliésteres alifáticos y, hasta incluso, algunos poliésteres aromáticos (**Figura I.5**).

ácido poliglicólico-PGA

polibutilén succinato-PBS

policaprolactona-PCL

poli(butilén succinato-*co*-adipato)-PBSA

poli(butilén succinato-*co*-tereftalato)-PBAT
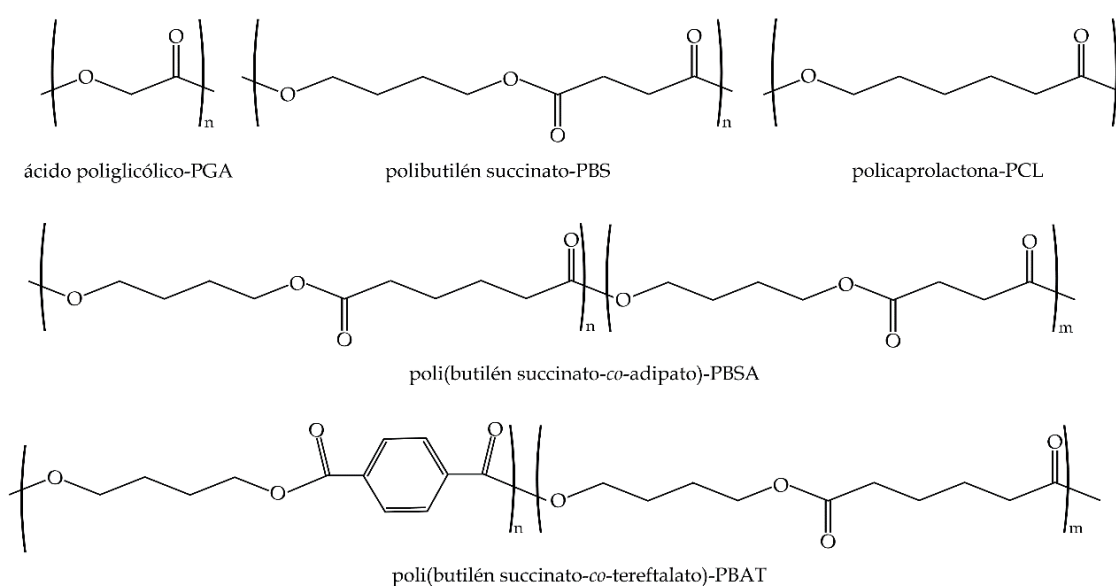
Figura I.5. Estructura química de algunos poliésteres y copoliésteres de origen petroquímico biodegradables.

Este tipo de polímeros tienen la peculiaridad de estar formados principalmente por estructuras de carbono muy estables, pero que poseen grupos funcionales que se pueden romper en ciertas condiciones. En particular, en estos polímeros, el grupo éster es fácilmente hidrolizable, con lo cual, en condiciones de compost, con una humedad controlada, se produce un proceso de fragmentación repetida de las cadenas poliméricas (despolimerización), hasta que dichos fragmentos pueden ser incorporados en los ciclos biológicos de determinados microorganismos, que acaban descomponiendo completamente el polímero tal y como se muestra en la figura siguiente (**Figura I.6**).
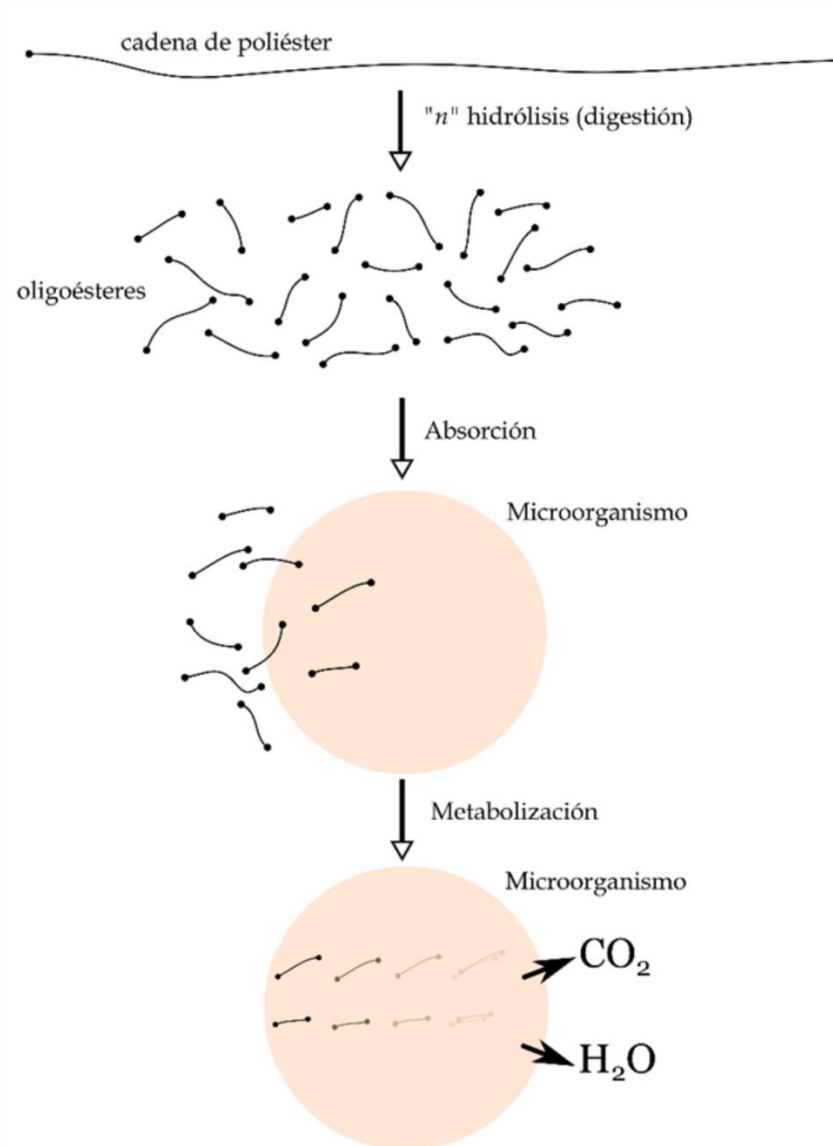
Figura I.6. Representación esquemática del proceso de biodegradación (desintegración en condiciones de compost) en poliésteres.

En los últimos años, sectores como el médico o el envase-embalaje han generado un gran aumento en el consumo y desarrollo de diferentes poliésteres. En particular, dentro del sector médico, materiales como el ácido poliglicólico (PGA), ácido poliláctico (PLA) o la policaprolactona (PCL), se están utilizando para la fabricación de prótesis, suturas y tornillos y placas de fijación [25, 26], estructuras óseas y tejidos [27, 28], o elementos vasculares [29]. Este gran auge de los poliésteres dentro de este sector se ha debido, fundamentalmente, a su capacidad de ser reabsorbidos por el organismo humano [30]. Además, este tipo de materiales poliméricos poseen un muy buen equilibrio entre propiedades mecánicas y térmicas, que los hacen muy viables para estas aplicaciones.

Debido a la problemática existente con la generación de residuos plásticos, se ha incrementado el uso de este tipo de materiales biodegradables en el sector del envase-

embalaje como una solución viable para paliar los efectos negativos en la cantidad de desechos generados. En este sentido, copoliésteres como el poli(butilén adipato-*co*-tereftalato) (PBAT) [31, 32] o poliésteres alifáticos como la poli(ε-caprolactona) (PCL) y poli(butilén succinato) (PBS) [33-35], se están introduciendo dentro de este sector gracias a su equilibrio de propiedades mecánicas y térmicas, sustituyendo a otros materiales con nulas capacidades de biodegradación.

Este grupo de polímeros ha conseguido, de manera muy positiva, reducir ciertos problemas relacionados con la contaminación de entornos y con las grandes cantidades de residuos que se estaban generando. No obstante, debido a que su origen sigue siendo petroquímico, se sigue dependiendo de compuestos derivados fósiles para su fabricación, por lo que el aumento de la huella de carbono crece con cada pieza que se fabrica con este tipo de polímeros. A pesar de las mejoras generadas gracias a la biodegradabilidad, se están ampliando de manera notable esfuerzos para encontrar y desarrollar polímeros con buenas capacidades para la aplicación en la industria a partir de recursos renovables y biodegradables.

I.1.3. Polímeros de origen renovables no biodegradables.

La fabricación de productos a partir de materias renovables, supone una gran reducción en el impacto ambiental que se genera con cada pieza y/o componente, ya que se permite prescindir de recursos como el petróleo para su fabricación, con la consiguiente reducción de la huella de carbono.

Dentro del grupo de polímeros de origen renovable y no biodegradable, se observa una gran utilización del etanol procedente de la industria de biodiesel, como fuente para la obtención de polietileno. Además, cabe resaltar la síntesis de algunas poliamidas derivadas de aceite de ricino o policarbonatos en los que el bisfenol A se ha substituido por isosorbida [36-39]. En la **Figura I.7** se muestra la estructura de diversas poliamidas de origen renovable con diferentes contenidos renovables. Destaca la poliamida 1010 (PA1010) que actualmente se obtiene 100% a partir de recursos renovables. Las otras poliamidas presentan diferentes contenidos renovables, ya que alguno de los componentes es de origen petroquímico, pero ya se han desarrollado las rutas "*bio*" para estos componentes y en los próximos años también alcanzarán un 100% de origen renovable.

poliamida 610 - PA610

poliamida 1010 - PA1010

poliamida 1012 - PA1012
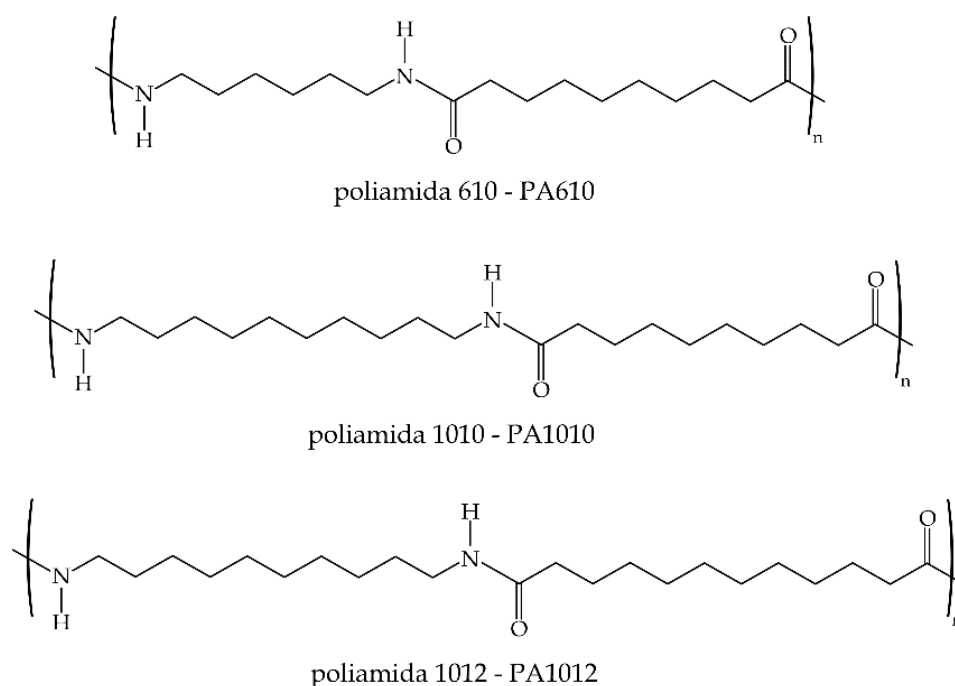
Figura I.7. Estructura química de diferentes poliamidas con distinto contenido de origen renovable.

Generalmente, estos polímeros presentan estructura y propiedades muy similares a sus equivalentes obtenidos mediante la ruta petroquímica, y es por ello, que no ofrecen propiedades de biodegradación. En relación al precio, suelen ser más caros que sus homónimos no renovables; no obstante, gracias a la conciencia social y las recientes investigaciones, empiezan a tener precios mucho más competitivos, donde la connotación "*bio*" empieza a aportar un nuevo valor añadido a este tipo de productos.

Como se puede intuir, en este grupo es posible encontrar plásticos de uso común como el PE, con gran participación en sector envase y embalaje y la consiguiente problemática de generación de residuos, y plásticos técnicos como las PAs y el PC que se emplean en aplicaciones técnicas, con un Ciclo de Vida largo y, en consecuencia, no contribuyen de forma significativa a la generación de grandes volúmenes de residuos.

I.1.4. Polímeros de origen renovable biodegradables.

Los problemas medioambientales derivados de la utilización de polímeros no renovables o que no tienen la capacidad para biodegradarse, han fomentado la investigación en un grupo de polímeros que se pueden obtener a partir de fuentes renovables y que, además, son capaces de desintegrarse en condiciones de compost. Este tipo de materiales poliméricos consiguen reducir al máximo la huella de carbono que se genera con cada producto fabricado y, además, reducen al máximo la generación de residuos, sirviendo en muchos casos como compost o abonos útiles para la industria agrícola. Como se muestra en la **Figura I.8**, estos nuevos polímeros

consiguen cerrar un ciclo completamente limpio, ya que desde su origen hasta el final de la vida útil, no solo no generan residuos nocivos, sino que son en algunos casos reciclados y, en otros casos, utilizados como abono, mejorando de manera directa el rendimiento de los cultivos y favoreciendo la fabricación de más materia prima.
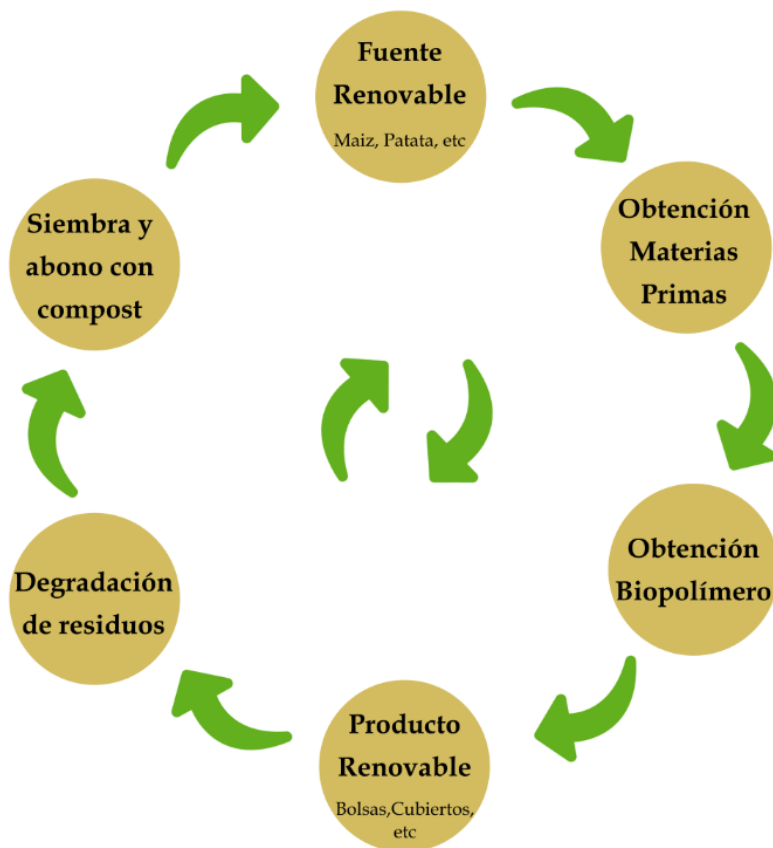
Figura I.8. Representación esquemática del Ciclo de Vida de un polímero renovable y biodegradable.

En ciertas industrias y, en particular, en el sector del envase y embalaje, este tipo de polímeros están teniendo gran repercusión en el ámbito de la I+D+i de nuevos productos y/o soluciones de alto rendimiento medioambiental. Estos esfuerzos se han centrado en el desarrollo de polímeros derivados completamente de fuentes renovables, con altas capacidades de biodegradabilidad. Entre estos polímeros merece la pena destacar el empleo de polisacáridos como el almidón, celulosa, quitina y derivados [40, 41]. Uno de los polímeros derivado de polisacáridos que mayor repercusión está teniendo en diversos sectores, es el ácido poliláctico (PLA), que se obtiene a partir de la fermentación de compuestos ricos en almidón. Otro grupo incluye a los denominados plásticos o polímeros bacterianos. Al igual que muchos vegetales almacenan reservas en forma de almidón, algunas cepas bacterianas son capaces de almacenar sus reservas en forma de polihidroxialcanoatos (más de 300 variedades) o PHAs. Si bien se ha investigado en la síntesis de un gran número de PHAs a partir de diversas cepas bacterianas, comercialmente, son el poli(3-hidroxibutirato) (PHB) y sus copolímeros como el poli(3-hidroxibutirato-*co*-3-hidroxivalerato) (PHBV), el poli(3-hidroxibutirato-*co*-3-hidroxihexanoato) (PHBH), etc., los que mayor interés han suscitado. Debido a su estructura química de poliéster

alifático, la cual se muestra en la **Figura I.9**, no solo poseen altas capacidades de degradación en condiciones de compost, sino que tienen un alto grado de biocompatibilidad [42, 43]. Este factor los hace materiales muy prometedores para sectores como el envasado de alimentos o el sector médico [33, 44, 45]. Junto con estos, en los últimos años también han adquirido relevancia en el sector envase y embalaje, así como en la alimentación, los polímeros derivados de proteínas como el gluten, colágeno, soja, queratina, etc [46].

poli(3-hidroxibutirato)-P3HB   poli(3-hidroxibutirato-*co*-3-hidroxivalerato)-PHBV
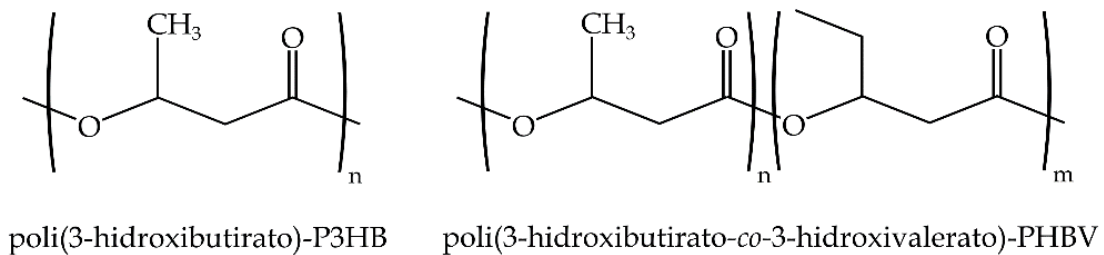
Figura I.9. Representación esquemática de la estructura de monómero de un polihidroxialcanoato homopolímero y un copolímero.

Como se ha descrito previamente, el PLA es uno de los materiales que más repercusión ha tenido en los últimos años, gracias a la buena conjunción de propiedades que posee. Además, ofrece un proceso de fabricación relativamente sencillo y un gran repertorio de fuentes renovables asequibles [47, 48]. Gracias a la fermentación de almidones, que pueden proceder de diferentes fuentes como el maíz, la caña de azúcar o la yuca, se pueden obtener moléculas de lactida y así, polimerizar para conseguir el producto final [49]. Con relación a los PHAs, entre los que destacan comercialmente el PHB [50-53] y el PHBV [54, 55], se trata de materiales con un futuro muy prometedor en la industria del plástico. No obstante, todavía deben superar ciertas limitaciones de costes de fabricación ligados a su origen bacteriano, así como temas técnicos ligados al procesado y envejecimiento a temperatura ambiente, para ser completamente competitivos en la industria actual.

A raíz de los graves problemas generados por los plásticos en los últimos años, y la concienciación social sobre la contaminación y el cambio climático, este último grupo de polímeros están destinados a convertirse en los nuevos plásticos del futuro, capaces de eliminar de manera directa los problemas medioambientales derivados de las fuentes no renovables y, en particular, la capacidad para descomponerse en condiciones de compost al final del Ciclo de Vida.

I.2. OBTENCIÓN Y TECNOLOGÍA DE POLIÉSTERES.

I.2.1. Obtención de poliésteres.

Desde el punto de vista químico, y como indica su nombre, los poliésteres se obtienen a partir de la unión de monómeros que contienen grupos éster (**Figura I.10**). Dentro de los poliésteres, se pueden encontrar multitud de polímeros diferentes, ya que, generalmente, la esterificación se produce por condensación de ácidos dicarboxílicos con alcoholes (dioles).
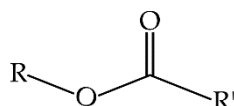
Figura I.10. Representación esquemática de la estructura general de un éster o sal orgánica de un ácido carboxílico.

Uno de los poliésteres más utilizados en la industria es el polietilén tereftalato (PET), aunque recientemente el ácido poliláctico (PLA) ha ganado interés debido a su notable eficiencia medioambiental.
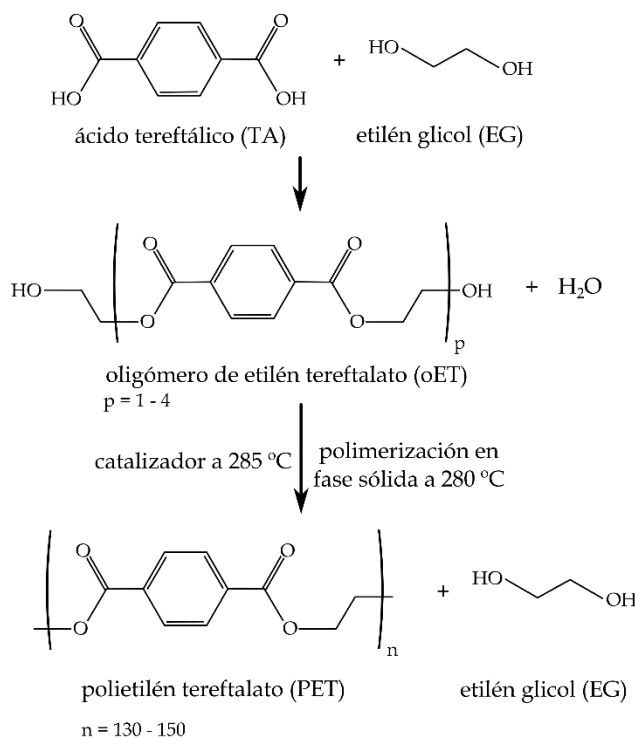
Figura I.11. Representación esquemática de la estructura monomérica de poliésteres de amplio uso a nivel industrial.

Muchos poliésteres se obtienen mediante procesos de policondensación de ácidos dicarboxílicos con alcoholes dihídricos. Las condensaciones repetidas conducen a la formación de cadenas lineales. En **Figura I.11** se muestra el proceso de polimerización del PET a partir de ácido tereftálico (TA) y del etilén glicol (EG) en diversas etapas [56]. En una primera etapa el etilén glicol reacciona con los dos grupos carboxílicos y da lugar a la formación de bis(2-hidroxietil) tereftalato (BHET), junto con oligómeros de bajo peso molecular. Para alcanzar el alto peso molecular, se produce un calentamiento de estos monómeros y oligómeros y, posteriormente, se lleva a cabo una polimerización en fase sólida mediante condensación de etilenglicol. Normalmente se trabaja con un exceso de etilenglicol para forzar este mecanismo de síntesis.

Otros poliésteres se obtienen mediante procesos de polimerización de adición por apertura de anillo ("*ring opening polymerization*" – ROP), como es el caso del PLA o la PCL, por apertura de la lactida y ε-caprolactona respectivamente, tal y como se muestra en la **Figura I.12** [57].
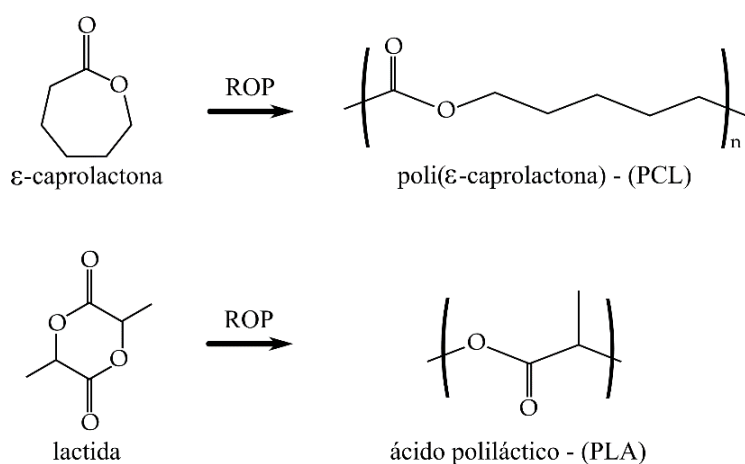
Figura I.12. Representación esquemática de la estructura de anillo y monómero de poliéster obtenido mediante ROP.

I.2.2. Clasificación de poliésteres.

De manera sencilla, los poliésteres se pueden clasificar en dos grandes grupos: origen petroquímico y origen renovable. No obstante, dentro de estos grandes grupos se pueden englobar dos subgrupos completamente diferentes y que basan sus diferencias en su composición estructural; hecho que condiciona, en gran medida, la susceptibilidad a la biodegradación. Así pues, otra forma de clasificar los poliésteres se basa en la presencia o no de grupos aromáticos, dando lugar a los poliésteres aromáticos y alifáticos. Antes de entrar en profundidad en los dos grupos principales, hay resaltar que, debido a las diferencias entre su estructura, los poliésteres alifáticos son más sencillas, lo que facilita en gran medida procesos como la biodegradación mediante hidrólisis de los grupos éster. En el caso de los poliésteres aromáticos, estos poseen una estructura más compleja y resistente debido a la presencia de los grupos aromáticos [58]. La **Figura I.13** muestra de forma gráfica la diferencia de estructura de diversos poliésteres.

politrimetilén tereftalato (PTT)   polibutilén adipato (PBA)
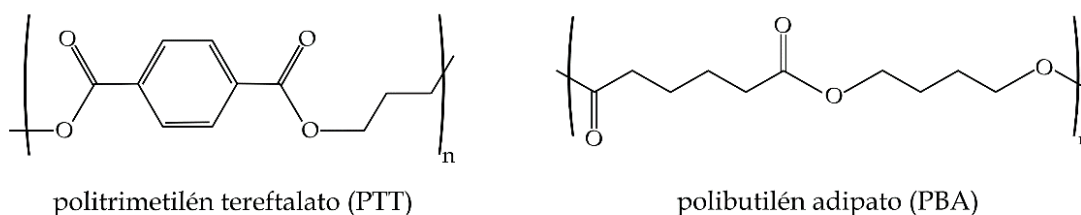
Figura I.13. Diferencias entre la estructura de un poliéster alifático, politrimetilén tereftalato (PTT) y uno aromático, polibutilén adipato (PBA).

Dentro de la industria de los plásticos, los poliésteres aromáticos han sido los más estudiados y utilizados a lo largo de la historia gracias a sus excelentes propiedades térmicas y mecánicas, lo que les ha supuesto en una muy buena posición comercial frente a los poliésteres alifáticos. No obstante, los nuevos intereses sociales derivados de la no utilización de polímeros derivados del petróleo y el deseo de reducir al máximo la generación de residuos, ha provocado que los poliésteres alifáticos hayan empezado a ser investigados en profundidad y utilizados en aplicaciones que antes cubrían algunos poliésteres aromáticos.

I.2.2.1 Poliésteres de origen petroquímico.

Los poliésteres obtenidos a partir de fuentes petroquímicas se han utilizado de manera continuada desde su descubrimiento, gracias a las excelentes propiedades y características que poseen. Dentro de estos poliésteres termoplásticos, el PET (poliéster aromático) ha sido, y continúa siendo, uno de los que presenta mayor consumo en la industria del envasado de productos gracias a las altas propiedades mecánicas, alta temperatura de fusión y excelentes propiedades barrera. Además, debido a la complejidad de su estructura química, poseen una gran estabilidad química, lo que les confiere una gran resistencia contra ataques microbianos y degradaciones en situaciones de compost. Este tipo de resistencia los ha convertido en soluciones viables para envases de todo tipo de productos con una gran estabilidad en el tiempo. Además del PET, otros poliésteres aromáticos derivados del ácido tereftálico se han sintetizado y encuentran aplicaciones de menor consumo, pero de mayor tecnicidad; es el caso del polibutilén tereftalato (PBT) y el politrimetilén tereftalato (PTT).

Los poliésteres aromáticos derivados del petróleo poseen, en general, una gran estabilidad química y a la degradación, lo que genera de manera directa un gran problema medioambiental ligado a la difícil eliminación de sus residuos.

Dentro de los poliésteres petroquímicos, también es posible encontrar un gran grupo de poliésteres alifáticos, con características muy lejanas a las que ofrecen los aromáticos, tanto a nivel de propiedades como a nivel de coste. Sin embargo, estos poliésteres alifáticos presentan gran susceptibilidad a la biodegradación debido a la sensibilidad de los grupos éster a los fenómenos de hidrólisis, hecho que facilita la desintegración en condiciones de compost con humedad controlada.

Como ya se ha comentado, este tipo de poliésteres, posee una estructura más simple, que favorece los procesos de degradación y siendo soluciones viables para reducir la generación de residuos [59, 60]. Polímeros como la PCL, el PLA o el polibutilén succinato (PBS) son poliésteres alifáticos que se pueden obtener a partir de monómeros derivados del petróleo [61, 62]. No obstante, muchas de los compuestos orgánicos que se emplean para la síntesis de estos poliésteres (ácidos dicarboxílicos y alcoholes dihídricos), también se pueden obtener mediante rutas "bio" que, actualmente, no se emplean debido a los elevados costes, pero que en un futuro desempeñarán un papel importante en la síntesis de estos poliésteres [63, 64].

I.2.2.2 Poliésteres de origen renovable parcial o total.

Los poliésteres derivados de materias primas renovables, vienen a solucionar muchos de los problemas ambientales generados por la utilización de polímeros derivados del petróleo, o aquellos materiales con bajas capacidades para ser degradados en condiciones de compost.

Con el objetivo de paliar los problemas medioambientales ligados a los poliésteres aromáticos, con un doble impacto tanto en origen (petroquímico) como la final del Ciclo de Vida (no biodegradables), muchas investigaciones se han centrado en la síntesis de poliésteres a partir de recursos renovables (total o parcialmente). Desde un punto de vista técnico, es posible obtener un PET 100% procedente de recursos renovables. Actualmente, se comercializa un bioPET con un contenido renovable de alrededor del 30%, que corresponde con el contenido en etilén glicol (EG) empleado en su síntesis, ya que, mediante procesos de fermentación de biomasa, es posible obtener glicoles con un coste razonable   [65]. Este material puede mantener las buenas propiedades de su homólogo de origen petroquímico, pero con el valor añadido de reducir el impacto medioambiental gracias a su origen parcialmente renovable. Sin embargo, el futuro bioPET puede alcanzar una fuente 100% renovable ya que existe una ruta biológica para sintetizar ácido tereftálico (TA) [66, 67].

En contrapartida, los poliésteres alifáticos de origen renovable son uno de los polímeros más prometedores dentro del sector del plástico. Atributos como un fácil proceso de compostaje y un buen equilibrio de propiedades, los sitúa como una alternativa de bajo impacto medioambiental en diferentes sectores industriales, entre los que destaca el envase y embalaje. Se pueden sintetizar mediante diferentes mecanismos a partir de materias como almidones, glucosas o celulosas para controlar de manera muy precisa las formulaciones y masa molar final, aspecto que repercute en las propiedades finales y aplicaciones [68]. En este sentido la **Figura I.14** muestra el proceso de obtención de algunos poliésteres de origen renovable total o parcial.
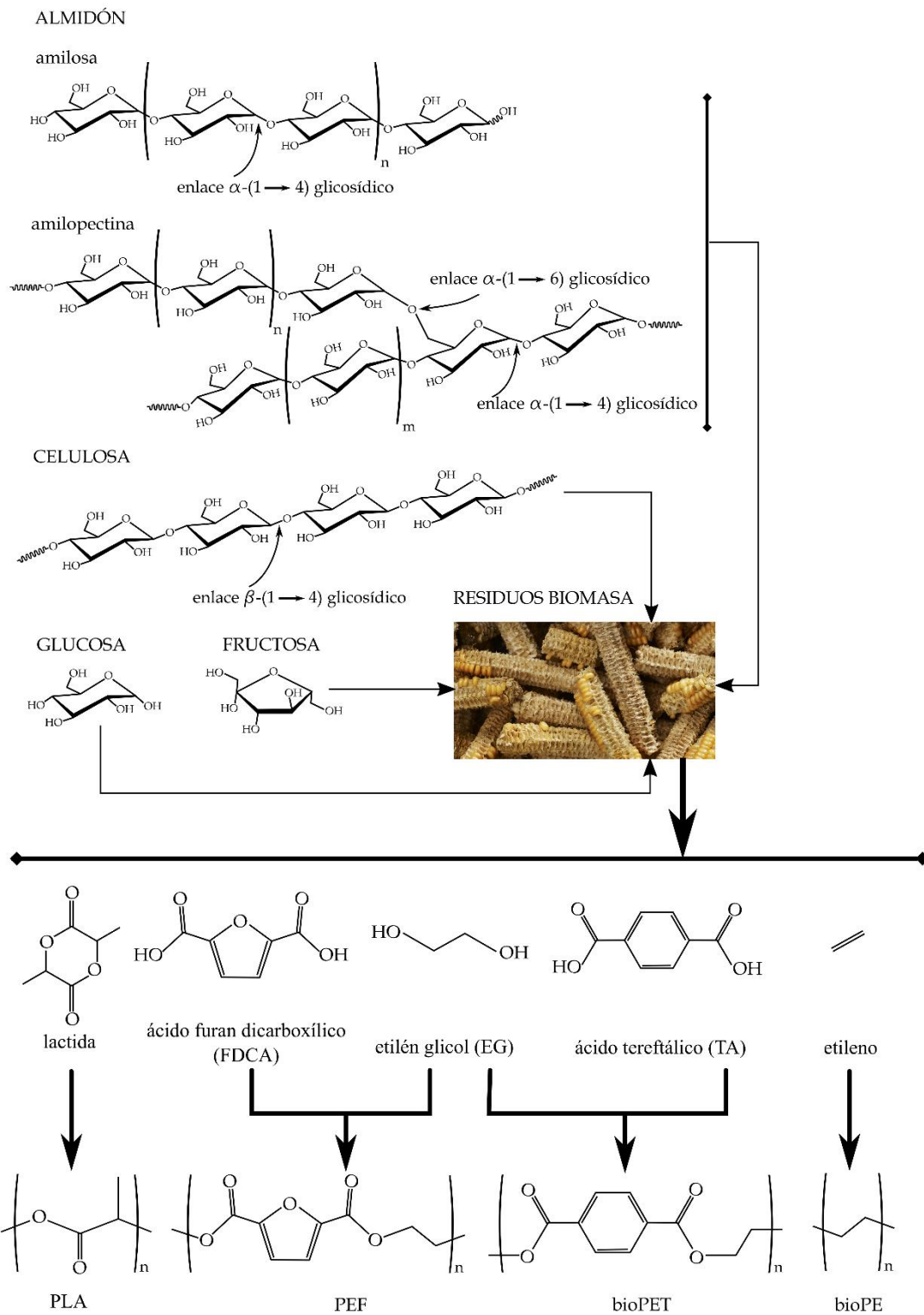
Figura I.14. Proceso de obtención de poliésteres de origen renovable y otros biopolímeros a partir de carbohidratos procedentes de residuos de biomasa ricos en almidón y celulosa.

Mediante fermentación de carbohidratos (almidones y celulosa, principalmente), es posible obtener pentosas y hexosas. Estas, representan la base para

la síntesis de monómeros para la obtención de biopolímeros. Uno de los poliésteres más relevantes, debido a su producción y consumo es el PLA, siendo el sector del envase y embalaje el que mayor uso hace de este biopolímero [69-71]. Uno de los polímeros más prometedores es el denominado polietilén Furanoato (PEF) que presenta una estructura muy similar a la del PET (presencia de un anillo), y puede obtenerse 100% de recursos renovables, sin embargo, actualmente, todavía no se encuentra totalmente introducido a escala comercial [72, 73].

I.2.3. Degradación/desintegración de poliésteres.

El gran aumento en el consumo de plásticos durante las últimas décadas, en conjunción con la gran durabilidad que poseen algunos polímeros, está generando, a día de hoy, grandes problemas en relación a la gestión de residuos o la contaminación de entornos naturales. La gran concienciación social generada en los últimos años a favor de una reducción del impacto medioambiental, ha entrado de manera muy directa en la industria del plástico, fundamentalmente en los residuos ligados al sector envase y embalaje, que son los que representan un mayor volumen. En este sentido, desde principios del siglo XXI, las investigaciones y desarrollos de nuevos polímeros capaces de paliar los problemas de contaminación y reducción del impacto ambiental han empezado a evolucionar de manera muy positiva.

Por este motivo, se han empezado a desarrollar, diseñar y modificar, polímeros capaces de degradarse/desintegrarse bajo condiciones determinadas. Este tipo de condiciones permiten a ciertos polímeros descomponerse en tiempos razonables, gracias a dos fenómenos: una fragmentación de las cadenas macromoleculares debido a la sensibilidad a la rotura de ciertos enlaces (por ejemplo, los grupos éster en poliésteres alifáticos son muy sensibles a la hidrólisis) y una incorporación de los segmentos fragmentados a los ciclos metabólicos de ciertos microorganismos en entornos activos. Este tipo de polímeros capaces de ser degradados en su totalidad, sin afectar en gran medida al entorno, se les ha denominado polímeros biodegradables.

I.2.3.1 Procesos de biodegradación enzimática.

Los poliésteres alifáticos son los materiales poliméricos con mayores capacidades desde el punto de vista de la biodegradación. Algunos ejemplos de poliésteres con grandes capacidades para ser degradados son el PHB [74, 75], la PCL [76] o el PLA [77].

Dentro de la degradación de los poliésteres, una de las técnicas empleadas para llevar a cabo este proceso, es el ataque de microorganismos o biodegradación catalizada por enzimas. Para que este ataque sea efectivo, es necesario convertir los polímeros en oligómeros de bajo peso molecular, para conseguir su solubilidad en agua. En estas condiciones, los microorganismos incorporan estos fragmentos de bajo peso molecular a su ciclo metabólico y para convertirlos en agua, dióxido de carbono o biomasa. En especial, este proceso se centra inicialmente en la despolimerización a través de ciertas enzimas. La **Figura I.15** muestra el mecanismo de degradación a

través de microorganismos, donde poliésteres alifáticos como la PCL o el PLA pueden desintegrarse completamente. Este tipo de biodegradación es la denominada enzimática o en presencia de enzimas. Los microorganismos excretan enzimas extracelulares que se anclan en la superficie del polímero, provocando una erosión o fragmentación de las cadenas poliméricas más externas. Con ello, se forman oligómeros de bajo peso molecular, solubles en medio acuoso que son asimilados a través del metabolismo del microorganismo, y después de este proceso desprenden H_2O, CO_2, CH_4 y otros productos resultado del proceso metabólico [78].
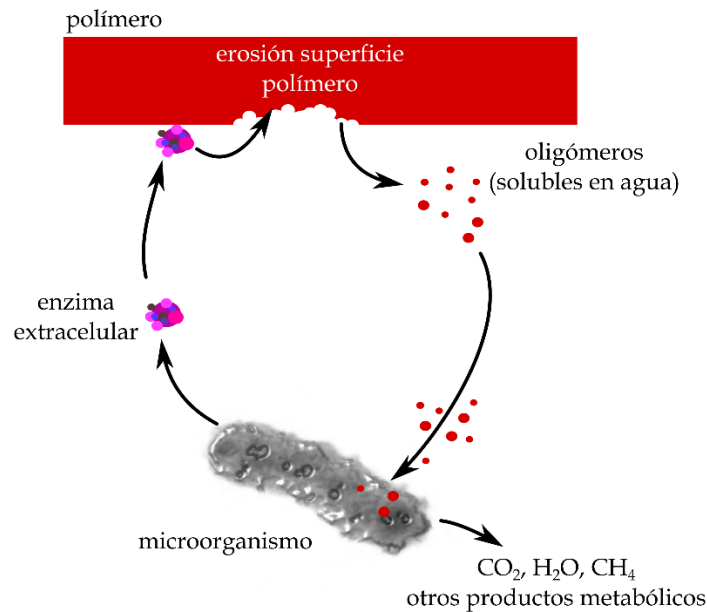
Figura I.15. Esquema del mecanismo general de degradación por microorganismos catalizada por enzimas.

Teniendo en cuenta este primer sistema, debido a su estructura, los poliésteres alifáticos son los candidatos principales para poder ser degradados [79]. Por este motivo, y como ya se ha comentado anteriormente, poliésteres aromáticos como el polietilén tereftalato (PET) o el polibutilén tereftalato (PBT) son materiales inviables para ser degradados de ésta forma ya que los grupos aromáticos confieren una mayor resistencia a la actividad enzimática de erosión. No obstante, a finales del siglo XX autores como Tokiwa y Suzuki [80], descubrieron que ciertas enzimas aisladas, eran capaces de atacar de manera directa a la superficie de estos polímeros. Así, han favorecido y abierto líneas de investigación para obtener ciertas enzimas modificadas que sean capaces de descomponer ciertos poliésteres que, hasta la fecha, son inertes a este tipo de degradación.

I.2.3.2 Procesos de degradación hidrolítica.

Además de la biodegradación a través de microorganismos mediante el empleo de enzimas, existen otros tipos de degradación o desintegración, que también se emplean en ciertos materiales y, fundamentalmente, poliésteres con el objetivo de reducir al máximo su impacto ambiental. En este caso, son los poliésteres alifáticos

como los polidroxialcanoatos (PHAs), el PLA, así como otros poliésteres de origen petroquímico como el PBS, PCL, PBSA, etc., los que son susceptibles de degradación por hidrólisis debido a la fuerte sensibilidad de los grupos éster, fácilmente hidrolizables por la acción del agua [81]. Si bien en el mecanismo de degradación enzimática es la acción de las enzimas la que provoca la erosión superficial del polímero a través de la fragmentación de las cadenas, la hidrólisis puede ejercer el mismo efecto de fragmentación hasta dar lugar a oligómeros de bajo peso molecular que pueden incorporarse en el metabolismo de determinados microorganismos. Este es el denominado proceso de compostaje o desintegración en condiciones de compost. El compost proporciona un medio para la desintegración que favorece, en primer lugar, los procesos hidrolíticos de fragmentación, que llevan asociados la formación de oligómeros de bajo peso molecular que progresivamente se acercan a las paredes celulares de los microrganismos y se incorporan a su metabolismo.
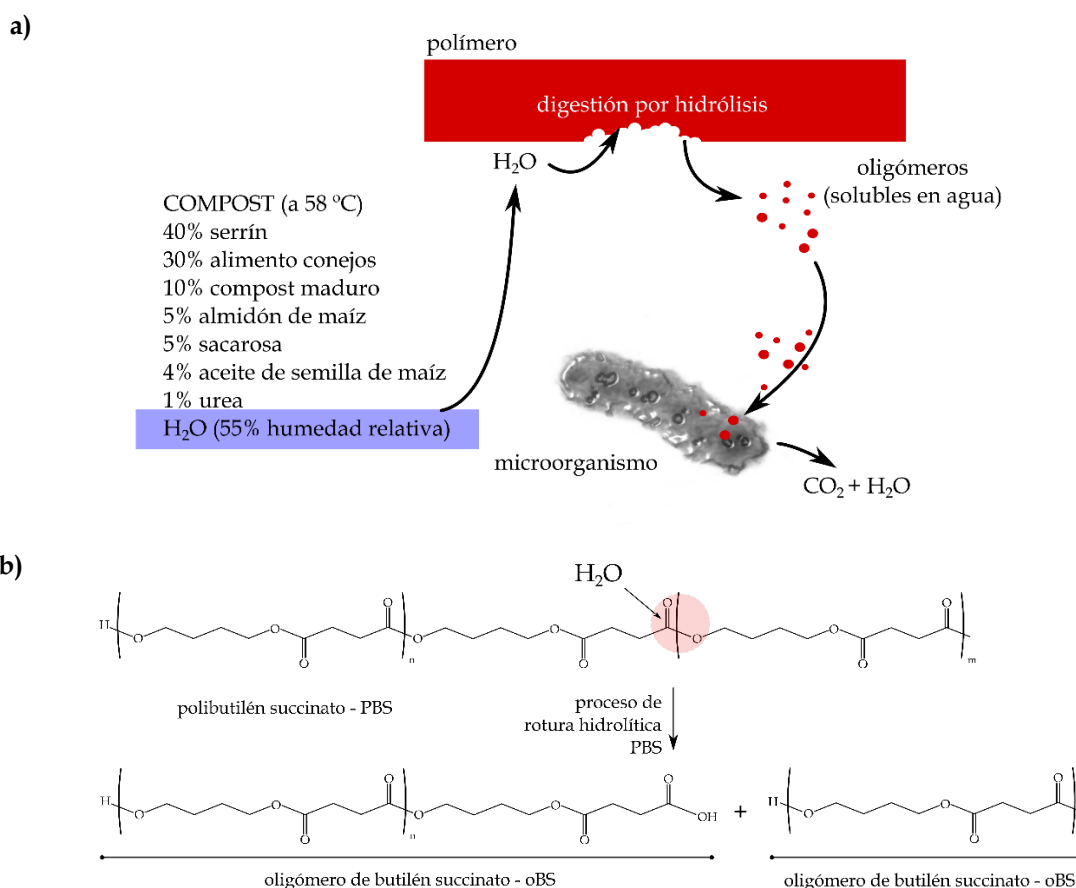
Figura I.16. Esquema del mecanismo general de degradación por hidrólisis/compostaje de un poliéster alifático, polibutilén succinato (PBS), a) esquema del proceso de compostaje y b) esquema de la formación de oligómeros de bajo peso molecular por hidrólisis.

La composición del compost viene definida en la norma UNE-EN-ISO 20200 [82]. El compost contiene (sobre peso en seco) un 40% de serrín, un 30% de alimento para conejos, un 10% de compost maduro, un 10% de almidón de maíz, 5% de sacarosa, 4% de aceite de semilla de maíz y, finalmente, un 1% de urea. Las condiciones de cultivo se establecen en una humedad relativa de 55% (debe revisarse

periódicamente y restituir el agua perdida por evaporación), a una temperatura de 58 ºC. En estas condiciones, si se entierra un poliéster en un medio de compost, se produce una hidrólisis progresiva que lleva a la fragmentación de las cadenas, dando lugar a la formación de oligómeros de bajo peso molecular que, finalmente, pueden incorporarse al metabolismo de los microorganismos presentes en el compost [83]. En la **Figura I.16** se muestra esquemáticamente el proceso de degradación hidrolítica/compostaje de un poliéster alifático.

Al igual que sucede en la degradación enzimática, la simplicidad en la estructura química de los poliésteres alifáticos, favorece en gran medida este tipo de degradaciones. En general los poliésteres alifáticos son más sensibles a la degradación por hidrólisis, ya que los aromáticos poseen una mayor resistencia. Con el fin de mejorar la degradación de algunos poliésteres aromáticos, estos se están combinando con poliésteres alifáticos para mejorar su degradación hidrolítica [84]. En este caso, copoliésteres alifáticos-aromáticos como el poli(butilén adipato-*co*-tereftalato) (PBAT), poseen una gran capacidad de degradación con valores molares aromáticos inferiores al 55%, manteniendo siempre un buen compromiso de propiedades mecánicas y térmicas [85].

I.2.4. Propiedades y aplicaciones de poliésteres.

El PET es, sin duda, uno de los polímeros más representativo de los poliésteres termoplásticos. En general, los poliésteres aromáticos poseen unas propiedades mecánicas, térmicas y resistencia química muy superiores a los poliésteres alifáticos, debido a la mayor complejidad de su estructura. En el caso del PET, este se caracteriza por tener una elevada tenacidad, una buena resistencia, tanto a la temperatura como a elementos externos, alta transparencia y gran resistencia al desgaste. Además, se caracteriza por ser uno de los materiales con un coste más bajo y con unas muy buenas propiedades barrera, que lo han situado como uno de los principales polímeros en la industria del envase y embalaje. Sin embargo, debido a su elevada resistencia química, no es susceptible de biodegradación en condiciones convencionales de compost.

El PET se ha utilizado masivamente en la fabricación de botellas de agua y bebidas carbónicas, todo tipo de envases alimentarios y algunos envases para detergentes o productos químicos [86]. Dentro del sector electrónico, debido a las excelentes propiedades al desgaste, la alta resistencia dieléctrica y la transparencia, el PET también se ha empleado en la fabricación de sensores piezoeléctricos, películas protectoras para aislamientos, circuitos integrados, células solares o, incluso, partes electromecánicas que antes se fabricaban con materiales termoestables, factor que facilita mucho el reciclaje de ciertos componentes electrónicos [87-89].

Otra de las aplicaciones más relevantes del PET a lo largo de la historia, ha sido en el sector textil, debido a la gran facilidad que tiene para ser procesado en forma de filamento/fibra y las excelentes propiedades mecánicas y térmicas que poseen. Otro poliéster aromático, el poli(trimetilén tereftalato) (PTT), posee unas cualidades muy elevadas para la obtención de fibras, incluso mejores que algunos *nylons* o poliamidas comerciales. Dentro del sector del automóvil y la industria mecánica, debido a las

excelentes propiedades técnicas de algunos poliésteres, se han utilizado como elementos capaces de soportar elevadas fuerzas tales como turbinas de bombas, engranajes o cojinetes.

Entre los poliésteres aromáticos-alifáticos, hay que destacar que el PBAT tiene unas propiedades muy similares a las del polietileno de baja densidad (LDPE), en relación a sus propiedades mecánicas, además de ser totalmente biodegradable. Estas propiedades le confieren la posibilidad de ser incorporado en multitud de aplicaciones [85], ligadas al sector envase y embalaje. También, debido a su buena biocompatibilidad y bioabsorción, el PBAT se ha empleado de forma creciente en el sector médico en forma de suturas, o estructuras que requieren soportar grandes esfuerzos, y que otros materiales no pueden proporcionar [90, 91].

Los poliésteres alifáticos, con relación a los aromáticos, ofrecen una reducción de algunas propiedades mecánicas como la tenacidad y, en algunos casos, la elongación, viéndose mermado su uso en ciertas aplicaciones. Por otro lado, suelen tener una menor temperatura de fusión, y una estabilidad térmica algo inferior. No obstante, debido a la menor resistencia química que poseen, son capaces de degradarse/desintegrarse en diversos medios, lo que los convierte en polímeros muy prometedores desde un punto de vista medioambiental.

Esta ventaja medioambiental, ligada a unas buenas propiedades barrera, los sitúa en la industria del envase y embalaje como opciones muy viables para reducir el impacto de los grandes volúmenes de residuos generados por este sector. Los poliésteres alifáticos como el PLA, la PCL, el PGA son materiales biocompatibles y, además, pueden ser absorbidos de manera controlada por el organismo humano, lo que amplía el uso de estos materiales en multitud de aplicaciones médicas en fabricación de placas de fijación, prótesis, tornillos de interferencia, suturas, estructuras de soporte y ciertos dispositivos médicos, situándose como materiales punteros dentro de este ámbito [92-94]. Otros sectores relevantes para estos poliésteres, son el de la automoción, la impresión 3D o el sector textil, donde su baja temperatura de procesado, alta eficiencia medioambiental y buenas propiedades mecánicas, les han permitido sustituir a materiales petroquímicos o no biodegradables de uso común [95, 96].

La conjunción de todos estos factores convierte a la mayoría de poliésteres alifáticos como el PLA, el PBS o la PCL en materiales con grandes posibilidades y multitud de aplicaciones. En la **Tabla I.1** se pueden apreciar las principales diferencias entre algunas propiedades de diversos poliésteres, tanto alifáticos como aromáticos [97-100].

**Tabla I.1.** Comparativa de propiedades mecánicas y térmicas de algunos poliésteres alifáticos y aromáticos.

Propiedad	PET	PBAT	PLA	PBS	PCL
Tipo	Aromático	Aromático-Alifático	Alifático	Alifático	Alifático
Densidad (g cm^{-3})	1,37-1,40	1,25-1,29	1,20-1,25	1,24-1,27	1,14-1,15
Módulo de Young (MPa)	2800-3100	50-80	3200-3800	400-600	200-350
Resistencia a tracción (MPa)	70-75	9-12	48-60	28-35	40-43
Alargamiento (%)	60-100	350-550	3-8	180-250	400-600
T_g (ºC)	75	-45 a -35	90 a 120	-30 a -20	-70 a -60
T_m (ºC)	260	60-120	160-180	115-120	50-65

Dentro de las aplicaciones más destacadas de los poliésteres alifáticos, se encuentra un gran sector como el del envase y embalaje [101-104]. Con la incorporación de este tipo de poliésteres en esta industria, se está contribuyendo, en gran medida, a mitigar los problemas medioambientales ligados con la generación y acumulación de residuos. La principal ventaja que aportan es que estos materiales son capaces de degradarse/desintegrarse bajo condiciones de compost/hidrólisis, evitando que se contaminen entornos naturales. En este sector, el PLA es, con diferencia, el poliéster alifático de mayor consumo y su coste se ha situado en parámetros competitivos. Sin embargo, alguna de las limitaciones que presenta el PLA están ligadas a su gran fragilidad (baja elongación) y propiedades barrera moderadas [105, 106]. Es por ello, que en el ámbito de la investigación se está trabajando intensamente en solucionar total o parcialmente estos inconvenientes, que limitan una utilización masiva de PLA [43, 107].

I.2.5. Tecnología de ácido poliláctico (PLA).

Dentro de los poliésteres alifáticos, el ácido poliláctico es uno de los materiales más relevantes, y que más repercusión ha tenido en las últimas décadas. Debido a su estructura, es un polímero totalmente biodegradable que, además, se puede obtener tanto de recursos petroquímicos como componentes 100% renovables, tales como el azúcar, el maíz o la patata [108-110]. Estos factores, junto con el buen equilibrio de propiedades mecánicas que posee, son los motivos por los que se ha convertido en una alternativa muy prometedora para reducir al máximo la acumulación de residuos plásticos generados por el ser humano y, disminuir al máximo la huella de carbono. Además, es importante destacar que el PLA puede obtenerse a partir de residuos de diversos orígenes procedentes del sector alimentación, agroforestal, etc., contribuyendo, de esta manera, a la generación de economías circulares [111, 112].

Para la obtención de PLA de origen renovable, se parte de recursos vegetales con un alto contenido en carbohidratos, para convertirlos en glucosa (dextrosa), y a partir de un proceso de fermentación bacteriana y procesos de polimerización, obtener un polímero completamente funcional. A modo de esquema, la **Figura I.17** muestra el proceso de obtención de PLA.
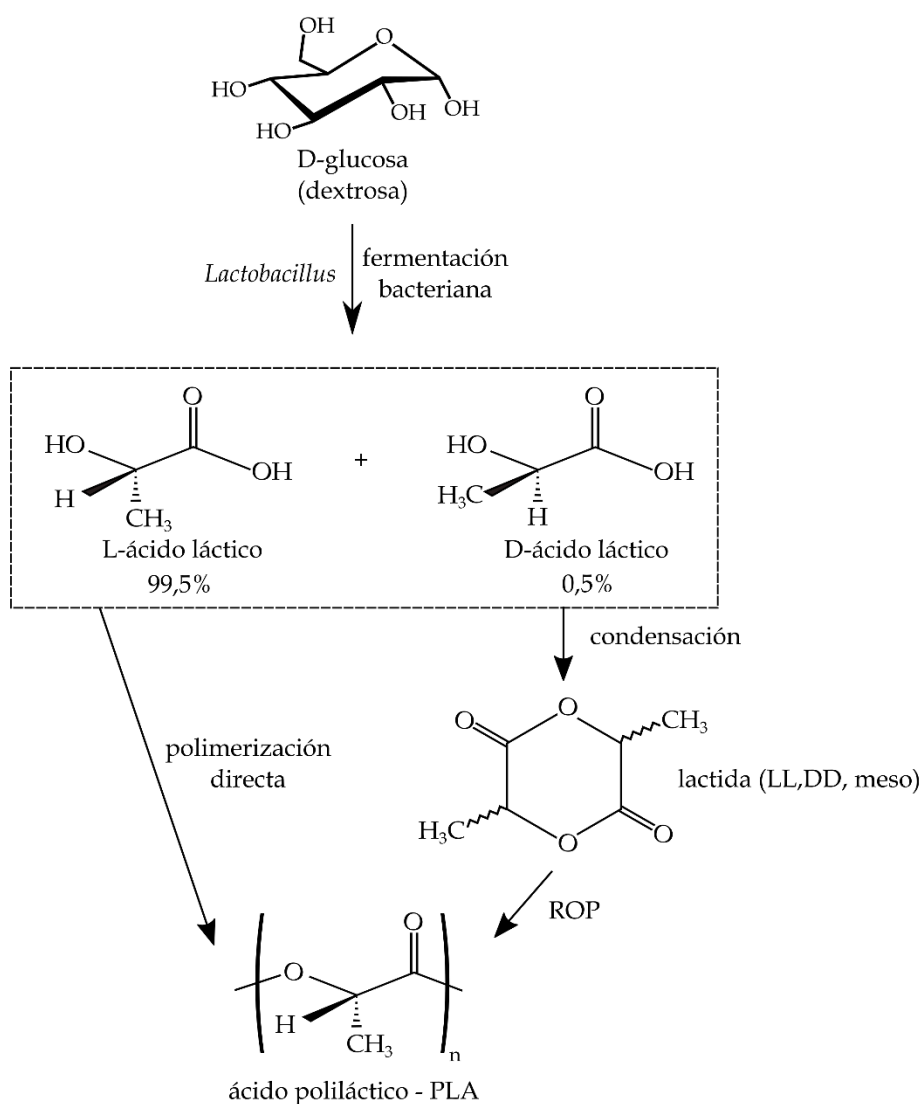
Figura I.17. Esquema del proceso de obtención del PLA.

Después del proceso de fermentación de la glucosa, se obtienen los primeros enantiómeros a causa de este proceso bacteriano [113]. Estos estereoisómeros de partida denominados L(+)-ácido láctico y D(-)-ácido láctico, son la base para la síntesis del ácido láctico.

Como muestra la **Figura I.17**, la producción de PLA a partir del ácido láctico se puede abordar de diferentes maneras. La primera de ellas es la ya conocida polimerización por condensación, la cual usa solventes, vacío y alta temperatura para eliminar el agua que genera el proceso y así obtener un polímero estable. Una de las principales desventajas de este proceso, es que el poliéster generado posee un bajo peso molecular y, además, se requieren diferentes agentes (extensores de cadena) para incrementar el peso molecular lo suficiente para ofrecer un uso industrial, factor que aumenta de manera notable el coste [114]. Este aumento en el coste, ha sido uno de los principales problemas que ha tenido este proceso de síntesis de PLA desde sus inicios,

lo que ha generado una reducción en su consumo, y dejado de lado este método de fabricación.

Por otro lado, otro proceso de síntesis de PLA es mediante la denominada polimerización por apertura de anillos o ROP de sus siglas en inglés *("ring opening polymerization")*. Este proceso se basa en la eliminación del agua bajo condiciones mucho menos agresivas que las que se generan en la policondensación, con el mismo objetivo de generar un polímero estable con un bajo peso molecular. Posteriormente, se aplica un proceso de despolimerización con la finalidad de formar un dímero intermedio cíclico, denominado lactida, que mediante un proceso de destilación es purificado como un nuevo polímero [115]. La **Figura I.18** muestra el proceso por apertura de anillos de manera más ampliada.
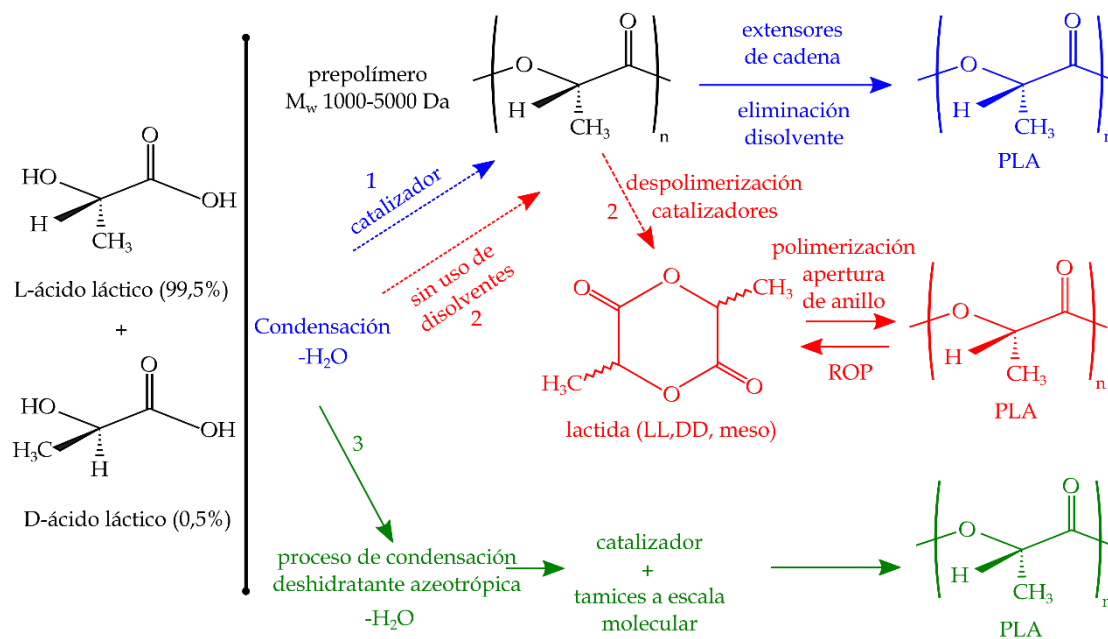
Figura I.18. Rutas de síntesis de PLA a partir de los productos de fermentación de la glucosa (dextrosa) en ácido láctico.

Con este proceso se puede obtener ácido poliláctico con un mayor peso molecular, además de poder controlar de manera mucho más precisa las reacciones químicas y procesos que definirán a posteriori las propiedades finales del polímero, pudiendo generar y decidir diversos grados en cada tipo de aplicación. Desde que en 1992 Cargill Inc. patentó este tipo de polimerización [116], los costes de fabricación de los polímeros fabricados con esta tecnología se han visto reducidos de manera contundente.

Un tercer método se basa en un proceso de condensación por deshidratación con el uso de disolventes azeotrópicos que, combinado con el empleo de catalizadores y tamices moleculares, permite obtener PLA con un peso molecular superior a los 100000 Da, al igual que en los procesos anteriores [117, 118].

Estas innovaciones, unidas a la creciente sensibilización social a favor de la reducción de los residuos plásticos, han situado al PLA como un material puntero dentro de diversos sectores. En sus inicios, su utilización estaba muy limitada a aplicaciones técnicas o sectores como el médico, debido a su elevado coste, pero a medida que se ha ido eliminando esta limitación y ha aumentado la concienciación social, se ha visto incrementado su consumo de manera notable. Desde hace más de una década, los investigadores han trabajado para solucionar/minimizar ciertos problemas ligados a su fragilidad intrínseca, lo que ha situado a este poliéster alifático como un candidato muy a tener en cuenta en el sector del envase y embalaje [69, 119, 120].

En definitiva, se puede apreciar cómo el PLA, además de su alta capacidad para la biodeagradabilidad, posee un muy buen equilibrio de propiedades mecánicas, térmicas, ópticas y barrera, las cuales son comparables a otros polímeros comerciales como el polipropileno (PP), el polietilén tereftalato (PET) o el poliestireno (PS) [116, 121], lo que le abre un gran abanico de posibilidades dentro de la industria. Todo esto teniendo un material totalmente renovable, y capaz de ser biodegradado sin dejar ningún residuo, mediante procesos de compostaje; sin perder de vista su biocompatibilidad y capacidad de reabsorción por parte del organismo.

I.2.6. Tecnología de polihidroxialcanoatos (PHAs).

Una de las familias más amplias y versátiles dentro de los poliésteres alifáticos son los polihidroxialcanoatos (PHAs) que, si bien todavía presentan un coste elevado, complejos procesos de fabricación y propiedades variables con el tiempo, están llamados a ser los plásticos del futuro. Estos poliésteres tienen la peculiaridad de que se obtienen mediante procesos de síntesis bacteriana ya que determinadas cepas bacterianas almacenan energía en forma de estos polímeros.

estructura genérica del monómero de un polihidroxialcanoato - PHA
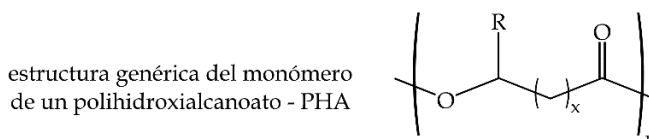
x	R	ácido carboxílico-monómero	abreviatura
1	-H	ácido 3-hidroxipropiónico	3HP
1	-CH$_3$	ácido 3-hidroxibutírico	3HB
1	-CH$_2$CH$_3$	ácido 3-hidroxivalérico	3HV
1	-CH$_2$CH$_2$CH$_3$	ácido 3-hidroxihexanoico	3HHx
1	-CH$_2$CH$_2$CH$_2$CH$_2$CH$_3$	ácido 3-hidroxioctanoico	3HO
2	-H	ácido 4-hidroxibutírico	4HB
2	-CH$_3$	ácido 4-hidroxivalérico	4HV

Figura I.19. Estructura genérica del monómero de los polihidroxialcanoatos y tabla con los ácidos carboxílicos de base para su síntesis.
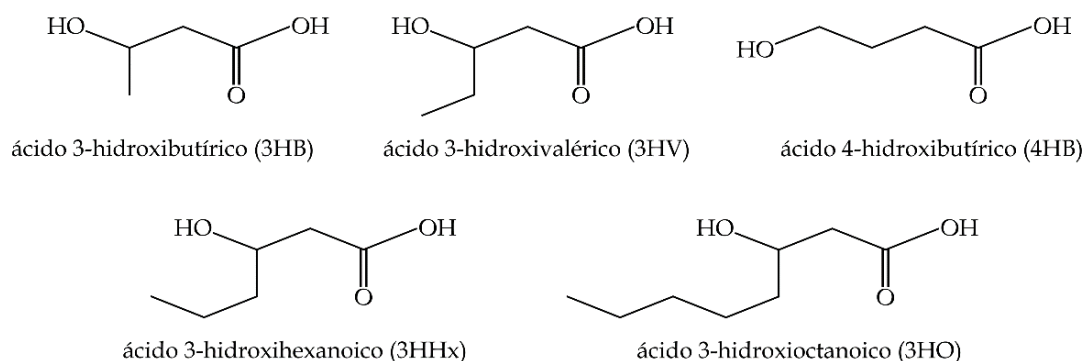
Su estructura básica se centra en la combinación de un enlace éster con monómeros de ácido R-hidroxialcanoico. La **Figura I.19** muestra la estructura química genérica de los PHAs. Generalmente, este tipo de polímeros se sintetizan y almacenan como carbono intracelular y, sobretodo, como depósitos de energía en bacterias Gram-negativas y Gram-positivas [122]. Debido a su origen bacteriano, existen una gran cantidad de variaciones dentro del grupo de PHAs, ya que, según el origen de la bacteria, la fuente del carbono o las condiciones durante el proceso de fabricación, se pueden obtener multitud de variantes y combinaciones, consiguiendo una gran cantidad de posibles poliésteres para diferentes aplicaciones. La **Tabla I.**2 muestra algunos de los PHAs más comunes en la industria, juntamente con su cepa bacteriana y el origen del carbono [123].

Tabla I.2. Diferentes polihidroxialcanoatos obtenidos con el empleo de distintas fuentes de carbono y cepas bacterianas.

PHA	Fuente Carbono	Cepa bacteriana
PHV/PHB	ácido acético, glucosa, fructosa	*Ralstonia eutropha*
PHB	sacarosa, gluconato	*Burkholderia sp.*
P(3HB-*co*-3HV)	xilosa, ácido levulínico	*Burkholderia cepacia*
P(3HB-*co*-3HV)	ácido propiónico, sacarosa	*Burkholderia sacchari*

Los PHAs se pueden clasificar por el número de átomos que se encuentran es su unidad monomérica, debido a la relevancia que tienen en sus propiedades y estructuras químicas. Por este motivo, se pueden encontrar PHAs de cadena corta (PHA$_{SC}$) y PHAs de cadena media (PHA$_{MC}$).

Los PHA$_{SC}$ se caracterizan por tener entre 3 y 5 átomos de carbono en su unidad monomérica. Este tipo de polímeros son los más comunes dentro de la familia de PHAs, y se caracterizan por tener valores de cristalinidad muy elevados, siendo muy rígidos y quebradizos. En relación a los PHA$_{MC}$, su cadena monomérica contiene entre 6 y 14 átomos de carbono y, al contrario que los de cadena corta, poseen una mayor flexibilidad y una cristalinidad más baja. Además, destacan por tener una temperatura de fusión elevada y una buena resistencia mecánica [124, 125]. La **Figura I.20** muestra varios ejemplos de ácidos R-hidroxialcanoicos, base para la síntesis de PHAs de cadena corta y cadena media. Existe algún tipo de PHAs, denominaos como híbridos, que están constituidos por la combinación de ácidos R-hidroxialcanoicos de cadena corta y cadena media. Autores como Urtuvia *et al.* [123], han constatado que actualmente hay más de 150 componentes monoméricos diferentes capaces de formar una amplia variedad de PHAs.

ácido 3-hidroxibutírico (3HB)   ácido 3-hidroxivalérico (3HV)   ácido 4-hidroxibutírico (4HB)

ácido 3-hidroxihexanoico (3HHx)   ácido 3-hidroxioctanoico (3HO)

Figura I.20. Estructura química de ácidos R-hidroxialcanoicos constituyentes de PHAs de cadena corta y cadena media.

Debido al origen bacteriano de los PHAs, existen una gran cantidad de bacterias capaces de formar y sinterizar este tipo de compuestos. Entre todas las posibles bacterias, solo unas pocas como las *pseudomonas olovorans*, *azotobacter vinelandii* o *escherichia coli* recombinante [126], son capaces de sintetizar estos polímeros a niveles suficientemente eficientes, para ser comercializadas y fabricadas a nivel industrial. Esta reducción en las posibles opciones, permite centrar de manera directa las investigaciones en estas bacterias, mejorando su proceso productivo, y generando una reducción directa en el coste final del polímero. Desde el punto de vista de la producción de PHAs, se requiere la implantación de tres etapas para su correcta síntesis a nivel industrial. Estas etapas son fermentación, extracción y purificación.

Durante la primera etapa, se fomenta un notable crecimiento de la biomasa, la cual genera de manera directa la formación y síntesis del polímero. Esta es una de las etapas principales para la obtención de PHAs, ya que según el tipo de bacterias y las condiciones que se establezcan durante el proceso, se puede variar el polímero final y, en consecuencia, las propiedades finales. En esta etapa, con el fin de aumentar al máximo el rendimiento durante el proceso de fermentación, se tienen en cuenta parámetros como el pH, el tipo de sustrato utilizado o el sistema de cultivo. En particular, es el sustrato utilizado uno de los factores que más relevancia tienen a la hora de obtener este tipo de polímeros, y que más afectan al coste final. El tipo de sustrato se basa principalmente en la fuente de carbono que se utiliza para la síntesis bacteriana, lo que condiciona la estructura y, sobretodo, el coste final del producto. Como se muestra en la **Tabla 1.2,** los principales sustratos que se utilizan en la actualidad a nivel industrial son la glucosa y la sacarosa; no obstante las investigaciones tratan de buscar sustratos lo más baratos posibles, para reducir al máximo el coste, mejorando así la incorporación de este tipo de poliésteres en la industria en mayor escala. En los últimos años, se han descrito diversas fuentes de residuos para la obtención de PHAs, contribuyendo al desarrollo sostenible y generación de economías circulares [127, 128].

Para la correcta fermentación de los PHAs a nivel industrial, existen dos tipos de procesos que se clasifican según el flujo de obtención. Con relación a este criterio, a nivel técnico se utiliza tanto el cultivo continuo como el cultivo por lotes alimentados,

siendo el proceso por lotes uno de los más empleados. El proceso en continuo se fundamenta en la entrada de nutrientes para una correcta fermentación durante un tiempo determinado en el reactor en continuo y, finalmente se recoge el producto de la fermentación de forma continua. Este es el caso de la síntesis de P3HB mediante *Ralstonia eutropha* [129]. Con respecto al proceso por lotes alimentados, debido a que no existe un flujo de salida continuo, es necesario realizar el proceso de fermentación en dos etapas separadas para aquellos PHAs que necesitan una limitación o restricción de nutrientes [125].

Una vez terminada la fermentación, se inicia la etapa de extracción y recuperación del material sintetizado durante la primera etapa. Los procesos más frecuentes para separar las células de PHA de la solución son la centrifugación, filtración o sedimentación. Según el proceso seleccionado y los materiales generados, se obtienen diferentes rendimientos durante todo el proceso.

Finalmente, una vez se ha recuperado la primera materia del caldo de cultivo, es necesario filtrar el polímero del conjunto de elementos que lo conforman. Una de las técnicas más simples y de mayor repercusión, es la utilización de disolventes para conseguir disolver selectivamente los polímeros, y separarlos del resto de elementos para, posteriormente, precipitarlos mediante el empleo de etanol y obtener el producto final. Existen otros procesos de recuperación más complejos a partir de sistemas mecánicos o digestión química, que suelen ser más complicados y caros, aunque, en muchos casos, permiten obtener mejores rendimientos o polímeros de mayor pureza [130]. Una vez se ha obtenido el producto final, se pueden aplicar procesos de purificación con el objetivo de aumentar al máximo el rendimiento en polímero y así, mejorar la calidad del mismo [131].

Como ya se ha descrito previamente, dentro del grupo de los PHAs, polímeros como el poli(3-hidroxibutirato) (PHB) y el poli(3-hidroxibutirato-*co*-3-hidroxivalerato) (PHBV), se han convertido en unos de los polímeros más estudiados debido a sus excelentes propiedades mecánicas, elevadas propiedades barrera, y su facilidad para ser desintegrados bajo la aplicación de ciertos microorganismos. Se trata de PHAs de cadena corta; esta composición estructural les confiere, en algunos casos, propiedades similares a los de algunos materiales derivados de recursos fósiles como el PP y el PE [53], situándolos como futuros sustitutos a niveles industriales.

Como ha sucedido en el caso del PLA, sus altos costes de fabricación y ciertas limitaciones (ligadas a las propiedades finales, envejecimiento físico por cristalización secundaria, ventanas de procesado estrechas, etc.), ha relegado a los PHAs, desde sus inicios, a aplicaciones en la industria farmacéutica o médica. No obstante, las continuas investigaciones y esfuerzos por mejorar sus costes y propiedades están generando, cada vez más, un aumento en las posibles aplicaciones de este tipo de materiales [132].

I.3. OBTENCIÓN Y TECNOLOGÍA DE POLIAMIDAS.

Las poliamidas son materiales poliméricos que han tenido una gran repercusión gracias a sus elevadas propiedades mecánicas y térmicas. Su obtención se basa, principalmente, en la integración de grupos amida en su estructura, la cual generalmente es lineal y semicristalina. Desde su descubrimiento en 1928 por Wallace Hume Carothers en la empresa DuPont, la poliamida o *nylon*, revolucionó el sector textil de manera muy positiva para el consumidor, consiguiendo fibras y tejidos con altísimas capacidades. Inicialmente, el sector militar fue el mayor receptor de este nuevo polímero, pero, después de la II Guerra Mundial, fue cuando entró de manera directa en la industria textil cotidiana. Debido a sus elevadas propiedades mecánicas, estos materiales termoplásticos son considerados como plásticos de ingeniería o de uso técnico, lo que les ha proporcionado el acceso a sectores como la automoción, maquinaria, filtración, o en el sector textil de altas prestaciones. Sus características están fuertemente ligadas a su estructura y obtención, la cual puede ser tanto de origen petroquímico como de origen renovable.

I.3.1. Estructura y obtención de poliamidas.

Las poliamidas representan un grupo de polímeros muy amplio que se caracteriza por la repetición de grupos amida en su estructura. Como se muestra en la **Figura I.21**, los grupos amida suelen obtenerse mediante la condensación de ácidos carboxílicos con aminas, con desprendimiento de agua. Los grupos amida son capaces de formar puentes de hidrógeno de manera sencilla, lo que supone uno de los factores más relevantes a la hora de obtener ciertas propiedades de estos polímeros.

Además, para la correcta síntesis de poliamidas, se requiere la combinación de grupos amida con grupos alifáticos, siendo esta combinación la encargada de aportar las propiedades finales a cada tipo de poliamida. Si en esta relación aparece un bajo número de grupos amida, el comportamiento de la poliamida se asemeja más a un polímero de uso convencional, mientras que con un mayor número de grupos amida, se generan estructuras con propiedades muy similares a las de las proteínas y polipéptidos, que no tienen gran interés industrial. Es importante destacar la similitud de las estructuras de las poliamidas con las de las proteínas. En general, las proteínas resultan de la polimerización de aminoácidos (estructuras base con grupos ácido carboxílico y grupos amina). Con la reacción de dos aminoácidos, se produce una condensación que da lugar a un dipéptido. Si son varios los ensamblajes de aminoácidos, se obtienen los oligopéptidos y, cuando son muchos los aminoácidos que se ensamblan de forma regular, se obtienen los polipétidos que tienen una estructura química similar a las poliamidas, y son la base de las estructuras proteicas. De hecho, el grupo amida, en el ámbito de la biología, se denomina enlace peptídico.

Por estos motivos, aquellas poliamidas que tienen un mayor interés comercial son las que poseen un equilibrio de grupos amida y grupos alifáticos. A modo de ejemplo, las poliamidas conocidas industrialmente como "*nylons*", son aquellas que poseen menos de un 85% de los grupos amida directamente conectados a dos grupos

aromáticos [133]. Hay que tener muy en cuenta, que el grupo amida realiza un papel estructural esencial, contribuyendo de manera directa a la extraordinaria resistencia mecánica y térmica que poseen las poliamidas, debido a su naturaleza fuertemente polar y su alta estabilidad química.
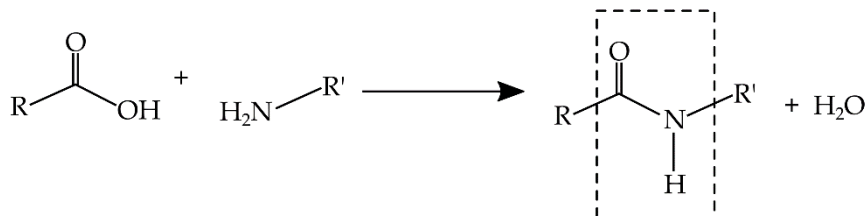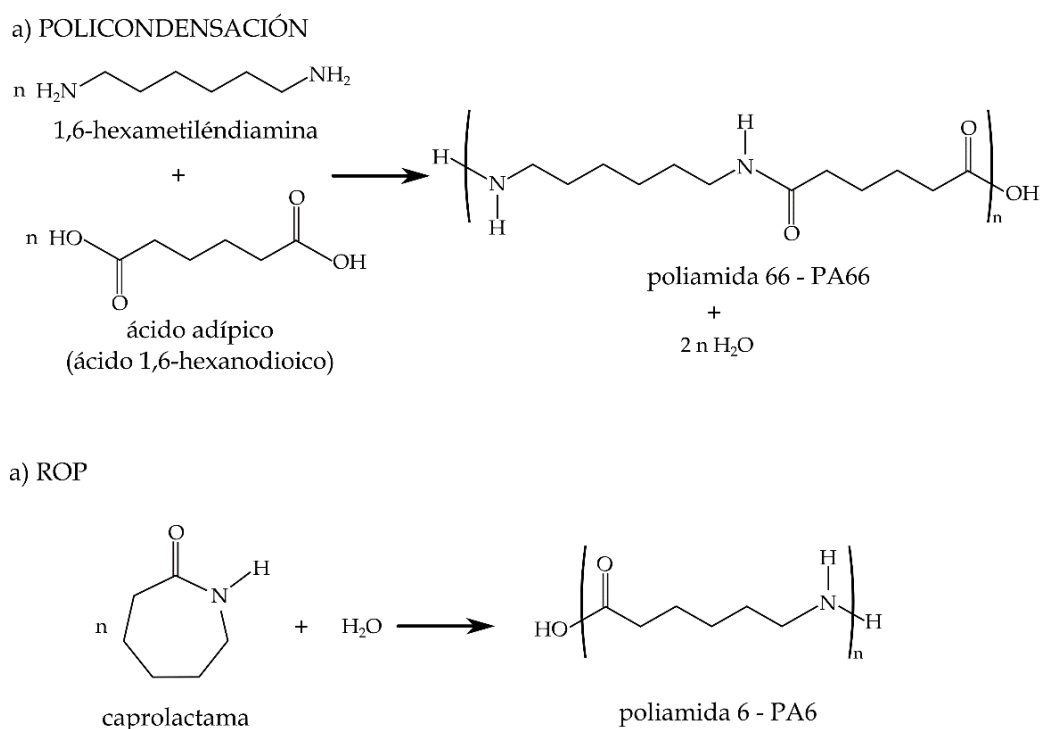

Figura I.21. Representación esquemática de la unidad de repetición del grupo amida, característico de las poliamidas.

Desde un punto de vista industrial, las poliamidas pueden obtenerse tanto por polimerización por apertura de anillos como por policondensación. La primera poliamida que se obtuvo fue la poliamida 6,6 (PA66). Generalmente, las poliamidas que se obtienen mediante polimerización por condensación, basan su síntesis en la reacción de un ácido dicarboxílico y una diamina en una relación de 1: 1; a partir de un aumento de temperatura y presión, es posible que la reacción de condensación tenga lugar [134].

No obstante, las poliamidas también pueden obtenerse mediante polimerización por apertura de anillo (ROP). Una importante característica de este tipo de polimerización, al igual que ocurre con el PLA, es la ventaja de no producir ningún tipo de subproducto (o producto de condensación), dando lugar a una polimerización limpia que permite obtener diferentes tipos de poliamidas con multitud de posibles aplicaciones. Este es el caso de la poliamida 6 (PA6), que puede obtenerse mediante ROP con la incorporación de agua a la ε-caprolactama y aumentar la temperatura por encima de los 240 °C. En estas condiciones, el oxígeno del grupo carbonilo dona un par de electrones al agua y esto permite, de manera simplificada, la apertura del anillo para la correcta formación de la PA6 sin ningún producto sobrante. La **Figura I.22** muestra dos ejemplos de polimerización de una PA6 y una PA66 a partir de un proceso ROP y policondensación respectivamente.

a) POLICONDENSACIÓN

1,6-hexametiléndiamina

+

ácido adípico
(ácido 1,6-hexanodioico)

poliamida 66 - PA66
+
$2 \, n \, H_2O$

a) ROP

caprolactama

poliamida 6 - PA6

Figura I.22. Representación esquemática de los procesos de obtención de poliamida por a) policondensación y b) apertura de anillo (ROP).

Dentro de la industria de los polímeros de alto rendimiento y, en particular, dentro de las poliamidas, estas, habitualmente se han sintetizado por la ruta petroquímica, debido a la facilidad de obtención, costes más reducidos y, sobretodo, por una investigación muy sólida desde su síntesis inicial. No obstante, gracias al impulso fomentado por los problemas medioambientales derivados del uso del petróleo, han surgido nuevas alternativas y posibilidades.

I.3.2. Clasificación y aplicaciones de poliamidas de origen petroquímico.

Antes de su descubrimiento como polímero sintético, la estructura de poliamida ha estado presentes en la naturaleza en forma de proteínas o polipéptidos y fibras naturales vegetales derivadas de la lana o la seda, tal y como se ha descrito previamente. Fue a partir de la primera mitad del siglo XX, cuando se empezó a investigar y producir las primeras poliamidas sintéticas. Durante estos años, el auge del petróleo y la escasez de recursos naturales derivados de la II Guerra Mundial, se impulsó en gran medida la utilización de recursos petroquímicos para la fabricación de estos polímeros técnicos. A continuación, se describen las particularidades de distintas poliamidas, así como su evolución hacia formulaciones de mayor rendimiento medioambiental.

I.3.2.1. Poliamidas alifáticas.

Como se ha mencionado con anterioridad, las poliamidas alifáticas fueron las primeras en aparecer en la industria gracias a la incursión del *nylon* en el mercado después de que fuese patentado por la empresa DuPont. Este tipo de poliamidas posee una estructura lineal, basada en hidrocarburos alifáticos. Su estructura es simple y según la longitud de su cadena alifática, se obtienen diferentes valores de tenacidad y flexibilidad, consiguiendo, de manera directa, diferentes propiedades mecánicas y térmicas. La **Figura I.23** muestra la estructura genérica de una poliamida alifática convencional.
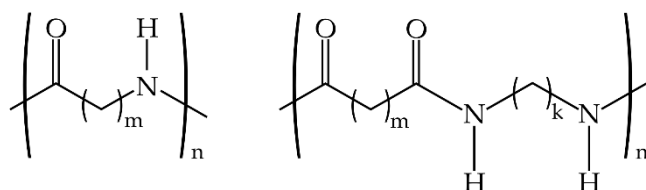
Figura I.23. Representación esquemática de la estructura de monómero de poliamidas alifáticas.

Dentro del grupo de poliamidas alifáticas, la PA6 y la PA66 son las más empleadas a escala industrial. Estos materiales poseen temperaturas de fusión relativamente altas, ya que funden alrededor de 215 ºC y 250 ºC para la PA6 y la PA66, respectivamente. Debido a su estructura química, presentan un gran número de enlaces secundarios (puentes de hidrógeno) entre cadenas (**Figura I.24**), aspecto que repercute en elevadas propiedades mecánicas como tenacidad, dureza y rigidez, lo que les ha dado una gran ventaja en algunos campos [135, 136]. Además, tienen una alta capacidad para absorber impactos y debido a su alta resistencia, se pueden utilizar en aplicaciones donde el desgaste de la pieza es un factor a tener en cuenta.
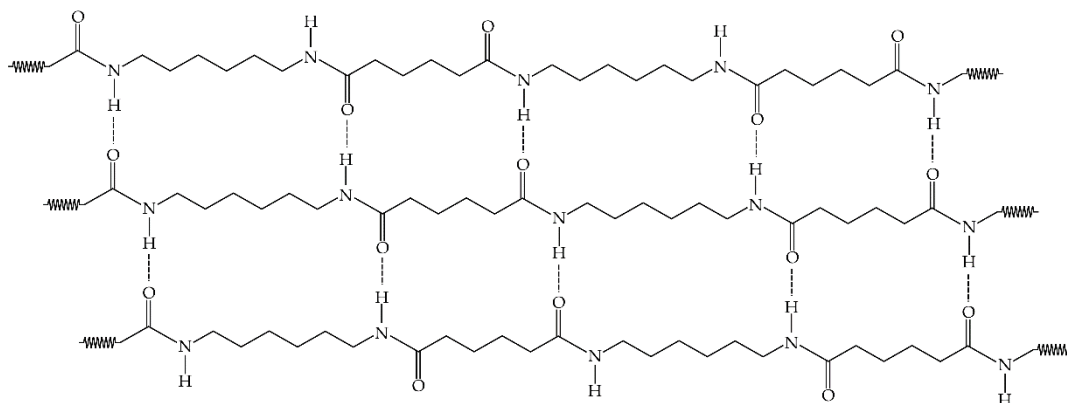
Figura I.24. Formación de enlaces secundarios (enlaces por puente de hidrógeno) en estructuras de poliamidas.

Con la aparición de la PA6 de manos de DuPont, el primer sector en incorporar este polímero fue el textil. Antes de su utilización de manera comercial, se utilizó para la fabricación de paracaídas. Posteriormente, se empleó en la fabricación de medias elásticas y tejidos técnicos, donde empezó a emplearse de forma extensiva en el sector textil. Actualmente, debido a su buen equilibrio entre propiedades y coste, se utiliza

para aplicaciones textiles más técnicas como tejidos retardantes a la llama o tejidos antimicrobianos [137-139].

Dentro del sector del envase y embalaje, estas poliamidas también han tenido cierta repercusión, sobre todo en las últimas décadas donde se están utilizando con la combinación de diferentes agentes y nanocompuestos [140] o, en algunos casos, como films con propiedades antimicrobianas [141]. Otro de los sectores donde la utilización de la PA6 y PA66 es de gran relevancia es en automoción. En este sector se emplean, sobretodo, en partes y componentes estructurales sometidos a condiciones de desgaste tales como tapas, engranajes o tubos, etc. [142, 143].

I.3.2.2. Poliamidas semiaromáticas. Poliftalamidas.

Otro grupo interesante dentro de las poliamidas, está constituido por las poliamidas semiaromáticas, también denominadas poliftalamidas (PPA), que proceden de hidrocarburos semiaromáticos. A diferencia de las poliamidas alifáticas, estas poseen en su estructura algún anillo aromático (**Figura I.25**), que da lugar a una estructura algo más compleja, que le otorga mejores prestaciones mecánicas.
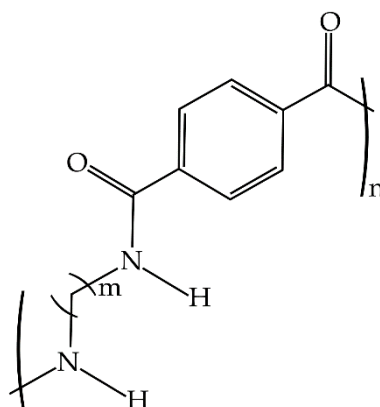
Figura I.25. Representación esquemática de la estructura de monómero de una poliamida semiaromática o poliftalamida.

Estas poliamidas poseen unas propiedades térmicas y mecánicas superiores a las alifáticas. Al igual que sucede en el ámbito de los poliésteres, una mayor complejidad en la estructura aporta una diferenciación de propiedades, resultando factores relevantes para ciertos ámbitos, pero acarreando normalmente, un aumento en el coste de fabricación.

Las aplicaciones de estas poliamidas están muy relacionadas con sus propiedades. En el caso de las propiedades térmicas, estos polímeros alcanzan temperaturas de fusión superiores a los 300 ºC, mientras que su estabilidad térmica se ve muy favorecida por tener una temperatura de transición vítrea (T_g), por encima de los 120 ºC. Estas prestaciones hacen que, sectores como automoción o componentes eléctricos, incorporen estas poliamidas para la fabricación de sus piezas y componentes. Además de estas elevadas propiedades térmicas, ofrecen gran resistencia

mecánica, sobre todo desde el punto de vista de la rigidez, y gran estabilidad química. Debido a la mayor complejidad de su estructura, las poliftalamidas se ven afectadas por la humedad en menor medida que las poliamidas alifáticas. De hecho, la absorción de humedad es una de las principales desventajas que poseen las poliamidas para su utilización en ciertas aplicaciones de ingeniería, no obstante, con la mayor complejidad de la estructura de las poliamidas semiaromáticas, este problema se ve minimizado en gran medida.

Como consecuencia de sus excelentes propiedades, este grupo de poliamidas se utilizan para sectores donde los requerimientos técnicos son muy elevados. En particular, en sectores como la automoción se emplean en la fabricación de componentes estructurales y tubos de presión que están sometidos a elevadas temperaturas o en contacto con productos químicos durante tiempos prolongados [144]. Actualmente, se están utilizando como base para la fabricación de materiales compuestos de altas prestaciones dentro de la industria del automóvil [145]. En otras industrias, como la de componentes electrónicos, se emplean para fabricar piezas y componentes que requieren de grandes prestaciones mecánicas a temperaturas elevadas, como carcasas para sensores o conectores [146].

I.3.2.3 Poliamidas aromáticas o aramidas.

Finalmente, las poliamidas aromáticas o aramidas, se diferencian de las anteriores por poseer una mayor cantidad de grupos aromáticos y por un cambio significativo en las propiedades, tanto mecánicas como térmicas.

Son materiales de muy altas prestaciones, ya que poseen altísimos valores de resistencia mecánica, térmica y química. Esto supone una ventaja notable ya que aportan excepcionales propiedades con valores de densidad muy bajos. Debido a la complejidad de su estructura (**Figura I.26**), y la gran resistencia térmica y química que poseen, la fabricación de este tipo de materiales supone un gran reto para los ingenieros. Sus altas temperaturas de fusión (T_m), y de transición vítrea (T_g), suponen un problema para que estos materiales se puedan procesar por inyección o extrusión. Por estos motivos es normal encontrar este tipo de polímeros en forma de fibras de altas prestaciones o como refuerzos de otros materiales.
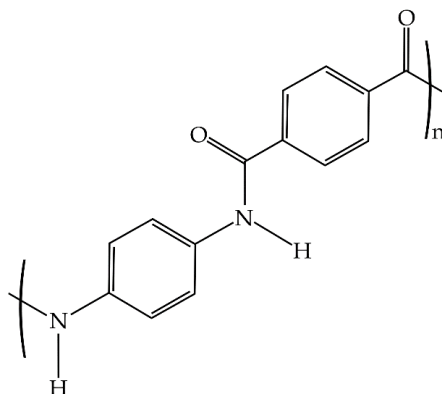
Figura I.26. Representación esquemática de la estructura de monómero de una poliamida aromática o aramida.

Las poliamidas aromáticas más estudiadas y que mayor repercusión han tenido en los últimos 30 años, son aquellas derivadas del ácido isoftálico y tereftálico. Este tipo de poliamidas son más conocidas por su denominación comercial como Nomex® y Kevlar® de la compañía DuPont. Estas fibras se sintetizaron a través del cloruro de isoftaloílo y m-fenilénisoftalamida para el caso del Nomex® o m-aramidas, y a través de la poli(p-feniléntereftalamida) para el Kevlar® o p-aramidas [147].

Estas poliamidas aromáticas o aramidas, poseen unas propiedades térmicas muy superiores a las poliamidas alifáticas. En el caso de las m-aramidas, el punto de fusión y degradación está en torno a unos 365 ºC, mientras que las p-aramidas, funden a temperaturas superiores a 500 ºC. La complejidad y elevado coste de fabricación que poseen las relega a aplicaciones muy técnicas y selectas, como balística, aeronáutica o utilización militar.

Normalmente este tipo de aramidas se emplean en forma de tejidos estructurales en la construcción de aviones y barcos, con la combinación de otros componentes como resinas termoestables. Gracias a los elevados valores de resistencia térmica y mecánica que poseen, se suelen aplicar en ropas y equipos de protección contra incendios, además de fabricación de chalecos antibala. Actualmente tienen diversas aplicaciones en el campo deportivo como en tablas de "*skate*" o como refuerzos en materiales deportivos de altas prestaciones [148].

I.3.3. Obtención de biopoliamidas a partir de recursos renovables.

La tendencia social de reducir al máximo el impacto ambiental derivado del uso de productos procedentes de recursos fósiles, ha fomentado el interés en I+D+i en polímeros de altas presentaciones a partir de recursos sostenibles. A priori, parece darse a entender que todos aquellos materiales de altas prestaciones provienen obligatoriamente de recursos petroquímicos. Por suerte, esta afirmación queda muy alejada de la realidad, ya que existen cadenas de polímeros de altas prestaciones provenientes de productos renovables [149].

En el ámbito de las poliamidas, sin tener en cuenta las proteínas y polipéptidos, existen varias maneras de obtener diaminas renovables, capaces de formar poliamidas total o parcialmente renovables. La fabricación de poliamidas a partir de materias renovables, supone una gran ventaja desde el punto de vista medioambiental, además de avanzar hacia materiales sostenibles alejados de recursos fósiles limitados.

Uno de los objetivos principales de las poliamidas de base biológica (bioPA), es conseguir propiedades lo más similares posibles a las que derivan de recursos fósiles. El primer punto de partida para la obtención de bioPAs, es la utilización de monómeros de origen biológico tales como el ácido brasílico, ácido sebácico, 1,4-diaminobutano (putrescina) o 1,5-diaminopentano (cadaverina) [150, 151] (**Figura I.27**).
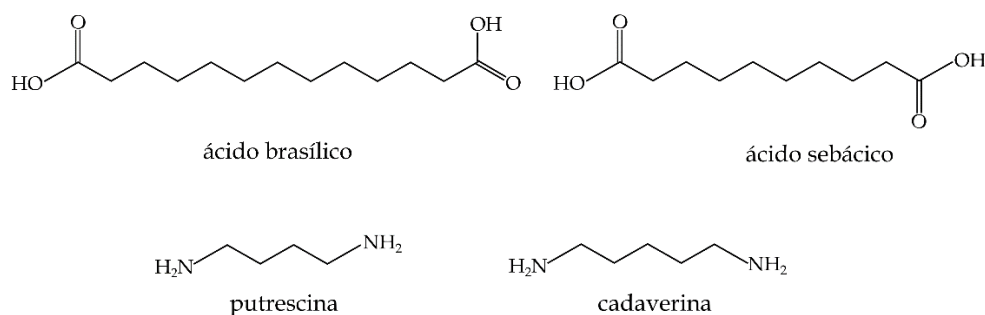
Figura I.27. Representación esquemática de diversos compuestos de origen renovable empleados en la obtención de biopoliamidas.

En los últimos años, se ha investigado en las mejores formas para la obtención de los componentes básicos a través de materias primas renovables. En este contexto, debido a la estructura química que poseen algunas poliamidas, tales como la poliamida 610 (PA610), la poliamida 1010 (PA1010), la poliamida 11 (PA11) o la poliamida 1012 (PA1012), la búsqueda de materias primas capaces de proporcionar ácidos carboxílicos y diaminas de diversa longitud, es de vital importancia.

Por estos motivos, para la síntesis de bioPAs, el aceite de ricino juega un papel muy importante como fuente principal. Este aceite natural de color amarillento, contiene un 85-95% de ácido ricinoleico, un ácido graso de 18 carbonos (C18), el cual está disponible en forma de éster en la estructura del triglicérido [152]. La **Figura I.28** muestra la estructura del aceite de ricino.
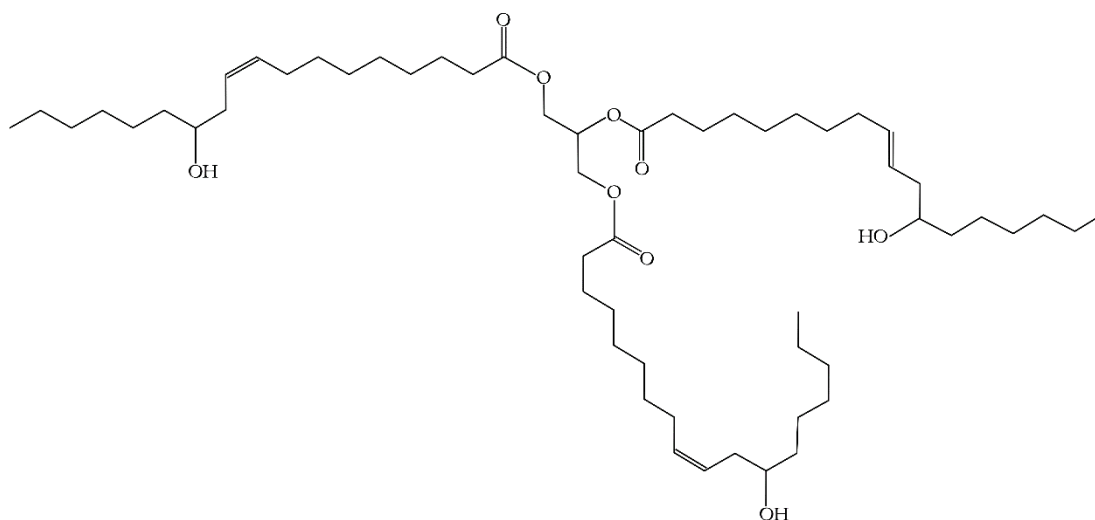
Figura I.28. Representación esquemática de la estructura química del aceite de ricino, triglicérido con un 85-95% de ácido ricinoleico.

Este aceite se extrae a partir de la semilla de una planta denominada *Ricinus communis*. La utilización de este tipo de aceite para la fabricación de bioPAs, aporta una serie de ventajas ligadas a la obtención de su semilla, la cual no es apta para el

consumo humano de manera directa y, además, crece en lugares donde la plantación de alimentos no es viable. Estos factores conducen a que este tipo de aceite sea viable tanto a nivel medioambiental como económico. En este contexto, en los últimos años se han generado anualmente cantidades de aceite de ricino por encima de las 600.000 toneladas, de las cuales, más de una tercera parte, ha ido destinado a la obtención de poliamidas de origen bio [153].
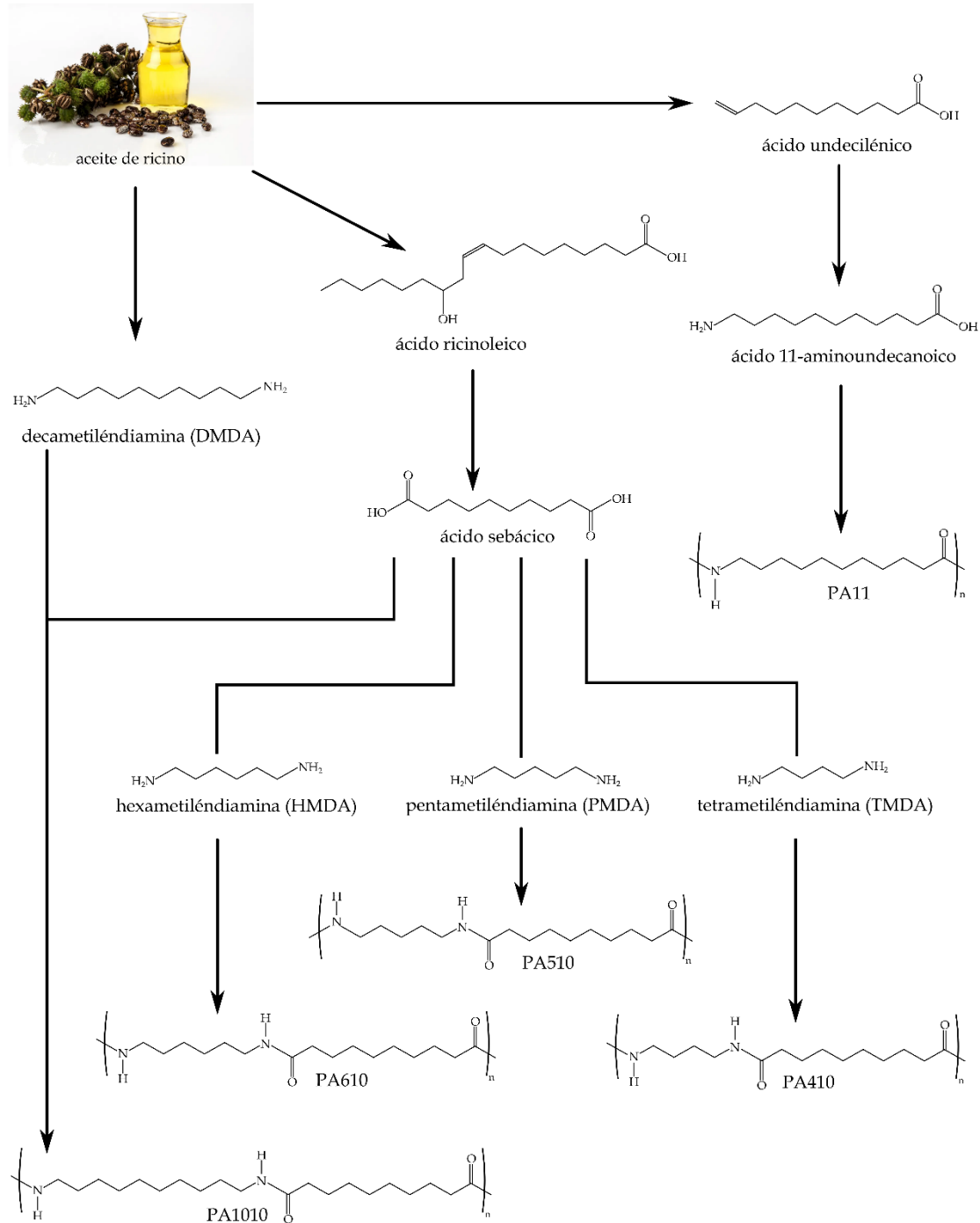

Figura I.29. Proceso de obtención de bio poliamidas a partir de aceite de ricino.

Para la obtención de los compuestos necesarios para sintetizar poliamidas de origen bio o bioPAs, es necesario someter al aceite de ricino a una serie de procesos iniciales. El primer paso se centra en la transesterficación o una etapa de saponificación, en la que se consigue obtener ácido ricinoleico, es decir, extraer los ácidos grasos libres de la estructura del triglicérido [154]. Una vez se obtiene el ácido ricinoleico, este se calienta a temperaturas cercanas a los 250 ºC con álcali, con el objetivo de extraer una de las estructuras fundamentales en la fabricación de bioPAs, el ácido sebácico o acido 1,10-decanodioco [155]. La **Figura I.29** muestra el proceso de obtención de diversas bioPAs a partir del aceite de ricino.

Además, hay que resaltar que a partir de procesos de hidrogenación y deshidratación, se puede obtener 1,10-decametilendiamina (DMDA) del ácido sebácico [156], factor de vital importancia para la polimerización entre el ácido sebácico y la DMDA de origen natural para la obtención de la PA1010 con un 100% de recursos naturales. Por otro lado, el ácido sebácico (C10), se puede combinar fácilmente con otras diaminas derivadas del petróleo, para obtener poliamidas con origen renovable parcial. A partir del proceso de policondensación, este ácido se puede combinar con 1,6-hexametilendiamina (HMDA) de origen petroquímico, para producir poliamida alifática 610 (PA610). Debido a esta combinación, la PA610 contiene alrededor de un 60% en peso derivado de recursos naturales [157].

Otro ejemplo dentro de las poliamidas derivadas de fuentes renovables, es la fabricación de la poliamida alifática 1012 (PA1012). Esta poliamida se obtiene a partir de la polimerización del DMDA de origen renovable, con el ácido 1,12-dodecanodioico, el cual se obtiene principalmente a partir de recursos fósiles. Con esta composición, la PA1012 puede llegar a tener un 45% de base renovable; no obstante, en los últimos años se ha conseguido obtener este ácido dicarboxílico a partir de fuentes renovables como el aceite de palma. Estos nuevos procesos generan la posibilidad de sintetizar una PA1012 totalmente de origen renovable.

I.3.4. Tecnología y aplicaciones de biopoliamidas.

Las biopoliamidas, tanto las de origen renovable parcial como total, aportan unas propiedades muy similares a las de sus homólogas petroquímicas. Estas características se basan en su estructura, la cual, en muchos casos, se obtiene a partir de los mismos compuestos, pero derivados de recursos renovables.

Como se ha descrito previamente, las PAs se consideran plásticos técnicos o de ingeniería. Entre sus propiedades, merece la pena destacar las excelentes propiedades mecánicas y térmicas, alta resistencia a la abrasión y a los aceites, la baja fricción que poseen o las buenas capacidades de procesabilidad. Al ser poliamidas alifáticas, debido a la mayor simplicidad de su estructura, pueden presentar ciertos problemas de estabilidad dimensional. En muchos casos, este tipo de problemas se pueden solucionar de manera sencilla con la aplicación de refuerzos como fibras.

Otro de los problemas derivado de su composición, al igual que sucede en las poliamidas petroquímicas, es la capacidad que tienen de absorber agua. Este fenómeno se basa en la afinidad que posee la estructura en absorber moléculas de agua en las regiones amorfas entre dos grupos amida[158]. La poliamida es un polímero con alta polaridad y ello repercute en niveles elevados de absorción de humedad, comparado con otros polímeros apolares como el PE o PP.

En general, la mayoría de bioPAs, muestran rendimientos mecánicos y térmicos muy elevados para ciertas aplicaciones; no obstante, la presencia de humedad en su estructura suele verse reflejada en un empeoramiento en ciertas propiedades. Otro tema de gran relevancia es que, debido a la afinidad por el vapor de agua, el procesado de PAs (incluidas las bioPAs), requiere una etapa previa de secado. Al igual que ocurre con los problemas de estabilidad dimensional, se están estudiando posibles soluciones que reduzcan al máximo la absorción de agua en las bioPAs; todo ello, con el fin de incrementar sus posibilidades técnicas y permitir su uso en diversos sectores.

Algunas de las aplicaciones más comunes de las bioPAs son sobre todo la fabricación de tuberías y mangueras para transporte de combustibles, gases o aceites. También se pueden encontrar en cables para aplicaciones eléctricas o electrónicas y, en algunos casos, para la industria del envasado de ciertos productos [159, 160]. Dentro de la industria del automóvil, se están utilizando materiales compuestos basados en bioPAs y fibras para sustituir ciertos plásticos de origen petroquímico [161].

En la industria del plástico, la tendencia del mercado a eliminar/reducir los productos derivados del petróleo, está generando un gran aumento en la utilización de bioPAs. En particular, la demanda mundial del mercado de estos nuevos polímeros renovables fue de aproximadamente 21.000 toneladas en 2014, y para el 2022 se espera una proyección de más de 22.000 toneladas [162]. Esta demanda de poliamidas derivadas de orígenes renovables, está generando un gran aumento en las investigaciones para solucionar o paliar los problemas derivados del elevado coste, baja estabilidad dimensional y su afinidad hacia la humedad y vapor de agua.

I.4. MODIFICACIÓN DE FORMULACIONES DE POLÍMEROS.

Habitualmente, el término "polímero" hace referencia al material de alto peso molecular obtenido mediante procesos de polimerización. No obstante, estos polímeros, raramente se emplean tal cual. En la mayoría de las ocasiones, se utilizan diversas materias para modificar, proteger, abaratar, etc. el polímero y convertirlo en una formulación de plástico industrial. Entre los materiales que se emplean merece la pena distinguir entre (**Figura I.30**):

- **Cargas.**
  Se trata de materiales que se incorporan para abaratar el coste del material polimérico. Las cargas se añaden en cantidades elevadas a las formulaciones, siempre y cuando, no modifiquen las prestaciones finales requeridas. Pueden ser inorgánicas u orgánicas y, habitualmente, se trata de materiales de bajo coste o, incluso, subproductos de otras industrias.

- **Aditivos.**
  Los aditivos son, en general, compuestos químicos que se incorporan en cantidades bajas con la finalidad de proteger al polímero frente agentes externos, o bien, para modificar alguna propiedad. Se trata de materiales caros y existe una amplia variedad según la propiedad que se pretenda modificar.

- **Refuerzos.**
  Los materiales plásticos o polímeros han ido ganando aplicaciones con el paso del tiempo. Actualmente, es posible encontrar plásticos en aplicaciones de contenido técnico medio-alto. En muchas de estas aplicaciones, los plásticos se emplean con fibras de refuerzo, cuya finalidad es la mejora de las propiedades mecánicas y la estabilidad del material.
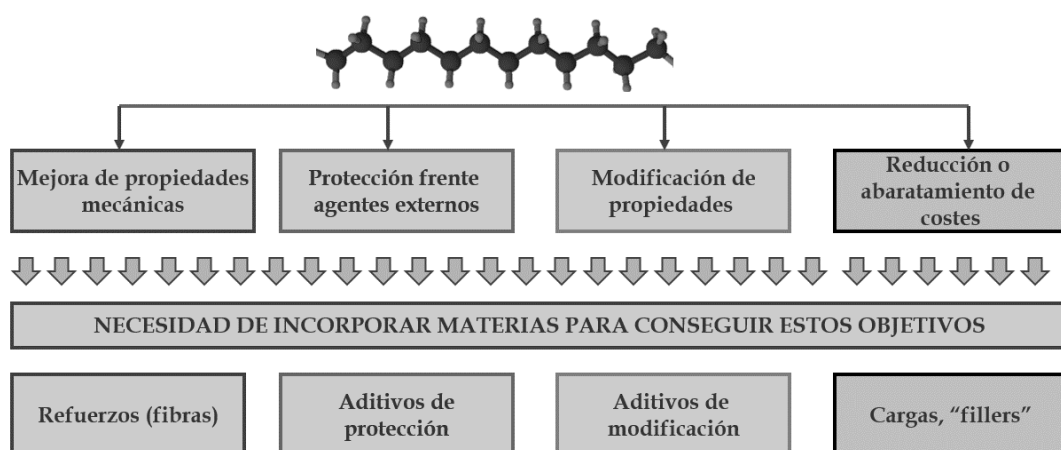

Figura I.30. Materias que se incorporan en las formulaciones de plásticos industriales con diversa finalidad.

La modificación de ciertos polímeros y formulaciones a través de técnicas como la incorporación de aditivos, mejoras del proceso de extrusión, mezclado de materiales o adición de cargas, son procesos que se han utilizado de manera habitual en la industria de los plásticos para mejorar ciertas propiedades y limitaciones que poseen, con el objetivo de ampliar las posibles aplicaciones de ciertos materiales. Estos procesos de modificación han sido ampliamente estudiados, pero en las últimas décadas se ha intensificado la búsqueda de alternativas y soluciones lo más respetuosas con el medio ambiente, para obtener productos de bajo impacto medioambiental.

I.4.1. Incorporación de aditivos.

Uno de los principales métodos para modificar las propiedades de los polímeros, es la utilización de aditivos. Estos productos son capaces de modificar, de manera relativamente sencilla, ciertas propiedades tales como el comportamiento mecánico, térmico, el color, la resistencia química y UV, densidad, etc. La gran mayoría de polímeros que se utilizan en la industria, llevan incorporados ciertos aditivos que les permiten mejorar su procesabilidad, modificar ciertas características físicas como el color, o elementos protectores (antioxidantes, estabilizantes a la luz, ignifugantes, etc.) capaces de aumentar la vida útil de los polímeros.

Al igual que sucede en la industria de los plásticos, las nuevas tendencias ligadas al desarrollo de materiales derivados de recursos renovables, están generando un creciente interés en la búsqueda de alterativas naturales a los aditivos más utilizados en la industria. Este factor, junto con la búsqueda de materiales poliméricos de origen renovable, generan un gran impacto positivo en el medio ambiente, obteniendo cada vez más alternativas renovables para la industria. En la **Figura I.31** se muestra un gráfico resumen de las posibilidades que ofrece la aditivación en el campo de los materiales plásticos.
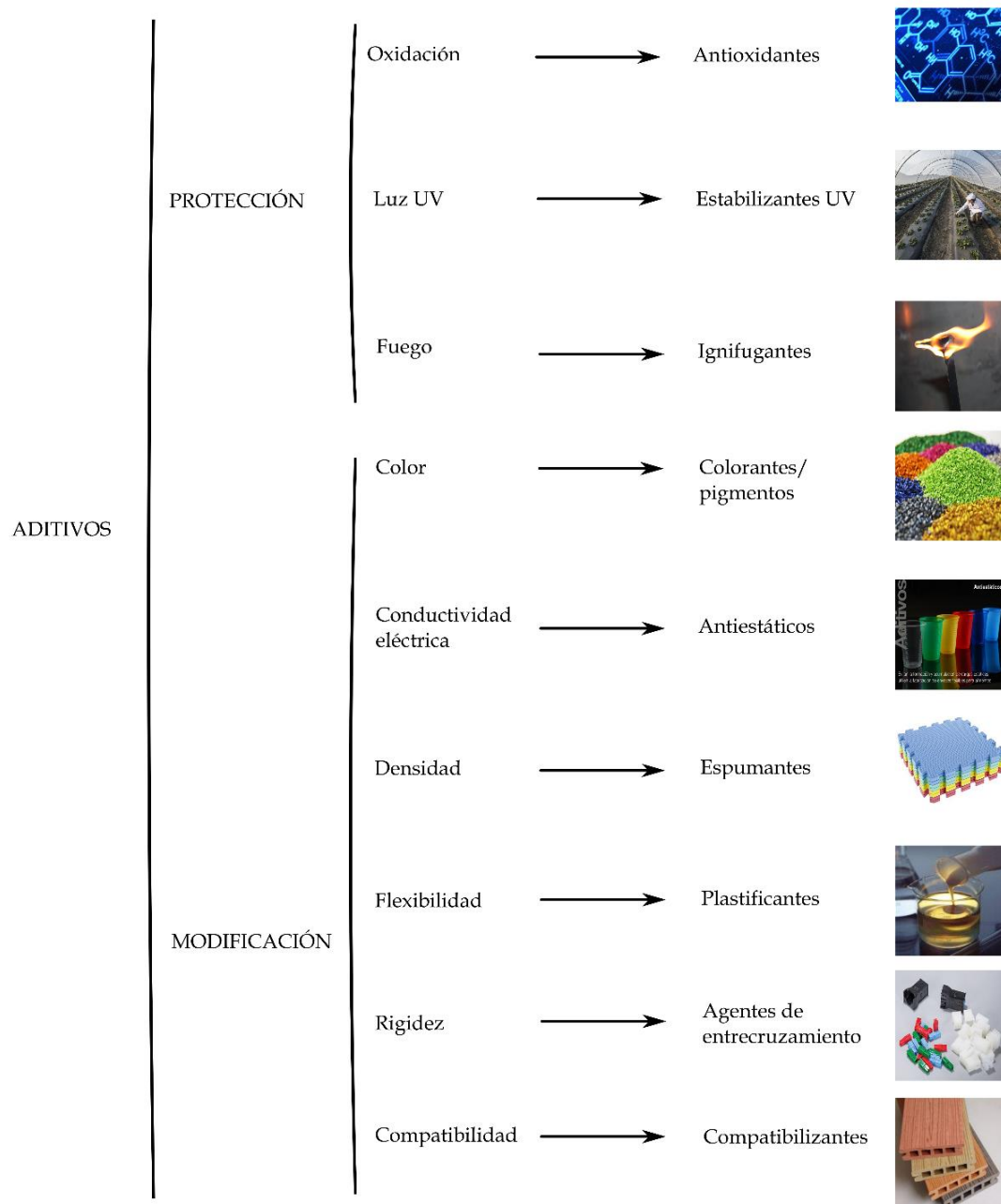
Figura I.31. Clasificación y tipos de aditivos empleados en formulaciones de plásticos industriales.

I.4.2. Mezclado industrial.

El mezclado industrial consiste en el proceso de combinación de dos o más polímeros mediante un proceso industrial. Las mezclas proporcionan una gran versatilidad a la hora de obtener materiales con nuevas propiedades, o simplemente, propiedades diferentes a las de los materiales individuales. El mezclado se centra, básicamente, en la combinación y distribución de diversos componentes separados, con el objetivo de obtener un producto final con una distribución y homogenización adecuada. El mezclado industrial aporta una gran serie de ventajas a la industria de los

plásticos, favoreciendo la obtención de nuevas mezclas y combinaciones que pueden ser utilizadas en aplicaciones que los materiales en estado puro no podrían alcanzar. El mezclado físico de dos o más polímeros es una alternativa de bajo coste a los copolímeros. No obstante, las propiedades que se pueden alcanzar mediante mezclado están muy lejos de las que se pueden obtener mediante copolimerización. La **Figura I.32** se muestra de forma esquemática, la diferencia entre una mezcla física y un copolímero.
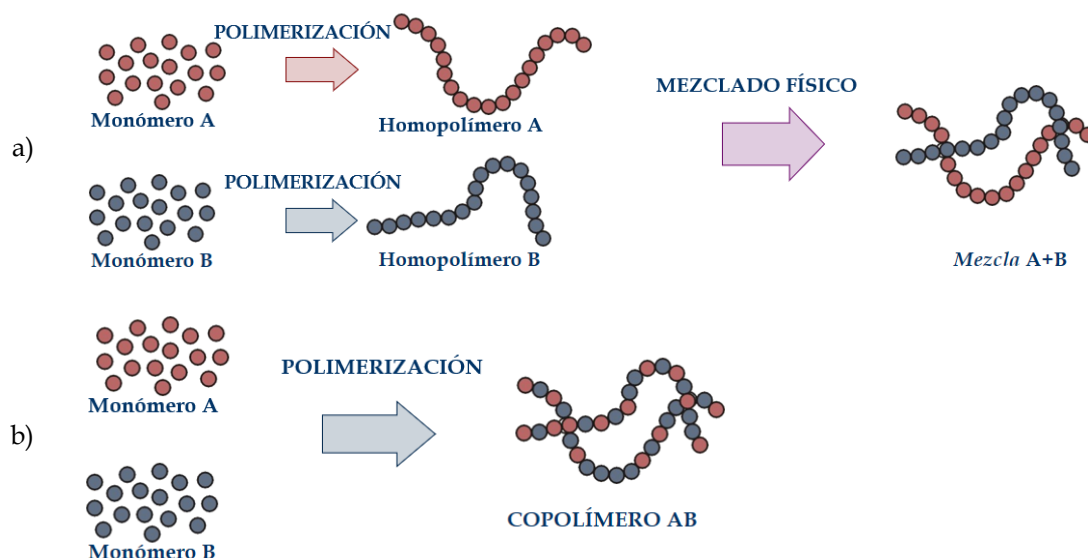
Figura I.32. Diferencias entre un proceso de a) copolimerización y b) mezclado industrial de dos componentes.

Para la obtención de mezclas poliméricas, uno de los métodos más utilizados es el mezclado por fusión, con el empleo de altas condiciones de cizallamiento, ya que se permite obtener una morfología lo más homogénea posible. Este método, permite obtener unas condiciones de mezcla adecuadas si se utilizan temperaturas y viscosidades lo suficientemente apropiadas, para favorecer fuerzas de cizalla y mejorar al máximo el mezclado. En particular, mezclas de polímeros renovables como el PHBV y el PLA, consiguen unas condiciones de viscosidad adecuada para lograr una buena dispersión de la fase PLA debido a la competencia entre las fuerzas de cizalla y las fuerzas de tensión superficial en la entrecara [163]. Debido a la facilidad de procesado que poseen los materiales termoplásticos, este tipo de mezclas y combinaciones están obteniendo cada vez más relevancia dentro de la industria gracias a los costes tan reducidos y la facilidad para producir en masa [164].

Actualmente, debido a su gran versatilidad, la gran mayoría de las veces se utiliza la extrusión de doble husillo co-rotante, tanto para la obtención de materiales compuestos poliméricos, como mezclas de polímeros o, simplemente, la incorporación de ciertos aditivos [165, 166].

I. INTRODUCCIÓN

I.4.3. Extrusión reactiva y extensión de cadena.

La extrusión reactiva (REX – reactive extrusion), se centra en la utilización de extrusoras de doble husillo co-rotante con el objetivo de unificar en el mismo proceso la producción y la modificación de polímeros [167, 168]. De esta manera, se permite obtener materiales en forma de granza completamente adaptados a las necesidades requeridas para su posterior transformación de una manera rápida y económica.

Como ya se ha comentado en el apartado anterior, las extrusoras de doble husillo co-rotantes permiten facilitar en gran medida la reacción durante todo su proceso, situando a la extrusión reactiva como un proceso muy interesante a la hora de obtener polímeros con mejoras de compatibilidad de una manera mucho más rentable y preferible que la adición de copolímeros, los cuales están hechos a medida para cada mezcla [169]. Otra ventaja reseñable a comentar, es la facilidad sobre el control de los tiempos de residencia que se obtiene con este proceso, los cuales suelen rondar entre 1 y 15 min para su correcto funcionamiento (precisamente para dar tiempo a que se produzcan ciertas reacciones). Este tiempo de residencia depende en gran medida de los materiales o reacciones químicas que se quieran llevar a cabo, teniendo en cuenta siempre las mejores condiciones para cada caso.

Entre algunas de las reacciones más utilizadas, se pueden encontrar procesos de poliadición y policondensación de diferentes polímeros, reacciones de funcionalización y compatibilización, entrecruzamientos y reticulaciones e, incluso, procesos de reciclado químico y degradación de materiales como el PET. Gracias a la gran versatilidad que posee este proceso, en los últimos años se han referenciado e investigado nuevas formas de obtener mezclas de materiales biodegradables multifuncionales [170], materiales obtenidos a partir de reacciones enzimáticas [171], mejora de materiales totalmente renovables [172] o, incluso, mejora de compatibilidad entre materiales poliméricos y nanopartículas [173].

Dentro de la modificación de polímeros, y relacionado muy de cerca con la extrusión reactiva (REX), los extensores de cadena son elementos muy utilizados para mejorar ciertas limitaciones que poseen algunos materiales o mezclas poliméricas, especialmente los polímeros de condensación de tipo poliéster. Los extensores de cadena son compuestos químicos (incluso polímeros), con pesos moleculares relativamente bajos, que sirven para ensamblar los extremos de las cadenas poliméricas de ciertos polímeros. En materiales como el PLA, debido a los problemas asociados a su estructura lineal y su sensibilidad a la hidrólisis, la incorporación de este tipo de extensores de cadena favorece de manera directa un aumento en su peso molecular, mejorando la temperatura de fusión y generando una estructura más resistente [174]. En este ámbito, diversos autores han mostrado cómo la incorporación de diferentes oligómeros acrílicos en materiales poliméricos con bajos valores de tenacidad, han conseguido mejorar estas limitaciones gracias a los procesos de extensión de cadena [175].

Generalmente, este tipo de extensores de cadena se basan en oligómeros basados en epóxidos provenientes de recursos petroquímicos. Estos extensores de cadena funcionan muy bien con los poliésteres, debido a que los grupos epoxi de estos

Tesis Doctoral   Página 83 de 602

oligómeros, desencadenan en la formación de enlaces covalentes con los grupos hidroxilo (- OH) presentes en las posiciones terminales de los poliésteres. A modo de ejemplo, la **Figura I.33** muestra como interactúa un extensor de cadena con un poliéster como el PHB [176].
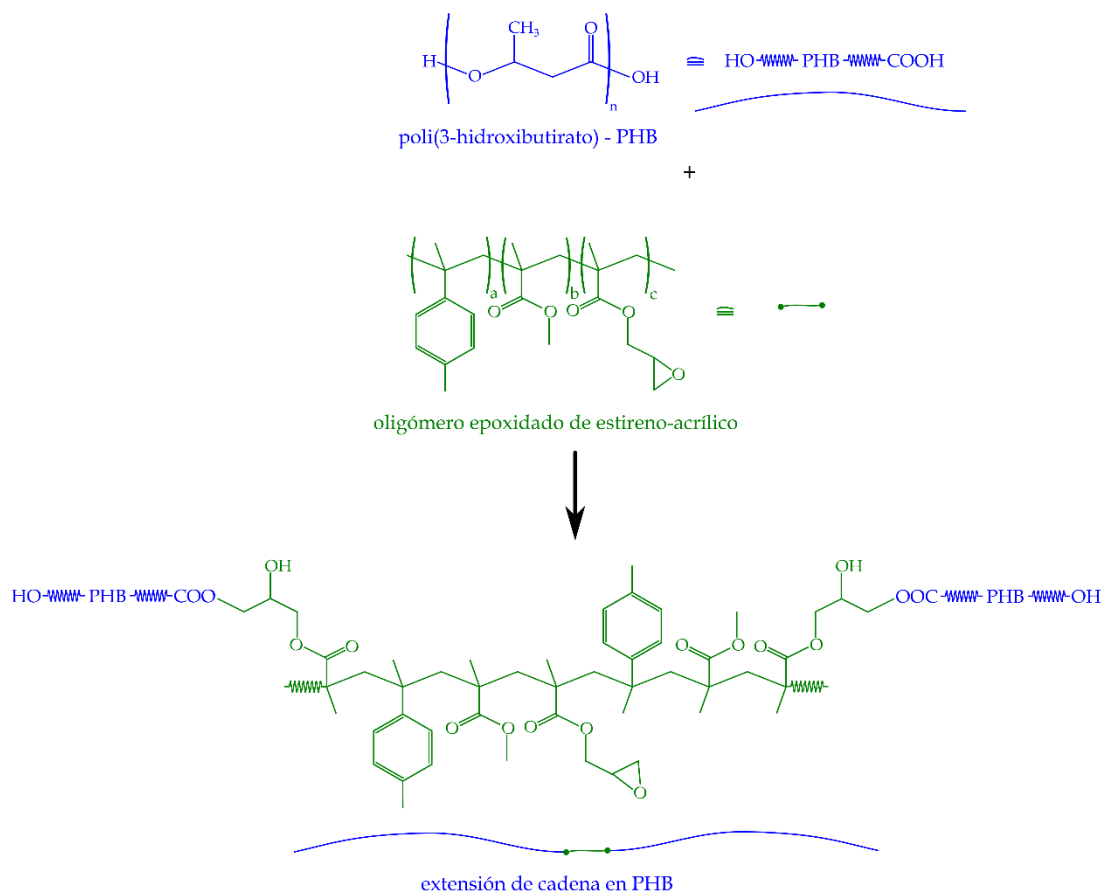
Figura I.33. Proceso de extensión de cadena de un PHB con un oligómero epoxidado de estireno-acrílico.

Debido a los problemas medioambientales generados desde hace años por los materiales poliméricos no renovables, y con nulas capacidades para ser degradados, los poliésteres alifáticos tales como los PHAs y el PLA, han empezado a utilizarse e investigarse en gran medida. En este ámbito, la utilización de los extensores de cadena para mejorar sus propiedades dúctiles o para crear mezclas poliméricas viables para la industria, han generado un gran impulso en el desarrollo y optimización de diversos extensores de cadena [100, 176]. Destaca la modificación de ciertos aceites vegetales a partir de epoxidación y apertura de anillos con alcoholes, aminas o ácidos carboxílicos [177]. Mediante estos procesos se pueden obtener compuestos con potencial uso como extensores de cadena, como es el caso de ciertos polioles derivados de aceite de ricino o aceite de algas marinas [178]. Es en la obtención de los poliuretanos, donde este tipo de elementos actúan de manera más efectiva, sustituyendo a los extensores derivados del petróleo [179].

I.4.4. Incorporación de "fillers" y/o refuerzos. Green composites.

Dentro de la industria de los polímeros, siempre se han utilizado diferentes tipos de cargas o refuerzos con el objetivo de modificar ciertas propiedades o, simplemente, para abaratar costes. Hasta hace relativamente pocos años, la utilización de materiales poliméricos petroquímicos con refuerzos como la fibra de vidrio, la fibra de carbono o la aramidas [180-182], parecían las únicas opciones para mejorar ciertas características y superar algunas limitaciones que tenían los polímeros desde el punto de vista de la resistencia mecánica, siendo materiales con mayor potencial que algunos metales, gracias a su bajo peso.

Actualmente, la incorporación de refuerzos o rellenos, a partir de fibras provenientes de recursos renovables y en muchos casos, generada como residuos de otras industrias, está siendo ampliamente estudiada por diferentes autores. Algunas fibras procedentes de residuos o cultivos como el lino, kenaf, yute, coco o arroz se están empezando a utilizar en gran medida en sectores importantes como la automoción, donde la búsqueda de materiales reciclables, con bajo impacto ambiental, y buen equilibrio de propiedades es de vital importancia. Además, la utilización de este tipo de desechos o subproductos, favorecen no solo de mejora directa en la reducción de residuos de la industria del plástico, sino también la valorización de residuos para alcanzar economías circulares. Autores como Ferrero *et al.* [183], han sido capaces de reutilizar residuos de algas de *Posidonia oceanica*, para obtener materiales compuestos de bajo impacto medioambiental, con matrices de gluten. Por este motivo, la utilización de residuos y desechos como cargas o refuerzos provenientes de entornos o empresas cercanas a cada sector, es una manera muy prometedora de obtener una gran revalorización y conseguir cerrar un ciclo industrial totalmente limpio. En este ámbito, las empresas agroalimentarias ligadas a un territorio, pueden verse ampliamente beneficiadas por la utilización de sus residuos en nuevos polímeros, desde un punto de vista de reducción y revalorización directa. Este tipo de materiales que se basan en un polímero con un refuerzo de fibra natural se denominan (NFRP) del inglés "*natural fiber reinforced plastic*".

Uno de los principales problemas de estos materiales naturales reforzados, es la mala adhesión existente entre la matriz polimérica y algunos refuerzos. Kim *et al.* [184] demuestran cómo la incorporación de diferentes porcentajes de fibras naturales como algodón o fibra de madera al polipropileno muestran resultados diferentes. En el caso de la madera, se ve reducida la resistencia a tracción en todos los casos, mientras que, con la incorporación de las fibras de algodón, es a partir de un 20% de refuerzo cuando empieza a distinguirse una mejora en la resistencia a tracción. Para la mejora de la compatibilidad entre las matrices poliméricas (habitualmente hidrofóbicas) con las cargas lignocelulósicas (altamente hidrofílicas), se requiere el empleo de agentes compatibilizantes. Avella *et al.* [185] demostraron cómo la incorporación de un compatibilizante derivado del anhídrico maleico (MA), puede favorecer en gran medida la interacción entre los grupos hidroxilo de la fibra natural de kenaf y el PLA. En particular, mostraron una mejora de propiedades mecánicas de hasta un 190% combinación de las fibras y el compatibilizante. Por su parte, Balart *et al.* [186] han mostrado resultados muy prometedores de mejoras en la interacción de un polímero

renovable como el PLA, con una carga derivada de la cáscara de avellana a partir de compatibilizantes naturales derivados de aceite de soja.

Dentro de la industria del plástico, la utilización de cargas o "fillers" lignocelulósicos provenientes de subproductos, se ha convertido en una opción muy viable para la obtención de materiales de alto contenido renovable y con un acabado similar a la madera. Se trata de los WPC ("*wood plastic composites*") ya que inicialmente empleaban el serrín de madera para reforzar matrices plásticas. Este tipo de materiales poseen una alta eficiencia ambiental gracias a su origen natural, que en muchos casos provienen de residuos de la industria agroalimentaria [187]. Por estos motivos, en las últimas décadas, ha aumentado de manera significativa la investigación en materiales compuestos a partir de cargas provenientes de residuos agroalimentarios, como la cascara de nuez, café molido, residuos de maíz o arroz [188-190]. Estos materiales ofrecen una solución atractiva para ciertos sectores como el de la automoción, el envase y embalaje, decoración y jardinería o la construcción [96, 191, 192]. Estas ventajas radican en su apariencia, similar a la madera, propiedades equilibradas y elevado contenido renovable.

I.5. ADITIVOS NATURALES EN FORMULACIONES DE POLÍMEROS.

Como se ha descrito previamente, la incorporación de aditivos es una parte importante en la industria de los polímeros, ya que pueden variar y modificar las propiedades de estos, según las necesidades o especificaciones que se requieran.

Las tendencias más recientes se centran en la búsqueda de materiales poliméricos respetuosos con el medio ambiente. Este hecho ha afectado de manera positiva a la I+D+i en aditivos renovables, capaces de ser reciclados con facilidad, y que no generen una gran carga final en el entorno. Este tipo de aditivos provenientes de fuentes naturales y renovables, juntamente con la utilización de materiales poliméricos respetuosos con el medio ambiente, está generando una sinergia, referente al conjunto de propiedades técnicas y bajo impacto medioambiental.

I.5.1. Utilización de nanoarcillas.

Las nanopartículas suponen una solución viable y novedosa para mejorar ciertas propiedades de los polímeros, con la aplicación de contenidos relativamente bajos, entre un 1 y un 10% en peso. Este tipo de aditivos se caracterizan principalmente por tener una gran superficie específica, debido a su elevada área en relación a su volumen, además de tamaños por debajo de los 100 nm en alguna de sus dimensiones. Debido a su elevada superficie específica y la gran reactividad que poseen, suelen generar problemas de aglomerados o agregados, que pueden provocar problemas de concentración de tensiones. Este tipo de aglomerados generados a partir de las fuerzas de van der Waals de las mismas nanopartículas, generan una baja dispersión, lo que puede derivar en una reducción en las propiedades deseadas del compuesto. No obstante, este tipo de inconvenientes se pueden solucionar mediante la modificación superficial de estas nanopartículas a través de procesos químicos, mejorando de manera directa la dispersión de estas dentro de las mezclas y favoreciendo en gran medida la aplicación de estos aditivos nanométricos [193].

Las nanoarcillas se han posicionado de manera muy positiva como una de las soluciones más viables y naturales en la utilización de nanocargas para la aditivación y mejora de las propiedades de polímeros. Las primeras investigaciones se centraron en nanoarcillas laminares, como la montmorillonita [194], la cual posee una estructura en forma de esmectita con una excelente superficie útil y un coste muy bajo. Con el empleo de este tipo de nanoarcillas se ha conseguido una notable mejora en el módulo de Young y excelentes propiedades barrera [193, 195].

No obstante, las recientes investigaciones han levantado un gran interés en la utilización de otras nanoarcillas como la haloisita y la sepiolita, entre otras, que, además, presentan una estructura tubular o con huecos, que permite cargar selectivamente estas nanoarcillas con compuestos activos para liberación controlada [196-198].

I.5.1.1. Nanotubos de haloisita (HNTs).

Este tipo de nanopartículas, están despertando un gran interés como aditivos dentro de diversos sectores, debido a sus buenas prestaciones y posibilidades tecnológicas. Al ser un elemento natural, se puede encontrar de manera directa en depósitos naturales en diferentes formatos, según la zona o las condiciones de formación. Este tipo de nanoarcillas, se pueden clasificar según sus dimensiones en forma tubular, laminar o en formato esférico. En particular, es la forma tubular o nanotubos de haloisita (HNT), la que mayor aplicación está teniendo actualmente, gracias a sus excelentes propiedades mecánicas, elevada superficie útil, capacidad para encapsular diferentes elementos, capacidades retardantes a la llama, o su relativo bajo coste de obtención [199, 200].

Desde un punto de vista químico, los HNTs se basan en aluminosilicatos, con una estructura muy similar a la de la caolinita, pero con un notable cambio dimensional y con moléculas de agua entre sus capas. A diferencia de la caolinita, los nanotubos de haloisita se caracterizan por formar su estructura de manera tubular a partir de una lámina de dicho material. La **Tabla I.3** muestra algunas de las principales propiedades físicas de los nanotubos de haloisita [201].

Tabla I.3. Características principales de los nanotubos de haloisita.

Fórmula química	$Al_2Si_2O_5(OH)_4$ nH_2O
Densidad	2,1-2,6 g cm^{-3}
Módulo elástico	230-340 GPa
Longitud	0,2-2,0 μm
Diámetro externo	40-70 nm
Diámetro interno	10-40 nm
Ratio (L/D)	10-50

Una vez se enrolla la lámina, la formación de la estructura tubular genera una diferencia directa entre la parte interna y la parte externa del tubo, obteniendo una variación en las propiedades iniciales, y formando el denominado nanotubo de haloisita. La lámina que sirve de base para la formación de los HNTs, se caracteriza por tener dos capas; una primera basada en alúmina y una segunda basada en sílice. Cada una de estas capas está en una de las caras del nanotubo, generando así grupos aluminol (Al−OH) en la parte interna y grupos siloxanos (Si−O−Si) en la capa externa. La clara diferenciación química entre cada una de las capas, genera un efecto muy favorable para ciertas aplicaciones, como es una diferencia de cargas entre la parte interna y la externa, favoreciendo un gran abanico de posibilidades para ciertas aplicaciones. La **Figura I.34** muestra la estructura final que adoptan los nanotubos de haloisita después de plegar la capa de caolinita, con sus grupos y la carga de cada uno de ellos
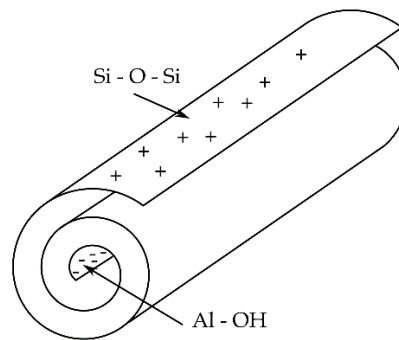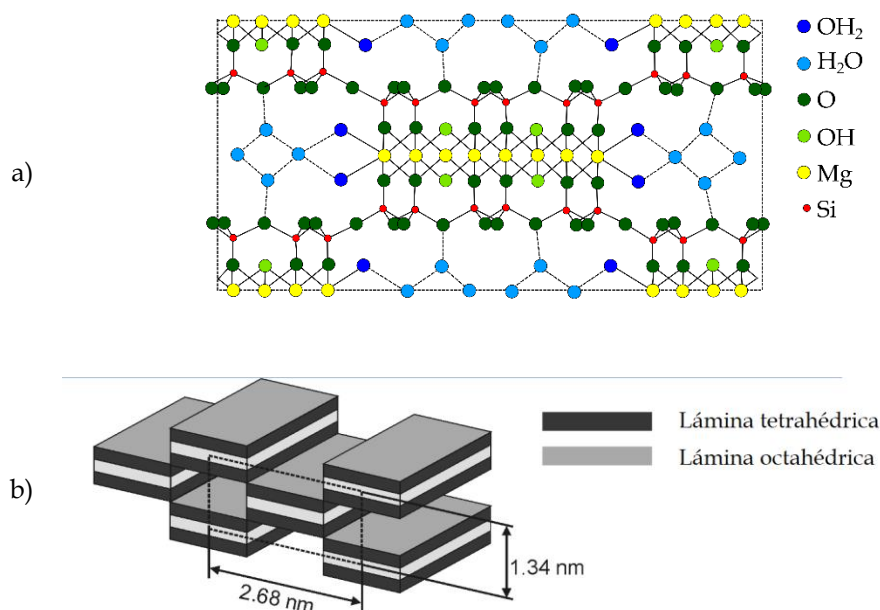
Figura I.34. Representación esquemática de la estructura tubular de la haloisita.

Sus excelentes propiedades y versatilidad, las han situado como un aditivo muy prometedor para mejorar ciertas aplicaciones de los polímeros. En este ámbito, Liu *et al.* [201] ha mostrado la relevancia que están teniendo este tipo de nanoarcillas en los últimos años, vislumbrando un aumento de las publicaciones en la utilización los HNTs en aplicaciones para refuerzos mecánicos, mejora en la estabilidad térmica, retardantes a la llama, funcionalización o encapsulación de principios activos.

I.5.1.2. Nanoarcillas derivadas de sepiolita.

Al igual que sucede en el caso de la haloisita, la utilización de la sepiolita como aditivo nanométrico, está generando cada vez más interés dentro de la industria de los aditivos naturales. En este caso, este auge se basa, principalmente, en la forma acicular o de aguja que posee, además de un bajo coste, facilidad de obtención y gran superficie de contacto. Este tipo de nanoarcillas basan su estructura en un filosilicato de magnesio hidratado complejo ($Mg_4Si_6O_{15}(OH)_2 \cdot 6H_2O$). En particular, los cristales de sepiolita se caracterizan por estar formados a partir de láminas de silicato, las cuales están estructuradas en dos capas tetraédricas de SiO_4, donde los átomos de oxígeno que no se comparten, se encuentran enfrentados entre sí. Además, estas capas están unidas con una capa octaédrica de átomos de magnesio coordinados [202]. Para ver de manera más clara la compleja su estructura, la **Figura I.35** muestra un esquema de su composición.

Esta composición estructural, da como resultado una estructura longitudinal discontinua, formando a su paso una serie de túneles abiertos o canales zeolíticos, con una sección transversal inferior a 1 nm^2 [203]. La configuración de su estructura proporciona un elemento nanométrico de origen natural en forma de aguja y unas dimensiones comprendidas entre 100–5000 nm de longitud, 10–30 nm de ancho y 5–10 nm de grosor. Las dimensiones, junto con la estructura de esta nanoarcilla, le proporcionan una gran superficie específica, un gran volumen poroso y una energía superficial elevada, generando unas excelentes propiedades coloidales y una alta capacidad de sorción [204].

Figura I.35. Representación esquemática de a) estructura química de la sepiolita y b) estructura 3D de las láminas de sepiolita con túneles.
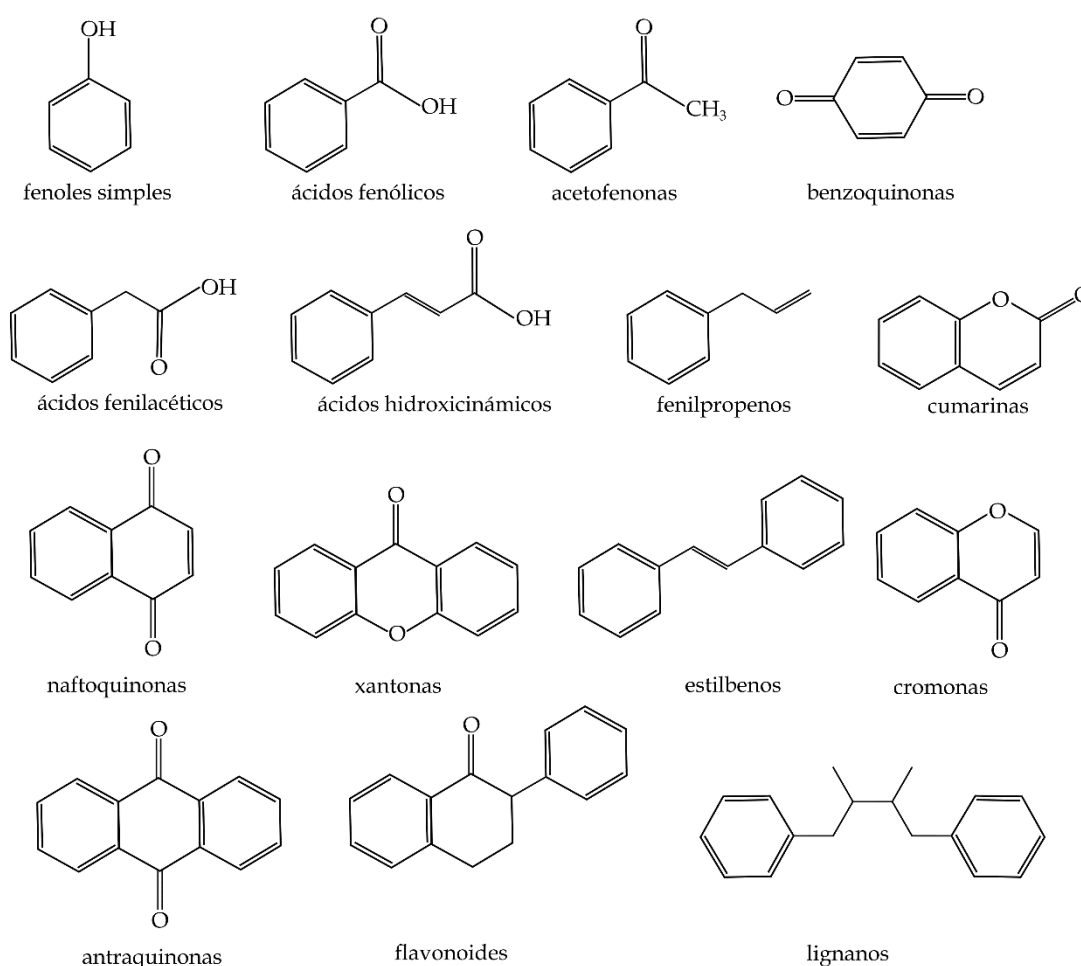
La utilización de este tipo de nanoarcillas como aditivos en polímeros, se ha estudiado en los últimos años por diversos autores, demostrando, de manera directa, cómo su incorporación genera ciertas ventajas en las características del polímero. Además, gracias a su estructura, con un tratamiento superficial adecuado, este tipo de nanoarcillas pueden dispersarse de manera adecuada en diferentes tipos de polímeros sin llegar a formar aglomerados. La sepiolita también actúa como agente nucleante en la cristalización de polímeros como el PP o el PLA, mejorando de manera notable la tenacidad y la resistencia a flexión de ciertos polímeros, y pueden actuar como aditivos ignífugos mejorando la estabilidad térmica del material [205, 206]. En materiales como el PLA o sus mezclas, se utiliza en gran medida la sepiolita, para mejorar las propiedades mecánicas y térmicas, para su uso en forma de lámina o de film, gracias a sus excelentes propiedades de dispersión. Maozeni *et al.* [207], observó una mejora de un 40% en el módulo de Young con la incorporación de cantidades entre 1 y un 3% de sepiolita en films de PLA.

I.5.2. Compuestos fenólicos naturales. Extracción y tecnologías de encapsulación.

La utilización de compuestos fenólicos provenientes de residuos agroalimentarios como aditivos naturales, supone una doble ventaja. A partir de los residuos agroalimentarios, no solo se consigue obtener un compuesto fenólico completamente funcional, sino que se revalorizan ciertos residuos que contribuyen a la generación de economías circulares. Estos compuestos fenólicos, presentes en muchos residuos agroalimentarios, representan una fuente de compuestos activos de gran utilidad en el sector envase y embalaje [208-210].

I.5.2.1. Compuestos fenólicos y polifenoles.

Los compuestos fenólicos o polifenoles, son elementos orgánicos que se encuentran de manera natural en plantas y frutas. Se caracterizan por tener en su estructura al menos un grupo fenólico unido con grupos aromáticos o grupos hidroxilo. Dentro de este tipo de compuestos, se pueden englobar diferentes familias, pero son los ácidos fenólicos y los flavonoides los que más abundan en la naturaleza, siendo un 30 y un 60% respectivamente del total de compuestos fenólicos existentes [211]. La **Figura I.36** muestra la estructura de diferentes familias de compuestos fenólicos más relevantes [212, 213]. Además de estas familias, también se contempla la lignina que responde a una fórmula de polímero donde se combinan muchos de estos compuestos para formar una estructura compleja [214].

fenoles simples   ácidos fenólicos   acetofenonas   benzoquinonas

ácidos fenilacéticos   ácidos hidroxicinámicos   fenilpropenos   cumarinas

naftoquinonas   xantonas   estilbenos   cromonas

antraquinonas   flavonoides   lignanos

Figura I.36. Representación esquemática de la estructura química de diferentes compuestos fenólicos.

Dentro de los polifenoles, existe una diferenciación estructural entre los ácidos fenólicos y los flavonoides. Esta diferenciación puede favorecer o modificar de manera

directa el proceso de extracción o la capacidad de degradación de cada uno de ellos. En relación a los ácidos fenólicos, estos se caracterizan por estar formados por formas más simples, a partir de esteres o ácidos fenólicos libres. Por el contrario, los flavonoides se centran en la formación de una estructura a partir de anillos aromáticos unidos mediante carbonos. Debido a la mayor complejidad y posibilidades de su estructura, los flavonoides pueden clasificarse en diferentes subclases como las chalconas, isoflavonas, auronas, catequinas, flavonas y flavonoles, flavanonas y flavanoles (catequinas) y taninos condensados entre otros [211].

Una de las principales ventajas que tienen los polifenoles, es una alta capacidad antioxidante. Con la ingesta de frutas y verduras, siempre se han utilizado como elementos importantes en la alimentación, ya que suponen un factor relevante a la hora de preservar la salud en el ser humano. Los polifenoles actúan como captadores de radicales, inhibiendo reacciones de oxidación, y consiguiendo un elemento primordial para la reducción del envejecimiento de las células y prevención de enfermedades. Desde un punto de vista químico, esta capacidad antioxidante de debe a la cantidad y posición de los grupos hidroxilo y carbonilo, aumentando su efectividad cuanto mayor es el grado de hidroxidación [215]. Este factor es de vital importancia, ya que su funcionamiento como antioxidantes, puede ser extrapolado a los materiales poliméricos, generando así un gran abanico de aditivos antioxidantes completamente naturales.

Si estos conocimientos se aplican a la industria del plástico y, sobre todo, a la industrial del envasado de alimentos, se pueden utilizar este tipo de compuestos fenólicos tanto para preservar alimentos frente a la oxidación, como mejorar la vida útil de materiales; todo esto, a partir de elementos completamente naturales. En este contexto, diversos autores han demostrado que la incorporación de compuestos fenólicos como la catequina, el carvacrol o el ácido gálico, como aditivos antioxidantes en films de PLA es altamente beneficioso para la industria del envasado de alimentos [216, 217]. La incorporación de este tipo de aditivos, no solo aporta una mejora notable en las propiedades antioxidantes y antimicrobianas, sino que componentes como el ácido gálico, han mejorado el alargamiento del PLA. En particular, Arcan *et al.* [218], observaron valores de alargamiento a la rotura del PLA superiores a un 100%, con la incorporación de cantidades inferiores al 3% de ácido gálico.

I.5.2.2. Tecnologías de extracción de compuestos fenólicos.

Debido a que los compuestos fenólicos están presentes en la mayoría de vegetales y frutas existentes en la naturaleza, se puede disponer de un amplio abanico de fuentes renovables para la obtención de polifenoles. En particular, las últimas investigaciones buscan obtener estos compuestos a partir de residuos provenientes del procesado industrial de productos alimentarios, con el objetivo de minimizar al máximo la contaminación y generar productos con baja huella de carbono. No obstante, estos compuestos no se pueden obtener de manera directa de su fuente vegetal, sino que deben ser extraídos de manera adecuada para poder ser utilizarlos posteriormente. Por este motivo, los procesos de extracción son de vital importancia, ya que son los encargados de separar los compuestos deseados del resto de elementos, consiguiendo así, el compuesto fenólico final.

Los primeros métodos de extracción utilizados, se basaban en técnicas de separación a partir de la utilización de disolventes orgánicos, con la finalidad de separar los polifenoles del resto de elementos presentes en la materia vegetal. Este método tradicional es denominado como extracción líquido-líquido, en el cual, se utilizan disolventes como el metanol, etanol y acetona, o diferentes mezclas con agua, con el objetivo de disolver los compuestos fenólicos y separarlos del resto de elementos.

Uno de los principales problemas de los compuestos fenólicos es que, según la naturaleza u origen de la materia prima, estas pueden contener cantidades variables de ácidos fenólicos, flavonoides o taninos, generando problemas de insolubilidad por la complejidad de los compuestos, o por la diferencia de polaridad de los disolventes utilizados. Estos factores generan grandes problemas cuando se plantea el uso de diferentes residuos o materias primas para la extracción de polifenoles, ya que es complicado desarrollar un procedimiento de extracción adecuado para la extracción de todos los fenoles existentes [219]. Por otro lado, desde un punto de vista medioambiental, este proceso requiere la utilización de disolventes orgánicos costosos y peligrosos, que no son adecuados ni para la salud ni para el medio ambiente, y que en ciertos casos pueden degradar de manera directa los elementos fenólicos. Actualmente, para ciertas extracciones se sigue utilizando este método debido a su simplicidad y bajo coste; no obstante, existen nuevas técnicas donde el rendimiento y la calidad del producto obtenido están muy por encima de los métodos convencionales basados en disolventes orgánicos.

Para obtener mayores rendimientos y, en especial, poder disponer de procesos menos agresivos para la obtención de los compuestos deseados de cada materia prima, se han desarrollado nuevas técnicas de extracción de compuestos fenólicos. Estas nuevas técnicas permiten mejorar de manera directa la calidad y la cantidad de compuestos por cada kilogramo de residuo, siendo procesos muy prometedores para la industria actual. Por estos motivos, las técnicas modernas de extracción son técnicas capaces de reducir considerablemente el consumo de disolventes y acelerar el proceso de extracción. Alguna de estas técnicas son la extracción de fluido supercrítico (SFE), la extracción asistida por ultrasonido (UAE) o la extracción asistida por microondas (MAE).

La técnica SFE se ha empezado a utilizar hace relativamente pocos años, presentando diversas ventajas con relación a las técnicas convencionales, como las bajas temperaturas y energía de procesado. Pero sobretodo, la SFE se caracteriza por la calidad que se obtiene de los compuestos fenólicos debido a la ausencia de solventes en las fases de obtención del soluto. No obstante, este tipo de técnicas, debido a la utilización de CO_2 como principal solvente supercrítico, está limitada a compuestos con polaridades medias y bajas, no siendo útil para la extracción de la mayoría de fenoles [220].

La extracción asistida por ultrasonido (UAE), permite acelerar los procesos de extracción, gracias a la simplicidad de su proceso y de equipamiento. Este método se centra básicamente en colocar la muestra triturada en el disolvente indicado, y se introduce en un baño ultrasónico, en el cual se establecen los parámetros de tiempo y

temperatura requeridos. Esta técnica permite mejorar de manera directa ciertos procesos de extracción existentes, consiguiendo rendimientos comprendidos entre un 5 y un 35%, y sí que están más indicadas para la extracción de compuestos fenólicos [221].

Por último, la extracción asistida por microondas (MAE), se ha convertido en una de las técnicas más prometedoras a nivel industrial, por diversos factores a tener en cuenta. Desde un punto de vista productivo, gracias a la utilización de la tecnología de microondas, este tipo de proceso presenta un alto rendimiento y un bajo coste, ofreciendo la posibilidad de que varias muestras se puedan extraer simultáneamente, proporcionando grandes velocidades de extracción y recuperaciones similares a tecnologías como SFE, pero con mayor capacidad para extraer fenoles. Teniendo en cuenta la reutilización de residuos, este método ya se ha empleado con diferentes residuos, tanto alimentarios como sedimentos para extraer compuestos fenólicos, aportando un gran valor añadido desde un punto de vista medioambiental. Al igual que sucede con la extracción por fluido supercrítico, al trabajar en entornos cerrados y controlados, los compuestos fenólicos no se degradan por contacto directo con la luz, generando así una gran ventaja para este tipo de extracciones, desde un punto de vista técnico. No obstante, esta técnica presenta ciertas limitaciones ligadas a la utilización de solventes inflamables y que ciertos compuestos pueden ser afines a la radiación de las microondas generando posibles situaciones altamente peligrosas por la temperatura que se pueden llegar a alcanzar durante el proceso.

Actualmente, debido a los excelentes rendimientos y, sobre todo, a la facilidad para extraer compuestos fenólicos de la mayoría de residuos provenientes de la industria agroalimentaria, la extracción por microondas está experimentando gran aceptación y crecimiento, otorgando una gran versatilidad para obtener polifenoles a partir de diferentes bases provenientes de alimentos o residuos alimentarios como hojas de olivo [222], residuos de cítricos [223, 224], residuos de tomate [225], o algunos residuos de alto valor añadido [226, 227].

I.5.2.2. Tecnologías de encapsulación de compuestos fenólicos.

Algo a tener muy en cuenta a la hora de utilizar compuestos fenólicos como aditivos en polímeros, es que, debido a su estructura química, suelen reaccionar de manera rápida con agentes externos como la temperatura, humedad, oxígeno o la luz visible, provocando una degradación de sus propiedades, y reduciendo, en gran, medida su vida útil. Por este motivo, es necesario para su correcto funcionamiento, que se puedan encapsular con la finalidad de preservar sus propiedades y mejorar su manipulación.

Básicamente, la encapsulación se centra en recubrir materiales o sustancias líquidas, sólidas o gaseosas mediante una película o capa, que proteja el elemento en cuestión frente a la acción de agentes externos para, posteriormente, ser liberado de manera controlada, y cubrir de manera eficaz su cometido inicial. Este tipo de tecnologías lleva en desarrollo durante muchos años, gracias a la gran aplicación que

tienen los compuestos fenólicos en industrias como la farmacéutica o la alimentación, donde el control de liberación y la protección de estos elementos está muy regulada.

Partiendo de esta base, actualmente existen diferentes métodos de encapsular compuestos biológicos como los polifenoles, algunos de los cuales se pueden aplicar de manera directa en la industria de los plásticos y, en particular, en la industria del envasado de alimentos. Existen diferentes tipos de tecnologías de encapsulación, las cuales varían según el método utilizado; no obstante, a continuación, se describen las más utilizadas en la encapsulación de compuestos para el sector del plástico.

- **Métodos físicos de encapsulación.**
Como su nombre indica, se centran en la utilización de procesos físicos, como aplicación de grandes presiones, líquidos o gases, para obtener productos totalmente encapsulados. En este contexto, el secado por pulverización o *spray-drying*, se utiliza de manera muy habitual, debido a su facilidad de implementación a escala industrial. En este proceso, se mezcla en disolución el compuesto a encapsular con un agente o polímero de recubrimiento para, posteriormente, ser atomizado a gran presión, obteniendo así nanoesferas con un núcleo cargado y una capa protector a[228].

- **Métodos físico-químicos de encapsulación.**
Los métodos físico-químicos, emplean ciertos compuestos químicos para obtener diversos procesos de encapsulación. En particular, crean recubrimientos a partir de emulsiones, con el objetivo de separar los compuestos activos del material que formará parte del recubrimiento. En este caso, se combina la parte química de las disoluciones, con propiedades físicas como interacciones iónicas o hidrofóbicas, con la finalidad de separar de manera eficaz los compuestos a partir de la carga de cada componente o su hidrofobicidad. De esta manera se consigue una diferenciación de fases, permitiendo obtener un recubrimiento de los compuestos de una manera adecuada [229].

- **Métodos químicos de encapsulación.**
Los métodos químicos, se centran en la polimerización *"in situ"* de nanocompuestos. Este proceso consiste en emulsionar el componente monómero (principalmente compuestos como el estireno o el metil metacrilato) en una fase acuosa añadida con un tensioactivo apropiado. Cuando empieza la polimerización, el polímero insoluble en agua resultante, da lugar a la formación de microesferas en las que se puede encapsular de manera efectiva los compuestos fenólicos [230].

En general, la encapsulación de compuestos fenólicos dentro del sector de los materiales poliméricos, genera ciertos inconvenientes que no pueden solucionarse de forma simple, ya que la mayoría de los procesos de transformación de plásticos implica el empleo de temperatura y, con ello, es posible degradar o, incluso perder, dichos compuestos fenólicos [231, 232]. Teniendo en cuenta estas consideraciones, en los últimos años se ha investigado sobre las técnicas más adecuadas para encapsular y utilizar compuestos fenólicos dentro de materiales poliméricos. En particular, la encapsulación de compuestos fenólicos a través de la pulverización o formación de nanofibras mediante novedosas técnicas como la electrohilatura o *"electrospinning"*, están ganando interés en la industria de los plásticos, y en particular en la obtención de

materiales para el envasado de alimentos con altas capacidades antioxidantes, así como materiales para el sector médico.

La electrohilatura o "*electrospinning*", es una manera directa de obtener encapsulados de diferentes compuestos fenólicos o agentes bioactivos, a escala nanométrica o micrométrica, a partir de soluciones de polímeros [233]. Estas técnicas utilizan fuerzas electrostáticas con el objetivo de producir flujos de disoluciones de polímeros que, al secarse por evaporación del solvente, dan lugar a fibras o esferas poliméricas. En especial, la técnica de "*electrospinning*" es una tecnología prometedora que puede realizarse fácilmente a temperatura ambiente, por lo que está generando un gran interés en relación a la encapsulación de compuestos y sustancias termolábiles y sensibles a la luz [234, 235]. Además, debido a la versatilidad que se puede obtener con las disoluciones, se pueden crear de manera rápida recubrimientos para elementos con propiedades activas [236]. La **Figura I.37** muestra, de forma esquemática, el proceso de obtención de nanopartículas y nanofibras a través del proceso de "*electrospinning*".
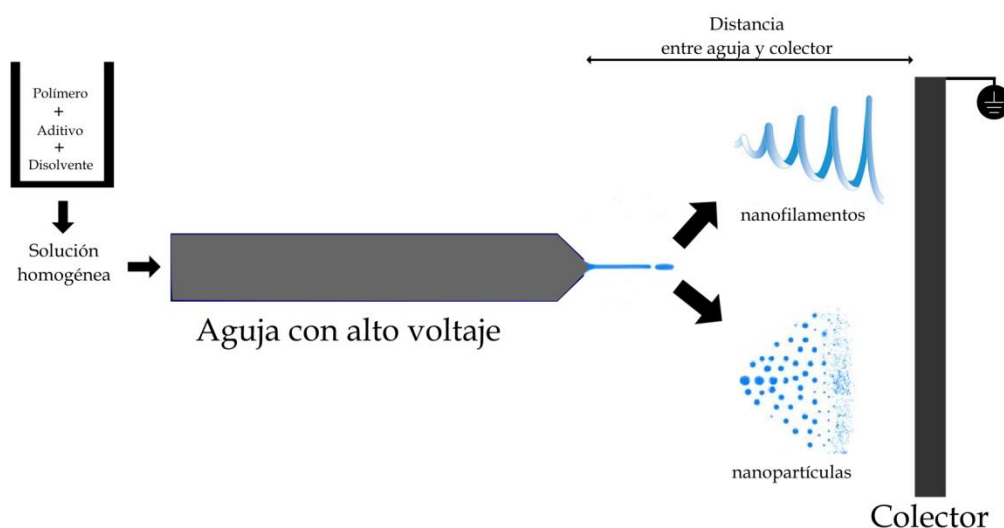
Figura I.37. Proceso de obtención de nanopartículas o nanofilamentos mediante "*electrospinning*".

Hay que tener en cuenta, que en este método de obtención de compuestos nanométricos, se pueden modificar diferentes parámetros, permitiendo así poder conseguir hilatura (nanofibras) o pulverizado (nanopartículas). Este proceso, se centra en la modificación de la diferencia de potencial entre la base de recolección, y la aguja de inyección, además de su distancia y el caudal inyectado en la aguja. Con estos parámetros es posible controlar de manera sencilla la calidad y geometría del material obtenido. No obstante, hay que seleccionar de forma adecuada tanto el polímero como el disolvente, ya que los parámetros de conductividad de la disolución, afectan de manera directa en los resultados finales.

Dentro de la industria de los materiales poliméricos, ya se han obtenido varios tejidos y materiales a partir de esta técnica, con capacidades bioactivas para el envasado de alimentos [237, 238]. Además de poder obtener materiales en forma de

nanoesferas cargados con compuestos fenólicos, se pueden obtener, de manera directa, películas continuas mediante la aplicación de un tratamiento térmico por debajo del punto de fusión del biopolímero, generando films activos de manera simple y sin someter al polímero a demasiadas acciones de procesado, reduciendo así la interacción de los compuestos con la temperatura.

I.5.3. Tecnología de aceites vegetales modificados.

En la última década, la gran sensibilización social sobre la búsqueda de materiales y aditivos naturales, ha generado nuevas tendencias en el desarrollo de plastificantes para materiales poliméricos. En este contexto, se ha empezado a investigar sobre nuevos plastificantes con orígenes renovables, con baja toxicidad, y que ofrezcan una baja migración, permitiendo mejorar, en gran medida, el abanico de posibilidades de estos nuevos plastificantes.

Actualmente, los aceites vegetales modificados, están teniendo una gran aceptación y aplicación en la industria del plástico, como plastificantes y compatibilizantes naturales, ya que su particular estructura, en forma de triglicérido con ácidos grasos insaturados, permite llevar a cabo diversas modificaciones químicas que permiten su uso en diversas aplicaciones.

I.5.3.1. Obtención de aceites vegetales.

Una de las principales formas de obtener los aceites vegetales, es por prensado de semillas. A partir de este proceso se elaboran la mayoría de estos aceites, debido a su bajo coste, simplicidad de proceso y gran capacidad de producción. No obstante, este método tan antiguo y rudimentario, posee un bajo rendimiento y suele generar una cantidad de residuos elevada. Actualmente, se están estudiando otras técnicas para extraer aceites, tales como la extracción asistida por microondas (MAE) o por ultrasonido (UAE). Estas técnicas, permiten mejorar, en cierta medida, el rendimiento final de la extracción, pero están muy limitadas en relación al coste y a la cantidad de material a procesar [238].

Los aceites vegetales están compuestos, en más de un 90%, por triglicéridos, con una estructura central de glicerina esterificada con 3 ácidos grasos. En este sentido, según el tipo de aceite y su origen, en el triglicérido se pueden encontrar diferentes tipos de ácidos grasos en su estructura [239], **Figura I.38**.
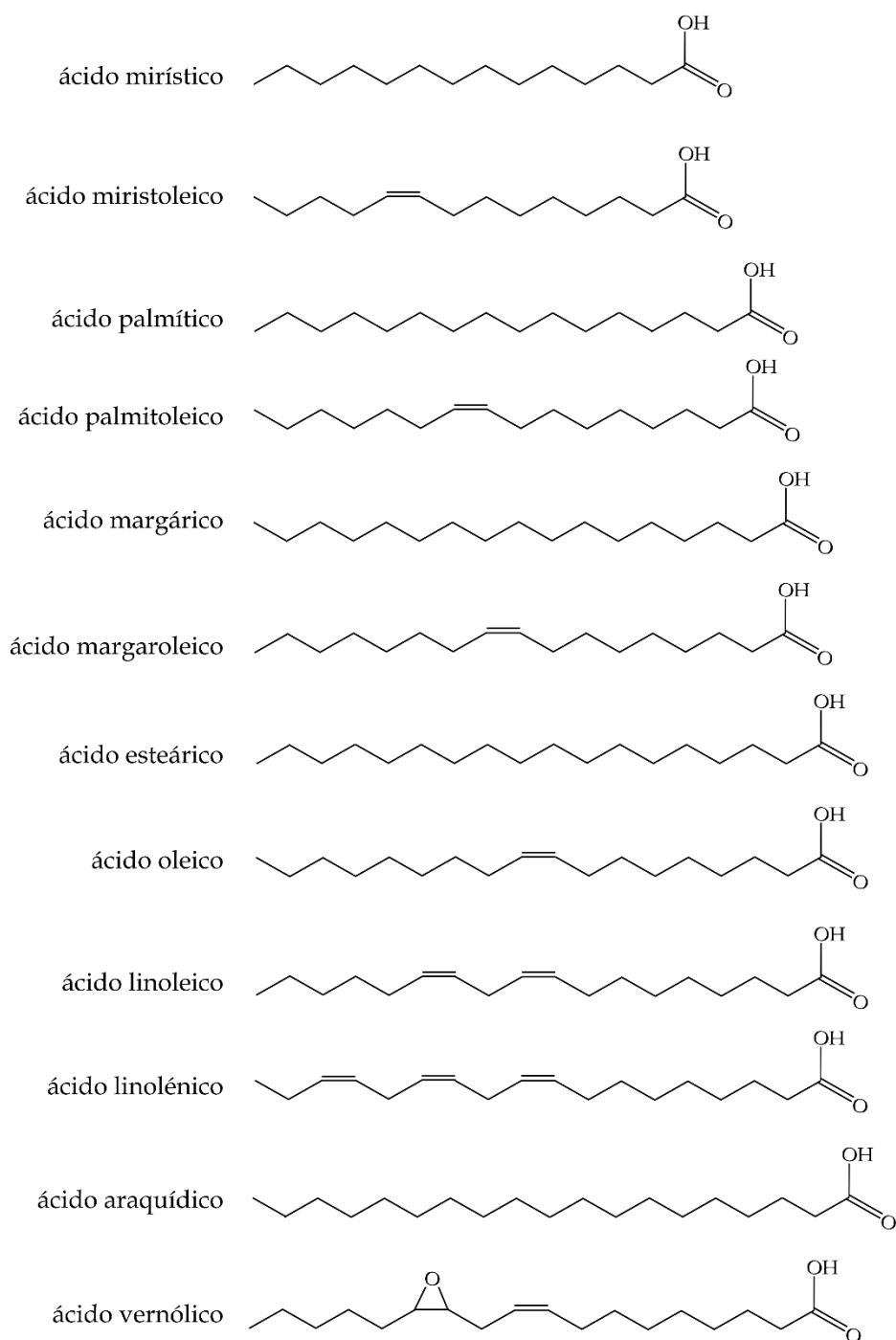
Figura I.38. Estructura general de diferentes ácidos grasos comunes que forman parte de aceites vegetales.

Para la utilización de esos aceites naturales como aditivos dentro de los polímeros, es necesario modificar químicamente su estructura, con la finalidad de que puedan actuar de manera adecuada en conjunción con el polímero o mezcla seleccionada. En particular, la estructura de los ácidos grasos es de vital importancia para que estos aceites trabajen como aditivos de manera adecuada, ya que deben ser

modificados mediante técnicas de epoxidación, acrilación, hidroxilación o maleinización para crear grupos funcionales capaces de ampliar el espectro de aplicación de estos aceites. A continuación, la **Tabla I.4** muestra la composición porcentual de ácidos grasos de los aceites vegetales más comunes utilizados para su modificación, mostrando de manera directa las diferentes posibilidades según en grado de insaturaciones contenidas.

Tabla I.4. Porcentaje de composición de ácidos grasos según cadena de átomos de carbono (a) y cantidad de insaturaciones (b), (a:b).

Aceite	14:0	14:1	16:0	16:1	17:0	17:1	18:0	18:1	18:2	18:3	20:0	20:1
Maíz	0,1	0,0	10,9	0,2	0,1	0,0	2,0	25,4	59,6	1,2	0,4	1,0
Linaza	0,0	0,0	5,5	0,0	0,0	0,0	3,5	19,1	15,3	56,6	0,0	0,0
Palma	1,0	0,0	44,4	0,2	0,1	0,0	4,1	39,3	10,0	0,4	0,3	0,0
Soja	0,1	0,0	11,0	0,1	0,0	0,0	4,0	23,4	53,2	7,8	0,3	0,0
Girasol	0,0	0,0	6,1	0,0	0,0	0,0	3,9	42,6	46,4	1,0	0,0	0,0
Aceituna	0,0	0,0	13,7	1,2	0,0	0,0	2,5	71,1	10,0	0,6	0,9	0,0

I.5.3.2. Modificación de aceites vegetales.

Los aceites vegetales, a pesar de su contenido en insaturaciones, no presentan una elevada reactividad química. A través de técnicas como la epoxidación, acrilación o maleinización, se puede mejorar la reactividad de los aceites vegetales, generando grupos altamente reactivos a partir de los diferentes ácidos grasos y los triglicéridos que los conforman. En particular, la presencia de dobles enlaces carbono-carbono (insaturaciones) que poseen algunos ácidos grasos, los hacen atractivos para su modificación y posterior uso en otros sectores industriales. Además, es importante destacar que muchos de los aceites que se emplean para su modificación química, no son aptos para consumo, por su alto contenido en ácidos grasos poliinsaturados.

Una de las técnicas más simples y más utilizadas para la modificación de aceites vegetales es la epoxidación, que da lugar a los denominados aceites vegetales epoxidados (EVO). Existen diversos métodos para dicha modificación; uno de estos se basa en la reacción de las insaturaciones con peroxoácidos, que da lugar a la oxidación de las insaturaciones formando grupos oxirano. En general, es un proceso químico relativamente sencillo, que permite aumentar la reactividad de los triglicéridos a partir de la conversión de las insaturaciones en grupos oxirano, proporcionando de manera directa, una funcionalidad epoxi al aceite [240]. La **Figura I.39** muestra el ejemplo de epoxidación de un aceite vegetal genérico con ácidos grasos insaturados, en el cual se utilizan reactivos como peróxido de hidrógeno o ácido peracético para introducir un átomo de oxígeno en la estructura y convertir el doble enlace de carbono en un anillo de oxirano [241]. Por este motivo, los aceites epoxidados son mucho más reactivos que el aceite vegetal en su estructura primaria.
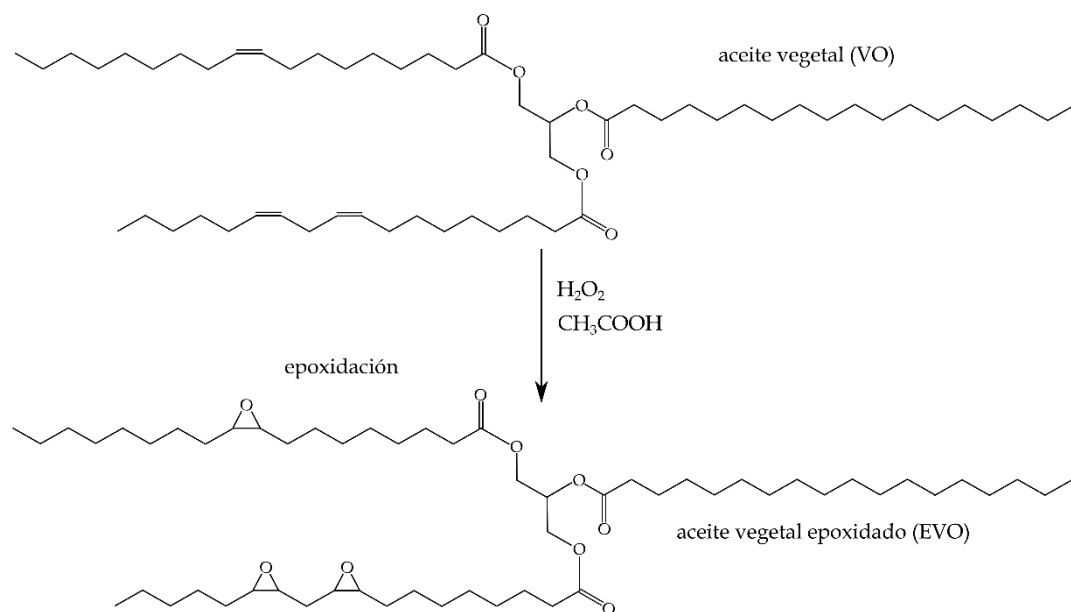
Figura I.39. Representación esquemática del proceso de epoxidación de un aceite vegetal con peroxoácidos generados "*in situ*".
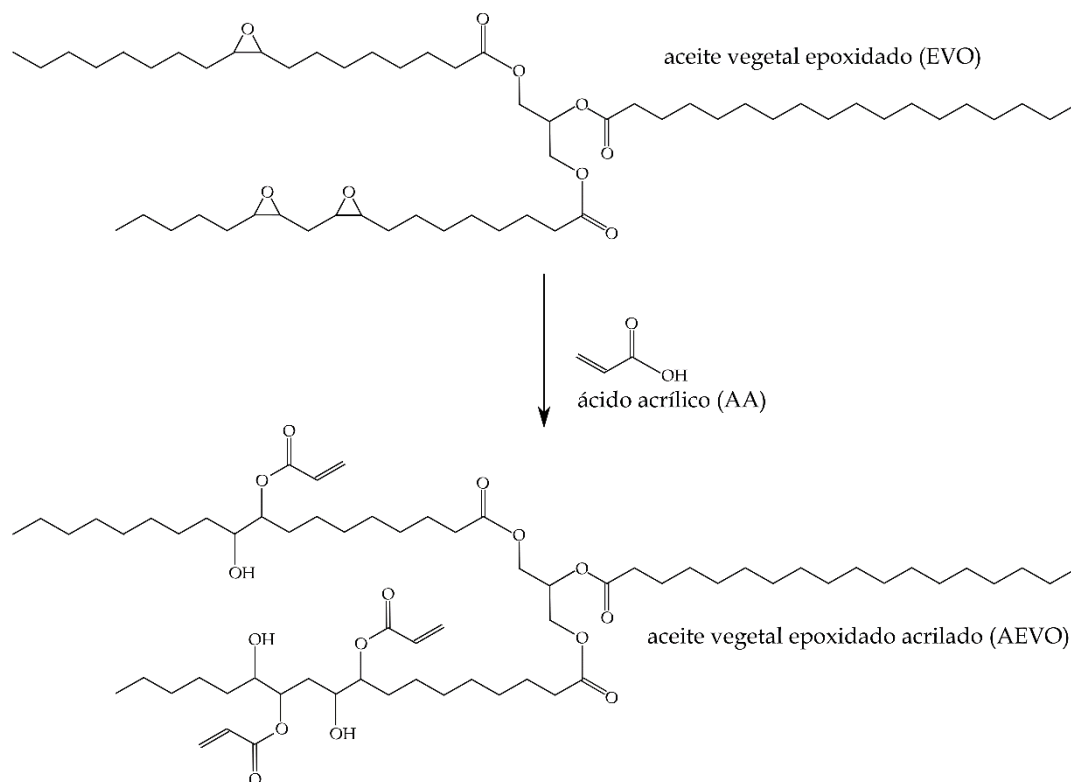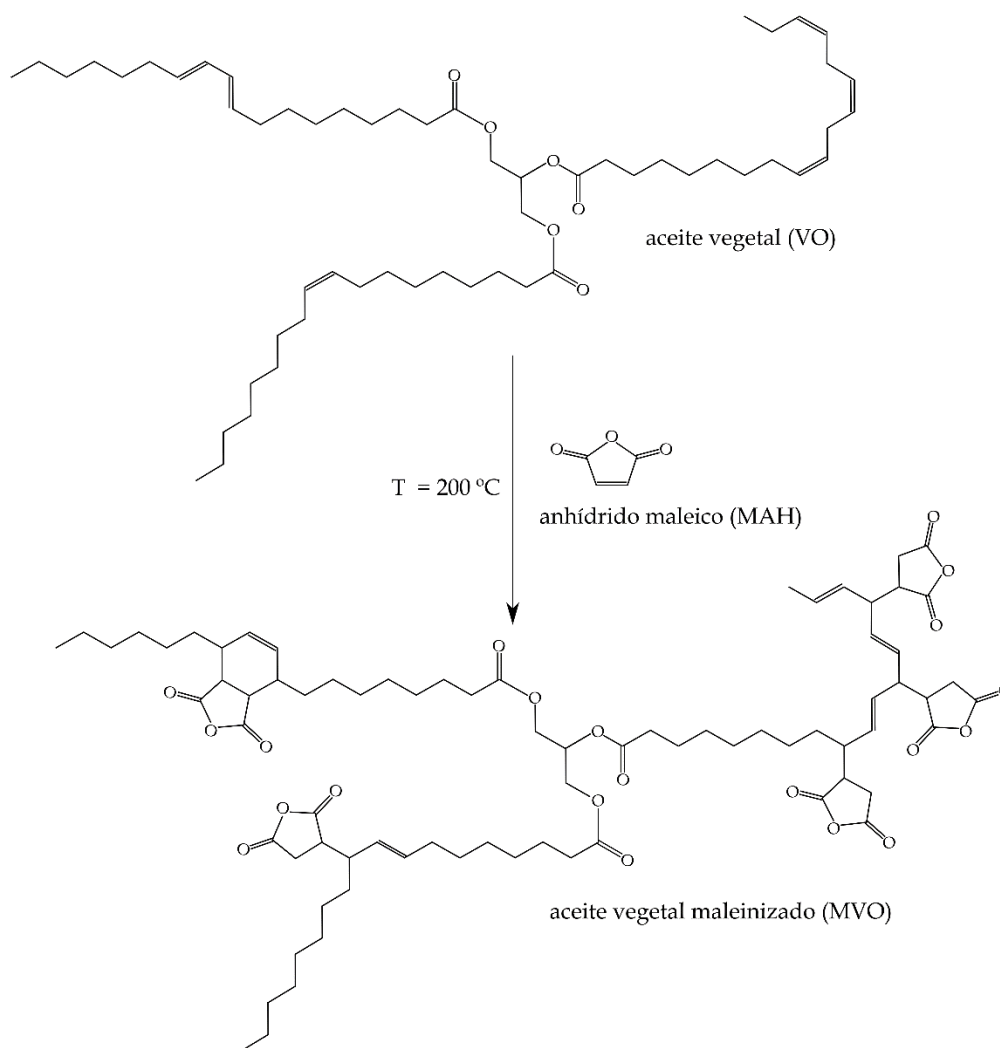

Figura I.40. Representación esquemática del proceso de acrilación de un aceite vegetal por reacción de aceite vegetal epoxidado con ácido acrílico.

Dentro del proceso de epoxidación, una modificación que se está utilizando para la mejora de ciertas propiedades mecánicas de materiales como el PLA, es la acrilación de aceites vegetales. Este proceso se basa en usar ácido acrílico (AA) en aceites vegetales epoxidados con la finalidad de abrir los grupos epóxido y así generar una estructura reactiva diferente a la obtenida con la epoxidación, tal y como se muestra en la **Figura I.40** [242].

Otra de las modificaciones relevantes para la incorporación de aceites vegetales como aditivos naturales en polímeros, es la maleinización. Este proceso químico es relativamente sencillo, ya que se centra en la incorporación de anhídridos, como el anhídrido maleico (MAH), a la estructura principal del aceite vegetal, con el objetivo principal de conseguir un anclaje de los grupos anhídrido en los dobles enlaces de los triglicéridos insaturados. Esto se lleva a cabo a partir de la reacción "eno" o la adición alílica de anhídrido maleico y, en algunos casos, por condensación de Diels-Alder cuando los dobles enlaces carbono-carbono conjugados están presentes [243]. La **Figura I.41** muestra la reacción de maleinización de un aceite vegetal con ácidos insaturados y poliinsaturados.

Figura I.41. Representación esquemática del proceso de maleinización de un aceite vegetal por reacción con anhídrido maleico.

I.5.3.2. Aplicaciones de aceites modificados en tecnología de polímeros.

La utilización de aceites modificados, como aditivos dentro de la industria de los materiales plásticos, se ha visto fuertemente reforzada, en gran medida, gracias a la actual tendencia centrada en la obtención de productos renovables, y con bajo impacto medioambiental. Estos aceites se han empleado, principalmente, como plastificantes o, en algunos casos, como compatibilizantes entre diferentes mezclas poliméricas o cargas naturales. Por este motivo, las principales aplicaciones se han observado en materiales totalmente renovables y biodegradables como poliésteres alifáticos como el PLA o los polihidroxialcanoatos.

En particular, el uso de aceites vegetales epoxidados (EVOs), representa una solución ecológica para plastificar polímeros de origen renovable. Como resultado, varios EVOs se han utilizado con éxito como plastificantes del PLA. En este contexto, el aceite de soja epoxidado (ESBO), el aceite de palma epoxidado (EPO), o el aceite de linaza (ELO) han aportado grandes mejoras en la plastificación de poliésteres naturales como el PLA [43, 244, 245]. La gran funcionalidad que poseen los grupos epoxi de estos aceites modificados, genera una alta compatibilización entre polímeros y cargas lignocelulósicas debido a la reacción del anillo epóxido con los grupos hidroxilo presentes en las cadenas de la celulosa [186]. Este factor, otorga un gran abanico de posibles aplicaciones de los EVOs en la mejora de las prestaciones de los WPC, permitiendo aumentar las aplicaciones de productos totalmente renovables y biodegradables. El ESBO o el ELO, se han empleado como plastificantes para diferentes PHAs con muy buenos resultados. En este sentido, Seydibeyoğlu *et al.* [246], concluyeron que la adición de 10% en peso de ELO y ESBO conduce a una mejora en el alargamiento a la rotura del PHBV, con una posterior reducción de la resistencia a la tracción y el módulo de Young. Este tipo de aditivos, aportan a estos materiales grandes posibilidades de incorporación en aplicaciones como en el sector del envase y embalaje, permitiendo mejorar sus propiedades dúctiles sin comprometer su estructura renovable.

Por otro lado, la incorporación de aceites maleinizados como aditivos, también generan una mejora en la ductilidad y tenacidad en poliésteres de base biológica. Por ejemplo, Ferri *et al.* [247], demostraron la eficiencia del aceite de linaza maleinizado (MLO) para mejorar la ductilidad de las formulaciones de PLA, únicamente con la incorporación de un 5% en peso de MLO. En este estudio se muestra una mejora en el alargamiento a la rotura del PLA de un 8% hasta un 25%, gracias a la reacción que provoca el aceite vegetal maleinizado en el polímero. Por último y debido a su estructura, la incorporación de este tipo de aceites en los PHAs, no genera una mejora tan notable como en los poliésteres, pero aportan resultados muy prometedores desde el punto de vista de la plastificación [248].

I.6. MEZCLAS DE POLÍMEROS DE ALTO RENDIMIENTO MEDIOAMBIENTAL.

Actualmente, los polímeros con alto rendimiento medioambiental ligado tanto a su origen renovable como altas capacidades de ser biodegradados, son excelentes candidatos para su empleo en aplicaciones desechables, o aquellas donde la generación de residuos está causando grandes problemas ecológicos. No obstante, este grupo de polímeros posee ciertas limitaciones debido a su compleja procesabilidad, menor estabilidad térmica, y ciertos problemas ligados a sus propiedades mecánicas.

Con el objetivo de superar estas limitaciones y poder aplicar este tipo de polímeros, se están desarrollando técnicas como la copolimerización o el mezclado. La copolimerización resulta un método excesivamente complejo y costoso; es por ello, que el mezclado físico se consolida como una solución económica y viable para proporcionar las propiedades deseadas, sin requerir necesariamente una etapa de síntesis o modificación química. En el ámbito de las mezclas de polímeros, las más extendidas son las que basan su estructura en dos o tres polímeros distintos (mezclas binarias y ternarias), ofreciendo un amplio abanico de posibilidades y nuevas opciones renovables. No obstante, la mayoría de mezclas presentan problemas de miscibilidad entre los componentes, necesitando, en muchas ocasiones, la incorporación de agentes compatibilizantes para mejorar la adhesión en la entrecara de las diferentes fases, reducir su tensión en la entrecara y disminuir el tamaño de la fase dispersa en la matriz de polímero base [249].

I.6.1. Mezclas binarias y ternarias de polímeros de origen renovable.

En este nuevo entorno, caracterizado por una fuerte sensibilidad por el desarrollo sostenible, aprovechamiento integral de residuos y generación de economías circulares, el empleo de poliésteres como el PLA, los PHAs o los almidones termoplásticos, están generando un gran interés en la industria actual, siendo las mezclas binarias y ternarias, soluciones muy viables para solucionar ciertas limitaciones mecánicas y térmicas.

En el caso del PLA, la baja ductilidad y tenacidad que posee, lo limita mucho en aplicaciones como el envasado de productos o alimentos. Las mezclas binarias de PLA con otros polímeros renovables han sido ampliamente estudiadas, reduciendo de manera directa la fragilidad intrínseca del PLA, pero sin perder su gran resistencia mecánica o mantener un equilibrio final en el coste del producto. En los últimos años, mezclas binarias de PLA con PHAs [97, 250], PBAT [251, 252], PAs [253, 254], TPS [255], PBSA [256], PCL [256, 257], o PBS [258], se han estudiado y analizado en profundidad, ofreciendo nuevas soluciones de formulaciones industriales con altas capacidades técnicas y productos relativamente económicos.

Dentro de estas mezclas binarias, se puede observar cómo unas de las principales inquietudes es la obtención de mezclas completamente renovables y, en algunos casos, buscar mezclas capaces de ser biodegradadas en condiciones de compost, permitiendo cerrar el ciclo de vida del producto con la mayor eficiencia

medioambiental. En algunos casos como el PBS o la PCL, aunque estos materiales tengan un origen petroquímico, poseen capacidad de biodegradación, además de unas excelentes propiedades dúctiles. En algunos casos como en el sector médico, las mezclas de PLA/PCL están muy presentes, generando un gran interés comercial. En particular, este tipo de mezclas están atrayendo nuevas aplicaciones, ya que los dominios flexibles del PCL pueden dispersarse con facilidad en el PLA, generando de manera directa una mayor tenacidad sin comprometer la biodegradación. Además, las mezclas resultantes son completamente reabsorbibles, potenciando aplicaciones interesantes como dispositivos biomédicos. Otro de los casos interesantes, es la utilización de las poliamidas para mejorar las prestaciones de polímeros bio como el PLA o los PHAs. Las poliamidas aportan una gran mejora en las características técnicas de las mezclas.

Con relación a los PHAs, materiales como el PHB o PHBV, están generando un gran interés desde un punto de vista tanto medioambiental como técnico. Se caracterizan por un alto grado de cristalinidad, y una temperatura de fusión relativamente alta, pero son unos de los materiales con mayores capacidades para ser degradados. A pesar de esto, su alto coste de producción en comparación con los plásticos comerciales, la alta fragilidad debido a la alta cristalinidad, así como la inestabilidad térmica a temperaturas moderadas, restringen su uso. Por estos motivos, las mezclas binarias de los polímeros bacterianos, se están investigando en profundidad, buscando una mejora de propiedades a un menor coste y, sobretodo, mejorar la eficiencia medioambiental. Por lo tanto, mezclas de PHA con materiales biodegradables como el PLA [259, 260], el PBS [261, 262], o la PCL [263, 264] han demostrado que son soluciones prometedoras para futuras aplicaciones industriales.

Además de las mezclas binarias, la utilización de mezclas ternarias consigue generar soluciones atractivas y equilibradas para diferentes aplicaciones. Este tipo de mezclas, son algo más complejas que las binarias, ya que es más complicado obtener un buen equilibrio entre tres polímeros distintos. En este contexto, son el PLA y los PHAs, los polímeros que más incursión y aplicación están teniendo en este tipo de mezclas. Merece la pena destacar la combinación del PLA/PCL y TPS, que ha sido ampliamente estudiada, debido a la combinación de propiedades de unir el PLA y PCL, y la reducción de coste que implica la utilización de almidón termoplástico, manteniendo siempre una combinación de materiales totalmente biodegradables [265]. La combinación de polihidroxialcanoatos PHAs con PLA supone una práctica muy prometedora desde un punto de vista medioambiental; además, debido a su estructura suelen presentar cierta afinidad. No obstante, debido a las limitaciones de fragilidad que poseen ambas, la utilización de otro componente polimérico con altas flexibilidad como el PBS, PBSA o PCL entre otros, se ha propuesto como alternativa para la mejora de las propiedades dúctiles y tenacidad [266, 267].

I.6.2. Compatibilización de mezclas poliméricas de alto rendimiento medioambiental.

La compatibilización es una técnica importante para obtener una mejora en los resultados y el rendimiento de las mezclas que, habitualmente, presentan falta de miscibilidad o compatibilidad entre los polímeros que las forman.

La compatibilización en mezclas de polímeros de alto rendimiento medioambiental, puede abordarse mediante métodos no reactivos ("*ex situ*") o métodos reactivos ("*in situ*"). La compatibilización "*ex situ*", resulta ser un proceso algo menos rentable en polímeros bio que en polímeros convencionales, ya que el diseño y la obtención de copolímeros capaces de interactuar entre estos nuevos materiales, debido a la novedad de estos, encarece de manera directa el proceso. Además, el gran abanico de posibles materiales altamente eficientes dentro de los materiales renovables y biodegradables, sobre todo dentro de los PHAs, incrementa las posibles soluciones haciendo poco eficiente la síntesis de copolímeros para estas mezclas. Desde un punto de vista industrial, este tipo de compatibilización solo está enfocada a mezclas y procesos donde el coste de fabricación no es relevante [268]. Por otro lado, desde un punto de vista de eficiencia, en mezclas con materiales altamente inmiscibles, resulta muy difícil que este tipo de copolímeros actúen de manera eficaz, ya que es complicado interactuar con las fases tan separadas [269].

Por otro lado, la compatibilización "*in situ*" o mediante extrusión reactiva (REX), representa una técnica simple y de bajo coste para mejorar la compatibilidad de mezclas poliméricas altamente eficientes. Debido a que se realiza en un único proceso, se pueden incorporar multitud de aditivos, con diferentes grupos funcionales capaces de reaccionar durante el proceso de extrusión con los grupos terminales de los polímeros y así, mejorar de manera directa la compatibilidad de las mezclas [270].

La mayoría de compatibilizantes reactivos comerciales, se basan en polímeros de bajo peso molecular u oligómeros en los que una cierta cantidad de grupos funcionales son altamente reactivos: epoxi, anhídrido maleico, acrílicos, etc. Estos grupos ofrecen altas posibilidades de reacción durante el procesado del material fundido [249]. En este sentido, los aceites vegetales pueden representar una alternativa interesante a los polímeros y aditivos derivados del petróleo [271, 272]; en particular, aceites epoxidados, acrilados, maleinizados, entre otros, ya que se pueden usar de manera directa como aditivos reactivos para mejorar las propiedades de mezclas de biopolímeros, y también para lograr compatibilidad en polímeros con cargas o refuerzos naturales.

Los aceites vegetales epoxidados y maleinizados se han empleado como elementos plastificantes y compatibilizantes, de manera eficaz, en mezclas de materiales como PLA y PHB, mejorando de manera significativa la tenacidad de ambos biopolímeros [244, 273]. Los aceites vegetales maleinizados han dado buenos resultados en mezclas binarias totalmente renovables y biodegradables como PLA y TPS. En este contexto, Ferri *et al.* [247], demostraron el efecto de compatibilización del aceite de linaza maleinizado (MLO) en mezclas de PLA con TPS, además de una clara mejora en la tenacidad del PLA puro. Por otro lado, García-Campo *et al.* [274],

utilizaron diferentes aceites de soja modificados (epoxidado, acrilado y maleinizado), como agente compatibilizante en mezclas ternarias de alto rendimiento medioambiental a partir de PLA/PHB y PCL. Los resultados son muy interesantes, ya que se consigue incrementar el alargamiento a la rotura desde un 15% (mezcla sin compatibilizar), hasta un 130% con la utilización del aceite epoxidado y un 65% para el aceite maleinizado. Todo esto únicamente con la incorporación de un 5% de la masa total en aceite vegetal.

O BJETIVOS

OBJETIVOS

II.1 OBJETIVO GENERAL

El objetivo principal de esta tesis doctoral se centra en el estudio y la búsqueda de nuevos materiales poliméricos de alto rendimiento medioambiental a partir de materiales renovables, con una alta capacidad para ser introducidos en el sector envase y embalaje. A lo largo de la etapa de investigación, se ha determinado que la utilización de poliésteres y poliamidas procedentes de recursos renovables con cargas y aditivos naturales, pueden solventar grandes problemas presentes en la actualidad ligados a la gran generación de residuos. En particular, se han analizado los problemas de fragilidad y falta de adhesión, ligados a las mezclas entre diferentes polímeros y cargas naturales, a partir de aditivos y compuestos respetuosos con el medio ambiente. La utilización de cargas, aditivos y antioxidantes procedentes de desechos y elementos naturales, permiten revalorizar ciertos residuos procedentes de la almendra, naranja o algarrobo, con el objetivo de obtener un producto respetuoso con el medio ambiente, capaz de solucionar los graves problemas de residuos que existen actualmente para poder ser aplicados en el sector envase y embalaje. El objetivo final de la presente tesis doctoral es obtener formulaciones de polímeros respetuosas con el medio ambiente, que resulten competitivas desde el punto de vista del sector del envase y embalaje, y que sean capaces de resolver la gran problemática existente con la actual generación de residuos.

II.2 OBJETIVOS PARCIALES

Con la finalidad de poder alcanzar el objetivo general que se ha programado desde el inicio de la tesis, se han planteado una serie de objetivos parciales que han permitido cumplir con el objetivo general. Dichos objetivos específicos se han englobado en cuatro grandes bloques según los materiales y el objetivo a perseguir:

Materiales de poliéster de base biológica con resistencia mejorada mediante mezcla y extrusión reactiva.

- Análisis de la incorporación de nanoarcillas de sepiolita sobre un biopolímero de P(3HB-co-4HB) y un compatibilizante como el ESAO, mediante extrusión reactiva, con el objetivo de ver el efecto en sus propiedades mecánicas, térmicas y morfológicas.
- Evaluación de la miscibilidad y de propiedades mecánicas, térmicas, termomecánicas y morfológicas de mezclas binarias y ternarias basadas en PLA con PCL y TPS para desarrollar plásticos totalmente compostables con ductilidad y tenacidad mejoradas.
- Estudio y evaluación del ESAO como elemento compatibilizante en mezclas ternarias inmiscibles hechas de PHBV, PLA y PBAT a partir de la extrusión reactiva para su aplicación en el sector envase y embalaje.
- Desarrollo de mezclas binarias de bio-HDPE y PLA con la incorporación de diferentes agentes compatibilizantes como PE-g-MA, PE-co-GMA, MLO y DCP para mejorar la miscibilidad entre la poliolefina verde y el biopoliéster.

Obtención de ácido poliláctico con tenacidad mejorada a partir de aditivos y rellenos naturales.

- Estudio del efecto de la adición del AESO sobre las propiedades mecánicas, térmicas y termomecánicas de las piezas PLA obtenidas por moldeo por inyección.
- Análisis y caracterizaron en términos de propiedades mecánicas, térmicas y termomecánicas del efecto del aceite de semilla de cáñamo maleinizado (MHO) en el rendimiento físico del PLA.
- Estudio de la viabilidad del empleo de piel de naranja como refuerzo y AESO como elemento compatibilizante para la fabricación de compuestos verdes basados en PLA.
- Evaluación de la incorporación de cáscara de almendra para la creación de compuestos verdes de PLA con un alto contenido en carga y la mejora de la adhesión interfacial a partir de diferentes compatibilizantes como ESAO, AC y MLO.
- Análisis y mejora de la viabilidad del compuesto verde basado en PLA y ASF a partir de la incorporación de diferentes porcentajes de un aditivo completamente natural como el MLO. Superar limitaciones de baja estabilidad térmica y mejora de la ductilidad del conjunto.

Usos y aplicaciones de las nuevas poliamidas biológicas respetuosas con el medio ambiente.

- Evaluación mecánica, térmica, termomecánica y absorción de agua de tres poliamidas de base biológica.
- Estudio de la viabilidad del empleo de fibras de pizarra como refuerzo en una poliamida de base biológica, y el análisis de propiedades mecánicas, térmicas y morfológicas después de la mejorar de la adhesión interfacial a partir de G-SF y A-SF
- Evaluación del efecto de la incorporación de fibras de coco en una poliamida completamente biobasada como es la PA1010 desde el punto de vista de las propiedades mecánicas, térmicas, termomecánicas, morfológicas y de absorción de agua, y la mejora de su adhesión a partir de aditivos naturlaes y comerciales.
- Evaluación y análisis de la fabricación y caracterización de nuevos materiales de ingeniería consistentes en mezclas totalmente biobasadas de PA1010 y PLA, mejorando su compatibilidad y propiedades a partir de elementos naturales como MLO y ELO y derivados del petróleo como ESAO y PS-GMA.

Extracción y aplicaciones de antioxidantes naturales en poliésteres biobasados y en mezclas respetuosas con el medio ambiente.

- Optimización de los parámetros de extracción mediante MAE de compuestos fenólicos antioxidantes a partir de residuos agroalimentarios provenientes de la algarroba.
- Estudio y desarrollo de películas bicapa y multicapa de PLA mediante la incorporación de GA a partir de electrospinning, para mejorar la creación de envases activos con altas capacidades antioxidantes.

- Evaluación del efecto del GA como antioxidantes para mejorar las propiedades térmicas y degradación UV de films de bio-HDPE en el sector envase y embalaje.
- Análisis sobre la mejora de la ventana de procesamiento y de las propiedades mecánicas y térmicas de las mezclas de biopolímeros PA1010 y bio-HDPE a partir de la incorporación de aditivos naturales y GA.

En la **Figura II.1** se puede apreciar la planificación para cada objetivo específico desde un punto de vista esquemático.
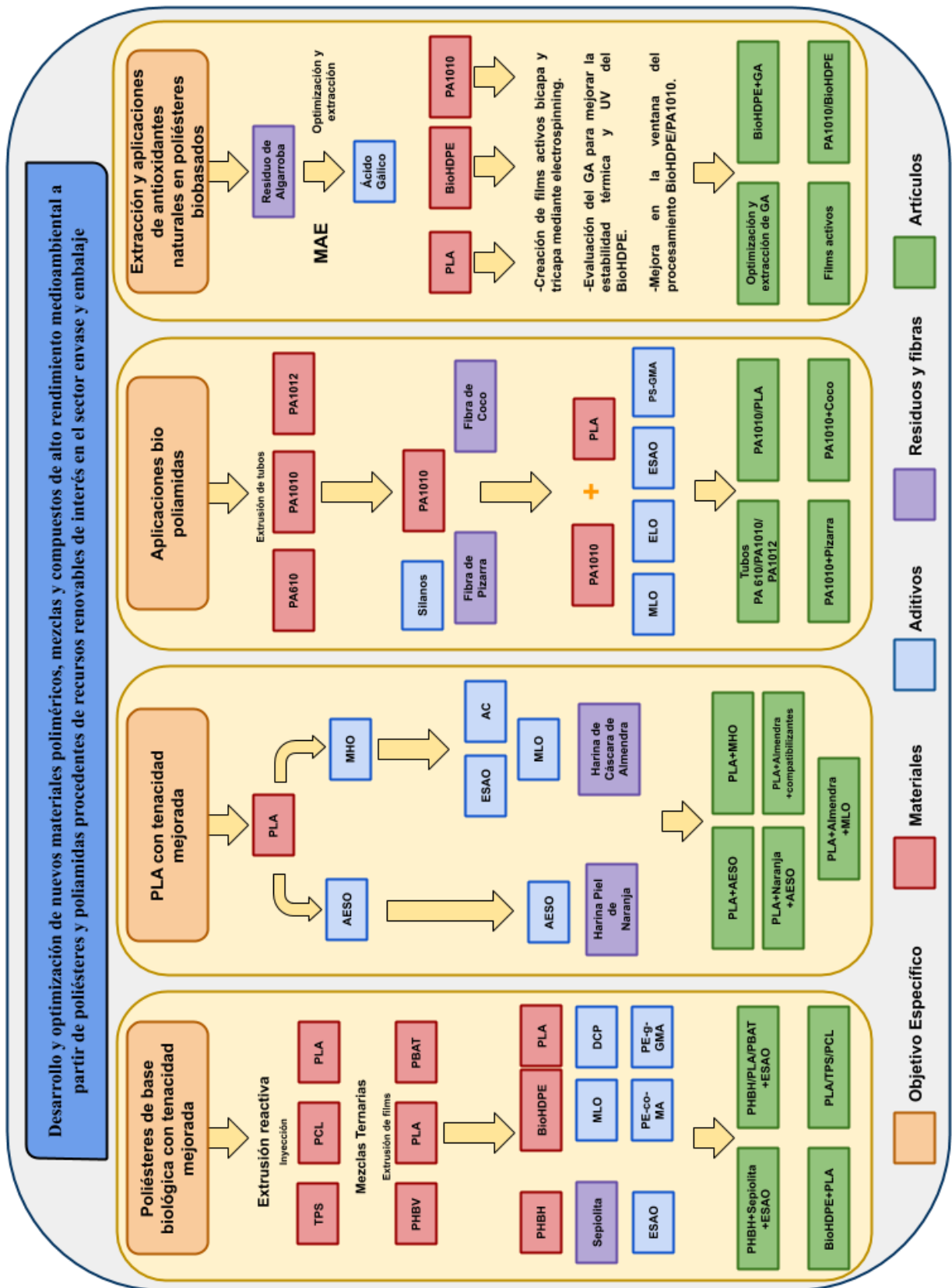
Figura II.1. Esquema del trabajo realizado en la presente tesis doctoral.

RESULTS & DISCUSSION

RESULTS & DISCUSSION

This research work focuses on the development, optimization and obtaining of polymeric materials and mixtures from natural fillers, residues and additives. The aim is to obtain alternatives with high environmental performance that are capable of being economical and capable of solving certain problems of rigidity and fragility for their subsequent application in the packaging sector.

In order to achieve different viable and totally renewable alternatives, different polyesters and polyamides have been analysed. Different natural fillers and additives have also been analysed with the aim of maintaining maximum environmental efficiency, trying to reduce costs as much as possible

The results obtained have been structured in 4 clearly differentiated blocks, with a total of 17 chapters. These main blocks have been grouped according to the type of materials used and the solutions proposed.

Biobased polyester materials with improved toughness by blending and reactive extrusion.

This block includes the main results of the improvement of the toughness and properties from the reactive extrusion of binary and ternary mixtures of different polyesters such as PLA, PCL, PBSs and PHAs. In addition, nano-loads such as sepiolite and plasticizers and compatibilizers have been used to improve miscibility between them.

The results of the different mixtures and formulations are described in the following sections:

Chapter III.1.1
Melt grafting of sepiolite nanoclay onto poly(3-hydroxybutyrate-co-4-hydroxybutyrate) by reactive extrusion with multi-functional epoxy-based styrene-acrylic oligomer.

Chapter III.1.2
Ductility and Toughness Improvement of Injection-Molded Compostable Pieces of Polylactide by Melt Blending with Poly(e-caprolactone) and Thermoplastic Starch.

Chapter III.1.3
In Situ Compatibilization of Biopolymer Ternary Blends by Reactive Extrusion with Low-Functionality Epoxy-Based Styrene Acrylic Oligomer

Chapter III.1.4
A comparative study on the effect of different reactive compatibilizers on injection-molded pieces of bio-based high-density polyethylene/polylactide blends

Poly(lactic acid) with improved toughness by natural additives and fillers.

This block includes the main results of the improvement of toughness and ductility of PLA from plasticizers and compatibilizers derived from natural elements such as MHO, MLO or AESO, and the use of natural fillers such as almond shell flour and orange peel flour to improve certain properties of PLA in the packaging industry.

The results of the different mixtures and formulations are described in the following sections:

Chapter III.2.1
Enhancement of the mechanical and thermal properties of injection-molded polylactide parts by the addition of acrylated epoxidized soybean oil

Chapter III.2.2
Reactive toughening of injection-molded polylactide pieces using maleinized hemp seed oil

Chapter III.2.3
On the use of acrylated epoxidized soybean oil as a reactive compatibilizer in injection-molded compostable pieces consisting of polylactide filled with orange peel flour

Chapter III.2.4
Effect of different compatibilizers on injection-molded green composite pieces based on polylactide filled with almond shell flour

Chapter III.2.5
Compatibilization of highly sustainable polylactide/almond shell flour composites by reactive extrusion with maleinized linseed oil

Uses and applications of new environmentally friendly partially or fully biobased polyamides.

This block includes the main results on the study and analysis of the different bio-based polyamides, and the cost improvement and strengthening from the incorporation of natural fillers such as slate or coconut fibre. In addition, the manufacture and characterization of new engineering materials consisting of fully biobased PA1010 and PLA blends has been evaluated, improving their compatibility and properties from natural elements such as MLO and ELO and oil derivatives such as ESAO and PS-GMA.

The results of the different blends and formulations are described in the following chapters:

Chapter III.3.1

III. RESULTS & DISCUSSION

Evaluation of the engineering performance of different bio-based aliphatic homopolyamide tubes prepared by profile extrusion

Chapter III.3.2
Injection-molded parts of fully bio-based polyamide 1010 strengthened by waste derived slate fibers pre-treated with glycidyl- and amino-silane coupling agents

Chapter III.3.3
Development of high-performance polyamide 1010/coconut fibers composites by reactive extrusion with natural and petrochemical derived compatibilizers

Chapter III.3.4
A comparative study on the reactive compatibilization of melt-processed polyamide 1010/polylactide blends by multi-functionalized additives derived from linseed oil and petroleum

Extraction and applications of natural antioxidants in a biobased polyesters and environmentally friendly blends.

This block includes the main results on the optimization of the extraction by MAE of antioxidant phenolic compounds from carob-based agro-food residues. Gallic acid extracted from this residue has been used as an element for the creation of packaging films with high antioxidant capacities by means of the electrospinning technique. In addition, the effect of GA as antioxidants has been evaluated to improve the thermal properties and UV degradation of bio-HDPE films in the packaging sector, and to improve their processing window in combination with other biopolymers such as PA1010.

The results of the different blends and formulations are described in the following chapters:

Chapter III.4.1
Optimization of microwave-assisted extraction of phenolic compounds with antioxidant activity from carob pods

Chapter III.4.2
Bioactive Multilayer Polylactide Films with Controlled Release Capacity of Gallic Acid Accomplished by Incorporating Electrospun Nanostructured Coatings and Interlayers

Chapter III.4.3
On the use of gallic acid as a natural antioxidant and ultraviolet light stabilizer in cast-extruded bio-based high-density polyethylene films

Chapter III.4.4

Enhancement of the processing window and performance of polyamide 1010/bio-based high-density polyethylene blends by melt mixing with natural additives.

III. RESULTS & DISCUSSION
RESULTS & DISCUSSION

B LOCK I
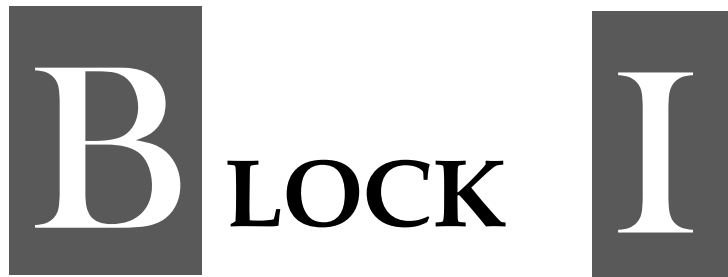
III.1. BIOBASED POLYESTER MATERIALS WITH IMPROVED TOUGHNESS BY BLENDING AND REACTIVE EXTRUSION.

III.1.1. Melt grafting of sepiolite nanoclay onto poly(3-hydroxybutyrate-co-4-hydroxybutyrate) by reactive extrusion with multi-functional epoxy-based styrene-acrylic oligomer.

S. Torres-Giner [1,2], N. Montanes [1], T. Boronat [1], L. Quiles-Carrillo [1] and R.Balart [1]

[1] Technological Institute of Materials (ITM), Universitat Politècnica de València (UPV), Plaza Ferrándiz y Carbonell 1, 03801 Alcoy, Spain;

[2] Novel Materials and Nanotechnology Group, Institute of Agrochemistry and Food Technology (IATA), Spanish National Research Council (CSIC), Calle Catedrático Agustín Escardino Benlloch 7, 46980 Paterna, Valencia, Spain

Melt grafting of sepiolite nanoclay onto poly(3-hydroxybutyrate-*co*-4-hydroxybutyrate) by reactive extrusion with multi-functional epoxy-based styrene-acrylic oligomer

Macromolecular Nanotechnology

Melt grafting of sepiolite nanoclay onto poly(3-hydroxybutyrate-*co*-4-hydroxybutyrate) by reactive extrusion with multi-functional epoxy-based styrene-acrylic oligomer

S. Torres-Giner *, N. Montanes, T. Boronat, L. Quiles-Carrillo, R. Balart

Technological Institute of Materials (ITM), Universitat Politècnica de València (UPV), Plaza Ferrándiz y Carbonell 1, 03801 Alcoy, Spain

ARTICLE INFO

ABSTRACT

This paper deals with grafting of sepiolite nanoclay onto poly(3-hydroxybutyrate-*co*-4-hydroxybutyrate) (P(3HB-*co*-4HB)) biopolymer by melt compounding. Reactive extrusion was performed in a twin-screw extruder in the presence of an epoxy-based styrene-acrylic oligomer (ESAO). The chemical interaction of sepiolite with P(3HB-*co*-4HB) were investigated using Fourier transform infrared (FTIR) spectroscopy. A novel grafting mechanism was proposed based on the multiple epoxy groups present in the reactive coupling agent. Epoxy ring-opening generated, on the one hand, the formation of alkoxy silanes bonds with the silanol groups exposed on the external surface of pristine sepiolite. On the other hand, ester bonds were produced with the terminal acid groups of the biopolymer chains. The newly formed sepiolite-grafted P(3HB-*co*-4HB) (sepiolite-g-P(3HB-*co*-4HB)) nanocomposite showed higher thermal, thermomechanical, and mechanical performance than the equivalent ungrafted nanocomposite. Melt grafting of sepiolite at different weight contents (1, 3, and 5 wt.-%) interestingly increased the thermal stability and stiffness of P(3HB-*co*-4HB) without impairing its ductility and toughness.

© 2016 Elsevier Ltd. All rights reserved.

1. Introduction

Bio-based and biodegradable polymers have received a great deal of attention over the last two decades due to environmental issues. Polyhydroxyalkanoates (PHAs) are a family of biodegradable polyesters that are intracellularly synthesized by microorganisms as carbon and energy reserves. Copolymerization of 3-hydroxybutyrate (3HB) units with of 4-hydroxybutyrate (4HB) units yields to poly(3-hydroxybutyrate-*co*-4-hydroxybutyrate) (P(3HB-*co*-4HB)), which represents the latest generation of PHAs [1]. The introduction of 4HB units induces defects in the crystal lattice, making P(3HB-*co*-4HB) more flexible and less crystalline for practical applications [2]. Different ratios of 3HB *vs.* 4HB can be achieved depending on the type of microorganism and supplied carbon substrates [3]. This bio-based copolyester can be therefore regarded as a potential candidate to replace polyolefins in packaging applications [4]. Main drawbacks of P(3HB-*co*-4HB) are related to

---

* Corresponding author.
  E-mail address: storresginer@hotmail.com (S. Torres-Giner).

Abstract

This paper deals with grafting of sepiolite nanoclay onto poly(3-hydroxybutyrate-*co*-4-hydroxybutyrate) (P(3HB-*co*-4HB)) biopolymer by melt compounding. Reactive extrusion was performed in a twin-screw extruder in the presence of an epoxy-based styrene-acrylic oligomer (ESAO). The chemical interaction of sepiolite with P(3HB-*co*-4HB) were investigated using Fourier transform infrared (FTIR) spectroscopy. A novel grafting mechanism was proposed based on the multiple epoxy groups present in the reactive coupling agent. Epoxy ring-opening generated, on the one hand, the formation of alkoxy silanes bonds with the silanol groups exposed on the external surface of pristine sepiolite. On the other hand, ester bonds were produced with the terminal acid groups of the biopolymer chains. The newly formed sepiolite-grafted P(3HB-*co*-4HB) (sepiolite-*g*-P(3HB-*co*-4HB)) nanocomposite showed higher thermal, thermomechanical, and mechanical performance than the equivalent ungrafted nanocomposite. Melt grafting of sepiolite at different weight contents (1, 3, and 5 wt.-%) interestingly increased the thermal stability and stiffness of P(3HB-*co*-4HB) without impairing its ductility and toughness.

Keywords: Polyhydroxyalkanoates; Sepiolite; Melt grafting; Reactive extrusion; Mechanical properties; Polymer nanocomposites

INTRODUCTION

Bio-based and biodegradable polymers have received a great deal of attention over the last two decades due to environmental issues. Polyhydroxyalkanoates (PHAs) are a family of biodegradable polyesters that are intracellularly synthesized by microorganisms as carbon and energy reserves. Copolymerization of 3-hydroxybutyrate (3HB) units with of 4-hydroxybutyrate (4HB) units yields to poly(3-hydroxybutyrate-co-4-hydroxybutyrate) (P(3HB-*co*-4HB)), which represents the latest generation of PHAs [1]. The introduction of 4HB units induces defects in the crystal lattice, making P(3HB-*co*-4HB) more flexible and less crystalline for practical applications [2]. Different ratios of 3HB vs. 4HB can be achieved depending on the type of microorganism and supplied carbon substrates [3]. This bio-based copolyester can be therefore regarded as a potential candidate to replace polyolefins in packaging applications [4]. Main drawbacks of P(3HB-*co*-4HB) are related to its poor mechanical strength and low thermal stability, which would restrict its access to the plastics industry when biodegradability is required [5], [6].

The incorporation of nanofillers, i.e., fillers below 100 nm, represents a novel solution to promote the industrial use of polymer materials [7]. Due to the ultrathin size of the fillers, polymer nanocomposites can markedly exhibit improved physical properties at low filler contents, *i.e.*, $\leqslant 5$ in weight (wt.-%) [8]. Up to recent years, the most intensive research was focused on polymer nanocomposites based on plate-like nanoclays, typically montmorillonite (MMT) [9]. However, sepiolite has recently gained increasing consideration because of its particular acicular form, low cost, availability, and extremely high surface area [10]. This nanoclay is a complex hydrated magnesium phyllosilicate ($Mg_4Si_6O_{15}(OH)_2 \cdot 6H_2O$). Sepiolite crystals are composed of sheet silicate units that consist of two layers of SiO_4 tetrahedrons in which the unshared oxygen atoms face each other [11]. Tetrahedral layers are bonded with an octahedral layer of coordinated magnesium atoms [12]. This results in a discontinuous longitudinal structure that forms open tunnels, i.e., the so-called "zeolitic channels", which run parallel to the axis and present a cross-section of *ca*. 1.1×0.4 nm^2 [13]. Naturally occurring sepiolite forms bundles of isolated needle-like particles with sizes between 100–5000 nm in length, 10–30 nm in width, and 5–10 nm in thickness [14]. This peculiar structure provides sepiolite with a porous volume of up to 0.4 cm^3/g [15], a surface energy of about 240 mJ/m^2 [16], and a specific surface above 350 m^2/g [17]. Such outstanding properties are responsible for its high sorption capacity and excellent colloidal properties.

Under ambient conditions, $Mg(OH_2)_2$ groups within the channels are completely filled by water [18]. Neither large molecules nor those of low polarity can penetrate the channels and displace the zeolitic water. On the contrary, polar molecules are well absorbed on the external surface of sepiolite, which accounts for 40–50% of its whole surface area [19]. This exposes around 2.2 silanol groups (Si—OH)/100 Å^2 [20], which are located every 0.5 nm along the side of the external channels [21]. Silanol groups are easily available for coupling reactions and favor the dispersion of sepiolite in polar matrices [22]. Up to the present, different polymers have been studied for hosting sepiolite such as polypropylene (PP) [10], [18], [23], [24], [25], [26], [27], poly(ε-caprolactone) (PCL) [11], [28], [29], thermoplastic starch (TPS) [12], chitosan [13], poly(ethyl methacrylate) (PEMA) and poly(2-hydroxyethyl methacrylate) (PHEMA) [14], poly(ethylene oxide) (PEO) [17], poly(butylene terephthalate) (PBT) [18],

polystyrene (PS) [27], ethylene vinyl acetate (EVA) [27], low-density polyethylene (LDPE) [27], [30], linear low-density polyethylene (LLDPE) [31], polyamide 6 (PA 6) [32], [33], [34], [35], polyamide 66 (PA 66) [36], [37], polyimide (PI) [38], polyurethane (PU) [39], [40], [41], epoxy resins [42], [43], [44], poly(lactic acid) (PLA) [28], [29], [45], [46], [47], [48], [49], poly(butylene adipate-co-terephthalate) (PBAT) [50], poly(hydroxyethyl acrylate) (PHEA) [51], gelatin [52], [53], poly(vinyl alcohol) (PVA) [54], and poly(sodium acrylate) (PSA) [55]. Additionally, sepiolite has been proposed to compatibilize immiscible polymer blends such as bio-based high-density polyethylene (bio-HDPE)/TPS [22], LDPE/TPS [56], LDPE/PLA [57], PLA/PP [58], and TPS/PBAT [59]. Most of these previous works have showed that the introduction of sepiolite habitually leads to a mechanical and thermal improvement due to the high aspect ratio of the nanoclay. Additionally, other materials properties can be improved such as rheology [25], [56], biocompatibility [47], [50], biodegradation [29], and flame retardancy [25], [26], [45]. Sepiolite can also enlarge the operating window of a given polymer, which certainly results advantageous for P(3HB-*co*-4HB) in the replacement of commodity plastics [24].

Effective reinforcement is related, however, to a good dispersion of the nanoclay within the polymer matrix. This can be only achieved when non-trivial prerequisites (*e.g.*, good nanofiller dispersion, orientation, and positive matrix-filler interactions) are fulfilled. Unfortunately, sepiolite, similar to other nanoclays, is habitually aggregated in nature and physical mixing can hardly provide desired dispersion at the nanometer scale. To attain effective disaggregation, diverse organic modifications can be applied on the sepiolite surface. These mainly include hydrophobic silanes such as 3-aminopropyl triethoxyl silane (3-APTS) [14], propyltrimethoxy silane (PTMS) [22], octyl trimethoxy silane (OTMS) [30], and vinyl triethoxy silane (VTES) [31]. Some authors have also employed other chemical treatments, for instance polyethylene glycol (PEG) [17], quaternary ammonium salts [18], cethyl trymethyl ammonium bromide (CTAB) [25], [26], dimethyl benzyl hydrogenated tallow quaternary ammonium (B2MTH) [35], trimethyl hydrogenated tallow quaternary ammonium (3MTH) [32], [35], and N-hydrogenated tallow-1,3-diaminopropane (DIAMIN T) [35]. Nevertheless, their application adds complexity and increases the manufacturing costs of the final polymer nanocomposite. Moreover, certain poor thermal stability can be induced, especially when used in combination with polymers that need to be processed at high temperatures.

The large concentration of silanol groups on sepiolite offers high functionality, which therefore opens up new coupling reactions with polar matrices. In particular, Si—OH can react with epoxides in vapor phase. This reaction opens the epoxy rings followed by combination with the resulting organic species on the silicate surface [60]. In the field of polymer science, bi-functional and multi-functional epoxy-based oligomers are currently used as "chain extenders". These are mainly applied for polyesters, recently including PHAs [61]. The use of the so-called chain extenders basically leads to an increase in the polymer molecular weight (M_W), which in turn improves melt strength and thermal stability. These have also been recently reported to perform as compatibilizer in blends of polyesters [62]. At high temperatures, the epoxy functions trigger the formation of covalent bonds with both nucleophilic terminal groups of polyesters chains, *i.e.*, hydroxyl (OH) and carboxyl (—COOH) groups [63]. This paper describes the first attempt to graft pristine sepiolite onto P(3HB-co-4HB)

biopolymer by reactive extrusion using a functional coupling agent containing multiple epoxy groups. The large concentration of silanol groups on sepiolite offers high functionality, which therefore opens up new coupling reactions with polar matrices. In particular, Si—OH can react with epoxies in vapor phase. This reaction opens the epoxy rings followed by combination with the resulting organic species on the silicate surface [60]. In the field of polymer science, bi-functional and multi-functional epoxy-based oligomers are currently used as "chain extenders". These are mainly applied for polyesters, recently including PHAs [61]. The use of the so-called chain extenders basically leads to an increase in the polymer molecular weight (M_W), which in turn improves melt strength and thermal stability. These have also been recently reported to perform as compatibilizer in blends of polyesters [62]. At high temperatures, the epoxy functions trigger the formation of covalent bonds with both nucleophilic terminal groups of polyesters chains, *i.e.*, hydroxyl (—OH) and carboxyl (—COOH) groups [63]. This paper describes the first attempt to graft pristine sepiolite onto P(3HB-*co*-4HB) biopolymer by reactive extrusion using a functional coupling agent containing multiple epoxy groups.

MATERIAL AND METHODS

Materials

Bacterial aliphatic copolyester P(3HB-*co*-4HB) was Mirel® P1004, supplied by Metabolix, Inc. (Woburn, USA). This is a home-compostable grade up to 488 µm designed for injection molding. The resin presents a M_W of 2.9×10^5 g/mol, with a polydispersitivity index (PDI) of 1.62, a melt flow rate of 14 g/10 min (190 °C/2.16 kg), and a density of 1.3 g/cm³. The molar fraction of 4HB in the copolymer is approximately 5%. Unmodified sepiolite was kindly supplied by Grupo Tolsa S.A. (Madrid, Spain) under the trade name of Pansil® 400. The nanoclay is obtained from the Tagus river basin and the bulk density of the powder is 60 ± 30 g/L. Joncryl® ADR 4368-C was provided by BASF S.A. (Barcelona, Spain) in the form of solid flakes. This is a proprietary epoxy-based styrene-acrylic oligomer (ESAO) with number average functionality (*f*) > 4. Styrene and acrylic building blocks are each between 1 and 20. M_W is 6800 g/mol, glass transition temperature (T_g) is 54 °C, and the epoxy equivalent weight (EE_W) is 285 g/mol. Recommended dosage by manufacturer is 0.1–1 wt.-% for appropriate processability of biodegradable polyesters.

Reactive extrusion

Prior to processing, to remove residual moisture, the P(3HB-*co*-4HB) pellets and sepiolite powder were stored at 60 °C for 36 h in a dehumidifying dryer MD from Industrial Marsé (Barcelona, Spain). P(3HB-*co*-4HB) and sepiolite were compounded in a co-rotating ZSK-18 MEGAlab laboratory twin-screw extruder from Coperion (Stuttgart, Germany). The screws feature 18 mm diameter with a length (L) to diameter (D) ratio, *i.e.*, L/D, of 48. The barrel is divided into 11 segments, including the strand die head. P(3HB-*co*-4HB) pellets were fed into the main hopper while sepiolite and ESAO were introduced through a ZS-B 18 twin-screw side feeder from K-Tron (Pitman, USA), located at segment number 4. Materials dosage was set to achieve a residence time of about 1 min. The screws speed was fixed at 300 rpm. The extrusion temperature profile, from the hopper to the die, was set as follow: 165–170–170–175–175–180–180 °C. The strand was cooled in a water bath and then pelletized using an air-knife

unit. **Table III.1.1.1** summarizes the different samples prepared during the melt compounding.

Table III.1.1.1. Samples prepared according to the content of poly(3-hydroxybutyrate-*co*-4-hydroxybutyrate) (P(3HB-*co*-4HB)), epoxy-based styrene-acrylic oligomer (ESAO), and sepiolite nanoclay.

Samples	Percentage (wt.-%)		
	P(3HB-*co*-4HB)	ESAO	Sepiolite
P(3HB-*co*-4HB)	100	0	0
P(3HB-*co*-4HB) + ESAO	99	1	0
P(3HB-*co*-4HB) + Sepiolite 1 wt.-%	99	0	1
P(3HB-*co*-4HB) + ESAO + Sepiolite 1 wt.-%	98	1	1
P(3HB-*co*-4HB) + ESAO + Sepiolite 3 wt.-%	96	1	3
P(3HB-*co*-4HB) + ESAO + Sepiolite 5 wt.-%	94	1	5

Injection molding

P(3HB-*co*-4HB)/sepiolite nanocomposites were shaped for characterization using an injection-molding machine 270/75 from Mateu & Solé (Barcelona, Spain). The profile temperature, from the feeding zone to the injection nozzle, was set as follows: 155–160–165–170 °C. A clamping force of 75 tons was applied. The cavity filling and cooling time were set at 1 and 10 s, respectively. Standard samples with a thickness of 4 mm were obtained and stored at room conditions, *i.e.*, 23 °C and 50% HR, for 15 days before characterization.

Morphology

Morphologies of the sepiolite powder and the fractured surfaces of the P(3HB-*co*-4HB) nanocomposites were observed by scanning electron microscope (SEM) with a Zeiss Ultra 55 from Oxford Instruments (Abingdon, UK). An acceleration voltage of 2 kV was applied. Surfaces were previously coated with a gold-palladium alloy in a sputter coater EMITECH model SC7620 from Quorum Technologies, Ltd. (East Sussex, UK). Detailed morphology of sepiolite was obtained by transmission electron microscopy (TEM) with a JEM-2010 microscope from JEOL (Tokyo, Japan) using an acceleration voltage of 100 kV. This was equipped with an ORIUSTM SC600 TEM CCD camera for image acquisition. Sepiolite sizes were measured using Image J software.

Infrared spectroscopy

Chemical analyses was performed using attenuated total reflection–Fourier transform infrared (ATR-FTIR) spectroscopy. Spectra were recorded with a Vector 22

from Bruker S.A. (Madrid, Spain) coupling a PIKE MIRacle™ ATR accessory from PIKE Technologies (Madison, USA). Ten scans were averaged from 4000 to 400 cm⁻¹ at a resolution of 4 cm⁻¹.

Thermal analysis

Crystallization and melting behavior of P(3HB-*co*-4HB) and its nanocomposites were conducted in a differential scanning calorimetry (DSC) 821 model from Mettler-Toledo, Inc. (Schwerzenbach, Switzerland). For this, approximately 5 mg of sample was placed in 40-μl hermetic aluminum sealed pans, previously calibrated with an indium standard. The analysis was performed in a dry reducing atmosphere in which nitrogen flowed at a constant rate of 66 mL/min. Samples were subjected to a three-step program at a heating rate of 10 °C/min. An initial heating cycle from 30 to 200 °C was applied to remove the thermal history, followed by a cooling to −50 °C, and a final increase to 350 °C to evaluate the thermal transitions. The crystallization temperature from the melt (T_c) and enthalpy of crystallization (ΔH_c) were obtained from the first cooling scan while the melting temperature (T_m), enthalpy of melting (ΔH_m), and cold crystallization (ΔH_{cc}) were determined from the second heating scan. The percentage of crystallinity (X_c) was obtained by the following **Equation III.1.1.1**:

$$Xc(\%) = \left(\frac{\Delta Hm - \Delta Hcc}{\Delta H_m^0 \cdot (1-w)}\right) \cdot 100 \qquad \textbf{Equation III.1.1.1}$$

Where J/g is the theoretical enthalpy corresponding to the melting of a 100% pure crystalline sample of poly(3-hydroxybutyrate) (PHB) [64] and w represents the filler weight fraction.

Thermogravimetric analysis (TGA) was used to evaluate the thermal stability of P(3HB-*co*-4HB) and its nanocomposites in a TGA/SDTA 851 thermobalance from Mettler Toledo, Inc. (Schwerzenbach, Switzerland). The heating program was set from 30 to 700 °C at a heating rate of 20 °C/min in nitrogen with a constant flow rate of 66 mL/min. Approximately 10 mg of each sample was used for the measurements. The onset degradation temperature was defined as the temperature at 5% weight loss ($T_{5\%}$) and the degradation temperature (T_{deg}) was obtained from the maximum value of the first derivative peak.

Thermomechanical characterization

Dynamic mechanical thermal analysis (DMTA) was performed using an AR-G2 device from TA Instruments (New Castle, USA) equipped with a torsion clamp system in torsion-shear mode. To determine the storage modulus (G'), loss storage modulus (G''), and loss tangent (tan δ), samples were scanned from −60 to 100 °C at a heating rate of 2 °C/min, a frequency of 1 Hz, and a strain amplitude (γ) of 0.1%. The dimensions of the tested samples were 4 × 10 × 40 mm³. All measurements were done in triplicate.

Mechanical tests

Injection-molded specimens with a dumbbell shape, a total length of 150 mm, and a cross-section of 10×4 mm² were tested in a universal test machine ELIB 30 from S.A.E. Ibertest (Madrid, Spain). Tensile and flexural tests were performed according to ISO 527 and 178, respectively. In both tests a 5 kN load cell and a cross-head speed of 5 mm/min were employed. Shore D hardness was determined in a durometer 676-D model from J. Bot S.A. (Barcelona, Spain) following ISO 868. Impact strength was tested in a 1-J Charpy pendulum from Metrotec S.A. (San Sebastián, Spain), as suggested by ISO 179. All specimens were tested in a controlled chamber at room conditions, *i.e.*, 23 °C and 50% RH. Six samples for each material were analyzed and averaged.

RESULTS

Morphology of nanoclay

Figure III.1.1.1 shows a SEM micrograph of the sepiolite powder. The image basically revealed the characteristic fiber-like structure of sepiolite, which was mainly presented as bundle-like aggregates of nano-sized needles. These micrometric assemblies are naturally produced because of the high surface interaction between individual nanoparticles [32]. To better ascertain the nanoclay morphology, TEM characterization was performed. As shown in Fig. 1b, sepiolite morphology was certainly based on a needle-shaped nanostructure with dissimilar sizes. In the TEM image, it can be observed that the large needles observed by SEM were actually formed by the presence of discontinuous shorter nanoparticles. Isolated nanoparticles also showed the typical tubular structure of sepiolite, which leads to its highly porous morphology. These tunnels, as previously indicated, are formed as a consequence of alternating tetrahedral-octahedral-tetrahedral plates along the longitudinal axis of the nanoclay.
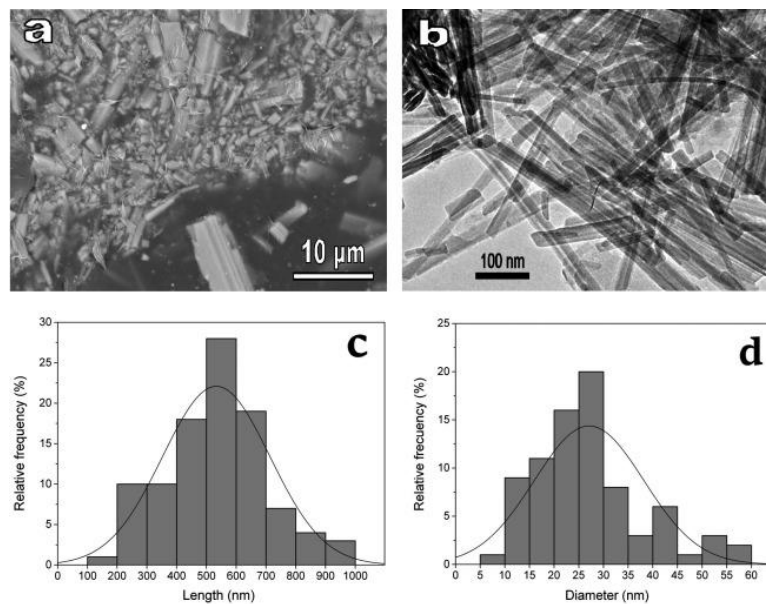
Figure III.1.1.1. (a) Scanning electron microscope (SEM) image of sepiolite powder. Scale marker of 10 μm; (b) Transmission electron microscopy (TEM) image of sepiolite powder. Scale marker of 100 nm; (c) Histogram of sepiolite length (L); (d) Histogram of sepiolite diameter (D).

The histograms of the nanoparticle length (L) and diameter (D) of sepiolite are shown in Fig. 1c and d. Mean values of L and D were *ca.* 540 and 27 nm, respectively. The aspect ratio, *i.e.*, L/D, was determined at 20, which is a positive geometric indicator for mechanical reinforcement in polymer matrices. In this sense, there is a positive correlation between the mechanical properties and the aspect ratio in fiber-reinforced nanocomposites: The higher the aspect ratio, the higher the tensile strength [65]. High values of L/D are therefore habitually needed for achieving optimal reinforcement. The observed aspect ratio of sepiolite is in agreement with Sabzi *et al.* [46], who reported values of L of 7 μm and D of 340 nm for Turkish sepiolite, *i.e.*, a mean L/D of 21. The average sizes of sepiolite nanoclay have been described elsewhere, showing values in the range of 1000–2000 nm for L and 20–30 nm for D [23], [32], [39].

Structural analysis

ATR-FTIR was performed to evaluate chemical interactions between P(3HB-*co*-4HB), sepiolite, and ESAO. FTIR spectra of the sepiolite powder, ESAO flakes, neat P(3HB-*co*-4HB), and its nanocomposites are gathered in **Figure III.1.1.2a**. In relation to the nanoclay, the spectrum of the pristine sepiolite powder showed a broad intensity in the region from 1100 to 900 cm^{-1}. Main peaks were particularly seen at 1008 and 976 cm^{-1}, which have been respectively identified as the SiO "cage-like" and "network" stretching modes [31], [66]. The main peak for the CO stretching vibration of the epoxy groups in the spectrum of ESAO appeared around 1180, 910, 850, and 760 cm^{-1} [67], [68], [69]. In the P(3HB-*co*-4HB)-based materials containing ESAO these peaks disappeared, indicating that these functional groups reacted and were consumed during the melt-compounding process. For the biopolymer, the stretching vibration of the carbonyl group (CO) produced a strong and sharp peak at ca. 1724 cm^{-1} that corresponds to the intramolecular bonding of the crystalline state of P(3HB-*co*-4HB) [70], [71]. The stretching bands of the carbon–carbon single bond (CC) also gave rise to complex and multiple peaks in the region from 1000 to 880 cm^{-1}, containing a sharp and intense band centered around 978 cm^{-1} [72].
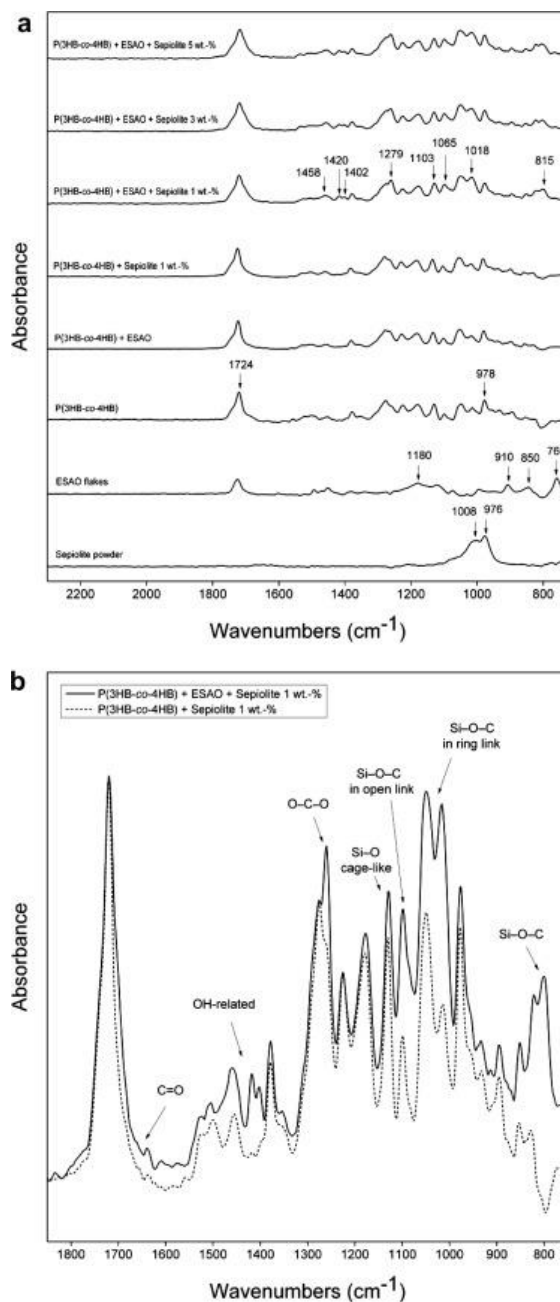
Figure III.1.1.2. (a) Fourier transform infrared (FTIR) spectra, from bottom to top, of: Sepiolite powder, epoxy-based styrene-acrylic oligomer (ESAO) flakes, poly(3-hydroxybutyrate-*co*-4-hydroxybutyrate) (P(3HB-*co*-4HB)), P(3HB-*co*-4HB) with ESAO, P(3HB-*co*-4HB) with sepiolite at 1 wt.-%, P(3HB-co-4HB) with ESAO and sepiolite at 1, 3, and 5 wt.-%. Arrows indicate the wavenumbers of the bands described in the text; (b) Detail of the FTIR spectra for the ungrafted and melt-grafted P(3HB-*co*-4HB)/sepiolite 1 wt.-% nanocomposites. Arrows indicate the chemical bonds described in the text.

Figure III.1.1.2b shows the spectra details for both P(3HB-*co*-4HB) nanocomposites containing 1 wt.-% of sepiolite prepared with and without ESAO. Arrows indicate the identified chemical groups formed in the spectra. By comparison of both spectra, it can be seen that the strongest band in the P(3HB-*co*-4HB) spectrum, which corresponds to the crystalline C=O stretching vibration, was kept at 1724 cm^{-1}.

Interestingly, combination of ESAO with sepiolite broadened the carbonyl peak and generated a shoulder at approximately 1705 cm^{-1}. This indicates that the hydrogen bonding in the molecular arrangement of P(3HB-*co*-4HB) was altered, which could be produced due to an intramolecular disruption of the biopolymer chains by the presence of sepiolite. Some authors have also ascribed shifts in this peak to the reaction between the epoxy groups of the chain extender and the carboxyl groups ($-COO$) in polyesters [73]. Additionally, an intensity increase in the $-O-C-O-$ stretching vibration peak, related to the carboxyl group at 1279 cm^{-1} [71], also proved the formation of new ester groups. The intense bonding mode observed at *ca.* 1150 cm^{-1} is for the Si--O cage-like stretching mode [66]. Interaction of the nanoclay with the P(3HB-*co*-4HB) matrix was also supported by the intensity increase in the band centered at 1103 cm^{-1} and both major bands at *ca.* 1065 and 1018 cm^{-1} that correspond to the $Si-O-C$ bands in their "open" and "ring" links, respectively [74]. The presence of this new $Si-O-C$ bond was further evidenced by the strong signal near 815 cm^{-1} [74]. Interestingly, the spectra of the P(3HB-*co*-4HB) nanocomposite produced with ESAO also showed a new group of bands at 1420–1500 cm^{-1}, with main intensities at *ca.* 1402, 1420, and 1459 cm^{-1}. These bands are ascribed to the $C-H$ bending in close proximity to the newly formed OH-related bonds during the hydroxyl side group formation [74], [75]. These peaks were not observed in the spectrum of the P(3HB-*co*-4HB)/sepiolite nanocomposite prepared without ESAO, which confirmed the chemical bonding of sepiolite to the biopolymer.

The above results clearly indicate that intramolecular changes took place in the P(3HB-*co*-4HB) structure. More importantly, the presence of new bands related to $Si-O-C$ bonds supports the fact that covalent bonds were formed between the biopolymer and the reactive $Si-OH$ groups of sepiolite. This chemical interaction could be intensified due to the high surface area of sepiolite. Based on the above FTIR results, **Figure III.1.1.3** suggests the possible grafting mechanism of sepiolite onto the biopolymer during reactive extrusion. On one hand, in the case of the biopolymer, ester bonds are formed by the reaction of terminal acid groups of P(3HB-*co*-4HB) with the epoxy functional groups of ESAO. The mechanisms of epoxy-based chain extension in polyesters by these highly reactive compounds have been long discussed in the literature [63]. This mainly consists on glycidyl esterification of carboxylic acid end groups, which precedes hydroxyl end group etherification. This latter reaction competes with etherification of secondary hydroxyl groups and main chain transesterification. In this sense, it has been reported that the reaction rate of the epoxide in polyesters is about 10–15 times higher with the carboxyl ($-COO$) than the hydroxyl ($-OH$) group [76]. On the other hand, an alkoxy carbonyl silane structure is proposed to take place through the reaction of the external $Si-OH$ groups of sepiolite with other epoxy groups present in the acrylic units of ESAO. This reaction involves epoxy ring-opening and the creation of covalent $Si-O-C$ bonds with hydroxyl side group formation [77]. Therefore, the reactive coupling agent successfully established strong chemical "bridges" between the biopolymer and sepiolite by $Si-O-C$ bonds. As a result it generated a new hybrid nanostructure, *i.e.*, a sepiolite-grafted P(3HB-*co*-4HB) (sepiolite-*g*-P(3HB-*co*-4HB)) nanocomposite.
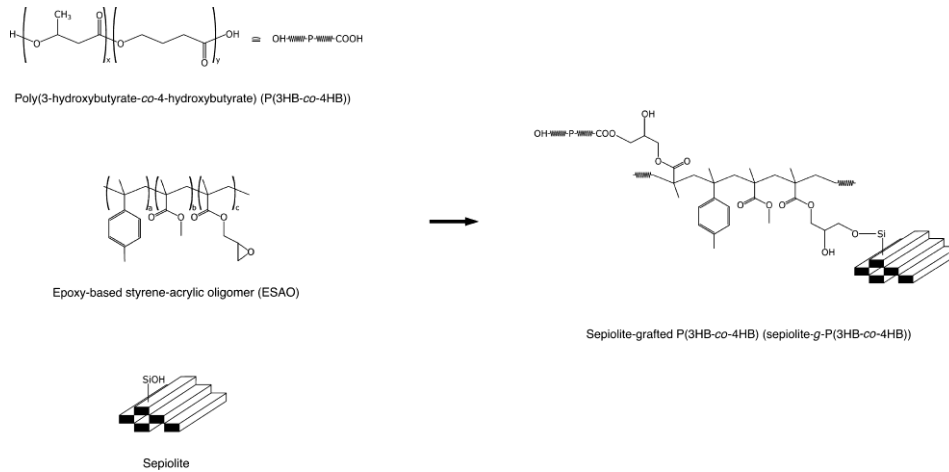
Figure III.1.1.3. Schematic representation of the melt grafting of sepiolite nanoclay onto poly(3-hydroxybutyrate-*co*-4-hydroxybutyrate) (P(3HB-*co*-4HB)) by epoxy-based styrene-acrylic oligomer (ESAO).

Thermal properties

As previously discussed, both the crystallinity and thermal stability of P(3HB-*co*-4HB) have great influence on its performance. DSC was carried out to determine the influence of sepiolite nanoclay on the thermal properties of the P(3HB-*co*-4HB) nanocomposites. DSC thermograms for the first cooling and second heating scans are given in **Figure III.1.1.4.** Thermal values, obtained from the DSC thermograms, are collected in **Table III.1.1.2**.

Table III.1.1.2. Thermal properties obtained from the differential scanning calorimetry (DSC) and thermogravimetric analysis (TGA) curves in terms of normalized enthalpy of crystallization (ΔH_c), crystallization temperature from the melt (T_c), normalized enthalpy of melting (ΔH_m), melting temperature (T_m), amount of crystallinity (X_c), degradation temperature at 5% of mass loss ($T_{5\%}$), degradation temperature (T_{deg}), mass loss at T_{deg}, and residual mass for poly(3-hydroxybutyrate-*co*-4-hydroxybutyrate) (P(3HB-*co*-4HB)) nanocomposites containing epoxy-based styrene-acrylic oligomer (ESAO) and sepiolite nanoclay.

Samples	DSC							TGA			
	ΔH_c (J/g)	T_c (°C)	ΔH_{m1} (J/g)	T_{m1} (°C)	ΔH_{m2} (J/g)	T_{m2} (°C)	X_c (%)	$T_{5\%}$ (°C)	T_{deg} (°C)	Mass loss (%)	Residual mass (%)
P(3HB-co-4HB)	30.2 ± 0.8	109.1 ± 1.3	7.4 ± 0.3	160.1 ± 1.2	25.0 ± 0.2	171.3 ± 0.7	32.4 ± 1.7	289.7 ± 1.2	305.3 ± 1.4	36.1 ± 0.5	3.8 ± 0.3
P(3HB-co-4HB)/ESAO	33.4 ± 0.6	108.7 ± 0.9	9.4 ± 0.5	160.0 ± 1.3	27.1 ± 0.3	171.1 ± 1.3	36.2 ± 1.0	290.1 ± 1.0	305.1 ± 2.5	35.8 ± 0.4	3.9 ± 0.2
P(3HB-co-4HB)/Sepiolite 1 wt.-%	32.0 ± 0.5	109.8 ± 1.1	6.7 ± 0.5	159.3 ± 1.1	26.8 ± 0.7	170.2 ± 0.8	33.2 ± 1.6	290.3 ± 0.8	305.2 ± 1.9	33.4 ± 0.2	5.7 ± 0.1
P(3HB-co-4HB)/ESAO/Sepiolite 1 wt.-%	31.8 ± 0.7	102.5 ± 0.5	8.4 ± 0.4	157.9 ± 0.3	29.9 ± 0.6	169.7 ± 0.6	37.4 ± 0.2	291.4 ± 0.9	306.8 ± 1.7	38.5 ± 0.3	5.0 ± 0.2
P(3HB-co-4HB)/ESAO/Sepiolite 3 wt.-%	33.9 ± 0.6	101.9 ± 0.8	12.8 ± 0.7	157.6 ± 0.7	24.7 ± 0.1	169.7 ± 0.9	36.5 ± 0.6	292.3 ± 0.5	309.7 ± 0.9	41.6 ± 0.9	6.5 ± 0.1
P(3HB-co-4HB) + ESAO + Sepiolite 5 wt.-%	31.9 ± 0.4	101.2 ± 0.2	15.6 ± 0.6	157.6 ± 0.4	19.9 ± 0.1	169.6 ± 0.4	34.4 ± 0.9	292.4 ± 0.7	310.0 ± 1.1	44.2 ± 0.8	7.4 ± 0.1
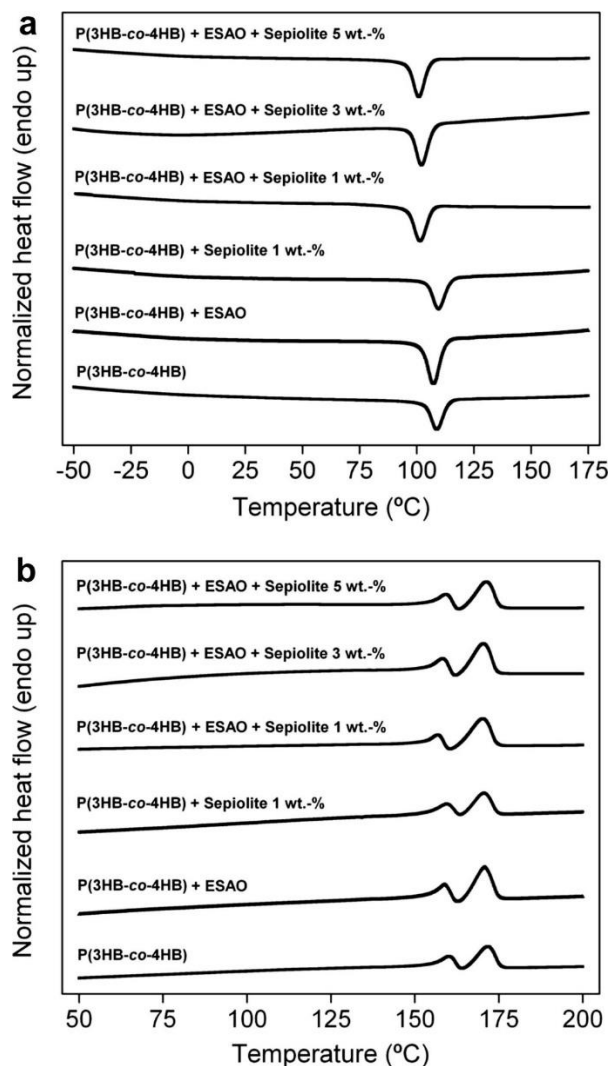
Figure III.1.1.4. Comparative plots of differential scanning calorimetry (DSC) thermograms for poly(3-hydroxybutyrate-*co*-4-hydroxybutyrate) (P(3HB-*co*-4HB)) nanocomposites containing sepiolite nanoclay and epoxy-based styrene-acrylic oligomer (ESAO) for: (a) First cooling run; (b) Second heating run.

Figure III.1.1.4a shows the cooling scans for P(3HB-*co*-4HB) and its nanocomposites. All samples showed crystallization from the melt during the cooling process, however this occurred at different temperatures. The unfilled biopolymer showed a T_c of about 109.1 °C, which is in agreement with the previous study done by Dagnon *et al.* [78]. For the ungrafted P(3HB-*co*-4HB) nanocomposite containing sepiolite at 1 wt.-%, Tc remained constant. However, T_c was found to decrease up to 101.2 °C in the sepiolite-*g*-P(3HB-*co*-4HB) nanocomposites. These results indicated that sepiolite nanoclay, when melt grafted, certainly disrupted the ordering of P(3HB-*co*-4HB) by hindering chain diffusion and folding into the crystalline lattice. In the second heating scan, shown in **Figure III.1.1.4b**, all P(3HB-*co*-4HB) samples showed negligible cold crystallization. This is known to occur by the formation of imperfect crystals from unmelted ones acting as nuclei [79]. The heating thermogram of P(3HB-*co*-4HB)

showed a bimodal endothermic peak: A first melting temperature at *ca.* 160.1 °C followed by a more intense second melting temperature at *ca.* 171.3 °C. Similar observations were previously found by Zhang *et al*. [80]. Multiple melting peaks in P(3HB-*co*-4HB) are certainly linked to crystal reorganization upon melting, by which imperfect crystals can order into spherulites with thicker lamellar thicknesses and then melt at higher temperatures. Lower melting peaks for P(3HB-*co*-4HB), which could be assigned to the crystalline phase of the 4HB-rich fractions [81], [82], were not observed due to the relatively low 4HB mol.-% content. As shown in **Table III.1.1.2**, melting temperatures of the P(3HB-*co*-4HB) nanocomposites slightly decreased with sepiolite. This can be attributed to a confinement effect of the nanoclay, which promoted less ordered structures.

Crystallinity values were calculated from ΔH_m evolved during the second heating scan. **Table III.1.1.2** shows that the resultant amount of crystallinity of P(3HB-*co*-4HB) increased from 32.4 to 36.2% with the addition of ESAO. This can be related to a M_W improvement due to linear chain extension of P(3HB-*co*-4HB) and/or prevention of random chain scission reactions (*e.g.*, hydrolysis) by which more mass of biopolymer crystallized [83]. Crystallinity was seen to slightly increase for a low content of sepiolite, *i.e.*, 37.4% at 1 wt.-%, and then decreased for higher contents, *i.e.*, 36.5 and 34.4% at 3 and 5 wt.-%, respectively. This suggests that crystal growth in the sepiolite-*g*-P(3HB-*co*-4HB) nanocomposites was controlled by two competing factors related to the nanoclay, i.e., the nucleation and confinement. The observed increase in crystallinity at the lowest sepiolite content indicates a dominant influence of the heterogeneous nucleation. At higher concentrations, however, certain agglomerations of sepiolite nanoparticles probably led to an excessive confinement that hindered molecular organization at the crystal growth front.

Relevant decomposition parameters, obtained from the TGA curves for P(3HB-*co*-4HB) and its nanocomposites, are also tabulated in **Table III.1.1.2**. Thermal degradation of all P(3HB-*co*-4HB) materials occurred through a single and sharp degradation step that ranged from about 290 to 315 °C. For the unfilled P(3HB-*co*-4HB) biopolymer, $T_{5\%}$ and T_{deg} were observed at *ca.* 289.7 and 305.3 °C, respectively. The single introduction of ESAO or pristine sepiolite had a negligible effect on the decomposition profile of P(3HB-*co*-4HB). Conversely, as shown in the table, grafted sepiolite slightly delayed the degradation temperature of P(3HB-*co*-4HB). For instance, in the sepiolite-*g*-P(3HB-*co*-4HB) 3 wt.-% nanocomposite, $T_{5\%}$ and Tdeg increased to 292.3 and 309.7 °C, respectively. This effect can be mainly ascribed to a mass transport barrier exerted by the nanoclay to the volatiles produced during decomposition [6]. Due to the high porosity of sepiolite, certain sorption during degradation could be also responsible for delaying the sample weight loss [12]. For instance, thermal stability of PLA in nitrogen was improved around 16 °C by addition of 5 wt.-% unmodified sepiolite [28]. In general, thermal degradation temperature of the sepiolite-*g*-P(3HB-*co*-4HB) nanocomposites significantly exceeds the processing temperature and their thermal stability can meet the requirement of the industrial production by injection molding.

As also shown in **Table III.1.1.2**, thermal degradation of unfilled P(3HB-*co*-4HB) was accompanied by the production of a residue of *ca.* 3.8% at 800 °C. This can be related to microbial residues after polymerization as well as small amounts of additives added during polymer production. The residual mass increased in the P(3HB-*co*-4HB)

nanocomposites with increasing the sepiolite content, which is known to produce a weight loss of *ca*. 20% at 850 °C [32], [40], [49]. It is also worthy to mention that the addition of sepiolite nanoclay accelerated the weight loss rate of P(3HB-*co*-4HB), *i.e.*, the percentage of mass loss increased with the degradation temperature. This confirmed that the nanoclay can function as a catalyst by which thermal degradation is accelerated [39]. A strong catalytic effect on the degradation of polyolefins by sepiolite has been also reported [27], underlining the drawbacks of the large presence of silanol groups on its surface.

Thermomechanical properties

Figure III.1.1.5 presents the temperature dependence expressed in terms of the storage modulus and tan δ of neat P(3HB-*co*-4HB) and the various nanocomposites. The storage modulus represents the stiffness of a viscoelastic material and it is proportional to the energy stored during a loading cycle. As shown in **Figure III.1.1.5a**, DMTA curves of P(3HB-*co*-4HB) distinguished two processes. In the temperature range from −50 to 25 °C, the storage modulus showed a significant decrease with increasing temperature. This is associated with the glass transition and it reflects the motions in connection with the biopolymer chains in the amorphous regions. From 25 °C, the modulus presented a smoother decrease with temperature. This is originated from the chain mobility between the crystalline and amorphous regions, which depends on the lamellae thickness of the biopolymer. In this sense, Dagnon *et al*. [78] showed that P(3HB-*co*-4HB) exhibits two transitions at around −104 and 2 °C, corresponding to beta (β) and alpha (α) relaxation processes, respectively. The β-relaxation (T_β) of the biopolymer is conventionally associated with local crankshaft motion of the $(CH_2)_n$ segment [84] whereas the α-relaxation constitutes the T_g of the biopolymer. It can be seen that the storage modulus decreased after the addition of ESAO at both glassy and rubbery states. This reduction was much more intense in the glassy state, *i.e.*, at −50 °C. The incorporation of sepiolite slightly increased the elastic properties of the P(3HB-*co*-4HB) matrix, which was more noticeable above 25 °C. From 50 °C, the modulus of the sepiolite-*g*-P(3HB-*co*-4HB) nanocomposites was similar than the neat biopolymer.
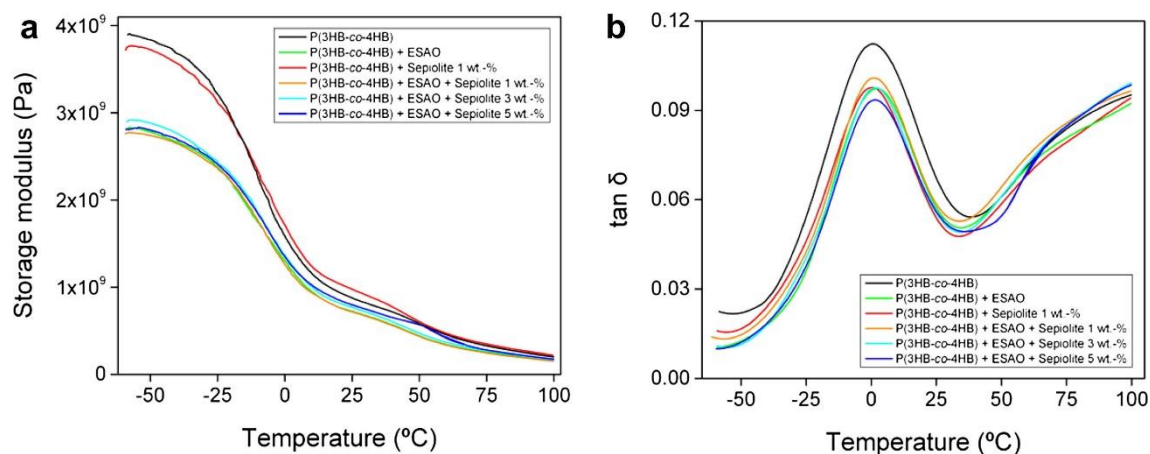
Figure III.1.1.5. Dynamic mechanical thermal analysis (DMTA) curves for poly(3-hydroxybutyrate-*co*-4-hydroxybutyrate) (P(3HB-*co*-4HB)) nanocomposites containing sepiolite nanoclay and epoxy-based styrene-acrylic oligomer (ESAO) for: (a) Storage modulus *vs.* temperature; (b) Damping factor (tan δ) *vs.* temperature.

Tan δ is defined as the ratio of loss modulus to storage modulus. It is a measure of the energy lost, expressed in terms of recoverable energy, which represents the mechanical damping or internal friction in a viscoelastic system. Tan δ plots in **Figure III.1.1.5b** showed that the neat P(3HB-*co*-4HB) exhibits a well-resolved single relaxation peak with a maximum value at *ca.* 0.7 °C, which defines the α-relaxation of the biopolymer. The incorporation of ESAO into P(3HB-*co*-4HB) slightly shifted the value to *ca.* 1.8 °C. This effect can be associated with a slight reduction of chain mobility due to chain length extension. Sepiolite showed negligible variation at both peak shift and broadening of P(3HB-*co*-4HB) chain dynamics during glass transition. However, intensity values of tan δ were reduced in the sepiolite-*g*-P(3HB-*co*-4HB) nanocomposites. Depression in the mechanical loss peak heights implies a reduction in the number of the mobile chains during the glass transition [85].

Mechanical properties

The tensile and flexural stress-strain curves of P(3HB-*co*-4HB) and its various nanocomposites are represented in **Figure III.1.1.6**. **Table III.1.1.3** includes the main mechanical values for each sample. It can be seen that the neat biopolymer behaves as an elastic material with a relatively low plastic deformation. The tensile modulus, strength, and elongation at break of P(3HB-*co*-4HB) were 689.3 MPa, 17.8 MPa, and 3.9%, respectively. In relation to the flexural properties, the flexural modulus, strength, and elongation at break were 1226 MPa, 27.4 MPa, and 3.8%, respectively. Similar mechanical values for injection-molded parts were obtained by Zhang *et al.* [80], who particularly reported a tensile strength at yield of about 17.5 MPa and an elongation at break below 5%. Notable enhancements in stiffness and yield stress were observed with the addition of ESAO, which can be related to the M_W improvement in the biopolymer structure. Elastic moduli of the P(3HB-*co*-4HB) nanocomposites also increased with the sepiolite content in the investigated concentration range, indicating that the nanoclay effectively enhanced the material stiffness. In particular, the sepiolite-*g*-P(3HB-*co*-4HB) 5 wt.-% nanocomposite increased the tensile modulus and strength up to 1012.1 and 21.9 MPa, respectively. The flexural modulus and strength also increased to 1635.6 and 29.8 MPa, respectively. In the case of the tensile and flexural moduli, this represents a percentage increase of about 47 and 35%, respectively.
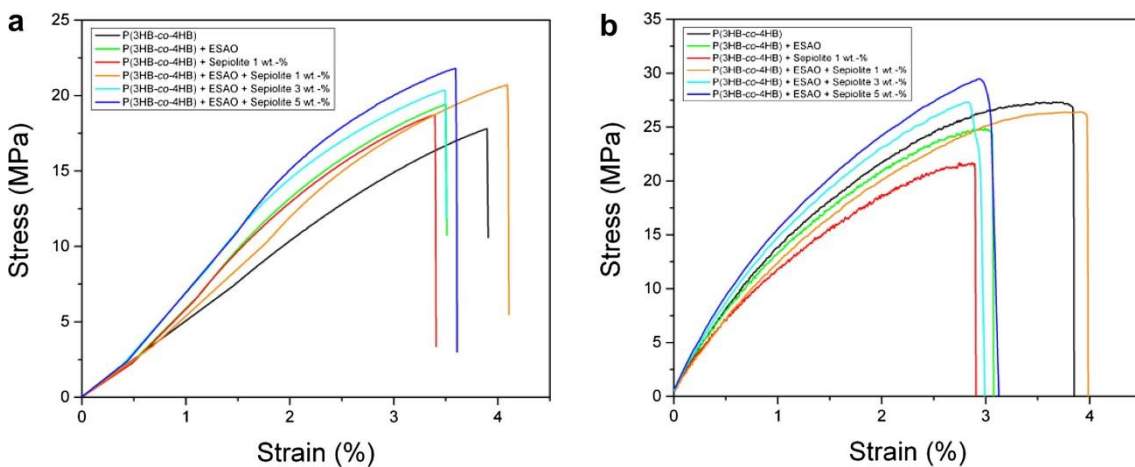
Figure III.1.1.6. Typical stress-strain curves of poly(3-hydroxybutyrate-*co*-4-hydroxybutyrate) (P(3HB-*co*-4HB)) nanocomposites containing sepiolite nanoclay and epoxy-based styrene-acrylic oligomer (ESAO) for: (a) Tensile tests; (b) Flexural tests.

Table III.1.1.3. Mechanical properties in terms of tensile modulus ($E_{tensile}$), tensile strength at yield ($\sigma_{tensile}$), tensile elongation at break ($\varepsilon_{tensile}$), flexural modulus ($E_{flexural}$), flexural strength at yield ($\sigma_{flexural}$), flexural elongation at break ($\varepsilon_{flexural}$), Shore D hardness, and Charpy impact strength for poly(3-hydroxybutyrate-*co*-4-hydroxybutyrate) (P(3HB-*co*-4HB)) nanocomposites containing epoxy-based styrene-acrylic oligomer (ESAO) and sepiolite nanoclay.

Samples	Tensile test			Flexural test			Shore D hardness	Charpy impact strength (kJ/m^2)
	$E_{tensile}$ (MPa)	$\sigma_{tensile}$ (MPa)	$\varepsilon_{tensile}$ (%)	$E_{flexural}$ (MPa)	$\sigma_{flexural}$ (MPa)	$\varepsilon_{flexural}$ (%)		
P(3HB-co-4HB)	689.3 ± 58.3	17.8 ± 0.9	3.9 ± 0.3	1226.0 ± 173.3	27.4 ± 2.9	3.8 ± 0.2	66.8 ± 1.3	3.0 ± 0.2
P(3HB-co-4HB)/ESAO	893.2 ± 60.2	19.4 ± 0.9	3.5 ± 0.3	1353.3 ± 154.1	24.9 ± 5.5	3.1 ± 0.4	67.0 ± 1.2	2.1 ± 0.5
P(3HB-co-4HB)/Sepiolite 1 wt.-%	897.0 ± 62.0	18.7 ± 0.9	3.3 ± 0.2	1207.8 ± 209.7	21.7 ± 3.7	2.9 ± 0.3	64.2 ± 2.0	2.1 ± 0.4
P(3HB-co-4HB)/ESAO/Sepiolite 1 wt.-%	938.1 ± 81.3	20.7 ± 0.8	4.1 ± 0.5	1381.9 ± 157.0	26.9 ± 3.6	4.0 ± 0.3	67.0 ± 0.7	2.4 ± 0.6
P(3HB-co-4HB)/ESAO/Sepiolite 3 wt.-%	977.6 ± 73.8	20.4 ± 1.1	3.5 ± 0.5	1489.0 ± 189.1	27.4 ± 4.3	3.0 ± 0.2	67.6 ± 0.5	2.2 ± 0.3
P(3HB-co-4HB) + ESAO + Sepiolite 5 wt.-%	1012.1 ± 51.9	21.9 ± 0.9	3.6 ± 0.2	1635.6 ± 165.5	29.8 ± 4.9	3.1 ± 0.5	69.4 ± 0.5	2.3 ± 0.6

The high reinforcement generated by sepiolite suggests that a good dispersion level of the nanoclay in the biopolymer matrix was reached. Indeed, without an effective interaction between the P(3HB-*co*-4HB) matrix and sepiolite, the nanoclay would act as a merely stress concentrator, *i.e.*, the so-called "notch effect". In agreement with previous studies, the high content of silanol groups exposed on the external surface of sepiolite can favor its compatibilization with polycondensation polymers such as polyesters and polyamides. For instance, the tensile modulus and yield strength of PA 66 was increased from 2.06 to 2.73 GPa and from 53.7 to 60.9 MPa, respectively, with 5 wt.-% of sepiolite in the study performed by Fernandez-Barranco *et al*. [36]. However, in the same study, the elongation-at-break value drastically decreased from 182 to 42%. In the research work carried out by Sabzi *et al.* [46], the incorporation of unmodified sepiolite into PLA at 10 wt.-% led to a 25% increase in the tensile modulus. Notable mechanical reinforcements were also reported for nanocomposites based on starch [12], PA 6 [33], [34], and gelatin [53], which proves that sepiolite can be effectively dispersed in polar polymer matrices by melt mixing. Nevertheless, it is also worthy to mention that, in most of the previous polymer nanocomposites, ductility decreased with increasing the sepiolite content. Indeed, in the present study the incorporation of 1 wt.-% of pristine sepiolite also reduced the elongation at break of P(3HB-*co*-4HB) from 3.9 to 3.3%. Interestingly, this strain reduction was not observed for the equivalent sepiolite-g-P(3HB-*co*-4HB) nanocomposite. The melt-grafted P(3HB-co-4HB) nanocomposites still preserved around 90% of the initial strain-at-break value, even at the highest sepiolite content, *i.e.*, 5 wt.-%. This evidences that mechanical stress can be effectively transferred from sepiolite to the P(3HB-*co*-4HB) matrix due to melt grafting.

Table III.1.1.3 also includes the mechanical values obtained from the Shore D hardness and Charpy impact tests. Hardness followed the same trend previously observed in the moduli, *i.e.*, the addition of both ESAO and sepiolite exerted a positive effect on the properties of P(3HB-*co*-4HB). It was noticeable the low value observed for the ungrafted nanocomposite. This suggests that pristine sepiolite presents a poor interfacial adhesion with the biopolymer matrix. As opposite, the incorporation of sepiolite nanoclay reduced the impact strength of P(3HB-*co*-4HB). This is an expected consequence of the rigidity increase and loss of toughness in the P(3HB-co-4HB) nanocomposites. Sepiolite embrittled the P(3HB-*co*-4HB) matrix by immobilizing the biopolymer chains and constraining plastic deformation. Nevertheless, similar to the other mechanical properties, this impairment was attenuated for the P(3HB-*co*-4HB) nanocomposites produced by reactive extrusion. This indicates that the sepiolite-*g*-P(3HB-*co*-4HB) nanocomposites were able to absorb higher amounts of energy before fracture.

Morphology of nanocomposites

The fractured surfaces of the P(3HB-*co*-4HB) nanocomposites, after the Charpy impact tests, were analyzed by SEM. Micrographs included in **Figure III.1.1.7** revealed the presence of sepiolite as needle-shaped structures embedded in the biopolymer matrix. All P(3HB-*co*-4HB) nanocomposites showed a high degree of dispersion and a relatively low number of sepiolite aggregates, even at high contents of nanoclay. As above stated, this finding can be related to the good chemical affinity between the polar P(3HB-*co*-4HB) chains with the silanol groups of sepiolite. In **Figure III.1.1.7a**, which corresponds to the ungrafted P(3HB-*co*-4HB) nanocomposite, it is possible to identify spherical voids and fiber-like gaps that correspond to sepiolite nanoparticles that were removed from the biopolymer matrix after fracture. Interfacial debonding supports the previous mechanical results in which the P(3HB-*co*-4HB) nanocomposite produced without ESAO lacked of sufficient adhesion with the nanoclay. As a result the ungrafted samples were more prone to produce mechanical failures at low strains.

The effect of melt grafting can be observed in **Figure III.1.1.7b** for the sepiolite-*g*-P(3HB-*co*-4HB) 1 wt.-% nanocomposite. This sample showed no fracture lines located at the sepiolite-biopolymer interface and the number of voids after fracture was significantly reduced too. The melt-grafted P(3HB-*co*-4HB) nanocomposites containing higher amounts of sepiolite, *i.e.*, 3 wt.-% (**Figure III.1.1.7c**) and 5 wt.-% (**Figure III.1.1.7d**), exhibited rougher and more irregular fracture surfaces. As it can be seen in these images, increasing the sepiolite content also produced some filler attrition, i.e., length reduction of sepiolite nanoparticles. This can be due to a higher number of nanofillers collision and increased shear stresses during melt compounding [86]. Additionally, sepiolite nanoparticles could also break during the mechanical test due to their strong interaction with the P(3HB-*co*-4HB) matrix. In any case, an optimal distribution of sepiolite was achieved since single nanoparticles were effectively dispersed and no sepiolite bundles were observed even at the highest concentration.
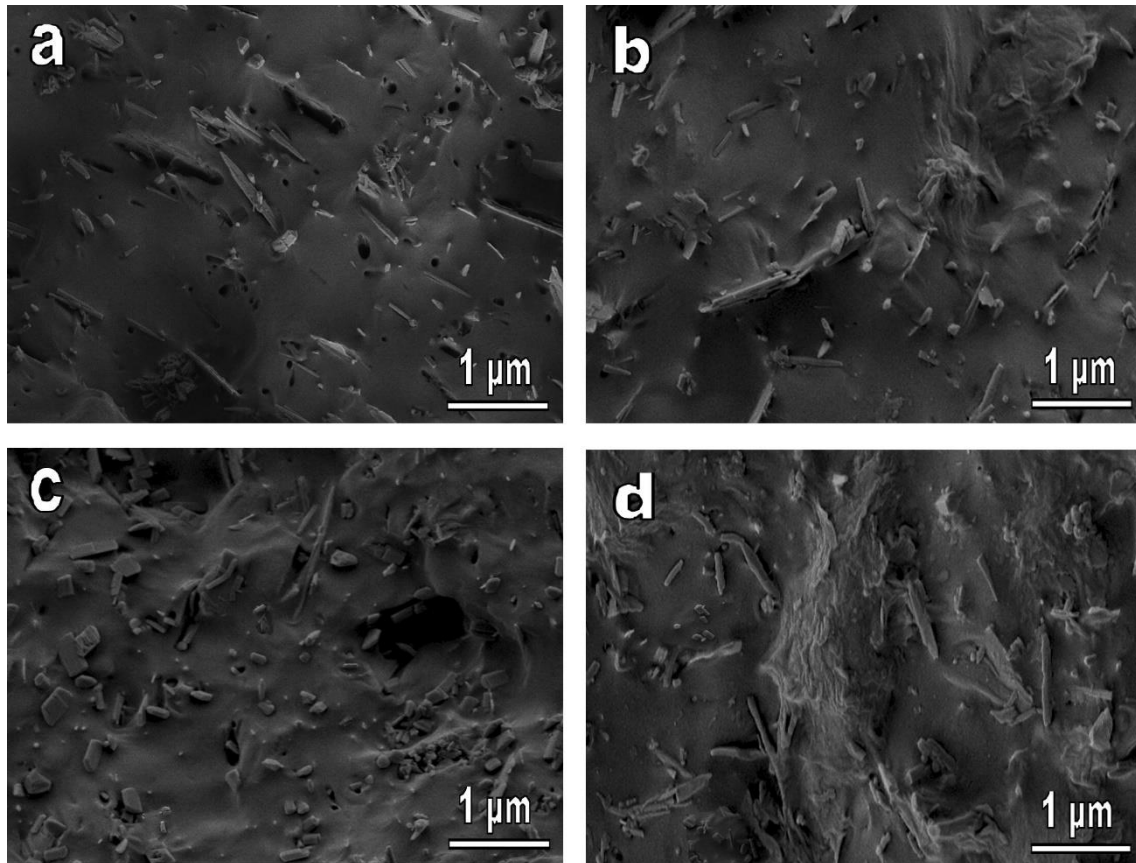
Figure III.1.1.7. Scanning electron microscope (SEM) images of the fractured surfaces of poly(3-hydroxybutyrate-*co*-4-hydroxybutyrate) (P(3HB-*co*-4HB)) nanocomposites based on: (a) Ungrafted sepiolite at 1 wt.-%; (b) Melt-grafted sepiolite at 1 wt.-%; (c) Melt-grafted sepiolite at 3 wt.-%; (d) Melt-grafted sepiolite at 5 wt.-%. Scale markers of 1 μm in all cases.

Conclusions

Sepiolite-*g*-P(3HB-*co*-4HB) nanocomposites were successfully obtained by reactive extrusion using a multi-functional epoxy-based oligomer in a twin-screw extruder. Silanol groups on the external surface of the nanoclay effectively grafted onto the biopolymer via alkoxy silanes bonds. Sepiolite interaction with the biopolymer was detected in the FTIR spectra of the melt-grafted P(3HB-*co*-4HB) nanocomposites by the formation of Si—O—C bands in the region of 1100–1000 cm^{-1} and at 815 cm^{-1}. Melt-grafted sepiolite improved the thermal stability and mechanical properties of P(3HB-co-4HB). In particular, T_{deg} was retarded about 5 °C while the tensile and flexural moduli increased up to 47 and 35%, respectively, for the sepiolite-*g*-P(3HB-*co*-4HB) 5 wt.-% nanocomposite. Melt-grafted P(3HB-*co*-4HB) nanocomposites also retained around 90% of the elongation-at-break and impact-strength values. SEM analysis revealed that sepiolite was efficiently embedded in the P(3HB-*co*-4HB) matrix. Melt grafting was supported in the fractured surfaces by the absence of voids and high interfacial interaction between sepiolite and the biopolymer. Future studies should be focused on assessing the potential benefits of multi-functional epoxy-based additives to increase the processability of biodegradable polymer nanocomposites and their influence on the biodegradation behavior.

Melt compounding with highly reactive coupling agents can be regarded as a novel tool to develop high-performing polymer nanocomposites. In particular, melt grafting of nanoclays can potentially enhance the thermal and mechanical performance of biopolymers. This may promote and revolutionize their accessibility to industrial sectors such as packaging, where both good performance and environmental concerns are requirements.

Acknowledgements

REFERENCES

1. Nakamura, S., Y. Doi and M. Scandola, *Microbial Synthesis and Characterization of poly(3-hydroxybutyrate-co-4-hydroxybutyrate)*. Macromolecules, 1992. **25**(17): 4237-4241.
2. Kunioka, M., A. Tamaki and Y. Doi, *Crystalline and Thermal Properties of Bacterial Copolyesters: Poly(3-hydroxybutyrate-co-3-hydroxyvalerate) and Poly(3-hydroxybutyrate-co-4-hydroxybutyrate)*. Macromolecules, 1989. **22**(2): 694-697.
3. Saito, Y., S. Nakamura, M. Hiramitsu and Y. Doi, *Microbial synthesis and properties of poly(3-hydroxybutyrate-co-4-hydroxybutyrate)*. Polymer International, 1996. **39**(3): 169-174.
4. Philip, S., T. Keshavarz and I. Roy, *Polyhydroxyalkanoates: Biodegradable polymers with a range of applications.* Journal of Chemical Technology and Biotechnology, 2007. **82**(3): 233-247.
5. Han, L.J., C.Y. Han, W.L. Cao, X.M. Wang, J.J. *Bian and L.S. Dong, Preparation and characterization of biodegradable poly(3-hydroxybutyrate-co-4-hydroxybutyrate)/silica nanocomposites*. Polymer Engineering and Science, 2012. **52**(2): 250-258.
6. Wang, X., H. Zhang, M. Liu and D. Jia, *Thermal stability of poly(3-hydroxybutyrate-co-4-hydroxybutyrate)/modified montmorillonite bio-nanocomposites*. Polymer Composites, 2015: n/a-n/a.
7. Feijoo-Gomez, J.L., S. Torres-Giner and C. Vazquez-Tomer. *INNOVEX® a new technology for masterbatch additives for the XPS industry. in 10th International Conference on Foam Materials and Technology*, FOAMS 2012. 2012. Society of Plastics Engineers.
8. Torres-Giner, S., A. Martinez-Abad and J.M. Lagaron, *Zein-based ultrathin fibers containing ceramic nanofillers obtained by electrospinning. II. Mechanical properties, gas barrier, and sustained release capacity of biocide thymol in multilayer polylactide films.* Journal of Applied Polymer Science, 2014. **131**(18): 9270-9276.
9. Angellier-Coussy, H., S. Torres-Giner, M.H. Morel, N. Gontard and E. Gastaldi, *Functional properties of thermoformed wheat gluten/montmorillonite materials with respect to formulation and processing conditions*. Journal of Applied Polymer Science, 2008. **107**(1): 487-496.
10. Bilotti, E., H.R. Fischer and T. Peijs, *Polymer nanocomposites based on needle-like sepiolite clays: Effect of functionalized polymers an the dispersion of nanofiller, crystallinity, and mechanical properties*. Journal of Applied Polymer Science, 2008. **107**(2): 1116-1123.
11. Duquesne, E., S. Moins, M. Alexandre and P. Dubois, *How can nanohybrids enhance polyester/sepiolite nanocomposite properties?* Macromolecular Chemistry and Physics, 2007. **208**(23): 2542-2550.
12. Chivrac, F., E. Pollet, M. Schmutz and L. Avérous, *Starch nano-biocomposites based on needle-like sepiolite clays.* Carbohydrate Polymers, 2010. **80**(1): 145-153.

13.   Darder, M., M. Lopez-Blanco, P. Aranda, A.J. Aznar, J. Bravo and E. Ruiz-Hitzky, *Microfibrous chitosan-sepiolite nanocomposites*. Chemistry of Materials, 2006. **18**(6): 1602-1610.

14.   Benlikaya, R., M. Alkan and I. Kaya, *Preparation and Characterization of Sepiolite-Poly(ethyl methacrylate) and Poly(2-hydroxyethyl methacrylate) Nanocomposites*. Polymer Composites, 2009. **30**(11): 1585-1594.

15.   Aranda, P., R. Kun, M.A. Martin-Luengo, S. Letaief, I. Dekany and E. Ruiz-Hitzky, *Titania-Sepiolite nanocomposites prepared by a surfactant templating colloidal route*. Chemistry of Materials, 2008. **20**(1): 84-91.

16.   Helmy, A.K. and S.G. de Bussetti, *The surface properties of sepiolite*. Applied Surface Science, 2008. **255**(5 PART 2): 2920-2924.

17.   Mejía, A., N. García, J. Guzmán and P. Tiemblo, *Confinement and nucleation effects in poly(ethylene oxide) melt-compounded with neat and coated sepiolite nanofibers: Modulation of the structure and semicrystalline morphology*. European Polymer Journal, 2013. **49**(1): 118-129.

18.   Tartaglione, G., D. Tabuani, G. Camino and M. Moisio, *PP and PBT composites filled with sepiolite: Morphology and thermal behaviour*. Composites Science and Technology, 2008. **68**(2): 451-460.

19.   Galan, E., *Properties and applications of palygorskite-sepiolite clays*. Clay Minerals, 1996. **31**(4): 443-453.

20.   Hermosin, M.C. and J. Cornejo, *Methylation of Sepiolite and Palygorskite with Diazomethane*. Clays and Clay Minerals, 1986. **34**(5): 591-596.

21.   Volle, N., F. Giulieri, A. Burr, S. Pagnotta and A.M. Chaze, *Controlled interactions between silanol groups at the surface of sepiolite and an acrylate matrix: Consequences on the thermal and mechanical properties.* Materials Chemistry and Physics, 2012. **134**(1): 417-424.

22.   Samper-Madrigal, M.D., O. Fenollar, F. Dominici, R. Balart and J.M. Kenny, *The effect of sepiolite on the compatibilization of polyethylene-thermoplastic starch blends for environmentally friendly films.* Journal of Materials Science, 2015. **50**(2): 863-872.

23.   Ma, J., E. Bilotti, T. Peijs and J.A. Darr, *Preparation of polypropylene/sepiolite nanocomposites using supercritical CO2 assisted mixing*. European Polymer Journal, 2007. **43**(12): 4931-4939.

24.   Bilotti, E., H. Deng, R. Zhang, D. Lu, W. Bras, H.R. Fischer and T. Peijs, *Synergistic reinforcement of highly oriented poly(propylene) tapes by sepiolite nanoclay*. Macromolecular Materials and Engineering, 2010. **295**(1): 37-47.

25.   Vargas, A.F., V.H. Orozco, F. Rault, S. Giraud, E. Devaux and B.L. Lopez, *Influence of fiber-like nanofillers on the rheological, mechanical, thermal and fire properties of polypropylene An application to multifilament yarn*. Composites Part a-Applied Science and Manufacturing, 2010. **41**(12): 1797-1806.

26.   Pappalardo, S., P. Russo, D. Acierno, S. Rabe and B. Schartel, *The synergistic effect of organically modified sepiolite in intumescent flame retardant polypropylene*. European Polymer Journal, 2016. **76**: 196-207.

27.   Marcilla, A., A. Gómez, S. Menargues and R. Ruiz, *Pyrolysis of polymers in the presence of a commercial clay.* Polymer Degradation and Stability, 2005. **88**(3): 456-460.

28.   Fukushima, K., D. Tabuani and G. Camino, *Nanocomposites of PLA and PCL based on montmorillonite and sepiolite.* Materials Science & Engineering C-Biomimetic and Supramolecular Systems, 2009. **29**(4): 1433-1441.

29.   Fukushima, K., D. Tabuani, C. Abbate, M. Arena and L. Ferreri, *Effect of sepiolite on the biodegradation of poly(lactic acid) and polycaprolactone.* Polymer Degradation and Stability, 2010. **95**(10): 2049-2056.

30.   García, N., M. Hoyos, J. Guzmán and P. Tiemblo, *Comparing the effect of nanofillers as thermal stabilizers in low density polyethylene.* Polymer Degradation and Stability, 2009. **94**(1): 39-48.

31. Shafiq, M., T. Yasin and S. Saeed, *Synthesis and Characterization of Linear Low-Density Polyethylene/Sepiolite Nanocomposites*. Journal of Applied Polymer Science, 2012. **123**(3): 1718-1723.

32. García-López, D., J.F. Fernández, J.C. Merino, J. Santarén and J.M. Pastor, *Effect of organic modification of sepiolite for PA 6 polymer/organoclay nanocomposites*. Composites Science and Technology, 2010. **70**(10): 1429-1436.

33. Bilotti, E., R. Zhang, H. Deng, F. Quero, H.R. Fischer and T. Peijs, *Sepiolite needle-like clay for PA6 nanocomposites: An alternative to layered silicates?* Composites Science and Technology, 2009. **69**(15-16): 2587-2595.

34. Xie, S., S. Zhang, F. Wang, M. Yang, R. Séguéla and J.-M. Lefebvre, *Preparation, structure and thermomechanical properties of nylon-6 nanocomposites with lamella-type and fiber-type sepiolite*. Composites Science and Technology, 2007. **67**(11–12): 2334-2341.

35. Garcia-Lopez, D., J.F. Fernandez, J.C. Merino and J.M. Pastor, *Influence of organic modifier characteristic on the mechanical properties of polyamide 6/organosepiolite nanocomposites.* Composites Part B-Engineering, 2013. **45**(1): 459-465.

36. Fernandez-Barranco, C., A. Yebra-Rodriguez, M.D. La Rubia-Garcia, F.J. Navas-Martos and P. Alvarez-Lloret, *Mechanical and crystallographic properties of injection-molded polyamide 66/sepiolite nanocomposites with different clay loading*. Polymer Composites, 2015. **36**(12): 2326-2333.

37. Fernandez-Barranco, C., A.E. Koziol, K. Skrzypiec, M. Rawski, M. Drewniak and A. Yebra-Rodriguez, *Study of spatial distribution of sepiolite in sepiolite/polyamide6,6 nanocomposites.* Applied Clay Science, 2016. **127**: 129-133.

38. Yu, Y., S.L. Qi, J.Y. Zhan, Z.P. Wu, X.P. Yang and D.Z. Wu, *Polyimide/sepiolite nanocomposite films: Preparation, morphology and properties*. Materials Research Bulletin, 2011. **46**(10): 1593-1599.

39. Chen, H., M. Zheng, H. Sun and Q. Jia, *Characterization and properties of sepiolite/polyurethane nanocomposites.* Materials Science and Engineering: A, 2007. **445–446**: 725-730.

40. Chen, H., H. Lu, Y. Zhou, M. Zheng, C. Ke and D. Zeng, *Study on thermal properties of polyurethane nanocomposites based on organo-sepiolite*. Polymer Degradation and Stability, 2012. **97**(3): 242-247.

41. Chen, H., D. Zeng, X. Xiao, M. Zheng, C. Ke and Y. Li, *Influence of organic modification on the structure and properties of polyurethane/sepiolite nanocomposites*. Materials Science and Engineering: A, 2011. **528**(3): 1656-1661.

42. Nohales, A., L. Solar, I. Porcar, C.I. Vallo and C.M. Gómez, *Morphology, flexural, and thermal properties of sepiolite modified epoxy resins with different curing agents*. European Polymer Journal, 2006. **42**(11): 3093-3101.

43. Nohales, A., R. Muñoz-Espí, P. Félix and C.M. Gómez, *Sepiolite-reinforced epoxy nanocomposites: Thermal, mechanical, and morphological behavior*. Journal of Applied Polymer Science, 2011. **119**(1): 539-547.

44. Franchini, E., J. Galy and J.F. Gérard, *Sepiolite-based epoxy nanocomposites: Relation between processing, rheology, and morphology*. Journal of Colloid and Interface Science, 2009. **329**(1): 38-47.

45. Hapuarachchi, T.D. and T. Peijs, *Multiwalled carbon nanotubes and sepiolite nanoclays as flame retardants for polylactide and its natural fibre reinforced composites*. Composites Part a-Applied Science and Manufacturing, 2010. **41**(8): 954-963.

46. Sabzi, M., L. Jiang, M. Atai and I. Ghasemi, *PLA/sepiolite and PLA/calcium carbonate nanocomposites: A comparison study.* Journal of Applied Polymer Science, 2013. **129**(4): 1734-1744.

47. Nieddu, E., L. Mazzucco, P. Gentile, T. Benko, V. Balbo, R. Mandrile and G. Ciardelli, *Preparation and biodegradation of clay composites of PLA*. Reactive & Functional Polymers, 2009. **69**(6): 371-379.

48. Fukushima, K., D. Tabuani and G. Camino, *Poly(lactic acid)/clay nanocomposites: effect of nature and content of clay on morphology, thermal and thermo-mechanical properties.*

Materials Science & Engineering C-Materials for Biological Applications, 2012. **32**(7): 1790-1795.

49. Fukushima, K., A. Fina, F. Geobaldo, A. Venturello and G. Camino, *Properties of poly (lactic acid) nanocomposites based on montmorillonite, sepiolite and zirconium phosphonate.* Express Polymer Letters, 2012. **6**(11).

50. Fukushima, K., A. Rasyida and M.C. Yang, *Characterization, degradation and biocompatibility of PBAT based nanocomposites.* Applied Clay Science, 2013. **80-81**: 291-298.

51. Bokobza, L., A. Burr, G. Garnaud, M.Y. Perrin and S. Pagnotta, *Fibre reinforcement of elastomers: Nanocomposites based on sepiolite and poly(hydroxyethyl acrylate).* Polymer International, 2004. **53**(8): 1060-1065.

52. Frydrych, M., C.Y. Wan, R. Stengler, K.U. O'Kelly and B.Q. Chen, *Structure and mechanical properties of gelatin/sepiolite nanocomposite foams.* Journal of Materials Chemistry, 2011. **21**(25): 9103-9111.

53. Miguel Fernandes, F., A. Isabel Ruiz, M. Darder, P. Aranda and E. Ruiz-Hitzky, *Gelatin-Clay Bio-Nanocomposites: Structural and Functional Properties as Advanced Materials.* Journal of Nanoscience and Nanotechnology, 2009. **9**(1): 221-229.

54. Can, M.F., L. Avdan and A.C. Bedeloglu, *Properties of biodegradable PVA/sepiolite-based nanocomposite fiber mats.* Polymer Composites, 2015. **36**(12): 2334-2342.

55. Santiago, F., A.E. Mucientes, M. Osorio and F.J. Poblete, *Synthesis and swelling behaviour of poly(sodiurn acrylate)/sepiolite superabsorbent composites and nanocomposites.* Polymer International, 2006. **55**(8): 843-848.

56. Mir, S., T. Yasin, P.J. Halley, H.M. Siddiqi, O. Ozdemir and A. Nguyen, *Thermal and rheological effects of sepiolite in linear low-density polyethylene/starch blend.* Journal of Applied Polymer Science, 2013. **127**(2): 1330-1337.

57. Nuñez, K., C. Rosales, R. Perera, N. Villarreal and J.M. Pastor, *Poly(lactic acid)/low-density polyethylene blends and its nanocomposites based on sepiolite.* Polymer Engineering and Science, 2012. **52**(5): 988-1004.

58. Nuñez, K., C. Rosales, R. Perera, N. Villarreal and J.M. Pastor, *Nanocomposites of PLA/PP blends based on sepiolite.* Polymer Bulletin, 2011. **67**(9): 1991-2016.

59. Olivato, J.B., J. Marini, E. Pollet, F. Yamashita, M.V.E. Grossmann and L. Avérous, *Elaboration, morphology and properties of starch/polyester nano-biocomposites based on sepiolite clay.* Carbohydrate Polymers, 2015. **118**: 250-256.

60. Frost, R.L. and E. Mendelovici, *Modification of fibrous silicates surfaces with organic derivatives: An infrared spectroscopic study.* Journal of Colloid and Interface Science, 2006. **294**(1): 47-52.

61. Duangphet, S., D. Szegda, J. Song and K. Tarverdi, *The Effect of Chain Extender on Poly(3-hydroxybutyrate-co-3-hydroxyvalerate): Thermal Degradation, Crystallization, and Rheological Behaviours.* Journal of Polymers and the Environment, 2014. **22**(1): 1-8.

62. Arruda, L.C., M. Magaton, R.E.S. Bretas and M.M. Ueki, *Influence of chain extender on mechanical, thermal and morphological properties of blown films of PLA/PBAT blends.* Polymer Testing, 2015. **43**: 27-37.

63. Villalobos, M., A. Awojulu, T. Greeley, G. Turco and G. Deeter, *Oligomeric chain extenders for economic reprocessing and recycling of condensation plastics.* Energy, 2006. **31**(15): 3227-3234.

64. Wen, X., X. Lu, Q. Peng, F. Zhu and N. Zheng, *Crystallization behaviors and morphology of biodegradable poly(3-hydroxybutyrate-co-4-hydroxybutyrate).* Journal of Thermal Analysis and Calorimetry, 2012. **109**(2): 959-966.

65. Torres-Giner, S., *Electrospun nanofibers for food packaging applications, in Multifunctional and nanoreinforced polymers for food packaging.* 2011, Elsevier. p. 108-125.

66. Chang, T.C., P.T. Liu, Y.S. Mor, S.M. Sze, Y.L. Yang, M.S. Feng, F.M. Pan, B.T. Dai and C.Y. Chang, *The novel improvement of low dielectric constant methylsilsesquioxane by N2O plasma treatment.* Journal of the Electrochemical Society, 1999. **146**(10): 3802-3806.

67.   Wang, Y., C. Fu, Y. Luo, C. Ruan, Y. Zhang and Y. Fu, *Melt synthesis and characterization of poly(L-lactic acid) chain linked by multifunctional epoxy compound.* Journal of Wuhan University of Technology-Mater. Sci. Ed., 2010. **25**(5): 774-779.

68.   Wei, D., H. Wang, H. Xiao, A. Zheng and Y. Yang, *Morphology and mechanical properties of poly(butylene adipate-co-terephthalate)/potato starch blends in the presence of synthesized reactive compatibilizer or modified poly(butylene adipate-co-terephthalate).* Carbohydrate Polymers, 2015. **123**: 275-282.

69.   Abdelwahab, M.A., S. Taylor, M. Misra and A.K. Mohanty, *Thermo-mechanical characterization of bioblends from polylactide and poly(butylene adipate-co-terephthalate) and lignin.* Macromolecular Materials and Engineering, 2015. **300**(3): 299-311.

70.   Guo, L.H., H. Sato, T. Hashimoto and Y. Ozaki, *FTIR Study on Hydrogen-Bonding Interactions in Biodegradable Polymer Blends of Poly(3-hydroxybutyrate) and Poly(4-vinylphenol).* Macromolecules, 2010. **43**(8): 3897-3902.

71.   Sato, H., R. Murakami, A. Padermshoke, F. Hirose, K. Senda, I. Noda and Y. Ozaki, *Infrared spectroscopy studies of CH···O hydrogen bondings and thermal behavior of biodegradable poly(hydroxyalkanoate).* Macromolecules, 2004. **37**(19): 7203-7213.

72.   Huang, H., Y. Hu, J.M. Zhang, H. Sato, H.T. Zhang, I. Noda and Y. Ozaki, *Miscibility and hydrogen-bonding interactions in biodegradable polymer blends of poly(3-hydroxybutyrate) and a partially hydrolyzed poly(vinyl alcohol*). Journal of Physical Chemistry B, 2005. **109**(41): 19175-19183.

73.   Sun, Q.R., T. Mekonnen, M. Misra and A.K. Mohanty, *Novel Biodegradable Cast Film from Carbon Dioxide Based Copolymer and Poly(Lactic Acid).* Journal of Polymers and the Environment, 2016. **24**(1): 23-36.

74.   Jing, S.Y., H.J. Lee and C.K. Choi, *Chemical bond structure on Si-O-C composite films with a low dielectric constant deposited by using inductively coupled plasma chemical vapor deposition.* Journal of the Korean Physical Society, 2002. **41**(5): 769-773.

75.   Yang, C.S., K.S. Oh, J.Y. Ryu, D.C. Kim, J. Shou-Yong, C.K. Choi, H.-J. Lee, S.H. Um and H.Y. Chang, *A study on the formation and characteristics of the SiOCH composite thin films with low dielectric constant for advanced semiconductor devices.* Thin Solid Films, 2001. **390**(1–2): 113-118.

76.   Al-Itry, R., K. Lamnawar and A. Maazouz, *Improvement of thermal stability, rheological and mechanical properties of PLA, PBAT and their blends by reactive extrusion with functionalized epoxy.* Polymer Degradation and Stability, 2012. **97**(10): 1898-1914.

77.   Corre, Y.-M., J. Duchet, J. Reignier and A. Maazouz, *Melt strengthening of poly (lactic acid) through reactive extrusion with epoxy-functionalized chains.* Rheologica Acta, 2011. **50**(7): 613-629.

78.   Dagnon, K.L., C. Thellen, J.A. Ratto and N.A. D'Souza, *Physical and Thermal Analysis of the Degradation of Poly(3-Hydroxybutyrate-co-4-Hydroxybutyrate) Coated Paper in a Constructed Soil Medium.* Journal of Polymers and the Environment, 2010. **18**(4): 510-522.

79.   An, Y.X., L.S. Dong, L.X. Li, Z.S. Mo and Z.L. Feng, *Isothermal crystallization kinetics and melting behavior of poly(beta-hydroxybutyrate)/poly(vinyl acetate) blends*. European Polymer Journal, 1999. **35**(3): 365-369.

80.   Zhang, K., M. Misra and A.K. Mohanty, *Toughened Sustainable Green Composites from Poly(3-hydroxybutyrate-co-3-hydroxyvalerate) Based Ternary Blends and Miscanthus Biofiber.* Acs Sustainable Chemistry & Engineering, 2014. **2**(10): 2345-2354.

81.   Hsieh, W., H. Mitomo, K. Kasuya and T. Komoto, *Enzymatic degradation and aminolysis of microbial poly(3-hydroxybutyrate-co-4-hydroxybutyrate) single crystals*. Journal of Polymers and the Environment, 2006. **14**(1): 79-87.

82.   Cong, C.B., S.Y. Zhang, R.W. Xu, W.C. Lu and D.S. Yu, *The influence of 4HB content on the properties of poly(3-hydroxylbutyrate-co-4-hydroxylbutyrate) based on melt molded sheets.* Journal of Applied Polymer Science, 2008. **109**(3): 1962-1967.

83.   Erceg, M., T. Kovacic and I. Klaric, *Thermal degradation of poly(3-hydroxybutyrate) plasticized with acetyl tributyl citrate.* Polymer Degradation and Stability, 2005. **90**(2): 313-318.

84.   Dagnon, K.L., H.H. Chen, L.H. Lnnocentini-Mei and N.A. D'Souza, *Poly (3-hydroxybutyrate)-co-(3-hydroxyvalerate) /layered double hydroxide nanocomposites*. Polymer International, 2009. **58**(2): 133-141.

85.   Torres-Giner, S., N. Montanes, O. Fenollar, D. García-Sanoguera and R. Balart, *Development and optimization of renewable vinyl plastisol/wood flour composites exposed to ultraviolet radiation.* Materials & Design, 2016. **108**: 648-658.

86.   Torres-Giner, S., A. Chiva-Flor and J.L. Feijoo, *Injection-molded parts of polypropylene/multi-wall carbon nanotubes composites with an electrically conductive tridimensional network.* Polymer Composites, 2016. **37**(2): 488-496.

III.1.2. Ductility and Toughness Improvement of Injection-Molded Compostable Pieces of Polylactide by Melt Blending with Poly(e-caprolactone) and Thermoplastic Starch.

L. Quiles-Carrillo [1], N. Montanes [1], F. Pineiro [1], A. Jorda-Vilaplana [1] and S. Torres-Giner [1,2]

[1] Technological Institute of Materials (ITM), Universitat Politècnica de València (UPV), Plaza Ferrándiz y Carbonell 1, 03801 Alcoy, Spain;

[2] Novel Materials and Nanotechnology Group, Institute of Agrochemistry and Food Technology (IATA), Spanish National Research Council (CSIC), Calle Catedrático Agustín Escardino Benlloch 7, 46980 Paterna, Valencia, Spain

materials

MDPI

Ductility and Toughness Improvement of Injection-Molded Compostable Pieces of Polylactide by Melt Blending with Poly(ε-caprolactone) and Thermoplastic Starch

Luis Quiles-Carrillo [1] , **Nestor Montanes** [1], **Fede Pineiro** [1], **Amparo Jorda-Vilaplana** [1] and **Sergio Torres-Giner** [1,2,]*

[1]   Technological Institute of Materials (ITM), Universitat Politècnica de València (UPV), Plaza Ferrándiz y Carbonell 1, 03801 Alcoy, Spain; luiquic1@epsa.upv.es (L.Q.-C.); nesmonmu@upvnet.upv.es (N.M.); fepival@epsa.upv.es (F.P.); amjorvi@upv.es (A.J.-V.)
[2]   Novel Materials and Nanotechnology Group, Institute of Agrochemistry and Food Technology (IATA), Spanish National Research Council (CSIC), Calle Catedrático Agustín Escardino Benlloch 7, 46980 Paterna, Spain
*   Correspondence: storresginer@iata.csic.es; Tel.: +34-963-900-022

check for updates

Abstract: The present study describes the preparation and characterization of binary and ternary blends based on polylactide (PLA) with poly(ε-caprolactone) (PCL) and thermoplastic starch (TPS) to develop fully compostable plastics with improved ductility and toughness. To this end, PLA was first melt-mixed in a co-rotating twin-screw extruder with up to 40 wt % of different PCL and TPS combinations and then shaped into pieces by injection molding. The mechanical, thermal, and thermomechanical properties of the resultant binary and ternary blend pieces were analyzed and related to their composition. Although the biopolymer blends were immiscible, the addition of both PCL and TPS remarkably increased the flexibility and impact strength of PLA while it slightly reduced its mechanical strength. The most balanced mechanical performance was achieved for the ternary blend pieces that combined high PCL contents with low amounts of TPS, suggesting a main phase change from PLA/TPS (comparatively rigid) to PLA/PCL (comparatively flexible). The PLA-based blends presented an "island-and-sea" morphology in which the TPS phase contributed to the fine dispersion of PCL as micro-sized spherical domains that acted as a rubber-like phase with the capacity to improve toughness. In addition, the here-prepared ternary blend pieces presented slightly higher thermal stability and lower thermomechanical stiffness than the neat PLA pieces. Finally, all biopolymer pieces fully disintegrated in a controlled compost soil after 28 days. Therefore, the inherently low ductility and toughness of PLA can be successfully improved by melt blending with PCL and TPS, resulting in compostable plastic materials with a great potential in, for instance, rigid packaging applications.

Keywords: PLA; PCL; TPS; biopolymer blends; mechanical properties; compostable plastics

---

1. Introduction

The extensive use of petroleum-derived polymers is responsible for the increasing concern about the environmental impact of plastics due to both their origin and end-of-cycle, since most of them are not biodegradable. Worldwide polymer production was estimated to be 260 million metric tons per year in 2007 and it is considered that in 2020 each person will consume around 40 kg of plastic annually [1]. Bioplastics emerge as an alternative to conventional plastics, including both natural-sourced polymers

Ductility and Toughness Improvement of Injection-Molded Compostable Pieces of Polylactide by Melt Blending with Poly(e-caprolactone) and Thermoplastic Starch.

Abstract

The present study describes the preparation and characterization of binary and ternary blends based on polylactide (PLA) with poly(ε-caprolactone) (PCL) and thermoplastic starch (TPS) to develop fully compostable plastics with improved ductility and toughness. To this end, PLA was first melt-mixed in a co-rotating twin-screw extruder with up to 40 wt% of different PCL and TPS combinations and then shaped into pieces by injection molding. The mechanical, thermal, and thermomechanical properties of the resultant binary and ternary blend pieces were analyzed and related to their composition. Although the biopolymer blends were immiscible, the addition of both PCL and TPS remarkably increased the flexibility and impact strength of PLA while it slightly reduced its mechanical strength. The most balanced mechanical performance was achieved for the ternary blend pieces that combined high PCL contents with low amounts of TPS, suggesting a main phase change from PLA/TPS (comparatively rigid) to PLA/PCL (comparatively flexible). The PLA-based blends presented an "island-and-sea" morphology in which the TPS phase contributed to the fine dispersion of PCL as micro-sized spherical domains that acted as a rubber-like phase with the capacity to improve toughness. In addition, the here-prepared ternary blend pieces presented slightly higher thermal stability and lower thermomechanical stiffness than the neat PLA pieces. Finally, all biopolymer pieces fully disintegrated in a controlled compost soil after 28 days. Therefore, the inherently low ductility and toughness of PLA can be successfully improved by melt blending with PCL and TPS, resulting in compostable plastic materials with a great potential in, for instance, rigid packaging applications.

Keywords: PLA; PCL; TPS; biopolymer blends; mechanical properties; compostable plastics

INTRODUCTION

The extensive use of petroleum-derived plastics is responsible for the increasing concern about their environmental impact due to both their origin and end-of-cycle, since most of them are not biodegradable. Worldwide polymer production was estimated to be 260 million metric tons per year in 2007 for all polymers, but it is considered that in 2020 each person will consume around 40 kg of plastic annually [1]. Bioplastics emerge as an alternative to conventional plastics, including both natural-sourced polymers and also petroleum-based polyesters that undergo biodegradation. Among biopolymers, polylactide (PLA) is currently considered one of the most promising biopolymers at industrial scale due to its good balance between physicochemical properties, low price, and sustainability [2]. PLA is obtained from lactide derived from starch fermentation and it is fully biodegradable. The increasing use of PLA in the last years is noticeable with a current worldwide production of about 140,000 tons/year [3]. The main uses of PLA cover a wide variety of industrial sectors for instance automotive [4–6], biomedical applications [7,8], packaging [9,10] or, lately, the growing industry of 3D printing [11,12]. Despite this, PLA presents several intrinsic restrictions that are mainly related to its relatively high price, low heat resistance, and high fragility [13]. As a result, PLA cannot fulfill the technical requirements of some industries, limiting its expansion to commodity areas such as food packaging [14].

To overcome or, at least, minimize the low ductility and toughness of PLA, several approaches have been considered with excellent results. The first approach is copolymerization. For instance, the simultaneous polymerization of lactide acid (LA) with glycolic acid (GA) leads to the synthesis of poly(lactic acid-*co*-glycolic acid) (PLGA). In general terms, PLGA copolymers exhibit improved solubility as well as better ductile properties than both PLA and poly(glycolic acid) (PGA) homopolymers [15,16]. Nevertheless, copolymers are frequently expensive and their use is not yet generalized at industrial scale. A second strategy to increase PLA toughness is focused on the use of plasticizers. Some of the widely used plasticizers for PLA include poly(ethylene glycol) (PEG) [17], triethyl citrate (TEC) [18,19], and lactic acid oligomers (OLAs) [20]. All these plasticizers contribute positively to increasing ductility by providing a relevant decrease in the glass transition temperature (T_g) of PLA but they can also reduce the heat resistance, tensile strength, and stiffness. In addition to these plasticizers, in recent years, new vegetable oil-derived plasticizers have been successfully developed for PLA formulations such as maleinized, acrylated, hydroxylated, and epoxidized vegetable oils [21–24]. Although their efficiency as primary plasticizers for PLA is lower than those indicated previously, the particular chemical structure of these multi-functionalized modified vegetable oils delivers chain extension, branching and, in some cases, cross-linking resulting in improved toughness without compromising the mechanical strength in a great extent [23]. The third route is related to the manufacturing of PLA-based blends. This represents a very cost-effective solution to reduce the intrinsic fragility of PLA materials without decreasing their tensile strength. A wide variety of binary blends based on PLA has been extensively studied in the last years. For instance, it is worthy to note the interest in binary blends of PLA with polyhydroxyalkanoates (PHAs) [25,26], polyamides (PAs) [27,28], poly(butylene adipate-co-terephthalate) (PBAT) [29,30], thermoplastic starch (TPS) [31], poly(ε-caprolactone) (PCL), poly(butylene succinate) (PBS), and poly(butylene succinate-*co*-adipate) (PBSA) [32–34]. These previous studies are based on the fact that,

to improve toughness, PLA is blended with flexible polymers that perform as a rubber-like phase inside a rigid polymer matrix as, for instance, polybutadiene rubbers (BRs) do in high-impact polystyrene (HIPS).

In addition to binary blends, a wide variety of ternary blends with PLA have been proposed to tailor the desired properties, particularly in terms of improved toughness [35–37]. On the one hand, PCL is a well-known synthetic aliphatic biopolyester, characterized by a high crystallinity, relatively fast biodegradability, and high ductility. However, PCL shows a low melting temperature (T_m), of about 60 °C, which restricts its use in a wide range of applications [38]. PLA/PCL blends are attracting some industrial uses since flexible PCL domains can be finely dispersed into the rigid PLA matrix leading to improved toughness without compromising biodegradation [39]. In addition, the resultant blends are fully resorbable, finding interesting applications as biomedical devices. On the other hand, starch is a versatile and useful biopolymer. Starch has to be modified by means of plasticizers (*e.g.*, glycerol and water) [40] and/or chemical reaction (*e.g.*, esterification) [41] in order to be melt-processed, which then results in TPS. The role of plasticizers is to destructurize granular starch by breaking hydrogen bonds between the starch macromolecules, accompanying with a partial depolymerization of starch backbone. As a result, TPS leads to compostable plastic materials offering interesting opportunities in the packaging field due to its low cost and tailor-made mechanical behavior by selecting the appropriate plasticizers [42]. Blending of PLA with TPS is, therefore, a good way to balance the price and develop materials that has new performances.

The aim of this work was to prepare and characterize ternary blends of PLA with PCL and TPS to overcome the intrinsic brittleness of PLA. To this end, different PCL and TPS contents were blended by melt compounding with PLA to obtain PLA-based materials with tailor-made properties. The resultant PLA/PCL/TPS ternary blends were, thereafter, injection-molded into pieces and subjected to mechanical, morphological, thermal, and thermomechanical analysis while their potential compostability was also ascertained.

MATERIALS AND METHODS

Materials

Commercial PLA Ingeo™ biopolymer 6201D was purchased from NatureWorks (Minnetonka, MN, USA). This PLA resin has a density of 1.24 g·cm⁻³, a met flow rate (MFR) of 15–30 g·10 min⁻¹ (210 °C, 2.16 kg), a T_g value in the 55–60 °C range, and a T_m value in the 165–175 °C range. This MFR allows the manufacturing of PLA articles by both extrusion and injection molding. PCL was a CapaTM 6800 commercial grade supplied by Perstorp UK Ltd (Warrington, UK) with a density of 1.15 g·cm⁻³, a T_g value of -60 °C, and a T_m value in the 58–62 °C range. The melt flow index (MFI) of PCL is 2–4 g·10 min⁻¹ (160 °C, 2.16 kg). TPS Mater-Bi® NF 866 was obtained from Novamont SPA (Novara, Italy), which is derived from maize starch. Its MFI is 3.5 g·10 min⁻¹ (150 °C, 2.16 kg). This TPS resin presents a density of 1.27 g·cm⁻³, a T_g value ranging from -35 to -40 °C, and a Tm value in the 110–120 °C range.

Manufacturing of Ternary PLA/PCL/TPS Blends

Prior to manufacturing, all the biopolymer pellets were dried at 45 °C for 48 h in a MDEO dehumidifier from Industrial Marsé (Barcelona, Spain). All blends contained 60 wt% PLA while PCL and TPS varied from 0 to 40 wt% to give a series of materials with different properties. The corresponding amounts of each biopolymer is summarized and coded in **Table III.1.2.1**.

Initially, the biopolymer pellets were weighed and manually mixed in a zipper bag. Then, the different mixtures were melt-compounded in a co-rotating twin-screw extruder from Construcciones Mecánicas Dupra S.L. (Alicante, Spain) at a rotating speed of 30 rpm. The screws had a diameter of 25 mm with a length-to-diameter ratio (L/D) of 24. The temperature profile, from the feeding hopper to the extrusion die (circular), was set at 165 °C–170 °C–175 °C–180 °C. The extruded materials were pelletized in an air-knife unit.

The compounded pellets were finally processed by injection molding in a Meteor 270/75 injection machine from Mateu and Solé (Barcelona, Spain). The temperature profile during the injection molding process was: 160 °C (hopper) – 165 °C–170 °C–180 °C (injection nozzle). A clamping force of 75 tons was applied while the cavity filling and cooling time were set at 1 and 10 s, respectively. Pieces with a thickness of 4 mm were produced.

Table III.1.2.1. Composition and coding of the polylactide (PLA), poly(ε-caprolactone) (PCL), and thermoplastic starch (TPS) blends.

Sample	PLA (wt%)	PCL (wt%)	TPS (wt%)
PLA	100	0	0
$PLA_{60}PCL_{40}TPS_0$	60	40	0
$PLA_{60}PCL_{30}TPS_{10}$	60	30	10
$PLA_{60}PCL_{20}TPS_{20}$	60	20	20
$PLA_{60}PCL_{10}TPS_{30}$	60	10	30
$PLA_{60}PCL_0TPS_{40}$	60	0	40

Mechanical Characterization

Tensile and flexural tests were performed on the injection-molded pieces of PLA and its blends using a universal test machine ELIB 50 from S.A.E. Ibertest (Madrid, Spain). Tensile tests were carried out following the guidelines of ISO 527-1:2012 using a cross-head speed rate of 10 mm · min^{-1}. Similarly, flexural tests were carried out according to the standard ISO 178 and the speed rate was 5 mm · min^{-1}. Both tests were carried out at 25 °C and with a load cell of 5 kN. At least six samples of each material were tested.

Shore D hardness of the biopolymer pieces were obtained in a Shore durometer 676-D from J. Bot Instruments (Barcelona, Spain), as recommended by ISO 868:2003. A type-D indenter with a load of 5 kg and an indentation time of 12–15 s was used to stabilize the measurement. The impact-absorbed energy, which is directly related to toughness, was estimated by using the Charpy impact test with a 1-J pendulum from Metrotec S.A. (San Sebastian, Spain). The average energy per unit cross-section area

was obtained on V-notched samples with a radius of 0.25 mm, as recommended by ISO 179-1:2010. Both mechanical tests were carried out at room temperature, that is, 25 °C, and five different samples of each material were tested.

Morphological Characterization

The morphology of the fracture surfaces was studied on the broken samples after the impact tests by field emission scanning electron microscopy (FESEM) in a ZEISS ULTRA 55 microscope from Oxford Instruments (Abingdon, UK). Before placing the samples into the vacuum chamber, all surfaces were covered with a thin metallic layer of gold-palladium by sputtering in an EMITECH mod. SC7620 from Quorum Technologies, Ltd. (East Sussex, UK). The acceleration voltage for the FESEM study was 2 kV.

Solubility

The relative affinity of the biopolymers was estimated by measuring the solubility parameters (δ) according to the Small's method [43]. To consider the blend miscible, the δ values of the polymers should be of the same order. This parameter was determined according to **Equation III.1.2.1**:

$$\delta = \frac{\rho \cdot \sum G}{M_n} \qquad\qquad \textbf{Equation III.1.2.1}$$

where ρ is the density of the polymer, M_n is the molar mass of the repeating unit, and $\sum G$ is the sum of the group contributions to the cohesive energy density.

Thermal Characterization

The thermal transitions of PLA and its blends were obtained by differential scanning calorimetry (DSC) in a Mettler-Toledo 821 calorimeter (Schwerzenbach, Switzerland). An average sample weight comprised in the 5–7 mg range was used for all DSC tests. The thermal program consisted of a first heating step from 25 °C to 190 °C, followed by a cooling step down to 25 °C, and a second heating step up to 300 °C. All heating rates were set at 10 °C $\cdot$ min^{-1}. A constant nitrogen flow-rate of 66 mL $\cdot$ min^{-1} was used to achieve inert atmosphere. Aluminum pans with a total volume capacity of 40 µL were used.

Thermal stability was determined by thermogravimetric analysis (TGA) in a Mettler-Toledo TGA/SDTA 851 thermobalance (Schwerzenbach, Switzerland). Samples with an average size of 5–7 mg were placed into standard alumina crucibles with a total volume of 70 µL and subjected to a heating program from 30 °C to 650 °C at a heating rate of 20 °C $\cdot$ min^{-1} in air atmosphere.

Thermomechanical Characterization

The effect of temperature on the mechanical properties was followed by dynamic mechanical thermal analysis (DMTA) in an oscillatory rheometer AR-G2 from TA Instruments (New Castle, DE, USA). This rheometer is equipped with a special clamp system to work with solid samples in a combined torsion/shear mode. Injection-molded pieces with dimensions of 4 mm × 10 mm × 40 mm were subjected to a

temperature sweep from −80 °C to 120 °C at a constant heating rate of 2 °C · min⁻¹. The selected frequency was 1 Hz and the maximum shear deformation was set at 0.1% (% γ).

The thermomechanical behavior of the ternary blends was also assessed by obtaining the Vicat softening temperature (VST) and the heat deflection temperature (HDT) in a Vicat/HDT station VHDT 20 from Metrotec S.A. (San Sebastián, Spain). VST was obtained following the procedure described in ISO 306, using the B50 heating method and applying a total force of 50 N at a heating rate of 50 °C · h⁻¹. Regarding HDT, ISO 75-1 recommendations were followed. To this end, samples sizing 4 mm × 10 mm × 80 mm were placed between two supports with a total span of 60 mm. After this, a load of 320 g was applied in the center using a heating rate of 120 °C · h⁻¹.

Disintegration Test

A disintegration test in controlled compost conditions was conducted following the guidelines of ISO 20200 at a temperature of 58 °C and a relative humidity (RH) of 55%. For this, squared samples with a size of 30 mm × 30 mm × 1 mm were placed in a carrier bag and buried in a controlled soil with the following composition (in dry weight): sawdust (40 wt%), rabbit-feed (30 wt%), ripe compost (10 wt%), corn starch (10 wt%), saccharose (5 wt%), corn seed oil (4 wt%), and urea (1 wt%). To follow the disintegration process, samples were periodically unburied, washed with distilled water, dried, and weighed in an analytic balance. In order to get a visual evolution of this process, pictures of the disintegration process were also collected. The weight loss due to disintegration in the controlled compost soil was calculated by means of **Equation III.1.2.2:**

$$Weight\ loss(\%) = \left(\frac{W_0 - W_t}{W_0}\right) \cdot 100 \qquad \textbf{Equation III.1.2.2}$$

where Wt is the weight of the sample after a bury time t and W0 is the initial dry weight of the sample. All tests were carried out in triplicate to ensure reliability.

Statistical Analysis

Ternary graphs were plotted using Origin Pro 2015 from OriginLab Corporation (Northampton, MA, USA) with the Ternary Contour function using the average and standard deviation values.

RESULTS

Mechanical Properties

The injection-molded pieces of PLA and of the binary and ternary blends of PLA with PCL and TPS were tested in order to determine their mechanical properties. The tensile strength ($\sigma_{tensile}$) and elongation at break (ε_b) were obtained under tensile conditions, while the flexural modulus ($E_{flexural}$) and flexural strength ($\sigma_{flexural}$) were determined under flexural conditions. **Figure III.1.2.1** shows the resultant stress–strain curves of the PLA-based pieces obtained during the tensile tests (**Figure III.1.2.1a**) and flexural tests (**Figure III.1.2.1b**).
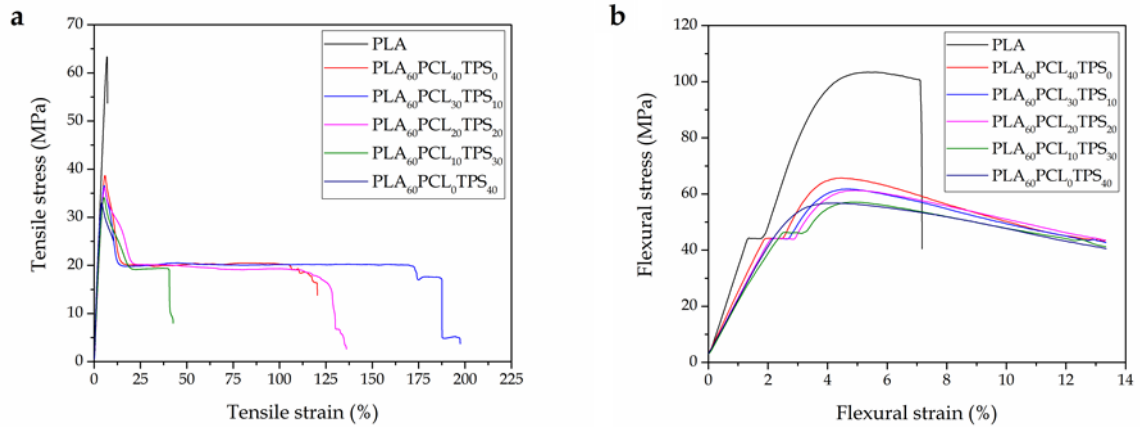
Figure III.1.2.1. Stress–strain curves of the polylactide (PLA), poly(ε-caprolactone) (PCL), and thermoplastic starch (TPS) blend pieces obtained from: (a) tensile test and (b) flexural test.

Figure III.1.2.2 summarizes in ternary graphs the evolution of the tensile properties, that is, ε_b and $\sigma_{tensile}$, of the injection-molded PLA-based pieces with the addition of PCL and TPS. One can observe in **Figure III.1.2.2a** that the neat PLA piece was very fragile, presenting a ε_b value of 4.9%. This value, together with a medium-to-high $\sigma_{tensile}$ value of 63.4 MPa, was responsible for its high brittleness. As one can see, the addition of both PCL and TPS provided a positive effect on the PLA's ductility, but this effect was much more pronounced with PCL due to its intrinsic higher flexibility compared to TPS. In particular, the $PLA_{60}PCL_{30}TPS_{10}$ and $PLA_{60}PCL_{20}TPS_{20}$ blend pieces showed a remarkable increase in elongation at break with values of 196.7% and 134.3%, respectively, which were noticeably higher than that of the neat PLA piece (4.9%). It is also worthy to note that these two blend pieces presented higher ductility than the blend piece containing only PCL, that is, $PLA_{60}PCL_{40}TPS_{0}$, which suggests a synergistic effect of both PCL and TPS on the overall material's ductility. With regard to the mechanical strength of the PLA-based pieces, as shown in **Figure III.1.2.2b**, one can observe that the pieces presented lower $\sigma_{tensile}$ values after the addition of PCL and TPS. In the case of the binary blend piece with PCL, that is, $PLA_{60}PCL_{40}TPS_{0}$, the value of $\sigma_{tensile}$ was reduced to 39.1 MPa, which is remarkable lower than that observed for the neat PLA piece, that is, 63.4 MPa. The binary blend piece with TPS, that is, $PLA_{60}PCL_{0}TPS_{40}$, resulted in even a lower $\sigma_{tensile}$ value, that is, 33.6 MPa. All intermediate compositions showed a proportional decrease depending on the PCL and TPS content. With regard to the blend pieces with 30 wt% and 40 wt% TPS contents, that is, $PLA_{60}PCL_{10}TPS_{30}$ and $PLA_{60}PCL_{0}TPS_{40}$, respectively, the ductility was poor when compared to the ternary blend piece with the highest PCL content, that is, $PLA_{60}PCL_{30}TPS_{10}$. This suggests that both individual PCL and TPS biopolymers have a positive effect on the ductile properties of PLA but the best results were obtained for the ternary blends that combined a high PCL content with low amounts of TPS. The addition of 40 wt% TPS to PLA without PCL, that is, $PLA_{60}PCL_{0}TPS_{40}$, produced the piece with the poorest mechanical performance. Although this piece doubled the ductility of the neat PLA piece, that is, ε_b increased from 4.9 to 8.8%, $\sigma_{tensile}$ also decreased to a value of 33.6 MPa. As previously indicated, the binary blend piece made

of PLA with 40 wt% PCL, that is, $PLA_{60}PCL_{40}TPS_0$, also provided non-optimum results showing a value of ε_b of 114.3%. However, interestingly, the ternary blend pieces containing 20–30 wt% PCL and 20–10 wt% TPS, that is, $PLA_{60}PCL_{20}TPS_{20}$ and $PLA_{60}PCL_{30}TPS_{10}$, offered the best ductile properties with remarkable high ε_b values.
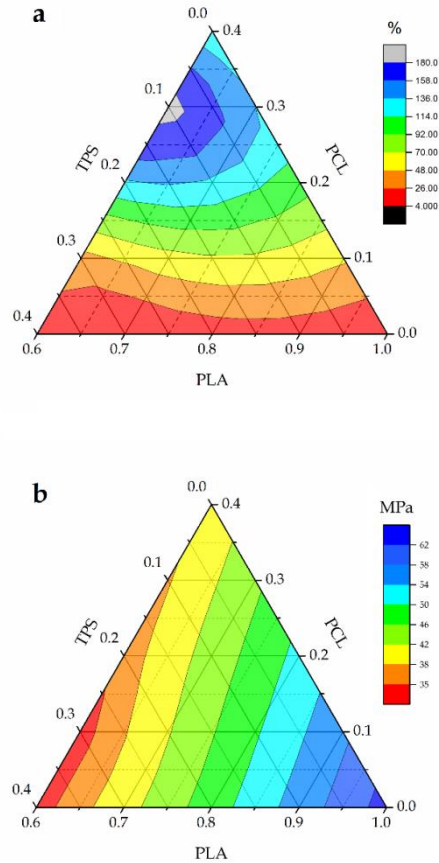
Figure III.1.2.2. Ternary graphs showing the evolution of the polylactide (PLA), poly(ε-caprolactone) (PCL), and thermoplastic starch (TPS) blend pieces in terms of: (**a**) elongation at break (ε_b), and (**b**) tensile strength ($\sigma_{tensile}$).

The above-described observation suggests that a main phase change, from PLA/TPS (comparatively rigid) to PLA/PCL (comparatively flexible), occurs in the ternary blends when relative high contents of PCL and low contents of TPS are blended with PLA. In this sense, other authors have reported that the ductility of PLA/TPS blends can be drastically increased by the incorporation of high amounts of flexible polyesters. For instance, Zhen *et al.* [44] observed that the addition of PBS led to a mechanical strength decrease and ductility increase in TPS/PLA blends. Whereas the tensile strength decreased from 28.54 MPa to 14.60 MPa with the increase of PBS content from 0% to 50 wt%, the elongation at break of the ternary blends also increased from 1.82% to 45.17%. However, the most significant mechanical changes were obtained for PBS contents above 20 wt%, which was ascribed to the main phase changing from TPS/PLA (comparatively rigid) to TPS/PBS (comparatively flexible). Similar results were previously obtained by Ren *et al.* [45] for ternary TPS/PLA/PBAT blends, in which the main phase changed from TPS/PLA (comparatively rigid) to

TPS/PBAT (comparatively flexible) when the PBAT reached contents between 20 and 30 wt%.

Figure III.1.2.3 shows a ternary graph with the evolution of flexural properties of the injection-molded PLA-based pieces, that is, $E_{flexural}$ and $\sigma_{flexural}$, when varying the composition of the blends. With regard to $E_{flexural}$, in Figure 3a it can be seen that a clear reduction was observed after the incorporation of PCL and/or TPS in comparison to the neat PLA piece. In fact, it was reduced from 3200 MPa, for the neat PLA piece, to 2100 MPa, for the binary PLA blend piece with 40 wt% PCL, that is, $PLA_{60}PCL_{40}TPS_{0}$. The value of $E_{flexural}$ followed the same tendency as reported by Ferry *et al.* [46], decreasing as the TPS content increased in the pieces. In particular, $E_{flexural}$ presented the lowest value, that is, 1780 MPa, for the binary blend piece with 40 wt% TPS, that is, $PLA_{60}PCL_{0}TPS_{40}$. As shown in Figure 3b, $\sigma_{flexural}$ decreased from 103 MPa, for the neat PLA piece, down to values of 65 MPa and 57 MPa for the binary blend pieces containing 40 wt% PCL, that is, $PLA_{60}PCL_{40}TPS_{0}$, and 40 wt% TPS, that is, $PLA_{60}PCL_{0}TPS_{40}$, respectively. Intermediate compositions of the ternary blends showed a proportional decrease in the flexural strength as a function of their composition. Similar results were reported by Garcia-Campo *et al.* [47] where intermediate compositions of the ternary PLA/PHB/PCL blends presented an intermediate mechanical behavior between the binary PLA/PHB and PLA/PCL blends.
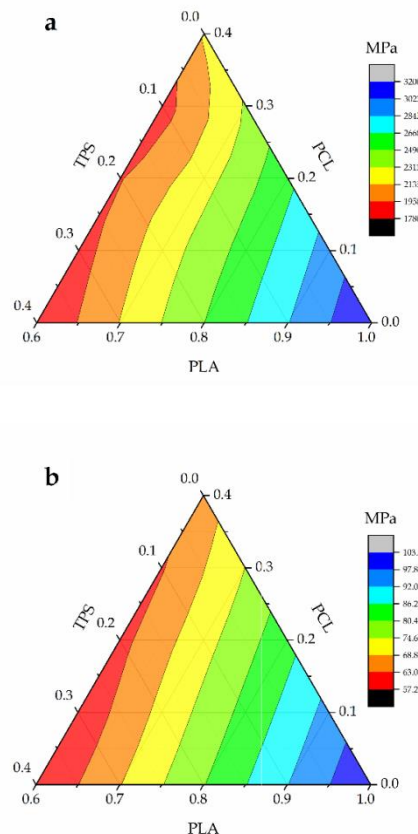
Figure III.1.2.3. Ternary graphs showing the evolution of the polylactide (PLA), poly(ε-caprolactone) (PCL), and thermoplastic starch (TPS) blend pieces in terms of: (a) flexural modulus ($E_{flexural}$), and (b) flexural strength ($\sigma_{flexural}$).

As stated above, one of the main drawbacks of PLA is its low toughness. **Table III.1.2.2** summarizes the main results obtained in Charpy impact test as well as the Shore D hardness values. As it can be observed, the typical energy absorption of the V-notched neat PLA piece was very low, of about 2.14 kJ · m^{-2}. With regard to the binary blend piece with 40 wt% PCL, that is, PLA$_{60}$PCL$_{40}$TPS$_0$, it resulted in an impact energy per unit cross-section of 6.52 kJ · m^{-2}, which represents an increase of more than three times compared to the neat PLA piece. Similar findings were reported for instance by Chen *et al*. [48], showing a remarkable improvement in the PLA toughness by the addition of PCL. The blend pieces with 10–30 wt% PCL also showed relatively high values of impact strength, thus, supporting the good effect of PCL on the overall PLA toughness. It is also important to remark that the binary blend piece with 40 wt% TPS, that is, PLA$_{60}$PCL$_0$TPS$_{40}$, provided increased toughness with an impact strength value of 5.46 kJ · m^{-2}. However, as observed above for other mechanical properties, the effect of PCL was more intense than that of TPS. In relation to the Shore D hardness, the hardness value of the neat PLA piece was 73.1. The Shore D hardness values decreased by approximately 10 units in all the developed blend pieces, thus, reaching a plateau at values of 63–64.

Table III.1.2.2. Impact strength and Shore D hardness of the polylactide (PLA), poly(ε-caprolactone) (PCL), and thermoplastic starch (TPS) blend pieces.

Sample	Impact Strength (kJ m^{-2})	Shore D Hardness
PLA	2.14 ± 0.28	73.1 ± 1.3
PLA$_{60}$PCL$_{40}$TPS$_0$	6.52 ± 0.62	63.0 ± 1.0
PLA$_{60}$PCL$_{30}$TPS$_{10}$	6.46 ± 0.39	63.6 ± 1.1
PLA$_{60}$PCL$_{20}$TPS$_{20}$	6.51 ± 0.27	63.7 ± 1.2
PLA$_{60}$PCL$_{10}$TPS$_{30}$	6.33 ± 0.24	64.3 ± 1.1
PLA$_{60}$PCL$_0$TPS$_{40}$	5.46 ± 0.88	64.6 ± 1.1

Morphology

Figure III.1.2.4 shows the FESEM images corresponding to fracture surfaces of the different PLA/PCL/TPS ternary blend pieces obtained after the impact tests. **Figure III.1.2.4a**, which corresponds to the neat PLA piece, shows the typical fracture surface of a brittle material with low roughness, that is, a smooth and relatively flat surface. Regarding the binary blend piece of PLA with 40 wt% PCL, that is, PLA$_{60}$PCL$_{40}$TPS$_0$, shown in **Figure III.1.2.4b**, a clearly different fracture surface can be observed. In particular, the surface roughness was higher and the flat surface changed to an "island-and-sea" morphology that was based on finely dispersed PCL-rich domains, sizing 1–5 μm, into the PLA matrix. Although PLA and PCL are thermodynamically immiscible [49], this particular structure positively contributed to improving toughness as the enclosed microdroplets of PCL were able to absorb energy, acting as a rubber-like dispersed in a brittle matrix [50]. Plastic deformation provided by PCL can be also observed by the presence of some filaments along the PLA matrix. Addition of 10 wt% TPS in the ternary blend piece, that is, PLA$_{60}$PCL$_{30}$TPS$_{10}$, produced a noticeable change in the morphology, which can be observed in **Figure III.1.2.4c**. In particular, one can observe that the TPS-rich domains presented a higher size, in the 1–35 μm range. A similar morphology was previously reported by Sarazin *et al*. [31]. In **Figure III.1.2.4d–f** one can observe that, as the TPS content increased, the TPS-rich
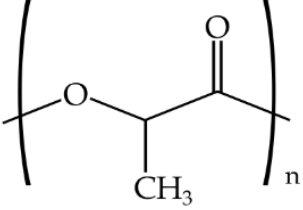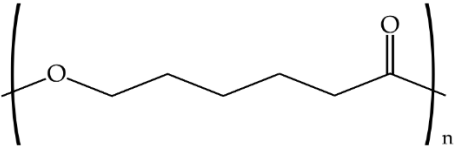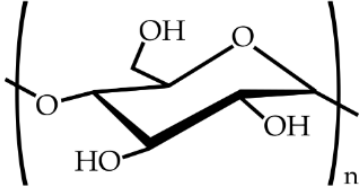
domains increased both in number and size, which is an indication of their poor interfacial interaction with the PLA-based matrix [51]. With regard to the blend pieces with the highest TPS contents, that is, both $PLA_{60}PCL_{10}TPS_{30}$ and $PLA_{60}PCL_0TPS_{40}$, the domains changed from spherical to a ribbon-like morphology due to stretching of the TPS phase during fracture. This morphological changes were also observed by Carmona *et al.* [52] at high TPS contents, that is, 33.3 wt% TPS. Ferri *et al.* [49] have previously related the formation of TPS flakes to the crystalline plane growth or "crystalline lamellae" located at the amylopectin branches that fold up during fracture. In particular, the mechanically-induced flakes structures form parallel-plane blocks and clusters, resulting in granules separated by porous of amorphous areas in which amylose and plasticizers can be allocated [49]. Since PLA is a hydrophobic biopolymer whilst TPS is highly hydrophilic, indeed one of the main drawbacks of TPS is related to its extremely high moisture sensitiveness, this results in the lack (or very low) affinity between the two biopolymers that frequently leads to a strong phase separation [53].
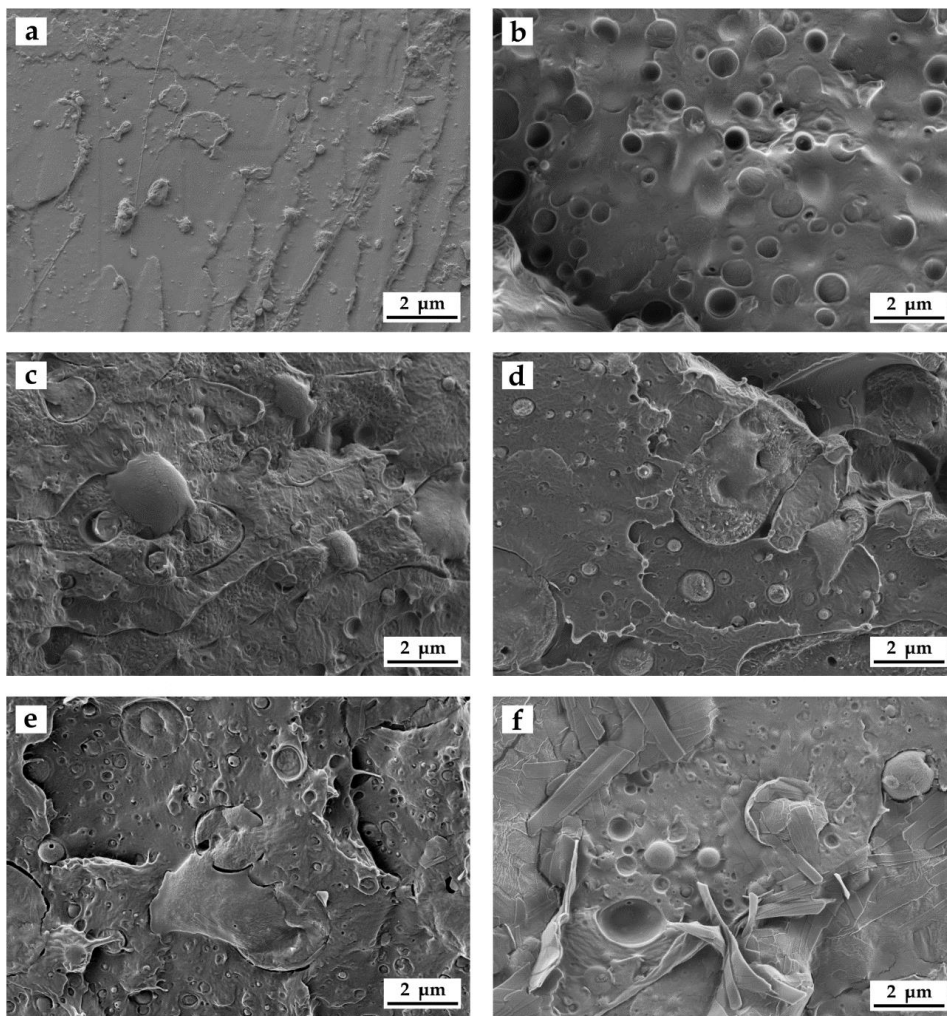
Figure III.1.2.4. Field emission scanning electron microscopy (FESEM) images of the fracture surfaces of the polylactide (PLA), poly(ε-caprolactone) (PCL), and thermoplastic starch (TPS) blend pieces: (a) Neat PLA; (b) $PLA_{60}PCL_{40}TPS_0$; (c) $PLA_{60}PCL_{30}TPS_{10}$; (d) $PLA_{60}PCL_{20}TPS_{20}$; (e) $PLA_{60}PCL_{10}TPS_{30}$; and (f) $PLA_{60}PCL_0TPS_{40}$. Images were taken at 5000x and scale markers are of 2 µm.

To further study the compatibility of the developed blends and also to ascertain their resultant morphologies, the miscibility of the biopolymer formulations was evaluated using the Small's method. According to this, the closer the δ values, the higher the miscibility of the polymers in the blend. **Table III.1.2.3** shows the chemical structure and the resultant δ values of the here-studied biopolymers. One can observe that both PLA and PCL presented a relatively similar δ value while TPS presented a considerably lower value, which support the above-described mechanical and morphological results. This difference in the δ values can be mainly related to the higher density of oxygen atoms in the chemical structure of TPS, mainly hydroxyl groups (–OH), which are certainly responsible for its high hydrophilicity. However, it is also worthy to mention that the δ values obtained for TPS can also vary considerably due to the thermoplastic carbohydrate is obtained by mixing with large quantities of plasticizers. The here-reported δ values are in agreement with Samper *et al*. [54] who obtained values for PLA and TPS of 19.1–20.1 and 8.4, respectively. Similarly, Bordes *et al*. [55] reported a δ value of 17 MPa$^{1/2}$ for PCL.

Table III.1.2.3. Values of the solubility parameters (δ) obtained for polylactide (PLA), poly(ε-caprolactone) (PCL), and thermoplastic starch (TPS).

Biopolymer	Chemical structure	$\sum G$ (cal/cc)$^{1/2}$ [56]	Δ (MPa$^{1/2}$)
PLA		587	20.8
PCL		1010	19.4
TPS		662	11.2

Thermal Properties

Figure III.1.2.5 shows a comparison plot of the DSC curves obtained during the second heating cycle. One can observe that the neat PLA piece showed a T_m value of 169.5 °C. In addition, PLA developed cold crystallization with a cold crystallization temperature (T_{CC}) located at approximately 103 °C and a value of T_g of around 63 °C. In the DSC curve for the binary PLA blend piece with 40 wt% PCL, that is,

$PLA_{60}PCL_{40}TPS_0$, it can be observed that the melt peak intensity for PLA was lower due to the diluting effect of PCL. An additional melting process with a peak located at ~59 °C appeared, which is attributable to the PCL's T_m. This melting process overlapped with the glass transition region of PLA so that it was not possible to separate both processes by conventional DSC. Similar results were also obtained by, for instance, Navarro-Baena *et al*. [57] for PLA/PCL blends using dynamic DSC measurements. In addition, the value of T_m for PLA did not remarkably change in the blends. As the PCL content in the ternary blends decreased, the corresponding peak intensity, that is, the melting enthalpy (ΔH_m), also decreased. In the case of the blend piece with 40 wt% TPS, that is, $PLA_{60}PCL_0TPS_{40}$, it also showed a slight shift of the cold crystallization region towards lower temperatures, which can be ascribed to a plasticizing effect of the PLA matrix by TPS. In this sense, it is worthy to note that TPS contains high amounts of plasticizers, such as glycerol, which can contribute to plasticizing PLA. The resultant plasticization is also evident by observing the PLA's T_g, which moved down to 61.2 °C. The glass transition regions of both PCL and TPS were not registered using the present thermal program since these peaks are located below room temperature, in particular from −50 to −65 °C for PCL [42] and from −75 to 10 °C for TPS [58,59].
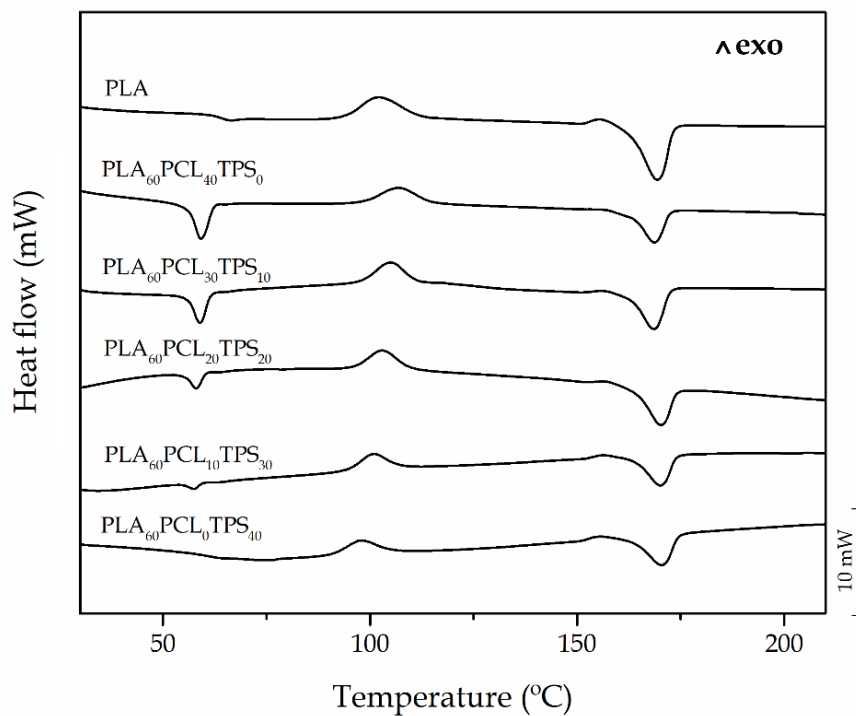
Figure III.1.2.5. Comparative plot of the differential scanning calorimetry (DSC) curves of the polylactide (PLA), poly(ε-caprolactone) (PCL), and thermoplastic starch (TPS) blend pieces.

Figure III.1.2.6 gathers the TGA thermograms (**Figure III.1.2.6a**) and their corresponding first derivative thermogravimetric (DTG) curves (**Figure III.1.2.6b**) for the neat PLA and its binary and ternary blend pieces in the temperature range comprised between 100 °C and 600 °C. Additionally, **Table III.1.2.4** summarizes the main thermal values obtained from these curves. It can be observed that the $PLA_{60}PCL_{30}TPS_{10}$ piece showed the lowest thermal stability, having the decomposition

process in two stages. Its typical thermal degradation parameters, that is, the onset degradation temperature ($T_{5\%}$) and degradation temperature (T_{deg}), were 303.5 °C and 348 °C, respectively. Regarding the neat PLA piece, although it showed a high $T_{5\%}$ value, that is, 322 °C, its degradation occurred in a single step at a relatively low T_{deg} value, that is, 360 °C. In contrast, the $PLA_{60}PCL_{30}TPS_{10}$ piece and, in particular, the $PLA_{60}PCL_{10}TPS_{30}$ piece, improved the thermal stability by having lower mass losses at high temperatures while their T_{deg} values showed an increase of up to 15 °C with regard to the neat PLA. Therefore, the addition of both PCL and TPS led to an increase of the thermal stability of PLA at high temperatures. In addition, the binary and ternary pieces presented a thermal degradation process in two steps. The first mass loss corresponds to the PLA degradation while the second, at higher temperatures, can be attributed to the PCL and TPS decompositions. Additionally, the PLA degradation onset was delayed by the presence of both PCL and TPS. In this sense, Patrício *et al*. [60] reported that the addition of PCL can successfully enhance the thermal stability of PLA. In particular, it was observed an increase in the T_{deg} value from 325 °C, for the neat PLA, up to 334 °C, for binary blends of PLA with PCL at different ratios. Mofokeng *et al*. [61] however suggested the lack of miscibility between PLA and PCL biopolymers, indicating completely independent degradation stages for each phase in the blend.

With regard to the residual mass, it can be observed that TPS contributed to generating a higher amount of residue. Whereas the neat PLA resulted in a very low char content, of approximately 1.5%, this value increased up to 6.4% in the binary blend with 40 wt % TPS, that is, $PLA_{60}PCL_{0}TPS_{40}$. Thus, intermediate compositions led to intermediate char residues. This result can be related to additives incorporated into the biopolymer by the manufacturer.
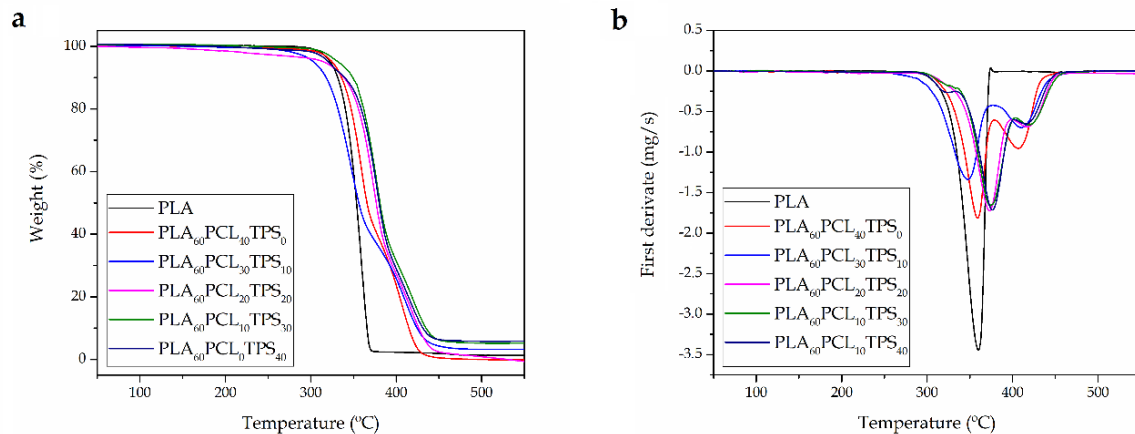
Figure III.1.2.6. Comparative plot of the polylactide (PLA), poly(ε-caprolactone) (PCL), and thermoplastic starch (TPS) blend pieces in terms of: (a) Thermogravimetric analysis (TGA) curves; and (b) first derivative thermogravimetric (DTG) curves.

Table III.1.2.4. Thermal degradation properties in terms of the onset degradation temperature ($T_{5\%}$), degradation temperature (T_{deg}), and residual mass of the polylactide (PLA), poly(ε-caprolactone) (PCL), and thermoplastic starch (TPS) blend pieces.

Sample	$T_{5\%}$ (°C)	T_{deg} (°C)	Residual Mass (%)
PLA	322.67 ± 1.36	359.74 ± 1.58	1.5 ± 0.3
$PLA_{60}PCL_{40}TPS_{0}$	325.03 ± 1.69	358.94 ± 2.14	0.4 ± 0.2
$PLA_{60}PCL_{30}TPS_{10}$	303.50 ± 1.74	347.99±2.36	3.2 ± 0.4
$PLA_{60}PCL_{20}TPS_{20}$	315.33 ± 1.95	373.18 ± 1.74	1.2 ± 0.2
$PLA_{60}PCL_{10}TPS_{30}$	332.06 ± 1.41	373.21 ± 1.95	5.7 ± 0.5
$PLA_{60}PCL_{0}TPS_{40}$	320.34 ± 1.25	376.61 ± 1.78	6.4 ± 0.4

Thermomechanical Properties

DMTA allows estimating the effect of temperature on the mechanical performance. Additionally, it is a more sensitive technique to evaluate potential changes in T_g that, in turn, can be directly related to miscibility in polymer blends [62]. **Figure III.1.2.7** shows the evolution of the storage modulus (G′) and the dynamic damping factor (tan δ) as a function of temperature in the PLA-based pieces. **Figure III.1.2.7a** presents the G′ curves for the neat PLA piece and for the binary and ternary PLA/PCL/TPS blend pieces. G′ is directly related to the stored elastic energy and, consequently, can be directly related to stiffness. Regarding the neat PLA piece, its G′ value was 1.69 GPa at −80 °C. One can also observe that the G′ value increased from 5.6 MPa, at 80 °C, to 76 MPa, above 90 °C. This stiffness increase is ascribed to the cold crystallization process of PLA due to the rearrangement of the biopolyester chains to give a more packed structure [63]. Addition of 40 wt% TPS led to lower G′ values. For instance, the $PLA_{60}PCL_{0}TPS_{40}$ piece presented a G′ value of 1.55 GPa at −80 °C and the same trend that in the case of PLA was observed at higher temperatures. The highest decrease in G′ was obtained for the binary blend piece with 40 wt% PCL, that is, $PLA_{60}PCL_{40}TPS_{0}$, with a value of 1.30 GPa at −80 °C. Therefore, the addition of both PCL and TPS represents an interesting strategy to obtain PLA-based toughened formulations. In relation to the intermediate compositions, for instance the $PLA_{60}PCL_{20}TPS_{20}$ piece, it is worthy to note the remarkable decrease in G′ observed at about −60 °C, which corresponds to the glass transition of PCL. Another important decrease in G′ was observed in the ternary blend pieces in the thermal region located from −20 °C to −30 °C, which is attributable to the glass transition of TPS.
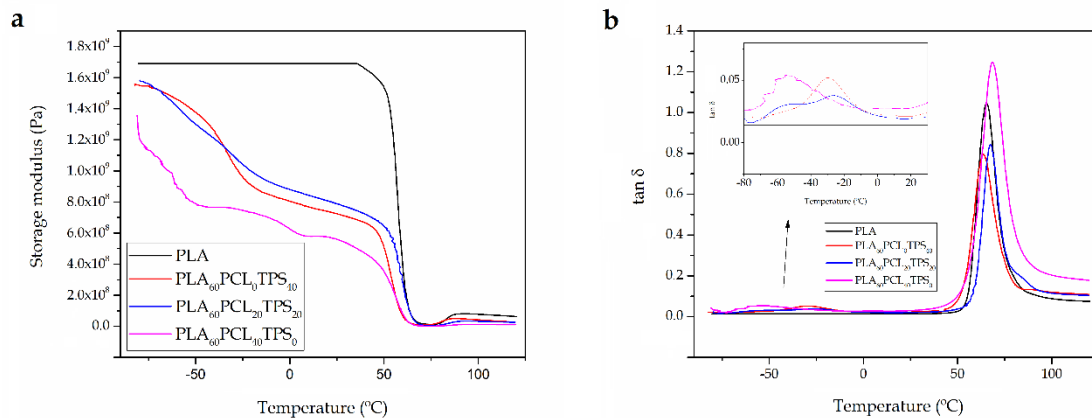
Figure III.1.2.7. Comparative plot of the polylactide (PLA), poly(ε-caprolactone) (PCL), and thermoplastic starch (TPS) blend pieces in terms of: (a) Storage modulus (G′) versus temperature, and (b) dynamic damping factor (tan δ) versus temperature.

Figure III.1.2.7b shows the evolution of tan δ that is, the ratio of G″ to G′, versus temperature. The alpha (α)-relaxation regions of each biopolymer can be clearly identified by the peaks of the tan δ plots, which are related to their T_{gs} and molecular motions [64]. Once can observe that the α-peak of the PLA phase slightly changed in the pieces when it was melt blended with the other biopolymers. In particular, it increased from 65.2 °C, for the neat PLA piece, to 68.4 °C, for the blend piece containing 40 wt% PCL, that is, $PLA_{60}PCL_{40}TPS_0$, while it was reduced to 64.0 °C, for the blend piece containing 40 wt% TPS, that is, $PLA_{60}PCL_0TPS_{40}$. In this sense, Martin *et al*. [65] observed that the α-relaxation region of the PLA phase presented a gradual decrease with increasing the amounts of TPS. In particular, the T_g of PLA decreased from 67 °C, for neat PLA, to about 55 °C, for PLA blends containing 10 wt% TPS. Since it was observed that glycerol has a relatively low effect on the glass transition of PLA, the shift of the α-relaxation to lower temperatures suggested some interaction between TPS and PLA and, as a result, partial miscibility between the two biopolymers was inferred. However, since this reduction was moderate, a small degree of miscibility between the blend components was concluded. In relation PCL, Mittal *et al*. [66] showed that the α-relaxation region of PLA occurred at higher temperatures as the amount of PCL in the binary blends was increased. In particular, the α-peak of the neat PLA increased from approximately 55 °C to 61 °C. This effect was ascribed by the authors to a better intermixing of the phases in the presence of PCL. Additionally, one can also observe that the α -peak values for the PCL- and TPS-rich phases were located at approximately −55 °C and −30 °C, respectively.

Furthermore, one can observe in **Table III.1.2.5** that the addition of both PCL and TPS yielded lower VST and HDT values than those observed for the neat PLA piece. These results are in agreement with the above-described mechanical and thermomechanical results due to both PCL and TPS provided increased ductility and, subsequently, the material's ability to deform was remarkably increased.

Table III.1.2.5. Thermomechanical properties in terms of the Vicat softening temperature (VST) and heat deflection temperature (HDT) of the polylactide (PLA), poly(ε-caprolactone) (PCL), and thermoplastic starch (TPS) blend pieces.

Sample	VST (°C)	HDT (°C)
PLA	53.2 ± 0.5	47.9 ± 0.5
$PLA_{60}PCL_{40}TPS_0$	51.2 ± 0.6	43.2 ± 0.4
$PLA_{60}PCL_{30}TPS_{10}$	50.2 ± 0.5	46.4 ± 0.5
$PLA_{60}PCL_{20}TPS_{20}$	48.8 ± 0.3	46.6 ± 0.4
$PLA_{60}PCL_{10}TPS_{30}$	47.1 ± 0.5	46.2 ± 0.4
$PLA_{60}PCL_0TPS_{40}$	47.4 ± 0.4	46.8 ± 0.3

Disintegration in Controlled Compost Soil

Figure III.1.2.8 shows the percentage of weight loss as a function of the elapsed time during disintegration in a controlled compost soil of the neat PLA piece and of its binary and ternary blend pieces with PCL and TPS. One can observe that all of the PLA-based pieces presented a significant loss of mass after only one week while they were fully disintegrated at the end of the test, that is, after a period of 28 days. The sample with the highest degradation rate was the neat PLA piece. In fact, after 21 days in the controlled compost soil, this sample already lost 100% of its initial weight. The addition of both PCL and TPS slightly reduced the biodegradation rate of PLA and this effect was more marked for the binary blend pieces, that is, $PLA_{60}PCL_{40}TPS_0$ and $PLA_{60}PCL_0TPS_{40}$, than for the ternary blend pieces. For instance, after 21 days, whereas the ternary $PLA_{60}PCL_{20}TPS_{20}$ piece showed a mass loss of 89.9%, this value was only 57.3% for the binary $PLA_{60}PCL_0TPS_{40}$ piece. This suggests that the biodegradation rate of PCL and TPS was lower than that observed for PLA in the selected compost soil. Therefore, the use of ternary blends improved the compostability profile of the binary blends made of PLA with PCL or TPS since, as shown during the morphological analysis, the regions of the secondary phases in the ternary blend pieces were smaller. Previous research studies, however, have reported that the PCL and TPS degradation rates are faster than that of PLA [67,68]. These differences can be ascribed to the type of culture present in the medium during disintegration. For instance, Thakore *et al*. [69] described that the different compost soils from municipal yard waste sites, which generally contains various types of microorganisms, can strongly affect the biodegradation profile of compostable polymers in a different manner. In particular, it was observed that the TPS degradation pathway was mainly produced due to two enzymes secreted by the microbes. In particular, esterase cleaves the ester bond, releasing free phthalic acid and starch, while amylase acts on starch to produce reducing sugars.
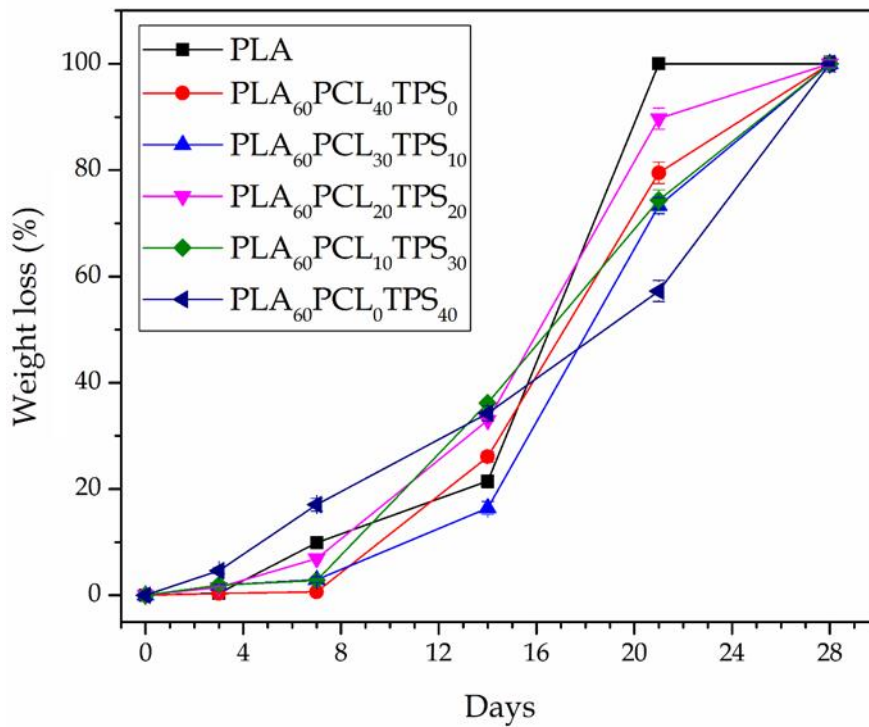
Figure III.1.2.8. Evolution plot of the percentage of weight loss as a function of the elapsed time during disintegration in controlled compost soil of the polylactide (PLA), poly(ε-caprolactone) (PCL), and thermoplastic starch (TPS) blend pieces.

Figure III.1.2.9 shows the visual aspect of the PLA-based pieces during the disintegration test, giving some further information about the compostability profile of each material. After analyzing the appearance of the samples, one can conclude that all the here-prepared PLA-based pieces were either fully disintegrated or significantly fragmented after 21 days. Regarding PLA, one can observe that its piece become opaque after only 3 days of incubation in the controlled compost soil due to hydrolysis of the biopolyester [70]. Although a slight weight decrease was observed, no significant alterations from a physical point of view (e.g. color changes, presence of micro-cracks, etc.) were seen during the first week. Over the second week, however, the PLA-based pieces revealed significant evidences of biodegradation. At this incubation time, the PLA piece as well as the $PLA_{60}PCL_{20}TPS_{20}$ and $PLA_{60}PCL_{10}TPS_{30}$ ternary blend pieces were extensively biodegraded producing small fragments. Although the other blend pieces, that is, the $PLA_{60}PCL_{40}TPS_0$, $PLA_{60}PCL_{10}TPS_{30}$, and $PLA_{60}PCL_0TPS_{40}$, remained into a single part, they visually presented a clear weight loss and develop a dark brown color. After 21 days, the neat PLA piece was fully biodegraded while the binary and ternary blend pieces were considerably disintegrated into small fragments, with the exemption of the binary blend piece of PLA containing 40 wt% TPS, that is, $PLA_{60}PCL_0TPS_{40}$. Therefore, as explained above, the addition of PCL and TPS slightly slowed down the degradation process of PLA. This delay was mostly visible in the PLA-based pieces with high contents of either PCL or TPS, thought in the case of the plasticized carbohydrate it was even more pronounced.
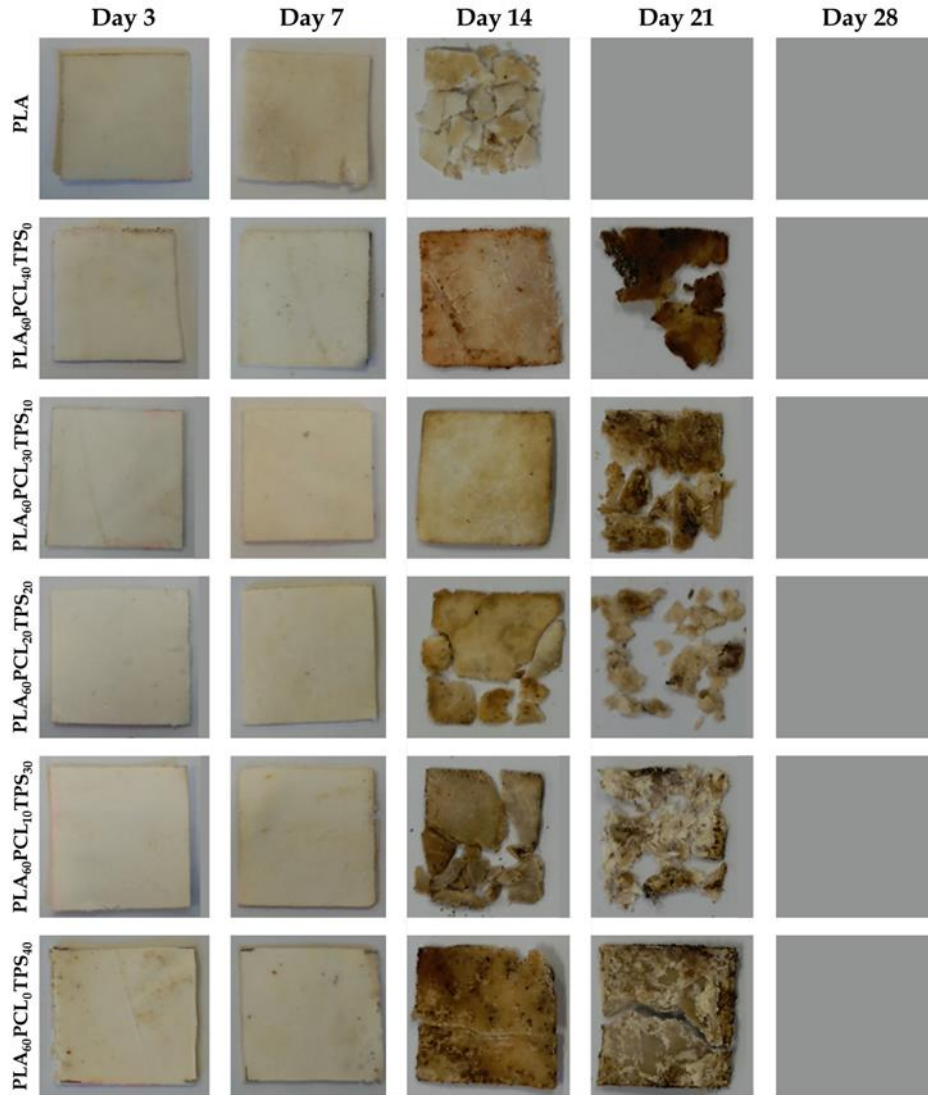
Figure III.1.2.9. Visual aspect at selected disintegration times of the polylactide (PLA), poly(ε-caprolactone) (PCL), and thermoplastic starch (TPS) blend pieces.

DISCUSSION

Binary and ternary blend pieces based on PLA with different PCL and TPS contents are herein presented as novel sustainable plastics with improved ductility and toughness. In the here-performed tensile and flexural tests, it was observed that the addition of PCL and TPS provided a positive effect on flexibility and impact strength but also a slight reduction in the mechanical resistance properties. Although both biopolymers individually produced a positive effect on the ductile properties of PLA, the best results were obtained for the ternary blends that combined high PCL contents with low amounts of TPS. In particular, the ternary blend piece containing 30 wt% PCL and 10 wt% TPS, that is, $PLA_{60}PCL_{30}TPS_{10}$, showed the highest flexibility with a ε_b value of 196.7%, approximately 40 times higher than that observed for the neat PLA piece. Similar findings were obtained in the impact tests, in which the ternary blends with the highest PCL contents provided toughness increases of more than three times

in comparison to the neat PLA piece. During the thermal analysis, DSC confirmed that the here-prepared binary and ternary blends are immiscible while TGA revealed that the ternary blend pieces present slightly higher thermal stability than the neat PLA piece and the binary blend pieces. Thermomechanical analysis, performed by means of DMTA, as well as VST and HDT measurements, also demonstrated that the blend pieces presented lower stiffness since both PCL and TPS effectively softened PLA. Finally, during the disintegration test in a controlled compost soil, it was observed that all PLA-based pieces presented a significant mass loss after only two weeks while the blend pieces disintegrated into small fragments after a period of 21 days. At the end of the test, that is, after 28 days, all pieces fully biodegraded. Although the addition of both PCL and TPS slightly reduced the PLA biodegradation rate, this impairment was more marked for the binary blend pieces, that is, $PLA_{60}PCL_{40}TPS_0$ and $PLA_{60}PCL_0TPS_{40}$. Interestingly, the ternary blend pieces with intermediate contents of PCL and TPS presented a biodegradation rate close to that observed for the neat PLA piece.

CONCLUSIONS

The development of ternary blends based on PLA with relatively high contents of PCL and low contents TPS can be successfully applied for the development of compostable plastics with improved ductility and toughness. Potential uses of the here-described injection-molded pieces can be found in, for instance, the rigid packaging industry where sustainable trays, lids, and bottles with high mechanical resistance, but also sufficient impact strength, are currently required.

Acknowledgments

REFERENCES

1. Hopewell, J., R. Dvorak and E. Kosior, *Plastics recycling: challenges and opportunities.* Philosophical Transactions of the Royal Society B: Biological Sciences, 2009. **364**(1526): 2115-2126.
2. Quiles-Carrillo, L., N. Montanes, D. Garcia-Garcia, A. Carbonell-Verdu, R. Balart and S. Torres-Giner, *Effect of different compatibilizers on injection-molded green composite pieces based on polylactide filled with almond shell flour.* Composites Part B: Engineering, 2018. **147**: 76-85.
3. Nampoothiri, K.M., N.R. Nair and R.P. John, *An overview of the recent developments in polylactide (PLA) research.* Bioresource technology, 2010. **101**(22): 8493-8501.
4. Kumar, N. and D. Das, *Fibrous biocomposites from nettle (Girardinia diversifolia) and poly (lactic acid) fibers for automotive dashboard panel application.* Composites Part B: Engineering, 2017. **130**: 54-63.
5. Bouzouita, A., D. Notta-Cuvier, J.-M. Raquez, F. Lauro and P. Dubois, *Poly (lactic acid)-Based Materials for Automotive Applications.* 2017.
6. Garces, J.M., D.J. Moll, J. Bicerano, R. Fibiger and D.G. McLeod, *Polymeric nanocomposites for automotive applications.* Advanced Materials, 2000. **12**(23): 1835-1839.
7. Lasprilla, A.J., G.A. Martinez, B.H. Lunelli, A.L. Jardini and R. Maciel Filho, *Poly-lactic acid synthesis for application in biomedical devices—A review.* Biotechnology advances, 2012. **30**(1): 321-328.

8. Santos, D., C.O. Correia, D.M. Silva, P.S. Gomes, M.H. Fernandes, J.D. Santos and V. Sencadas, *Incorporation of glass-reinforced hydroxyapatite microparticles into poly (lactic acid) electrospun fibre mats for biomedical applications.* Materials Science and Engineering: C, 2017. **75**: 1184-1190.

9. Muller, J., C. González-Martínez and A. Chiralt, *Combination of poly (lactic) acid and starch for biodegradable food packaging.* Materials, 2017. **10**(8): 952.

10. Kakroodi, A.R., Y. Kazemi, M. Nofar and C.B. Park, *Tailoring poly (lactic acid) for packaging applications via the production of fully bio-based in situ microfibrillar composite films.* Chemical Engineering Journal, 2017. **308**: 772-782.

11. Kao, C.-T., C.-C. Lin, Y.-W. Chen, C.-H. Yeh, H.-Y. Fang and M.-Y. Shie, *Poly (dopamine) coating of 3D printed poly (lactic acid) scaffolds for bone tissue engineering.* Materials Science and Engineering: C, 2015. **56**: 165-173.

12. Chen, Q., J.D. Mangadlao, J. Wallat, A. De Leon, J.K. Pokorski and R.C. Advincula, *3D Printing Biocompatible Polyurethane/Poly (lactic acid)/Graphene Oxide Nanocomposites: Anisotropic Properties.* ACS applied materials & interfaces, 2017. **9**(4): 4015-4023.

13. Quiles-Carrillo, L., S. Duart, N. Montanes, S. Torres-Giner and R. Balart, *Enhancement of the mechanical and thermal properties of injection-molded polylactide parts by the addition of acrylated epoxidized soybean oil.* Materials and Design, 2018. **140**: 54-63.

14. Torres-Giner, S., L. Gil, L. Pascual-Ramírez and J.A. Garde-Belza, *Packaging: Food Waste Reduction*, in *Encyclopedia of Polymer Applications*, M. Mishra, Editor. 2018, CRC Press, Taylor and Francis Group: Boca Raton, FL, US.

15. Mooney, D., C. Breuer, K. McNamara, J. Vacanti and R. Langer, *Fabricating tubular devices from polymers of lactic and glycolic acid for tissue engineering.* Tissue engineering, 1995. **1**(2): 107-118.

16. Elsawy, M.A., K.-H. Kim, J.-W. Park and A. Deep, *Hydrolytic degradation of polylactic acid (PLA) and its composites.* Renewable and Sustainable Energy Reviews, 2017. **79**: 1346-1352.

17. Pluta, M. and E. Piorkowska, *Tough crystalline blends of polylactide with block copolymers of ethylene glycol and propylene glycol.* Polymer Testing, 2015. **46**: 79-87.

18. Maiza, M., M.T. Benaniba, G. Quintard and V. Massardier-Nageotte, *Biobased additive plasticizing Polylactic acid (PLA).* Polímeros, 2015. **25**(6): 581-590.

19. Ljungberg, N. and B. Wesslen, *The effects of plasticizers on the dynamic mechanical and thermal properties of poly (lactic acid).* Journal of Applied Polymer Science, 2002. **86**(5): 1227-1234.

20. Darie-Niţă, R.N., C. Vasile, A. Irimia, R. Lipşa and M. Râpă, *Evaluation of some eco-friendly plasticizers for PLA films processing.* Journal of Applied Polymer Science, 2016. **133**(13).

21. Quiles-Carrillo, L., M. Blanes-Martínez, N. Montanes, O. Fenollar, S. Torres-Giner and R. Balart, *Reactive toughening of injection-molded polylactide pieces using maleinized hemp seed oil.* European Polymer Journal, 2018. **98**: 402-410.

22. Ferri, J.M., D. Garcia-Garcia, N. Montanes, O. Fenollar and R. Balart, *The effect of maleinized linseed oil as biobased plasticizer in poly (lactic acid)-based formulations.* Polymer International, 2017. **66**(6): 882-891.

23. Carbonell-Verdu, A., D. Garcia-Garcia, F. Dominici, L. Torre, L. Sanchez-Nacher and R. Balart, *PLA films with improved flexibility properties by using maleinized cottonseed oil.* European Polymer Journal, 2017. **91**: 248-259.

24. Quiles-Carrillo, L., N. Montanes, C. Sammon, R. Balart and S. Torres-Giner, *Compatibilization of highly sustainable polylactide/almond shell flour composites by reactive extrusion with maleinized linseed oil.* Industrial Crops and Products, 2018. **111**: 878-888.

25. Gerard, T. and T. Budtova, *Morphology and molten-state rheology of polylactide and polyhydroxyalkanoate blends.* European polymer journal, 2012. **48**(6): 1110-1117.

26. Yu, L., K. Dean and L. Li, *Polymer blends and composites from renewable resources.* Progress in polymer science, 2006. **31**(6): 576-602.

27.   Gug, J.-I., B. Tan, J. Soule, M. Downie, J. Barrington and M. Sobkowicz, *Analysis of models predicting morphology transitions in reactive twin-screw extrusion of bio-based polyester/polyamide blends.* International Polymer Processing, 2017. **32**(3): 363-377.

28.   Stoclet, G., R. Seguela and J.-M. Lefebvre, *Morphology, thermal behavior and mechanical properties of binary blends of compatible biosourced polymers: polylactide/polyamide11.* Polymer, 2011. **52**(6): 1417-1425.

29.   Al-Itry, R., K. Lamnawar and A. Maazouz, *Improvement of thermal stability, rheological and mechanical properties of PLA, PBAT and their blends by reactive extrusion with functionalized epoxy.* Polymer Degradation and Stability, 2012. **97**(10): 1898-1914.

30.   Wu, N. and H. Zhang, *Mechanical properties and phase morphology of super-tough PLA/PBAT/EMA-GMA multicomponent blends.* Materials Letters, 2017. **192**: 17-20.

31.   Sarazin, P., G. Li, W.J. Orts and B.D. Favis, *Binary and ternary blends of polylactide, polycaprolactone and thermoplastic starch.* Polymer, 2008. **49**(2): 599-609.

32.   Valerio, O., M. Misra and A.K. Mohanty, *Statistical design of sustainable thermoplastic blends of poly (glycerol succinate-co-maleate)(PGSMA), poly (lactic acid)(PLA) and poly (butylene succinate)(PBS).* Polymer Testing, 2017.

33.   Ostafinska, A., I. Fortelný, J. Hodan, S. Krejčíková, M. Nevoralová, J. Kredatusová, Z. Kruliš, J. Kotek and M. Šlouf, *Strong synergistic effects in PLA/PCL blends: Impact of PLA matrix viscosity.* Journal of the mechanical behavior of biomedical materials, 2017. **69**: 229-241.

34.   Wu, D., D. Lin, J. Zhang, W. Zhou, M. Zhang, Y. Zhang, D. Wang and B. Lin, *Selective localization of nanofillers: effect on morphology and crystallization of PLA/PCL blends.* Macromolecular Chemistry and Physics, 2011. **212**(6): 613-626.

35.   Liu, H., W. Song, F. Chen, L. Guo and J. Zhang, *Interaction of microstructure and interfacial adhesion on impact performance of polylactide (PLA) ternary blends.* Macromolecules, 2011. **44**(6): 1513-1522.

36.   Ren, J., H. Fu, T. Ren and W. Yuan, *Preparation, characterization and properties of binary and ternary blends with thermoplastic starch, poly (lactic acid) and poly (butylene adipate-co-terephthalate).* Carbohydrate polymers, 2009. **77**(3): 576-582.

37.   Zolali, A.M. and B.D. Favis, *Partial to complete wetting transitions in immiscible ternary blends with PLA: the influence of interfacial confinement.* Soft Matter, 2017. **13**(15): 2844-2856.

38.   Matzinos, P., V. Tserki, A. Kontoyiannis and C. Panayiotou, *Processing and characterization of starch/polycaprolactone products.* Polymer Degradation and Stability, 2002. **77**(1): 17-24.

39.   Maglio, G., M. Malinconico, A. Migliozzi and G. Groeninckx, *Immiscible Poly (L-lactide)/Poly (ε-caprolactone) Blends: Influence of the Addition of a Poly (L-lactide)-Poly (oxyethylene) Block Copolymer on Thermal Behavior and Morphology.* Macromolecular chemistry and physics, 2004. **205**(7): 946-950.

40.   Forssell, P., J. Mikkilä, T. Suortti, J. Seppälä and K. Poutanen, *Plasticization of Barley Starch with Glycerol and Water.* Journal of Macromolecular Science, Part A, 1996. **33**(5): 703-715.

41.   Raquez, J.M., Y. Nabar, M. Srinivasan, B.Y. Shin, R. Narayan and P. Dubois, *Maleated thermoplastic starch by reactive extrusion.* Carbohydrate Polymers, 2008. **74**(2): 159-169.

42.   Averous, L., L. Moro, P. Dole and C. Fringant, *Properties of thermoplastic blends: starch–polycaprolactone.* Polymer, 2000. **41**(11): 4157-4167.

43.   Odelius, K., M. Ohlson, A. Höglund and A.C. Albertsson, *Polyesters with small structural variations improve the mechanical properties of polylactide.* Journal of Applied Polymer Science, 2013. **127**(1): 27-33.

44.   Zhen, Z., S. Ying, F. Hongye, R. Jie and R. Tianbin, *Preparation, Characterization and Properties of Binary and Ternary Blends with Thermoplastic Starch, Poly(Lactic Acid) and Poly(Butylene Succinate).* Polymers from Renewable Resources, 2011. **2**(2): 49-62.

45. Ren, J., H. Fu, T. Ren and W. Yuan, *Preparation, characterization and properties of binary and ternary blends with thermoplastic starch, poly(lactic acid) and poly(butylene adipate-co-terephthalate).* Carbohydrate Polymers, 2009. **77**(3): 576-582.

46. Ferri, J., D. Garcia-Garcia, L. Sánchez-Nacher, O. Fenollar and R. Balart, *The effect of maleinized linseed oil (MLO) on mechanical performance of poly (lactic acid)-thermoplastic starch (PLA-TPS) blends.* Carbohydrate polymers, 2016. **147**: 60-68.

47. García-Campo, M., T. Boronat, L. Quiles-Carrillo, R. Balart and N. Montanes, *Manufacturing and Characterization of Toughened Poly(lactic acid) (PLA) Formulations by Ternary Blends with Biopolyesters.* Polymers, 2018. **10**(1): 3.

48. Chen, C.-C., J.-Y. Chueh, H. Tseng, H.-M. Huang and S.-Y. Lee, *Preparation and characterization of biodegradable PLA polymeric blends.* Biomaterials, 2003. **24**(7): 1167-1173.

49. Ferri, J.M., O. Fenollar, A. Jorda-Vilaplana, D. García-Sanoguera and R. Balart, *Effect of miscibility on mechanical and thermal properties of poly (lactic acid)/polycaprolactone blends.* Polymer International, 2016. **65**(4): 453-463.

50. Tang, L., L. Wang, P. Chen, J. Fu, P. Xiao, N. Ye and M. Zhang, *Toughness of ABS/PBT blends: The relationship between composition, morphology, and fracture behavior.* Journal of Applied Polymer Science, 2018. **135**(13).

51. Muthuraj, R., M. Misra and A.K. Mohanty, *Biodegradable compatibilized polymer blends for packaging applications: A literature review.* Journal of Applied Polymer Science, 2018. **135**(24): 45726.

52. Carmona, V.B., A.C. Corrêa, J.M. Marconcini and L.H.C. Mattoso, *Properties of a biodegradable ternary blend of thermoplastic starch (TPS), poly (ε-caprolactone)(PCL) and poly (lactic acid)(PLA).* Journal of Polymers and the Environment, 2015. **23**(1): 83-89.

53. Kim, H.-Y., S.S. Park and S.-T. Lim, *Preparation, characterization and utilization of starch nanoparticles.* Colloids and Surfaces B: Biointerfaces, 2015. **126**: 607-620.

54. Samper, M., A. Marina Patricia, F. Santiago and L. Juan, *Influence of biodegradable materials in the recycled polystyrene.* Journal of Applied Polymer Science, 2014. **131**(23).

55. Bordes, C., V. Fréville, E. Ruffin, P. Marote, J. Gauvrit, S. Briançon and P. Lantéri, *Determination of poly (ε-caprolactone) solubility parameters: Application to solvent substitution in a microencapsulation process.* International journal of pharmaceutics, 2010. **383**(1-2): 236-243.

56. Small, P., *Some factors affecting the solubility of polymers.* Journal of Applied Chemistry, 1953. **3**(2): 71-80.

57. Navarro-Baena, I., V. Sessini, F. Dominici, L. Torre, J.M. Kenny and L. Peponi, *Design of biodegradable blends based on PLA and PCL: From morphological, thermal and mechanical studies to shape memory behavior.* Polymer Degradation and Stability, 2016. **132**: 97-108.

58. Averous, L. and N. Boquillon, *Biocomposites based on plasticized starch: thermal and mechanical behaviours.* Carbohydrate Polymers, 2004. **56**(2): 111-122.

59. Zhang, Y., C. Rempel and Q. Liu, *Thermoplastic Starch Processing and Characteristics—A Review.* Critical Reviews in Food Science and Nutrition, 2014. **54**(10): 1353-1370.

60. Patrício, T. and P. Bártolo, *Thermal stability of PCL/PLA blends produced by physical blending process.* Procedia Engineering, 2013. **59**: 292-297.

61. Mofokeng, J. and A. Luyt, *Morphology and thermal degradation studies of melt-mixed poly (lactic acid)(PLA)/poly (ε-caprolactone)(PCL) biodegradable polymer blend nanocomposites with TiO 2 as filler.* Polymer Testing, 2015. **45**: 93-100.

62. Quiles-Carillo, L., N. Montanes, J.M. Lagaron, R. Balart and S. Torres-Giner, *In Situ Compatibilization of Biopolymer Ternary Blends by Reactive Extrusion with Low-Functionality Epoxy-Based Styrene–Acrylic Oligomer.* Journal of Polymers and the Environment, 2018. DOI: 10.1007/s10924-018-1324-2.

63. Garcia-Campo, M.J., L. Quiles-Carrillo, J. Masia, M.J. Reig-Pérez, N. Montanes and R. Balart, *Environmentally friendly compatibilizers from soybean oil for ternary blends of poly (lactic acid)-PLA, poly (ε-caprolactone)-PCL and poly (3-hydroxybutyrate)-PHB.* Materials, 2017. **10**(11): 1339.

64. Torres-Giner, S., N. Montanes, O. Fenollar, D. García-Sanoguera and R. Balart, *Development and optimization of renewable vinyl plastisol/wood flour composites exposed to ultraviolet radiation.* Materials & Design, 2016. **108**: 648-658.

65. Martin, O. and L. Averous, *Poly (lactic acid): plasticization and properties of biodegradable multiphase systems.* Polymer, 2001. **42**(14): 6209-6219.

66. Mittal, V., T. Akhtar and N. Matsko, *Mechanical, thermal, rheological and morphological properties of binary and ternary blends of PLA, TPS and PCL.* Macromolecular Materials and Engineering, 2015. **300**(4): 423-435.

67. Di Franco, C., V. Cyras, J. Busalmen, R. Ruseckaite and A. Vázquez, *Degradation of polycaprolactone/starch blends and composites with sisal fibre.* Polymer Degradation and Stability, 2004. **86**(1): 95-103.

68. Iovino, R., R. Zullo, M. Rao, L. Cassar and L. Gianfreda, *Biodegradation of poly (lactic acid)/starch/coir biocomposites under controlled composting conditions.* Polymer Degradation and Stability, 2008. **93**(1): 147-157.

69. Thakore, I., S. Desai, B. Sarawade and S. Devi, *Studies on biodegradability, morphology and thermo-mechanical properties of LDPE/modified starch blends.* European Polymer Journal, 2001. **37**(1): 151-160.

70. Sikorska, W., M. Musiol, B. Nowak, J. Pajak, S. Labuzek, M. Kowalczuk and G. Adamus, *Degradability of polylactide and its blend with poly [(R, S)-3-hydroxybutyrate] in industrial composting and compost extract.* International Biodeterioration & Biodegradation, 2015. **101**: 32-41.

III.1.3. In Situ Compatibilization of Biopolymer Ternary Blends by Reactive Extrusion with Low-Functionality Epoxy-Based Styrene Acrylic Oligomer

L. Quiles-Carrillo[1], N. Montanes[1], J.M. Lagaron[2], R. Balart[1], S. Torres-Giner[1,2]

[1] Technological Institute of Materials (ITM), Universitat Politècnica de València (UPV), Plaza Ferrándiz y Carbonell 1, Alcoy 03801, Spain

[2] Novel Materials and Nanotechnology Group, Institute of Agrochemistry and Food Technology (IATA), Spanish Council for Scientific Research (CSIC), Calle Catedrático Agustín Escardino Benlloch 7, Paterna 46980, Spain

ORIGINAL PAPER

In Situ Compatibilization of Biopolymer Ternary Blends by Reactive Extrusion with Low-Functionality Epoxy-Based Styrene–Acrylic Oligomer

L. Quiles-Carrillo[1] · N. Montanes[1] · J. M. Lagaron[2] · R. Balart[1] · S. Torres-Giner[1,2]

Abstract

The present study reports on the use of low-functionality epoxy-based styrene–acrylic oligomer (ESAO) to compatibilize immiscible ternary blends made of poly(3-hydroxybutyrate-*co*-3-hydroxyvalerate) (PHBV), polylactide (PLA), and poly(butylene adipate-*co*-terephthalate) (PBAT). The addition during melt processing of low-functionality ESAO at two parts per hundred resin (phr) of biopolymer successfully changed the soften inclusion phase in the blend system to a thinner morphology, yielding biopolymer ternary blends with higher mechanical ductility and also improved oxygen barrier performance. The compatibilization achieved was ascribed to the in situ formation of a newly block terpolymer, i.e. PHBV-*b*-PLA-*b*-PBAT, which was produced at the blend interface by the reaction of the multiple epoxy groups present in ESAO with the functional terminal groups of the biopolymers. This chemical reaction was mainly linear due to the inherently low functionality of ESAO and the more favorable reactivity of the epoxy groups with the carboxyl groups of the biopolymers, which avoided the formation of highly branched and/or cross-linked structures and thus facilitated the films processability. Therefore, the reactive blending of biopolymers at different mixing ratios with low-functionality ESAO represents a straightforward methodology to prepare sustainable plastics at industrial scale with different physical properties that can be of interest in, for instance, food packaging applications.

Keywords PHBV · PLA · PBAT · Reactive extrusion · Biopolymer blends

Introduction

The future scarcity of petroleum and the strong awareness of post-consumer plastic wastes are the two main drivers behind the interest, at both academic and industrial levels, in biopolymers. The terms "bio-based polymers" and "biodegradable polymers" are extensively used in the polymer literature when referring to biopolymers [1]. Bio-based polymers include both naturally occurring macromolecules, such as proteins and carbohydrates, and polymers synthetized from renewable monomers. Biodegradable polymers undergo rapidly and completely disintegration through the action of enzymes and/or chemical deterioration associated with living microorganisms. Articles fully made of biodegradable polymers can be also compostable according to the specifications of international standards (e.g. EN 13432 and ASTM D6400). Bio-based polymers can be either non-degradable, such as bio-based polyethylene (bio-PE) [2] and bio-based polyamides (bio-PAs) [3], or biodegradable polymers. Among biodegradable polymers, bio-based aliphatic polyesters, including polyhydroxyalkanoates (PHAs) and polylactides (PLAs), play a predominant role due to their potentially hydrolysable ester bonds. Some biodegradable polyesters can be produced from non-renewable petroleum resources, which is the case of, for instance, poly(butylene succinate) (PBS), poly(butylene succinate-*co*-adipate) (PBSA), and poly(butylene adipate-*co*-terephthalate) (PBAT) [4].

PHAs are aliphatic polyesters produced by bacterial fermentation with the highest potential to replace polyolefins. PHAs generally consist of 3–6 hydroxycarboxylic acids

✉ S. Torres-Giner
storreginer@iata.csic.es; storresginer@upv.es

[1] Technological Institute of Materials (ITM), Universitat Politècnica de València (UPV), Plaza Ferrándiz y Carbonell 1, 03801 Alcoy, Spain

[2] Novel Materials and Nanotechnology Group, Institute of Agrochemistry and Food Technology (IATA), Spanish Council for Scientific Research (CSIC), Calle Catedrático Agustín Escardino Benlloch 7, 46980 Paterna, Spain

Ⓐ Springer

In Situ Compatibilization of Biopolymer Ternary Blends with Tunable Properties by Reactive Extrusion with Low-functionality Epoxy-based Styrene–Acrylic Oligomer

Abstract

The present study originally reports on the use of low-functionality epoxy-based styrene–acrylic oligomer (ESAO) to compatibilize immiscible ternary blends made of poly(3-hydroxybutyrate-co-3-hydroxyvalerate) (PHBV), polylactide (PLA), and poly(butylene adipate-co-terephthalate) (PBAT). The addition of 2 parts per hundred resin (phr) of low-functionality ESAO during melt processing successfully changed the soften inclusion phase in the blend system to a thinner morphology, yielding biopolymer ternary blends with exceptionally higher mechanical ductility and improved oxygen barrier performance. The compatibilization achieved was ascribed to the *in situ* formation of a newly block terpolymer, i.e. PHBV-b-PLA-b-PBAT, which was produced at the blend interface by the reaction of the multiple epoxy groups present in ESAO with the functional terminal groups of the biopolymers. Additionally, this reaction was mainly linear due to the inherent low functionality of ESAO and the more favorable reactivity of the epoxy groups with the biopolymer carboxyl groups, avoiding the formation of highly branched and/or cross-linked structures and facilitating the films processability. The here-described reactive blending of the selected biopolymers at different mixing ratios represents a suitable industrial methodology to prepare sustainable plastics with tunable properties, excluding any synthesis stage or chemical modification, and of potential application interest in the food packaging field.

Keywords: PHBV; PLA; PBAT; Reactive extrusion; Sustainable packaging

INTRODUCTION

The future scarcity of petroleum and the strong awareness of post-consumer plastic wastes are the two main drivers behind the interest, at both academic and industrial levels, in biopolymers. The terms "bio-based polymers" and "biodegradable polymers" are extensively used in the polymer literature when referring to biopolymers [1]. Bio-based polymers include both naturally occurring macromolecules, such as proteins and carbohydrates, or polymers synthetized from renewable monomers. Biodegradable polymers undergo rapidly and completely disintegration through the action of enzymes and/or chemical deterioration associated with living microorganisms. Bio-based polymers can be either non-degradable, such as bio-based polyethylene (bio-PE)[2] and bio-based polyamides (bio-PAs)[3], or biodegradable. Among biodegradable polymers, bio-based aliphatic polyesters, including polyhydroxyalkanoates (PHAs) and polylactides (PLAs), play a predominant role due to their potentially hydrolysable ester bonds. Some other biodegradable polyesters can be produced from non-renewable petroleum resources, which is the case of, for instance, poly(butylene succinate) (PBS), poly(butylene succinate-co-adipate) (PBSA), and poly(butylene adipate-co-terephthalate) (PBAT).

PHAs are aliphatic polyesters produced by bacterial fermentation with the highest potential to replace polyolefins. PHAs generally consist of 3 to 6 hydroxycarboxylic acids and more than 150 monomers have been identified as their constituents [4]. Such diversity allows the production of biopolymers with a wide range of properties [5]. Poly(3-hydroxybutyrate) (PHB) homopolyester and its copolymer with 3-hydroxyvalerate (HV), *i.e.* poly(3-hydroxybutyrate-co-3-hydroxyvalerate) (PHBV) are the most important PHAs. The copolyester has lower crystallinity and stiffness while improved flexibility and toughness, broadening both their processing window and applications [6]. However, most PHA materials cannot be easily processed in current processing equipment and are excessively rigid and brittle for a large number of packaging applications.

PLA also belongs to the family of aliphatic polyesters and it is synthetically produced in continuous *via* ring-opening polymerization (ROP) of the lactide dimer [7]. This monomer is habitually obtained from carbohydrate resources, including agricultural by-products [8]. Since it contains two chiral carbon centers, PLA can coexist in three stereochemical forms: poly(L-lactide) (PLLA), poly(D-lactide) (PDLA), and poly(DL-lactide) (PDLLA) [9]. Most commercial grades of PLA are indeed copolymers of PLLA and PDLLA[10], which can be easily melt processed in conventional processing methodologies, including film and sheet extrusion, injection molding, thermoforming, foaming, and fiber spinning, to produce habitually rigid articles [11]. However, the major drawbacks of PLA are related to its low heat distortion temperature (HDT) and toughness due to its glass transition temperature (T_g ~60 °C) and intrinsic brittleness, respectively. Therefore, to overcome these drawbacks, a large research activity is being carried out by melt mixing with both natural fillers [12] and plasticizers [13, 14].

PBAT is a semi-aromatic copolyester that is synthetically obtained by polycondensation reaction between 1,4-butanediol and a mixture of adipic acid and terephathalic acid (TPA), mainly derived from petroleum sources. A range from approximately 35 to 55 mol.-% TPA usually offers an optimal compromise between

biodegradability and useful properties [15]. Because of their high flexibility, PBAT copolyesters are mostly interesting for flexible applications (*e.g.* bags and mulch films) [16]. In view of their high toughness, good heat resistance, and high-impact performance, blends of PBAT with other biopolymers, such as PLA [17], thermoplastic starch (TPS) [18], and PBS [19], have been studied.

Biodegradable polymers are suitable candidates for disposable material applications, particularly in short-term uses, such as packaging and hygiene. However, the use of biopolymers is currently restricted for most industrial applications due to both their poor processability and lower thermal stability and mechanical performance (when taken alone) than commodity polymers. The development of copolymers and biopolymer blends with satisfactory properties can straightforwardly overcome these limitations. In comparison to copolymerization, polymer blends represent an economic and more convenient way to provide the desired properties by physical mixing without any synthesis stage or chemical modification. However, most of the existing polymer blends are not thermodynamically miscible, which is mainly influenced by interactions such as dipole–dipole, ion–dipole, hydrogen bonding, acid–base, and donor and acceptor [20, 21]. As a result, immiscible polymer blends habitually need to be compatibilized to improve the adhesion between the phase components, reduce their interfacial tension, and generate limited inclusion phase sizes [22].

Compatibilization in biopolymer blends can be effectively addressed by either *ex situ* (non-reactive) or *in situ* (reactive) methods [22]. *Ex situ* compatibilization is based on the use of a premade (block or grafted) copolymer, being highly miscible with the blend components. However, this is a two-step strategy that is not habitually desirable from an industrial point of view and it is only suitable for specialty polymer systems where the cost of manufacturing and addition of the copolymer is economically feasible [23, 24]. In addition, it habitually yields a low compatibilizing effect due to it is almost impossible to reach all the added copolymer at the interface of the immiscible blend [25-27]. Alternatively, *in situ* compatibilization is performed by means of polymers, oligomers, and additives containing multi-functional groups (*e.g.* anhydride, epoxy, oxazoline, isocyanates, etc.). These are capable of reacting during melt processing with the hydroxyl and carboxyl functional groups of condensation polymers [28]. For this, it is important that the reactive compatibilizers possess low melt viscosity so that they can easily diffuse to the blends interface within a short processing time [22].

In situ compatibilization of biopolymer blends with additives of low-molecular weight (M_W), such as reactive oligomers and oils, is both economically and environmentally more favorable because it involves the use of a relatively low concentration of compatibilizer, typically below 5 wt.-%, in a one-step process [22, 29]. Recent studies have concluded that it results in the formation of *in situ* copolymers that improve drop breakup and stabilize coalescence in the blend systems [30, 31]. Among the studied reactive compatibilizers, epoxy-based styrene–acrylic oligomers (ESAOs) with different degree of functionalities and a low M_W, well below 9000 g/mol, can easily form new ester bonds through reaction of their epoxy groups with the terminal functional groups of the biopolymer chains. This mainly consists on glycidyl esterification of carboxylic acid end groups, which precedes hydroxyl end group etherification [32]. In ESAOs, styrene and acrylate building blocks are each typically 1–

20 and 2–20, respectively, having glycidyl and epoxy groups incorporated as side chains [33]. By the epoxy ring-opening and subsequent reaction with both the hydroxyl and carboxylic acid end groups, ESAOs can efficiently reconnect the polyester chains that break down during melt processing. These additives are habitually termed as ''chain extenders'' since the M_W of the biopolymers is increased (or recovered if hydrolysis simultaneously occurs) [34]. The resultant biopolymer articles typically present enhanced mechanical performance and thermal stability due to their increased M_W [35, 36]. Since the melt-processing time is sufficient to accomplish chain reaction, this method presents a great deal of potential for *in situ* compatibilization of polymer blends at industrial scale [37].

In ESAOs, the average number of epoxy groups per chain habitually lies between 4 and 9. This reactive oligomer can form *in situ* block copolymers by the hydrogen abstraction from the carboxyl group of blended polyesters [38]. However, most tested ESAO grades present high number average functionality (f), typically ~9, *i.e.* the so-called multi-functional ESAO (Joncryl® ADR 4368-C)[33], which can easily lead to the formation of highly chain-branched and/or cross-linked structures [38]. This may result in a dramatic reduction of the melt flow index (MFI) of the blended system, which could both limit its processing (*e.g.* injection molding) and originate gel formation. On the contrary, both bi-functional ESAO, *i.e.* with f values of ~2, and low-functionality ESAO, *i.e.* with f values of 4–5, can raise melt viscosity through linear chain-extension or moderate branching [39].

The present study reports, for the first time, the use of low-functionality ESAO to *in situ* compatibilize ternary blends of three commercial biodegradable polyesters, namely PHBV, PLA, and PBAT, by reactive extrusion (REX). These biopolymers were selected as they are currently produced in relatively large volumes and present a very dissimilar performance, so their combination can provide tunable properties for a broad packaging application range.

EXPERIMENTAL

Materials

Bacterial aliphatic copolyester PHBV was ENMAT™ Y1000P, produced by Tianan Biologic Materials (Ningbo, China). This biopolymer resin presents a density of 1.23 g/cm³ and a melt flow index (MFI) of 5–10 g/10 min (190 °C, 2.16 kg). The HV fraction in the copolyester is 2–3 mol.-%.

Homopolyester PLA, grade Ingeo™ biopolymer 2003D, was obtained from NatureWorks (Minnetonka, MN, USA). Density is 1.24 g/cm³ and MFI is ~6 g/10 min (210 ºC, 2.16 kg). The D-lactide isomer content is 3.8–4.2 wt.-%.

Petrochemical copolyester PBAT, termed as Biocosafe 2003F, was purchased from Xinfu Pharmaceutical Co. Ltd. (Zhejiang, China). This resin presents a MFI value of ≤ 5 g/10 min (150 °C, 2.16 Kg) and a density of 1.18–1.28 g/cm³. The butylene adipate (BA)-to-butylene terephthalate (BT) ratio in the copolyester is approximately 55/45 (mol/mol).

Low-functionality ESAO was obtained from BASF S.A. (Barcelona, Spain), in the form of solid granules, under the trade name Joncryl® ADR 4300. Its M_W is 5500

g/mol, T_g is 56 °C, the epoxy equivalent weight (EEW) is 445 g/mol, and f is $\leq$ 5. Manufacturer recommends a dosage of 0.4–2wt.-% in polyesters.

Melt processing

Prior to processing, all biopolymer pellets were dried in an Industrial Marsé MDEO dehumidifier (Barcelona, Spain) at 60 °C for at least 12 h. Drying was necessary to minimize hydrolytic degradation of the biopolyesters.

The neat biopolymers and their ternary blends were melt compounded in a co-rotating ZSK-18 MEGAlab laboratory twin-screw extruder from Coperion (Stuttgart, Germany). The screws feature 18 mm diameter with a length (L) to diameter (D) ratio, *i.e.* L/D, of 48. The biopolymer pellets and ESAO granules were manually pre-homogenized in a zipper bag and then fed into the main hopper. The materials dosage was set to achieve a residence time of about 1 min, measured by a blue masterbatch. The extrusion temperature profile, from the hopper to the die, was set as follow: 155, 160, 160, 165, 165, 170, and 175 °C. The strand was cooled in a water bath at 15 °C and pelletized using an air-knife unit.

Films with a mean thickness of 200–250 µm were obtained by thermo-compression in a hydraulic press 3850-model from Carver, Inc. (Wabash, IN, USA). The process was performed at 180 °C and 8 bar for 10 min, followed by fast cooling inside the press using an internal water system at 15 °C for 5 min. The films were stored at room conditions, *i.e.* 23 °C and 50% HR, for at least 15 days before characterization.

Table III.1.3.1 summarizes the composition of the here-prepared biopolymer films. Addition of low-functionality ESAO was set at a fixed content of 2 parts per hundred resin (phr) of biopolymer.

Table III.1.3.1. Films composition according to the weight content (wt.-%) of poly(3-hydroxybutyrate-*co*-3-hydroxyvalerate) (PHBV), polylactide (PLA), and poly(butylene adipate-*co*-terephthalate) (PBAT). Low-functionality epoxy-based styrene–acrylic oligomer (ESAO) was added as parts per hundred resin (phr) of biopolymer.

Sample	PHBV (wt.-%)	PLA (wt.-%)	PBAT (wt.-%)	ESAO (phr)
PHBV	100	0	0	0
PLA	0	100	0	0
PBAT	0	0	100	0
PHBV/PLA/PBAT 1:1:1	33.33	33.33	33.33	0
PHBV/PLA/PBAT 1:1:1 + ESAO	33.33	33.33	33.33	2
PHBV/PLA/PBAT 2:1:1 + ESAO	50	25	25	2
PHBV/PLA/PBAT 3:1:1 + ESAO	60	20	20	2

Films characterization

Morphology

The film cross-sections were observed by field emission scanning electron microscopy (FESEM) in a ZEISS ULTRA 55 from Oxford Instruments (Abingdon, United Kingdom). Film specimens were cryo-fractured by immersion in liquid nitrogen and then mounted on aluminum stubs perpendicularly to their surface. The working distance (WD) varied in the 6–7 mm range and an extra high tension (EHT) of 2 kV was applied to the electron beam. Due to their non-conducting nature, samples were subjected to a sputtering process with a gold-palladium alloy in a sputter coater EMITECH-SC7620 from Quorum Technologies, Ltd. (East Sussex, United Kingdom). The sizes of the inclusion phase were determined using Image J Launcher v 1.41 and the data presented were based on measurements from a minimum of 20 SEM micrographs per sample.

Infrared Spectroscopy

Chemical analyses on the film surfaces were performed using attenuated total reflection–Fourier transform infrared (ATR-FTIR) spectroscopy. Spectra were recorded with a Vector 22 from Bruker S.A. (Madrid, Spain) coupling a PIKE MIRacle™ ATR accessory from PIKE Technologies (Madison, USA). Ten scans were averaged from 4000 to 400 cm^{-1} at a resolution of 4 cm^{-1}.

Thermal analysis

Main thermal transitions of the biopolymer films were obtained by differential scanning calorimetry (DSC) in a Mettler-Toledo 821 calorimeter (Schwerzenbach, Switzerland). An average sample weight ranging from 5 to 7 mg was subjected to a heating program from 30 °C to 200 °C at a heating rate of 10 °C min^{-1} in nitrogen atmosphere (66 mL min^{-1}). Standard sealed aluminum crucibles of a volume capacity of 40 μl were used. DSC runs were performed in triplicate.

Thermal stability was determined by thermogravimetric analysis (TGA) in a Mettler-Toledo TGA/SDTA 851 thermobalance. Samples, with an average weight between 5 and 7 mg, were placed in standard alumina crucibles of 70 μl and subjected to a heating program from 30 °C to 700 °C at a heating rate of 20 °C min^{-1} in air atmosphere. TGA experiments were performed in triplicate.

Thermomechanical tests

Dynamic mechanical thermal analysis (DMTA) was conducted in a DMA-1 model from Mettler-Toledo, working in tension mode, single cantilever. Film samples sizing 10 x 5 x 0.2 mm^3 were subjected to a temperature sweep program from -40 °C to 130 °C at a heating rate of 2 °C min^{-1}, an offset strength of 1N, an offset deformation of 150%, and a control deformation of 6 μm. DMTA tests were run in triplicate.

Mechanical tests

Tensile tests of films were carried out by analyzing standard samples (type-2), as indicated in ISO 527-3, with a total length and width of 160 mm and 10 mm, respectively. The tests were performed in a universal testing machine ELIB 30 from

S.A.E. Ibertest (Madrid, Spain), equipped with a 5-kN load cell, and using specific pneumatic clamps at a cross-head speed of 5 mm min^{-1}. At least six specimens per sample were tested.

Permeability tests

The water vapor permeability (WVP) was determined according to the ASTM 2011 gravimetric method. For this, 5 mL of distilled water were poured into a Payne permeability cup ($\emptyset = 3.5$ cm) from Elcometer Sprl (Hermalle-sous-Argenteau, Belgium). The films were placed in the cups so that on one side they were exposed to 100% relative humidity (RH), avoiding direct film contact with water. The cups containing the films were then secured with silicon rings and stored in a desiccator at 25 °C and 0% RH. Identical cups with aluminum foils were used as control samples to estimate water loss through the sealing. The cups were weighed periodically using an analytical balance with ±0.0001 g accuracy. Water vapor permeation rate (WVPR), also called water permeance when corrected for permeant partial pressure, was determined from the steady-state permeation slope obtained from the regression analysis of weight loss data per unit area vs. time, in which the weight loss was calculated as the total cell loss minus the loss through the sealing. WVP was obtained, in triplicate, by correcting the permeance by the average film thicknesses.

Limonene permeability (LP) was also determined according to ASTM 2011 gravimetric method. Similarly, 5 mL of D-limonene, obtained from Sigma-Aldrich S.A. (Madrid, Spain) with 98% purity, was placed inside the Payne permeability cups and the cups containing the films were stored under controlled conditions, *i.e.* 25 °C and 40% RH. Limonene permeation rate (LPR) was obtained from the steady-state permeation slopes. The weight loss was calculated as the total cell loss minus the loss through the sealing plus the water sorption gained from the environment measured in samples with no permeant. LP was calculated taking into account the average sheet thickness in each case, measuring three replicates per sample.

Oxygen permeability (OP) was obtained from the oxygen transmission rate (OTR) measurements using an Oxygen Permeation Analyzer M8001 from Systech Illinois (Thame, UK). The samples were previously purged with nitrogen in the humidity equilibrated samples and then exposed to an oxygen flow of 10 mL min^{-1}. The exposure area during the test was 5 cm^2. Test were performed at 25 °C and 60% RH and recorded in duplicate.

RESULTS AND DISCUSSION

Morphology

Figure III.1.3.1 shows the FESEM images, taken at low (left) and high (right) magnification, of the biopolymer film cross-sections obtained by cryo-fracture. As it can be seen in **Figure III.1.3.1a-c**, all neat biopolymer films presented a relatively homogenous fracture surface with different degrees of roughness. In the case of PHBV and PLA, respectively shown in **Figure III.1.3.1a** and **1b**, one can also observe that both biopolymer films followed a similar pattern of breakage, showing a rough surface that is representative of brittle materials. This was more noticeable for the PLA film where several micro-cracks were also formed during the fracture. On the contrary, as seen in

Figure III.1.3.1c, the PBAT film showed a softer surface, evidencing certain plastic deformation by the presence of long filaments.
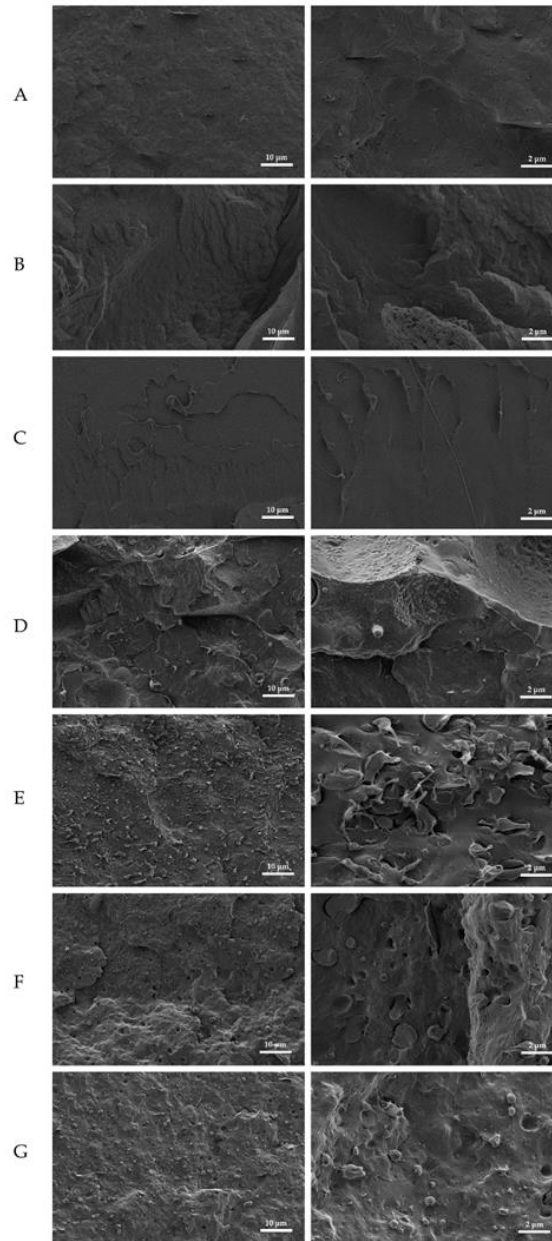
Figure III.1.3.1. Field emission scanning electron microscopy (FESEM) images of the cryofracture surfaces taken at 1000x (left) and 5000x (right) corresponding to the films made of: a) Poly(3-hydroxybutyrate-co-3-hydroxyvalerate) (PHBV); b) Polylactide (PLA); c) Poly(butylene adipate-co-terephthalate) (PBAT); d) PHBV/PLA/PBAT 1:1:1; e) PHBV/PLA/PBAT 1:1:1 with low-functionality epoxy-based styrene–acrylic oligomer (ESAO); f) PHBV/PLA/PBAT 2:1:1 with ESAO; g) PHBV/PLA/PBAT 3:1:1 with ESAO.

In relation to the biopolymer blends, gathered in **Figure III.1.3.1d-g**, these exhibited heterogeneous surfaces that were based on an "island-and-sea" morphology

in which a part of each phase was dispersed as small droplets in the others. The absence of a co-continues phase morphology in the blends supports previous studies indicating that, at the here-studied mixing ratios, these biopolymers are thermodynamically immiscible[40]. However, the droplet sizes of the embedded inclusion phases were considerably larger in the ternary blend film processed without ESAO, in the range of 2–10 µm, as it can be seen in **Figure III.1.3.1d**. This indicates a rapid coalescence and also a poor interface adhesion between the biopolymer phases. In the case of the ternary blend films melt processed with low-functionality ESAO, the inclusion phases were stretched into submicron droplets, *i.e.* lower than 1 µm, indicating that a higher coalescence stabilization of the biopolymer phases was achieved. As seen in **Figure III.1.3.1g**, for the ternary blend film melt processed with ESAO and with the highest PHBV content, *i.e.* 80 wt.-%, the droplets size achieved the lowest value, presenting a mean diameter of approximately 600 nm. This morphological change can be attributed to the achievement of a partial miscibility in the biopolymer ternary blends that, as one can expect, increased as the PHBV content was higher. A similar effect of ESAO was observed, for instance, by Ojijo *et al.* [38] on PLA/PBSA blends, in which the inclusion phase size was significantly reduced from 2.69 to 0.7 µm due to a reduced surface tension between the phases. A previous study consisting of PLA and PBAT blends compatibilized using ESAO also suggested that partial miscibility is achieved through the *in situ* formation of a block copolymer [41].

One can additionally observe that, after melt processing the ternary blends with ESAO, the fracture surface behavior of their films predominantly changed from brittle to ductile. In the case of the uncompatibilized blend film, *i.e.* the ternary blend melt processed without ESAO, it presented a clear pull-out of the inclusion phase after fracture, which is supported by the presence of large holes in **Figure III.1.3.1d**. However, the submicron droplets in the ternary blend films processed with ESAO induced a notable plastic deformation with no evidence of phase separation. Therefore, the addition of low-functionality ESAO also improved the adhesion between the blended components, facilitating a better stress transfer from one phase to another phase. In this sense, Lin *et al.* [42] also reported a significant adhesion improvement in PLA/PBAT blends by means of tetrabutyl titanate (TBT), which decreased the interface between the two biopolymers. Indeed, the resulting biopolymer binary blends only acquired improved performance when the stress transfer between the two blended components was effective. In another work, Arruda *et al.* [43] studied the morphology both in machine direction (MD) and transverse direction (TD) of a blown film made of PLA/PBAT processed with and without multi-functional ESAO. The incorporation of ESAO into the blend changed the PBAT inclusion phase shape, in both MD and TD, from platelet to refined fibrilar structure. This morphological change was attributed to the improved compatibility between the phases due to a PLA-*b*-PBAT copolymer formation at the interface of both biopolymers.

Chemical properties

FTIR was carried out in order to ascertain the chemical interactions of the biopolymer phases after the addition of low-functionality ESAO. **Figure III.1.3.2** shows the FTIR spectra of the ESAO granules and the films of the ternary blend PHBV/PLA/PBAT 1:1:1 melt-processed with and without low-functionality ESAO. In relation to the ESAO spectrum, the main peaks related to C–O stretching vibration of

the epoxy groups appeared at ~1180, 910, and 840 cm^{-1} [33, 44-46]. These peaks were not observed in the spectrum of the ternary blend processed with low-functionality ESAO, indicating that the functional groups of the oligomer reacted and were consumed during melt compounding. In this sense, the ESAO reaction in a binary PLA/PBSA blend was previously confirmed by FTIR spectroscopy as a result of the disappearance of the epoxy group bands at 907 and 843 cm^{-1} [38].
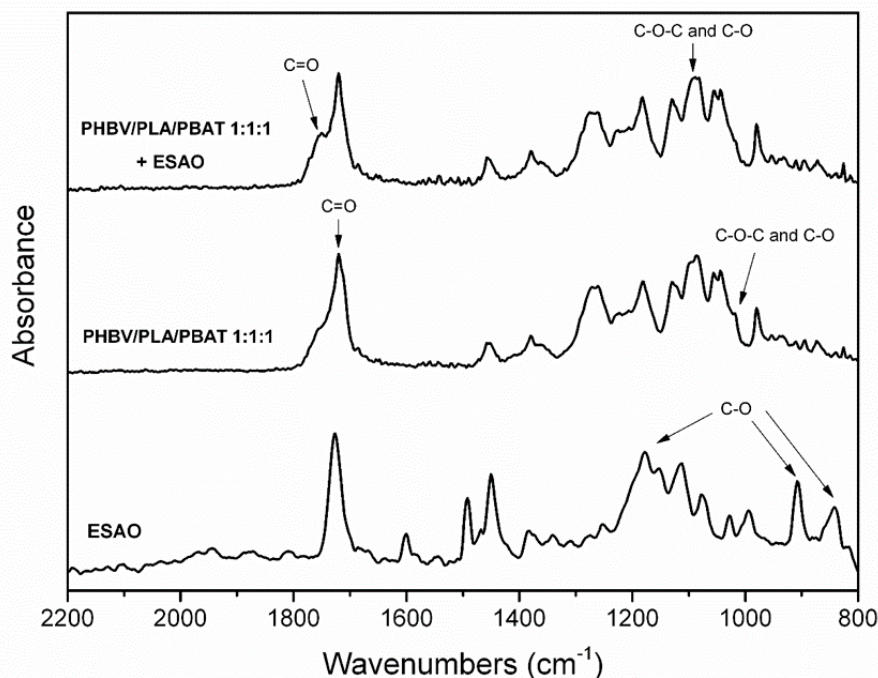
Figure III.1.3.2. Fourier transform infrared (FTIR) spectra, from bottom to top, of: low-functionality epoxy-based styrene–acrylic oligomer (ESAO) and the ternary blends of poly(3-hydroxybutyrate-*co*-3-hydroxyvalerate) (PHBV), polylactide (PLA), and poly(butylene adipate-*co*-terephthalate) (PBAT) processed with and without ESAO. Arrows indicate the chemical bonds described in the text.

In relation to the spectra of the biopolymer blends one can observe that the strongest band of the polyesters, attributed to their C=O stretching [12], slightly broadened and shifted from 1721 cm^{-1}, for the uncompatibilized ternary blend, to 1718 cm^{-1}, for the ternary blend melt processed with ESAO. The shoulder of the carbonyl peak centered at ~1750 cm^{-1} also became more intense in the compatibilized film. A similar peak change was previously ascribed to the reaction between the epoxy groups of multi-functional ESAO and the carboxyl groups (–COO) in polyesters [47]. This observation has been also related to a disruption of the hydrogen bonding in the molecular arrangement of the PHA chains[33], which further supports the presence of a newly formed copolyester. It is also worthy to mention the slight increase observed for the ester-related band at ~1080 cm^{-1} that was accompanied to the reduction of the band at ~1020 cm^{-1}, which are known to arise from C–O and C–O–C stretching vibrations of ester groups in biopolyesters [48]. Though these changes were subtle, they may suggest a reduction of the former ester bonds in the biopolymers as well as the formation of new ones.
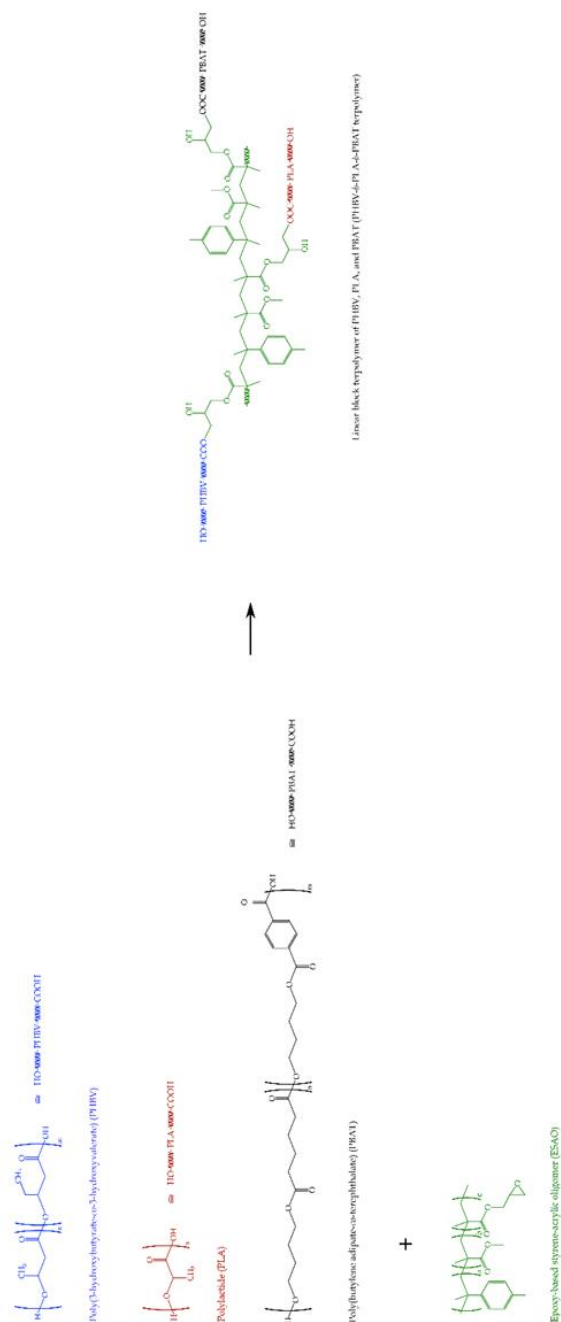
Figure III.1.3.3. Schematic representation of the *in situ* formed block terpolymer of poly(3-hydroxybutyrate-*co*-3-hydroxyvalerate) (PHBV), polylactide (PLA), and poly(butylene adipate-*co*-terephthalate) (PBAT) by low-functionality epoxy-based styrene–acrylic oligomer (ESAO). An average functionality (*f*) value of 3 was considered for the proposed reaction.

According to the above-described chemical interactions, **Figure III.1.3.3** proposes the chemical reaction of the three biopolymers with the epoxy functional groups of low-functionality ESAO during melt processing. The proposed scheme suggests the formation of a new copolyester, which first involves the ring-opening of epoxy groups in ESAO and their subsequent reaction with the carboxyl groups of the

terminal acids of the biopolymers to create new covalent C–O–C bonds. This chain-linking process is considered to be mainly linear based on the fact that, on the one hand, the reaction rate between epoxy groups with the carboxyl groups in polyesters is about 10–15 times more favorable than with the hydroxyl groups [41] and, on the other, the here-selected ESAO inherently presents a low functionality. As a result, a linear block terpolymer consisting of PHBV, PLA, and PBAT chains, *i.e.* a PHBV-*b*-PLA-*b*-PBAT terpolymer, and the copolymers based on binary combinations of thereof are proposed to be formed.

Thermal properties

Figure III.1.3.4 shows the DSC heating thermograms of the biopolymer films. One can observe that the neat PHBV film presented a sharp melting peak at ~175 °C, showing no evidences of cold crystallization during heating. For both PLA and PBAT, the curves showed a slight and poorly defined endothermic peak centered at 151 °C and 124 °C, respectively. This observation suggests that the neat PLA and PBAT films were predominantly amorphous. Since the crystallization behavior is closely related to the biopolymers thermal history, it is considered that PLA and PBAT developed an amorphous structure at the cooling rate of the films. In this sense, Miyata and Masuko [49] studied the non-isothermal crystallization of PLLA materials at various cooling rates, observing that samples cooled at rates greater than 10 °C min^{-1} did not crystallize and remained amorphous. In the case of the PLA film, a glass transition phenomenon can be seen at ~62 °C. This second thermal transition was not observed for the other biopolymer films as it is known to occur under ambient temperature, i.e. Tg ranges from −40 °C to 5 °C for PHAs [5] while it is around −20 °C for PBAT [19, 50]. In relation to the biopolymer ternary blend films, the DSC curves presented a low-intense glass transition in the 55–65 °C range and a melting process in the temperature range of 165–180 °C corresponding to the PLA and PHBV phases, respectively. Additionally, it can be observed that the Tm values gradually increased with increasing the PHBV content, ranging from ~171 °C, for the 1:1:1 blends, to 174 °C, for the 3:1:1 blend. The melting enthalpies were also higher in the blend films with higher PHBV content.
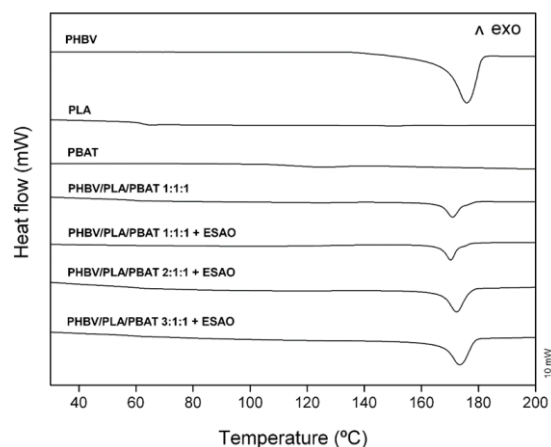
Figure III.1.3.4. Differential scanning calorimetry (DSC) thermograms of the ternary blend films made of poly(3-hydroxybutyrate-*co*-3-hydroxyvalerate) (PHBV), polylactide (PLA), and poly(butylene adipate-*co*-terephthalate) (PBAT) processed with and without low-functionality epoxy-based styrene–acrylic oligomer (ESAO).

Figure III.1.3.5 includes both the TGA curves, in **Figure III.1.3.5a**, and their corresponding derivative thermogravimetric (DTG) curves, in **Figure III.1.3.5b**, of the biopolymer films in the 100–700 °C range. One can clearly observe that PHBV presented the lowest thermal stability, fully decomposing in a sharp single step. The values of onset degradation temperature, determined as the degradation temperature at 5% of mass loss ($T_{5\%}$), and degradation temperature (T_{deg}) were ~294 °C and 310 °C, respectively. On the contrary, both PLA and PBAT, particularly the latter, presented a relatively high thermal stability, showing $T_{5\%}$ values around 340 °C. Both biopolymers decomposed in two stages with T_{deg} values at approximately 390 °C and 480 °C, for PLA, and 430 °C and 510 °C, for PBAT. All ternary blends showed a thermal stability profile relatively close to that of neat PHBV, though the onset was slightly delayed up to ~300 °C. It is also worthy to mention that the thermal decomposition of the blends took place in three different stages, in which the second mass loss, which was observed in the 325–375 °C range, is mainly related to the PHBV phase. Therefore, the effect of the low-functionality ESAO addition on the thermal behavior and stability of the blends was relatively low, whereas PHBV played the major role in their thermal degradation.
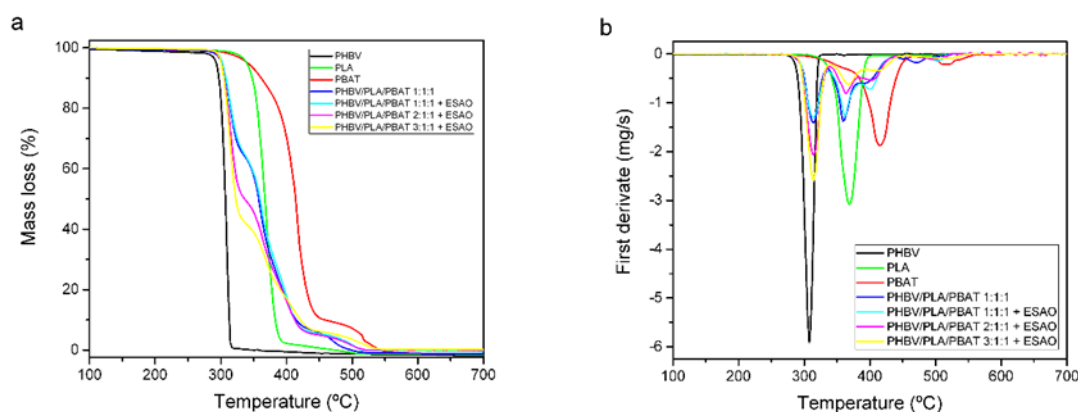
Figure III.1.3.5. a) Thermogravimetric analysis (TGA) and b) derivative thermogravimetric (DTG) curves of the ternary blend films made of poly(3-hydroxybutyrate-co-3-hydroxyvalerate) (PHBV), polylactide (PLA), and poly(butylene adipate-co-terephthalate) (PBAT) processed with and without low-functionality epoxy-based styrene–acrylic oligomer (ESAO).

Thermomechanical properties

In order to fully determine the T_g of the biopolymer blends and also to further ascertain the potential effect of low-functionality ESAO on their miscibility, DMTA was carried out from –40 °C to 130 °C. The evolution of the storage modulus, loss modulus, and damping factor (tan δ) *vs.* temperature of the biopolymer films are included in **Figure III.1.3.6**. The storage modulus is a measure of the energy stored and recovered in a cyclic deformation and it represents the stiffness of the films. As shown in **Figure III.1.3.6a**, at −40 °C, the neat PHBV film showed a value around 5600 MPa. This was significantly higher than those of PLA and PBAT, which then resulted in more flexible films, having values of 3450 MPa and 2400 MPa, respectively. The storage modulus of PHBV started to decrease at approximately 0 °C, which corresponds to the initiation of alpha (α)-transition region of this biopolymer. In the case of the PLA film, this

thermomechanical change was observed at ~55 °C, while for the PBAT film this overlapped with the beginning of the measurement, *i.e.* −40 °C. In addition, the softening of the PLA and PBAT films with increasing temperature was also more intense. This confirms that a higher fraction of the biopolymer molecules underwent glass transition, as previously observed by DSC analysis. Similar DMTA curves were reported for PLA and PBAT binary blends by Abdelwahab *et al.* [46], who also revealed that the addition of 1 phr ESAO increased the storage modulus for samples containing lignin. In the present study, all biopolymer blend films presented intermediate values of storage modulus, which increased as the PHBV content was increased. Comparison of the ternary blend with and without low-functionality ESAO indicated that the addition of this reactive additive slightly reduced the storage modulus, *i.e.* the film samples became more flexible. This effect was especially notable at low temperatures, indicating that this reactive oligomer acted as a plasticizer.
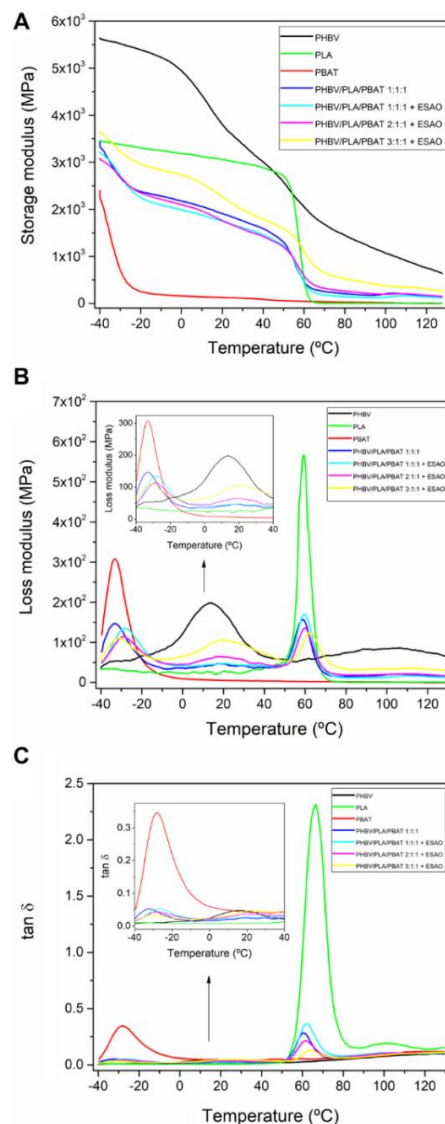
Figure III.1.3.6. Dynamic mechanical thermal analysis (DMTA) curves of the ternary blend films made of poly(3-hydroxybutyrate-*co*-3-hydroxyvalerate) (PHBV), polylactide (PLA), and poly(butylene adipate-*co*-terephthalate) (PBAT) processed with and without low-functionality epoxy-based styrene–acrylic oligomer (ESAO).

The evolution of loss modulus *vs.* temperature is depicted in **Figure III.1.3.6b**. These curves showed a sharp peak during the α-transition, which is related to the biopolymers T_gs and it is proportional to the energy increase that is dissipated in the films during the loading cycle. This further confirms that each biopolymer undergoes its glass−rubber transition at very different temperatures. The maximum values of loss modulus were particularly observed at approximately -34 °C (0.31 GPa), 13 °C (0.2 GPa), and 58 °C (0.56 GPa) for PBAT, PHBV, and PLA, respectively. In the case of the uncompatibilized blend, this film sample presented three α-peaks related to each biopolymer phase, at temperatures very similar to the ones observed for the neat biopolymers. Interestingly, the ternary blends compatibilized with low-functionality ESAO presented a clear shift of α-peaks to intermediate temperatures of the blended biopolymers. For instance, the α-peak related to the PBAT phase of the 1:1:1 blend moved to −34 °C (0.31 GPa), *i.e.* an increase of 4.5 °C. Similarly, for ternary blend films with higher contents of this biopolymer, the α-peak related to the PHBV increased to values in the 19 ° C range. Indeed, the study of T_g, in addition to morphology, can be efficiently used to differentiate the level of miscibility in polymer blends. Whereas thermodynamically immiscible blends show different distinguishable T_g values, blends made of two polymers that constitute a completely miscible blend present a single Tg and partially miscible blends have tendency to shift the T_g value of the one component toward that of the other. The here-observed shifts of T_g thus support the partial miscibility of the ternary blends. Similarly, Ren *et al*. [51] also observed a slight Tg decrease in binary and ternary blends of TPS, PLA, and PBAT with increasing contents of the latter biopolymer.

Analogous observations were further found in **Figure III.1.3.6c** for the damping factor, which relates the ratio of the energy lost to the energy stored in a cyclic deformation. However, the peak displacements related to state changes in the films presented a lower intensity than in the case of the loss modulus. It is also worthy to note the observed enhancement in the tan δ peak with the addition of low-functionality ESAO. For instance, at 60 °C, it increased from a value of 0.275, for the uncompatibilized blend, up to a value of 0.36, in the case of compatibilized blend, *i.e.* an improvement close to 30%. This directly implies a greater energy dissipation and improved toughness for the ternary blends processed with low-functionality ESAO.

Mechanical properties of ternary blends

Table III.1.3.2 summarizes the tensile properties of the neat biopolymers and their ternary blends. One can observe that both PHBV and PLA biopolymers produced rigid films with relatively high modulus (E), *i.e.* 800–1200 MPa, and tensile strength ($σ_y$), *i.e.* 30–40 MPa. As a result, both biopolymers share some mechanical similarities with traditional rigid polymers, such as polyethylene terephthalate (PET), polystyrene (PS), polypropylene (PP), and polycarbonate (PC), making them as an attractive alternative for disposable and compostable rigid articles [52, 53]. However, these films were also very brittle, presenting values of elongation at break ($ε_b$) lower than 6%, which limits their application in flexible packaging. In contrast, the PBAT film was very flexible and ductile, reaching $ε_b$ values of ~900%. In this sense, it has been reported that PBAT has mechanical properties similar to that of low-density polyethylene (LDPE) [54].

Melt blending of the three biopolymers without ESAO compatibilizer resulted in a film with intermediate mechanical strength values but still with poor ductility. Due to insufficient adhesion between the different phases, it is considered that the soft PBAT domains acted as stress concentrators because of the different elasticity, favoring mechanical failure during the tensile test. A similar effect was recently observed for uncompatibilized PLA/PBAT/PBS blends, in which the stress concentration resulted in a high triaxial stress in the PBAT domain that provoked debonding at the particle–matrix interface [55]. This observation correlates well with the FESEM images shown above. Interestingly, the same ternary biopolymer blend melt processed with low-functionality ESAO presented higher mechanical values but with an extraordinary improvement in ductility. In particular, if the PHBV/PLA/PBAT 1:1:1 blend is compared to the neat PHBV film, E and σ_y values were improved by more than 10% and 35%, respectively, while ε_b value was almost 8 times higher. For the whole studied composition range, higher contents of PHBV in the ternary blends gradually provided greater mechanical strength properties but also lower ductility. Therefore, the preparation of different mixing ratios remarkably resulted in biopolymer films with tunable mechanical properties.

Table III.1.3.2. Mechanical properties of the films made of poly(3-hydroxybutyrate-*co*-3-hydroxyvalerate) (PHBV), polylactide (PLA), and poly(butylene adipate-*co*-terephthalate) (PBAT) processed with and without low-functionality epoxy-based styrene–acrylic oligomer (ESAO) in terms of elastic modulus (E), tensile strength at yield (σ_y), and elongation at break (ε_b).

Sample	E (MPa)	σ_y (MPa)	ε_b (%)
PHBV	1151.2 ± 63.8	30.4 ± 1.2	2.1 ± 0.1
PLA	822.5 ± 18.3	39.6 ± 1.3	5.5 ± 0.3
PBAT	42.6 ± 1.5	11.6 ± 0.5	901.2 ± 39.6
PHBV/PLA/PBAT 1:1:1	583.1 ± 17.4	14.1 ± 0.9	4.4 ± 0.2
PHBV/PLA/PBAT 1:1:1 + ESAO	644.8 ± 29.6	19.1 ± 0.7	35.1 ± 1.6
PHBV/PLA/PBAT 2:1:1 + ESAO	756.8 ± 28.3	20.2 ± 0.8	7.2 ± 0.5
PHBV/PLA/PBAT 3:1:1 + ESAO	788.6 ± 23.7	21.0 ± 0.9	4.6 ± 0.3

The here-observed mechanical improvement is in agreement with some previous works related to biopolymer blends obtained by REX. For instance, addition

of either 2 or 5 wt.-% of glycidyl methacrylate (GMA) during melt compounding to an immiscible PLA/PBAT binary blend resulted in an increase of the tensile toughness of the binary blend without severe loss in tensile strength [56]. In another work, Ojijo *et al*. [38] also reported that the elongation at break and impact strength of compression-molded PLA/PBSA 3:2 blend sheets improved from ca. 100% to 200% and from 9.8 to 34.7 kJ/m^2, respectively, with the incorporation of 1 phr multi-functional ESAO. More importantly, the blends also presented a relatively high tensile strength while simultaneously exhibiting improved thermal stability and favorable crystallinity. More recently, blown PLA/PBAT 8:2 films prepared by reactive blending with 1 phr multi-functional ESAO showed a remarkably high ε_b value of ~250% in comparison to the very low ε_b value of 4% of the neat PLA film [57]. Those binary blend films also possessed high E and σ_y values, *i.e.* 2 GPa and 50–60 MPa, respectively. However, in these previous studies the use of multi-functional ESAO also resulted in a high increase of the melt viscosity, which could limit the industrial applicability of the biopolymer blends.

Barrier properties of ternary blends

Table III.1.3.3 shows the barrier properties in terms of WPV, LP, and OP for the here-developed biopolymer films. The barrier performance is, indeed, one of the main parameters of application interest in the food packaging field. Whereas both water vapor and oxygen barrier properties are important to avoid physical and chemical deterioration, limonene transport properties are usually used as a standard system to test aroma barrier. In the case of the neat biopolymers, one can observe that the PHBV film presented the highest barrier performance in relation to both water vapor and oxygen, showing WVP and OP values of approximately 1.8×10^{-15} kg·m·m^{-2}·Pa^{-1}·s^{-1} and 2×10^{-19} m^3·m·m^{-2}·Pa^{-1}·s^{-1}, respectively. The PLA film showed the lowest LP value and intermediate values of WVP and OP, while the permeability values of the PBAT film were the highest. In this sense, it has been reported that the water vapor barrier of PLA films is lower than PS but still in the range of PET [58]. Similarly, it has been reported that the oxygen barrier property of PBAT is around 50% lower than LDPE [54], which is already a low barrier material to oxygen. In the case of limonene, as opposed to moisture, this is a strong plasticizing component for PHAs and, then, solubility plays a key role in permeability. For instance, solvent-cast films of PHBV with 12 mol.-% HV have been reported to uptake up to 12.7 wt.-% limonene, reaching a LP value of $\sim2 \times 10^{-13}$ kg·m·m^{-2}·Pa^{-1}·s^{-1}.[59] The here-obtained PHBV film was around 20 times more barrier to limonene, which can be ascribed to both the preparation methodology and its lower HV content.

Table III.1.3.3. Barrier properties of the films made of poly(3-hydroxybutyrate-*co*-3-hydroxyvalerate) (PHBV), polylactide (PLA), and poly(butylene adipate-*co*-terephthalate) (PBAT) processed with and without low-functionality epoxy-based styrene–acrylic oligomer (ESAO) in terms of water vapor permeability (WVP), limonene permeability (LP), and oxygen permeability (OP).

Sample	WVP x 10^{15} (kg $\cdot$ m $\cdot$ m^{-2} $\cdot$ Pa^{-1} $\cdot$ s^{-1})	LP x 10^{15} (kg $\cdot$ m $\cdot$ m^{-2} $\cdot$ Pa^{-1} $\cdot$ s^{-1})	OP x 10^{18} (m^3 $\cdot$ m $\cdot$ m^{-2} $\cdot$ Pa^{-1} $\cdot$ s^{-1})
PHBV	1.82 ± 0.37	10.26 ± 0.57	0.21 ± 0.03
PLA	12.31 ± 0.98	3.30 ± 0.41	2.22 ± 0.24
PBAT	33.13 ± 1.46	72.58 ± 3.07	9.14 ± 0.86
PHBV/PLA/PBAT 1:1:1	5.11 ± 0.67	3.14 ± 0.82	1.31 ± 0.14
PHBV/PLA/PBAT 1:1:1 + ESAO	5.86 ± 0.29	3.73 ± 0.79	0.49 ± 0.03
PHBV/PLA/PBAT 2:1:1 + ESAO	4.78 ± 0.79	4.34 ± 0.37	0.35 ± 0.19
PHBV/PLA/PBAT 3:1:1 + ESAO	2.75 ± 0.68	4.99 ± 0.96	0.30 ± 0.18

The biopolymer blend films presented intermediate barrier properties in comparison to the films made of the neat biopolymers. The PHBV/PLA/PBAT 1:1:1 blend film processed with low-functionality ESAO showed slightly higher WVP and LP values than the uncompatibilized blend film, but a significantly lower OP value. As supported above during the morphology analysis, low-functionality ESAO induced a reduction of both the inclusion phase size and interface of the biopolymer regions in the blend, which could favor plasticization by water and/or limonene vapors. Alternatively, since oxygen is a noncondensable small permeant, the presence of the newly formed PHBV-*b*-PLA-*b*-PBAT terpolymer may also reduce the free volume of the ternary blend and, then, lower diffusion of the oxygen molecules. A previous work performed on the barrier properties of biopolymer blends has reported that PLA/poly(propylene carbonate) (PPC) cast films processed with 0.5 phr multi-functional ESAO exhibited optimum performance and certain compatibility, but it did not experience any positive influence on the WVP and OP compared to their corresponding uncompatibilized binary blend [47]. In general, increasing the content of PHBV in the biopolymer blends increased the barrier performance to both water vapor and oxygen, whereas it decreased the limonene barrier properties. In particular, the PHBV/PLA/PBAT 3:1:1 compatibilized by low-functionality ESAO showed the most balanced barrier performance. This biopolymer blend film presented a WVP value similar to that of compression-molded films of petroleum-derived PET, *i.e.* 2.30 × 10−15

kg·m·m^{-2}·Pa^{-1}·s^{-1}, but with considerably lower LP and OP values, *i.e.* 1.17 × 10−13 kg·m·m^{-2}·Pa^{-1}·s^{-1} and 1.35 × 10−19 m^3·m·m^{-2}·Pa^{-1}·s^{-1}, respectively [60, 61]. Therefore, a potential application of the here-developed biopolymer ternary blends in medium and medium-to-high barrier packaging applications are foreseen.

CONCLUSIONS

The present study describes the preparation and characterization of novel biopolymer ternary blends made of PHBV, PLA, and PBAT. The neat PHBV film, which was the major component of the blends, presented poor thermal stability, extremely low ductility, and low barrier to limonene (aroma) but high crystallinity, sufficient mechanical strength, and good barrier properties to water and oxygen. The incorporation of PLA improved both processability and aroma barrier while PBAT offered higher ductility and slightly better thermal stability. The resultant uncompatibilized biopolymer blends then showed an intermediate mechanical and barrier performance, however these were immiscible and still presented a relatively low thermal stability and poor ductility.

The addition of low-functionality ESAO successfully increased the miscibility of the blended biopolymers, acting as a reactive compatibilizer during melt compounding. After the achievement of partial compatibilization, the coarse morphology of the soften inclusion phase in the immiscible blend changed to a finer morphology, inducing a more ductile fracture behavior. Though the effect of low-functionality ESAO on the thermal stability of the biopolymer blends was low, this reactive additive provided enhanced overall mechanical performance, particularly in terms of elongation at break, as well as higher oxygen barrier. This enhancement was proposed to be achieved by the *in situ* formation of a newly linear PHBV-*b*-PLA-*b*-PBAT terpolymer and the copolymers of thereof, which were produced at the biopolymers interface due to reaction between the multiple epoxy groups of ESAO with the functional terminal groups of the biopolymers. Due to the inherent low functionality of ESAO and the more favorable reactivity of the epoxy groups with the carboxyl groups in polyesters, the reaction mainly produced a linear connection of the biopolymer chains, avoiding the formation of highly branched and/or cross-linked structures and facilitating the processability of the films.

Finally, the here-prepared biopolymer ternary blends presented tunable properties, depending on the selected mixing ratio. The ternary blends with high contents of PHBV share some similarities with traditional rigid polymers such as PET, PS, and PC, which makes them attractive as a sustainable alternative in the food packaging field for disposable and compostable articles. These biopolymer articles can find potential uses as packaging materials requiring moderate barrier performance such as, among others, food trays and lids.

Acknowledgements

REFERENCES

1. Babu, R.P., K. O'Connor and R. Seeram, *Current progress on bio-based polymers and their future trends.* Progress in Biomaterials, 2013. **2**: 8.

2. Torres-Giner, S., A. Torres, M. Ferrándiz, V. Fombuena and R. Balart, *Antimicrobial activity of metal cation-exchanged zeolites and their evaluation on injection-molded pieces of bio-based high-density polyethylene*. Journal of Food Safety, 2017. 37(4): e12348-n/a.

3. Quiles-Carrillo, L., N. Montanes, T. Boronat, R. Balart and S. Torres-Giner, *Evaluation of the engineering performance of different bio-based aliphatic homopolyamide tubes prepared by profile extrusion*. Polymer Testing, 2017. **61**(Supplement C): 421-429.

4. Steinbüchel, A. and H.E. Valentin, *Diversity of bacterial polyhydroxyalkanoic acids*. FEMS Microbiology Letters, 1995. **128**(3): 219-228.

5. McChalicher, C.W.J. and F. Srienc, *Investigating the structure–property relationship of bacterial PHA block copolymers*. Journal of Biotechnology, 2007. **132**(3): 296-302.

6. Reis, K.C., J. Pereira, A.C. Smith, C.W.P. Carvalho, N. Wellner and I. Yakimets, *Characterization of polyhydroxybutyrate-hydroxyvalerate (PHB-HV)/maize starch blend films*. Journal of Food Engineering, 2008. **89**(4): 361-369.

7. Vink, E.T.H. and S. Davies, *Life Cycle Inventory and Impact Assessment Data for 2014 Ingeo™ Polylactide Production*. Industrial Biotechnology, 2015. **11**(3): 167-180.

8. John, R.P., K.M. Nampoothiri and A. Pandey, *Solid-state fermentation for l-lactic acid production from agro wastes using Lactobacillus delbrueckii*. Process Biochemistry, 2006. **41**(4): 759-763.

9. Madhavan Nampoothiri, K., N.R. Nair and R.P. John, *An overview of the recent developments in polylactide (PLA) research*. Bioresource Technology, 2010. **101**(22): 8493-8501.

10. Garlotta, D., *A Literature Review of Poly(Lactic Acid)*. Journal of Polymers and the Environment, 2001. **9**(2): 63-84.

11. Lim, L.T., R. Auras and M. Rubino, *Processing technologies for poly(lactic acid).* Progress in Polymer Science, 2008. **33**(8): 820-852.

12. Quiles-Carrillo, L., N. Montanes, C. Sammon, R. Balart and S. Torres-Giner, *Compatibilization of highly sustainable polylactide/almond shell flour composites by reactive extrusion with maleinized linseed oil*. Industrial Crops and Products, 2018. **111**(Supplement C): 878-888.

13. Quiles-Carrillo, L., M.M. Blanes-Martínez, N. Montanes, O. Fenollar, S. Torres-Giner and R. Balart, *Reactive toughening of injection-molded polylactide pieces using maleinized hemp seed oil*. European Polymer Journal, 2018. **98**: 402-410.

14. Quiles-Carrillo, L., S. Duart, N. Montanes, S. Torres-Giner and R. Balart, *Enhancement of the mechanical and thermal properties of injection-molded polylactide parts by the addition of acrylated epoxidized soybean oil*. Materials & Design, 2018. **140**(Supplement C): 54-63.

15. Witt, U., R.-J. Müller and W.-D. Deckwer, *Biodegradation behavior and material properties of aliphatic/aromatic polyesters of commercial importance*. Journal of environmental polymer degradation, 1997. 5(2): 81-89.

16. Siegenthaler, K.O., A. Künkel, G. Skupin and M. Yamamoto, *Ecoflex® and Ecovio®: Biodegradable, Performance-Enabling Plastics, in Synthetic Biodegradable Polymers*, B. Rieger, et al., Editors. 2012, Springer Berlin Heidelberg: Berlin, Heidelberg. p. 91-136.

17. Jiang, L., M.P. Wolcott and J. Zhang, *Study of Biodegradable Polylactide/Poly(butylene adipate-co-terephthalate) Blends*. Biomacromolecules, 2006. **7**(1): 199-207.

18. Brandelero, R.P.H., F. Yamashita and M.V.E. Grossmann, *The effect of surfactant Tween 80 on the hydrophilicity, water vapor permeation, and the mechanical properties of cassava starch*

and poly(butylene adipate-co-terephthalate) (PBAT) blend films. Carbohydrate Polymers, 2010. **82**(4): 1102-1109.

19. Muthuraj, R., M. Misra and A.K. Mohanty, *Biodegradable Poly(butylene succinate) and Poly(butylene adipate-co-terephthalate) Blends: Reactive Extrusion and Performance Evaluation.* Journal of Polymers and the Environment, 2014. **22**(3): 336-349.

20. Porter, R.S. and L.-H. Wang, *Compatibility and transesterification in binary polymer blends.* Polymer, 1992. **33**(10): 2019-2030.

21. Koning, C., M. Van Duin, C. Pagnoulle and R. Jerome, *Strategies for compatibilization of polymer blends.* Progress in Polymer Science, 1998. 23(4): 707-757.

22. Muthuraj, R., M. Misra and A.K. Mohanty, *Biodegradable compatibilized polymer blends for packaging applications: A literature review.* Journal of Applied Polymer Science, 2017: 45726-n/a.

23. Ryan, A.J., *Designer polymer blends.* Nature Materials, 2002. **1**: 8.

24. Wu, D., Y. Zhang, L. Yuan, M. Zhang and W. Zhou, *Viscoelastic interfacial properties of compatibilized poly(ε-caprolactone)/polylactide blend.* Journal of Polymer Science Part B: Polymer Physics, 2010. **48**(7): 756-765.

25. Kim, C.H., K.Y. Cho, E.J. Choi and J.K. Park, *Effect of P(lLA-co-εCL) on the Compatibility and Crystallization Behavior of PCL/PLLA Blends.* Journal of Applied Polymer Science, 2000. **77**(1): 226-231.

26. Supthanyakul, R., N. Kaabbuathong and S. Chirachanchai, *Random poly(butylene succinate-co-lactic acid) as a multi-functional additive for miscibility, toughness, and clarity of PLA/PBS blends.* Polymer, 2016. **105**(Supplement C): 1-9.

27. Na, Y.-H., Y. He, X. Shuai, Y. Kikkawa, Y. Doi and Y. Inoue, *Compatibilization Effect of Poly(ε-caprolactone)-b-poly(ethylene glycol) Block Copolymers and Phase Morphology Analysis in Immiscible Poly(lactide)/Poly(ε-caprolactone) Blends.* Biomacromolecules, 2002. **3**(6): 1179-1186.

28. Zeng, J.-B., K.-A. Li and A.-K. Du, *Compatibilization strategies in poly(lactic acid)-based blends.* RSC Advances, 2015. **5**(41): 32546-32565.

29. Xanthos, M. and S.S. Dagli, *Compatibilization of polymer blends by reactive processing.* Polymer Engineering & Science, 1991. **31**(13): 929-935.

30. Sundararaj, U. and C.W. Macosko, *Drop Breakup and Coalescence in Polymer Blends: The Effects of Concentration and Compatibilization.* Macromolecules, 1995. **28**(8): 2647-2657.

31. Milner, S.T. and H. Xi, *How copolymers promote mixing of immiscible homopolymers.* Journal of Rheology, 1996. **40**(4): 663-687.

32. Villalobos, M., A. Awojulu, T. Greeley, G. Turco and G. Deeter, *Oligomeric chain extenders for economic reprocessing and recycling of condensation plastics.* Energy, 2006. **31**(15): 3227-3234.

33. Torres-Giner, S., N. Montanes, T. Boronat, L. Quiles-Carrillo and R. Balart, *Melt grafting of sepiolite nanoclay onto poly(3-hydroxybutyrate-co-4-hydroxybutyrate) by reactive extrusion with multi-functional epoxy-based styrene-acrylic oligomer.* European Polymer Journal, 2016. **84**(Supplement C): 693-707.

34. Lehermeier, H.J. and J.R. Dorgan, *Melt rheology of poly(lactic acid): Consequences of blending chain architectures.* Polymer Engineering & Science, 2001. **41**(12): 2172-2184.

35. Liu, B. and Q. Xu, *Effects of Bifunctional Chain Extender on the Crystallinity and Thermal Stability of PET.* Journal of Materials Science and Chemical Engineering, 2013. **1**(6): 9-15.

36. Eslami, H. and M.R. Kamal, *Effect of a chain extender on the rheological and mechanical properties of biodegradable poly(lactic acid)/poly[(butylene succinate)-co-adipate] blends.* Journal of Applied Polymer Science, 2013. **129**(5): 2418-2428.

37. Loontjens, T., K. Pauwels, F. Derks, M. Neilen, C.K. Sham and M. Serné, *The action of chain extenders in nylon-6, PET, and model compounds.* Journal of Applied Polymer Science, 1997. **65**(9): 1813-1819.

38. Ojijo, V. and S.S. Ray, *Super toughened biodegradable polylactide blends with non-linear copolymer interfacial architecture obtained via facile in-situ reactive compatibilization.* Polymer, 2015. **80**(Supplement C): 1-17.

39. Frenz, V., D. Scherzer, M. Villalobos, A.A. Awojulu, M. Edison and R. Van Der Meer. *Multifunctional polymers as chain extenders and compatibilizers for polycondensates and biopolymers. in Technical Papers*, Regional Technical Conference - Society of Plastics Engineers. 2008.

40. Utracki, L.A., *Compatibilization of Polymer Blends*. The Canadian Journal of Chemical Engineering, 2002. **80**(6): 1008-1016.

41. Al-Itry, R., K. Lamnawar and A. Maazouz, *Improvement of thermal stability, rheological and mechanical properties of PLA, PBAT and their blends by reactive extrusion with functionalized epoxy.* Polymer Degradation and Stability, 2012. **97**(10): 1898-1914.

42. Lin, S., W. Guo, C. Chen, J. Ma and B. Wang, *Mechanical properties and morphology of biodegradable poly(lactic acid)/poly(butylene adipate-co-terephthalate) blends compatibilized by transesterification*. Materials & Design (1980-2015), 2012. **36**(Supplement C): 604-608.

43. Arruda, L.C., M. Magaton, R.E.S. Bretas and M.M. Ueki, *Influence of chain extender on mechanical, thermal and morphological properties of blown films of PLA/PBAT blends.* Polymer Testing, 2015. **43**(Supplement C): 27-37.

44. Wang, Y., C. Fu, Y. Luo, C. Ruan, Y. Zhang and Y. Fu, *Melt synthesis and characterization of poly(L-lactic acid) chain linked by multifunctional epoxy compound*. Journal Wuhan University of Technology, Materials Science Edition, 2010. **25**(5): 774-779.

45. Wei, D., H. Wang, H. Xiao, A. Zheng and Y. Yang, *Morphology and mechanical properties of poly(butylene adipate-co-terephthalate)/potato starch blends in the presence of synthesized reactive compatibilizer or modified poly(butylene adipate-co-terephthalate)*. Carbohydrate Polymers, 2015. **123**: 275-282.

46. Abdelwahab, M.A., S. Taylor, M. Misra and A.K. Mohanty, *Thermo-mechanical characterization of bioblends from polylactide and poly(butylene adipate-co-terephthalate) and lignin*. Macromolecular Materials and Engineering, 2015. **300**(3): 299-311.

47. Sun, Q., T. Mekonnen, M. Misra and A.K. Mohanty, *Novel Biodegradable Cast Film from Carbon Dioxide Based Copolymer and Poly(Lactic Acid)*. Journal of Polymers and the Environment, 2016. **24**(1): 23-36.

48. Torres-Giner, S., J.V. Gimeno-Alcañiz, M.J. Ocio and J.M. Lagaron, *Optimization of electrospun polylactide-based ultrathin fibers for osteoconductive bone scaffolds*. Journal of Applied Polymer Science, 2011. **122**(2): 914-925.

49. Miyata, T. and T. Masuko, *Crystallization behaviour of poly(l-lactide)*. Polymer, 1998. **39**(22): 5515-5521.

50. Muthuraj, R., M. Misra and A.K. Mohanty, *Hydrolytic degradation of biodegradable polyesters under simulated environmental conditions*. Journal of Applied Polymer Science, 2015. **132**(27): n/a-n/a.

51. Ren, J., H. Fu, T. Ren and W. Yuan, *Preparation, characterization and properties of binary and ternary blends with thermoplastic starch, poly(lactic acid) and poly(butylene adipate-co-terephthalate)*. Carbohydrate Polymers, 2009. **77**(3): 576-582.

52. Jamshidian, M., E.A. Tehrany, M. Imran, M. Jacquot and S. Desobry, *Poly-Lactic Acid: Production, Applications, Nanocomposites, and Release Studies*. Comprehensive Reviews in Food Science and Food Safety, 2010. **9**(5): 552-571.

53. Savenkova, L., Z. Gercberga, V. Nikolaeva, A. Dzene, I. Bibers and M. Kalnin, *Mechanical properties and biodegradation characteristics of PHB-based films.* Process Biochemistry, 2000. **35**(6): 573-579.

54. Costa, A.R.M., T.G. Almeida, S.M.L. Silva, L.H. Carvalho and E.L. Canedo, Chain extension in poly(butylene-adipate-terephthalate). *Inline testing in a laboratory internal mixer*. Polymer Testing, 2015. **42**(Supplement C): 115-121.

55. Zhang, K., A.K. Mohanty and M. Misra, *Fully Biodegradable and Biorenewable Ternary Blends from Polylactide, Poly(3-hydroxybutyrate-co-hydroxyvalerate) and Poly(butylene succinate) with Balanced Properties*. ACS Applied Materials & Interfaces, 2012. **4**(6): 3091-3101.

56.   Zhang, N., Q. Wang, J. Ren and L. Wang, *Preparation and properties of biodegradable poly(lactic acid)/poly(butylene adipate-co-terephthalate) blend with glycidyl methacrylate as reactive processing agent*. Journal of Materials Science, 2009. **44**(1): 250-256.

57.   Chinsirikul, W., J. Rojsatean, B. Hararak, N. Kerddonfag, A. Aontee, K. Jaieau, P. Kumsang and C. Sripethdee, *Flexible and Tough Poly(lactic acid) Films for Packaging Applications: Property and Processability Improvement by Effective Reactive Blending*. Packaging Technology and Science, 2015. **28**(8): 741-759.

58.   Auras, R., B. Harte and S. Selke, *Effect of water on the oxygen barrier properties of poly(ethylene terephthalate) and polylactide films*. Journal of Applied Polymer Science, 2004. **92**(3): 1790-1803.

59.   Sanchez-Garcia, M.D., E. Gimenez and J.M. Lagaron, *Morphology and barrier properties of solvent cast composites of thermoplastic biopolymers and purified cellulose fibers*. Carbohydrate Polymers, 2008. **71**(2): 235-244.

60.   Sanchez-Garcia, M.D., E. Gimenez and J.M. Lagaron, *Novel PET Nanocomposites of Interest in Food Packaging Applications and Comparative Barrier Performance With Biopolyester Nanocomposites*. Journal of Plastic Film & Sheeting, 2007. **23**(2): 133-148.

61.   Lagaron, J.M., 1 - *Multifunctional and nanoreinforced polymers for food packaging, in Multifunctional and Nanoreinforced Polymers for Food Packaging*. 2011, Woodhead Publishing: Cambridge, UK. p. 1-28.

III.1.4. A comparative study on the effect of different reactive compatibilizers on injection-molded pieces of bio-based high-density polyethylene/polylactide blends

L. Quiles-Carrillo [1], N. Montanes [1], A. Jorda-Vilaplana [1], R.Balart [1] and S. Torres-Giner [1,2,]

[1] Technological Institute of Materials (ITM), Universitat Politècnica de València (UPV), Plaza Ferrándiz y Carbonell 1, 03801 Alcoy, Spain;

[2] Novel Materials and Nanotechnology Group, Institute of Agrochemistry and Food Technology (IATA), Spanish National Research Council (CSIC), Calle Catedrático Agustín Escardino Benlloch 7, 46980 Paterna, Valencia, Spain

JOURNAL OF
Applied Polymer
SCIENCE

A comparative study on the effect of different reactive compatibilizers on injection-molded pieces of bio-based high-density polyethylene/polylactide blends

L. Quiles-Carrillo,[1] N. Montanes,[1] A. Jorda-Vilaplana [ORCID],[1] R. Balart,[1] S. Torres-Giner [ORCID][1,2]

[1]Technological Institute of Materials (ITM), Universitat Politècnica de València, Plaza Ferrándiz y Carbonell s/n, Alcoy, 03801, Spain
[2]Novel Materials and Nanotechnology Group, Institute of Agrochemistry and Food Technology (IATA), Spanish Council for Scientific Research (CSIC), Avenida Agustín Escardino 7, Paterna, 46980, Spain
Correspondence to: A. Jorda-Vilaplana (E-mail: amjorvi@upv.es)

ABSTRACT: The present study reports on the development of binary blends consisting of bio-based high-density polyethylene (bio-HDPE) with polylactide (PLA), in the 5–20 wt % range, prepared by melt compounding and then shaped into pieces by injection molding. In order to enhance the miscibility between the green polyolefin and the biopolyester, different reactive compatibilizers were added during the melt-blending process, namely polyethylene-grafted maleic anhydride (PE-g-MA), poly(ethylene-co-glycidyl methacrylate) (PE-co-GMA), maleinized linseed oil (MLO), and a combination of MLO with dicumyl peroxide (DCP). Among the tested compatibilizers, the dual addition of MLO and DCP provided the binary blend pieces with the most balanced mechanical performance in terms of rigidity and impact strength as well as the highest thermal stability. The fracture surface of the binary blend piece processed with MLO and DCP revealed the formation of a continuous structure in which the dispersed PLA phase was nearly no discerned in the bio-HDPE matrix. The resultant miscibility improvement was ascribed to both the high solubility and plasticizing effect of MLO on the PLA phase as well as the crosslinking effect of DCP on both biopolymers. The latter effect was particularly related to the formation of macroradicals of each biopolymer that, thereafter, led to the *in situ* formation of bio-HDPE-co-PLA copolymers and also to the development of a partially crosslinked network in the binary blend. As a result, cost-effective and fully bio-based polymer pieces with improved mechanical strength, high toughness, and enhanced thermal resistance were obtained. © 2018 Wiley Periodicals, Inc. J. Appl. Polym. Sci. **2019**, *136*, 47396.

INTRODUCTION

Current awareness of environmental issues related to the extensive use of plastics and the increasing necessity of reducing the carbon footprint is generating a great interest in the use of polymer materials derived from natural resources and with great capacity to be recycled. This trend has significantly raised both the interest and use of bio-based and biodegradable polymers, which are capable of decomposing in composting conditions and show similar technical characteristics than their fossil-derived counterparts.[1] Although the price and performance of most biopolymers are still far to those of petrochemical polymers,[2] the development of either green composites[3,4] or biopolymer blends[5,6] can certainly contribute to promote the use of biopolymers at industrial scale.

The use of binary blends represents a cost-effective strategy to obtain a good combination of physical properties and also to reduce the final cost of the biopolymers. This consists of mixing two dissimilar biopolymers in order to obtain formulations with intermediate or better performance than those of the neat biopolymers. In this sense, on the one hand, bio-based polyethylene (bio-PE) combines natural origin with the easy processability and optimal performance of polyolefins. In this sense, high-density polyethylene (HDPE) is among the top five plastic materials in the world in terms of volume, reaching 31.3 million tons in 2009.[7] On the other hand, polylactide (PLA) is currently the most used bio-based and biodegradable polyester. PLA is obtained through the polycondensation reaction of lactides, the dimers that are, in turn, obtained from the fermentation of sugars based on starch.[8] Currently, PLA is considered the front runner in the emerging market of bioplastics due to its good balance between mechanical, thermal, and barrier properties, and its double environmental advantage of being a bio-based and biodegradable material. For these reasons, it is now widely used in 3D printing,[9] biomedical applications,[10,11] automotive and textiles,[12] packaging,[13] and so forth.

ADVANCED SCIENCE NEWS
advancedsciencenews.com

A comparative study on the effect of different reactive compatibilizers on injection-molded pieces of bio-based high-density polyethylene/polylactide blends

Abstract

The present study reports on the development of binary blends consisting of bio-based high-density polyethylene (bio-HDPE) with polylactide (PLA), in the 5−20 wt% range, prepared by melt compounding and then shaped into pieces by injection molding. In order to enhance the miscibility between the green polyolefin and the biopolyester, different reactive compatibilizers were added during the melt blending process, namely polyethylene-grafted maleic anhydride (PE-*g*-MA), poly(ethylene-*co*-glycidyl methacrylate) (PE-*co*-GMA), maleinized linseed oil (MLO), and a combination of MLO with dicumyl peroxide (DCP). Among the tested compatibilizers, the dual addition of MLO and DCP provided the binary blend pieces with the most balanced mechanical performance in terms of rigidity and impact strength as well as the highest thermal stability. The fracture surface of the binary blend piece processed with MLO and DCP revealed the formation of a continuous structure in which the dispersed PLA phase was nearly no discerned in the bio-HDPE matrix. The resultant miscibility improvement was ascribed to both the high solubility and plasticizing effect of MLO on the PLA phase as well as the cross-linking effect of DCP on both biopolymers. The latter effect was particularly related to the formation of macroradicals of each biopolymer that, thereafter, led to the *in situ* formation of bio-HDPE-*co*-PLA copolymers and also to the development of a partially cross-linked network in the binary blend. As a result, cost-effective and fully bio-based polymer pieces with improved mechanical strength, high toughness, and enhanced thermal resistance were obtained.

Keywords: Green polyolefins, PLA, reactive extrusion, multi-functionalized vegetable oils, peroxides, mechanical properties

INTRODUCTION

Current awareness of environmental issues related to the extensive use of plastics and the increasing necessity of reducing the carbon footprint is generating a great interest in the use of polymer materials derived from natural resources and with great capacity to be recycled. This trend has significantly raised both the interest and use of bio-based and biodegradable polymers, which are capable of decomposing in composting conditions and show similar technical characteristics than their fossil-derived counterparts [1]. Although the price and performance of most biopolymers are still far to those of petrochemical polymers [2], the development of either green composites [3, 4] or biopolymer blends [5, 6] can certainly contribute to promote the use of biopolymers at industrial scale.

The use of binary blends represents a cost-effective strategy to obtain a good combination of physical properties and also to reduce the final cost of the biopolymers. This consists of mixing two dissimilar biopolymers in order to obtain formulations with intermediate or better performance than those of the neat biopolymers. In this sense, on the one hand, bio-based polyethylene (bio-PE) combines natural origin with the easy processability and optimal performance of polyolefins. In this sense, high-density polyethylene (HDPE) is among the top five plastic materials in the world in terms of volume, reaching 31.3 million tons in 2009 [7]. On the other hand, polylactide (PLA) is currently the most used bio-based and biodegradable polyester. PLA is obtained through the polycondensation reaction of lactides, the dimers that are, in turn, obtained from the fermentation of sugars based on starch [8]. Currently, PLA is considered the front runner in the emerging market of bioplastics due to its good balance between mechanical, thermal, and barrier properties, and its double environmental advantage of being a bio-based and biodegradable material. For these reasons, it is now widely used in 3D printing,[9] biomedical applications [10, 11], automotive and textiles [12], packaging [13], etc.

Recycling is an interesting solution to minimize plastic wastes but its main drawbacks are related to collection and separation, particularly in the case of multilayers. Polyolefins such as polyethylene (PE) and polypropylene (PP) are, with difference, the most recycled polymers but sometimes, due to the difficulty in separating polymers, they can be recycled with low amounts of other polymers (even immiscible) without compromising their overall performance. As mentioned above, PLA is gaining interest at industrial scale and, therefore, it is everyday more present in plastic wastes that can be potentially subjected to recycling. As it is a relatively new polymer in plastic waste streams (with a relatively low percentage in comparison to other polymers), separation is still complex and expensive at this stage, so that, PLA could be present in low amounts in recycled PE and PP streams, leading to complex blends. Polyolefins are highly hydrophobic polymers (non-polar) while, in general, thermoplastic polyesters are more hydrophilic (polar) due to the presence of ester groups and other oxygen-based groups. This difference in polarity leads to a high difference between their solubility parameters (δ). In fact, the δ value of PE is close to 16.0 MPa$^{1/2}$ while PLA shows a typical value of 20 MPa$^{1/2}$, resulting in a poor or lack of miscibility between them [4, 14-17].

The mixture of polymers with a dissimilar physical properties is widely considered as an economic technique to produce plastic materials that have a desirable

combination of properties and may also have the ability to recycle or degrade after usage [18, 19]. However, one of the main problems of the blends made of polyolefins and polyesters is that they present total immiscibility. When mixed together, the resultant polymer blends turn out to have a two-phase morphology in which the main component forms a matrix and the minor component appears as the dispersion phase in the form of spheres, platelets or even fibrils [20]. Unfortunately, immiscible mixtures are frequently characterized by a poor adhesion between the phases and they generally require compatibility for achieving improved performance [21].

Two main methods can be applied to improve the miscibility between two or more immiscible polymers, namely *ex situ* (non-reactive) or *in situ* (reactive) compatibilization [22]. *Ex situ* compatibilization is based on the use of a premade (block or grafted) copolymer, being highly miscible with the blend components that are obtained under careful design and synthesis. Usually, these copolymers possess dual functionality, which means that a chain segment (with a particular chemical structure) can interact with one polymer in the blend and the other segment chain (with other chemical groups) can establish some interactions with the other polymer in the blend, thus acting as a bridge between them. These tailor-made copolymers can reduce particle size, increase morphological stability and interfacial adhesion, and improve final mechanical properties [23]. Some copolymers have been specifically designed for PLA [24, 25] or PE [22, 26], providing good results as compatibilizers [27]. The second method to improve the compatibility in polymer blends is the use of in situ (reactive) compatibilization, the so-called reactive extrusion (REX), during the compounding of the polymer formulation [28, 29]. *In situ* compatibilization is carried out by means of polymers, oligomers, and additives containing multi-functional groups (*e.g.* anhydride, epoxy, oxazoline, isocyanates, etc.) that are capable of reacting during the extrusion process with the functional groups (*e.g.* hydroxyl and carboxyl terminal groups of condensation polymers) to form new copolymers [29, 30]. REX is a straightforward and cost-effective technique for polymer processing in which dicumyl peroxide (DCP), a free radical initiator widely used in polymerization processes, can be additionally used as an initiator and cross-linker [31]. Indeed, DCP has been used to promote the compatibilization of immiscible polymers in different polymer binary blends with good results. For instance, Garcia-Garcia *et al*. [32] improved the compatibility between poly(3-hydrobutyrate) (PHB) and poly(ε-caprolactone) (PCL) by the addition of DCP. Moreover, in a more sustainable context, derivatives of natural oils, such as acrylated [4], epoxidized [32] or maleinized vegetable oils [4, 33], can be used as reactive additives to improve the properties of biopolymers and also to achieve compatibility in polymer blends or even in green composites. Among them, epoxidized linseed oil and, more lately, maleinized linseed oil (MLO) currently represent a sustainable solution in PLA-based formulations [4, 34-36].

Bio-based high-density polyethylene (bio-HDPE), also called "microbial" or "green" HDPE, is a polyolefin produced by conventional polymerization of ethylene obtained by catalytic dehydration of bioethanol [37]. Bio-HDPE has the same physical properties than its counterpart petrochemical resin, particularly having a good mechanical resistance, high ductility, and improved water resistance [38]. Injection-molded pieces of bio-HDPE can be targeted to manufacture rigid plastic parts for packaging materials and surfaces (*e.g.* cutting boards, kitchen utensils and countertops, and storage containers) [39].

The aim of this study was to prepare binary blends of bio-HDPE with PLA by melt compounding in order to develop a cost-effective and fully renewable material with high mechanical strength and rigidity but with still sufficient mechanical ductility. To this end, this work explores the use of different reactive additives as compatibilizers, such as copolymers and grafted polymers, multi-functionalized vegetable oils, and a cross-linking agent, to enhance the miscibility between both biopolymers and obtain the more balanced mechanical performance.

EXPERIMENTAL

Materials

Bio-HDPE was SHA7260, a grade for injection molding supplied by FKuR Kunststoff GmbH (Willich, Germany) and manufactured by Braskem (São Paulo, Brazil). It has a density of 0.955 g/cm³ and a melt flow index (MFI) of 20 g/10 min measured at 190 ºC and 2.16 kg. Its minimum bio-based content is 94%, as determined by the manufacturer according to ASTM D6866. Commercial PLA Ingeo™ biopolymer 6201D was obtained from NatureWorks (Minnetonka, MN, USA). This PLA grade has a density of 1.24 g/cm³ and a melt flow rate (MFR) of 15–30 g/10 min, measured at 210 °C and 2.16 kg, which makes it suitable for injection molding.
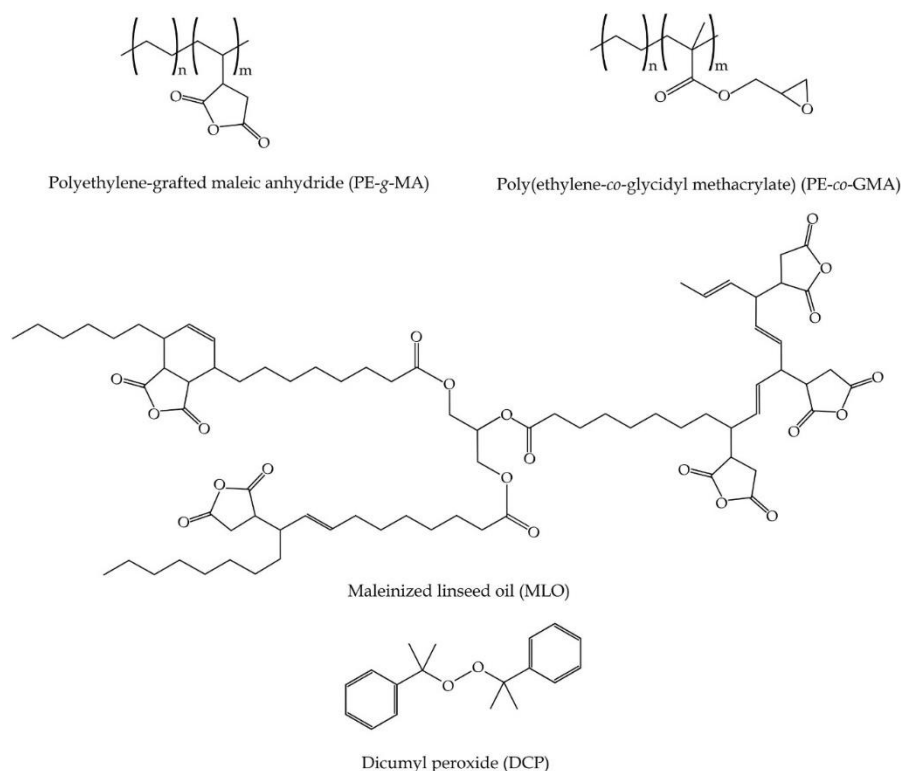
Figure III.1.4.1. Chemical structure of the different compatibilizers used in this work.

Polyethylene-grafted maleic anhydride (PE-*g*-MA) and poly(ethylene-*co*-glycidyl methacrylate) (PE-*co*-GMA), with reference numbers 456624 and 430862, respectively, and MFI values of 5 g/10 min (190 °C/2.16 kg), were obtained from Sigma-Aldrich S.A. (Madrid, Spain). These two PE-based copolymers were selected due to their dual functionality: non-polar polyethylene segments and polar segments,

either with maleic anhydride (MA) or glycidyl methacrylate (GMA) groups, that can readily react with the hydroxyl groups of the PLA end-chains. MLO, a maleinized vegetable oil from linseed oil, was obtained from Vandeputte (Mouscron, Belgium) as VEOMER LIN. This multi-functional reactive oil was selected due to its dual functionality since it contains non-polar fatty acids and polar maleic anhydride-grafted fatty acids. The oil has a viscosity of 1000 cP at 20 °C and an acid value of 105–130 mg potassium hydroxide (KOH)/g. Finally, DCP, with 98% purity, was purchased from Sigma-Aldrich S.A. (Madrid, Spain) and used to provide free radicals during the REX process. **Figure III.1.4.1** shows the chemical structure of each compatibilizer.

Preparation of biopolymer blends

REX was carried out in a co-rotating twin-screw extruder from Construcciones Mecánicas Dupra, S.L. (Alicante, Spain). The speed of the screws, having a diameter of 25 mm with a ratio of length (L) to diameter (D), that is, L / D of 24, was set at 25 rpm and the extrusion temperature profile, from the hopper to the die, was set as follows: 165–170–175–180 °C. All materials were fed through the main hopper, being previously pre-homogenized in a zipper bag. These were extruded through a round die to produce strands and pelletized using an air-knife unit. In all cases, residence time was approximately 1 min. **Table III.1.4.1** gathers the set of materials prepared during extrusion. The additives were added as parts per hundred resin (phr) of biopolymer.

Table III.1.4.1. Summary of compositions according to the weight content (wt%) of bio-based high-density polyethylene (bio-HDPE) and polylactide (PLA) in which polyethylene-grafted maleic anhydride (PE-*g*-MA), poly(ethylene-*co*-glycidyl methacrylate) (PE-*co*-GMA), maleinized linseed oil (MLO), and dicumyl peroxide (DCP) were added as parts per hundred resin (phr) of biopolymer blend.

Sample	Bio-HDPE (wt%)	PLA (wt%)	PE-*g*-MA (phr)	PE-*co*-GMA (phr)	MLO (phr)	DCP (phr)
Bio-HDPE	100	0	0	0	0	0
Bio-HDPE/5PLA	95	5	0	0	0	0
Bio-HDPE/10PLA	90	10	0	0	0	0
Bio-HDPE/15PLA	85	15	0	0	0	0
Bio-HDPE/20PLA	80	20	0	0	0	0
Bio-HDPE/20PLA+PE-*g*-MA	80	20	3	0	0	0
Bio-HDPE/20PLA+PE-*co*-GMA	80	20	0	3	0	0
Bio-HDPE/20PLA+MLO	80	20	0	0	5	0
Bio-HDPE/20PLA+MLO+DCP	80	20	0	0	5	1

The compounded pellets were, thereafter, shaped into pieces by injection molding in a Meteor 270/75 from Mateu & Solé (Barcelona, Spain). The temperature profile was 165 °C (hopper), 170 °C, 175 °C, and 180 °C (injection nozzle). A clamping force of 75 tons was applied while the cavity filling and cooling time were set at 1 and 10 s, respectively. Pieces with a thickness of 4 mm were produced. **Figure III.1.4.2** shows a schematic representation of the manufacturing process.
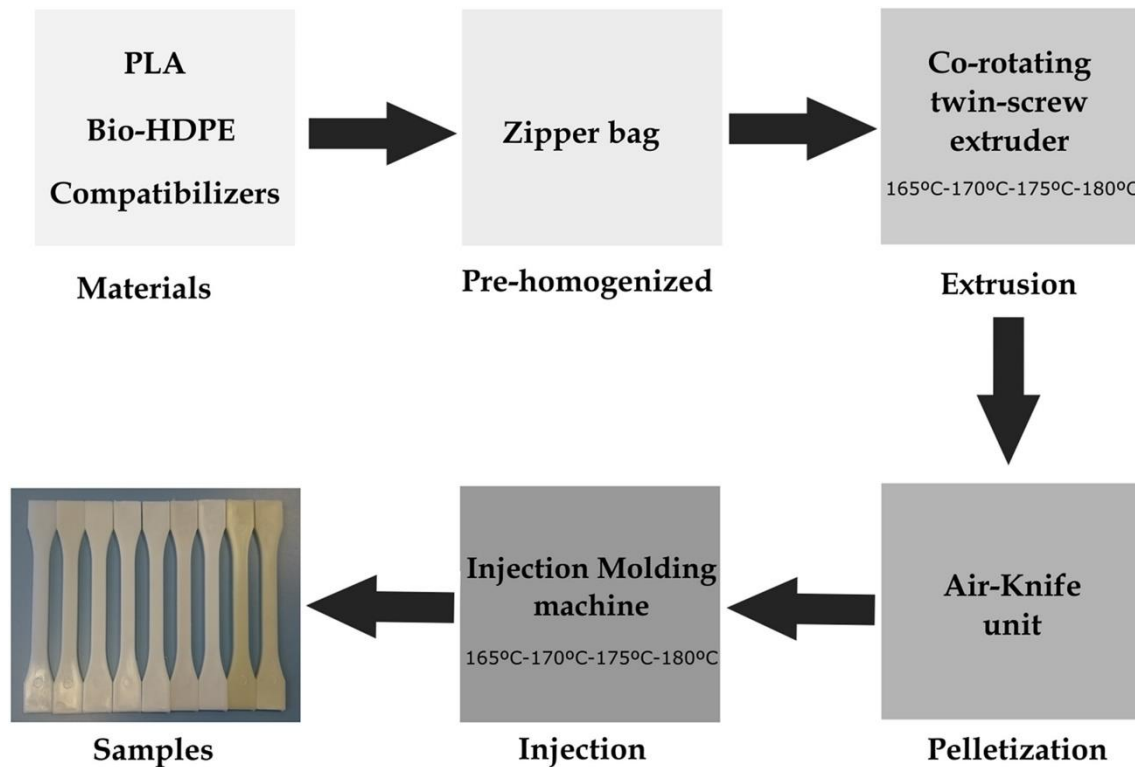
Figure III.1.4.2. Schematic representation of the manufacturing process of the injection-molded pieces of bio-based high-density polyethylene (bio-HDPE)/polylactide (PLA) blends.

Mechanical characterization

The tensile tests were performed in a universal testing machine ELIB 50 of S.A.E. Ibertest (Madrid, Spain) as recommended by ISO 527-1:2012. The tests were carried out with a load cell of 5 kN and the loading speed was set to 40 mm/min.

The hardness measurements were done according to ISO 868:2003, using a Model 676-D durometer (J. Bot Instruments S.A., Barcelona, Spain). The impact resistance was measured using a 1-J Charpy pendulum test machine from Metrotec S.A. (San Sebastián, Spain) in rectangular pieces with dimensions of 4x10x80 mm^3 and a 0.25-mm radius v-notch, according to the specifications of ISO 179-1:2010.

All samples were analyzed at room temperature, that is, 25 ° C, and at least 6 samples of each material were tested and their values averaged.

Morphological characterization

The morphology of the fracture surfaces of the biopolymer pieces obtained from the impact tests was observed by field emission scanning electron microscopy (FESEM) in a ZEISS ULTRA 55 from Oxford Instruments (Abingdon, UK). Prior to placing the samples in the vacuum chamber, the surfaces were sputtered with a gold-palladium alloy in an EMITECH sputter coating SC7620 model from Quorum Technologies, Ltd. (East Sussex, UK). An acceleration voltage of 2 kV was applied.

Thermal characterization

The main thermal transitions of the biopolymer pieces were obtained by differential scanning calorimetry (DSC) in a Mettler-Toledo 821 calorimeter (Schwerzenbach, Switzerland). An average sample weight of 5 to 7 mg was subjected to a thermal cycle as follows: initial heating from 25 °C to 200 °C, cooling to -50 °C, and second heating to 300 °C, at a heating rate of 10 °C/min. All tests were performed under a nitrogen atmosphere (66 mL/min) with standard sealed aluminum crucibles with a volume capacity of 40 µL.

Thermogravimetric analysis (TGA) was carried out in a Mettler-Toledo TGA/SDTA 851 thermobalance (Schwerzenbach, Switzerland). Samples, with an average weight between 5 and 7 mg, were placed in standard alumina crucibles (70 µL) and subjected to a heating program from 30 °C to 700 °C at a heating rate of 20 °C/min in air atmosphere. All thermal tests were performed in triplicate.

Thermomechanical characterization

Dynamical mechanical thermal analysis (DMTA) was carried out in a DMA1 dynamic analyzer from Mettler-Toledo (Schwerzenbach, Switzerland), working in single cantilever flexural conditions. Samples with dimensions of 20x6x2.7 mm^3 were subjected to a temperature sweep from -160 °C to 100 °C at a constant heating rate of 2 °C/min. The selected frequency was 1 Hz while the maximum flexural deformation was 10 µm.

The dimensional stability of the injection-molded pieces was estimated by thermomechanical analysis (TMA) in a Q-400 thermoanalyzer from TA Instruments (Newcastle, DE, USA) using rectangular samples of 10x10x4 mm^3. A dynamic temperature ramp was programmed from -160 °C to 100 °C, at a heating rate of 3 °C/min and a constant load of 0.02 N. All thermomechanical tests were run in triplicate.

RESULTS ANS DISCUSION

Mechanical properties

The mechanical characterization of the injection-molded pieces made of bio-HDPE and its blends with PLA provides relevant information in terms of the effect of the blend composition and the tested additives as well as their most suitable applications. **Table III.1.4.2** shows the values of tensile modulus ($E_{tensile}$), maximum tensile strength (σ_{max}), elongation at break (ε_b) of the pieces obtained from the tensile tests. One can observe that the neat bio-HDPE piece presented values of $E_{tensile}$ and σ_{max}

of 408.4 MPa and 21.6 MPa, respectively, while ε_b was 545.2%, indicating that the material was relatively rigid and with a high ductility. The incorporation of PLA into bio-HDPE resulted in rigidity increase of the pieces, that is, the $E_{tensile}$ values varied from 492.9 MPa, for the piece containing 5 wt% PLA, up to 563 MPa, for the piece with 20 wt% PLA. However, while the σ_{max} was kept in the same range or even showed slightly higher values than the neat bio-HDPE piece, that is, in the 21.5−23.5 MPa range, the ε_b values of the pieces significantly decreased with the PLA content. For instance, the bio-HDPE/20PLA piece showed a ε_b value of 54%, that is, approximately 10 times lower than that observed for the neat bio-HDPE. The reduction induced in the ductile properties suggests a poor stress transfer between the two biopolymer phases in which, more likely, the PLA phase acted as a stress concentrator in the bio-HDPE matrix favoring the rupture of the pieces.

Table III.1.4.2. Mechanical properties in terms of tensile modulus ($E_{tensile}$), maximum tensile strength (σ_{max}), elongation at break (ε_b), Shore D hardness, and impact strength of the injection-molded pieces of bio-based high-density polyethylene (bio-HDPE) blended with different percentages of polylactide (PLA) and compatibilized with polyethylene-grafted maleic anhydride (PE-*g*-MA), poly(ethylene-*co*-glycidyl methacrylate) (PE-*co*-GMA), maleinized linseed oil (MLO), and dicumyl peroxide (DCP).

Sample	$E_{tensile}$ (MPa)	σ_{max} (MPa)	ε_b (%)	Shore D hardness	Impact strength (kJ/m²)
Bio-HDPE	408.4 ± 16.6	21.6 ± 0.4	545.2 ± 56,1	61.8 ± 0.8	3.77 ± 0.2
Bio-HDPE/5PLA	492.9 ± 11.1	21.7 ± 0.2	499.0 ± 74.5	62.0 ± 0.7	2.83 ± 0.2
Bio-HDPE/10PLA	500.0 ± 9.10	21.5 ± 0.2	253.2 ± 35.8	63.2 ± 0.8	1.88 ± 0.2
Bio-HDPE/15PLA	538.6 ± 6.34	22.2 ± 0.1	122.4 ± 6.73	66.2 ± 0.8	1.76 ± 0.2
Bio-HDPE/20PLA	563.0 ± 10.3	23.2 ± 0.3	54.0 ± 6.09	67.4 ± 1.1	1.70 ± 0.2
Bio-HDPE/20PLA+PE-*g*-MA	568.1 ± 8.84	22.7 ± 0.2	57.6 ± 4.33	68.0 ± 0.7	1.57 ± 0.2
Bio-HDPE/20PLA+PE-*co*-GMA	570.1 ± 6.38	22.1 ± 0.1	34.4 ± 4.28	67.5 ± 0.9	2.01 ± 0.3
Bio-HDPE/20PLA+MLO	496.1 ± 17.4	18.9 ± 0.2	50.5 ± 2.71	58.8 ± 1.5	3.96 ± 0.3
Bio-HDPE/20PLA+MLO+DCP	582.0 ± 6.07	22.0 ± 0.2	23.2 ± 1.16	65.8 ± 0.8	3.71 ± 0.5

The addition of the different compatibilizers was analyzed on the bio-HDPE/20PLA pieces. It can be observed that the studied compatibilizers induced very dissimilar effects on the mechanical properties of the binary blend pieces. In relation to the PE-based compatibilizers, both PE-*g*-MA and PE-*co*-GMA delivered a similar improvement in E*tensile*, reaching values of approximately 570 MPa, and a slight reduction in σ*max*. In contrast, the addition of PE-*g*-MA slightly increased ε_b, reaching a value of 57.7%, while PE-*co*-GMA induced a significant reduction in ductility down to a value of 34.4%. This suggests that the latter additive could produce certain cross-linking in the biopolymer blend. Similar results were obtained, for instance, by Abdolrasouli *et al*. [40] using PE-*g*-MA as compatibilizer in PLA/PE blends containing organoclays. In particular, it was observed that the PLA/PE/PE-*g*-MA 80/12/8 (wt/wt) blends increased ε_b around 30%, while the tensile strength properties

remained almost constant in comparison to an unmodified PLA/PE blend. In this sense, it is worthy to note that the selected PE-based compatibilizers show dual functionality. On one hand, the hydrophobic PE blocks and, on the other hand, the highly polar and reactive MA and GMA groups. The PE blocks/segments can then interact with the bio-HDPE chains in the blend while both the MA and GMA groups can readily react/interact with the hydroxyl groups of PLA through esterification and etherification reactions, respectively. This way, the PE-based compatibilizer chains tended to place at the interface between the bio-HDPE and PLA phases thus acting as a bridge between the two immiscible phases. This partial compatibilization has been reported to yield improved miscibility and allows somewhat load transfer between both polymers in the blend, thus, overcoming (or minimizing) the negative effects of immiscibility [41, 42].

In the case of MLO, the addition of the vegetable oil generated pieces with similar or slightly lower mechanical properties than the neat bio-HDPE/20PLA piece. This reduction in the mechanical strength has been previously related to the plasticizing effect of MLO on the PLA matrix, in which the multi-functionalized oil also produced an increase in ductility [4, 35]. However, the absence of improvement in the ε_b value of the here-described pieces suggests that the vegetable oil presented a low solubility and, thus, a poor effect on the bio-HDPE matrix. Interestingly, the combination of MLO and DCP resulted in more rigid injection-molded pieces, showing the highest Etensile value among the tested pieces, that is, 582 MPa, and the lowest ε_b value, that is, 23.2%. As similar to the PE-*co*-GMA-treated piece, it can be considered that the addition of the peroxide additive generated a cross-linked structure in the polymer blend. The cross-linking effect of DCP has been tested in different polymers, blends, and composites [43-46]. Similar results were observed, for instance, by Sen-lin Yang *et al.* [47] where the DCP addition resulted in a cross-linking of the PLA structure, yielding a stiffened material with a higher $E_{tensile}$ and lower ε_b.

Table III.1.4.2 also shows the values of Shore D hardness and impact strength of the biopolymer pieces. Similar to the tensile tests, the addition of PLA induced an increase in hardness and a reduction in toughness in comparison to the neat bio-HDPE piece. In particular, while the neat bio-HDPE piece presented a Shore D hardness of 61.8 and an impact-strength value of 3.77 kJ/m², the addition of PLA progressively increased hardness up to 67.4, while it decreased impact strength up to 1.70 kJ/m², both values for the bio-HDPE/20PLA piece. Similar to the tensile properties, the use of PE-g-MA slightly increased hardness but reduced impact strength. As opposite, PE-co-GMA produced pieces with similar hardness but a higher toughness. In particular, the impact-strength value increased to 2.01 kJ/m², that is, an increase of approximately 18%. For the MLO-containing piece, hardness was lower, that is, 58.8, while the impact strength was significantly increased, reaching a value of 3.96 kJ/m², representing an improvement close to 133%. This observation points to the fact that the multi-functionalized oil was probably preferentially incorporated in the PLA-rich regions as a dispersed phase. A similar effect was previously observed for PLA pieces containing acrylated epoxidized soybean oil [4], in which the multi-functionalized oil was dispersed in the form of fine droplets contributing to increasing the impact-absorbed energy in a similar way as, for instance, polybutadiene rubbers do in high-impact polystyrene. This remarkable toughening effect was maintained for the injection-

molded piece produced with MLO in combination to DCP, which also showed hardness values close to those of the neat bio-HDPE/20PLA.

Although the dual incorporation of DCP and MLO improved the impact strength of the bio-HDPE/20PLA piece it also resulted in a slight reduction of 0.25 kJ/m^2 with respect to the MLO-containing bio-HDPE/20PLA piece. This effect can be thus ascribed to the cross-linking effect of DPC on the binary blend, which resulted in a more interconnected network of biopolymer chains that increased the mechanical resistance of the pieces but also reduced its toughness. In this sense, it has been reported that DCP can be effectively applied as a reactive compatibilizer in polymers blends since it decomposes and acts as a free radical initiator [42]. For instance, Garcia-Garcia *et al.* [48] prepared PHB and PCL blends compatibilized with DCP. It was observed that DCP not only promoted the formation of macroradicals of each biopolymer that, thereafter, led to the formation of in situ PHB-*co*-PCL copolymers that contributed to improving compatibilization and forming partially cross-linked networks in the blends, but also the PCL-rich domains could establish stronger interactions with the PHB polymer matrix. Hence, the use of DCP during the melt mixing of polymer blends can yield a series of grafted, branched, and/or cross-linked structures in polymer blends [49].

Morphological characterization

Figure III.1.4.3 includes the FESEM images of the fracture surfaces of the biopolymer pieces after the impact tests. **Figure III.1.4.3a**, corresponding to the neat bio-HDPE piece, shows a fracture surface with a very irregular and rough appearance presenting the typical cavernous formations of a polymer with a ductile behavior. Due to the low miscibility between both biopolymers, one can observe in **Figure III.1.4.3e** that PLA remained incorporated into the bio-HDPE matrix as a dispersed phase in the form of micro-sized spherical domains or droplets generating an "island-and-sea" morphology. The absence of a co-continues phase morphology in the blends supports previous studies indicating that, at the here-studied mixing ratios, these biopolymers are thermodynamically immiscible [50]. Additionally, these droplets were larger as the percentage of the added PLA was increased. In particular, the size of these droplets ranged between 1−2 µm for the bio-HDPE/5PLA piece, 2−3 µm for the bio-HDPE/10PLA piece, 3−5 µm for the bio-HDPE/15PLA piece, and 4−8 µm for the bio-HDPE/20PLA piece. One can also observe the existence of a gap or a lack of continuity between the PLA droplets and the bio-HDPE matrix, which was more noticeable in the pieces with the highest PLA contents, shown in **Figure III.1.4.3d** and **3e**. In addition, the fracture surfaces presented several holes, suggesting a phenomenon of phase debonding after breakage. Both the presence of gaps and holes further indicates the lack of compatibility between the two phases, therefore suggesting that the presence of the PLA microdroplets acted as stress concentrators rather than a reinforcing element. This would explain the above-described mechanical performance of the bio-HDPE/PLA pieces, by which when the pieces are subjected to external stresses the microdroplets are responsible for their loss of intrinsic ductility.
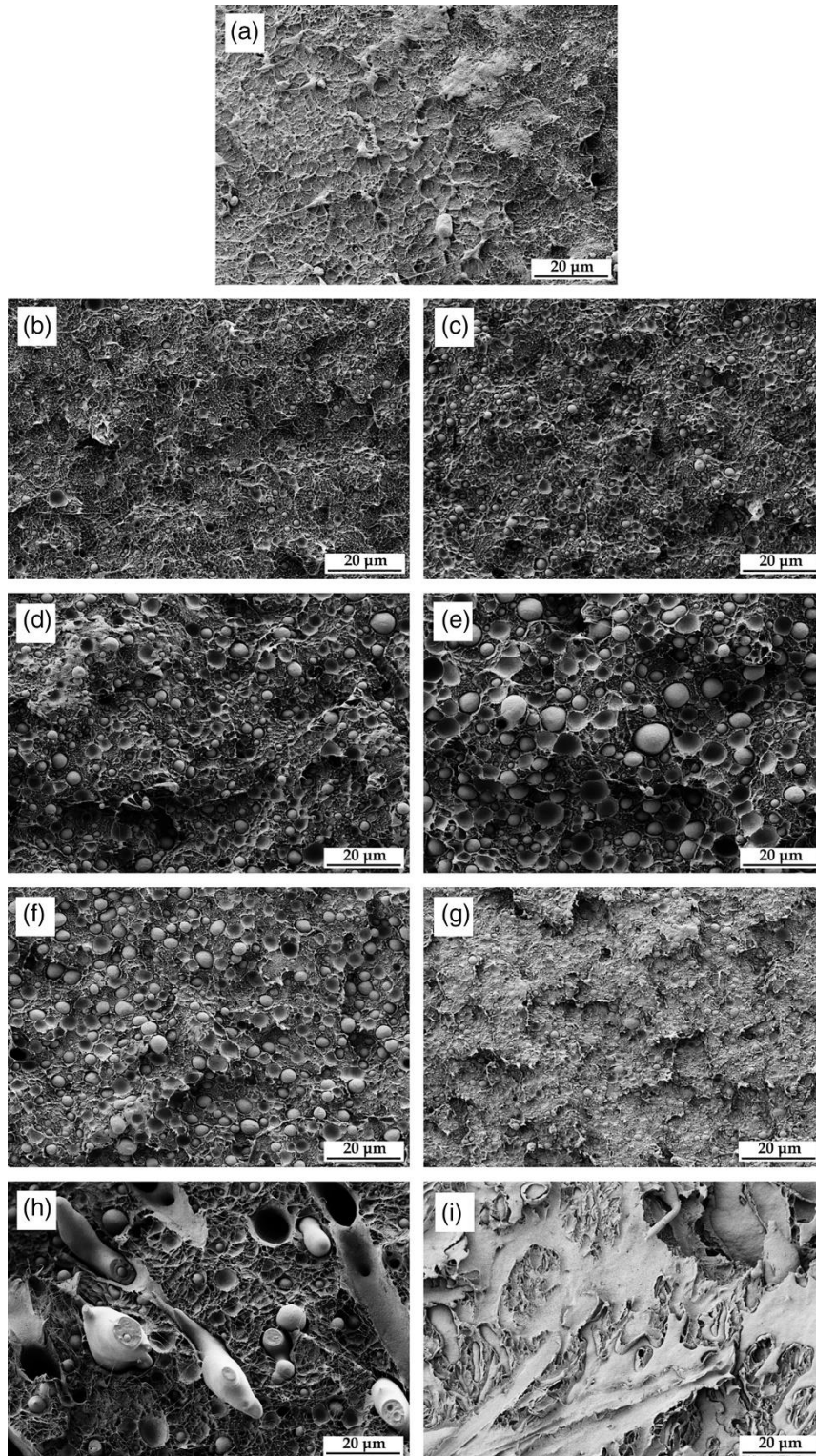
Figure III.1.4.3. Field emission scanning electron microscopy (FESEM) images, taken at 1000×, of the surface fractures of the injection-molded pieces of: a) Neat bio-based high-density polyethylene (bio-HDPE); b) Bio-HDPE/5 polylactide (PLA); c) Bio-HDPE/10PLA; d) Bio-HDPE/15PLA; e) Bio-HDPE/20PLA; f) Bio-HDPE/20PLA + polyethylene-grafted maleic anhydride (PE-*g*-MA); g) Bio-HDPE/20PLA + poly(ethylene-*co*-glycidyl methacrylate) (PE-*co*-GMA); h) Bio-HDPE/20PLA + maleinized linseed oil (MLO); i) Bio-HDPE/20PLA+MLO + dicumyl peroxide (DCP). Scale markers of 20 µm.

In relation to the effect of the different tested compatibilizers, one can observe that the surface fracture of the piece treated with PE-*g*-MA, shown in Figure 3f, presented a similar morphology than that of the neat bio-HDPE/20PLA piece. However, the mean size of the PLA droplets was slightly lower, that is, 4-6 μm, and the number of voids was also reduced. This reduction of the PLA domains was more evident in the case of the pieces treated with PE-*co*-GMA, where the mean droplets size was in the 1−2 μm range. Moreover, the gap at the interface between the two polymers was significantly reduced. This suggests that a higher coalescence stabilization in the biopolymer blend was successfully achieved due to a reduced surface tension between the phases. This phenomenon would then explain the improved capacity of energy absorption observed during the impact tests. A similar morphological effect was previously observed by Wang *et al*. [51] when PE-*g*-MA was used as a compatibilizer between HDPE and poly(ethylene-co-vinyl alcohol) (EVOH). It was observed that the domain size of EVOH decreased in the HDPE matrix when 10 phr PE-*g*-MA were used while the phase boundaries disappeared as its content was higher than 20 phr. Similarly, Quiroz-Castillo *et al*. [52] showed positive results in low-density polyethylene (LDPE)/chitosan blends due to the incorporation of 5 wt% PE-*g*-MAH.

Figure III.1.4.3g one can observe the surface fracture of the blend piece processed with MLO. Noticeably, the droplets became larger, leading to the formation of big droplets that also presented some stretching phenomenon along the bio-HDPE matrix. Further observation at the droplet cross-sections revealed the presence of ultrathin enclosed droplets or pores, which supports the above-described hypothesis that MLO was mainly incorporated into the PLA phase. In any case, a large gap between the bio-HDPE and PLA phases could be still discerned and, hence, the multi-functionalized vegetable oil failed to yield compatibilization to the blend. Interestingly, the surface fracture of the bio-HDPE/20PLA piece processed with MLO and DCP revealed the presence of a continuous structure. Indeed, the dispersed PLA droplets were mostly no longer discerned and it gave rise to the formation of a morphology in which the bio-HDPE matrix fully covered the enclosed PLA regions. In particular, these PLA regions showed a dendritic or branch-like shape, being produced during fracture as a result of the high interaction between the two biopolymers. The fracture also produced a rougher surface with certain plastic deformation where no evidence of phase separation or pull-out of the inclusion phase after fracture was observed. This morphological change can be attributed to both the *in situ* formation of bio-HDPE-*co*-PLA copolymers to achieve compatibilization and the cross-linking effect of DCP, above described during the mechanical analysis, which produced a fully interconnected bio-HDPE/PLA structure. The previous work carried out by Ma *et al*. [53] showed that DCP is able to compatibilize PLA/PBAT blends by the formation of an in-situ formed PLA-g-PBAT copolymer, reducing the size of the PBAT domains embedded in the PLA matrix from 1.0 μm to 0.6 μm after addition of 0.1 wt% DCP. In another work, Li *et al*. [54] observed that the addition of 0.5% DCP to polyamide 11/EVOH blends favored the formation of more fine spherical domains. Moreover, large number of thinner and longer embedded flat-like structures of EVOH were obtained when 1.5% DCP was added.

Thermal characterization

Figure III.1.4.4 shows the DSC curves during the second heating of the biopolymer pieces. One can observe that the neat bio-HDPE presented a melting temperature (T_m) of 132.2 ± 1.5 °C. The addition of PLA generated a second endothermic peak, related to the melting of PLA, which was observed in the 160−180 °C range. For the bio-HDPE/20PLA blend instance, this peak was centered at approximately at 169.6 ± 0.7 °C. The second peak intensity was relatively low though it was more noticeable at high PLA contents, that is, 15 and 20 wt%. Additionally, it can be observed that the T_m values of the bio-HDPE phase slightly decreased gradually with increasing the PLA content, up to 131.4 ± 1.1 °C, for the bio-HDPE/20PLA blend. The melting enthalpies were also lower in the blend formulations with higher PLA contents. In overall, the thermal values remained almost constant, which confirmed the poor compatibility or absence of miscibility between both biopolymers. A similar observation was previously obtained in, for instance, PLA/PP blends [55].
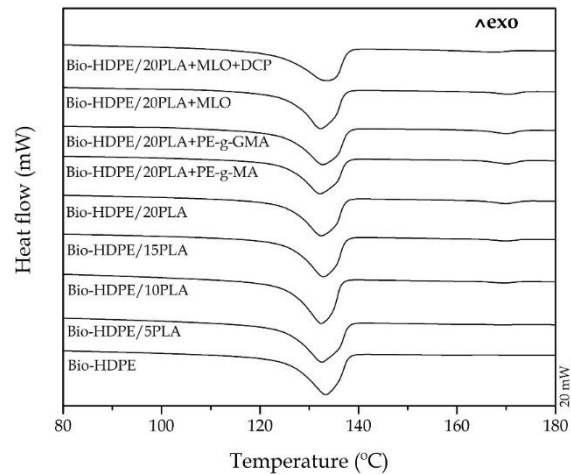
Figure III.1.4.4. Differential scanning calorimetry (DSC) curves of the injection-molded pieces of bio-based high-density polyethylene (bio-HDPE) blended with different percentages of polylactide (PLA) and compatibilized with polyethylene-grafted maleic anhydride (PE-*g*-MA), poly(ethylene-*co*-glycidyl methacrylate) (PE-*co*-GMA), maleinized linseed oil (MLO), and dicumyl peroxide (DCP).

With the incorporation of the different compatibilizers, some interesting changes in the thermal properties of the injection-molded pieces could be observed. While the melting profile of the blends remained nearly constant with the addition of both PE-*g*-MA and PE-*co*-GMA, the use of MLO in combination with DCP produced both an increase in the T_m value related to the bio-HDPE phase, that is, 134.5 ± 1.0 °C, and a decrease for the PLA phase, that is, 167.2 ± 0.8 °C. This slight shift in the characteristic melting profiles of HDPE and PLA can be related to the formation of some HDPE-*g*-PLA copolymer chains due to the action of DCP, which can provide free radicals to attach the HDPE chains, and MLO, which can react with the hydroxyl groups in PLA and also provide plasticization. Although the change was not substantial, it gives some evidence of the synergistic compatibilizing effect of DCP and MLO on the blends of bio-HDPE with PLA. Similar findings were reported by, for instance, Lai *et al*. [56] in binary blends of PLA with thermoplastic polyurethane (TPU) compatibilized with aminosilane. A depression in the characteristic melting peak of

PLA was attributed to a lubrication provided by the compatibilized chains with a low molecular weight (M_W). Although MLO, as similar to other vegetable oils, is able to plasticize PLA and then to increase its free volume and reduce the biopolymer-biopolymer interactions [4], this effect was not observed in the neat MLO-containing blend piece, suggesting that the addition of DCP favored certain miscibility for the whole blend system. In any case, the absence of significant melting peak shifts towards intermediate temperatures, in between the melting peaks of each polymer in the blend, confirmed the presence of two phases with different crystal types and therefore the absence of a fully miscible structure [22].
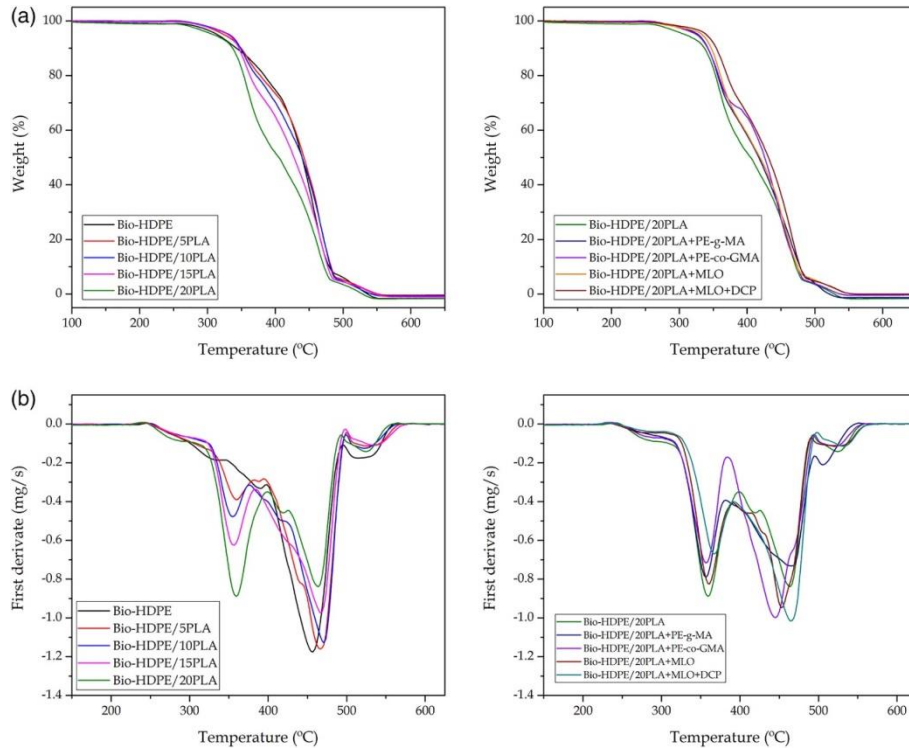
Figure III.1.4.5. Thermogravimetric analysis (TGA) curves of the injection-molded pieces of bio-based high-density polyethylene (bio-HDPE) blended with different percentages of polylactide (PLA) and compatibilized with polyethylene-grafted maleic anhydride (PE-*g*-MA), poly(ethylene-*co*-glycidyl methacrylate) (PE-*co*-GMA), maleinized linseed oil (MLO), and dicumyl peroxide (DCP): a) Weight loss and b) First derivate.

In relation to thermal stability, **Figure III.1.4.5** shows the TGA curves for the here-prepared biopolymer pieces whereas **Table III.1.4.3** summarizes the obtained values from the curves. The neat bio-HDPE piece presented an onset degradation temperature, defined as the temperature at which the material losses 5% of its mass ($T_{5\%}$), of 312.5 ± 1.7 °C. Its degradation temperature (T_{deg}), determined at the temperature when the mass loss was maximum, was 455.2 ± 1.5 °C. Additionally, the green polyolefin degraded in a single stage, giving a residual mass of 0.3 ± 0.2 %. A similar thermal degradation profile has been recently observed by Montanes *et al*. [57] for bio-HDPE. Interestingly, it can be seen that the incorporation of PLA positively delayed the degradation onset of bio-HDPE, up to values in the range of 324−329 °C, but it also reduced the values of T_{deg}. In particular, the TGA curves presented two main weight losses. The first one occurred from 320 °C to 390 °C, which can be related to the

initial thermal decomposition of bio-HDPE and mainly to the whole thermal degradation of the PLA phase. The second one was observed in the 400−510 ºC range, which can be ascribed to the chain-scission process of bio-HDPE. In this sense, Garcia-Campo *et al.* [58] has recently analyzed the thermal degradation of PLA, showing that the thermal decomposition of the biopolyester occurs in one single step, in the 300−400 ºC range, with $T_{5\%}$ and T_{deg} values of 328.5 °C and 368.5 °C, respectively.

Table III.1.4.3. Thermal properties in terms of onset degradation temperature ($T_{5\%}$), degradation temperature (T_{deg}), and residual mass at 700 °C of the injection-molded pieces of bio-based high-density polyethylene (bio-HDPE) blended with different percentages of polylactide (PLA) and compatibilized with polyethylene-grafted maleic anhydride (PE-*g*-MA), poly(ethylene-*co*-glycidyl methacrylate) (PE-*co*-GMA), maleinized linseed oil (MLO), and dicumyl peroxide (DCP).

Sample	$T_{5\%}$ (ºC)	$T_{deg\,1}$ (ºC)	$T_{deg\,2}$ (ºC)	Residual mass (%)
Bio-HDPE	312.5 ± 1.7	-	455.2 ± 1.5	0.2 ± 0.3
Bio-HDPE/5PLA	324.1 ± 1.4	359.5 ± 1.6	466.5 ± 1.8	0.3 ± 0.2
Bio-HDPE/10PLA	327.2 ± 1.8	356.2 ± 1.8	470.9 ± 1.5	0.2 ± 0.3
Bio-HDPE/15PLA	328.9 ± 1.5	355.2 ± 1.7	466.5 ± 1.6	0.3 ± 0.2
Bio-HDPE/20PLA	324.9 ± 1.6	358.1 ± 2.0	465.1 ± 1.9	0.1 ± 0.1
Bio-HDPE/20PLA+PE-*g*-MA	329.6 ± 1.9	356.6 ± 1.9	465.1 ± 1.4	0.3 ± 0.2
Bio-HDPE/20PLA+PE-*co*-GMA	327.3 ± 1.7	356.6 ± 1.7	445.2 ± 1.8	0.4 ± 0.1
Bio-HDPE/20PLA+MLO	332.9 ± 2.1	360.9 ± 2.1	453.7 ± 1.9	0.3 ± 0.2
Bio-HDPE/20PLA+MLO+DCP	338.9 ± 1.4	365.1 ± 1.9	465.1 ± 2.0	0.5 ± 0.3

While the incorporation of both PE-*g*-MA and PE-*co*-GMA compatibilizers induced no changes in the thermal stability of the bio-HDPE/20PLA pieces, the MLO-containing pieces presented a slight improvement. In particular, the values of $T_{5\%}$ increased from 324.9 ± 1.6 ºC, for the neat the bio-HDPE/20PLA piece, to 332.9 ± 2.1 ºC and 338.9 ± 1.4 ºC, for the pieces containing MLO and MLO with DPC, respectively. In the case of T_{deg}, the first degradation peak was also delayed from 358.1 ± 2.0 ºC, for the neat the bio-HDPE/20PLA piece, to 360.9 ± 2.1 ºC and 365.1 ± 1.9 ºC, for the pieces containing MLO and MLO with DPC, respectively. An increase in thermal stability by the incorporation of multi-functionalized vegetable oils has already been reported in some of our previous works [4, 34], which was related to the development of a macromolecule with a higher M_W. In the case of the piece treated with MLO and DCP, the thermal stability improvement can be ascribed to the partial cross-linking achieved in the blend. In this sense, it has been reported that the thermal stability of biopolymers can be improved, to a certain extent, with the addition DCP [32, 59]. In relation to the residual mass, it can be seen that, in all cases, small residual amounts in the 0.1−0.5% range were produced.

Thermomechanical characterization

Figure III.1.4.6a presents the evolution of the storage module (G ') in the here-developed bio-HDPE/PLA pieces from -150 °C to 100 °C. In relation to the neat bio-HDPE piece, a sharp decrease of G′ was produced up to -100 °C, which can be related to the glass-to-rubber transition of the green polyolefin. Then, it progressively decreased as the test temperature increased due to a softening effect of the bio-HDPE matrix. The incorporation of PLA into the bio-HDPE matrix induced a slight decrease in G′, which was more pronounced as the percentage of PLA increased. In particular, at -150 °C, it decreased from 2493 MPa, for the neat bio-HDPE piece, to 2140 MPa, for the bio-HDPE/20PLA piece. This reduction was observed up to temperatures close to 0 °C, which supposed a decrease in the overall rigidity of the material. Similar to other physical properties, the addition of both PE-*g*-MA and PE-*co*-GMA resulted in a similar thermomechanical profile whereas the MLO induced some relevant changes. In the case of the neat MLO-treated bio-HDPE/PLA piece, lower G′ values were observed in the whole temperature range. This reduction has been ascribed to the intrinsic plasticizing effect provided by MLO on polyesters [4]. In any case, the G ' reduction was relatively low, indicating that the oil mainly plasticized the dispersed PLA phase, as described above during the morphological analysis. The combined use of MLO and DCP provided, in a similar way to the mechanical and thermal properties described above, the highest rigidity increase. This change was mainly seen in the temperature range from -100 °C to -25 °C, while at higher temperatures all pieces presented a similar thermomechanical performance. For instance, at -25 °C, the G′ value increased from 1229.5 MPa, for the neat bio-HDPE/20PLA piece, to 1369.6 MPa, for the same piece processed with MLO and DCP.
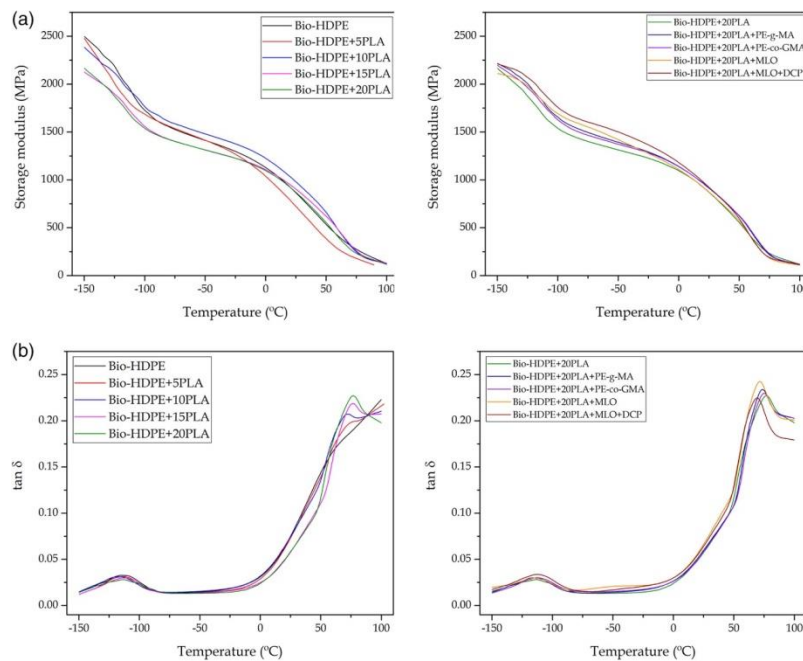
Figure III.1.4.6. Dynamical mechanical thermal analysis (DMTA) curves of the injection-molded pieces of bio-based high-density polyethylene (bio-HDPE) blended with different percentages of polylactide (PLA) and compatibilized with polyethylene-grafted maleic anhydride (PE-*g*-MA), poly(ethylene-*co*-glycidyl methacrylate) (PE-*co*-GMA), maleinized linseed oil (MLO), and dicumyl peroxide (DCP): a) Storage modulus (G′) and b) damping factor (tan ∂).

Figure III.1.4.6b shows the evolution of the damping factor (tan ∂) in the bio-HDPE/PLA pieces. The peak located between -112 °C and -116 °C in the bio-HDPE piece sample corresponds to alpha (α)-relaxation of the green polyolefin, which is related to its glass transition temperature (T_g). The PLA blending generated a second peak, seen in the 65−75 °C range, which can be similarly related to the α-relaxation of PLA. The addition of the compatibilizers induced almost no change in the α-relaxation peak of bio-HDPE, while they slightly reduced that of PLA. In the case of PE-*g*-MA and PE-*co*-GMA, this reduction was of only 3−4 °C while the MLO and MLO combined with DCP reduced approximately by 7 and 11 °C, respectively, the α-relaxation peak of PLA. This thermomechanical change can be ascribed to the above-mentioned process of plasticization of the PLA phase by MLO while, particularly for the piece also treated with DCP, this further confirms the improved compatibilization by the peroxide. Indeed, the study of T_g gives an indication of the level of miscibility in polymer blends. Briefly, thermodynamically immiscible blends show different distinguishable Tg values, partially miscible blends have tendency to shift the Tg value of one component toward that of the other, and blends made of two polymers that constitute a completely miscible blend present a single T_g [22]. Therefore, the here-observed shift of T_g for the PLA phase with the combined used of MLO and DCP further supports the partial miscibility with bio-HDPE in the binary blends. Similar results were obtained by Wang *et al.* [60] for thermoplastic dry starch (DTPS) blends with PLA compatibilized by MA in the presence of DCP. In particular, T_g of DTPS shifted to a higher temperature, while PLA's T_g moved to a lower temperature.

In addition to DMTA, the dimensional stability was evaluated by TMA. To this end, the coefficient of linear thermal expansion (CLTE) was studied in the injection-molded pieces and the obtained results are summarized in **Table III.1.4.4**. Below T_g of bio-HDPE, that is, -110 °C, one can observe that the PLA addition to the mixture slightly reduced the CLTE values, making the pieces somewhat stiffer in their glassy region. In particular, it was decreased from 112.7 ± 0.3 μm/m°C, for the neat bio-HDPE piece, to 107.6 ± 1.2 μm/m°C, for the bio-HDPE/20PLA piece. The incorporation of the different compatibilizers further enhanced the reduction of the CLTE values, reaching the lowest CLTE value for the piece processed with MLO and DCP, that is, 90.6 ± 1.3 μm/m°C. As the temperature was increased during the test, the CLTE values also increased. In the temperature range between both T_gs, that is, from -110 °C to 70 °C, the same trend was observed. The addition of PLA reduced the CLTE values from 134.0 ± 0.4 μm/m°C, for the neat bio-HDPE piece, to 94.3 ± 1.1 μm/m°C, for the bio-HDPE/20PLA piece. However, only the piece treated with MLO in combination with DCP showed an improvement in the thermomechanical response, having a value of 85.8 ± 1.2 μm/m°C. The greatest thermomechanical changes were observed at temperatures higher than 70 °C, that is, above Tg of PLA. While the neat bio-HDPE piece showed a CLTE value of 465.3 ± 0.6 μm/m°C, the addition of PLA positively reduced this values up to 342.1 ± 0.96 μm/m°C, for the piece containing 20 wt% PLA. This implies a lower expansion with temperature, thus improving the service conditions of the injection-molded pieces. Although the addition of all compatibilizers increased the CLTE values of the bio-HDPE/20 PLA pieces, the combined use of MLO and DCP again successfully kept this value in the same order of magnitude, that is, 359.4 ± 1.1 μm/m°C. It is worthy to mention the high increase observed for the MLO-treated piece, reaching a CLTE value of 525.1 ± 1.0 μm/m°C. This further supports the

plasticization produced in the dispersed PLA phase, as described in detail in our previous studies [4, 6, 61].

Table III.1.4.4. Coefficients of linear thermal expansion (CLTE) of the injection-molded pieces of bio-based high-density polyethylene (bio-HDPE) blended with different percentages of polylactide (PLA) and compatibilized with polyethylene-grafted maleic anhydride (PE-*g*-MA), poly(ethylene-*co*-glycidyl methacrylate) (PE-*co*-GMA), maleinized linseed oil (MLO), and dicumyl peroxide (DCP).

Sample	CLTE (µm/m ºC)		
	T < -110 ºC	-110 ºC ≥ T ≤ 70 ºC	T > 70 ºC
Bio-HDPE	112.7 ± 0.3	134.0 ± 0.4	465.3 ± 0.6
Bio-HDPE/5PLA	110.7 ± 0.8	103.9 ± 0.6	457.2 ± 0.9
Bio-HDPE/10PLA	107.3 ± 1.3	110.2 ± 0.9	408.9 ± 0.5
Bio-HDPE/15PLA	109.2 ± 0.9	98.2 ± 0.7	408.7 ± 0.6
Bio-HDPE/20PLA	107.6 ± 1.2	94.3 ± 1.1	342.1 ± 0.9
Bio-HDPE/20PLA+PE-*g*-MA	109.5 ± 0.9	101.7 ± 0.8	356.8 ± 1.5
Bio-HDPE/20PLA+PE-*co*-GMA	101.2 ± 1.1	101.3 ± 0.9	499.2 ± 1.1
Bio-HDPE/20PLA+MLO	99.6 ± 0.9	102.1 ± 1.3	525.1 ± 1.0
Bio-HDPE/20PLA+MLO+DCP	90.6 ± 1.3	85.8 ± 1.2	359.4 ± 1.1

CONCLUSIONS

The present study describes the preparation by melt compounding and subsequent injection molding of binary blend pieces of bio-HDPE/PLA, at PLA contents from 5 wt% to 20 wt%, with the aim to develop a cost-effective and fully renewable plastic articles with high mechanical strength and rigidity but with still sufficient mechanical ductility. Whereas the incorporation of PLA into bio-HDPE resulted in an increase of the mechanical strength of the pieces, their toughness significantly decreased with the PLA content. The reduction observed in the ductile properties suggested a poor stress transfer between the two biopolymer phases, due their lack of compatibility, in which the dispersed PLA phase potentially acted as a stress concentrator in the bio-HDPE matrix favoring the piece rupture. The low of miscibility, at the here-studied mixing ratios, between both biopolymers was confirmed by morphological analysis of the fracture surfaces of pieces after the impact tests. In particular, it was observed that PLA remained mainly incorporated into the bio-HDPE matrix as a dispersed phase in the form of micro-sized spherical domains or droplets to generate an "island-and-sea" morphology. The thermal and thermomechanical studies carried out on the biopolymer pieces further confirmed the poor compatibility or absence of miscibility between bio-HDPE and PLA.

In order to increase miscibility and, thus, the mechanical and thermal performance of the pieces, different reactive compatibilizers were tested on the blend pieces of bio-HDPE with 20 wt% PLA, that is, bio-HDPE/20PLA. In particular, it was explored the use of a grafted polymer, that is, PE-*g*-MA, a copolymer, that is, PE-*co*-GMA, a multi-functionalized vegetable oils, that is, MLO, and a combination of MLO with a peroxide, that is, DCP. The obtained results showed that the addition of either PE-*g*-MA or PE-*co*-GMA induced a low improvement on the physical performance of the pieces since these additives were not able to interact with both biopolymers and the binary blend pieces still presented a marked phase separation. In relation to MLO, it was observed that the multi-functionalized vegetable oil was mainly solubilized in the dispersed PLA phase, which became highly plasticized so that it induced an overall enhancement of the ductile properties in the binary blend pieces. Interestingly, the optimal performance was attained for the binary blend piece simultaneously treated with MLO and DCP, which presented the highest modulus, that is, 582 MPa, and also a relatively high value of impact strength, that is, 3.71 kJ/m^2. The fracture surface of the bio-HDPE/20PLA piece processed with MLO and DCP revealed the presence of a continuous structure where the dispersed MLO-containing PLA droplets were mostly no longer discerned and the bio-HDPE matrix fully covered the enclosed PLA regions. This morphological change was attributed to the cross-linking effect of DCP, which resulted in a more polymer interconnected network. The latter effect was related to the formation of macroradicals of each biopolymer that, thereafter, led to the in situ formation of bio-HDPE-*co*-PLA copolymers and also to the development of a partially cross-linked network in the blend. Furthermore, the combined use of both compatibilizers yielded a thermal stability increase of up to 14 °C.

It can be concluded that the combination of multi-functionalizes vegetable oils and peroxides represents an attractive strategy to enhance the miscibility between green polyolefins and biopolyesters and it can potentially contribute to the development of sustainable polymer technologies. The here-obtained injection-molded pieces made of bio-HDPE with up to 20 wt% PLA present higher mechanical resistance and similar impact strength than those of neat bio-HDPE. These pieces, which are fully bio-based, can be then regarded as great candidates for being use in sustainable rigid packaging. Potential uses include, for instance, rigid packaging articles such as food trays and lids, kitchen utensils and countertops, and storage containers, or surfaces such as cutting boards.

Acknowledgements

REFERENCES

1.   Tahir, N., H.N. Bhatti, M. Iqbal and S. Noreen, *Biopolymers composites with peanut hull waste biomass and application for Crystal Violet adsorption.* International journal of biological macromolecules, 2017. **94**: 210-220.

2.   Imre, B. and B. Pukánszky, *Compatibilization in bio-based and biodegradable polymer blends.* European Polymer Journal, 2013. **49**(6): 1215-1233.

3.   Quiles-Carrillo, L., N. Montanes, J. Lagaron, R. Balart and S. Torres-Giner, *On the use of acrylated epoxidized soybean oil as a reactive compatibilizer in injection-molded compostable pieces consisting of polylactide filled with orange peel flour.* Polymer International, 2018. **67**: 1341-1351.

4.   Quiles-Carrillo, L., M. Blanes-Martínez, N. Montanes, O. Fenollar, S. Torres-Giner and R. Balart, *Reactive toughening of injection-molded polylactide pieces using maleinized hemp seed oil.* European Polymer Journal, 2018. **98**: 402-410.

5.   Yu, L., K. Dean and L. Li, *Polymer blends and composites from renewable resources.* Progress in polymer science, 2006. **31**(6): 576-602.

6.   Quiles-Carrillo, L., F. Pineiro, A. Jorda-Vilaplana, N. Montanes and S. Torres-Giner, *Ductility and Toughness Improvement of Injection-Molded Compostable Pieces of Polylactide by Melt Blending with Poly(ε-caprolactone) and Thermoplastic Starch.* Materials, 2018.

7.   Kumar, S., A.K. Panda and R. Singh, *A review on tertiary recycling of high-density polyethylene to fuel.* Resources, Conservation and Recycling, 2011. **55**(11): 893-910.

8.   Biresaw, G. and C. Carriere, *Interfacial tension of poly (lactic acid)/polystyrene blends.* Journal of Polymer Science Part B: Polymer Physics, 2002. **40**(19): 2248-2258.

9.   Li, N., Y. Li and S. Liu, *Rapid prototyping of continuous carbon fiber reinforced polylactic acid composites by 3D printing.* Journal of Materials Processing Technology, 2016. **238**: 218-225.

10.   Lasprilla, A.J., G.A. Martinez, B.H. Lunelli, A.L. Jardini and R. Maciel Filho, *Poly-lactic acid synthesis for application in biomedical devices—A review.* Biotechnology advances, 2012. **30**(1): 321-328.

11.   da Silva, D., M. Kaduri, M. Poley, O. Adir, N. Krinsky, J. Shainsky-Roitman and A. Schroeder, *Biocompatibility, biodegradation and excretion of polylactic acid (PLA) in medical implants and theranostic systems.* Chemical Engineering Journal, 2018.

12.   Oksman, K., M. Skrifvars and J.-F. Selin, *Natural fibres as reinforcement in polylactic acid (PLA) composites.* Composites science and technology, 2003. **63**(9): 1317-1324.

13.   Auras, R., B. Harte and S. Selke, *An overview of polylactides as packaging materials.* Macromolecular Bioscience, 2004. **4**(9): 835-864.

14.   Agrawal, A., A.D. Saran, S.S. Rath and A. Khanna, *Constrained nonlinear optimization for solubility parameters of poly(lactic acid) and poly(glycolic acid) - validation and comparison.* Polymer, 2004. **45**(25): 8603-8612.

15.   Camacho, J., E. Diez, I. Diaz and G. Ovejero, *Hansen solubility parameter: from polyethylene and poly(vinyl acetate) homopolymers to ethylene-vinyl acetate copolymers.* Polymer International, 2017. **66**(7): 1013-1020.

16.   Ferri, J.M., M.D. Samper, D. Garcia-Sanoguera, M.J. Reig, O. Fenollar and R. Balart, *Plasticizing effect of biobased epoxidized fatty acid esters on mechanical and thermal properties of poly(lactic acid).* Journal of Materials Science, 2016. **51**(11): 5356-5366.

17.   Patricia Arrieta, M., M. Dolores Samper, M. Aldas and J. Lopez, *On the Use of PLA-PHB Blends for Sustainable Food Packaging Applications.* Materials, 2017. **10**(9).

18.   Ying-Chen, Z., W. Hong-Yan and Q. Yi-Ping, *Morphology and properties of hybrid composites based on polypropylene/polylactic acid blend and bamboo fiber.* Bioresource technology, 2010. **101**(20): 7944-7950.

19.   Garcia, D., R. Balart, L. Sanchez and J. Lopez, *Compatibility of recycled PVC/ABS blends. Effect of previous degradation.* Polymer Engineering and Science, 2007. **47**(6): 789-796.

20.   Afshari, M., R. Kotek, M.H. Kish, H.N. Dast and B.S. Gupta, *Effect of blend ratio on bulk properties and matrix–fibril morphology of polypropylene/nylon 6 polyblend fibers.* Polymer, 2002. **43**(4): 1331-1341.

21.   Palabiyik, M. and S. Bahadur, *Mechanical and tribological properties of polyamide 6 and high density polyethylene polyblends with and without compatibilizer.* Wear, 2000. **246**(1-2): 149-158.

22.   Muthuraj, R., M. Misra and A.K. Mohanty, *Biodegradable compatibilized polymer blends for packaging applications: A literature review.* Journal of Applied Polymer Science, 2017: 45726-n/a.

23.   Macosko, C., P. Guegan, A.K. Khandpur, A. Nakayama, P. Marechal and T. Inoue, *Compatibilizers for melt blending: Premade block copolymers.* Macromolecules, 1996. **29**(17): 5590-5598.

24.   Wang, Y. and M.A. Hillmyer, *Polyethylene-poly (l-lactide) diblock copolymers: synthesis and compatibilization of poly (l-lactide)/polyethylene blends.* Journal of Polymer Science Part A: Polymer Chemistry, 2001. **39**(16): 2755-2766.

25.   Nehra, R., S. Maiti and J. Jacob, *Poly (lactic acid)/(styrene-ethylene-butylene-styrene)-g-maleic anhydride copolymer/sepiolite nanocomposites: Investigation of thermo-mechanical and morphological properties.* Polymers for Advanced Technologies, 2018. **29**(1): 234-243.

26.   Arostegui, A. and J. Nazabal, *Supertoughness and critical interparticle distance dependence in poly (butylene terephthalate) and poly (ethylene-co-glycidyl methacrylate) blends.* Journal of Polymer Science Part B: Polymer Physics, 2003. **41**(19): 2236-2247.

27.   Li, Z., B.H. Tan, T. Lin and C. He, *Recent advances in stereocomplexation of enantiomeric PLA-based copolymers and applications.* Progress in Polymer Science, 2016. **62**: 22-72.

28.   Torres-Giner, S., N. Montanes, T. Boronat, L. Quiles-Carrillo and R. Balart, *Melt grafting of sepiolite nanoclay onto poly (3-hydroxybutyrate-co-4-hydroxybutyrate) by reactive extrusion with multi-functional epoxy-based styrene-acrylic oligomer.* European Polymer Journal, 2016. **84**: 693-707.

29.   Quiles-Carillo, L., N. Montanes, J.M. Lagaron, R. Balart and S. Torres-Giner, *In Situ Compatibilization of Biopolymer Ternary Blends by Reactive Extrusion with Low-Functionality Epoxy-Based Styrene–Acrylic Oligomer.* Journal of Polymers and the Environment, 2018. DOI: 10.1007/s10924-018-1324-2**.**

30.   Zeng, J.-B., K.-A. Li and A.-K. Du, *Compatibilization strategies in poly (lactic acid)-based blends.* Rsc Advances, 2015. **5**(41): 32546-32565.

31.   Yang, L., J. Huang, X. Lu, S. Jia, H. Zhang, G. Jin and J. Qu, *Influences of dicumyl peroxide on morphology and mechanical properties of polypropylene/poly (styrene-b-butadiene-b-styrene) blends via vane-extruder.* Journal of Applied Polymer Science, 2015. **132**(9).

32.   Carbonell-Verdu, A., M.D. Samper, D. Garcia-Garcia, L. Sanchez-Nacher and R. Balart, *Plasticization effect of epoxidized cottonseed oil (ECSO) on poly (lactic acid).* Industrial Crops and Products, 2017. **104**: 278-286.

33.   Garcia-Campo, M.J., L. Quiles-Carrillo, J. Masia, M.J. Reig-Pérez, N. Montanes and R. Balart, *Environmentally friendly compatibilizers from soybean oil for ternary blends of poly (lactic acid)-PLA, poly (ε-caprolactone)-PCL and poly (3-hydroxybutyrate)-PHB.* Materials, 2017. **10**(11): 1339.

34.   Ferri, J., D. Garcia-Garcia, L. Sánchez-Nacher, O. Fenollar and R. Balart, *The effect of maleinized linseed oil (MLO) on mechanical performance of poly (lactic acid)-thermoplastic starch (PLA-TPS) blends.* Carbohydrate polymers, 2016. **147**: 60-68.

35.   Ferri, J.M., D. Garcia-Garcia, N. Montanes, O. Fenollar and R. Balart, *The effect of maleinized linseed oil as biobased plasticizer in poly (lactic acid)-based formulations.* Polymer International, 2017. **66**(6): 882-891.

36.   Miao, S., P. Wang, Z. Su and S. Zhang, *Vegetable-oil-based polymers as future polymeric biomaterials.* Acta biomaterialia, 2014. **10**(4): 1692-1704.

37.   Chen, G., S. Li, F. Jiao and Q. Yuan, *Catalytic dehydration of bioethanol to ethylene over TiO2/γ-Al2O3 catalysts in microchannel reactors.* Catalysis Today, 2007. **125**(1-2): 111-119.

38.   Babu, R.P., K. O'connor and R. Seeram, *Current progress on bio-based polymers and their future trends.* Progress in Biomaterials, 2013. **2**(1): 8.

39.   Torres-Giner, S., A. Torres, M. Ferrándiz, V. Fombuena and R. Balart, *Antimicrobial activity of metal cation-exchanged zeolites and their evaluation on injection-molded pieces of bio-based high-density polyethylene.* Journal of Food Safety, 2017. **37**(4).

40. Abdolrasouli, M.H., G.M.M. Sadeghi, H. Nazockdast and A. Babaei, *Polylactide/polyethylene/organoclay blend nanocomposites: structure, mechanical and thermal properties.* Polymer-Plastics Technology and Engineering, 2014. **53**(13): 1417-1424.

41. Abdolrasouli, M.H., H. Nazockdast, G.M.M. Sadeghi and J. Kaschta, *Morphology Development, Melt Linear Viscoelastic Properties and Crystallinity of Polylactide/Polyethylene/Organoclay Blend Nanocomposites.* Journal of Applied Polymer Science, 2015. **132**(3).

42. Madhu, G., H. Bhunia, P.K. Bajpai and V. Chaudhary, *Mechanical and morphological properties of high density polyethylene and polylactide blends.* Journal of Polymer Engineering, 2014. **34**(9): 813-821.

43. Betron, C., P. Cassagnau and V. Bounor-Legare, *EPDM crosslinking from bio-based vegetable oil and Diels-Alder reactions.* Materials Chemistry and Physics, 2018. **211**: 361-374.

44. Minhaz-Ul Haque, M., N. Herrera, S. Geng and K. Oksman, *Melt compounded nanocomposites with semi-interpenetrated network structure based on natural rubber, polyethylene, and carrot nanofibers.* Journal of Applied Polymer Science, 2018. **135**(10).

45. Pourshooshtar, R., Z. Ahmadi and F.A. Taromi, *Formation of 3D networks in polylactic acid by adjusting the cross-linking agent content with respect to processing variables: a simple approach.* Iranian Polymer Journal, 2018. **27**(5): 329-337.

46. Zhou, L., H. He, M.-c. Li, S. Huang, C. Mei and Q. Wu, *Enhancing mechanical properties of poly(lactic acid) through its in-situ crosslinking with maleic anhydride-modified cellulose nanocrystals from cottonseed hulls.* Industrial Crops and Products, 2018. **112**: 449-459.

47. Yang, S.-l., Z.-H. Wu, W. Yang and M.-B. Yang, *Thermal and mechanical properties of chemical crosslinked polylactide (PLA).* Polymer Testing, 2008. **27**(8): 957-963.

48. Garcia-Garcia, D., E. Rayón, A. Carbonell-Verdu, J. Lopez-Martinez and R. Balart, *Improvement of the compatibility between poly (3-hydroxybutyrate) and poly (ε-caprolactone) by reactive extrusion with dicumyl peroxide.* European Polymer Journal, 2017. **86**: 41-57.

49. Ma, P., D.G. Hristova-Bogaerds, P.J. Lemstra, Y. Zhang and S. Wang, *Toughening of PHBV/PBS and PHB/PBS Blends via In situ Compatibilization Using Dicumyl Peroxide as a Free-Radical Grafting Initiator.* Macromolecular Materials and Engineering, 2012. **297**(5): 402-410.

50. Utracki, L.A., *Compatibilization of Polymer Blends.* The Canadian Journal of Chemical Engineering, 2002. **80**(6): 1008-1016.

51. Wang, Q., R. Qi, Y. Shen, Q. Liu and C. Zhou, *Effect of high-density polyethylene-g-maleic anhydride on the morphology and properties of (high-density polyethylene)/(ethylene–vinyl alcohol) copolymer alloys.* Journal of applied polymer science, 2007. **106**(5): 3220-3226.

52. Quiroz-Castillo, J., D. Rodríguez-Félix, H. Grijalva-Monteverde, T. del Castillo-Castro, M. Plascencia-Jatomea, F. Rodríguez-Félix and P. Herrera-Franco, *Preparation of extruded polyethylene/chitosan blends compatibilized with polyethylene-graft-maleic anhydride.* Carbohydrate polymers, 2014. **101**: 1094-1100.

53. Ma, P., X. Cai, Y. Zhang, S. Wang, W. Dong, M. Chen and P. Lemstra, *In-situ compatibilization of poly (lactic acid) and poly (butylene adipate-co-terephthalate) blends by using dicumyl peroxide as a free-radical initiator.* Polymer Degradation and Stability, 2014. **102**: 145-151.

54. Li, Y., G. Hu and B. Wang, *Morphology development and non-isothermal crystallization behavior of polyamide 11/ethylene-vinyl alcohol blends.* Journal of applied polymer science, 2010. **118**(4): 2126-2133.

55. Yoo, T.W., H.G. Yoon, S.J. Choi, M.S. Kim, Y.H. Kim and W.N. Kim, *Effects of compatibilizers on the mechanical properties and interfacial tension of polypropylene and poly (lactic acid) blends.* Macromolecular Research, 2010. **18**(6): 583-588.

56. Lai, S.-M., Y.-C. Lan, W.-L. Wu and Y.-J. Wang, *Compatibility improvement of poly(lactic acid)/thermoplastic polyurethane blends with 3-aminopropyl triethoxysilane.* Journal of Applied Polymer Science, 2015. **132**(30).

57.   Montanes, N., D. Garcia-Sanoguera, V. Segui, O. Fenollar and T. Boronat, *Processing and Characterization of Environmentally Friendly Composites from Biobased Polyethylene and Natural Fillers from Thyme Herbs.* Journal of Polymers and the Environment, 2018. **26**(3): 1218-1230.

58.   García-Campo, M.J., T. Boronat, L. Quiles-Carrillo, R. Balart and N. Montanes, *Manufacturing and Characterization of Toughened Poly (lactic acid)(PLA) Formulations by Ternary Blends with Biopolyesters.* Polymers, 2017. **10**(1): 3.

59.   Huang, Y., C. Zhang, Y. Pan, W. Wang, L. Jiang and Y. Dan, *Study on the effect of dicumyl peroxide on structure and properties of poly (lactic acid)/natural rubber blend.* Journal of Polymers and the Environment, 2013. **21**(2): 375-387.

60.   Wang, N., J. Yu and X. Ma, *Preparation and characterization of thermoplastic starch/PLA blends by one-step reactive extrusion.* Polymer International, 2007. **56**(11): 1440-1447.

61.   Ferri, J.M., D. Garcia-Garcia, L. Sanchez-Nacher, O. Fenollar and R. Balart, *The effect of maleinized linseed oil (MLO) on mechanical performance of poly(lactic acid)-thermoplastic starch (PLA-TPS) blends.* Carbohydrate Polymers, 2016. **147**: 60-68.

III. RESULTS & DISCUSSION

RESULTS & DISCUSSION

BLOCK II

III.2. POLY(LACTIC ACID) WITH IMPROVED TOUGHNESS BY NATURAL ADDITIVES AND FILLERS.

III.2.1. Enhancement of the mechanical and thermal properties of injection-molded polylactide parts by the addition of acrylated epoxidized soybean oil

L. Quiles-Carrillo[1], S.Duart[1], N. Montanes[1], S. Torres-Giner[1, 2] and R. Balart[1]

[1] Technological Institute of Materials (ITM), Universitat Politècnica de València (UPV), Plaza Ferrándiz y Carbonell 1, Alcoy 03801, Spain

[2] Novel Materials and Nanotechnology Group, Institute of Agrochemistry and Food Technology (IATA), Spanish Council for Scientific Research (CSIC), Calle Catedrático Agustín Escardino Benlloch 7, Paterna 46980, Spain

Enhancement of the mechanical and thermal properties of injection-molded polylactide parts by the addition of acrylated epoxidized soybean oil

L. Quiles-Carrillo [a], S. Duart [a], N. Montanes [a], S. Torres-Giner [b], R. Balart [a],*

[a] Technological Institute of Materials (ITM), Universitat Politècnica de València (UPV), Plaza Ferrándiz y Carbonell 1, 03801 Alcoy, Spain
[b] Novel Materials and Nanotechnology Group, Institute of Agrochemistry and Food Technology (IATA), Spanish Council for Scientific Research (CSIC), Calle Catedrático Agustín Escardino Benlloch 7, 46980 Paterna, Spain

HIGHLIGHTS

- Polylactide (PLA) formulations with acrylated epoxidized soybean oil (AESO) give new features to designers by widening PLA applications.
- The intrinsic brittleness of PLA is remarkably improved by the addition of AESO.
- The impact-absorbed energy is noticeably increased with relatively low AESO contents of 2.5–7.5 wt%.
- Although phase separation occurs, the submicron AESO droplets finely dispersed in PLA contribute to improving toughness.
- AESO also provides increased thermal stability to PLA parts.

GRAPHICAL ABSTRACT

ABSTRACT

This work reports the effect of acrylated epoxidized soybean oil (AESO) addition on the mechanical, thermal, and thermomechanical properties of polylactide (PLA) parts obtained by injection molding. To this end, AESO, a chemically multi-functionalized vegetable oil, was incorporated into PLA during melt processing. The PLA parts with AESO contents in the 2.5–7.5 wt% range showed a remarkable enhancement in both elongation at break and impact-absorbed energy while their tensile and flexural strength as well as thermomechanical properties were maintained or slightly improved. Additionally, the AESO-containing PLA parts presented higher thermal stability and lower crystallinity. The improvement achieved was ascribed to a dual effect of plasticization in combination with a chain-extension and/or cross-linking process of the PLA chains by the highly reactive acrylate and epoxy groups present in AESO. The use of AESO thus represents an environmentally friendly solution to obtain toughened PLA materials of high interest in, for instance, rigid packaging, automotive or building and construction applications.

© 2017 Elsevier Ltd. All rights reserved.

* Corresponding author.
  E-mail address: rbalart@mcm.upv.es (R. Balart).

Enhancement of mechanical and thermal properties of injection-molded polylactide parts by addition of acrylated epoxidized soybean oil

Abstract

This work reports the effect of acrylated epoxidized soybean oil (AESO) addition on the mechanical, thermal, and thermomechanical properties of polylactide (PLA) parts obtained by injection molding. To this end, AESO, a chemically multi-functionalized vegetable oil, was incorporated into PLA during melt processing. The PLA parts with AESO contents in the 2.5–7.5 wt% range showed a remarkable enhancement in both elongation at break and impact-absorbed energy while their tensile and flexural strength as well as thermomechanical properties were maintained or slightly improved. Additionally, the AESO-containing PLA parts presented higher thermal stability and lower crystallinity. The improvement achieved was ascribed to a dual effect of plasticization in combination with a chain-extension and/or cross-linking process of the PLA chains by the highly reactive acrylate and epoxy groups present in AESO. The use of AESO thus represents an environmentally friendly solution to obtain toughened PLA materials of high interest in, for instance, rigid packaging, automotive or building and construction applications.

INTRODUCTION

Polylactide (PLA) is currently considered the front runner in the emerging bioplastics market due to its good balance between physical properties, *i.e.* mechanical, thermal, optical, and barrier properties, and its two-fold environmental advantage of being a bio-based and biodegradable material. For these reasons it is nowadays widely used in 3D printing, biomedical devices, rigid packaging, drug delivery systems, textiles, automotive parts, building and construction materials, etc. [1-5]

The main drawbacks of PLA, however, are related to its intrinsic brittleness, which is a limiting factor to further expand its applications in commodity areas (*e.g.* packaging) [6, 7]. Today, with the increasing use of PLA as the base material for 3D printing and short-term uses [8, 9], the fragility of PLA is certainly an important issue to overcome [10-13]. For this reason, the vast majority of PLA industrial formulations are based on either plasticized formulations by means of additives or polymer blends [14-19].

A wide variety of plasticizers have been previously proposed for PLA. Different monomeric, oligomeric, and polymeric esters from adipic [20], citric [21-24], succinic [25], and lactic acid [26, 27], among others, have offered interesting results for PLA materials in terms of plasticization and/or compatibilization with other bio-based polyesters [28]. Another interesting family is that corresponding to polyhydric alcohols and their esters. Although glycerol is known to exert a poor plasticizing effect on PLA, both oligomeric and polymeric glycols and some related esters have been successfully used to plasticize PLA [29]. It is worthy to note the good plasticizing effect that poly(ethylene glycol) (PEG) [21, 30], poly(propylene glycol) (PPG) [31, 32], and their copolymers [33] can provide on PLA. Isosorbide esters have also been reported as good plasticizers for PLA and other polymers [34, 35]. Acrylic/acrylated oligomers and polymers have also been reported to offer a good plasticizing effect on PLA in combination with a chain extension phenomenon, which improves toughness [36, 37].

With regard to vegetable oils, it is worthy to note their increasing use in the polymer industry as both the starting materials for polymer synthesis and additives [38-40]. Vegetable oils consist on a triglyceride structure in which different fatty acids are chemically bonded to a glycerol molecule through ester bonds. The main feature of some fatty acids is the presence of carbon–carbon double bonds that allows for a wide variety of chemical modifications. Unmodified vegetable oils have been used as PLA plasticizers but their performance is restricted due to the high difference in their solubility parameter (around 16 MPa $^{1/2}$) compared to that of PLA, in the 19.5–20.5 MPa $^{1/2}$ range [41, 42], which typically results in a migration process. For this reason, chemically modified vegetable oils offer a better plasticizing efficiency since their solubility parameters are closer to that of PLA [43].

In particular, the use of epoxidized vegetable oils (EVOs) represents an environmentally friendly solution to plasticize PLA and other polymers. As a result, several EVOs have been successfully used as PLA plasticizers. It is worthy to note the good plasticizing effect exerted by epoxidized fatty acid esters (EFAE) [44, 45], epoxidized soybean oil (ESBO) and palm oil [46, 47], and epoxidized linseed oil (ELO) [48]. The epoxy functionality present in EVOs also offers a high compatibilization on green composites with lignocellulosic fillers due to the reaction of the epoxide ring

with the hydroxyl groups present in both PLA end-chains and cellulose [49]. This effect of compatibilization provided by EVOs has also been observed in vinyl plastisol/wood flour composites [50], thus emphasizing the extraordinary reactivity of the epoxy group.

Another interesting modification of vegetable oils is maleinization, which allows the formation of several maleic anhydride (MAH) groups, *i.e.* multiple functionalities, from the different degrees of unsaturation originally present in the fatty acids. Maleinized vegetable oils such as maleinized linseed oil (MLO), maleinized cottonseed oil (MCSO), and maleinized tung oil (MTO) have been successfully used in toughened PLA formulations with an interesting combination of plasticization, chain-extension, and compatibilizing effects [51-54]. Acrylated epoxidized vegetable oils (AEVOs) are obtained by reaction of EVOs with acrylic acid (AA). Specifically, acrylated epoxidized soybean oil (AESO) has been reported as an environmentally friendly additive for toughening PLA-based blends [55].

Injection molding of PLA has to face some challenges related to its chemical structure [56]. Similar to other biopolyesters, PLA is particularly sensitive to moisture, which decreases its molecular weight (M_W) during processing [57], inducing a remarkable impairment on the mechanical performance. Additionally, its intrinsic brittleness also restricts a wider use of PLA materials in injection molding. In this sense, the injection molding industry uses different additives to control crystallization phenomena to improve mechanical properties [58, 59]. Another increasing trend within the injection-molded PLA context is related to use of green composites based on natural fibers [60, 61]. Finally, PLA blends also represent a relevant alternative for toughened-PLA formulations processed by injection molding but, usually, compatibilizers are needed [62].

Although several works have been previously focused on AESO-modified PLA films, the effect of AESO on PLA materials obtained by injection molding has not been evaluated. This work aims to carry out, for the first time, an in-depth study of the influence of AESO on the properties of injection-molded PLA parts. To this end, the effect of different AESO contents in the 2.5–10 wt% range were evaluated on the performance of the PLA parts.

EXPERIMENTAL

Materials

A commercial PLA grade IngeoTM biopolymer 6201D was obtained from NatureWorks (Minnetonka, Minnesota, USA). This is a PLA grade with a density of 1.24 g cm^{-3} and a melt flow rate (MFR) of 15-30 g/10 min measured at 210 °C which makes it suitable for injection molding. AESO was supplied by Sigma Aldrich S.A. (Madrid, Spain). This commercial grade comes with 4,000 ppm hydroquinone as inhibitor to avoid polymerization. **Figure III.2.1.1** shows the chemical process to obtain AESO from epoxidized soybean oil (ESO) by treatment with AA.
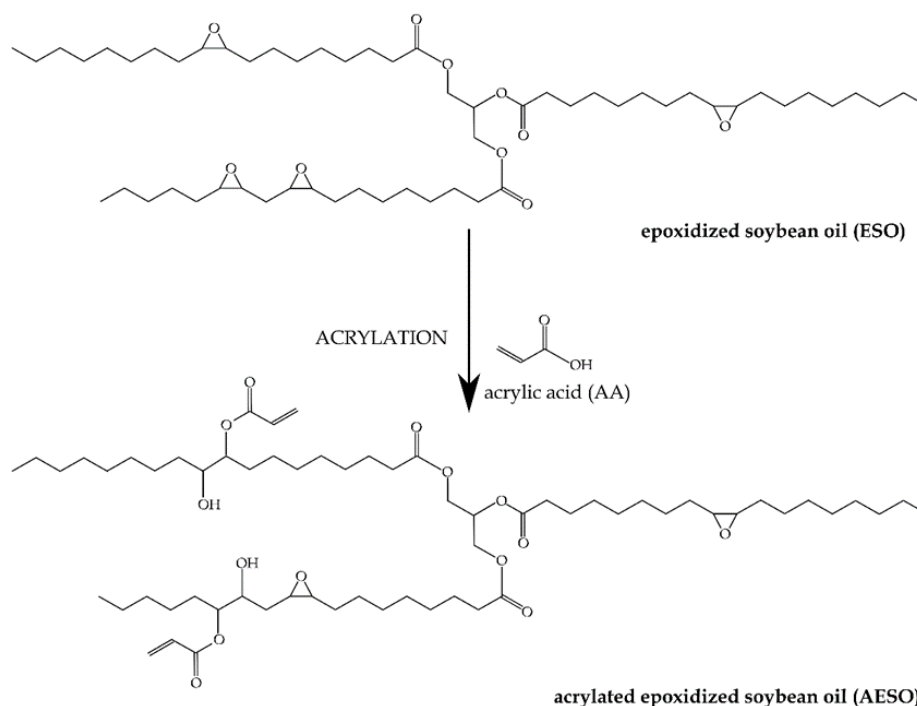
Figure III.2.1.1 Schematic representation of the chemical structure of acrylated epoxidized soybean oil (AESO) obtained by acrylation of epoxidized soybean oil (ESO), previously produced from epoxidation of soybean oil (SO), with acrylic acid (AA).

Preparation of PLA parts

Prior to processing, all materials were dried in a dehumidifier MDEO from Industrial Marsé (Barcelona, Spain) at a temperature of 60 ºC for 36 h to remove residual moisture due to the high sensitiveness of PLA to hydrolysis. The AESO content varied in the 0-10 wt% range as summarized in **Table III.2.1.1**.

The PLA and AESO formulations were then melt compounded in a co-rotating twin-screw extruder from Dupra, S.L. (Alicante, Spain) with a diameter of 25 mm and a length/diameter (L/D) ratio of 24. The temperature profile of the barrel was set to 180 ºC (feeding zone), 185 ºC, 190 ºC, and 195 ºC (die) and the rotating speed was 20 rpm. The extruded materials were pelletized and subsequently shaped into plastic parts by injection molding by means of a Sprinter 11t from Erinca S.L (Barcelona, Spain) using a temperature profile of 165 ºC (hopper), 170 ºC, 175 ºC, and 180 ºC (injection nozzle).

Table III.2.1.1. Composition and coding of the different prepared formulations based on polylactide (PLA) and acrylated epoxidized soybean oil (AESO).

Sample	PLA content (wt%)	AESO content (wt%)
0 wt% AESO	100	0
2.5 wt% AESO	97.5	2.5
5 wt% AESO	95.0	5.0
7.5 wt% AESO	92.5	7.5
10 wt% AESO	90.0	10.0

Mechanical characterization

Mechanical properties of AESO-toughened PLA parts were obtained by both tensile and flexural tests in a universal test machine ELIB 50 from S.A.E. Ibertest (Madrid, Spain), equipped with a load cell of 5 kN. Tensile tests followed the guidelines of the ISO527-1:2012 while flexural tests were carried out as recommended by ISO 178:2011. The cross-head speed was set to 5 mm min^{-1} for both tests.

Shore hardness of the injection-molded parts was measured in a 676-D durometer from J. Bot Instruments (Barcelona, Spain), using the D-scale as recommended in ISO 868:2003. Toughness was also studied on the un-notched samples using the Charpy impact test with a 6-J pendulum from Metrotec S.A. (San Sebastián, Spain) following the guidelines of the ISO 179-1:2010. All samples were tested at room temperature and at least six samples per formulation were evaluated to obtain the average values of the corresponding parameters.

Thermal characterization

Main thermal transitions, *i.e.* glass transition (T_g), cold crystallization (T_c), and melting (T_m) of the injection-molded parts were obtained using differential scanning calorimetry (DSC) with a Mettler-Toledo 821 calorimeter (Schwerzenbach, Switzerland). The average sample weight ranged from 5 to 7 mg and it was placed in standard aluminium crucibles with a volume capacity of 40 µL. Thermal analysis was programmed as follows: initial heating scan from 30 °C to 200 °C at 10 °C min^{-1}, then a cooling scan from 200 °C down to 0 °C at 10 °C min-1, and finally a second heating scan from 0 °C to 350 °C at 10 °C min^{-1}. All tests were run under nitrogen atmosphere with a flow-rate of 66 mL min^{-1}. In addition to above-mentioned temperatures, the degree of crystallinity (X_c) was calculated by using the following equation (**Equation III.2.1.1**):

$$X_C = \left[\frac{\Delta H_m - \Delta H_{CC}}{\Delta H_m^0 \cdot (1-w)} \right] \cdot 100 \qquad \textbf{Equation III.2.1.1}$$

Where ΔH_m and ΔH_{CC} (J g^{-1}) correspond to the enthalpies of melting and cold crystallization, respectively. ΔH_m^0 (J g^{-1}) stands for the melting enthalpy of a fully crystalline PLA, with a value of 93.0 J g^{-1} [63], and w represents the weight fraction of AESO in the PLA formulation.

The effect of AESO on the overall thermal stability up to decomposition was studied by thermogravimetric analysis (TGA) in a TGA/SDTA 851 thermobalance from Mettler-Toledo, LLC (Columbus, Ohio, USA). The samples weight ranged 5-7 mg and these were placed on standard aluminum oxide (Al_2O_3) crucibles with a volume capacity of 70 µL. A dynamic heating program from 30 °C to 700 °C at a heating rate of 20 °C min-1 in air atmosphere was used.

Thermomechanical characterization

Dynamic mechanical thermal characterization (DMTA) was performed using an AR-G2 oscillatory rheometer from TA Instruments (New Castle, Delaware, USA),

equipped with a clamp system for solid samples working in torsion/shear mode. The samples, with a size of 4x10x40 mm³, were subjected to a temperature sweep from 30 º up to 140 ºC at a constant heating rate of 2 ºC min⁻¹. The maximum deformation percentage (γ) was set to 0.1%. The storage modulus (G′) and the dynamic damping factor (tan δ) were obtained as a function of temperature at a constant frequency of 1 Hz.

Thermomechanical properties were further analyzed by means of Vicat softening temperature (VST) and heat deflection temperature (HDT) tests in a Vicat/HDT station model VHDT 20 from Metrotec S.A. (San Sebastián, Spain). VST values were obtained according to ISO 306 using the B50 method, with an applied load of 50 N and a heating rate of 50 ºC h⁻¹. HDT measurements were carried out following ISO 75-1 on samples sizing 4x10x80 mm³. The distance between supports was 60 mm and the applied force was 320 g while the heating rate was 120 ºC h⁻¹.

In addition, the dimensional stability was studied by thermomechanical analysis (TMA) in a thermomechanical analyzer Q400 from TA Instruments on samples with a size of 10x10x4 mm³. A dynamic heating program from 0 ºC to 140 ºC at a constant heating rate of 2 ºC min⁻¹ was used to obtain the coefficient of linear thermal expansion (CLTE) using a constant load of 0.02 N. All samples were tested in triplicate.

Morphology

The morphology of the injection-molded parts was observed on their fracture surfaces from impact tests. For this, field emission scanning electron microscopy (FESEM) in a ZEISS ULTRA 55 from Oxford Instruments (Abingdon, United Kingdom) was performed. The working distance (WD) varied in the 6-7 mm range and an extra high tension (EHT) of 2 kV was applied to the electron beam. Due to the non-conducting nature of the samples, these were subjected to a sputtering process with a gold-palladium alloy in a sputter coater EMITECH-SC7620 from Quorum Technologies, Ltd. (East Sussex, United Kingdom).

RESULTS AND DISCUSION

Mechanical properties of AESO-containing PLA parts

Figure III.2.1.2 shows the evolution of tensile properties of the injection-molded PLA parts varying the AESO content. As it can be observed in the graph, the incorporation of AESO induced a slight increase in the tensile modulus, *i.e.* from 2 GPa (for the neat PLA part) to 2.2 GPa (for PLA parts containing 10 wt% AESO). Regarding tensile strength, the neat PLA part was characterized by a value of 66 MPa. One can observe a slight decrease in tensile strength with increasing the AESO content. However, tensile strength remained relatively constant at high values, *i.e.* 63-64 MPa, for up to 7.5 wt% AESO, and a significant decrease (below 60 MPa) was only noticed at the highest content, *i.e.* 10 wt%. A similar effect was previously reported in the study carried out by Mauck *et al.* [55] in which PLA films containing 5 wt% AESO were prepared by solvent casting following by drying at 190 ºC.

Incorporation of AESO into PLA led to a considerable increase in elongation at break. The highest value of elongation at break was observed for the PLA parts containing 10 wt% AESO. In particular, this value was 10.6%, representing a percentage increase of 113% in comparison to the unmodified PLA part. Mauck *et al.* [55] previously reported a remarkable increase in elongation at break, from 4.1%, for a neat PLA film, up to 31%, for PLA films with 5 wt% AESO. This increment is substantially higher than the reported values herein for the same AESO content. However, this previous study also reported high variability on the mechanical properties, which was ascribed to the lack of homogeneity of the manufacturing process. A similar plasticizing effect was also reported by Ferri *et al.* [51] for PLA formulations containing 10-13 wt% MLO, showing an increase in elongation at break of up to 70-80%. Nevertheless, a remarkable decrease in tensile strength, in particular from 64 MPa down to 40 MPa, was also observed. Carbonell-Verdu *et al.* [52] similarly reported a ductility improvement on PLA films by means of MCSO, showing an increment in elongation at break of 11%. However, a reduction in the tensile strength of 24% was also observed. Therefore, these previous plasticizers promoted certain decrease in both the strength and modulus of PLA materials. Interestingly, the here-developed PLA parts showed a similar mechanical strength for AESO contents up to 7.5 wt% than the neat PLA part, while maintaining a similar improvement in ductility than previously studied plasticizers.
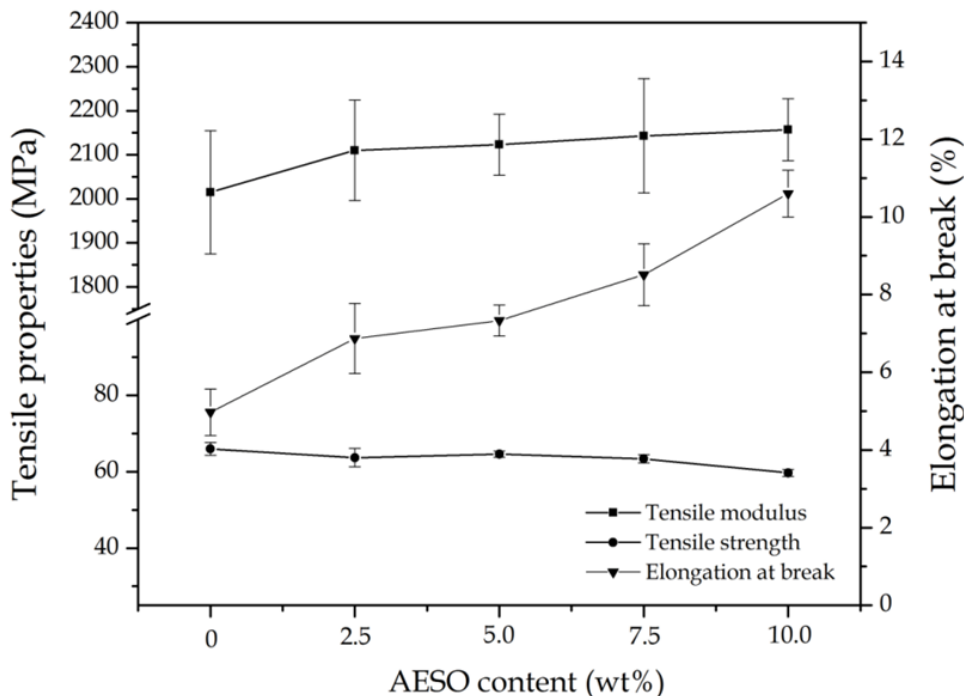
Figure III.2.1.2. Plot evolution of the tensile properties of the injection-molded polylactide (PLA) parts varying the acrylated epoxidized soybean oil (AESO) content.

Figure III.2.1.3 shows the flexural properties of the PLA parts containing AESO. In relation to the flexural modulus, a slight increase from 3.3 GPa (neat PLA part) up to

3.4-3.5 GPa (for PLA parts containing 7.5-10 wt% AESO) was observed. One can also observe in the graph that AESO improved flexural strength. In particular, flexural strength increased from 89.9 MPa, for the neat PLA part, up to 100.7 MPa, for the PLA part with 10 wt% AESO. This somewhat suggests an interaction between the multiple acrylic functionalities of AESO with the PLA chains. In this sense, Mauk *et al.* [55] suggested a potential cross-linking reaction of AESO during melt processing at high temperature. Therefore, this mechanism can be responsible for the above-described mechanical performance, i.e. a significant ductility improvement in combination to a moderate increase in the mechanical resistant properties.
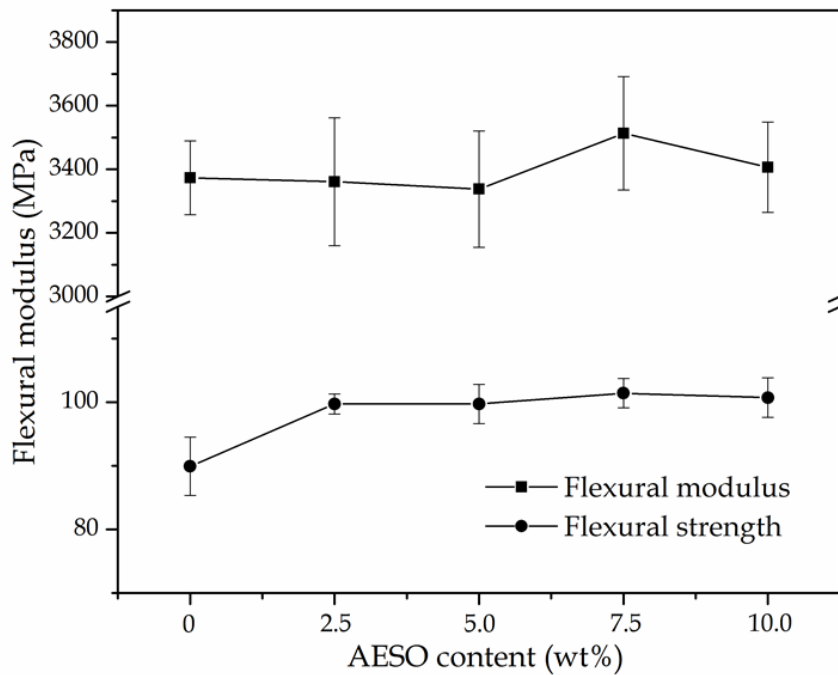
Figure III.2.1.3. Plot evolution of the flexural properties of the injection-molded polylactide (PLA) parts varying the acrylated epoxidized soybean oil (AESO) content.

In relation to hardness, no significant changes were observed for the Shore D measurements of the AESO-toughened PLA parts (see **Table III.2.1.2**). In general, all PLA parts showed values around 79, except the sample containing 2.5 wt%, which presented a slight increase up to approximately 81. The PLA parts containing AESO also presented a remarkable increase in toughness, as measured through the Charpy impact test. Whereas the neat PLA part showed a Charpy impact resistance of 19.5 kJ m^{-2}, the addition of only 2.5 wt% AESO increased the impact-absorbed energy up to 30.6 kJ m^{-2}, i.e. an increase of about 57%. The impact-strength values gradually improved up to 35.1 kJ m^{-2} for the PLA parts containing AESO at 10 wt%. This further confirms the high effect of AESO on the toughness of the PLA parts. Similar findings were previously reported by Ferri *et al.* [51] for MLO-plasticized PLA materials, showing an increase in the absorbed energy from 30.9 kJ m^{-2}, for neat PLA, to 62.9 kJ m^{-2}, for PLA materials with 3.6 wt% MLO. This previous study also pointed out

that plasticizer saturation habitually occurs at relatively low concentrations, inducing a negative effect on the overall mechanical properties. Plasticizer saturation was also observed in PLA formulations containing EFAE in the same range of concentrations, which was detectable by a clear phase separation [44]. In the present study, however, the impact-strength values of the PLA parts linearly increased with the AESO content for all studied formulations. In this sense, Nagarajan *et al.* [64] also reported interesting results in polytrimethylene terephthalate (PTT)/PLA blends by reactive compatibilization with an acrylic terpolymer, showing a remarkable increase in toughness.

Table III.2.1.2. Shore D hardness and Charpy impact values of the injection-molded polylactide (PLA) parts varying the acrylated epoxidized soybean oil (AESO) content.

AESO content (wt%)	Shore D hardness	Charpy impact (kJ m^{-2})
0	79.0 ± 0.6	19.5 ± 2.6
2.5	81.7 ± 0.8	30.6 ± 0.1
5.0	79.6 ± 0.9	31.9 ± 0.1
7.5	79.0 ± 0.4	33.7 ± 1.7
10.0	79.0 ± 0.5	35.1 ± 2.3

Morphology of AESO-containing PLA parts

Mechanical properties are directly related to the material-specific morphology. **Figure III.2.1.4** gathers the FESEM images, taken at 500x, of the fracture surfaces of the neat PLA and AESO-toughened PLA parts after the Charpy impact tests. As shown in **Figure III.2.1.4a**, the neat PLA part is a rigid material, showing the fracture surface morphology of a typical brittle polymer in which micro-crack formation and growth can be observed. One can also observe that there was no evidence of plastic deformation due to the intrinsic brittleness of PLA, which is related to its low energy absorption, as mentioned above. However, as it can be observed from **Figure III.2.1.4b** to **Figure III.2.1.4e**, the morphology of the fracture surfaces of all AESO-toughened parts was remarkably different. The fracture surface changed from brittle to ductile, showing different flat levels with a certain degree of plastic deformation. Nevertheless, it is also worth to mention the presence of small spherical voids, which were more noticeable as the AESO content increased (see for instance **Figure III.2.1.4e**). The presence of these droplets suggests phase separation that is known to exert two opposing effects on a polymer matrix. On the one hand, this phenomenon occurs due to a given additive saturation that may cause migration. As a result, it has a negative influence on the mechanical properties, which has been already observed in PLA and other bio-based polyesters [44, 48, 51, 52]. On the other hand, an excess of plasticizer can also change the morphology of the material matrix. In particular, the presence of small droplets with a spherical shape can positively contribute to improve toughness as, for instance, polybutadiene rubbers (BR) do in high-impact polystyrene (HIPS). Both phenomena can occur and overlap. Their overall effect depends on the droplet size, distribution, potential interactions, etc. This phenomenon has been previously observed in PPG-plasticized PLA formulations [31].
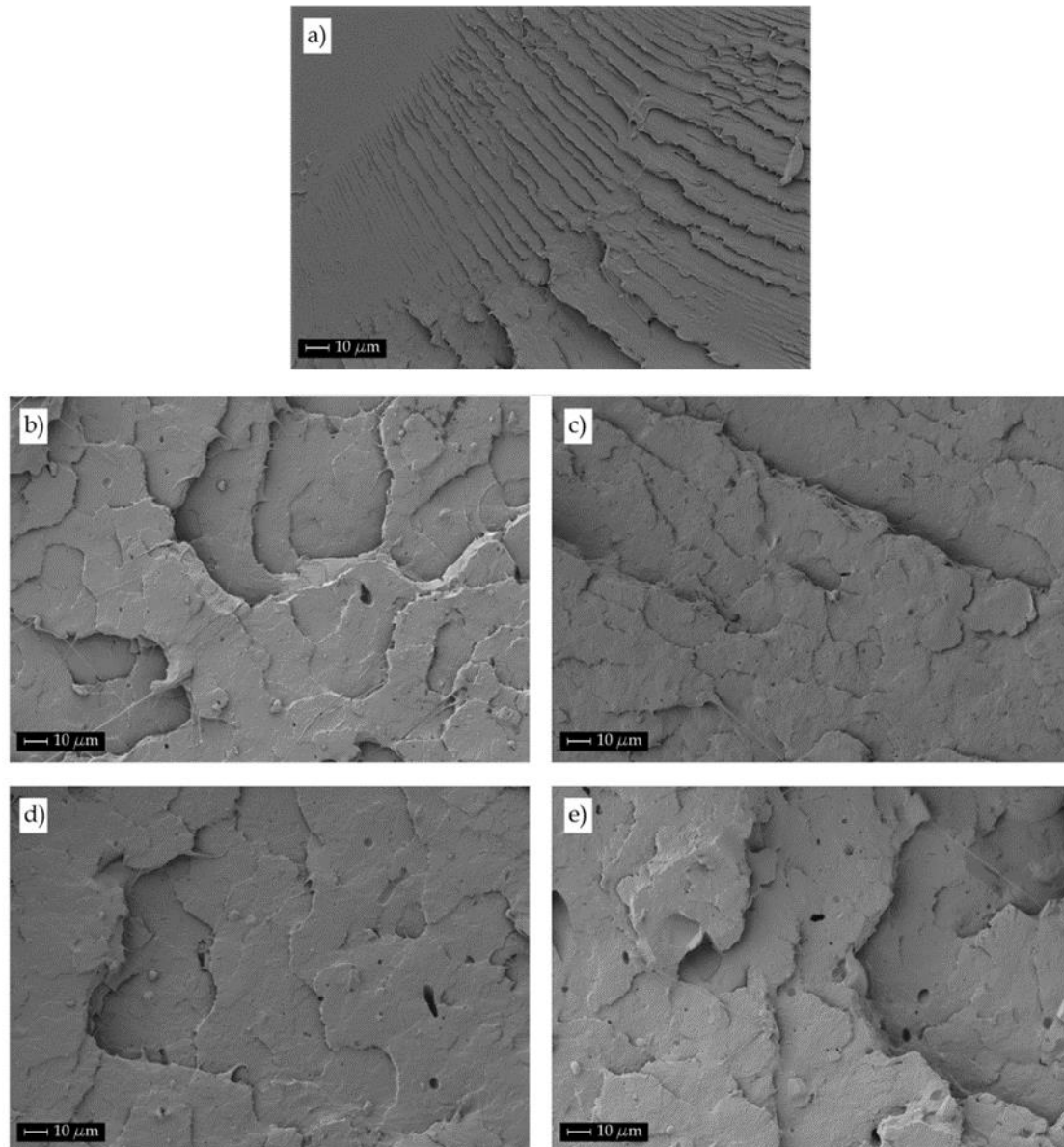
Figure III.2.1.4. Field emission scanning electron microscopy (FESEM) images of the surface fractures of the injection-molded polylactide (PLA) parts with acrylated epoxidized soybean oil (AESO) taken at 500x: a) neat PLA; b) 2.5 wt% AESO; c) 5.0 wt% AESO; d) 7.5% AESO; e) 10.0 wt% AESO. Scale markers of 10 μm.

       Figure III.2.1.5 shows the FESEM images taken at higher magnifications, *i.e.* 2,000x and 5,000x. These micrographs confirm, in a clear way, the morphology of the fracture surfaces of the injection-molded PLA parts. At 2,000x, some spherical holes with a mean diameter of 1-2 μm can be observed in both parts of PLA with 2.5 wt% (**Figure III.2.1.5a**) and 10 wt% (**Figure III.2.1.5c**) AESO. The plasticizing effect exerted by AESO on the PLA matrix was supported by the presence of some filaments on the flat fracture planes resulting from plastic deformation. FESEM images taken at 5,000x confirmed phase separation at high AESO contents. PLA parts with 2.5 wt%, shown in **Figure III.2.1.5b**, presented some spherical voids but the overall surface was quite

homogeneous, thus indicating good miscibility. Nevertheless, PLA parts containing 10 wt% AESO, in **Figure III.2.1.5d**, showed a noticeably phase separation since small droplets below 0.5 μm can be easily identified. Despite this, the sizes of these AESO droplets were relatively low, producing the above-described positive effect on the mechanical ductile properties. Similar findings were reported by Mauck *et al*. [55] for AESO-toughened PLA films at 5 wt%, which presented higher miscibility and then lower phase separation than soybean oil. In fact, it was reported a droplet size of 4.5 μm for the PLA films containing soybean oil while the films made of PLA with AESO at 5 wt% presented a droplet size of 2.2 μm. Ferri *et al*. [44] also observed phase separation in PLA plasticized with 13 wt% EFAE with droplet sizes similar to those observed in the here-prepared developed materials, *i.e.* around 1 μm. Therefore, this particular morphology based on submicron AESO droplets finely dispersed in the PLA matrix can be certainly responsible for the achieved toughness improvement.
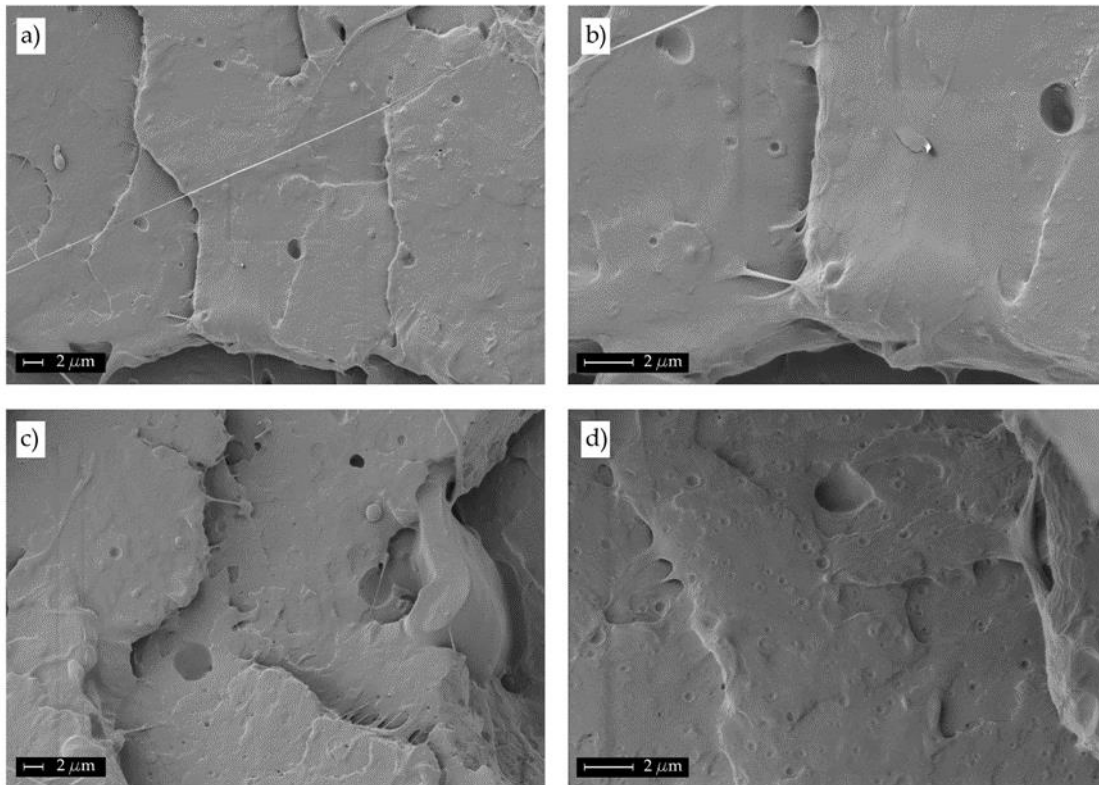
Figure III.2.1.5. Field emission scanning electron microscopy (FESEM) images of the surface fractures of the injection-molded polylactide (PLA) parts with acrylated epoxidized soybean oil (AESO) taken at different magnifications: a) 2.5 wt% AESO at 2,000x; b) 2.5 wt% AESO at 5,000x; c) 10 wt% AESO at 2,000x; d) 10 wt% AESO at 5,000x. Scale markers of 2 μm.

Thermal properties of AESO-containing PLA parts

DSC thermograms for neat PLA and AESO-toughened PLA parts are shown in **Figure III.2.1.6**. A baseline step located between 60–70 °C corresponds to Tg of PLA. The exothermic peak located between 90 °C and 120 °C stands for the cold crystallization process due to the rearrangement of the PLA polymer chains in a

packed structure during heating. Finally, the melting process was observed in the 150–170 °C range. As it can be seen in the thermograms, the addition of AESO shifted the cold crystallization process to higher temperatures, which is not the usual effect of a plasticizer. That was particularly noticeable for the PLA part containing 2.5 wt% AESO. In general, a plasticizer increases free volume and reduces the polymer-polymer interactions, allowing higher chain mobility and lowering T_{CC} values [23, 46]. This unexpected anti-nucleating effect of AESO on PLA materials suggests that certain chain extension or cross-linking occurred due to its multiple acrylate and epoxy functionalities, thus leading to a chain mobility restriction. This effect was more intense for the PLA part containing 2.5 wt% AESO, as it can be seen in **Figure III.2.1.6**. At higher AESO contents, however, its plasticizing effect overlapped the chain extension/cross-linking process resulting in a decrease in cold crystallization. Therefore, the AESO-containing PLA parts at 5-10 wt% presented intermediate T_{CC} values. Similar phenomenon was previously observed by Choi *et al.* [36] by using poly(ethylene glycol) acrylate (PEGA) as additive in toughened PLA formulations. However, it is also worth to note that these previous formulations were processed with a radical initiator that promoted reactive extrusion with PLA polymer chains.
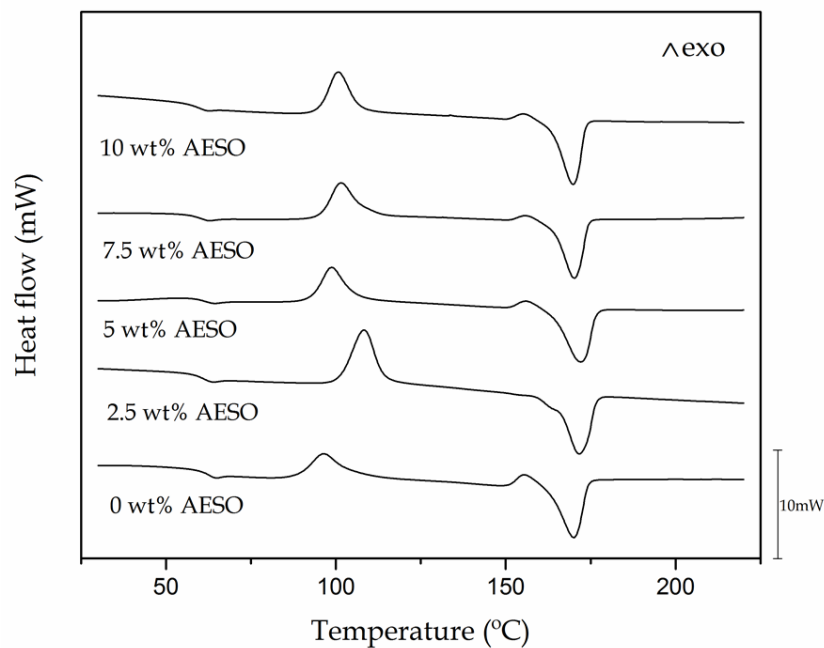
Figure III.2.1.6. Comparative plot of differential scanning calorimetry (DSC) thermograms of the injection-molded polylactide (PLA) parts varying the acrylated epoxidized soybean oil (AESO) content.

The main thermal properties of the AESO-toughened PLA formulations are summarized in **Table III.2.1.3**. It is worthy to note the relatively low decrease observed in the T_g values from 62.8 °C, for the neat PLA part, to 59.4 °C, *i.e.* a reduction of 2-3 °C. Indeed, the efficiency of a given plasticizer is habitually directly related to their ability to lower polymer T_g. The obtained results further confirm that AESO does not play the typical plasticization role in PLA. In fact, other plasticizers, such as PEG, ATBC, PPG, OLAs, etc., are known to be capable to decrease T_g by 25–30 °C with a plasticizer content in the 10–20 wt% range [23, 26, 31, 33]. Similar findings were reported by

Mauck *et al*. [55] in plasticized PLA by 5 wt% AESO, showing a T_g decrease of *ca*. 1 ºC with regard to the unplasticized PLA film. This can be related to the restricted chain motion to form a packed structure with AESO addition. Regarding the cold crystallization process, as above described, this occurred at higher temperatures. In particular, T_{CC} increased from 96.3 ºC, for the neat PLA part, to up 105.9 ºC, for the PLA part containing 2.5 wt% AESO. Another important observation was the X_C decrease. This reduction was particularly high for the PLA part formulated with 2.5 wt%, supporting the chain extension/cross-linking process between the acrylate and epoxy groups and the hydroxyl groups of the PLA chains. However, even though the degree of crystallization was reduced, the mechanical strength of the PLA parts toughened by AESO was similar to that of the neat PLA part.

Table III.2.1.3. Thermal properties obtained from the differential scanning calorimetry (DSC) curves in terms of glass transition temperature (T_g), cold crystallization temperature (T_{CC}), enthalpy of crystallization (ΔH_{CC}), melting temperature (T_m), enthalpy of melting (ΔH_m), and degree of crystallinity (X_c) for the injection-molded polylactide (PLA) parts varying the acrylated epoxidized soybean oil (AESO) content.

AESO content (wt%)	T_g (ºC)	T_{CC} (ºC)	ΔH_{CC} (J g^{-1})	T_m (ºC)	ΔH_m (J g^{-1})	X_C(%)
0	62.8 ± 0.26	96.3 ± 0.62	12.5 ± 0.29	169.6 ± 0.66	34.5 ± 0.37	23.6 ± 0.75
2.5	61.7 ± 0.62	105.9 ± 0.56	30.4 ± 0.67	171.6 ± 0.59	35.2 ± 0.52	5.2 ± 0.98
5.0	61.6 ± 0.48	98.9 ± 0.56	24.9 ± 0.58	171.2 ± 0.49	36.9 ± 0.47	11.8 ± 0.94
7.5	59.9 ± 0.28	101.6 ± 0.45	26.8 ± 0.41	169.8 ± 0.82	35.0 ± 0.62	11.9 ± 0.86
10.0	59.4 ± 0.45	100.8 ± 0.36	26.6 ± 0.39	169.3 ± 0.47	38.2 ± 0.64	13.5 ± 0.85

Another important feature that AESO provided to the PLA parts was an improvement on thermal stability, which can be observed in **Figure III.2.1.7**. This is an interesting result since one of the main drawbacks of most plasticizers (*e.g*. PEG, PPG, ATBC, etc.) is that they contribute to lower the thermal stability of PLA [23, 36]. Thermal stability impairment is habitually related to a process of plasticizer evaporation, which becomes especially important for additives of low MW that are not clearly detected by DSC. However, this phenomenon can be easily detected by TGA, allowing to evaluate whether the additive improves or not the thermal stability. This is a key issue in defining the processing window of PLA formulations, which are typically processed at 180–190 ºC or even at higher temperatures, being thus necessary to ensure that plasticizer evaporation does not occur in this temperature range. Moreover, TGA also gave evidence of the thermal stabilization effect that AESO provides to PLA. As reported by Carrasco *et al*. [65, 66], PLA degradation habitually occurs in a single step, following a chain scission mechanism. It was also reported an increase in thermal stability by using reactive extrusion, which gave partially branched PLA chains [67]. **Figure III.2.1.7a** shows a comparison plot of the TGA thermograms of the neat PLA and AESO-toughened PLA parts varying the AESO content. Inset in **Figure III.2.1.7a** shows a detailed graph of the degradation onset. It is clearly observable the displacement of the degradation curves to higher temperatures. The decomposition process proceeded in a one-stage weight loss for all PLA materials as it can be concluded from the derivative thermogravimetric (DTG) curves (see **Figure III.2.1.7b**). The most striking fact is that AESO increased thermal stability at high

temperatures, thus leading to a significant delay in the degradation process. Degradation temperature (T_{deg}), corresponding to the maximum degradation rate and shown by the temperature peak in the DTG graphs, increased from is 361 °C, for the neat PLA part, up to 370 °C, for PLA parts with 5.0–7.5 wt% AESO contents. Similar to that mentioned above during DSC characterization, the PLA part with 2.5 wt% AESO showed a slightly different thermal behavior. This AESO content also led to the highest thermal stability of all studied compositions. This is related to the fact that both overlapping effects, *i.e.* plasticization and chain extension/cross-linking, took place simultaneously and the predominance of one over the other depends on the additive amount. This feature has been also observed for other modified vegetable oils in PLA formulations and represents a positive issue with regard to other conventional plasticizing/toughening agents for bio-based polyesters [44, 46, 48, 51].
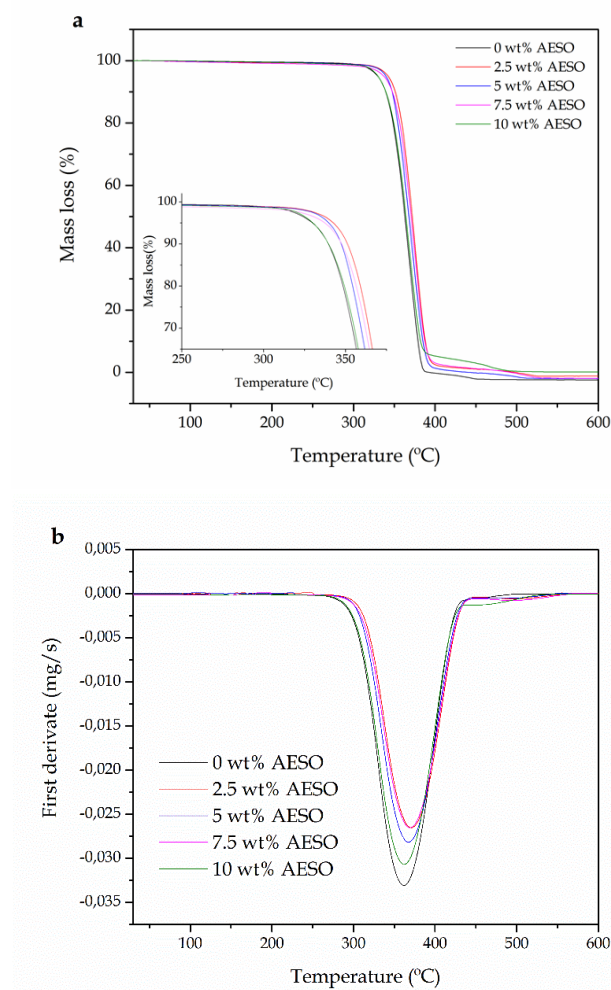
Figure III.2.1.7. Thermal stability of the injection-molded polylactide (PLA) parts varying the acrylated epoxidized soybean oil (AESO) content in terms of: a) Thermogravimetric analysis (TGA) curves; b) Derivative thermogravimetric (DTG) curves.

Thermomechanical properties of AESO-containing PLA parts

With regard to DMTA analysis, **Figure III.2.1.8** gathers a comparative plot of the evolution of G′ and tan δ shown in **Figure III.2.1.8a** and **Figure III.2.1.8b**, respectively. In **Figure III.2.1.8a**, a two-fold reduction in G′ can be observed. The curves showed a first G′ decrease from 50 °C to 70 °C, related to Tg of PLA, followed by the cold crystallization process of the biopolymer that was discernable by a G′ increase in the 75–90 °C range. It is worthy to note that the PLA parts containing AESO presented lower G′ values, which represents a positive effect on toughness. This effect was more noticeable for the PLA part with 10 wt% AESO. Furthermore, in relation to the cold crystallization process, it can be clearly observed a displacement to higher temperatures, thus indicating that AESO addition delayed the crystallization process, as previously described in the DSC analysis. Fig. 8b shows the evolution of tan δ, the so-called damping factor, for the neat PLA and AESO-toughened PLA parts. The α-relaxation peak, which is ascribed to the biopolymer T_g, was located in the 60–70 °C range. One can observe that the decrease in T_g was relatively small, of about 5 °C, as also described during DSC. Nevertheless, all AESO-containing PLA parts were characterized by higher tan δ values, which can be related to the formation of a macromolecular structure with a higher energy dissipation capacity and correlates well with the improved toughness described during mechanical analysis.

Finally, **Table III.2.1.4** shows the evolution of the CLTE values, below and above T_g, obtained by TMA. It can be observed that all PLA parts presented higher CLTE values above T_g since the movement of the biopolymer chains was favored. Below T_g, the CLTE value of the neat PLA part was 94.4 μm m^{-1} °C^{-1} and the AESO-containing PLA parts showed slightly reduced CLTE values. On the contrary, above T_g, the neat PLA part presented a CLTE value of 146.9 μm m^{-1} °C^{-1}, which considerably increased for the PLA parts with AESO. This phenomenon correlates well with the previously described mechanical and thermomechanical properties. Dimensional stability was measured by means of other two thermomechanical parameters, *i.e.* VST and HDT, which are also included in **Table III.2.1.4**. One can observe that VST and HDT values for the neat PLA part were 56.3 °C and 55.4 °C, respectively, and these thermomechanical values were slightly lower after AESO addition. In fact, the decrease observed in VST and HDT was in the 2–3 °C range, thus indicating an extraordinary thermomechanical response.

Table III.2.1.4. Variation of the coefficient of linear thermal expansion (CLTE) below and above glass transition temperature (T_g), Vicat softening temperature (VST), and heat deflection temperature (HDT) of the injection-molded polylactide (PLA) parts varying the acrylated epoxidized soybean oil (AESO) content.

AESO content (wt%)	CLTE below T_g (μm m^{-1} °C^{-1})	CLTE above T_g (μm m^{-1} °C^{-1})	VST (°C)	HDT (°C)
0	94.4 ± 0.4	146.9 ± 0.4	56.3 ± 0.5	55.4 ± 1.6
2.5	89.6 ± 0.8	155.5 ± 1.2	56.0 ± 0.4	54.4 ± 0.4
5.0	90.6 ± 0.5	182.3 ± 7.2	55.8 ± 0.5	54.8 ± 0.6
7.5	90.7 ± 0.8	172.8 ± 2.4	54.0 ± 0.3	53.8 ± 0.4
10.0	92.4 ± 0.6	178.2 ± 3.8	53.6 ± 0.5	53.9 ± 0.7

a)

b)
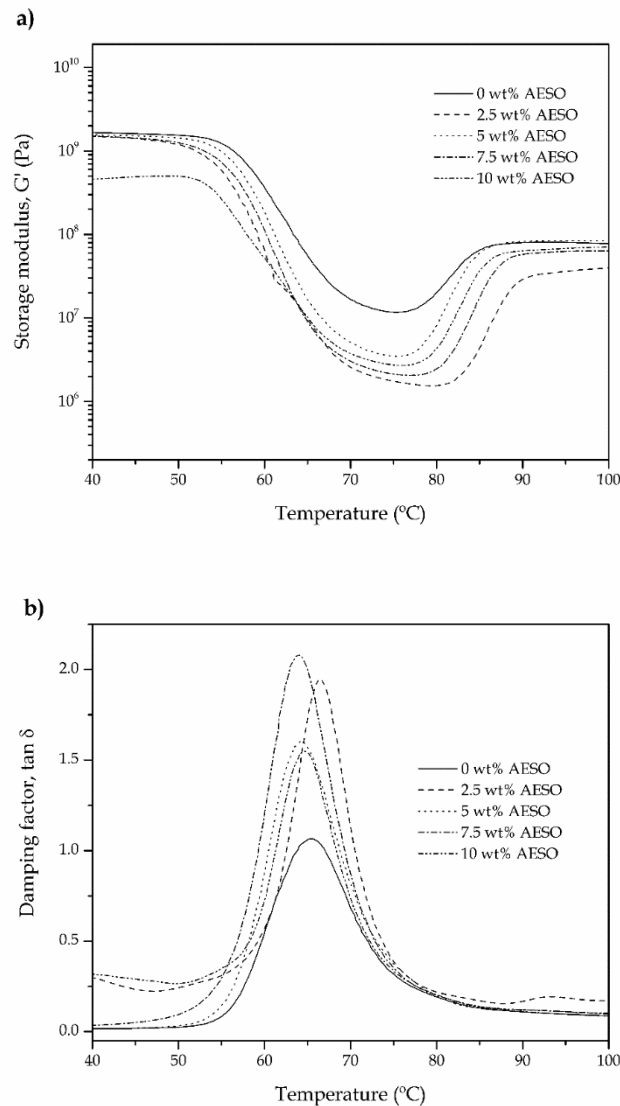
Figure III.2.1.8. Dynamic mechanical thermal analysis (DMTA) curves of the injection-molded polylactide (PLA) parts varying the acrylated epoxidized soybean oil (AESO) content: a) Storage modulus (G′); b) Damping factor (tan δ).

CONCLUSIONS

In the present study, AESO has been proposed as a novel additive for toughening PLA parts obtained by injection molding. Although the plasticizing effect of AESO in terms of T_g decrease was not remarkable, PLA toughness was noticeably improved. In particular, AESO had a positive effect on elongation at break, which increased from 4.97 %, for the neat PLA part, up to 10.6%, for the PLA part with 10 wt% AESO, though the most balanced performance was observed for an AESO content of 2.5 wt%. Furthermore, the mechanical strength of the AESO-toughened PLA parts was in the same range of the neat PLA part more likely due to a chain-extension

and/or cross-linking process of the biopolymer chains induced by the acrylate and epoxy groups present in AESO. Additionally, impact strength increased from 19.5 kJ m^{-2}, for the neat PLA part, up to 35.1 kJ m^{-2}, for the PLA part with 10 wt% AESO. FESEM analysis also revealed good miscibility, in particular for the lowest AESO concentration (2.5 wt%) while AESO saturation occurred at concentrations above 7.5 wt%. The fracture surfaces showed a characteristic morphology defined by a PLA-rich matrix phase in which submicron spherical droplets of AESO appeared fully dispersed. With regard to the thermal properties, AESO addition favored the formation of a more amorphous structure and increased thermal stability of PLA as evidenced by DSC and TGA analysis, respectively. In addition, the thermomechanical measurements indicated that the AESO-containing PLA parts can be applied in technical applications at similar temperatures than the neat PLA part. Therefore, AESO represents an environmentally friendly solution to reduce the intrinsic brittleness of PLA materials, widening and balancing their performance. These toughened PLA parts can be particularly interesting for rigid packaging, automotive or building and construction applications, in which elastic materials but with enhanced ductility and sufficient impact strength are highly demanded.

Acknowledgements

REFERENCES

1. Arrieta, M.P., M.D. Samper, M. Aldas and J. Lopez, *On the Use of PLA-PHB Blends for Sustainable Food Packaging Applications.* Materials, 2017. **10**(9): 26.
2. Bajpai, P.K., I. Singh and J. Madaan, *Development and characterization of PLA-based green composites: A review.* Journal of Thermoplastic Composite Materials, 2014. **27**(1): 52-81.
3. Bergstrom, J.S. and D. Hayman, *An Overview of Mechanical Properties and Material Modeling of Polylactide (PLA) for Medical Applications.* Annals of Biomedical Engineering, 2016. **44**(2): 330-340.
4. Jozwicka, J., K. Gzyra-Jagiela, A. Gutowska, K. Twarowska-Schmidt and M. Cieplinski, *Chemical Purity of PLA Fibres for Medical Devices.* Fibres & Textiles in Eastern Europe, 2012. **20**(6B): 135-141.
5. Notta-Cuvier, D., J. Odent, R. Delille, M. Murariu, F. Lauro, J.M. Raquez, B. Bennani and P. Dubois, *Tailoring polylactide (PLA) properties for automotive applications: Effect of addition of designed additives on main mechanical properties.* Polymer Testing, 2014. **36**: 1-9.
6. Herrera, N., H. Roch, A.M. Salaberria, M.A. Pino-Orellana, J. Labidi, S.C.M. Fernandes, D. Radic, A. Leiva and K. Oksman, *Functionalized blown films of plasticized polylactic acid/chitin nanocomposite: Preparation and characterization.* Materials & Design, 2016. **92**: 846-852.
7. Luckachan, G.E. and C.K.S. Pillai, *Biodegradable Polymers- A Review on Recent Trends and Emerging Perspectives.* Journal of Polymers and the Environment, 2011. **19**(3): 637-676.
8. Chacon, J.M., M.A. Caminero, E. Garcia-Plaza and P.J. Nunez, *Additive manufacturing of PLA structures using fused deposition modelling: Effect of process parameters on mechanical properties and their optimal selection.* Materials & Design, 2017. **124**: 143-157.

9.   Le Duigou, A., M. Castro, R. Bevan and N. Martin, *3D printing of wood fibre biocomposites: From mechanical to actuation functionality.* Materials & Design, 2016. **96**: 106-114.

10.   Tsouknidas, A., M. Pantazopoulos, I. Katsoulis, D. Fasnakis, S. Maropoulos and N. Michailidis, *Impact absorption capacity of 3D-printed components fabricated by fused deposition modelling.* Materials & Design, 2016. **102**: 41-44.

11.   Balakrishnan, H., A. Hassan, M.U. Wahit, A.A. Yussuf and S.B.A. Razak, *Novel toughened polylactic acid nanocomposite: Mechanical, thermal and morphological properties.* Materials & Design, 2010. **31**(7): 3289-3298.

12.   Liu, H.Z. and J.W. Zhang, *Research Progress in Toughening Modification of Poly(lactic acid).* Journal of Polymer Science Part B-Polymer Physics, 2011. **49**(15): 1051-1083.

13.   Wang, M., Y. Wu, Y.D. Li and J.B. Zeng, *Progress in Toughening Poly(Lactic Acid) with Renewable Polymers.* Polymer Reviews, 2017. **57**(4): 557-593.

14.   Aghjeh, M.R., M. Nazari, H.A. Khonakdar, S.H. Jafari, U. Wagenknecht and G. Heinrich, *In depth analysis of micro-mechanism of mechanical property alternations in PLA/EVA/clay nanocomposites: A combined theoretical and experimental approach.* Materials & Design, 2015. **88**: 1277-1289.

15.   Jiang, W.R., R.Y. Bao, W. Yang, Z.Y. Liu, B.H. Xie and M.B. Yang, *Morphology, interfacial and mechanical properties of polylactide/poly(ethylene terephthalate glycol) blends compatibilized by polylactide-g-maleic anhydride.* Materials & Design, 2014. **59**: 524-531.

16.   Nampoothiri, K.M., N.R. Nair and R.P. John, *An overview of the recent developments in polylactide (PLA) research.* Bioresource Technology, 2010. **101**(22): 8493-8501.

17.   Lasprilla, A.J.R., G.A.R. Martinez, B.H. Lunelli, A.L. Jardini and R. Maciel, *Poly-lactic acid synthesis for application in biomedical devices - A review.* Biotechnology Advances, 2012. **30**(1): 321-328.

18.   Kfoury, G., J.M. Raquez, F. Hassouna, J. Odent, V. Toniazzo, D. Ruch and P. Dubois, *Recent advances in high performance poly(lactide): from "green" plasticization to super -tough materials via (reactive) compounding.* Frontiers in Chemistry, 2013. **1**: 46.

19.   Zeng, J.B., K.A. Li and A.K. Du, *Compatibilization strategies in poly(lactic acid)-based blends.* Rsc Advances, 2015. **5**(41): 32546-32565.

20.   Martino, V.P., R.A. Ruseckaite and A. Jimenez, *Thermal and mechanical characterization of plasticized poly (L-lactide-co-D,L-lactide) films for food packaging.* Journal of Thermal Analysis and Calorimetry, 2006. **86**(3): 707-712.

21.   Baiardo, M., G. Frisoni, M. Scandola, M. Rimelen, D. Lips, K. Ruffieux and E. Wintermantel, *Thermal and mechanical properties of plasticized poly(L-lactic acid).* Journal of Applied Polymer Science, 2003. **90**(7): 1731-1738.

22.   Arrieta, M.P., E. Fortunati, F. Dominici, J. Lopez and J.M. Kenny, *Bionanocomposite films based on plasticized PLA-PHB/cellulose nanocrystal blends.* Carbohydrate Polymers, 2015. **121**: 265-275.

23.   Arrieta, M.P., M.D. Castro-Lopez, E. Rayon, L.F. Barral-Losada, J.M. Lopez-Vilarino, J. Lopez and M.V. Gonzalez-Rodriguez, *Plasticized Poly(lactic acid)-Poly(hydroxybutyrate) (PLA-PHB) Blends Incorporated with Catechin Intended for Active Food-Packaging Applications.* Journal of Agricultural and Food Chemistry, 2014. **62**(41): 10170-10180.

24.   Maiza, M., M.T. Benaniba, G. Quintard and V. Massardier-Nageotte, *Biobased additive plasticizing Polylactic acid (PLA).* Polimeros-Ciencia E Tecnologia, 2015. **25**(6): 581-590.

25.   Park, S.B., S.Y. Hwang, C.W. Moon, S.S. Im and E.S. Yoo, *Plasticizer Effect of Novel PBS Ionomer in PLA/PBS Ionomer Blends.* Macromolecular Research, 2010. **18**(5): 463-471.

26.   Burgos, N., V.P. Martino and A. Jimenez, *Characterization and ageing study of poly(lactic acid) films plasticized with oligomeric lactic acid.* Polymer Degradation and Stability, 2013. **98**(2): 651-658.

27.   Armentano, I., et al., *Processing and characterization of plasticized PLA/PHB blends for biodegradable multiphase systems.* Express Polymer Letters, 2015. **9**(7): 583-596.

28.   Arrieta, M.P., J. Lopez, E. Rayon and A. Jimenez, *Disintegrability under composting conditions of plasticized PLA-PHB blends.* Polymer Degradation and Stability, 2014. **108**: 307-318.

29.   Ge, H.H., F. Yang, Y.P. Hao, G.F. Wu, H.L. Zhang and L.S. Dong, *Thermal, Mechanical, and Rheological Properties of Plasticized Poly(L-lactic acid).* Journal of Applied Polymer Science, 2013. **127**(4): 2832-2839.

30.   Sungsanit, K., N. Kao and S.N. Bhattacharya, *Properties of linear poly(lactic acid)/polyethylene glycol blends.* Polymer Engineering and Science, 2012. **52**(1): 108-116.

31.   Kulinski, Z., E. Piorkowska, K. Gadzinowska and M. Stasiak, *Plasticization of poly(L-lactide) with poly(propylene glycol).* Biomacromolecules, 2006. **7**(7): 2128-2135.

32.   Piorkowska, E., Z. Kulinski, A. Galeski and R. Masirek, *Plasticization of semicrystalline poly(L-lactide) with poly(propylene glycol).* Polymer, 2006. **47**(20): 7178-7188.

33.   Kowalczyk, M., M. Pluta, E. Piorkowska and N. Krasnikova, *Plasticization of polylactide with block copolymers of ethylene glycol and propylene glycol.* Journal of Applied Polymer Science, 2012. **125**(6): 4292-4301.

34.   Yang, Y., J.C. Huang, R.Y. Zhang and J. Zhu, *Designing bio-based plasticizers: Effect of alkyl chain length on plasticization properties of isosorbide diesters in PVC blends.* Materials & Design, 2017. **126**: 29-36.

35.   Yang, Y., Z. Xiong, L.S. Zhang, Z.B. Tang, R.Y. Zhang and J. Zhu, *Isosorbide dioctoate as a "green" plasticizer for poly(lactic acid).* Materials & Design, 2016. **91**: 262-268.

36.   Choi, K.M., S.W. Lim, M.C. Choi, Y.M. Kim, D.H. Han and C.S. Ha, *Thermal and mechanical properties of poly(lactic acid) modified by poly(ethylene glycol) acrylate through reactive blending.* Polymer Bulletin, 2014. **71**(12): 3305-3321.

37.   Torres-Giner, S., N. Montanes, T. Boronat, L. Quiles-Carrillo and R. Balart, *Melt grafting of sepiolite nanoclay onto poly(3-hydroxybutyrate-co-4-hydroxybutyrate) by reactive extrusion with multi-functional epoxy-based styrene-acrylic oligomer.* European Polymer Journal, 2016. **84**: 693-707.

38.   Islam, M.R., M.D.H. Beg and S.S. Jamari, *Development of Vegetable-Oil-Based Polymers.* Journal of Applied Polymer Science, 2014. **131**(18): 13.

39.   Gandini, A., T.M. Lacerda, A.J.F. Carvalho and E. Trovatti, *Progress of Polymers from Renewable Resources: Furans, Vegetable Oils, and Polysaccharides.* Chemical Reviews, 2016. **116**(3): 1637-1669.

40.   Kozlowski, R. and K. Bujnowicz, *Polymers from vegetable oils.* Przemysl Chemiczny, 2008. **87**(12): 1168-1170.

41.   King, J.W., *Determination of the solubility parameter os soybean oil by inverse gas-chromatography.* Food Science and Technology-Lebensmittel-Wissenschaft & Technologie, 1995. **28**(2): 190-195.

42.   Arrieta, M.P., M.D. Samper, J. Lopez and A. Jimenez, *Combined Effect of Poly(hydroxybutyrate) and Plasticizers on Polylactic acid Properties for Film Intended for Food Packaging.* Journal of Polymers and the Environment, 2014. **22**(4): 460-470.

43.   Wang, Q., Y.L. Chen, J. Tang and Z.F. Zhang, *Determination of the Solubility Parameter of Epoxidized Soybean Oil by Inverse Gas Chromatography.* Journal of Macromolecular Science Part B-Physics, 2013. **52**(10): 1405-1413.

44.   Ferri, J.M., M.D. Samper, D. Garcia-Sanoguera, M.J. Reig, O. Fenollar and R. Balart, *Plasticizing effect of biobased epoxidized fatty acid esters on mechanical and thermal properties of poly(lactic acid).* Journal of Materials Science, 2016. **51**(11): 5356-5366.

45.   Li, M., S.H. Li, J.L. Xia, C.X. Ding, M. Wang, L.N. Xu, X.H. Yang and K. Huang, *Tung oil based plasticizer and auxiliary stabilizer for poly(vinyl chloride).* Materials & Design, 2017. **122**: 366-375.

46.   Chieng, B.W., N.A. Ibrahim, Y.Y. Then and Y.Y. Loo, *Epoxidized Vegetable Oils Plasticized Poly(lactic acid) Biocomposites: Mechanical, Thermal and Morphology Properties.* Molecules, 2014. **19**(10): 16024-16038.

47.   Xu, Y.Q. and J.P. Qu, *Mechanical and Rheological Properties of Epoxidized Soybean Oil Plasticized Poly(lactic acid).* Journal of Applied Polymer Science, 2009. **112**(6): 3185-3191.

48.   Garcia-Garcia, D., J.M. Ferri, N. Montanes, J. Lopez-Martinez and R. Balart, *Plasticization effects of epoxidized vegetable oils on mechanical properties of poly(3-hydroxybutyrate).* Polymer International, 2016. **65**(10): 1157-1164.

49.   Balart, J.F., V. Fombuena, O. Fenollar, T. Boronat and L. Sanchez-Nacher, *Processing and characterization of high environmental efficiency composites based on PLA and hazelnut shell flour (HSF) with biobased plasticizers derived from epoxidized linseed oil (ELO).* Composites Part B-Engineering, 2016. **86**: 168-177.

50.   Torres-Giner, S., N. Montanes, O. Fenollar, D. García-Sanoguera and R. Balart, *Development and optimization of renewable vinyl plastisol/wood flour composites exposed to ultraviolet radiation.* Materials & Design, 2016. **108**: 648-658.

51.   Ferri, J.M., D. Garcia-Garcia, N. Montanes, O. Fenollar and R. Balart, *The effect of maleinized linseed oil as biobased plasticizer in poly(lactic acid)-based formulations.* Polymer International, 2017. **66**(6): 882-891.

52.   Carbonell-Verdu, A., D. Garcia-Garcia, F. Dominici, L. Torre, L. Sanchez-Nacher and R. Balart, *PLA films with improved flexibility properties by using maleinized cottonseed oil.* European Polymer Journal, 2017. **91**: 248-259.

53.   Xiong, Z., C. Li, S.Q. Ma, J.X. Feng, Y. Yang, R.Y. Zhang and J. Zhu, *The properties of poly(lactic acid)/starch blends with a functionalized plant oil: Tung oil anhydride.* Carbohydrate Polymers, 2013. **95**(1): 77-84.

54.   Quiles-Carrillo, L., N. Montanes, S. Sammon, R. Balart and S. Torres-Giner, *Compatibilization of highly sustainable polylactide/almond shell flour composites by reactive extrusion with maleinized linseed oil.* Industrial Crops and Products, 2017. **111**: 878-888.

55.   Mauck, S.C., S. Wang, W.Y. Ding, B.J. Rohde, C.K. Fortune, G.Z. Yang, S.K. Ahn and M.L. Robertson, *Biorenewable Tough Blends of Polylactide and Acrylated Epoxidized Soybean Oil Compatibilized by a Polylactide Star Polymer.* Macromolecules, 2016. **49**(5): 1605-1615.

56.   Najafi, N., M.C. Heuzey, P.J. Carreau, D. Therriault and C.B. Park, *Mechanical and morphological properties of injection molded linear and branched-polylactide (PLA) nanocomposite foams.* European Polymer Journal, 2015. **73**: 455-465.

57.   Lim, L.T., R. Auras and M. Rubino, *Processing technologies for poly(lactic acid).* Progress in Polymer Science, 2008. **33**(8): 820-852.

58.   Takayama, T., K. Uchiumi, H. Ito, T. Kawai and M. Todo, *Particle size distribution effects on physical properties of injection molded HA/PLA composites.* Advanced Composite Materials, 2013. **22**(5): 327-337.

59.   Harris, A.M. and E.C. Lee, *Improving mechanical performance of injection molded PLA by controlling crystallinity.* Journal of Applied Polymer Science, 2008. **107**(4): 2246-2255.

60.   Mofokeng, J.P., A.S. Luyt, T. Tabi and J. Kovacs, *Comparison of injection moulded, natural fibre-reinforced composites with PP and PLA as matrices.* Journal of Thermoplastic Composite Materials, 2012. **25**(8): 927-948.

61.   Chaitanya, S. and I. Singh, *Processing of PLA/sisal fiber biocomposites using direct- and extrusion-injection molding.* Materials and Manufacturing Processes, 2017. **32**(5): 468-474.

62.   Pivsa-Art, S., J. Kord-Sa-Ard, W. Pivsa-Art, R. Wongpajan, N. O-Charoen, S. Pavasupree and H. Hamada, *Effect of Compatibilizer on PLA/PP Blend for Injection Molding*, in *Coe on Sustainable Energy System*, B. Plangklang, H. Ohgaki, and S. PivsaArt, Editors. 2016, Elsevier Science Bv: Amsterdam. p. 353-360.

63.   Tábi, T., A.Z. Égerházi, P. Tamás, T. Czigány and J.G. Kovács, *Investigation of injection moulded poly (lactic acid) reinforced with long basalt fibres.* Composites Part A: Applied Science and Manufacturing, 2014. **64**: 99-106.

64.   Nagarajan, V., A.K. Mohanty and M. Misra, *Reactive compatibilization of poly trimethylene terephthalate (PTT) and polylactic acid (PLA) using terpolymer: Factorial design optimization of mechanical properties.* Materials & Design, 2016. **110**: 581-591.

65.   Carrasco, F., L.A. Perez-Maqueda, O.O. Santana and M.L. Maspoch, *Enhanced general analytical equation for the kinetics of the thermal degradation of poly(lactic acid)/montmorillonite nanocomposites driven by random scission.* Polymer Degradation and Stability, 2014. **101**: 52-59.

66.   Carrasco, F., L.A. Perez-Maqueda, P.E. Sanchez-Jimenez, A. Perejon, O.O. Santana and M.L. Maspoch, *Enhanced general analytical equation for the kinetics of the thermal*

degradation of poly(lactic acid) driven by random scission. Polymer Testing, 2013. **32**(5): 937-945.

67.   Carrasco, F., J. Cailloux, P.E. Sanchez-Jimenez and M.L. Maspoch, *Improvement of the thermal stability of branched poly(lactic acid) obtained by reactive extrusion.* Polymer Degradation and Stability, 2014. **104**: 40-49.

III.2.2. Reactive toughening of injection-molded polylactide pieces using maleinized hemp seed oil

L. Quiles-Carrillo[1], M.M.Blanes-Martínez[1], N. Montanes[1], O. Fenollar[1], S. Torres-Giner[1, 2] and R. Balart[1]

[1] Technological Institute of Materials (ITM), Universitat Politècnica de València (UPV), Plaza Ferrándiz y Carbonell 1, Alcoy 03801, Spain

[2] Novel Materials and Nanotechnology Group, Institute of Agrochemistry and Food Technology (IATA), Spanish Council for Scientific Research (CSIC), Calle Catedrático Agustín Escardino Benlloch 7, Paterna 46980, Spain
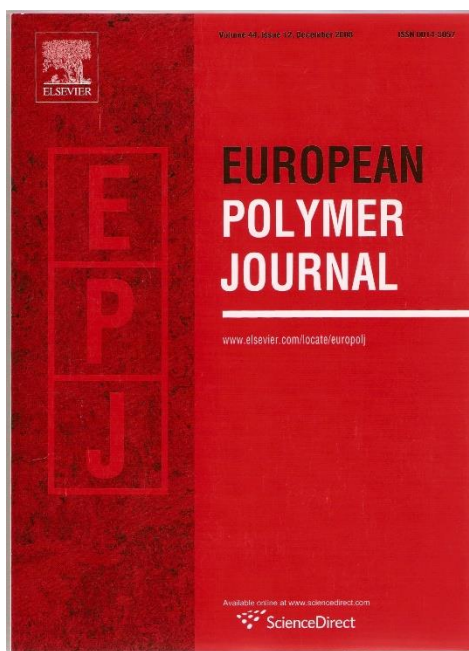
Contents lists available at ScienceDirect

European Polymer Journal

journal homepage: www.elsevier.com/locate/europolj

Reactive toughening of injection-molded polylactide pieces using maleinized hemp seed oil

L. Quiles-Carrillo[a], M.M. Blanes-Martínez[a], N. Montanes[a], O. Fenollar[a], S. Torres-Giner[b], R. Balart[a],*

[a] Technological Institute of Materials (ITM), Universitat Politècnica de València (UPV), Plaza Ferrándiz y Carbonell 1, Alcoy 03801, Spain
[b] Novel Materials and Nanotechnology Group, Institute of Agrochemistry and Food Technology (IATA), Spanish Council for Scientific Research (CSIC), Calle Catedrático Agustín Escardino Benlloch 7, Paterna 46980, Spain

ARTICLE INFO

ABSTRACT

The present study describes the effect of maleinized hemp seed oil (MHO) on the physical performance of polylactide (PLA) pieces. To this end, PLA pieces with varying MHO contents in the 0–10 wt% range were manufactured by twin-screw extrusion (TSE) followed by injection molding. The resultant pieces were characterized in terms of their mechanical, thermal, and thermomechanical properties. The obtained properties suggested that, unlike typical plasticizers, MHO does not only induce an increment in elongation at break and impact resistance but it also enhances both elastic modulus and tensile strength. In addition, a moderate decrease in the glass transition temperature (T_g) was observed. This was ascribed to simultaneous linear chain-extension, branching, and/or cross-linking phenomena due to the reaction of the multiple maleic anhydride (MAH) groups present in MHO with the terminal hydroxyl groups of the PLA chains. Furthermore, morphology characterization revealed that, though certain phase separation occurred at its highest content, MHO was finely dispersed as submicron droplets within the PLA matrix contributing to improving toughness. The use of multi-functionalized reactive vegetable oils thus represents a highly sustainable solution to reduce the intrinsic brittleness of PLA materials without compromising their mechanical resistance and the toughened biopolymer pieces described herein can find interesting applications in, for instance, rigid packaging.

1. Introduction

The use of biopolymers is gaining interest and relevance due to an increasing environmental concern. Some petroleum-derived polymers are being currently employed due to their ability to disintegrate in a controlled compost soil such as poly(ε-caprolactone) (PCL), poly(butylene succinate) (PBS), and poly(butylene succinate-co-adipate) (PBSA), etc. [1–3]. More interestingly, other biopolymers can be obtained from renewable resources as it is the case of polylactide (PLA), prepared by starch fermentation, and polyhydroxyalkanoates (PHAs), obtained from bacterial fermentation [4–7]. Among them, PLA is nowadays the most close-to-market biopolymer from both technical and economical standpoints [8]. PLA can be processed by conventional manufacturing techniques at industrial scale with an annual volume of 140,000 t [9]. Currently, PLA finds several applications in the rigid packaging industry [10]. In particular, PLA offers an unusual range of physical properties that can be tailored by the processing conditions, molecular weight (M_W), and type of isomers [11].

However, one of the main drawbacks of PLA is its extremely low toughness. For this reason, plasticization and blending with flexible and rubber-like polymers are currently being investigated as economical and technical solutions to obtain toughened PLA-based industrial formulations [12–15]. Plasticizers represent a well-known strategy as they can increase elongation at break by reducing the glass transition temperature (T_g), but mechanical resistant properties usually decrease in a great extent. For this reason, other alternatives such as reactive extrusion by means of functionalized oligomers or copolymers are preferred as the technical solution to improve toughness. For instance, Wang et al. [16] proposed the use of an epoxy-functionalized rubber copolymer with excellent performance on both toughness and mechanical resistant properties. A wide variety of plasticizers for PLA have been proposed. Oligomeric lactic acid (OLA) has proved its high compatibility with PLA, showing a remarkable decrease in T_g and a high increase in elongation at break of the biopolymer, as reported by Burgos et al. [17]. It is also worthy to note the efficiency of citrate-derived plasticizers, such as acetyl tri-n-butyl citrate (ATBC), triethyl citrate

---

* Corresponding author.
  E-mail address: rbalart@mcm.upv.es (R. Balart).

Reactive toughening of injection-molded polylactide pieces using maleinized hemp seed oil

Abstract

The present study describes the effect of maleinized hemp seed oil (MHO) on the physical performance of polylactide (PLA) pieces. To this end, PLA pieces with varying MHO contents in the 0–10 wt% range were manufactured by twin-screw extrusion (TSE) followed by injection molding. The resultant pieces were characterized in terms of their mechanical, thermal, and thermomechanical properties. The obtained properties suggested that, unlike typical plasticizers, MHO does not only induce an increment in elongation at break and impact resistance but it also enhances both elastic modulus and tensile strength. In addition, a moderate decrease in the glass transition temperature (T_g) was observed. This was ascribed to simultaneous linear chain-extension, branching, and/or cross-linking phenomena due to the reaction of the multiple maleic anhydride (MAH) groups present in MHO with the terminal hydroxyl groups of the PLA chains. Furthermore, morphology characterization revealed that, though certain phase separation occurred at its highest content, MHO was finely dispersed as submicron droplets within the PLA matrix contributing to improving toughness. The use of multi-functionalized reactive vegetable oils thus represents a highly sustainable solution to reduce the intrinsic brittleness of PLA materials without compromising their mechanical resistance and the toughened biopolymer pieces described herein can find interesting applications in, for instance, rigid packaging.

INTRODUCTION

The use of biopolymers is gaining interest and relevance due to an increasing environmental concern. Some petroleum-derived polymers are being currently employed due to their ability to disintegrate in a controlled compost soil such as poly(ε-caprolactone) (PCL), poly(butylene succinate) (PBS), and poly(butylene succinate-co-adipate) (PBSA), etc. [1], [2], [3]. More interestingly, other biopolymers can be obtained from renewable resources as it is the case of polylactide (PLA), prepared by starch fermentation, and polyhydroxyalkanoates (PHAs), obtained from bacterial fermentation [4], [5], [6], [7]. Among them, PLA is nowadays the most close-to-market biopolymer from both technical and economical standpoints [8]. PLA can be processed by conventional manufacturing techniques at industrial scale with an annual volume of 140,000 t [9]. Currently, PLA finds several applications in the rigid packaging industry [10]. In particular, PLA offers an unusual range of physical properties that can be tailored by the processing conditions, molecular weight (M_W), and type of isomers [11].

However, one of the main drawbacks of PLA is its extremely low toughness. For this reason, plasticization and blending with flexible and rubber-like polymers are currently being investigated as economical and technical solutions to obtain toughened PLA-based industrial formulations [12], [13], [14], [15]. Plasticizers represent a well-known strategy as they can increase elongation at break by reducing the glass transition temperature (T_g), but mechanical resistant properties usually decrease in a great extent. For this reason, other alternatives such as reactive extrusion by means of functionalized oligomers or copolymers are preferred as the technical solution to improve toughness. For instance, Wang *et al*. [16] proposed the use of an epoxy-functionalized rubber copolymer with excellent performance on both toughness and mechanical resistant properties. A wide variety of plasticizers for PLA have been proposed. Oligomeric lactic acid (OLA) has proved its high compatibility with PLA, showing a remarkable decrease in T_g and a high increase in elongation at break of the biopolymer, as reported by Burgos *et al*. [17]. It is also worthy to note the efficiency of citrate-derived plasticizers, such as acetyl tri-n-butyl citrate (ATBC), triethyl citrate (TEC), among others [18], [19], [20]. Another important family of PLA plasticizers are derived from polymeric glycols, such as poly(ethylene glycol) (PEG), poly(propylene glycol) (PPG), etc. By selecting the appropriate M_W and/or type of copolymers, the properties of PLA formulations can be tailored [18], [21], [22].

In the last years, vegetable oils (VOs) have acquired a relevant role in polymer synthesis and modification [23], [24], [25]. VOs, obtained from plants, offer a great potential to partially or fully substitute petroleum-derived materials in the polymer industry [26], [27], [28]. These consist on a glycerol base skeleton in which three different fatty acids are linked through ester bonds, thus leading to the typical triglyceride structure. Fatty acids consist, generally, on aliphatic long-chains made of 13–21 carbon atoms. The fatty acid composition varies with the plant, crop, and growing conditions. Some fatty acids (*e.g*. oleic, linoleic, linolenic, etc.) are characterized by the presence of one, two or more degrees of unsaturation, *i.e*. highly reactive points, which make fatty acids and triglycerides suitable for a wide variety of chemical modifications. In general, this chemical modification is necessary to induce

certain reactivity to VOs and to achieve good interactions with the PLA chains [29], [30]. Epoxidized vegetable oils (EVOs) and epoxidized fatty acid esters (EFAE) have been successfully used as PLA plasticizers, however certain saturation occurs at relatively low contents [31], [32], [33]. Although the plasticizing efficiency of EVOs is lower to that reported for citrates, adipates, and polymeric glycols, their main benefit when adding to PLA is a considerable toughness improvement and a noticeable increase in thermal stability [34].

Hemp seed oil (HO) is an interesting vegetable oil obtained from Cannabis sativa L. with a high potential in the polymer industry due to its typical lipid profile (wt%): 55.3% linoleic acid, 20.3% α-linolenic acid, 9.0% oleic acid, 5.9% palmitic acid, 4.4% γ-linolenic acid, 2.2% stearic acid, and 1.7% arachidic acid [35]. HO can be easily obtained by cold-press processing the hemp seeds [36] and possesses high oxidative stability [37]. It is worthy to note that an important fraction of HO comes from the crops of hemp plants for the textile industry, so that, it can be considered a by-product (or co-product) of this industry, leading to a cost-effective raw material for chemical modification. Its high unsaturation content (similar or slightly lower to linseed oil, which is widely used in polymer synthesis and additives) allows a wide variety of modifications (*e.g.* epoxidation, acrylation, hydroxylation, etc.) that makes it interesting for polymer synthesis, modification, and composite manufacturing [38], [39], [40], [41], [42]. Shuttleworth *et al.* [43] have recently reported the fabrication of flexible bio-based nanocomposites from epoxidized hemp seed oil (EHO) as thermosetting resin with halloysite nanotubes (HNTs). Manthey *et al.* [40] reported interesting green composites based on EHO thermosetting matrix and hemp fiber reinforcement. The main use of modified HO has been so far focused on thermosetting resins. In particular, both EHO and acrylated epoxidized hemp seed oil (AEHO) have been proposed as bio-derived thermosetting resins for uses in polymer composites. The works of Francucci *et al.* [44] reported the cure mechanism of these bio-based thermosets with interesting uses at industrial scale.

Cyclic anhydrides, *i.e.* itaconic, phthalic, maleic anhydride (MAH), and derivatives, are readily reactive groups towards hydroxyl groups. Marsilla *et al.* [45] reported the grafting of itaconic anhydride to improve the overall properties of PLA. In fact, maleinized copolymers have been widely used to compatibilize polymer blends and polymers with cellulosic fillers [46]. Maleinization is a straightforward chemical modification carried out on VOs that proceeds mainly by "*ene*" reaction or allylic addition of MAH and, in some cases, by Diels-Alder condensation when conjugated carbon-carbon double bonds are present [47]. Depending on stoichiometry, maleinization reaction can be performed to a partial extent, thus leading to tailored functionalities [48], [49]. The application of maleinized vegetable oils (MVOs) as additives in PLA and other bio-based polyesters has proved to provide increased ductility and toughness. For instance, Ferri *et al.* [50] reported the efficiency of maleinized linseed oil (MLO) for toughening PLA formulations by the only addition of 4.3 wt% MLO. Despite this, the efficiency of MLO on poly(3-hydroxybutyrate) (PHB) was not as high as that reported for PLA [51]. Carbonell-Verdu *et al.* [52] also reported the usefulness of maleinized cottonseed oil (MCSO) as another green alternative to MLO, showing a good plasticizing effect on PLA films. MVOs can also provide a compatibilizing effect, as previously described by Xiong *et al.* [53]. Depending on both

the maleinization degree and the particular chemical profile of the base vegetable oil, different degrees of plasticization can be achieved.

This works focuses on the maleinization process of HO to produce maleinized hemp seed oil (MHO) and its use, for the first time, as an environmentally friendly additive for toughening PLA pieces obtained by twin-screw extrusion (TSE) followed by injection molding.

EXPERIEMNTAL

Materials

PLA Ingeo™ Biopolymer 6201D grade was supplied by NatureWorks (Minnetonka, Minnesota, USA). This is a commercial grade with a density of $1.24\,\mathrm{g\,cm^{-3}}$ and a melt flow index (MFI) of 15–30 g/10 min (190 °C, 2.16 kg), which is suitable for injection molding. HO, obtained from hemp seeds by a cold-press process, was provided by Suministros Agropecuarios Jordà (Concentaina, Spain). MAH was obtained from Sigma-Aldrich S.A. (Madrid, Spain).

Maleinization of hemp seed oil

The extracted HO was subjected to a maleinization process with MAH. To this end, a three-necked round bottom reactor equipped with a magnetic stirrer-heating mantle was used. In the first neck, a digital thermometer was introduced to control the temperature of the process. In the second neck, a nitrogen gas dispenser with a flow-rate of $1.5\,\mathrm{L\,min^{-1}}$ was added to achieve an inert atmosphere. A reflux condenser was coupled in the third neck to minimize the MAH loss during the process.

The production consisted on introducing into the reactor 20 g of MAH per 100 g of HO to achieve a stoichiometric ratio. For this, taking into account the most abundant fatty acids present in HO [35], it was considered that each molecule of linolenic acid, linoleic acid, and oleic acid, will react with an average of 2.5, 2, and 1 molecules of MAH, respectively. The mixture was heated at 200 °C and allowed to react for four hours under constant stirring, maintaining the nitrogen atmosphere to avoid oil oxidation. **Figure III.2.2.1** shows a schematic representation of the process.
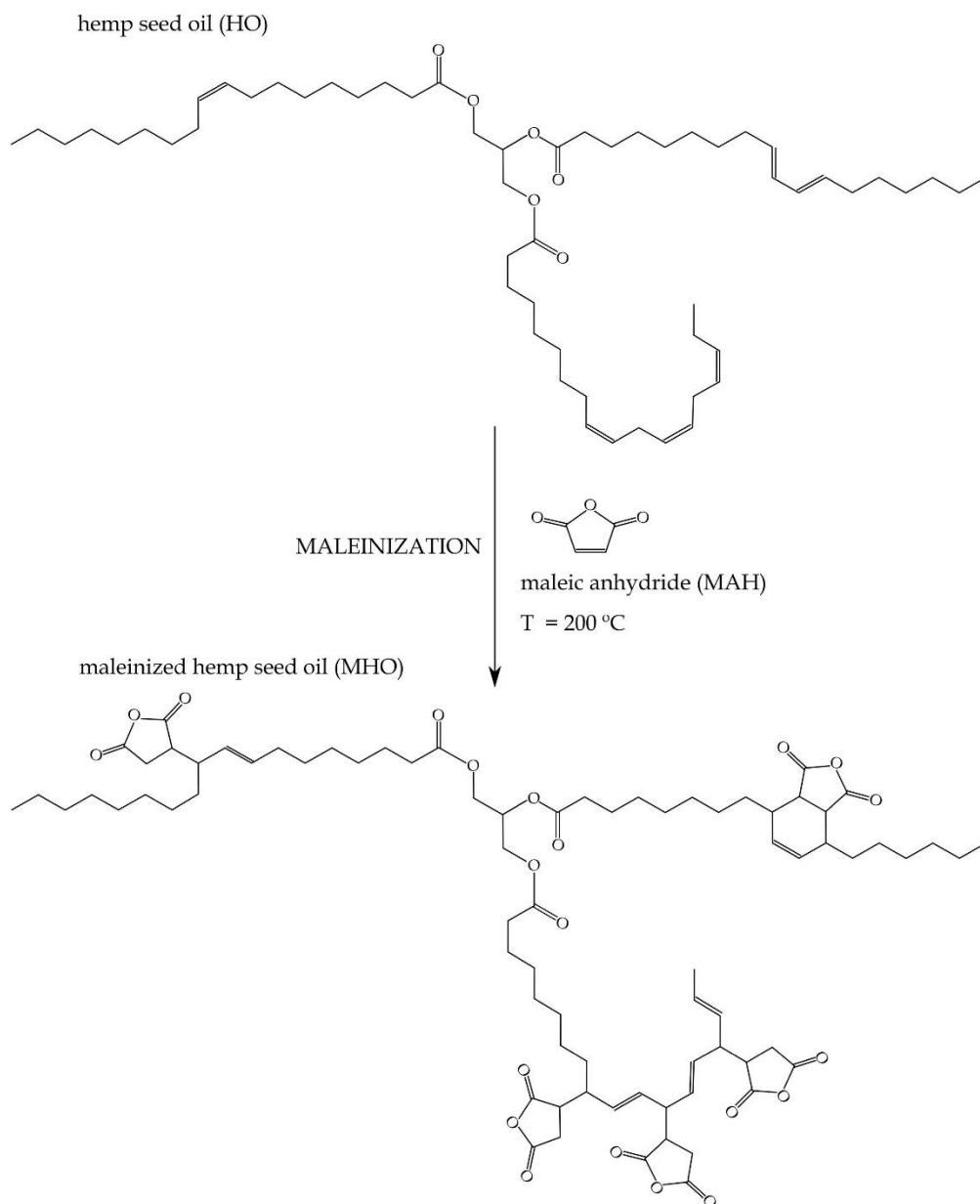
Figure III.2.2.1. Schematic representation of the maleinization process of hemp seed oil (HO) by maleic anhydride (MAH) to obtain maleinized hemp seed oil (MHO).

Manufacturing of injection-molded pieces

Prior to processing, all materials were dried for 36 h in a dehumidifier model MDEO provided by Industrial Marsé (Barcelona, Spain). The selected temperature was 60 °C. Then, different PLA formulations with MHO contents of 2.5, 5, 7.5, and 10 wt% were prepared by melt compounding in a co-rotating twin-screw extruder from Dupra S.L. (Castalla, Spain). The two screws had a diameter of 25 mm and a length-to-diameter ratio (L/D) of 24. All raw materials were fed into the main hoper, being previously pre-homogenized in a zipper bag. The temperature profile for the extrusion process was, from hopper to die, 180 °C, 185 °C, 190 °C, and 195 °C while the rotation speed was 20 rpm. The compounded materials were pelletized using an air-knife unit and subsequently processed by injection molding in a Sprinter 11 t injection machine

from Erinca S.L. (Barcelona, Spain). The pelletized materials were fed at 165 °C and injected at 180 °C into a mirror-finishing steel mold with standard shapes for sample characterization. Pieces with a thickness of 4 mm were obtained for characterization.

Mechanical characterization

Tensile tests were carried out in a universal test machine Elib 50 from S.A.E. Ibertest (Madrid, Spain) following the guidelines of ISO 527-1:2012. The selected load cell was 5 kN and the cross-head speed was 5 mm min^{-1}. Shore D hardness values were measured with a 676-D durometer from J. Bot (Barcelona, Spain) as indicated in ISO 868:2003. The improvement in toughness was estimated by standard Charpy's test with a 6-J pendulum from Metrotec (San Sebastián, Spain) as suggested by ISO 179-1:2010. To obtain reliable values, at least five different samples were subjected to each mechanical test and the values were averaged. All tests were performed at room temperature.

Morphology characterization

Fractured samples from the Charpy's tests were used to observe the morphology of the MHO-containing PLA pieces using a field emission scanning electron microscope (FESEM) model ZEISS ULTRA 55 from Oxford Instruments (Abingdon, United Kingdom). All fracture surfaces were coated with an ultrathin metallic layer (Au-Pd alloy) to provide electrical conductivity. This process was conducted in vacuum conditions inside a sputter chamber EMITECH mod. SC7620 provided by Quorum Technologies (East Sussex, United Kingdom).

Thermal characterization

Thermal characterization was carried out by differential scanning calorimetry (DSC) and thermogravimetric analysis (TGA). The main transition temperatures and enthalpies were obtained by dynamic DSC in a Mettler-Toledo 821 calorimeter (Schwerzenbach, Switzerland) with a temperature program consisting on three stages: a first heating process from 30 °C to 200 °C, followed by a cooling process from 200 °C down to 0 °C, and finally a second heating process from 0 °C to 350 °C. The heating/cooling rate was 10 °C min^{-1} for all three stages. The main thermal parameters were obtained from the second heating program. The sample size ranged from 5 mg to 7 mg and it was placed in standard aluminium crucibles (40 µL). All the DSC runs were carried out in nitrogen atmosphere with a flow-rate of 66 mL min^{-1}. The degree of crystallinity (X_c) was calculated by means of **Equation III.2.2.1**.

$$X_C = \left[\frac{\Delta H_m - \Delta H_{CC}}{\Delta H_m^0 \cdot (1-w)} \right] \cdot 100 \qquad \textbf{Equation III.2.2.1}$$

ΔH_m Melt enthalpy (J g^{-1})

ΔH_{CC} Cold crystallization enthalpy (J g^{-1})

ΔH_m^0 Melt enthalpy of a theoretical 100% crystalline PLA (J g^{-1}) [54]

w   weight fraction of the maleinized hemp oil

Thermal stability was studied in a TGA/SDTA 851 thermobalance also from Mettler-Toledo using a weight sample of 5–7 mg and standard alumina crucibles (70 µL). The thermal program was set from 30 °C to 700 °C at a constant heating rate of 20 °C min^{-1} in air.

Thermomechanical characterization

Thermomechanical properties were obtained by standard Vicat softening temperature (VST) and heat deflection temperature (HDT) tests following the recommendation of ISO 306 and ISO 75-1, respectively. Both VST and HDT values were obtained in a Vicat/HDT station model VHDT 20 from Metrotec S.A. (San Sebastián, Spain). VST values were obtained using the B50 method, which stands for an applied force of 50 N and a heating rate of 50 °C h^{-1}. Regarding HDT values, samples with dimensions 4 × 10 × 80 mm^3, were subjected to a load of 320 g (three-point bending with a distance between supports of 60 mm) and a heating rate of 120 °C h^{-1}. Three different measurements of VST and HDT values were carried out and averaged.

Dimensional stability was studied by thermomechanical analysis (TMA) in a Q400 TMA analyser from TA Instruments (New Castle, Delaware, USA). Squared samples with parallel faces (4 × 10 × 10 mm^3) were subjected to a constant load of 0.02 N and to a temperature sweep from 0 °C to 140 °C at a constant heating rate of 2 °C min^{-1}. The coefficient of linear thermal expansion (CLTE) was calculated below and above T_g. All measurements were done in triplicate.

The effect of temperature on the thermomechanical properties was also followed by dynamic mechanical thermal analysis (DMTA) in an oscillatory rheometer AR-G2 from TA Instruments. This device was equipped with a special clamp system for solid samples, working in torsion-shear conditions. Rectangular samples (4 × 10 × 40 mm^3) were subjected to a dynamic heating program from 30 °C to 140 °C using a heating rate of 2 °C min^{-1} at a constant frequency of 1 Hz. The maximum deformation (γ) was set to 0.1%. Both the storage modulus (G') and the damping factor (tan δ) were recorded as function of increasing temperature.

RESULT AND DISCUSSION

Mechanical properties of PLA pieces containing MHO

In **Figure III.2.2.2** it can be observed the effect of MHO on the tensile properties of the injection-molded PLA pieces. As a plasticizer, an increase in the ductile properties was expected and results showed that the elongation at break was remarkably improved from 4.97%, for the neat PLA piece, up to 11.6%, for the PLA piece containing 10 wt% MHO. In addition, it was also observed an increase in both the tensile modulus and strength, which is an effect that differs from conventional plasticizers. In particular, the tensile modulus of the neat PLA piece was close to 2.0 GPa and addition of MHO led to an increase up to values of 2.7 GPa, which represents a percentage increase of about 35%. Similar tendency was observed for the tensile strength, which increased from 66.0 MPa, for the neat PLA piece, up to 75 MPa, for the PLA pieces containing MHO at 2.5–5.0 wt%. However, for higher MHO contents than 5.0 wt%, the tensile strength started to decrease, which can be ascribed to a saturation phenomenon of the plasticizer in the PLA matrix.
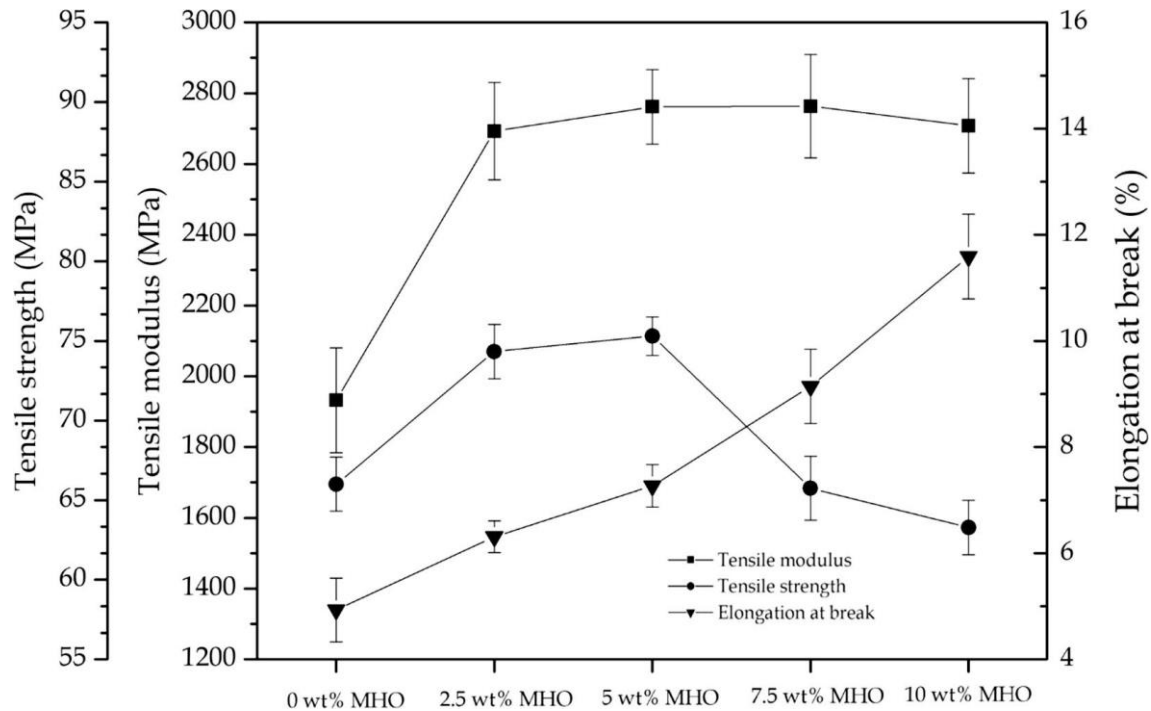
Figure III.2.2.2. Plot evolution of the mechanical properties for the injection-molded polylactide (PLA) pieces varying the maleinized hemp seed oil (MHO) content.

Whereas typical plasticizers habitually produce an increase in the mechanical ductile properties, such as elongation at break and impact resistance, they also produce a decrease in the mechanical resistant properties, such as modulus and strength. For instance, Xiong *et al.* [53] reported that the addition of 5 wt% maleinized tung oil (MTO) led to a decrease in tensile strength with no remarkable improvement of elongation at break. The main benefit of MTO was as compatibilizer in immiscible PLA/starch blends. Ferri *et al.* [50] also showed interesting plasticizing effects of MLO on PLA with a remarkable increase in elongation at break from values below 15%, for neat PLA, up to almost 80%, for a MLO content of 13 wt%. However, they also reported the typical decrease in both tensile modulus and tensile strength. In this study, interestingly, it was observed that MHO exerted a different effect on PLA. This behavior can be related to a chain-extension effect provided by MHO. The MAH groups present in MHO are considered to react with the terminal hydroxyl (OH) groups of the PLA chains, generating a macromolecule of higher MW based on a linear chain-extended, branched or even cross-linked structure and, thus, with an improved molecular entanglement to resist mechanical deformation. **Figure III.2.2.3** illustrates the here-described possible chemical reactions between the biopolymer molecules with the reactive VO.
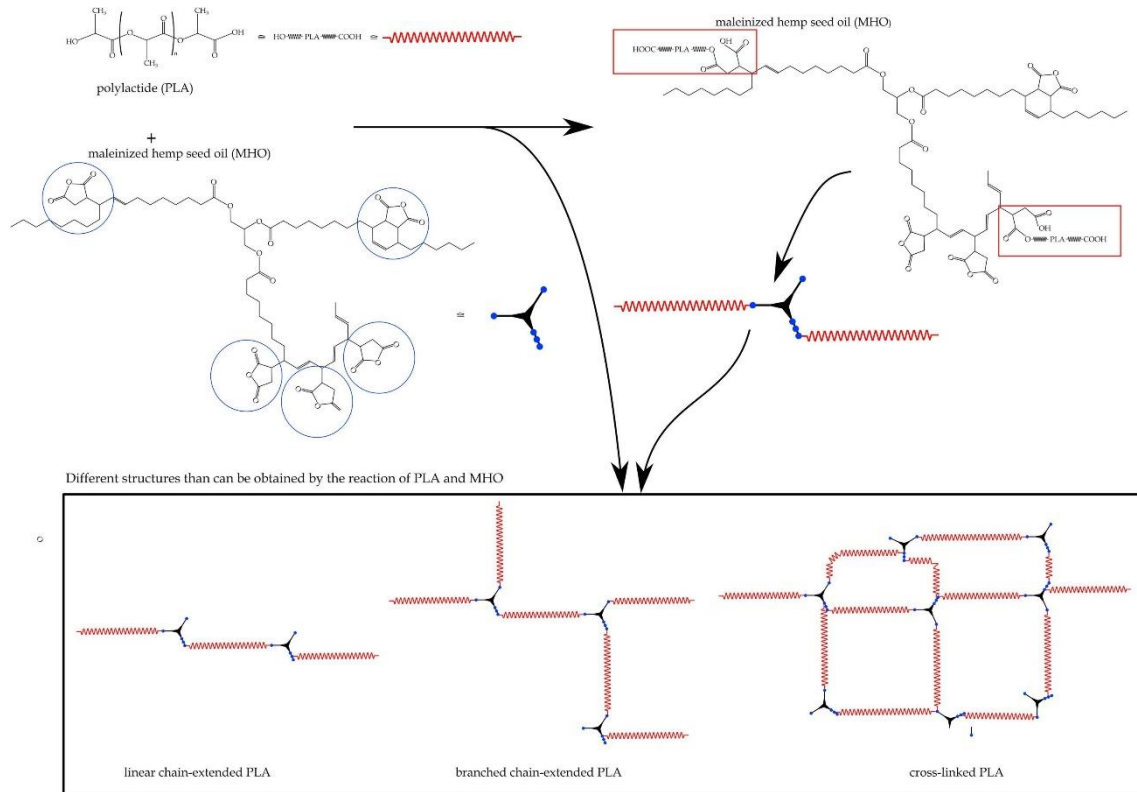
Figure III.2.2.3. Schematic representation of the proposed linear chain-extension (left), branching (middle), and cross-linking (right) processes of polylactide (PLA) by means of maleinized hemp seed oil (MHO).

As a result, depending on the number of MAH groups in MHO, *i.e.* its average functionality (*f*), a combined effect of different processes such as linear chain extension, branching, and/or cross-linking can be achieved. A similar effect was observed by Mauk *et al.* [55] who suggested that using acrylated epoxidized soybean oil (AESO) and a thermal initiator, reactive extrusion of PLA was achieved. The work developed by Yuryev *et al.* gave clear evidences of certain toughness improvement on PLA by using reactive extrusion with an acrylic-co-glycidyl copolymer [56]. Due to the multi-functionality of MHO and the tendency of the MAH groups to react with the hydroxyl groups at the end of the PLA chains, the above-described simultaneous phenomena are considered to take place, which can contribute to an increase in mechanical resistance. This effect is then proposed to occur in combination with the typical plasticization process due to the interactions of MHO individual molecules with the PLA chains, being responsible for the observed increase in the elongation at break.

The above-mentioned behavior can be also observed by analysing the Shore D and the Charpy's impact resistance, as shown in **Table III.2.2.1**. All the MHO-containing PLA pieces showed higher hardness values compared to the neat PLA piece. It is worthy to note the remarkable increase in the impact-absorbed energy that was obtained by the Charpy's test. While the neat PLA piece was characterized by an absorbed-energy of 19.5 kJ m^{-2}, the only addition of 2.5 wt% MHO led to an absorbed-energy of 32.1 kJ m^{-2}. This property even increased further up to a value of 43.4 kJ m^{-2} for the PLA piece additivated with 10 wt% MHO, which represents an increase of

122.6% with regard to the unmodified PLA piece. In this sense, it is important to take into account that the impact resistance is highly dependent on both mechanical ductile and resistant properties. Therefore, for the PLA pieces containing MHO it is expectable to have a higher contribution of the improved tensile strength (resistant property) in the overall toughness improvement, compared to the increase in elongation (ductile property). Although similar improvements of toughness have been previously reported by means of other chemically modified VOs (*e.g.* MLO), their main contribution was related to an increase in elongation at break since the mechanical resistant properties usually decrease with the plasticizer addition [31], [50], [53].

Table III.2.2.1. Shore D hardness and Charpy's impact strength for the injection-molded polylactide (PLA) pieces varying the maleinized hemp seed oil (MHO) content.

MHO content wt%	Shore D hardness	Charpy's impact resistance (kJ m^{-2})
0	79.0 ± 0.6	19.5 ± 2.6
2.5	83.1 ± 0.5	32.1 ± 1.5
5.0	84.4 ± 0.9	34.0 ± 1.9
7.5	83.3 ± 0.8	37.1 ± 1.7
10.0	82.1 ± 0.7	43.4 ± 1.9

Fracture surfaces of PLA pieces containing MHO

As it can be observed in the FESEM micrographs of the fracture surfaces included in **Figure III.2.2.4**, PLA and MHO are not fully miscible. Indeed, these images suggest that phase separation occurred at a relative low MHO content. In **Figure III.2.2.4a–c**, one can observe that neat PLA showed the typical brittle fracture with several crack growths and a very soft surface. This was mainly observable at higher magnification (**Figure III.2.2.4c**). This fracture morphology is representative for a material with a low deformation during the impact test, leading to lower impact-absorbed energy values.

The fracture surface of the injection-molded PLA piece containing 5 wt% MHO, as it can be seen from **Figure III.2.2.4d** to **f**, showed clear evidences of plastic deformation. This is emphasized with white circles in the images taken at 2,000× and 5,000×. At these magnifications, shown in **Figure III.2.2.4e** and **f**, respectively, some evidences of phase separation can be detected due to the presence of small spherical shapes, which can be ascribed to MHO, that appeared finely dispersed in the PLA-rich phase (marked with white arrows). At a higher magnification (5,000×, **Figure III.2.2.4f**) these spherical shapes were more evident with a diameter of 0.5 μm, *i.e.* in the submicron scale. Presence of filaments gives support to the higher elongation at break of the PLA piece with 5 wt% MHO. With regard to the PLA piece with the highest plasticizer content, *i.e.* 10 wt% MHO, phase separation was evident even at low magnification (500×, **Figure III.2.2.4g**). At magnifications of 2,000× and 5,000× (**Figure III.2.2.4h** and **i**, respectively), the MHO droplets were clearly distinguishable with

diameters ranging from hundred nanometres to 1–2 µm. This submicron MHO domains within the biopolymer matrix are expected to exert a positive effect on energy absorption in a similar way that, for instance, a rubber phase that is finely dispersed in a brittle polymer matrix [50], [52].
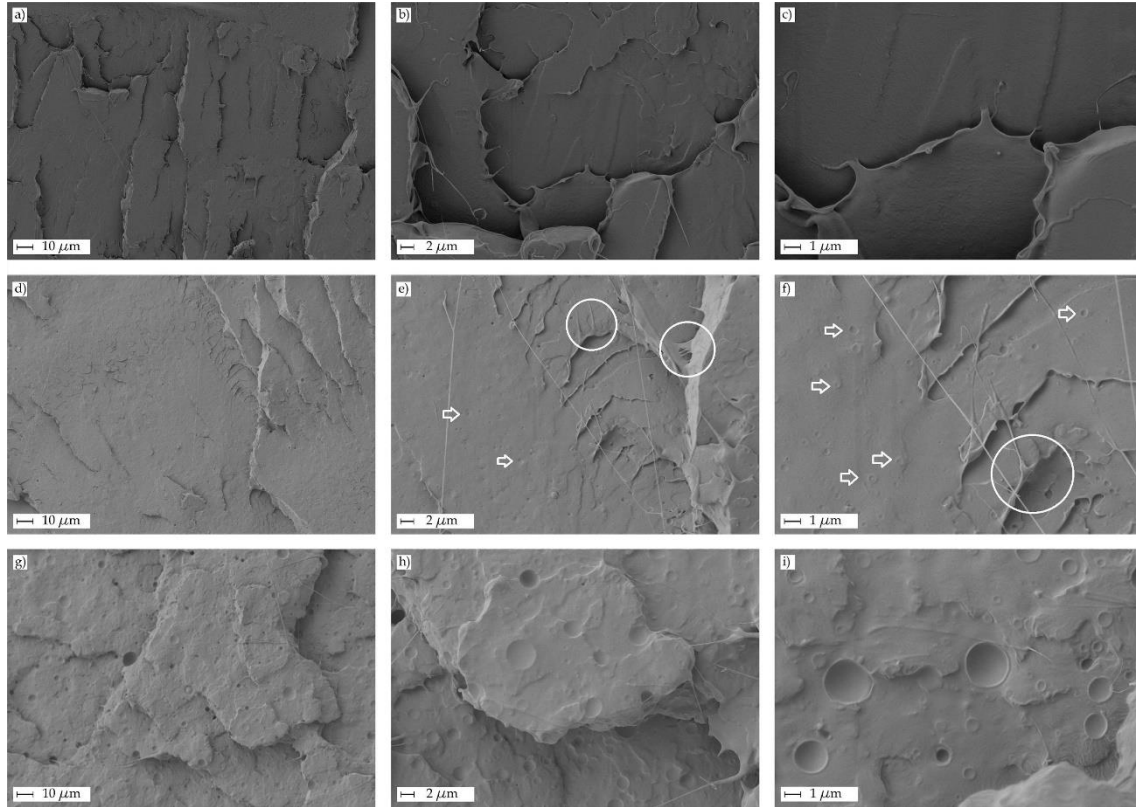
Figure III.2.4. Field emission scanning electron microscopy (FESEM) images of the injection-molded polylactide (PLA) pieces varying the maleinized hemp seed oil (MHO) content at different magnifications: (**a**, **b**, and **c**) neat PLA at 500×, 2,000×, and 5,000×; (**d**, **e**, and **f**) PLA with 5 wt% MHO at 500×, 2,000×, and 5,000×; (**g**, **h**, and **i**) PLA with 10 wt% MHO at 500×, 2,000×, and 5,000×.

Thermal properties of PLA pieces containing MHO

The DSC curves of the neat and MHO-containing PLA pieces are included in **Figure III.2.5**. **Table III.2.2.2** summarizes the main thermal parameters obtained from the DSC analysis. The baseline step in the 55–65 °C range corresponds to T_g of the biopolymer. The typical cold crystallization process of PLA, due to the rearrangement of the biopolymer chains in a packed way, was observed for neat PLA in the temperature range between 80 °C and 110 °C. Finally, the melting process can be identified as an endothermic peak in the 160–175 °C range. All these three thermal transitions were clearly identified for neat PLA. Its T_g was 62.8 °C, cold crystallization temperature (T_{CC}) was located at 96.3 °C and, finally, melting temperature (T_m) was around 169.6 °C.
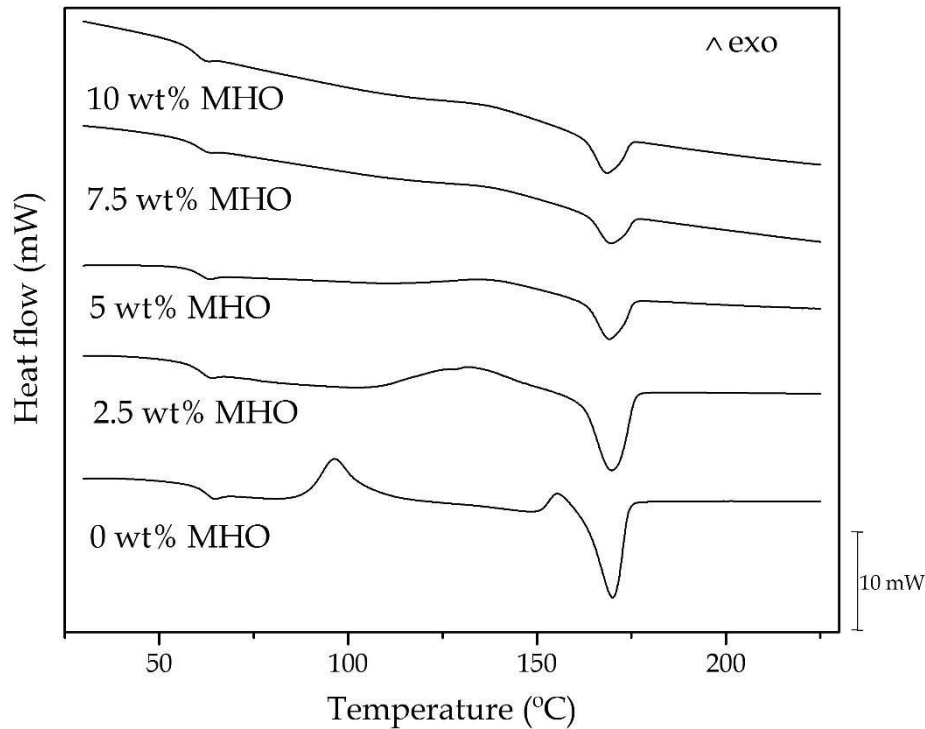
Figure III.2.2.5. Differential scanning calorimetry (DSC) thermograms of the injection-molded polylactide (PLA) pieces varying the maleinized hemp seed oil (MHO) content.

Table III.2.2.2. Thermal values in terms of glass transition temperature (T_g), cold crystallization temperature (T_{CC}), enthalpy of crystallization (ΔH_{CC}), melting temperature (T_m), enthalpy of melting (ΔH_m), and degree of crystallinity (X_c) for the injection-molded polylactide (PLA) pieces varying the maleinized hemp seed oil (MHO) content.

MHO content wt%	T_g (°C)	T_{CC} (°C)	ΔH_{CC} (J g^{-1})	T_m (°C)	ΔH_m (J g^{-1})	X_c%
0	62.8 ± 0.26	96.3 ± 0.62	12.5 ± 0.29	169.6 ± 0.66	34.5 ± 0.37	23.6 ± 0.75
2.5	61.4 ± 0.54	132.6 ± 0.76	11.7 ± 0.67	169.5 ± 0.48	28.8 ± 0.52	18.9 ± 0.85
5.0	60.6 ± 0.36	137.1 ± 0.46	3.0 ± 0.58	168.9 ± 0.67	13.7 ± 0.47	12.1 ± 0.77
7.5	60.6 ± 0.34	137.1 ± 1.03	1.7 ± 0.37	169.1 ± 0.52	9.3 ± 0.62	10.7 ± 0.69
10.0	59.8 ± 0.42	135.8 ± 1.24	1.4 ± 0.42	168.0 ± 0.72	7.9 ± 0.64	9.4 ± 0.74

The plasticization efficiency of a given additive is directly related to the T_g decrease it provides. Many studies have reported a remarkable decrease in T_g for PLA-based materials, particularly down to values in the range of 25–35 °C, by using common plasticizers such as ATBC, TEC, OLA, PEG, PPG, etc. [17], [20], [21], [22], [30]. As it can be seen in the DSC runs, a slight decrease of 2–3 °C in T_g was produced after incorporation of MHO, thus giving evidences of a low plasticization. As described above, MHO could induce certain chain extension, branching or cross-linking to the

PLA chains by which it promoted a moderate increase in elongation at break in combination to a significant improvement of the mechanical resistant properties (both tensile modulus and strength).

This macromolecular change can be reflected based on the fact that the cold crystallization peak was broader or even vanished as the MHO content increased and the melting peak slightly shifted to lower temperatures whereas the crystallization degree was noticeably reduced. In particular, T_{CC} of PLA formulations with 2.5 wt% and 5.0 wt% MHO moved up to 132.6 °C and 137.0 °C, respectively. Similar T_{CC} of PLA was observed for formulations with 7.5 wt% and 10 wt% MHO with values of 137.1 °C and 135.8 °C, respectively. In addition, neat PLA showed a X_c of 23.6% and this value presented a decreasing tendency down to 7.8% for the formulation containing 10 wt% MHO. As it can be observed in **Table III.2.2.2**, ΔH_{CC} changed from 12.5 J g^{-1}, with a narrow and well defined peak (see **Figure III.2.2.5**), for the unmodified PLA piece, down to values of 1–2 J g^{-1}, for the PLA formulations with 7.5–10 wt% MHO, showing a broader and poorly defined peak. This suggests a rupture of the crystalline structure in PLA. A similar effect was previously observed for PLA-based formulations cross-linked with acrylic monomers, as reported by Kaczmarek *et al.* [57]. They also observed a T_m decrease due to the PLA crystallites were less perfect in the cross-linked structure. Yang *et al.* [58] reported a similar thermal behavior for PLA cross-linked with triallyl isocyanurate (TAIC) and dicumyl peroxide (DCP) as the thermal initiator. It was concluded that the shift in the cold crystallization process was related to the network formation of PLA molecules of higher M_W that inhibits chain motion during the packed rearrangement.

With regard to thermal stability, PLA degraded in a one-stage decomposition process, which can be seen in **Figure III.2.2.6**. As it was formerly reported by Carrasco *et al.* [59], [60], PLA degradation proceeds with a typical chain-scission reaction through breakage of its ester groups. One can observe that MHO provided enhanced thermal stability as it delayed the degradation/decomposition process at elevated temperatures. As shown in **Table III.2.2.3**, both the onset temperature of degradation ($T_{5\%}$), measured at a constant weight loss of 5 wt%, and the degradation temperature (T_{deg}) slightly shifted to higher values with increasing the MHO content. This increase was more evident in the case of $T_{5\%}$ for which it changed from 331.2 °C, in neat PLA, up to values around 338 °C, for the PLA compositions containing 7.5–10 wt% MHO. In this sense, it is well known that, due to the high thermal stability of VOs and their chemically modified ones, some of them are used as thermal stabilizers in poly(vinyl chloride) (PVC) formulations [61]. Recently, it has been reported the efficiency of EVOs and other vegetable oil-derived materials as thermal stabilizers for PLA formulations [62], [63], [64].
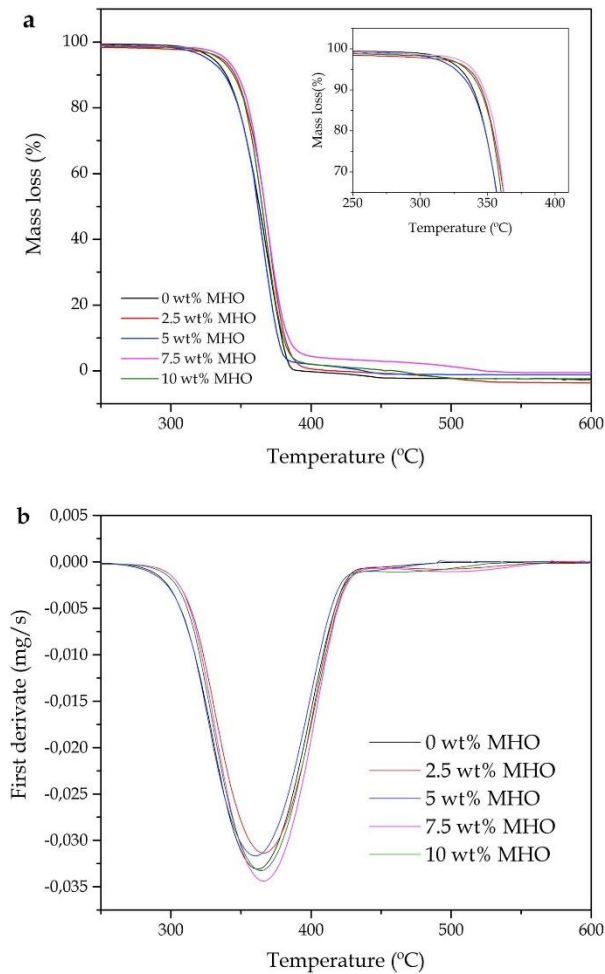
Figure III.2.2.6. Comparative plot of the injection-molded polylactide (PLA) pieces varying the maleinized hemp seed oil (MHO) content in terms of: (a) Thermogravimetric analysis (TGA) curves; (b) derivative thermogravimetric (DTG) curves.

Table III.2.2.3. Thermal degradation parameters in terms of onset temperature of degradation ($T_{5\%}$), degradation temperature (T_{deg}), and residual mass at 700 °C for the injection-molded polylactide (PLA) pieces varying the maleinized hemp seed oil (MHO) content.

MHO content wt%	$T_{5\%}$ (°C)	T_{deg} (°C)	Residual mass (%)
0	331.2 ± 1.13	361.7 ± 1.74	0.81 ± 0.10
2.5	334.5 ± 0.96	366.4 ± 1.63	0.51 ± 0.09
5.0	335.0 ± 1.32	365.9 ± 1.55	1.42 ± 0.12
7.5	338.7 ± 1.08	365.9 ± 1.82	1.96 ± 0.23
10.0	337.9 ± 1.41	363.4 ± 1.77	0.91 ± 0.15

The present results suggest that the linear chain-extension, branching and/or, even more intensely, cross-linking effects of MHO are responsible for the achieved

thermal stabilization. This is related to the fact that these phenomena are considered to counteract chain scission, potentially leading to a more branched structure. In this sense, Carrasco *et al*. [65] and Torres-Giner *et al*. [66] also reported similar findings on the thermal stability of PLA and poly(3-hydroxybutyrate-*co*-4-hydroxybutyrate) ((P(3HB-*co*-4HB)), respectively, by reactive extrusion (REX) with a multi-functional epoxy-based styrene-acrylic oligomer (ESAO), which provided a chain-extension effect by which a long-chain branched structure with a higher thermal stability was generated.

Thermomechanical properties of PLA pieces containing MHO

Figure III.2.2.7 gathers the dynamic behavior, obtained from DMTA in torsion mode, of the neat and MHO-containing PLA pieces corresponding to the evolution of G′ and tan δ *vs.* temperature. In the case of G′, this is representative for the elastic behavior of these PLA materials. As it has been described in the previous section, DSC revealed a slight T_g decrease and a T_{CC} shift until it disappeared for increasing MHO contents. Both the glass transition and cold crystallization processes can be clearly detected by DMTA. In particular, T_g for neat PLA was detected by a G′ drop of 2 orders of magnitude in the 52–75 °C range. With regard to the MHO-containing PLA pieces, this reduction in G′ was even more accentuated, *i.e.* almost 3 orders of magnitude, and moved to a lower temperature range, *i.e.* 47–72 °C, thus indicating a clear decrease in T_g as previously observed by DSC. The cold crystallization process can be assessed by observing the rise in G′ with increasing temperature due to the crystallinity increase achieved, which leads to a stiffer material. For the neat PLA piece, the cold crystallization process ranged from 75 °C to 90 °C. This can be also observed for all toughened PLA pieces by MHO but it is worthy to note that cold crystallization occurred at higher temperature values, which is in accordance with the above-mentioned behavior observed by DSC analysis. A similar effect on the cold crystallization process was observed by Yang *et al*. [58] for PLA materials cross-linked with TAIC and DCP. Even more, they also reported a remarkable change in the melt behavior. Another relevant property that can be observed in **Figure III.2.2.7b** is the slight decrease of the tan δ peak. This indicates that the α-relaxation of the biopolymer, which is related to its T_g, shifted down from 65 °C, for the neat PLA piece, to 62 °C, for the PLA pieces containing 7.5–10 wt% MHO.
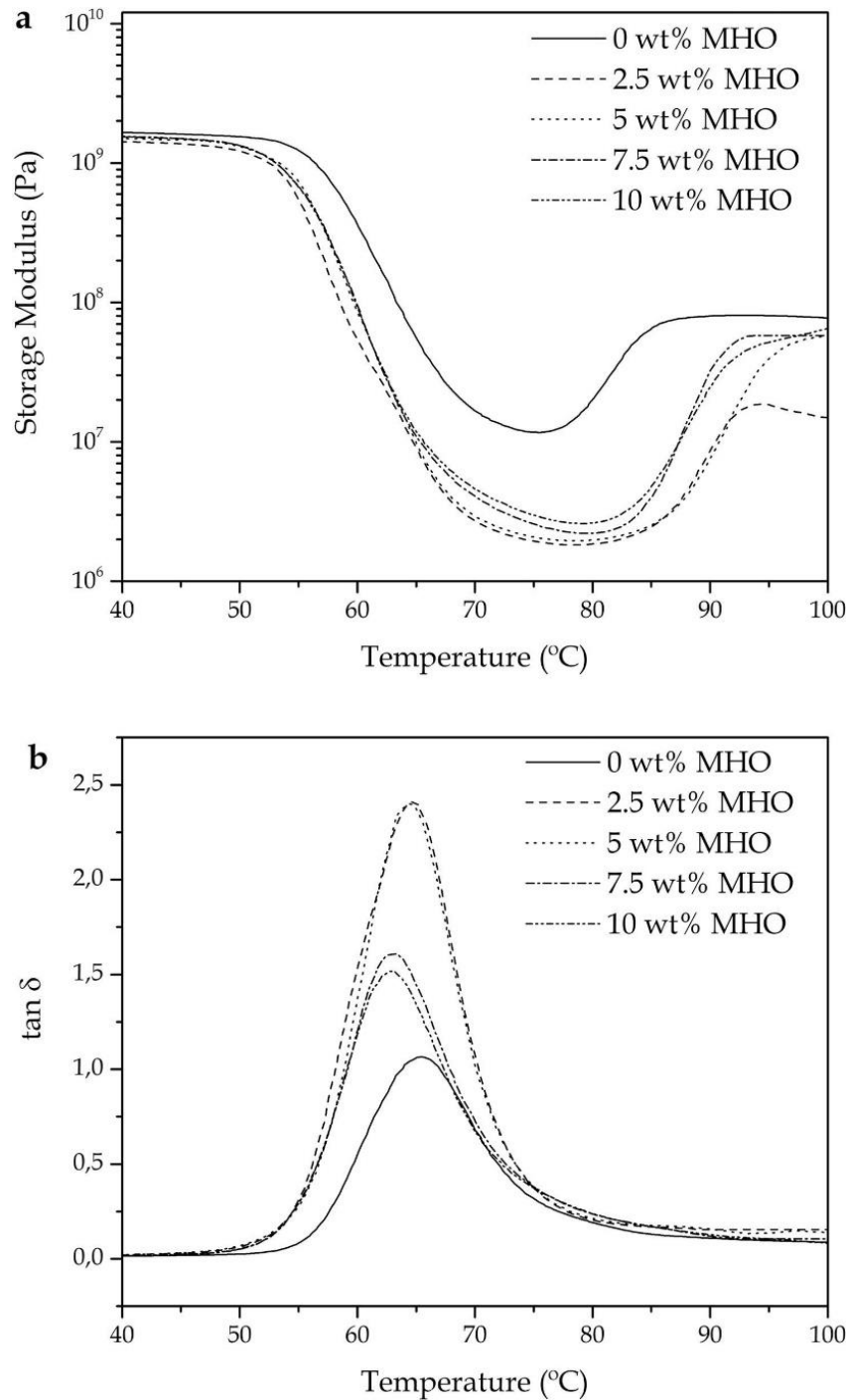
Figure III.2.2.7. Dynamic mechanical thermal analysis (DMTA) curves of the injection-molded polylactide (PLA) pieces varying the maleinized hemp seed oil (MHO) content: (a) storage modulus (G'); (b) damping factor (tan δ).

As it can be seen in **Table III.2.2.4**, similar values were observed in the VST and HDT values after the incorporation of MHO into PLA. Only a slight reduction in the thermomechanical properties occurred for the highest MHO contents, *i.e.* 7.5 and 10 wt%.

Table III.2.2.4. Thermomechanical values in terms of Vicat softening temperature (VST), heat deflection temperature (HDT), and coefficient of linear thermal expansion (CLTE) below and above glass transition temperature (T_g) for the injection-molded polylactide (PLA) pieces varying the maleinized hemp seed oil (MHO) content.

MHO content wt%	VST (ºC)	HDT (ºC)	CLTE (µm/m ºC) by TMA	
			Below T_g	Above T_g
0	56.3 ± 0.5	55.4 ± 1.6	94.4 ± 0.42	146.9 ± 0.39
2.5	57.2 ± 2.4	57.2 ± 2.6	80.7 ± 0.65	160.3 ± 0.56
5.0	55.6 ± 1.3	55.2 ± 2.2	85.6 ± 0.59	160.4 ± 0.79
7.5	54.6 ± 2.5	54.6 ± 2.6	90.8 ± 0.67	168.6 ± 0.52
10.0	54.6 ± 2.4	54.2 ± 1.9	91.4 ± 0.62	172.8 ± 0.62

However, these changes were comprised within the typical error associated to these two techniques. In relation to the dimensional stability, all PLA formulations presented higher CLTE values above T_g since the biopolymer chains can more readily move. However, MHO provided certain changes in the CLTE values. Specifically, below T_g, these values decreased from 94.4 µm/m °C to 80.7 µm/m °C after the only addition of 2.5 wt% MHO. The CLTE values then increased with further increasing the MHO content up to values close to the neat PLA piece. This effect can be ascribed to the formation of a linear chain-extended, branched, and/or cross-linked (or even a combination of all three possible mechanisms) structure. Nevertheless, a positive dimensional stabilization was observed for all MHO contents above T_g. The CLTE values increased from 146.9 µm/m °C, for the neat PLA piece, to 172.8 µm/m °C, for the PLA piece containing 10 wt% MHO. This is an indication of the formation of a more compacted structure, indicating an extraordinary thermomechanical response.

CONCLUSIONS

In the present study, MHO has been assessed as an environmentally friendly and cost-effective reactive additive for producing injection-molded PLA pieces with improved toughness. PLA pieces containing 2.5–7.5 wt% MHO offered a more balanced combination of mechanical and thermomechanical properties whilst the thermal properties remained nearly constant. As opposite to typical plasticizers, MHO generated PLA pieces with not only higher mechanical ductility, in terms of improved elongation at break and impact resistance, but also enhanced mechanical strength. As suggested by the obtained results, the MAH groups present in MHO reacted with the terminal hydroxyl groups of the PLA chains to form a linear chain-extended, branched, and/or cross-linked structure with improved energy absorption. Morphological observation performed on the fracture surface revealed good miscibility at low MHO concentrations. However, over 5 wt% MHO, saturation of MHO in PLA occurred and some MHO-rich domains appeared as finely dispersed submicron droplets, which were also considered to positively improve toughness of the biopolymer. Therefore, the use of multi-functionalized reactive VOs represents an environmentally friendly solution to overcome the high inherent brittleness of PLA articles with interesting

applications in, for instance, the rigid packaging industry or as parts or components for the automotive and building and construction industries, etc.

Acknowledgements

REFERENCES

1. Nurul Fazita, M.R., K. Jayaraman, D. Bhattacharyya, M.K. Mohamad Haafiz, C.K. Saurabh, M.H. Hussin and H.P.S. Abdul Khalil, *Green composites made of bamboo fabric and poly (lactic) acid for packaging applications – a review*. Materials, 2016. **9**(6): 435.

2. Torres, E., V. Fombuena, A. Valles-Lluch and T. Ellingham, *Improvement of mechanical and biological properties of Polycaprolactone loaded with Hydroxyapatite and Halloysite nanotubes.* Materials Science & Engineering C-Materials for Biological Applications, 2017. **75**: 418-424.

3. Al-Duhaidahwi, H.R.H., E.A.J. Al-Mulla and H.a.A. Ali, *Enhancement of properties and biodegradability of polybutylene succinate by epoxidized palm oil.* Epitoanyag-Journal of Silicate Based and Composite Materials, 2016. **68**(1): 2-5.

4. Schneiderman, D.K., C. Gilmer, M.T. Wentzel, M.T. Martello, T. Kubo and J.E. Wissinger, *Sustainable Polymers in the Organic Chemistry Laboratory: Synthesis and Characterization of a Renewable Polymer from δ-Decalactone and L-Lactide.* Journal of Chemical Education, 2013. **91**(1): 131-135.

5. Mohanty, A., M. Misra and L. Drzal, *Sustainable bio-composites from renewable resources: opportunities and challenges in the green materials world.* Journal of Polymers and the Environment, 2002. **10**(1): 19-26.

6. Torres-Tello, E.V., J.R. Robledo-Ortiz, Y. Gonzalez-Garcia, A.A. Perez-Fonseca, C.F. Jasso-Gastinel and E. Mendizabal, *Effect of agave fiber content in the thermal and mechanical properties of green composites based on polyhydroxybutyrate or poly(hydroxybutyrate-co-hydroxyvalerate).* Industrial Crops and Products, 2017. **99**: 117-125.

7. Uzun, G. and D. Aydemir, *Biocomposites from polyhydroxybutyrate and bio-fillers by solvent casting method.* Bulletin of Materials Science, 2017. **40**(2): 383-393.

8. Drumright, R.E., P.R. Gruber and D.E. Henton, *Polylactic acid technology*. Advanced materials, 2000. **12**(23): 1841-1846.

9. Nampoothiri, K.M., N.R. Nair and R.P. John, *An overview of the recent developments in polylactide (PLA) research*. Bioresource technology, 2010. **101**(22): 8493-8501.

10. Lunt, J., *Large-scale production, properties and commercial applications of polylactic acid polymers.* Polymer degradation and stability, 1998. **59**(1-3): 145-152.

11. Ajioka, M., K. Enomoto, K. Suzuki and A. Yamaguchi, *Basic properties of polylactic acid produced by the direct condensation polymerization of lactic acid.* Bulletin of the Chemical Society of Japan, 1995. **68**(8): 2125-2131.

12. Martin, O. and L. Averous, *Poly (lactic acid): plasticization and properties of biodegradable multiphase systems.* Polymer, 2001. **42**(14): 6209-6219.

13. Pillin, I., N. Montrelay and Y. Grohens, *Thermo-mechanical characterization of plasticized PLA: Is the miscibility the only significant factor?* Polymer, 2006. **47**(13): 4676-4682.

14. Deng, Y. and N.L. Thomas, *Blending poly(butylene succinate) with poly(lactic acid): Ductility and phase inversion effects.* European Polymer Journal, 2015. **71**: 534-546.

15. Lebarbe, T., E. Grau, C. Alfos and H. Cramail, *Fatty acid-based thermoplastic poly(ester-amide) as toughening and crystallization improver of poly(L-lactide)*. European Polymer Journal, 2015. **65**: 276-285.

16. Wang, Y.S., Z.Y. Wei and Y. Li, *Highly toughened polylactide/epoxidized poly(styrene-b-butadiene-b-styrene) blends with excellent tensile performance*. European Polymer Journal, 2016. **85**: 92-104.

17. Burgos, N., V.P. Martino and A. Jimenez, *Characterization and ageing study of poly(lactic acid) films plasticized with oligomeric lactic acid*. Polymer Degradation and Stability, 2013. **98**(2): 651-658.

18. Baiardo, M., G. Frisoni, M. Scandola, M. Rimelen, D. Lips, K. Ruffieux and E. Wintermantel, *Thermal and mechanical properties of plasticized poly(L-lactic acid)*. Journal of Applied Polymer Science, 2003. **90**(7): 1731-1738.

19. Arrieta, M.P., E. Fortunati, F. Dominici, J. Lopez and J.M. Kenny, *Bionanocomposite films based on plasticized PLA-PHB/cellulose nanocrystal blends*. Carbohydrate Polymers, 2015. **121**: 265-275.

20. Arrieta, M.P., M.D. Castro-Lopez, E. Rayon, L.F. Barral-Losada, J.M. Lopez-Vilarino, J. Lopez and M.V. Gonzalez-Rodriguez, *Plasticized Poly(lactic acid)-Poly(hydroxybutyrate) (PLA-PHB) Blends Incorporated with Catechin Intended for Active Food-Packaging Applications*. Journal of Agricultural and Food Chemistry, 2014. **62**(41): 10170-10180.

21. Piorkowska, E., Z. Kulinski, A. Galeski and R. Masirek, *Plasticization of semicrystalline poly(L-lactide) with poly(propylene glycol)*. Polymer, 2006. **47**(20): 7178-7188.

22. Sungsanit, K., N. Kao and S.N. Bhattacharya, *Properties of linear poly(lactic acid)/polyethylene glycol blends*. Polymer Engineering and Science, 2012. **52**(1): 108-116.

23. de Espinosa, L.M. and M.A. Meier, *Plant oils: the perfect renewable resource for polymer science?!* European Polymer Journal, 2011. **47**(5): 837-852.

24. Güner, F.S., Y. Yağcı and A.T. Erciyes, *Polymers from triglyceride oils*. Progress in Polymer Science, 2006. **31**(7): 633-670.

25. Meier, M.A., J.O. Metzger and U.S. Schubert, *Plant oil renewable resources as green alternatives in polymer science*. Chemical Society Reviews, 2007. 36(11): 1788-1802.

26. Sharma, V. and P. Kundu, *Condensation polymers from natural oils*. Progress in Polymer Science, 2008. **33**(12): 1199-1215.

27. Meier, M.A., *Metathesis with oleochemicals: new approaches for the utilization of plant oils as renewable resources in polymer science*. Macromolecular Chemistry and Physics, 2009. **210**(13-14): 1073-1079.

28. Lu, Y. and R.C. Larock, *Novel polymeric materials from vegetable oils and vinyl monomers: preparation, properties, and applications*. ChemSusChem, 2009. **2**(2): 136-147.

29. King, J.W., *Determination of the solubility parameter os soybean oil by inverse gas-chromatography*. Food Science and Technology-Lebensmittel-Wissenschaft & Technologie, 1995. **28**(2): 190-195.

30. Arrieta, M.P., M.D. Samper, J. Lopez and A. Jimenez, *Combined Effect of Poly(hydroxybutyrate) and Plasticizers on Polylactic acid Properties for Film Intended for Food Packaging*. Journal of Polymers and the Environment, 2014. **22**(4): 460-470.

31. Ferri, J.M., M.D. Samper, D. Garcia-Sanoguera, M.J. Reig, O. Fenollar and R. Balart, *Plasticizing effect of biobased epoxidized fatty acid esters on mechanical and thermal properties of poly(lactic acid)*. Journal of Materials Science, 2016. **51**(11): 5356-5366.

32. Chieng, B.W., N.A. Ibrahim, Y.Y. Then and Y.Y. Loo, *Epoxidized Vegetable Oils Plasticized Poly(lactic acid) Biocomposites: Mechanical, Thermal and Morphology Properties*. Molecules, 2014. **19**(10): 16024-16038.

33. Xu, Y.Q. and J.P. Qu, *Mechanical and Rheological Properties of Epoxidized Soybean Oil Plasticized Poly(lactic acid)*. Journal of Applied Polymer Science, 2009. **112**(6): 3185-3191.

34. Garcia-Garcia, D., J.M. Ferri, N. Montanes, J. Lopez-Martinez and R. Balart, *Plasticization effects of epoxidized vegetable oils on mechanical properties of poly(3-hydroxybutyrate)*. Polymer International, 2016. **65**(10): 1157-1164.

35. Mikulcova, V., V. Kasparkova, P. Humpolicek and L. Bunkova, *Formulation, Characterization and Properties of Hemp Seed Oil and Its Emulsions.* Molecules (Basel, Switzerland), 2017. **22**(5).

36. Kyari, M., *Extraction and characterization of seed oils.* International Agrophysics, 2008. **22**(2): 139.

37. Abuzaytoun, R. and F. Shahidi, *Oxidative stability of flax and hemp oils.* Journal of the American Oil Chemists' Society, 2006. **83**(10): 855-861.

38. Cardona, F., M.T. Sultan, A.R. Abu Talib, F. Ezzah and A. Derahman, *Interpenetrating Polymer Network (IPN) with Epoxidized and Acrylated Bioresins and their Composites with Glass and Jute Fibres.* Bioresources, 2016. **11**(1): 2820-2838.

39. Francucci, G., N.W. Manthey, F. Cardona and T. Aravinthan, *Processing and characterization of 100% hemp-based biocomposites obtained by vacuum infusion.* Journal of Composite Materials, 2014. **48**(11): 1323-1335.

40. Manthey, N.W., F. Cardona, G. Francucci and T. Aravinthan, *Thermo-mechanical properties of epoxidized hemp oil-based bioresins and biocomposites.* Journal of Reinforced Plastics and Composites, 2013. **32**(19): 1444-1456.

41. Manthey, N.W., F. Cardona, G. Francucci and T. Aravinthan, *Thermo-mechanical properties of acrylated epoxidized hemp oil based biocomposites.* Journal of Composite Materials, 2014. **48**(13): 1611-1622.

42. Surender, R., A.R. Mahendran, G. Wuzella and C.T. Vijayakumar, *Synthesis, characterization and degradation behavior of thermoplastic polyurethane from hydroxylated hemp seed oil.* Journal of Thermal Analysis and Calorimetry, 2016. **123**(1): 525-533.

43. Shuttleworth, P.S., A.M. Diez-Pascual, C. Marco and G. Ellis, Flexible *Bionanocomposites from Epoxidized Hemp Seed Oil Thermosetting Resin Reinforced with Halloysite Nanotubes.* Journal of Physical Chemistry B, 2017. **121**(11): 2454-2467.

44. Francucci, G., F. Cardona and N.W. Manthey, *Cure kinetics of an acrylated epoxidized hemp oil-based bioresin system.* Journal of Applied Polymer Science, 2013. **128**(3): 2030-2037.

45. Marsilla, K.I.K. and C.J.R. Verbeek, *Modification of poly(lactic acid) using itaconic anhydride by reactive extrusion.* European Polymer Journal, 2015. **67**: 213-223.

46. Csikos, A., G. Faludi, A. Domjan, K. Renner, J. Moczo and B. Pukanszky, *Modification of interfacial adhesion with a functionalized polymer in PLA/wood composites.* European Polymer Journal, 2015. **68**: 592-600.

47. Hoffmann, H., *The ene reaction.* Angewandte Chemie International Edition in English, 1969. **8**(8): 556-577.

48. Sclavons, M., M. Laurent, J. Devaux and V. Carlier, *Maleic anhydride-grafted polypropylene: FTIR study of a model polymer grafted by ene-reaction.* Polymer, 2005. **46**(19): 8062-8067.

49. Nahm, S. and H. Cheng, *Transition-state geometry and stereochemistry of the ene reaction between olefins and maleic anhydride.* The Journal of Organic Chemistry, 1986. **51**(26): 5093-5100.

50. Ferri, J.M., D. Garcia-Garcia, N. Montanes, O. Fenollar and R. Balart, *The effect of maleinized linseed oil as biobased plasticizer in poly(lactic acid)-based formulations.* Polymer International, 2017. **66**(6): 882-891.

51. Garcia-Garcia, D., O. Fenollar, V. Fombuena, J. Lopez-Martinez and R. Balart, *Improvement of Mechanical Ductile Properties of Poly(3-hydroxybutyrate) by Using Vegetable Oil Derivatives.* Macromolecular Materials and Engineering, 2017. **302**(2): 12.

52. Carbonell-Verdu, A., D. Garcia-Garcia, F. Dominici, L. Torre, L. Sanchez-Nacher and R. Balart, *PLA films with improved flexibility properties by using maleinized cottonseed oil.* European Polymer Journal, 2017. **91**: 248-259.

53. Xiong, Z., C. Li, S.Q. Ma, J.X. Feng, Y. Yang, R.Y. Zhang and J. Zhu, *The properties of poly(lactic acid)/starch blends with a functionalized plant oil: Tung oil anhydride.* Carbohydrate Polymers, 2013. **95**(1): 77-84.

54. Tábi, T., A.Z. Égerházi, P. Tamás, T. Czigány and J.G. Kovács, *Investigation of injection moulded poly (lactic acid) reinforced with long basalt fibres*. Composites Part A: Applied Science and Manufacturing, 2014. **64**: 99-106.

55. Mauck, S.C., S. Wang, W.Y. Ding, B.J. Rohde, C.K. Fortune, G.Z. Yang, S.K. Ahn and M.L. Robertson, *Biorenewable Tough Blends of Polylactide and Acrylated Epoxidized Soybean Oil Compatibilized by a Polylactide Star Polymer*. Macromolecules, 2016. **49**(5): 1605-1615.

56. Yuryev, Y., A.K. Mohanty and M. Misra, *Novel super-toughened bio-based blend from polycarbonate and poly(lactic acid) for durable applications*. Rsc Advances, 2016. **6**(107): 105094-105104.

57. Kaczmarek, H., M. Nowicki, I. Vukovic-Kwiatkowska and S. Nowakowska, *Crosslinked blends of poly(lactic acid) and polyacrylates: AFM, DSC and XRD studies*. Journal of Polymer Research, 2013. **20**(3): 12.

58. Yang, S.L., Z.H. Wu, W. Yang and M.B. Yang, *Thermal and mechanical properties of chemical crosslinked polylactide (PLA)*. Polymer Testing, 2008. **27**(8): 957-963.

59. Carrasco, F., L.A. Perez-Maqueda, P.E. Sanchez-Jimenez, A. Perejon, O.O. Santana and M.L. Maspoch, *Enhanced general analytical equation for the kinetics of the thermal degradation of poly(lactic acid) driven by random scission*. Polymer Testing, 2013. **32**(5): 937-945.

60. Sanchez-Jimenez, P.E., L.A. Perez-Maqueda, A. Perejon and J.M. Criado, *Generalized Kinetic Master Plots for the Thermal Degradation of Polymers Following a Random Scission Mechanism*. Journal of Physical Chemistry A, 2010. **114**(30): 7868-7876.

61. Li, M., S.H. Li, J.L. Xia, C.X. Ding, M. Wang, L.N. Xu, X.H. Yang and K. Huang, *Tung oil based plasticizer and auxiliary stabilizer for poly(vinyl chloride)*. Materials & Design, 2017. **122**: 366-375.

62. Carrasco, F., P. Pages, J. Gamez-Perez, O.O. Santana and M.L. Maspoch, *Processing of poly(lactic acid): Characterization of chemical structure, thermal stability and mechanical properties*. Polymer Degradation and Stability, 2010. **95**(2): 116-125.

63. Chieng, B.W., N.A. Ibrahim, Y.Y. Then and Y.Y. Loo, *Epoxidized Jatropha Oil as a Sustainable Plasticizer to Poly(lactic Acid)*. Polymers, 2017. **9**(6): 10.

64. Polym. Sci. Ser. A+Prempeh, N., J.L. Li, D.G. Liu, K. Das, S. Maiti and Y. Zhang, *Plasticizing Effects of Epoxidized Sun Flower Oil on Biodegradable Polylactide Films: A Comparative Study*. Polymer Science Series A, 2014. **56**(6): 856-863.

65. Carrasco, F., J. Cailloux, P.E. Sanchez-Jimenez and M.L. Maspoch, *Improvement of the thermal stability of branched poly(lactic acid) obtained by reactive extrusion*. Polymer Degradation and Stability, 2014. **104**: 40-49.

66. Torres-Giner, S., N. Montanes, T. Boronat, L. Quiles-Carrillo and R. Balart, *Melt grafting of sepiolite nanoclay onto poly(3-hydroxybutyrate-co-4-hydroxybutyrate) by reactive extrusion with multi-functional epoxy-based styrene-acrylic oligomer*. European Polymer Journal, 2016. **84**: 693-707.

III.2.3. On the use of acrylated epoxidized soybean oil as a reactive compatibilizer in injection-molded compostable pieces consisting of polylactide filled with orange peel flour

L. Quiles-Carrillo[1], N. Montanes[1], J.M. Lagaron[2], R. Balart[1], S. Torres-Giner[1,2]

[1] Technological Institute of Materials (ITM), Universitat Politècnica de València (UPV), Plaza Ferrándiz y Carbonell 1, Alcoy 03801, Spain

[2] Novel Materials and Nanotechnology Group, Institute of Agrochemistry and Food Technology (IATA), Spanish Council for Scientific Research (CSIC), Calle Catedrático Agustín Escardino Benlloch 7, Paterna 46980, Spain

Research Article

On the use of acrylated epoxidized soybean oil as a reactive compatibilizer in injection-molded compostable pieces consisting of polylactide filled with orange peel flour

Luis Quiles-Carrillo,[a] Nestor Montanes,[a] Jose Maria Lagaron,[b] Rafael Balart[a] and Sergio Torres-Giner[a,b]*

Abstract

Novel green composites made of polylactide (PLA) and orange peel flour (OPF) were melt-compounded using twin-screw extrusion and shaped into pieces by injection molding. Orange peel, a major by-product of the juice industry, was first ground to flour and then incorporated as a lignocellulosic filler into the biopolymer at 10, 20 and 30 wt%. Since both components of the green composite presented low compatibility, the resultant injection-molded pieces showed poor ductility and impaired thermomechanical performance. As a new bio-based reactive compatibilizer, acrylated epoxidized soybean oil (AESO) was added at five parts per hundred resin to the PLA/OPF formulations during the extrusion process. The addition of AESO increased the filler–biopolymer adhesion and led to compostable green composite pieces with improved physical properties. The enhancement achieved was related to a dual effect of plasticization and melt grafting of the OPF particles onto the PLA chains provided by the multiple acrylate and epoxy groups present in AESO. The use of multi-functionalized vegetable oils to improve the performance of green composites certainly opens up new opportunities for the expansion of fully bio-based and biodegradable materials that are partially obtained from agro-food waste.
© 2018 Society of Chemical Industry

Keywords: PLA; green composites; multi-functionalized vegetable oils; reactive extrusion; waste valorization

INTRODUCTION

Nowadays, the increasing environmental concerns about the extensive use of petroleum-derived polymers are leading the research of new environmentally friendly polymer materials obtained from natural resources.[1] The development of green composites is a leap forward to solve these environmental problems since these novel materials combine a bio-based polymer with a natural filler obtained either from plants or agro-food wastes.[2,3] Additionally, the use of biodegradable polymers, that is, polymers that undergo rapid and complete disintegration through the action of enzymes and/or chemical deterioration associated with living microorganisms, represents the most valuable approach in green composites since fully bio-based and biodegradable materials are produced.[4,5]

The use of polylactide (PLA) as a matrix in green composites is currently gaining great importance.[6,7] Indeed, this biopolyester is nowadays considered the front runner in the bioplastics market, which is already surpassing some conventional polymers derived from petroleum with an annual consumption of 140 000 tons.[8] PLA is of particular interest in the manufacturing of green composites due to its dual advantages of being bio-based and biodegradable.[9,10] In addition, it shows the required mechanical strength for various industrial applications (e.g. automotive, rigid packaging or building and construction) as well as adequate thermal stability and rheological characteristics for being easily processable and recyclable on a large scale.[11–13]

The latest research performed on green composites shows that the use of lignocellulosic materials obtained from industrial by-products and food or agroforestry wastes is increasing as cost-effective fillers since they provide a sustainability enhancement and improve physical performance.[14,15] Some recent examples include, for instance, wood flour,[16] banana fibers,[17] rice husk,[18,19] peanut skin,[20,21] wheat and soy fibers,[22] pita fibers[23] and *Posidonia oceanica* seaweed.[24] In the study reported in the present paper, for the first time, orange peel flour (OPF) was used as a lignocellulosic filler to develop green composites of PLA. The use of this lignocellulosic filler provides a further positive sustainable effect on the resultant green composite due to the large world

---

* Correspondence to: S Torres-Giner, Novel Materials and Nanotechnology Group, Institute of Agrochemistry and Food Technology (IATA), Spanish Council for Scientific Research (CSIC), 46980 Paterna, Spain. E-mail: storresginer@iata.csic.es; storresginer@upv.es

a Technological Institute of Materials (ITM), Universitat Politècnica de València, Alcoy, Spain

b Novel Materials and Nanotechnology Group, Institute of Agrochemistry and Food Technology (IATA), Spanish Council for Scientific Research (CSIC), Paterna, Spain

1341

On the use of acrylated epoxidized soybean oil as a reactive compatibilizer in injection-molded compostable pieces consisting of polylactide filled with orange peel flour

Abstract

Novel green composites made of polylactide (PLA) and orange peel flour (OPF) were melt-compounded using twin-screw extrusion and shaped into pieces by injection molding. Orange peel, a major by-product of the juice industry, was first ground to flour and then incorporated as a lignocellulosic filler into the biopolymer at 10, 20 and 30 wt%. Since both components of the green composite presented low compatibility, the resultant injection-molded pieces showed poor ductility and impaired thermomechanical performance. As a new bio-based reactive compatibilizer, acrylated epoxidized soybean oil (AESO) was added at five parts per hundred resin to the PLA/OPF formulations during the extrusion process. The addition of AESO increased the filler–biopolymer adhesion and led to compostable green composite pieces with improved physical properties. The enhancement achieved was related to a dual effect of plasticization and melt grafting of the OPF particles onto the PLA chains provided by the multiple acrylate and epoxy groups present in AESO. The use of multi-functionalized vegetable oils to improve the performance of green composites certainly opens up new opportunities for the expansion of fully bio-based and biodegradable materials that are partially obtained from agro-food waste.

Keywords: PLA, Cellulose, Multi-functionalized vegetable oils, Green composites, Reactive extrusion, Waste valorization.

INTRODUCTION

Nowadays, the increasing environmental concerns about the extensive use of petroleum-derived polymers are leading the research of new environmentally friendly polymer materials obtained from natural resources [1]. The development of green composites is a leap forward to solve these environmental problems since these novel materials combine a bio-based polymer with a natural filler obtained either from plants or agro-food wastes [2, 3]. Additionally, the use of biodegradable polymers, that is, polymers that undergo rapid and complete disintegration through the action of enzymes and/or chemical deterioration associated with living microorganisms, represents the most valuable approach in green composites since fully bio-based and biodegradable materials are produced [4, 5].

The use of polylactide (PLA) as a matrix in green composites is currently gaining great importance [6, 7]. Indeed, this biopolyester is nowadays considered the front runner in the bioplastics market, which is already surpassing some conventional polymers derived from petroleum with an annual consumption of 140 000 tons [8]. PLA is of particular interest in the manufacturing of green composites due to its dual advantages of being bio-based and biodegradable [9, 10]. In addition, it shows the required mechanical strength for various industrial applications (*e.g.* automotive, rigid packaging or building and construction) as well as adequate thermal stability and rheological characteristics for being easily processable and recyclable on a large scale [11-13].

The latest research performed on green composites shows that the use of lignocellulosic materials obtained from industrial by-products and food or agroforestry wastes is increasing as cost-effective fillers since they provide a sustainability enhancement and improve physical performance [14, 15]. Some recent examples include, for instance, wood flour[16], banana fibers [17], rice husk [18, 19], peanut skin [20, 21], wheat and soy fibers [22], pita fibers [23] and Posidonia oceanica seaweed [24]. In the study reported in the present paper, for the first time, orange peel flour (OPF) was used as a lignocellulosic filler to develop green composites of PLA. The use of this lignocellulosic filler provides a further positive sustainable effect on the resultant green composite due to the large world production of oranges and, especially, to the possibility of generating a high added value from a readily available residue produced by the juice industry. Indeed, around 20 million tons of solid and liquid wastes derived from orange juice production are globally generated. In this sense, Spain is one of the main world producers of oranges, among other countries like Brazil, the USA and China, the Valencian Community being one of the areas with the highest production rate with approximately 1.7 million tons of oranges [25]. Although at present orange peel is not of economic value, it is rich in cellulose, sugars, hemicellulose, pectin and essential oils, which opens up new opportunities for diverse applications [26].

There are some general drawbacks related to the use of lignocellulosic fillers in polymer composites, which are mainly derived from their poor interfacial adhesion with most polymer and biopolymer matrices. In general, polymers are highly hydrophobic whilst lignocellulosic materials are extremely hydrophilic. This low chemical affinity is certainly responsible for the lack of compatibility, thus leading to the formation of particle aggregates and, overall, to poor physical properties [17, 27, 28]. In this sense, reactive extrusion (REX) has been proposed as a smart strategy for

enhancing the properties of polymer materials, being particularly interesting for the preparation of biopolymer blends [29]. Based on this concept, REX has been recently proposed as a novel route for grafting inorganic nanoparticles with polar surface onto biopolymer matrices, which results in polymer nanocomposites with enhanced physical properties [30]. This process is based on the addition during melt mixing of reactive additives capable of acting as interfacial agents between both components of the polymer composite. This process particularly involves the chemical attachment of the fillers to the biopolymer chains by the action of reactive molecules with an average functionality (*f*) value of at least 2. These additives not only can act as interfacial agents but also they can potentially react with hydrolyzed polymer chains to provide a chain-extension effect, inducing a positive effect on melt stability [31, 32].

Most conventional and commercially available reactive additives consist of polymers with a low molecular weight or oligomers based on various functional groups, such as anhydride, epoxy, oxazoline, isocyanates, acrylates, etc [33, 34]. More recently, however, the use of chemically modified vegetable oils (*e.g.* maleinized, acrylated and epoxidized oils), the so-called multi-functionalized vegetable oils, has been expanded [35, 36]. These multi-functionalized vegetable oils present the dual advantages of being derived from natural resources and of acting as plasticizers due to their intrinsic lubricant effect on polymer matrices [37]. This is of great interest from an environmental point of view since they allow one to obtain totally ecofriendly and fully bio-based polymer formulations with improved toughness [38-40]. In this regard, chemically modified oils, such as maleinized linseed oil [41] or epoxidized soybean oil [42], have been recently used to increase the filler–matrix compatibility in PLA-based composites with very promising results. The main objective of the work present here was to evaluate the effect of acrylated epoxidized soybean oil (AESO) on the compatibility and physical properties of injection-molded green composite pieces consisting of PLA and OPF.

EXPERIMENTAL

Materials

Commercial PLA grade Ingeo™ biopolymer 6201D was obtained from NatureWorks (Minnetonka, MN, USA). This PLA resin is characterized by a density of $1.24\,g\,cm^{-3}$ and a melt flow index of 15–30 g/10 min (210 °C and 2.16 kg), which makes it suitable for injection molding. Fresh oranges were purchased in a local market in Valencia, Spain. AESO was supplied by Sigma-Aldrich SA (Madrid, Spain). According to the supplier, this contains 4000 ppm of monomethyl ether hydroquinone as inhibitor to avoid polymerization.

Preparation of OPF

The orange peels were first allowed to dry for 48 h at 40 °C using a dehumidifying stove (MCP Vacuum Casting System, Lubeck, Germany) to remove any residual moisture. Then, the dried peels were crushed in a Maype mill (Manises, Spain) to reduce their particle size for facilitating their incorporation into the centrifugal mill. The resultant particles were further allowed to dry at 40 °C for 12 h. The peel particles were then milled by means of a ZM 200 centrifugal mill from Retsch (Düsseldorf,

Germany) at a speed of 12 000 rpm and finally sieved with a 250-μm mesh filter. The various stages carried out during the preparation of OPF are shown in **Figure III.2.3.1**.
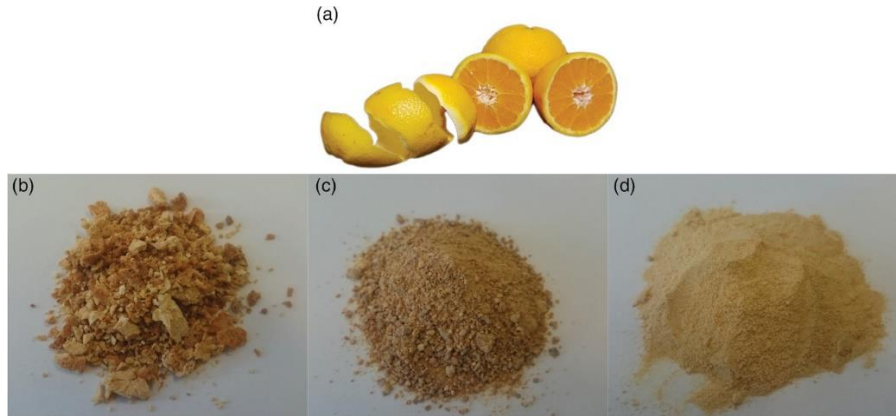
Figure III.2.3.1. (a) As-received fresh oranges, (b) dried orange peel, (c) crushed orange peel particles and (d) OPF obtained after milling.

Preparation of green composite pieces

Prior to processing, all materials were dried at 60 °C for 36 h in a dehumidifying dryer (MDEO, Industrial Marsé, Barcelona, Spain) to remove any residual moisture due to the high sensitiveness of PLA to hydrolysis. Materials were then melt-compounded in a co-rotating twin-screw extruder from Construcciones Mecanicas Dupra SL (Alicante, Spain). The screws have a 25 mm diameter with a length-to-diameter ratio of 24. All materials, namely PLA, OPF and AESO, were fed using the main hopper. The temperature profile was set as follows: 180 °C (feeding zone), 185, 190 and 195 °C (die). A rotating speed of 20 rpm was selected. Residence time was about 1 min, measured by means of a blue masterbatch. The AESO content was fixed at 5 parts per hundred resin (phr) based on recent previous research performed for this multi-functionalized vegetable oil [43], while the amount of OPF in the PLA formulations varied from 10 to 30 wt%. A neat PLA sample and a green composite sample at 10 wt% without AESO were produced under the same conditions for use as control materials. **Table III.2.3.1** summarizes the set of prepared formulations.

Table III.2.3.1. Summary of compositions according to amount of polylactide (PLA) and orange peel flour (OPF) in which acrylated epoxidized soybean oil (AESO) was added as parts per hundred resin (phr) of PLA/OPF composite.

Sample	PLA (wt%)	OPF(wt%)	AESO (phr)
PLA	100	0	0
PLA+AESO	100	0	5
PLA+10 wt% OPF	90	10	0
PLA+AESO+10 wt% OPF	90	10	5
PLA+AESO+20 wt% OPF	90	20	5
PLA+AESO+30 wt% OPF	90	30	5

The resultant PLA and green composite pellets were shaped into pieces by injection molding. This was carried out in a Sprinter 11 machine from Erinca SL (Cornellá, Spain). The temperature profile was set as follows: 170 °C (hopper), 175, 180 and 185 °C (injection nozzle). The materials were injected into a mirror-finishing steel mold with standard geometries for sample characterization. A clamping force of 11 tons was applied. The cavity filling and cooling times were set at 1 and 10 s, respectively. Standard samples with a thickness of 4 mm were obtained. The obtained pieces were stored in a desiccator at 25 °C and 0% relative humidity (RH) for 1 week.

Morphology

The morphologies of the OPF particles and the fracture surfaces of the green composite pieces after the impact tests were observed using field emission scanning electron microscopy (FESEM) with a Zeiss Ultra 55 from Oxford Instruments (Abingdon, UK). The working distance varied in the range 6–7 mm and an extra-high tension of 2 kV was applied to the electron beam. Before placing samples in the FESEM vacuum chamber, the surfaces were coated with a gold–palladium alloy in an EMITECH sputter coater (SC7620 from Quorum Technologies Ltd, UK). OPF sizes were determined using ImageJ Launcher v. 1.41 and the data presented were based on measurements from a minimum of 50 FESEM micrographs.

Thermal characterization

Main thermal transitions of the green composites were obtained using differential scanning calorimetry (DSC) with a Mettler-Toledo 821 calorimeter (Schwerzenbach, Switzerland). Samples with average weight ranging from 5 to 7 mg were subjected to a heating step from 40 to 190 °C at a heating rate of 10 °C min^{-1}. All tests were run in nitrogen atmosphere with a flow rate of 66 mL min^{-1} using standard sealed aluminium crucibles of a volume capacity of 40 µL. The degree of crystallinity (X_C) was determined using the following expression:

$$X_C = \left[\frac{\Delta H_m - \Delta H_{CC}}{\Delta H_m^0 \cdot (1-w)} \right] \cdot 100 \qquad \textbf{Equation III.2.3.1}$$

where ΔH_m and ΔH_{CC} (J g^{-1}) stand for the normalized melt and cold crystallization enthalpies, respectively, ΔHm^0 (J g^{-1}) represents the melt enthalpy of a theoretically fully crystalline PLA, that is, 93 J g^{-1} [44], and $1 - w$ corresponds to the weight fraction of PLA in the formulation.

Thermal stability was determined using thermogravimetric analysis (TGA) with a Mettler-Toledo TGA/SDTA 851 thermobalance (Schwerzenbach, Switzerland). Samples with an average weight of 5–7 mg were placed in standard alumina crucibles of 70 µL and subjected to a heating program from 30 to 700 °C at a heating rate of 20 °C min^{-1} in air atmosphere.

Mechanical characterization

Tensile tests were carried out on injection-molded pieces with a size of $75 \times 5 \times 4$ mm^3 using a universal testing machine (ELIB 50, SAE Ibertest, Madrid, Spain) equipped with a 5-kN load cell. The tests were performed as recommended by ISO 527–1:2012. The crosshead speed was set to 5 mm min^{-1}.

Shore D hardness was measured with a 676-D durometer from J Bot Instruments (Barcelona, Spain) according to ISO 868:2003. Impact strength was also studied using unnotched pieces with dimensions of $80 \times 10 \times 4$ mm^3 using a 6-J Charpy pendulum from Metrotec SA (San Sebastián, Spain) following the guidelines of ISO 179–1:2010.

All samples were tested under ambient conditions, that is, 23 °C and 50% RH, using at least six samples per formulation.

Thermomechanical characterization

Dynamic mechanical thermal analysis (DMTA) was performed using an AR-G2 oscillatory rheometer from TA Instruments (New Castle, DE, USA), which was equipped with a special clamp system for solid samples working in combined torsion–shear mode. The samples, with dimensions of $40 \times 10 \times 4$ mm^3, were subjected to a temperature sweep from 30 to 140 °C at a constant heating rate of 2 °C min^{-1}. The maximum deformation percentage (γ) was set to 0.1%. The storage modulus and the dynamic damping factor (tan δ) were obtained as a function of increasing temperature at a constant frequency of 1 Hz. DMTA tests were run in triplicate.

Dimensional stability was studied by measuring the coefficient of linear thermal expansion (CLTE) using a thermomechanical analyzer (Q400, TA Instruments). The test was performed on injection-molded pieces of size $10 \times 10 \times 4$ mm^3. The heating program was set from 0 to 140 °C with a constant heating rate of 2 °C min^{-1} and a load of 0.02 N. CLTE measurements were performed in triplicate.

Disintegration tests

Disintegration in simulated composting conditions was conducted at 58 °C and 55% RH as indicated by ISO 20200. Injection-molded pieces of size $10 \times 10 \times 4$ mm^3 were placed in a carrier bag and buried in a controlled soil compost made of sawdust (40 wt%), rabbit-feed (30 wt%), ripe compost (10 wt%), corn starch (10 wt%), saccharose (5 wt%), corn seed oil (4 wt%) and urea (1 wt%). Samples were periodically unburied from the composting facility, washed with distilled water, dried and weighed with an analytical balance. The weight loss during disintegration was calculated using **Equation III.2.3.2**:

$$Weight\ loss(\%) = \left(\frac{W_0 - W_t}{W_0}\right) \cdot 100 \qquad \textbf{Equation III.2.3.2}$$

where W_0 is the initial dry weight of the sample and W_t is the weight of the sample after a bury time t. All tests were carried out in triplicate to ensure reliability.

RESULTS AND DISCUSSION

Morphology of OPF

Figure III.2.3.2 shows the size distribution of the OPF particles used for the preparation of the green composites. One can observe that the mean particle size was approximately 25 µm, most of the particles being smaller than 75 µm. The micro-sized structure of the OPF particles is considered a positive aspect for their adhesion to the biopolymer matrix due to the increased total surface area of the fillers [45, 46]. The FESEM image of OPF, shown in the inset, also indicates that particle morphology was mostly heterogeneous. In addition, a rough perimeter was observed, which can be a consequence of the intensive crushing and milling processes applied to obtain the flour.
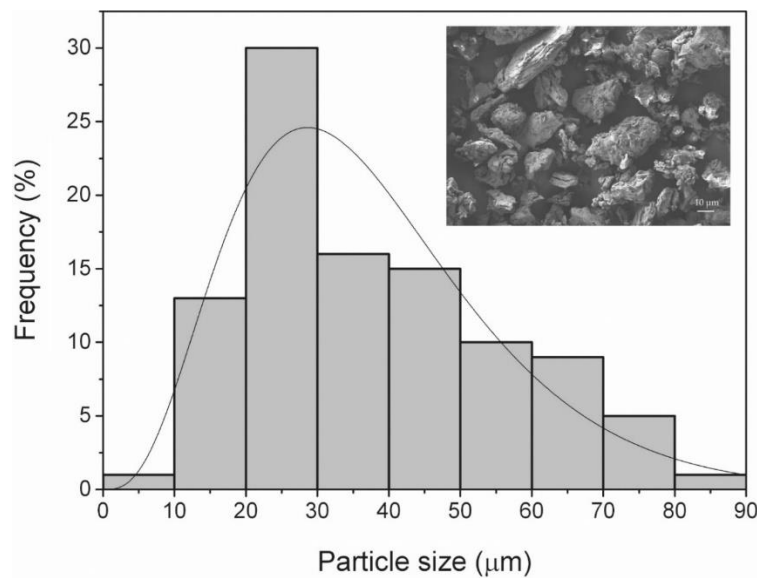
Figure III.2.3.2. Histogram of OPF particles with FESEM image of OPF. Image was taken with a magnification of 500× and scale marker is 10 µm.

Thermal properties

Figure III.2.3.3 shows the DSC thermograms of PLA and its green composite pieces with OPF obtained by injection molding. The main thermal parameters obtained using DSC are summarized in **Table III.2.3.2**. The neat PLA pieces were characterized as having a glass transition temperature (T_g) and melting temperature (T_m) of approximately 64 and 171.5 °C, respectively, and an X_C value close to 24%. In addition, the biopolymer showed a cold crystallization process with a cold crystallization temperature (T_{CC}) of ca 93 °C. The incorporation of AESO slightly increased the degree of crystallinity, that is, the X_C value for the AESO-containing PLA piece was 28.5%. The value of T_g was reduced to ca 60 °C while T_{CC} and T_m remained nearly constant.
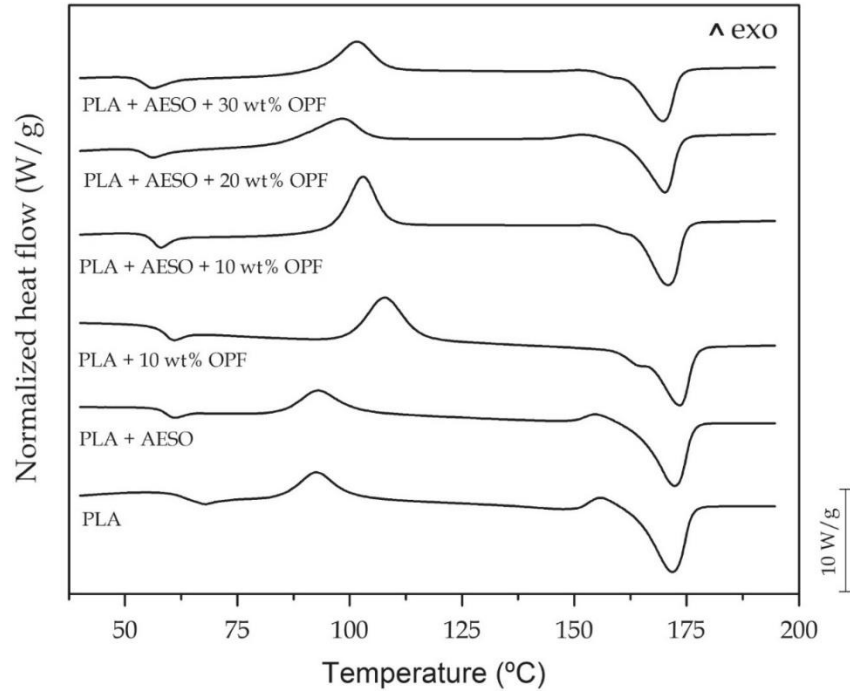
Figure III.2.3.3. DSC thermograms of injection-molded green composite pieces based on PLA, OPF and AESO.

Table III.2.3.2. Summary of main thermal parameters obtained using DSC in terms of glass transition temperature (T_g), normalized enthalpy of crystallization (ΔH_{CC}), cold crystallization temperature (T_{CC}), normalized enthalpy of melting (ΔH_m), melting temperature (T_m) and degree of crystallinity (X_C) of injection-molded green composite pieces based on polylactide (PLA), orange peel flour (OPF) and acrylated epoxidized soybean oil (AESO).

Sample	T_g (ºC)	ΔH_{CC} (J g^{-1})	T_{CC} (ºC)	ΔH_m (J g^{-1})	T_m (ºC)	$Xc\%$
PLA	63.9 ± 0.5	16.7 ± 0.3	92.7 ± 0.4	38.9 ± 0.3	171.5 ± 0.4	23.8 ± 0.9
PLA + AESO	59.9 ± 0.7	17.0 ± 0.5	92.9 ± 0.9	42.3 ± 0.6	171.9 ± 0.5	28.5 ± 0.9
PLA + 10 wt% OPF	59.1 ± 1.9	26.9 ± 0.4	107.8 ± 0.8	32.0 ± 0.5	172.4 ± 0.8	6.0 ± 0.8
PLA + AESO +10 wt% OPF	55.9 ± 1.5	28.1 ± 0.3	103.1 ± 0.4	34.7 ± 0.4	170.6 ± 0.7	8.3 ± 0.4
PLA + AESO +20 wt% OPF	54.4 ± 0.8	19.9 ± 0.4	98.9 ± 0.2	32.4 ± 0.5	170.0 ± 0.3	17.6 ± 0.3
PLA + AESO +30 wt% OPF	54.1 ± 0.6	19.0 ± 0.3	101.5 ± 0.4	28.2 ± 0.4	169.6 ± 0.6	14.8 ± 0.4

The incorporation of OPF also reduced T_g to ca 59 °C and induced a pronounced reduction in the crystallinity of the PLA pieces, that is, X_C was reduced to values of ca 6%. This marked reduction of crystallinity can be produced due to transesterification between the particles and the PLA chains, leading to the formation of a more amorphous structure. However, it is worth noting that the green composite pieces presented T_m values similar to that of the neat PLA piece, which indicates that the presence of OPF did not alter the crystal type of the biopolymer or the lamellar thickness of its spherulites. In relation to T_{CC}, one can observe that there was a notable delay in the cold crystallization process. In particular, the green composite piece containing 10 wt% OPF without AESO showed TCC close to 108 °C, that is, 15 °C higher than that of the neat PLA piece. Therefore, this confirms that the OPF particles predominantly acted as anti-nucleating agents for PLA [47], interrupting the folding or packing process of the PLA chains.

The green composite pieces containing AESO presented lower values of T_g, particularly in the range 54–56 °C. The incorporation of AESO also affected the process of cold crystallization of the pieces, which moved towards lower temperatures in relation to the green composite piece without AESO. The lowest value was observed for the AESO-containing green composite with 20 wt% OPF, showing a T_{CC} value of around 99 °C. In this sense, one can consider that AESO acts as a plasticizer in the green composites. It typically increases free volume and reduces polymer–polymer interactions, allowing a greater mobility of the polymer chains and reducing both T_g and T_{CC} [48, 49]. Nevertheless, this effect was relatively small in comparison to that of other plasticizers, such as poly(ethylene glycol) and poly(propylene glycol) [50, 51], acetyl tri-*n*-butyl citrate [52], oligomeric lactic acid [53], etc., which have been reported to decrease T_g of PLA materials by 25–30 °C with contents in the range 10–20 wt%. In this sense, a reduction of T_g of only 2–3 °C has been recently observed in AESO-toughened PLA pieces.40 The incorporation of higher percentages of lignocellulosic fillers, that is, 20–30 wt% OPF, into the PLA formulations containing 5 phr AESO produced a slight reduction in both T_{CC} and T_m while it resulted in an increase of X_C.

Figure III.2.3.4 shows the TGA curves of PLA and its green composite pieces. It can be observed that the incorporation of OPF significantly reduced the thermal stability of PLA. This also induced the development of two degradation stages, which are summarized in **Table III.2.3.3**. The first occurred in the temperature range 200–350 °C, which corresponds to the decomposition of hemicelluloses at 200–300 °C and of celluloses at 300–350 °C [54]. This step overlapped with the PLA degradation and it became more significant as the percentage of OPF in the composite increased. The second stage took place from 400 to 500 °C and it can be related to the degradation of the lignin fraction present in OPF [55]. The incorporation of OPF also resulted in a direct increase of the residual mass at 600 °C, producing values of ca 3% for the green composite pieces with the highest filler content.
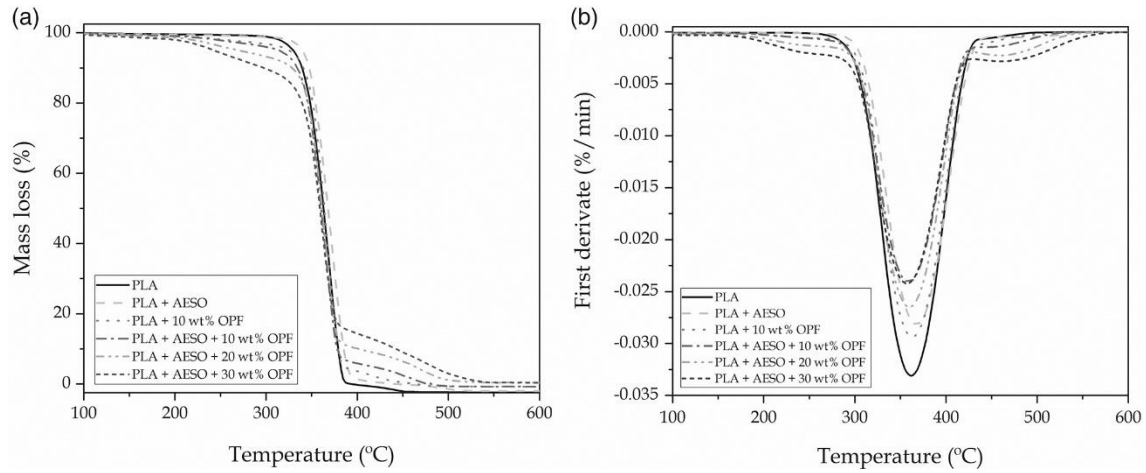
Figure III.2.3.4. TGA curves of injection-molded green composite pieces based on PLA, OPF and AESO: **(a)** mass loss versus temperature; **(b)** first derivative versus temperature.

Table III.2.3.3. Thermal degradation steps and degradation temperature (T_{deg}) obtained using TGA of injection-molded green composite pieces based on polylactide (PLA), orange peel flour (OPF) and acrylated epoxidized soybean oil (AESO).

Sample	First step			Second step			T_{deg} (°C)
	Onset (°C)	Endset (°C)	Mass loss (%)	Onset (°C)	Endset (°C)	Mass loss (%)	
PLA	329.8 ± 1.0	386.3 ± 0.9	99.5 ± 0.1	—	—	—	361.8 ± 1.5
PLA + AESO	339.9 ± 1.0	396.2 ± 1.1	98.8 ± 0.2	—	—	—	366.8 ± 1.2
PLA + 10 wt% OPF	335.6 ± 1.6	384.1 ± 0.8	92.5 ± 0.9	384.1 ± 0.9	488.8 ± 1.1	98.3 ± 0.1	362.6 ± 1.8
PLA + AESO +10 wt% OPF	329.5 ± 1.0	381.3 ± 1.1	89.5 ± 0.6	381.3 ± 1.1	483.9 ± 1.0	98.3 ± 0.1	358.5 ± 1.4
PLA + AESO +20 wt% OPF	328.4 ± 1.2	380.5 ± 0.9	85.2 ± 0.9	380.5 ± 1.2	507.9 ± 1.1	96.9 ± 0.1	359.3 ± 1.1
PLA + AESO +30 wt% OPF	326.2 ± 1.1	373.9 ± 0.8	80.1 ± 0.8	376.9 ± 1.1	541.4 ± 0.9	96.9 ± 0.1	357.6 ± 1.4

Interestingly, the addition of AESO slightly improved the thermal stability of PLA. In particular, T_{deg} of the neat PLA piece was around 362 °C and the addition of 5 phr AESO reduced it by 5 °C. A similar effect has been recently observed for PLA materials containing AESO [40] and epoxidized linseed oil [56] and, hence, potentially suggesting that the molecular structure of the biopolymer was altered. This enhancement in the thermal stability suggests certain chemical interaction of AESO with both components of the green composite, by which the resultant linked

lignocellulosic fillers are expected to act as a physical barrier that obstructs the removal of volatile products produced during decomposition. This is an interesting result since one of the main drawbacks of most PLA plasticizers is related to the fact that they habitually reduce the thermal stability of the biopolymer [52, 57]. This thermal degradation improvement was also observed for the green composite pieces containing AESO, though their resultant thermal stability was still slightly lower than that of the neat PLA.

Mechanical properties

Table III.2.3.4 summarizes the effect of both OPF and AESO on the mechanical properties of the injection-molded PLA pieces. In relation to the tensile properties, one can observe that the PLA modulus increased with the addition of the multi-functionalized vegetable oil and, more significantly, of the lignocellulosic filler. While the neat PLA piece showed a Young's modulus of *ca* 1.97 GPa, it slightly increased to 2.12 and 2.71 GPa with the addition of 5 phr AESO and 10 wt% OPF, respectively. Furthermore, the modulus remained almost constant, that is, around 2.70–2.80 GPa, for green composite pieces containing AESO at all OPF loadings. For the lowest OPF content, that is, 10 wt%, the values of tensile strength also remained close to that of the neat PLA piece, that is, 66 MPa. However, higher filler contents reduced the tensile strength to values of approximately 50 and 40 MPa for the green composite pieces filled with 20 and 30 wt% OPF, respectively.

Table III.2.3.4. Mechanical properties in terms of tensile modulus (E), tensile strength at yield (σ_y), elongation at break (ϵ_b), Shore D hardness and impact strength of injection-molded green composite pieces based on polylactide (PLA), orange peel flour (OPF) and acrylated epoxidized soybean oil (AESO).

Sample	E (MPa)	σ_y (MPa)	ϵ_b (%)	Shore D hardness	Impact strength (kJ m^{-2})
PLA	1972.4 ± 95.4	65.9 ± 1.8	5.3 ± 1.0	80.2 ± 1.1	22.8 ± 1.1
PLA + AESO	2118.9 ± 65.9	64.6 ± 0.7	7.3 ± 0.4	81.4 ± 0.6	29.7 ± 0.8
PLA + 10 wt% OPF	2713.9 ± 103.5	64.3 ± 0.9	4.5 ± 0.3	84.4 ± 1.1	18.1 ± 0.7
PLA + AESO +10 wt% OPF	2679.2 ± 81.4	63.4 ± 1.1	4.9 ± 0.2	84.6 ± 0.5	20.8 ± 0.5
PLA + AESO +20 wt% OPF	2670.9 ± 115.0	50.3 ± 2.1	4.5 ± 0.4	84.7 ± 1.1	14.6 ± 0.8
PLA + AESO +30 wt% OPF	2750.4 ± 103.6	40.1 ± 0.9	4.0 ± 0.4	85.2 ± 1.8	11.9 ± 0.7

Since the elongation at break was also reduced in the green composite pieces, it can be considered that the lignocellulosic fillers acted as a stress concentrator. In particular, the elongation at break values decreased from 5.3% for the neat PLA piece to 4.5% for the green composite piece containing 10 wt% OPF without AESO. This

result points to the poor adhesion of the OPF particles to the biopolymer and probably their low dispersion in the PLA matrix. Therefore, the lignocellulosic fillers acted as a defect rather than a reinforcement so that these cannot efficiently absorb the stresses or prevent the propagation of cracks [58]. However, the addition of 5 phr AESO led to a considerable increase in elongation at break up to 7.3%. This value represents an increase of approximately 40%, further indicating that the multi-functionalized vegetable oil provided some plasticization to the PLA matrix. Interestingly, AESO also improved the ductility of the green composite pieces. A comparison of the injection-molded green composite piece at 10 wt% OPF with and without AESO shows that the addition of the multi-functionalized vegetable oil improved the elongation at break from 4.5 to 4.9%, that is, around 9%, while the tensile modulus and strength remained nearly constant. This improvement in the elongation at break allowed the realization of a green composite piece with ductility similar to that observed for the neat PLA piece.

Regarding hardness, addition of OPF also produced a moderate increase. In particular, the hardness value increased from 80.2 for the neat PLA piece to 84.4 for the green composite piece containing 10 wt% OPF without AESO, which is the typical effect of a hard filler on a polymer matrix. While the addition of AESO did not provide any marked effect on the PLA hardness, the green composites containing AESO and with high contents of OPF showed further increase in hardness. In particular, the highest Shore D hardness was observed for the PLA piece filled with 30 wt% OPF, that is, a value of 85.2.

In contrast to hardness, the impact strength decreased after the OPF incorporation. This was reduced from 22.8 kJ m^{-2} for the neat PLA piece to 18.1 kJ m^{-2} for the green composite piece with 10 wt% OPF. Interestingly, the addition of AESO markedly improved the toughness of the PLA piece, increasing its impact strength up to 29.7 kJ m^{-2}, which means an improvement of approximately 30%. Similar results were also observed, for instance, by Ferri *et al*. [59] for PLA plasticized with maleinized linseed oil, though a saturation effect was also observed at a very low concentration. In the case of the AESO-containing green composite piece with 10 wt% OPF, a slight increase in the impact strength was also observed. This green composite piece presented an impact strength of 20.8 kJ m^{-2}, being very close to that of the neat PLA piece. However, for the green composite pieces with 20 and 30 wt% OPF, the decrease in impact strength was significant due to the relatively high filler content, which clearly compromises the capacity for energy absorption.

Thermomechanical properties

Figure III.2.3.5 shows the dynamic behavior, obtained from DMTA in torsion mode, of the neat PLA and green composite pieces. In **Figure III.2.3.5a**, which shows the evolution of the storage modulus versus temperature, both the glass transition and cold crystallization processes can be observed. For the neat PLA piece, T_g was detected by a drop of the storage modulus of two orders of magnitude in the range 55–65 °C. Besides, the cold crystallization process occurred from 80 °C, showing a slight increase in the storage modulus due to the formation of a stiffer material by a crystallinity increase. The incorporation of OPF produced a marked increase of the storage modulus at temperatures below T_g and a slight delay in the temperature at which cold crystallization occurred, as was stated above in the discussion of DSC analysis. For instance, at 40 °C, the storage modulus increased from a value of 1.5 GPa for the neat

PLA piece to a value of 1.8 GPa in the case of the green composite piece with 10 wt% OPF. The addition of AESO also increased the storage modulus of PLA up to a value of 1.6 GPa at 40 °C. In general, the curves for all green composite pieces shifted towards lower temperatures, thus indicating a slight decrease in T_g of PLA with an additional positive effect on the toughness.
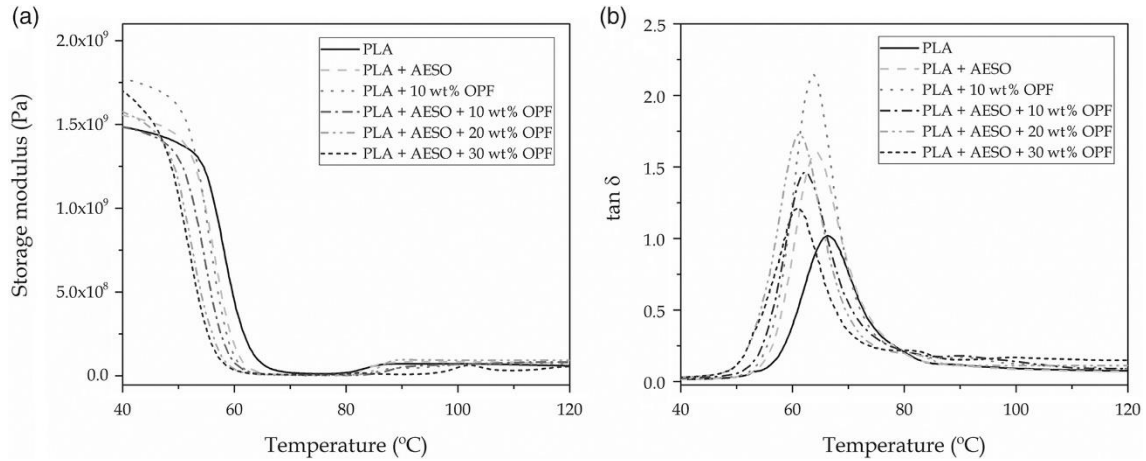
Figure III.2.3.5. DMTA curves of injection-molded green composite pieces based on PLA, OPF and AESO: (a) Storage modulus; (b) damping factor (tan δ).

In relation to the damping factor, in **Figure III.2.3.5b** it can be observed that the peak of the neat PLA piece shifted to lower temperatures for the pieces containing both OPF and AESO. This decrease of the tan δ peak indicates a reduction of the α-relaxation of the biopolymer, which is related to T_g. Although this effect was noticeable for all the materials, it was more intense in the case of the green composites containing AESO in which it was reduced by ca 5 °C. In addition, all green composite pieces presented higher values of tan δ than the neat PLA piece, which is a direct indication that the pieces presented higher energy dissipation with improved toughness [16].

In relation to the dimensional stability, as is evident from **Table III.2.3.5**, all PLA pieces presented higher CLTE values above T_g than below T_g since the biopolymer chains were more readily able to move. Interestingly, AESO also provided certain interesting changes in the CLTE values. Specifically, below T_g, it decreased from 95.3 $\mu m\,m^{-1}\,°C^{-1}$ for the neat PLA piece to 91.7 $\mu m\,m^{-1}\,°C^{-1}$ for the AESO-containing PLA piece. This effect has been previously ascribed to the formation of a long-chained or partially cross-linked structure due to the reaction of PLA with the multiple epoxy or acrylate groups present in AESO [40]. The addition of OPF further decreased the CLTE values below T_g, indicating that the pieces acquired more thermomechanical resistance. Above T_g, CLTE increased from 148.8 $\mu m\,m^{-1}\,°C^{-1}$ for the neat PLA piece to 202.5 $\mu m\,m^{-1}\,°C^{-1}$ for the PLA piece containing AESO. However, for the AESO-containing green composite pieces, a positive dimensional stabilization was observed. In particular, the green composites showed CLTE values in the range 175-185 $\mu m\,m^{-1}\,°C^{-1}$, therefore presenting an extraordinary thermomechanical response at high temperatures. One can also observe that the incorporation of OPF also reduced T_g of PLA, presenting values very similar to those reported above in relation to DSC. For instance, for the green composite piece with the highest OPF content, that is, 30 wt%, the reduction was higher than 10 °C in relation to the neat PLA piece.

Table III.2.3.5. Coefficient of linear thermal expansion (CLTE) and glass transition temperature (T_g) of injection-molded green composite pieces based on polylactide (PLA), orange peel flour (OPF) and acrylated epoxidized soybean oil (AESO).

Sample	CLTE below T_g (μm m^{-1}°C)	CLTE above T_g (μm m^{-1}°C)	T_g (°C)
PLA	95.3 ± 3.5	148.8 ± 2.3	65.7 ± 1.3
PLA + AESO	91.7 ± 2.2	202.5 ± 3.8	62.6 ± 2.2
PLA + 10 wt% OPF	83.8 ± 2.9	172.7 ± 1.9	60.8 ± 1.9
PLA + AESO +10 wt% OPF	88.4 ± 3.1	173.8 ± 2.8	58.6 ± 1.5
PLA + AESO +20 wt% OPF	88.2 ± 4.2	175.6 ± 2.6	56.9 ± 1.8
PLA + AESO +30 wt% OPF	86.6 ± 2.6	184.5 ± 4.0	56.1 ± 1.9

Morphology of green composites

Figure III.2.3.6 shows the fracture surfaces after impact testing of the injection-molded pieces of PLA and its green composites with OPF. The fracture surface of the neat PLA piece, depicted in **Figure III.2.3.6a**, shows the characteristic morphology of a brittle material with a low energy absorption. Both a micro-crack formation and a high roughness can be observed, showing no evidence of plastic deformation. In **Figure III.2.3.6b**, in contrast, one can observe that the addition of AESO modified the fracture surface of the PLA piece. It changed from a rough surface to plastic-like morphology with the presence of some long filaments. This confirms the increase in toughness described above in relation to the mechanical analysis. **Figure III.2.3.6c** shows the fracture surface of the green composite containing 10 wt% OPF without AESO. This FESEM image reveals the presence of some voids, more likely produced from particle debonding during breaking, and also large gaps in the interface between the lignocellulosic particles and the biopolymer matrix. Therefore, the observed morphology fully confirmed the poor compatibility between both components of the green composite.
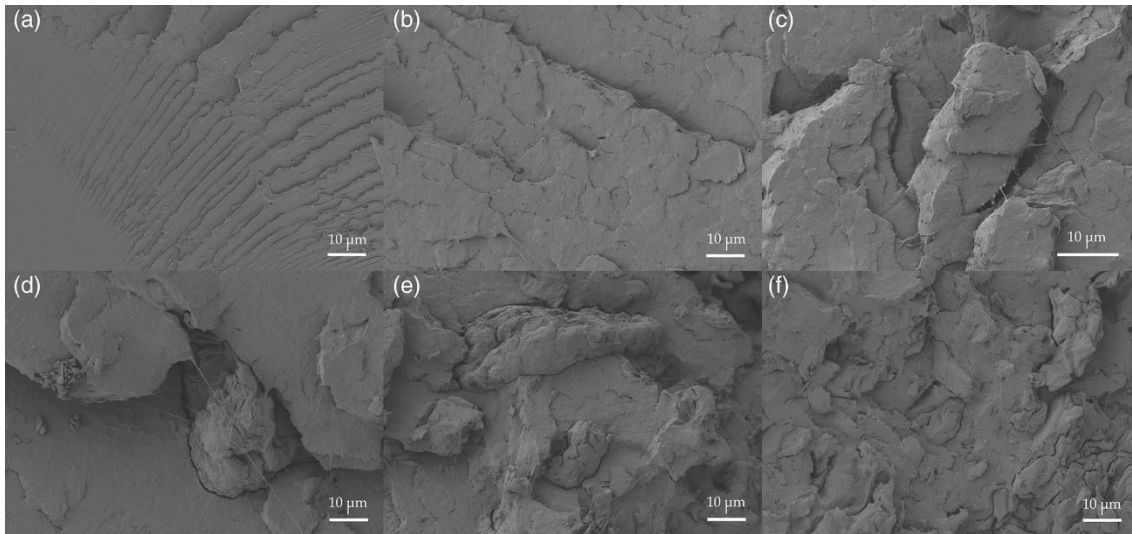
Figure III.2.3.6. FESEM images of fracture surfaces of injection-molded pieces: (a) PLA; (b) PLA containing AESO; (c) PLA filled with 10 wt% OPF; (d) PLA + AESO +10 wt% OPF; (e) PLA + AESO +20 wt% OPF; (f) PLA + AESO +30 wt% OPF.

Interestingly, as shown in **Figure III.2.3.6d** and **f**, one can observe that the morphology of the fracture surfaces of all AESO-toughened green composites was markedly different. Comparison of both FESEM images shown in **Figure III.2.3.6d** and **c**, that is, the fracture surfaces of the green composite with 10 wt% OPF with and without AESO, respectively, indicates that the presence of the multi-functionalized vegetable oil notably reduced the number of voids and also produced smaller gaps between the OPF particles and the PLA biopolymer. In addition, as can be observed in **Figure III.2.3.6f** for the green composite piece with the highest OPF loading, that is, 30 wt%, the dispersion of the lignocellulosic fillers was relatively high.

Compatibilization of green composites

From the improvement in morphology discussed above, it can be established that the PLA–OPF adhesion increased in the injection-molded pieces after the addition of AESO. Furthermore, AESO offered a more balanced mechanical and thermomechanical performance whilst the thermal properties were slightly improved. It is considered that AESO induced certain plasticization to the PLA matrix, which increased ductility and toughness of the PLA and its green composite pieces. However, changes in T_g were relatively small, as determined from both DMTA and CLTE analysis. In the addition, the elongation at break, which is a direct measurement of the mechanical ductile properties, did not increase in a marked way as other plasticizers certainly do [43]. Therefore, in addition to a plasticizing effect, AESO induced certain interfacial adhesion between the OPF particles and the PLA matrix by which it promoted a moderate increase in elongation at break in combination with a significant improvement of the mechanical properties. This improvement was further assessed based on the fact that the cold crystallization peak was delayed and the melting peak slightly shifted to lower temperatures while the degree of crystallization was noticeably reduced.

Based on our previous research findings related to biopolymer composites and nanocomposites processed using REX with multi-functional low-molecular-weight additives [30, 41], it is proposed that AESO also acted as a reactive compatibilizer during melt processing, successfully establishing strong chemical 'bridges' between the biopolymer chains and the lignocellulosic fillers. AESO, which is feasibly obtained from epoxidized soybean oil by treatment with acrylic acid (AA) [40], is based on a chemical structure containing multiple acrylate and epoxy groups. These functional groups are highly reactive, being then able to provide a chain-extension and/or cross-linking effect to polymers also containing functional groups. Indeed, AESO has been recently reported as an environmentally friendly additive for toughening PLA-based materials [40, 43].
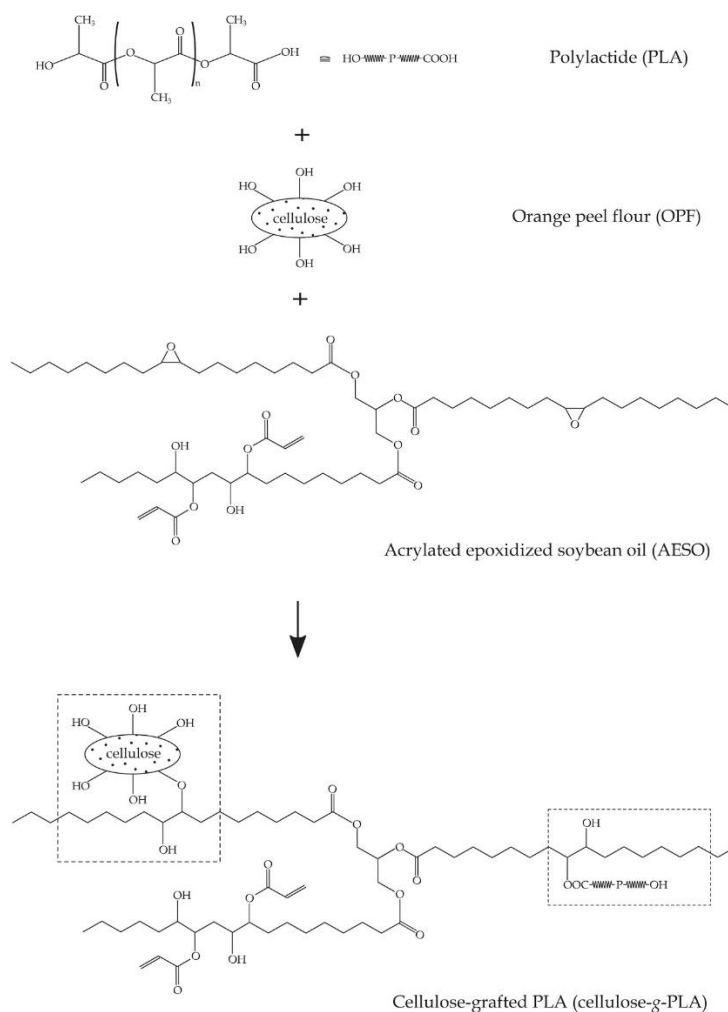
Figure III.2.3.7. Schematic of melt grafting of OPF onto PLA by AESO.

Therefore, **Figure III.2.3.7** suggests a possible grafting mechanism of OPF onto the PLA macromolecular structure during melt processing. On the one hand, in the case of the biopolymer, ester bonds are proposed to be formed by the reaction of the terminal acid groups of the PLA chains with some of the multiple epoxy groups of AESO. In this sense, the mechanism of epoxy ring-opening to produce chain extension in polyesters typically consists of glycidyl esterification of the carboxylic acid end

groups, which precedes hydroxyl end-group etherification [60]. In the case of polyesters, the reaction rate of the epoxy groups is known to be approximately 10–15 times higher with the carboxyl group (-COOH) than with the hydroxyl group (-OH) [61]. On the other hand, other epoxy groups present in AESO can simultaneously react with the -OH groups of the cellulose available on the surface of the OPF particles. This reaction generates C-O-C bonds with hydroxyl side-group formation. Therefore, a new hybrid structure, namely a cellulose-grafted PLA composite, that is, cellulose-g-PLA composite, was formed.

Disintegration of green composites

Finally, disintegration tests in a controlled compost soil were carried out in order to ascertain the effect of both OPF and AESO on the PLA compostability. The weight loss of the injection-molded PLA-based pieces during disintegration in compost is plotted in **Figure III.2.3.8**. In addition, **Figure III.2.3.9** shows the visual aspect of the pieces evaluated during the disintegration test. One can observe that, after an incubation period of about 2 weeks, all pieces started an embrittlement process accompanied by the development of a dark-to-black color and a quick weight loss. It is also worth remarking that the test was conducted at 58 °C and 50% RH, that is, a relatively high temperature and humidity, which are certainly favorable conditions for the hydrolytic degradation of PLA. Although it has been previously reported in the polymer literature that neat PLA disintegrates notably faster than its composites based on lignocellulosic fillers [62, 63], the here-developed green composites presented similar degradation rates. In the case of the AESO-containing PLA piece and the green composite piece with 10 wt% OPF, the disintegration rate was even slightly faster than that of the neat PLA piece during the first 4 weeks. In the case of the green composites containing AESO, these pieces showed a slightly slower degradation profile in the final weeks, particularly for the piece filled with 30 wt% OPF. After 8 weeks, the neat PLA piece lost over 98% of its initial weight while both the AESO-containing PLA piece and the green composite piece filled with 10 wt% OPF were fully degraded. For the AESO-containing green composites the weight loss reached values around 95%. Therefore, it can be concluded that neither the multi-functional vegetable oil nor the lignocellulosic filler impair the compostability of the PLA pieces.
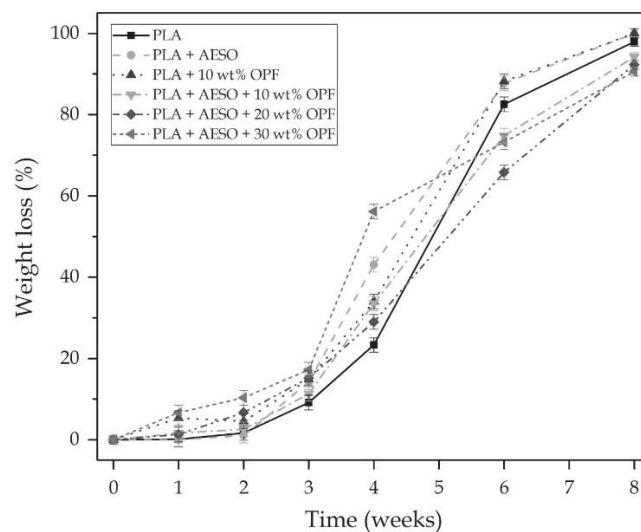
Figure III.2.3.8. Weight loss as a function of elapsed time during disintegration test in controlled compost soil of injection-molded green composite pieces based on PLA, OPF and AESO.
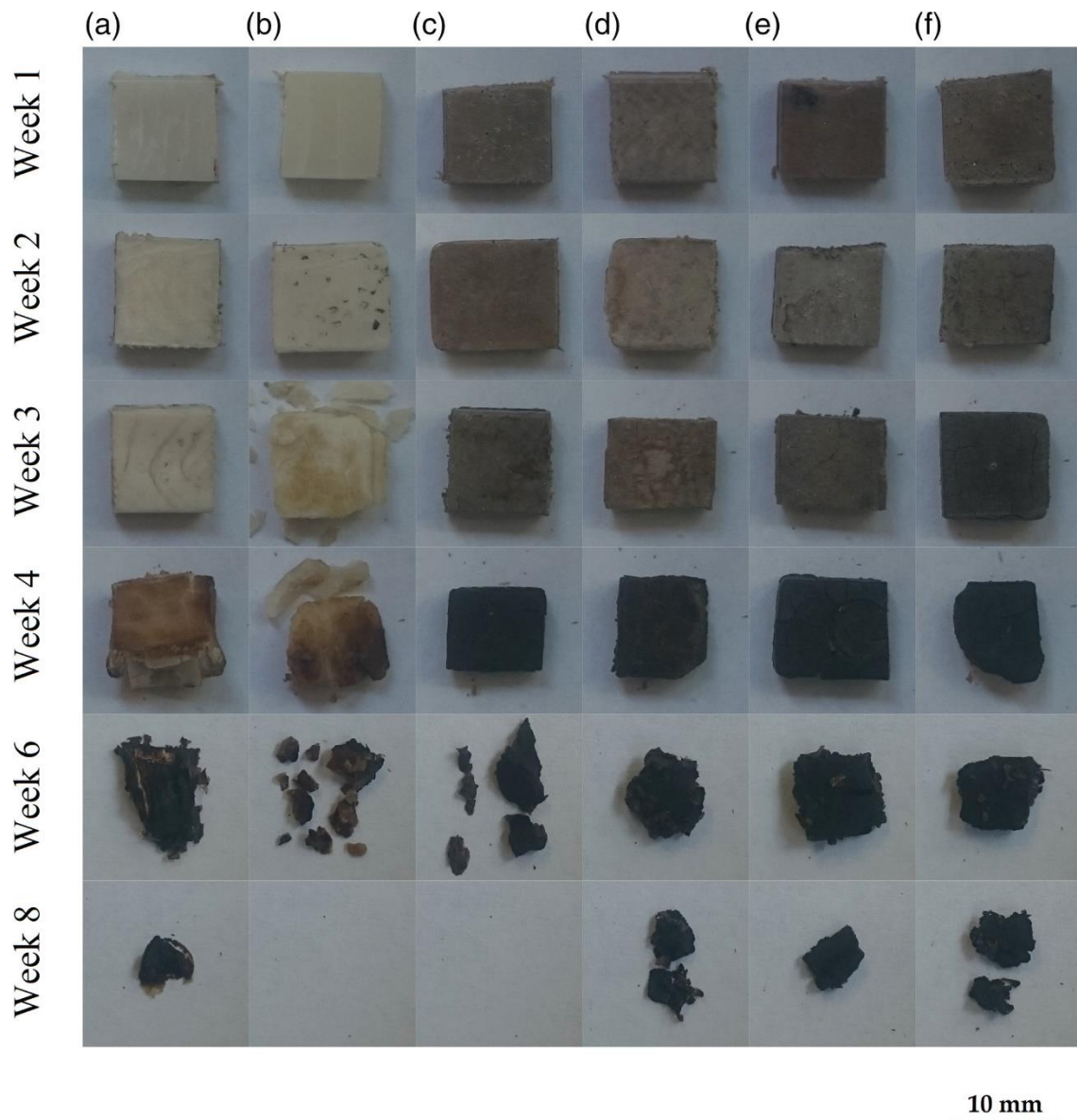
Figure III.2.3.9. Visual aspect during disintegration test in controlled compost soil of injection-molded pieces: (a) PLA; (b) PLA containing AESO; (c) PLA filled with 10 wt% OPF; (d) PLA + AESO +10 wt% OPF; (e) PLA + AESO +20 wt% OPF; (f) PLA + AESO +30 wt% OPF.

CONCLUSIONS

The present study describes the preparation and characterization of PLA/OPF composite pieces compatibilized with AESO, an environmentally friendly multi-functionalized additive that can be easily obtained from natural soybean oil. While the incorporation of OPF into PLA induced a marked reduction of both thermal stability and mechanical ductility, showing values of T_{deg} of 363 °C and values of elongation at

break and impact strength of 4.5% and 18.1 kJ m⁻², respectively, the addition of only 5 phr AESO successfully enhanced the thermal, mechanical and thermomechanical properties of the green composites. In particular, for the AESO-compatibilized green composite piece filled with 10 wt%, the elongation at break and impact strength were approximately 9 and 13% higher, respectively. However, in the case of the green composite pieces with higher filler contents, that is, 20 and 30 wt% OPF, a significant decrease in ductility was observed. The compatibilization achieved was ascribed to a dual effect of plasticization in combination with melt grafting of the OPF particles onto the PLA chains provided by the multiple functional groups present in the chemical structure of AESO.

The results obtained indicate that OPF, a major by-product of the food juice industry, can be successfully incorporated up to 10 wt% into PLA by melt processing in the presence of AESO without compromising the physical properties and compostability of the biopolymer. It can be concluded that AESO, similar to other multi-functionalized vegetable oils, can be used as a reactive additive to enhance the compatibility between biopolymers and lignocellulosic fillers in green composite materials and, thus, it can potentially contribute to the development of sustainable polymer technologies.

Acknowledgements

REFERENCES

1. Quiles-Carrillo, L., N. Montanes, T. Boronat, R. Balart and S. Torres-Giner, *Evaluation of the engineering performance of different bio-based aliphatic homopolyamide tubes prepared by profile extrusion.* Polymer Testing, 2017. **61**: 421-429.
2. Chiellini, E., P. Cinelli, F. Chiellini and S.H. Imam, *Environmentally Degradable Bio-Based Polymeric Blends and Composites.* Macromolecular bioscience, 2004. **4**(3): 218-231.
3. Majhi, S.K., S.K. Nayak, S. Mohanty and L. Unnikrishnan, *Mechanical and fracture behavior of banana fiber reinforced Polylactic acid biocomposites.* International Journal of Plastics Technology, 2010. **14**: 57-75.
4. Thakur, V.K., M.K. Thakur, P. Raghavan and M.R. Kessler, *Progress in green polymer composites from lignin for multifunctional applications: a review.* ACS Sustainable Chemistry & Engineering, 2014. **2**(5): 1072-1092.
5. Yang, H.-S., H.-J. Kim, J. Son, H.-J. Park, B.-J. Lee and T.-S. Hwang, *Rice-husk flour filled polypropylene composites; mechanical and morphological study.* Composite Structures, 2004. **63**(3): 305-312.
6. Cheng, S., K.-t. Lau, T. Liu, Y. Zhao, P.-M. Lam and Y. Yin, *Mechanical and thermal properties of chicken feather fiber/PLA green composites.* Composites Part B: Engineering, 2009. **40**(7): 650-654.
7. Huda, M., A. Mohanty, L. Drzal, E. Schut and M. Misra, "*Green" composites from recycled cellulose and poly (lactic acid): Physico-mechanical and morphological properties evaluation.* Journal of Materials Science, 2005. **40**(16): 4221-4229.
8. Nampoothiri, K.M., N.R. Nair and R.P. John, *An overview of the recent developments in polylactide (PLA) research.* Bioresource technology, 2010. **101**(22): 8493-8501.

9.   Koronis, G., A. Silva and M. Fontul, *Green composites: A review of adequate materials for automotive applications*. Composites Part B: Engineering, 2013. **44**(1): 120-127.

10.   Dicker, M.P., P.F. Duckworth, A.B. Baker, G. Francois, M.K. Hazzard and P.M. Weaver, *Green composites: A review of material attributes and complementary applications.* Composites part A: applied science and manufacturing, 2014. **56**: 280-289.

11.   Bajpai, P.K., I. Singh and J. Madaan, *Development and characterization of PLA-based green composites: A review*. Journal of Thermoplastic Composite Materials, 2014. **27**(1): 52-81.

12.   Zini, E. and M. Scandola, *Green composites: an overview.* Polymer composites, 2011. **32**(12): 1905-1915.

13.   Shih, Y.-F. and C.-C. Huang, *Polylactic acid (PLA)/banana fiber (BF) biodegradable green composites.* Journal of polymer Research, 2011. **18**(6): 2335-2340.

14.   Laka, M., S. Chernyavskaya and M. Maskavs, *Cellulose-containing fillers for polymer composites.* Mechanics of composite materials, 2003. **39**(2): 183-188.

15.   Khalil, H.A., A. Bhat and A.I. Yusra, *Green composites from sustainable cellulose nanofibrils: a review*. Carbohydrate Polymers, 2012. **87**(2): 963-979.

16.   Torres-Giner, S., N. Montanes, O. Fenollar, D. García-Sanoguera and R. Balart, *Development and optimization of renewable vinyl plastisol/wood flour composites exposed to ultraviolet radiation*. Materials & Design, 2016. **108**: 648-658.

17.   Rai, B., G. Kumar, V. Tyagi, R. Diwan and U. Niyogi, *Development and Characterization of Green Composite from Euphorbia Coagulum and Banana Fiber*. Journal of Polymer Materials, 2015. **32**(3): 305.

18.   Karlssion, S. and B.S. Ndazi, *Characterization of hydrolytic degradation of polylactic acid/rice hulls composites in water at different temperatures*. 2011.

19.   Yussuf, A., I. Massoumi and A. Hassan, *Comparison of polylactic acid/kenaf and polylactic acid/rise husk composites: the influence of the natural fibers on the mechanical, thermal and biodegradability properties*. Journal of Polymers and the Environment, 2010. **18**(3): 422-429.

20.   Nishikawa, Y., N. Nagase and K. Fukushima, *Application of Peanut Hulls as Filler for Plastics.* Journal of Environment and Engineering, 2009. **4**(1): 124-134.

21.   Garcia-Garcia, D., A. Carbonell-Verdu, A. Jordá-Vilaplana, R. Balart and D. Garcia-Sanoguera, *Development and characterization of green composites from bio-based polyethylene and peanut shell.* Journal of Applied Polymer Science, 2016. **133**(37).

22.   Sanchez-Vazquez, S., H. Hailes and J. Evans, *Hydrophobic polymers from food waste: resources and synthesis.* Polymer Reviews, 2013. **53**(4): 627-694.

23.   Torres-Giner, S., N. Montanes, V. Fombuena, T. Boronat and L. Sanchez-Nacher, *Preparation and characterization of compression-molded green composite sheets made of poly(3-hydroxybutyrate) reinforced with long pita fibers.* Advances in Polymer Technology, 2016: n/a-n/a.

24.   Ferrero, B., V. Fombuena, O. Fenollar, T. Boronat and R. Balart, *Development of natural fiber-reinforced plastics (NFRP) based on biobased polyethylene and waste fibers from Posidonia oceanica seaweed.* Polymer Composites, 2015. **36**(8): 1378-1385.

25.   Coltro, L., A.L. Mourad, R.M. Kletecke, T.A. Mendonça and S.P. Germer, *Assessing the environmental profile of orange production in Brazil*. The International Journal of Life Cycle Assessment, 2009. **14**(7): 656-664.

26.   Rezzadori, K., S. Benedetti and E. Amante, *Proposals for the residues recovery: orange waste as raw material for new products.* Food and bioproducts processing, 2012. 90(4): 606-614.

27.   Borah, J.S. and D.S. Kim, *Recent development in thermoplastic/wood composites and nanocomposites: A review*. Korean Journal of Chemical Engineering, 2016. **33**(11): 3035-3049.

28.   Yang, H.-S., H.-J. Kim, H.-J. Park, B.-J. Lee and T.-S. Hwang, *Water absorption behavior and mechanical properties of lignocellulosic filler–polyolefin bio-composites*. Composite Structures, 2006. **72**(4): 429-437.

29. Raquez, J.-M., P. Degée, Y. Nabar, R. Narayan and P. Dubois, *Biodegradable materials by reactive extrusion: from catalyzed polymerization to functionalization and blend compatibilization.* Comptes Rendus Chimie, 2006. **9**(11): 1370-1379.

30. Torres-Giner, S., N. Montanes, T. Boronat, L. Quiles-Carrillo and R. Balart, *Melt grafting of sepiolite nanoclay onto poly (3-hydroxybutyrate-co-4-hydroxybutyrate) by reactive extrusion with multi-functional epoxy-based styrene-acrylic oligomer.* European Polymer Journal, 2016. **84**: 693-707.

31. Meng, Q.-K., M.-C. Heuzey and P. Carreau, *Effects of a multifunctional polymeric chain extender on the properties of polylactide and polylactide/clay nanocomposites.* International Polymer Processing, 2012. **27**(5): 505-516.

32. Najafi, N., M. Heuzey and P. Carreau, *Polylactide (PLA)-clay nanocomposites prepared by melt compounding in the presence of a chain extender.* Composites Science and Technology, 2012. **72**(5): 608-615.

33. Zhang, J.-F. and X. Sun, *Mechanical properties of poly (lactic acid)/starch composites compatibilized by maleic anhydride.* Biomacromolecules, 2004. **5**(4): 1446-1451.

34. Orozco, V.H., W. Brostow, W. Chonkaew and B.L. Lopez. *Preparation and characterization of poly (Lactic acid)-g-maleic anhydride+ starch blends.* in Macromolecular symposia. 2009. Wiley Online Library.

35. Xiong, Z., L. Zhang, S. Ma, Y. Yang, C. Zhang, Z. Tang and J. Zhu, *Effect of castor oil enrichment layer produced by reaction on the properties of PLA/HDI-g-starch blends.* Carbohydrate polymers, 2013. **94**(1): 235-243.

36. Mamun, A.A., H.-P. Heim, D.H. Beg, T.S. Kim and S.H. Ahmad, *PLA and PP composites with enzyme modified oil palm fibre: A comparative study.* Composites Part A: Applied Science and Manufacturing, 2013. **53**: 160-167.

37. García-García, D., A. Carbonell, M. Samper, D. García-Sanoguera and R. Balart, *Green composites based on polypropylene matrix and hydrophobized spend coffee ground (SCG) powder.* Composites Part B: Engineering, 2015. **78**: 256-265.

38. Garcia-Garcia, D., O. Fenollar, V. Fombuena, J. Lopez-Martinez and R. Balart, *Improvement of Mechanical Ductile Properties of Poly (3-hydroxybutyrate) by Using Vegetable Oil Derivatives.* Macromolecular Materials and Engineering, 2016.

39. Quiles-Carrillo, L., M. Blanes-Martínez, N. Montanes, O. Fenollar, S. Torres-Giner and R. Balart, *Reactive toughening of injection-molded polylactide pieces using maleinized hemp seed oil.* European Polymer Journal, 2018. **98**: 402-410.

40. Quiles-Carrillo, L., S. Duart, N. Montanes, S. Torres-Giner and R. Balart, *Enhancement of the mechanical and thermal properties of injection-molded polylactide parts by the addition of acrylated epoxidized soybean oil.* Materials & Design, 2018. **140**: 54-63.

41. Quiles-Carrillo, L., N. Montanes, C. Sammon, R. Balart and S. Torres-Giner, *Compatibilization of highly sustainable polylactide/almond shell flour composites by reactive extrusion with maleinized linseed oil.* Industrial crops and products, 2018. **111**: 878-888.

42. Xiong, Z., Y. Yang, J. Feng, X. Zhang, C. Zhang, Z. Tang and J. Zhu, *Preparation and characterization of poly (lactic acid)/starch composites toughened with epoxidized soybean oil.* Carbohydrate polymers, 2013. **92**(1): 810-816.

43. Mauck, S.C., S. Wang, W. Ding, B.J. Rohde, C.K. Fortune, G. Yang, S.-K. Ahn and M.L. Robertson, *Biorenewable tough blends of polylactide and acrylated epoxidized soybean oil compatibilized by a polylactide star polymer.* Macromolecules, 2016. **49**(5): 1605-1615.

44. Torres-Giner, S., J.V. Gimeno-Alcañiz, M.J. Ocio and J.M. Lagaron, *Optimization of electrospun polylactide-based ultrathin fibers for osteoconductive bone scaffolds.* Journal of Applied Polymer Science, 2011. **122**(2): 914-925.

45. Crespo, J., R. Balart, L. Sanchez and J. Lopez, *Mechanical behaviour of vinyl plastisols with cellulosic fillers. Analysis of the interface between particles and matrices.* International journal of adhesion and adhesives, 2007. **27**(5): 422-428.

46. Crespo, J., L. Sanchez, F. Parres and J. Lopez, *Mechanical and morphological characterization of PVC plastisol composites with almond husk fillers.* Polymer composites, 2007. **28**(1): 71-77.

47.   Hosseinihashemi, S.K., A. Eshghi, N. Ayrilmis and H. Khademieslam, *Thermal Analysis and Morphological Characterization of Thermoplastic Composites Filled with Almond Shell Flour/Montmorillonite.* BioResources, 2016. **11**(3): 6768-6779.

48.   Arrieta, M.P., M.D. Samper, J. López and A. Jiménez, *Combined effect of poly (hydroxybutyrate) and plasticizers on polylactic acid properties for film intended for food packaging.* Journal of Polymers and the Environment, 2014. **22**(4): 460-470.

49.   Chieng, B.W., N.A. Ibrahim, Y.Y. Then and Y.Y. Loo, *Epoxidized vegetable oils plasticized poly (lactic acid) biocomposites: mechanical, thermal and morphology properties.* Molecules, 2014. **19**(10): 16024-16038.

50.   Kulinski, Z., E. Piorkowska, K. Gadzinowska and M. Stasiak, *Plasticization of poly (L-lactide) with poly (propylene glycol).* Biomacromolecules, 2006. **7**(7): 2128-2135.

51.   Kowalczyk, M., M. Pluta, E. Piorkowska and N. Krasnikova, *Plasticization of polylactide with block copolymers of ethylene glycol and propylene glycol.* Journal of applied polymer science, 2012. **125**(6): 4292-4301.

52.   Arrieta, M.P., M.d.M. Castro-Lopez, E. Rayón, L.F. Barral-Losada, J.M. López-Vilariño, J. López and M.V. González-Rodríguez, *Plasticized poly (lactic acid)–poly (hydroxybutyrate)(PLA–PHB) blends incorporated with catechin intended for active food-packaging applications.* Journal of agricultural and food chemistry, 2014. **62**(41): 10170-10180.

53.   Burgos, N., V.P. Martino and A. Jiménez, *Characterization and ageing study of poly (lactic acid) films plasticized with oligomeric lactic acid.* Polymer degradation and stability, 2013. **98**(2): 651-658.

54.   Chun, K.S., S. Husseinsyah and H. Osman, *Mechanical and thermal properties of coconut shell powder filled polylactic acid biocomposites: effects of the filler content and silane coupling agent.* Journal of Polymer Research, 2012. **19**(5): 9859.

55.   Lee, S.-H. and S. Wang, *Biodegradable polymers/bamboo fiber biocomposite with bio-based coupling agent.* Composites Part A: Applied Science and Manufacturing, 2006. **37**(1): 80-91.

56.   Balart, J., V. Fombuena, O. Fenollar, T. Boronat and L. Sánchez-Nacher, *Processing and characterization of high environmental efficiency composites based on PLA and hazelnut shell flour (HSF) with biobased plasticizers derived from epoxidized linseed oil (ELO).* Composites Part B: Engineering, 2016. **86**: 168-177.

57.   Choi, K.-M., S.-W. Lim, M.-C. Choi, Y.-M. Kim, D.-H. Han and C.-S. Ha, *Thermal and mechanical properties of poly (lactic acid) modified by poly (ethylene glycol) acrylate through reactive blending.* Polymer bulletin, 2014. **71**(12): 3305-3321.

58.   Delgado, P.S., S.L.B. Lana, E. Ayres, P.O.S. Patrício and R.L. Oréfice, *The potential of bamboo in the design of polymer composites.* Materials Research, 2012. **15**(4): 639-644.

59.   Ferri, J.M., D. Garcia-Garcia, N. Montanes, O. Fenollar and R. Balart, *The effect of maleinized linseed oil as biobased plasticizer in poly (lactic acid)-based formulations.* Polymer International, 2017. **66**(6): 882-891.

60.   Villalobos, M., A. Awojulu, T. Greeley, G. Turco and G. Deeter, *Oligomeric chain extenders for economic reprocessing and recycling of condensation plastics.* Energy, 2006. **31**(15): 3227-3234.

61.   Al-Itry, R., K. Lamnawar and A. Maazouz, *Improvement of thermal stability, rheological and mechanical properties of PLA, PBAT and their blends by reactive extrusion with functionalized epoxy.* Polymer Degradation and Stability, 2012. **97**(10): 1898-1914.

62.   Kumar, R., M. Yakubu and R. Anandjiwala, *Biodegradation of flax fiber reinforced poly lactic acid.* 2010.

63.   Mathew, A.P., K. Oksman and M. Sain, *Mechanical properties of biodegradable composites from poly lactic acid (PLA) and microcrystalline cellulose (MCC).* Journal of applied polymer science, 2005. **97**(5): 2014-2025.

III.2.4. Effect of different compatibilizers on injection-molded green composite pieces based on polylactide filled with almond shell flour

L. Quiles-Carrillo [1], N. Montanes [1], D. Garcia-Garcia [1], A. Carbonell-Verdu [1], R.Balart [1] and S. Torres-Giner [1,2,]

[1] Technological Institute of Materials (ITM), Universitat Politècnica de València (UPV), Plaza Ferrándiz y Carbonell 1, 03801 Alcoy, Spain;

[2] Novel Materials and Nanotechnology Group, Institute of Agrochemistry and Food Technology (IATA), Spanish National Research Council (CSIC), Calle Catedrático Agustín Escardino Benlloch 7, 46980 Paterna, Valencia, Spain

Composites Part B: engineering

2018, 147:76-85

Effect of different compatibilizers on injection-molded green composite pieces based on polylactide filled with almond shell flour

L. Quiles-Carrillo[a], N. Montanes[a], D. Garcia-Garcia[a], A. Carbonell-Verdu[a], R. Balart[a], S. Torres-Giner[a,b,*]

[a] Technological Institute of Materials (ITM), Universitat Politècnica de València (UPV), Plaza Ferrándiz y Carbonell 1, 03801 Alcoy, Spain
[b] Novel Materials and Nanotechnology Group, Institute of Agrochemistry and Food Technology (IATA), Spanish Council for Scientific Research (CSIC), Calle Catedrático Agustín Escardino Benlloch 7, 46980 Paterna, Spain

A B S T R A C T

Green composites made of polylactide (PLA) filled with almond shell flour (ASF), at a constant weight content of 25 wt.-%, were manufactured by injection molding. In order to increase the interfacial adhesion between the biopolymer and the lignocellulosic filler, three different compatibilizers were tested, namely multi-functional epoxy-based styrene-acrylic oligomer (ESAO), aromatic carbodiimide (AC), and maleinized linseed oil (MLO). The effect of each compatibilizer on the thermal, mechanical, and thermomechanical properties and water uptake of the injection-molded PLA/ASF pieces was analyzed. The obtained results indicated that all the here-studied compatibilizers had a positive influence on both the thermal stability and the mechanical and thermomechanical performance of the green composite pieces but a low impact on their water uptake profile. In addition, the morphological analysis performed at the fracture surfaces of the green composite pieces revealed that the filler–matrix gap was substantially reduced. Among the tested compatibilizers, ESAO and MLO yielded the highest performance in terms of mechanical strength and ductility, respectively. In the case of MLO, it also offers the advantage of being a plant-derived additive so that its application in green composites positively contributes to the development of sustainable polymer technologies.

1. Introduction

Nowadays, the increasing concern about environmental issues derived from the use of non-recyclable and petroleum-derived materials is promoting the development of environmentally friendly high-performance polymer materials [1]. Green composites represent an interesting sustainable solution as they are typically made of a biopolymer matrix and a plant-derived filler [2,3]. These materials are being increasingly applied in a wide variety of sectors such as automotive, building and construction, packaging, etc. [4–8]. Furthermore, the use of green composites is gaining an increasing interest in the Circular Economy since these materials are not only obtained from natural resources but they can also be fully disintegrated under controlled compost conditions [9]. In the emerging bioplastics market, polylactide (PLA) is currently considered the front runner due to its good balance between physical properties and its two-fold environmental advantage of being a bio-based and biodegradable material [10].

From an environmental point of view, lignocellulosic materials obtained from industrial by-products and food or agroforestry waste are also gaining certain relevance as cost-effective fillers due to their positive dual contribution on natural origin and biodegradability, i.e. disintegration in compost soil [11,12]. In recent years, it has been reported the use of a wide variety of these plant-derived fillers such as rice hull [13–15], peanut skin [16,17], Posidonia oceanica seagrass [18], corn cob and sunflower hull [19], pineapple flour [20], etc. In this context, almond shell flour (ASF) particles are very promising fillers in green composites due to the increasing consumption of pastries, almond milk, and other almond-derived products in the food industry [21,22]. In particular, the worldwide annual production of almond (Prunus amygdalus L.) is 2.31 million tons from a land area of 1.7 million hectare [23], being Spain the second biggest producer with approximately 0.3 million tons. Since the almond by-products, i.e. hulls and shells, account for more than 50% by dry weight of the almond fruit [24], it is estimated that around 0.8–1.7 million tons of them are annually wasted [25]. Therefore, the use of this agro-food waste currently represents a smart solution to generate high-added value materials in the plastic industry [26,27].

* Corresponding author. Institute of Agrochemistry and Food Technology (IATA), Spanish Council for Scientific Research (CSIC), Calle Catedrático Agustín Escardino Benlloch 7, 46980 Paterna, Spain.
E-mail addresses: storresginer@iata.csic.es, storresginer@upv.es (S. Torres-Giner).

Effect of different compatibilizers on injection-molded green composite pieces based on polylactide filled with almond shell flour

Abstract.

Green composites made of polylactide (PLA) filled with almond shell flour (ASF), at a constant weight content of 25 wt.-%, were manufactured by injection molding. In order to increase the interfacial adhesion between the biopolymer and the lignocellulosic fillers, three different compatibilizers were tested, namely multi-functional epoxy-based styrene-acrylic oligomer (ESAO), aromatic carbodiimide (AC), and maleinized linseed oil (MLO). The effect of each compatibilizer on the thermal, mechanical, and thermomechanical properties and water uptake of the injection-molded PLA/ASF pieces was analyzed. The obtained results indicated that all the here-studied compatibilizers had a positive influence on both the thermal stability and the mechanical and thermomechanical performance of the green composite pieces but a low impact on their water uptake profile. In addition, the morphological analysis performed at the fracture surfaces of the green composite pieces revealed that the filler–matrix gap was substantially reduced. Among the tested compatibilizers, ESAO and MLO yielded the highest performance in terms of mechanical strength and ductility, respectively. In the case of MLO, it also offers the advantage of being a plant-derived additive so that its application in green composites positively contributes to the development of sustainable polymer technologies.

INTRODUCTION

Nowadays, the increasing concern about environmental issues derived from the use of non-recyclable and petroleum-derived materials is promoting the development of environmentally friendly high-performance polymer materials [1]. Green composites represent an interesting sustainable solution as they are typically made of a biopolymer matrix and a plant-derived filler [2, 3]. These materials are being increasingly applied in a wide variety of sectors such as automotive, building and construction, packaging, etc. [4-8]. Furthermore, the use of green composites is gaining an increasing interest in the Circular Economy since these materials are not only obtained from natural resources but they can also be fully disintegrated under controlled compost conditions [9]. In the emerging bioplastics market, polylactide (PLA) is currently considered the front runner due to its good balance between physical properties and its two-fold environmental advantage of being a bio-based and biodegradable material [10].

From an environmental point of view, lignocellulosic materials obtained from industrial by-products and food or agroforestry waste are also gaining certain relevance as cost-effective fillers due to their positive dual contribution on natural origin and biodegradability, i.e. disintegration in compost soil [11,12]. In recent years, it has been reported the use of a wide variety of these plant-derived fillers such as rice hull [13-15], peanut skin [16, 17], Posidonia oceanica seagrass [18], corn cob and sunflower hull [19], pineapple flour [20], etc. In this context, almond shell flour (ASF) particles are very promising fillers in green composites due to the increasing consumption of pastries, almond milk, and other almond-derived products in the food industry [21, 22]. In particular, the worldwide annual production of almond (*Prunus amygdalus L.*) is 2.31 million tons from a land area of 1.7 million hectare [23], being Spain the second biggest producer with approximately 0.3 million tons. Since the almond by-products, i.e. hulls and shells, account for more than 50% by dry weight of the almond fruit [24], it is estimated that around 0.8–1.7 million tons of them are annually wasted [25]. Therefore, the use of this agro-food waste currently represents a smart solution to generate high-added value materials in the plastic industry [26, 27].

Unfortunately, there are some drawbacks related to the incorporation of lignocellulosic fillers into polymers, which are mainly ascribed to their poor filler–matrix interfacial adhesion and the potential formation of particle aggregates. In general, polymers, including biopolyesters, are highly hydrophobic or low hydrophilic whereas the lignocellulosic fillers are extremely hydrophilic [28]. Such low chemical affinity is certainly responsible for their lack of compatibility, thus leading to green composite materials with poor overall physical properties [29-31]. In most cases, this fact particularly induces an impairment on the mechanical ductility and thermal stability of the resultant green composites [32].

The use of compatibilizers currently represents a straightforward strategy to enhance the interfacial adhesion between the lignocellulosic fillers and a wide range of polymer matrices [16, 33, 34]. Reactive compatibilizers are specifically designed to form chemical bridges during the melt processing between the two distinct phases that constitute the polymer composites, the so-called reactive extrusion (REX) [35].

Compatibilization in composites is achieved by the melt grafting of the fillers onto the biopolymer through the use of chemical structures with at least two average functionalities (*f*) [36]. Indeed, most commercially available reactive compatibilizers consist of polymers with low molecular weight (M_W) or oligomers in which a certain number of functional groups (*e.g.* epoxy and maleic anhydride groups) are prone to react during melt processing [37]. If the main polar polymer chains that constitute the matrix of the polymer composite are characterized by terminal hydroxyl and carboxylic acid groups, these can then establish chemical reactions with some functional groups of the compatibilizer. In addition, due to the compatibilizer presents $f \geq 2$, other functional groups can also react with the hydroxyl groups exposed on the surface of the lignocellulosic filler. In this sense, both epoxy and maleic anhydride groups have been reported to efficiently react with the hydroxyl groups of both the PLA chains and cellulose on the fillers surface [38, 39]. Moreover, as these additives can additionally offer a chain-extension effect, these can positively reduce hydrolytic degradation during manufacturing and then improve melt stability [40-43].
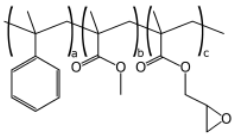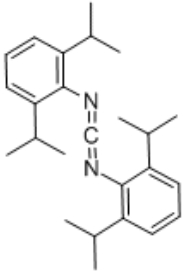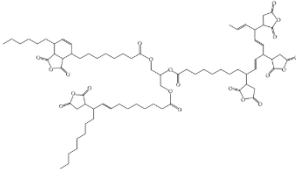
This work originally reports on the effect of three reactive compatibilizers based on different chemical functionalities, namely epoxy, carbodiimide, and maleic anhydride on PLA/ASF composite pieces obtained by injection molding. To this end, the thermal, mechanical, thermomechanical properties as well as morphology and water uptake of the injection-molded green composite pieces were characterized and related to the type of compatibilizer employed.

EXPERIMENTAL

Materials

Aliphatic polyester PLA was Ingeo™ biopolymer 6201D, obtained from NatureWorks (Minnetonka, MN, USA). This is a PLA grade with a density of 1.24 g cm^{-3} and a met flow rate (MFR) of 15–30 g/10 min (210 °C and 2.16 kg), which makes it suitable for injection molding. Almond was collected in the Sierra Mariola region and the shells were provided by Jesol Materias Primas S.A. (Valencia, Spain) as an industrial by-product after seed extraction. Multi-functional epoxy-based styrene-acrylic oligomer (ESAO), aromatic carbodiimide (AC), and maleinized linseed oil (MLO) were used as the compatibilizers. **Table III.2.4.1** summarizes their commercial information, chemical structures, and relevant properties provided by the manufacturers.

Table III.2.4.1. Summary of the different compatibilizers with their main relevant information.

Compatibilizer	Commercial name	Supplier	Chemical structure	Description
Epoxidized styrene-acrylic oligomer (ESAO)	Joncryl® ADR 4368-C	BASF S.A. (Barcelona, Spain)		Molecular weight (M_w) = 6800 g/mol Glass transition temperature (T_g) = 54 ºC Epoxy equivalent weight (EE_w) = 285 g/mol
Aromatic carbodiimide (AC)	BioAdimide® 500 XT	Rhein Chemie Rheinau GmbH (Mannheim, Germany)		Carbodiimide content (CC) > 13%
Maleinized linseed oil (MLO)	VEOMER LIN	Vandeputte (Mouscron, Belgium)		Viscosity = 1,000 cP (20°C) Acid value (AV) = 105–130 mg KOH/g

Preparation of green composites

Prior to processing, ASF was prepared as described in our previous research [39]. Briefly, the as-received almond shells were ground in an SK 100 Cross Beater mill from Retsch GmbH (Düsseldorf, Germany) at a rotating speed of 10,000 rpm. The resultant flour was then processed in a RP09 CISA® (Barcelona, Spain) sieve shaker to obtain a flour with a homogenous particle size distribution with a top-cut of 150 μm.

All materials were dried in a dehumidifier MDEO from Industrial Marsé (Barcelona, Spain) at a temperature of 60 °C for 36 h. ESAO was not dried due to its low glass transition temperature (T_g = 54 °C). A fixed weight content of 25 wt.-% of ASF in PLA was set while each compatibilizer was added at 1 part per hundred resin (phr) of composite. A neat PLA sample and a PLA/ASF sample without any compatibilizer were produced in the same conditions as the control materials.

Materials were melt compounded in a co-rotating twin-screw extruder from Construcciones Mecanicas Dupra, S.L. (Alicante, Spain). The screws feature 25 mm diameter with a length-to-diameter ratio, *i.e.* L/D, of 24. All materials were fed through the main hopper. The temperature profile was set as follows: 180 °C (feeding zone), 185 °C, 190 °C, and 195 °C (die). A rotating speed of 20 rpm was selected. Residence time was approximately 1 min. The extruded materials were finally pelletized using an air-knife unit.

The resultant green composite pellets were shaped into pieces by injection molding in a Meteor 270/75 from Mateu & Solé (Barcelona, Spain). The temperature profile was set as follows: 170 °C (hopper), 175 °C, 180 °C, and 185 °C (injection nozzle). A clamping force of 75 tons was applied. The cavity filling and cooling time were set at 1 and 10 s, respectively. Pieces with a thickness of approximately 4 mm were obtained.

Scanning electron microscopy

The morphologies of the ASF particles and the fractured surfaces of the green composite samples after the impact test were observed by field emission scanning electron microscopy (FESEM). This was performed in a ZEISS ULTRA 55 from Oxford Instruments (Abingdon, United Kingdom). Samples surfaces were coated, prior to analysis, with a gold-palladium alloy in a Quorum Technologies Ltd EMITECH model SC7620 sputter coater (East Sussex, UK). An acceleration voltage of 2 kV was applied. Sizes were determined using Image J Launcher v 1.41 and the data presented were based on measurements from a minimum of 50 SEM micrographs.

Color measurements

A Konica CM-3600d Colorflex-DIFF2, from Hunter Associates Laboratory, Inc. (Reston, Virginia, USA) was used for the color measurement. Color indexes (L*, a*, and b*) were measured according to following criteria: L* = 0, darkness; L* = 100, lightness; +a* = red, -a* = green; and +b* = yellow, -b* = blue. Measurements were done in triplicate.

Thermal characterization

Main thermal transitions of green composite pieces were obtained by differential scanning calorimetry (DSC) in a Mettler-Toledo 821 calorimeter (Schwerzenbach, Switzerland). An average sample weight ranging from 5 to 7 mg was subjected to a thermal cycle as follows: First heating from 30 °C to 200 °C, cooling down to 0 °C, and second heating to 350 °C. Heating and cooling rates were set at 10 °C·min^{-1}. All tests were run in nitrogen atmosphere (66 mL min^{-1}) with standard sealed aluminium crucibles of a volume capacity of 40 µL. The degree of crystallinity (X_c) was calculated by using the following expression (**Equation III.2.4.1**):

$$X_C = \left[\frac{\Delta H_m - \Delta H_{CC}}{\Delta H_m^0 \cdot (1 - w)} \right] \cdot 100 \qquad \textbf{Equation III.2.4.1}$$

Where ΔH_m and ΔH_{CC} (J g⁻¹) stand for the melt and cold crystallization enthalpies respectively, (ΔH_m^0) (J g⁻¹) represents the theoretical melt enthalpy of a fully crystalline PLA, i.e. 93.0 J g−1 [44], and 1-w corresponds to the weight fraction of PLA in the sample.

Thermal stability (degradation/decomposition) was determined by thermogravimetric analysis (TGA) in a Mettler-Toledo TGA/SDTA 851 thermobalance. Samples with an average weight comprised between 5 and 7 mg were placed in standard alumina crucibles of 70 µL and subjected to a heating program from 30 °C to 700 °C at a heating rate of 20 °C·min⁻¹ in air atmosphere.

Mechanical characterization

Tensile and flexural tests were carried out in a mechanical universal testing machine ELIB 50 from S.A.E. Ibertest (Madrid, Spain) as recommended by ISO 527 and ISO 178, respectively. This was equipped with a 5-kN load cell. A cross-head speed was set to 5 mm min⁻¹ in both tests. Hardness was measured using the Shore D scale in a durometer model 676-D from J. Bot Instruments (Barcelona, Spain) as recommended by ISO 868. Impact strength was obtained in a 6-J Charpy pendulum from Metrotec (San Sebastián, Spain) following ISO 179. All mechanical tests were performed at room temperature testing at least six different specimens per sample.

Thermomechanical characterization

The thermomechanical properties of the green composite pieces were studied by measuring the Vicat softening temperature (VST) and the heat deflection temperature (HDT) in a Vicat/HDT station VHDT 20 from Metrotec S.A. (San Sebastián, Spain). VST values were obtained according ISO 306 by the B50 method. The applied force was 50 N and the heating rate was 50 °C·h⁻¹. HDT measurements were carried out according to ISO 75 with a distance between supporting edges of 60 mm and an applied weight of 320 g. Samples sizing $4 \times 10 \times 80$ mm³ were heated at 120 °C·h⁻¹. Tests were performed in triplicate.

Dynamical mechanical thermal analysis (DMTA) was conducted in an oscillatory rheometer AR-G2 from TA Instruments (New Castle, USA) equipped with a special clamps system for solid samples working in torsion-shear mode. Samples with dimensions of $4 \times 10 \times 40$ mm³ were subjected to a temperature sweep program from 40 °C to 100 °C at a heating rate of 2 °C·min⁻¹, a frequency of 1 Hz, and a maximum shear deformation (ɣ) of 0.1%.

Water uptake characterization

Injection-molded samples of $4 \times 10 \times 80$ mm³ were immersed in distilled water at 23 ± 1 °C. The samples were taken out and weighed weekly using an analytical balance with a precision of ± 0.1 mg, after removing the residual water with a dry cloth. The evolution of the water absorption was followed for a period of 15 weeks. Measurements were performed in triplicate.

RESULTS AND DISCUSSION

Fillers morphology

The morphology of the ASF particles is shown in the FESEM images of **Figure III.2.4.1**. As it can be observed in **Figure III.2.4.1a**, the fillers presented an irregular shape with a great variety of diameters. The particle size was approximately 75 µm, as it can be seen in the histogram of the ASF powder. Further magnification of the particles, shown in **Figure III.2.4.1b**, revealed the presence of some voids and granular features in their surface, which resemble the original porous-like structure of almond shell. The ASF particles also showed a rough surface, which can be a consequence of the crushing process due to the high hardness of the almond shell. A similar morphology for ASF particles has been reported in previous studies of polymer composites [26, 39, 45].
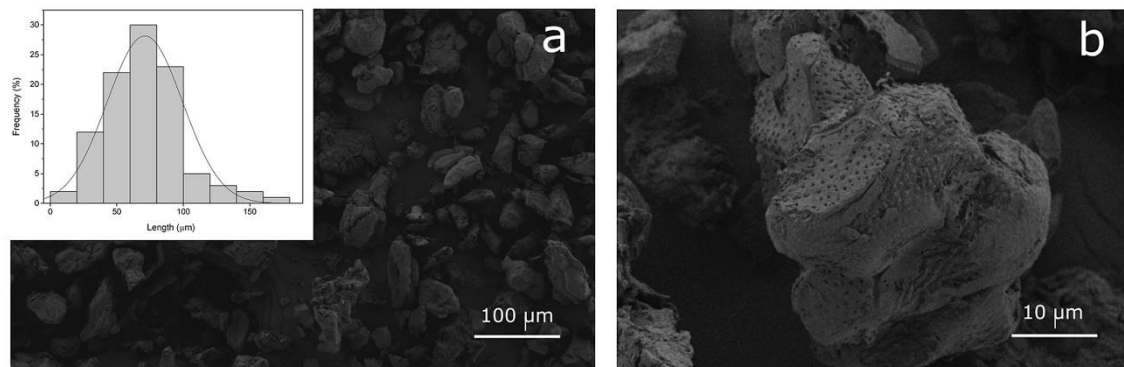
Figure III.2.4.1. Field emission scanning electron microscopy (FESEM) images of almond shell flour (ASF) particles taken at: a) 100x with a scale marker of 100 µm and the ASF powder histogram; b) 500x with a scale marker of 10 µm.

Appearance of green composite pieces

Figure III.2.4.2 shows the appearance of the resultant injection-molded green composite pieces. It can be seen that the incorporation of ASF into PLA resulted in pieces with a dark brown color, which corresponds to the natural color of almond shell. In general, all green composites presented similar color characteristics with different intensities depending on the compatibilizer used. **Table III.2.4.2** summarizes the color indexes ($L^*a^*b^*$) of the injection-molded pieces. The piece with the darkest color, i.e. the sample with the lowest lightness, corresponded to the uncompatibilized green composite. This presented a L^* value of 26.4, while the a^* and b^* color coordinates were 3.5 and 3.6, respectively. Indeed, all injection-molded pieces showed positive values for the a^* and b^* color coordinates, confirming that the incorporation of ASF produced a reddish- or brownish-like color. The three compatibilizers generated pieces with a lighter brown color, showing L^* values in the 28–32 range, being the lightest coloration observed for the MLO-treated piece. Therefore, the ASF incorporation delivered a wood-like color and surface finish, which can be interesting from an aesthetical perspective in packaging materials such as food trays for fruits and vegetables.
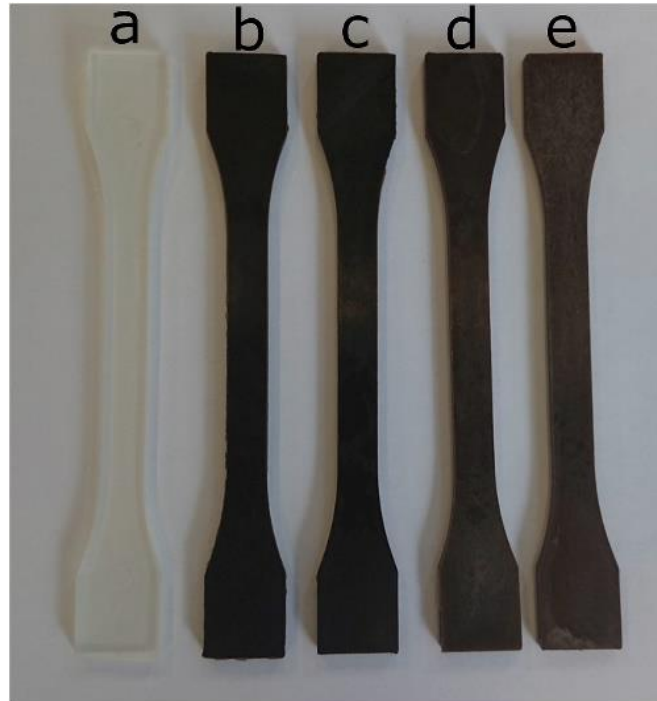
Figure III.2.4.2. Surface aspect of the injection-molded pieces made of: a) Neat polylactide (PLA); b) Uncompatibilized PLA/almond shell flour (ASF); c) Compatibilized PLA/ASF with multi-functional epoxy-based styrene-acrylic oligomer (ESAO); d) Compatibilized PLA/ASF with aromatic carbodiimide (AC); e) Compatibilized PLA/ASF with maleinized linseed oil (MLO).

Table III.2.4.2. Color indexes ($L*$, $a*$, $b*$) of the injection-molded pieces made of neat polylactide (PLA) and its green composites with almond shell flour (ASF) compatibilized with multi-functional epoxy-based styrene-acrylic oligomer (ESAO), aromatic carbodiimide (AC), and maleinized linseed oil (MLO).

Sample	L^*	a^*	b^*
PLA	94.1±0.15	-1.1±0.05	1.4±0.1
PLA/AHF	26.4±0.18	3.49±0.12	3.61±0.23
PLA/AHF + ESAO	28.43±0.27	3.41±0.19	3.28±0.14
PLA/AHF + AC	29.52±0.22	4.95±0.16	6.48±0.20
PLA/AHF + MLO	31.95±0.14	5.31±0.22	6.34±0.0.15

Thermal properties of green composite pieces

Figure III.2.4.3 shows the DSC curves corresponding to the second heating run of the injection-molded pieces of neat PLA and its green composites processed with the different compatibilizers. Their main thermal parameters are included in **Table III.2.4.3**.
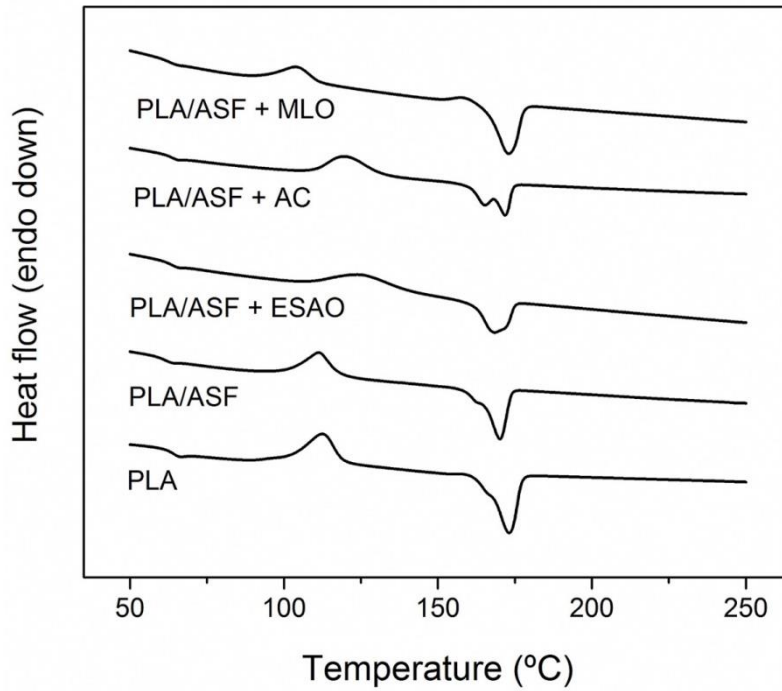
Figure III.2.4.3. Differential scanning calorimetry (DSC) curves of the injection-molded pieces made of neat polylactide (PLA) and its green composites with almond shell flour (ASF) compatibilized with multi-functional epoxy-based styrene-acrylic oligomer (ESAO), aromatic carbodiimide (AC), and maleinized linseed oil (MLO).

Table III.2.4.3. Thermal properties obtained from the differential scanning calorimetry (DSC) curves in terms of normalized enthalpy of cold crystallization (ΔH_{cc}), cold crystallization temperature (T_{cc}), normalized enthalpy of melting (ΔH_m), melting temperature (Tm), and percentage of crystallinity (X_c) of the injection-molded pieces made of neat polylactide (PLA) and its green composites with almond shell flour (ASF) compatibilized with multi-functional epoxy-based styrene-acrylic oligomer (ESAO), aromatic carbodiimide (AC), and maleinized linseed oil (MLO).

Sample	ΔH_c (J g^{-1})	T_c (°C)	ΔH_m (J g^{-1})	T_m (°C)	X_c (%)
PLA	25.1±0.6	112.5±1.1	33.7±0.4	172.1±1.1	14.8±0.4
PLA/AHF	22.6±0.6	111.4±0.9	30.9±0.3	169.6±0.9	11.9±0.3
PLA/AHF + ESAO	22.3±0.7	125.3±0.8	24.6±0.3	167.8±1.0	3.4±0.4
PLA/AHF + AC	25.5±0.5	120.0±0.9	25.0±0.3	171.3±0.8	1.0±0.3
PLA/AHF + MLO	10.6±0.6	103.9±1.0	31.6±0.4	172.3±0.9	30.5±0.4

In relation to the neat PLA piece, the initial change in slope located between 55 °C and 65 °C is associated to its glass transition temperature (T_g). The exothermic peak in the 105–130 °C range corresponds to the cold crystallization process, showing a crystallization temperature (T_{cc}) of 112.5 °C. Cold crystallization is typically observed

in PLA-based articles, which is produced due to an internal rearrangement of the quenched-in amorphous domains from cooling into ordered/packed (crystalline) regions when chain mobility increases above T_g [46]. During this process, imperfect crystals of PLA are formed from unmelted ones acting as nuclei. The ASF incorporation into PLA slightly reduced the cold crystallization temperature, i.e. Tcc was 111.4 °C, which can be related to a nucleation ability of the fillers [46]. The addition of different compatibilizers generated more intense effects on the cold crystallization process. Whereas the green composite pieces compatibilized with ESAO and AC presented the cold crystallization process at higher temperatures, T_{cc} of *ca.* 125 and 120 °C, respectively, MLO induced the opposite effect and T_{cc} moved towards lower temperatures, *i.e.* 103.9 °C. This can be related to the significant plasticizing effect that MLO, similar to other multi-functionalized vegetable oils, can provide to the PLA matrix [10, 39, 47].

With regard to the melting temperature (T_m), it can be observed that the presence of ASF also reduced T_m by approximately 3 °C. It is then expected that the presence of ASF slightly disrupted the folding process of the PLA chains, avoiding the formation of more perfect crystals. A similar value of T_m was observed for the green composite piece compatibilized with ESAO. However, interestingly, the addition of AC and MLO maintained the original T_m of PLA, *i.e.* approximately 172 °C, which indicates that both compatibilizers did not interfere with the lamellae growth of the spherulites. For the case of AC, however, melting took place in two peaks. This can be related a process of crystal reorganization upon melting, by which less perfect crystals can order into spherulites with thicker lamellar thicknesses than thereafter melt at higher temperatures. In relation to the degree of crystallinity (X_c), it can be observed that the neat PLA piece and the uncompatibilized green composite piece presented a similar degree of crystallinity of approximately 9% and 12%, respectively. However, the addition of ESAO and AC considerably reduced the amount of crystallinity of the green composite pieces down to values of 3.3% and 0.9%, respectively. Therefore, ESAO and AC seem to restrict crystallization in PLA, which can be caused by intermolecular chain-extension reactions that would contribute to avoid the formation of more packed and ordered regions [48]. Interestingly, MLO provided the opposite effect in comparison to the two other compatibilizers. In particular, X_c increased up to values of 30.5% in the MLO-treated green composite piece. Similar findings have been recently reported by Balart *et al.* [38] for PLA/hazelnut shell flour (HSF) composites compatibilized with epoxidized linseed oil (ELO). This increase was related to the plasticizing effect of the vegetable oil, which both enhanced chain mobility and lowered polymer–polymer interactions. As a result, the PLA chains in the green composites compatibilized with MLO were more prone to order.

TGA curves of the ASF powder as well as of the neat PLA and the PLA/ASF composite pieces treated with the different compatibilizers are gathered in **Figure III.2.4.4**. Regarding the ASF powder, its degradation was similar to that observed for other lignocellulosic materials [49, 50]. First weight loss is related to residual water removal, produced at 80–150 °C. The second degradation step was observed in the 220–300 °C range, which was the highest weight loss, and it corresponds to the hemicelluloses and cellulose degradation. Although lignin starts degradation around 250 °C, it degrades more slowly, contributing for the progressive weight loss up to

500 °C. Early stages of lignin degradation overlap with cellulose and hemicellulose degradation [51].
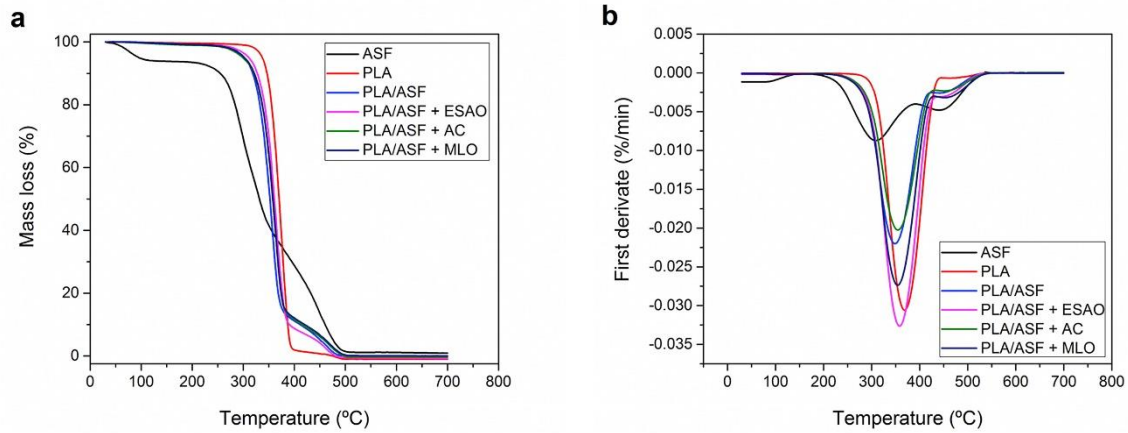
Figure III.2.4.4. Thermal stability of the injection-molded pieces made of neat polylactide (PLA) and its green composites with almond shell flour (ASF) compatibilized with multi-functional epoxy-based styrene-acrylic oligomer (ESAO), aromatic carbodiimide (AC), and maleinized linseed oil (MLO) in terms of: a) Thermogravimetric analysis (TGA) curves; b) Derivative thermogravimetric (DTG) curves.

In relation to the thermal degradation profile of injection-molded pieces, one can observe that PLA decomposed in a single step, starting approximately at 320 °C and with a degradation temperature (T_{deg}) located at 370 °C. Degradation of the uncompatibilized PLA/ASF composite piece differed from that of the neat PLA and it proceeded in two steps. First weight loss initiated at 300 °C, which indicates that the ASF incorporation reduced the thermal stability of PLA by around 30 °C. This may involve the initial degradation of low-M_W components of almond shell such as hemicellulose. Second weight loss was less pronounced. It appeared in the 370–490 °C range, which corresponds to the thermal degradation of both PLA and cellulose. This slope change, observed between 400 and 420 °C, can be attributed to the above-indicated degradation of the lignin present in ASF.

As it can be seen in **Table III.2.4.4**, the addition of all compatibilizers induced a positive effect on the thermal stability of the green composites. Thermal degradation values were delayed up to 10 °C in comparison to the unmodified green composite, being the highest improvement observed for the ESAO-compatibilized piece. This enhancement in the thermal stability suggests certain chemical interaction of the compatibilizers with both components of the composite, by which the resultant linked fillers are expected to act as a physical barrier that obstructs the removal of volatile products produced during decomposition.

Table III.2.4.4. Thermal properties obtained from the thermogravimetry analysis (TGA) curves of the injection-molded pieces made of neat polylactide (PLA) and its green composites with almond shell flour (ASF) compatibilized with multi-functional epoxy-based styrene-acrylic oligomer (ESAO), aromatic carbodiimide (AC), and maleinized linseed oil (MLO). Residual mass was determined at 700 °C.

Sample	1st step			2nd step		
	Onset (°C)	EndSet (°C)	Residual mass (%)	Onset (°C)	EndSet (°C)	Residual mass (%)
PLA	334.6±1.1	392.6±1.0	2.1±0.2	-	-	0.7±0.1
PLA/AHF	315.5±1.0	373.3±1.2	15.0±0.3	373.3±1.0	486.0±0.9	0.9±0.1
PLA/AHF + ESAO	317.3±0.1	383.7±1.1	10.2±0.2	383.7±1.0	490.9±1.0	0.6±0.1
PLA/AHF + AC	311.0±0.9	377.6±1.0	14.0±0.2	377.6±1.0	494.8±1.1	0.7±0.1
PLA/AHF + MLO	315.5±1.0	378.8±1.0	14.2±0.2	378.8±.0	463.0±1.0	0.8±0.1

Mechanical properties of green composite pieces

Figure III.2.4.5 shows the effect of the different compatibilizers on both the tensile and flexural properties. With regard to the tensile properties, the incorporation of ASF into PLA produced an increase of the elastic modulus values. While the neat PLA piece presented a tensile modulus of 1.96 GPa, the green composite piece showed a value 2.54 GPa. However, the injection-molded piece also became more brittle since the elongation at break was reduced from 5.2%, for the neat PLA piece, to 2.1%, for the uncompatibilized green composite piece. This can be related to the absence (or very poor) interaction of ASF with the PLA matrix. As a matter of fact, the tensile strength varied from 63.3 MPa, for the neat PLA piece, down to 39.7 MPa, for the uncompatibilized green composite piece. It is considered that the lignocellulosic filler acted as a stress concentrator, being responsible for lowering the elongation at break and the tensile strength. Since the elastic modulus relates both the tensile strength and elongation at break, and the reduction of the latter property was much more pronounced, this supports the increase observed in the modulus after the ASF incorporation into the PLA pieces.

Interestingly, the addition of all three compatibilizers provided a positive effect on the green composite pieces in terms of tensile strength and, particularly, elongation at break. The highest improvement in tensile strength was observed for the green composite pieces compatibilized with ESAO and AC. In particular, the values of tensile strength increased in the ESAO- and AC-treated green composite pieces up to 52.2 MPa and 51.2 MPa, respectively. This is an indication of the positive effect of the compatibilizers on the material cohesion, which provided a more efficient load transfer from the dispersed ASF particles to the PLA matrix. In this regard, Awal *et al.* [52] reported similar effects on PLA/cellulose composites compatibilized with carbodiimide. However, although AC offered enhanced mechanical properties for the green composite, the compatibilizing effect of ESAO was still superior since the

mechanical strength increase was accompanied by a higher improvement in ductility. In particular, the elongation at break reached values of 2.6% and 3.3% for the AC- and ESAO-compatibilized green composite pieces, respectively. The latter represents an increase of approximately 55% in relation to the uncompatibilized green composite piece. This effect can be ascribed to the fact that the multiple epoxy groups of ESAO, in addition to react with the terminal groups of PLA, are also able to react with hydroxyl groups exposed on the fillers surface [36]. In this sense, Nagaranjan *et al.* have also reported that epoxy-based chain extenders can be also interesting additives for compatibilization of cellulose and cellulose-derived materials purposes and not only for biopolymer blends [53, 54].
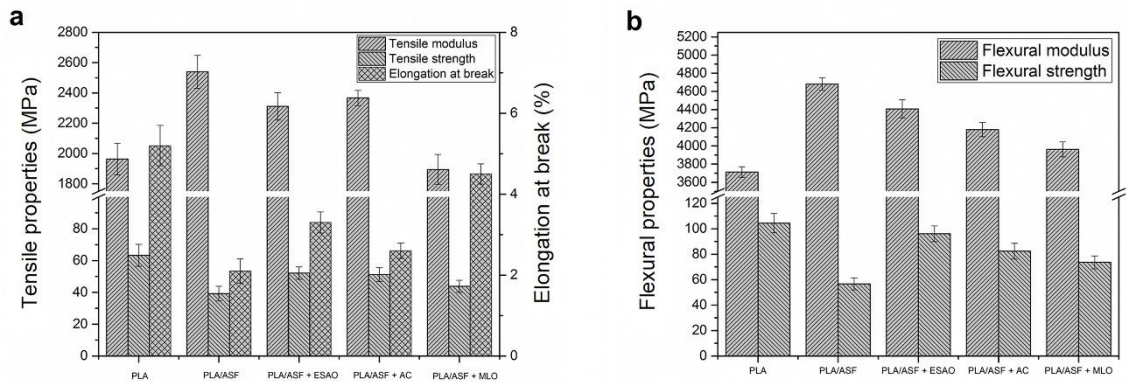
Figure III.2.4.5. Mechanical properties of the injection-molded pieces made of neat polylactide (PLA) and its green composites with almond shell flour (ASF) compatibilized with multi-functional epoxy-based styrene-acrylic oligomer (ESAO), aromatic carbodiimide (AC), and maleinized linseed oil (MLO) in terms of: a) Tensile properties (tensile modulus and tensile strength) and elongation at break); b) Flexural properties (flexural modulus and flexural strength).

In relation to the compatibilizing effect of MLO on the tensile properties of the green composite pieces, this additive provided lower values of tensile modulus and strength than the other two compatibilizers but an extraordinary improvement in mechanical ductility. In particular, the elongation at break increased to 4.5%, which represents an increase of approximately 115% in relation to the uncompatibilized green composite piece. Similar results have been recently observed for PLA/ASF composites compatibilized with different amounts of MLO [39], which was ascribed to the strong plasticization provided by this multi-functionalized vegetable oil. Since the vegetable oil molecules can readily place among the biopolymer chains, then these act as a lubricant with an enhanced influence on chain mobility [55].

The effect of the three compatibilizers was further evaluated by flexural tests. The neat PLA piece presented a flexural modulus of 3.71 GPa and a flexural strength of 104.5 MPa. The uncompatibilized PLA/ASF composite piece showed an increase in the flexural modulus up to 4.68 GPa, but a noticeable decrease in the flexural strength down to 58 MPa. This further supports the poor biopolymer–filler interfacial adhesion. A similar mechanical improvement than that described above for the tensile tests were observed for the different compatibilizers. In particular, ESAO showed the highest flexural improvement since, in comparison to the uncompatibilized green composite, it presented both the lowest reduction in flexural modulus and the highest increase in

flexural strength. In particular, the ESAO-treated green composite piece showed a flexural strength of about 96.1 MPa, which is very close that observed for the neat PLA piece. The green composite pieces compatibilized with AC and MLO presented values of flexural strength of 82.4 and 73.6 MPa, respectively. Therefore, all compatibilizers provided an improvement in the mechanical properties of the PLA/ASF pieces.

As it can be seen in **Table III.2.4.5**, the incorporation of ASF resulted in a noticeable increase of the Shore D hardness. In particular, it increased from 78 to approximately 84, which can be related to the reinforcing effect of a hard filler on the biopolymer matrix. The addition of all three compatibilizers produced similar Shore D hardness values, in the range of the unmodified green composite piece. In relation to impact strength, as opposite to hardness, this was highly affected by both the introduction of ASF and the addition of the different compatibilizers. While the neat PLA piece showed an impact strength of 16.1 kJ m^{-2}, which indicates that it is inherently a brittle material, the uncompatibilized green composite piece presented a value of only 6.2 kJ m^{-2}. This fact can be related to the high content of ASF, *i.e.* 25 wt.-%, that potentially produced high tensile stresses and very low deformation levels along the piece, leading to a low impact-energy absorption. Since the ability of the green composite pieces to absorb energy was remarkably compromised, this represents a crucial drawback of the green composites for most applications from a technical standpoint. Interestingly, the three tested compatibilizers induced a positive effect on impact strength, which were in the range of 8–11 kJ m^{-2}. The highest toughness was observed for the green composite piece compatibilized with MLO, yielding an impact-strength value of 10.1 kJ m^{-2}, which represents a percentage increase of about 63% in comparison to the uncompatibilized PLA/ASF composite piece.

Table III.2.4.5. Shore D hardness, impact strength, Vicat softening temperature (VST), and heat deflection temperature (HDT) of the injection-molded pieces made of neat polylactide (PLA) and its green composites with almond shell flour (ASF) compatibilized with multi-functional epoxy-based styrene-acrylic oligomer (ESAO), aromatic carbodiimide (AC), and maleinized linseed oil (MLO).

Sample	Shore D hardness	Charpy (KJ m^{-2})	VST (°C)	HDT (°C)
PLA	78.0 ± 1.2	16.1 ± 6.1	56.0 ± 1.0	53.9 ± 0.7
PLA/AHF	83.8 ± 1.3	6.2 ± 1.1	77.0 ± 1.2	64.0 ± 1.2
PLA/AHF + ESAO	83.8 ± 1.8	10.1 ± 1.5	79.6 ± 1.6	67.0 ± 0.8
PLA/AHF + AC	83.0 ± 1.6	8.5 ± 1.6	81.8 ± 1.2	67.7 ± 1.2
PLA/AHF + MLO	83.2 ± 2.5	9.1 ± 1.9	81.9 ± 1.3	66.9 ± 1.7

Thermomechanical properties of green composite pieces

Table III.2.4.5 also includes the VST and HDT values of the injection-molded PLA/ASF composite pieces. The neat PLA piece showed a VST of 56 °C while this value increased to 77 °C for the green composite piece containing 25 wt.-% ASF. The addition of the compatibilizers further induced a slight increase in VST, showing values close to 80 °C in all cases. A similar tendency was observed in the case of the HDT values. Whereas the neat PLA piece was characterized by having a HDT value of approximately 54 °C, the unmodified green composite piece presented a value of 64 °C. The three tested compatibilizers slightly improved HDT of the pieces to values in the 66–68 °C range, which is an additional indication of their effect on enhancing the filler–biopolymer interfacial adhesion. Therefore, the service temperature of the PLA-based pieces was increased with the incorporation of ASF while the addition of the compatibilizers reinforced this thermomechanical enhancement.

Figure III.2.4.6 represents the evolution of the storage modulus and damping factor (tan δ) *vs.* temperature for the injection-molded pieces obtained from DMTA. **Figure III.2.4.6a** shows the evolution of the storage modulus for the neat PLA and its green composite pieces. In the case of the neat PLA piece, this presented a storage modulus value of 1.5–1.6 GPa up to 50 °C. Then, the storage modulus sharply decreased by three orders of magnitude in the 50–70 °C range, down to values of 2–3 MPa. This phenomenon corresponds to the alpha (α)-relaxation of the biopolymer, which is ascribed to the glass–rubber transition behavior and relates to the biopolymer's T_g. A second important change was observed in the 80–100 °C range, which is attributed to the cold crystallization process. As previously discussed during the DSC analysis, once the T_{cc} is reached, PLA chains tend to rearrange in a more ordered structure that provides a more thermomechanical resistance. In particular, the storage modulus reached values of approximately 100 MPa. The incorporation of ASF into PLA increased the storage modulus values in the glass region to 1.75–1.9 GPa. Additionally, cold crystallization occurred at lower temperatures, *i.e.* 75–85 °C. This observation confirms that the lignocellulosic fillers acted as a nucleating agent for PLA. In addition, higher storage values, of around 250 MPa, were obtained after the cold crystallization process.
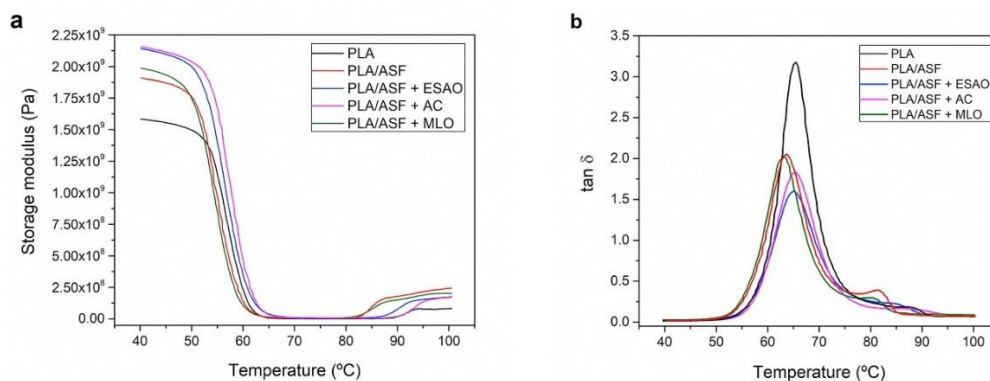
Figure III.2.4.6. Dynamical mechanical thermal analysis (DMTA) curves of the injection-molded pieces made of neat polylactide (PLA) and its green composites with almond shell flour (ASF) compatibilized with multi-functional epoxy-based styrene-acrylic oligomer (ESAO), aromatic carbodiimide (AC), and maleinized linseed oil (MLO) in terms of: a) Storage modulus; b) Damping factor.

In relation to the effect of the different compatibilizers, both ESAO and AC provided a similar thermomechanical improvement. In particular, for these two compatibilizers, the storage modulus increased in the glassy region of the biopolymer up to values of 2–2.2 GPa while the cold crystallization process was observed in a temperature range similar to that of the neat PLA piece. In the case of MLO, the piece presented lower values of storage modulus, particularly below T_g. Indeed, the curve of the green composite piece compatibilized with MLO was located below that of the uncompatibilized green composite at the whole temperature range. This confirms the plasticizing effect provided by MLO. Moreover, a decrease in the cold crystallization process was observed, as previously detected by DSC. According to these findings, the addition of MLO interestingly provided two simultaneous effects. On the one hand, MLO acted as typical plasticizer with a lubricant effect and, on the other hand, it contributed to increasing the PLA–ASF interfacial adhesion. These two phenomena had a positive effect on the overall polymer chain mobility, lowering both T_g and T_{cc} [56, 57].

Figure III.2.4.6b shows the evolution of tan δ versus temperature for PLA and its green composite pieces. The peak represents the α-relaxation of the biopolymer, which relates to its T_g. As it can be observed, the neat PLA piece presented a T_g value of about 63 °C and this value was slightly reduced to the 61–62 °C range for all PLA/ASF composite pieces, with the exception of the MLO-treated piece in which Tg was even lower due to its above-described plasticizing effect on PLA. Therefore, MLO provided increased mobility and free volume, which reduced the biopolymer chain interactions with a direct effect on lowering T_g [58]. Another important behavior to note is the relatively low damping factor observed for the green composite pieces. Whereas the neat PLA piece showed a maximum damping factor of approximately 3.2, this decreased down to values in the 1.5–2 range in the green composite pieces. This reduction implies a lower energy dissipation and reduced toughness due to the presence of the lignocellulosic filler [28]. In particular, the PLA/ASF composite piece with the lowest damping factor, *i.e.* ~1.6, corresponded to the ESAO-compatibilized piece.

Morphology of green composite pieces

Figure III.2.4.7 gathers the FESEM images of the fracture surfaces of the green composite pieces, obtained after the impact tests. The fracture surface of the unmodified green composite, shown in **Figure III.2.4.7a**, revealed the absence of ASF particles. Indeed, the uncompatibilized green composite presented several voids that would correspond to the detached particles after impact, which also copied the granular surface of the ASF particles. It is expected that, as the lignocellulosic fillers did not interact with the PLA matrix, these subsequently acted as stress concentrators. This supports the above-described mechanical results, indicating that the uncompatibilized green composite pieces presented a brittle behavior. **Figure III.2.4.7b** shows the FESEM micrograph corresponding to the green composite piece compatibilized with ESAO. Although some voids can be yet observed after fracture, some ASF particles were attained to the PLA matrix. Interestingly, the embedded ASF particles also broke during fracture, which is an indication of their higher interfacial adhesion with PLA. In addition, the gap between the ASF particles and the surrounding biopolymer matrix was relatively low. This gap can be still detected in some particles (see black arrows)

while it was fully indiscernible in others (see white arrows). With regard to the AC-compatibilized PLA/ASF composite piece, shown in **Figure III.2.4.7c**, it also showed the presence of ASF particles embedded in the PLA matrix. Nevertheless, in this case, a larger gap between the ASF particles and the surrounding PLA matrix was observed (see white arrows). The piece also showed some voids due to the phenomenon of particle debonding while certain plastic deformation of the PLA matrix can be also observed by the presence of long filaments. Finally, the green composite piece compatibilized with MLO, included in **Figure III.2.4.7d**, presented a softer fracture surface with the presence of fully embedded ASF particles. This image also supports the hypothesis that the presence of MLO in the green composites improved ASF wettability based on the plasticization of the PLA matrix [59]. The filler–matrix gaps were relatively low (see white arrows) though some few voids were also discerned. In addition, phase separation of the vegetable oil was not detectable. As a result, the addition of the three here-studied compatibilizers successfully improved the adhesion between the blended components, facilitating a better stress transfer from the filler to the biopolymer matrix.
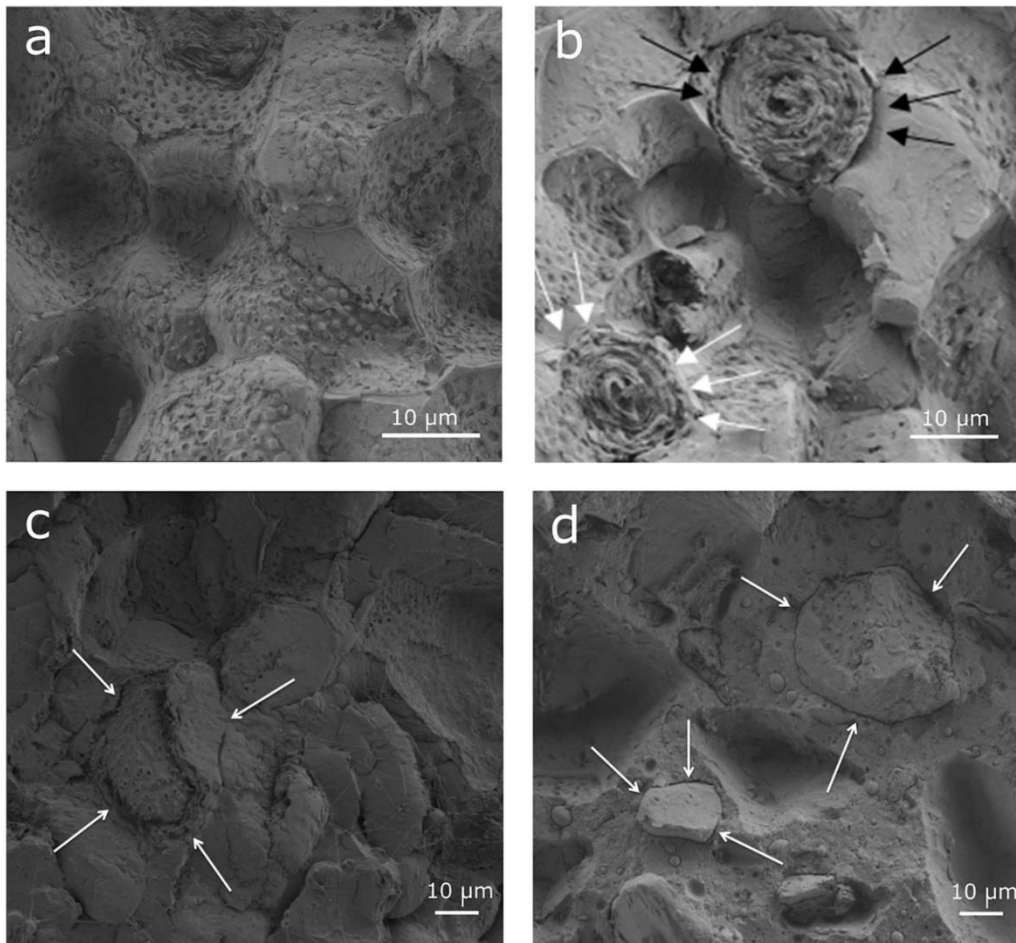
Figure III.2.4.7. Field emission scanning electron microscopy (FESEM) images of the fracture surfaces of the injection-molded pieces made of: a) Uncompatibilized polylactide (PLA)/almond shell flour (ASF); b) Compatibilized PLA/ASF with multi-functional epoxy-based styrene-acrylic oligomer (ESAO); c) Compatibilized PLA/ASF with aromatic carbodiimide (AC); d) Compatibilized PLA/ASF with maleinized linseed oil (MLO). Scale markers of 10 μm.

Water uptake of green composite pieces

One of the most important drawbacks of green composites or any material based on hydrophilic fillers is their tendency to absorb water. **Figure III.2.4.8** shows the evolution of the water uptake of the injection-molded pieces for a period of 15 weeks of immersion in water. The neat PLA piece presented a relatively low water absorption for the whole tested period, with an asymptotic value of approximately 0.7 wt.-%. This observation demonstrates the intrinsic hydrophobic behavior of PLA. However, after the incorporation of ASF, all pieces showed a considerable increase in the values of water uptake up to 4–5 wt.-%. In the case of the unmodified green composite piece, after 15 weeks, the uptake value stabilized at a water content of approximately 4.8 wt.-%. Therefore, the ASF fillers, due to its high number of hydroxyl groups, present a high tendency to trap moisture [60]. The incorporation of ESAO and AC compatibilizers slightly reduced the water uptake profile of the green composite pieces, indicating that the available number of hydroxyl groups exposed to water was reduced. The highest improvement was particularly observed for the ESAO-compatibilized PLA/ASF composite piece, which showed a final water content of approximately 4.2 wt.-%, *i.e.* an improvement of around 14% *vs.* the uncompatibilized green composite piece. Nevertheless, the water uptake increased for the green composite piece compatibilized with MLO. Particularly, its slope during the first weeks was more pronounced, showing a more typical Fickean behavior. This can be related to the above-described plasticizing effect of MLO on the PLA matrix by which its free volume was enlarged, favoring water diffusion.
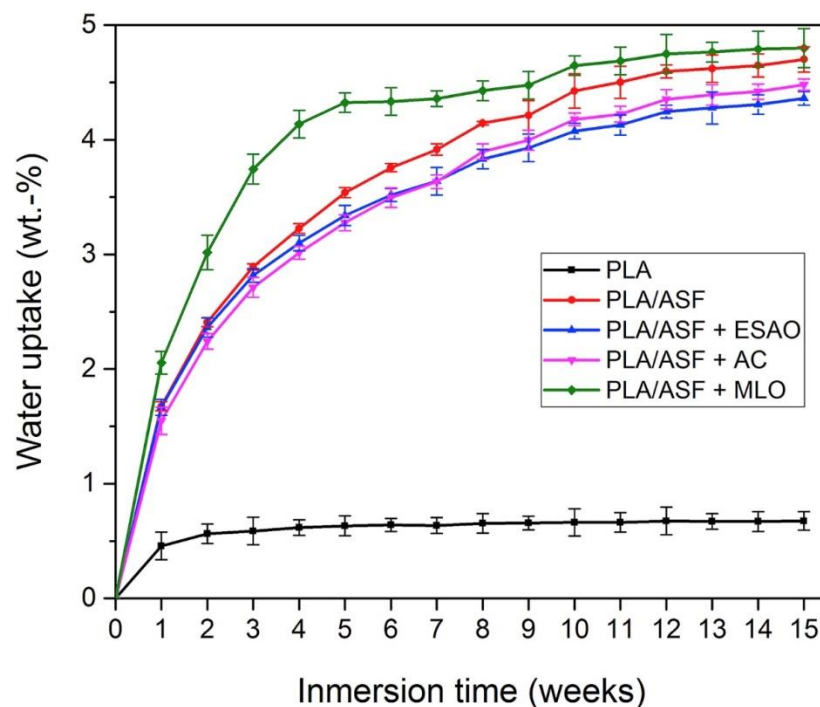
Figure III.2.4.8. Water uptake of the injection-molded pieces made of neat polylactide (PLA) and its green composites with almond shell flour (ASF) compatibilized with multi-functional epoxy-based styrene-acrylic oligomer (ESAO), aromatic carbodiimide (AC), and maleinized linseed oil (MLO).

CONCLUSIONS

Injection-molded green composite pieces based on PLA and ASF at 25 wt.-% are herein presented as an interesting sustainable solution within the Circular Economy concept since these materials are able to upgrade agro-food wastes as well as contribute to reducing the cost of bioplastics. The resultant green composite pieces, however, presented poor physical properties due to the lack of compatibility between PLA and the ASF fillers. The addition of different compatibilizers based on three different chemical functionalities, namely epoxy, carbodiimide, and maleic anhydride, was tested. All three compatibilizers successfully improved the thermal stability, mechanical performance, and thermomechanical properties of the green composite pieces though their effect on water uptake was relatively low. Compatibilization achieved was also supported by the analysis of the fracture surface of the green composites, which showed an enhancement of the interfacial adhesion between the ASF fillers and the PLA matrix. In particular, both ESAO and MLO compatibilizers provided the highest improvement in terms of mechanical strength and ductility, respectively. It was proposed that these compatibilizers, based on multi-functional epoxy and maleic anhydride groups, respectively, are able to enhance the interfacial adhesion of the green composite components by a process of melt grafting of the ASF fillers onto the PLA chains (and partially hydrolyzed PLA chains). In the case of the multi-functionalized vegetable oil, it additionally provided certain plasticization on the PLA matrix. Additionally, compatibilization by MLO represents a more sustainable strategy for providing property enhancement solutions in green composites due to its intrinsic eco-friendly condition. Future in-depth studies are being currently conducted to optimize the content of each compatibilizer as well as to explore the use of novel low-MW additives with different functionalities for the compatibilization of green composites and biopolymer blends.

Acknowledgements

REFERENCES

1. Quiles-Carrillo, L., N. Montanes, T. Boronat, R. Balart and S. Torres-Giner, *Evaluation of the engineering performance of different bio-based aliphatic homopolyamide tubes prepared by profile extrusion.* Polymer Testing, 2017. **61**: 421-429.
2. Faruk, O., A.K. Bledzki, H.-P. Fink and M. Sain, *Biocomposites reinforced with natural fibers: 2000–2010.* Progress in polymer science, 2012. **37**(11): 1552-1596.
3. Shah, D.U., *Developing plant fibre composites for structural applications by optimising composite parameters: a critical review.* Journal of materials science, 2013. **48**(18): 6083-6107.

4.   Dicker, M.P., P.F. Duckworth, A.B. Baker, G. Francois, M.K. Hazzard and P.M. Weaver, *Green composites: A review of material attributes and complementary applications.* Composites part A: applied science and manufacturing, 2014. **56**: 280-289.

5.   Koronis, G., A. Silva and M. Fontul, *Green composites: A review of adequate materials for automotive applications.* Composites Part B: Engineering, 2013. **44**(1): 120-127.

6.   Mohanty, A.K., M. Misra and L. Drzal, *Sustainable bio-composites from renewable resources: opportunities and challenges in the green materials world.* Journal of Polymers and the Environment, 2002. **10**(1-2): 19-26.

7.   Zini, E. and M. Scandola, *Green composites: an overview.* Polymer composites, 2011. **32**(12): 1905-1915.

8.   Masmoudi, F., A. Bessadok, M. Dammak, M. Jaziri and E. Ammar, *Biodegradable packaging materials conception based on starch and polylactic acid (PLA) reinforced with cellulose.* Environmental Science and Pollution Research, 2016. **23**(20): 20904-20914.

9.   Torres-Giner, S., N. Montanes, V. Fombuena, T. Boronat and L. Sanchez-Nacher, *Preparation and characterization of compression-molded green composite sheets made of poly (3-hydroxybutyrate) reinforced with long pita fibers.* Advances in Polymer Technology, 2018. **37**(5): 1305-1315.

10.   Quiles-Carrillo, L., S. Duart, N. Montanes, S. Torres-Giner and R. Balart, *Enhancement of the mechanical and thermal properties of injection-molded polylactide parts by the addition of acrylated epoxidized soybean oil.* Materials & Design, 2018. **140**: 54-63.

11.   Laka, M., S. Chernyavskaya and M. Maskavs, *Cellulose-containing fillers for polymer composites.* Mechanics of composite materials, 2003. **39**(2): 183-188.

12.   Liu, R., Y. Peng, J. Cao and Y. Chen, *Comparison on properties of lignocellulosic flour/polymer composites by using wood, cellulose, and lignin flours as fillers.* Composites Science and Technology, 2014. **103**: 1-7.

13.   Arjmandi, R., A. Hassan, K. Majeed and Z. Zakaria, *Rice husk filled polymer composites.* International Journal of Polymer Science, 2015. **2015**.

14.   Ismail, M., A.A. Yassen and M. Afify, *Mechanical properties of rice straw fiber-reinforced polymer composites.* Fibers and Polymers, 2011. **12**(5): 648.

15.   Wiebeck, H., F.R. Valenzuela-Díaz, F.J. Esper, G.R. Martín-Cortés, W.T. Hennies and M.V. Costa. *Tire Rubber Powder/Rice Husk Ash Polymer Compound*. in *Materials Science Forum*. 2012. Trans Tech Publ.

16.   Garcia-Garcia, D., A. Carbonell-Verdu, A. Jordá-Vilaplana, R. Balart and D. Garcia-Sanoguera, *Development and characterization of green composites from bio-based polyethylene and peanut shell.* Journal of Applied Polymer Science, 2016. **133**(37).

17.   Zaaba, N.F., H. Ismail and M. Jaafar, *Effect of peanut shell powder content on the properties of recycled polypropylene (RPP)/peanut shell powder (PSP) composites.* BioResources, 2013. **8**(4): 5826-5841.

18.   Ferrero, B., V. Fombuena, O. Fenollar, T. Boronat and R. Balart, *Development of natural fiber-reinforced plastics (NFRP) based on biobased polyethylene and waste fibers from Posidonia oceanica seaweed.* Polymer Composites, 2015. **36**(8): 1378-1385.

19.   Fuqua, M.A., V.S. Chevali and C.A. Ulven, *Lignocellulosic byproducts as filler in polypropylene: Comprehensive study on the effects of compatibilization and loading.* Journal of applied polymer science, 2013. **127**(2): 862-868.

20.   Kim, K.-W., B.-H. Lee, H.-J. Kim, K. Sriroth and J.R. Dorgan, *Thermal and mechanical properties of cassava and pineapple flours-filled PLA bio-composites.* Journal of thermal analysis and calorimetry, 2012. **108**(3): 1131-1139.

21.   Valdés, A., O. Fenollar, A. Beltrán, R. Balart, E. Fortunati, J.M. Kenny and M.C. Garrigós, *Characterization and enzymatic degradation study of poly (ε-caprolactone)-based biocomposites from almond agricultural by-products.* Polymer degradation and stability, 2016. **132**: 181-190.

22.   García, A.V., M.R. Santonja, A.B. Sanahuja and M.d.C.G. Selva, *Characterization and degradation characteristics of poly (ε-caprolactone)-based composites reinforced with almond skin residues.* Polymer degradation and stability, 2014. **108**: 269-279.

23. Pirayesh, H., H. Khanjanzadeh and A. Salari, *Effect of using walnut/almond shells on the physical, mechanical properties and formaldehyde emission of particleboard.* Composites Part B: Engineering, 2013. **45**(1): 858-863.

24. Fadel, J., *Quantitative analyses of selected plant by-product feedstuffs, a global perspective.* Animal Feed Science and Technology, 1999. **79**(4): 255-268.

25. Pirayesh, H. and A. Khazaeian, *Using almond (Prunus amygdalus L.) shell as a bio-waste resource in wood based composite.* Composites Part B: Engineering, 2012. **43**(3): 1475-1479.

26. Crespo, J., L. Sanchez, F. Parres and J. Lopez, *Mechanical and morphological characterization of PVC plastisol composites with almond husk fillers.* Polymer composites, 2007. **28**(1): 71-77.

27. Gordobil, O., I. Egüés, R. Llano-Ponte and J. Labidi, *Physicochemical properties of PLA lignin blends.* Polymer Degradation and Stability, 2014. **108**: 330-338.

28. Torres-Giner, S., N. Montanes, O. Fenollar, D. García-Sanoguera and R. Balart, *Development and optimization of renewable vinyl plastisol/wood flour composites exposed to ultraviolet radiation.* Materials & Design, 2016. **108**: 648-658.

29. Borah, J.S. and D.S. Kim, *Recent development in thermoplastic/wood composites and nanocomposites: A review.* Korean Journal of Chemical Engineering, 2016. **33**(11): 3035-3049.

30. La Mantia, F., N.T. Dintcheva, M. Morreale and C. Vaca-Garcia, *Green composites of organic materials and recycled post-consumer polyethylene.* Polymer international, 2004. **53**(11): 1888-1891.

31. Rai, B., G. Kumar, V. Tyagi, R. Diwan and U. Niyogi, *Development and Characterization of Green Composite from Euphorbia Coagulum and Banana Fiber.* Journal of Polymer Materials, 2015. **32**(3): 305.

32. Labidi, S., N. Alqahtani and M. Alejji, *Effect of Compatibilizer on Mechanical and Physical Properties of Green Composites Based on High Density Polyethylene and Date Palm Fiber.* Composite Science and Technology, 2013.

33. García-García, D., A. Carbonell, M. Samper, D. García-Sanoguera and R. Balart, *Green composites based on polypropylene matrix and hydrophobized spend coffee ground (SCG) powder.* Composites part B: engineering, 2015. **78**: 256-265.

34. Nyambo, C., A.K. Mohanty and M. Misra, *Effect of maleated compatibilizer on performance of PLA/wheat Straw-Based green composites.* Macromolecular Materials and Engineering, 2011. **296**(8): 710-718.

35. Wei, L. and A.G. McDonald, *A review on grafting of biofibers for biocomposites.* Materials, 2016. **9**(4): 303.

36. Torres-Giner, S., N. Montanes, T. Boronat, L. Quiles-Carrillo and R. Balart, *Melt grafting of sepiolite nanoclay onto poly (3-hydroxybutyrate-co-4-hydroxybutyrate) by reactive extrusion with multi-functional epoxy-based styrene-acrylic oligomer.* European Polymer Journal, 2016. **84**: 693-707.

37. Muthuraj, R., M. Misra and A.K. Mohanty, *Biodegradable compatibilized polymer blends for packaging applications: A literature review.* Journal of Applied Polymer Science, 2018. **135**(24): 45726.

38. Balart, J., V. Fombuena, O. Fenollar, T. Boronat and L. Sánchez-Nacher, *Processing and characterization of high environmental efficiency composites based on PLA and hazelnut shell flour (HSF) with biobased plasticizers derived from epoxidized linseed oil (ELO).* Composites Part B: Engineering, 2016. **86**: 168-177.

39. Quiles-Carrillo, L., N. Montanes, C. Sammon, R. Balart and S. Torres-Giner, *Compatibilization of highly sustainable polylactide/almond shell flour composites by reactive extrusion with maleinized linseed oil.* Industrial crops and products, 2018. **111**: 878-888.

40. Duarte, I.S., A.A. Tavares, P.S. Lima, D.L. Andrade, L.H. Carvalho, E.L. Canedo and S.M. Silva, *Chain extension of virgin and recycled poly (ethylene terephthalate): effect of processing conditions and reprocessing.* Polymer degradation and stability, 2016. **124**: 26-34.

41.   Meng, Q.-K., M.-C. Heuzey and P. Carreau, *Effects of a multifunctional polymeric chain extender on the properties of polylactide and polylactide/clay nanocomposites.* International Polymer Processing, 2012. **27**(5): 505-516.

42.   Najafi, N., M. Heuzey and P. Carreau, *Polylactide (PLA)-clay nanocomposites prepared by melt compounding in the presence of a chain extender.* Composites Science and Technology, 2012. **72**(5): 608-615.

43.   Zhang, Y., X. Yuan, Q. Liu and A. Hrymak, *The effect of polymeric chain extenders on physical properties of thermoplastic starch and polylactic acid blends.* Journal of Polymers and the Environment, 2012. **20**(2): 315-325.

44.   Torres-Giner, S., J.V. Gimeno-Alcañiz, M.J. Ocio and J.M. Lagaron, *Optimization of electrospun polylactide-based ultrathin fibers for osteoconductive bone scaffolds.* Journal of Applied Polymer Science, 2011. **122**(2): 914-925.

45.   Crespo, J., R. Balart, L. Sanchez and J. Lopez, *Mechanical behaviour of vinyl plastisols with cellulosic fillers. Analysis of the interface between particles and matrices.* International journal of adhesion and adhesives, 2007. **27**(5): 422-428.

46.   Jandas, P., S. Mohanty and S. Nayak, *Thermal properties and cold crystallization kinetics of surface-treated banana fiber (BF)-reinforced poly (lactic acid)(PLA) nanocomposites.* Journal of thermal analysis and calorimetry, 2013. **114**(3): 1265-1278.

47.   Quiles-Carrillo, L., M. Blanes-Martínez, N. Montanes, O. Fenollar, S. Torres-Giner and R. Balart, *Reactive toughening of injection-molded polylactide pieces using maleinized hemp seed oil.* European Polymer Journal, 2018. **98**: 402-410.

48.   Baimark, Y. and P. Srihanam, *Influence of chain extender on thermal properties and melt flow index of stereocomplex PLA.* Polymer Testing, 2015. **45**: 52-57.

49.   Kim, S.-K. and T. Lee, *Degradation of lignocellulosic materials under sulfidogenic and methanogenic conditions.* Waste management, 2009. **29**(1): 224-227.

50.   Morrell, J.J., *Degradation of lignocellulosic materials and its prevention.* JOM, 2014. **66**(4): 580-587.

51.   Tserki, V., P. Matzinos, S. Kokkou and C. Panayiotou, *Novel biodegradable composites based on treated lignocellulosic waste flour as filler. Part I. Surface chemical modification and characterization of waste flour.* Composites Part A: Applied Science and Manufacturing, 2005. **36**(7): 965-974.

52.   Awal, A., M. Rana and M. Sain, *Thermorheological and mechanical properties of cellulose reinforced PLA bio-composites.* Mechanics of Materials, 2015. **80**: 87-95.

53.   Nagarajan, V., A.K. Mohanty and M. Misra, *Perspective on polylactic acid (PLA) based sustainable materials for durable applications: Focus on toughness and heat resistance.* ACS Sustainable Chemistry & Engineering, 2016. **4**(6): 2899-2916.

54.   Frenz, V., D. Scherzer, M. Villalobos, A. Awojulu, M. Edison and R. Van Der Meer. *Multifunctional polymers as chain extenders and compatibilizers for polycondensates and biopolymers*. in *Tech. Pap. Reg. Tech. Conf. Soc. Plast. Eng*. 2008.

55.   Chieng, B.W., N.A. Ibrahim, Y.Y. Then and Y.Y. Loo, *Epoxidized vegetable oils plasticized poly (lactic acid) biocomposites: mechanical, thermal and morphology properties.* Molecules, 2014. **19**(10): 16024-16038.

56.   Ferri, J., D. Garcia-Garcia, L. Sánchez-Nacher, O. Fenollar and R. Balart, *The effect of maleinized linseed oil (MLO) on mechanical performance of poly (lactic acid)-thermoplastic starch (PLA-TPS) blends.* Carbohydrate polymers, 2016. **147**: 60-68.

57.   Pivsa-Art, W., K. Fujii, K. Nomura, Y. Aso, H. Ohara and H. Yamane, *The effect of poly (ethylene glycol) as plasticizer in blends of poly (lactic acid) and poly (butylene succinate).* Journal of Applied Polymer Science, 2016. **133**(8).

58.   Qiu, Z. and W. Yang, *Crystallization kinetics and morphology of poly (butylene succinate)/poly (vinyl phenol) blend.* Polymer, 2006. **47**(18): 6429-6437.

59.   Ferri, J.M., D. Garcia-Garcia, N. Montanes, O. Fenollar and R. Balart, *The effect of maleinized linseed oil as biobased plasticizer in poly (lactic acid)-based formulations.* Polymer International, 2017. **66**(6): 882-891.

60.   Kuciel, S., P. Jakubowska and P. Kuźniar, *A study on the mechanical properties and the influence of water uptake and temperature on biocomposites based on polyethylene from renewable sources.* Composites Part B: Engineering, 2014. **64**: 72-77.

III.2.5. Compatibilization of highly sustainable polylactide/almond shell flour composites by reactive extrusion with maleinized linseed oil

L. Quiles-Carrillo [1], N. Montanes [1], C. Sammon [2], R.Balart [1] and S. Torres-Giner [3, 4]

[1] Technological Institute of Materials (ITM), Universitat Politècnica de València (UPV), Plaza Ferrándiz y Carbonell 1, 03801 Alcoy, Spain;

[2] Materials and Engineering Research Institute, Sheffield Hallam University, Sheffield, UK;

[3] Novel Materials and Nanotechnology Group, Institute of Agrochemistry and Food Technology (IATA), Spanish National Research Council (CSIC), Calle Catedrático Agustín Escardino Benlloch 7, 46980 Paterna, Valencia, Spain

[4] School of Technology and Experimental Sciences (ESTCE), Universitat Jaume I (UJI), Castellón, Spain
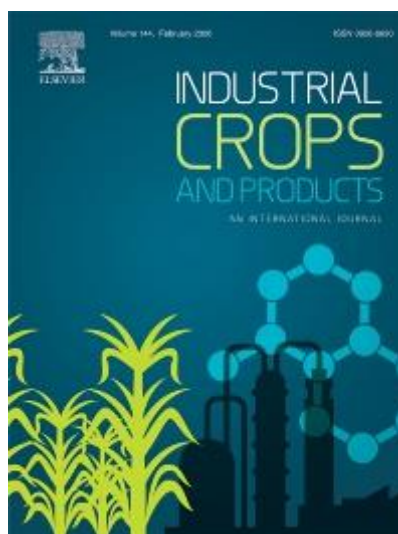
Contents lists available at ScienceDirect

Industrial Crops & Products
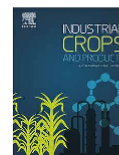
Compatibilization of highly sustainable polylactide/almond shell flour composites by reactive extrusion with maleinized linseed oil

L. Quiles-Carrillo[a], N. Montanes[a], C. Sammon[b], R. Balart[a], S. Torres-Giner[c,d,*]

[a] Technological Institute of Materials (ITM), Universitat Politècnica de València (UPV), Alcoy, Spain
[b] Materials and Engineering Research Institute, Sheffield Hallam University, Sheffield, UK
[c] Novel Materials and Nanotechnology Group, Institute of Agrochemistry and Food Technology (IATA), Spanish National Research Council (CSIC), Paterna, Spain
[d] School of Technology and Experimental Sciences (ESTCE), Universitat Jaume I (UJI), Castellón, Spain

ABSTRACT

Highly sustainable composites were produced by melt compounding polylactide (PLA) with almond shell flour (ASF), a processed by-product of the food industry, at a constant weight content of 30 wt.-%. However, due to the lack of miscibility between PLA and ASF, both being raw materials obtained from crops, resultant green composite presented poor ductility and low thermal stability. To overcome this limitation, maleinized linseed oil (MLO), a multi-functionalized plant-derived additive, was originally incorporated as a reactive compatibilizer during the extrusion process. Both chemical and physical characterizations showed that 1–5 parts per hundred resin (phr) of MLO successfully serve to obtain PLA/ASF composites with improved mechanical, thermal, and thermomechanical properties. The enhancement achieved was particularly related to a dual compatibilizing effect of plasticization in combination with melt grafting. The latter process was specifically ascribed to the formation of new carboxylic ester bonds through the reaction of the multiple maleic anhydride functionalities present in MLO with the hydroxyl groups of both the PLA terminal chains and cellulose on the ASF surface. The fully bio-based and biodegradable composites described herein give an efficient sustainable solution to upgrade agro-food wastes as well as contributing to reducing the cost of PLA-based materials.

1. Introduction

Poly(lactic acid), or more correctly, polylactide (PLA), is a bio-based and biodegradable linear aliphatic polyester. Lactic acid, i.e. 2-hydroxypropionic acid, comprises its basic building block, which is in turn derived from the fermentation of starch sources (e.g. corn, potato, sugarcane, tapioca, etc.). To attain high molecular weights (M_w), PLA is habitually prepared by ring-opening polymerization (ROP) of lactide, i.e. the six-membered cyclic diester of lactic acid, using tin octanoate as catalyst (Garlotta, 2001). PLA is nowadays considered the front runner in the emerging bioplastics market, showing an annual consumption of 140,000 tons (Madhavan Nampoothiri et al., 2010). This biopolyester is particularly interesting for short-term applications (e.g. food packaging) due to its two-fold environmental advantage of being bio-based, i.e. obtained from renewable resources, and biodegradable, though durable applications can be also possible (Nagarajan et al., 2016). The physical properties of PLA are fairly similar to those of petrochemical-based polymers with high strength and low toughness, such as polystyrene (PS) and

poly(ethylene terephthalate) (PET) (Auras et al., 2010). Most common uses include disposable and compostable glasses for cold drinks, food trays and rigid containers, teabags, lids, disposable plates, cutlery, etc. (Lim et al., 2008). By using natural fillers (e.g. cellulosic materials) as reinforcement for PLA matrices, fully bio-based and biodegrable composites can be manufactured (Johari et al., 2016; Oksman et al., 2003; Plackett et al., 2003; Yusoff et al., 2016). These constitute the so-called "green composites", which represent an emerging area in materials science and sustainable chemistry (La Mantia and Morreale, 2011).

Almond (Prunus amygdalus L.) is a very important crop throughout the world's temperate regions with an annual production of 2.31 million tons from a land area of 1.7 million hectare (Pirayesh et al., 2013). The almond tree fruit, the drupe, is considered to comprise of four parts, namely, the almond kernel, the almond brown skin, the almond green shell cover (hull), and the almond shell (Esfahlan et al., 2010). The latter constitutes the thick endocarp of the almond fruit that is composed, on a dry basis, of approximately 38 wt.-% of hemicellulose, 31 wt.-% cellulose (Kürschner), 28 wt.-% of lignin (Klason), and 3 wt.-

---

Compatibilization of highly sustainable polylactide/almond shell flour composites by reactive extrusion with maleinized linseed oil

Abstract.

Highly sustainable composites were produced by melt compounding polylactide (PLA) with almond shell flour (ASF), a processed by-product of the food industry, at a constant weight content of 30 wt.-%. However, due to the lack of miscibility between PLA and ASF, both being raw materials obtained from crops, resultant green composite presented poor ductility and low thermal stability. To overcome this limitation, maleinized linseed oil (MLO), a multi-functionalized plant-derived additive, was originally incorporated as a reactive compatibilizer during the extrusion process. Both chemical and physical characterizations showed that 1–5 parts per hundred resin (phr) of MLO successfully serve to obtain PLA/ASF composites with improved mechanical, thermal, and thermomechanical properties. The enhancement achieved was particularly related to a dual compatibilizing effect of plasticization in combination with melt grafting. The latter process was specifically ascribed to the formation of new carboxylic ester bonds through the reaction of the multiple maleic anhydride functionalities present in MLO with the hydroxyl groups of both the PLA terminal chains and cellulose on the ASF surface. The fully bio-based and biodegradable composites described herein give an efficient sustainable solution to upgrade agro-food wastes as well as contributing to reducing the cost of PLA-based materials.

Keywords: PLA; Cellulose; Green composites; Multi-functionalized vegetable oils; Reactive extrusion; Waste valorization

INTRODUCTION

Poly(lactic acid), or more correctly, polylactide (PLA), is a bio-based and biodegradable linear aliphatic polyester. Lactic acid, *i.e.* 2-hydroxypropionic acid, comprises its basic building block, which is in turn derived from the fermentation of starch sources (*e.g.* corn, potato, sugarcane, tapioca, etc.). To attain high molecular weights (M_w), PLA is habitually prepared by ring-opening polymerization (ROP) of lactide, i.e. the six-membered cyclic diester of lactic acid, using tin octanoate as catalyst [1]. PLA is nowadays considered the front runner in the emerging bioplastics market, showing an annual consumption of 140,000 tons [2]. This biopolyester is particularly interesting for short-term applications (*e.g.* food packaging) due to its two-fold environmental advantage of being bio-based, i.e. obtained from renewable resources, and biodegradable, though durable applications can be also possible[3]. The physical properties of PLA are fairly similar to those of petrochemical-based polymers with high strength and low toughness, such as polystyrene (PS) and poly(ethylene terephthalate) (PET) [4]. Most common uses include disposable and compostable glasses for cold drinks, food trays and rigid containers, teabags, lids, disposable plates, cutlery, etc. [5]. By using natural fillers (*e.g.* cellulosic materials) as reinforcement for PLA matrices, fully bio-based and biodegrable composites can be manufactured [6-9]. These constitute the so-called "green composites", which represent an emerging area in materials science and sustainable chemistry [10].

Almond (*Prunus amygdalus L.*) is a very important crop throughout the world's temperate regions with an annual production of 2.31 million tons from a land area of 1.7 million hectare [11]. The almond tree fruit, the drupe, is considered to comprise of four parts, namely, the almond kernel, the almond brown skin, the almond green shell cover (hull), and the almond shell [12]. The latter constitutes the thick endocarp of the almond fruit that is composed, on a dry basis, of approximately 38 wt.-% of hemicellulose, 31 wt.-% cellulose (Kürschner), 28 wt.-% of lignin (Klason), and 3 wt.-% of other components [13, 14]. After harvesting, these woody shells are separated to obtain the edible seeds, which are widely employed in the food industry, remaining available as a solid residue for which no relevant industrial use has been developed to date [12]. Some novel applications of almond shells are being continuously proposed, such as heavy metal adsorbents, dye absorbents, growing media, activated carbon preparation, and additives for the preparation of xylo-oligosaccharides (XOs) [12, 15-18]. However, currently almond shells are mainly incinerated [19] or used as animal feed [20]. Additionally, it is worth to note that the processing by-products, *i.e.* hulls and shells, account for more than 50% by dry weight of the almond fruit [21]. Consequently, it is estimated that around 0.8–1.7 million tons of this agro-food waste are generated annually [22]. As a result, these highly lignified materials are potential candidates to be applied as renewable fillers to reinforce polymer and biopolymer matrices. For this application, the shells are required to be ground and dried to obtain a more easy-to-handle product in a powder form, *i.e.* the almond shell flour (ASF).

Previous studies on green composites based on ASF are not very extensive and these are limited to the use of urea-formaldehyde (UF) resin [11, 22, 23], epoxy resin [24], polypropylene (PP) [25-27], polyvinyl chloride (PVC) [28, 29], and poly(ε-caprolactone) (PCL) [30, 31]. In relation to thermoplastic materials, these previous studies have shown that the incorporation of ASF can bring important advantages such as

mechanical reinforcement, reduce environmental impact, and lower costs. Besides intrinsic properties of each component, the mechanical and thermomechanical properties of the resultant green composites are dependent on filler aspect ratio, filler content and orientation, and adhesion at the filler–matrix interface [32]. The latter, *i.e.* the interfacial filler–matrix adhesion, is crucial since it is responsible for promoting a good stress transfer from the continuous phase to the dispersed fillers that must carry the load. Nevertheless, the high inherent hydrophilicity of cellulosic fillers does not habitually offer good adhesion with the hydrophobic or low hydrophilic polymers used as the composite matrix [33]. Poor filler wetting causes a non-uniform distribution of fillers in the matrix, consequently aggregation and void formation are commonly observed during melt processing. Many different approaches, reported in multiple reviews [34-37], have explored different strategies to improve adhesion in cellulose-reinforced polymer materials. These methods mainly include surface modification of the cellulosic filler prior to composite manufacture via chemical (*e.g.* esterification, etherification, treatment with silanes or isocyanates) or physical means (*e.g.* plasma, corona treatments, and radiation) as well as modification of the polymer matrix. Among them, the exposure to ultraviolet (UV) radiation has been recently demonstrated to be very effective on the activation of the cellulosic filler surface in order to improve the physical properties of the resultant polymer composites [38].

An alternative approach to improve both filler–matrix adhesion and filler dispersion in polymer composites is the use of a compatibilizer, playing the role of an adhesion promoter [39]. In this sense, reactive extrusion (REX) is a well-known and cost-effective methodology to introduce a variety of functional groups into biopolymer chains [40, 41]. Based on this concept, REX has been recently proposed as novel route for grafting inorganic nanoparticles onto biopolymer matrices, resulting in sustainable polymer nanocomposites with enhanced physical performance [42]. This is due to biopolyester chains are characterized by hydroxyl and carboxylic acid terminal groups, which can establish chemical interactions during melt processing. This process mainly involves the chemical attachment of the fillers to the biopolymer chains by the action of reactive molecules with, on average, two or more functionalities (*f*), *i.e.* molecules with at least two functional sites. These bi- or multi-functional additives actually act as interfacial agents and improve adhesion between filler and the polymer continuous phase by the creation of covalent bonds.

Maleinized linseed oil (MLO) is a natural cross-linker that is industrially prepared from linseed oil, which is extracted from oilseed flax (*Linum usitatissimum* L.), a plant widely cultivated in Europe. Linseed oil contains approximately 9–11% saturated (mainly 5–6% palmitic acid and 4–5% stearic acid) and 75–90% unsaturated fatty acids (mainly 50–55% linolenic acid, 15–20% oleic acid, and 10–15% linoleic acid) [43]. This unsaturated fatty acid content results in one of the highest unsaturation levels amongst common vegetable oils, comparable only to tung oil, thus leading to a highly versatile additive, ripe for chemical functionalization. In particular, the maleinization process provides multiple maleic anhydride functionalities to the MLO structure, which could easily react thereafter with hydroxyl groups [44, 45]. Moreover, MLO offers an important advantage in comparison to other maleinized oils since it is commercially available at a competitive price due to its alternative uses as biolubricant. Additionally, small amounts of MLO can also act as a sustainable plasticizer for PLA-based materials, allowing chain motion and improving their processing conditions,

thermal stability, and ductility [46]. Moreover, the use of vegetable oils is of great interest from an environmental point of view as these lend themselves to obtaining fully bio-based and compostable formulations [47]. Based on recent research findings [48], the present study reports the compatibilization by MLO of cellulosic ASF with PLA biopolymer. The influence of different contents of MLO on the thermal, mechanical, and morphological properties of these novel green composites is evaluated and related to its compatibilizing effect.

MATERIALS AND METHODS

Materials

The PLA used was Ingeo™ Biopolymer 3251D, supplied by NatureWorks (Minnetonka, Minnesota, USA). According to the manufacturer, this is an injection molding-grade resin made primarily from dextrose that is derived from field corn grown for industrial and functional end-uses. The biopolymer has a M_W of 5.5×10^4 g/mol, with a polydispersity index (PI) of 1.62, a melt flow rate (MFR) of 30–40 g/10 min (190 °C, 2.16 kg), and a true density of 1.24 g/cm^3. Almond was collected in the Sierra Mariola region and the shells were provided by Jesol Materias Primas S.A. (Valencia, Spain) as an industrial by-product after seed extraction. MLO was obtained from Vandeputte (Mouscron, Belgium) as VEOMER LIN. This agent has a viscosity of 1,000 cP at 20 °C and an acid value of 105–130 mg potassium hydroxide (KOH)/g.

Preparation of almond shell flour

The as-received almond shells were ground in a Retsch GmbH (Düsseldorf, Germany) SK 100 Cross Beater mill at a rotating speed of 10,000 rpm. Resultant particles were then sieved using a Cisa® Sieve Shaker model RP09 (Barcelona, Spain) to obtain a flour with a homogenous particle size distribution with a top-cut of 150 µm. **Figure III.2.5.1** shows the almond shells and the obtained ASF in powder form. Subsequently, ASF was UV irradiated in a Honle UV Technology (Barcelona, Spain) UVASPOT 1000RF2 cabinet for 4 min, based on previous research [38] using a high pressure mercury lamp with a power of 1,000 W at a wavelength at 350 nm.
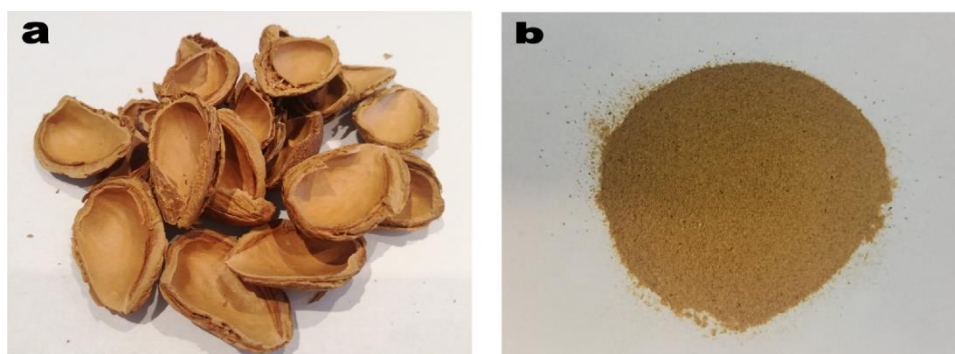
Figure III.2.5.1. (a) As-received almond shells; (b) Processed almond shell flour (ASF).

Prior to processing and to remove any residual moisture, the biopolymer pellets and ASF were stored at 60 °C for 36 h in an Industrial Marsé (Barcelona, Spain) dehumidifying dryer MD. The final water content of ASF was kept at 1–2%.

Reactive extrusion

A constant weight percentage of 30 wt.-% of ASF in PLA was selected to evaluate the influence of MLO on the measured physical properties. This composite composition was chosen based on previous reported results observed for other PLA green composites [49]. The MLO range composition was subsequently varied in the range of 0–10 parts per hundred resin (phr) since previous studies with other vegetable oils indicated saturation with contents below 10 phr [50]. **Table III.2.5.1** summarizes the set of the prepared green composite formulations.

Table III.2.5.1. Summary of compositions according to the weight content (wt.-%) of polylactide (PLA) and almond shell flour (ASF) in which maleinized linseed oil (MLO) was added as parts per hundred resin (phr) of PLA/ASF composite.

Samples	Percentage (wt.-%)		MLO (phr)
	PLA	AHF	
PLA	100	-	-
PLA/AHF	70	30	-
PLA/AHF + MLO 1 phr	70	30	1
PLA/AHF + MLO 2.5 phr	70	30	2.5
PLA/AHF + MLO 5 phr	70	30	5
PLA/AHF + MLO 7.5 phr	70	30	7.5
PLA/AHF + MLO 10 phr	70	30	10

Extrusion was performed on a co-rotating twin-screw extruder ZSK-18 MEGAlab from Coperion (Stuttgart, Germany). The screws feature 18 mm diameter with a length (L) to diameter (D) ratio, *i.e.* L/D, of 48. The materials dosage was set to achieve a residence time of about 1 min, measured by a blue masterbatch and based on a previously described configuration [42]. To this end, ASF was fed into a ZS-B 18 twin-screw side feeder from K-Tron (Pitman, New Jersey, USA) while MLO was added through a loss-in-weight (LIW) liquid feeder FDDW-MD2-DKMP-6 from Brabender Technologie GmbH (Duisburg, Germany). The screw speed was fixed at 300 rpm and the temperature profile, from the hopper to die, was set as follows: 170–180–180–180–190–190–190 °C. The extruded material was cooled in a water bath at 15 °C and pelletized using an air-knife unit.

Injection molding

Green composite pellets were shaped into pieces by injection molding in a Meteor 270/75 from Mateu & Solé (Barcelona, Spain) prior to characterization. The profile temperature, from the feeding zone to the injection nozzle, was set as follows: 170–175–180–185 °C. A clamping force of 75 tons was applied. The cavity filling and

cooling time were set at 1 and 10 s, respectively. Standard samples with a thickness of 4 mm were obtained.

Scanning electron microscopy

The morphology of the ASF particles and fracture surfaces of the green composite pieces after the impact tests were characterized using scanning electron microscope (SEM). An Oxford Instruments Zeiss Ultra 55 (Abingdon, UK) was used and an acceleration voltage of 2 kV was applied. Samples surfaces were coated with a gold-palladium alloy in a Quorum Technologies Ltd EMITECH model SC7620 sputter coater (East Sussex, UK) prior to analysis. ASF sizes were determined using Image J Launcher v 1.41 and the data presented were based on measurements from a minimum of 50 SEM micrographs.

Infrared spectroscopy

Chemical analysis was performed via attenuated total reflection–Fourier transform infrared (ATR-FTIR) spectroscopy. Spectra were recorded using a Bruker S.A. Vector 22 (Madrid, Spain) coupled to a PIKE MIRacle™ single reflection diamond ATR accessory (Madison, Wisconsin, USA). Data were collected as the average of ten scans between 4000 and 400 cm^{-1} at a spectral resolution of 4 cm^{-1}.

Mechanical tests

Injection-molded specimens with a dumbbell shape, a total length of 150 mm, and a cross-section of 10×4 mm^2 were tested in a universal test machine ELIB 30 from S.A.E. Ibertest (Madrid, Spain). Tensile tests were performed according to ISO 527. A 5-kN load cell and a cross-head speed of 5 mm/min were employed. Impact strength was tested on unnotched samples in a 1-J Charpy pendulum from Metrotec S.A. (San Sebastián, Spain), as suggested by ISO 179. Shore D hardness was determined in a durometer 676-D model from J. Bot S.A. (Barcelona, Spain) following ISO 868. All specimens were tested in a controlled chamber at room conditions, *i.e.* 23 °C and 50% RH. Six samples for each material were analyzed and averaged.

Thermal analysis

Thermal transitions of PLA and its green composites were evaluated by differential scanning calorimetry (DSC) using an 821 DSC model from Mettler-Toledo, Inc. (Schwerzenbach, Switzerland). For this, *ca.* 5 mg samples were placed in 40 µL hermetic aluminum sealed pans, previously calibrated with an indium standard. The analysis was performed in a dry reducing atmosphere in which nitrogen flowed at a constant rate of 66 mL/min. Samples were subjected to a two-step regime based on an initial heating step from 30 to 200 °C followed by a cooling step down to 0 °C at a heating rate of 10 °C/min. The cold crystallization temperature (T_{cc}), enthalpy of cold crystallization (ΔH_{cc}), melting temperature (T_m), and enthalpy of melting (ΔH_m) were obtained from the heating scan while the crystallization temperature from the melt (T_c) and enthalpy of crystallization (ΔH_c) were determined from the cooling scan. The percentage of crystallinity (X_c) in the samples was determined using the following **Equation III.2.5.1**:

$$X_C = \left[\frac{\Delta H_m - \Delta H_{CC}}{\Delta H_m^0 \cdot (1-w)}\right] \cdot 100 \qquad \textbf{Equation III.2.5.1}$$

where ΔH_m^0 = 93.7 J/g is the theoretical enthalpy corresponding to the melting of a 100% crystalline PLA sample [51], while the term 1-w represents the PLA weight fraction in the composite.

Thermogravimetric analysis (TGA) was used to evaluate the thermal stability of the materials using a TGA/SDTA 851 thermobalance from Mettler Toledo, Inc. The heating program was set from 30 to 650 °C at a heating rate of 20 °C/min in nitrogen with a constant flow-rate of 66 mL/min. Approximately 10 mg of each sample was used for the measurements. The onset degradation temperature was defined as the temperature at 5% weight loss ($T_{5\%}$) and the degradation temperature (T_{deg}) was obtained from the maximum value of the first derivative.

Thermomechanical tests

Vicat softening point and heat deflection temperature (HDT) of the injection-molded pieces were both measured using a DEFLEX 687-A2 standard Vicat/HDT station from Metrotec S.A. (San Sebastián, Spain). Vicat softening point was determined following the UNE-EN 727 and ISO 306, in accordance with the B50 method. The protocol involved the placement of specimens in the testing apparatus so that the penetrating needle rested on its surface at least 1 mm from the edge. A load of 50 N was applied to the sample. This was then lowered into an oil bath in which the temperature was raised at a rate of 50 °C/h until the needle penetrated 1 mm. HDT measurements were carried out according to UNE-EN ISO 75-Method A and ASTM D648, heating the medium (oil) at a rate of 120 °C/h. A specimen of 80 × 10 × 4 mm³ was loaded in three-point bending mode in the edgewise direction with a distance of 60 cm. The outer stress used for testing was 1.8 MPa and the temperature was increased at 120 °C/h until the sample deflected 0.31 mm.

Dimensional stability was studied by determining the coefficient of linear thermal expansion (CLTE) using a thermomechanical analyzer (TMA) Q400 model from TA Instruments (New Castle, Delaware, USA). The heating program was set between 0 and 140 °C with a constant heating rate of 2 °C/min and a load of 0.02 N. The test was performed on injection-molded rectangular samples with dimensions of 40 × 10 × 4 mm³.

RESULTS

Filler morphology

One of the most important adhesion mechanisms in polymer composites is mechanical interlocking, which is influenced by the filler shape. **Figure III.2.5.2a** shows the morphology of the ASF powder observed by SEM. In this image a rough perimeter can be seen, which can be a consequence of the crushing process due to the high hardness of this type of filler. A closer observation of the filler surface reveals the presence of some voids and granular features. This unusual porous-like structure on the surface of almond shell contributes to its high degree of roughness. A similar morphology was previously reported for ASF in PVC-based composites [28, 29], which was hypothesized to play a significant role in the adhesion with the polymer. The

particle size histogram for ASF, determined from the SEM images, is shown in **Figure III.2.5.2b**. The predominant particle size was approximately 75 µm. Habitually this is another relevant parameter in the mechanical properties of green composites. Previous studies also reported that mechanical impairment was much more pronounced in systems compromising large almond shell particles, in particular for those particle sizes greater than 150 µm [28, 29]. This effect is related to the arrangement of the fillers within the polymer matrix, which undoubtedly becomes more heterogeneous.
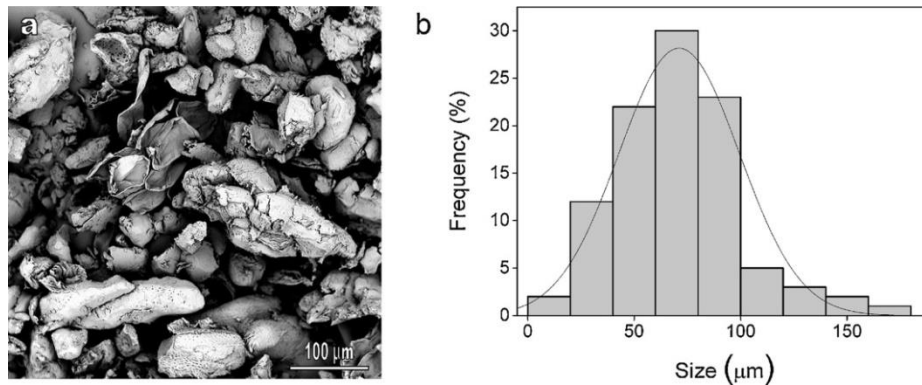
Figure III.2.5.2. (a) Scanning electron microscope (SEM) image of almond shell flour (ASF). Image was taken with a magnification of 500 × and a scale marker of 100 µm; (b) Histogram of ASF powder.

Chemical properties

Figure III.2.5.3a shows the FTIR spectra of the ASF powder, MLO liquid, neat PLA, the unmodified PLA/ASF composite, and the PLA/ASF composite containing 2.5 phr MLO.

The main bands of interest within each sample are described as follows. For ASF, the strongest absorption peak ~1032 cm^{-1} is ascribed to the C-O and C-OH stretching vibrations of polysaccharide rings in cellulose [52]. There is evidence of a broad absorption band between 3600 and 3000 cm^{-1}, which corresponds to the characteristic OH stretching vibrations of hydrogen bonded of hydroxyl groups (–OH) [53]. Considering that the ASF particles were dried and exposed to UV radiation, these peaks should be mostly derived from OH on the pyranose rings of cellulose [54], but the presence of small quantities of sorbed water cannot be excluded. The band centered at 1735 cm^{-1} represents the carbonyl (C=O) stretching [16]. The low intensity bands observed in the range 1400–1300 cm^{-1} are attributed to the bending vibrations of C-H and C-O groups of the polysaccharide ring [55]. The absorbance band at ~1234 cm^{-1} corresponds to the C-O-C stretching vibration of the acetyl group in lignin and hemicellulose component, respectively [16, 56].

Principal absorption bands for MLO are observed at ~3008 cm^{-1}, which has been identified as the =C-H stretching of the carbon–carbon double bonds, and at ~2924 cm^{-1} and ~2853 cm^{-1} as the antisymmetric and symmetric CH stretching of the saturated carbon–carbon (C-C) bonds, respectively [57]. Other main bands can be observed at ~1742 cm^{-1} and 1708 cm^{-1}, being associated to the C=O stretching of the carbonyl functionalities from the ester and maleic anhydride groups respectively, at

1161 cm^{-1} for the C-O-C, C-O and C-C stretching to the ester functionalities, and at 719 cm^{-1} to the C-H out of the plane stretching of the saturated C-C bonds [57]. The band centered at ~1458 cm^{-1} is ascribed to C-H bending while peaks related to the anhydride groups are seen as shoulders on the ester carbonyl at ~1810 and 1777 cm^{-1}.
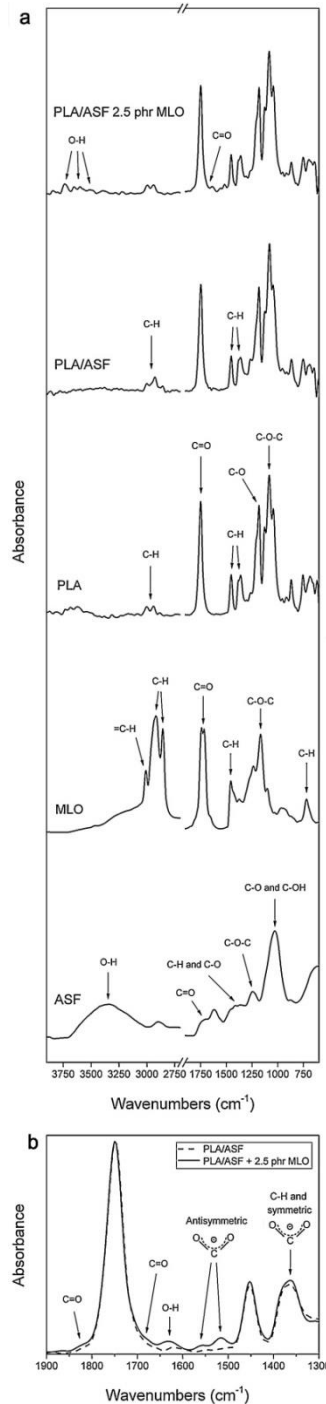
Figure III.2.5.3. (a) Fourier transform infrared (FTIR) spectra, from bottom to top, of almond shell flour (ASF), maleinized linseed oil (MLO), polylactide (PLA), uncompatibilized PLA/ASF composite, and compatibilized PLA/ASF composite by 2.5 parts per hundred resin (phr) of MLO. (b) Detail of the FTIR spectra for the uncompatibilized and compatibilized PLA/ASF composite. Arrows indicate the bands discussed in the text.

One of the strongest peak of neat PLA spectrum appears at 1751 cm^{-1} and is assigned to C=O stretching of the biopolymer [58]. Other strong bands observed are seen in between 1250 and 1050 cm^{-1}, which arise from the ester C-O and C-O-C stretching vibrations [51]. Bands in the range 1500–1300 cm^{-1} are ascribed to symmetric and antisymmetric deformational vibrations of C-H in the methyl (CH$_3$) groups [59], in which the peak centered at 1450 cm^{-1} is related to C-H bends from lactic acid moieties. The weak bands located at *ca*. 3000 and 2850 cm^{-1} are assigned to the antisymmetric and symmetric stretching vibrations of -CH$_2$ [59]. Incorporation of ASF certainly disrupted the CH vibrations (see subtle changes in the regions 3000–2850 and 1500–1300 cm^{-1}) of the biopolymer backbone chain, but it did not produce further significant changes in the spectrum of PLA.

Interestingly, the addition of MLO produced additional changes with regard to the uncompatibilized PLA/ASF composite. One can observe in **Figure III.2.5.3b** the formation of a shoulder in the carbonyl peak of PLA at approximately 1690 cm^{-1}. This can be related to the C=O stretching group of hydrolyzed anhydride groups of MLO in the green composite [60]. There is another weak increased absorption band in the range 1780–1850 cm^{-1} that can be ascribed to the symmetric stretching and asymmetric stretching of C=O of remaining cyclic maleic anhydride (MAH) groups [61, 62]. The presence of new weak peaks in the region 3600–3300 cm^{-1} can be further attributed to O-H stretch of the newly formed free carboxylic acid and may also indicate the presence of sorbed water in the green composite due to the presence of ASF. This is in agreement with Eren *et al.* [63] who observed a new carbonyl band of the carboxylic acid at 1709 cm^{-1} and a broad carboxylic O-H centered at 3286 cm^{-1} during the polyesterification reaction of diols with maleinized soybean oil (MSO). Additionally, the formation of two new bands at ~1560 and 1518 cm^{-1}, which are most likely to be derived from the antisymmetric stretches of delocalized deprotonated carboxylic acid end groups, can be produced as a result of interaction with sorbed water [64]. The symmetric stretch of these newly formed functional groups, expected to appear close to 1350 cm^{-1}, are not explicitly visible to permit verification of this hypothesis due to the proximity of C-H band associated with PLA. Nevertheless, it is clear that the incorporation of MLO into the green composite perturbed the band shape at the peak ~1360 cm^{-1} and formation of these delocalized carboxyl groups would readily explain this phenomenon.

These FTIR results suggest that new esters and carboxylic acids were produced after MLO addition to the green composites. The expected chemical reaction of MLO with PLA biopolymer and the cellulose component of ASF is given in **Figure III.2.5.4**. This scheme proposes that carboxylic ester linkages are formed upon elevated temperature during melt processing. The MLO structure provides multiple chemical reaction sites, by the presence of a various number of MAH groups, giving therefore reliable bond strength for hydroxyl groups of both the PLA terminal chains (and partially hydrolyzed PLA chains) and cellulose on the ASF surface. As a result of the esterification reaction, a cellulose-grafted PLA (cellulose-*g*-PLA) structure was generated.
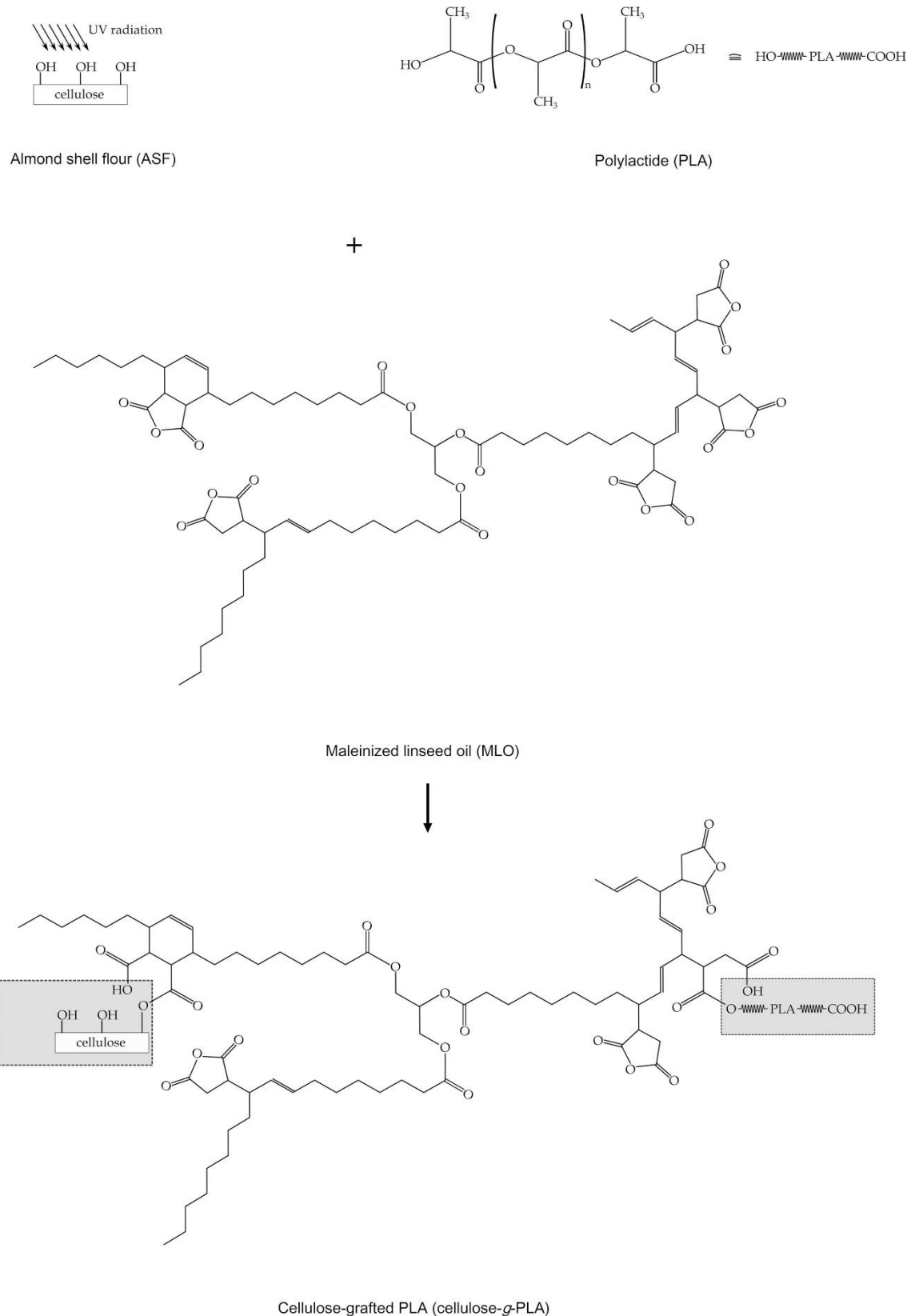
Figure III.2.5.4. Schematic representation of the reactive compatibilization between polylactide (PLA) and almond shell flour (ASF) by means of maleinized linseed oil (MLO).

Mechanical properties

Figure III.2.5.5 summarizes the mechanical properties of the neat PLA and its green composites with varying the MLO content. Unreinforced PLA displayed a tensile modulus and strength of 1960 and 63 MPa, respectively (**Figure III.2.5.5a** and **b**). In addition, Shore D hardness was ~79.6 (**Figure III.2.5.5e**). These values indicate that PLA is intrinsically a rigid and hard material. Nevertheless, PLA is also brittle, showing a low elongation-at-break value of 5.3% and poor energy absorption with an impact-strength value of 15.7 kJ/m^2 (**Figure III.2.5.5c** and **d**). Filling PLA with 30 wt.-% ASF led to a considerable decrease in mechanical properties, particularly for those related to material cohesion such as tensile strength, elongation at break, and impact strength. In particular, tensile modulus and strength were reduced to 1520 and 18 MPa, respectively (**Figure III.2.5.5a** and **b**). Elongation at break was also reduced to 2.5% and impact strength to 7 kJ/m^2 (**Figure III.2.5.5c** and **d**), which represents an overall percentage reduction of approximately 55% in the mechanical ductility with regard to unfilled PLA. As a positive effect, the filler addition contributed to a slight increase in Shore D hardness to a value of 84.7, *i.e.* about 7% (**Figure III.2.5.5e**). Similar mechanical results have been observed recently for other PLA-based green composites in which impact-absorbed energy was reduced by about 40% and Shore D hardness increased 9% by the presence of 30 wt.-% of hazelnut shell flour (HSF) [49]. Here, the reported results clearly confirm the lack of compatibility between the PLA matrix and ASF. Additionally the low aspect ratio of the filler also contributed to a poor mechanical improvement, which significantly differs from fiber-based PLA composites[8].
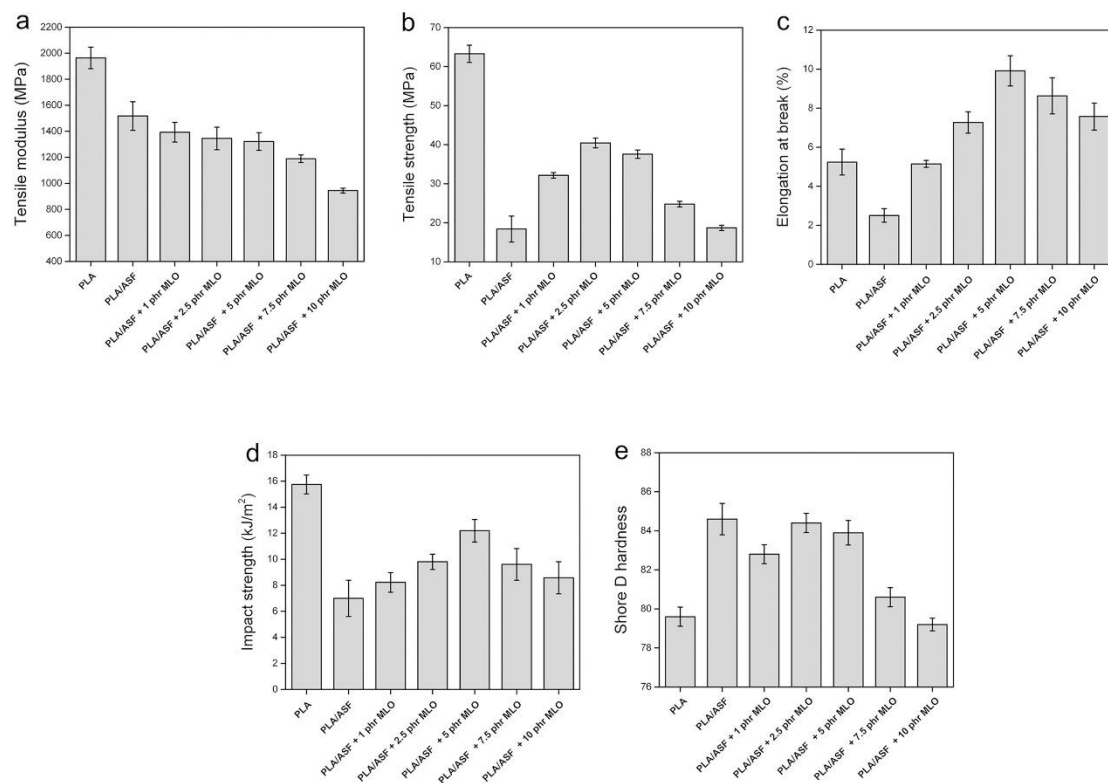
Figure III.2.5.5. Mechanical properties of polylactide (PLA) and its green composites with almond shell flour (ASF) varying the content of maleinized linseed oil (MLO) in terms of: (a) Tensile modulus; (b) Tensile strength at yield; (c) Elongation at break; (d) Charpy impact strength; (e) Shore D hardness. MLO content is expressed as parts per hundred resin (phr).

As an efficient plasticizer, MLO remarkably improved the ductility of the green composites. Elongation-at-break values gradually increased up to 9.8%, for the green composites containing 5 phr MLO, *i.e.* an increase of about 292% and 84% in relation to the uncompatibilized green composite and to the neat PLA, respectively (**Figure III.2.5.5c**). This is due to the strong plasticization effect provided by MLO on the PLA matrix, where the molecules place among the biopolymer chains acting as a lubricant with an enhanced influence on chain mobility [65]. Additionally, MLO could move into the free volume of the green composite, improving its impact-absorbed energy. As a result, incorporation of 5 phr MLO increased the impact-strength value up to 12.1 kJ/m^2 (**Figure III.2.5.5d**), which represents a percentage increase of about 73% with regard to unmodified green composite. In relation to the Shore D hardness, green composites with MLO contents of 2.5 and 5 phr presented similar values than the unmodified composite, *i.e.* 84.4 and 83.9, respectively, which can be regarded as a positive effect too (**Figure III.2.5.5e**). However, for the green composites with the highest MLO contents, *i.e.* 7.5 and 10 phr, it was observed an overall decrease in the mechanical properties. This indicates that saturation occurred from 7.5 phr MLO, resulting in a phase separation in the green composites [48].

Both the increase in elongation at break and impact strength indicate that the addition of MLO led to more ductile green composites, which can be explained by the previously described plasticization effect. However, interestingly, the addition of MLO in the range of 1–5 phr MLO also resulted in a noticeable increase in the tensile strength of the green composites. For instance, incorporation of 2.5 phr MLO showed a tensile strength value of 40.1 MPa (**Figure III.2.5.5b**), which represents an increase of 118% in comparison to the uncompatibilized green composite. For contents over 7.5 phr MLO, a clear decrease in both mechanical strength and ductility was observed. This negative effect can be related to the above-described phase separation of MLO in the green composite due to an excess of concentration. This suggests that an optimal and balanced performance from a mechanical perspective is achieved for MLO contents close to 5 phr. Here, the reported improvement of both mechanical strength and ductility gives some evidences that, in addition to plasticization, a degree of grafting occurred. This supports the previously described infrared data of the MLO-treated green composites in which ester bonds are potentially formed between the multiple MAH groups present in MLO with the hydroxyl groups of both PLA and ASF. This successfully induced an effective stress transfer from the biopolymer to the reinforcing fillers.

Thermal properties

Table III.2.5.2 shows a summary of the main thermal parameters obtained from DSC and TGA for PLA and its green composites treated with different amounts of MLO. As it can be seen in the table, PLA was characterized by a T_g of ~67 °C, a T_m of ~172 °C, and a X_c of ~15%. In addition, the biopolymer showed cold crystallization phenomenon with a T_{cc} of approximately 111 °C. After ASF incorporation, the value of T_m was reduced to 168.5 °C and crystallinity also decreased to ~9%. These results indicate that the presence of ASF can potentially disrupt the folding process of PLA chains, which avoids the formation of more perfect crystals and supports the findings from the infrared data. Although Hosseinihashemi *et al.* [26] have recently reported that almond shell particles are capable of acting as a nucleating agent that is able to

increase T_c of the resultant polymer composites, ASF could also interfere with the growing stage by which the overall crystallinity level of PLA in the composite decreased.

Table III.2.5.2. Thermal properties obtained from the differential scanning calorimetry (DSC) and thermogravimetric analysis (TGA) curves in terms of glass transition temperature (T_g), cold crystallization temperature (T_{cc}), melting temperature (T_m), normalized enthalpy of cold crystallization (ΔH_{cc}), normalized enthalpy of melting (ΔH_m), percentage of crystallinity (X_c), degradation temperature at 5% of mass loss ($T_{5\%}$), degradation temperature (T_{deg}), and residual mass at 650 °C for polylactide (PLA) and its green composites with almond shell flour (ASF) varying the content of maleinized linseed oil (MLO). MLO content is expressed as parts per hundred resin (phr) of PLA/ASF composite.

Samples	DSC parameters						TGA parameters		
	T_g (°C)	T_{cc} (°C)	T_m (°C)	ΔH_{cc} (J/g)	ΔH_m (J/g)	X_c (%)	$T_{5\%}$ (°C)	T_{deg} (°C)	Residual mass (%)
AHF	-	-	-	-	-	-	221.2 ±0.3	259.2 ±0.5	1.1 ±0.2
PLA	66.7 ± 0.3	111.3 ± 0.3	172.1 ± 0.4	21.1 ± 0.3	35.1 ± 0.3	15.0 ± 0.3	295.0 ±0.5	339.3 ±0.5	0.5 ±0.2
PLA/AHF	58.1 ± 0.3	110.1 ± 0.1	168.5 ± 0.5	22.6 ± 0.3	28.6 ± 0.3	9.1 ± 0.2	289.8±0.4	308.6±0.4	0.8 ±0.3
PLA/AHF + MLO 1 phr	62.1 ± 0.2	96.9 ± 0.3	171.4 ± 0.4	17.0 ± 0.2	31.9 ± 0.3	23.0 ± 0.3	299.3±0.5	322.1±0.3	0.6 ±0.3
PLA/AHF + MLO 2.5 phr	59.9 ± 0.5	103.6 ± 0.3	172.2 ± 0.3	17.7 ± 0.4	28.2 ± 0.2	17.2 ± 0.3	300.6±0.4	322.2±0.4	0.7 ±0.2
PLA/AHF + MLO 5 phr	58.7 ± 0.3	106.7 ± 0.5	171.9 ± 0.3	18.1 ± 0.3	26.6 ± 0.4	13.6 ± 0.2	297.2±0.5	317.3±0.5	0.6 ±0.3
PLA/AHF + MLO 7.5 phr	55.2 ± 0.2	103.4 ± 0.4	171.9 ± 0.4	19.9 ± 0.2	27.5 ± 0.3	12.5 ± 0.3	302.2±0.4	325.2±0.2	0.7 ±0.3
PLA/AHF + MLO 10 phr	54.9 ± 0.3	102.9 ± 0.3	172.3 ± 0.3	20.1 ± 0.2	27.4 ± 0.2	12.4 ± 0.2	304.3±0.3	327.1±0.3	0.7 ±0.2

For the MLO-treated green composites, the addition of MLO increased X_c and also, interestingly, induced a significant reduction in T_{cc}. It is important to remark that only the addition of 1 phr MLO led to a significant decrease in T_{cc} of approximately 12 °C and a value of X_c of ~23%. The presence of MLO in the green composites improved the compatibilization and subsequently the dispersion of ASF in the PLA matrix, which contributes to fewer polymer–polymer interactions and favors the formation of PLA crystals [65]. In addition, as described previously, MLO can readily react with hydroxyl groups in both PLA end chains and the cellulosic surface of ASF, leading to a combined effect of grafting and chain extension. Alternatively, as expected, T_g decreased as a function of the MLO content. This is related to an overall increase in the PLA chain mobility. It can be considered that MLO, due to its low Mw as well as good chemical affinity with the biopolymer, facilitates the reduction of secondary forces (*e.g.* hydrogen bonding, van der Waals forces, etc.) among the PLA chains by occupying intermolecular spaces and increasing the free volume.

As also included in **Table III.2.5.2**, the evaluation of thermal stability of the unmodified green composite showed a downward shift in T_{deg} from 339.3 °C, for the neat PLA, to 308.6 °C, for the untreated PLA/ASF composite. The unmodified green composite also began to degrade at a lower temperature, of around 5 °C, *i.e.* a $T_{5\%}$ of approximately 290 °C. Therefore, a significant decrease in the thermal stability of PLA was clearly noticeable after the incorporation of ASF. This fact is related to the relatively low thermal stability of the lignocellulosic filler, which initiated degradation at 221.2 °C and, one assumes, negatively contributed to the reduction of the global thermal stability of the green composite. In the present study, the observed impairment is in agreement with previous studies concerning the thermal stability of polymer composites based on almond shell [25, 26, 31]. It was specifically reported that the degradation of these natural fillers initially occurs in the range 250–350 °C, which is assigned to the thermal decomposition of cellulose and lignin [26]. Interestingly, the addition of MLO exerted a positive effect on the overall thermal stability of the green composites. Specifically, the onset degradation temperature, corresponding to 5% weight loss, increased to values in the range of 300–305 °C for the green composites compatibilized by MLO. Thermal degradation was also significantly improved in comparison to the unmodified green composite. In particular, Tdeg was delayed up to about 20 °C for the green composites treated with MLO. This remarkable increase in the thermal stability can be directly related to the chemical interaction achieved by MLO due to the covalent bonds established between the lignocellulosic fillers and the biopolymer matrix. In addition, MLO could also provide a physical barrier that obstructs the removal of volatile products produced during decomposition. A similar positive effect on the thermal stability was recently reported for PLA and epoxidized palm oil (EPO) blends [65, 66],. Indeed, Chieng *et al.* [65] observed a remarkable increase of 40 °C in the onset degradation of PLA by incorporating 5 wt.-% EPO.

Thermomechanical properties

Table III.2.5.3 shows the values of Vicat softening temperature, HDT, and CLTE, which are representative parameters for the thermomechanical properties of the green composites. With regard to the Vicat softening temperature, the value of unfilled PLA was 56.2 °C and this increased to 73.4 °C after the addition of 30 wt.-% ASF. This is in agreement with previous studies conducted on PLA/HSF composites [49] Interestingly, the incorporation of MLO also showed a considerable increase in the softening point, reaching a maximum value of 87.3 °C. This represents an increase of about 55% in relation to the unfilled PLA, further supporting the chemical interaction of ASF with the biopolymer. It is also worthy to indicate that the highest value was observed for the green composite containing 1 phr MLO, which further confirms that higher MLO amounts plasticize the PLA matrix and therefore reduce the service temperature of the green composites. A similar trend was also observed for HDT, in which the highest value was attained for the green composite containing 2.5 phr MLO. In particular, HDT increased from 53.1 and 61.6 °C for the neat PLA and unmodified green composite, respectively, up to 63.6 °C.

Table III.2.5.3. Vicat softening point, heat deflection temperature (HDT), and coefficient of linear thermal expansion (CLTE) below and above glass transition temperature (T_g) for polylactide (PLA) and its green composites with almond shell flour (ASF) varying the content of maleinized linseed oil (MLO). MLO content is expressed as parts per hundred resin (phr) of PLA/ASF composite.

Sample	Vicat (°C)	HDT (°C)	CLTE below T_g (μm/m°C)	CLTE above T_g (μm/m°C)
PLA	56.2 ± 1.9	53.1 ± 1.0	79.1 ± 1.9	170.9 ± 1.9
PLA/AHF	73.4 ± 1.2	61.6 ± 0.4	64.4 ± 1.9	116.4 ± 1.9
PLA/AHF + MLO 1 phr	87.3 ± 1.8	62.7 ± 2.3	63.3 ± 1.9	145.9 ± 1.9
PLA/AHF + MLO 2.5 phr	86.2 ± 0.8	63.6 ± 2.5	72.4 ± 1.9	146.8 ± 1.9
PLA/AHF + MLO 5 phr	81.9 ± 1.8	62.3 ± 1.8	73.8 ± 1.9	149.3 ± 1.9
PLA/AHF + MLO 7.5 phr	81.2 ± 0.4	61.3 ± 1.9	79.8 ± 1.9	151.1 ± 1.9
PLA/AHF + MLO 10 phr	81.3 ± 2.9	62.0 ± 1.6	81.0 ± 1.9	152.6 ± 1.9

The effect of compatibilization of MLO on the green composites was additionally determined by TMA. **Table III.2.5.3** also includes the CLTE values, below and above T_g, which are indicative of the dimensional stability of the green composites. As it can be seen in the table, the linear expansion was lower in the range of temperatures below T_g, which are ascribed to restrictions in the biopolymer chain mobility. Comparison of CLTE values below T_g shows that the incorporation of ASF reduced them from 79.1 to 64.4 μm/m°C. This indicates that ASF successfully reinforced the PLA matrix and improved the dimensional stability of the biopolymer, producing analogous findings to those recently described for PLA/HSF composites [49]. With regard to the evolution of the CLTE values in the compatibilized green composites, these increased with increasing the MLO content and ranged from about 63 to 81 μm/m°C. This can be explained by the plasticization effect provided by MLO, which facilitates the PLA chains mobility and increases free volume. The evolution of the CLTE values over T_g followed a similar tendency, showing a significant increase from 116.4 μm/m°C, for the unmodified green composite, up to 152.6 μm/m°C for the green composite containing 10 phr MLO. Plasticization was then more pronounced at higher temperatures, which is in agreement with previously studies looking at PLA-based green composites plasticized by epoxidized linseed oil (ELO) [50]. All green composites showed higher dimensional stability than the neat PLA. This can be considered as a positive finding, facilitating the technical applications of PLA materials at elevated temperatures.

Morphology of green composites

Figure III.2.5.6 shows the SEM images of the fracture surfaces of PLA and its green composites after the impact tests. **Figure III.2.5.6a**, which corresponds to the uncompatibilized PLA/ASF composite, clearly illustrates the typical brittle fracture of

the biopolymer showing a rough fracture surface due to nonexistent or very low plastic deformation. In addition, the lack of interaction between ASF and PLA was clearly detectable by the presence of several voids, which correspond to the detached particles after impact. Interestingly, some of the voids also showed the marks of the ASF surface. This supports a recent finding in which it was indicated that particle debonding was the main failure mechanism of cellulosic fillers in biopolymer matrices [33]. This occurs due to the lack of adhesion or cohesion at the particle–matrix interface of the green composite. This morphological observation correlates satisfactorily with the above-described physical performance of the unmodified green composites in which the presence of ASF did not contribute to an improvement of the mechanical and thermal properties but it rather decreased them.
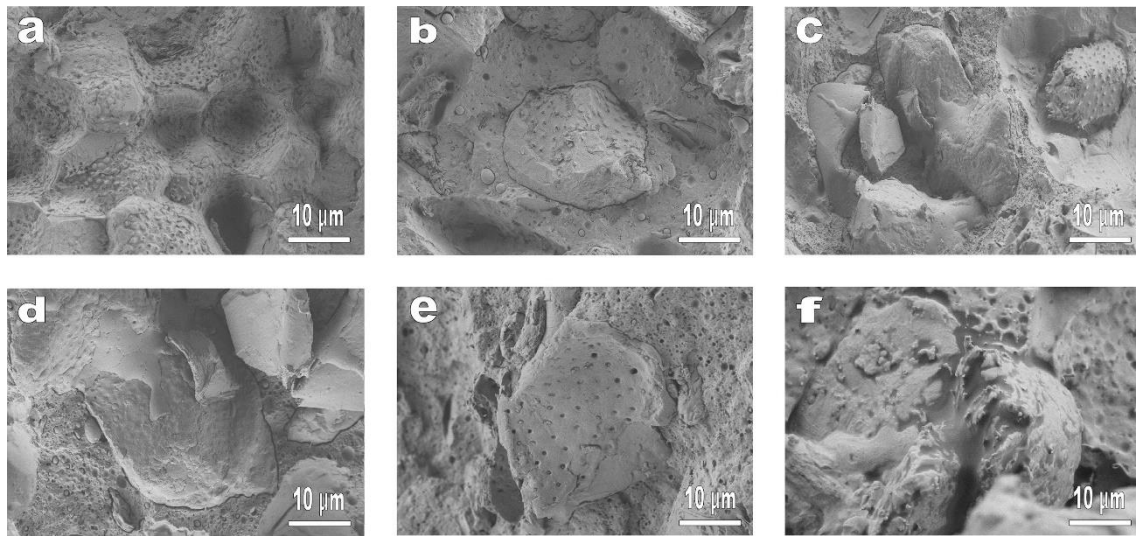
Figure III.2.5.6. Scanning electron microscope (SEM) images of the fracture surfaces of: (a) Uncompatibilized polylactide (PLA)/almond shell flour (ASF) composite; (b) PLA/ASF composite compatibilized with 1 part per hundred resin (phr) of maleinized linseed oil (MLO); (c) PLA/ASF composite compatibilized with 2.5 phr MLO; (d) PLA/ASF composite compatibilized with 5 phr MLO; (e) PLA/ASF composite compatibilized with 7.5 phr MLO; (f) PLA/ASF composite compatibilized with 10 phr MLO. Images were taken with a magnification of 1500 × and a scale marker of 10 µm.

The positive effect of MLO addition on the morphology of the green composites can be seen in **Figure III.2.5.6b** to **f**. Although it is possible to still detect some voids in the PLA matrix after the addition of 1 phr MLO (**Figure III.2.5.6b**), the presence of finely dispersed ASF particles into PLA indicates that MLO certainly improved compatibility. The addition of 2.5 phr (**Figure III.2.5.6c**) and 5 phr MLO (**Figure III.2.5.6d**) clearly led to an improvement of the particle–polymer continuity, which is subsequently responsible for reducing stress concentration phenomena and increasing load transfer between the biopolymer matrix and the lignocellulosic filler. One can also observe that the filler–matrix gap was reduced as the MLO content increased. **Figure III.2.5.6e** shows the good dispersion of the ASF particles within the PLA matrix containing 7.5 phr MLO. This image supports the hypothesis that the presence of MLO in the green composites improved ASF wettability. This can be confirmed by **Figure III.2.5.6f**, for the PLA/ASF composite containing 10 phr MLO, in which the lignocellulosic fillers were completely covered by MLO. It can be also observed the

absence of gaps with the surrounding PLA, which points towards improved interfacial affinity. However, certain phase separation was also detectable due to the MLO saturation, which is in turn considered to be responsible for impairing the performance of the green composites at high MLO contents.

CONCLUSIONS

The present study described the compatibilization of PLA and ASF by the addition of MLO during melt compounding. It was observed that the incorporation of high amounts of ASF into PLA resulted in green composites with increased hardness, potentially offering a remarkable cost reduction and improved waste valorization. However, it considerably reduced ductility and also thermal stability. Interestingly, the addition of relatively low contents of MLO, *i.e.* 1–5 phr, successfully improved the mechanical, thermal, and thermomechanical properties of the green composites. The achieved compatibilization was ascribed to a dual effect of plasticization and grafting provided by MLO. As supported by FTIR analysis, new ester bonds were formed during the extrusion process most likely between the multiple MAH groups of MLO with the hydroxyl groups present on the ASF surface and PLA terminal chains. For PLA/ASF composites containing high MLO amounts, *i.e.* 7.5 and 10 phr, an overall decrease in the physical properties occurred probably due to plasticizer saturation.

The results obtained in this study indicate that ASF, derived as a by-product from the food industry, can be used to reinforce PLA matrices when combined with low amounts of MLO due to its multi-functional reactivity. Moreover, the resultant MLO-containing green composites are highly sustainable because of their completely biodegradable and renewable characteristics. These can be applied as monolayers, in bio-based packaging materials, such as trays and lids, or even as replacements for wood boards or docks in building and construction applications.

In general terms, MLO and other multi-functionalized vegetable oils can be regarded as an attractive additive to enhance compatibility in immiscible or low miscible green composites based on biopolyesters and fillers with polar groups. In addition, due to their natural origin, MLO represents an environmentally friendly solution to improve industrial formulations and can positively contribute to the development of sustainable polymer technologies.

Acknowledgements

REFERENCES

1. Garlotta, D., *A literature review of poly (lactic acid).* Journal of Polymers and the Environment, 2001. **9**(2): 63-84.
2. Nampoothiri, K.M., N.R. Nair and R.P. John, *An overview of the recent developments in polylactide (PLA) research.* Bioresource technology, 2010. **101**(22): 8493-8501.

3.   Nagarajan, V., A.K. Mohanty and M. Misra, *Perspective on polylactic acid (PLA) based sustainable materials for durable applications: Focus on toughness and heat resistance.* ACS Sustainable Chemistry & Engineering, 2016. **4**(6): 2899-2916.

4.   Auras, R.A., L.-T. Lim, S.E. Selke and H. Tsuji, *Poly (lactic acid): synthesis, structures, properties, processing, and applications*. Vol. 10. 2011: John Wiley & Sons.

5.   Lim, L.-T., R. Auras and M. Rubino, *Processing technologies for poly (lactic acid).* Progress in polymer science, 2008. **33**(8): 820-852.

6.   Johari, A.P., S. Mohanty, S.K. Kurmvanshi and S.K. Nayak, *Influence of different treated cellulose fibers on the mechanical and thermal properties of poly (lactic acid).* ACS Sustainable Chemistry & Engineering, 2016. **4**(3): 1619-1629.

7.   Oksman, K., M. Skrifvars and J.-F. Selin, *Natural fibres as reinforcement in polylactic acid (PLA) composites.* Composites science and technology, 2003. **63**(9): 1317-1324.

8.   Plackett, D., T.L. Andersen, W.B. Pedersen and L. Nielsen, *Biodegradable composites based on L-polylactide and jute fibres.* Composites Science and Technology, 2003. **63**(9): 1287-1296.

9.   Yusoff, R.B., H. Takagi and A.N. Nakagaito, *Tensile and flexural properties of polylactic acid-based hybrid green composites reinforced by kenaf, bamboo and coir fibers.* Industrial Crops and Products, 2016. **94**: 562-573.

10.   La Mantia, F. and M. Morreale, *Green composites: A brief review.* Composites Part A: Applied Science and Manufacturing, 2011. **42**(6): 579-588.

11.   Pirayesh, H., H. Khanjanzadeh and A. Salari, *Effect of using walnut/almond shells on the physical, mechanical properties and formaldehyde emission of particleboard.* Composites Part B: Engineering, 2013. **45**(1): 858-863.

12.   Esfahlan, A.J., R. Jamei and R.J. Esfahlan, *The importance of almond (Prunus amygdalus L.) and its by-products.* Food chemistry, 2010. **120**(2): 349-360.

13.   Caballero, J., J. Conesa, R. Font and A. Marcilla, *Pyrolysis kinetics of almond shells and olive stones considering their organic fractions.* Journal of Analytical and Applied Pyrolysis, 1997. **42**(2): 159-175.

14.   Martinez, J., J. Granado, D. Montane, J. Salvado and X. Farriol, *Fractionation of residual lignocellulosics by dilute-acid prehydrolysis and alkaline extraction: application to almond shells.* Bioresource Technology, 1995. **52**(1): 59-67.

15.   Deniz, F., *Dye removal by almond shell residues: Studies on biosorption performance and process design.* Materials Science and Engineering C, 2013. **33**(5): 2821-2826.

16.   Doulati Ardejani, F., K. Badii, N.Y. Limaee, S.Z. Shafaei and A.R. Mirhabibi, *Adsorption of Direct Red 80 dye from aqueous solution onto almond shells: Effect of pH, initial concentration and shell type.* Journal of Hazardous Materials, 2008. **151**(2-3): 730-737.

17.   Ebringerová, A., Z. Hromádková, Z. Košt'álová and V. Sasinková, *Chemical valorization of agricultural by-products: Isolation and characterization of xylan-based antioxidants from almond shell biomass.* BioResources, 2008. **3**(1): 60-70.

18.   Urrestarazu, M., G.A. Martínez and M.D.C. Salas, *Almond shell waste: Possible local rockwool substitute in soilless crop culture.* Scientia Horticulturae, 2005. **103**(4): 453-460.

19.   Chiou, B.S., D. Valenzuela-Medina, C. Bilbao-Sainz, A.P. Klamczynski, R.J. Avena-Bustillos, R.R. Milczarek, W.X. Du, G.M. Glenn and W.J. Orts, *Torrefaction of almond shells: Effects of torrefaction conditions on properties of solid and condensate products.* Industrial Crops and Products, 2016. **86**: 40-48.

20.   Ledbetter, C.A., *Shell cracking strength in almond (Prunus dulcis [Mill.] D.A. Webb.) and its implication in uses as a value-added product.* Bioresource Technology, 2008. **99**(13): 5567-5573.

21.   Fadel, J.G., *Quantitative analyses of selected plant by-product feedstuffs, a global perspective.* Animal Feed Science and Technology, 1999. **79**(4): 255-268.

22.   Pirayesh, H. and A. Khazaeian, *Using almond (Prunus amygdalus L.) shell as a bio-waste resource in wood based composite.* Composites Part B: Engineering, 2012. **43**(3): 1475-1479.

23.   Gürü, M., S. Tekeli and I. Bilici, *Manufacturing of urea-formaldehyde-based composite particleboard from almond shell.* Materials and Design, 2006. **27**(10): 1148-1151.

24. Chaudhary, A.K., P.C. Gope and V.K. Singh, *Effect of almond shell particles on tensile property of particleboard.* Journal of Materials and Environmental Science, 2013. **4**(1): 109-112.

25. Essabir, H., S. Nekhlaoui, M. Malha, M.O. Bensalah, F.Z. Arrakhiz, A. Qaiss and R. Bouhfid, *Bio-composites based on polypropylene reinforced with Almond Shells particles: Mechanical and thermal properties.* Materials and Design, 2013. **51**: 225-230.

26. Hosseinihashemi, S.K., A. Eshghi, N. Ayrilmis and H. Khademieslam, *Thermal analysis and morphological characterization of thermoplastic composites filled with almond shell flour/montmorillonite.* BioResources, 2016. **11**(3): 6768-6779.

27. Lashgari, A., A. Eshghi and M. Farsi, *A study on some properties of polypropylene based nanocomposites made using almond shell flour and organoclay.* Asian Journal of Chemistry, 2013. **25**(2): 1043-1049.

28. Crespo, J.E., R. Balart, L. Sanchez and J. Lopez, *Mechanical behaviour of vinyl plastisols with cellulosic fillers. Analysis of the interface between particles and matrices.* International Journal of Adhesion and Adhesives, 2007. **27**(5): 422-428.

29. Crespo, J.E., L. Sanchez, F. Parres and J. López, *Mechanical and morphological characterization of PVC plastisol composites with almond husk fillers.* Polymer Composites, 2007. **28**(1): 71-77.

30. Valdés, A., O. Fenollar, A. Beltrán, R. Balart, E. Fortunati, J.M. Kenny and M.C. Garrigós, *Characterization and enzymatic degradation study of poly(ε-caprolactone)-based biocomposites from almond agricultural by-products.* Polymer Degradation and Stability, 2016. **132**: 181-190.

31. Valdés García, A., M. Ramos Santonja, A.B. Sanahuja and M. Del Carmen Garrigós Selva, *Characterization and degradation characteristics of poly(ε-caprolactone)-based composites reinforced with almond skin residues.* Polymer Degradation and Stability, 2014. **108**: 269-279.

32. Nagarajan, V., A.K. Mohanty and M. Misra, *Sustainable green composites: Value addition to agricultural residues and perennial grasses.* ACS Sustainable Chemistry and Engineering, 2013. **1**(3): 325-333.

33. Torres-Giner, S., N. Montanes, V. Fombuena, T. Boronat and L. Sanchez-Nacher, *Preparation and characterization of compression-molded green composite sheets made of poly(3-hydroxybutyrate) reinforced with long pita fibers.* Advances in Polymer Technology, 2018. **37**(5): 1305-1315.

34. Bledzki, A.K. and J. Gassan, *Composites reinforced with cellulose based fibres.* Progress in Polymer Science (Oxford), 1999. **24**(2): 221-274.

35. Bledzki, A.K., S. Reihmane and J. Gassan, *Properties and modification methods for vegetable fibers for natural fiber composites.* Journal of Applied Polymer Science, 1996. **59**(8): 1329-1336.

36. La Mantia, F.P. and M. Morreale, *Green composites: A brief review.* Composites Part A: Applied Science and Manufacturing, 2011. **42**(6): 579-588.

37. Wei, L. and A.G. McDonald, *A review on grafting of biofibers for biocomposites.* Materials, 2016. **9**(4).

38. Torres-Giner, S., N. Montanes, O. Fenollar, D. García-Sanoguera and R. Balart, *Development and optimization of renewable vinyl plastisol/wood flour composites exposed to ultraviolet radiation.* Materials and Design, 2016. **108**: 648-658.

39. Sengupta, S., D. Ray and A. Mukhopadhyay, *Sustainable materials: Value-added composites from recycled polypropylene and fly ash using a green coupling agent.* ACS Sustainable Chemistry and Engineering, 2013. **1**(6): 574-584.

40. Miladinov, V.D. and M.A. Hanna, *Starch esterification by reactive extrusion.* Industrial Crops and Products, 2000. **11**(1): 51-57.

41. Raquez, J.M., P. Degée, Y. Nabar, R. Narayan and P. Dubois, *Biodegradable materials by reactive extrusion: from catalyzed polymerization to functionalization and blend compatibilization.* Comptes Rendus Chimie, 2006. **9**(11-12): 1370-1379.

42.   Torres-Giner, S., N. Montanes, T. Boronat, L. Quiles-Carrillo and R. Balart, *Melt grafting of sepiolite nanoclay onto poly(3-hydroxybutyrate-co-4-hydroxybutyrate) by reactive extrusion with multi-functional epoxy-based styrene-acrylic oligomer.* European Polymer Journal, 2016. **84**: 693-707.

43.   Bayrak, A., M. Kiralan, A. Ipek, N. Arslan, B. Cosge and K.M. Khawar, *Fatty acid compositions of linseed (Linum Usitatissimum L.) genotypes of different origin cultivated in Turkey.* Biotechnology and Biotechnological Equipment, 2010. **24**(2): 1836-1842.

44.   Ford, E.N.J., S.K. Mendon, J.W. Rawlins and S.F. Thames, *Spectroscopic analysis of cotton treated with neutralized maleinized soybean oil.* JAOCS, Journal of the American Oil Chemists' Society, 2011. **88**(5): 681-687.

45.   Ford, E.N.J., J.W. Rawlins, S.K. Mendon and S.F. Thames, *Effect of acid value on the esterification mechanism of maleinized soybean oil with cotton.* Journal of Coatings Technology and Research, 2012. **9**(5): 637-641.

46.   Ferri, J.M., D. Garcia-Garcia, N. Montanes, O. Fenollar and R. Balart, *The effect of maleinized linseed oil as biobased plasticizer in poly(lactic acid)-based formulations.* Polymer International, 2017. **66**(6): 882-891.

47.   Garcia-Garcia, D., O. Fenollar, V. Fombuena, J. Lopez-Martinez and R. Balart, *Improvement of Mechanical Ductile Properties of Poly(3-hydroxybutyrate) by Using Vegetable Oil Derivatives.* Macromolecular Materials and Engineering, 2017. **302**(2).

48.   Ferri, J.M., D. Garcia-Garcia, L. Sánchez-Nacher, O. Fenollar and R. Balart, *The effect of maleinized linseed oil (MLO) on mechanical performance of poly(lactic acid)-thermoplastic starch (PLA-TPS) blends.* Carbohydrate Polymers, 2016. **147**: 60-68.

49.   Balart, J.F., D. García-Sanoguera, R. Balart, T. Boronat and L. Sánchez-Nacher, *Manufacturing and properties of biobased thermoplastic composites from poly(lactid acid) and hazelnut shell wastes.* Polymer Composites, 2018. **39**(3): 848-857.

50.   Balart, J.F., V. Fombuena, O. Fenollar, T. Boronat and L. Sánchez-Nacher, *Processing and characterization of high environmental efficiency composites based on PLA and hazelnut shell flour (HSF) with biobased plasticizers derived from epoxidized linseed oil (ELO).* Composites Part B: Engineering, 2016. **86**: 168-177.

51.   Torres-Giner, S., J.V. Gimeno-Alcañiz, M.J. Ocio and J.M. Lagaron, *Optimization of electrospun polylactide-based ultrathin fibers for osteoconductive bone scaffolds.* Journal of Applied Polymer Science, 2011. **122**(2): 914-925.

52.   Liu, D., G. Han, J. Huang and Y. Zhang, *Composition and structure study of natural Nelumbo nucifera fiber.* Carbohydrate Polymers, 2009. **75**(1): 39-43.

53.   Spinacé, M.A.S., C.S. Lambert, K.K.G. Fermoselli and M.A. De Paoli, *Characterization of lignocellulosic curaua fibres.* Carbohydrate Polymers, 2009. **77**(1): 47-53.

54.   Lin, N. and A. Dufresne, *Supramolecular hydrogels from in situ host-guest inclusion between chemically modified cellulose nanocrystals and cyclodextrin.* Biomacromolecules, 2013. **14**(3): 871-880.

55.   Olsson, A.M. and L. Salmén, *The association of water to cellulose and hemicellulose in paper examined by FTIR spectroscopy.* Carbohydrate Research, 2004. **339**(4): 813-818.

56.   Essabir, H., E. Hilali, A. Elgharad, H. El Minor, A. Imad, A. Elamraoui and O. Al Gaoudi, *Mechanical and thermal properties of bio-composites based on polypropylene reinforced with Nut-shells of Argan particles.* Materials and Design, 2013. **49**: 442-448.

57.   Gomez, N.A., R. Abonia, H. Cadavid and I.H. Vargas, *Chemical and spectroscopic characterization of a vegetable oil used as dielectric coolant in distribution transformers.* Journal of the Brazilian Chemical Society, 2011. **22**(12): 2292-2303.

58.   Paragkumar N, T., D. Edith and J.L. Six, *Surface characteristics of PLA and PLGA films.* Applied Surface Science, 2006. **253**(5): 2758-2764.

59.   Braun, B., J.R. Dorgan and S.F. Dec, *Infrared spectroscopic determination of lactide concentration in polylactide: An improved methodology.* Macromolecules, 2006. **39**(26): 9302-9310.

60.   Wu, C.H. and A.C. Su, *Functionalization of ethylene-propylene rubber via melt mixing.* Polymer Engineering & Science, 1991. **31**(23): 1629-1636.

61.   John, J., J. Tang, Z. Yang and M. Bhattacharya, *Synthesis and characterization of anhydride-functional polycaprolactone.* Journal of Polymer Science, Part A: Polymer Chemistry, 1997. **35**(6): 1139-1148.

62.   Zhu, R., H. Liu and J. Zhang, *Compatibilizing effects of maleated poly(lactic acid) (PLA) on properties of PLA/soy protein composites.* Industrial and Engineering Chemistry Research, 2012. **51**(22): 7786-7792.

63.   Eren, T., S.H. Küsefoğlu and R. Wool, *Polymerization of maleic anhydride-modified plant oils with polyols.* Journal of Applied Polymer Science, 2003. **90**(1): 197-202.

64.   Cabaniss, S.E., J.A. Leenheer and I.F. McVey, *Aqueous infrared carboxylate absorbances: Aliphatic di-acids.* Spectrochimica Acta - Part A: Molecular and Biomolecular Spectroscopy, 1998. **54**(3): 449-458.

III. RESULTS & DISCUSSION
RESULTS & DISCUSSION

BLOCK III

III.3. USES AND APPLICATIONS OF NEW ENVITONMENTALLY FRIENDLY BIOBASED POLYAMIDES.

III.3.1. Evaluation of the engineering performance of different bio-based aliphatic homopolyamide tubes prepared by profile extrusion

L. Quiles-Carrillo [1], N. Montanes [1], T. Boronat [1], R.Balart [1] and S. Torres-Giner [2, 3]

[1] Technological Institute of Materials (ITM), Universitat Politècnica de València (UPV), Plaza Ferrándiz y Carbonell 1, 03801 Alcoy, Spain;

[2] Novel Materials and Nanotechnology Group, Institute of Agrochemistry and Food Technology (IATA), Spanish National Research Council (CSIC), Calle Catedrático Agustín Escardino Benlloch 7, 46980 Paterna, Valencia, Spain

[3] School of Technology and Experimental Sciences (ESTCE), Universitat Jaume I (UJI), Castellón, Spain
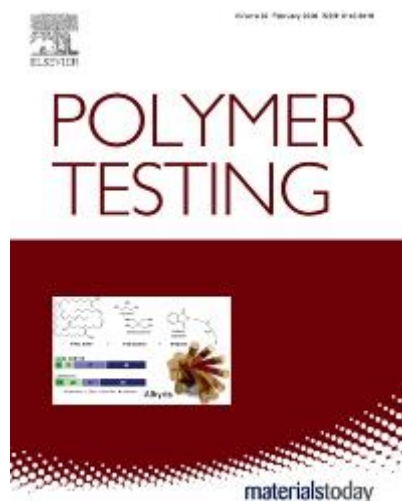
Evaluation of the engineering performance of different bio-based aliphatic homopolyamide tubes prepared by profile extrusion

L. Quiles-Carrillo [a], N. Montanes [a], T. Boronat [a], R. Balart [a], S. Torres-Giner [b, c, *]

[a] Technological Institute of Materials (ITM), Universitat Politècnica de València (UPV), Plaza Ferrándiz y Carbonell 1, Alcoy 03801, Spain
[b] Novel Materials and Nanotechnology Group, Institute of Agrochemistry and Food Technology (IATA), Spanish Council for Scientific Research (CSIC), Calle Agustín Escardino Benlloch 7, Paterna 46980, Spain
[c] School of Technology and Experimental Sciences (ESTCE), Universitat Jaume I (UJI), Avenida de Vicent Sos Baynat s/n, Castellón 12071, Spain

ARTICLE INFO

ABSTRACT

In the present study, three different commercial bio-based polyamides (bio-PAs), namely polyamide 610 (PA610), polyamide 1010 (PA1010), and polyamide 1012 (PA1012), were processed by profile extrusion with an annular die. These aliphatic homopolyamides, also known as "green nylons", are industrially produced by polycondensation reaction of diamines and dicarboxylic acids that are partially or fully obtained from naturally occurring castor oil. The profile-extruded bio-PA tubes were characterized and compared in terms of their thermal, thermomechanical, and mechanical properties and also water uptake. Resultant comparative evaluation indicated that both the methylene-to-amide (CH_2/CONH) ratio and the crystallinity degree of the bio-PAs played the main role in determining the performance of the tubes. Due to significant differences in their CH_2/CONH ratio, the PA610 tubes showed the highest thermal properties while the tubes made of PA1012 presented the highest flexibility and lowest water uptake. Interestingly, the fully bio-based PA1010 tubes offered the most balanced and enhanced engineering performance, which was ascribed to the high crystallinity achieved during profile extrusion. The here-developed bio-PA tubes can fulfil demanding technical requirements and these also certainly represent a sustainable answer to the rising demand for new high-performance biopolymers for engineering applications.

1. Introduction

Polyamides are polymers, generally linear and semi-crystalline, with recurring amide groups as an integral part of the main polymer chain. These are commonly known in the plastics industry as "nylons", which are referred to any polyamide having less than 85% of the amide groups directly connected to two aromatic groups [1]. Discovered by Wallace Carothers and early commercialized in the 1940s by DuPont, polyamides can be either obtained by ring-opening polymerization (ROP) of lactams, *i.e.* their bi-functional monomer, or polycondensation, *i.e.* condensation polymerization of diamines and diacids at elevated temperature [2]. The latter reaction is based on a "nylon salt" solution, where the corresponding salt is previously formed at room temperature using a molar ratio dicarboxylic acid/diamine 1:1. The amide group, along with its essential structural role, contributes to the extraordinary mechanical strength and thermal resistance of polyamides due to its polar nature and high chemical stability. As a result, these thermoplastic materials are traditionally considered as "engineering plastics", being currently manufactured for a wide variety of technically demanding applications such as fibers for clothing for carpets, injection-molded car parts, oil delivery lines and gas pressure pipes, barrier films for food packaging, and soles for high-quality sports shoes [3]. Nowadays, the global plastics market annually requires over 6 million tons of polyamides with a growing rate close to 5% [4]. Traditional polyamide 6 (PA6) and polyamide 66 (PA66), and recently polyamide 12 (PA12), constitute more than 90% of their overall usage in the plastics industry [5].

Even though high-performance plastics are classical petro-chemistry products, polymer chains can also be partially or completely synthesized from bio-based components [6]. In particular, the development of a sustainable route to the production of

 * Corresponding author. Novel Materials and Nanotechnology Group, Institute of Agrochemistry and Food Technology (IATA), Spanish Council for Scientific Research (CSIC), Calle Agustín Escardino Benlloch 7, Paterna 46980, Spain.
 E-mail addresses: storresginer@iata.csic.es, storresginer@hotmail.com (S. Torres-Giner).

Evaluation of the engineering performance of different bio-based aliphatic homopolyamide tubes prepared by profile extrusion

Abstract.

In the present study, three different commercial bio-based polyamides (bio-PAs), namely polyamide 610 (PA610), polyamide 1010 (PA1010), and polyamide 1012 (PA1012), were processed by profile extrusion with an annular die. These aliphatic homopolyamides, also known as "green nylons", are industrially produced by polycondensation reaction of diamines and dicarboxylic acids that are partially or fully obtained from naturally occurring castor oil. The profile-extruded bio-PA tubes were characterized and compared in terms of their thermal, thermomechanical, and mechanical properties and also water uptake. Resultant comparative evaluation indicated that both the methylene-to-amide ($CH_2/CONH$) ratio and the crystallinity degree of the bio-PAs played the main role in determining the performance of the tubes. Due to significant differences in their $CH_2/CONH$ ratio, the PA610 tubes showed the highest thermal properties while the tubes made of PA1012 presented the highest flexibility and lowest water uptake. Interestingly, the fully bio-based PA1010 tubes offered the most balanced and enhanced engineering performance, which was ascribed to the high crystallinity achieved during profile extrusion. The here-developed bio-PA tubes can fulfil demanding technical requirements and these also certainly represent a sustainable answer to the rising demand for new high-performance biopolymers for engineering applications.

Keywords: Green nylons, Methylene-to-amide ratio, Plastics engineering, Structure-property relationships, Tubing extrusion.

INTRODUCTION

Polyamides are polymers, generally linear and semi-crystalline, with recurring amide groups as an integral parts of the main polymer chain. These are commonly known in the plastics industry as "nylons", which are referred to any polyamide having less than 85% of the amide groups directly connected to two aromatic groups [1]. Discovered by Wallace Carothers and early commercialized in the 1940s by DuPont, polyamides can be either obtained by ring-opening polymerization (ROP) of lactams, *i.e.* their bi-functional monomer, or condensation polymerization, i.e. polycondensation of diamines and diacids at elevated temperature [2]. The latter reaction is based on a "nylon salt" solution, where the corresponding salt is previously formed at room temperature using exact ratio dicarboxylic acid/diamine 1:1. The amide group, along with its essential structural role, contributes to the extraordinary mechanical strength and thermal resistance of polyamides due to its polar nature and high chemical stability. As a result, these thermoplastic materials are traditionally considered as "engineering plastics", being currently applied in a wide variety of technically demanding applications such as the manufacturing of fibers for clothing for carpets, injection-molded car parts, oil delivery lines and gas pressure pipes, barrier films for food packaging, and soles for high-quality sports shoes [3]. Nowadays, the global plastics market annually requires over 6 million tons of polyamides with a growing rate close to 5% [4]. Traditional polyamide 6 (PA6) and polyamide 66 (PA66), and more recently polyamide 12 (PA12), constitute more than 90% of their overall usage in the plastics industry [5].

Even though high-performance plastics are classical petrochemistry products, polymer chains can also be partially or completely synthesized from bio-based components [6]. In particular, the development of a sustainable route to the production of bio-based polyamides (bio-PAs) has recently received a high interest due to the growing awareness of the damage sustained by environment [7]. In particular, the synthesis of both traditional and new polyamides from renewable resources could exceptionally reduce high amounts of fossil energy, which is particularly favorable in the light of the growing shortage and rising price of fossil resources [8]. Unfortunately, the use of fully bio-PAs, excluding polypeptides and proteins, is still restricted due to the limited availability of renewable diamines [9]. Thus, increasing the applications of bioPAs is certainly of major interest.

Without doubt, castor oil is nowadays playing the biggest role as the raw material to yield the building blocks for the production of bio-Pas [10]. This is a natural, viscous, pale yellow, non-volatile and non-drying oil with an unusual homogeneous composition. Structurally, castor oil contains 85–95% ricinoleic acid, a 18-carbon (C18) fatty acid, which is available in its triglyceride ester [11]. The oil is obtained from the seed of the Ricinus communis plant, which belongs to the family Eurphorbiacae and predominantly grows in the wild of tropical and sub-tropical countries (*e.g.* Africa, India, Brazil, and China) [12]. Castor oil is not only a naturally occurring resource, but it is also inexpensive and environmentally friendly. Due to its extreme drought resistance, the plant is primarily cultivated in sites that are unsuitable for food production so that it does not compete directly with food purposes [13]. It is estimated that over 600,000 metric tons of castor oil are produced annually, of which at least one third are used for the synthesis of bioPAs [14].

Ricinoleic acid is the starting compound for the different bio-routes, which is obtained by subjecting castor oil either to a transesterfication step or a saponification step [15]. Sebacic acid, *i.e.* 1,10-decanedioic acid, a C10 dicarboxylic acid, is manufactured by heating ricinoleic acid to high temperatures, typically about 250°C, with alkali [16]. Although its manufacturing yields are lower than those of current petrochemical monomers used in the synthesis of traditional polyamides, this route has been found to be cost competitive [17]. Sebacic acid can readily react with petroleum-based 1,6-hexamethylene diamine (HMDA), obtained from butadiene, via polycondensation to produce aliphatic polyamide 610 (PA610). As a result, PA610 is typically 60–63% based on natural resources [18]. Sebacic acid can also polymerize with 1,10-decamethylene diamine (DMDA) to produce aliphatic polyamide 1010 (PA1010). Interestingly, DMDA, a C10 diamine, can be obtained by exposing sebacic acid to ammonia followed by dehydration and hydrogenation [19]. Since both monomers are obtained from castor oil, resultant PA1010 is fully bio-based. Finally, aliphatic polyamide 1012 (PA1012) is a polycondensation product of DMDA and 1,12-dodecanedioic acid. The C12 dicarboxylic acid is typically fossil-based, being 45% the bio-based content of PA1012. However, this can be also obtained from palm kernel oil via a biotechnological process [20]. As a result, PA1012 can also consists up to 100% of renewable raw materials.

Figure III.3.1.1 shows the chemical structure of PA610, PA1010, and PA1012, indicating the weight percentage of renewably sourced ingredients. As it can be observed, these bio-PAs consist of amide groups separated by alkane segments of different length, which results in different amide concentration per polymer chain. Therefore, the methylene-to-amide ($CH_2/CONH$) ratio results in 7, 9, and 10 for PA610, PA1010, and PA1012, respectively. Polyamides with longer aliphatic segments, *i.e.* with higher $CH_2/CONH$ ratios, have reasonably lower amide densities per unit length of chain. Interestingly, the $CH_2/CONH$ ratio, in combination with the chain symmetry, is known to determine the final properties of polyamides [21]. Even-even polyamides form chain-folded sheets in which the amide groups participate in linear hydrogen bonding to one another. Lower $CH_2/CONH$ ratios result in a density increase of hydrogen bonds, which restricts the segmental inter-chain mobility of the long-chain aliphatic methylene groups in the polymer backbone and then increases thermal resistance [21], mechanical strength and abrasive wear performance [22] and, hence, tribological behavior [23]. In addition, hydrogen bonding pulls many of the polyamide chains into more ordered crystalline regions, which further increases the polyamide melting point. In particular, it is considered that resultant hydrogen bonds are able to retain the polyamide chains in an ordered solid phase after the alkane segments have effectively melted [21]. Hydrogen bonding also takes place between polyamide and water or polar absorbed substances, which act as a plasticizer, lowering the glass transition temperature (T_g) and impairing the mechanical performance significantly [24].
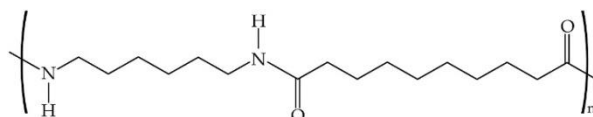
PA610
Based up to 63% on renewable raw materials
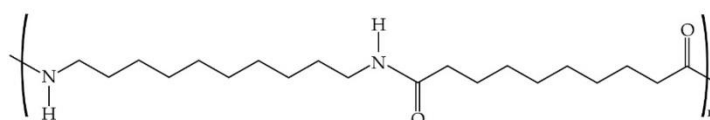
PA1010
Based up to 100% on renewable raw materials
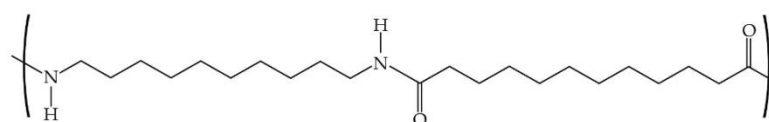
PA1012
Based from 45 to 100% on renewable raw materials

Figure III.3.1.1. Chemical structure and bio-based weight content of polyamide 610 (PA610), polyamide 1010 (PA1010), and polyamide 1012 (PA1012).

Profile extrusion is the high-volume process of making continuous shapes of plastic, ranging from solid to hollow forms, but not including sheet and film. When the polymer melt is extruded through an annular die, round cross-sections such as tubes and pipes are obtained. This is specifically called pipe extrusion or tubing extrusion [25]. During this process, polymer resins, habitually in the form of pellets, flow from the main hopper to the gap between the rotating screw and heated barrel of the extruder. Once the polymer is melted, mixed, and pressurized in the extruder, it is then pumped through the annular die. The extruded product, while being pulled, passes through a vacuum sizer in which it attains its final dimensions. This is followed by cooling via chilled water immersion or spraying and cutting to fixed lengths. Pipes, with a diameter of 2 m or greater, and tubes, from 10 mm down to below 1 mm, can be processed by profile extrusion [26]. The annular dies used in this process are normally of spider or spiral mandrel design [27].

The present study reports, for the first time, the preparation by profile extrusion of tubes made of three different bio-PAs, namely PA610, PA1010, and PA1012. Since the amide group concentration controls the physical properties of aliphatic polyamides, the thermal, thermomechanical, and mechanical performance and water uptake of these bio-PA tubes were evaluated and compared. The obtained results were ascribed to the chemical structure of the bio-PAs, based on different $CH_2/CONH$ ratios, and the processing conditions in which the tubes were obtained.

EXPERIMENTAL

Materials

PA610 was supplied by DuPont (Solingen, Germany) as medium-viscosity grade Zytel® RS LC4601. This homopolyamide is developed for extrusion applications, has a density of 1.04 g/cm^3, and contains approximately 60 wt.-% of renewably sourced ingredients. Commercial PA1010 was Grilamid® XE 4181 provided by EMS-Chemie A.G. (Domat/Ems, Switzerland). This is a fully bio-based high-viscosity extrusion-grade homopolyamide with a density of 1.05 g/cm^3. Finally, PA1012 was Vestamid® Terra DD 2230 (CW1120), distributed by Evonik Industries (Essen, Germany). This is a high-viscosity homopolyamide with a density of 1.03 g/cm^3 and 45 wt.-% based on bio-renewables. The renewable weight contents were provided by the manufacturers according to ASTM D6866 standard.

Profile extrusion

Extrusion of tubes was performed using a Collin E30M single-screw extruder equipped with a 15-mm annular die based on a spider ring design. The barrel extruder presented a length/diameter (L/D) of 30 and screw speed was 40 rpm. Temperature profile was set accordingly to provide a melt temperature during extrusion of 250 °C, for PA610, and 225 °C, for PA1010 and PA1012. In all cases die temperature was set at 275 °C. The process is illustrated in **Figure III.3.1.2**, showing its different sections. Briefly, the extruded tube exiting the die travelled a short distance in air, allowing a thin skin to form. Then it passed through a vacuum sizing chamber, which was equipped with sizing rings and operated at 230 mbar. The tubes, while being pulled, entered a cooling bath with chilled water at 15 °C to dissipate the heat. The pull-out system was a caterpillar-type puller (capstan). Finally, annealing was performed in a reheat station working with an open flame. Line speed was 5 m/min. Tube specimens of different lengths with an outer diameter of 10 mm and wall thickness of 1 mm were ejected from the cutting station.
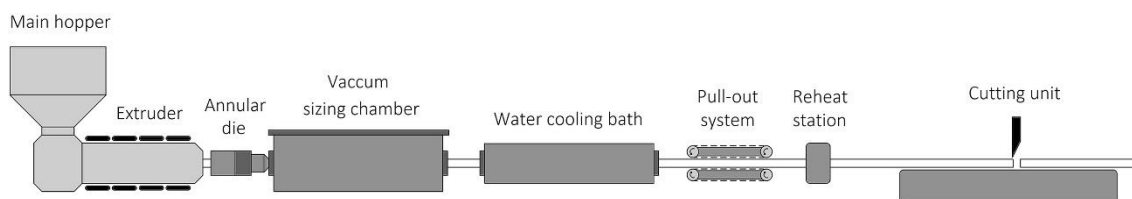
Figure III.3.1.2. Schematic representation of the profile extrusion process.

Infrared spectroscopy

Chemical analysis was performed via attenuated total reflection–Fourier transform infrared (ATR-FTIR) spectroscopy. Spectra were recorded using a Bruker S.A. Vector 22 (Madrid, Spain) coupled to a PIKE MIRacle™ single reflection diamond ATR accessory (Madison, USA). Data were collected as the average of ten scans from 4000 to 400 cm^{-1} at a spectral resolution of 4 cm^{-1}.

Thermal characterization

Thermal transitions were obtained by differential scanning calorimetry (DSC) using a Mettler-Toledo, Inc. (Schwerzenbach, Switzerland) 821 model. For this, *ca.* 5 mg of tube sample was placed in 40-µl hermetic aluminum sealed pans, previously calibrated with an indium standard. The analysis was performed in a dry reducing atmosphere in which nitrogen flowed at a constant rate of 66 mL/min. Samples were subjected to a two-step regime at a heating rate of 10 °C/min to evaluate the thermal transitions. An initial heating scan from 30 to 250 °C was followed by a cooling scan to 30 °C. The cold crystallization temperature (T_{cc}), normalized cold crystallization enthalpy (ΔH_{cc}), melting temperature (T_m), and normalized enthalpy of melting (ΔH_m) were obtained from the heating scan while the crystallization temperature from the melt (T_c) and normalized enthalpy of crystallization (ΔH_c) were determined from the cooling scan. The percentage of crystallinity (X_c) was determined using the following **Equation III.3.1.1**:

$$X_C = \left[\frac{\Delta H_m - \Delta H_{CC}}{\Delta H_m^0}\right] \cdot 100 \qquad \textbf{Equation III.3.1.1}$$

Where ΔH_m^0 (J/g) represents the theoretical melt enthalpy of a fully crystalline bio-PA, considering 197 J/g for PA610 [28], 244 J/g for PA1010 [29], and 209.2 J/g for PA1012 [30].

Thermal stability was determined by thermogravimetric analysis (TGA) in a TGA/SDTA 851 thermobalance from Mettler-Toledo, LLC (Columbus, OH, USA). The heating program was set from 30 to 700 °C at a heating rate of 20 °C/min in air atmosphere with a constant flow-rate of 66 mL/min. Approximately 5–7 mg of tube sample was used for the measurements. The onset degradation temperature was defined as the temperature at 5% weight loss ($T_{5\%}$) and the degradation temperature (T_{deg}) was obtained from the maximum value of the first derivative.

Thermomechanical characterization

Dynamic mechanical thermal analysis (DMTA) was conducted with a single cantilever in flexion mode using a DMA-1 from Mettler-Toledo GmbH (Greifensee, Switzerland). Tube samples of 10 mm were cut longitudinally into stripes of 10 × 5 × 1 mm^3 and subjected to a temperature program ranging from 0 to 140 °C at a heating rate of 2 °C/min, a deformation frequency of 1 Hz, and a strain of 0.1%.

Vicat softening temperature and heat deflection temperature (HDT) were both measured in a Vicat/HDT station VHDT 20 from Metrotec S.A. (San Sebastián, Spain). Vicat values were obtained according ISO 306, following B50 method. This was performed on circular compression-molded samples with a diameter of 2.5 cm and a thickness of 4 mm prepared in a 10-Tn hydraulic press from Robima S.A. (Valencia, Spain) equipped with two hot aluminum plates and a temperature controller from Dupra S.A. (Castalla, Spain) [31]. Specimens were cut using a die on a hydraulic press model MEGA KCK-15A from Melchor Gabilondo S.A. (Vizcaya, Spain) [32]. During this test, each specimen was placed in the testing apparatus so that the penetrating

needle rested on its surface at least 1 mm from the edge. The applied force was 50 N and the heating rate was 50 °C/h.

Regarding HDT characterization, this was carried out using 80-mm long tubes based on ISO 75. The bio-PA tubes were placed at a distance between supporting edges of 60 mm and a weight of 320 g was applied, which corresponds to a pressure of 1.8 MPa. The heating rate was 120 °C/h as recommended in the corresponding standard.

Dimensional stability was studied by measuring the coefficient of linear thermal expansion (CLTE) using a thermomechanical analyzer (TMA) Q400 model from TA Instruments (Delaware, USA). Test was performed on 7-mm long tubes. The heating program was set from 0 to 140 °C with a constant heating rate of 2 °C/min and a load of 0.02 N. All measurements were done in triplicate.

Mechanical characterization

Tube specimens with a total length of 150 mm were tested in a universal test machine ELIB 30 from S.A.E. Ibertest (Madrid, Spain). Tensile tests were performed according to ISO 527. A 5-kN load cell and a cross-head speed of 5 mm/min were employed. Shore D hardness was determined in a durometer 676-D model from J. Bot S.A. (Barcelona, Spain) following ISO 868. All specimens were tested in a controlled chamber at room conditions, *i.e.* 23 °C and 50% RH. At least six samples for each material were analyzed and averaged.

Water uptake measurements

Tube specimens of 80 mm were immersed in distilled water at 23 ± 1 °C. Samples were extracted weekly and weighed in an analytical balance with an accuracy of ±0.1 mg after removing the residual water with a dry cloth. The evolution of water uptake was followed over a whole period of 9 weeks. Measurements were done in triplicate.

RESULTS AND DISCUSSION

Visual aspect

Figure III.3.1.3 shows the resultant profile-extruded tubes of the here-studied bio-PAs. One can observe in this image that continuous tubes with a diameter of 10 mm and a homogenous surface were produced. In general, the obtained bio-PA tubes presented high translucency but low transparency, as expected for semi-crystalline polymers. No visual differences among the tubes were noticeable.
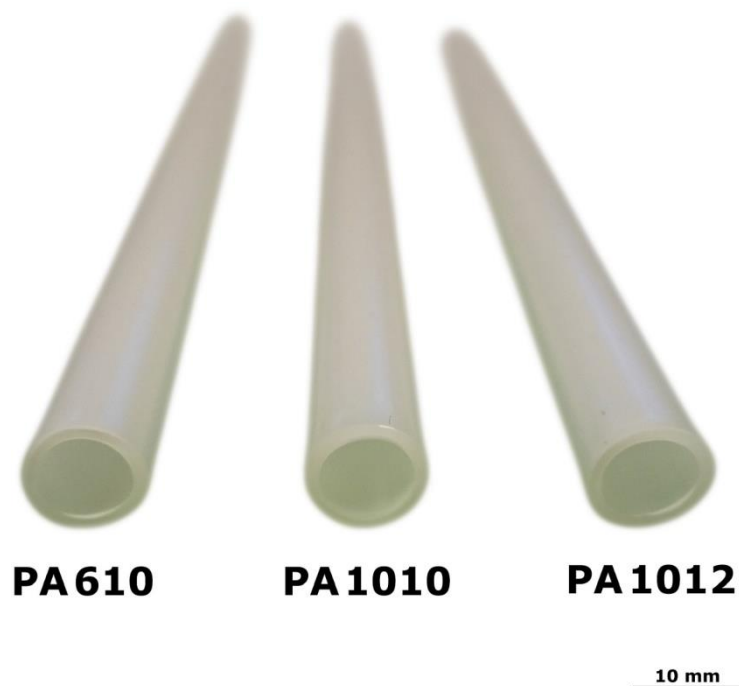
Figure III.3.1.3. Profile-extruded tubes of polyamide 610 (PA610), polyamide 1010 (PA1010), and polyamide 1012 (PA1012).

Chemical properties

Figure III.3.1.4 shows the FTIR characteristic absorption peaks of the here-studied bio-based PAs. The broad absorption peak at ~3300 cm^{-1} has been mainly reported for the valence stretch vibrations of hydrogen atoms bonded as N–H of terminal amine groups [33-35]. The intense peaks observed at 2919 and 2851 cm^{-1} are caused from the asymmetric and symmetric C–H stretching vibration of methylene groups, respectively [28]. These peaks were very similar for the three bio-PAs. However, some interesting changes can be observed in these spectra at lower wavenumbers.

For the PA1012 and PA1010 spectra the main absorption peak was seen at 1635 cm^{-1}, which has been well assigned to the C=O of Amide I in both α- and β-crystalline phases [29], [34, 35]. This moved down to 1632 cm^{-1} in the case of PA610, which can be either related to its higher amide density or changes in crystallinity. In addition, the strong peak at 1540 cm^{-1} in the spectra of both PA1012 and PA610, which belongs to the bending vibration of N–H in Amide II [34, 36], shifted to 1535 cm^{-1} for PA1010. This band displacement to a lower frequency region has recently been ascribed to crystallization increases in polyamides [37]. The band at 1462 cm^{-1} has been related to the contribution of the C–N stretching vibration of amide groups [29] and C–H bending vibration in methylene groups [35]. The group of bands in the range 1300–1200 cm^{-1} are attributed to the gauche nitrogen-methylene group, *i.e.* N–H and C–H twisting [28], [38]. These absorption bands, showing a main peak centered at 1238 cm^{-1}, became sharper and more intense in the spectrum of PA1010. This suggests that chain conformation of the methylene sequences in PA1010 was more ordered. The aforementioned changes can be therefore ascribed to the more symmetrical chain

structure of PA1010, which favors molecular folding and subsequent crystallization. The low-intense bands at 1160 and 940 cm^{-1} that can be observed for both PA1010 and PA1012 are attributed to the skeletal motion and in-plane modes of CO–NH bonds, respectively, which are characteristic of amide groups in semi-crystalline polyamides [39]. For PA610, this peak shifted towards 922 cm^{-1}. In this sense, the bands located at 936 and 922 cm^{-1} have been attributed to the amide C–C=O vibration stretching that are related to the crystalline and amorphous phases in PA66, respectively [28]. This indicates that the structure of PA610 was predominantly amorphous. Finally, the peak at 720 cm^{-1} corresponds to the shear vibration of methylene groups, *i.e.* C–H rocking [35]. This was more intense in the spectra of PA1012 and PA1010 than in the PA610 spectrum possibly due to the lower CH2/CONH ratio of the latter bio-PA.
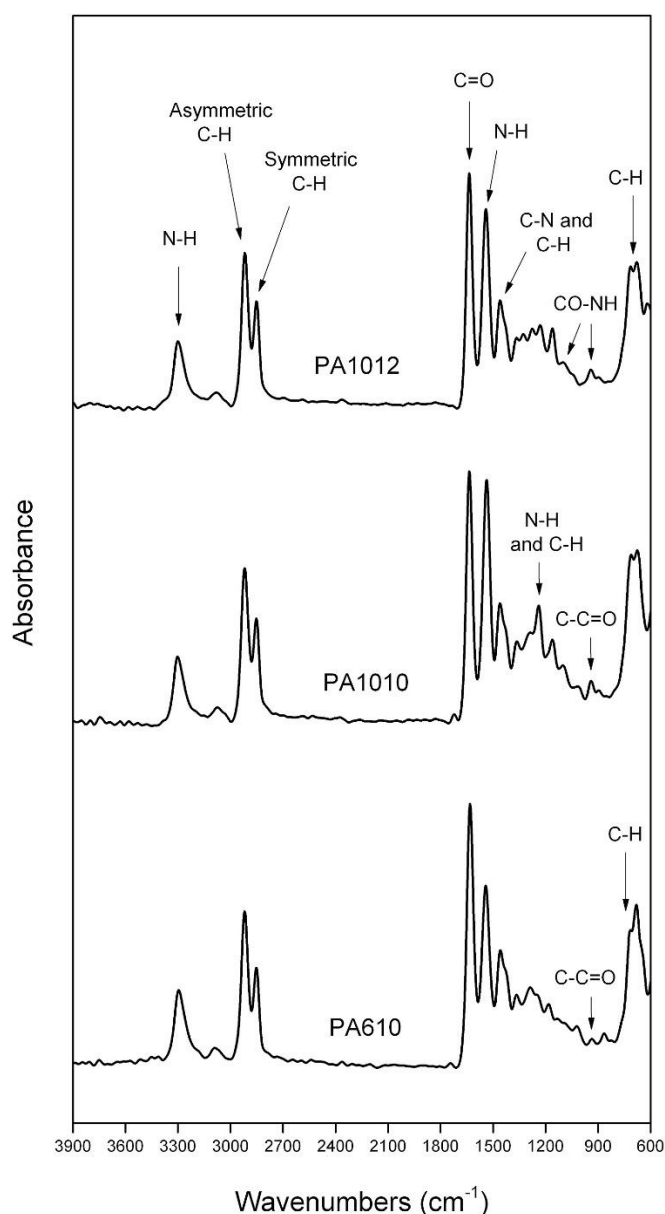
Figure III.3.1.4. Fourier transform infrared (FTIR) spectra, from bottom to top, of polyamide 610 (PA610), polyamide 1010 (PA1010), and polyamide 1012 (PA1012). Arrows indicate the bands discussed in the text.

Thermal properties

Figure III.3.1.5 includes the heating and cooling DSC scans of the bio-PA tubes and the results obtained from these curves are summarized in **Table III.3.1.1**. The melting thermograms, gathered in **Figure III.3.1.5a**, indicate that all bio-PAs showed T_g values in the range of 40–60 °C. However, these were difficult to elucidate, particularly for PA1010 and PA1012, probably due to their reduced amorphous phase. It can also be observed that the bio-PA tubes did not show any cold crystallization peak before melting, which can be related to the efficient cooling conditions and annealing treatment performed in the last stage of profile extrusion.
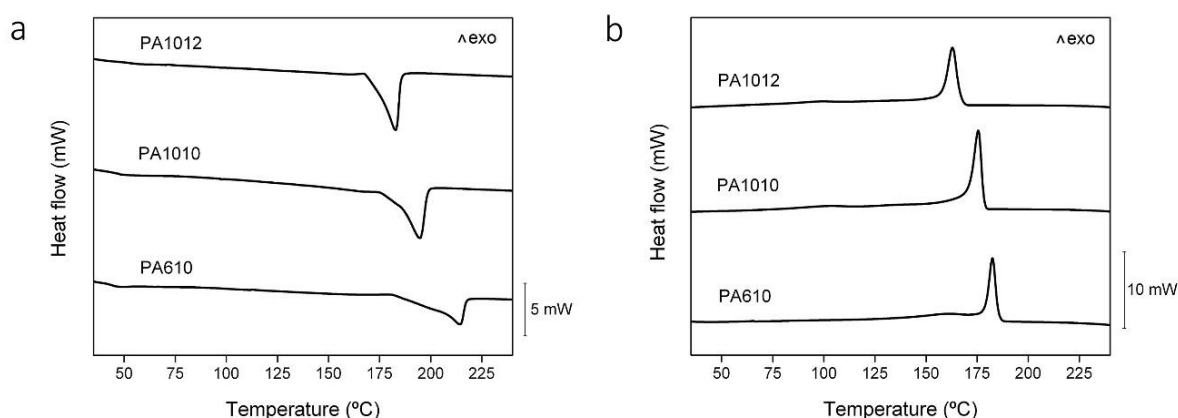
Figure III.3.1.5. Differential scanning calorimetry (DSC) curves of polyamide 610 (PA610), polyamide 1010 (PA1010), and polyamide 1012 (PA1012) for: a) Heating scan; b) Cooling scan.

Table III.3.1.1. Thermal properties obtained from the differential scanning calorimetry (DSC) and thermogravimetric analysis (TGA) curves in terms of normalized enthalpy of crystallization (ΔH_c), crystallization temperature (T_c), normalized enthalpy of melting (ΔH_m), melting temperature (T_m), amount of crystallinity (X_c), degradation temperature at 5% of mass loss ($T_{5\%}$), degradation temperature (T_{deg}), mass loss at T_{deg}, and residual mass at 650 °C for polyamide 610 (PA610), polyamide 1010 (PA1010), and polyamide 1012 (PA1012).

	DSC					TGA			
Sample	ΔH_c (J g^{-1})	T_c (°C)	ΔH_m (J g^{-1})	T_m (°C)	X_c (%)	$T_{5\%}$ (°C)	T_{deg} (°C)	Mass loss (%)	Residual mass (%)
PA610	22.51 ± 1.03	182.6 ± 1.1	15.24 ± 0.85	215.5 ± 1.2	7.8 ± 0.8	331.9± 1.5	462.4 ± 1.6	47.3 ± 0.9	0.62 ± 0.06
PA1010	30.77 ± 1.18	176.5 ± 0.9	65.91 ± 0.94	195.4 ± 0.9	27.1 ± 1.2	323.3 ± 1.9	460.7 ± 1.1	47.6 ± 1.3	0.09 ± 0.03
PA1012	25.56 ± 0.96	163.4 ± 0.6	33.59 ± 1.05	183.4 ± 1.1	16.1 ± 0.9	337.6 ± 2.4	463.9 ± 1.3	45.3 ± 1.1	0.21 ± 0.04

All three bio-PAs presented one intense melting peak, suggesting the presence of a predominant single crystalline form in the tubes that can be ascribed to the slow

cooling rate applied during profile extrusion. This observation differentiates the here-evaluated bio-PAs from short-chain polyamides (*e.g.* PA6) that typically exhibit a polymorphism behavior, showing multiple melting peaks of different intensities due to the presence of different crystalline forms where distinct crystalline lamellae coexist, *i.e.* α, β, and γ [40]. In particular, the α-form is the most stable and perfect crystalline phase, in which hydrogen bonds are formed between antiparallel chains, stretching to a lower extent the rotation of the polymer chains and, therefore, increasing chains packing [41]. However, one can also observe that the melting peaks were relatively broad, showing the presence of a shoulder at lower temperatures. This was particularly noticeable for PA610, which can denote the presence of an additional crystallite population. According to Thompson-Gibbs relationship, this reflects the melt recrystallization of less perfect crystals, which has been well reported for either conventional polyamides (e.g. PA6, PA66) [42, 43] but also for newly PA610 [36] and PA1010 [44].

Due to its lower $CH_2/CONH$ ratio, PA610 presented the highest value of T_m (~216 °C) while PA1010 and PA1012 melted at approximately 195 and 183 °C, respectively. Therefore, the here-studied bio-PAs followed perfectly correlation between melting temperature and $CH_2/CONH$ ratio. For instance, a similar melting point for PA1012 has been recently reported [45]. Regarding PA1010, this melting point has been precisely ascribed to the above-described α-form crystals, which are based on a triclinic system [44]. This value certainly places the thermal properties of these bio-PAs in between those of conventional medium- or long-chain PA12 (~179 °C) [46] and short-chain PA6 (~221 °C) [47]. Furthermore, as commented above, the melting peaks of PA1010 and PA1012 were clearly sharper than that of PA610.

Figure III.3.1.5b shows the DSC thermograms taken during the cooling scan. All bio-PAs crystallized from the melt in a single peak according to their $CH_2/CONH$ ratio too. In particular, values of T_c were observed at 183, 177, and 163 °C for PA610, PA1010, and PA1012, respectively. It can be observed that PA1010 presented the highest X_c value (~27%) while PA610 showed the lowest (~8%), even though the latter bio-PA is based on a shorter chain structure, *i.e.* its amide density per chain is higher [24]. The larger crystallinity degree observed for PA1010 can be related to its more symmetrical chain structure in which the diamine and dicarboxylic acid are both based on a C10 chemical structure. This can potentially result in a high regular spacing of the amide groups along the polymer chains that, in turns, favors the formation of orderly regions of crystallinity. In relation to the crystallinity degree observed for PA1012 (~16%), which was higher than PA610 but lower than PA1010, this can be explained by a decrease in the average number of inter-chain hydrogen bonds caused by the increase of the diacid chain length [28].

Table III.3.1.1 also includes thermal stability values of the profile-extruded bio-PA tubes. All samples presented similar values of thermal degradation. No moisture content was observed in the samples since no noticeable weight loss occurred below 100 °C. In particular, the bio-PA tubes remained stable up to approximately 320–340 °C, showing a T_{deg} of *ca.* 460 °C. Similar thermal degradation profiles in bio-PAs have been previously reported [44], [48]. It was particularly indicated that this mainly involves a β-C-H transfer reaction mechanism, producing ketoamides as the primary decomposition products [49].

Thermomechanical properties

Figure III.3.1.6 presents the temperature dependence of the storage modulus (G') and damping factor (tan δ) of the bio-PA tubes. It can be clearly observed in **Figure III.3.1.6a** that, as temperature increased, the storage modulus gradually decreased. At the glassy plateau region, for instance 25 °C, PA610 displayed higher storage modulus (~1225 MPa) than PA1010 (~1030 MPa) and, more significantly, than PA1012 (~618 MPa). This value was expected due to the lower $CH_2/CONH$ ratio of PA610. However, comparison of the biopolymer tubes in the rubbery plateau region, for instance 100 °C, indicated that the storage modulus of PA1010 was considerably higher (~259 MPa) than that observed for both PA1012 (~164 MPa) and PA610 (~107 MPa). This interesting observation confirms previous chemical and thermal analyses, indicating that PA610 is a highly amorphous material. As a result, in the rubber-like state, *i.e.* above T_g, mechanical strength of PA610 was considerably reduced. On the contrary, the higher crystallinity of PA1012 and, particularly, of PA1010, potentially restricted the movement of the polymer chains and improved elasticity as temperature was increased.
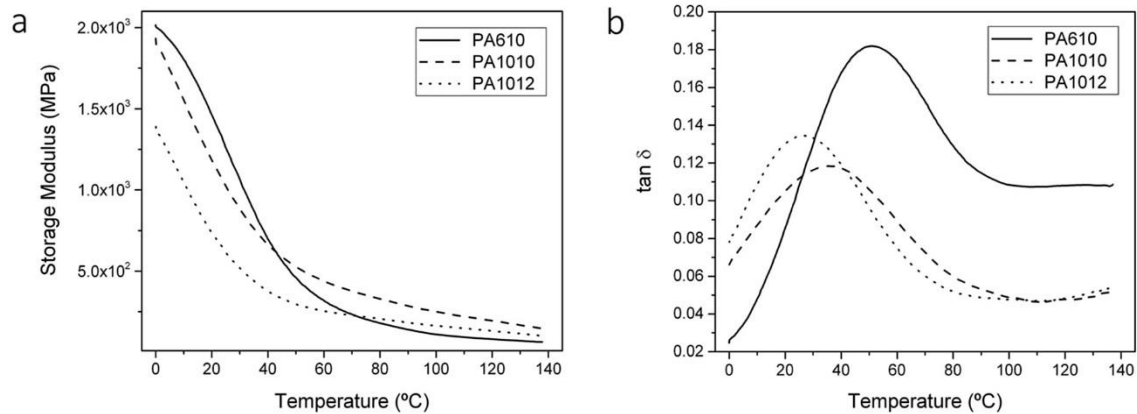
Figure III.3.1.6. Dynamic mechanical thermal analysis (DMTA) curves of polyamide 610 (PA610), polyamide 1010 (PA1010), and polyamide 1012 (PA1012) for: **a)** Storage modulus *vs.* temperature; **b)** Damping factor (tan δ) *vs.* temperature.

Figure III.3.1.6b shows the damping factor as a function of temperature for the PA610, PA1010, and PA1012 tubes measured by DMTA. A loss peak can be seen in the curves that points out the α-relaxation of the bio-PAs, which is related to their T_g. Due to PA610 presents the lowest $CH_2/CONH$ ratio, *i.e.* the highest amide density, this bio-PA exhibited the highest α-relaxation value (~51 °C). This was followed by PA1010 (~38 °C) and PA1012 (~27 °C). Therefore, the α-relaxation values perfectly correlated with the CH2/CONH ratio. In addition, the peak intensities for both PA1010 and PA1012 did not only shift towards lower temperatures but, more importantly, these were also significantly lower than that for PA610. This observation clearly confirms that a lower amount of amorphous part underwent glass transition in both PA1010 and PA1012 when compared to PA610.

Table III.3.1.2 includes the CLTE values of the bio-PA tubes, below and above T_g. All samples showed lower CLTE values below T_g than above T_g. By increasing temperature, the bio-PA tubes offered less resistance against thermal expansion,

leading higher CLTE values. The highest CLTE values were clearly observed for PA1010, which is related to the formation of a stronger crystal network that certainly reduces the biopolymer degree of freedom. Similar values were recently reported for compression-molded PA610 parts [48]. From the thermal expansion test, T_g values were also obtained, defined as the temperature in which the slope of CLTE changes. As one can observe in the table, these values ranged from 40 to 50 °C, following the same trend as the α-relaxation values determined above by DMTA. In general, all bio-PAs presented T_g values close to that of PA6 (~53 °C) [47]. Indeed, variations in the aliphatic chain length within the repeating unit are known to have a small effect on T_g of short- and medium-chain polyamides [50].

Table III.3.1.2. Thermomechanical properties in terms of the coefficient of linear thermal expansion (CLTE) below and above glass transition temperature (T_g), Vicat softening point, and heat deflection temperature (HDT) for polyamide 610 (PA610), polyamide 1010 (PA1010), and polyamide 1012 (PA1012).

Sample	CLTE test			VST (°C)	HDT (°C)
	CLTE below T_g (μm/m°C)	CLTE above T_g (μm/m°C)	T_g (°C)		
PA610	124.6 ± 1.4	139.8 ± 1.9	49.8 ± 1.2	87.2 ± 1.1	46.3 ± 1.6
PA1010	171.3 ± 1.6	254.6 ± 1.5	42.9 ± 1.4	137.4 ± 1.2	58.6 ± 1.8
PA1012	120.6 ± 1.3	142.2 ± 1.4	45.2 ± 1.3	120.3 ± 1.4	53.4 ± 1.2

In **Table III.3.1.2** the values of Vicat softening point and HDT are also listed. These are two important factors when selecting a plastic material for a high-temperature application. In this regard, Vicat reflects the softening degree that would be reached when the bio-PAs are subjected to indentation conditions at a given temperature. In relation to HDT, it determines their upper mechanical use in terms of the temperature limit. In this table, it can be observed that, while PA1010 presented the highest values of both thermomechanical factors, the lowest values were observed for PA610. From the above discussion, these results can be certainly ascribed to the degree of crystallinity observed for the different bio-PAs, showing a good correlation with previous DMTA results. In particular, the here-obtained HDT value for the PA1010 tubes (~60 °C) is positively close to that previously reported for injection-molded pieces of PA6 (62 °C) [51].

Mechanical properties

Figure III.3.1.7 shows the tensile stress-strain curves at room temperature for the bio-PA tubes. The mechanical results, in terms of tensile modulus (E), tensile strength at yield (σ_y), and elongation at break (ε_b), are summarized in **Table III.3.1.3**. The mechanical curve of PA610 showed a double yielding while the PA1010 and PA1012 curves displayed a more pronounced ductile behavior. Interestingly, all tensile curves presented strain-hardening phenomenon at large strains. This has been well explained in semi-crystalline polyamides by an induced mechanism of crystals lamellae reorientation process or, in some cases, by a change of both crystal form and

size during plastic deformation [52], [53]. The tensile moduli were obtained from the initial linear regions of the curves in the lower strain range, *i.e.* <0.025%. As it was previously observed during DMTA, PA610 showed the highest tensile modulus, *i.e.* 516.8 MPa. This was very similar to that of PA1010, *i.e.* 507.4 MPa, but higher than that of PA1012, *i.e.* 408.6 MPa. However, in relation to tensile strength, the PA1010 tube presented the highest value, *i.e.* ~40 MPa, which was approximately 14% and 28% higher than those observed for PA1012 and PA610, respectively. As previously described during the thermomechanical analysis, the enhanced mechanical strength of PA1010 in comparison to the other bio-PA tubes can be ascribed to its higher degree of crystallinity. Furthermore, PA1012 produced the most flexible tubes, showing an elongation-at-break value of approximately 245% due to this bio-PA presents the highest methylene content [54]. Regarding the ductility of the other tubes, PA1010 showed a slightly higher value of elongation at break than PA610, *i.e.* 197% vs. 186%. It is also worthy to note that the here-studied bio-PA tubes presented intermediate elongation-at-break values between those observed for more elastic PA6 (140%) [55] and more ductile PA12 (286%) [56], both processed by injection molding.
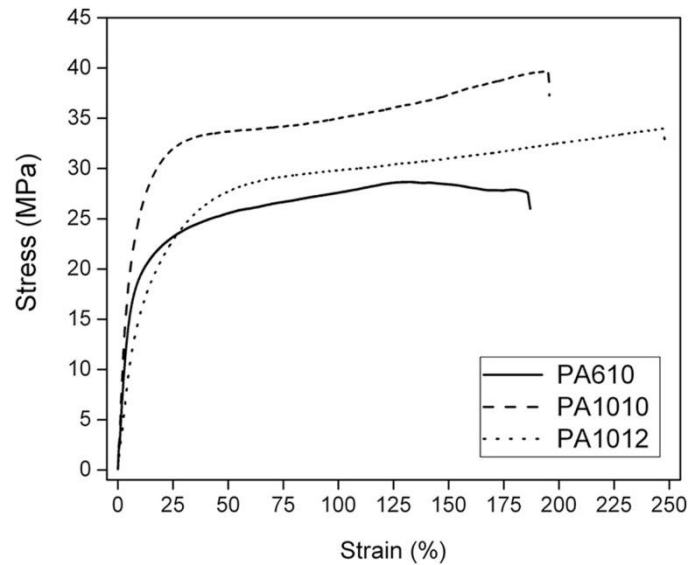
Figure III.3.1.7. Typical tensile stress-strain curves of polyamide 610 (PA610), polyamide 1010 (PA1010), and polyamide 1012 (PA1012) tubes.

Table III.3.1.3. Mechanical properties in terms of tensile modulus (E), tensile strength at yield (σ_y), elongation at break (ε_b), and Shore D hardness for polyamide 610 (PA610), polyamide 1010 (PA1010), and polyamide 1012 (PA1012).

Sample	Tensile test			Shore D hardness
	$E_{tensile}$ **(MPa)**	$\sigma_{tensile}$ **(MPa)**	$\varepsilon_{tensile}$ **(%)**	
PA610	516.8 ± 12.1	28.7 ± 0.3	185.6 ± 12.3	64.8 ± 0.8
PA1010	507.4 ± 24.9	39.9 ± 1.3	196.7 ± 11.7	64.2 ± 0.9
PA1012	408.6 ± 15.1	34.3 ± 0.5	245.3 ± 14.4	61.6 ± 1.0

Finally, in **Table III.3.1.3** the values of Shore D hardness are also included. One can observe that hardness followed the same trend previously observed in the tensile modulus, having the PA610 and PA1010 tubes the highest values. Thus, higher values of hardness can be related to an enhancement of the biopolymer elasticity [57]. However, differences in hardness among the bio-PA tubes were relatively small. In summary, from a mechanical point of view, it can be concluded that PA1010 certainly offers enhanced flexibility with the additional benefit of a relatively high mechanical strength and hardness.

Water uptake

Water absorption is one of the most important characteristics of polyamide-based parts for plastics engineering applications. In particular, this phenomenon has been widely studied for polyamides, indicating that water molecules are sorbed only in the amorphous regions by involving two neighboring amide groups in an accessible region [58]. In the first amide, a water molecule is bound by dipole-dipole interactions to the carbonyl groups, *i.e.* hydrogen bonds, while two other water molecules remain loosely bonded in the other amide between the C–O and N–H groups [49]. As it can be observed in **Figure III.3.1.8**, the immersed bio-PA tubes absorbed different weight amounts of water until these reached a plateau after approximately 4 weeks. In particular, water absorption values of 1.93, 1.20, and 0.95 wt.-% were observed for PA610, PA1010, and PA1012, respectively. Therefore, as it has been already established in previous studies concerning polyamides [59], an increase in the $CH_2/CONH$ ratio resulted in a decrease in the water uptake at equilibrium. However, since water is known to be only absorbed by the amorphous phase, crystallinity had a noticeable effect on water uptake too. This explains the significant difference observed between PA610, more amorphous, and the other two bio-PAs. In particular, it is considered that polymer crystallites can hinder translational mobility of water molecules that are sorbed in the amorphous phase [60]. Overall, the water absorption of the here-developed bio-PA tubes was relatively low, in particular when these values are compared to that of conventional PA6 (~8.5 wt.-%) [61]. This encouragingly suggests that their mechanical properties would be scarcely affected by atmospheric humidity.
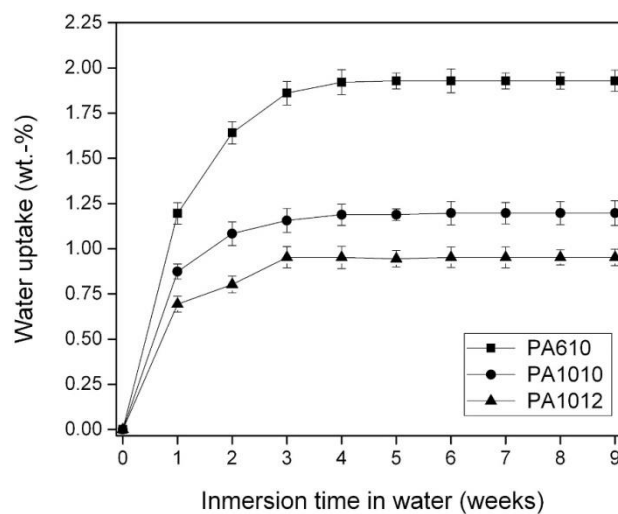
Figure III.3.1.8. Water uptake of polyamide 610 (PA610), polyamide 1010 (PA1010), and polyamide 1012 (PA1012) tubes.

CONCLUSIONS

The present study ruled out the differences in the thermal, thermomechanical, and mechanical properties and also water uptake of profile-extruded tubes of PA610, PA1010, and PA1012. The obtained data were analyzed and compared in view of their different chemical structures and degrees of crystallinity. It was observed that the $CH_2/CONH$ ratio had a main role in determining the thermal properties, *i.e.* T_g, T_c, and T_m, and water uptake, but it had a lower impact on the thermomechanical and mechanical performance than the crystallinity degree. In particular, it was observed that the PA610 tubes presented a similar thermal performance but lower thermomechanical and mechanical properties than short-chain polyamides, for instance PA6, being relatively rigid at room temperature. Meanwhile, PA1010 interestingly produced highly semi-crystalline tubes with very balanced physical properties, showing peculiar properties of an engineering thermoplastic. Finally, the PA1012 tubes were much more flexible and these may find applications in the same domain as, for instance, those made of PA12. In general, the PA1010 and PA1012 chemical structures have longer aliphatic segments and lower amide densities than PA610, but these still show higher melting transition temperature than general-purpose plastics such as polyolefins. Therefore, these novel bio-PA tubes can be a good candidate for engineering applications with enhanced sustainable characteristics. Additionally, the effect of chemical agents, fuels, and industrial fluids on the stability and performance of these bio-PA tubes would warrant further investigation.

Acknowledgements

REFERENCES

1. Marchildon, K., *Polyamides – Still Strong After Seventy Years*. Macromolecular Reaction Engineering, 2011. **5**(1): 22-54.
2. Carothers, W.H., *Studies on polymerization and ring formation. I. An introduction to the general theory of condensation polymers*. Journal of the American Chemical Society, 1929. **51**(8): 2548-2559.
3. Pervaiz, M., M. Faruq, M. Jawaid and M. Sain, *Polyamides: Developments and applications towards next-generation engineered plastics*. Current Organic Synthesis, 2017. **14**(2): 146-155.
4. Fischer, M., *Polyamides (PA)*. Kunststoffe Plast Europe, 2004. **94**(10): 90-95.
5. Siejak, V. and H.B. Lüchtefeld, *Global market for high-tenacity polyamide and polyester filament yams 2008-2010*. Chemical Fibers International, 2011. **61**(3): 135-136.
6. Carole, T.M., J. Pellegrino and M.D. Paster, *Opportunities in the industrial biobased products industry*. Applied Biochemistry and Biotechnology - Part A Enzyme Engineering and Biotechnology, 2004. **115**(1-3): 871-885.
7. Nakayama, A., *Development of biobased polyamides*. Sen'i Gakkaishi, 2010. **66**(11): 368-372.
8. Shen, L., E. Worrell and M. Patel, *Present and future development in plastics from biomass*. Biofuels, Bioproducts and Biorefining, 2010. **4**(1): 25-40.

9.   Pardal, F., S. Salhi, B. Rousseau, M. Tessier, S. Claude and A. Fradet, *Unsaturated Polyamides from Bio-Based Z-octadec-9-enedioic Acid.* Macromolecular Chemistry and Physics, 2008. **209**(1): 64-74.

10.   Ogunniyi, D.S., *Castor oil: A vital industrial raw material*. Bioresource Technology, 2006. **97**(9): 1086-1091.

11.   Desroches, M., M. Escouvois, R. Auvergne, S. Caillol and B. Boutevin, *From vegetable oils to polyurethanes: synthetic routes to polyols and main industrial products*. Polymer Reviews, 2012. **52**(1): 38-79.

12.   Olsnes, S., *The history of ricin, abrin and related toxins*. Toxicon, 2004. 44(4): 361-370.

13.   Koigeldina, A.E., T. Nurgasenov and B.S. Rahmetolaevich, *Structure of a crop and productivity of a castor-oil plant depending on periods of sowing, norms of sowing and seeding depth.* Biosciences Biotechnology Research Asia, 2015. 12(1): 51-57.

14.   Severino, L.S., et al., *A review on the challenges for increased production of castor*. Agronomy Journal, 2012. **104**(4): 853-880.

15.   Jiang, Y. and K. Loos, *Enzymatic synthesis of biobased polyesters and polyamides*. Polymers, 2016. 8(7).

16.   Yasuda, M. and A. Miyabo, *Polyamide derived from castor oil*. Sen'i Gakkaishi, 2010. **66**(4): P137-P142.

17.   Vasishtha, A.K., R.K. Trivedi and G. Das, *Sebacic acid and 2-octanol from castor oil*. Journal of the American Oil Chemists' Society, 1990. **67**(5): 333-337.

18.   Ogunsona, E.O., M. Misra and A.K. Mohanty, *Sustainable biocomposites from biobased polyamide 6,10 and biocarbon from pyrolyzed miscanthus fibers*. Journal of Applied Polymer Science, 2017. **134**(4): n/a-n/a.

19.   Winnacker, M. and B. Rieger, *Biobased Polyamides: Recent Advances in Basic and Applied Research*. Macromolecular Rapid Communications, 2016. **37**(17): 1391-1413.

20.   Niaounakis, M., *Biopolymers: Processing and Products*. 2015, William Andrew Publishing: Oxford.

21.   Jones, N.A., E.D.T. Atkins, M.J. Hill, S.J. Cooper and L. Franco, *Chain-folded lamellar crystals of aliphatic polyamides.* Investigation of nylons 4 8, 4 10, 4 12, 6 10, 6 12, 6 18 and 8 12. Polymer, 1997. **38**(11): 2689-2699.

22.   Rajesh, J.J., J. Bijwe and U. Tewari, *Abrasive wear performance of various polyamides*. Wear, 2002. **252**(9): 769-776.

23.   John Rajesh, J., J. Bijwe, B. Venkataraman and U.S. Tewari, *Effect of impinging velocity on the erosive wear behaviour of polyamides.* Tribology International, 2004. **37**(3): 219-226.

24.   Adriaensens, P., A. Pollaris, R. Rulkens, V.M. Litvinov and J. Gelan, *Study of the water uptake of polyamide 46 based copolymers by magnetic resonance imaging relaxometry*. Polymer, 2004. **45**(8): 2465-2473.

25.   Giles Jr, H.F., J.R. Wagner Jr and E.M. Mount Iii, 50 - *Pipe and Tubing Extrusion, in Extrusion. 2005*, William Andrew Publishing: Norwich, NY. p. 487-496.

26.   Vlachopoulos, J. and D. Strutt, *Polymer processing*. Materials Science and Technology, 2003. **19**(9): 1161-1169.

27.   Vlachopoulos, J. and D. Strutt, *The SPE Guide on Extrusion Technology and Troubleshooting*. 2001, Brookfield, CT: Society of Plastics Engineers.

28.   Elzein, T., M. Brogly and J. Schultz, *Crystallinity measurements of polyamides adsorbed as thin films*. Polymer, 2002. **43**(17): 4811-4822.

29.   Yan, M. and H. Yang, *Improvement of polyamide 1010 with silica nanospheres via in situ melt polycondensation.* Polymer Composites, 2012. **33**(10): 1770-1776.

30.   Gogolewski, S., K. Czerntawska and M. Gastorek, *Effect of annealing on thermal properties and crystalline structure of polyamides*. Nylon 12 (polylaurolactam). Colloid and Polymer Science Kolloid Zeitschrift & Zeitschrift für Polymere, 1980. **258**(10): 1130-1136.

31.   Torres-Giner, S., N. Montanes, V. Fombuena, T. Boronat and L. Sanchez-Nacher, *Preparation and characterization of compression-molded green composite sheets made of poly(3-hydroxybutyrate) reinforced with long pita fibers*. Advances in Polymer Technology, 2016: DOI: 10.1002/adv.21789.

32. Torres-Giner, S., N. Montanes, O. Fenollar, D. García-Sanoguera and R. Balart, *Development and optimization of renewable vinyl plastisol/wood flour composites exposed to ultraviolet radiation*. Materials & Design, 2016. **108**: 648-658.

33. Kong, W., K. Hu, X. Fu, D. Guo and J. Lei, *Preparation and Characterization of Thermoplastic Elastomer Based on Amino-terminated Polyamide-6 and Diisocyanate-terminated Polytetramethylene Glycol*. Polymer-Plastics Technology and Engineering, 2016. **55**(1): 1-8.

34. Li, H. and Z. Li, *The effect of reactive compatibilization of carboxylated polystyrene on morphology and toughness of polyamide-1010/polystyrene blends*. Polymer International, 1999. **48**(2): 124-128.

35. Porubská, M., O. Szöllős, A. Kóňová, I. Janigová, M. Jašková, K. Jomová and I. Chodák, *FTIR spectroscopy study of polyamide-6 irradiated by electron and proton beams*. Polymer Degradation and Stability, 2012. **97**(4): 523-531.

36. Pai, F.-C., S.-M. Lai and H.-H. Chu, *Characterization and Properties of Reactive Poly(lactic acid)/Polyamide 610 Biomass Blends*. Journal of Applied Polymer Science, 2013. **130**(4): 2563-2571.

37. Wan, C., F. Zhao, X. Bao, B. Kandasubramanian and M. Duggan, *Effect of POSS on crystalline transitions and physical properties of polyamide 12*. Journal of Polymer Science Part B: Polymer Physics, 2009. **47**(2): 121-129.

38. Rhee, S. and J.L. White, *Investigation of structure development in polyamide 11 and polyamide 12 tubular film extrusion*. Polymer Engineering & Science, 2002. **42**(1): 134-145.

39. Vasanthan, N. and D.R. Salem, *FTIR spectroscopic characterization of structural changes in polyamide-6 fibers during annealing and drawing*. Journal of Polymer Science Part B: Polymer Physics, 2001. **39**(5): 536-547.

40. Logakis, E., C. Pandis, V. Peoglos, P. Pissis, C. Stergiou, J. Pionteck, P. Pötschke, M. Mičušík and M. Omastová, *Structure–property relationships in polyamide 6/multi-walled carbon nanotubes nanocomposites*. Journal of Polymer Science Part B: Polymer Physics, 2009. **47**(8): 764-774.

41. Jiang, J., D. Zhang, Y. Zhang, K. Zhang and G. Wu, *Influences of Carbon Nanotube Networking on the Conductive, Crystallization, and Thermal Expansion Behaviors of PA610-Based Nanocomposites*. Journal of Macromolecular Science, Part B, 2013. **52**(7): 910-923.

42. Bell, J.P., P.E. Slade and J.H. Dumbleton, *Multiple melting in nylon 66*. Journal of Polymer Science Part A-2: Polymer Physics, 1968. **6**(10): 1773-1781.

43. Zhang, Q.-X., Z.-Z. Yu, M. Yang, J. Ma and Y.-W. Mai, *Multiple melting and crystallization of nylon-66/montmorillonite nanocomposites*. Journal of Polymer Science Part B: Polymer Physics, 2003. **41**(22): 2861-2869.

44. Xiuwei, F., L. Xiaohong, Y. Laigui and Z. Zhijun, *Effect of in situ surface-modified nano-SiO2 on the thermal and mechanical properties and crystallization behavior of nylon 1010*. Journal of Applied Polymer Science, 2010. **115**(6): 3339-3347.

45. Song, J., J. Liu, Y. Zhang, L. Chen, Y. Zhong and W. Yang, *Basalt fibre-reinforced PA1012 composites: Morphology, mechanical properties, crystallization behaviours, structure and water contact angle*. Journal of Composite Materials, 2014. **49**(4): 415-424.

46. Yan, C., L. Hao, L. Xu and Y. Shi, *Preparation, characterisation and processing of carbon fibre/polyamide-12 composites for selective laser sintering*. Composites Science and Technology, 2011. **71**(16): 1834-1841.

47. Cho, J.W. and D.R. Paul, *Nylon 6 nanocomposites by melt compounding*. Polymer, 2001. **42**(3): 1083-1094.

48. Ghaffari Mosanenzadeh, S., M.W. Liu, A. Osia and H.E. Naguib, *Thermal Composites of Biobased Polyamide with Boron Nitride Micro Networks*. Journal of Polymers and the Environment, 2015. **23**(4): 566-579.

49. Botelho, E.C. and M.C. Rezende, *Monitoring of Carbon Fiber/Polyamide Composites Processing by Rheological and Thermal Analyses*. Polymer-Plastics Technology and Engineering, 2006. **45**(1): 61-69.

50. Prevorsek, D.C., R.H. Butler and H.K. Reimschuessel, *Mechanical relaxations in polyamides*. Journal of Polymer Science Part A-2: Polymer Physics, 1971. **9**(5): 867-886.

51.   Xie, S., S. Zhang, F. Wang, M. Yang, R. Séguéla and J.-M. Lefebvre, *Preparation, structure and thermomechanical properties of nylon-6 nanocomposites with lamella-type and fiber-type sepiolite.* Composites Science and Technology, 2007. **67**(11–12): 2334-2341.

52.   Shan, G.-F., W. Yang, B.-h. Xie, Z.-m. Li, J. Chen and M.-b. Yang, *Double yielding behaviors of polyamide 6 and glass bead filled polyamide 6 composites.* Polymer Testing, 2005. **24**(6): 704-711.

53.   Shan, G.-F., W. Yang, M.-b. Yang, B.-h. Xie, Z.-m. Li and J.-m. Feng, *Effect of crystallinity level on the double yielding behavior of polyamide 6.* Polymer Testing, 2006. **25**(4): 452-459.

54.   Rajesh, J.J. and J. Bijwe, *Investigations on scratch behaviour of various polyamides.* Wear, 2005. **259**(1–6): 661-668.

55.   Isik-Gulsac, I., U. Yilmazer and G. Bayram, *Mechanical and rheological properties, and morphology of polyamide-6/organoclay/elastomer nanocomposites.* Journal of Applied Polymer Science, 2012. **125**(5): 4060-4073.

56.   Fornes, T.D. and D.R. Paul, *Structure and Properties of Nanocomposites Based on Nylon-11 and -12 Compared with Those Based on Nylon-6.* Macromolecules, 2004. **37**(20): 7698-7709.

57.   Torres-Giner, S., N. Montanes, T. Boronat, L. Quiles-Carrillo and R. Balart, *Melt grafting of sepiolite nanoclay onto poly (3-hydroxybutyrate-co-4-hydroxybutyrate) by reactive extrusion with multi-functional epoxy-based styrene-acrylic oligomer.* European Polymer Journal, 2016. **84**: 693-707.

58.   Paterson, M.W.A. and J.R. White, *Effect of water absorption on residual stresses in injection-moulded nylon 6,6.* Journal of Materials Science, 1992. 27(22): 6229-6240.

59.   Razumovskii, L.P., V.S. Markin and G.Y. Zaikov, *Sorption of water by aliphatic polyamides. Review.* Polymer Science U.S.S.R., 1985. **27**(4): 751-768.

60.   Adriaensens, P., A. Pollaris, R. Carleer, D. Vanderzande, J. Gelan, V.M. Litvinov and J. Tijssen, *Quantitative magnetic resonance imaging study of water uptake by polyamide 4,6.* Polymer, 2001. **42**(19): 7943-7952.

61.   Jördens, C., S. Wietzke, M. Scheller and M. Koch, *Investigation of the water absorption in polyamide and wood plastic composite by terahertz time-domain spectroscopy.* Polymer Testing, 2010. **29**(2): 209-215.

III.3.2. Injection-molded parts of fully bio-based polyamide 1010 strengthened by waste derived slate fibers pre-treated with glycidyl- and amino-silane coupling agents

L. Quiles-Carrillo [1], T. Boronat [1], N. Montanes [1], R. Balart [1] and S. Torres-Giner [1,2],

[1] Technological Institute of Materials (ITM), Universitat Politècnica de València (UPV), Plaza Ferrándiz y Carbonell 1, 03801 Alcoy, Spain;

[2] Novel Materials and Nanotechnology Group, Institute of Agrochemistry and Food Technology (IATA), Spanish National Research Council (CSIC), Calle Catedrático Agustín Escardino Benlloch 7, 46980 Paterna, Valencia, Spain

Injection-molded parts of fully bio-based polyamide 1010 strengthened with waste derived slate fibers pretreated with glycidyl- and amino-silane coupling agents

Luis Quiles-Carrillo[a,*], Teodomiro Boronat[a], Nestor Montanes[a], Rafael Balart[a], Sergio Torres-Giner[b,**]

[a] Technological Institute of Materials (ITM), Universitat Politècnica de València (UPV), Plaza Ferrándiz y Carbonell 1, 03801, Alcoy, Spain
[b] Novel Materials and Nanotechnology Group, Institute of Agrochemistry and Food Technology (IATA), Spanish National Research Council (CSIC), Calle Catedrático Agustín Escardino Benlloch 7, 46980, Paterna, Spain

ARTICLE INFO

ABSTRACT

Fully bio-based polyamide 1010 (PA1010) was melt-compounded with 15 wt% of slate fibers (SFs), which were obtained from wastes of the tile industry, and the resultant composites were shaped into parts by injection molding. The as-received fibers were first thermally treated and afterwards subjected to surface modification with glycidyl- and amino-silane coupling agents to improve the interfacial adhesion of the composites. The incorporation of both the glycidyl-silane slate fiber (G-SF) and amino-silane slate fiber (A-SF) remarkably improved the mechanical strength of PA1010, inducing a 3-fold increase in tensile modulus. The composite parts prepared with the silanized SFs also presented higher thermal stability and improved thermomechanical resistance. Water uptake was reduced below 1 wt%, encouragingly suggesting that the mechanical performance of the PA1010/SF composites would be scarcely affected by atmospheric humidity. G-SF was the most effective in strengthening PA1010. This improvement was ascribed to the higher reactivity of the cyclic anhydride in the coupled silane with the terminal hydroxyl groups of the biopolymer.

1. Introduction

Polyamides (PAs) are linear and semi-crystalline polymers that are composed of repeating amide groups. PAs are classically petroleum derived materials though, in the last years, several aliphatic PAs have been obtained partially or totally from bio-based building blocks [1]. Bio-sourced monomers include brassylic acid, sebacid acid, 1,4-diaminobutane (putrescine), and 1,5-diaminopentane (cadaverine) [2–4]. Making the properties of the newly so-called bio-based polyamides (bio-PA) similar to those of polyamide 6 (PA6) and polyamide 66 (PA66), for rigid applications, and of polyamide 12 (PA12), for flexible applications, is becoming increasingly important for economical and sustainable reasons [5]. In particular, the 10-carbon (10C), 11-carbon (11C), and 12-carbon (12C) comprising bio-PAs, such as polyamide 610 (PA610), polyamide 1010 (PA1010), polyamide 11 (PA11) or polyamide 1012 (PA1012), have mild and soft physical properties due to their long aliphatic segments, that is, its high methylene-to-amide ($CH_2/CONH$) ratios, which make them prized for applications that

require more flexibility [6]. In this context, recent developments have led to the cost-effective production of bio-based sebacic acid, a C10 dicarboxylic acid derived from castor oil [7]. Sebacic acid can readily react via polycondensation with 1,10-decamethylene diamine (DMDA), which can be obtained by exposing sebacic acid to ammonia followed by dehydration and hydrogenation, to produce fully bio-based PA1010 [8]. Besides its relatively low melting temperature (T_m), PA1010 is attractive for engineering applications that require high-impact resistance and resilience such as automotive fuel lines, bike tubing, and cable coating [9,10]. The long alkyl chains of PA1010 also result in a lower water uptake so that its mechanical properties can be less affected by atmospheric humidity [11].

Although most bio-PAs show engineering performance, they still have some technical drawbacks related to their tendency to moisture absorption due to the presence of amide groups. These phenomena are known to have a negative effect on the mechanical and thermal performance of PA-based materials [12]. Moreover, bio-PAs still present higher prices, in the range of US$15,000–20,000 a ton, than

Injection-molded parts of fully bio-based polyamide 1010 strengthened with waste derived slate fibers pretreated with glycidyl- and amino-silane coupling agents

Abstract.

Fully bio-based polyamide 1010 (PA1010) was melt-compounded with 15 wt% of slate fibers (SFs), which were obtained from wastes of the tile industry, and the resultant composites were shaped into parts by injection molding. The as-received fibers were first thermally treated and afterwards subjected to surface modification with glycidyl- and amino-silane coupling agents to improve the interfacial adhesion of the composites. The incorporation of both the glycidyl-silane slate fiber (G-SF) and amino-silane slate fiber (A-SF) remarkably improved the mechanical strength of PA1010, inducing a 3-fold increase in tensile modulus. The composite parts prepared with the silanized SFs also presented higher thermal stability and improved thermomechanical resistance. Water uptake was reduced below 1 wt%, encouragingly suggesting that the mechanical performance of the PA1010/SF composites would be scarcely affected by atmospheric humidity. G-SF was the most effective in strengthening PA1010. This improvement was ascribed to the higher reactivity of the cyclic anhydride in the coupled silane with the terminal hydroxyl groups of the biopolymer.

Keywords: PA1010; Environmentally friendly composites; Engineering bioplastics; Waste valorization.

INTRODUCTION

Polyamides (PAs) are linear and semi-crystalline polymers that are composed of repeating amide groups. PAs are classically petroleum derived materials though, in the last years, several aliphatic PAs have been obtained partially or totally from bio-based building blocks [1]. Bio-sourced monomers include brassylic acid, sebacid acid, 1,4-diaminobutane (putrescine), and 1,5-diaminopentane (cadaverine) [2-4]. Making the properties of the newly so-called bio-based polyamides (bio-PA) similar to those of polyamide 6 (PA6) and polyamide 66 (PA66), for rigid applications, and of polyamide 12 (PA12), for flexible applications, is becoming increasingly important for economical and sustainable reasons [5]. In particular, the 10-carbon (10C), 11-carbon (11C), and 12-carbon (12C) comprising bio-PAs, such as polyamide 610 (PA610), polyamide 1010 (PA1010), polyamide 11 (PA11) or polyamide 1012 (PA1012), have mild and soft physical properties due to their long aliphatic segments, that is, its high methylene-to-amide ($CH_2/CONH$) ratios, which make them prized for applications that require more flexibility [6]. In this context, recent developments have led to the cost-effective production of bio-based sebacic acid, a C10 dicarboxylic acid derived from castor oil [7]. Sebacic acid can readily react via polycondensation with 1,10-decamethylene diamine (DMDA), which can be obtained by exposing sebacic acid to ammonia followed by dehydration and hydrogenation, to produce fully bio-based PA1010 [8]. Besides its relatively low melting temperature (T_m), PA1010 is attractive for engineering applications that require high-impact resistance and resilience such as automotive fuel lines, bike tubing, and cable coating [9,10]. The long alkyl chains of PA1010 also result in a lower water uptake so that its mechanical properties can be less affected by atmospheric humidity [11].

Although most bio-PAs show engineering performance, they still have some technical drawbacks related to their tendency to moisture absorption due to the presence of amide groups. These phenomena are known to have a negative effect on the mechanical and thermal performance of PA-based materials [12]. Moreover, bio-PAs still present higher prices, in the range of US$ 15,000–20,000 a ton, than conventional PA6 and PA66, that is, US$ 2,000–4,000 a ton, or even specialty PA12, that is, US$ 8,000–12,000 a ton. The global bio-PA market demand was approximately 21,000 tons in 2014, which represents around 1% of the worldwide capacity of bioplastics, whereas the growth projection indicates that it is expected to reach over 50,000 tons by 2022 [13]. Fiber reinforcement represents an efficient method to both overcome the above-described technical limitations and reduce cost. Glass fiber (GF) is, with difference, the most used reinforcing filler in PAs [[14], [15], [16], [17]]. Also carbon fiber (CF) and aramid fiber (AF) have being increasingly used for numerous mechanical and tribological applications [18-21]. Nevertheless, the high melt viscosity of PAs together with the chemical inertness of most of these reinforcing elements result in poor matrix–filler interactions that, in turn, are responsible for the performance impairment of the composites [22]. Therefore, surface modification of fibers and/or the use of coupling agents are usually required to enhance the overall performance [18,23, 24]. In addition, melt grafting of fillers onto polymers is an effective method to achieve compatibilization and, thus, enhance the mechanical strength of composites [25]. For instance, Hui *et al*. [26] reported the usefulness of grafting chemically oxidized CF onto PA6, thus leading to fiber-reinforced composites with increased mechanical properties. Several coupling agents and compatibilizers have been extensively explored to

enhance PA–fiber interfacial interactions [27-30]. Among them, silanes and chemically modified silanes are one of the most used coupling agents employed in PA-reinforced composites [31].

In the last years, some silica-based fibers have been introduced at commercial scale. One of the most promising ones is basalt fiber (BF), which has been proposed in several engineering applications [32-34]. More recently, slate fiber (SF) has also attracted some academic interest as it can be obtained from wastes of the building and construction industry. Slate is a natural rock, typically of a dark grey color, which is widely used in roofs and for tiling due to its attractive rustic appearance, high wear resistance, and good frost resistance [35]. More than 1 billion tons per year are manufactured in the world, being the Galicia region in northwest Spain one of the largest producers in Europe. However, in spite of the broad use of slate, these manufacturing processes have remained unaltered for many years and are highly inefficient. Indeed, it is estimated that more than 90% of the material is wasted during the transformation stages from the quarry up to the final slate tile [36]. As a result, a huge amount of slate wastes is being currently generated in the tile industry. For instance, one ton end product could potentially give 30 tons waste [37]. Estimated price of SF varies from US$ 300 to US$ 700 a ton, which is comparable or even lower than that of chopped strands of GF. Therefore, not only can this add value to an industrial by-product, but it can also reduce the overall cost of bio-PA articles. However, a limited number of studies have reported so far the use of slate waste as reinforcing filler in thermoplastic matrices. For instance, the incorporation of slate powder into polypropylene (PP) resulted in cost-competitive composites with mechanical and optical properties comparable to neat PP [38]. More recently, new composite laminates based on epoxidized linseed oil (ELO)/SF fabrics were successfully manufactured as alternative to epoxy/GF composites [39]. In another work, it was demonstrated the potential of bio-based high-density polyethylene (bio-HDPE) composites reinforced with short SFs, thus broadening its use for engineering materials [40].

This research work aims to develop, for the first time, new environmentally friendly and high-performance composite materials from fully bio-based PA1010 and SF. The use of two different reactive silane coupling agents, that is, a glycidyl- and an amino-silane, were also investigated in order to modify the fiber surface to improve the biopolymer–fiber interactions and facilitate a better load transfer from the composite components. The mechanical, morphological, thermal, and thermomechanical properties as well as water uptake of the newly developed composite parts were evaluated to ascertain their potential in automotive and also building and construction applications.

MATERIALS AND METHODS

Materials

PA1010 was provided as NP BioPA1010-201 by NaturePlast (Ifs, France). The manufacturer supplies this homopolyamide in pellets as fully bio-based and medium-viscosity grade for injection molding applications. It presents a density of 1.05 g/cm^3 and a viscosity number (VN) of 160 cm^3/g. A roving of SFs was provided by Mifibra S.L. (Ourense, Spain) obtained from wastes of the tile industry. The monofilaments show a dark brown color, being 4–8 mm in length.

A glycidyl-silane, namely (3-glycidyloxypropyl) trimethoxysilane (GPTMS), with CAS number 2530-83-8, molecular weight (M_W) of 236.34 g/mol, and density of 1.07 g/cm³, and an amino-silane, namely [3-(2-aminoethylamino)propyl] trimethoxysilane (AEAPTMS), with CAS number 1760-24-3, M_W of 222.36 g/mol, and density of 1.03 g/cm³, were both purchased at Sigma-Aldrich S.A. (Madrid, Spain). **Figure III.3.2.1** shows the chemical structures of both silanes.
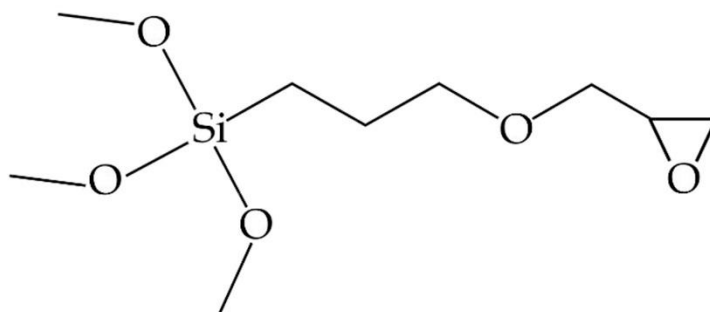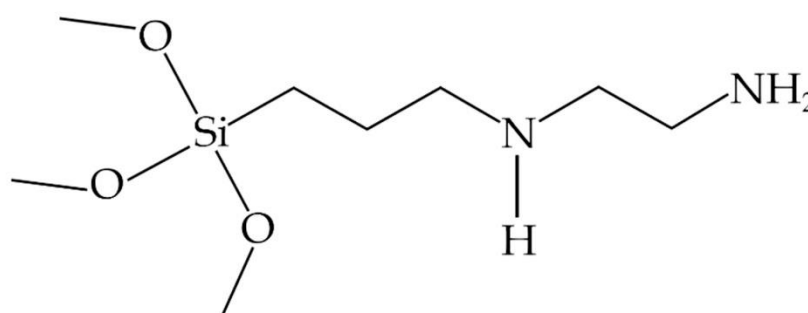
Figure III.3.2.1. Chemical structure of the silane coupling agents: (a) (3-glycidyloxypropyl) trimethoxysilane (GPTMS); (b) [3-(2-aminoethylamino)propyl] trimethoxysilane (AEAPTMS).

Fiber pre-treatment

SFs were first washed extensively with distilled water and then placed in a dehumidifying dryer MDEO from Industrial Marsé (Barcelona, Spain) at 350 °C for 6 h to remove their organic coatings (sizings). The resultant thermally treated fibers were afterwards subjected to surface modification with GPTMS or AEAPTMS to produce, respectively, the here-called silanized slate fiber with glycidyl-silane (G-SF) and amino-silane (A-SF). To this end, both reactive coupling agents were added to distilled water at a concentration of 1 wt%. The fibers were then submerged into the aqueous dissolutions containing each silane and magnetically stirred at 25 °C for 1 h to promote hydrolysis and homogenization. After this, the fibers were extracted from the solution, washed several times with distilled water and, finally, dried at 60 °C for 72 h. A sample of thermally treated slate fiber (TT-SF), without any silane modification, was also obtained as control to compare the effect of silanes on the properties of the composite parts.

Composite parts preparation

Prior to processing, PA1010 was dried at 60 °C for 36 h in the dehumidifying dryer MDEO to remove any residual moisture. PA1010 and the different SFs were manually pre-homogenized in a zipper bag. In all cases, a fixed weight content of 15 wt% SF in PA1010 was set. Extrusion was performed using a co-rotating twin-screw extruder from Construcciones Mecánicas Dupra, S.L. (Alicante, Spain), featuring screws of 25 mm diameter with a length-to-diameter ratio (L/D) of 24. The materials were then fed into the main hopper and the rotating speed during extrusion was 20 rpm. The following temperature profile was set: 210 °C (hopper) – 215 °C – 220 °C – 225 °C (die). The PA1010/SF composites were extruded through a round die producing strands that were finally pelletized using an air-knife unit. Residence time was approximately 1 min. **Table III.3.2.1** gathers the set of compositions melt-processed by twin-screw extrusion.

Table III.3.2.1. Summary of compositions according to the weight content (wt%) of polyamide 1010 (PA1010), thermally treated slate fiber (TT-SF), glycidyl-silane slate fiber (G-SF), and amino-silane slate fiber (A-SF).

Code	PA1010 (wt%)	TT-SF (wt%)	G-SF (wt%)	A-SF (wt%)
PA1010	100	0	0	0
PA1010/TT-SF	85	15	0	0
PA1010/G-SF	85	0	15	0
PA1010/A-SF	85	0	0	15

The compounded pellets were dried in the same conditions applied prior to extrusion. Thereafter, they were processed by injection molding using a Meteor 270/75 (Mateu & Solé, Barcelona, Spain). The temperature profile in the injection molding unit was 210 °C (hopper) – 215 °C – 225 °C – 230 °C (injection nozzle). The injected material was shaped in a mold by applying a clamping force of 75 tons to obtain the different parts with an average thickness of approximately 4 mm. The cavity filling and cooling times were set to 1 and 10 s, respectively.

MATERIAL CHARACTERIZATION

XRF spectroscopy

A basic chemical characterization of SF was carried out by X-ray fluorescence (XRF) spectroscopy in a sequential X-ray spectrometer PHILIPS MagiX Pro PW2400 (Amsterdam, The Netherlands). This device was equipped with a rhodium tube and a beryllium window. The chemical composition was analyzed using the SuperQ analytical software (Malvern Panalytical Ltd, Malvern, UK).

Morphology

The morphology of the SF fillers as well as the fracture surfaces of the PA1010/SF composite parts, which were obtained from the impact tests, was observed by field emission scanning electron microscopy (FESEM). The samples were first sputtered with a gold-palladium alloy in an EMITECH sputter coating SC7620 model from Quorum Technologies, Ltd (East Sussex, UK). Analysis was carried out in a ZEISS

ULTRA 55 microscope from Oxford Instruments (Abingdon, UK) using 2 kV as the acceleration voltage.

Mechanical tests

A universal testing machine ELIB 50 (S A E. Ibertest, Madrid, Spain) was used to perform tensile tests on injection-molded dog bone-shaped parts sizing $150 \times 10 \times 4$ mm³. The test was carried out as indicated by ISO 527–1:2012. The cross-head speed was 5 mm/min and the load cell was 5 kN. A 676-D durometer (J. Bot Instruments, Barcelona, Spain), using the Shore D-scale, was employed to measure hardness on injection-molded parts with dimensions of $80 \times 10 \times 4$ mm³. The principles of ISO 868:2003 were followed. A 6-J pendulum (Metrotec S.A., San Sebastián, Spain) was employed to determine toughness by the Charpy impact test on injection-molded 0.25-mm V-notched parts with dimensions of $80 \times 10 \times 4$ mm³. The test was done based on the specifications of ISO 179–1:2010. All the mechanical tests were performed at controlled conditions of 25 °C and 40% of relative humidity (RH) for which, at least, 6 samples of each material were evaluated.

Thermal analysis

A Mettler-Toledo 821 calorimeter (Mettler-Toledo, Schwerzenbach, Switzerland) was employed to analyze the main thermal transitions of the injection-molded PA1010/SF composite parts by differential scanning calorimetry (DSC). Samples with an average weight between 5 mg and 7 mg were placed in standard sealed aluminum crucibles (40 µL). The samples were then subjected to a three stage dynamic thermal cycle at 10 °C/min in a nitrogen atmosphere with a flow-rate of 66 mL/min. It consisted of a first heating from 30 °C to 250 °C, followed by cooling to 0 °C, and a second heating to 350 °C. The following **Equation III.3.2.1** was used to determine the degree of crystallinity (X_c):

$$\chi_c(\%) = \left[\frac{\Delta H_m}{\Delta H_m^0 \cdot (1-w)} \right] \cdot 100 \qquad \textbf{Equation III.3.2.1}$$

Where ΔH_m (J/g) is the melting enthalpy of the sample, ΔH_m^0 (J/g) = 244 J/g [41] is the theoretical melting enthalpy of a fully crystalline PA1010, and w is the SF weight fraction.

A Mettler-Toledo TGA/SDTA 851 thermobalance (Mettler-Toledo, Schwerzenbach, Switzerland) was employed for thermogravimetric analysis (TGA). Samples with an average weight in the 5–7 mg range were placed in standard alumina crucibles (70 µl) and thus subjected to a heating program at 20 °C/min in air atmosphere from 30 °C to 700 °C. The first derivative thermogravimetry (DTG) curves, expressing the weight loss rate as the function of time, were also determined. All thermal tests were carried out in triplicate.

Thermomechanical tests

A DMA1 dynamic analyzer from Mettler-Toledo was used for dynamic mechanical thermal analysis (DMTA). Tests were performed on injection-molded parts sizing $20 \times 6 \times 2.7$ mm³ in single cantilever flexural conditions. Samples were subjected to a dynamic temperature sweep at 2 °C/min from −60 °C to 160 °C. The selected

frequency and maximum flexural deformation or deflection were 1 Hz and 10 μm, respectively. All thermomechanical tests were done in triplicate.

Water uptake measurements

The evolution of water absorption was studied on injection-molded parts of $80 \times 10 \times 4$ mm^3 for a whole period of 12 weeks of immersion in distilled water at 24 ± 1 °C. This procedure followed ISO 62:2008. Weight measurements were collected weekly in an AG245 analytical balance from Mettler-Toledo with a precision of ±0.1 mg. Tests were performed in triplicate.

RESULTS AND DISCUSSION

Characterization of SF

Table III.3.2.2 shows a summary of the chemical composition of the as-received SFs obtained by XRF. The results confirmed that SF is mainly constituted by silica (SiO_2). **Figure III.3.2.2** shows the FESEM images of TT-SF and of the SFs pretreated with GPTMS and AEAPTMS, respectively called G-SF and A-SF. It can be observed that all the fibers were straight and circular in the cross-section, having a mean diameter in the 5–10 μm range. In **Figure III.3.2.2a** one can see that the non-silanized fibers, that is, TT-SFs, presented a clean and very smooth surface. This morphology suggests successful removal of any previous sizings during thermal treatment. Further details of the TT-SF morphology are shown in **Figure III.3.2.2b** in the FESEM image taken at higher magnification. It revealed that the TT-SF surface was not actually smooth but relatively rough based on a wavy morphology with clear steps across the fiber section. In the case of the silane-treated fibers, shown in **Figure III.3.2.2c** and e for G-SF and A-SF, respectively, one can clearly observe that the fibers presented the same morphology than TT-SF. However, as seen in the magnified FESEM images shown in **Figure III.3.2.2d** and **f**, the fiber surface became significantly rougher due to the formation of nano-sized precipitates. A similar morphology has been recently reported by Yu *et al.* [42] for amino-silane-treated BFs during topographical analysis carried out by atomic force microscopy (AFM) analysis. Roughness was ascribed to the presence of spherical silane molecules with radius below 50 nm. One can also observe that the fiber surfaces were also little glossier after silanization, which relates to the formation of thin silane layers that were strongly attached to the SF surface. In this context, it has been reported that layers resulting from the anchorage of silane coupling agents are produced by the formation of a siloxane (Si-O-Si) through reaction between the hydrolyzed alkoxy groups in the silane and hydroxyl functional groups available on the inorganic fibers surface [43]. Coupled silanes can then play a key role in establishing strong interactions among fiber and matrix since, as one can see in previous **Figure III.3.2.1**, the amino or glycidyl functionality remain still suitable to react with the organic component of the composite.

Table III.3.2.2. Chemical composition of the as-received slate fiber (SF) obtained by X-ray fluorescence (XRF) spectroscopy.

Constituent	Percentage (wt%)
SiO_2	91.5 ± 2.8
ZnO	8.5 ± 2.3
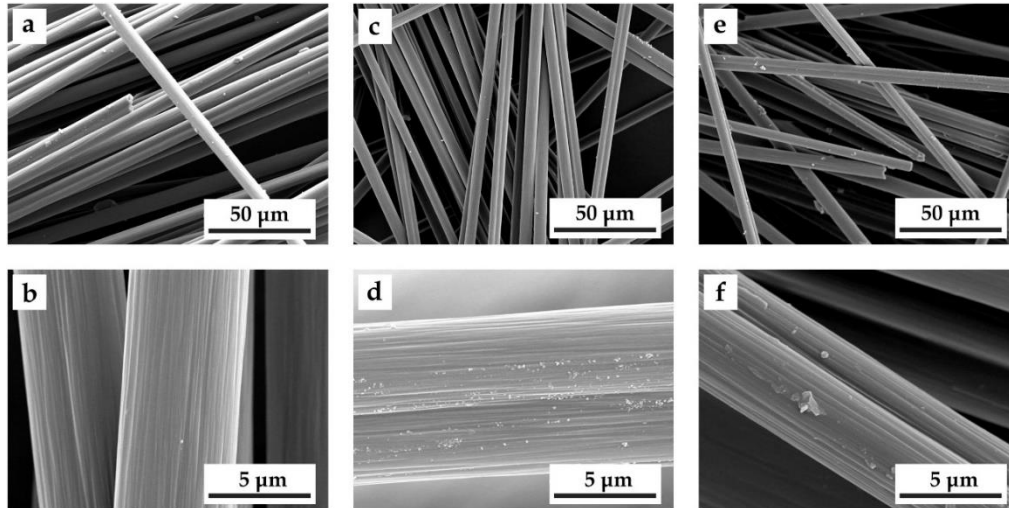
Figure III.3.2.2. Field emission scanning electron microscopy (FESEM) micrographs of: (a, b) Thermally treated slate fiber (TT-SF); (c, d) Glycidyl-silane slate fiber (G-SF); (e, f) Amino-silane slate fiber (A-SF).

Mechanical properties of PA1010/SF composite parts

Table III.3.2.3 shows the values of modulus (E), maximum tensile strength (σ_{max}), and elongation at break (ε_b) of the PA1010/SF composite parts obtained from the tensile tests. In relation to the neat PA1010 part, E and σ_{max} were 541 MPa and 56.7 MPa, respectively, while ε_b was 622.2%. These mechanical properties indicate that PA1010 generates injection-molded parts with a high ductile behavior but a relatively elasticity. The incorporation of 15 wt% TT-SF into PA1010 induced a significant increase in the mechanical strength of the parts. In particular, E increased to 1560 MPa, that is, nearly a 3-fold increase in comparison to the neat PA1010 part. The value of σ_{max} also increased up to a value of 102.5 MPa, that is, a percentage increase of approximately 81%. In contrast, the ductility was dramatically reduced, showing a ε_b value of 14.3%. Similar mechanical changes were reported by Carbonell-Verdú *et al.* [40], who showed that the incorporation of SF at 20 wt% into bio-HDPE pieces led to a noticeable increase in stiffness, increasing E from 373 MPa to 1483 MPa, and also to a decrease in ductility, reducing ε_b from 520% to 18.7%.

Table III.3.2.3. Summary of the mechanical properties of polyamide 1010 (PA1010) and its composites with thermally treated slate fiber (TT-SF) and slate fibers pretreated with glycidyl-silane (G-SF) and amino-silane (A-SF) in terms of tensile modulus (E), maximum tensile strength (σ_{max}), elongation at break (ε_b), Shore D hardness, and impact strength.

Parts	E (MPa)	σ_{max} (MPa)	ε_b (%)	Shore D hardness	Impact strength (kJ/m²)
PA1010	541 ± 12	56.7 ± 1.3	622.2 ± 18.5	74.8 ± 1.1	10.9 ± 0.2
PA1010/TT-SF	1560 ± 31	102.5 ± 1.2	14.3 ± 0.4	79.8 ± 0.8	8.9 ± 0.4
PA1010/G-SF	1850 ± 63	111.2 ± 1.4	13.1 ± 0.8	79.6 ± 0.5	9.8 ± 0.1
PA1010/A-SF	1770 ± 48	110.4 ± 1.9	13.4 ± 0.5	80.0 ± 0.7	9.8 ± 0.5

Both silanized SFs, that is, G-SF and A-SF, positively contributed to further increasing stiffness of the parts without, interestingly, compromising the ductility of the PA1010/TT-SF part. Thus, addition of G-SF led to an increase in E and σmax to values of 1850 MPa and 111.2 MPa, respectively, while ϵb was 13.1%. Similarly, the PA1010/A-SF composite part showed an E value of 1770 MPa, a σ_{max} of 110.4 MPa, and a ϵ_b of 13.4%. Therefore, the mechanical stiffness was slightly higher in the case of the composite prepared with G-SF. In this context, Nishitani *et al*. [10] showed previously the influence of various silane coupling agents on hemp fiber (HF) that were used to reinforce PA1010. It was demonstrated that the combination of an alkali pre-treatment with sodium hydroxide (NaOH) and a subsequent surface treatment with an ureidosilane was the most effective approach to improve the mechanical strength and hardness of the composite. The effect obtained was mainly attributed to an interfacial interaction improvement between the HF reinforcement element and the PA1010 matrix. Laura *et al*. [44] also developed PA6-based composites reinforced with GF subjected to previous silanization with different functionalities, that is, amino, epoxy, and anhydride. Authors concluded that the epoxy- and anhydride-silanized GFs offer the optimal mechanical performance, which is also thought to occur due to the highest interfacial interaction between GF and PA6.

With regards to the Shore D hardness values, all the tested SFs offered a similar increase. Hardness values increased from 74.8, for the neat PA1010 part, up to values around 80, for the PA1010/SF composite parts. This increase is directly related to the intrinsic hardness of SF. It should be noted that the here-prepared SF-reinforced PA1010 composites are still softer than that of GF-reinforced ones [45], which has the advantage of reducing the wear of the extruder screws. Regarding impact strength, which gives a measurement of the material toughness, both PA1010/SF composite parts produced with the silanized SFs showed intermediate values between the neat PA1010 part and the PA1010/TT-SF composite part. In particular, one can observe that the impact strength was reduced from 10.9 kJ/m2, for the neat bio-PA part, to 8.9 kJ/m2, for the PA1010/TT-SF composite part. Since impact strength is related to both mechanical ductile and resistant properties, it is considered that the addition of SFs led to a remarkable decrease in elongation at break (ductile property) but, in contrast, improved noticeably the tensile strength, which then further confirms the reinforcing effect of SF. In addition, the efficiency of the silanization on the SF surface and their positive effect on the biopolymer–fiber interactions were evidenced by the fact that the impact-strength values of both the PA1010/G-SF and PA1010/A-SF composite parts were 9.8 kJ/m2. Similarly, Samper *et al*. [39] showed that the impact-strength energy for composites prepared with untreated SF was 66.0 kJ/m2 whereas equivalent composite laminates with G-SF presented an absorbed energy of 77.9 kJ/m2, that is, 18% higher. This enhancement is, therefore, representative of a good fiber–matrix interaction that allows good load transfer from the matrix to fiber.

Morphology of PA1010/SF composite parts

Figure III.3.2.3 shows the FESEM images corresponding to the fracture surfaces of the injection-molded parts after the impact test. **Figure III.3.2.3a** and **b** presents the fracture surfaces of the neat PA1010 part taken at 500x and 1000x, respectively. One can observe that the fracture surface was relatively smooth, with several crack fronts, typical of a brittle material. The low plastic deformation observed, however, can be

related to the impact test conditions and the use of V-notched parts [46]. **Figure III.3.2.3c** and **d** shows the FESEM images corresponding to the fracture surfaces of the PA1010/TT-SF composite pieces. It can be observed that TT-SF presented a relatively poor interaction with the PA1010 matrix, which was evidenced by the presence of several holes. The formation of holes and voids indicates that some fibers were pulled out during fracture. In this context, Carbonell-Verdu *et al.* [40] showed similar fracture surfaces that were ascribed to the absence or poor fiber–matrix interactions between bio-HDPE and SFs. As it can be seen in **Figure III.3.2.3e** and **f**, the use of SF pretreated with glycidyl silane, the so-called G-SF, successfully modified the morphology of the fracture surfaces of the resultant composite parts. Although some cavities and holes were still visible, due to the pulled-out phenomenon described above, they became less intense and the polymer–fiber interaction was also stronger. In fact, in the magnified FESEM image one can observe that the fibers were intensely attached to the biopolymer matrix as an indication of good interaction. Incorporation of the pretreated SFs with amino-silane, that is, A-SF, yielded similar biopolymer–fiber interaction. This can be evidenced in **Figure III.3.2.3g** and **h**, where the number of cavities/holes was reduced and the fibers were highly adhered to the biopolymer matrix.

Thus, silanes successfully acted as coupling agents and provided an effective bridge between the inorganic fibers and the PA1010 matrix. In this sense, the use of silanes has given excellent results for different composite materials by improving significantly the interfacial adhesion between inorganic and/or organic fibers and different thermoplastics and thermosets in composite materials. For instance, as reported by Xie *et al.* [47], the organo-functionality of silane can effectively interact with the polymer matrix depending on the polymer chemistry. Briefly, a non-reactive alkyl group in a silane coupling agent may increase the compatibility with non-polar matrices due to their similar polarities. In other cases, specific reactive organo-functionalities (amino, mercapto, glycidoxy, vinyl, or methacryloxy groups, etc.) in silane can react with some chemical groups of the polymer chains to form newly covalent bonds or, at least, to favor certain interaction between them. Therefore, the functional groups of silanes can respond selectively to the chemical structure of the base resin. In this study, the coupling mechanism of glycidyl-silane is proposed to occur based on the two-step reaction scheme described recently by Samper *et al.* [43] for epoxy resins. Briefly, in a first stage, the cyclic anhydride would react with the terminal hydroxyl groups (-OH) of PA1010, opening the cyclic anhydride and leading to formation of a free carboxylic acid group (-COO) that, thereafter, can further react with more available cyclic anhydride rings to form new carboxylic groups. On the other hand, amino-silanes have been reported to successfully act as coupling agents in PA66 by forming strong intramolecular hydrogen interactions with its amide (-CONH-) groups [42]. Based on the two coupling mechanisms reported earlier, one can consider that the effect of glycidyl-silane on bio-PAs is more intense than that of the amino-silane. The first approach implies the formation of newly covalent bonds whereas the latter depends on intramolecular interactions. This dissimilar coupling mechanism can potentially explain the slightly different mechanical performance observed above.
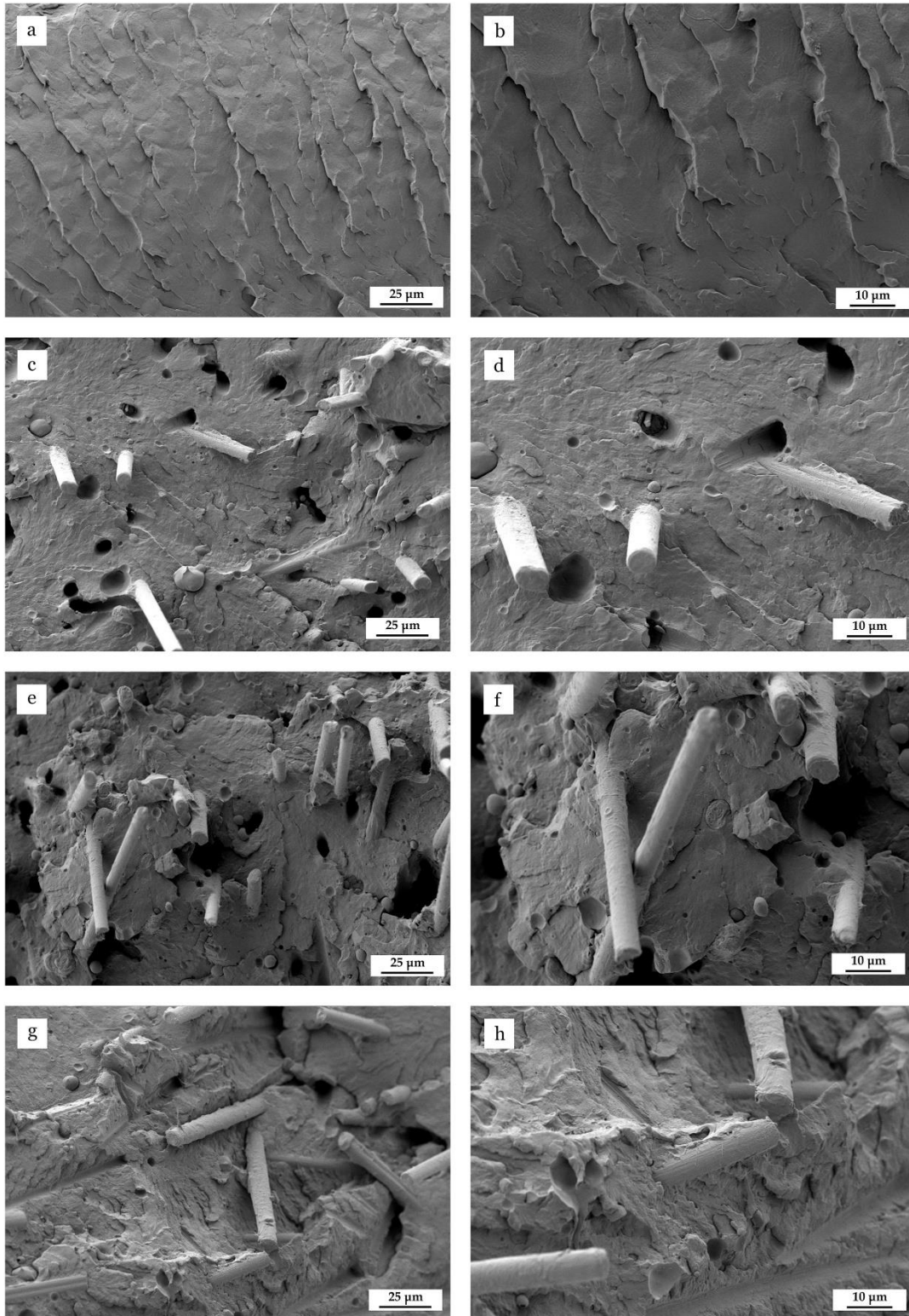
Figure III.3.2.3. Field emission scanning electron microscopy (FESEM) images of the fracture surfaces of: (a, b) Polyamide 1010 (PA1010); (c, d) PA1010/thermally treated slate fiber (TT-SF); (e, f) PA1010/glycidyl-silane slate fiber (G-SF); (g, h) PA1010/amino-silane slate fiber (A-SF).

Thermal properties of PA1010/SF composite parts

Figure III.3.2.4 shows the DSC thermograms during the second heating step of the neat PA1010 and PA1010/SF composites. **Table III.3.2.4** gathers the main thermal parameters obtained from DSC. The heating thermogram was plotted in the 100–250 °C range in order to better elucidate the melting profile of the samples since glass transition of PA1010 is known to be very subtle [11]. It can be observed that the neat PA1010 sample did not show any cold crystallization peak before melting. One can also observe that PA1010 showed a T_m value nearly at 202 °C, melting in a single peak. The value of T_m was slightly reduced by 1–2 °C after the addition of all types of SF. More interestingly, the biopolymer developed a double-melting peak phenomenon, showing a first melting point around 191 °C, which is characteristic of the well-known phenomenon of melt recrystallization during heating [48]. Briefly, the first peak is due to melting of the polymer fraction that crystallized previously, during cooling or cold crystallization, whereas in the second peak contributes the melting of the recrystallized polymer fraction during heating. In this context, Zhang *et al.* [49] indicated that the incorporation of montmorillonite (MMT) can restrict the crystallization of PA1010, shifting T_m to lower values. Also, the physical hindrance of silicate layers affected the second melting peak more than the first one. Therefore, one can consider that the presence of SF slightly disrupted the chain-folding process of the biopolymer. This effect can be attributed to segmental immobilization of the biopolymer chains at the fiber surface, which induced a double-melting behavior since the PA1010 chains were more restricted and difficult to recrystallize into thickened, perfect, and stable crystals. A similar observation was also reported by Zeng *et al.* [50] who showed that the T_m values of PA1010 decreased uniformly with increasing the multi-walled carbon nanotubes (MWCNTs) content. In particular, the highest temperature peak decreased with increasing the MWCNTs content and disappeared when the content reached 30 wt%, implying that the movement and re-arrangement of the PA1010 chains were completely restricted in the composites with high MWCNTs loadings. Neat PA1010 was also characterized by a X_c value of 18%, which is related to its symmetrical chain structure in which the diamine and the dicarboxylic acid are both based on a C10 carbon chain [11]. This structure potentially results in a high regular spacing of the amide groups along the biopolymer chains that, in turn, favors the formation of ordered regions. One can observe that the incorporation of SF slightly increased the percentage of crystallinity of PA1010 up to values in the 20–22% range. This observation suggests that the fibers nucleated the formation of more crystals though less perfect due to the above-described molecular restriction. Similar results have been reported by Mittal *et al.* [51] who described a significant ΔH_m increase in PA with the graphene addition.
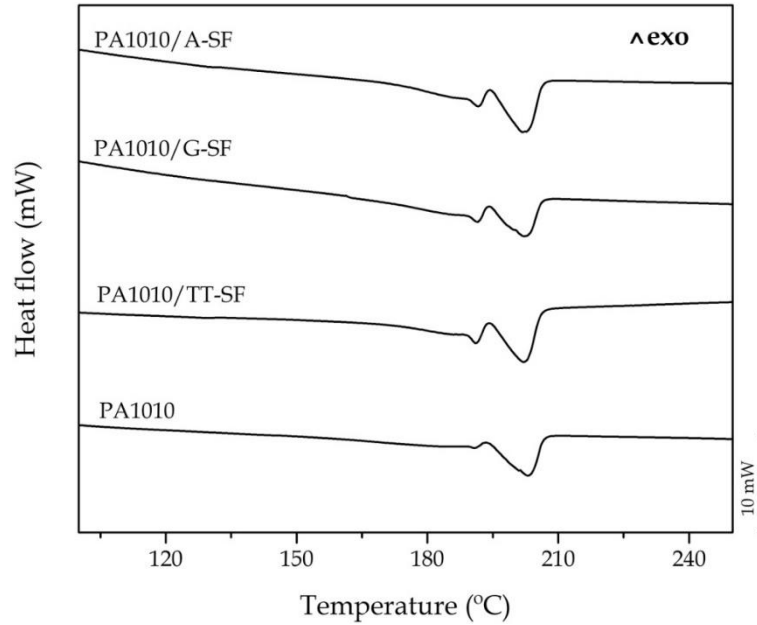
Figure III.3.2.4. Differential scanning calorimetry (DSC) thermograms of polyamide 1010 (PA1010) and its composites with thermally treated slate fiber (TT-SF) and slate fibers pretreated with glycidyl-silane (G-SF) and amino-silane (A-SF).

Table III.3.2.4. Main thermal parameters of polyamide 1010 (PA1010) and its composites with thermally treated slate fiber (TT-SF) and slate fibers pretreated with glycidyl-silane (G-SF) and amino-silane (A-SF) in terms of melting temperature (T_m), normalized melting enthalpy (ΔH_m), and percentage of crystallinity (χ_c).

Parts	T_m (°C)	ΔH_m (J/g)	χ_c (%)
PA1010	202.4 ± 1.0	43.9 ± 0.4	18.0 ± 0.2
PA1010/TT-SF	190.9 ± 0.8 / 201.5 ± 1.1	43.2 ± 0.5	20.8 ± 0.3
PA1010/G-SF	191.4 ± 1.1 / 201.1 ± 0.9	46.9 ± 0.7	22.6 ± 0.4
PA1010/A-SF	191.5 ± 0.9 / 200.8 ± 0.8	45.3 ± 0.6	21.8 ± 0.3

TGA curves are plotted in **Figure III.3.2.5** and the most relevant properties obtained from the curves are listed in **Table III.3.2.5**. This shows that $T_{5\%}$, which corresponds to the characteristic temperature for a weight loss of 5% and reflects the thermal degradation onset, of the neat PA1010 part was 410.3 °C whereas T_{deg}, determined at the maximum weight loss rate, was located at 473.5 °C. It is also worthy to note that no residual moisture was observed as there was not any significant weight loss in the 100–150 °C range. Similar thermal degradation profiles in bio-PAs have been previously described [52, 53]. It has been reported that PA1010 degradation involves a β-C-H transfer reaction mechanism, producing ketoamides as the primary decomposition products [11]. In relation to the composite parts, addition of all types of SF yielded a slight increase in both $T_{5\%}$ and T_{deg} of 2–8 °C and 8–10 °C, respectively. In particular, the PA1010/G-SF composite presented the highest thermal stability,

showing a T_{deg} value of 483.1 °C. This increase can be related mainly to a mass transport barrier exerted by the inorganic filler to the volatiles produced during the polymer decomposition [54]. The higher thermal improvement observed for the composites prepared with the silanized fibers can be ascribed to the higher material's cohesion achieved by the silane pre-treatment on the fibers, which enhanced the overall thermal stability of PA1010 in the composites. In this sense, Shen *et al.* [55] demonstrated that the addition of MWCNTs improves the thermal stability of PA6 by a free radical scavenging effect of the fillers. Then, organic groups in silanes can also potentially contribute to delaying chain cleavage and radical formation during thermal degradation of PA1010. It also worthy to mention that the composites prepared with TT-SF showed a minor mass loss (of approximately 5%) at a temperature below 200 °C. This observation may indicate the presence of some residual water and/or volatiles in the non-silanized SF even though the fibers were subjected to a long thermal pre-treatment. Interestingly, this mass loss was not observed in the composites prepared with G-SF and A-SF, suggesting that a more effective moisture removal was also accomplished during silanization. With regards to the residual mass, all composite samples showed residues of around 15–17% due to the inorganic nature of SF.
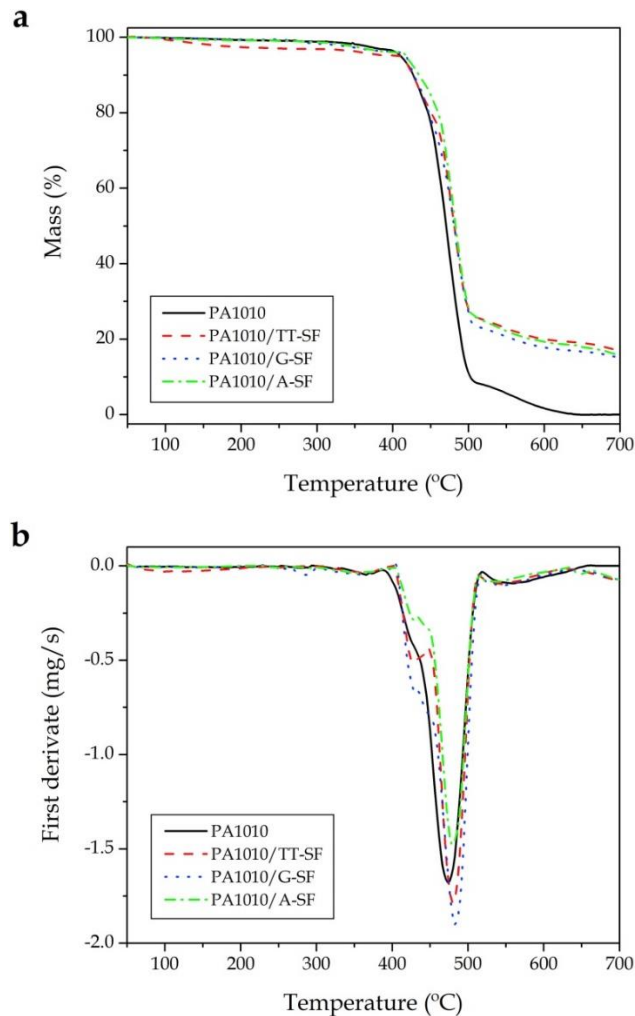
Figure III.3.2.5. (a) Thermogravimetric analysis (TGA) and (b) first derivative (DTG) curves of polyamide 1010 (PA1010) and its composites with thermally treated slate fiber (TT-SF) and slate fibers pretreated with glycidyl-silane (G-SF) and amino-silane (A-SF).

Table III.3.2.5. Main thermal degradation parameters of polyamide 1010 (PA1010) and its composites with thermally treated slate fiber (TT-SF) and slate fibers pretreated with glycidyl-silane (G-SF) and amino-silane (A-SF) in terms of temperature at mass loss of 5% ($T_{5\%}$), degradation temperature (T_{deg}), and residual mass at 700 °C.

Parts	$T_{5\%}$ (°C)	T_{deg} (°C)	Residual mass (%)
PA1010	410.3 ± 0.8	473.5 ± 1.0	0.3 ± 0.1
PA1010/TT-SF	411.9 ± 0.9	480.3 ± 1.1	16.7 ± 0.3
PA1010/G-SF	417.6 ± 1.1	483.1 ± 0.9	15.1 ± 0.4
PA1010/A-SF	418.4 ± 0.9	480.5 ± 0.8	15.4 ± 0.3

Thermomechanical properties of PA1010/SF composite parts

Figure III.3.2.6 shows the DMTA curves of the neat PA1010 and the PA1010/SF composite parts. **Table III.3.2.6** summarizes some of the thermomechanical properties obtained from the curves. In **Figure III.3.2.6a** one can observe the evolution of the storage modulus (E′) as a function of temperature. The dynamic thermomechanical behavior of PA1010 was characterized by an E′ value in the range of 700–825 MPa from −50 °C to 25 °C. In the temperature range comprised between 30 °C and 60 °C, the storage modulus decreased progressively down to values of 100–200 MPa. This drop in mechanical stiffness is attributed to the alpha (α)-transition region of PA1010 in which the amorphous phase of the biopolymer changes from the glassy to rubbery state. The composite parts showed a similar evolution of E′ with temperature than that observed for the neat PA1010 part, however the samples presented considerably higher values in the whole temperature range. This stiffness increase was more evident below the α-transition region, where E′ reached values over 1500 MPa, that is, it was multiplied by a factor two compared to the unfilled biopolymer part. In addition, E′ reached values above 600 MPa at 90 °C. The thermomechanical enhancement observed was more intense in the composite parts prepared with the silanized fibers. The PA1010/G-SF composite part presented the highest E′ value at temperatures below the α-transition region, reaching a value 1685 MPa at 0 °C, whereas the PA1010/A-SF composite part showed similar but slightly higher values above this region. These results are in agreement with the above-described mechanical characterization, performed at room temperature, which showed that the incorporation of SF resulted in a rigidity increase. The further improvement of the mechanical resistant properties for the PA1010/G-SF and PA1010/A-SF composite parts can be attributed to the adhesion increase between fibers and matrix at the interface, as also observed during the morphological analysis. In this regard, Abdelmouleh *et al.* [56] reported a similar increase in the thermomechanical performance of low-density polyethylene (LDPE) when silane-treated cellulose fibers were incorporated.
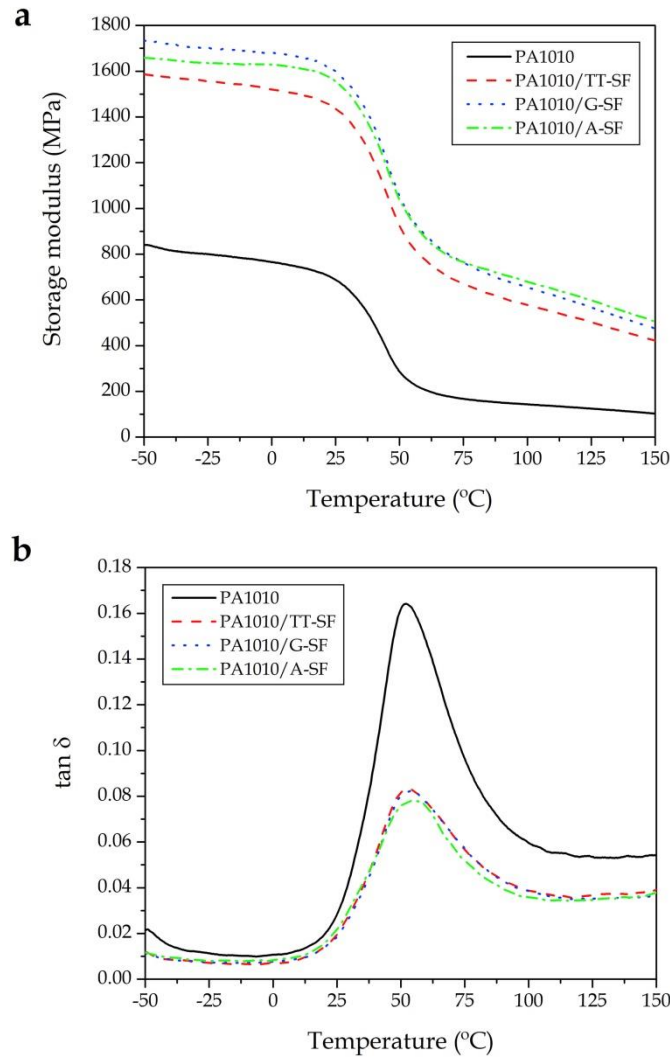
Figure III.3.2.6. (a) Storage modulus (E′) and (b) dynamic damping factor (tan δ) of polyamide 1010 (PA1010) and its composites with thermally treated slate fiber (TT-SF) and slate fibers pretreated with glycidyl-silane (G-SF) and amino-silane (A-SF).

Table III.3.2.6. Main thermomechanical parameters of polyamide 1010 (PA1010) and its composites with thermally treated slate fiber (TT-SF) and slate fibers pretreated with glycidyl-silane (G-SF) and amino-silane (A-SF) in terms of storage modulus (E′) measured at 0 °C and 90 °C and glass transition temperature (T_g).

Parts	E (MPa) at 0 °C	E (MPa) at 90 °C	T_g (°C)
PA1010	759 ± 20	146.2 ± 2.3	51.9 ± 0.9
PA1010/TT-SF	1523 ± 22	609.1 ± 2.3	52.7 ± 0.7
PA1010/G-SF	1685 ± 16	688.4 ± 1.2	54.0 ± 0.8
PA1010/A-SF	1618 ± 17	725.3 ± 1.4	55.2 ± 1.1

Figure III.3.2.6b shows the evolution of the damping factor (tan δ) as a function of temperature. It can be observed that the tan δ peak for the neat PA1010 was 51.9 °C. This value is representative of the α-transition of the biopolymer, which relates to its glass transition temperature (T_g). One can observe that the α-peak was slightly shifted to higher temperatures in the PA1010/TT-SF part, that is, 52.7 °C. The shift observed in the composite parts prepared with silanized fibers was also higher, showing values of 54.0 °C and 55.2 °C for PA1010/G-SF and PA1010/A-SF, respectively. The higher T_g values observed for both PA1010/G-SF and PA1010/A-SF composites also confirm the interfacial adhesion improvement achieved by both silane pre-treatments. This supports the previous observation outlined during DSC analysis, indicating that the movement of the biopolymer chains became more restricted and, therefore, the relaxation peak shifted to higher temperatures. It is also worthy to mention the significant reduction of the α-peak values in the composite parts. Since tan δ represents the ratio between the lost energy (E″) and E′, the lower values observed suggest a lower energy dissipation. This reduction is directly related to the higher E′ values due to fiber reinforcement. However, it can also be ascribed partially to the higher crystallinity achieved in the pieces since a reduced percentage of amorphous phase undergoes glass transition [57].

Water uptake of PA1010/SFs composite parts

One of the most serious handicap related to the use of fiber-reinforced composites, especially those made of condensation polymers, is their high sensitivity to water that may reduce dramatically their mechanical performance in a damp atmosphere [58]. In general, PAs have high tendency to water absorption due to their relatively high polarity. **Figure III.3.2.7** shows the evolution of the water uptake of the neat PA1010 part and the PA1010/SF composite parts at room temperature. For all the immersed parts, the water absorption was found to increase with immersion time reaching a plateau after approximately 7 weeks. Although PA1010 is not extremely prone to moisture due its relatively high $CH_2/CONH$ ratio, the unfilled part absorbed approximately 1.35 wt% of water. This result is slightly higher than that previously observed for profile-extruded PA1010 tubes [11], that is, 1.20 wt%, possibly due to the lower crystallinity attained in the injection-molded parts. For the composite parts, the equilibrium water uptake was positively reduced to values in the 0.9–1.1 wt% range. This effect was also found to slightly depend on the pre-treatment applied to SF. Thus, PA1010 composites containing TT-SF absorbed 0.97 wt% of water whereas the composites based on G-SF and A-SF showed saturation moisture contents of 0.96 wt% and 1.04 wt%, respectively. It seems therefore that, despite the marked hydrophobic character of SFs, fiber adhesion plays a minor role in water uptake and the silanization pre-treatment performed on the fiber surface did not bring about significant reduction in water absorption. The water uptake reduction observed can be also ascribed to the higher crystallinity achieved in the parts since water molecules are absorbed only in the amorphous regions by involving two close amide groups in an accessible region [59]. Indeed, it has been reported that the use of coupling agents can potentially reduce the water absorption of several fiber-based composites, especially in cellulose-based fibers, though they do not provide a long-term performance [60]. In any case, the low water absorption obtained suggests that the mechanical properties of the composite parts will be nearly unaffected by atmospheric humidity.
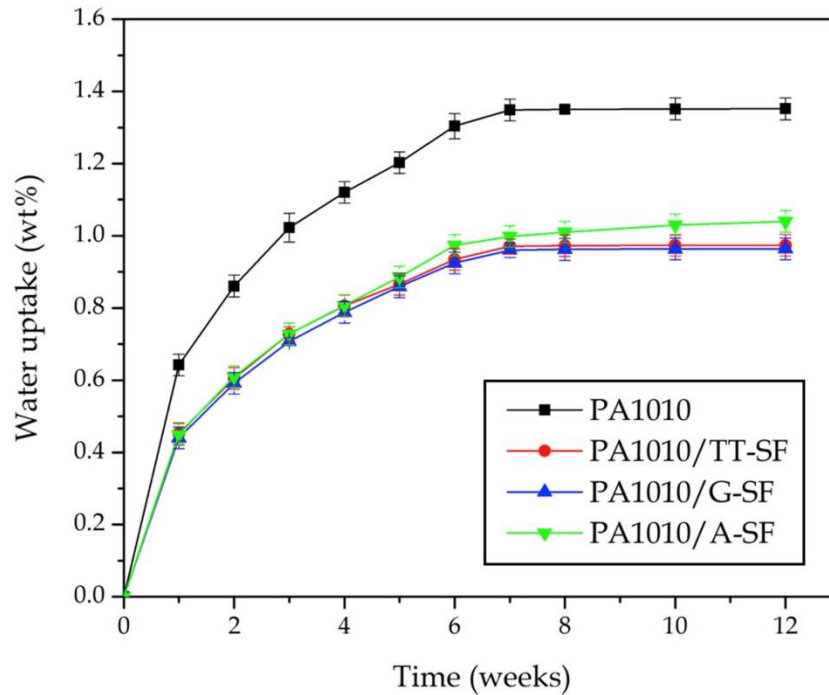
Figure III.3.2.7. Water uptake of polyamide 1010 (PA1010) and its composites with thermally treated slate fiber (TT-SF) and slate fibers pretreated with glycidyl-silane (G-SF) and amino-silane (A-SF).

CONCLUSIONS

This work shows that industrial waste derived SFs can be effectively used as novel reinforcing elements in fully bio-based PA1010 parts prepared by conventional industrial processes for thermoplastic materials, as it is the case of injection molding. In particular, the here-prepared injection-molded PA1010/SF composite parts presented a 3-fold increase in the tensile modulus whereas the tensile strength was doubled when compared to the unfilled PA1010 part. This approach was further improved by the pre-treatment of the inorganic fibers with coupling agents from silane family. The incorporation of the pretreated SF with glycidyl- and amino-silanes, called G-SF and A-SF, resulted in an additional increase of the mechanical strength and hardness without impairing the ductility and toughness of the PA1010/TT-SF composite. The mechanical improvement achieved was related to an enhanced adhesion at the biopolymer–fiber interface due to the specific reactive organo-functionalities of each silane. The thermal analysis indicated that the presence of SFs slightly increased the sample crystallinity. However, the fibers also confined the motion of the PA1010 chains, restricting their chain-folding process so that less perfect crystals with a thinner lamellae thickness were developed. The composite parts containing G-SF and A-SF also presented slightly higher thermal stability and improved thermomechanical resistance. In particular, thermal degradation was improved by up to 10 °C mainly due to an effect of mass transport barrier to the volatiles produced during decomposition offered by the inorganic fibers, which was further improved in the composites prepared with the silanized fibers. Water uptake was also reduced down to values below 1 wt% in the composite parts, though the effect of the silane pre-treatments was relatively low. Although both silane pre-treatments provided a significant improvement in the

mechanical and thermal properties of the PA1010/SF composite parts, the use of G-SF generated parts with slightly higher performance. This effect was ascribed to the more effective coupling mechanism of glycidyl-silane with PA1010. From the above, it can be concluded that G-SF constitutes a good alternative to replace GF, commonly used to reinforce PAs in engineering applications, and the resultant biopolymer composite parts can be of interest for the automotive or the building and construction industries. The use of PA1010 and SFs can contribute positively to the development of sustainable polymer technologies by decoupling raw materials to petroleum and also promoting the valorization of industrial wastes. Future works are also under progress to verify whether the glycidyl-silane reactive coupling agent can effectively enhance the interfacial adhesion of other environmentally friendly polymer composites.

Acknowledgments

REFERENCES

1. Winnacker, M. and B. Rieger, *Biobased Polyamides: Recent Advances in Basic and Applied Research.* Macromolecular Rapid Communications, 2016. **37**(17): 1391-1413.
2. Kind, S., S. Neubauer, J. Becker, M. Yamamoto, M. Völkert, G. von Abendroth, O. Zelder and C. Wittmann, *From zero to hero–production of bio-based nylon from renewable resources using engineered Corynebacterium glutamicum.* Metabolic engineering, 2014. **25**: 113-123.
3. Nguyen, A.Q., J. Schneider, G.K. Reddy and V.F. Wendisch, *Fermentative production of the diamine putrescine: system metabolic engineering of Corynebacterium glutamicum.* Metabolites, 2015. **5**(2): 211-231.
4. Wu, J., L. Jasinska-Walc, D. Dudenko, A. Rozanski, M.R. Hansen, D. Van Es and C.E. Koning, *An investigation of polyamides based on isoidide-2, 5-dimethyleneamine as a green rigid building block with enhanced reactivity.* Macromolecules, 2012. **45**(23): 9333-9346.
5. Jasinska, L., M. Villani, J. Wu, D. van Es, E. Klop, S. Rastogi and C.E. Koning, *Novel, fully biobased semicrystalline polyamides.* Macromolecules, 2011. **44**(9): 3458-3466.
6. Nakajima, H., P. Dijkstra and K. Loos, *The recent developments in biobased polymers toward general and engineering applications: Polymers that are upgraded from biodegradable polymers, analogous to petroleum-derived polymers, and newly developed.* Polymers, 2017. 9(10): 523.
7. Yasuda, M. and A. Miyabo, *Polyamide derived from castor oil.* Journal of Fiber Science and Technology, 2010. **66**(4): P137-P142.
8. Mutlu, H. and M.A. Meier, *Castor oil as a renewable resource for the chemical industry.* European Journal of Lipid Science and Technology, 2010. **112**(1): 10-30.
9. Kausar, A., *Polyamide 1010/Polythioamide Blend Reinforced with Graphene Nanoplatelet for Automotive Part Application.* Advances in Materials Science, 2017. **17**(3): 24-36.
10. Nishitani, Y., T. Kajiyama and T. Yamanaka, *Effect of silane coupling agent on tribological properties of hemp fiber-reinforced plant-derived polyamide 1010 biomass composites.* Materials, 2017. **10**(9): 1040.
11. Quiles-Carrillo, L., N. Montanes, T. Boronat, R. Balart and S. Torres-Giner, *Evaluation of the engineering performance of different bio-based aliphatic homopolyamide tubes prepared by profile extrusion.* Polymer Testing, 2017. **61**: 421-429.

12. Karsli, N.G., T. Yilmaz and O. Gul, *Effects of coupling agent addition on the adhesive wear, frictional and thermal properties of glass fiber-reinforced polyamide 6, 6 composites.* Polymer Bulletin, 2018. **75**(10): 4429-4444.

13. GmbH, n.-I., *Bio-Polyamide Market Expected To Reach USD 220.6 Million By 2022*. 2015.

14. Belmonte, E., M. De Monte, C.-J. Hoffmann and M. Quaresimin, *Damage mechanisms in a short glass fiber reinforced polyamide under fatigue loading*. International Journal of Fatigue, 2017. **94**: 145-157.

15. Zhang, S., Z. Huang, Y. Zhang and H. Zhou, *Experimental investigation of moisture diffusion in short glass fiber reinforced polyamide 6, 6*. Journal of Applied Polymer Science, 2015. **132**(37).

16. Bernasconi, A., F. Cosmi and D. Taylor, *Analisys of the fatigue properties of different specimens of a 10% by weight short glass fibre reinforced polyamide 6.6*. Polymer Testing, 2014. **40**: 149-155.

17. Sasayama, T., T. Okabe, Y. Aoyagi and M. Nishikawa, *Prediction of failure properties of injection-molded short glass fiber-reinforced polyamide 6, 6*. Composites Part A: Applied Science and Manufacturing, 2013. **52**: 45-54.

18. Loureiro, L., V.H. Carvalho and S.H.P. Bettini, *Reuse of p-aramid from industrial waste as reinforcement fiber in polyamide 6.6*. Polymer Testing, 2016. **56**: 124-130.

19. Dorigato, A. and L. Fambri, *Effect of aramid regenerated fibers on thermo-mechanical behaviour of polyamide 12 composites*. Journal of Reinforced Plastics and Composites, 2013. **32**(17): 1243-1256.

20. Wu, S.H., F.Y. Wang, C.C. Ma, W.C. Chang, C.T. Kuo, H.C. Kuan and W.J. Chen, *Mechanical, thermal and morphological properties of glass fiber and carbon fiber reinforced polyamide-6 and polyamide-6/clay nanocomposites*. Materials Letters, 2001. **49**(6): 327-333.

21. Karsli, N.G. and A. Aytac, *Tensile and thermomechanical properties of short carbon fiber reinforced polyamide 6 composites*. Composites Part B: Engineering, 2013. **51**: 270-275.

22. Ma, Y., C. Yan, H. Xu, D. Liu, P. Shi, Y. Zhu and J. Liu, *Enhanced interfacial properties of carbon fiber reinforced polyamide 6 composites by grafting graphene oxide onto fiber surface*. Applied Surface Science, 2018. **452**: 286-298.

23. Yao, S.-S., F.-L. Jin, K.Y. Rhee, D. Hui and S.-J. Park, *Recent advances in carbon-fiber-reinforced thermoplastic composites: a review.* Composites Part B: Engineering, 2017.

24. Bao, J. and J. Li. *The effect of surface treatment on the mechanical properties of glass fiber reinforced polyamide 6 composite*. in Applied Mechanics and Materials. 2011. Trans Tech Publ.

25. Quiles-Carrillo, L., N. Montanes, C. Sammon, R. Balart and S. Torres-Giner, *Compatibilization of highly sustainable polylactide/almond shell flour composites by reactive extrusion with maleinized linseed oil*. Industrial Crops and Products, 2018. **111**: 878-888.

26. Hui, C., C. Qingyu, W. Jing, X. Xiaohong, L. Hongbo and L. Zhanjun, *Interfacial enhancement of carbon fiber/nylon 12 composites by grafting nylon 6 to the surface of carbon fiber*. Applied Surface Science, 2018. **441**: 538-545.

27. Liu, J. and X.G. Liu. *The Studying on the Influence of Coupling Agents to Short Glass Fiber Reinforced Polyamide Composites*. in Advanced Materials Research. 2011. Trans Tech Publ.

28. Aparna, S., D. Purnima and R. Adusumalli, *Effect of Compatibilizer on the Properties of Polyamide 6 Blend Based Carbon Fiber Reinforced Composites*. Fibers and Polymers, 2018. **19**(6): 1335-1346.

29. Jenneskens, L., H. Schuurs, D.-J. Simons and L. Willems, *Molecular mechanisms of adhesion promotion by silane coupling agents in glass bead-reinforced polyamide-6 model composites.* Composites, 1994. **25**(7): 504-511.

30. Rudzinski, S., L. Häussler, C. Harnisch, E. Mäder and G. Heinrich, *Glass fibre reinforced polyamide composites: Thermal behaviour of sizings*. Composites Part A: Applied Science and Manufacturing, 2011. **42**(2): 157-164.

31. Kim, B.-J., S.-H. Cha, K. Kong, W. Ji, H.W. Park and Y.-B. Park, *Synergistic interfacial reinforcement of carbon fiber/polyamide 6 composites using carbon-nanotube-modified silane*

coating on ZnO-nanorod-grown carbon fiber. Composites Science and Technology, 2018. **165**: 362-372.

32. Zhang, Z. and Y. Xin, *Mechanical properties of basalt-fiber-reinforced polyamide-6/polypropylene composites*. Mechanics of Composite Materials, 2014. **50**(4): 509-514.

33. Nguyen, V., J. Hao and W. Wang, *Ultraviolet Weathering Performance of High-Density Polyethylene/Wood-Flour Composites with a Basalt-Fiber-Included Shell*. Polymers, 2018. **10**(8): 831.

34. Pak, S., S. Park, Y.S. Song and D. Lee, *Micromechanical and dynamic mechanical analyses for characterizing improved interfacial strength of maleic anhydride compatibilized basalt fiber/polypropylene composites*. Composite Structures, 2018. **193**: 73-79.

35. Siegesmund, S. and R. Snethlage, *Stone in Architecture: Properties, Durability*. 2011, Berlin, Germany: Springer.

36. Penide, J., et al., *Laser Microdrilling of Slate Tiles*. Materials, 2019. **12**(3): 398.

37. Barluenga, G. and F. Hernández-Olivares, *Self-levelling cement mortar containing grounded slate from quarrying waste.* Construction and Building Materials, 2010. **24**(9): 1601-1607.

38. Carvalho, G.M.X.d., H.S. Mansur, W.L. Vasconcelos and R.L. Oréfice, *Composites obtained by the combination of slate powder and polypropylene.* Polímeros, 2007. **17**: 98-103.

39. 39. Samper, M., R. Petrucci, L. Sánchez-Nacher, R. Balart and J. Kenny, *New environmentally friendly composite laminates with epoxidized linseed oil (ELO) and slate fiber fabrics.* Composites Part B: Engineering, 2015. **71**: 203-209.

40. Carbonell-Verdú, A., D. García-García, A. Jordá, M. Samper and R. Balart, *Development of slate fiber reinforced high density polyethylene composites for injection molding*. Composites Part B: Engineering, 2015. **69**: 460-466.

41. Yan, M. and H. Yang, *Improvement of polyamide 1010 with silica nanospheres via in situ melt polycondensation.* Polymer Composites, 2012. **33**(10): 1770-1776.

42. Yu, S., K.H. Oh, J.Y. Hwang and S.H. Hong, *The effect of amino-silane coupling agents having different molecular structures on the mechanical properties of basalt fiber-reinforced polyamide 6,6 composites.* Composites Part B: Engineering, 2019. **163**: 511-521.

43. Samper, M.D., R. Petrucci, L. Sánchez-Nacher, R. Balart and J.M. Kenny, *Effect of silane coupling agents on basalt fiber–epoxidized vegetable oil matrix composite materials analyzed by the single fiber fragmentation technique*. Polymer Composites, 2015. **36**(7): 1205-1212.

44. Laura, D., H. Keskkula, J. Barlow and D. Paul, *Effect of glass fiber surface chemistry on the mechanical properties of glass fiber reinforced, rubber-toughened nylon 6*. Polymer, 2002. **43**(17): 4673-4687.

45. Chen, J., L. Qu, W. Han, X. Li and Z. Wang, *Study on radiation stability of glass-fiber reinforced nylon-1010.* Gaofenzi Cailiao Kexue Yu Gongcheng/Polymeric Materials Science and Engineering, 1995. **11**(2): 127-129.

46. Zhang, S.L., G.B. Wang, Z.H. Jiang, D. Wang, R.T. Ma and Z.W. Wu, *Impact properties, phase structure, compatibility, and fracture morphology of polyamide 1010/thermoplastic poly (ester urethane) elastomer blends.* Journal of Polymer Science Part B: Polymer Physics, 2005. **43**(10): 1177-1185.

47. Xie, Y., C.A. Hill, Z. Xiao, H. Militz and C. Mai, *Silane coupling agents used for natural fiber/polymer composites: A review.* Composites Part A: Applied Science and Manufacturing, 2010. **41**(7): 806-819.

48. Philip, B., J. Xie, A. Chandrasekhar, J. Abraham and V.K. Varadan, *A novel nanocomposite from multiwalled carbon nanotubes functionalized with a conducting polymer.* Smart materials and structures, 2004. **13**(2): 295.

49. Zhang, G. and D. Yan, *Crystallization kinetics and melting behavior of nylon 10, 10 in nylon 10, 10–montmorillonite nanocomposites*. Journal of applied polymer science, 2003. **88**(9): 2181-2188.

50. Zeng, H., C. Gao, Y. Wang, P.C. Watts, H. Kong, X. Cui and D. Yan, *In situ polymerization approach to multiwalled carbon nanotubes-reinforced nylon 1010 composites: mechanical properties and crystallization behavior.* Polymer, 2006. **47**(1): 113-122.

51.   Mittal, V., A.U. Chaudhry and G.E. Luckachan, *Biopolymer–thermally reduced graphene nanocomposites: structural characterization and properties.* Materials Chemistry and Physics, 2014. **147**(1-2): 319-332.

52.   Xiuwei, F., L. Xiaohong, Y. Laigui and Z. Zhijun, *Effect of in situ surface modified nano SiO2 on the thermal and mechanical properties and crystallization behavior of nylon 1010.* Journal of applied polymer science, 2010. **115**(6): 3339-3347.

53.   Mosanenzadeh, S.G., M.W. Liu, A. Osia and H.E. Naguib, *Thermal composites of biobased polyamide with boron nitride micro networks.* Journal of Polymers and the Environment, 2015. **23**(4): 566-579.

54.   Torres-Giner, S., N. Montanes, T. Boronat, L. Quiles-Carrillo and R. Balart, *Melt grafting of sepiolite nanoclay onto poly(3-hydroxybutyrate-co-4-hydroxybutyrate) by reactive extrusion with multi-functional epoxy-based styrene-acrylic oligomer.* European Polymer Journal, 2016. **84**: 693-707.

55.   Shen, Z., S. Bateman, D.Y. Wu, P. McMahon, M. Dell'Olio and J. Gotama, *The effects of carbon nanotubes on mechanical and thermal properties of woven glass fibre reinforced polyamide-6 nanocomposites.* Composites Science and Technology, 2009. **69**(2): 239-244.

56.   Abdelmouleh, M., S. Boufi, M.N. Belgacem and A. Dufresne, *Short natural-fibre reinforced polyethylene and natural rubber composites: effect of silane coupling agents and fibres loading.* Composites science and technology, 2007. **67**(7-8): 1627-1639.

57.   Torres-Giner, S., N. Montanes, O. Fenollar, D. García-Sanoguera and R. Balart, *Development and optimization of renewable vinyl plastisol/wood flour composites exposed to ultraviolet radiation.* Materials and Design, 2016. **108**: 648-658.

58.   Lassila, L., T. Nohrström and P. Vallittu, *The influence of short-term water storage on the flexural properties of unidirectional glass fiber-reinforced composites.* Biomaterials, 2002. **23**(10): 2221-2229.

59.   Paterson, M. and J. White, *Effect of water absorption on residual stresses in injection-moulded nylon 6, 6.* Journal of materials science, 1992. **27**(22): 6229-6240.

60.   Faruk, O., A.K. Bledzki, H.P. Fink and M. Sain, *Progress report on natural fiber reinforced composites.* Macromolecular Materials and Engineering, 2014. **299**(1): 9-26.

III.3.3. Development of high-performance polyamide 1010/coconut fibers composites by reactive extrusion with natural and petrochemical derived compatibilizers

L. Quiles-Carrillo [1], N. Montanes [1], V. Fombuena [1], R.Balart [1] and S. Torres-Giner [1,2,]

[1] Technological Institute of Materials (ITM), Universitat Politècnica de València (UPV), Plaza Ferrándiz y Carbonell 1, 03801 Alcoy, Spain;

[2] Novel Materials and Nanotechnology Group, Institute of Agrochemistry and Food Technology (IATA), Spanish National Research Council (CSIC), Calle Catedrático Agustín Escardino Benlloch 7, 46980 Paterna, Valencia, Spain

Development of high-performance polyamide 1010/coconut fibers composites by reactive extrusion with linseed oil derived and petrochemical compatibilizers with multi-functionalities

Abstract.

This work reports the preparation and characterization of fully biobased polymer composites with coconut fibers (CFs) as an alternative to wood-plastic composites, typically based on petroleum-derived materials. Polyamide 1010 (PA1010) was melt-extruded with 20 wt% of natural coconut fibers (CFs) and, after that, shaped into pieces by injection molding. Four different multi-functionalized compatibilizers were tested to increase the polymer-fiber interactions with the subsequent improvement on toughness. These consisted of two chemically modified vegetable oils, namely maleinized and epoxidized linseed oil, MLO, and ELO respectively, and two commercial additives derived from petroleum and based on glycidyl functionality, that is, low-functionality epoxy-based styrene-acrylic oligomer (ESAO) and polystyrene-glycidyl methacrylate random copolymer (PS-GMA). The addition of all four compatibilizers improved both the mechanical and thermomechanical properties of the composites, thus resulting in high-performance composite materials with relatively low water uptake. Furthermore, the morphology of the obtained composites revealed an extraordinary embedment of the fibers into the biopolymer matrix, which plays a crucial role in improving toughness. Among all the tested compatibilizers, those derived from vegetable oils can be considered the most interesting due to they offer a complete sustainable solution.

Keywords: Bio-based polyamides; natural fibers; high-performance composites; polymer-matrix interaction; multi-functionalized vegetable oils.

INTRODUCTION

In the last years, natural fibers are gaining an essential role in developing high environmentally-friendly composites to overcome the current ecological and environmental problems related to the recyclability of glass fiber-reinforced plastics (GFRP). Besides, by using natural fibers, it is possible to upgrade a wide variety of natural waste or by-products. For this reason, natural fibers such as hemp [1, 2], flax [3, 4], jute [5, 6] or sisal [7, 8] are becoming particularly attractive in technological sectors such automotive and transportation industries because of their lower cost and lower density, therefore leading to lightweight composites as realistic alternatives to glass-reinforced composites in many applications [9]. Moreover, one of the primary wastes from agriculture, agroforestry and other food-related industries are lignocellulosic materials that offer high potential as reinforcing materials as they are readily available and characterized by having a low weight, being fully bio-sourced and biodegradable (disintegrable in compost soil), showing low abrasive properties and, in most cases, they represent a cost-effective solution to other conventional reinforcing fibers. In particular, coir palms (*Cocos nucifera L.*) are abundantly growing in tropical countries, and their wide variety of products are being applied in both food and non-food products. Coconut palms are grown in more than 100 countries and autonomous regions of the world, which results in annual worldwide production of about 60.5 million tons in 2014 [10]. They represent an essential agribusiness in developing countries with a tropical climate [11]. A variety of uses have been proposed for the husks and shells, which remain after harvesting and processing of coconuts. For example, coconut husks and shells are widely used as an alternative energy source in some countries. In particular, the coconut husk is constituted of 30 wt% fiber and 70 wt% pith material [12]. This 30 wt% represents a colossal waste that does not have a great value, and it is discarded entirety. Coconut husks can be further processed into new useful fiber-like products known as coir when the fibers completely ground up. Nowadays, only 15 wt% of the husk fibers are recovered for different uses [13]. A much more efficient utilization is possible, especially using shorter fibers (sometimes called fiber bits) that cannot be used for high-value products [10].

As already mentioned, an interesting approach is the use of coconut fibers as reinforcement in composites with a thermoplastic polymeric matrix, thus leading to the so-called "natural fiber-reinforced plastics" (NFRP) or "wood-plastic composites" (WPC) that are gaining a considerable interest due to the increasing environmental concerns as they positively contribute to lowering the carbon footprint and give rise to new solutions for a sustainable development in the frame of a new paradigm based on the Circular Economy [14-17]. The use of wood-plastic composites (WPCs) offers significant advantages from both economic and environmental standpoints, but they also are attractive from a technical point of view as they can be shaped by conventional manufacturing processes such as hot-press molding, extrusion, injection processes, and so on [18, 19].

Typical polymer matrices in WPC include commodity polymers such as low- and high-density polyethylene (LDPE and HDPE) [20, 21], polypropylene (PP) [22, 23], polystyrene (PS) [24] and polyvinyl chloride (PVC) [25]. Nevertheless, in accordance with the increasing environmental concern, new biopolymer matrices are being increasingly used in WPCs, such as polylactide (PLA), poly(ε-caprolactone) (PCL),

poly(butylene succinate) (PBS), poly(butylene succinate-*co*-adipate) (PBSA), among others [26-28]. These polymers offer similar properties to those based on commodities but, also, they are disintegrable in controlled compost soil, that is, compostable. Additionally, to these aliphatic polyesters, new polymers are being synthesized from renewable resources. This is particularly noticeable in engineering plastics such as polycarbonate (PC), polyethylene terephthalate (PET), polyethylene furanoate (PEF), and polyamides (PAs) and their blends, which can be totally or partially obtained from renewable resources [29-31]. Polyamide 1010 (PA1010) is a new material from different standpoints; on the one hand, it is fully bio-derived from castor-oil derivatives and, on the other hand, it has comparable properties, or even higher than those of petroleum-derived polyamide 12 (PA12). For these reasons, PA1010 offers interesting uses in engineering applications such as the automotive industry. PA1010 are flexible, high-impact resistance materials with improved heat resistance and low extraction [32, 33]. These balanced properties make PA1010 suitable for thermal management and complex parts in the automotive industry and also food packaging applications [34-36].

One of the main drawbacks related to natural fiber thermoplastic reinforced plastics is the poor compatibility between the typical hydrophobic polymer matrix and the highly hydrophilic reinforcement, which are typically lignin, hemicellulose, and cellulose. This weak polymer-fiber interactions, together with some other drawbacks related to the high polar nature of the lignocellulosic fibers, such as poor fiber dispersion into the hydrophobic polymer matrix or high moisture gaining, do not allow to benefit from the excellent properties of the thermoplastic matrix and it leads to low-performance materials [37]. To overcome or, at least, minimize these effects, it is necessary to improve the polymer-fiber interaction, and this process can be achieved by different approaches. Conventional chemical processes on fibers such as esterification, acetylation, and so on, allow reducing the hydrophilicity of natural fibers with a positive effect on improved interactions between the polymer matrix and the chemically modified fiber. In some cases, specific additives can be used, which contain functional molecules that can react with both the polymeric matrix and the natural fiber. In general, bi-functional copolymers give good results [38-40]. In this sense, Jeng *et al.* [41] have used polypropylene-*grafted*-maleic anhydride (PP-*g*-MA) to make PP compounds compatible with natural fibers with excellent results. Other approaches include the use of other functional molecules such as stearic acid [42], maleic anhydride [43] or silane and isocyanate [44], which can positively contribute to improved interface interactions. Recent researches are being focused on the development of highly environmentally friendly functional materials that could potentially help in increasing polymer-fiber interactions. The use of compatibilizers represents a powerful strategy to enhance interfacial adhesion between the lignocellulosic fillers/fibers and a wide range of polymer matrices [39, 45]. Multi-functionalized vegetable oils (VOs) represent a real solution to a range of new materials with different uses. For instance, epoxidized linseed oil (ELO) and maleinized linseed oil (MLO) have been successfully used as compatibilizers in polymer blends and polymer composites with polyester-type matrices such as PLA, PBS, PCL, PBSA, etc. [26, 46-48], due to the high reactivity of the oxirane and maleic anhydride groups towards hydroxyl groups in both aliphatic polyester and lignocellulosic fiber. As an example, Garcia-Garcia *et al*. [49] recently reported that the use of vegetable oil derivatives does not compromise the overall biodegradation of poly(3-hydroxybutyrate) (PHB) aliphatic polyester.

These environmentally friendly additives derived from vegetable oils are gaining interest against petroleum-derived conventional chain-extenders or compatibilizers such as typical epoxy-based styrene-acrylic oligomers (ESAOs), commercially known as Joncryl®. These oligomers can quickly form new ester bonds through reaction of their epoxy groups with the hydroxyl terminal groups of the biopolymer chains during melt processing [50] and, obviously, these epoxy rings can also react with hydroxyl groups of the lignocellulosic fillers/fibers to provide improved polymer-fiber interactions [51-53].

In this research work, highly environmentally friendly composite materials have been obtained with a PA1010 matrix and coir fiber as reinforcement. The effect of CFs on the mechanical, thermal, morphological, and thermomechanical properties was studied as a function of the different compatibilizers employed. The efficiency of the two bio-based compatibilizers obtained from linseed oil, namely ELO and MLO, respectively, was compared with two commercial petroleum-based compatibilizers widely used as chain extenders in polyester formulations, that is, the ESAO supplied as Joncryl® ADR 4300 and the polystyrene-glycidyl methacrylate random copolymer (PS-GMA) as Xibond™ 920.

EXPERIEMNTAL

Materials

Fully bio-based homopolyamide PA1010 commercial-grade NP BioPA1010-201 was provided, in pellets form, by NaturePlast (Ifs, France). According to the manufactured information, this PA1010 is a medium-viscosity injection-grade with a density of 1.05 g.cm^{-3} and a viscosity number (VN) of about 160 cm^3.g^{-1}.
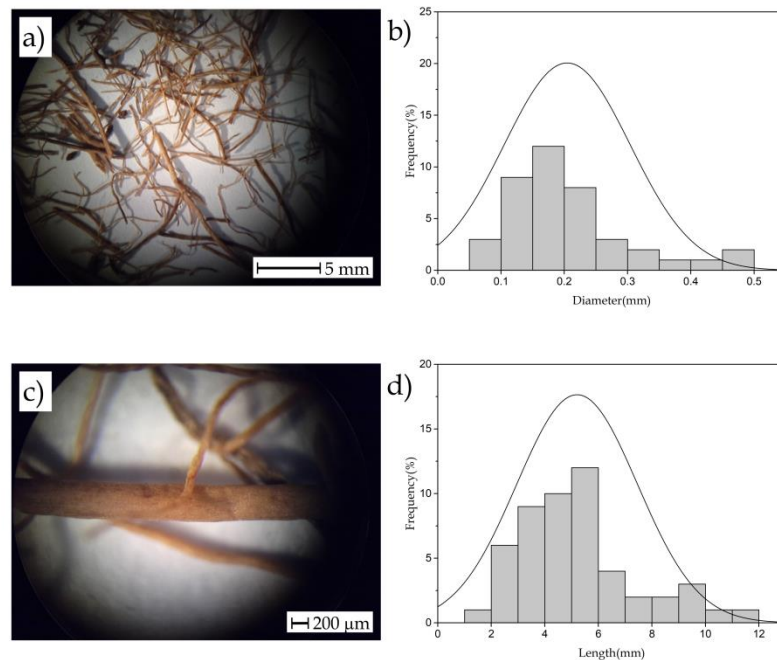
Figure III.3.3.1. Optical images of coconut fiber (CFs) (a & c) at different magnifications and statistical distribution of the length (b) and diameter (d).

CF was supplied by BCK Barnacork S.L (Barcelona, Spain). The fibers present an average length of 5.2 ± 2.2 mm and an average diameter of 205 ± 98 μm. **Figure III.3.3.1** shows the optical images of CFs used to measure the average diameter and length together with the corresponding histogram profiles. As can be seen, both distributions have a high standard deviation due to the high heterogeneity of CFs.

MLO was VEOMER LIN supplied from Vandeputte (Mouscron, Belgium). It has a viscosity of 1000 cP at 20°C and an acid value comprised in the 105 and 130 mg KOH.g^{-1} range. ELO was supplied by Traquisa S.L. (Barcelona, Spain). This has a molecular weight (M_W) of about 1037 g.mol^{-1}, a density between 1.05 and 1.06 g.cm^{-3} at 20 °C, and a viscosity of 8–11 p (at 25 °C). Regarding the petroleum-derived compatibilizers, a low-functionality ESAO, Joncryl® ADR 4300, was obtained from BASF S.A. (Barcelona, Spain) in flakes form. Its average M_W is 5500 g.mol^{-1}, and it shows a glass transition temperature (T_g) of 56 °C. Its epoxy equivalent weight (EEW) is 445 g mol^{-1}, and its functionality (*f*) is ≤ 5. PS-GMA was Xibond™ 920 kindly supplied by Polyscope (Geleen, The Netherlands). Its M_W is 50000 g.mol^{-1}, its T_g is 95 ºC, and its glycidyl methacrylate (GMA) content is 20 m/m%. **Figure III.3.3.2** shows the chemical structure of all four compatibilizers used in this study.

a) vegetable oil-derived compatibilizers

epoxidized linseed oil (ELO)

maleinized linseed oil (MLO)

b) petroleum-derived compatibilizers

R$_1$, R$_2$ are H or alkyl
R$_3$ is alkyl
x and y are 1 to 20
z is 2 to 20

poly(styrene-*ran*-glycidyl methacrylate) PS-GMA [Xibond™ 920]

epoxy styrene-acrylic oligomer - ESAO [Joncryl(R) ADR-4300]
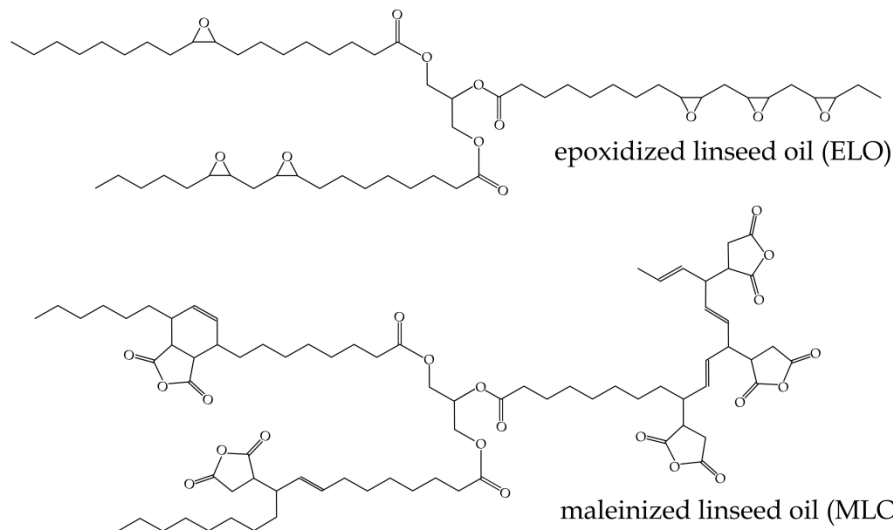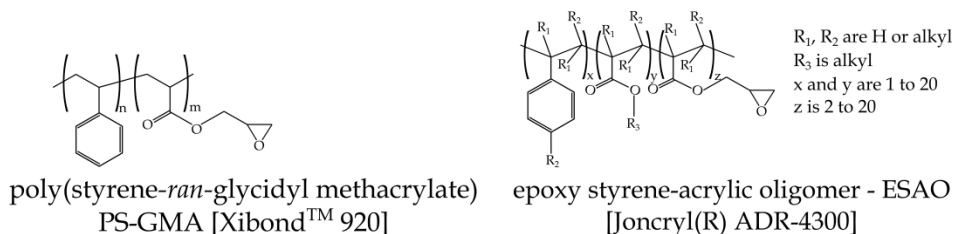
Figure III.3.3.2. Schematic representation of the chemical structure of a) bio-based and b) petroleum-derived functional compounds used.

Manufacturing of PA1010/CF composites

In a previous stage, to remove any residual moisture which could affect processing, both PA1010 and coir fiber were dried at 60 °C for 45 h in a dehumidifying dryer MDEO from Industrial Marsé (Barcelona, Spain). After this stage, an initial mechanical mixing of the appropriate components, which are summarized in **Table III.3.3.1**, was obtained in a zipper bag and then the different mixtures were subjected to a compounding process in a twin-screw co-rotating extruder from Construcciones Mecánicas DUPRA S.L. (Alicante, Spain). The screws had a diameter of 25 mm and a length (L) to diameter (D) ratio (L/D) of 24. The mixtures were subjected to the following temperature program during extrusion from the hopper to the extrusion die: 200 °C – 210 °C – 215 °C and 220 °C. **Figure III.3.3.3** shows an image of the injection-molded composites together with the starting materials.
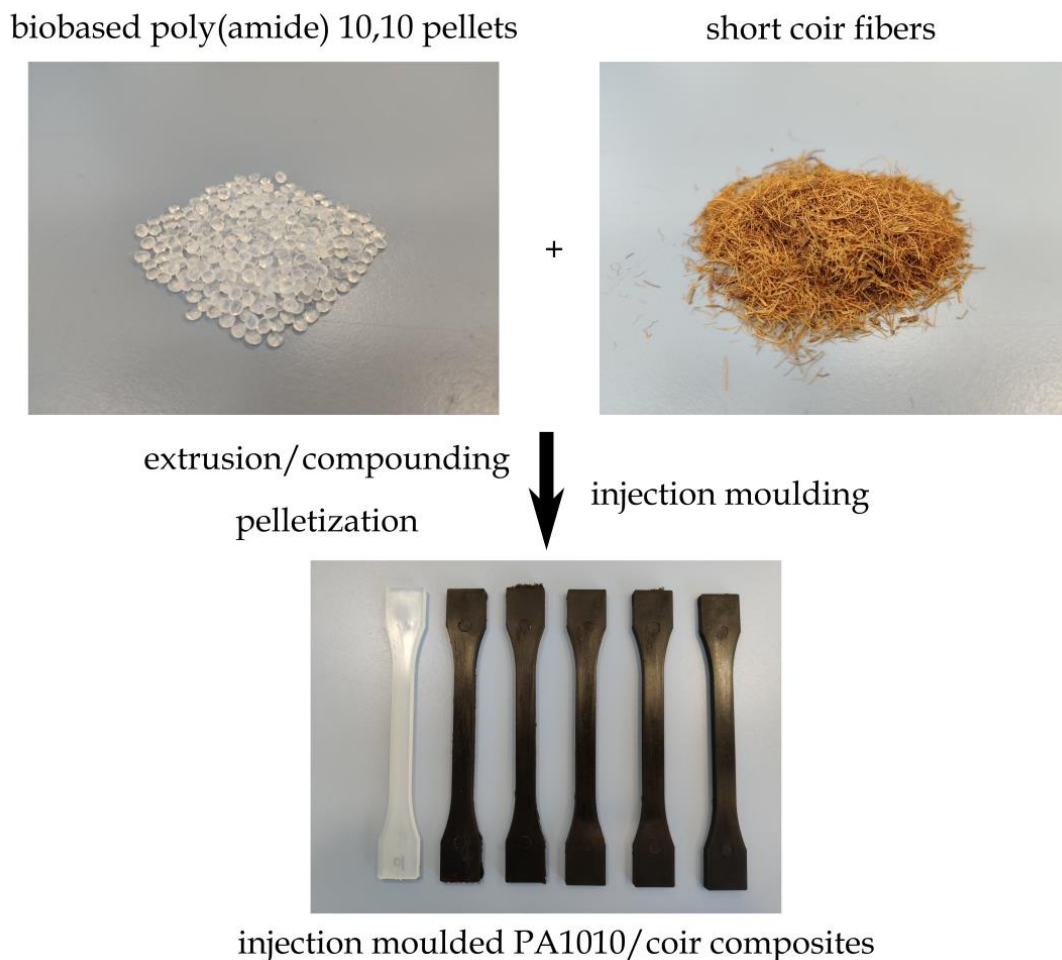
Figure III.3.3.3. Image of the starting materials polyamide 1010 (PA1010) and coconut fibers (CFs) and of the obtained pieces after melt compounding and injection molding.

Table III.3.3.1. Summary of codes and compositions according to the weight content (wt %) of polyamide 1010 (PA1010) and coconut fibers (CFs) in which maleinized linseed oil (MLO), epoxidized linseed oil (ELO), epoxy-based styren-–acrylic oligomer (ESAO), and polystyrene-glycidyl methacrylate random copolymer (PS-GMA) were added as parts per hundred resin (phr) of PA1010/CFs composite.

Code	PA1010 (wt%)	CFs (wt%)	MLO (phr)	ELO (phr)	ESAO (phr)	PS-GMA (phr)
PA1010	100	0	0	0	0	0
PA1010/CF	80	20	0	0	0	0
PA1010/CF + MLO	80	20	7.5	0	0	0
PA1010/CF + ELO	80	20	0	7.5	0	0
PA1010/CF + ESAO	80	20	0	0	2.5	0
PA1010/CF + PS-GMA	80	20	0	0	0	2.5

The compounded pellets corresponding to the different formulations were further processed by injection molding in a Meteor 270/75 from Mateu & Solé (Barcelona, Spain). The selected temperature profile in the injection molding machine was the following (from the feeding zone to the injection nozzle): 205 °C, 205 °C, 210 °C, and 210 °C. A clamping force of 75 tons was applied. Concerning the cavity filling and cooling times, they were set to 1 s and 10 s, respectively. Standard samples for characterization were obtained by injection molding.

Mechanical characterization.

Different mechanical tests were used to assess the compatibilization effectiveness of different compatibilizers mentioned above on mechanical performance. In particular, tensile, hardness, and Charpy impact tests were carried out. Concerning tensile tests, they were carried out in a universal test machine LLOYD 30 K (Hampshire, United Kingdom) on dog bone-shaped samples following the recommendations of ISO 527-1:2012. The selected load cell was 30 kN, and the cross-head speed was set to 1 mm min^{-1}. Hardness values were measured by using a hardness tester durometer Brevetti AFFRI – Model ART. 13 durometer, (Induno Olona, Italy). The measurements were taken at 10 different points on injection-molded samples with a size of 80x10x4 mm^3, according to ISO 868:2003. Toughness was also assessed on rectangular samples with dimensions 80x10x4 mm^3 by the Charpy impact test with a 6J pendulum from Metrotec S.A. (San Sebastián, Spain) on notched samples (V-notch with a radius of 0.25 mm), following the specifications of ISO 179-1:2010. To obtain reliable results, all tests were carried out on at least 6 different samples of each material, and the main parameters from each mechanical test were obtained and averaged.

Thermal characterization.

Thermal characterizations were carried out by differential scanning calorimetry (DSC) and thermogravimetric analysis (TGA). To evaluate the main thermal transitions of PA1010/CFs composites, a differential scanning calorimeter (DSC) Q200 from TA Instruments (Schwerzenbach, Switzerland) was used. Samples (average weight of 5 – 8 mg) were placed into standard sealed aluminum crucibles characterized by a total volume of 40 µL. Then, samples were subjected to a dynamic thermal program scheduled in three different stages: a first heating step from 25 °C to 150 °C was followed by a cooling down to 25 °C and then a second heating step was programmed from 25 °C up to 350 °C. The heating/cooling rate was set to 10 °C min^{-1}, and the selected atmosphere was nitrogen at a constant flow rate of 66 mL min^{-1}. In addition to the melt peak temperature (T_m), additional information about the melting enthalpy (ΔH_m) was collected to calculate the degree of crystallinity (χ_c) as indicated in **Equation III.3.3.1**.

$$\chi_c(\%) = \left[\frac{\Delta H_m}{\Delta H_m^0 \cdot (1-w)} \right] \cdot 100 \qquad \textbf{Equation III.3.3.1}$$

Where ΔH_m (J.g^{-1}) corresponds to the melting enthalpy of the crystalline fraction in PA1010 and ΔH_m^0 (J.g^{-1}) stands for the melting enthalpy of a theoretically fully crystalline PA1010, that is, 244 J.g^{-1} [54]. Finally, the term 1-w represents the weight fraction of PA1010 where w represents the weight fraction of all components except PA1010.

In addition to thermal transitions, thermal stability was assessed by TGA in a Seiko Exstar 6300 analyzer (Tokyo, Japan). Samples amounts of 5–7 mg were placed in standard alumina crucibles of 70 µL and subjected to a dynamic heating program from 30 °C to 700 °C at a heating rate of 10 °C min^{-1} under nitrogen atmosphere at 60 mL/min.

Thermomechanical characterization.

Complementary to other thermal analysis techniques, dynamical thermomechanical properties were obtained in a dynamic mechanical thermal analyzer (DMTA) DMA1 from Mettler-Toledo (Schwerzenbach, Switzerland). The selected setup was dynamic flexural load in a single cantilever. Rectangular samples with dimensions of 20×6×2.7 mm[3] were subjected to dynamic temperature heating program from -150°C up to 150 °C at a constant heating rate of 2 °C min^{-1}. The maximum flexural deformation in the cantilever was set to 10 µm, and the selected frequency was 1 Hz.

Morphology characterization.

The morphology of the developed composites was studied by field emission electron microscopy (FESEM) in a microscope ZEISS SUPRA 25 from Oxford Instruments (Abingdon, UK) working art an acceleration voltage of 2 kV. To provide electrical conducting properties to fractured samples, these were covered with a thin platinum layer in a high vacuum sputter coater EM MED20 from Leica Microsystem (Milton Keynes, United Kingdom).

Water uptake characterization.

To evaluate the effect of natural fiber on the water uptake, injection-molded samples sizing 4x10x80 mm^3 were immersed in distilled water at 24 ± 1 $^{\circ}$C. The evolution of water absorption was followed for a whole period of 14 weeks. Samples were extracted weekly. The residual water was removed with a dry cloth, and then, samples were weighed on an analytical balance with a precision of ± 0.1 mg to give high accuracy. All measurements were performed in triplicate to obtain reliable data. The weight of the samples during the water uptake period was obtained using an ABT 220-SDM analytical balance from Kern&Sohn (Balingen-Frommern, Germany). The analysis was carried out according to ISO 62: 2008. To obtain the diffusion coefficient (D), the ISO 62:2008 allows the application of Fick's first law. The diffusion coefficient can be estimated according to **Equation III.3.2**. In this sense, $W_t/W_s \leq 0.5$ is a linear plot of $\Delta m_t = f(\sqrt{t})$ that allows calculation of the diffusion coefficient from the slope (θ) [55, 56].

$$\frac{W_t}{W_S} = \frac{4}{d}\left(\frac{D\,t}{\pi}\right)^{\frac{1}{2}} \qquad \textbf{Equation III.3.3.2}$$

Where d is the initial thickness of the sample, D is the diffusion coefficient, and W_s is the saturation weight in the linear region. The slope is calculated from the plot representation of W_t/W_S versus $t^{1/2}$. To obtain the diffusion coefficient, **Equation III.3.3.3** was used [57]:

$$D = 0.0625\,\pi\,d^2\theta^2 \qquad \textbf{Equation III.3.3.3}$$

where θ is the slope, and d is the initial thickness of the sample. Since this expression is only correct for a one-dimensional shape such as a film, new **Equation III.3.3.4** considers different corrections to make this expression useful for three-dimensional samples:

$$D_c = D\left(1 + \frac{d}{h} + \frac{d}{w}\right)^{-2} \qquad \textbf{Equation III.3.3.4}$$

where D_c is the corrected diffusion coefficient (geometry), h is the total length, w is the width, and d is the sample thickness. The use of this equation assumes that the velocity of diffusion is equal in all directions. [56-58].

RESULTS AND DISCUSSION

Mechanical characterization of PA1010/CFs composites

Table III.3.3.2 shows the mechanical results of PA1010/coir fiber composite with different compatibilizers, obtained from tensile tests. Concerning neat PA1010, the tensile modulus, E and σ_{max} were 636 MPa and 41.2 MPa, respectively. About the elongation, it is important to remark two different values, both the elongation at break

(ε_b) of 256% [59] and the elongation at the maximum tensile stress σ_{max}, which was only 11.8%. These mechanical properties are typical of a tough engineering material. It is important to bear in mind that due to the low polymer-fiber interaction, the uncompatibilized PA1010/CFs piece showed an increased rigidity. In particular, reinforcement with 20 wt% CF yielded an increase in the tensile modulus of about two times the value of neat PA1010, that is, 940 MPa. On the contrary, the maximum tensile strength was remarkably reduced down to values of 20.2 MPa, which represents about half the value of neat PA1010. Similarly, the elongation at break is coincident with the elongation at the maximum stress since the material lost certain cohesion. This poor material's cohesion is responsible for this dramatic decrease in elongation down to values of 3.1%. Similar findings were reported by L.H. Staffa *et al.* [60] with PP composites containing 30 wt% coir fiber with a decrease in elongation at break from >350% down to 3.69% with slight improvements achieved by using different compatibilizers. This is the typical behavior of fibers with weak interactions with the polymer matrix, as reported by other authors. For instance, Rozman *et al.* [61] reported that the addition of coir fiber to PP provided a dramatic reduction of elongation at break and, subsequently, an increase in Young's modulus of the obtained composites. This is evident if it is taken into account the definition of the tensile or Young's modulus, which represents the stress to elongation ratio in the linear region of a tensile test. As the elongation is in the denominator, a high decrease in elongation provides increased tensile modulus. This behavior has been reported in a wide variety of polymer-fiber composites with poor or absence of fiber-polymer interactions and is much more pronounced in polymers characterized by high elongation at break. Following this, Carbonell-Verdú *et al.* [62] reported this effect on bio-based high-density polyethylene (bio-HDPE) reinforced with 20 wt% slate fiber (SF). The modulus was increased from 373 MPa, for neat bio-HDPE, up to 1483 MPa in the composite containing 20 wt% SF. On the contrary, the elongation at break decreased dramatically from 520% for neat bio-HDPE down to 18.7% for the above-mentioned uncompatibilized composites. For this reason, it is necessary to improve polymer-fiber interactions. In this work, different bio-based and petroleum-derived compatibilizers were used with the main aim of overcoming this drawback related to poor polymer-fiber interactions. The addition of 7.5 phr of MLO or ELO provided interesting changes in the mechanical behavior of PA1010/CFs composites. Both chemically modified vegetable oils contributed to slightly increasing tensile strength (σ_{max}) and in particular, an increase in the elongation at break (ε_b) of PA1010/CF composites.

Following the definition of the tensile modulus, as the ε_b increases, the modulus decreases. The addition of MLO and ELO led to E and σ_{max} values of about 780 MPa and 22–23 MPa, respectively, which are improved properties compared to uncompatibilized PA1010/CF composite. It is worthy to note that both modified vegetable oils can provide different overlapping phenomena to binary systems such as chain extension, compatibilization, plasticization, branching, and, in some cases, some cross-linking. It is worthy to note the significant increase in ε_b that ELO can provide to the PA1010/CFs composites with an ε_b value of 7.1%, which is more than double the value of the uncompatibilized composite. This phenomenon could be related to two mechanisms, one related to the plasticization ELO can provide and, on the other hand, to an increase in polymer-fiber interaction that, in turn, is responsible for an increase in material's cohesion and this has a positive effect on cohesion-related properties such as tensile strength and elongation. Balart *et al.* [48] reported that the incorporation of 7.5%

ELO into a PLA composite with hazelnut waste powder provided some plasticization and compatibilization between the polymer and the lignocellulosic filler. This was particularly observed by observation of completely embedded hazelnut particles in the PLA matrix after the ELO addition. As indicated previously, modified vegetable oils can provide some plasticization to the matrix [63, 64], but the increase in tensile strength suggests an improvement of the compatibility between the fiber and the surrounding biopolymer matrix. Concerning the petroleum-derived compatibilizers, their effects were not so remarkable as those provided by the chemically modified vegetable oils. The amount of petroleum-derived compatibilizers was lower than that of MLO or ELO but previous works have demonstrated that vegetable oil contents of 7.5–10 phr provided optimum balanced properties [49, 64, 65], while the typical content of these two petroleum-derived compatibilizers is lower than 3 phr [50, 66]. Both petroleum-derived compatibilizers offered a slight increase in the tensile modulus, which is directly related to the compatibilizing effect as the elongation at break is also slightly increased up to values of 3.6%, but, in general, their effect on the tensile properties was not remarkable.

Table III.3.3.2. Summary of the mechanical properties of the polyamide 1010 (PA1010)/coconut fibers (CFs) composites processed with maleinized linseed oil (MLO), epoxidized linseed oil (ELO), epoxy-based styren-–acrylic oligomer (ESAO), and polystyrene-glycidyl methacrylate random copolymer (PS-GMA).

Sample	E (MPa)	σ_{max} (MPa)	ε_b (%)	Shore D hardness	Impact strength (kJ m^{-2})
PA1010	636 ± 29	41.2 ± 2.1	256.5 ± 26.8	70.2 ± 1.1	11.3 ± 0.4
PA1010/CF	940 ± 26	20.2 ± 0.6	3.1 ± 0.2	74.2 ± 0.8	1.7 ± 0.3
PA1010/CF + MLO	785 ± 23	22.0 ± 1.0	4.2 ± 0.4	71.6 ± 0.5	2.4 ± 0.3
PA1010/CF + ELO	777 ± 20	23.3 ± 0.6	7.1 ± 0.5	75.0 ± 0.7	2.0 ± 0.1
PA1010/CF + ESAO	941 ± 32	19.2 ± 0.4	3.6 ± 0.2	75.0 ± 0.8	1.6 ± 0.2
PA1010/CF + PS-GMA	884 ± 22	18.9 ± 0.3	3.6 ± 0.3	74.1 ± 0.9	1.4 ± 0.2

About the Shore D hardness values, all the tested PA1010/CFs composites, except that for the MLO-containing composite, offered similar values. Shore D hardness values increased from 70.2, for neat PA1010, up to values around 74-75 for all the composite pieces. This increase is directly related to the intrinsic hardness of the lignocellulosic components of CF. In the case of the PA1010/CG+MLO, the Shore D hardness was slightly lower than other composites, and this could be due to the plasticization that MLO can provide. Regarding impact strength, the trend is identical to the elongation at break as the impact strength is highly sensitive to the material's cohesion. Neat PA1010 is a tough material with a relatively high impact strength of 11.3 kJ m^{-2}, even on notched samples. It is worthy to note that the impact strength is directly related to two mechanical parameters, that is, the applied stress and the

deformation before failure. As it has been described previously, the elongation at break for neat PA1010 was very high with relatively high tensile strength. Subsequently, the impact strength was also high. Identically to the elongation at break, the addition of 20 wt% CFs promoted a dramatic decrease in toughness down to values of 1.7 kJ m^{-2}. The effect of both linseed oil derived compatibilizers, resulted in improved toughness up to values of 2.4 kJ m^{-2} and 2.0 kJ m^{-2} for MLO and ELO-compatibilized composites, respectively. This is directly related somewhat to the compatibilization attained, as observed with the elongation at break. Regarding ESAO and PS-GMA, both produced similar results with no remarkable improvement in toughness. Nevertheless, both petroleum-derived compatibilizers resulted in stiffer materials.

Morphology of PA1010/CF composites

Figure III.3.3.4 shows the morphology of an individual CF. The average diameter calculated from the optical images was 205 ± 98 μm, and **Figure III.3.3.4a** shows a short fiber with a diameter of 78 μm, but it is worthy to note that typical CFs are quite heterogeneous with diameters changing from 90 to 400 μm. The cross-section of this fiber is shown in **Figure III.3.3.4b**, where the typical tubular formations (see white circle) can be observed [67]. This structure is responsible for the lightness of the CFs together with its excellent thermal insulation properties as air is located into these tubular formations, thus contributing to good insulation properties [68]. Indeed, CFs have not only been used in polymer matrices but also in concrete for construction and building materials due to the excellent insulating properties [69]. CFs are among the thickest fibers commercially available. Depending on the variety, single fibers can reach average diameters above 200 μm [70].
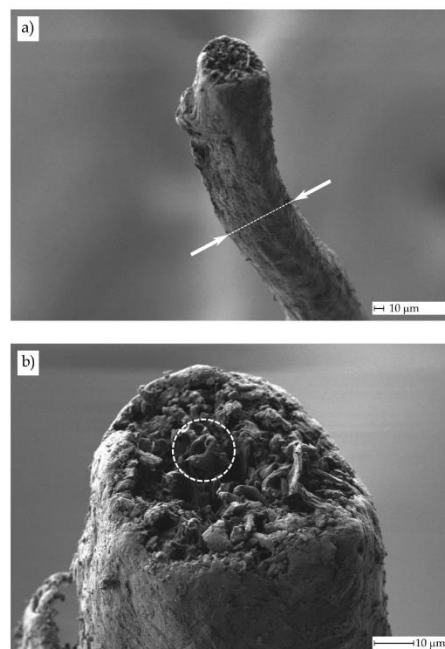
Figure III.3.3.4. Morphology of a single coconut fiber (CF) obtained by field emission electron microscopy (FESEM): **a)** longitudinal (axis) direction taken at 250x and **b)** cross-section taken at 1000x. Scale markers of 10 μm.
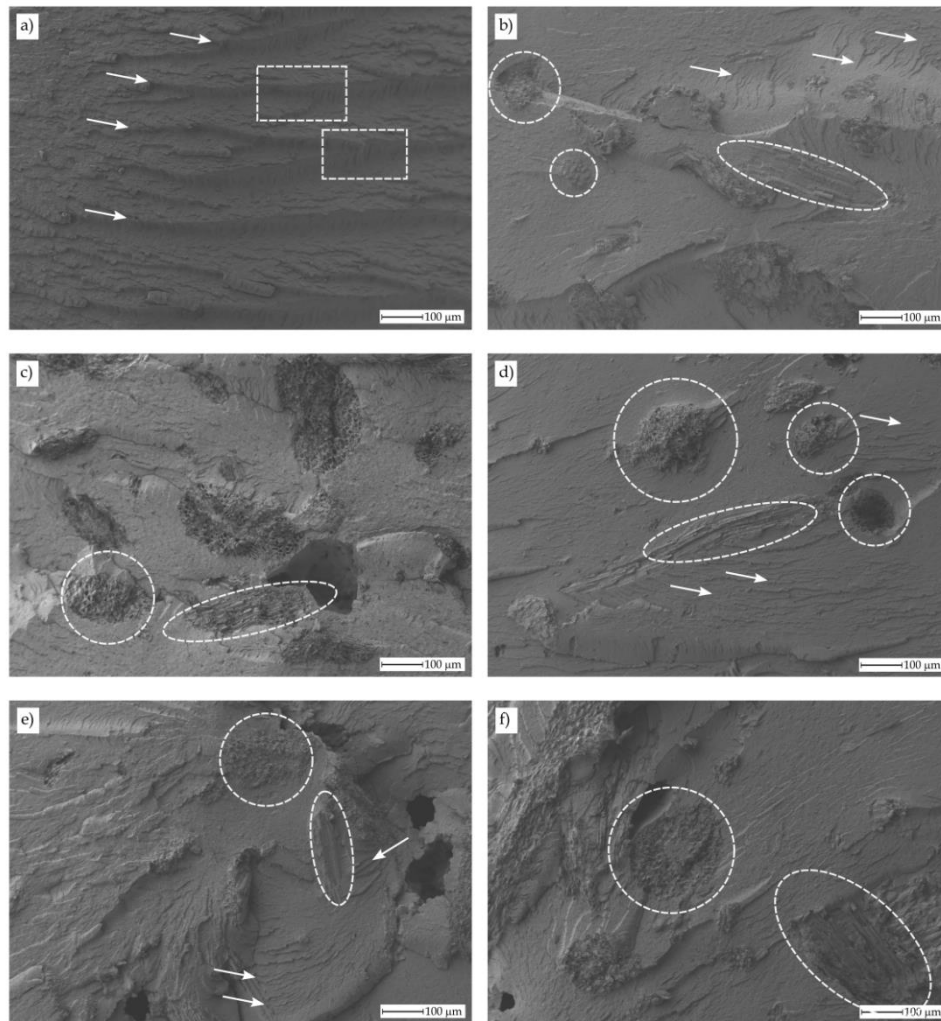
Figure III.3.5. Field emission electron microscopy (FESEM) images taken at 100x, showing the morphology of fractured images from impact tests corresponding to: a) neat polyamide 1010 (PA1010); b) PA1010/coconut fibers (CFs); c) PA1010/CF + maleinized linseed oil (MLO); d) PA1010/CF+ epoxidized linseed oil (ELO); e) PA1010/CF + epoxy-based styrene–acrylic oligomer (ESAO); f) PA1010/CF + polystyrene-glycidyl methacrylate random copolymer (PS-GMA).

Figure III.3.5 gathers the FESEM images corresponding to the fracture surfaces of the injection-molded pieces after the impact test. Regarding neat PA1010, the fracture is typical from an impact test on notched samples. As the material is rather tough, the surface was very rough, and this effect is visible by the presence of crack fronts (white arrows) and the coalescence of microcracks during crack growth (see white rectangles in **Figure III.3.5a**. Despite this material is very ductile and allows substantial plastic deformation, the conditions of the impact test (notched samples) promoted stress concentration with lower energy absorption, and, subsequently, with lower evident deformation. Nevertheless, the high roughness observed is representative for deformation as completely brittle materials typically show a very smooth surface. Uncompatibilized composites with 20 wt% CFs (**Figure III.3.5b**) showed a remarkably different surface morphology after the failure by the impact. The

relative high diameter of CFs, with an average diameter of 95 μm but with some bigger fibers of up to 200 μm, promoted a stress concentration effect due to the loss of material continuity. This led to a more brittle fracture surface (see the white arrows indicating micro-crack formation and a smoother fracture surface). Even after the achievement of high polymer-filler interaction, one assumes that the short fiber and its high diameter did not contribute to improving mechanical properties. K. Mustapha *et al.* [71] established a threshold at about 10 wt% short CFs on a polyolefin matrix. Above this threshold content value, mechanical properties suffered a dramatic decrease. L.H. Staffa *et al.* [60] also demonstrated the poor compatibility of composites based on a PP matrix and 30 wt% CFs. A SEM analysis reported some evidence of pulled-out fibers for the uncompatibilized PP/CFs composites. It was also observed that the use of PP-*g*-MA copolymer improved the interaction, but mechanical properties were only slightly improved due to the high content of short CFs in these composites.

The interaction between the lignocellulosic fibers and the PA1010 matrix is not deficient since PAs are more polar than PP, LDPE or HDPE, widely used as matrices in these composites. As it can be seen in **Figure III.3.3.5b**, the uncompatibilized PA1010/CFs presented some embedded fibers in the cross-section direction (circles) while some longitudinal fibers were pulled-out (see the white elliptical shape). The addition of compatibilizers resulted in a better fiber dispersion with a clear cross-section of CFs that were rather good embedded in the PA1010 matrix. One can expect somewhat improved interactions for all four compatibilizers since the mechanical properties were slightly improved, as shown in previous **Table III.3.3.2**, specifically for the bio-based compatibilizers derived from linseed oil, although both petroleum-derived compatibilizers also provided improved stiffness. As it can be seen in **Figure III.3.3.5c** and **Figure III.3.3.5d**, the normal/perpendicular fibers appeared well embedded in the PA1010 matrix (white circles) while some debonding occurred with CFs in the longitudinal direction (parallel to fracture surface).

In the case of ELO (**Figure III.3.3.5d**), CFs were fully embedded in the PA1010 matrix. The above-reported brittleness is also evident by the presence of micro-crack formation (white arrows). Similar behavior can be observed for both petroleum-derived compatibilizers. **Figure III.3.3.5e**, shows the compatibilized composite with EASO and the morphology of its fracture surface was similar, with perfectly embedded perpendicular CFs (white circles) and some debonded CFs in the longitudinal direction (white elliptical shapes). Moreover, an identical morphology is detectable by using PS-GMA as a compatibilizer, thus indicating its effectiveness (**Figure III.3.3.5f**).

Figure III.3.3.6 shows zoomed FESEM images showing the fracture surface of a perpendicular CF and its surrounding area. These zoomed images allow precise observation of the individual microfibrils. The diameter of these hollow microfibrils can be as high as 12 μm, as reported by F.Z. Semlali Aouragh Hassani *et al.*[70]. The diameters of the CFs used in this study were about 5 to 10 μm, and it plays an essential role in composites. As can be seen for the uncompatibilized PA1010/CF composites in **Figure III.3.3.6a**, the lumen of these microfibrils was full as the biopolymer chains could enter these macro-tubes. Nevertheless, the morphology and shape of the individual microfibrillar tubes were lost during processing. The fiber-polymer interaction is considered to be good enough as a tiny gap was observed. The fiber seems to be fully embedded in the PA1010 matrix. Both vegetable oil-derived

compatibilizers produced different morphologies. As expected, these molecules increased the free volume of the PA1010 matrix due to their plasticizing effect and, thus, the polymer chains could enter the tubular microfibrils more easily. It can be noted in **Figure III.3.3.6b** and **Figure III.3.3.6c** that the tubular shape of the microfibrils was not altered after processing these composites due to the plasticization provided by both MLO and ELO. In the case of MLO, it is possible to see some biopolymer tubes out of the tubular microfibrils that indicate deformation during the fracture test. Concerning the petroleum-derived compatibilizers, both ESAO (**Figure III.3.3.6d**) and PS-GMA (**Figure III.3.3.6e**) broke up the tubular morphology, but their compatibilizing effect was evident as the CFs were wholly embedded in the biopolymer matrix without any gap between the fibers and the surrounding PA1010 matrix. Similar findings have been reported by L. Quiles Carrillo *et al*. [53] in PLA/almond shell flour (ASF) green composites with a decreased the gap between the dispersed particles and the surrounding biopolymer matrix.
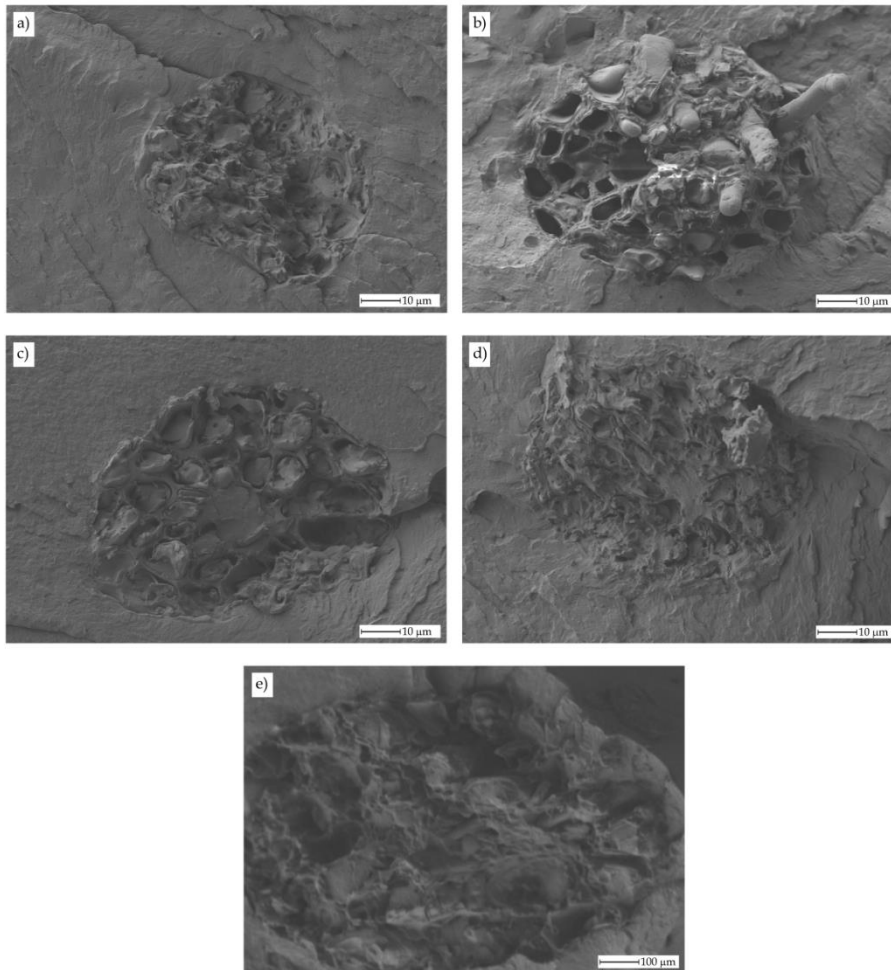
Figure III.3.3.6. Field emission electron microscopy (FESEM) images taken at 1000x, showing the morphology of the cross-section of the embedded coconut fibers (CFs) in polyamide 1010 (PA1010) corresponding to: a) PA1010/CF; b) PA1010/CF + maleinized linseed oil (MLO); c) PA1010/CF + epoxidized linseed oil (ELO); d) PA1010/CF + epoxy-based styrene–acrylic oligomer (ESAO); e) PA1010/CF + polystyrene-glycidyl methacrylate random copolymer (PS-GMA).

Thermal properties of PA1010/CF composites

Figure III.3.3.7 gathers a comparative plot of the DSC thermograms of the PA1010/CFs composites processed with the different compatibilizers, while **Table III.3.3.3** shows a summary of the main thermal parameters obtained by DSC for these composites. Neat PA1010 was characterized by melting temperature (T_m) of 203.9 °C and a degree of crystallinity (χ_c) of approximately 21%. The addition of CFs did not provide any relevant change in Tm, showing a similar value of 203.4 °C whereas the crystallinity was not profoundly affected, with a χ_c value of 20.7%. It has been widely reported the nucleating effect of lignocellulosic fillers, such as hemp or rice straw fibers, on different polymers and biopolymers with the subsequent increase in the crystallinity [72, 73]. However, it has been previously observed that CF itself shows a low nucleating effect in other natural filled composites [74, 75]. With the addition of MLO and ELO, crystallinity in the green composites remarkably increased up to values of about 28%. This increase can be related to two different phenomena. On the one hand, the increased polymer-particle interactions could favor the nucleating effect of the lignocellulosic CFs and, on the other hand, both chemically modified vegetable oils provided a plasticization that promoted chain mobility, thus favoring folding of polymer chains into a packed structure [26]. However, the effect of MLO and ELO on the Tm values, inducing a decrease by 1 °C and 2 °C, respectively, was neglected as it is within the typical deviation range. With the incorporation of both petroleum-derived compatibilizers, that is, and, a slight increase in T_m was observes for the composites containing PS-GMA while it remains almost constant for the ESAO-containing composites. About the χ_c values, the crystallinity of PA1010/CF composites, both ESAO and PS-GMA induced a decrease down to values around 17%. This phenomenon is ascribed to the characteristic chain-extension effect of these additives, which could restrict the formation of more packed and ordered regions. According to this, Qian *et al*. [76] reported that the addition of chain extenders, particularly epoxides, led to an apparent decrease in crystallinity in PA1010. A similar effect was also observed in our study for PLA/ASF composites compatibilized by ESAO [53].

Table III.3.3.3. Main thermal properties of polyamide 1010 (PA1010) and the PA1010/coconut fibers (CFs) composites processed with maleinized linseed oil (MLO), epoxidized linseed oil (ELO), epoxy-based styren-–acrylic oligomer (ESAO), and polystyrene-glycidyl methacrylate random copolymer (PS-GMA,. in terms o: melting temperature (T_m), and normalized melting enthalpy (ΔH_m), and degree of crystallinity (X_c).

Sample	T_m (°C)	ΔH_m (J·g^{-1})	χ_c (%)
PA1010	203.9 ± 1.5	52.3 ± 1.9	21.4 ± 1.2
PA1010/CF	203.4 ± 1.2	40.4 ± 1.7	20.7 ± 0.8
PA1010/CF + MLO	202.5 ± 0.9	50.3 ± 1.6	27.7 ± 0.7
PA1010/CF + ELO	201.5 ± 1.2	51.9 ± 1.5	28.6 ± 0.8
PA1010/CF + ESAO	204.9 ± 1.1	31.9 ± 1.7	17.7 ± 0.8
PA1010/CF + PS-GMA	203.1 ± 1.1	31.4 ± 1.4	16.5 ± 0.9
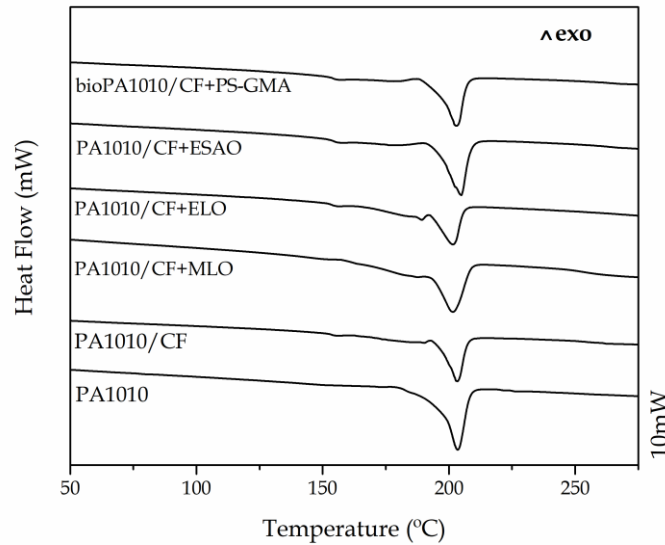
Figure III.3.7. Differential scanning calorimetry (DSC) thermograms of polyamide 1010 (PA1010) and the PA1010/coconut fibers (CFs) composites processed with maleinized linseed oil (MLO), epoxidized linseed oil (ELO), epoxy-based styrene–acrylic oligomer (ESAO), and polystyrene-glycidyl methacrylate random copolymer (PS-GMA).

Regarding degradation at high temperatures, that is, thermal decomposition, **Figure III.3.8** shows a comparative plot of the characteristic TGA curve of neat PA1010 and the uncompatibilized and compatibilized PA1010/CFs composites as well as the raw CFs. The most relevant information obtained from TGA is gathered in **Table III.3.4**. In particular, the temperature at which a 5 wt% mass loss occurs ($T_{5\%}$) and the maximum degradation rate temperature (T_{max}) are shown. CF is a lignocellulosic material, and it shows relatively low thermal stability compared to PA1010. In the graph, it can be observed an initial weight loss in the temperature range of 80–120 °C that is attributable to the residual water removal. At moderate temperatures of 250 °C degradation of hemicelluloses occurred, and this has a negative effect on the overall thermal stability, as both lignin and cellulose are much more thermally stable. Although the thermal degradation of lignin starts at similar temperatures of hemicellulose, that is, at about 250 °C, its degradation rate is remarkably lower and is extended up to temperatures above 500 °C. The residual mass of CF was close to 30%, which is a relatively high value, as reported by Rosa *et al*. [77]. Rosa *et al*. [78] also reported similar results regarding coir husk fibers. This was characterized by a first weight loss up to 120 °C due to water evaporation while lignin removal was reflected in the amount of final mass, measured in the temperature range comprised between 350 °C and 500 °C. Hemicellulose removal can be observed by the disappearance of the shoulder at 275 °C, as shown by the first derivative of the TGA curves. As expected, the low $T_{5\%}$, which can be considered as the onset degradation, of CF contributed to a decrease in the overall thermal stability of the composites. Whereas neat PA1010 showed remarkable thermal stability and its characteristic $T_{5\%}$ was 420.3 °C, the $T_{5\%}$ value for the uncompatibilized PA1010/CF was remarkably lower, that is, 292.8 °C. Although PA1010 can withstand higher temperatures, the thermal stability of its

composites with CF was compromised due to CF degrades at relatively low temperatures. As it can be seen in **Table III.3.4**, the T_{max} value of PA1010 was 466.6 °C. It is also worthy to note that the residual moisture in the neat PA1010 was very low since the weight loss in the 100–150 °C range was neglected. Similar thermal degradation profiles for different bioPAs have been described in the literature [59, 79, 80]. As PA1010 was the main component of the composites, the T_{max} values remained almost constant, showing values of around 465 °C, independently of the compatibilizer used. The most visible effect of the different compatibilizers was observed by a slight increase in the $T_{5\%}$ values, specifically for ELO and PS-GMA, which provided higher values of 12 °C and 17 °C, respectively. This slight increase in thermal stability can be directly related to increased fiber-polymer interactions, which gives some evidence of partial compatibilization. In this regard, Chieng *et al.* [81] have reported that epoxidized vegetable oils can establish covalent links between lignocellulosic fillers and the PLA matrix. As indicated previously, this enhanced chemical interactions successfully act as a physical barrier that obstructs the removal of volatile products during decomposition. In our previous work [53], it was suggested that the increased thermal stability of the PLA-based composites was achieved by favoring the polymer-particle interactions by processing with ESAO. Concerning the residual mass, all the PA1010/CF composites showed residues of around 6–7%, mainly due to the presence of CF.

Table III.3.4. Main thermal degradation parameters of polyamide 1010 (PA1010) and the PA1010/coconut fibers (CFs) composites processed with maleinized linseed oil (MLO), epoxidized linseed oil (ELO), epoxy-based styren-–acrylic oligomer (ESAO), and polystyrene-glycidyl methacrylate random copolymer (PS-GMA) in terms of the temperature required for a mass loss of 5% ($T_{5\%}$), the maximum degradation rate temperature (T_{max}), and residual mass at 700 °C.

Sample	$T_{5\%}$ (°C)	T_{max} (°C)	Residual weight (%)
PA1010	420.3± 0.7	466.6± 1.0	1.1± 0.2
PA1010/CF	292.8± 1.2	463.5± 1.1	7.2± 0.8
PA1010/CF + MLO	290.5± 1.1	461.7± 0.9	7.3± 0.9
PA1010/CF + ELO	304.6± 1.7	469.9± 0.8	7.2± 0.8
PA1010/CF + ESAO	299.3± 1.3	459.7± 1.0	6.8± 0.2
PA1010/CF + PS-GMA	309.5± 1.4	461.3± 0.9	6.9± 0.2
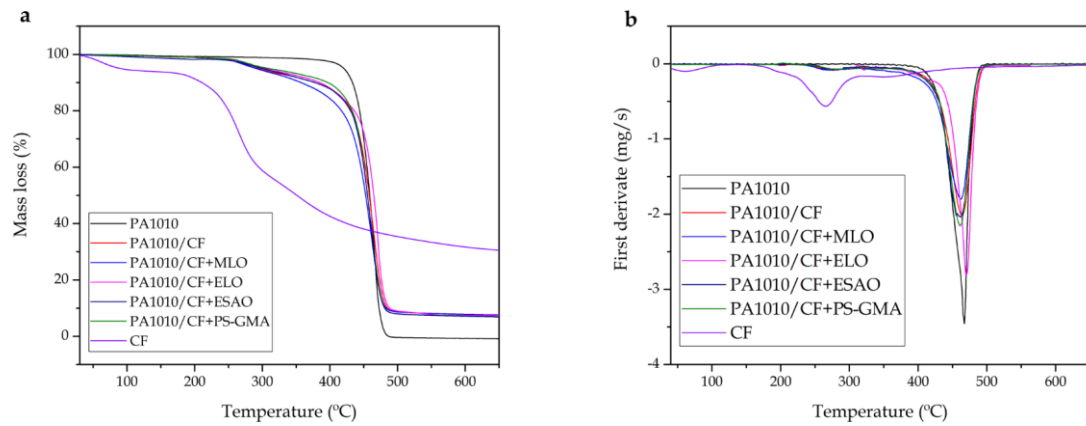
Figure III.3.3.8. a) Thermogravimetric analysis (TGA) curves and b) first derivative (DTG) curves of polyamide 1010 (PA1010) and the PA1010/coconut fibers (CFs) composites processed with maleinized linseed oil (MLO), epoxidized linseed oil (ELO), epoxy-based styrene–acrylic oligomer (ESAO), and polystyrene-glycidyl methacrylate random copolymer (PS-GMA).

Thermomechanical properties of PA1010/CF composites

Figure III.3.3.9 shows the evolution of DMTA curves of the neat PA1010 and the PA1010/CFs with different compatibilizers. In particular, **Table III.3.3.5** summarizes some of the thermomechanical properties obtained from these curves. In this sense, in **Figure III.3.3.9a** one can observe the evolution of the storage modulus (E') as a function of temperature. The dynamic thermomechanical behavior of PA1010 was characterized by an E' value in the of 1250–800 MPa range from -100 °C to 25 °C. Similar results were shown by other authors [59]. Above 50 °C, the storage modulus dropped down to a value of 200 MPa. This reduction is directly related to the alpha α-transition of PA1010 in which the amorphous phase of the biopolymer changes from the glassy to a rubbery state.

Table III.3.3.5. Main thermomechanical parameters of polyamide 1010 (PA1010) and the PA1010/coconut fibers (CFs) composites processed with maleinized linseed oil (MLO), epoxidized linseed oil (ELO), epoxy-based styren-–acrylic oligomer (ESAO), and polystyrene-glycidyl methacrylate random copolymer (PS-GMA) in terms of: storage modulus (E') measured at -100 °C and 100 °C and glass transition temperature (T_g).

Sample	E' (MPa) at -100 °C	E' (MPa) at 100 °C	T_g (°C)
PA1010	1245 ± 21	155 ± 2	52.6 ± 0.8
PA1010/CF	1515 ± 25	235 ± 3	45.1 ± 1.0
PA1010/CF + MLO	1610 ± 16	215 ± 3	48.1 ± 0.8
PA1010/CF + ELO	1585 ± 20	225 ± 1	50.1 ± 0.9
PA1010/CF + ESAO	1600 ± 17	240 ± 2	44.1 ± 1.1
PA1010/CF + PS-GMA	1610 ± 19	260 ± 2	54.2 ± 0.9

The addition of CF produced an increase in E′, below and above the α-transition. For the uncompatibilized PA1010/CF composite, a value of 1515 MPa at -100 °C was obtained, which represents 20% more than the neat biopolymer. In general, the addition of synthetics and naturals fibers in a polymer matrix increases the stiffness of the material. In this sense, other authors have shown that the incorporation of short natural fibers increases in an obvious way the values of E′ of the obtained composites [82-84]. Concerning the presence of compatibilizers, it is worthy to note they provide increased rigidity on composites at temperatures below the glass transition region.
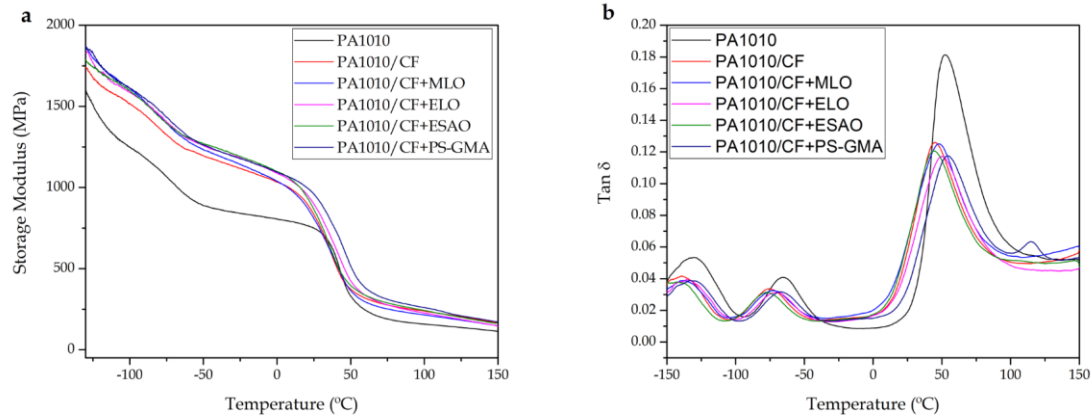
Figure III.3.3.9. Dynamic mechanical thermal analysis (DMTA) curves of polyamide 1010 (PA1010) and the PA1010/coconut fibers (CFs) composites processed with maleinized linseed oil (MLO), epoxidized linseed oil (ELO), epoxy-based styren-–acrylic oligomer (ESAO), and polystyrene-glycidyl methacrylate random copolymer (PS-GMA): a) Storage modulus (E′) and b) Dynamic damping factor (tan δ).

This increase observed in stiffness may be due to a direct improvement in the compatibility between the matrix and the dispersed fibers. Although the vegetable oil-derived compatibilizers provided additional plasticization, as mentioned above, the interaction of the glycidyl and maleic anhydride groups with both PA1010 and CFs led to improved cohesion between both components of the composite. This phenomenon increases the stiffness of the composite at low temperatures, significantly improving their potential uses for technical applications. In all cases, the improvement in stiffness was very similar since it changed from a value of 1500 MPa, for the uncompatibilized PA1010/CFs composite, up to about 1600 MPa after the addition of the different compatibilizers. In this sense, Michaz-Ul Haque *et al.* [85] reported that the addition of glycidyl methacrylate (GMA) to ethylene-vinyl acetate (EVA) composite filled with cellulose fibers increased the stiffness and the effectiveness of the fillers based on the E′ values of the obtained composites.

About the dynamic damping factor (tan δ), it represents the ratio between the lost energy (E″) and the stored energy (E′), so that low values indicate low energy dissipation. Figure 9b shows the evolution of tan δ as a function of temperature. It can be observed that the tan δ peak for neat PA1010 was 52.6 °C. This value is representative of the α-transition of the biopolymer, which relates to its T_g. Moreover, two additional peaks were located at temperatures of -65 °C and -130 °C, which are attributed to the β- and γ-relaxations of PA1010. For instance, Pagacz et al. [86]

reported that the peak around −130 °C reflects the γ-relaxation, which has been attributed to motions of methylene groups [87]. The peak located at about −80 °C represents the β-relaxation, typically attributed to non-hydrogen-bonded amide groups [87] and, more specifically, to water-bound on carbonyl groups. Finally, the prominent peak above 50 °C is typically attributed to the dynamic glass transition of this type of polyamide [88, 89]. One can observe that the tan δ peak of neat PA1010 was remarkably higher than the peaks seen for the PA1010/CFs composites. This observation suggests that all composites showed a higher elastic behavior, that is they performed as stiffer materials with higher E' values, and this contributes to lowering tan δ. In particular, the PA1010/CF + ELO showed the lowest tan δ value, in terms of temperature value and peak intensity, thus indicating improved fiber-matrix interactions as outlined previously.

The addition of CF to PA1010 reduced its T_g by 7.5 °C, which could be related to the presence of some inherent low-MW components in the fibers. The compatibilizing or coupling effect of MLO, ELO, and PS-GMA was evidenced by an increase in T_g up to values of 48.1 °C, 50.1 °C, and 54.2 °C, respectively, which are significantly higher than the T_g value for the uncompatibilized PA1010/CFs composite, that is, 45.1 °C. This increase in T_g is representative of improved fiber-matrix interaction as these interactions restrict the biopolymer chains' mobility and lead to an increased T_g. Other authors have reported similar results for PAs with other lignocellulosic fibers [59].

Evolution of the water uptake and water diffusion process

Since the here-developed PA1010/CFs composites contain a substantial amount of a lignocellulosic filler, they are characterized by extremely high hydrophilic behavior. Therefore, the study of their water absorption or uptake becomes indeed crucial for real applications. The study of the water uptake and diffusion of the PA1010/CFs composites is shown in **Figure III.3.3.10**. Water absorption is a diffusion-controlled process and, subsequently, it follows Fick's Law. This fact can be observed in **Figure III.3.3.10a**, which represents the water uptake during the first 24 h, and it is useful to calculate D and Dc that can be seen in **Table III.3.3.6**. One can observe that the D_c value indicates the hydrophilic nature of the developed materials. Neat PA1010 is a polar polymer, and it tends to absorb water as similar to other PAs (see **Figure III.3.3.10b**). It resulted in an asymptotic value of about 1.69 wt%, which is remarkably higher compared to non-polar polymers such as polyolefins with values close to 0.1–0.3 wt% [90, 91]. Besides, it is essential to remark that water absorption in polymer composites also highly depends on the nature of the lignocellulosic filler [92].
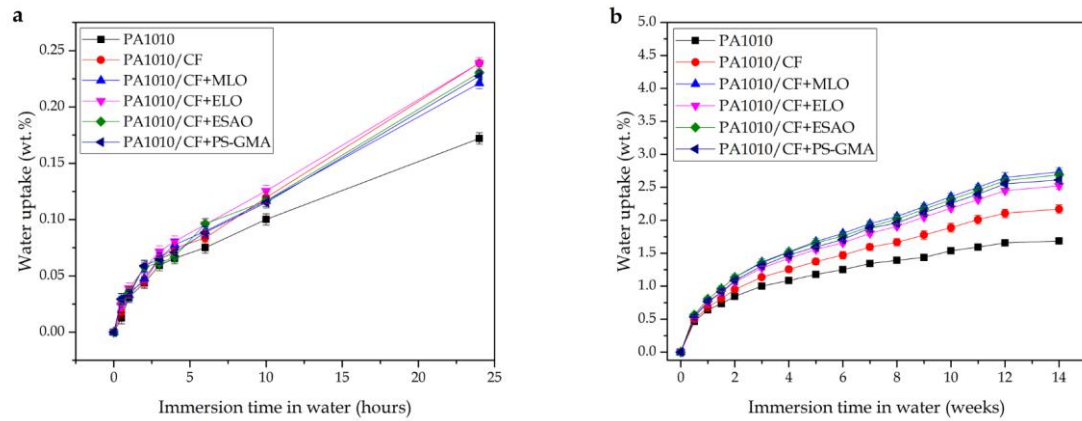
Figure III.3.3.10. Water uptake of polyamide 1010 (PA1010) and the PA1010/coconut fibers (CFs) composites processed with maleinized linseed oil (MLO), epoxidized linseed oil (ELO), epoxy-based styren-–acrylic oligomer (ESAO), and polystyrene-glycidyl methacrylate random copolymer (PS-GMA): a) Water absorption during the first 24 h; b) Evolution of the water uptake for 14 weeks.

Table III.3.3.6. Values of the diffusion coefficient (D) and the corrected diffusion coefficient (D_c) for polyamide 1010 (PA1010) and the PA1010/coconut fibers (CFs) composites processed with maleinized linseed oil (MLO), epoxidized linseed oil (ELO), epoxy-based styren-–acrylic oligomer (ESAO), and polystyrene-glycidyl methacrylate random copolymer (PS-GMA).

Sample	D x 10^8 (cm$^2 \cdot$s^{-1})	D_c x 10^8 (cm$^2 \cdot$s^{-1})
PA1010	1.13± 0.08	0.54± 0.02
PA1010/CF	2.42± 0.09	1.15± 0.04
PA1010/CF + MLO	2.02± 0.07	0.96± 0.03
PA1010/CF + ELO	2.28± 0.06	1.08± 0.04
PA1010/CF + ESAO	2.17± 0.05	1.03± 0.05
PA1010/CF + PS-GMA	2.08± 0.06	0.99± 0.03

The values of D_c were calculated considering the saturation mass. This resulted in a Dc value of $0.54 \cdot 10^{-8}$ cm$^2 \cdot$ s^{-1} for neat PA1010. The addition of a lignocellulosic filler, highly hydrophilic, promoted an increase in D_c up to values of $1.15 \cdot 10^{-8}$ cm$^2 \cdot$ s^{-1}. In general, all four compatibilizers provided slightly lower Dc values, close to $1 \cdot 10^{-8}$ cm$^2 \cdot$ s^{-1}, which indicates that in a first approach, at short immersion times, all four compatibilizers reduce the water diffusion rate. Nevertheless, as can be seen in **Figure III.3.3.10b**, the saturation values for the uncompatibilized PA1010/CFs composite were around 2.18 wt% while all the compatibilized PA1010/CFs composites tended to stabilize water absorption at an average value of 2.68 wt%. This result indicates that, despite the reduction attained in water uptake observed for early immersion stages, the use of compatibilizers promotes the absorption of water in composite in the long term. Our previous work [53] also demonstrated the effect of different compatibilizers on the water uptake of PLA composites filled with 25 wt% ASF. It was observed a very low

water saturation for neat PLA of 0.7 wt% after 14 weeks, while the uncompatibilized composite containing 25 wt% ASF reached water saturation at 4.8 wt%. This points out that the water uptake impairment of the PA1010/CFs composites is lower. This fact can be related to the entrance of the compatibilized polymer into the tubular-shaped microfibrils, which leads to exposure of the lignocellulosic walls that, in turn, contribute to slightly higher water uptake values for long periods.

On the other hand, the presence of compatibilizers, such as MLO or ELO, increases the biopolymer free volume, and this phenomenon enhances new paths for water from entering into the composite structure. Balart *et al.* [93] reported similar findings for PLA/hazelnut shell flour (HSF) composites. In particular, the uncompatibilized composite with 20 wt% HSF showed an asymptotic water absorption of 3.5 wt% after 14 weeks, while these composites when compatibilized with different amounts of ELO reached an asymptotic water absorption of almost 4.5 wt%.

CONCLUSIONS

This work demonstrated the feasibility of manufacturing highly environmentally friendly and wood-plastic composites with high performance based on a fully bio-based matrix of PA1010 and a reinforcement phase of 20 wt% CFs. These composites were manufactured by melt compounding followed by injection molding to develop materials with a wood appearance. Mechanical characterization revealed the remarkable effect that CF delivers on the final properties of composites. In particular, the elongation at break is dramatically reduced from 256%, for neat PA1010, down to values of 3.1%, for the uncompatibilized composite. The incorporation of multi-functionalized vegetable oil derived compatibilizers, namely MLO and ELO, resulted in a noticeable improvement of all the mechanical properties, including toughness. The two tested commercial petroleum-derived compatibilizers based on GMA multi-functionality, that is, Joncryl® 4300 and Xibond™ 920, also provided some enhancement of the composite performance. The water uptake remained at relatively low values, thus leading to materials that could replace wood in different industrial applications.

Acknowledgments.

REFERENCES

1.	Shahzad, A., *Hemp fiber and its composites–a review*. Journal of Composite Materials, 2012. **46**(8): 973-986.
2.	Ashori, A., *Wood–plastic composites as promising green-composites for automotive industries!* Bioresource technology, 2008. **99**(11): 4661-4667.

3. Herrmann, A., J. Nickel and U. Riedel, *Construction materials based upon biologically renewable resources – from components to finished parts*. Polymer Degradation and Stability, 1998. **59**(1-3): 251-261.

4. Holbery, J. and D. Houston, *Natural-fiber-reinforced polymer composites in automotive applications*. Jom, 2006. **58**(11): 80-86.

5. Alves, C., A. Silva, L. Reis, M. Freitas, L. Rodrigues and D. Alves, *Ecodesign of automotive components making use of natural jute fiber composite*s. Journal of Cleaner Production, 2010. **18**(4): 313-327.

6. Zafar, M.T., S.N. Maiti and A.K. Ghosh, *Effect of surface treatment of jute fibers on the interfacial adhesion in poly (lactic acid)/jute fiber biocomposites*. Fibers and Polymers, 2016. **17**(2): 266-274.

7. Jayaraman, K., *Manufacturing sisal–polypropylene composites with minimum fibre degradation.* Composites Science and technology, 2003. **63**(3-4): 367-374.

8. Wu, L., S. Lu, L. Pan, Q. Luo, J. Yang, L. Hou, Y. Li and J. Yu, *Enhanced thermal and mechanical properties of polypropylene composites with hyperbranched polyester grafted sisal microcrystalline*. Fibers and Polymers, 2016. **17**(12): 2153-2161.

9. Joshi, S.V., L. Drzal, A. Mohanty and S. Arora, *Are natural fiber composites environmentally superior to glass fiber reinforced composites?* Composites Part A: Applied science and manufacturing, 2004. **35**(3): 371-376.

10. Stelte, W., S.T. Barsberg, C. Clemons, J.P.S. Morais, M. de Freitas Rosa and A.R. Sanadi, *Coir Fibers as Valuable Raw Material for Biofuel Pellet Production.* Waste and Biomass Valorization, 2018: 1-9.

11. Harish, S., D.P. Michael, A. Bensely, D.M. Lal and A. Rajadurai, *Mechanical property evaluation of natural fiber coir composite.* Materials characterization, 2009. **60**(1): 44-49.

12. Van Dam, J.E., M.J. van den Oever, W. Teunissen, E.R. Keijsers and A.G. Peralta, *Process for production of high density/high performance binderless boards from whole coconut husk: Part 1: Lignin as intrinsic thermosetting binder resin*. Industrial Crops and products, 2004. **19**(3): 207-216.

13. Gu, H., *Tensile behaviours of the coir fibre and related composites after NaOH treatment*. Materials & Design, 2009. **30**(9): 3931-3934.

14. Tapper, R.J., M.L. Longana, H. Yu, I. Hamerton and K.D. Potter, *Development of a closed-loop recycling process for discontinuous carbon fibre polypropylene composites*. Composites Part B: Engineering, 2018. **146**: 222-231.

15. Mohanty, A.K., M. Misra and L. Drzal, *Sustainable bio-composites from renewable resources: opportunities and challenges in the green materials world*. Journal of Polymers and the Environment, 2002. **10**(1-2): 19-26.

16. Bachmann, J., C. Hidalgo and S. Bricout, *Environmental analysis of innovative sustainable composites with potential use in aviation sector – A life cycle assessment review.* Science China Technological Sciences, 2017. **60**(9): 1301-1317.

17. Enciso, B., J. Abenojar, E. Paz and M. Martínez, *Influence of low pressure plasma treatment on the durability of thermoplastic composites LDPE-flax/coconut under thermal and humidity conditions*. Fibers and Polymers, 2018. **19**(6): 1327-1334.

18. TabkhPaz, M., A.H. Behravesh, P. Shahi and A. Zolfaghari, *Procedure effect on the physical and mechanical properties of the extruded wood plastic composites*. Polymer Composites, 2013. **34**(8): 1349-1356.

19. Torres-Giner, S., L. Hilliou, B. Melendez-Rodriguez, K.J. Figueroa-Lopez, D. Madalena, L. Cabedo, J. Covas, A.A. Vicente and J. Lagaron, *Melt processability, characterization, and antibacterial activity of compression-molded green composite sheets made of poly (3-hydroxybutyrate-co-3-hydroxyvalerate) reinforced with coconut fibers impregnated with oregano essential oil.* Food packaging and shelf life, 2018. **17**: 39-49.

20. Mahdavi, S., H. Kermanian and A. Varshoei, *Comparison of mechanical properties of date palm fiber-polyethylene composite*. BioResources, 2010. **5**(4): 2391-2403.

21. Mosavi-Mirkolaei, S.T., S.K. Najafi and M. Tajvidi, *Physical and Mechanical Properties of Wood-Plastic Composites Made with Microfibrillar Blends of LDPE, HDPE and PET*. Fibers and Polymers, 2019. **20**(10): 2156-2165.

22. Kaymakci, A., E. Birinci and N. *Ayrilmis, Surface characteristics of wood polypropylene nanocomposites reinforced with multi-walled carbon nanotubes*. Composites Part B: Engineering, 2019. **157**: 43-46.

23. Pham, L.H., H.D. Nguyen, J. Kim and D. Hoang, *Thermal Properties and Fire Retardancy of Polypropylene/Wood Flour Composites Containing Eco-friendly Flame Retardants*. Fibers and Polymers, 2019. **20**(11): 2383-2389.

24. Chun, K.S., N.M.Y. Fahamy, C.Y. Yeng, H.L. Choo, P.M. Ming and K.Y. Tshai, *Wood Plastic Composites Made From Corn Husk Fiber and Recycled Polystyrene Foam*. Journal of Engineering Science and Technology, 2018. **13**(11): 3445-3456.

25. Wang, L., C. He and X. Yang, *Effects of Pretreatment on the Soil Aging Behavior of Rice Husk Fibers/Polyvinyl Chloride Composites*. BioResources, 2019. **14**(1): 59-69.

26. Liminana, P., D. Garcia-Sanoguera, L. Quiles-Carrillo, R. Balart and N. Montanes, *Development and characterization of environmentally friendly composites from poly (butylene succinate)(PBS) and almond shell flour with different compatibilizers*. Composites Part B: Engineering, 2018. **144**: 153-162.

27. Yang, T.-C., *Effect of extrusion temperature on the physico-mechanical properties of unidirectional wood fiber-reinforced polylactic acid composite (WFRPC) components using fused deposition modeling*. Polymers, 2018. **10**(9): 976.

28. Zhang, L., S. Lv, C. Sun, L. Wan, H. Tan and Y. Zhang, *Effect of mah-g-pla on the properties of wood fiber/polylactic acid composites.* Polymers, 2017. **9**(11): 591.

29. Durand, P.-L., A. Brège, G. Chollet, E. Grau and H. Cramail, *Simple and Efficient Approach toward Photosensitive Biobased Aliphatic Polycarbonate Materials*. ACS Macro Letters, 2018. **7**(2): 250-254.

30. Pang, C., X. Jiang, Y. Yu, X. Liu, J. Lian, J. Ma and H. Gao, *Sustainable Polycarbonates from a Citric Acid-Based Rigid Diol and Recycled BPA-PC: From Synthesis to Properties.* ACS Sustainable Chemistry & Engineering, 2018. **6**(12): 17059-17067.

31. Eerhart, A., A. Faaij and M.K. Patel, *Replacing fossil based PET with biobased PEF; process analysis, energy and GHG balance*. Energy & environmental science, 2012. **5**(4): 6407-6422.

32. Kausar, A., *Polyamide 1010/polythioamide blend reinforced with graphene nanoplatelet for automotive part application*. Advances in Materials Science, 2017. **17**(3): 24-36.

33. Nishitani, Y., T. Kajiyama and T. Yamanaka, *Effect of silane coupling agent on tribological properties of hemp fiber-reinforced plant-derived polyamide 1010 biomass composites.* Materials, 2017. **10**(9): 1040.

34. Glasscock, D., W. Atolino, G. Kozielski and M. Martens, *High performance polyamides fulfill demanding requirements for automotive thermal management components*. DuPont Engineering Polymers, 2008.

35. Boros, R., P. Rajamani and J. Kovács, *Thermoplastic Overmolding onto Injection-Molded and In Situ Polymerization-Based Polyamides*. Materials, 2018. **11**(11): 2140.

36. Del Nobile, M., G. Buonocore, L. Palmieri, A. Aldi and D. Acierno, *Moisture transport properties of polyamides copolymers intended for food packaging applications*. Journal of food engineering, 2002. **53**(3): 287-293.

37. Pracella, M., M. Haque and V. Alvarez, *Functionalization, compatibilization and properties of polyolefin composites with natural fibers*. Polymers, 2010. **2**(4): 554-574.

38. Garcia-Garcia, D., A. Carbonell-Verdu, A. Jordá-Vilaplana, R. Balart and D. Garcia-Sanoguera, *Development and characterization of green composites from bio-based polyethylene and peanut shell*. Journal of Applied Polymer Science, 2016. **133**(37).

39. García-García, D., A. Carbonell, M. Samper, D. García-Sanoguera and R. Balart, *Green composites based on polypropylene matrix and hydrophobized spend coffee ground (SCG) powder.* Composites part B: engineering, 2015. **78**: 256-265.

40. Du, J., Y.-m. Song, Z.-j. Zhang, Y.-q. Fang, W.-h. Wang and Q.-w. Wang, *Influence of Maleic Anhydride/Glycidyl Methacrylate Cografted Polylactic Acid on Properties of Wood*

Flour/PLA Composites. Cailiao Gongcheng-Journal of Materials Engineering, 2017. **45**(12): 30-36.

41.   Saheb, D.N. and J.P. Jog, *Natural fiber polymer composites: a review.* Advances in Polymer Technology: Journal of the Polymer Processing Institute, 1999. **18**(4): 351-363.

42.   Zafeiropoulos, N., D. Williams, C. Baillie and F. Matthews, *Engineering and characterisation of the interface in flax fibre/polypropylene composite materials. Part I. Development and investigation of surface treatments.* Composites Part A: Applied Science and Manufacturing, 2002. **33**(8): 1083-1093.

43.   López Manchado, M., M. Arroyo, J. Biagiotti and J. Kenny, *Enhancement of mechanical properties and interfacial adhesion of PP/EPDM/flax fiber composites using maleic anhydride as a compatibilizer.* Journal of Applied Polymer Science, 2003. **90**(8): 2170-2178.

44.   George, J., M. Sreekala and S. Thomas, *A review on interface modification and characterization of natural fiber reinforced plastic composites.* Polymer Engineering & Science, 2001. **41**(9): 1471-1485.

45.   Nyambo, C., A.K. Mohanty and M. Misra, *Effect of maleated compatibilizer on performance of PLA/wheat Straw-Based green composites.* Macromolecular Materials and Engineering, 2011. **296**(8): 710-718.

46.   Valdés, A., O. Fenollar, A. Beltrán, R. Balart, E. *Fortunati, J.M. Kenny and M.C. Garrigós, Characterization and enzymatic degradation study of poly (ε-caprolactone)-based biocomposites from almond agricultural by-products.* Polymer Degradation and Stability, 2016. **132**: 181-190.

47.   Quiles-Carrillo, L., M. Blanes-Martínez, N. Montanes, O. Fenollar, S. Torres-Giner and R. Balart, *Reactive toughening of injection-molded polylactide pieces using maleinized hemp seed oil.* European Polymer Journal, 2018. **98**: 402-410.

48.   Balart, J., V. Fombuena, O. Fenollar, T. Boronat and L. Sánchez-Nacher, *Processing and characterization of high environmental efficiency composites based on PLA and hazelnut shell flour (HSF) with biobased plasticizers derived from epoxidized linseed oil (ELO).* Composites Part B: Engineering, 2016. **86**: 168-177.

49.   Garcia-Garcia, D., O. Fenollar, V. Fombuena, J. Lopez-Martinez and R. Balart, *Improvement of Mechanical Ductile Properties of Poly (3-hydroxybutyrate) by Using Vegetable Oil Derivatives.* Macromolecular Materials and Engineering, 2017. **302**(2): 1600330.

50.   Quiles-Carrillo, L., N. Montanes, J. Lagaron, R. Balart and S. Torres-Giner, *In situ compatibilization of biopolymer ternary blends by reactive extrusion with low-functionality epoxy-based styrene–acrylic oligomer.* Journal of Polymers and the Environment, 2019. **27**(1): 84-96.

51.   Pérez Amaro, L., H. Chen, A. Barghini, A. Corti and E. Chiellini, *High performance compostable biocomposites based on bacterial polyesters suitable for injection molding and blow extrusion.* Chemical and biochemical engineering quarterly, 2015. **29**(2): 261-274.

52.   Smith, M.J. and C.J. Verbeek, *Compatibilization effects in thermoplastic protein/polyester blends.* Journal of Applied Polymer Science, 2018. **135**(6): 45808.

53.   Quiles-Carrillo, L., N. Montanes, D. Garcia-Garcia, A. Carbonell-Verdu, R. Balart and S. Torres-Giner, *Effect of different compatibilizers on injection-molded green composite pieces based on polylactide filled with almond shell flour.* Composites Part B: Engineering, 2018. **147**: 76-85.

54.   Yan, M. and H. Yang, *Improvement of polyamide 1010 with silica nanospheres via in situ melt polycondensation.* Polymer Composites, 2012. **33**(10): 1770-1776.

55.   Tham, W.L., B.T. Poh, Z.A.M. Ishak and W.S. Chow, *Water Absorption Kinetics and Hygrothermal Aging of Poly(lactic acid) Containing Halloysite Nanoclay and Maleated Rubber.* Journal of Polymers and the Environment, 2015. **23**(2): 242-250.

56.   Arbelaiz, A., B. Fernandez, J.A. Ramos, A. Retegi, R. Llano-Ponte and I. Mondragon, *Mechanical properties of short flax fibre bundle/polypropylene composites: Influence of matrix/fibre modification, fibre content, water uptake and recycling.* Composites Science and Technology, 2005. **65**(10): 1582-1592.

57. Gil-Castell, O., J.D. Badia, T. Kittikorn, E. Stromberg, A. Martinez-Felipe, M. Ek, S. Karlsson and A. Ribes-Greus, *Hydrothermal ageing of polylactide/sisal biocomposites. Studies of water absorption behaviour and Physico-Chemical performance*. Polymer Degradation and Stability, 2014. **108**: 212-222.

58. Deroine, M., A. Le Duigou, Y.-M. Corre, P.-Y. Le Gac, P. Davies, G. Cesar and S. Bruzaud, *Accelerated ageing of polylactide in aqueous environments: Comparative study between distilled water and seawater*. Polymer Degradation and Stability, 2014. **108**: 319-329.

59. Quiles-Carrillo, L., T. Boronat, N. Montanes, R. Balart and S. Torres-Giner, *Injection-molded parts of fully bio-based polyamide 1010 strengthened by waste derived slate fibers pre-treated with glycidyl-and amino-silane coupling agents*. Polymer Testing, 2019.

60. Staffa, L.H., J.A.M. Agnelli, M.L. de Souza and S.H. Bettini, *Evaluation of interactions between compatibilizers and photostabilizers in coir fiber reinforced polypropylene composites*. Polymer Engineering & Science, 2017. **57**(11): 1179-1185.

61. Rozman, H., K. Tan, R. Kumar, A. Abubakar, Z.M. Ishak and H. Ismail, *The effect of lignin as a compatibilizer on the physical properties of coconut fiber–polypropylene composites*. European Polymer Journal, 2000. **36**(7): 1483-1494.

62. Carbonell-Verdú, A., D. García-García, A. Jordá, M. Samper and R. Balart, *Development of slate fiber reinforced high density polyethylene composites for injection molding*. Composites Part B: Engineering, 2015. **69**: 460-466.

63. Quiles-Carrillo, L., N. Montanes, C. Sammon, R. Balart and S. Torres-Giner, *Compatibilization of highly sustainable polylactide/almond shell flour composites by reactive extrusion with maleinized linseed oil*. Industrial Crops and Products, 2018. **111**: 878-888.

64. Ferri, J., M. Samper, D. García-Sanoguera, M. Reig, O. Fenollar and R. Balart, *Plasticizing effect of biobased epoxidized fatty acid esters on mechanical and thermal properties of poly (lactic acid)*. Journal of materials science, 2016. **51**(11): 5356-5366.

65. Ferri, J.M., D. Garcia-Garcia, N. Montanes, O. Fenollar and R. Balart, *The effect of maleinized linseed oil as biobased plasticizer in poly (lactic acid)- based formulations*. Polymer International, 2017. **66**(6): 882-891.

66. Nofar, M. and H. Oğuz, *Development of PBT/Recycled-PET Blends and the Influence of Using Chain Extender*. Journal of Polymers and the Environment, 2019. **27**(7): 1404-1417.

67. Silva, G.G., D. De Souza, J. Machado and D. Hourston, *Mechanical and thermal characterization of native Brazilian coir fiber*. Journal of applied polymer science, 2000. **76**(7): 1197-1206.

68. Chuen, K.W., C.W. Qian, C.C. Hwa and M.H. Fouladi, *Effect of using coconut fibre and polypropylene for thermal insulation in a flat plate collector*. J Eng Sci Technol, 2015. **10**: 41-9.

69. Yan, L., S. Su and N. Chouw, *Microstructure, flexural properties and durability of coir fibre reinforced concrete beams externally strengthened with flax FRP composites*. Composites Part B: Engineering, 2015. **80**: 343-354.

70. Semlali Aouragh Hassani, F.Z., W. Ouarhim, M.O. Bensalah, H. Essabir, D. Rodrigue, R. Bouhfid and A.e.K. Qaiss, *Mechanical properties prediction of polypropylene/short coir fibers composites using a self- consistent approach*. Polymer Composites, 2019. **40**(5): 1919-1929.

71. Mustapha, K., S.A. Bello, Y. Danyuo and T. Oshifowora, *Uniaxial tensile response of coconut coir fiber-reinforced polyethylene Composites*. Journal of Materials and Engineering Structures, 2019. **6**(1): 15-23.

72. Pracella, M., D. Chionna, I. Anguillesi, Z. Kulinski and E. Piorkowska, *Functionalization, compatibilization and properties of polypropylene composites with hemp fibres*. Composites Science and Technology, 2006. **66**(13): 2218-2230.

73. Qin, L., J. Qiu, M. Liu, S. Ding, L. Shao, S. Lü, G. Zhang, Y. Zhao and X. Fu, *Mechanical and thermal properties of poly (lactic acid) composites with rice straw fiber modified by poly (butyl acrylate)*. Chemical Engineering Journal, 2011. **166**(2): 772-778.

74. Hosseinihashemi, S.K., A. Eshghi, N. Ayrilmis and H. Khademieslam, *Thermal Analysis and Morphological Characterization of Thermoplastic Composites Filled with Almond Shell Flour/Montmorillonite*. BioResources, 2016. **11**(3): 6768-6779.

75. Fasihah Zaaba, N., H. Ismail and M. Jaafar, *Recycled polypropylene/peanut shell powder (RPP/PSP) composites: Property comparison before and after electron beam irradiation.* Polymer Composites, 2018. **39**(9): 3048-3056.

76. Qian, Z., X. Chen, J. Xu and B. Guo, *Chain extension of PA1010 by reactive extrusion by diepoxide 711 and diepoxide TDE85 as chain extenders.* Journal of applied polymer science, 2004. **94**(6): 2347-2355.

77. Rosa, M.F., B.-s. Chiou, E.S. Medeiros, D.F. Wood, T.G. Williams, L.H. Mattoso, W.J. Orts and S.H. Imam, *Effect of fiber treatments on tensile and thermal properties of starch/ethylene vinyl alcohol copolymers/coir biocomposites.* Bioresource technology, 2009. **100**(21): 5196-5202.

78. Rosa, M., E. Medeiros, J. Malmonge, K. Gregorski, D. Wood, L. Mattoso, G. Glenn, W. Orts and S. Imam, *Cellulose nanowhiskers from coconut husk fibers: Effect of preparation conditions on their thermal and morphological behavior.* Carbohydrate Polymers, 2010. **81**(1): 83-92.

79. Xiuwei, F., L. Xiaohong, Y. Laigui and Z. Zhijun, *Effect of in situ surface-modified nano-SiO2 on the thermal and mechanical properties and crystallization behavior of nylon 1010.* Journal of applied polymer science, 2010. **115**(6): 3339-3347.

80. Mosanenzadeh, S.G., M.W. Liu, A. Osia and H.E. Naguib, *Thermal composites of biobased polyamide with boron nitride micro networks.* Journal of Polymers and the Environment, 2015. **23**(4): 566-579.

81. Chieng, B., N. Ibrahim, Y. Then and Y. Loo, *Epoxidized vegetable oils plasticized poly (lactic acid) biocomposites: mechanical, thermal and morphology properties.* Molecules, 2014. **19**(10): 16024-16038.

82. Tao, Y., L. Yan and R. Jie, *Preparation and properties of short natural fiber reinforced poly (lactic acid) composites.* Transactions of Nonferrous Metals Society of China, 2009. **19**: s651-s655.

83. Saba, N., O.Y. Alothman, Z. Almutairi and M. Jawaid, *Magnesium hydroxide reinforced kenaf fibers/epoxy hybrid composites: Mechanical and thermomechanical properties.* Construction and Building Materials, 2019. **201**: 138-148.

84. Kalusuraman, G., I. Siva, J.W. Jappes, X.-Z. Gao and S.C. *Amico, Fibre loading effects on dynamic mechanical properties of compression moulded luffa fibre polyester composites.* International Journal of Computer Aided Engineering and Technology, 2018. **10**(1-2): 157-165.

85. Haque, M.M.-U. and M. Pracella, *Reactive compatibilization of composites of ethylene–vinyl acetate copolymers with cellulose fibres.* Composites Part A: Applied Science and Manufacturing, 2010. **41**(10): 1545-1550.

86. Pagacz, J., K.N. Raftopoulos, A. Leszczyńska and K. Pielichowski, *Bio-polyamides based on renewable raw materials.* Journal of Thermal Analysis and Calorimetry, 2016. **123**(2): 1225-1237.

87. Prevorsek, D., R. Butler and H. *Reimschuessel, Mechanical relaxations in polyamides.* Journal of Polymer Science Part A-2: Polymer Physics, 1971. **9**(5): 867-886.

88. Zhao, C., G. Hu, R. Justice, D.W. Schaefer, S. Zhang, M. Yang and C.C. Han, *Synthesis and characterization of multi-walled carbon nanotubes reinforced polyamide 6 via in situ polymerization.* Polymer, 2005. **46**(14): 5125-5132.

89. Urman, K. and J. Otaigbe, *Novel phosphate glass/polyamide 6 hybrids: miscibility, crystallization kinetics, and mechanical properties.* Journal of Polymer Science Part B: Polymer Physics, 2006. **44**(2): 441-450.

90. Quiles-Carrillo, L., N. Montanes, T. Boronat, R. Balart and S. Torres-Giner, *Evaluation of the engineering performance of different bio-based aliphatic homopolyamide tubes prepared by profile extrusion.* Polymer Testing, 2017. **61**: 421-429.

91. Ferrero, B., V. Fombuena, O. Fenollar, T. Boronat and R. Balart, *Development of natural fiber- reinforced plastics (NFRP) based on biobased polyethylene and waste fibers from Posidonia oceanica seaweed.* Polymer Composites, 2015. **36**(8): 1378-1385.

92. Zabihzadeh, S.M., *Effect of Lignocellulosic Type on Long-Term Hygroscopic Behavior of Natural Filler/HDPE Composites.* Journal of Polymers and the Environment, 2011. **19**(1): 133-136.

93. Balart, J.F., N. Montanes, V. Fombuena, T. Boronat and L. Sanchez-Nacher, *Disintegration in Compost Conditions and Water Uptake of Green Composites from Poly(Lactic Acid) and Hazelnut Shell Flour*. Journal of Polymers and the Environment, 2018. **26**(2): 701-715.

III.3.4. A comparative study on the reactive compatibilization of melt-processed polyamide 1010/polylactide blends by multi-functionalized additives derived from linseed oil and petroleum

L. Quiles-Carrillo [1], O. Fenollar [1], R.Balart [1], S. Torres-Giner [2], M.Rallini [3], F.Dominici [3] and L. Torre [3]

[1] Technological Institute of Materials (ITM), Universitat Politècnica de València (UPV), Plaza Ferrándiz y Carbonell 1, 03801 Alcoy, Spain;

[2] Novel Materials and Nanotechnology Group, Institute of Agrochemistry and Food Technology (IATA), Spanish National Research Council (CSIC), Calle Catedrático Agustín Escardino Benlloch 7, 46980 Paterna, Valencia, Spain

[3] Dipartimento di Ingegneria Civile ed Ambientale, University of Perugia, UdR INSTM, Strada di Pentima, 4 - 05100 Terni, Italy

L1 **A comparative study on the reactive compatibilization of**
L2 **melt-processed polyamide 1010/polylactide blends by**
L3 **multi-functionalized additives derived from linseed oil and**
L4 **petroleum**

L5 *L. Quiles-Carrillo[1*], O. Fenollar[1], R. Balart[1], S. Torres-Giner[2], M. Rallini[3], F. Dominici[3], L. Torre[3]*

L6 [1]Technological Institute of Materials (ITM), Universitat Politècnica de València (UPV), Plaza Ferrándiz y Carbonell 1,
L7 03801 Alcoy, Spain.
L8 [2]Novel Materials and Nanotechnology Group, Institute of Agrochemistry and Food Technology (IATA), Spanish National
L9 Research Council (CSIC), Calle Catedrático Agustín Escardino Benlloch 7, 46980 Paterna, Spain.
L10 [3]Dipartimento di Ingegneria Civile ed Ambientale, University of Perugia, UdR INSTM, Strada di Pentima, 4-05100 Terni,
L11 Italy

L13 **Abstract.** This research work describes the manufacturing and characterization of novel engineering materials consisted of
L14 fully bio-based blends of polyamide 1010 (PA1010) with 20 wt% of polylactide (PLA). Four different compatibilizers were
L15 used to enhance the miscibility and the performance of the biopolymer blends. Two multi-functionalized vegetable oils
L16 (maleinized linseed oil (MLO) and epoxidized linseed oil (ELO)) and two petroleum-derived glycidyl-based additives (epoxy
L17 styrene-acrylic oligomer (ESAO) and styrene-glycidyl methacrylate copolymer (PS-GMA)) were tested during melt com-
L18 pounding. The resultant biopolymer blends were processed by either cast film extrusion or injection molding to obtain films
L19 and pieces, respectively. Thin films with an average thickness of 50–60 μm and thick pieces of 4 mm were obtained, and
L20 their mechanical, morphological, thermal, thermomechanical, barrier and, optical properties were characterized. Although
L21 all four compatibilizers successfully provided compatibilization to the blends, the chemically modified vegetable oils, that
L22 is, MLO and ELO yielded the injection-molded pieces with the most balanced mechanical properties in terms of strength
L23 and toughness. Besides, the resultant films showed very low oxygen transmission rate values, thus broadening the potential
L24 of these biopolymer blends for the food packaging industry.

L25 ***Keywords:*** *biopolymers, biocomposites, bio-based polyamides, multi-functionalized vegetable oils, reactive compatibilization*

L26 **1. Introduction**
L27 The increasing awareness about sustainable devel-
L28 opment, petroleum depletion, carbon footprint, and
L29 so on, have recently been consolidated as the leading
L30 forces for the development of environmentally
L31 friendly materials [1]. For this reason, the plastic in-
L32 dustry is every day more concerned about this issue,
L33 and bio-based and/or biodegradable polymers are
L34 gaining interest. This transition is not only affecting

R1 commodity plastics, but also engineering polymers.
R2 Aliphatic polyamides (PAs), also known as nylons,
R3 have received considerable attention in the last years
R4 since they can be fully or partially biobased and can
R5 offer similar properties to conventional petroleum-
R6 derived PAs such as polyamide 6 (PA6) or poly-
R7 amide 66 (PA66), representative for rigid uses or poly-
R8 amide 12 (PA12) for flexible applications [2]. Today,
R9 some recent developments have been successful

*Corresponding author, e-mail: luiquic1@epsa.upv.es
© BME-PT

1

A comparative study on the reactive compatibilization of melt-processed polyamide 1010/polylactide blends by multi-functionalized additives derived from linseed oil and petroleum

Abstract.

This research work describes the manufacturing and characterization of novel engineering materials consisted of fully bio-based blends of polyamide 1010 (PA1010) with 20 wt% of polylactide (PLA). Four different compatibilizers were used to enhance the miscibility and the performance of the biopolymer blends. Two multi-functionalized vegetable oils (MLO and ELO) and two petroleum-derived glycidyl-based additives (ESAO and PS-GMA) were tested during melt compounding. The resultant biopolymer blends were processed by either cast film extrusion or injection molding to obtain films and pieces, respectively. Thin films with an average thickness of 50–60 µm and thick pieces of 4 mm were obtained, and their mechanical, morphological, thermal, thermomechanical, barrier and, optical properties were characterized. Although all four compatibilizers successfully provided compatibilization to the blends, the chemically modified vegetable oils, that is, MLO and ELO yielded the injection-molded pieces with the most balanced mechanical properties in terms of strength and toughness. Besides, the resultant films showed very low oxygen transmission rate values, thus broadening the potential of these biopolymer blends for the food packaging industry.

Keywords: Biopolymers, biocomposites; Bio-based polyamides; Multi-functionalized vegetable oils; Reactive compatibilization.

INTRODUCTION

The increasing awareness about sustainable development, petroleum depletion, carbon footprint, and so on, have recently been consolidated as the leading forces for the development of environmentally friendly materials [1]. For this reason, the plastic industry is every day more concerned about this issue, and bio-based and/or biodegradable polymers are gaining interest [2]. This transition is not only affecting commodity plastics, but also engineering polymers. Aliphatic polyamides (PAs), also known as nylons, have received considerable attention in the last years since they can be fully or partially biobased and can offer similar properties to conventional petroleum-derived PAs such as polyamide 6 (PA6) or polyamide 66 (PA66), representative for rigid uses or polyamide 12 (PA12) for flexible applications [3]. Today, some recent developments have been successful both from technical and economic standpoints to obtain sebacic acid from castor oil (CO) [4]. Sebacic acid, a C10 dicarboxylic acid, can readily react by conventional polycondensation with 1,10-decamethylene diamine (DMDA). DMDA can be bio-sourced through the exposure of sebacic acid to ammonia and, subsequently, subjected to dehydration and hydrogenation process, thus leading to fully bio-based polyamide 1010 (PA1010) [5]. PA1010 shows a relatively low melting temperature (T_m) compared to other PAs, and it can be used in engineering applications, which require high resistance (mechanical and chemical) such as fuel lines for cars, bike tubes, cable coating, tubes for high-temperature fluids, among others [6]. The long alkyl chains of PA1010 are responsible for low water absorption and, therefore, their mechanical properties are less sensitive to moisture [7]. Bio-based polyamides (bioPAs) are being introduced slowly in the packaging industry due to their cost and some technical restrictions. Despite this, some amorphous polyamides (aPA) have been reported, together with ethylene-vinyl alcohol copolymer (EVOH), as interesting films in multilayer systems intended for oxygen-sensitive food packages [8].

Polymer blending is one of the most cost-effective ways to obtain tailored properties that individual polymer cannot achieve[9]. The increasing availability of bio-based polymers and, particularly, polylactide (PLA) due to an excellent combination of processability, cost, and overall properties, represent interesting alternatives to high environmentally friendly polymer blends with improved properties[10, 11]. PLA owns a privileged position in the bio-based polymer industry and, currently, it is worldwide available with several tradenames and increasing production facilities and industrial applications [12, 13]. In particular, PLA finds important applications as a rigid polymer in the packaging industry [14]. Even though many of the uses of PLA are for single-use applications, it has been described that PLA can also be successfully used for long-term engineering applications [15]. This polymer is obtained from starch-rich materials through a fermentation process, with high capacities to be degraded under hydrolytic or compost conditions. The worldwide consumption of PLA is estimated in 140,000 tons [16], and it is expected a growth of the production capability of 0.8 Mt up to 2020 [17]. PLA shows some properties similar to polystyrene (PS), which makes it suitable for blending with PA to provide tailored properties for uses in the packaging industry [18]. Another interesting topic related to the increasing use of polymer blends is the recycling of single-use plastics and/or disposable plastics. The separation of polymers during recycling is one of the most expensive stages, so polymers blending is an interesting solution. However, the lack of

miscibility between materials must be taken into account. This restriction is related to miscibility, which plays a key role in obtaining high-performance polymer blends. In fact, most of the polymer blend systems are immiscible (or with very restricted miscibility) from a thermodynamic standpoint, which is highly affected by dipole-dipole, ion-dipole, hydrogen bonds, acid-base interactions, among others [19].

To overcome this drawback related to miscibility, several strategies can be approached by *ex-situ* (non-reactive) and *in situ* (reactive) extrusion processes [20]. *Ex-situ* extrusion involves the use of a copolymer that is highly miscible with one of the components in the blend. This process consists of a two-stage process that increases overall costs so that it is only used in such applications in which the cost is not a restriction [21]. On the contrary, *in situ* compatibilization (reactive extrusion) is much more attractive as it can be obtained by using polymers, oligomers, and additives with highly reactive groups such as anhydride, epoxy, and isocyanate, among others. These compatibilizers can react during the extrusion process in the melt state to minimize the effects of immiscibility by reacting with hydroxyl, carboxyl, amine, and so on, groups that are typically present in condensation polymers [22].

In the last decade, vegetable oils (VOs) have gained considerable interest as bio-based building blocks for the polymer industry. Also, the particular chemical structure of unsaturated fatty acids, with one or more carbon-carbon unsaturations, allows a wide variety of chemical modifications that increase their reactive and, subsequently, their possibilities. Vegetable oils can be functionalized by acrylation [23], epoxidation [24-26], or maleinization [27], among others, with the main aim of increasing their reactivity which can be used for different purposes. Maleinized linseed oil (MLO) and epoxidized linseed oil (ELO) have been successfully used as reactive compatibilizers in different binary systems [23, 28, 29]. On the other hand, condensation polymers such as aliphatic polyesters and PAs are highly sensitive to hydrolytic degradation. Therefore, these polymers usually require a chain extender to minimize the effects of hydrolytic degradation. Usually, these chain extenders are glycidyl methacrylate (GMA) copolymers that are commercially available with different tradenames and compositions such as Joncryl® from BASF or Xibond™ from Polyscope. The glycidyl group is highly reactive and can react with hydroxyl or amine end-chain groups in condensation polymers during melting and extrusion [30]. This highly reactive copolymers can in-situ react to give block copolymers by reactive extrusion by the extraction of the hydrogen of an amine or carboxylic acid end-chain group of different condensation polymers to provide increased compatibility [31].

The main aim of this work is to improve the mechanical, thermal and gas barrier properties of a fully bio-based PA1010 by blending with PLA as the minor component, to widen the potential use of PA1010 in the packaging industry. To overcome the expected drawbacks related to the poor miscibility between these two polymers, different highly reactive compatibilizers were proposed. On the one hand, two vegetable oil derived compatibilizers, namely maleinized linseed oil (MLO) and epoxidized linseed oil (ELO), and on the other hand, two conventional petroleum-derived chain extenders, based on glycidyl methacrylate copolymers, namely Joncryl© ADR 4300 and Xibond™ 920.

EXPERIMENTAL

Materials

PA1010 with the tradename NP PA1010-201 was supplied by NaturePlast (Ifs, France) in the form of pellets. According to the manufacturer, this is a fully bio-based, medium-viscosity, injection-grade homopolyamide with a density of 1.05 g cm-3 and a viscosity number (VN) of 160 cm^3 g^{-1}. PLA grade Ingeo™ Biopolymer 2003 D was supplied by Nature Works LLC (Minnetonka, USA) in pellet form with a typical density of 1.24 g m^{-3} and a melt flow index of 6 g/(10 min) measured at 210 °C.

Regarding the bio-based compatibilizers, maleinized linseed oil (MLO) with the tradename of VEOMER LIN was obtained from Vandeputte (Mouscron, Belgium). This has a viscosity of 1000 cP (20 °C) and an acid value of 105–130 mg KOH g^{-1}. Epoxidized linseed oil (ELO), CAS number 8016-11-3, was supplied by Traquisa S.L. (Barcelona, Spain) and was used as a biosourced compatibilizer. This epoxidized vegetable oil is characterized by a molecular weight of about 1037 g mol^{-1}, a density of 1.05 – 1.06 g cm^{-3} at 20 °C and a viscosity of 8–11 p at 25 °C.
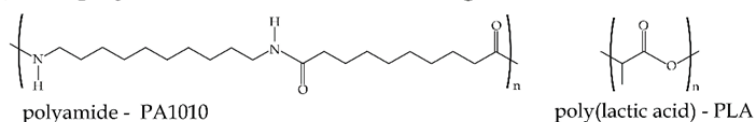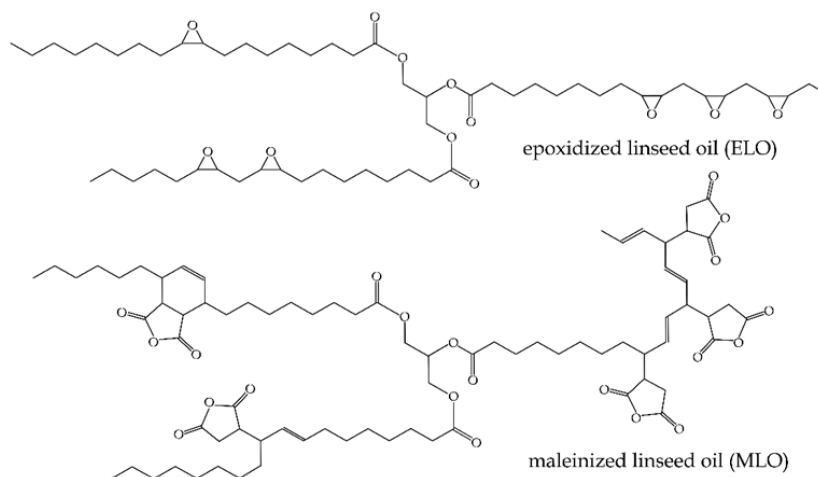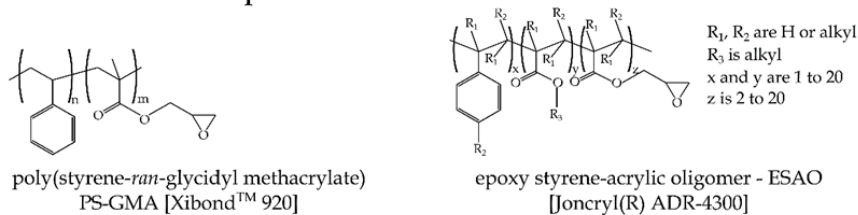
Figure III.3.4.1. Schematic representation of the chemical structure of base polymers, bio-based compatibilizers, and petroleum-derived chain extenders/compatibilizers.

Regarding the petroleum-derived chain extenders/compatibilizers, a low functionality epoxy styrene-acrylic oligomer (ESAO) with the tradename of Joncryl® ADR 4300 was obtained from BASF S.A. (Barcelona, Spain) in the form of solid granules with a molecular weight (M_W) of 5500 g mol^{-1}. This copolymer shows a T_g value of 56 ºC with an epoxy equivalent weight (EE$_W$) of 445 g mol^{-1}. The functionality (*f*) is ≤ 5. The manufacturer recommends a dosage comprised between 0.4 – 2 wt% for polyesters to avoid gel formation. A random styrene-glycidyl methacrylate (PS-GMA) copolymer from Polyscope (Geleen, The Netherlands) was used as a chain extender/compatibilizer in the binary blend. Xibond™ 920 was kindly supplied by Polyscope. This is a typical chain extender for poly(esters) with a molecular weight (M_W) of 50000 g mol^{-1} and a T_g of 95 ºC. The glycidyl methacrylate (GMA) content was 20% (mol fraction). **Figure III.3.4.1** shows a schematic representation of all the materials used in this study.

Manufacturing of PA1010/PLA blends

PA1010/PLA blends were manufactured with different compositions, as summarized in **Table III.3.4.1**. The amount of ESAO and PS-GMA was set to 2 phr (weight parts of compatibilizer/additive per hundred weight parts of the PA1010/PLA blend) since the manufacturer recommends this chain extender in the 0.25-2.5 wt% range to avoid gel formation (branching and crosslinking). Regarding the linseed oil derivatives, 5 parts per hundred resin (phr) of the blend was used. This loading was selected from previous papers of the group in which, over 5-10 phr, saturation can occur [32, 33].

Table III.3.4.1. Summary of codes and compositions according to the weight content (wt%) of polyamide 1010 (PA1010) and polylactide (PLA) in which maleinized linseed oil (MLO), epoxidized linseed oil (ELO), epoxy-based styrene-acrylic oligomer (ESAO), and polystyrene-glycidyl methacrylate random copolymer (PS-GMA) were added as parts per hundred resin (phr) of PA1010/PLA blend.

Code	PA1010 (wt%)	PLA (wt%)	MLO (phr)*	ELO (phr)*	Joncryl® ADR 4300 (phr)*	Xibond™ 920 (phr)*
PA1010	100	0	0	0	0	0
PA1010/PLA	80	20	0	0	0	0
PA1010/PLA + MLO	80	20	5	0	0	0
PA1010/PLA + ELO	80	20	0	5	0	0
PA1010/PLA + ESAO	80	20	0	0	2	0
PA1010/PLA + PS-GMA	80	20	0	0	0	2

* phr denotes the weight parts of additives per hundred parts by weight of PA1010/PLA blend.

PLA was dried for 24 h at 60 °C while PA was dried 6 h at 80 °C. The corresponding amounts of each component described in **Table III.3.4.1** were weighed

and mixed in a zipper bag as pre-homogenization stage. All materials were processed by extrusion in a DSM Xplore MC 15 micro compounder at 210-215-220 °C. The pre-mixing time inside the plasticization chamber was set to 1 min at a rotating speed of 100 rpm. After this time, the compounded material was forced to exit the plasticization chamber and extruded through a nozzle connected to a chill-roll system to obtain a continuous film, 60 mm width, and 60 μm thick films at 10 rpm and a controlled force of 700 N.

In addition to films, solid samples for further characterization were obtained by a coupled injection moulding unit to the DSC Xploere. The extrusion process was carried out identically as above-mentioned. Nevertheless, the chill-roll unit was changed to a 10-mL micro-injection moulding unit with the corresponding transfer chamber. This allows direct injection moulding of solid samples sizing ($80x10x4$ mm^3) after the mixing process in the DSM Xplore without a previous cooling stage of the extrudate and pelletization. The injection pressure cycle was set in three stages: 8 bar-0.3 s; 7 bar-0.2 s; and the last stage 7 bar-5.5 s. The temperature of the mould was kept at 35 °C.

Mechanical characterization

Tensile tests were carried out in a universal test machine LLOYD 30 K (Hampshire, England) on film samples of 100 mm length, 10 mm width, and an average thickness of 60 μm following the indications of ISO 527-1:2012. The selected load cell was 500 N, and the cross-head speed was set to 10 mm min^{-1}. Hardness values were measured using a hardness tester durometer Brevetti AFFRI – Mod. ART. 13 (Induno Olona, Italy). Ten different measures were collected from injection-molded samples sizing $80x10x4$ mm^3, according to ISO 868:2003.

Although the main aim of this work was to characterize films, some mechanical properties were obtained on injection-moulded samples to evaluate some properties that cannot be tested on film samples. For this reason, toughness was studied on injection-molded rectangular samples with dimensions of $80x10x4$ mm^3 by the Charpy impact test with a 6-J pendulum from Metrotec S.A. (San Sebastián, Spain) on notched samples (0.25 mm radius v-notch), following the specifications of ISO 179-1:2010. All mechanical tests were performed at room temperature, and at least 6 different samples of each formulation in **Table III.3.4.1** were tested, and the most relevant parameters of each test were calculated and averaged. The average has been calculated from the 6 values obtained while the dispersion was obtained by calculating the standard deviation.

Thermal characterization

The main thermal transitions of uncompatibilized and compatibilized PA1010/PLA films were obtained by differential scanning calorimetry (DSC) in a Q200 calorimeter from TA Instrument (Schwerzenbach, Switzerland). An average sample weight of 5-8 mg was subjected to a three-stage dynamic thermal cycle as follows: first heating from 25 °C to 180 °C, followed by cooling to 25 °C, and second heating to 350 °C. Heating and cooling rates were all run at 10 °C min^{-1}. All tests were run in a nitrogen atmosphere with a flow of 66 mL min^{-1} using standard sealed aluminium

crucibles (40 μL). The percentage degree of crystallinity, %X_c was determined following **Equation III.3.4.1**.

$$\%\chi_c = \left[\frac{\Delta H_m - \Delta H_{cc}}{\Delta H_m^0 \cdot (1-w)}\right] \cdot 100 \qquad \textbf{Equation III.3.4.1}$$

Where ΔH_m (J g^{-1}) corresponds to the melting enthalpy. ΔH_{cc} (J g^{-1}) corresponds to the cold crystallization enthalpy. ΔH_m^0 (J g^{-1}) stands for the melting enthalpy of a theoretically fully crystalline PA1010 and PLA, that is, 244 J g^{-1} [34] and 93 J g^{-1} [35] respectively. (1-w) represents the weight fraction of PA1010.

The thermal stability (degradation/decomposition) of PA1010/PLA films was determined by thermogravimetric analysis (TGA) in a Seiko Exstar 6300 analyzer (Tokyo, Japan). Samples with an average weight comprised between 5 and 7 mg were placed in standard alumina crucibles of 70 μL and subjected to a heating program from 30 to 700 °C at a heating rate of 10 °C min^{-1} in a nitrogen atmosphere.

Thermomechanical characterization

Dynamic mechanical thermal analysis (DMTA) was conducted in a DMA-1 model from Mettler-Toledo S.A. (Barcelona, Spain), with a special clamp system for films working in tension mode. Film samples sizing 10x5x0.06 mm^3 were subjected to a temperature sweep program from -100 °C to 150 °C at a heating rate of 2 °C min^{-1}. The initial pretension force was 0.5 N, and the displacement amplitude was set to 6 μm. The selected frequency was 1 Hz, and DMTA tests were run in triplicate to obtain reliable data.

Morphology characterization

The surface morphology after failure from impact tests on injection-moulded samples was observed by field emission scanning electron microscopy (FESEM). The samples were first sputtered with a palladium alloy in a sputter coater EM MED20 from Leica Microsystem (Milton Keynes, United Kingdom). The analysis was carried out in a ZEISS ULTRA 55 FESEM microscope from Oxford Instruments (Abingdon, UK) using 2 kV as the acceleration voltage. To evaluate the extent of the phase separation, selective extraction of PLA was applied with chloroform supplied by Sigma Aldrich (Madrid, Spain). Film samples were immersed in chloroform solution for 24 h and 48h, and then, dried and prepared for FESEM observation. In order to see the phase separation, analysis was carried out in a FESEM, ZEISS SUPRA 25 microscope from Oxford Instruments (Abingdon, UK) using 2 kV as the acceleration voltage. The samples were first sputtered with a palladium alloy in a sputter coater Agar Sputter Coater - Automatic from Agar Scientific Ltd (Stansted, United Kingdom). A freeware software called Image J, developed by the Laboratory for Optical and Computational Instrumentation (LOCI, University of Wisconsin) and the National Institutes of Health in Bethesda (NIH) has been used to determine the dimensions of the droplets.

Color measurement

Color coordinates were determined on films using a spectrophotometer CM-2300d Konica Minolta (Tokio, Japan). Data were acquired by using the SCI 10/D65 method, while CIELAB color variables, as defined by the Commission Internationale de 1'Éclairage (CIE 1995), were used as reported in [36]. This equipment provides the $L*$ (lightness), $a*$ (red-green coordinate), and $b*$ (yellow-blue coordinate) parameters. The color difference between the two samples ($\Delta E_{ab}*$) was calculated using **Equation III.3.4.2**.

$$\Delta E_{ab}\ *= \sqrt{\Delta L^{*2} + \Delta a^{*2} + \Delta b^{*2}}$$ **Equation III.3.4.2**

Where $\Delta L*$ is the difference in $L*$ (lightness) between two samples (neat PA1010 film and films of PA1010/PLA blends) while $\Delta a*$ and $\Delta b*$ are the differences in the $a*$ (green/red) and $b*$ (blue/yellow) coordinates, respectively. For each film, five readings were taken, and the average values were calculated. $\Delta Eab*$ values indicate the intensity in the color change. $\Delta Eab* < 0.5$ means imperceptible difference in color; $0.5 \leq \Delta Eab* < 1.5$ means a slight difference; $1.5 \leq \Delta Eab* < 3.0$ stands for a noticeable difference; $3.0 \leq \Delta Eab* < 6.0$ represents a marked difference; $6.0 \leq \Delta Eab* \leq 12.0$ an extremely marked difference, and $\Delta Eab* > 12.0$ indicates a color of a different shade.

Oxygen transmission rate

The oxygen transmission rate (OTR) was measured in triplicate using a Systech Instruments 8500 oxygen permeation analyzer from Metrotec S.A. (San Sebastián, Spain) at room temperature and 2.5 atm. Films were cut into 5 cm diameter circles and were compressed between the upper and lower diffusion chamber. Pure oxygen (99.9% purity) was introduced into the upper half of the sample chamber while nitrogen was injected into the lower half. A Mitutoyo digimatic micrometer model 293–832 (Illinois, USA) was used to calculate the average thickness – h of the samples all around their perimeter. The thickness of the samples was between 50 and 60 μm.

RESULTS AND DISCUSSION

Mechanical characterization of PA1010/PLA blends

Table III.3.4.2 summarizes the mechanical properties of PA1010/PLA films with different compatibilizers, paying particular attention to tensile properties (tensile modulus, maximum tensile strength, and elongation at break), with regard to hardness an impact strength, (Charpy test) has been studied based on standardized samples. Neat PA1010 is an engineering plastic with a modulus of 700 MPa and a tensile strength of 52 MPa. It was also characterized by a high elongation at break of 490% in the film form. These mechanical properties are similar to other bio-PAs [30]. The addition of 20 wt% PLA to PA1010 produced an increase in the tensile modulus up to 980 MPa (which represents a % increase of 39%). It is important to remark that PLA is stiffer than PA1010.

Table III.3.4.2. Summary of the mechanical properties of the polyamide 1010 (PA1010)/polylactide (PLA) blends processed with maleinized linseed oil (MLO), epoxidized linseed oil (ELO), epoxy-based styrene-acrylic oligomer (ESAO), and polystyrene-glycidyl methacrylate random copolymer (PS-GMA).

Films	E (MPa)	σ_{max} (MPa)	ε_b (%)	Shore D hardness*	Impact strength* (kJ/m²)
PA1010	700 ± 40	52 ± 5	490 ± 30	70.2 ± 0.8	6.7 ± 0.6
PLA	1900 ± 90	44 ± 5	15 ± 3	69.1 ± 0.7	1.8 ± 0.6
PA1010/PLA	980 ± 55	50 ± 4	470 ± 30	71.4 ± 0.5	3.0 ± 0.2
PA1010/PLA+MLO	900 ± 25	46 ± 3	550 ± 20	69.4 ± 0.4	5.7 ± 0.6
PA1010/PLA+ELO	1240 ± 50	77 ± 1	490 ± 18	71.0 ± 0.7	3.9 ± 0.2
PA1010/PLA+ESAO	1000 ± 30	57 ± 2	470 ± 35	74.1 ± 0.8	3.3 ± 0.3
PA1010/PLA+PS-GMA	1060 ± 40	59 ± 4	469 ± 34	72.4 ± 0.9	3.1 ± 0.2

On the contrary, a slight decrease in cohesion-related properties can be detected. In particular, the maximum tensile stretch decreases down to 50 MPa and the elongation at break decreases to 470%. The % decrease in these two mechanical properties is less than 5%. This is a very positive effect since the typical behaviour of immiscible polymer blends is a remarkable decrease in cohesion-related properties such as elongation at break, tensile strength, and toughness. It is worthy to note that even these two polymers are immiscible; addition of PLA can improve some properties of PA1010. Rashmi *et al.* [37], reported how the addition of 20 wt% PA in a brittle PLA matrix gave increased elongation and stiffness, even they observed immiscibility. As we will discuss later, the more negative effect of blending PA1010 and 20 wt% PLA is a clear decrease in toughness. Compatibilizers can overcome or minimize these adverse effects. Both vegetable oil-derived compatibilizers give two different effects on the base PA1010/PLA blend. The stiffness is almost the same with a tensile modulus of 900 MPa and the tensile strength decreases by 4 MPa which is not critical. It remains at high values of more than 45 MPa, which is unusual for an engineering plastic. On the contrary, the elongation at break increases in a dramatic way up to 550%, which is indicating two potential effects of MLO: on the one hand, a plasticization effect and, on the other hand, a compatibilization effect both contributing to improved ductile properties. As it has been reported in the literature, modified vegetable oils can positively improve ductile properties in immiscible binary/ternary blends as well as in wood-plastic composites with polyester-type matrices and natural fillers [27, 38]. Regarding ELO, the first thing that strikes is a remarkable increase in the tensile strength up to values above neat PA1010 (77 MPa) with a noticeable increase in elongation at break, also superior to neat PA1010 (490%). As expected, the stiffness also increases as the tensile modulus represents the stress to strain ratio in the linear region of a tensile diagram. As the stress is in the numerator and increases in a remarkable way, compared to the denominator (elongation), the ratio increases, thus leading to a tensile modulus of 1240 MPa, the highest of the developed materials. Therefore, it is

possible to hypothesize the synergistic effect of ELO on this binary blend. Xiong et al. [39], reported that the addition of epoxidized soybean oil (ESO) on a PLA matrix led to a slight decrease in stiffness but a noticeable improvement in elongation at break. In a previous work, Quiles-Carrillo *et al.* [23], reported the positive effect of epoxidized-acrylated vegetable oils on both the tensile strength and the elongation at break of PLA showing this synergistic effect.

Concerning the petroleum-derived chain extenders, it is worthy to note that they can also provide increased properties to the base PA1010/PLA blend. The most relevant effect of both Joncryl® ADR 4300 and Xibond™ 920 was an increase in the maximum tensile strength up to values of 56.9 MPa and 59.0 MPa, respectively, while the elongation at break remained almost invariable compared to the uncompatibilized PA1010/PLA blend with values around 468–469%. Because of the increase in tensile strength, the stiffness was also improved up to values above 1000 MPa for both chain extenders. So that, both petroleum-derived chain extenders can also provide compatibilization to this blend as it is composed of two condensation polymers with hydroxyl groups end-chains (from carboxylic acids in PLA and amines in PA1010). Rasselet *et al.* [40], showed a remarkable increase in stiffness due to the improved interface between PLA and PA11 by reactive compatibilization with ESAO, showing the additional efficiency of this chain extender on blend compatibilization. In this sense, the use of chain extensors derived from petroleum, usually give good results in poly(esters) thanks to the reaction of epoxy groups with hydroxyl terminal groups in poly(esters) like PLA [41].

Concerning hardness, the addition of 20 wt% PLA to PA1010 gave an increase of about 1.2 Shore D units due to the stiffness of PLA compared to that of PA1010. Both MLO and ELO showed a slight plasticization effect with lower Shore D hardness values, while both ESAO and PS-GMA copolymers delivered a slight increase in Shore D values in accordance with the increase in tensile strength.

As it has been above-mentioned, mechanical properties of immiscible polymer blends are highly sensitive to cohesion-related properties such as the strength and the elongation at break. It is important to remark that both of them play a critical role in toughness. Neat PA1010 showed an impact-absorbed energy of 6.7 kJ m^{-2} (on notched samples), and this was dramatically reduced down to half the initial value by blending with 20 wt% PLA (3.0 kJ m^{-2}). This is directly related to weak interface interactions between both polymers in the binary blend, which gives poor cohesion and, subsequently, the low ability for load transfer between the two base polymers in the blend. As it can be seen in **Table III.3.4.2**, all four compatibilizers/chain extenders, resulted in materials with improved toughness with impact strength values above 3 kJ m^{-2} for all of them. Both Joncryl® ADR 4300 and Xibond™ 920 show the efficiency of GMA-based copolymers/oligomers in improving tensile strength, while the impact toughness is only slightly improved. V. Narajan *et al.* [42], have reported the exceptional properties that GMA-derived copolymers can give to PLA-based materials to improve toughness.

Nevertheless, both vegetable oil-derived compatibilizers give better results in terms of improved toughness. Addition of 5 phr ELO to the base PA1010/PLA blend produced an impact strength of almost 4 kJ m^{-2}, which is indicating the synergistic effect above-mentioned but among all values, it strikes the high impact strength MLO

can provide to this blend with an absorbed-energy of 5.7 kJ m^{-2}, very close to neat PA1010. Similar findings have been reported by Garcia-Campo *et al.* [43], in ternary blends of PLA/poly(ε-caprolactone) (PCL)/poly(3-hydroxybutyrate) (PHB) with soybean-derived compatibilizers. On the other hand, Ferri *et al.*[44] reported a remarkable improvement in toughness in binary PLA/TPS blends by using MLO.

Morphological characterization of PA1010/PLA blends

Figure III.3.4.2 gathers FESEM images taken at 5000x of neat PA1010 and its blends with PLA with and without compatibilizers (fractured samples from Charpy impact test). **Figure III.3.4.2a** shows the fracture surface of neat PA1010. It is important to remark that these images were taken from fractured samples from impact tests (notched samples), and these conditions do not allow high plastic deformation. It can be seen a very rough surface, which corresponds to a ductile polymer. Brittle polymers show a very smooth surface with micro-crack formation and coalescence. In this case, this morphology could not be seen. The immiscibility between PA1010 and PLA can be clearly observed in **Figure III.3.4.2b** with a PA1010-rich matrix with embedded PLA-rich droplet-like shapes. This is the typical island-in-the-sea morphology of an immiscible polymer blend. The smaller is the droplet size, the better are the overall properties of the obtained blends. The average diameter of the PLA-rich domains on uncompatibilized PA1010/PLA blend was 1.7 ± 0.4 μm, which is a relatively small size and, consequently, the mechanical properties were not profoundly affected, as observed previously. This droplet size was obtained using Image J software, and it is an estimation of the diameter of spherical shapes (dispersed droplets) in the fractured surface, and an average value and the corresponding standard deviation were calculated. The effect of the compatibilizers is noticeably different depending on their nature. Both vegetable oil-derived compatibilizers produced a decrease in the average diameter of the embedded PLA-rich droplets. When using MLO as a reactive compatibilizer, the average size was 1.6 ± 0.5 μm, which is slightly smaller than the uncompatibilized blend.

Nevertheless, ELO was the one that provided the most remarkable decrease in the droplet size to 0.9 ± 0.4 μm. This is representative of an increase in compatibility between PA1010 and PLA due to the reaction of epoxy groups contained in ELO with end-chain hydroxyl groups of condensation polymers (mainly in carboxylic acid and amine groups). A similar behavior has been reported by Lin *et al*. [45] who reported a decreasing droplet size of the PA6 embedded droplets in a recycled polyethylene terephthalate (PET) matrix with increasing the content of the reactive compatibilizer, namely poly(ethylene octene-co-glycidyl methacrylate) (POE-*co*-GMA), with elastomeric properties characterized by high flexibility. They attribute this phenomenon to the reaction of epoxy groups with COOH or OH groups in recycled PET [46], and COOH or NH$_2$ groups in PA6 [47]. This assertion can be extended to the herein studied binary system with a PA and a polyester component.
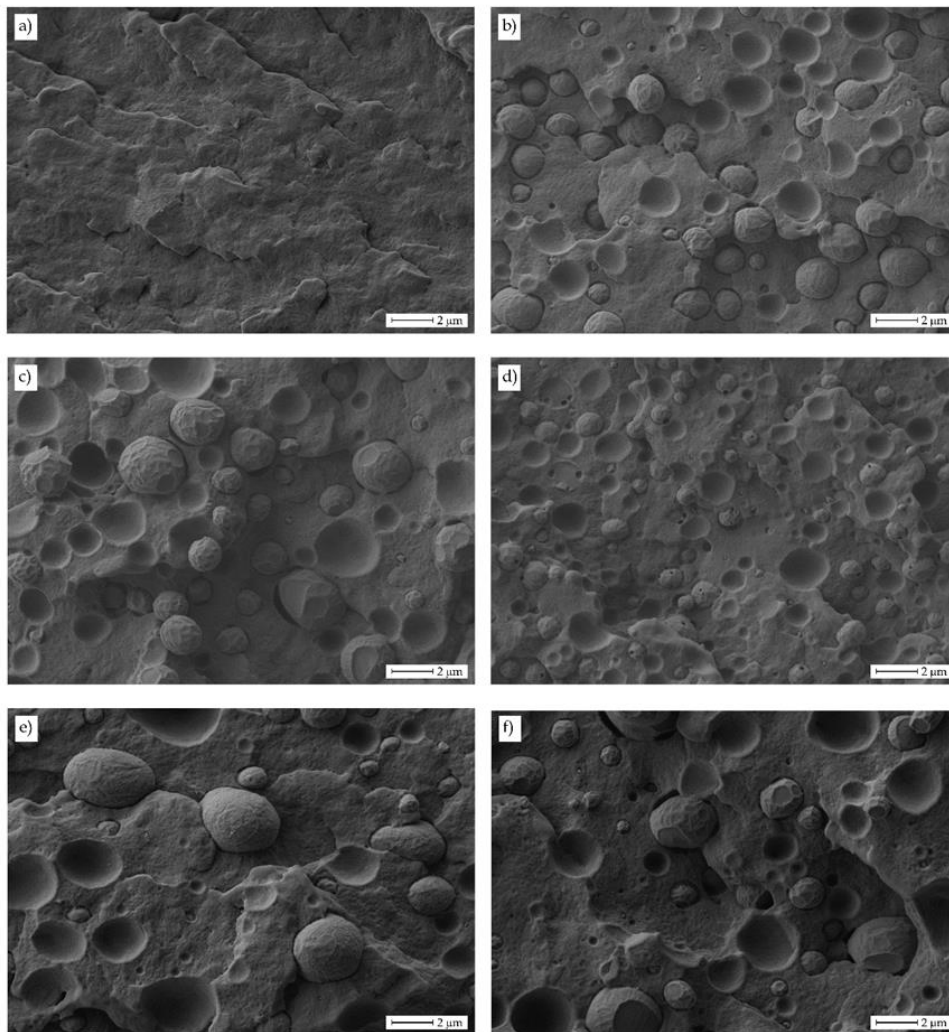
Figure III.3.4.2. Field emission scanning electron microscopy (FESEM) images of the fracture surfaces from the impact tests at 5000x corresponding to: a) Polyamide 1010 (PA1010); b) PA1010/polylactide (PLA); c) PA1010/PLA + maleinized linseed oil (MLO); d) PA1010/PLA + epoxidized linseed oil (ELO); e) PA1010/PLA + epoxy-based styrene–acrylic oligomer (ESAO); f) polystyrene-glycidyl methacrylate random copolymer (PS-GMA).

Regarding the effect of ESAO (Joncryl® ADR 4300) and PS-GMA (Xibond™ 920), the average size of the droplets does not decrease. In fact, it increased for ESAO up to 2.1 ± 0.8 µm, which indicates high size dispersion from tiny droplets to large particles. As it has been described previously, this chain extender provided a remarkable increase in tensile strength, but other ductile properties were not remarkably improved. In the case of PS-GMA, the droplet size decreased to an average value of 1.7 ± 0.7 µm, which is almost identical to the uncompatibilized blend but with higher size dispersion. Therefore, it is possible to expect that the main mechanism of these GMA derived compatibilizers is chain extension, as that is their primary purpose. Both GMA derived chain extenders showed a rigid chain with high T_g values, and this probably favors chain extension instead of compatibilization.
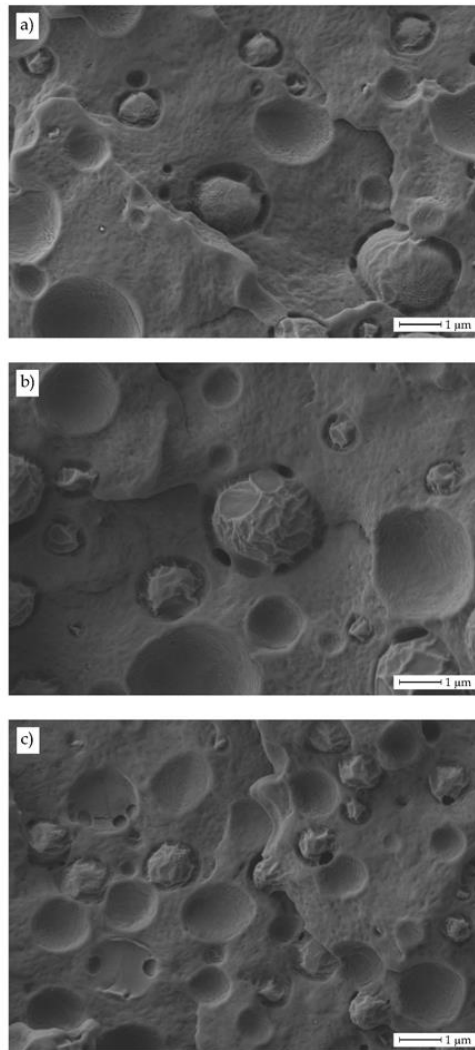
Figure III.3.4.3. Field emission scanning electron microscopy (FESEM) images of the fracture surfaces from impact tests at 10000x corresponding to a) polyamide 1010 (PA1010)/polylactide (PLA; b) PA1010/PLA + maleinized linseed oil (MLO); c) PA1010/PLA + epoxidized linseed oil (ELO), showing interface phenomena between polymers.

Figure III.3.4.3 shows FESEM images of the uncompatibilized PA1010/PLA blend and the corresponding images with vegetable oil-derived compatibilizers at higher magnification. As can be seen in **Figure III.3.4.3a**, there is some intrinsic interaction between PA1010 and PLA as the gap between the PLA-rich droplets was not homogeneous, which is representative of somewhat interactions or entanglement. Nevertheless, these interactions were much more intense in the MLO-compatibilized blend (**Figure III.3.4.3b**) in which some filament formations surrounding the dispersed PLA-rich domains can be observed and, in general, the PLA-rich droplets seem to be more embedded in the PA1010 matrix (smaller gap size). This situation is even more pronounced in the ELO-compatibilized blend (**Figure III.3.4.3c**) that shows an apparent decrease in the droplet size and, besides, the gap surrounding the PLA-rich droplets was almost inexistent. Anyway, it is worthy to remark that both MLO and ELO did not provide full miscibility as some voids (crater-like) can be detected in all

FESEM images, which indicates some PLA-rich droplets have been pulled-out during the impact test. These images are in accordance with Walha *et al*.[48] that showed the reactivity (reaction rates) of the epoxy group with primary and secondary hydroxyl, carboxyl and secondary amine groups, and reported the effect of reaction of epoxy groups with both PLA and PA11 end groups, with a decrease in droplet size. They also studied the effect of a Paraloid BPMS- 260 (BPMS), which is a styrene–acrylic copolymer (SM) with a noticeable compatibilization effect on PLA/PA11 blends, detectable by improved interfacial adhesion between both polymers.

Despite the above-mentioned images corresponding to the impact tests of fractured injection-molded samples, they give a clear idea of the mechanical properties, both tensile and impact strength. **Figure III.3.4.4** gathers FESEM images of the films subjected to a selective extraction with chloroform for 2 days, as reported by Rasselet *et al*. [49], to selectively etch the PLA-rich nodules. The morphology is in total agreement with the previous images and gives support to the obtained mechanical properties of films. Neat PA1010 (**Figure III.3.4.4a**) film showed a smooth surface as it was not blended. Nevertheless, the morphology of the uncompatibilized PA1010/PLA film was remarkably different, as it can be detected in **Figure III.3.4.4b**. There is a preferential orientation of the PLA domains obtained after the stretching process during film formation. This preferential orientation plays a crucial role in mechanical properties; therefore, all tensile tests were carried out on film samples in the stretching, longitudinal direction. It has been widely reported the different mechanical performance of films in the longitudinal (stretching) and perpendicular directions. In this work, the main aim was to relate the morphology of stretched films with the morphology of fractured solid samples to assess the compatibilization effect of the different compatibilizers. For this reason, mechanical properties in the transversal (perpendicular) direction were not evaluated as these FESEM images were in accordance with the comments on the morphology of fractured solid samples, in terms of compatibilization. So that, instead of spherical PLA-rich domains, these appeared as longitudinal voids with a length of 6 to 10 μm. This is giving clear evidence of phase separation, and despite the morphology is remarkably different from that in **Figure III.3.4.2b**, in the end, it is the same, but, in the film, the spherical PLA-rich droplets are stretched during film formation and rolling. This phase-separation was responsible for the slight decrease in tensile strength and elongation at break, as described in **Table III.3.4.2**.

Concerning the vegetable oil-compatibilized blends, the first thing that strikes is that the longitudinal voids or grooves were smaller in both length and width, which is representative for good compatibilization. These grooves were almost undetectable in the ELO-compatibilized blend (**Figure III.3.4.4d**), which gave improved tensile strength and enhanced elongation. In the case of MLO-compatibilized blend (**Figure III.3.4.4c**), these grooves were detectable, but the compatibilizing effect was evident as MLO provided the highest elongation at break on PA1010/PLA films. The mechanical properties provided by both petroleum-derived compatibilizers, with increased tensile strength and negligible change in elongation (ductility), can be easily related to the FESEM images. As it can be seen in **Figure III.3.4.4e** (ESAO-compatibilized) and **Figure III.3.4.4f** (PS-GMA) compatibilized) in which spherical (or elliptical) PLA-rich shapes have been selectively extracted thus giving evidence of poor compatibilization. Therefore, it is expectable that the improvement in tensile strength is directly related to

chain extension. As the processing conditions are different from injection-molded samples, the size of the PLA-rich droplets was smaller than that observed in the fracture surface of the injection-molded materials (see **Figure III.3.4.2** and **Figure III.3.4.3**).
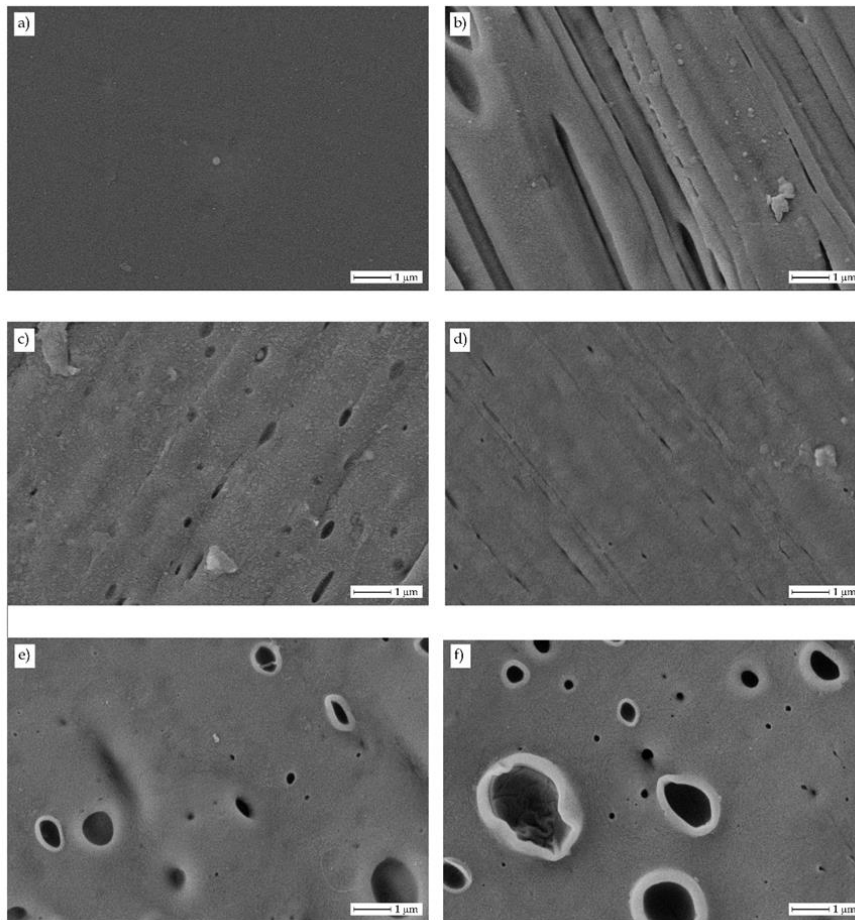
Figure III.3.4.4. Field emission scanning electron microscopy (FESEM) images of selective etched films at 25000x corresponding to: a) Polyamide 1010 (PA1010); b) PA1010/polylactide (PLA); c) PA1010/PLA + maleinized linseed oil (MLO); d) PA1010/PLA + epoxidized linseed oil (ELO); e) PA1010/PLA + epoxy-based styrene–acrylic oligomer (ESAO); f) polystyrene-glycidyl methacrylate random copolymer (PS-GMA).

Thermal properties of PA1010/PLA blends

From a thermal standpoint, **Figure III.3.4.5** gathers a comparative of the DSC plots during the second heating cycle corresponding to PA1010/PLA blends with and without compatibilizers. Besides, the most relevant information from DSC characterization is gathered in **Table III.3.4.3**. Neat PA1010 showed a double melting peak with a lower peak at 182 °C and the central peak located at 201 °C. This is related to a polymorphism on crystallites, which lead to multiple melting peaks of different intensities due to the presence of different crystalline forms, *i.e.* α, β, and γ [50], crystal forms of packed PA1010, with different characteristic melting peaks. As it can be seen

in **Table III.3.4.3**, PLA did not affect the characteristic melting points of PA1010. This identical behaviour has been observed in PA1010 blends with bio-based poly(ethylene), HDPE. Neat PLA (see **Figure III.3.4.5**) shows a melt peak temperature of 152.3 ± 1.2 °C. Its cold crystallization enthalpy is around 20.9 ± 0.9 J g^{-1}, while the melt peak enthalpy is close to 21.5 ± 0.8 J g^{-1}. These values indicate that this PLA grade shows very low crystallinity (0.7% ± 0.1) as the cold crystallization and the melt enthalpies (ΔH_{cc} and ΔH_m, respectively) show almost identical values. When blended with PA1010, due to the diluting effect, its specific melting point did not appear clearly in the DSC plots. Carbonell *et al.* [51] reported a similar thermal behavior of this PLA commercial-grade, specially intended for film manufacturing with an average melt peak temperature of 147 °C. All four compatibilizers exert a different effect on thermal properties and, mainly, on PA1010 crystallinity (%X_c). The thermal profile of the melting process of PA1010 remains almost invariable with all four compatibilizers. Another thing that strikes was a decrease in the degree of crystallinity in the blend from 35.8% to 23.6% in the uncompatibilized PA1010/PLA blend. Y. Huang *et al.* [52], reported the critical role of the interface on crystallization by two different phenomena: crystal nucleation and crystal growth. In this case, uncompatibilized blends suggested somewhat interactions as discussed in morphology study. So, this can affect the nucleation and crystal growth. Both MLO and ELO, offer lower crystallinity values compared to neat PA1010 and ELO shows the highest decrease in crystallinity. Crystallinity is directly related to ductile properties, and both MLO and ELO showed improved elongation at break. It is worthy to note that FESEM gives clear evidence of the compatibilization effect. Nevertheless, mechanical properties are also profoundly affected by the crystallinity and, in this case, as the blends are manufactured in a film form, the rapid cooling due to the small cross-section could influence mechanical properties. As can be seen, both petroleum-derived compatibilizers led to an increase in crystallinity up to values above 32%. This packed structure could be responsible for the increase in tensile strength as reported in **Table III.3.4.2** while the elongation at break remained invariable. Presence of ESAO and, in particular, PS-GMA favoured formation of more stable PA1010 crystals, and this has a positive effect on mechanical properties. Concerning PLA, the overall crystallinity was almost disrupted, as the peak intensity is very low for ESAO- and PS-GMA-compatibilized blends. Najafi *et al.* [53], reported that the addition of a GMA-based chain extender on PLA led to formation of a branched structure that critically affects crystal formation. Y. Huang *et al.*[52], showed the relevance of an epoxy-based compatibilizer on the crystallinity of PET/PA6 blends. They indicate that the potential reaction of the epoxy group towards -COOH, -OH and NH$_2$ groups in both condensation polymers, could affect crystal formation with more imperfections. Therefore, this dosage for both petroleum-derived compatibilizers seems to be the optimum as recommended by the suppliers since over this, branching and crosslinking (gel formation) can occur with a negative effect on crystallinity and, subsequently, on mechanical performance. About the melting peak characteristic temperatures, ELO increased the melting peak of neat PLA by 4 °C (and by 1.7 °C the characteristic peak of PA1010). This effect was also previously reported by Ferri *et al.* [28], by the addition of MLO to a PLA matrix with an increase in the melt peak temperature of 5 °C with 5% MLO.
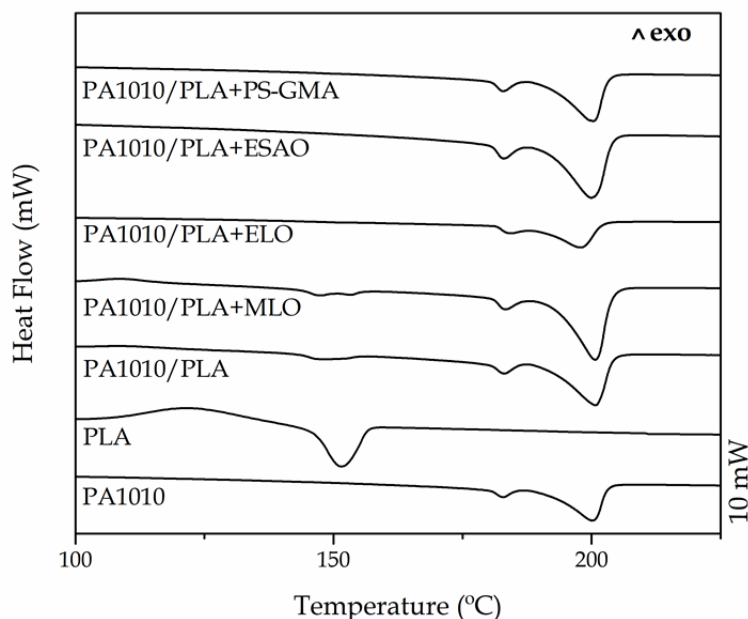
Figure III.3.4.5. Differential scanning calorimetry (DSC) curves of the polyamide 1010 (PA1010)/polylactide (PLA) blends compatibilized with maleinized linseed oil (MLO), epoxidized linseed oil (ELO), epoxy-based styrene-acrylic oligomer (ESAO), and polystyrene-glycidyl methacrylate random copolymer (PS-GMA).

Table III.3.4.3. Main thermal parameters of the polyamide 1010 (PA1010)/polylactide (PLA) blends compatibilized with maleinized linseed oil (MLO), epoxidized linseed oil (ELO), epoxy-based styrene-acrylic oligomer (ESAO), and polystyrene-glycidyl methacrylate random copolymer (PS-GMA) in terms of: melting temperature (T_m), and normalized melting enthalpy (ΔH_m), and degree of crystallinity (X_c).

Films	T_m (ºC)	ΔH_{cc} (J g^{-1})	ΔH_m (J g^{-1})	X_c (%)
PA1010	182.2 ± 1.5 /200.1± 1.5	-	87.3 ± 1.1	35.8 ± 1.1
PA1010/PLA	182.5 ± 1.5 /200.8± 1.1	-	46.2 ± 1.2	23.6 ± 1.2
PA1010/PLA + MLO	182.9 ± 1.0 /200.7± 0.9	-	46.6 ± 1.1	23.8 ± 1.0
PA1010/PLA + ELO	183.9 ± 0.9 /198.1± 0.8	-	35.7 ± 1.0	18.3 ± 1.0
PA1010/PLA + ESAO	182.4 ± 0.8 /200.0± 0.7	-	62.5 ± 1.5	32.0 ± 1.4
PA1010/PLA + PS-GMA	182.6 ± 0.7 /200.3± 0.6	-	67.1 ± 1.5	34.3 ± 1.4

TGA characterization also provided evidence of the degradation at high temperatures. **Figure III.3.4.6** shows a comparative plot of the characteristic TGA thermograms, while the main thermal parameters of the degradation process are summarized in **Table III.3.4.4**. PA1010 showed excellent thermal stability. Its onset degradation temperature (taken at a weight loss of 5%, $T_{5\%}$) was 407 ºC while the

maximum degradation rate (T_{max}) was close to 464.1 °C. Moreover, PA1010 degraded in a single step process with a residual mass of 0.2%. Yang *et al.* [54] reported similar results for the degradation of PA1010 with an onset degradation temperature of 414 °C. The addition of 20 wt% to PA1010 produced a decrease in thermal stability. The onset degradation temperature moved down to 324 °C, and the maximum degradation rate temperature decreased to 458 °C, thus indicating that the main effect of PLA was on the initial degradation stages with a remarkable decrease in $T_{5\%}$. It is also worthy to note that PLA was much more sensitive to thermal degradation than PA1010. Carbonell *et al.* [51] showed a similar PLA degradation profile with an onset degradation temperature located at 321 °C. Despite this low thermal stability of PLA compared to PA1010, the maximum degradation rate remained almost invariable above 450 °C. The addition of the vegetable oil derived compatibilizers did not affect significantly the compatibilized blends. In fact, $T_{5\%}$ was almost identical for the MLO-compatibilized blend, while a decrease of 9 °C was seen for the ELO-compatibilized blend. This decrease could be related to the plasticization that the chemically modified vegetable oils can provide to condensation polymers based on an increased free volume that could, potentially, lead to a decrease in thermal stability. Other authors have reported a decrease in the onset degradation temperatures of different polymers modified by multi-functionalized vegetable oils, namely acrylated, maleinized, and epoxidized oils [29, 38].
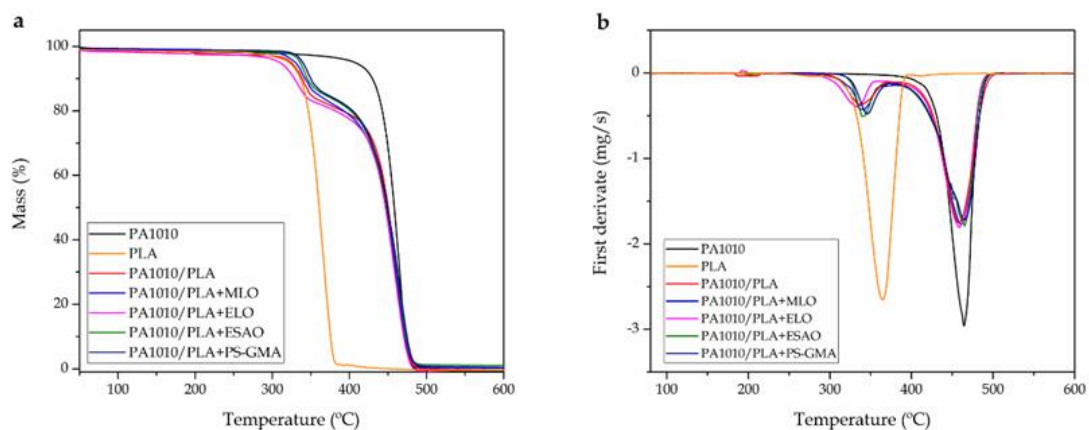
Figure III.3.4.6. Thermogravimetric analysis (TGA) curves of the polyamide 1010 (PA1010)/polylactide (PLA) blends compatibilized with maleinized linseed oil (MLO), epoxidized linseed oil (ELO), epoxy-based styrene-acrylic oligomer (ESAO), and polystyrene-glycidyl methacrylate random copolymer (PS-GMA): a) % weight loss and b) first derivative (DTG) curves.

Concerning the effect of both petroleum-derived compatibilizers, it is worthy to note that both positively contributed to improving thermal stability. In fact, the specific $T_{5\%}$ temperature moved up by 12 °C and 15 °C for the ESAO- and PS-GMA-compatibilized blends, respectively. Concerning the degradation characteristics, T_{max} increased by 7 °C for both compatibilizers. This improvement in thermal stability is directly linked to the internal structure obtained during the melt mixing due to the reactivity of the GMA contained in both chain extenders towards end-chain groups in both PA1010 (-COOH and NH_2) and PLA (-COOH and -OH). Lascano *et al.* [41]

demonstrated that the addition of ESAO to PLA/PBSA binary blends gave a slight increase in thermal stability. Moreover, Abdelwahab *et al.* [55] reported that the improvement in thermal stability of PLA/PBAT blends using Joncryl® as chain extender/compatibilizer was due to an increase in the molecular weight and increased chain stiffness. Identical findings were reported by Duangphet *et al.* [56] for poly(3-hydroxybutyrate-*co*-3-hydroxyvalerate) (PHBV) with a chain extender.

Table III.3.4.4. Main thermal degradation parameters of the polyamide 1010 (PA1010)/polylactide (PLA) blends compatibilized with maleinized linseed oil (MLO), epoxidized linseed oil (ELO), epoxy-based styrene-acrylic oligomer (ESAO), and polystyrene-glycidyl methacrylate random copolymer (PS-GMA) in terms of: temperature at mass loss of 5% ($T_{5\%}$), degradation temperature (T_{max}), and residual mass at 700 °C.

Films	$T_{5\%}$ (°C)	T_{max} (°C)	Residual weight (%)
PA1010	407.2 ± 1.2	464.1 ± 1.2	0.2 ± 0.1
PLA	320.2± 0.1	363.4± 0.1	0.1± 0.1
PA1010/PLA	324.2 ± 0.9	458.4 ± 1.3	0.3 ± 0.1
PA1010/PLA + MLO	330.3 ± 1.3	460.9 ± 0.9	0.4 ± 0.2
PA1010/PLA + ELO	316.8 ± 1.5	458.5 ± 1.0	0.1 ± 0.1
PA1010/PLA + ESAO	336.2 ± 1.3	465.4 ± 0.9	0.7 ± 0.2
PA1010/PLA + PS-GMA	339.5 ± 1.5	464.8 ± 1.1	0.2 ± 0.1

Thermomechanical properties of PA1010/PLA blends

Figure III.3.4.7 shows the evolution of dynamic-mechanical thermal analysis (DMTA) curves of neat PA1010 and the uncompatibilized and compatibilized PA1010/PLA blends by the different compatibilizers. **Table III.3.4.5** contains some quantitative values of the thermomechanical properties obtained from DMTA curves. In **Figure III.3.4.7a**, it can be seen the evolution of the storage modulus (E′) as a function of the increasing temperature. The dynamic thermomechanical behavior of PA1010 was characterized by an E′ value in the 1750-1000 MPa range in a wide temperature range comprised between -100 °C and 25 °C. Similar results can be found in the recent literature about bio-PAs [41]. Above 100 °C, the storage modulus dropped down to 177 MPa that represents a dramatic decrease. This is directly related to the α-relaxation process of PA1010 chains in which the amorphous phase of the biopolymer changes from the glassy to rubbery state. This α-relaxation is the most intense transition, and it is directly related to the glass transition process and its characteristic T_g. The addition of 20 wt% PLA provided an increase in the storage modulus below T_g. According to this, some authors have reported storage modulus values for PLA of 2500 MPa at temperatures below -40 °C [51]. The addition of PLA enhanced the stiffness values of neat PLA. All four compatibilizers provided a slight decrease in stiffness, which can be detected by characteristic DMTA curves below that corresponding to the uncompatibilized PA1010/PLA blend. This could be related to somewhat improved

polymer-polymer interactions, and it is in accordance with the previous observed morphology and mechanical properties. It is important to bear in mind that increased polymer-polymer interactions provide a slight increase in elongation ability due to improved stress transfer. If we consider the modulus as an estimation of the material's stiffness, the modulus shows the ratio between the applied stress and the obtained elongation. If the elongation increases while the applied stress remains almost constant, as it is in the denominator, it leads to a decrease in modulus and, subsequently, the stiffness is slightly reduced.
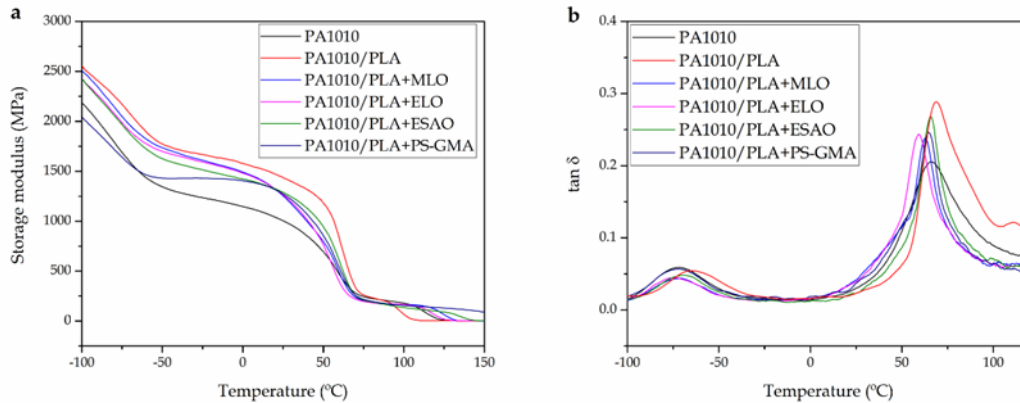
Figure III.3.4.7. Dynamic mechanical thermal analysis (DMTA) curves of the polyamide 1010 (PA1010)/polylactide (PLA) blend films compatibilized with maleinized linseed oil (MLO), epoxidized linseed oil (ELO), epoxy-based styrene-acrylic oligomer (ESAO), and polystyrene-glycidyl methacrylate random copolymer (PS-GMA): a) Storage modulus, E' and b) Dynamic damping factor (tan δ).

As can be seen in **Table III.3.4.5**, the storage modulus changed in a remarkable way below and above T_g. It is also worthy to note the effect of all the four compatibilizers on the characteristic T_g of the blends. Neat PA1010 showed a Tg of 66.0 °C, which overlaps with that of PLA, as reported by Choi *et al*.[57] with a T_g value of 59.1 °C. As PLA is the minor component in the PA1010/PLA blends, the dilution effect did not allow to identify this T_g. The T_g of the uncompatibilized PA1010/PLA blend was located at 68.2 °C, which is not a significant variation. Nevertheless, both vegetable oil-derived compatibilizers promoted a decrease in T_g to values of 62.7 °C and 58.9 °C, which is somewhat indicating a plasticizing effect of both MLO and ELO, as reported earlier in other polymer systems [24, 58]. It has been reported that chemically modified vegetable oils can contribute to a wide range of processes such as plasticization, compatibilization, chain extension, branching and cross-linking, but plasticization is always occurring with the use of these additives. Regarding the petroleum-derived compatibilizers, namely ESAO and PS-GMA, they did not provide any plasticizing effect as the T_g remained almost invariable compared to the uncompatibilized PA1010/PLA blend. Similar changes have been observed by Arruda *et al.* [59] in PLA/poly(butylene adipate-*co*-terephthalate) (PBAT) blends with very slight changes in T_g in the presence of chain extenders.

Table III.3.4.5. Main thermomechanical parameters of the polyamide 1010 (PA1010)/polylactide (PLA) blend films compatibilized with maleinized linseed oil (MLO), epoxidized linseed oil (ELO), epoxy-based styrene-acrylic oligomer (ESAO), and polystyrene-glycidyl methacrylate random copolymer (PS-GMA) in terms of: the storage modulus (E') measured at -100°C and 150 °C and the glass transition temperature (T_g).

Films	E' (MPa) at -100 °C	E' (MPa) at 100 °C	T_g (°C)*
PA1010	2183 ± 31	177 ± 3	66.0 ± 0.8
PA1010/PLA	2542 ± 35	59 ± 4	68.2 ± 1.0
PA1010/PLA + MLO	2501 ± 41	164 ± 3	62.7 ± 0.8
PA1010/PLA + ELO	2410 ± 30	167 ± 4	58.9 ± 0.9
PA1010/PLA + ESAO	2414 ± 27	134 ± 5	65.7 ± 1.1
PA1010/PLA + PS-GMA	2041 ± 29	156 ± 4	64.6 ± 0.9

* The Tg was measured as the peak temperature of the α-relaxation process related to PA1010 thorough the dynamic damping factor plots.

Colour measurement and visual appearance of PA1010/PLA blends

Colour and transparency are essential factors to be considered for food packaging, as they can influence consumer perception. **Figure III.3.4.8** shows the visual aspect of the developed PA1010/PLA blend films melt-processed with different compatibilizers. Initially, the addition of 20 wt% to PA1010 did not change remarkably the transparency. Some improvements in the film quality can be observed due to the disappearance of flow lines derived from PA1010 crystallization during extrusion. As one can also see, all the developed films showed high contact transparency. The biopolymer blend films were relatively transparent due to the low crystalline nature of the base polymers in the blend [60]. Some compatibilizers, namely MLO and PS-GMA, led to an increased opacity. From and end-use point of view, prevention of light penetration, especially in the ultraviolet (UV) region, could help in reducing the photo-oxidation processes of the organic compounds contained in packed food. This reduction in transparency after the addition of these compatibilizers produces films with UV-block capacity with significant potential for uses in the food packaging industry [61].
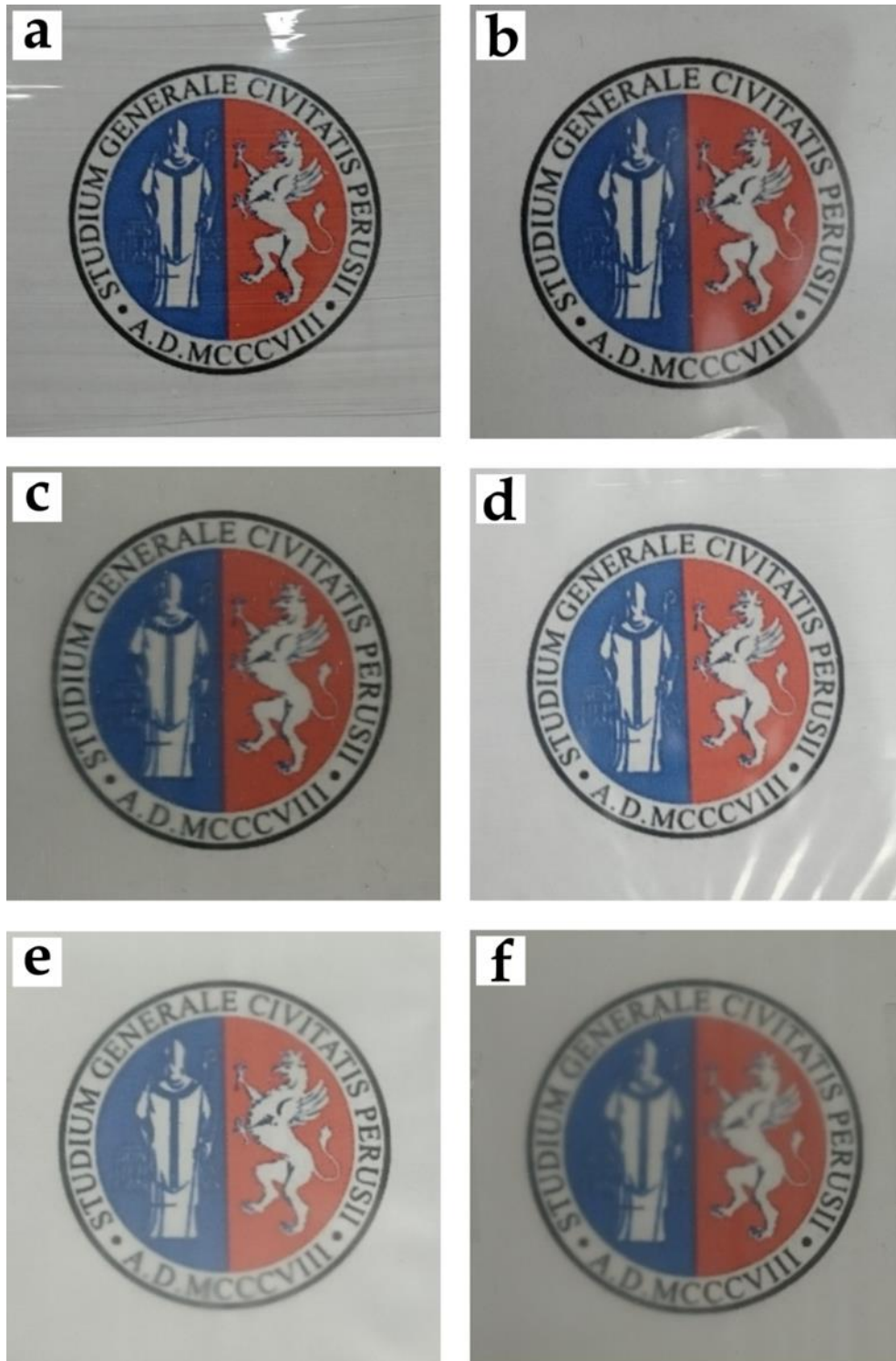
Figure III.3.4.8. Visual appearance and contact transparency of films of: a) Polyamide 1010 (PA1010); b) PA1010/polylactide (PLA); c) PA1010/PLA + epoxidized linseed oil (MLO)d) PA1010/PLA + epoxidized linseed oil (ELO); e) PA1010/PLA + epoxy-based styrene–acrylic oligomer (ESAO); f) polystyrene-glycidyl methacrylate random copolymer (PS-GMA).

In addition to the visual inspection, the color coordinates were measured. **Table III.3.4.6** gathers information about transparency, $L*a*b*$ coordinates, and color change

(*ΔE**) for all the developed films with PA1010 and PLA with and without compatibilizers. The addition of PLA to PA1010 did not yield a significant change in the color coordinates, but transparency was reduced from 294 to 175. The ELO-compatibilized films maintained the same transparency compared to the uncompatibilized PA1010/PLA film (see **Table III.3.4.6** with then lowest *ΔE** values). Nevertheless, all the other three compatibilizers showed an apparent decrease in transparency with values of 140, 77, and 70 for the MLO, PS-GMA and ESAO compatibilized biopolymer blend films, respectively.

Table III.3.4.6. Transparency and color parameters (*L*a*b**, and *ΔE**) of the polyamide 1010 (PA1010)/polylactide (PLA) blend films compatibilized with maleinized linseed oil (MLO), epoxidized linseed oil (ELO), epoxy-based styrene-acrylic oligomer (ESAO), and polystyrene-glycidyl methacrylate random copolymer (PS-GMA).

Films	Gloss	L*	a*	b*	ΔE_{ab}^{*}
PA1010	G294	99.32 ± 0.31	-0.16 ± 0.03	0.50 ± 0.06	-
PA1010/PLA	G175	99.26 ± 0.20	-0.17 ± 0.04	0.38 ± 0.05	0.13± 0.02
PA1010/PLA + MLO	G140	98.41 ± 0.23	-0.74 ± 0.02	3.91 ± 0.04	3.58± 0.08
PA1010/PLA + ELO	G207	98.99 ± 0.29	-0.20 ± 0.02	0.61 ± 0.03	0.35± 0.04
PA1010/PLA + ESAO	G70	98.21 ± 0.18	-0.41 ± 0.04	2.19 ± 0.04	2.04± 0.06
PA1010/PLA + PS-GMA	G77	98.84 ± 0.21	-0.44 ± 0.03	1.72 ± 0.06	1.34± 0.08

Regarding color coordinates, it is important to remark that the *a** coordinate (green to red) changed slightly to negative values (to the green) while the *b** coordinate (blue to yellow) changed remarkably to negative values towards positive values (to the yellow), in particular for the MLO-compatibilized films [62]. These differences could be attributable to the natural color of the used additives [63]. Thus, as it has been above-mentioned regarding the visual inspection, addition of PLA and, in particular, addition of some compatibilizers led to an increased opacity and yellowing, which could be an essential restriction for applications that require extremely high transparency, but, as opposite, this same phenomenon could represent an important advantage for some applications. For example, this optical property could be desirable for some packaging materials to enhance food protection against UV light, which could cause lipid oxidation if packed food [64].

Oxygen transmission rate of PA1010/PLA films

One of the most critical issues related to using polymer materials in the packaging industry is the oxygen permeation. This can be easily assessed from OTR tests. This property is, sometimes, a common quality control to assess the oxygen barrier properties or to assess the potential of a polymer for packaging in controlled atmosphere conditions. **Figure III.3.4.9** shows the oxygen barrier properties of PA1010/PLA blend films with different compatibilizers. Neat PA1010 showed a stabilized OTR value of 17 cm^3 mm m^{-2} day^{-1}. This is a low value if compared to other

PAs, such as PA6 that shows an OTR value of 55 cm³ mm m⁻² day⁻¹ [65], which can broaden the potential use of the herein developed materials in the packaging industry.
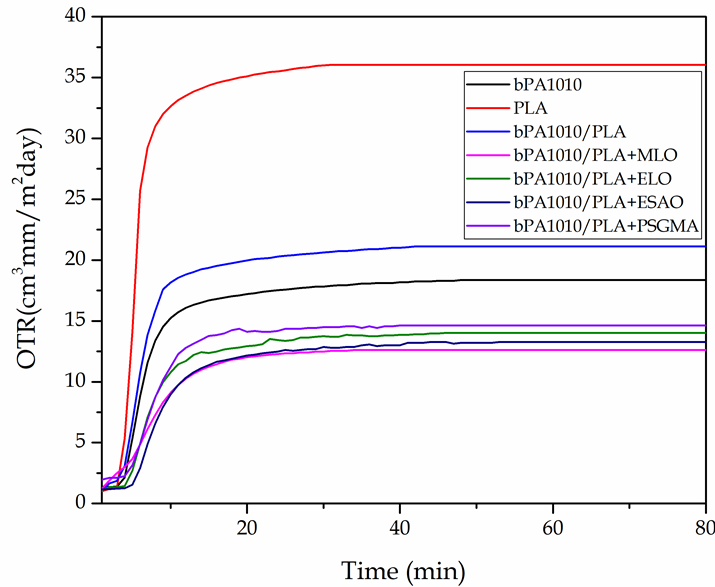
Figure III.3.4.9. Oxygen transmission rate (OTR) curves of the polyamide 1010 (PA1010)/polylactide (PLA) blend films compatibilized with maleinized linseed oil (MLO), epoxidized linseed oil (ELO), epoxy-based styrene-acrylic oligomer (ESAO), and polystyrene-glycidyl methacrylate random copolymer (PS-GMA) as a function of time.

On the other hand, it is crucial to bear in mind that PLA also offers good oxygen permeability with values about 35 cm³ mm m⁻² day⁻¹. Arrieta *et al*. [66] reported an OTR value of 30.5 mm m⁻² day⁻¹ for PLA thus, corroborating this balanced oxygen barrier properties. As expected, the addition of 20 wt% PLA into the PA1010 matrix led to an increase in OTR of about 20 cm³ mm m⁻² day⁻¹. This increase is related to the poor miscibility between these two biopolymers as corroborated through this research work. All four compatibilizers interestingly provided lower OTR values of 14.6, 14, and 13.3 cm³ mm m⁻² day⁻¹ for the PS-GMA, ELO, and ESAO compatibilized films, respectively. Therefore, all four compatibilizers exerted a positive effect on the barrier properties against oxygen. It is worthy to note that the lowest OTR value was obtained for the MLO-compatibilized films with an OTR value of 12.6 cm³ mm m⁻² day⁻¹. This could be related to a remarkable improvement in the interfacial adhesion between PA1010 and PLA (see morphology of films). Other authors have reported that using plasticizers on individual polymers can increase the free volume and, subsequently, increase the oxygen permeability [67]. Nevertheless, these compatibilizers successfully improved the barrier properties to the blend, probably due to improved interactions between these two polymers. According to this, Arrieta *et al.* [66] showed that the addition of cellulose nanocrystals (CNCs) into a PLA/PHB blend gave improved barrier properties due to improved interactions between both polymers thorough CNCs. The low OTR values obtained for PA1010/PLA films indicate these materials can be candidates for the packaging industry. In fact, the obtained OTR results are impressive if compared with

conventional packaging materials such as PET or LDPE with OTR values of 3 and 160 cm^3 mm m^{-2} day^{-1}, respectively. For these reasons, the obtained materials offer exciting properties for the industrial application in the food packaging sector [68].

CONCLUSIONS

This study reports the potential of reactive extrusion to compatibilize binary blends with engineering properties from the fully bio-based polymers PA1010 and PLA. A 20 wt% PLA was kept constant in the biopolymer blend formulations, and four different compatibilizers were tested. Two vegetable oil derived compatibilizers from linseed oil, namely MLO and ELO, which gave improved elongation at break and toughness, and two GMA-based additives, namely ESAO (Joncryl® ADR 4300) and PS-GMA (Xibond™ 920), which also provided excellent balanced properties. These materials were manufactured by cast film and injection molding, and the morphology was similar in both types of materials. Phase separation occurred, and it was more pronounced on the injection-molded materials.

Nevertheless, the vegetable oil derived compatibilizers provided a remarkable increase in elongation and toughness, and, mainly, ELO delivered an improved tensile strength. Besides, the addition of ELO produced high transparent films. Regarding the use of GMA-based additives, as well as MLO, resulted in films with improved tensile strength with a slight increase in opacity that could be helpful to protect food against UV light. Regarding the oxygen permeability, all four compatibilizers decreased OTR values compared to neat PA1010 and the uncompatibilized PA1010/PLA blend, thus giving evidence of the usefulness of all four compatibilizers to manufacture highly environmentally friendly films for the packaging industry without compromising the engineering properties. Depending on the final application, each compatibilizer could yield tailored properties.

Acknowledgments

REFERENCES

1. Quiles-Carrillo, L., N. Montanes, D. Garcia-Garcia, A. Carbonell-Verdu, R. Balart and S. Torres-Giner, *Effect of different compatibilizers on injection-molded green composite pieces based on polylactide filled with almond shell flour.* Composites Part B: Engineering, 2018. **147**: 76-85.
2. Battegazzore, D., A. Sattin, M.L. Maspoch and A. Frache, *Mechanical and Barrier Properties Enhancement in Film Extruded Bio-Polyamides With Modified Nanoclay.* Polymer Composites, 2018.
3. Jasinska, L., M. Villani, J. Wu, D. van Es, E. Klop, S. Rastogi and C.E. Koning, *Novel, Fully Biobased Semicrystalline Polyamides.* Macromolecules, 2011. **44**(9): 3458-3466.

4. Yasuda, M. and A. Miyabo, *Polyamide derived from castor oil.* Journal of Fiber Science and Technology, 2010. **66**(4): P137-P142.

5. Mutlu, H. and M.A. Meier, *Castor oil as a renewable resource for the chemical industry.* European Journal of Lipid Science and Technology, 2010. **112**(1): 10-30.

6. Kausar, A., *Polyamide 1010/polythioamide blend reinforced with graphene nanoplatelet for automotive part application.* Advances in Materials Science, 2017. **17**(3): 24-36.

7. Quiles-Carrillo, L., N. Montanes, T. Boronat, R. Balart and S. Torres-Giner, *Evaluation of the engineering performance of different bio-based aliphatic homopolyamide tubes prepared by profile extrusion.* Polymer Testing, 2017. **61**: 421-429.

8. Lagaron, J.M., E. Gimenez, R. Catala and R. Gavara, *Mechanisms of Moisture Sorption in Barrier Polymers Used in Food Packaging: Amorphous Polyamide vs. High-Barrier Ethylene-Vinyl Alcohol Copolymer Studied by Vibrational Spectroscopy.* Macromolecular Chemistry and Physics, 2003. **204**(4): 704-713.

9. Fenni, S., O. Monticelli, L. Conzatti, R. Doufnoune, P. Stagnaro, N. Haddaoui and D. Cavallo, *Correlating the morphology of poly (L-lactide)/poly (butylene succinate)/graphene oxide blends nanocomposites with their crystallization behavior.* Express Polymer Letters, 2018. **12**(1).

10. Haque, M.M.-U., D. Puglia, E. Fortunati and M. Pracella, *Effect of reactive functionalization on properties and degradability of poly (lactic acid)/poly (vinyl acetate) nanocomposites with cellulose nanocrystals.* Reactive and Functional Polymers, 2017. **110**: 1-9.

11. Rocha-Hoyos, J., E. Llanes-Cedeño, D. Peralta-Zurita and M. Pucha-Tambo, *Mechanical Flexural Characterization of Composite Materials with Photopolymer Matrix Reinforced with Abaca and Cabuya Fibers Using 3D Printing.* INGENIUS, 2019. **22**.

12. Tyler, B., D. Gullotti, A. Mangraviti, T. Utsuki and H. Brem, *Polylactic acid (PLA) controlled delivery carriers for biomedical applications.* Advanced Drug Delivery Reviews, 2016. **107**: 163-175.

13. Nagarajan, V., A.K. Mohanty and M. Misra, *Perspective on polylactic acid (PLA) based sustainable materials for durable applications: Focus on toughness and heat resistance.* ACS Sustainable Chemistry & Engineering, 2016. **4**(6): 2899-2916.

14. Vasile, C., et al., *New PLA/ZnO: Cu/Ag bionanocomposites for food packaging.* eXPRESS Polymer Letters, 2017. **11**(7).

15. Van Wouwe, P., M. Dusselier, E. Vanleeuw and B. Sels, *Lactide synthesis and chirality control for polylactic acid production.* ChemSusChem, 2016. **9**(9): 907-921.

16. Nampoothiri, K.M., N.R. Nair and R.P. John, *An overview of the recent developments in polylactide (PLA) research.* Bioresource technology, 2010. **101**(22): 8493-8501.

17. Hayat, K., S. Hussain, S. Abbas, U. Farooq, B. Ding, S. Xia, C. Jia, X. Zhang and W. Xia, *Optimized microwave-assisted extraction of phenolic acids from citrus mandarin peels and evaluation of antioxidant activity in vitro.* Separation and Purification Technology, 2009. **70**(1): 63-70.

18. Castro-Aguirre, E., F. Iñiguez-Franco, H. Samsudin, X. Fang and R. Auras, *Poly (lactic acid)—Mass production, processing, industrial applications, and end of life.* Advanced drug delivery reviews, 2016. **107**: 333-366.

19. Mazinani, S., S. Darvishmanesh, R. Ramazani and B. Van der Bruggen, *Miscibility of polyimide blends: Physicochemical characterization of two high performance polyimide polymers.* Reactive and Functional Polymers, 2017. **111**: 88-101.

20. Muthuraj, R., M. Misra and A.K. Mohanty, *Biodegradable compatibilized polymer blends for packaging applications: A literature review.* Journal of Applied Polymer Science, 2017: 45726-n/a.

21. Wu, D., Y. Zhang, L. Yuan, M. Zhang and W. Zhou, *Viscoelastic interfacial properties of compatibilized poly(ε-caprolactone)/polylactide blend.* Journal of Polymer Science Part B: Polymer Physics, 2010. **48**(7): 756-765.

22. Zeng, J.-B., K.-A. Li and A.-K. Du, *Compatibilization strategies in poly(lactic acid)-based blends.* RSC Advances, 2015. **5**(41): 32546-32565.

23. Quiles-Carrillo, L., N. Montanes, C. Sammon, R. Balart and S. Torres-Giner, *Compatibilization of highly sustainable polylactide/almond shell flour composites by reactive extrusion with maleinized linseed oil.* Industrial Crops and Products, 2018. **111**: 878-888.

24. Carbonell-Verdu, A., D. Garcia-Garcia, F. Dominici, L. Torre, L. Sanchez-Nacher and R. Balart, *PLA films with improved flexibility properties by using maleinized cottonseed oil.* European Polymer Journal, 2017. **91**: 248-259.

25. Liu, W., J. Qiu, M. Fei, R. Qiu, E. Sakai and M. Zhang, *Balancing performance of epoxidized soybean oil (ESO)/poly (lactic acid) composites: Synergistic effects of carbon nanotubes and tannic acid-induced crosslinking of ESO.* Express Polymer Letters, 2019. **13**(2): 109.

26. Samper, M.-D., J.M. Ferri, A. Carbonell-Verdu, R. Balart and O. Fenollar, *Properties of biobased epoxy resins from epoxidized linseed oil (ELO) crosslinked with a mixture of cyclic anhydride and maleinized linseed oil.* eXPRESS Polymer Letters, 2019. **13**(5): 407-418.

27. Liminana, P., D. Garcia-Sanoguera, L. Quiles-Carrillo, R. Balart and N. Montanes, *Development and characterization of environmentally friendly composites from poly (butylene succinate)(PBS) and almond shell flour with different compatibilizers.* Composites Part B: Engineering, 2018. **144**: 153-162.

28. Ferri, J.M., D. Garcia-Garcia, N. Montanes, O. Fenollar and R. Balart, *The effect of maleinized linseed oil as biobased plasticizer in poly (lactic acid)-based formulations.* Polymer International, 2017. **66**(6): 882-891.

29. Garcia-Campo, M., L. Quiles-Carrillo, J. Masia, M. Reig-Pérez, N. Montanes and R. Balart, *Environmentally friendly compatibilizers from soybean oil for ternary blends of poly (lactic acid)-PLA, poly (ε-caprolactone)-PCL and poly (3-hydroxybutyrate)-PHB.* Materials, 2017. **10**(11): 1339.

30. Quiles-Carrillo, L., N. Montanes, J. Lagaron, R. Balart and S. Torres-Giner, *In situ compatibilization of biopolymer ternary blends by reactive extrusion with low-functionality epoxy-based styrene–acrylic oligomer.* Journal of Polymers and the Environment, 2019. **27**(1): 84-96.

31. Ojijo, V. and S.S. Ray, *Super toughened biodegradable polylactide blends with non-linear copolymer interfacial architecture obtained via facile in-situ reactive compatibilization.* Polymer, 2015. **80**(Supplement C): 1-17.

32. Garcia-Garcia, D., J.M. Ferri, T. Boronat, J. Lopez-Martinez and R. Balart, *Processing and characterization of binary poly(hydroxybutyrate) (PHB) and poly(caprolactone) (PCL) blends with improved impact properties.* Polymer Bulletin, 2016. **73**(12): 3333-3350.

33. Ferri, J.M., M.D. Samper, D. Garcia-Sanoguera, M.J. Reig, O. Fenollar and R. Balart, *Plasticizing effect of biobased epoxidized fatty acid esters on mechanical and thermal properties of poly(lactic acid).* Journal of Materials Science, 2016. **51**(11): 5356-5366.

34. Yan, M. and H. Yang, *Improvement of polyamide 1010 with silica nanospheres via in situ melt polycondensation.* Polymer Composites, 2012. **33**(10): 1770-1776.

35. Arrieta, M.P., M.D. Samper, J. López and A. Jiménez, *Combined effect of poly (hydroxybutyrate) and plasticizers on polylactic acid properties for film intended for food packaging.* Journal of Polymers and the Environment, 2014. **22**(4): 460-470.

36. Pisello, A.L., E. Fortunati, C. Fabiani, S. Mattioli, F. Dominici, L. Torre, L.F. Cabeza and F. Cotana, *PCM for improving polyurethane-based cool roof membranes durability.* Solar Energy Materials and Solar Cells, 2017. **160**: 34-42.

37. Rashmi, B.J., K. Prashantha, M.-F. Lacrampe and P. Krawczak. *Toughening of poly (lactic acid) without sacrificing stiffness and strength by melt-blending with polyamide 11 and selective localization of halloysite nanotubes.* in *AIP Conference Proceedings.* 2016. AIP Publishing.

38. Ferri, J., M. Samper, D. García-Sanoguera, M. Reig, O. Fenollar and R. Balart, *Plasticizing effect of biobased epoxidized fatty acid esters on mechanical and thermal properties of poly (lactic acid).* Journal of materials science, 2016. **51**(11): 5356-5366.

39. Xiong, Z., Y. Yang, J. Feng, X. Zhang, C. Zhang, Z. Tang and J. Zhu, *Preparation and characterization of poly (lactic acid)/starch composites toughened with epoxidized soybean oil.* Carbohydrate polymers, 2013. **92**(1): 810-816.

40. Rasselet, D., A.-S. Caro-Bretelle, A. Taguet and J.-M. Lopez-Cuesta, *Reactive Compatibilization of PLA/PA11 Blends and Their Application in Additive Manufacturing.* Materials, 2019. **12**(3): 485.

41. Lascano, D., L. Quiles-Carrillo, R. Balart, T. Boronat and N. Montanes, *Toughened Poly (Lactic Acid) — PLA Formulations by Binary Blends with Poly (Butylene Succinate-co-Adipate) — PBSA and Their Shape Memory Behaviour.* Materials, 2019. **12**(4): 622.

42. Nagarajan, V., A.K. Mohanty and M. Misratt, *Perspective on Polylactic Acid (PLA) based Sustainable Materials for Durable Applications: Focus on Toughness and Heat Resistance.* Acs Sustainable Chemistry & Engineering, 2016. **4**(6): 2899-2916.

43. Garcia-Campo, M.J., L. Quiles-Carrillo, J. Masia, M.J. Reig-Perez, N. Montanes and R. Balart, *Environmentally Friendly Compatibilizers from Soybean Oil for Ternary Blends of Poly(lactic acid)-PLA, Poly(epsilon-caprolactone)-PCL and Poly(3-hydroxybutyrate)-PHB.* Materials, 2017. **10**(11): 19.

44. Ferri, J.M., D. Garcia-Garcia, L. Sanchez-Nacher, O. Fenollar and R. Balart, *The effect of maleinized linseed oil (MLO) on mechanical performance of poly(lactic acid)-thermoplastic starch (PLA-TPS) blends.* Carbohydrate Polymers, 2016. **147**: 60-68.

45. Lin, X.T., Q.R. Qian, L.R. Xiao, Q.H. Chen, Q.L. Huang and H.J. Zhang, *Influence of Reactive Compatibilizer on the Morphology, Rheological, and Mechanical Properties of Recycled Poly(Ethylene Terephthalate)/Polyamide 6 Blends.* Journal of Macromolecular Science Part B-Physics, 2014. **53**(9): 1543-1552.

46. Liu, Y.J., Z.Z. Su, W.H. Guo, B.Y. Li and C.F. Wu, *Reactive Compatibilization and Properties of Recycled Poly(ethylene terephthalate)/Poly(ethylene-octene) Blends.* Journal of Macromolecular Science Part B-Physics, 2010. **49**(4): 615-628.

47. Wei, Q., D. Chionna and M. Pracella, *Reactive compatibilization of PA6/LDPE blends with glycidyl methacrylate functionalized polyolefins.* Macromolecular Chemistry and Physics, 2005. **206**(7): 777-786.

48. Walha, F., K. Lamnawar, A. Maazouz and M. Jaziri, *Biosourced blends based on poly (lactic acid) and polyamide 11: Structure-properties relationships and enhancement of film blowing processability.* Advances in Polymer Technology, 2018. **37**(6): 2061-2074.

49. Rasselet, D., A.S. Caro-Bretelle, A. Taguet and J.M. Lopez-Cuesta, *Reactive Compatibilization of PLA/PA11 Blends and Their Application in Additive Manufacturing.* Materials, 2019. **12**(3): 18.

50. Logakis, E., C. Pandis, V. Peoglos, P. Pissis, C. Stergiou, J. Pionteck, P. Pötschke, M. Mičušík and M. Omastová, *Structure–property relationships in polyamide 6/multi-walled carbon nanotubes nanocomposites.* Journal of Polymer Science Part B: Polymer Physics, 2009. **47**(8): 764-774.

51. Carbonell-Verdu, A., J. Ferri, F. Dominici, T. Boronat, L. Sanchez-Nacher, R. Balart and L. Torre, *Manufacturing and compatibilization of PLA/PBAT binary blends by cottonseed oil-based derivatives.* Express Polymer Letters, 2018. **12**(9): 808-823.

52. Huang, Y.Q., Y.X. Liu and C.H. Zhao, *Morphology and properties of PET/PA-6/E-44 blends.* Journal of Applied Polymer Science, 1998. **69**(8): 1505-1515.

53. Najafi, N., M. Heuzey and P. Carreau, *Polylactide (PLA)-clay nanocomposites prepared by melt compounding in the presence of a chain extender.* Composites Science and Technology, 2012. **72**(5): 608-615.

54. Yang, J., W. Dong, Y. Luan, J. Liu, S. Liu, X. Guo, X. Zhao and W. Su, *Crystallization and crosslinking of polyamide-1010 under elevated pressure.* Journal of applied polymer science, 2002. **83**(12): 2522-2527.

55. Abdelwahab, M.A., S. Taylor, M. Misra and A.K. Mohanty, *Thermo-mechanical characterization of bioblends from polylactide and poly (butylene adipate-co-terephthalate) and lignin.* Macromolecular Materials and Engineering, 2015. **300**(3): 299-311.

56. Duangphet, S., D. Szegda, J. Song and K. Tarverdi, *The effect of chain extender on poly (3-hydroxybutyrate-co-3-hydroxyvalerate): Thermal degradation, crystallization, and rheological behaviours.* Journal of Polymers and the Environment, 2014. **22**(1): 1-8.

57. Choi, K.M., M.C. Choi, D.H. Han, T.S. Park and C.S. Ha, *Plasticization of poly(lactic acid) (PLA) through chemical grafting of poly(ethylene glycol) (PEG) via in situ reactive blending.* European Polymer Journal, 2013. **49**(8): 2356-2364.

58. Garcia-Garcia, D., J.M. Ferri, N. Montanes, J. Lopez-Martinez and R. Balart, *Plasticization effects of epoxidized vegetable oils on mechanical properties of poly(3-hydroxybutyrate).* Polymer International, 2016. **65**(10): 1157-1164.

59. Arruda, L.C., M. Magaton, R.E.S. Bretas and M.M. Ueki, *Influence of chain extender on mechanical, thermal and morphological properties of blown films of PLA/PBAT blends.* Polymer Testing, 2015. **43**: 27-37.

60. Liu, Z. and D. Yan, *Non-isothermal crystallization kinetics of polyamide 1010/montmorillonite nanocomposite.* Polymer Engineering & Science, 2004. **44**(5): 861-867.

61. Lasprilla-Botero, J., S. Torres-Giner, M. Pardo-Figuerez, M. Álvarez-Láinez and J. M Lagaron, *Superhydrophobic bilayer coating based on annealed electrospun ultrathin poly (ε-caprolactone) fibers and electrosprayed nanostructured silica microparticles for easy emptying packaging applications.* Coatings, 2018. **8**(5): 173.

62. Fenollar, O., D. García, L. Sánchez, J. López and R. Balart, *Optimization of the curing conditions of PVC plastisols based on the use of an epoxidized fatty acid ester plasticizer.* European Polymer Journal, 2009. **45**(9): 2674-2684.

63. Ramos, M., A. Jiménez, M. Peltzer and M.C. Garrigós, *Development of novel nano-biocomposite antioxidant films based on poly (lactic acid) and thymol for active packaging.* Food chemistry, 2014. **162**: 149-155.

64. Melendez-Rodriguez, B., K.J. Figueroa-Lopez, A. Bernardos, R. Martínez-Máñez, L. Cabedo, S. Torres-Giner and J.M. Lagaron, *Electrospun Antimicrobial Films of Poly (3-hydroxybutyrate-co-3-hydroxyvalerate) Containing Eugenol Essential Oil Encapsulated in Mesoporous Silica Nanoparticles.* Nanomaterials, 2019. **9**(2): 227.

65. Pereira, D., P.P. Losada, I. Angulo, W. Greaves and J.M. Cruz, *Development of a polyamide nanocomposite for food industry: morphological structure, processing, and properties.* Polymer Composites, 2009. **30**(4): 436-444.

66. Arrieta, M.P., E. Fortunati, F. Dominici, J. López and J.M. Kenny, *Bionanocomposite films based on plasticized PLA–PHB/cellulose nanocrystal blends.* Carbohydrate polymers, 2015. **121**: 265-275.

67. Martino, V.P., A. Jiménez and R.A. Ruseckaite, *Processing and characterization of poly (lactic acid) films plasticized with commercial adipates.* Journal of Applied Polymer Science, 2009. **112**(4): 2010-2018.

68. Burgos, N., V.P. Martino and A. Jiménez, *Characterization and ageing study of poly (lactic acid) films plasticized with oligomeric lactic acid.* Polymer degradation and stability, 2013. **98**(2): 651-658.

III. RESULTS & DISCUSSION
RESULTS & DISCUSSION

BLOCK IV

III.4. USES AND APPLICATIONS OF NEW ENVITONMENTALLY FRIENDLY PARTIALLY OR FULLY BIOBASED POLYAMIDES.

III.4.1. Optimization of microwave-assisted extraction of phenolic compounds with antioxidant activity from carob pods

L. Quiles-Carrillo [1], C. Mellinas [2], M.C. Garrigos [2], R.Balart [1] and S. Torres-Giner [3],

[1] Technological Institute of Materials (ITM), Universitat Politècnica de València (UPV), Plaza Ferrándiz y Carbonell 1, 03801 Alcoy, Spain;

[2] Analytical Chemistry, Nutrition and Food Sciencies Department, University of Alicante, P.O. Box 99, E-03080, Alicante, Spain;

[2] Novel Materials and Nanotechnology Group, Institute of Agrochemistry and Food Technology (IATA), Spanish National Research Council (CSIC), Calle Catedrático Agustín Escardino Benlloch 7, 46980 Paterna, Valencia, Spain

Optimization of Microwave-Assisted Extraction of Phenolic Compounds with Antioxidant Activity from Carob Pods

L. Quiles-Carrillo[1] · C. Mellinas[2] · M. C. Garrigos[2] · R. Balart[1] · S. Torres-Giner[3]

Abstract

A microwave-assisted extraction (MAE) procedure to obtain phenolic compounds from carob bark was optimized by using response surface methodology. A four-factor, three-level Box–Behnken design with five central points was used to evaluate the influence of temperature, solid-liquid ratio, ethanol concentration, and time in carob bark extraction in terms of antioxidant activity (DPPH) and total extraction yield. Optimal extraction conditions were found using 80 °C, 35% (v/v) ethanol, a ratio of 35 mL/g, and 29.5 min. Total phenolics content (TPC), antioxidant activity (DPPH, FRAP, ABTS), carbohydrate content, and main polyphenols composition (HPLC) were determined at optimal conditions. An experimental total yield of 66.5% was obtained with a TPC value of 33.6 mg GAE/g DW and polysaccharides content of 345.4 mg glucose/g DW. A high antioxidant activity was also shown by the three methods tested. The results showed the potential of carob pods skin as a natural source of phenolic compounds, in particular gallic acid, and the effectiveness of MAE as extraction technique for the revalorization of this agro-food waste.

Keywords Microwave-assisted extraction · Antioxidant activity · Carob pods · Gallic acid · Phenolic compounds · Box–Behnken design

Introduction

Currently, the packaging sector is requesting the use of polymer materials of renewable origin due to the great awareness of existing environmental problems. Therefore, the number of both natural and recyclable biopolymer materials that are suitable for their use in the packaging sector is gaining a greater relevance (Kumar et al. 2017; TĂNASE et al. 2016; Tang et al. 2012). This type of biopolymers is intended to be combined with active ingredients that may have antioxidant effect for the development of active packaging systems to improve the shelf-life of foods (Arrieta et al. 2017). It is also aimed that these compounds could be obtained from agro-food waste (Di Donato et al. 2017; Manousaki et al. 2016), with the aim of increasing the added value of industrial by-products and reducing the total price of the final packaging system. Antioxidants obtained from agro-food waste could greatly enhance the preservation of packaged food in a remarkable way increasing the benefits of this type of products. In this sense, the carob tree fruit is a characteristic product of the Mediterranean area that is currently discarded which is known to have good antioxidant properties, being its valorization very interesting (Kumazawa et al. 2002).

Carob tree (*Ceratonia siliqua* L.) is one of the most useful native Mediterranean trees. In producing countries, carob pods have been traditionally used as human and animal food, but currently, their main use is related to the extraction of rubber from their seeds (Owis and El-Naggar 2016). Carob trees grow around the Mediterranean basin and countries such as Portugal, Spain, Italy, Greece, Turkey, and Morocco and several regions of North America. In 2010, world carob production was 163 kt, a considerably low amount due to the fact that it is an abandoned plantation. In 2011, the production was doubled reaching 310 kt worldwide, with Spain being the main producer of carob with 135 kt, followed by Italy, Portugal, and Morocco (Vourdoubas and Skoulou 2017).

✉ L. Quiles-Carrillo
   luiquic1@epsa.upv.es

[1] Instituto de Tecnología de Materiales (ITM), Universitat Politècnica de València, Plaza Ferrándiz y Carbonell s/n, Alcoy (Alicante), Spain

[2] Analytical Chemistry, Nutrition and Food Sciences Department, University of Alicante, P.O. Box 99, E-03080 Alicante, Spain

[3] Novel Materials and Nanotechnology Group, Institute of Agrochemistry and Food Technology (IATA), Spanish Council for Scientific Research (CSIC), Calle Catedrático Agustín Escardino Benlloch 7, 46980 Paterna, Spain

Ⓢ Springer

Optimization of microwave-assisted extraction of phenolic compounds with antioxidant activity from carob pods

Abstract.

A microwave-assisted extraction (MAE) procedure to obtain phenolic compounds from carob bark was optimized by using response surface methodology. A four-factor, three-level Box-Behnken design with five central points was used to evaluate the influence of temperature, solid-liquid ratio, ethanol concentration and time in carob bark extraction in terms of antioxidant activity (DPPH) and total extraction yield. Optimal extraction conditions were found using 80 °C, 35% (v/v) ethanol, a ratio of 35 mL/g and 29.5 min. Total phenolics content (TPC), antioxidant activity (DPPH, FRAP, ABTS), carbohydrates content and main polyphenols composition (HPLC) were determined at optimal conditions. An experimental total yield of 66.5% was obtained with a TPC value of 33.6 mg GAE/g DW and polysaccharides content of 345.4 mg glucose/g DW. A high antioxidant activity was also shown by the three methods tested. The results showed the potential of carob pods skin as a natural source of phenolic compounds, in particular gallic acid, and the effectiveness of MAE as extraction technique for the revalorization of this agro-food waste.

INTRODUCTION

Currently, the packaging sector is requesting the use of polymer materials of renewable origin due to the great awareness of existing environmental problems. Therefore, the number of both natural and recyclable biopolymer materials that are suitable for their use in the packaging sector is gaining a greater relevance [1-3]. This type of biopolymers, are intended to be combined with active ingredients that may have antioxidant effect for the development of active packaging systems to improve the shelf-life of foods [4]. It is also aimed that these compounds could be obtained from agro-food waste [5, 6], with the aim of increasing the added value of industrial by-products and reducing the total price of the final packaging system. Antioxidants obtained from agro-food waste could greatly enhance the preservation of packaged food in a remarkable way increasing the benefits of this type of products. In this sense, the carob tree fruit is a characteristic product of the Mediterranean area that is currently discarded which is known to have good antioxidant properties, being its valorisation very interesting [7].

Carob tree (*Ceratonia siliqua L.*) is one of the most useful native Mediterranean trees. In producing countries, carob pods have been traditionally used as human and animal food, but currently their main use is related to the extraction of rubber from their seeds [8]. Carob trees grow around the Mediterranean basin and countries such as Portugal, Spain, Italy, Greece, Turkey, as well as Morocco and several regions of North America. In 2010, world carob production was 163 kt, a considerably low amount due to the fact that it is an abandoned plantation. In 2011, the production was doubled reaching 310 kt worldwide, with Spain being the main producer of carob with 135 kt, followed by Italy, Portugal, and Morocco [9].

Carob pods are characterized by their high content in water-soluble sugars (approximately 40-50%, mainly sucrose) and low content in proteins (3-4%) and lipids (0.4-0.8%). Carob pods also contain considerable amounts of polyphenols [10, 11], in particular gallic acid [11]. Polyphenols have a wide range of biological properties and, among them, the antioxidant activity is the best known, which can prevent oxidative damage of some biomolecules. Polyphenols have received much attention in recent years due to their ability to act as powerful antioxidants. Polyphenolic compounds are found in the tissues of plants and are important for their growth and development as they provide a defence mechanism against infections and injuries [12]. In addition, carob pod extracts have been reported to exhibit a very strong antimicrobial activity against several bacteria and fungi [13].

For the determination of the main polyphenols present in the carob pod and the evaluation of potential applications of these compounds, the optimization of the extraction process of phenolic compounds must be previously carried out [14]. For this purpose, microwave-assisted extraction (MAE) shows several advantages over conventional extraction techniques such as the reduction of solvent volume and energy consumption used for extraction, obtaining high recoveries and good reproducibility [15, 16]. Nowadays, this technique has been successfully used for the extraction of different food waste matrices such as peanut [17] and tangerine [18] skins and tomato [19], among other wastes with high added value.[20-22] Regarding the extraction of carob pods, some studies have analysed the antioxidant capacity of the obtained extracts but in very few cases MAE has been used [7, 23, 24].

The objective of the present study is to revalorize carob bark as a main source of polyphenols giving an added value to this waste. For this purpose, carob beans not suitable for consumption or sale were selected and the seeds were manually extracted and discarded, in order to use as residue only the bark part of the pod. In this work, the optimal MAE conditions to extract polyphenol compounds were determined by using response surface methodology in terms of total yield and antioxidant capacity (DPPH). Independent variables studied included temperature, time, liquid:solvent ratio, and ethanol concentration. Total phenolics (TPC) and carbohydrates content, antioxidant capacity by using FRAP, DPPH and ABTS methods, total yield and quantification of main polyphenols were also determined in the extracts obtained at optimal conditions.

MATERIALS AND METHODS

Raw material and chemical reagents

Carob pods were obtained from the European carob tree *Ceratonia Silicua* of the variety "*ramillete*", which is original of Alicante and Murcia regions (Spain). The obtained bark (**Figure III.4.1.1a**) was oven-dried for 48 h at 40 °C (MCP Vacuum Casting System, Lubeck, Germany). As a first step, carob bark was manually crushed and then introduced into a centrifugal mill (Maype, Manises, Spain). The obtained powder (Figure 1b) was oven-dried at 40 °C for 12 h and grinded in a Mill ZM 200 centrifugal mill (Retsch, Düsseldorf, Germany) at 12000 rpm. The milled sample was passed through a 0.25 mm sieve. This residue (**Figure III.4.1.1c**) was oven-dried again during 24 h at 40 °C.

Figure III.4.1.1. Carob pods (a) and grinding process to obtain carob flour (b and c).

Quercetin, sodium carbonate, Folin−Ciocalteu reagent (2 N), 2,2-diphenyl-1-picrylhydrazyl (DPPH), (±) 6-hydroxy-2,5,7,8-tetramethylchromane-2-carboxylic acid (Trolox), ethanol (96%), ethanol (absolute grade), methanol (HPLC grade), acetonitrile (HPLC grade), 2,2'azinobis(3-ethylbenzthiazoline)-6-sulfonic acid (ABTS), potassium persulfate, and calcium chloride were purchased from Sigma–Aldrich(Madrid, Spain).

Microwave-assisted extraction (MAE) of polyphenols: experimental design

Extraction of polyphenols was carried out by using a commercial microwaves oven (Milestone flexiWAVE, Shelton, Connecticut, USA). 2g of sample was introduced and the microwave agitator was set at 300 rpm during the extraction process. Response surface methodology (RSM) was used to determine the optimal extraction conditions of polyphenols from carob bark. A Box-Behnken design (BBD) was used to determine the effect of four variables which may affect phytochemical contents in plants [25]: extraction temperature, liquid:solid ratio, ethanol concentration and extraction time. **Table III.4.1.1** shows the selected variables and levels which were set according to experimental limitations and related bibliography [26]. This design consisted of 29 experiments including five central points to estimate the model's pure error. All experiments were carried out in random order and were performed once. The responses obtained from the experimental design were evaluated in terms of overall yield and antioxidant activity (DPPH method).

Table III.4.1.1. Independent variables and selected levels used in the BBD for polyphenols extraction from carob bark.

Factors	-1	0	+1
Temperature (ºC)	60	70	80
Ratio (mL/g)	25	35	45
Concentration (%)	35	60	85
Time (min)	5.0	17.5	30.0

After extraction, extracts were centrifuged at 5300 rpm and 4 ºC (Digicen 21, Ortoalresa, Ajalvir, Spain) for 15 min to separate the remaining solid residues from the extraction. The supernatant obtained from the centrifugation process was oven-dried (J.P Selecta S.A, Spain) at 40 °C for 24 h and then re-dissolved in 20 mL ethanol 50% (v/v) and frozen at -20 ºC until analysis was performed. Due to some precipitation after this preservation process, samples were centrifuged again at 5300 rpm and 4 ºC for 15 minutes before analysis to separate any precipitated solid residues.

A multiple linear regression analysis was performed to obtain the regression coefficients following a second-order polynomial model (**Equation III.4.1.1**):

$$Y = \beta_0 + \sum \beta_i X_i + \sum \beta_{ii} X_i^2 + \sum \sum \beta_{ij} X_i X_j \qquad \textbf{Equation III.4.1.1}$$

where Y is the predicted response, X represents the variables of the system, i and j are design variables, β_0 is a constant, β_i is the linear coefficient, β_{ii} is the quadratic coefficient, and β_{ij} is the interaction coefficient of variables i and j.

The extracts obtained at optimal conditions were also analysed to evaluate the antioxidant performance by FRAP and ABTS methods; total phenolics (TPC) and carbohydrates content. Main polyphenols present in carob extracts were also monitored by HPLC analysis.

Total extraction yield

The total yield after each extraction was determined as follows:

$$Extraction\ yield(\%) = \frac{W_{ext}}{W_0} \cdot 100 \qquad \textbf{Equation III.4.1.2}$$

where W_{ext} is the mass of the dried extract (g) and W_0 is the mass of dried carob bark used for extraction (g). Samples were weighed by means of an Atilon ATL-224-I analytical balance (Acculab, Bradford, England).

Determination of antioxidant capacity

DPPH assay

The 2,2-diphenyl-1-picrylhydrazyl (DPPH) assay was performed according to the methodology described by Sengul Uysal *et al*. [27]. A solution of DPPH 10^{-4} M was prepared by dissolving 0.0039 g of DPPH radical in 100 mL of absolute ethanol. This stock solution was daily prepared. 1 mL of the extract was mixed with 4 mL of DPPH ethanolic solution and kept in darkness conditions at room temperature for 30 min. The decrease in absorbance was determined at 517 nm using a Biomate-3 UV-VIS spectrophotometer (Thermospetronic, Mobile, AL, USA).

The antioxidant capacity of the extracts was expressed as percentage of DPPH inhibition by using the following **Equation III.4.1.3**:

$$I(\%) = \frac{A_0 - A_1}{A_0} \cdot 100 \qquad \textbf{Equation III.4.1.3}$$

where A_0 is the absorbance of the control and A_1 is the absorbance of the extract after 30 min.

FRAP assay

The ferric ion reducing antioxidant power (FRAP) was also determined as described by Sengul Uysal *et al*. [27]. The FRAP reagent was prepared freshly by mixing 300 mM acetate buffer (pH = 3.6), 10 mM/ TPTZ and 20 mM ferric chloride in a mixing ratio of 10:1:1 (v/v/v), respectively. Then, 2 mL of reagent and 200 µL of the sample solution were mixed and incubated at 30 °C for 30 min. The absorbance was then determined at 593 nm. Trolox was used as standard and the results were expressed as mg trolox equivalents per gram dry weight (mg TE/g DW). All samples were analysed in triplicate.

ABTS assay

The antioxidant capacity against 2,2'-azino-bis(3-ethylbenzothiazoline-6-sulphonic acid) (ABTS) was also measured according to the method described by S. Uysal *et al*. [27]. ABTS radical cation was produced directly by reacting 7 mM ABTS solution with 2.45 mM potassium persulfate and allowing the mixture to stand for 12–16 hours in darkness conditions at room temperature. Prior to the assay, the solution was diluted with ethanol to an absorbance of 0.700 ± 0.02 at 734 nm. 1 mL of extract was then added to 2 mL of ABTS solution and mixed at room temperature for 30 min.

The absorbance was determined at 734 nm. ABTS scavenging activity was also expressed as mg TE/g DW and measurements were carried out in triplicate.

Total phenolics content (TPC)

Total phenolics content was determined according to the Folin-Ciocalteu colorimetric assay following the method described by Meziani *et al*. [13]. 0.5 mL of extract was mixed with 0.9 mL of Folin-Ciocalteu reagent and 3.6 mL of sodium carbonate solution at a concentration of 75 g/L. The test tubes were stored in darkness conditions at room temperature for 30 min. Absorbance was determined at 765 nm and the total phenolics content of samples were expressed as milligrams of gallic acid equivalents per g dry weight (mg GAE/g DW). All samples were analysed in triplicate.

Phenol-sulfuric acid method

The basic principle of this method is that carbohydrates, when dehydrated by reaction with concentrated sulfuric acid, can produce furfural derivatives. The subsequent reaction between furfural derivatives and phenol results in a compound with a detectable colour. 2 mL of the carbohydrate solution (extract) was mixed with 1 mL of 5% aqueous solution (v/v) of phenol in a test tube. Subsequently, 5 mL of concentrated sulfuric acid were rapidly added to the mixture. After 10 min, the mixture was vortexed for 30 s and placed for 20 minutes in a water bath at room temperature for colour development. Then, absorbance at 490 nm was recorded. Reference solutions were identically prepared using a calibration curve between 40 and 180 ppm. The results were expressed in mg glucose/g DW.

Main polyphenols profile by HPLC analysis

Prior to the quantification of polyphenols, these were verified using an Agilent high-performance liquid chromatograph model 1100 Series trailer at the same time a variable wavelength UV-visible detector and analyser of ion trap mass spectrometer. The wavelength used was 280 nm and mass spectrometric detection was performed in the negative ionization mode (ESI). After passing through the flow cell of the diode array detector, the column eluate was split (1:10) and the sample was directed to an LCQ ion trap mass spectrometer fitted. Scan range was 50-900 m/z and scan rate, 1 scan/sec. The desolvation temperature was 350 °C. High spray voltage was set at 4500 V. Nitrogen was used as the dry gas at a flow rate of 10 mL/min.

The identification and quantification of main polyphenols present in carob bark extracts was carried out following the method proposed by SuJung *et al.* [28] with some modifications. 34 mg of dried carob extract was diluted with 50 mL of ultrapure miliQ water. The diluted solution (1:100 v/v) was analysed for polyphenols content using an Agilent 1260 infinity HPLC system coupled with DAD detector. A BRISA LC2 C18 column (250 mm x 4.6 mm x 5µm, Teknokroma) at 30 °C was used. The mobile phase consisted of two solvents: 0.1% acetic acid (A) and 100% acetonitrile (B). The gradient used was: 100% A (1 min) linearly decreasing to 60% A at 25 min (5 min). The flow rate was 0.5 mL/min and the injection volume was 20 µL. Quantification of polyphenols was based on retention times compared with corresponding standards (Sigma-Aldrich, Germany) and their verification were done with Agilent high-performance liquid chromatograph model 1100 Series trailer at the same time a variable wavelength UV-

visible detector and Analyzer of ion trap mass spectrometer (Agilent model 1100 Series LC/MSD Trap SL). Analysis was performed in triplicate and mean values were reported. Polyphenols content was calculated from mean peak areas using external calibration method and expressed as mg/g DW.

Statistical analysis

Analysis of variance (ANOVA) was carried out from experimental data and mean values were compared at confidence level of 95% ($p < 0.05$) using the Tukey test.

Statgraphics Centurion XVI (Statistical Graphics, Rockville, MD, USA) was used to generate and analyse the results of the BBD. A graphic analysis of the main effects and interactions between the variables was used for results interpretation. Response surface methodology (RSM) was used to determine optimal extraction conditions. Multiple linear regression was performed to obtain regression coefficients of the quadratic polynomial model previously described. Lack of fit, determination coefficient (R^2) and F test of the model were evaluated from analysis of variance (ANOVA) at confidence level of 95% ($p < 0.05$).

RESULTS

MAE optimization

The influence of several factors on the MAE extraction efficiency of polyphenols from carob bark, such as extraction time (min), ethanol concentration (% v/v), liquid:solid ratio (mL/g), and extraction temperature (ºC), was studied in terms of total yield (%) and DPPH inhibition (%) using surface response methodology. The experimental values selected for each variable in the Box-Behnken design and the responses obtained are given in **Table III.4.1.2**.

Figure III.4.1.2 shows Pareto charts and significant effects at 95% confidence obtained for the studied responses. The total yield obtained from carob bark ranged from 57.9 to 67.5%. As it can be seen in the Pareto chart, the yield was significantly affected by ethanol concentration and liquid:solid ratio. The ethanol concentration used was the main significant variable influencing extraction yield with a negative effect. So, the yield was increased within the studied levels with the decrease of ethanol concentration. The solvent constitution is one of the most important factors in an extraction process as it could influence the polarity of solvent, being crucial for the solubility of the extracted compounds [29]. The presence of water in the solvent could facilitate an increase in extraction yield by improving the swelling of the plant material, which is favourable to increase the surface area of contact between the matrix and the solvent [18] [30]. A high concentration of ethanol could interrupt the extraction of phenolic compounds possibly due to a lower penetration of ethanol into the plant matrix through the protective function and a lower solubility of some extractable phenolic compounds [31]. The increase in water content in the solvent composition was statistically influential to improve the overall extraction yield [32]. In this sense, with decreasing ethanol concentration and adding water, the polarity of the solvent is increased and not only polyphenols could be extracted but also other polar compounds such as fructose, glucose or sucrose (present in carob pods) which may result in increasing the total yield [33]. It was also observed that an increase in the liquid: solid

ratio resulted in increasing the total yield. A high solvent volume could accelerate substance transfer and promote solubility by increasing the contact surface of the plant material with the solvent, improving the extraction efficiency [29].

Table III.4.1.2. Box-Behnken Experimental Design used and MAE responses obtained from carob bark.

Experiment	Time (min)	Ethanol (%)	Ratio (mL/g)	Temperature (°C)	Yield (%)	DPPH (%)
1	30	35	35	70	62.5	87
2	5	60	35	60	62.1	79
3	30	60	35	80	63.7	81
4	5	35	35	70	63.4	68
5	17.5	35	25	70	62.7	78
6	17.5	85	35	80	60.0	74
7	17.5	85	25	70	57.9	81
8	17.5	85	45	70	62.4	79
9	17.5	60	45	60	64.6	80
10	30	60	25	70	61.8	77
11	30	60	35	60	63.4	75
12	17.5	60	35	70	62.5	77
13	5	60	35	80	64.5	80
14	17.5	35	35	80	66.1	89
15	5	60	25	70	61.7	79
16	17.5	60	35	70	64.2	80
17	17.5	60	35	70	65.1	81
18	17.5	60	35	70	64.1	75
19	17.5	60	25	60	62.1	71
20	17.5	35	45	70	67.5	76
21	17.5	60	35	70	66.1	81
22	30	85	35	70	58.1	73
23	30	60	45	70	65.1	84
24	17.5	85	35	60	60.8	71
25	17.5	35	35	60	64.0	74
26	17.5	60	25	80	62.3	78
27	5	85	35	70	61.6	81
28	17.5	60	45	80	64.8	77
29	5	60	45	70	64.7	70

Regarding antioxidant capacity, a higher extraction temperature improved the antioxidant capacity which ranged from 68 to 89 % of DPPH inhibition. A high temperature could speed up intermolecular interactions and facilitate molecular motion, which could increase the solubility of the solutes into the solution [29]. A significant negative interaction was also observed between time and ethanol concentration, with a lower concentration of ethanol generally improving the antioxidant activity of the extracts. Ethanol changes the dielectric properties of the

solvent towards microwave heating and the degree of microwave absorption usually increases with the dielectric constant. The decrease in ethanol results in an increase in the dielectric constant of the system due to higher water content, increasing the absorption of more microwave energy by the system and increasing the temperature inside the sample leading to the rupture of cells [34]. Some studies have shown that small amounts of water in the extracting solvent during MAE make possible the diffusion of water into the cells of the matrix, leading to better heating and thus facilitating the transport of compounds into the solvent at higher mass transfer rates [35]. Finally, a significant positive interaction between time and liquid:solid ratio also affected the antioxidant capacity, increasing DPPH inhibition with higher extraction times and solvent volume.
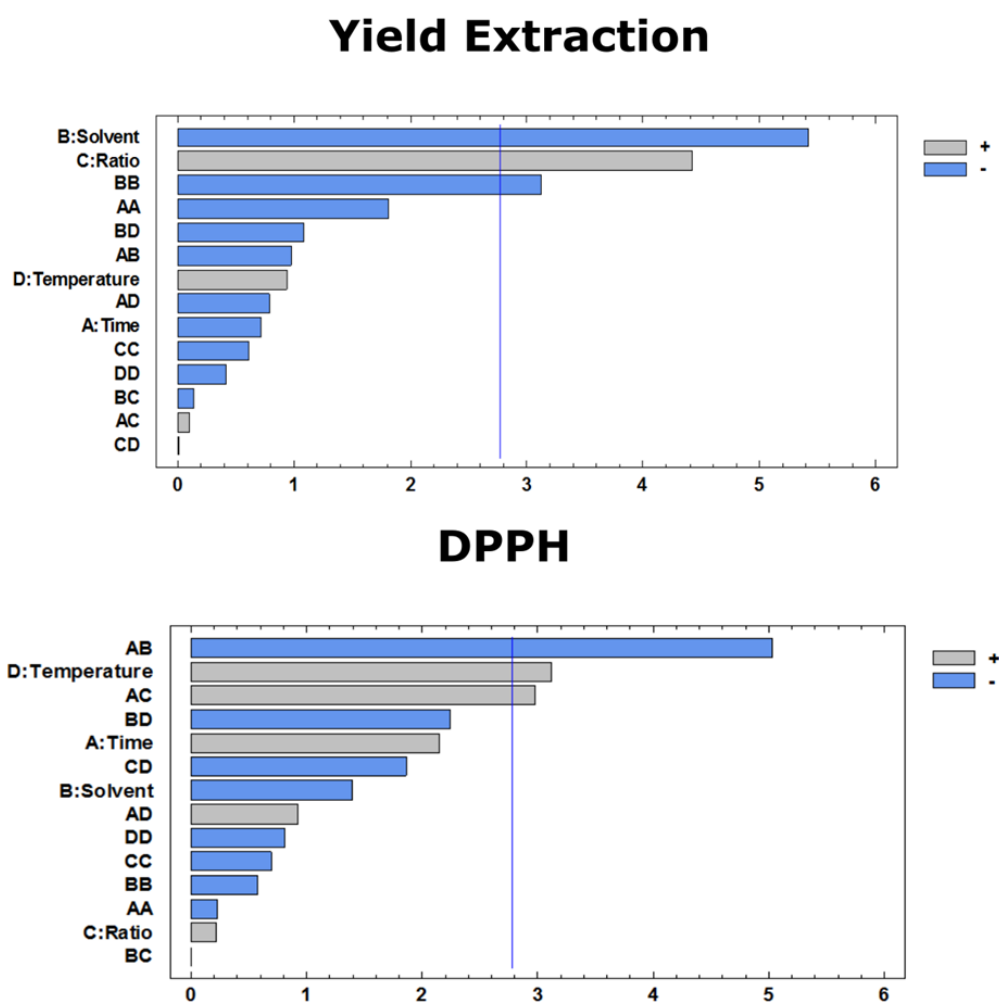
Figure III.4.1.2. Pareto charts obtained for extraction yield and antioxidant capacity (DPPH) of carob bark.

As a result of the analysis performed, it was decided to focus on the antioxidant capacity as this variable is more directly correlated with the extraction of phenolic compounds compared with the total yield that could be more influenced by the co-extraction of different compounds together with the target polyphenols.

A graphical analysis in terms of response surfaces was performed to study the interactions present in the antioxidant capacity of the obtained extracts (**Figure III.4.1.3**). These surface graphics represent in a visual way the interactions between the different factors, giving very valuable information for the analysis and optimization of the extraction. The interaction between time and ethanol concentration is plotted in **Figure III.4.1.3a**. As it can be seen, the best results for antioxidant capacity were obtained for a high time and a low ethanol concentration (approaching a 90% inhibition of DPPH) or for a low time and a high ethanol percentage.
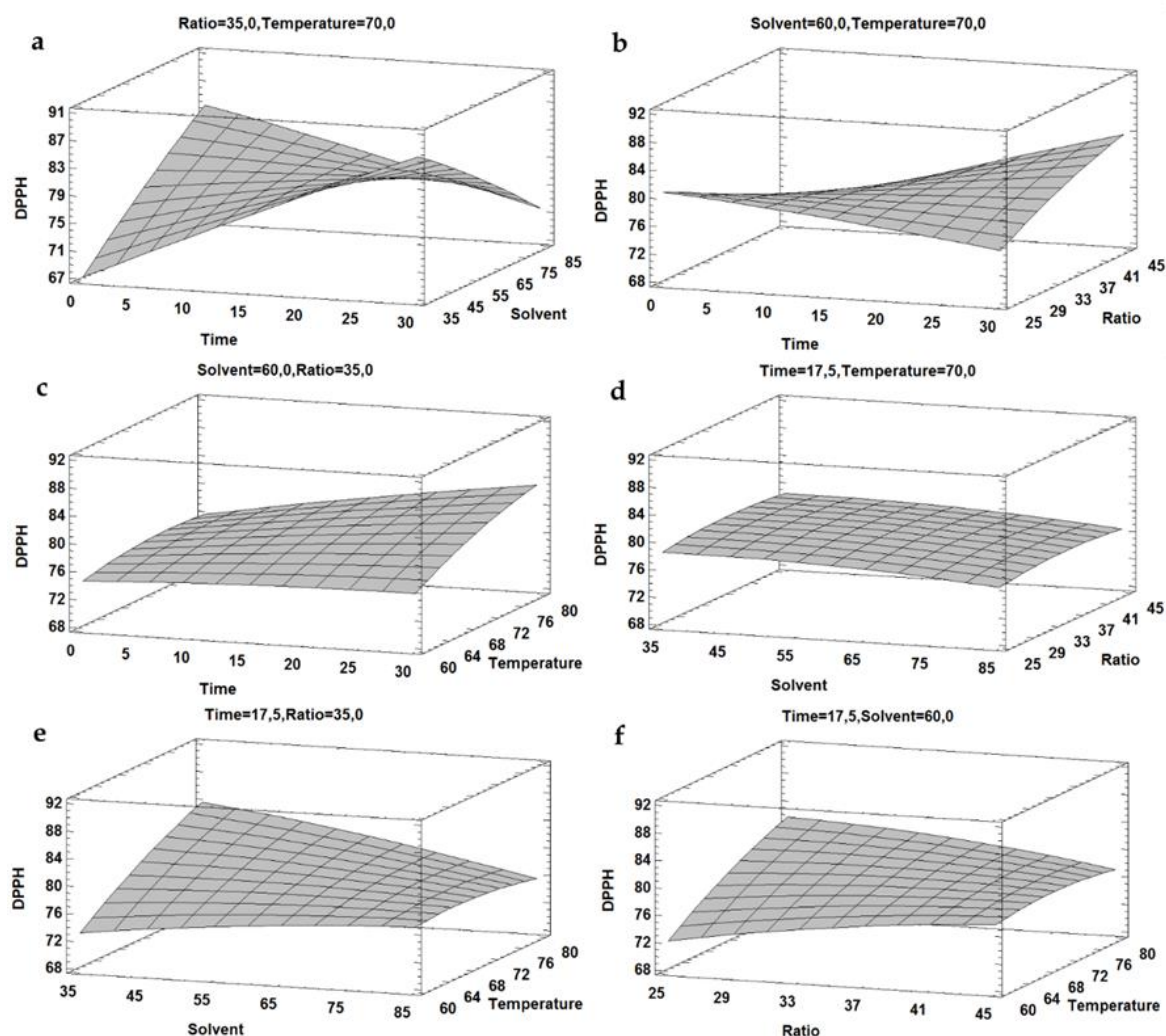
Figure III.4.1.3. Response surface plots showing the effect of the studied variables on the antioxidant capacity (DPPH) of extracts obtained from carob bark.

Figure III.4.1.3b shows the interaction between extraction time and liquid:solid ratio, where it can be appreciated that high time values and an intermediate liquid:solid ratio favours obtaining a high percentage of DPPH inhibition. Regarding extraction temperature, the effect of this variable was similar when studying the interaction between the other studied variables, showing an increase in temperature a significant improvement in the antioxidant capacity of the obtained extracts (**Figure III.4.1.3c**, **3e** and **3f**). In particular, the interactions between temperature and

liquid:solid ratio or ethanol concentration showed that an intermediate value of these variables together with a high temperature could remarkably improve the antioxidant capacity.

Finally, it can be seen in **Figure III.4.1.3d**, the interaction between liquid:solid ratio and ethanol concentration with no significant effect on the extraction process under the conditions studied to improve the antioxidant capacity.

The experimental data obtained from all 29 combinations for DPPH was fitted to a second-order polynomial model giving the following **Equation III.4.1.4**:

DPPH (%) = $-95.9163 - 0.3384 \cdot X_1 + 1.29147 \cdot X_2 + 1.72 \cdot X_3 + 2.86333 \cdot X_4 - 0.00149333 \cdot X_1^2 - 0.0216 \cdot X_1 \cdot X_2 + 0.032 \cdot X_1 \cdot X_3 + 0.01 \cdot X_1 \cdot X_4 - 0.000973333 \cdot X_2^2 + 0.0 \cdot X_2 \cdot X_3 - 0.012 \cdot X_2 \cdot X_4 - 0.00733333 \cdot X_3^2 - 0.025 \cdot X_3 \cdot X_4 - 0.00858333 \cdot X_4^2$

Where X_1, X_2, X_3 y X_4 correspond to extraction time, ethanol concentration, liquid:solid ratio and extraction temperature, respectively.

The ANOVA was used for the statistical testing of the model. The non-significance of the lack-of-fit tests ($p=0.2069$) verified the suitability of the selected model. The R^2 value obtained was 0.69, indicating a certain degree of correlation between experimental and predicted values. The optimal extraction conditions predicted by the model to optimize the extraction of carob bark in terms of antioxidant capacity are: a high extraction time (29.5 min), a low ethanol percentage (35%), an elevated temperature (80 °C) and an intermediate liquid:solid ratio of 35 mL/g. These conditions will be tested to verify the degree of confidence of the model.

Chemical analysis of extracts at optimal conditions

The selection of optimal conditions was considered taking into account the conditions predicted by the model and the behaviour observed from the response surface plots. As a result, it was decided to maintain the extraction conditions already predicted but modifying the value of the extraction time (**Table III.4.1.3**), which was previously established in 29.5 min (a high value of time). So, it was intended to analyse in a experimental way if the application of a shorter time with the same conditions for the rest of the studied variables could imply some improvement in antioxidant activity. The results obtained for total yield, antioxidant activity (FRAP, DPPH and ABTS methods), TPC and polysaccharides are shown in **Table III.4.1.4**.

Table III.4.1.3. Optimal conditions found for polyphenols extraction from carob bark.

Optimal extraction conditions	Factors			
	Temperature (°C)	Ratio (mL/g)	Ethanol (%)	Time(min)
A	80	35	35	5
B	80	35	35	29.5

Antioxidant capacity

Table III.4.1.4 shows the results obtained for antioxidant activity at the different extraction conditions, A and B, which were significantly different for all methods analyzed, obtaining the best results for the extraction performed at B conditions by using a longer extraction time, as predicted by the model. The extended time of microwaves irradiation also resulted in some increase in the extraction yield, obtaining 66.5% for B extraction which could be considered a high level of extraction capacity at an industrial level for the revalorization of carob waste. It has been reported that, in some cases, polyphenols recovery could be affected by the extension of microwaves extraction time due to some degradation of phenolic compounds [36]. In this study, however, an increase in extraction time was directly related to an improvement in the antioxidant capacity [37]; in particular from the results obtained for ABTS and DPPH methods. The used conditions seemed to significantly improve the antioxidant capacity compared to similar carob bean reported extractions [38].

Table III.4.1.4. Results obtained at different extraction times to optimize the extraction of carob bark.

Optimal extraction conditions	A	B
Extraction yield (%)	65.2 ± 0.5[a]	66.5 ± 0.4[b]
FRAP(μMTEs/g DW)	85.0 ± 2.0[a]	107.2 ± 1.7[b]
DPPH (% inhibition)	73.0 ± 1.0[a]	82.0 ± 1.0[b]
ABTS (mg TE/g DW)	14.9 ± 0.5[a]	22.0 ± 1.0[b]
TPC (mg GAE/g DW)	25.6 ± 0.3[a]	33.6 ± 0.4[b]
Polysaccharides (mg glucose/g DW)	336.4 ± 11.1[a]	345.4± 14.3[b]

(n=3) mean ± SD // Different superscripts within the same row indicate significant differences between values (p < 0.05)

The efficacy of MAE was compared with a conventional Soxhlet extraction (cold water and allowed to stand for 12 h at 3 °C and boiled for 10 min with stirring). With this method, a maximum of 20% to 60% DPPH inhibition was obtained by using final concentrations of extracts of 10 μg/mL and 50 μg/mL, respectively [7]. Compared to Soxhlet extraction, MAE cost less solvent and required lower extraction temperature and time.

The variety of the tree is a relevant issue when evaluating the antioxidant capacity. In this sense, no previous study has been found in the literature dealing with the antioxidant capacity of carob pods from the Alicante region of Spain. Worse antioxidant capacities but more polyphenols has been obtained with other pod species. Furthermore, carob pods as industrial product could be a potential source of polyphenol which can possibly substitute the use of synthetic antioxidants, thus improving the functional properties of a range of food products. Studies carried out on carob polyphenols have shown good antioxidant potential in microsomal lipid peroxidation and erythrocyte ghost systems [39].

The experimental results have demonstrated that MAE allows obtaining high values of antioxidant capacity. Even more, it has to be taken into account the origin of the carob pod, and especially its quality, as only poor quality pods and their bark, considered as waste, were used for this study. So, the antioxidant capacity results obtained could be considered very positive for the use of this type of residue as a source of antioxidant compounds.

Total polyphenols content (TPC)

Table III.4.1.5 shows the results obtained for total polyphenols content (TPC) at different extraction conditions. As it can be seen, only by varying the extraction time from 5 to 29.5 min the amount of polyphenols obtained from the residue was improved by more than 30%, demonstrating also the extraction of phenolic compounds from carob at tested conditions by MAE. A high content of polyphenols were obtained for both extractions when compared to conventional extractions of carobs beans previously reported, showing an average of around 20 mg GAE/g [40]. Comparing the obtained results by MAE with other extraction methods such as ultrasound assisted extraction (UAE) and supercritical fluid extraction (SFE) the improvement obtained in this work for TPC was around 100% and 20%, respectively [41].

Table III.4.1.5. Quantification of main compounds found in carob by HPLC.

	Time (min)	*Detected compound*	*mg/g DW**
1	*11.5*	Gallic acid	25.37 ± 0.26
2	14.2	Cathequin	18.70 ± 0.19
3	15.4	4-hidroxybenzoic acid	2.59 ± 0.10
4	16.8	Epigallocathequin	1.10 ± 0.09

*(mean± sd, n=3)

In relation to other similar extractions by microwaves, the values obtained have remained below due to the selected conditions. For TPC optimization conditions, values of 70 mg GAE / g were obtained for a time of 4.5 min and an ethanol concentration of 45% [35]. This reduction in the TPC values is due to the selection of the factors for a better obtaining of antioxidant properties instead of a greater amount of TPC. If we compare the results obtained with other residues, and in particular the use of the MAE, we can see how the residue studied has very good TPC values. Values of 15.1 mg GAE / g have been obtained for red grape peel and 20.6 mg GAE / g for olive leaves [42].

In relation with MAE, Huma *et al.*[35] said that the improvement with other techniques such as UAE and CSE cannot be excessively high with high extraction times. This factor is due to the due to degradation of plant cell walls by microwave irradiation as observed through scanning electron microscopy. However, the same quantities are extracted in very short time with MAE in comparison with other techniques.

The extraction of polyphenols by using MAE supposes a great opportunity to extract these compounds from the dried residue of carob bark, in a quick and easy way. Depending on the thermal stability of these compounds, they can be further encapsulating to preserve them for further applications. From an industrial point of view, the revalorization of this waste should be optimized, including extraction time, in order to reach a confidence value to optimize the final process.

Total polysaccharides content

Although the main objective of this work was not focused on the determination of the total amount of polysaccharides that could be extracted under the tested conditions, it was decided also to evaluate the amount of total polysaccharides present in the obtained extracts due to the complexity of the sample and the visible co-extraction in the process of other compounds such as carob beam gum. **Table III.4.1.4** shows the results obtained for the total polysaccharides content at different extraction conditions. As it can be seen, no significance differences were observed between the polysaccharides content obtained at A and B conditions.

These results show how this type of waste has a large amount of polysaccharides. When analyzing the chemical composition of carob bean pods, Khlifa *et al*. showed how the polysaccharide compositions of the carob pod are about 50% of the total amount in its chemical structure [43]. The residue studied has 35% polysaccharides in relation to the dry sample. This value indicates a smaller amount of polysaccharides, which can be positive when it comes to obtaining better results of antioxidant capacity.

From the obtained results, it has been shown that this residue contains a large amount of polyphenols, but it is also known that it is a residue rich in sugars, which could be directly related to the obtained results for the carbohydrate analysis [33].

HPLC analysis of main polyphenols

The identification of the type and content of phenolic compounds present in carob bark is essential to determine the potential of the obtained extracts for further applications. Detection and quantification of main phenolic compounds present in carob extract obtained at optimum conditions (80 °C; 29.5 min; 35% ethanol and 35 mL/g ratio) was performed by HPLC-DAD. **Figure III.4.1.4** shows polyphenols detected, highlighting the presence of gallic acid as the main polyphenolic compound present in carob extract in accordance with previous works [44-47]. Other polyphenols also detected are presented in **Table III.4.1.5**. Other authors have reported the presence of other compounds, not detected in this work, such as vanillic acid or rutin [48]. This difference in results could be due to many factors such as environmental differences, extraction procedures, genetic characteristics of the plant, and state of maturity [49].
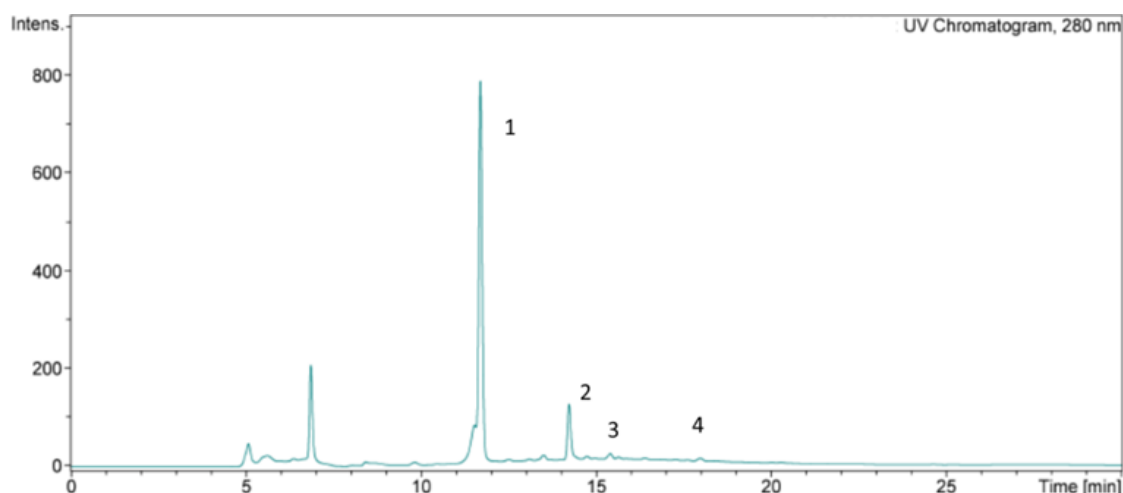
Figure III.4.1.4. Chromatogram of main compounds found in carob (**Table III.4.1.5**) at 280 nm.

CONCLUSIONS

Microwave assisted extraction (MAE) was demonstrated to be an efficient process for the extraction of phenolic compounds with antioxidant activity, in particular gallic acid, from the European carob tree *Ceratonia Silicua* of the variety "*ramillete*". A Box Behnken design was used to optimize the MAE experimental conditions by using RSM, obtaining a value of R^2 of 0.69. The best extraction conditions were as follows: 80 ºC; 29.5 min; 35% ethanol and 35 mL/g ratio. The TPC value and overall yield obtained were 33.6 ± 0.4 mg GAE/g DW and 66.5 ± 0.4%, respectively. A high concentration of polysaccharides was also co-extracted at optimized conditions. The obtained results from carob tree will contribute to the revalorization of this type of agro-food waste for different applications in the food industry sector, such as the encapsulation of phenolic compounds for functional food or the development of active films. In conclusion, the results from this work have shown the potential of carob barks as a natural source of phenolic compounds with antioxidant performance and the effectiveness of MAE for the reutilization of this agro-food waste.

Acknowledgements

REFERENCES

1.	Tang, X., P. Kumar, S. Alavi and K. Sandeep, *Recent advances in biopolymers and biopolymer-based nanocomposites for food packaging materials*. Critical reviews in food science and nutrition, 2012. **52**(5): 426-442.
2.	TĂNASE, E.E., V.I. POPA, M.E. POPA, M. RÂPĂ and O. POPA, *Biodegradation study of some food packaging biopolymers based on PVA*. Bulletin UASVM Animal Science and Biotechnologies, 2016. **73**: 1.

3. Kumar, N., P. Kaur and S. Bhatia, *Advances in bio-nanocomposite materials for food packaging: a review*. Nutrition & Food Science, 2017. **47**(4).

4. Arrieta, M., V. Sessini and L. Peponi, *Biodegradable poly (ester-urethane) incorporated with catechin with shape memory and antioxidant activity for food packaging*. European Polymer Journal, 2017.

5. Manousaki, A., M. Jancheva, S. Grigorakis and D.P. Makris, *Extraction of antioxidant phenolics from agri-food waste biomass using a newly designed glycerol-based natural low-transition temperature mixture: A comparison with conventional eco-friendly solvents*. Recycling, 2016. **1**(1): 194-204.

6. Di Donato, P., V. Taurisano, G. Tommonaro, V. Pasquale, J.M.S. Jiménez, S. de Pascual-Teresa, A. Poli and B. Nicolaus, *Biological Properties of Polyphenols Extracts from Agro Industry's Wastes*. Waste and Biomass Valorization, 2017: 1-12.

7. Kumazawa, S., M. Taniguchi, Y. Suzuki, M. Shimura, M.-S. Kwon and T. Nakayama, *Antioxidant activity of polyphenols in carob pods*. Journal of agricultural and food chemistry, 2002. **50**(2): 373-377.

8. Owis, A.I. and E.-M.B. El-Naggar, *Identification and quantification of the major constituents in Egyptian carob extract by liquid chromatography–electrospray ionization-tandem mass spectrometry*. Pharmacognosy magazine, 2016. **12**(Suppl 1): S1.

9. Vourdoubas, J. and V.K. Skoulou, *Possibilities of Upgrading Solid Underutilized Lingo-cellulosic Feedstock (Carob Pods) to Liquid Bio-fuel: Bio-ethanol Production and Electricity Generation in Fuel Cells-A Critical Appraisal of the Required Processes*. Studies in Engineering and Technology, 2017. **4**(1): 25-34.

10. Sęczyk, Ł., M. Świeca and U. Gawlik-Dziki, *Effect of carob (Ceratonia siliqua L.) flour on the antioxidant potential, nutritional quality, and sensory characteristics of fortified durum wheat pasta.* Food chemistry, 2016. **194**: 637-642.

11. Hadrich, B., K. Dimitrov and K. Kriaa, *Modelling Investigation and Parameters Study of Polyphenols Extraction from Carob (Ceratonia siliqua L.) Using Experimental Factorial Design.* Journal of Food Processing and Preservation, 2017. **41**(2).

12. Karakaya, S.E., AA Taş, S, *Antioxidant activity of some foods containing phenolic compounds.* International journal of food sciences and nutrition, 2001. **52**(6): 501-508.

13. Meziani, S., B.D. Oomah, F. Zaidi, A. Simon-Levert, C. Bertrand and R. Zaidi-Yahiaoui, *Antibacterial activity of carob (Ceratonia siliqua L.) extracts against phytopathogenic bacteria Pectobacterium atrosepticum*. Microbial pathogenesis, 2015. **78**: 95-102.

14. Bai, X.L., T.L. Yue, Y.H. Yuan and H.W. Zhang, *Optimization of microwave-assisted extraction of polyphenols from apple pomace using response surface methodology and HPLC analysis.* Journal of separation science, 2010. **33**(23-24): 3751-3758.

15. Valdés, A., L. Vidal, A. Beltrán, A. Canals and M.C. Garrigós, *Microwave-assisted extraction of phenolic compounds from almond skin byproducts (prunus amygdalus): A multivariate analysis approach.* Journal of agricultural and food chemistry, 2015. **63**(22): 5395-5402.

16. Filip, S., B. Pavlić, S. Vidović, J. Vladić and Z. Zeković, *Optimization of microwave-assisted extraction of polyphenolic compounds from Ocimum basilicum by response surface methodology.* Food Analytical Methods, 2017. **10**(7): 2270-2280.

17. Ballard, T.S., P. Mallikarjunan, K. Zhou and S. O'Keefe, *Microwave-assisted extraction of phenolic antioxidant compounds from peanut skins*. Food Chemistry, 2010. **120**(4): 1185-1192.

18. Hayat, K., S. Hussain, S. Abbas, U. Farooq, B. Ding, S. Xia, C. Jia, X. Zhang and W. Xia, *Optimized microwave-assisted extraction of phenolic acids from citrus mandarin peels and evaluation of antioxidant activity in vitro*. Separation and Purification Technology, 2009. **70**(1): 63-70.

19. Pinela, J., M. Prieto, A.M. Carvalho, M.F. Barreiro, M.B.P. Oliveira, L. Barros and I.C. Ferreira, *Microwave-assisted extraction of phenolic acids and flavonoids and production of antioxidant ingredients from tomato: A nutraceutical-oriented optimization study*. Separation and Purification Technology, 2016. **164**: 114-124.

20. Moreira, M.M., M.F. Barroso, A. Boeykens, H. Withouck, S. Morais and C. Delerue-Matos, *Valorization of apple tree wood residues by polyphenols extraction: Comparison between conventional and microwave-assisted extraction*. Industrial Crops and Products, 2017. **104**: 210-220.

21. Ferreres, F., C. Grosso, A. Gil-Izquierdo, P. Valentão, A.T. Mota and P.B. Andrade, *Optimization of the recovery of high-value compounds from pitaya fruit by-products using microwave-assisted extraction*. Food Chemistry, 2017. **230**: 463-474.

22. Rosa, R., L. Tassi, G. Orteca, M. Saladini, C. Villa, P. Veronesi, C. Leonelli and E. Ferrari, *Process intensification by experimental design application to microwave-assisted extraction of phenolic compounds from Juglans regia L.* Food analytical methods, 2017. **10**(3): 575-586.

23. Makris, D.P. and P. Kefalas, *Carob pods (Ceratonia siliqua L.) as a source of polyphenolic antioxidants.* Food technology and biotechnology, 2004. **42**(2): 105-108.

24. Piñeiro, Z., A. Marrufo-Curtido, C. Vela and M. Palma, *Microwave-assisted extraction of stilbenes from woody vine material*. Food and Bioproducts Processing, 2017. **103**: 18-26.

25. Dai, J. and R.J. Mumper, *Plant phenolics: extraction, analysis and their antioxidant and anticancer properties*. Molecules, 2010. **15**(10): 7313-7352.

26. Yang, Z. and W. Zhai, *Optimization of microwave-assisted extraction of anthocyanins from purple corn (Zea mays L.) cob and identification with HPLC–MS*. Innovative food science & emerging technologies, 2010. **11**(3): 470-476.

27. Uysal, S., G. Zengin, A. Aktumsek and S. Karatas, *Chemical and biological approaches on nine fruit tree leaves collected from the Mediterranean region of Turkey*. Journal of Functional Foods, 2016. **22**: 518-532.

28. Hu, S., B.-Y. Kim and M.-Y. Baik, *Physicochemical properties and antioxidant capacity of raw, roasted and puffed cacao beans*. Food chemistry, 2016. **194**: 1089-1094.

29. Zhao, C.-N., J.-J. Zhang, Y. Li, X. Meng and H.-B. Li, *Microwave-assisted extraction of phenolic compounds from Melastoma sanguineum fruit: Optimization and identification.* Molecules, 2018. **23**(10): 2498.

30. Pan, X., G. Niu and H. Liu, *Microwave-assisted extraction of tea polyphenols and tea caffeine from green tea leaves.* Chemical Engineering and Processing: Process Intensification, 2003. **42**(2): 129-133.

31. Tóth, M.E., L. Vígh and M. Sántha, *Alcohol stress, membranes, and chaperones*. Cell Stress and Chaperones, 2014. **19**(3): 299-309.

32. Spigno, G., L. Tramelli and D.M. De Faveri, *Effects of extraction time, temperature and solvent on concentration and antioxidant activity of grape marc phenolics*. Journal of food engineering, 2007. **81**(1): 200-208.

33. Biner, B., H. Gubbuk, M. Karhan, M. Aksu and M. Pekmezci, *Sugar profiles of the pods of cultivated and wild types of carob bean (Ceratonia siliqua L.) in Turkey*. Food Chemistry, 2007. **100**(4): 1453-1455.

34. Chemat, F. and G. Cravotto, *Microwave-assisted extraction for bioactive compounds: theory and practice*. Vol. **4**. 2012: Springer Science & Business Media.

35. Huma, Z.E., V. Jayasena, S.M. Nasar-Abbas, M. Imran and M.K. Khan, *Process optimization of polyphenol extraction from carob (Ceratonia siliqua) kibbles using microwave-assisted technique*. Journal of Food Processing and Preservation, 2018. **42**(2): e13450.

36. Song, J., D. Li, C. Liu and Y. Zhang, *Optimized microwave-assisted extraction of total phenolics (TP) from Ipomoea batatas leaves and its antioxidant activity*. Innovative food science & emerging technologies, 2011. **12**(3): 282-287.

37. Karami, Z., Z. Emam-Djomeh, H.A. Mirzaee, M. Khomeiri, A.S. Mahoonak and E. Aydani, *Optimization of microwave assisted extraction (MAE) and soxhlet extraction of phenolic compound from licorice root*. Journal of food science and technology, 2015. **52**(6): 3242-3253.

38. Roseiro, L.B., C.S. Tavares, J.C. Roseiro and A.P. Rauter, *Antioxidants from aqueous decoction of carob pods biomass (Ceretonia siliqua L.): Optimisation using response surface methodology and phenolic profile by capillary electrophoresis*. Industrial crops and products, 2013. **44**: 119-126.

39.   Huma, Z.E., V. Jayasena, S.M. Nasar-Abbas, M. Imran and M.K. Khan, *Process optimization of polyphenol extraction from carob (Ceratonia siliqua) kibbles using microwave-assisted technique*. Journal of Food Processing and Preservation, 2017.

40.   Turhan, I., N. Tetik, M. Aksu, M. Karhan and M. Certel, *Liquid–solid extraction of soluble solids and total phenolic compounds of carob bean (Ceratonia siliqua L.)*. Journal of food process engineering, 2006. **29**(5): 498-507.

41.   Roseiro, L.B., et al., *Supercritical, ultrasound and conventional extracts from carob (Ceratonia siliqua L.) biomass: Effect on the phenolic profile and antiproliferative activity*. Industrial crops and products, 2013. **47**: 132-138.

42.   Makris, D.P., G. Boskou and N.K. *Andrikopoulos, Polyphenolic content and in vitro antioxidant characteristics of wine industry and other agri-food solid waste extracts*. Journal of Food Composition and Analysis, 2007. **20**(2): 125-132.

43.   Khlifa, M., A. Bahloul and S. Kitane, *Determination of chemical composition of carob pod (Ceratonia siliqua L.) and its morphological study*. J. Mater. Environ. Sci, 2013. **4**(3): 348-353.

44.   Almanasrah, M., L.B. Roseiro, R. Bogel-Lukasik, F. Carvalheiro, C. Brazinha, J. Crespo, M. Kallioinen, M. Mänttäri and L.C. Duarte, *Selective recovery of phenolic compounds and carbohydrates from carob kibbles using water-based extraction*. Industrial Crops and Products, 2015. **70**: 443-450.

45.   Papagiannopoulos, M., H.R. Wollseifen, A. Mellenthin, B. Haber and R. Galensa, *Identification and quantification of polyphenols in Carob Fruits (Ceratonia siliqua L.) and derived products by HPLC-UV-ESI/MS n*. Journal of agricultural and food chemistry, 2004. **52**(12): 3784-3791.

46.   El Ansari Zineb, B.M., B. Alain and L. Ahmed, *Total Polyphenols and Gallic Acid Contents in Domesticated Carob (Ceratonia siliqua L.) Pods and Leaves*. Int. J. Pure App. Biosci, 2017. **5**(4): 22-30.

47.   Bouli, A.A., M. Hansali and R.W. Owen, *Determination of phenolic composition of carob pods grown in different regions of Morocco*. Journal of Natural Products, 2010. **3**.

48.   Balaban, M., *Identification of the main phenolic compounds in wood of Ceratonia siliqua by GC-MS*. Phytochemical Analysis: An International Journal of Plant Chemical and Biochemical Techniques, 2004. **15**(6): 385-388.

49.   Stavrou, I.J., A. Christou and C.P. Kapnissi-Christodoulou, *Polyphenols in carobs: A review on their composition, antioxidant capacity and cytotoxic effects, and health impact*. Food chemistry, 2018.

III.4.2. Bioactive Multilayer Polylactide Films with Controlled Release Capacity of Gallic Acid Accomplished by Incorporating Electrospun Nanostructured Coatings and Interlayers

L. Quiles-Carrillo [1], N. Montanes [1], J.M. Lagaron [2], R.Balart [1] and S. Torres-Giner [2]

[1] Technological Institute of Materials (ITM), Universitat Politècnica de València (UPV), Plaza Ferrándiz y Carbonell 1, 03801 Alcoy, Spain;

[2] Novel Materials and Nanotechnology Group, Institute of Agrochemistry and Food Technology (IATA), Spanish National Research Council (CSIC), Calle Catedrático Agustín Escardino Benlloch 7, 46980 Paterna, Valencia, Spain

applied sciences

MDPI

Article

Bioactive Multilayer Polylactide Films with Controlled Release Capacity of Gallic Acid Accomplished by Incorporating Electrospun Nanostructured Coatings and Interlayers

Luis Quiles-Carrillo [1], Nestor Montanes [1], José M. Lagaron [2], Rafael Balart [1] and Sergio Torres-Giner [2,*]

[1] Technological Institute of Materials (ITM), Universitat Politècnica de València (UPV), Plaza Ferrándiz y Carbonell 1, 03801 Alcoy, Spain; luiquic1@epsa.upv.es (L.Q.-C.); nesmonmu@upvnet.upv.es (N.M.); rbalart@mcm.upv.es (R.B.)

[2] Novel Materials and Nanotechnology Group, Institute of Agrochemistry and Food Technology (IATA), Spanish National Research Council (CSIC), Calle Catedrático Agustín Escardino Benlloch 7, 46980 Paterna, Valencia, Spain; lagaron@iata.csic.es

* Correspondence: storresginer@iata.csic.es; Tel.: +34-963-900-022

check for updates

Featured Application: The electrospinning coating technology is herein proposed to develop multilayer polylactide (PLA) films with controlled release rates of gallic acid (GA), a natural antioxidant, into saline medium. The bioactivity of the PLA films described here is based on their potential capacity to incorporate a large amount of GA into the packaging structure until its eventual release into the food product either through fast release, by means of coatings, or sustained release, in the form of interlayers, during storage. Therefore, their application in bioactive packaging for both short- and long-term storage of food products can advantageously permit the development of functional food, enhancing the food impact over the consumer's health.

Abstract: The present research reports on the development of bi- and multilayer polylactide (PLA) films by the incorporation of electrospun nanostructured PLA coatings and interlayers containing the antioxidant gallic acid (GA) at 40 wt% onto cast-extruded PLA films. To achieve the bilayer structures, submicron GA-loaded PLA fibers were applied on 200-µm cast PLA films in the form of coatings by electrospinning for 1, 2, and 3 h. For the multilayers, the cast PLA films were first coated on one side by electrospinning, then sandwiched with 10-µm PLA film on the other side, and the resultant whole structure was finally thermally post-treated at 150 °C without pressure. Whereas the bilayer PLA films easily delaminated and lacked transparency, the multilayers showed sufficient adhesion between layers and high transparency for deposition times during electrospinning of up to 2 h. The incorporation of GA positively contributed to delaying the thermal degradation of PLA for approximately 10 °C, as all films were thermally stable up to 345 °C. The in vitro release studies performed in saline medium indicated that the GA released from the bilayer PLA films rapidly increased during the first 5 h of immersion while it stabilized after 45–250 h. Interestingly, the PLA multilayers offered a high sustained release of GA, having the capacity to deliver the bioactive for over 1000 h. In addition, in the whole tested period, the GA released from the PLA films retained most of its antioxidant functionality. Thus, during the first days, the bilayer PLA films can perform as potent vehicles to deliver GA while the multilayer PLA films are able to show a sustained release of the natural antioxidant for extended periods.

Keywords: PLA; GA; electrospinning; multilayer films; bioactive packaging

Bioactive Multilayer Polylactide Films with Controlled Release Capacity of Gallic Acid Accomplished by Incorporating Electrospun Nanostructured Coatings and Interlayers

Abstract.

The present research reports on the development of bi- and multilayer polylactide (PLA) films by the incorporation of electrospun nanostructured PLA coatings and interlayers containing the antioxidant gallic acid (GA) at 40 wt% onto cast-extruded PLA films. To achieve the bilayer structures, submicron GA-loaded PLA fibers were applied on 200-µm cast PLA films in the form of coatings by electrospinning for 1, 2, and 3 h. For the multilayers, the cast PLA films were first coated on one side by electrospinning, then sandwiched with 10-µm PLA film on the other side, and the resultant whole structure was finally thermally post-treated at 150 °C without pressure. Whereas the bilayer PLA films easily delaminated and lacked transparency, the multilayers showed sufficient adhesion between layers and high transparency for deposition times during electrospinning of up to 2 h. The incorporation of GA positively contributed to delaying the thermal degradation of PLA for approximately 10 °C, as all films were thermally stable up to 345 °C. The in vitro release studies performed in saline medium indicated that the GA released from the bilayer PLA films rapidly increased during the first 5 h of immersion while it stabilized after 45–250 h. Interestingly, the PLA multilayers offered a high sustained release of GA, having the capacity to deliver the bioactive for over 1000 h. In addition, in the whole tested period, the GA released from the PLA films retained most of its antioxidant functionality. Thus, during the first days, the bilayer PLA films can perform as potent vehicles to deliver GA while the multilayer PLA films are able to show a sustained release of the natural antioxidant for extended periods.

Keywords: PLA; GA; electrospinning; multilayer films; bioactive packaging.

INTRODUCTION

The development of novel "functional foods" is a great opportunity to improve the quality of foods available to consumers to benefit their health and well-being in most modern societies. Indeed, the European Union (EU) is fighting diseases characteristic of a modern age, such as obesity, osteoporosis, cancer, diabetes, allergies, and dental problems [1]. A food can be regarded as functional if, beyond its inherent nutritional effects, it does satisfactorily demonstrate to provide added physiologic benefits (*e.g.*, reduction of chronic disease risk) [2]. Currently, the majority of commercial functional foods are presented with the bioactive components contained within compatible foods. However, this aspect imposes to the food industry a number of limitations and difficulties during processing and storage such as the loss of product functionality, the development of undesirable flavors, or the modification of the food product texture [3]. The functional, or more precisely, "bioactive packaging" concept, is based on the incorporation into the packaging structure of the desired bioactive principles in optimum conditions until their eventual release into the food product either through controlled or fast release during storage, or just before consumption, taking into account the specific product/functional substance characteristics or requirements [4]. Indeed, the so-called bioactive packaging differs from the well-known active packaging technologies in the fact that while active packaging primarily deals with maintaining or increasing quality and safety of packaged foods (*e.g.*, antimicrobial and antioxidant packaging), bioactive packaging provides a direct impact on the health of the consumer by generating healthier packaged foods.

Biodegradable polymers and sustainable plastics are nowadays essential elements involved in novel bioactive packaging technologies. Biopolymers are very advantageous to develop compostable (including edible) active and bioactive films due to their availability, non-toxicity, biodegradability and renewability, and their unique properties [5]. Biodegradable and/or sustainable polymer materials, such as synthetic biodegradable polymers, bio-based polyesters and polyamides, and naturally occurring polymers (*e.g.*, proteins and polysaccharides and derivatives) are considered among the most suitable materials for the controlled release of bioactive substances [6]. Biopolymers will also act as an "added value" argument within the food chain for the upward use of sustainable packaging. In this sense, polylactide (PLA) is a commercially available bio-based and biodegradable polymer, which is gaining acceptance for both existing and novel applications in the packaging field in the form of different articles such as films or injection-molded pieces and parts [7]. Creating a fully based PLA film with control release ability of bioactives is certainly a new concept of sustainable functional packaging. Additionally, PLA is also a Food and Drug Administration (FDA) approved material because it is degraded by hydrolysis to products that can be metabolized and excreted [8].

In this context, gallic acid (GA), that is, 3,4,5-trihydroxybenzoic acid, is a naturally occurring polyphenol commonly found in a variety of fruits and vegetables, such as grapes, cherry, tea leaves, and longan seeds [9], either in its free or bound form (*e.g.*, gallotannins) [10]. Moreover, GA can be obtained from both liquid and solid wastes of the agro-food industry, for instance the wine industry [11], resulting in a good candidate of a waste material converted into an added-value product. GA has been shown to exhibit bioactive properties such as antioxidant, anti-inflammatory,

anticarcinogenic, and antifungal properties [12]. Nevertheless, GA is unstable at high temperatures or in the presence of oxygen or light, conditions that are common in food processing and storage [13]. Due to these factors, there is a very large trend to encapsulate and control the release of GA to improve its stability and bioactivity over time [14]. To this end, the composition of the encapsulating material is a major determinant of both the capsule's functional properties and the way it can be applied to improve the performance and release of a particular bioactive compound [15].

Novel methods are, therefore, pursued in a particular effort to incorporate GA in sustainable packaging materials avoiding losses in antioxidant activity during film formation or packaging structure development. In this regards, the electrohydrodynamic processing (EHDP), also called electrospinning when fibrilar structures are produced, has been recently suggested as being a simple and straightforward method of generating nanostructured encapsulation structures for a variety of bioactive agents [16]. The electrospinning technique makes use of electrostatic forces to produce electrically charged jets from viscoelastic polymer solutions that upon drying, by the evaporation of the solvent, give rise to submicro- and nano-sized polymer-based fibers [17]. In this sense, EHDP is a promising technology that can be easily performed at room temperature so that it has recently attracted increased interest both for the nanoencapsulation and stabilization of thermolabile and light-sensitive substances [18–20] and for the development of fiber-based active coatings [21–24]. As a result, various bioactive-loaded electrospun biopolymer nanofibrous mats have been recently intended for food biopackaging purposes [25–27]. Moreover, in a more packaging application context, the electrospun fiber mats can be further converted into continuous films by the application of a thermal post-treatment below the biopolymer's melting point, the so-called annealing [28–30].

According to the above, the aim of this research work is to originally develop innovative multilayer structures of PLA with controlled release capacity of antioxidant GA that could serve as bioactive films for food and pharmaceutical packaging. To develop the bilayer structures, the electrospun PLA fibers containing GA were applied in the form of coating on PLA films previously prepared by cast extrusion. For the multilayers, a cast film of PLA was, first, coated on one side with different amounts of electrospun GA-loaded PLA fibers and then sandwiched with another PLA film on the other side. Thereafter, the three layers were annealed to generate a continuous film of PLA containing GA in the interlayer. The morphology, transparency, thermal properties, release profile, and antioxidant activity of the resultant PLA bi- and multilayer films were evaluated to ascertain their potential in bioactive packaging applications.

MATERIALS AND METHODS

Materials

Ingeo™ 6201D grade, provided by NatureWorks (Minnetonka, MN, USA), was used for electrospinning. This is a fiber-grade PLA resin, derived primarily from annually renewable resources and supplied in pellet form. It has a density of 1.24 g/cm^3 and a met flow rate (MFR) of 15–30 g/10 min (210 °C and 2.16 kg). For the manufacture of the films, a PLA Ingeo™ 2003D grade also supplied by NatureWorks

was used. This is general-purpose extrusion-grade PLA resin with a density of 1.24 g/cm^3 and a MFR of 6 g/10 min (210 °C and 2.16 kg).

Gallic acid (GA) with commercial reference G7384, having 97.5–102.5% (titration) and 170.12 g/mol, was supplied in powder form by Sigma-Aldrich S.A. (Madrid, Spain). This is a water-soluble phenolic acid obtained from grapes and the leaves of different plants.

Dichloromethane (DCM), N,N-dimethylformamide (DMF), and methanol, all with 99.8% purity, were supplied by Sigma-Aldrich S.A. The agent 2,2-diphenyl-1-picrylhydrazyl (DPPH), with a 394.32 g/mol, was also obtained from Sigma-Aldrich S.A.

Film Extrusion

Initially, all PLA pellets were dried at 60 °C for 24 h. PLA films with an average thickness of approximately 10 µm and 200 µm were obtained in a cast-roll machine MINI CAST 25 from EUR.EX.MA. (Venegono, Italy). The temperature profile was set at 195 (feeding)–195–200–200–205–210–210 (head) °C for both thicknesses. The extrusion speed was set at 30 rpm and 48 rpm for the 10-µm and 200-µm films, respectively. The speed of the calendar and the drag was adjusted to obtain the thickness requested in each case. The resultant films were annealed at 70 °C to develop crystallinity and release the remaining stresses in a vacuum drying oven Vaciotem-TV from S.P. Selecta S.A. (Barcelona, Spain). As a result, the PLA films achieved a completely smooth and flat surface. Finally, the films were then cut using a die on a hydraulic press model MEGA KCK-15A from Melchor Gabilondo S.A. (Vizcaya, Spain) to obtain square samples of 15 × 15 cm^2 [31].

Solution Preparation

A PLA solution was prepared for electrospinning by dissolving 10% (*w/v*) of the biopolymer in a DCM/DMF 7:3 (*v/v*) mixture at room temperature. GA was then added to the solution at a fixed content of 40 wt% based on the PLA weight. The resultant solution was gently stirred for up to 8 h at room temperature until a homogenous solution was obtained.

Solution Characterization

Prior to electrospinning, all PLA solutions were characterized in terms of surface tension, conductivity, and viscosity. Surface tension was measured following the Wilhemy plate method using an EasyDyne K20 tensiometer from Krüss GmbH (Hamburg, Germany). Conductivity was evaluated using a conductivity meter XS Con6 from Lab-box (Barcelona, Spain). Apparent viscosity (ηa) was determined at 100 s^{-1} using a rotational viscosity meter Visco BasicPlus L from Fungilab S.A. (San Feliu de Llobregat, Spain) equipped with a low viscosity adapter (LCP). All measurements were performed in triplicate at room temperature.

Electrospinning

Electrospinning was performed using a Fluidnatek® LE-50 benchtop line with temperature and relative humidity (RH) control system from Bioinicia S.L. (Valencia,

Spain) with a variable high-voltage 0–30 kV power supply. This device was equipped with a motorized injector able to scan towards a metallic collector to obtain a homogeneous electrospun deposition. The PLA solution was first transferred to a 60-mL plastic syringe, which was connected through polytetrafluoroethylene (PTFE) tubes to a stainless-steel needle (Ø = 0.9 mm) whereas the needle tip was connected to the power supply. A 200-µm film of PLA was placed on the collector and the PLA solution containing GA was electrospun for 1, 2, and 3 h under a steady flow-rate of 2.2 mL/h using the motorized injector. The distance between the injector and collector was optimal at 18 cm and the voltage was set at 18 kV. PLA fibers without GA were also electrospun for 1 h in identical conditions as the control material. The process was carried out at 25 °C and 40% RH.

Multilayer Preparation

The PLA films one side coated with the electrospun PLA fibers were first sandwiched with a 10-µm PLA film and then subjected to thermal post-treatment in a 4122-model press from Carver, Inc. (Wabash, IN, USA). This process was performed at 150 °C, without pressure, for 120 ± 1 s. The resultant films were air cooled at room temperature for 240 ± 1 s. Prior to annealing, the electrospun mats were equilibrated for, at least, 1 week in a desiccator at 25 °C and 0% RH by using silica gel.

Before testing, the thickness of films was measured using a digital micrometer (S00014, Mitutoyo, Corp., Kawasaki, Japan) with ± 0.001 mm accuracy. Measurements were performed and averaged in five different points, two in each corner and one in the middle. **Table III.4.2.1** shows the codification and structure of the different prepared films with their corresponding thicknesses.

Table III.4.2.1. Code and total thickness of the polylactide (PLA) films containing gallic acid (GA) according to their structure and deposition time during electrospinning.

Film	Structure	Time (h)	Thickness (µm)
Monolayer	200-µm PLA	0	200.1 ± 0.9
Bilayer 1h	200-µm PLA/Electrospun PLA+GA fibers	1	210.2 ± 2.8
Bilayer 2h	200-µm PLA / Electrospun PLA+GA fibers	2	215.0 ± 3.1
Bilayer 3h	200-µm PLA / Electrospun PLA+GA fibers	3	225.2 ± 2.0
Multilayer 1h	200-µm PLA/ Electrospun PLA+GA film/10-µm PLA	1	213.3 ± 1.8
Multilayer 2h	200-µm PLA/ Electrospun PLA+GA film/10-µm PLA	2	214.8 ± 1.9
Multilayer 3h	200-µm PLA/ Electrospun PLA+GA film/10-µm PLA	3	220.1 ± 2.1

MATERIAL CHARACTERIZATION

Morphology

The morphology of the electrospun fibers and the cross-sections of the films were observed by field emission scanning electron microscopy (FESEM) in a ZEISS ULTRA 55 from Oxford Instruments (Abingdon, United Kingdom). Film specimens were cryo-fractured by immersion in liquid nitrogen and then mounted on aluminum stubs perpendicularly to their surface. The working distance (WD) varied in the 6–7 mm range and an extra high tension (EHT) of 2 kV was applied to the electron beam. Due to their non-conducting nature, the films were subjected to a sputtering process with a gold-palladium alloy in a sputter coater EMITECH-SC7620 from Quorum Technologies, Ltd. (East Sussex, United Kingdom). The average fiber diameter was determined via ImageJ Launcher v 1.41 software using, at least, 20 FESEM images.

Thermal Analysis

Thermal stability was determined by thermogravimetric analysis (TGA) in a Mettler-Toledo TGA/SDTA 851 thermobalance (Schwerzenbach, Switzerland). Samples with an average weight between 5 and 7 mg were placed in standard alumina crucibles of 70 µL and subjected to a heating program from 30 °C to 700 °C at a heating rate of 20 °C/min in air atmosphere. The first derivative thermogravimetry (DTG) curves were also determined, expressing the weight loss rate as the function of time. All tests were carried out in triplicate.

Release Measurements

The release of GA was determined in saline medium following the procedure described by Chuysinuan *et al.* [32]. This type of medium was selected due to both the improved water retention behavior of the electrospun PLA mats and the high release rates of GA achieved. For this, the bi- and multilayer films containing GA were initially cut in square pieces of 20x20 mm^2 in randomly selected areas. The films were weighted and submerged in 30 mL of saline medium, prepared by dissolving 9 g of NaCl in 1 L of distilled water and stored for a whole period of 10 weeks, that is, 1680 h, without darkness and at room temperature, that is, 23 + 2 °C. At different submersion times, 1 mL of the medium solution was withdrawn (hereafter, a sample solution) and an equal amount of the fresh medium was refilled. The amount of GA in the sample solutions was determined in an Ultraviolet–Visible (UV–VIS) UV 4000 spectrophotometer (Thermo Scientific, Waltham, MA, USA) at a wavelength of 259 nm. The obtained data were calculated to determine the amount of GA released from the specimens at each submersion time point. For this, a calibration curve of GA in normal saline was previously determined, resulting in the following regression equation Y = 0.0227X + 0.0156 (R^2 = 0.9989), where "Y" is the absorbance and "X" the GA content, in ppm, of the sample. All measurements were carried out in triplicate.

Antioxidant Activity

The antioxidant activity of the GA released from the PLA films was determined by the DPPH inhibition assay. Measurements were taken after 2, 6, and 12 weeks of submersion in the saline medium. To this end, a modification of the procedure carried out by Chuysinuan *et al*. [32] was followed. Briefly, an aliquot of 1 mL of the sample

solution was diluted with 5 mL methanol. Later, 1 mL of the resultant solution was mixed with 3 mL of 9.4×10^{-2} M DPPH solution and the resulting solution was incubated for 30 min at room temperature in darkness. The absorbance of the final solution was recorded at the wavelength of 517 nm in the UV–VIS UV 4000 spectrophotometer. The antioxidant capacity of the extract was expressed as a percentage of inhibition of DPPH radical (% inhibition of DPPH radical) using the following **Equation III.4.2.1**:

$$I(\%) = \frac{A_0 - A_1}{A_0} \cdot 100 \qquad \textbf{Equation III.4.2.1}$$

where A_0 is the absorbance of the control and A_1 is the absorbance of the extract/standard. All measurements performed in triplicate.

Statistical Analysis

The solution properties, release of GA, and the antioxidant activity were evaluated through analysis of variance (ANOVA) using STATGRAPHICS Centurion XVI v 16.1.03 from StatPoint Technologies, Inc. (Warrenton, VA, USA). Fisher's least significant difference (LSD) was used at the 95% confidence level ($p < 0.05$). Mean values and standard deviations were also calculated.

RESULTS

Solution Properties

Prior to electrospinning, the properties of the neat PLA and the GA-containing PLA solutions were measured. **Table III.4.2.2** shows the values of surface tension, conductivity, and viscosity. The determination of these parameters is certainly relevant to explain the behavior of each biopolymer solution during electrospinning and a combined optimization of them is needed to tune the fiber into the required form [19]. As one can observe, the addition of GA to the PLA solution mainly induced an increase in conductivity as well as a slight decrease in viscosity and a negligible effect on the surface tension. On the one hand, the conductivity increase observed when GA was dissolved in the biopolymer solution can be ascribed to ionic factors that induced a greater charge carrying capacity. A moderate increase in conductivity is preferred in PLA solutions since fiber formation habitually improves by an increase of surface charge of the spinning jet [33]. Indeed, if the conductivity of the polymer solution is relatively high, the force required for a polymer droplet to fall on the metallic target will be comparatively lesser and, thus, fiber formation will be enhanced. In other words, the fiber jet of higher conductive solutions will be subjected to a greater tensile force in the presence of a given electric field. On the other hand, the slight reduction attained in viscosity suggests that the presence of GA also induces a plasticizing effect on PLA.

Table III.4.2.2. Values of surface tension, conductivity, and viscosity of the neat polylactide (PLA) and PLA containing gallic acid (GA) solutions.

Solution	Surface tension (mN/m)	Conductivity (µS/cm)	Viscosity (cP)
PLA	30.6 ± 0.1[a]	1.52 ± 0.08[b]	204.4 ± 0.4[c]
PLA + GA	30.7 ± 0.1[a]	5.83 ± 0.11[b]	195.9 ± 0.7[c]

[a-c] Different letters in the same column indicate a significant difference ($p < 0.05$).

Morphology

Figure III.4.2.1 shows the morphology of the electrospun mats obtained from the FESEM analysis. One can observe in Figure 1a that the neat PLA solution yielded smooth and homogenous fibers with a mean diameter of 1.1 ± 0.3 µm. Similar fibers, though slightly thinner, were obtained after the incorporation of GA. As shown in Figure 1b, the GA-containing PLA fibers presented a mean diameter of 0.9 ± 0.2 µm. In both cases, the electrospun PLA fibers were homogeneous and fully free of beads or beaded regions. The study of Aytac *et al.* [34] describing the preparation of electrospun PLA containing GA also reported a diameter decrease in the fibers when the bioactive was encapsulated. This previously observed morphological change was related to both a viscosity increase and a conductivity decrease due to the presence of GA in the PLA solution. As the conductivity of the solution increases, the diameter of the submicron fibers decreases owing to the increment in the number of charges leading greater stretching of the polymer jet [35]. Another relevant observation produced after the incorporation of GA was the change of fibers surface from smooth to a rough or nearly ribbon-like shape. This morphological change can be related to an increase of the electrostatic repulsion between charges encountered on the jet surface during electrospinning of the solution containing GA, which induced the formation of slightly thinner PLA fibers but also impaired the formation of a continuous surface along the fibers.
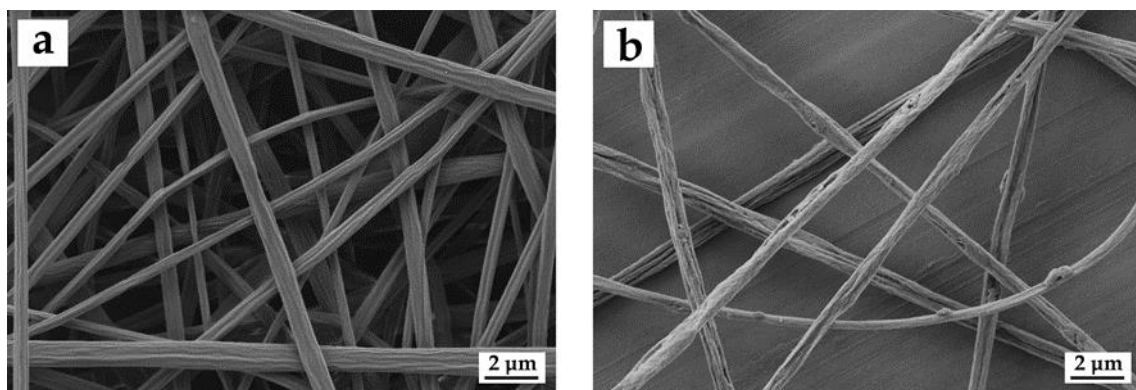
Figure III.4.2.1. Field emission scanning electron microscopy (FESEM) micrographs of the electrospun fibers of: (a) Neat polylactide (PLA); and (b) PLA containing gallic acid (GA). Both images were taken at 5000× and scale markers of 2 µm.
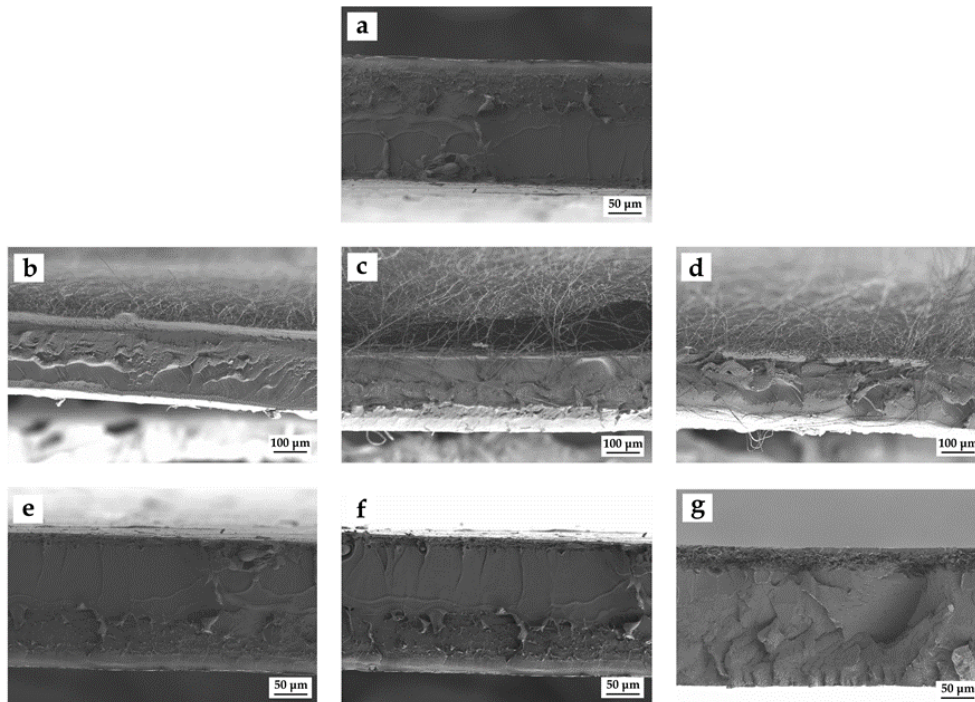
Figure III.4.2.2. Field emission scanning electron microscopy (FESEM) micrographs of the gallic acid (GA)-containing polylactide (PLA) films of: (a) monolayer; (b) bilayer 1 h; (c) bilayer 2 h; (d) bilayer 3 h; (e) multilayer 1 h; (f) multilayer 2 h; (g) multilayer 3 h.

In **Figure III.4.2.2** one can observe the FESEM images of the cross-sections of the PLA films prepared by cryo-fracture. **Figure III.4.2.2a** shows the neat PLA film, which presented a smooth surface fracture that is representative of a brittle material. **Figure III.4.2.2b–d** correspond to the bilayer films obtained after one, two, and three hours of electrospinning deposition of the GA-containing PLA fibers, respectively, without any thermal post-treatment. In these images one can clearly observe the presence of electrospun coatings of PLA fibers on the PLA films. As expected, the thickness of the electrospun coatings increased as a function of the deposition time during the electrospinning process. Thus, electrospun layers of PLA fibers of approximately 60, 85, and 100 µm were respectively obtained for the bilayers after one, two, and three hours of electrospinning. Although the electrospinning process yielded the formation of a continuous coating, one can also observe that it lacked of adhesion and a gap between the PLA film and the electrospun mat was observed, which most likely produced during cryo-fracture. Similar observations were recently described by Cherpinski *et al*. [36] where different biopolymer electrospun mats were not strongly adhered to a paper substrate. On the contrary, in the case of the multilayers, shown in **Figure III.4.2.2e–g**, a continuous film structure without gaps was attained after annealing. In the case of the multilayers produced for 1 and 2 h of electrospinning deposition, the so-called multilayer 1 h and multilayer 2 h samples, respectively shown in **Figure III.4.2.2e, f**, the electrospun interlayers were extremely thin in comparison to the overall multilayer thickness and then they were difficult to discern. In the case of the multilayer obtained after three hours of electrospinning deposition, that is, the so-called multilayer 3 h, shown in **Figure III.4.2.2g**, a nanostructured interlayer with a

total thickness of about 15 μm can be seen in the top region of the PLA film. The electrospun interlayers of GA-containing PLA also showed very little porosity, in the nanometric range, which can be ascribed to the large surface-to-volume ratio of the electrospun submicron fibers that efficiently coalesced and strongly adhered to both PLA films during the thermal post-treatment. In the multilayer 3h the fibrilar morphology was still kept in the electrospun interlayer, which can be mainly ascribed to an insufficient heat transmission due to the higher thickness of the electrospun interlay.

Film Transparency

Figure III.4.2.3 shows the optical appearance of the resultant PLA bi- and multilayers as a function of the deposition time during electrospinning. Simple naked eye examination of this image indicates that in the case of the bilayer structures, shown in the top images, the PLA films were mainly opaque. This effect is due to the inherent opacity of the electrospun coating, which is composed of fibers placed randomly that generate a significant level of porosity and hence refract the light very strongly [28,37]. Oppositely, the PLA multilayers, shown in the bottom images, highly retained the intrinsic transparency of PLA for up to 2 h of electrospinning. This optical effect can be related to the thermal post-treatment performed at 150 °C, below the biopolymer's T_m, the so-called annealing. This process effectively changed the electrospun interlayer morphology from a fiber-based mat structure to a continuous nanostructured film and hence reduced the porosity of the electrospun interlayer. During annealing a compact packing rearrangement of the electrospun nanofibers is produced by a phenomenon of coalescence [28, 29]. For the multilayer 3h sample, however, the PLA film developed certain opacity due to the longer electrospinning deposition time. This effect can be ascribed to the high porosity of the electrospun interlayer since this film sample still retained partially the original fiber morphology, as previously shown in **Figure III.4.2.2g**. From an application viewpoint, light penetration prevention (especially in the UV region) can also help reducing photoxidation of GA or any organic compounds present in foods. In any case, the annealing step applied on the PLA multilayers containing the electrospun interlayers resulted in continuous films with at least contact transparency, which have significant potential for use in food packaging applications [38]. This result indicates that the here-obtained nanostructured GA-containing fiber interlayers can be incorporated into PLA and the whole structure turned into actual films, which may be advantageous for encapsulation purposes and bioactive packaging applications.
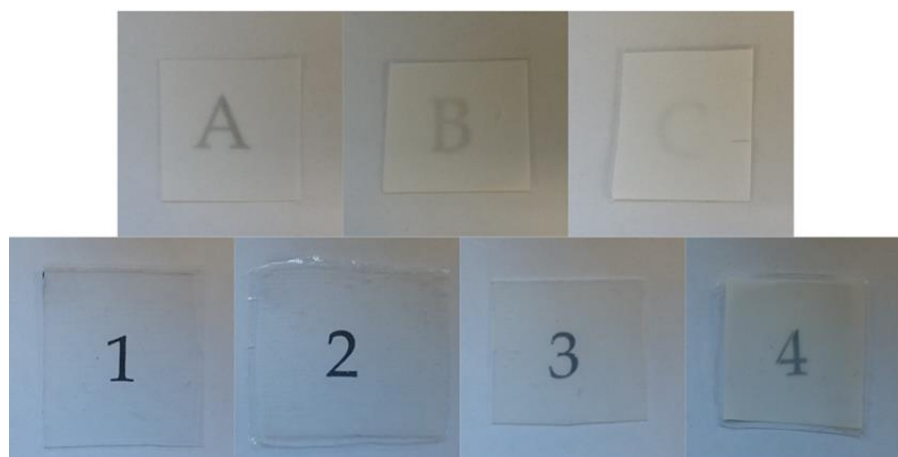
Figure III.4.2.3. Visual appearance and contact transparency of the gallic acid (GA)-containing polylactide (PLA) films of: (A) bilayer 1 h; (B) bilayer 2 h; (C) bilayer 3 h; (1) monolayer; (2) multilayer 1 h; (3) multilayer 2 h; and (4) multilayer 3 h.

Thermal Stability

Figure III.4.2.4 shows the TGA curves of the neat GA powder and the PLA films, whereas **Table III.4.2.3** summarizes the values obtained from these curves. On the one hand, it can be seen that the thermal decomposition of GA presented four peaks. The first mass loss occurred in the 70–130 °C range, which has been attributed to the degradation of volatile compounds of low molecular weight [39] as well as to the mass-loss event attributed to the water content [40]. The second and third peaks were centered at ca. 291 °C and 338 °C, respectively, which correspond to the main chain scission of GA and the loss of hydroxyl groups (–OH) [41]. Finally, minor and progressive degradation phenomena of lower intensity were observed at temperatures above 400 °C, which are related to the residual decomposition of GA at high temperature [39, 40]. On the other hand, one can observe that all PLA films presented a practically identical pattern of mass loss, similar to that of the neat PLA film. In particular, PLA decomposed in a single step, starting at ~340 °C, with a main degradation temperature (T_{deg}) slightly above 375 °C [42]. The incorporation of GA provided a thermal stability improvement, even at the lowest GA content, due to the intrinsic antioxidant activity of the polyphenol. The onset degradation temperature, measured at the 5% of mass loss ($T_{5\%}$), was delayed for up to 10 °C, whereas the values of T_{deg} also increased up to 5 °C. It is also worthy to mention that the thermal stability of the bilayer films was slightly better than that observed for the multilayer film, indicating that the capacity of GA to counteract the thermal effect was more effective when it was incorporated onto the film surface. For all film samples, the residual mass was nearly zero.
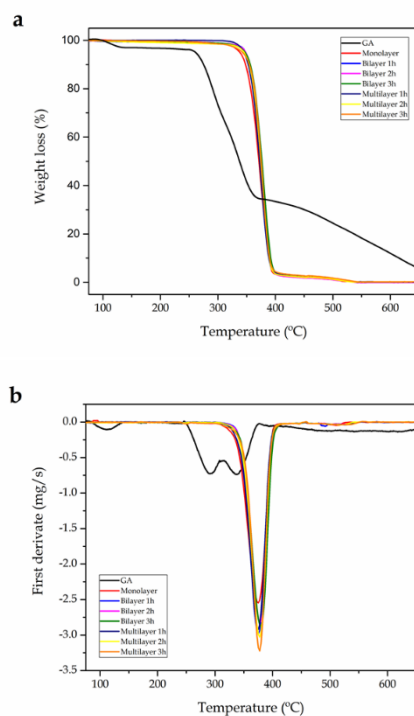
Figure III.4.2.4. Comparative plot of the gallic acid (GA)-containing polylactide (PLA) films in terms of: (a) Thermogravimetric analysis (TGA) curves; and (b) first derivative thermogravimetric (DTG) curves.

Table III.4.2.3. Thermal degradation properties in terms of the onset degradation temperature ($T_{5\%}$), degradation temperature (T_{deg}), and residual mass at 650 °C of gallic acid (GA) and the GA-containing polylactide (PLA) films.

Film	$T_{5\%}$ (°C)	T_{deg} (°C)	Residual mass (%)
GA	261.5 ± 1.1	290.6 ± 1.1 / 337.5 ± 1.2	5.32 ± 0.12
Monolayer	338.1 ± 1.3	375.1 ± 1.4	0.12 ± 0.04
Bilayer 1h	348.2 ± 1.2	375.2 ± 1.1	0.11 ± 0.05
Bilayer 2h	348.9 ± 1.0	378.7 ± 1.2	0.12 ± 0.03
Bilayer 3h	349.1 ± 1.4	379.5 ± 1.3	0.19 ± 0.04
Multilayer 1h	345.3 ± 0.9	375.1 ± 1.1	0.14 ± 0.03
Multilayer 2h	346.4 ± 1.2	377.4 ± 1.0	0.20 ± 0.05
Multilayer 3h	347.3 ± 1.4	377.5 ± 1.2	0.18 ± 0.04

A similar behavior has been previously observed for other GA-containing films. For instance, Luzi *et al*. [41] recently described that the addition of 5 wt% GA delayed thermal degradation of poly(ethylene-*co*-vinyl alcohol) (EVOH) for up to about 20 °C respect to the neat EVOH film. In another study, Wu *et al*. [43] developed an active film

based on gelatin with green tea extract (GTE), which contained 294.59 mg GA/g. It was observed that the thermal stability of the GTE-containing gelatin films was higher than that of the neat gelatin film and improved with increasing the concentration of GTE in the 0.3–0.7 wt% range. The increase of GTE did not only cause the Tdeg values of the gelatin films to increase but also decreased the maximum rate of mass loss. It is considered that interactions between the terminal –OH groups of the biopolymer chain with –OH, –CO, and/or –COOH chemical groups of the GA components via hydrogen bonding are responsible for the observed thermal stability improvement.

In vitro Release Studies

Figure III.4.2.5 shows the GA release from the bi- and multilayer PLA films as a function of the immersion time in saline medium for a span time of 1680 h. The in vitro release kinetics data are depicted in terms of the total amount release of GA (**Figure III.4.2.5a**) and its cumulative release to the medium based on the theoretical content of GA in the PLA films (**Figure III.4.2.5b**). One can observe that the release profile of the PLA films considerably varied according to their structure and, as one could expect, the total amount of GA released to the medium increased with increasing the GA content in the film samples. As a general observation, all bilayer films showed a Fickean diffusion release mechanism. During the first 5 h, a burst release profile was attained, showing cumulative release values of approximately 83%, 46%, and 35% for the PLA films coated by electrospun mats for 1 h, 2 h, and 3 h, respectively. Upon immersion in saline media, it is considered that the PLA fibers' coating is rapidly hydrated and swells, thus allowing the dissolution of the embedded polyphenols and their subsequent release at a relatively high rate due to the highly porosity of the electrospun mat. It is worthy to note that this phenomenon of burst release was observed even though the coated films were immersed in a water-based medium, for which PLA presents a low chemical affinity. It can be considered that the Fickean diffusion process was overlapped by the swelling behavior of the electrospun PLA fibers, leading to high release rates and thus accelerating the process. One can also observe that the GA release rate was higher in the bilayer films processed for shorter electrospinning deposition times, which can be related to the lower thickness of the electrospun coating and, thus, to a more favored diffusion of the polyphenol to the saline medium. In a second step, the release rates progressively decreased for all PLA films coated at different electrospinning deposition times. For the bilayer film obtained by 1 h of electrospinning deposition, the GA release rate stabilized after only ~45 h. In the PLA films coated for 2 and 3 h, stabilization was attained after approximately 250 h. At the end of the experiment, all bilayer films completed a theoretical cumulative release of GA in the 82–92% range. The deviation from the ideal value of 100% can be related to the inhomogeneous distribution of GA in different parts of the obtained electrospun PLA layers, partial losses during processing, and also a minor accumulation of GA in the PLA fibers during the whole tested immersion time.
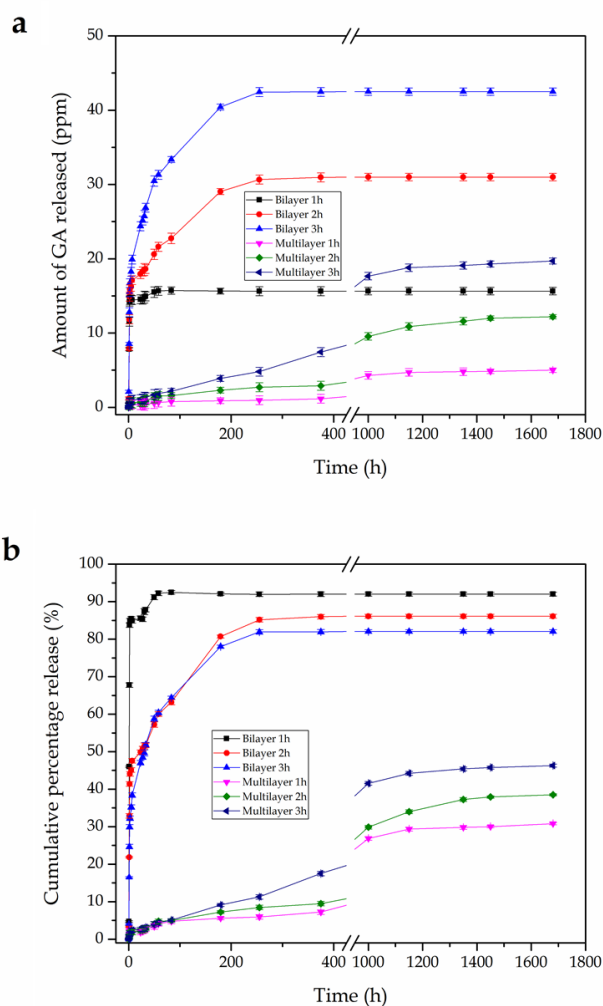
Figure III.4.2.5. Gallic acid (GA) release from the GA-containing polylactide (PLA) films as a function to the immersion time in saline medium: (a) Total amount released; and (b) cumulative release.

The above-described short or short-to-medium release can be of interest for most food packaging materials, based on the fact that the mean shelf life of a food-packaging product is typically below two weeks [44]. In this sense, Chuysinuan *et al.* [32] also studied the release behavior of GA from a single electrospun mat of PLA fibers in saline medium for 48 h. A similar release profile was reported, showing that the cumulative amount of GA released rapidly increased during the initial immersion time. Specifically, at 30 min after immersion, the cumulative amount of GA released into the normal saline was 21%. Further increase in the immersion time resulted in a gradual increase in the cumulative amount up to a plateau value of approximately 90% was reached. This burst release was related to the high water retention behavior of the GA-loaded PLA fibers, as well as potential dissociation of the polyphenol into ionic species due to the difference between the pKa value of GA and the pH of the normal saline, that is, 4.41 *vs*. 7. Moreover, the dissociation of the carboxylic acid chain ends of PLA into carboxylate groups (and protons) could additionally help promote the diffusion of the gallate ions out of the electrospun fibers due to electrostatic repulsion.

Similarly, Phiriyawirut and Phaechamud [45] reported the release of GA encapsulated at different rations into electrospun cellulose acetate (CA) nanofibers. It was observed that the release from 7.5–10 wt% GA-loaded electrospun CA fiber mats in phosphate buffer medium at room temperature was also rather rapid during the first 2 h, reaching cumulative release values of 35–45% after 100 h. The release profile reported was related to relative high content of GA, suggesting that the polyphenol was mainly located on the surface of electrospun fibers due to its limited solubility in the CA solution for electrospinning.

Oppositely, the multilayer PLA films exhibited a highly sustained release profile of GA to the selected simulant, that is, the saline medium. It can be observed that the multilayer PLA films smoothly delivered the bioactive and also still retained high amounts of GA during the whole tested period, that is, 10 weeks. In particular, at 375 h, when the release rates of bilayer films were already stabilized, the cumulative GA release values were only 7.4%, 10.8%, and 17.3% for the PLA films based on interlayers electrospun for 1 h, 2 h, and 3 h, respectively. Then, the three multilayers started to stabilize at approximately 1000 h, nearly reaching a plateau. The final cumulative GA values for the multilayers containing the electrospun interlayers processed for 1 h, 2 h, and 3 h were approximately 30%, 38%, and 46%, respectively. It can be then considered that the loaded GA was highly confined in the electrospun PLA interlayer due to the presence of the 10-µm top PLA layer. Therefore, although the release rate was stabilized, a slow and prolonged release is expected to occur for longer immersion times (no more data was collected). Since the GA release is the result of the diffusion and equilibrium process involving its transfer from the electrospun interlayer into the food simulant, the top PLA layer acted as an efficient barrier against the GA diffusion due to its intrinsic hydrophobic behavior. In this regard, it has been reported that the water absorption of PLA is only 0.7 wt% [46]. Therefore, the release mechanism in the fully PLA-based multilayer system can be easily further controlled and then tuned by not only adjusting the deposition time of the electrospun interlayer but also by selecting the appropriate thickness of the top layer prior to the thermal post-treatment.

Antioxidant Activity

Finally, the antioxidant capacity of the GA released from the PLA films was evaluated by the DPPH radical scavenging assay to assess their potential in bioactive packaging applications. DPPH is a stable radical with a maximum absorption at 517 nm that can readily undergo scavenging by an antioxidant such as polyphenols [47]. This method is based on the reduction of the relatively stable radical, that is, DPPH, to the formation of a non-radical form in the presence of hydrogen donating antioxidants. GA is a phenolic compound containing hydroxyl groups attached to the benzene ring in the ortho position so that it possesses electron and/or hydrogen donor ability [48]. Indeed, the antioxidant activity of these compounds is mainly due to their redox properties, which allows them to act as reducing agents, hydrogen donators, and singlet oxygen quenchers having metal–chelating capacities [49]. **Table III.4.2.4** shows the antioxidant capacity of the GA released from the bi- and multilayer PLA films after their immersion for two, six, and 12 weeks in the saline medium.

Table III.4.2.4. Inhibition (%) of 2,2-diphenyl-1-picrylhydrazyl radical (DPPH) of the gallic acid (GA) released from the polylactide (PLA) films.

Film	Inhibition (%)		
	2 weeks	**6 weeks**	**10 weeks**
Bilayer 1h	42.4 ± 0.7[a]	38.4 ± 0.9[a]	25.6 ± 1.2[a]
Bilayer 2h	65.7 ± 0.9[a]	54.9 ± 1.2[a]	47.7 ± 0.9[a]
Bilayer 3h	96.0 ± 2.4[a]	78.9 ± 1.3[a]	54.7 ± 1.3[a]
Multilayer 1h	5.9 ± 0.8[b]	29.2 ± 0.7[b]	38.1 ± 0.7[b]
Multilayer 2h	8.1 ± 0.8[b]	37.4 ± 1.0[b]	52.4 ± 1.2[b]
Multilayer 3h	12.3 ± 1.2[b]	48.7 ± 0.9[b]	71.4 ± 0.8[b]

[a-b] Different letters in the same column indicate a significant difference ($p < 0.05$).

As one can observe in the table above, the GA released from all the PLA films showed antioxidant activity confirming that electrospinning process was successful in retaining the bioactivity of GA [14, 50], even after the electrospun mats had been subjected to a high electrical potential during the fiber producing process as well as the thermal post-treatment. The antioxidant activity of the GA released from the PLA films was in agreement with the total amounts of the as-released GA, previously shown in **Figure III.4.2.5a**. Therefore, in the case of the bilayer PLA films, a strong antioxidant activity was attained after two weeks of immersion in the medium while it progressively decreased over time. On the contrary, the multilayer PLA films provided a release of GA that showed a relatively low DPPH inhibition in first weeks. However, after 10 weeks, the PLA films containing the electrospun GA-loaded interlayer achieved a stronger DPPH inhibition, indicating that it effectively protects the polyphenol over longer periods. Based on the present observations, it can be considered that the GA release and, thus, the GA antioxidant functionality can be controlled by the appropriate design of PLA films containing electrospun coating and interlayers.

In this sense, other previous studies have shown the potential of electrospinning to encapsulate GA in order to retain its antioxidant activity for active packaging applications. In the study performed by Neo *et al*. [14], GA was successfully encapsulated at 5–20 wt% in zein nanofibers by electrospinning. It was found that the DPPH scavenging abilities of the GA-loaded zein electrospun fibres varied from 58% to 89%, showing that there was no significant difference for DPPH scavenging activity of GA before and after the electrospinning process. Similar antioxidant properties have been recently observed by Aydogdu *et al*. [27], who loaded GA at 2–10 wt% into electrospun hydroxypropyl methylcellulose (HPMC)/ polyethylene oxide (PEO) blend nanofibers. The antioxidant activity of the electrospun HPMC/PEO nanofibers considerably increased as the GA content increased, reaching an antioxidant activity of up to 24.74 mg DPPH/g dry weight and 50.35%. However, in both studies the electrospun nanofibers had first to be fully dissolved in ethanol aqueous solutions in order to effectively release the encapsulated GA and then achieve the reported antioxidant activity.

DISCUSSION

In this study, homogenous ultrathin PLA fibers incorporating GA polyphenol at 40 wt% with a mean diameter of *ca*. 0.9 μm were successfully produced by the electrospinning technique. The incorporation of GA into the PLA fibers increased the roughness surface and also slightly flattened the fibers shape mainly due to the conductivity increase observed in the solutions used for electrospinning. The GA-containing submicron PLA fibers were then used to build nano-sized bi- and multilayers structures based on previously prepared cast-extruded 200–μm PLA films. For the bilayer structures, the electrospun mats were applied as a coating on the PLA films for 1, 2, and 3 h. Electrospun coatings of approximately 60, 85, and 100 μm were then obtained on the PLA films after 1, 2, and 3 h of deposition during electrospinning. The electrospinning process successfully yielded the formation of continuous coatings made of submicron PLA fibers, but they were not strongly adhered to the PLA film and the resultant bilayer PLA films also lacked of transparency. To produce the multilayer PLA films, the cast films of PLA were first one side coated with electrospun GA-loaded PLA fibers, also processed for 1, 2, and 3 h, and then sandwiched with a thin PLA film of 10 μm on the other side by the application of a thermal post-treatment without pressure, the so-called annealing. It was also observed that the thickness of the electrospun nanostructured interlayers increased as a function of the during the electrospinning process though they were relatively difficult to discern due to their low thicknesses. The resultant multilayer films interestingly presented sufficient adhesion between layers as a result of the large surface-to-volume ratio of the electrospun fibers that efficiently coalesced and adhered strongly to both PLA film sides during annealing. The multilayer PLA films showed relative high transparency when the containing nanostructured interlayers were produced for up to 2 h of electrospinning due to their very little porosity.

Results also showed that the incorporation of the natural polyphenol positively delayed the thermal degradation of PLA for up to 10 °C and all films were thermally stable up to 345 °C. This thermal enhancement was more pronounced in the case of the bilayer films, being this phenomenon ascribed to the presence of the antioxidant in regions close to the films surface. During the in vitro release studies, the GA release amounts from all PLA films increased but the release rates decreased with increasing the thickness of the electrospun GA-containing layer. The bilayer PLA films showed that the cumulative release amount of GA increased rather rapidly for the first 5 h of immersion time. Further increase in the submersion time resulted in a gradual increase in the cumulative amount of the polyphenol up to it finally reached a plateau value after 45–250 h. On the contrary, the PLA multilayers offered a highly sustained release of GA, having the capacity to release the polyphenol for over 1000 h and being the release diffusionally controlled. Therefore, whereas the bilayer PLA films can provide a quick release of antioxidant into saline food simulant that can be of interest for functional food in packaging materials of a relatively short life cycles, that is, 1–2 weeks, the multilayer systems can be interesting from a point of view of food products stored in water-based media with a much longer shelf life. Finally, the antioxidant activity assessment of the GA released from the PLA films was carried out by measuring its capacity to scavenge the DPPH radicals. During the first days, the bilayer PLA films performed as a potent source of antioxidant while the multilayer films

offered comparatively weaker activities. In the long term, however, the GA released from the multilayer PLA films were able to show a stronger DDPH inhibition.

This work has demonstrated that it is possible to develop multilayer PLA films containing electrospun nanostructured coatings and interlayers that provide specific release rates of the antioxidant GA into saline medium. The fabricated multilayer films connect the rising technology of bioactive packaging intended to aid in the production of functional foods, that is, to enhance the impact of food on the consumer's health. Further studies should be focused on studying the GA release profiles of the here-developed multilayers study in different solutions and also to apply them in real food products.

Author Contributions

Conceptualization was devised by R.B, J.M.L., and S.T.-G.; methodology, validation, and formal analysis was carried out by L.Q.-C., N.M., and S.T.-G.; investigation, resources, data curation, and writing—original draft preparation was performed by L.Q.-C. and S.T.-G.; writing—review and editing: L.Q.-C., R.B., and S. T.-G.; supervision: J.M.L., R.B., and S.T.-G; project administration: J.M.L. and R.B.

Funding

Acknowledgments

REFERENCES

1. Cencic, A.; Chingwaru, W. *The role of functional foods, nutraceuticals, and food supplements in intestinal health*. Nutrients 2010, **2**, 611–625.
2. Hasler, C.M. Functional foods: *Benefits, concerns and challenges—A position paper from the american council on science and health*. J. Nutr. 2002, **132**, 3772–3781.
3. Fogliano, V.; Vitaglione, P. *Functional foods: Planning and development*. Mol. Nutr. Food Res. 2005, **49**, 256–262.
4. Lopez-Rubio, A.; Gavara, R.; Lagaron, J.M. *Bioactive packaging: Turning foods into healthier foods through biomaterials*. Trends Food Sci. Technol. 2006, **17**, 567–575.
5. Mellinas, C.; Valdés, A.; Ramos, M.; Burgos, N.; Del Carmen Garrigós, M.; Jiménez, A. *Active edible films: Current state and future trends*. J. Appl. Polym. Sci. 2016, **133**, 42631.
6. Lopez-Rubio, A.; *Bioactive food packaging strategies. In Multifunctional and Nanoreinforced Polymers for Food Packaging*; Lagaron, J.M., Ed.; Woodhead Publishing Ltd.: Cambridge, UK, 2011; pp. 460–482.
7. Castro-Aguirre, E.; Iñiguez-Franco, F.; Samsudin, H.; Fang, X.; Auras, R. *Poly (lactic acid)—Mass production, processing, industrial applications, and end of life*. Adv. Drug Deliv. Rev. 2016, **107**, 333–366.

8. Lazzeri, L.; Cascone, M.G.; Quiriconi, S.; Morabito, L.; Giusti, P. *Biodegradable hollow microfibres to produce bioactive scaffolds.* Polym. Int. 2005, **54**, 101–107.

9. Ma, J.; Luo, X.D.; Protiva, P.; Yang, H.; Ma, C.; Basile, M.J.; Weinstein, I.B.; Kennelly, E.J. *Bioactive novel polyphenols from the fruit of manilkara zapota (sapodilla).* J. Nat. Prod. 2003, **66**, 983–986.

10. Rangkadilok, N.; Sitthimonchai, S.; Worasuttayangkurn, L.; Mahidol, C.; Ruchirawat, M.; Satayavivad, J. *Evaluation of free radical scavenging and antityrosinase activities of standardized longan fruit extract. Food Chem.* Toxicol. 2007, **45**, 328–336.

11. Makris, D.P.; Boskou, G.; Andrikopoulos, N.K. *Polyphenolic content and in vitro antioxidant characteristics of wine industry and other agri-food solid waste extracts.* J. Food Compos. Anal. 2007, **20**, 125–132.

12. Kim, J.H.; Kang, N.J.; Lee, B.K.; Lee, K.W.; Lee, H.J. *Gallic acid, a metabolite of the antioxidant propyl gallate, inhibits gap junctional intercellular communication via phosphorylation of connexin 43 and extracellular-signal-regulated kinase1/2 in rat liver epithelial cells.* Mutat. Res. Fundam. Mol. Mech. Mutagen. 2008, **638**, 175–183.

13. da Rosa, C.G.; Borges, C.D.; Zambiazi, R.C.; Nunes, M.R.; Benvenutti, E.V.; da Luz, S.R.; D'Avila, R.F.; Rutz, J.K. *Microencapsulation of gallic acid in chitosan, β-cyclodextrin and xanthan.* Ind. Crops Prod. 2013, **46**, 138–146.

14. Neo, Y.P.; Ray, S.; Jin, J.; Gizdavic-Nikolaidis, M.; Nieuwoudt, M.K.; Liu, D.; Quek, S.Y. *Encapsulation of food grade antioxidant in natural biopolymer by electrospinning technique: A physicochemical study based on zein–gallic acid system.* Food Chem. 2013, 136, 1013–1021.

15. Desai, K.G.H.; Jin Park, H. *Recent developments in microencapsulation of food ingredients.* Dry. Technol. 2005, **23**, 1361–1394.

16. Torres-Giner, S.; Pérez-Masiá, R.; Lagaron, J.M. *A review on electrospun polymer nanostructures as advanced bioactive platforms.* Polym. Eng. Sci. 2016, 56, 500–527.

17. Li, D.; Xia, Y. *Electrospinning of nanofibers: Reinventing the wheel?* Adv. Mater. 2004, **16**, 1151–1170.

18. Busolo, M.A.; Torres-Giner, S.; Prieto, C.; Lagaron, J.M. *Electrospraying assisted by pressurized gas as an innovative high-throughput process for the microencapsulation and stabilization of docosahexaenoic acid-enriched fish oil in zein prolamine.* Innov. Food Sci. Emerg. Technol. 2018, doi:10.1016/j.ifset.2018.04.007.

19. Torres-Giner, S.; Wilkanowicz, S.; Melendez-Rodriguez, B.; Lagaron, J.M. *Nanoencapsulation of aloe vera in synthetic and naturally occurring polymers by electrohydrodynamic processing of interest in food technology and bioactive packaging.* J. Agric. Food Chem. 2017, **65**, 4439–4448.

20. Horuz, T.İ.; Belibağlı, K.B. *Nanoencapsulation of carotenoids extracted from tomato peels into zein fibers by electrospinning.* J. Sci. Food Agric. 2019, **99**, 759–766.

21. Fabra, M.J.; López-Rubio, A.; Lagaron, J.M. *Use of the electrohydrodynamic process to develop active/bioactive bilayer films for food packaging applications.* Food Hydrocoll. 2016, **55**, 11–18.

22. Torres-Giner, S. *Electrospun nanofibers for food packaging applications. In Multifunctional and Nanoreinforced Polymers for Food Packaging;* Lagaron, J.M., Ed.; Woodhead Publishing Ltd.: Cambridge, UK, 2011; pp. 108–125.

23. Torres-Giner, S.; Busolo, M.; Cherpinski, A.; Lagaron, J.M. *Electrospinning in the packaging industry. In Electrospinning: From Basic Research to Commercialization;* Kny, E., Ghosal, K., Thomas, S., Eds.; The Royal Society of Chemistry: Cambridge, UK, 2018; pp. 238–260.

24. Torres-Giner, S.; Martinez-Abad, A.; Lagaron, J.M. *Zein-based ultrathin fibers containing ceramic nanofillers obtained by electrospinning. II. Mechanical properties, gas barrier, and sustained release capacity of biocide thymol in multilayer polylactide films.* J. Appl. Polym. Sci. 2014, **131**, 9270–9276.

25. Hosseini, S.F.; Nahvi, Z.; Zandi, M. *Antioxidant peptide-loaded electrospun chitosan/poly(vinyl alcohol) nanofibrous mat intended for food biopackaging purposes.* Food Hydrocoll. 2019, **89**, 637–648.

26.   Alehosseini, A.; Gómez-Mascaraque, L.G.; Martínez-Sanz, M.; López-Rubio, A. *Electrospun curcumin-loaded protein nanofiber mats as active/bioactive coatings for food packaging applications.* Food Hydrocoll. 2019, **87**, 758–771.

27.   Aydogdu, A.; Sumnu, G.; Sahin, S. *Fabrication of gallic acid loaded hydroxypropyl methylcellulose nanofibers by electrospinning technique as active packaging material. Carbohydr*. Polym. 2019, **208**, 241–250.

28.   Cherpinski, A.; Torres-Giner, S.; Cabedo, L.; Lagaron, J.M. *Post-processing optimization of electrospun submicron poly(3-hydroxybutyrate) fibers to obtain continuous films of interest in food packaging applications.* Food Addit. Contam. Part A 2017, **34**, 1817–1830.

29.   Melendez-Rodriguez, B.; Castro-Mayorga, J.L.; Reis, M.A.M.; Sammon, C.; Cabedo, L.; Torres-Giner, S.; Lagaron, J.M. *Preparation and characterization of electrospun food biopackaging films of poly(3-hydroxybutyrate-co-3-hydroxyvalerate) derived from fruit pulp biowaste.* Front. Sustain. Food Syst. 2018, **2**, 38.

30.   Cherpinski, A.; Kossel, C.; Torres-Giner, S.; Lagaron, J.M. Electrospun Hydrophilic/Hydrophobic *Double Coating for Property Enhanced Fiber Based Biopackaging Applications*; TAPPI Press: London, UK, 2018; pp. 145–150.

31.   Torres-Giner, S.; Montanes, N.; Fenollar, O.; García-Sanoguera, D.; Balart, R. *Development and optimization of renewable vinyl plastisol/wood flour composites exposed to ultraviolet radiation*. Mater. Des. 2016, **108**, 648–658.

32.   Chuysinuan, P.; Chimnoi, N.; Techasakul, S.; Supaphol, P. *Gallic acid-loaded electrospun poly (l-lactic acid) fiber mats and their release characteristic*. Macromol. Chem. Phys. 2009, **210**, 814–822.

33.   Casasola, R.; Thomas, N.L.; Trybala, A.; Georgiadou, S. *Electrospun poly lactic acid (pla) fibres: Effect of different solvent systems on fibre morphology and diameter*. Polymer 2014, **55**, 4728–4737.

34.   Aytac, Z.; Kusku, S.I.; Durgun, E.; Uyar, T. *Encapsulation of gallic acid/cyclodextrin inclusion complex in electrospun polylactic acid nanofibers: Release behavior and antioxidant activity of gallic acid.* Mater. Sci. Eng. C 2016, **63**, 231–239.

35.   Ramakrishna, S.; Fujihara, K.; Teo, W.E.; Lim, T.C.; Ma, Z. *An Introduction to Electrospinning and Nanofibers*; World Scientific Publishing Co. Pte. Ltd.: Singapore, 2005.

36.   Cherpinski, A.; Torres-Giner, S.; Cabedo, L.; Méndez, J.A.; Lagaron, J.M. *Multilayer structures based on annealed electrospun biopolymer coatings of interest in water and aroma barrier fiber-based food packaging applications.* J. Appl. Polym. Sci. 2018, **135**, 45501.

37.   Cherpinski, A.; Gozutok, M.; Sasmazel, H.; Torres-Giner, S.; Lagaron, J. *Electrospun oxygen scavenging films of poly(3-hydroxybutyrate) containing palladium nanoparticles for active packaging applications.* Nanomaterials 2018, **8**, 469.

38.   Lasprilla-Botero, J.; Torres-Giner, S.; Pardo-Figuerez, M.; Álvarez-Láinez, M.; M. Lagaron, J. *Superhydrophobic bilayer coating based on annealed electrospun ultrathin poly(ε-caprolactone) fibers and electrosprayed nanostructured silica microparticles for easy emptying packaging applications*. Coatings 2018, **8**, 173.

39.   Santos, N.A.; Cordeiro, A.M.T.M.; Damasceno, S.S.; Aguiar, R.T.; Rosenhaim, R.; Carvalho Filho, J.R.; Santos, I.M.G.; Maia, A.S.; Souza, A.G. *Commercial antioxidants and thermal stability evaluations.* Fuel 2012, **97**, 638–643.

40.   Garro Galvez, J.M.; Fechtal, M.; Riedl, B. *Gallic acid a model of tannins in condensation with formaldehyde. Thermochim*. Acta 1996, **274**, 149–163.

41.   Luzi, F.; Puglia, D.; Dominici, F.; Fortunati, E.; Giovanale, G.; Balestra, G.M.; Torre, L. *Effect of gallic acid and umbelliferone on thermal, mechanical, antioxidant and antimicrobial properties of poly (vinyl alcohol-co-ethylene) films*. Polym. Degrad. Stabil. 2018, **152**, 162–176.

42.   Quiles-Carrillo, L.; Montanes, N.; Lagaron, J.M.; Balart, R.; Torres-Giner, S. *In situ compatibilization of biopolymer ternary blends by reactive extrusion with low-functionality epoxy-based styrene–acrylic oligomer.* J. Polym. Environ. 2019, **27**, 84–96.

43. Wu, J.; Chen, S.; Ge, S.; Miao, J.; Li, J.; Zhang, Q. *Preparation, properties and antioxidant activity of an active film from silver carp (hypophthalmichthys molitrix) skin gelatin incorporated with green tea extract*. Food Hydrocoll. 2013, **32**, 42–51.

44. Torres-Giner, S.; Gil, L.; Pascual-Ramírez, L.; Garde-Belza, J.A. *Packaging: Food waste reduction. In Encyclopedia of Polymer Applications*; Mishra, M., Ed.; CRC Press, Taylor and Francis Group: Boca Raton, FL, USA, 2018; pp. 1990–2009.

45. Phiriyawirut, M.; Phaechamud, T. *Gallic acid-loaded cellulose acetate electrospun nanofibers: Thermal properties, mechanical properties, and drug release behavior*. Open J. Polym. Chem. 2012, **2,** 17550.

46. Quiles-Carrillo, L.; Montanes, N.; Garcia-Garcia, D.; Carbonell-Verdu, A.; Balart, R.; Torres-Giner, S. *Effect of different compatibilizers on injection-molded green composite pieces based on polylactide filled with almond shell flour*. Compos. Part B Eng. 2018, **147**, 76–85.

47. Lu, Y.; Yeap Foo, L. *Antioxidant activities of polyphenols from sage (salvia officinalis).* Food Chem. 2001, **75**, 197–202.

48. Ghitescu, R.-E.; Popa, A.-M.; Popa, V.I.; Rossi, R.M.; Fortunato, G. *Encapsulation of polyphenols into phema e-spun fibers and determination of their antioxidant activities*. Int. J. Pharm. 2015, **494**, 278–287.

49. Kähkönen, M.P.; Hopia, A.I.; Vuorela, H.J.; Rauha, J.-P.; Pihlaja, K.; Kujala, T.S.; Heinonen, M. *Antioxidant activity of plant extracts containing phenolic compounds*. J. Agric. Food Chem. 1999, **47**, 3954–3962.

50. Han, J.; Chen, T.-X.; Branford-White, C.J.; Zhu, L.-M. *Electrospun shikonin-loaded pcl/ptmc composite fiber mats with potential biomedical applications*. Int. J. Pharm. 2009, **382**, 215–221.

III.4.3. On the use of gallic acid as a natural antioxidant and ultraviolet light stabilizer in cast-extruded bio-based high-density polyethylene films

L. Quiles-Carrillo [1], S. Montava-Jordà [1], T. Boronat [1], C. Sammon [2], R.Balart [1] and S. Torres-Giner [3]

[1] Technological Institute of Materials (ITM), Universitat Politècnica de València (UPV), Plaza Ferrándiz y Carbonell 1, 03801 Alcoy, Spain;

[2] Materials and Engineering Research Institute, Sheffield Hallam University, Howard Street, Sheffield S1 1WB, UK;

[3] Novel Materials and Nanotechnology Group, Institute of Agrochemistry and Food Technology (IATA), Spanish National Research Council (CSIC), Calle Catedrático Agustín Escardino Benlloch 7, 46980 Paterna, Valencia, Spain;

polymers

MDPI

On the Use of Gallic Acid as a Potential Natural Antioxidant and Ultraviolet Light Stabilizer in Cast-Extruded Bio-Based High-Density Polyethylene Films

Luis Quiles-Carrillo [1,*], **Sergi Montava-Jordà** [1], **Teodomiro Boronat** [1], **Chris Sammon** [2], **Rafael Balart** [1] **and Sergio Torres-Giner** [3,*]

[1] Technological Institute of Materials (ITM), Universitat Politècnica de València (UPV), Plaza Ferrándiz y Carbonell 1, 03801 Alcoy, Spain; sermonjo@mcm.upv.es (S.M.-J.); tboronat@dimm.upv.es (T.B.); rbalart@mcm.upv.es (R.B.)

[2] Materials and Engineering Research Institute, Sheffield Hallam University, Howard Street, Sheffield S1 1WB, UK; C.Sammon@shu.ac.uk

[3] Novel Materials and Nanotechnology Group, Institute of Agrochemistry and Food Technology (IATA), Spanish National Research Council (CSIC), Calle Catedrático Agustín Escardino Benlloch 7, 46980 Paterna, Spain

[*] Correspondence: luiquic1@epsa.upv.es (L.Q.-C.); storresginer@iata.csic.es (S.T.-G.); Tel.: +34-966-528-433 (L.Q.-C.); +34-963-900-022 (S.T.-G.)

check for updates

Abstract: This study originally explores the use of gallic acid (GA) as a natural additive in bio-based high-density polyethylene (bio-HDPE) formulations. Thus, bio-HDPE was first melt-compounded with two different loadings of GA, namely 0.3 and 0.8 parts per hundred resin (phr) of biopolymer, by twin-screw extrusion and thereafter shaped into films using a cast-roll machine. The resultant bio-HDPE films containing GA were characterized in terms of their mechanical, morphological, and thermal performance as well as ultraviolet (UV) light stability to evaluate their potential application in food packaging. The incorporation of 0.3 and 0.8 phr of GA reduced the mechanical ductility and crystallinity of bio-HDPE, but it positively contributed to delaying the onset oxidation temperature (OOT) by 36.5 °C and nearly 44 °C, respectively. Moreover, the oxidation induction time (OIT) of bio-HDPE, measured at 210 °C, was delayed for up to approximately 56 and 240 min, respectively. Furthermore, the UV light stability of the bio-HDPE films was remarkably improved, remaining stable for an exposure time of 10 h even at the lowest GA content. The addition of the natural antioxidant slightly induced a yellow color in the bio-HDPE films and it also reduced their transparency, although a high contact transparency level was maintained. This property can be desirable in some packaging materials for light protection, especially UV radiation, which causes lipid oxidation in food products. Therefore, GA can successfully improve the thermal resistance and UV light stability of green polyolefins and will potentially promote the use of natural additives for sustainable food packaging applications.

Keywords: bio-HDPE; GA; natural additives; thermal resistance; UV stability; food packaging

---

1. Introduction

The scarcity of petroleum and the great awareness about plastic waste have recently generated a great interest in the use of biopolymers for packaging applications [1]. Biopolymers include bio-based polymers, biodegradable polymers, and polymers featuring both characteristics. Bio-based polymers

On the use of gallic acid as a potential natural antioxidant and ultraviolet light stabilizer in cast-extruded bio-based high-density polyethylene films

Abstract.

This study originally explores the use of gallic acid (GA) as a natural additive in bio-based high-density polyethylene (bio-HDPE) formulations. Thus, bio-HDPE was first melt-compounded with two different loadings of GA, namely 0.3 and 0.8 parts per hundred resin (phr) of biopolymer, by twin-screw extrusion and thereafter shaped into films using a cast-roll machine. The resultant bio-HDPE films containing GA were characterized in terms of their mechanical, morphological, and thermal performance as well as ultraviolet (UV) light stability to evaluate their potential application in food packaging. The incorporation of 0.3 and 0.8 phr of GA reduced the mechanical ductility and crystallinity of bio-HDPE, but it positively contributed to delaying the onset oxidation temperature (OOT) by 36.5 °C and nearly 44 °C, respectively. Moreover, the oxidation induction time (OIT) of bio-HDPE, measured at 210 °C, was delayed for up to approximately 56 and 240 min, respectively. Furthermore, the UV light stability of the bio-HDPE films was remarkably improved, remaining stable for an exposure time of 10 h even at the lowest GA content. The addition of the natural antioxidant slightly induced a yellow color in the bio-HDPE films and it also reduced their transparency, although a high contact transparency level was maintained. This property can be desirable in some packaging materials for light protection, especially UV radiation, which causes lipid oxidation in food products. Therefore, GA can successfully improve the thermal resistance and UV light stability of green polyolefins and will potentially promote the use of natural additives for sustainable food packaging applications.

Keywords: bio-HDPE; GA; natural additives; thermal resistance; UV stability; food packaging

INTRODUCTION

The scarcity of petroleum and the great awareness about plastic waste have recently generated a great interest in the use of biopolymers for packaging applications [1]. Biopolymers include bio-based polymers, derived primarily from natural and renewable sources, biodegradable polymers, and polymers featuring both characteristics. Bio-based polymers can successfully save fossil resources by using biomass that regenerates annually and provides the unique potential of carbon neutrality [2]. Bio-based high-density polyethylene (bio-HDPE), also called "green" polyethylene, is a highly cristalline polyolefin produced by addition polymerization of ethylene obtained by catalytic dehydration of bioethanol [3]. Bio-HDPE has the same physical properties than its counterpart petrochemical resin, that is, high-density polyethylene (HDPE), showing good mechanical strength, high ductility, and improved water resistance [4, 5]. In 2018, bio-based but non-biodegradable polyethylenes represented approximately 9.5% of the global bioplastics' production capacity, reaching nearly 200,000 tons/year [6].

Polyolefins are excellent materials as the base of industrial plastic formulations due to their excellent balance between performance and processability by conventional processing routes such as extrusion and injection molding [7]. However, they are highly sensitive to degradation when exposed to oxidant atmospheres or ultraviolet (UV) light [8]. Polyethylenes may undergo degradation, with subsequent increase in fragility, both during processing conditions by extrusion, that is, typically around 140–160 °C [9], or injection molding, that is, above 200 °C [10], and by the presence of light, heat, and chemicals. Hence, the addition of antioxidants and/or UV light stabilizers is habitually required to preserve its original physical properties for long periods. In this regard, phenolic compounds have been extensively used to extend the life service of low-density polyethylene (LDPE) [11, 12]. Nevertheless, several synthetic polymer additives have been associated with toxicity effects on human health and the environment as well as other side effects such as carcinogenesis, which has led to some restraint in their use in plastics [13, 14]. For instance, synthetic antioxidants, such as polyphenol, organophosphate, and thioester compounds can potentially induce some toxicity derived from their migration into food products [15].

While scientific evidence on the exact implications is not conclusive, especially due to the difficulty of assessing complex long-term exposure, there are sufficient indications that warrant further research of natural additives for packaging manufacturers. For instance, tocopherol, plant extracts, and essential oils from herbs and spices have been proposed as natural antioxidants in polyolefins [16-18]. Other research works have reported the use of dihydromyricetin (DHM), quercetin or rosmarinic acid as UV light stabilizers [19, 20]. Gallic acid (GA), that is, 3,4,5-trihydroxybenzoic acid, is a naturally occurring polyphenol commonly found in a variety of fruits and vegetables such as grapes, green tea, tea leaves, or tomatoes [21, 22]. Bioactive phenolic compounds can be effectively obtained by classical solid–liquid extraction employing organic solvents in heat-reflux systems [23] as well as other novel techniques including the use of supercritical fluids, high pressure processes, microwave-assisted extraction (MAE), and ultrasound-assisted extraction [24, 25]. Therefore, GA is a good candidate to be applied as a natural polymer additive due to

its natural origin, inherently low toxicity, and high bioactive activity such as antioxidant, anti-inflammatory, anticarcinogenic, and antifungal properties [26, 27].

This study originally focuses on the use of the GA natural antioxidant to protect bio-HDPE from thermal and UV degradation. To this end, two contents of GA were melt-mixed during extrusion with bio-HDPE and the resultant materials were shaped into films by cast extrusion. The films were characterized in terms of their mechanical, morphological, and thermal performance as well as UV light stability to ascertain their potential in packaging applications.

EXPERIMENTAL

Materials

Bio-HDPE, SHA7260 grade, was manufactured by Braskem (São Paulo, Brazil) and supplied in pellets form by FKuR Kunststoff GmbH (Willich, Germany). This resin has a density of 0.955 g cm^{-3} and a melt flow index (MFI) of 20 (2.16 kg, 190 °C). It has been developed for injection molding applications and its minimum bio-based content is 94%, determined by ASTM D6866. GA, with commercial reference G7384, having 97.5–102.5% (titration) and 170.12 g mol^{-1}, was supplied in powder form by Sigma-Aldrich S.A. (Madrid, Spain). This is a water-soluble phenolic acid obtained from grapes and the leaves of different plants.

Manufacturing of Films

Different mixtures of bio-HDPE and GA were manually premixed in a zipper bag and melt-compounded in a co-rotating twin-screw extruder from Construcciones Mecánicas Dupra, S.L. (Alicante, Spain). This extruder has a ratio of length (L) to diameter (D) ratio, that is, L/D, of 24 whereas its screws have a diameter of 25 mm. The speed of the screws was set at 20 rpm and the temperature profile was adjusted as follows: 145 °C (hopper) – 150 °C – 160 °C – 165 °C (die). The extruded materials were cooled in air and then pelletized using an air-knife unit. GA was added at 0.3 and 0.8 parts per hundred resin (phr) of bio-HDPE whereas a neat bio-HDPE sample was prepared in the same conditions as the control sample.

The compounded pellets were, thereafter, cast-extruded into films using a cast-roll machine MINI CAST 25 from EUR.EX.MA. (Venegono, Italy). The extrusion speed was set at 25 rpm and the temperature profile was 150 °C (feeding) – 155 °C – 160 °C – 165 °C – 165 °C – 170 °C – 170 °C (head). Bio-HDPE films with an average thickness of approximately 150 µm were obtained by adjusting the speed of the calender and the drag.

Color Measurements

A Hunter Mod. CFLX-DIF-2 colorimeter (Hunterlab, Murnau, Germany) was used to determine the color coordinates of the film samples. The values of L^* (lightness), a^* (red to green), and b^* (yellow to blue) parameters were determined while the color difference between two samples (ΔE_{ab}^*) was calculated using **Equation III.4.3.1**:

$$\Delta E_{ab}^* = \sqrt{\Delta L^{*2} + \Delta a^{*2} + \Delta b^{*2}} \qquad \text{Equation III.4.3.1}$$

Where ΔL^*, Δa^*, and Δb^* represent the differences in L^* and the a^* and b^* coordinates, respectively, between the neat bio-HDPE film and the GA-containing bio-HDPE films. At least 5 readings were taken for each film and the average values were reported. The following assessment was used to evaluate the color change of the films based on the ΔE_{ab}^* values: below 1 indicates an unnoticeable difference in color, 1–2 a slight difference that can only be noticed by an experienced observer, 2–3.5 a noticeable difference by an unexperienced observer, 3.5–5 a clear noticeable difference, and above 5 different colors are noticeable [28].

Mechanical Tests

A universal test machine Elib 50 from S.A.E. Ibertest (Madrid, Spain) was used to perform tensile tests in the bio-HDPE film samples following the guidelines of ISO 527-1:2012. The selected load cell was 5 kN and the cross-head speed was set at 10 mm min^{-1}. Standard tensile samples (type 2) with a total length and width of 160 mm and 10 mm, respectively, were tested as indicated in ISO 527-3. Tests were performed at room conditions and at least six samples per film were analyzed.

Thermal Characterization

The main thermal transitions of the bio-HDPE film samples were obtained by differential scanning calorimetry (DSC) in a Mettler-Toledo 821 calorimeter (Mettler-Toledo, Schwerzenbach, Switzerland). Samples with a total weight of about 5–10 mg were placed into aluminum crucibles. Two types of DSC tests were carried out to evaluate the antioxidant efficiency of GA. The first test was based on a dynamic program from 30 °C to 350 °C in air atmosphere at a heating rate of 5 °C.min^{-1} where the oxidative degradation was identified as the onset oxidation temperature (OOT). The second test consisted of a heating ramp from 30 °C to 210 °C in air atmosphere at a heating rate of 5 °C min^{-1} followed by an isotherm at 210 °C for a whole period of 400 min. The latter test allowed obtaining the oxidation induction time (OIT). Furthermore, the degree of crystallinity (X_c) was calculated following **Equation III.4.3.2**:

$$X_C = \left[\frac{\Delta H_m - \Delta H_{CC}}{\Delta H_m^0 \cdot (1 - w)} \right] \cdot 100 \qquad \textbf{Equation III.4.3.2}$$

Where ΔH_m (J g^{-1}) and ΔH_{CC} (J g^{-1}) correspond to the melt and cold crystallization enthalpies, respectively. ΔH_m^0 (J g^{-1}) stands for the melt enthalpy of a theoretically fully crystalline of bio-HDPE with a value of 293.0 J g^{-1} [29] and the term 1-w represents the weight fraction of bio-HDPE.

Thermal stability was also determined by thermogravimetric analysis (TGA) in a Mettler-Toledo TGA/SDTA 851 thermobalance (Mettler-Toledo, Schwerzenbach, Switzerland). Samples with an average weight of 5–7 mg were placed in standard alumina crucibles (70 µL) and subjected to a heating program from 30 °C to 700 °C in air atmosphere at heating rates of 20 °C min^{-1}. All the thermal tests were performed by triplicate.

Aging Treatment

The aging treatment of materials was performed by means of a high-pressure mercury lamp, with 1000 W and 350 nm wavelength, model UVASPOT 1000RF2 (Honle Spain S.A., Barcelona, Spain) in a closed chamber at room conditions. Samples were exposed for a period of up to 10 h and tests were carried out in triplicate.

Infrared Spectroscopy

Attenuated total reflection–Fourier transform infrared (ATR-FTIR) spectroscopy was used to perform chemical analysis of the films. A Vector 22 from Bruker S.A. (Madrid, Spain) coupling a PIKE MIRacle™ ATR accessory from PIKE Technologies (Madison, WI, USA) were used to record the FTIR spectra. Ten scans were averaged from 4000 cm^{-1} to 450 cm^{-1} at a resolution of 4 cm^{-1}. Film samples that were UV treated at 30 min intervals were used to collect variable time FTIR spectra for a whole span time of 10 h.

Microscopy

The morphology of the fracture surfaces of the UV-treated films of bio-HDPE was observed by field emission scanning electron microscopy (FESEM) in a ZEISS ULTRA 55 from Oxford Instruments (Abingdon, UK). Samples were obtained by cryo-fracture and an acceleration voltage of 2 kV was applied during FESEM observation. The surfaces were previously coated with a gold-palladium alloy in an EMITECH sputter coating SC7620 model from Quorum Technologies, Ltd. (East Sussex, UK).

RESULTS AND DISCUSSION

Optical Properties

Figure III.4.3.1 show the surface view of the bio-HDPE films varying the GA contents. Simple naked eye examination of these images indicated that all the biopolymer films showed a high contact transparency. Indeed, bio-HDPE is highly transparent due to its high crystalline nature [30]. All the film samples exhibited a smooth, defect-free, and uniform surface, in which GA yielded a yellow color and also certain opacity. The latter effect can be ascribed to the presence of the GA particles, which reduced the transparency properties by blocking the passage of UV-Vis light and scattering light. A similar yellowing effect was observed by Al-Malaica *et al*. [31] who reported the effect of changing the concentration of tocopherol and Irganox 1010 (a commercial phenolic antioxidant) on the color stability of PP. At low additive concentrations, both antioxidants showed low influence on the color sample, expressed in terms of differences in yellow index, whereas higher concentrations of tocopherol led to noticeable color changes. In order to quantify the optical parameters, **Table III.4.3.1** gathers the values of *L**, *a**, and *b** of all the bio-HDPE films and also the $\Delta E_{ab}*$ values of the bio-HDPE films containing GA. One can observe that, as the GA content increased, the film the luminance decreased, confirming that the films became less transparent. It can be also observed that the *a** coordinate slightly changed from negative values (green) to nearly neutral values, while the *b** coordinate remarkably changed also from negative values (blue) to positive values (yellow) [32]. Therefore, the incorporation of the here-tested GA loadings induced an increase in both opacity and the hue of yellow color, which could restrict the use of the biopolymer films for

transparent applications. Furthermore, the development of a different color in the bio-HDPE film after the GA addition was noticeable ($\Delta E_{ab}^* \geq 5$). However, the GA-containing bio-HDPE films can also offer some advantages for certain packaging applications. For instance, this optical property can be desirable for the protection of foodstuff from light, especially UV radiation, which can cause lipid oxidation in the food products [33, 34]. Examples include snack products that are made with refined vegetable oils and dried soups such as chicken soup that are sensitive to UV light because they contain highly sensitive unsaturated fatty acids or dry broccoli cream soup that is sensitive to visible light because it contains the photosensitisers chlorophyll from broccoli and riboflavin from dairy ingredients. Another potential application of the here-developed films is to avoid the discoloration of sliced sausage, which is a well-known adverse effect of light that often occurs even if the product is packed under vacuum [35].

Figure III.4.3.1. Visual appearance of the bio-based high-density polyethylene (bio-HDPE) films containing different amounts of gallic acid (GA): a) Bio-HDPE; b) Bio-HDPE + 0.3GA; **c)** Bio-HDPE + 0.8GA.

Table III.4.3.1. Color parameters (L^*, a^*, b^*, and ΔE_{ab}^*) of the bio-based high-density polyethylene (bio-HDPE) films containing different amounts of gallic acid (GA).

Film	L^*	a^*	b^*	ΔE_{ab}^*
Bio-HDPE	82.9 ± 1.0	-1.9 ± 0.1	-2.8 ± 0.3	-
Bio-HDPE + 0.3GA	75.3 ± 0.9	-0.7 ± 0.3	8.8 ± 0.4	13.9 ± 0.9
Bio-HDPE + 0.8GA	70.6 ± 0.5	-0.1 ± 0.1	10.9 ± 0.2	18.5 ± 0.4

Mechanical Properties

Tensile tests were carried out in order to analyze the mechanical properties of the GA-containing bio-HDPE films. **Table III.4.3.2** summarizes the values of tensile modulus ($E_{tensile}$), maximum tensile strength (σ_{max}), and elongation at break (ε_b). One can observe that $E_{tensile}$ of the neat bio-HDPE film was 292.5 MPa and this value was reduced to 222.1 MPa and 243.6 MPa with the incorporation of 0.3 phr and 0.8 phr of GA, respectively. The value of σ_{max} was in the 20−21 MPa range for all the bio-HDPE film samples, which is similar to the values reported by other authors [36]. In relation to ε_b, the neat bio-HDPE film showed a value of 45.2%, which was also reduced to 18.6% and 20.2% after the incorporation of 0.3 phr and 0.8 phr of GA, respectively.

Significantly higher ε_b values, around 450−550%, have been reported for injection-molded articles of bio-HDPE [5, 37], which can be ascribed to the testing conditions, manufacturing method, and differences in the percentage of crystallinity as well as crystals orientation. Therefore, the incorporation of GA resulted in a reduction in both elasticity and ductility of bio-HDPE. In this regard, crystallinity can play a significant role in the mechanical and durability performance in rigid applications. A decrease in the polymer's crystallinity can lead to a reduction of Etensile and σ_{max}, which are parameters ascribed to mechanical strength [38]. For instance, Jamshidian et al. [39] showed that the use of different antioxidants in PLA films yielded lower values $E_{tensile}$, σ_{max}, and ε_b. Whereas the reduction in mechanical strength was related to an effect of reduced crystallinity, the ductility impairment observed was ascribed to a phenomenon of stress concentration by the presence of additives with a low interfacial adhesion with the biopolymer matrix. Similarly, another research work performed by Jamshidian et al. [40] demonstrated that the addition of antioxidants in PLA films yielded a reduction in the mechanical performance of PLA due to the additive was not homogenously distributed throughout the entire polymer structure, which could lead to polymer inconstancy and be another reason for decreased mechanical parameters. In general, the incorporation of antioxidants and other polymer additives can alter the film continuity and then decrease the movement of the polymer chains, leading to a ductility decrease [41]. In the particular case of HDPE, its mechanical performance reduction has been attributed to direct reaction of the antioxidant with oxygen that lowers the efficiency of the inhibitor, pro-oxidant transformation products that may be formed during the processing operations and can participate in oxidative degradation and, more importantly, to limitations in the solubility of antioxidants in the polyolefin matrix [42]. This effect differs from that of UV stabilizers, which tend to be more soluble in low-molecular weight (M_W) organic solvents [43].

Table III.4.3.2. Summary of the tensile properties of the bio-based high-density polyethylene (bio-HDPE) films containing different amounts of gallic acid (GA) in terms of tensile modulus ($E_{tensile}$), maximum tensile strength (σ_{max}), and elongation at break (ε_b).

Film	$E_{tensile}$ (MPa)	σ_{max} (MPa)	ε_b (%)
Bio-HDPE	292.5 ± 22.1	21.3 ± 1.2	45.2 ± 3.5
Bio-HDPE + 0.3GA	222.1 ± 24.2	20.1 ± 0.6	18.6 ± 2.1
Bio-HDPE + 0.8GA	243.6 ± 31.5	20.8 ± 0.9	20.2 ± 2.3

Thermal Properties

Both DSC and TGA tests were carried out in order to ascertain the influence of the GA addition on the thermal stability of the bio-based polyolefin. **Figure III.4.3.2** shows the dynamical DSC curves of the cast-extruded bio-HDPE films, whereas **Table III.4.3.3** summarizes the main thermal parameters obtained from the curves. One can observe that, in all cases, the polyolefin melted sharply in a single peak at approximately 132 °C. A similar melting profile has been observed previously for this polyolefin, regardless the origin and the methodology followed to prepare the articles

[37, 44]. It can be also seen that the ΔH_m values of bio-HDPE slightly reduced as the GA content in the green polyolefin increased. In particular, the crystallinity degree, that is, X_c, was slightly reduced from 54.8%, for the neat bio-HDPE film, to 53.5% and 52.1% for the bio-HDPE films containing 0.3 phr and 0.8 phr GA, respectively. This result suggests that the presence of the GA antioxidant decreased the lamellae size of the bio-HDPE crystals by inducing imperfections [45]. For instance, Lopez-de-Dicastillo *et al.* [46] similarly reported that the incorporation of ascorbic acid, ferulic acid, quercetin or green tea extract, induced a lower and more deficient crystallinity structure for poly(ethylene-*co*-vinyl alcohol) (EVOH).

Table III.4.3.3. Main thermal parameters of the bio-based high-density polyethylene (bio-HDPE) films containing different amounts of gallic acid (GA) in terms of melting temperature (T_m), normalized melting enthalpy (ΔH_m), degree of crystallinity (X_c), onset oxidation temperature (OOT), and oxidation induction time (OIT).

Film	T_m (°C)	ΔH_m (J g^{-1})	X_C (%)	OTT (°C)	OIT (min)
Bio-HDPE	132.1 ± 0.3	160.6 ± 1.5	54.8± 0.8	226.3 ± 1.5	4.9 ± 0.3
Bio-HDPE + 0.3GA	132.4 ± 0.5	156.5 ± 1.4	53.4± 0.7	262.8 ± 2.1	60.8 ± 0.5
Bio-HDPE + 0.8GA	132.2 ± 0.7	152.7 ± 2.0	52.0 ± 0.9	270.2 ± 1.9	244.7 ± 1.0
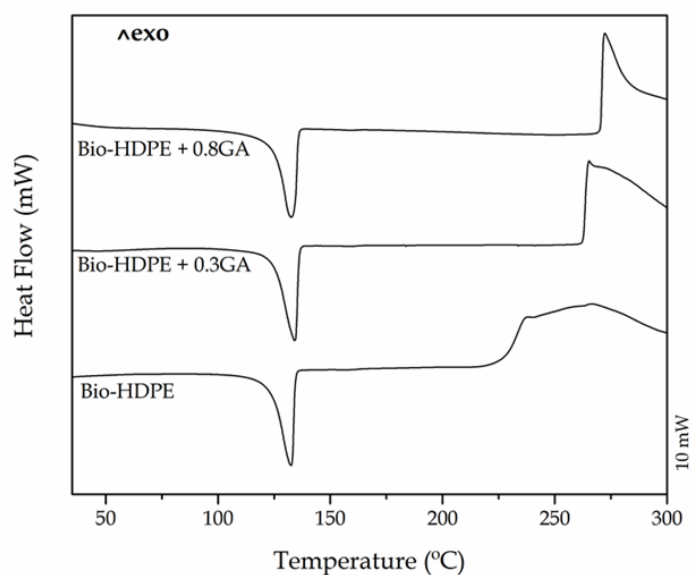
Figure III.4.3.2. Heating curves obtained by dynamic differential scanning calorimetry (DSC) of the bio-based high-density polyethylene (bio-HDPE) films containing different amounts of gallic acid (GA).

More interestingly, the DSC plots also revealed the significant oxidative retardant effect of GA on bio-HDPE. It can be observed that the onset of thermal degradation (T_{onset}), also called OOT when the DSC run is carried out in an oxygen-rich environment, started at 226.3 °C in the neat bio-HDPE film. This value is relatively

similar to that reported by Jorda-Vilaplana *et al*. [47], who showed that bio-HDPE started thermal degradation at approximately 232.5 °C. The value of T_{onset} then increased by 36.5 °C and nearly 44 °C in the bio-HDPE films containing 0.3 phr and 0.8 phr GA, respectively. Similar results were obtained by Samper *et al*. [17] in which 0.5 wt% silibinin and quercetin acted as oxidative retardants for PP as both natural additives successfully delayed the thermal oxidation onset. In this sense, Dopico-Garcia *et al*. [48] showed that the use of natural antioxidants can successfully result in polyolefins with enhanced stabilization against thermal-oxidation degradation. The criteria for the antioxidant activity is based on the o-dihydroxy structure of their B-ring, which confers higher stability to the radical form and participates in electron delocalization for effective radical scavenging.

Figure III.4.3.3 shows the isothermal DSC curves of the cast-extruded bio-HDPE films measured at 210 °C for a span time of 400 min. It can be observed that, after a heating ramp of 36 min, all the DSC pans reached 210 °C and green polyolefin samples already melted and then showed similar curves in which, thereafter, oxidation occurred at different times. The OIT value, that is, the time between melting and the decomposition onset in isothermal conditions, was seen as an exothermic peak. One can notice that in the neat bio-HDPE film oxidation initiated at approximately 5 min. The addition of 0.3 phr and 0.8 phr GA delayed oxidative thermal degradation of bio-HDPE by approximately 56 min and 240 min. It is worth to remark the high performance achieved using GA, a natural antioxidant, in comparison to other antioxidants. For instance, the use of other phenolic compounds such as the natural antioxidants naringin or silbinin at 0.5 wt% resulted in an OIT value of 17 min at 210 °C in PP [17]. In relation to synthetic antioxidants, Li *et al*. [49] showed that the incorporation of 0.1 wt% of dendritic antioxidant delayed the oxidation of PP and LDPE in 40 min and 50 min, respectively.
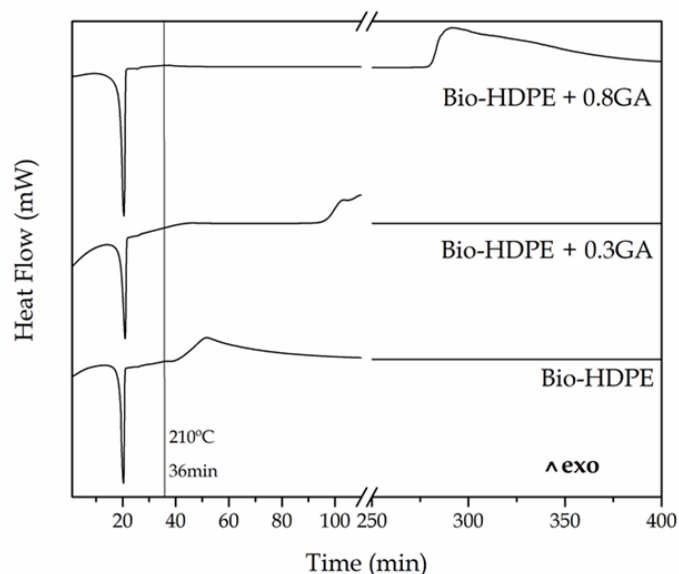
Figure III.4.3.3. Isothermal curves obtained by differential scanning calorimetry (DSC) of the bio-based high-density polyethylene (bio-HDPE) films containing different amounts of gallic acid (GA).

The improvement attained with the incorporation of the GA can be also related to the good dispersion of GA achieved within the bio-HDPE matrix. Thus, the additive chemically better contacts the peroxyradical on the polymer chains to inhibit the oxidation reaction. In this regard, Koontz *et al.* [50] showed that the addition of tocopherol improved in 68 min the OIT value of linear low-density polyethylene (LLDPE) when it was uniformly dispersed in the polyolefin matrix. Furthermore, the particular chemical structure of GA provides a great antioxidant capacity, which has been widely reported in food technology, medicine, pharmacy, etc. [51-53]. Consistent with most polyphenolic antioxidants, both the configuration and total number of hydroxyl groups can influence substantially its antioxidant activity mechanism [54, 55]. In particular, GA is a free radical scavenger that is based on the high reactivity of the hydroxyl substituents (F-OH) that participate in the next reaction [56]:

$$F - OH + R^{\cdot} \rightarrow F - O^{\cdot} + RH$$
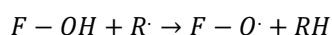
Hence, when a free radical (R$^{\cdot}$) is formed by thermo-oxidation, the phenolic compounds move toward this unstable point to block further degradation and thus producing a stabilization effect. Thus, F-OH donate hydrogen to become peroxyl (F-O$^{\cdot}$), stabilizing the free radical. Among structurally homologous flavones and flavanones, peroxyl and hydroxyl scavenging increases linearly and curvy-linearly, respectively, according to the total number of hydroxyl groups [57].

Figure III.4.3.4 shows the TGA curves (**Figure III.4.3.4a**) and DTG curves (**Figure III.4.3.4b**) of the cast-extruded bio-HDPE films while **Table III.4.3.4** summarizes the main thermal parameters obtained from the curves. The neat bio-based polyolefin presented an onset degradation temperature (T_{onset}) of 256.9 °C. The temperature of maximum degradation (T_{deg}), which corresponds to the temperature with the maximum degradation rate, was 427.8 °C. Although the thermal degradation of the green polyolefin was produced in a single step, a lower decomposition rate was observed up to approximately 370 °C, which can be seen as a shoulder in the DTG curve of the neat bio-HDPE. In this thermal range, the decomposition of the C–C covalent bond started and free radicals were generated. At higher temperatures, the free radicals formed led to sequential thermal degradation and breakdown of the main polyolefin chain [58]. Finally, all the film samples showed a similar residual mass of 0.2–0.3%, indicating fully thermal decomposition at 700 °C. In this sense, Montanes *et al.* [59] observed a similar thermal degradation profile for this green polyolefin, based on a one-step weight loss that ranged between 390 °C and 508 °C. The addition of 0.3 phr and 0.8 phr of GA successfully induced an improvement in the bio-based HDPE film of approximately 27 °C and 35 °C in the T_{onset} value and suppressing the formation of the above-described free radicals. This thermal stability enhancement was relatively similar to that obtained above by DSC, shown in previous **Table III.4.3.3**, which is related to the intrinsic antioxidant activity of the natural polyphenol. In comparison to previous works using synthetic antioxidants, Zeinalov *et al.* [60] showed that thermal degradation of neat polystyrene (PS) starts at around 270 °C, while the addition of 1% of antioxidant (Fullerene C60) delayed it up to 300 °C. In relation to other works reporting the use of GA, Luzi *et al.* [61] recently described that the addition of 5 wt% GA successfully increased by nearly 20 °C the thermal stability of EVOH films.
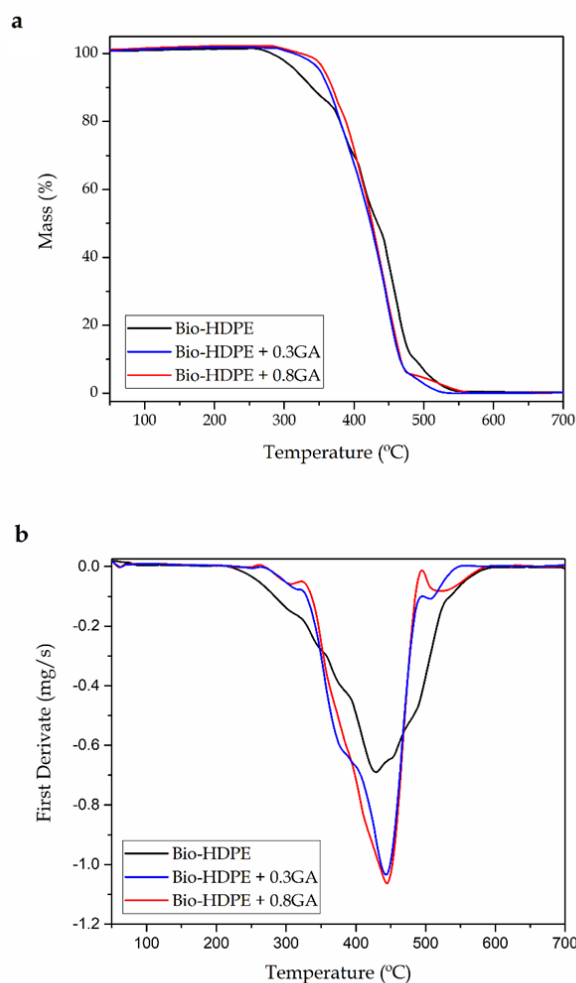
Figure III.4.3.4. (a) Thermogravimetric analysis (TGA) curves and (b) first derivative (DTG) of the bio-based high-density polyethylene (bio-HDPE) films containing different amounts of gallic acid (GA).

Table III.4.3.4. Summary of the main thermal decomposition parameters of the bio-based high-density polyethylene (bio-HDPE) films containing different amounts of gallic acid (GA) in terms of onset degradation temperature (T_{onset}), temperature of maximum degradation (T_{deg}), and residual mass at 700 °C.

Film	T_{onset} (°C)	T_{deg} (°C)	Residual mass (%)
Bio-HDPE	256.9 ± 1.8	427.8 ± 1.3	0.22 ± 0.05
Bio-HDPE + 0.3GA	283.9 ± 2.0	442.9 ± 1.1	0.20 ± 0.04
Bio-HDPE + 0.8GA	291.6 ± 2.1	444.6 ± 1.2	0.17± 0.05

It is also worthy to note that the GA addition increased the values of T_{deg} by approximately 15 °C but it also increased the of mass loss rate during thermal degradation. In general, the incorporation of different natural antioxidants can

significantly improve the thermal stability of polymers. In particular, some authors have reported similar results with other naturals antioxidant [62, 63]. For instance, España *et al*. [64] showed that the incorporation of phenolic compounds successfully improved the T_{deg} values of green composites made of a mixture of lignin and organic coconut fibers (CFs) with an excellent stabilization provided by tannic acid.

Chemical Characterization

The chemical changes in the bio-HDPE films after the GA addition were analyzed by means of FTIR spectroscopy. **Figure III.4.3.5** shows the FTIR absorbance spectra of the GA, in powder form, and the bio-HDPE and GA-containing bio-HDPE films. The main peaks of GA were observed at the 3100−3500 cm-1 region and, more intensely, from 1650 cm-1 to 560 cm-1. The peak located at 3491 cm−1 was ascribed to the O–H stretching vibration of the hydroxyl groups of polyphenols [65]. Xu *et al*. [66] showed that the strong absorption peak at around 1614 cm−1 and some bands from 1400 cm−1 to 1200 cm−1 are characteristic of polysaccharides. The peaks in the 1200–1000 cm−1 region are originated from ring vibrations that overlapped with stretching vibrations of C–OH side groups and the C–O–C glycosidic band vibration [67]. In relation to the green polyethylene, the intense peaks at 2925 cm−1, 2850 cm−1, 1460 cm−1, and 725 cm−1 are respectively assigned to stretching vibrations and bending and rocking deformations of the methylene (CH_2) groups [68]. Furthermore, the low-intense bands located between at 1377 cm−1 and 1351 cm−1 are assignable to the wagging deformation and symmetric deformation of the CH_2 and CH_3 groups, respectively. The peaks in the 1700–1800 cm−1 and 1200–1300 cm−1 regions have been ascribed to carbonyl compounds formed in the oxidation products of polyethylene [69].
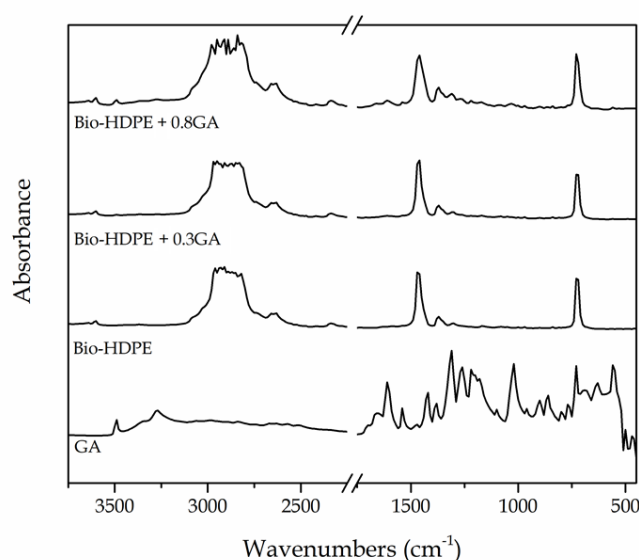
Figure III.4.3.5. Fourier transform infrared (FTIR) spectra, from bottom to top, of gallic acid (GA) powder, bio-based high-density polyethylene (bio-HDPE) film and bio-HDPE films containing 0.3 phr and 0.8 phr of GA.

The incorporation of GA into the bio-HDPE film generated the appearance of a series of peaks, particularly noticeable for the film containing 0.8 phr, which confirmed the presence of the natural antioxidant in the polyolefin. Briefly, the hydroxyl groups of GA altered the bands related to the CH_2 groups of bio-HDPE in the 3100−3500 cm^{-1} region. In addition, the formation of a new low-intense band at 1607 cm^{-1} can be ascribed to the stretching and bending vibrations of the aromatic ring of GA [65]. One can also observe the formation of a new low-intensity peak centered around 1030 cm^{-1}. Bands formed between 1021 cm^{-1} and 1037 cm^{-1} may be ascribed to the formation of dimers or oligomers of GA that can result from the stretching vibration of C−C and C−O bonds [65, 70]. Indeed, GA is known to be auto-oxidized to its semiquinone free radicals, which can consequently generate hydroquinone [71].

UV Light Stability

The bio-HDPE films were subjected to UV light for a span time of up to 10 h, herein referred as the aging time, in order to ascertain the influence of the GA addition on their UV light stability. Based on the above spectra, FTIR spectroscopy was used to analyze the chemical changes on the samples after being exposed to UV light. **Figure III.4.3.6** shows the 3D plots of the FTIR spectra taken across the exposure time to UV light. In the case of the neat bio-HDPE film, the UV exposure greatly increased the relative intensity of the strongest peaks observed at 2919 cm^{-1} and 2851 cm^{-1}, which are assigned to the CH_2 asymmetric and symmetric stretching, respectively [68]. Furthermore, the peaks centered at 1463 cm^{-1} and 720 cm^{-1} that are respectively ascribed to bending and rocking deformations in polyethylene [68] also increased. These chemical changes suggested an increase of the CH_2 groups in the film sample, which can be related to the partial breakdown of the polyolefin chain by UV degradation and the formation of more terminal groups. It is also worthy to mention that UV degradation was already noticeable after 30 min of UV light treatment, whereas it increased slightly in the whole aging time tested. No further changes were observed in the bands related to oxidized groups since changes are very subtle and also appear after longer UV exposure periods and higher temperatures [72]. The fast degradation changes observed in bio-HDPE can be ascribed to the above-reported mechanism based on free radicals with high reactivity. Interestingly, these absorbance bands related to CH_2 compounds of both GA-containing bio-HDPE films nearly remained constant and a slight increase was observed after 4h of UV light exposure. Therefore, the addition of GA successfully improved the oxidation stability of the green polyolefin, also offering long-term UV stability. As also explained above during the thermal analysis, the chemical configuration of GA and the significant number of hydroxyl groups could successfully stabilized the free radical formed during UV exposure.
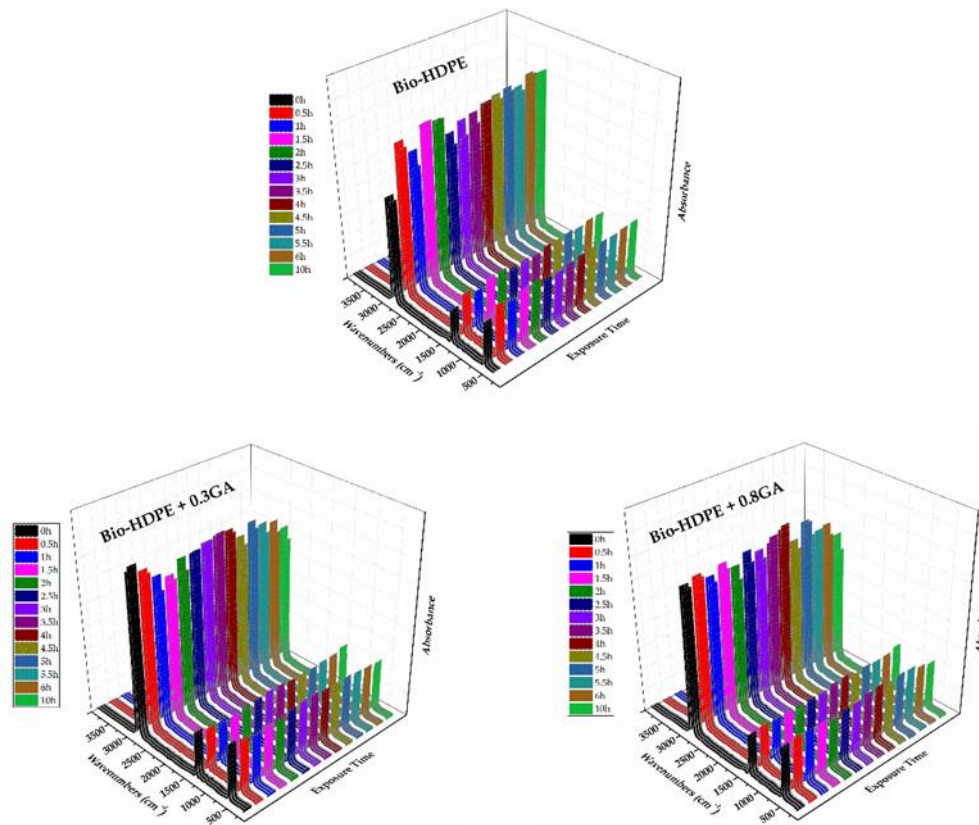
Figure III.4.3.6. Fourier transform infrared (FTIR) spectra taken across exposure time to ultraviolet (UV) light of the bio-based high-density polyethylene (bio-HDPE) films containing different amounts of gallic acid (GA).

Finally, **Figure III.4.3.7** shows the SEM images of the bio-HDPE films exposed to 5 hours UV light. One can observe that, prior to UV light exposure, all the films presented a similar fracture surface without any cracks or wrinkles. After 1h of exposure, the films developed an increase in roughness on their fracture surfaces. However, the GA-containing films generated a smoother surface, which is representative for a slower or negligible UV light aging. One can also observe that the fracture surface of the neat bio-HDPE suffered a remarkable modification after 2.5 h of exposure. Indeed, the life time of an article made of HDPE without stabilizers can be as low as one year since the polyolefin decomposes rapidly by the UV action [73]. This phenomenon is related to the presence of impurities that are formed during their synthesis, such as carbonyl, peroxide, hydroxyl, hydroxyperoxide or any substances with unsaturated groups, which absorb light at higher wavelength and thus yield the generation of free radicals. The incorporation of 0.3 phr GA significantly reduced the UV degradation of bio-HDPE and the fracture surfaces remained similar for up to 2.5 h, time at which some wrinkles were formed. Furthermore, 0.8 phr GA successfully achieved maintaining the film samples stable until 5 h of UV light exposure, showing fracture surfaces free of cracks. Therefore, the morphological analysis correlates well with the FTIR spectroscopy results and confirmed the UV light stability provided by GA to the bio-HDPE films, which can thus improve the shelf life of the green polyolefin. The antioxidant effect of GA is then considered to also protect the free

residues that are generated during polymer synthesis with improved degradation stability [74]. Indeed, UV stabilizers have always been categorized as a subgroup within the antioxidant additive group. Similarly, Du *et al.* [75] showed that HDPE/wood flour composites containing pigments presented fewer cracks on the surface than composites without pigment after accelerated UV weathering. The authors suggested that pigments can mask some UV radiation and prevent HDPE against UV radiation damage. Similar results were previously reported by Samper *et al.* [17] by the use of quercetin and silibinin as UV light stabilizers for PP.
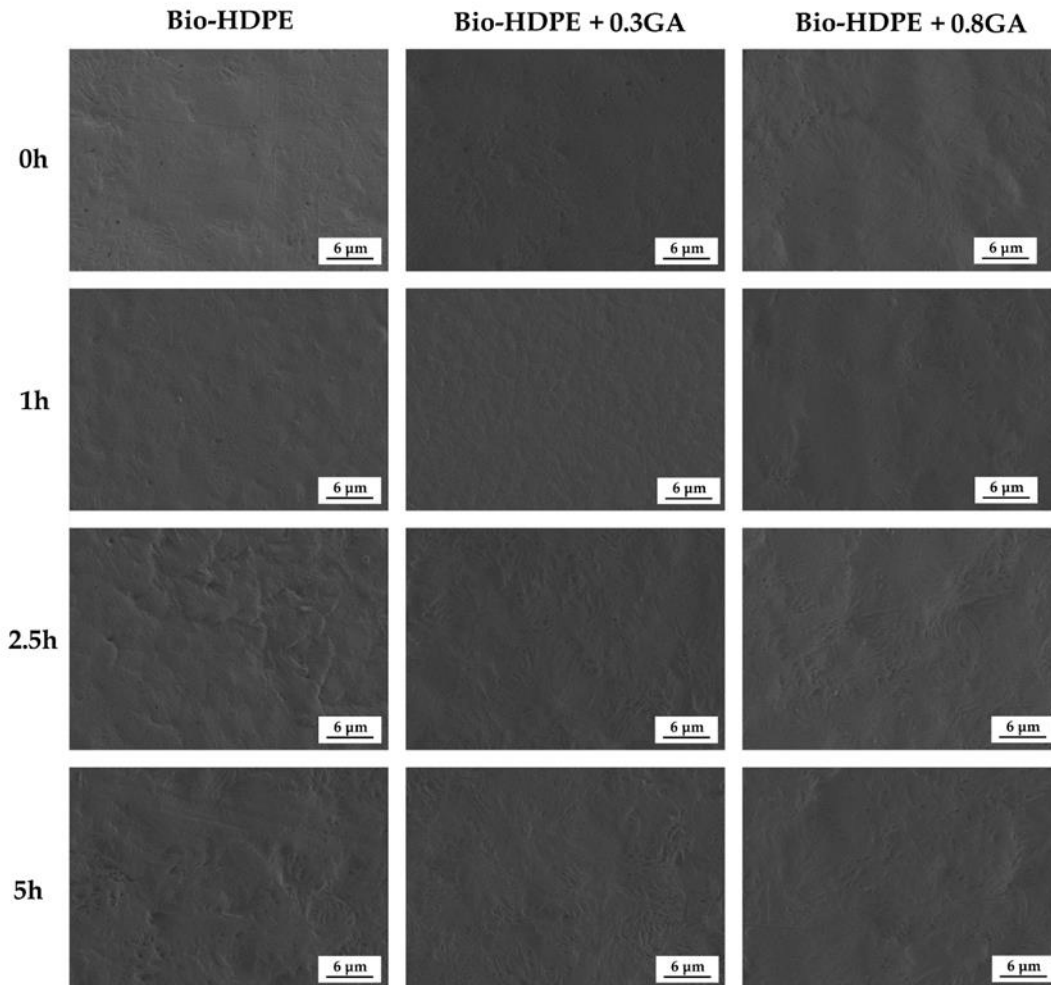
Figure III.4.3.7. Scanning electron microscopy (SEM) micrographs of the bio-based high-density polyethylene (bio-HDPE) films containing different amounts of gallic acid (GA) exposed to different ultraviolet (UV) light exposure times.

CONCLUSIONS

This work describes the development and characterization of cast-extruded bio-HDPE films containing the natural antioxidant GA in order to ascertain their potential application in food packaging. The incorporation of GA at 0.3 phr and 0.8 phr contents induced a mechanical elasticity and ductility impairment and also a crystallinity reduction of bio-HDPE due to its limited solubility in the green polyolefin matrix. The

films also developed a low-intense yellow color but they were still contact transparent. Interestingly, the OOT values was delayed by 36.5 °C and nearly 44 °C while the OIT values were reduced by approximately 56 min and 240 min in the bio-HDPE films containing 0.3 phr and 0.8 phr GA, respectively. Furthermore, the UV light stability of bio-HDPE was significantly improved after the GA addition for an aging time monitored by FTIR spectroscopy of 10h. The enhancement attained was ascribed to the high capacity of the phenolic compounds present in the natural antioxidant to stabilize the free radicals formed during degradation of the green polyolefin. As a result, GA can be regarded as a natural antioxidant and UV light stabilizer that can potentially replace synthetic additives in biopolymer formulations for food packaging applications following the Bioeconomy principles. Nevertheless, future studies should be addressed to increase the ductility of the resultant biopolymer films by, for instance, the addition of natural plasticizers, while the analysis of their barrier properties and the performance of specific migration tests will also be required according to the targeted application.

Author Contributions

Conceptualization, R.B., L.Q.-C., and S.T.-G; methodology, L.Q., S.M.-J. and C.S.; validation, C.S., R.B. and S.T.-G.; formal analysis, L.Q-C., T.B. and R.B.; investigation, C.S. and S.T.-G.; data curation, L.Q.-C., T.B., and S.M.-J.; writing—original draft preparation, L.Q.-C and S.T.-G.; writing—review and editing, R.B., S.T.-G; supervision, R.B., S.T.-G..; project administration, R.B and S.T.-G.

Funding

Acknowledgments

REFERENCES

1. Torres-Giner, S., L. Gil, L. Pascual-Ramírez and J. Garde-Belza, *Packaging: Food waste reduction.* Encyclopedia of Polymer Applications; Mishra, M., Ed.; CRC Press: Boca Raton, FL, USA, 2018.
2. Babu, R.P., K. O'connor and R. Seeram, *Current progress on bio-based polymers and their future trends.* Progress in Biomaterials, 2013. **2**(1): 8.
3. Chen, G., S. Li, F. Jiao and Q. Yuan, *Catalytic dehydration of bioethanol to ethylene over TiO2/γ-Al2O3 catalysts in microchannel reactors.* Catalysis Today, 2007. **125**(1-2): 111-119.
4. Quiles-Carrillo, L., N. Montanes, A. Jorda-Vilaplana, R. Balart and S. Torres-Giner, *A comparative study on the effect of different reactive compatibilizers on injection-molded pieces of bio-based high-density polyethylene/polylactide blends.* Journal of Applied Polymer Science, 2019. **136**(16): 47396.

5. Torres-Giner, S., A. Torres, M. Ferrándiz, V. Fombuena and R. Balart, *Antimicrobial activity of metal cation-exchanged zeolites and their evaluation on injection-molded pieces of bio-based high-density polyethylene.* Journal of Food Safety, 2017. **37**(4).

6. Vasile, C., et al., *New PLA/ZnO: Cu/Ag bionanocomposites for food packaging*. Express Polymer Letters, 2017. **11**(7): 531-544.

7. Carbonell-Verdú, A., D. García-García, A. Jordá, M. Samper and R. Balart, *Development of slate fiber reinforced high density polyethylene composites for injection molding*. Composites Part B: Engineering, 2015. **69**: 460-466.

8. Araújo, J., W. Waldman and M. De Paoli, *Thermal properties of high density polyethylene composites with natural fibres: Coupling agent effect*. Polymer Degradation and stability, 2008. **93**(10): 1770-1775.

9. Wang, J., Z. Du and T. Lian, *Extrusion–calendering process of single-polymer composites based on polyethylene*. Polymer Engineering & Science, 2018. **58**(12): 2156-2165.

10. Quiles-Carrillo, L., N. Montanes, V. Fombuena, R. Balart and S. Torres-Giner, *Enhancement of the processing window and performance of polyamide 1010/bio-based high-density polyethylene blends by melt mixing with natural additives*. Polymer International. n/a(n/a).

11. Gao, X., G. Hu, Z. Qian, Y. Ding, S. Zhang, D. Wang and M. Yang, *Immobilization of antioxidant on nanosilica and the antioxidative behavior in low density polyethylene*. Polymer, 2007. **48**(25): 7309-7315.

12. Yu, W., T. Reitberger, T. Hjertberg, J. Oderkerk, F. Costa, V. Englund and U.W. Gedde, *Chlorine dioxide resistance of different phenolic antioxidants in polyethylene*. Polymer degradation and stability, 2015. **111**: 1-6.

13. Ito, N., S. Fukushima, A. Haqlwara, M. Shibata and T. Ogiso, *Carcinogenicity of butylated hydroxyanisole in F344 rats.* Journal of the National Cancer Institute, 1983. 70(2): 343-352.

14. Reddy, V., A. Urooj and A. Kumar, *Evaluation of antioxidant activity of some plant extracts and their application in biscuits*. Food Chemistry, 2005. **90**(1-2): 317-321.

15. Gómez-Estaca, J., C. López-de-Dicastillo, P. Hernández-Muñoz, R. Catalá and R. Gavara, *Advances in antioxidant active food packaging*. Trends in Food Science & Technology, 2014. **35**(1): 42-51.

16. Peltzer, M., J. Wagner and A. Jiménez, *Thermal characterization of UHMWPE stabilized with natural antioxidants.* Journal of Thermal Analysis and Calorimetry, 2007. **87**(2): 493-497.

17. Samper, M., E. Fages, O. Fenollar, T. Boronat and R. Balart, *The potential of flavonoids as natural antioxidants and UV light stabilizers for polypropylene*. Journal of Applied Polymer Science, 2013. **129**(4): 1707-1716.

18. Tovar, L., J. Salafranca, C. Sánchez and C. Nerín, *Migration studies to assess the safety in use of a new antioxidant active packaging*. Journal of agricultural and food chemistry, 2005. **53**(13): 5270-5275.

19. Kirschweng, B., et al., *Melt stabilization of polyethylene with dihydromyricetin, a natural antioxidant.* Polymer Degradation and Stability, 2016. **133**: 192-200.

20. Doudin, K., S. Al-Malaika, H. Sheena, V. Tverezovskiy and P. Fowler, *New genre of antioxidants from renewable natural resources: Synthesis and characterisation of rosemary plant-derived antioxidants and their performance in polyolefins*. Polymer Degradation and Stability, 2016. **130**: 126-134.

21. Graham, H.N., *Green tea composition, consumption, and polyphenol chemistry*. Preventive medicine, 1992. **21**(3): 334-350.

22. Yilmaz, Y. and R.T. Toledo, *Major flavonoids in grape seeds and skins: antioxidant capacity of catechin, epicatechin, and gallic acid*. Journal of agricultural and food chemistry, 2004. **52**(2): 255-260.

23. Martins, S., C.N. Aguilar, I.d.l. Garza-Rodriguez, S.I. Mussatto and J.A. Teixeira, *Kinetic study of nordihydroguaiaretic acid recovery from Larrea tridentata by microwave-assisted extraction.* Journal of Chemical Technology & Biotechnology, 2010. **85**(8): 1142-1147.

24.   Valdés, A., L. Vidal, A. Beltran, A. Canals and M.C. Garrigós, *Microwave-assisted extraction of phenolic compounds from almond skin byproducts (Prunus amygdalus): A multivariate analysis approach.* Journal of agricultural and food chemistry, 2015. **63**(22): 5395-5402.

25.   Martins, S., S.I. Mussatto, G. Martínez-Avila, J. Montañez-Saenz, C.N. Aguilar and J.A. Teixeira, *Bioactive phenolic compounds: production and extraction by solid-state fermentation. A review.* Biotechnology advances, 2011. **29**(3): 365-373.

26.   Kim, J.H., N.J. Kang, B.K. Lee, K.W. Lee and H.J. Lee, *Gallic acid, a metabolite of the antioxidant propyl gallate, inhibits gap junctional intercellular communication via phosphorylation of connexin 43 and extracellular-signal-regulated kinase1/2 in rat liver epithelial cells.* Mutation Research/Fundamental and Molecular Mechanisms of Mutagenesis, 2008. **638**(1-2): 175-183.

27.   Quiles-Carrillo, L., N. Montanes, J.M. Lagaron, R. Balart and S. Torres-Giner, *Bioactive Multilayer Polylactide Films with Controlled Release Capacity of Gallic Acid Accomplished by Incorporating Electrospun Nanostructured Coatings and Interlayers.* Applied Sciences, 2019. **9**(3): 533.

28.   Agüero, A., M.d.C. Morcillo, L. Quiles-Carrillo, R. Balart, T. Boronat, D. Lascano, S. Torres-Giner and O. Fenollar, *Study of the Influence of the Reprocessing Cycles on the Final Properties of Polylactide Pieces Obtained by Injection Molding.* Polymers, 2019. **11**(12): 1908.

29.   Castro, D., A. Ruvolo-Filho and E. Frollini, *Materials prepared from biopolyethylene and curaua fibers: Composites from biomass.* Polymer Testing, 2012. **31**(7): 880-888.

30.   Paradkar, R., S. Sakhalkar, X. He and M. Ellison, *Estimating crystallinity in high density polyethylene fibers using online Raman spectroscopy.* Journal of applied polymer science, 2003. **88**(2): 545-549.

31.   Al-Malaika, S., C. Goodwin, S. Issenhuth and D. Burdick, *The antioxidant role of α-tocopherol in polymers II. Melt stabilising effect in polypropylene.* Polymer degradation and stability, 1999. **64**(1): 145-156.

32.   Fenollar, O., D. García, L. Sánchez, J. López and R. Balart, *Optimization of the curing conditions of PVC plastisols based on the use of an epoxidized fatty acid ester plasticizer.* European Polymer Journal, 2009. **45**(9): 2674-2684.

33.   Figueroa-Lopez, K.J., A.A. Vicente, M.A.M. Reis, S. Torres-Giner and J.M. Lagaron, *Antimicrobial and antioxidant performance of various essential oils and natural extracts and their incorporation into biowaste derived poly(3-hydroxybutyrate-co-3-hydroxyvalerate) layers made from electrospun ultrathin fibers.* Nanomaterials, 2019. **9**(2).

34.   Melendez-Rodriguez, B., K.J. Figueroa-Lopez, A. Bernardos, R. Martínez-Máñez, L. Cabedo, S. Torres-Giner and J.M. Lagaron, *Electrospun antimicrobial films of poly(3-hydroxybutyrate-co-3-hydroxyvalerate) containing eugenol essential oil encapsulated in mesoporous silica nanoparticles.* Nanomaterials, 2019. **9**(2).

35.   Møller, J.K.S., G. Bertelsen and L.H. Skibsted, *Photooxidation of nitrosylmyoglobin at low oxygen pressure. Quantum yields and reaction stoechiometries.* Meat Science, 2002. **60**(4): 421-425.

36.   Zhong, Y., D. Janes, Y. Zheng, M. Hetzer and D. De Kee, *Mechanical and oxygen barrier properties of organoclay-polyethylene nanocomposite films.* Polymer Engineering & Science, 2007. **47**(7): 1101-1107.

37.   Ferrero, B., V. Fombuena, O. Fenollar, T. Boronat and R. Balart, *Development of natural fiber-reinforced plastics (NFRP) based on biobased polyethylene and waste fibers from Posidonia oceanica seaweed.* Polymer Composites, 2015. **36**(8): 1378-1385.

38.   Harris, A.M. and E.C. Lee, *Improving mechanical performance of injection molded PLA by controlling crystallinity.* Journal of applied polymer science, 2008. **107**(4): 2246-2255.

39.   Jamshidian, M., E.A. Tehrany, F. Cleymand, S. Leconte, T. Falher and S. Desobry, *Effects of synthetic phenolic antioxidants on physical, structural, mechanical and barrier properties of poly lactic acid film.* Carbohydrate Polymers, 2012. **87**(2): 1763-1773.

40. Jamshidian, M., E.A. Tehrany, M. Imran, M.J. Akhtar, F. Cleymand and S. Desobry, *Structural, mechanical and barrier properties of active PLA–antioxidant films*. Journal of Food Engineering, 2012. **110**(3): 380-389.

41. Jongjareonrak, A., S. Benjakul, W. Visessanguan and M. Tanaka, *Antioxidative activity and properties of fish skin gelatin films incorporated with BHT and a-tocopherol*. Food Hydrocolloids, 2008. **22**(3): 449-458.

42. Chirinos Padrón, A.J., M.A. Colmenares, Z. Rubinztain and L.A. Albornoz, *Influence of additives on some physical properties of high density polyethylene-I. commercial antioxidants*. European Polymer Journal, 1987. **23**(9): 723-727.

43. Chirinos Padrón, A.J., Z. Rubinztain and M.A. Colmenares, *Influence of additives on some physical properties of high density polyethylene-II. commercial u.v. stabilizers*. European Polymer Journal, 1987. **23**(9): 729-732.

44. López-Naranjo, E.J., L.M. Alzate-Gaviria, G. Hernández-Zárate, J. Reyes-Trujeque, C.V. Cupul-Manzano and R.H. Cruz-Estrada, *Effect of biological degradation by termites on the flexural properties of pinewood residue/recycled high-density polyethylene composites*. Journal of Applied Polymer Science, 2013. **128**(5): 2595-2603.

45. Xu, T., H. Lei and C. Xie, *The effect of nucleating agent on the crystalline morphology of polypropylene (PP)*. Materials & design, 2003. **24**(3): 227-230.

46. López-de-Dicastillo, C., J. Gómez-Estaca, R. Catalá, R. Gavara and P. Hernández-Muñoz, *Active antioxidant packaging films: development and effect on lipid stability of brined sardines*. Food Chemistry, 2012. **131**(4): 1376-1384.

47. Jordá-Vilaplana, A., A. Carbonell-Verdú, M.-D. Samper, A. Pop and D. Garcia-Sanoguera, *Development and characterization of a new natural fiber reinforced thermoplastic (NFRP) with Cortaderia selloana (Pampa grass) short fibers*. Composites Science and Technology, 2017. **145**: 1-9.

48. Dopico-García, M., M. Castro-López, J. López-Vilariño, M. González-Rodríguez, P. Valentao, P. Andrade, S. García-Garabal and M. Abad, *Natural extracts as potential source of antioxidants to stabilize polyolefins*. Journal of Applied Polymer Science, 2011. **119**(6): 3553-3559.

49. Li, C., J. Wang, M. Ning and H. Zhang, *Synthesis and antioxidant activities in polyolefin of dendritic antioxidants with hindered phenolic groups and tertiary amine*. Journal of Applied Polymer Science, 2012. **124**(5): 4127-4135.

50. Koontz, J.L., J.E. Marcy, S.F. O'Keefe, S.E. Duncan, T.E. Long and R.D. Moffitt, *Polymer processing and characterization of LLDPE films loaded with a-tocopherol, quercetin, and their cyclodextrin inclusion complexes*. Journal of applied polymer science, 2010. **117**(4): 2299-2309.

51. Brewer, M., *Natural antioxidants: sources, compounds, mechanisms of action, and potential applications*. Comprehensive reviews in food science and food safety, 2011. **10**(4): 221-247.

52. Fogliano, V., V. Verde, G. Randazzo and A. Ritieni, *Method for measuring antioxidant activity and its application to monitoring the antioxidant capacity of wines*. Journal of agricultural and food chemistry, 1999. **47**(3): 1035-1040.

53. Choubey, S., L.R. Varughese, V. Kumar and V. Beniwal, *Medicinal importance of gallic acid and its ester derivatives: a patent review*. Pharmaceutical patent analyst, 2015. **4**(4): 305-315.

54. Burda, S. and W. Oleszek, *Antioxidant and antiradical activities of flavonoids*. Journal of agricultural and food chemistry, 2001. **49**(6): 2774-2779.

55. Pannala, A.S., T.S. Chan, P.J. O'Brien and C.A. Rice-Evans, *Flavonoid B-ring chemistry and antioxidant activity: fast reaction kinetics*. Biochemical and Biophysical Research Communications, 2001. **282**(5): 1161-1168.

56. Heim, K.E., A.R. Tagliaferro and D.J. Bobilya, *Flavonoid antioxidants: chemistry, metabolism and structure-activity relationships*. The Journal of nutritional biochemistry, 2002. **13**(10): 572-584.

57.	Cao, G., E. Sofic and R.L. Prior, *Antioxidant and prooxidant behavior of flavonoids: structure-activity relationships*. Free Radical Biology and Medicine, 1997. **22**(5): 749-760.

58.	Jana, R.N., P.G. Mukunda and G.B. Nando, *Thermogravimetric analysis of compatibilized blends of low density polyethylene and poly(dimethyl siloxane) rubber*. Polymer Degradation and Stability, 2003. **80**(1): 75-82.

59.	Montanes, N., D. Garcia-Sanoguera, V. Segui, O. Fenollar and T. Boronat, *Processing and characterization of environmentally friendly composites from biobased polyethylene and natural fillers from thyme herbs.* Journal of Polymers and the Environment, 2018. **26**(3): 1218-1230.

60.	Zeinalov, E.B. and G. Koßmehl, *Fullerene C60 as an antioxidant for polymers*. Polymer degradation and stability, 2001. **71**(2): 197-202.

61.	Luzi, F., D. Puglia, F. Dominici, E. Fortunati, G. Giovanale, G. Balestra and L. Torre, *Effect of gallic acid and umbelliferone on thermal, mechanical, antioxidant and antimicrobial properties of poly (vinyl alcohol-co-ethylene) films*. Polymer degradation and stability, 2018. **152**: 162-176.

62.	Cerruti, P., M. Malinconico, J. Rychly, L. Matisova-Rychla and C. Carfagna, *Effect of natural antioxidants on the stability of polypropylene films.* Polymer Degradation and Stability, 2009. **94**(11): 2095-2100.

63.	Ambrogi, V., P. Cerruti, C. Carfagna, M. Malinconico, V. Marturano, M. Perrotti and P. Persico, *Natural antioxidants for polypropylene stabilization*. Polymer degradation and stability, 2011. **96**(12): 2152-2158.

64.	España, J., E. Fages, R. Moriana, T. Boronat and R. Balart, *Antioxidant and antibacterial effects of natural phenolic compounds on green composite materials*. Polymer Composites, 2012. **33**(8): 1288-1294.

65.	Neo, Y.P., S. Ray, J. Jin, M. Gizdavic-Nikolaidis, M.K. Nieuwoudt, D. Liu and S.Y. Quek, *Encapsulation of food grade antioxidant in natural biopolymer by electrospinning technique: A physicochemical study based on zein–gallic acid system*. Food chemistry, 2013. **136**(2): 1013-1021.

66.	Xu, W., F. Zhang, Y. Luo, L. Ma, X. Kou and K. Huang, *Antioxidant activity of a water-soluble polysaccharide purified from Pteridium aquilinum*. Carbohydrate research, 2009. **344**(2): 217-222.

67.	Kacurakova, M., P. Capek, V. Sasinkova, N. Wellner and A. Ebringerova, *FT-IR study of plant cell wall model compounds: pectic polysaccharides and hemicelluloses*. Carbohydrate polymers, 2000. **43**(2): 195-203.

68.	Gulmine, J.V., P.R. Janissek, H.M. Heise and L. Akcelrud, *Polyethylene characterization by FTIR*. Polymer Testing, 2002. **21**(5): 557-563.

69.	Sugimoto, M., A. Shimada, H. Kudoh, K. Tamura and T. Seguchi, *Product analysis for polyethylene degradation by radiation and thermal ageing*. Radiation Physics and Chemistry, 2013. **82**: 69-73.

70.	Markarian, S.A., A.L. Zatikyan, S. Bonora and C. Fagnano, *Raman and FT IR ATR study of diethylsulfoxide/water mixtures*. Journal of molecular structure, 2003. **655**(2): 285-292.

71.	Gil-Longo, J. and C. González-Vázquez, *Vascular pro-oxidant effects secondary to the autoxidation of gallic acid in rat aorta.* The Journal of nutritional biochemistry, 2010. **21**(4): 304-309.

72.	Qin, H., C. Zhao, S. Zhang, G. Chen and M. Yang, *Photo-oxidative degradation of polyethylene/montmorillonite nanocomposite.* Polymer Degradation and Stability, 2003. **81**(3): 497-500.

73.	Grigoriadou, I., K. Paraskevopoulos, K. Chrissafis, E. Pavlidou, T.-G. Stamkopoulos and D. Bikiaris, *Effect of different nanoparticles on HDPE UV stability*. Polymer Degradation and Stability, 2011. **96**(1): 151-163.

74.	Scott, G., *The antioxidant role of UV stabilisers.* Pure and Applied Chemistry, 1980. **52**(2): 365-387.

75.	Du, H., W. Wang, Q. Wang, Z. Zhang, S. Sui and Y. Zhang, *Effects of pigments on the UV degradation of wood-flour/HDPE composites.* Journal of applied polymer science, 2010. **118**(2): 1068-1076.

III.4.4. Enhancement of the processing window and performance of polyamide 1010/bio-based high-density polyethylene blends by melt mixing with natural additives

L. Quiles-Carrillo [1], N. Montanes [1], V. Fombuena [1], R.Balart [1] and S. Torres-Giner [2]

[1] Technological Institute of Materials (ITM), Universitat Politècnica de València (UPV), Plaza Ferrándiz y Carbonell 1, 03801 Alcoy, Spain;

[2] Novel Materials and Nanotechnology Group, Institute of Agrochemistry and Food Technology (IATA), Spanish National Research Council (CSIC), Calle Catedrático Agustín Escardino Benlloch 7, 46980 Paterna, Valencia, Spain

Research Article

SCI

Enhancement of the processing window and performance of polyamide 1010/bio-based high-density polyethylene blends by melt mixing with natural additives

Luis Quiles-Carrillo,[a]* Nestor Montanes,[a] Vicent Fombuena,[a] Rafael Balart[a] and Sergio Torres-Giner[b]

ABSTRACT

This work reports the enhancement of the processing window and of the mechanical and thermal properties of biopolymer blends of polyamide 1010 (PA1010) and bio-based high-density polyethylene (bio-HDPE) at 70/30 (w/w) achieved by means of natural additives. The overall performance of the binary blend melt-mixed without additives was poor due to both the relatively low thermal stability of bio-HDPE at the processing temperatures of PA1010, that is, 210–240 °C, and the lack of or poor miscibility between the two biopolymers. Gallic acid, a natural phenolic compound, was added at 0.8 parts per hundred resin (phr) of biopolymer blend to enhance the thermal stability of the green polyolefin and therefore enlarge the processing window of the binary blend. Maleinized linseed oil, a multi-functionalized vegetable oil, was then incorporated at 5 phr to compatibilize the biopolymers and the performance of the blend was also compared with that of a conventional petroleum-derived copolymer, namely poly[ethylene-co-(acrylic acid)]. The resultant biopolymer blends showed a marked enhancement in thermal stability and also improved toughness when both natural additives were combined. This work can potentially serve as a sound base study for the mechanical recycling of similar blends containing bio-based but non-biodegradable polymers.
© 2019 Society of Chemical Industry

Keywords: PA1010; green polyethylene; thermal stability; mechanical properties; secondary recycling

INTRODUCTION

In the last few years, several aliphatic polyamides (PAs) have been totally or partially obtained from bio-based building blocks.[1] In this regard, polyamide 1010 (PA1010) can be produced using 1,10-decamethylenediamine and sebacic acid, which can be synthesized from a natural source, that is, castor oil, which certainly plays a key role in bio-based PAs.[2] PA1010 is fully bio-based and it is especially useful in engineering applications requiring flexibility, heat resistance and low extraction.[3,4] Aligned with the principles of the circular economy, the possibility of the recycling of PAs has also raised great interest.[5–7] Chemical or tertiary recycling of PAs by depolymerization to obtain the original monomers is, however, still not fully technologically and economically feasible.[8] Also, the environmental benefits of plastic incineration are questionable. For these reasons, mechanical or secondary recycling is nowadays regarded as the most sustainable alternative, with excellent balance between technical viability, costs and environmental benefits.[9]

Some of the drawbacks related to mechanical recycling are contamination with other polymers, thermal degradation and poor (or lack of) miscibility, which result in a marked deterioration in mechanical properties.[10] It is worth noting the increasing use of PA/polyolefin laminates, such as those based on high-density polyethylene (HDPE), in the packaging industry.[11] The selection of the optimal processing window for the mechanical recycling

of PA/HDPE blends is critical since the processing temperature of PA is higher than the onset degradation temperature of HDPE. Therefore, the polyolefin component may undergo thermal degradation during melt processing at temperatures in the range 220–240 °C, or due to the presence of light, heat or chemicals.[12] Moreover, since both polymers in such blends are immiscible, their melt-reprocessed blends show phase separation and poor mechanical properties.[13,14]

The use of antioxidants can improve the stability and enlarge the processing window of polyolefins and their blends. Nevertheless, bearing in mind the strong environmental concerns related to plastic additives, the use of natural antioxidants is currently preferred over petroleum-derived antioxidants.[15] Indeed, natural antioxidants can successfully provide stabilizing properties in polymers similar to those of synthetic phenolic-type

* Correspondence to: L Quiles-Carrillo, Technological Institute of Materials (ITM), Universitat Politècnica de València (UPV), Plaza Ferrándiz y Carbonell 1, 03801 Alcoy, Spain. E-mail: luiquic1@epsa.upv.es

a Technological Institute of Materials (ITM), Universitat Politècnica de València (UPV), Alcoy, Spain

b Novel Materials and Nanotechnology Group, Institute of Agrochemistry and Food Technology (IATA), Spanish National Research Council (CSIC), Paterna, Spain

61

Enhancement of the processing window and performance of polyamide 1010/bio-based high-density polyethylene blends by melt mixing with natural additives

Abstract.

This work reports the enhancement of the processing window and the mechanical and thermal properties of biopolymer blends of polyamide 1010 (PA1010) and bio-based high-density polyethylene (bio-HDPE) at 70/30 (wt/wt) achieved by means of natural additives. The overall performance of the binary blend melt-mixed without additives was poor due to both the relatively low thermal stability of bio-HDPE at the processing temperatures of PA1010, that is, 210–240 °C, and the lack or poor miscibility between the two biopolymers. Gallic acid (GA), a natural phenolic compound, was added at 0.8 parts per hundred resin (phr) of biopolymer blend to enhance the thermal stability of the green polyolefin and therefore enlarge the processing window of the binary blend. Maleinized linseed oil (MLO), a multi-functionalized vegetable oil, was then incorporated at 5 phr to compatibilize the biopolymers and its performance was also compared with that of a conventional petroleum-derived copolymer, namely, poly(ethylene-co-acrylic acid) (PE-co-AA). The resultant biopolymer blends showed a remarkable enhancement in the thermal stability and also improved toughness when both natural additives were combined. This work can potentially serve as a sound base study for the mechanical recycling of similar blends based on bio-based but non-biodegradable polymers.

Keywords: PA1010; Green polyethylene; Thermal stability; Mechanical properties; Secondary Recycling

INTRODUCTION

In the last years, several aliphatic polyamides (PAs) have been totally or partially obtained from bio-based building blocks [1]. In this regard, polyamide 1010 (PA1010) can be produced using 1,10-decametylene diamine (DMDA) and sebacic acid, which can be synthesized from a natural source, that is, castor oil, which certainly plays a key role in bio-based polyamides (bio-PAs) [2]. PA1010 is fully bio-based and it is especially useful in engineering applications requiring flexibility, heat resistance, and low extraction [3, 4]. Aligned with the principles of the Circular Economy, the possibility of PAs to be recycled has also raised a great interest [5-7]. Chemical or tertiary recycling of PAs by depolymerization to obtain the original monomers is, however, still not fully technological and economically feasible [8]. Alternatively, the environment benefits of plastic incineration are questionable. For these reasons, mechanical or secondary recycling is nowadays regarded as the most sustainable alternative, with excellent balance between technical viability, costs, and environmental benefits [9].

Some of the drawbacks related to mechanical recycling are the contamination with other polymers, thermal degradation, and the poor (or lack of) miscibility, which result in a remarkable decrease in mechanical properties [10]. It is worthy to note the increasing use of PA/polyolefin laminates, such as those based on high-density polyethylene (HDPE), in the packaging industry [11]. The selection of the optimal processing window for the mechanical recycling of PA/HDPE blends is critical since the processing temperature of the PA is higher than the onset degradation temperature of HDPE. Therefore, the polyolefin may undergo thermal degradation during melt processing at temperatures in the 220-240 °C range, or due to the presence of light, heat, or chemicals [12]. Moreover, since both polymers in article are immiscible, their melt-reprocessed blends show phase separation and poor mechanical properties [13, 14].

The use of antioxidants can improve the stability and enlarge the processing window of polyolefins and their blends. Nevertheless, bearing in mind the strong environmental concern related to plastic additives, the use of natural antioxidants is currently preferred over petroleum-derived antioxidants [15]. Indeed, natural antioxidants can successfully provide similar stabilizing properties in polymers than synthetic phenolic-type antioxidants [16, 17]. In this sense, gallic acid (GA) is one of the most interesting natural antioxidants, and it can be found in a variety of fruits and vegetables such as grapes, green tea, tea leaves, tomatoes and carob pods [18, 19]. Spain is the main producer of carob, followed by Italy, Portugal, and Morocco [20]. Moreover, GA can be effectively obtained from carob pods microwave-assisted extraction [21].

The addition of copolymers to polymer blends can increase the morphological stability and interfacial adhesion of polymer blends to overcome or minimize the effects of immiscibility [22]. For instance, poly(ethylene-*co*-glycidyl methacrylate) polymers yield interesting compatibilization properties due to the reactivity of the glycidyl methacrylate group [23, 24], thus leading to blends with enhanced properties [25]. From a more sustainable point of view, the use of multi-functionalized vegetable oil derivatives represents an environmentally friendly solution to achieve compatibilization [26, 27]. To this end, vegetable oils are subjected to chemical

modifications, such as acrylation [28], epoxidation [29, 30] or maleinization [31, 32]. In this regard, maleinized linseed oil (MLO) has shown interesting results as a compatibilizer for polymer blends [33-37].

The aim of this work is to improve the thermal stability and the mechanical and thermomechanical properties of binary blends made of PA1010 and bio-based high-density polyethylene (bio-HDPE) by means of natural additives. On the one hand, the use of GA was intended to extend the processing window of bio-HDPE to avoid degradation during processing of the biopolymer blends. On the other, MLO was added to increase the chemical interactions between the two immiscible biopolymers.

EXPERIMENTAL

Materials

PA1010, was supplied as NP-PA1010-201, in a pellet forms by NaturePlast (Ifs, France). This grade is a long chain PA, fully bio-based and characterized by a medium viscosity. It is an injection-grade homopolyamide with a density of 1.05 g/cm^3 and a viscosity number (VN) of 160 cm^3/g. Bio-HDPE, commercial grade of HDPE SHA7260, was supplied by Braskem (São Paulo, Brazil). This green polyethylene has a density of 0.955 g/cm^3 and a melt flow index (MFI) of 20 g/10 min, measured with a load of 2.16 kg at a temperature of 190 ºC.
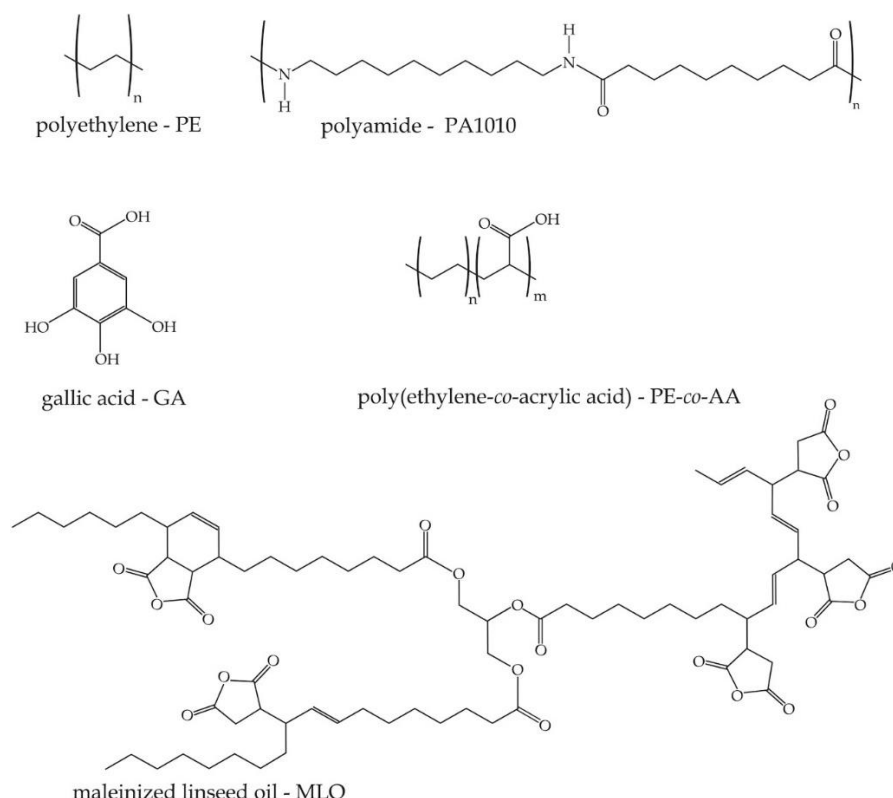
Figure III.4.4.1. Schematic representation of the chemical structure of the base polymers polyamide 1010 (PA1010) and bio-based high-density polyethylene (bio-HDPE) and the additives gallic acid (GA), maleinized linseed oil (MLO), and poly(ethylene-*co*-acrylic acid) copolymer (PE-*co*-AA).

GA, with commercial reference G7384 and 170.12 g/mol was supplied in powder form by Sigma-Aldrich S.A. (Madrid, Spain). This is a water-soluble phenolic acid obtained from grapes and the leaves of different plants. MLO was obtained from Vandeputte (Mouscron, Belgium) as VEOMER LIN. This has a viscosity of 1,000 cP (20°C) and an acid value of 105–130 mg KOH/g. Poly(ethylene-co-acrylic acid) (PE-*co*-AA), with CAS Number 9010-77-9, an acrylic acid content of 20 wt%, and density of 0.96 g/cm³ at 25 ºC was supplied by Sigma-Aldrich S.A. (Madrid, Spain). **Figure III.4.4.1** summarizes the chemical structures of all these materials. All materials were used as received without any purification process.

Manufacturing of blends

Prior to processing, PA1010 and Bio-HDPE were subjected to a drying process at 60 °C for 48 h in a dehumidifying dryer MDEO to remove any residual moisture. The extrusion was carried out in a co-rotating twin-screw extruder manufactured by Construcciones Mecánicas Dupra, S.L. (Alicante, Spain). The rotating speed of the screws was relatively low to enhance good mixing and was stablished at 20 rpm. The temperature profile was adjusted as follows: 220 (hopper)-230-235-240 (die) °C. The screws had a diameter of 25 mm with a L/D ratio of 24 (length to diameter ratio). **Table III.4.4.1** summarizes the composition of the blends.

Table III.4.4.1. Summary of compositions according to the weight content (wt%) of polyamide 1010 (PA1010) and bio-based high-density polyethylene (bio-HDPE) blends in which gallic acid (GA), maleinized linseed oil (MLO), and poly(ethylene-*co*-acrylic acid) copolymer (PE-*co*-AA) were added as parts per hundred resin (phr) of biopolymer blend.

Code	PA1010 (wt%)	Bio-HDPE (wt%)	GA (phr)	MLO (phr)	PE-*co*-AA (phr)
PA1010	100	0	0	0	0
PA1010/bio-HDPE	70	30	0	0	0
PA1010/bio-HDPE /GA	70	30	0.8	0	0
PA1010/bio-HDPE/GA/MLO	70	30	0.8	5	0
PA1010/bio-HDPE/GA/PE-*co*-AA	70	30	0.8	0	5

The compounded pellets obtained after extrusion were, thereafter, shaped into standard samples by injection molding using a Meteor 270/75 from Mateu & Solé (Barcelona, Spain), using a temperature profile of 210 °C (hopper), 220 °C, 230 °C, and 240 °C (injection nozzle). A clamping force of 75 tons was applied while the cavity filling and cooling times were set to 1 and 10 s, respectively. Different standard samples with an average thickness of 4 mm were obtained for further characterization.

Mechanical characterization

Characterization of the tensile properties of PA1010/bio-HDPE blends was carried out in a universal test machine Elib 50 from S.A.E. Ibertest (Madrid, Spain)

using injection-molded dog bone-shaped samples according to ISO 527-1:2012. A 5 kN load cell was used for all tensile tests while the cross-head speed was set to 10 mm/min. Shore hardness values of the samples were collected using a 676-D durometer from J. Bot Instruments (Barcelona, Spain), using the D-scale. Shore D measurements were conducted on injection-molded samples sizing 80x10x4 mm3, according to ISO 868:2003. Toughness was also assessed on rectangular samples (80x10x4 mm³) by measuring the impact strength on a 6-J Charpy pendulum from Metrotec S.A. (San Sebastián, Spain) on notched samples with a "V" type notch (0.25 mm radius, as recommended by ISO 179-1:2010. All tests were performed at room temperature and, at least, 6 samples of each material were tested, and the corresponding mechanical parameters obtained from each test were averaged.

Morphology characterization

Due to the immiscibility of Bio-HDPE and PA1010, the morphology of the fractured surfaces obtained after impact tests, was observed by field emission scanning electron microscopy (FESEM) in a ZEISS ULTRA 55 from Oxford Instruments (Abingdon, United Kingdom) working at an acceleration voltage of 2 kV. As these polymer blends were not electrical conducting materials, the surfaces were subjected to a sputtering process to deposit an ultrathin gold-palladium alloy using an EMITECH sputter coating SC7620 supplied by Quorum Technologies, Ltd. (East Sussex, UK).

Infrared spectroscopy

Chemical analysis was performed using attenuated total reflection–Fourier transform infrared (ATR-FTIR) spectroscopy. Spectra were recorded with a Vector 22 from Bruker S.A. (Madrid, Spain) coupling a PIKE MIRacle™ ATR accessory from PIKE Technologies (Madison, WI, USA). Ten scans were averaged from 4000 cm^{-1} to 500 cm^{-1} at a resolution of 4 cm^{-1}.

Thermal characterization

Thermal characterization of PA1010/bio-HDPE blends was studied by differential scanning calorimetry (DSC) in a Mettler-Toledo 821 calorimeter (Schwerzenbach, Switzerland). A sample weight comprised between 5-7 mg was subjected to a dynamic thermal program divided in three different stages: initially, a first heating cycle from 30 °C to 220 °C was, followed by controlled cooling to -50 °C. Finally, a second heating stage from -50 °C up to 350 °C was scheduled. The heating and cooling rates were set to 10 °C/min. All tests were run in nitrogen atmosphere with a flow of 66 mL/min using standard sealed aluminum pans with a total volume of 40 µL. The degree of crystallinity (χ_c) (in percentage, %) was calculated for both semicrystalline PA101o and bio-HDPE polymers following **Equation III.4.4.1**:

$$\chi_C = \left[\frac{\Delta H_m}{\Delta H_m^0 \cdot (1-w)} \right] \cdot 100 \qquad \textbf{Equation III.4.4.1}$$

In the previous equation, ΔH_m corresponds to the melt crystallization enthalpy obtained after integration of the corresponding endothermic peak of bio-HDPE or PA1010. ΔH_m^0 (J/g) stands for the melt enthalpy of a theoretically fully crystalline polymer. This value is 293.0 J/g for bio-HDPE and 244 J/g for PA1010 [38]. Finally, (1-

w) represents the weight fraction the polymer whose crystallinity is being calculated, with their corresponding ΔH_m and ΔH_m^0 values.

Thermal stability in more aggressive conditions (degradation/decomposition) was studied by thermogravimetry (TGA) in a Mettler-Toledo TGA/SDTA 851 thermobalance (Schwerzenbach, Switzerland). The sample weight was also set to 5-7 mg to enhance reproducibility. Samples were placed into standard alumina crucibles of 70 μL and then, subjected to a dynamic heating cycle from 30 up to 700 °C. The selected heating rate was 20 °C/min. All TGA tests were conducted in air atmosphere.

Thermomechanical characterization

Dynamical mechanical properties as a function of temperature were obtained in a DMA1 dynamic analyzer from Mettler-Toledo (Schwerzenbach, Switzerland), working in flexural conditions (single cantilever). The sample size for these tests were rectangular shapes with dimensions 20×6×2.7 mm³. A dynamic temperature sweep was scheduled to evaluate dynamic-mechanical properties in terms of increasing temperature from -160 °C up to 150 °C at a constant heating rate of 2 °C/min. The frequency was set to 1 Hz while the maximum allowed deflection was 10 μm.

In addition to DMTA characterization, the dimensional stability of PA1010/bio-HDPE blends was estimated by thermomechanical analysis (TMA) in a Q-400 thermoanalyzer from TA Instruments (Newcastle, DE, USA). Rectangular samples with dimensions 10×10×4 mm³ were subjected to a dynamic temperature ramp from -150 °C up to 150 °C using a constant heating rate of 3 °C/min and a constant applied load of 20 mN.

RESULTS ANS DISCUSION

Mechanical characterization

Table III.4.4.2 shows the mechanical properties of the PA1010/bio-HDPE blends. In particular, the values of the tensile modulus, maximum tensile strength, elongation at break, hardness and impact strength are displayed. Neat PA1010 showed values of tensile modulus and strength of 639.2 MPa and 48.6 MPa, respectively, with a high elongation at break of 515.8%. This tensile strength is typical of engineering plastics [39]. One can observe that neat PA1010 is not a stiff material but it shows a high toughness. The addition of 30 wt% of bio-HDPE to PA1010 resulted in a lower tensile modulus, down to 300 MPa, increasing the material's ductility. Nevertheless, it is worthy to note the decrease observed in tensile strength, down to 26.9 MPa, which represents almost half the value of neat PA1010. This decrease is directly related to the poor miscibility between both biopolymers in the blend. In addition, a dramatic decrease in elongation at break from 515.8% to 72.8% was observed. In this sense, Scaffaro *et al*. [40] reported similar results in polyamide 6 (PA6)/HDPE blends. It was indicated that the decrease in elongation at break was more pronounced at high HDPE contents in the blend. For instance, the HDPE25/PA675 was reduced down to 4.7%, while the effect of the addition of 25 wt% HDPE on the elongation at break of PA6 was not significant, resulting in a final elongation at break of 20%.

Table III.4.4.2. Summary of the mechanical properties of polyamide 1010 (PA1010)/bio-based high-density polyethylene (bio-HDPE) blends processed with gallic acid (GA), maleinized linseed oil (MLO), and poly(ethylene-*co*-acrylic acid) copolymer (PE-*co*-AA) in terms of: tensile modulus (E), maximum tensile strength (σ_{max}), elongation at break (ε_b), Shore D hardness, and impact strength.

Sample	E (MPa)	σ_{max} (MPa)	ε_b (%)	Shore D hardness	Impact strength (kJ/m²)
PA1010	639.2 ± 24	48.6 ± 1.5	515.8 ± 16.8	73.4 ± 0.8	8.3 ± 0.6
Bio-HDPE	364.6 ± 18	19.4 ± 0.8	518.2 ± 22.3	59.6 ± 0.9	3.5 ± 0.2
PA1010/bio-HDPE	298.3 ± 29	26.9 ± 1.9	72.8 ± 14.6	70.0 ± 1.0	2.8 ± 0.2
PA1010/bio-HDPE /GA	266.0 ± 23	26.1 ± 0.5	134.3 ± 11.7	70.2 ± 1.1	3.7 ± 0.6
PA1010/bio-HDPE/GA/MLO	237.5 ± 12	23.3 ± 0.6	139.6 ± 9.1	67.8 ± 0.7	4.3 ± 0.5
PA1010/bio-HDPE/GA/PE-*co*-AA	240.1 ± 19	30.6 ± 0.4	150.8 ± 14.8	70.6 ± 0.9	3.5 ± 0.2

The loss in mechanical properties is highly affected by the poor miscibility between both materials. Similar results were shown by Chen *et al.* [41] for PA6/HDPE blends. In particular, they demonstrated a dramatic decrease in elongation at break in comparison to neat PA6 and HDPE, which was attributed to the poor interfacial adhesion between the HDPE matrix and the dispersed PA6 phase. In addition to poor miscibility, the here-obtained poor mechanical properties could also be related to somewhat thermal degradation of bio-HDPE during. One can observe that the addition of GA had a positive effect on overall mechanical properties of PA1010/bio-HDPE blend. The tensile strength remained almost constant with a value of 26.1 MPa but the elongation at break was almost doubled. So that, in addition to the antioxidant properties that 0.8 phr GA can provide to the binary blend, a clear positive effect on mechanical properties was attained. In particular, it resulted in a remarkable increase in elongation at break. This could be related to a plasticizing effect or even an improvement related to the thermal stability that GA provides to bio-HDPE during processing. In this regard, Ambrogi *et al.* [42] reported a similar mechanical behavior with some natural antioxidants in PP. In particular, it was indicated an increase in elongation at break by using different natural antioxidants, namely, Pycnogenol® from maritime pine bark, carotenoids from tomato oleoresin, and a derivative from Cabernet pomace grape. Accordingly, this observation suggests that the addition of natural antioxidants also produces a slight decrease in both tensile modulus and strength. The presence of antioxidants could also impair crystallinity with the subsequent decrease in tensile modulus and strength [43]. For instance, Jamshidian *et al.* [43] reported that the incorporation of several natural antioxidants such as ascorbyl palmitate (AP) and α-tocopherol (AT) exerted a clear plasticization on polylactide (PLA).

The addition of the different compatibilizers also provided some changes in the mechanical properties of the PA1010/bio-HDPE blend. The addition of MLO slightly reduced the tensile modulus and strength by 10% but increased elongation at break by

5%. In this sense, MLO can successfully provide additional plasticization properties to the blend, thus leading to an improvement in ductile properties. Similar results have been reported in binary systems such as PLA/thermoplastic starch (TPS) blends [44] and polybutylene succinate (PBS) composites with almond shell flour (ASF) [45]. In both systems, the overall effect of MLO addition was remarkable on the improvement ductility and compatibility between the different components. With regard to PE-*co*-AA, it provided superior properties to the PA1010/bio-HDPE blend when compared to MLO. The most relevant changes were related to the increase in both tensile strength and elongation at break, which is a clear evidence of the compatibilizing effect that PE-*co*-AA can provide to the binary blend. Halldén *et al.* [46] showed very similar results in binary blends of low-density polyethylene (LDPE) and PA6, where the addition of PE-*co*-AA into the mixture markedly improved the elongation at break. It was also indicated the high efficiency of poly(ethylene-*graft*-ethylene oxide) (PE-*g*-PEO) as compatibilizer in this binary blend.

After the addition of bio-HDPE to PA1010, a nearly 4-fold reduction of hardness was observed. This can be related to the intrinsically lower hardness of bio-HDPE than PA1010, being the latter an engineering polymer. The incorporation of the GA and the PE-*co*-AA did not affect this hardness but the addition of MLO provided lower hardness due to its plasticizing effect. With regard to the overall toughness, estimated by the impact strength, the blend of PA1010 containing 30 wt% bio-HDPE showed a remarkable decrease in the impact strength from 8.3 kJ/m^2, for neat PA1010, down to 2.8 kJ/m^2, for the PA1010 blend with 30 wt% bio-HDPE. Impact strength is directly related to material's cohesion and, as expected, PA1010 and bio-HDPE are not miscible, as it will be discussed further. In any case, the plasticizing effect of the natural additive was enough to improved impact strength up to values of 3.7 kJ/m^2. Despite this, the highest impact strength was obtained by the combination of both GA and MLO, showing values of 4.3 kJ/m^2 that are still far from the values of neat PA1010. Despite this, the positive effect of the GA and MLO combination is clearly observed due to the impact strength was improved in comparison with the uncompatibilized PA1010/bio-HDPE blend. Several works have reported that MLO can perform as a bio-based solution to improve toughness in brittle materials such as PLA and its green composites with hazelnut shell flour (HSF) [28, 47]. Furthermore, as one can observe, PE-co-AA compatibilizer also increased both tensile strength and elongation at break, both parameters having a positive effect on the overall material's toughness. Scaffaro *et al*. [40] showed a similar improvement in PA6/LDPE blends.

Morphological characterization

Figure III.4.4.2 shows the FESEM images of the fracture surfaces of the PA1010/bio-HDPE blends from the impact tests. **Figure III.4.4.2a-b** correspond to the fracture surfaces of neat PA1010. These micrographs revealed a fracture surface with a very irregular and rough appearance, showing the typical cavernous formations of a polymer with a ductile behavior. **Figure III.4.4.2c-d** show that the addition of bio-HDPE to the PA1010 matrix resulted in a phenomenon of phase separation. The aforementioned low miscibility between both biopolymers can be clearly seen in the blend sample containing 30 wt% bio-HDPE, presenting the typical droplet like structure. Bio-HDPE appeared as micro-sized spherical domains or droplets with an average diameter comprised in a wide range from 4 to 17 µm. This morphology is

responsible for the decrease observed in tensile strength, elongation at break and impact strength, due to the lack of material's cohesion. The two components of the blend were then strongly incompatible and the blend showed a biphasic structure with large voids and poor adhesion between the two phases [48]. In this sense, Utraki *et al.* [49] reported that the absence of a co-continuous phase morphology is representative for immiscibility. The presence of small gaps of 1-3 μm surrounding the polyolefin domains supported the poor material's cohesion that, in turn, was responsible for the decrease in both elongation at break and tensile strength. The addition of GA to the blend system resulted in a better homogenization of the particle size but the immiscible droplets of bio-HDPE were still clearly discerned in the PA1010 matrix so that its effect on morphology was relatively low. Although plasticization was pointed out during the mechanical properties, this effect was not detectable during the morphological analysis.
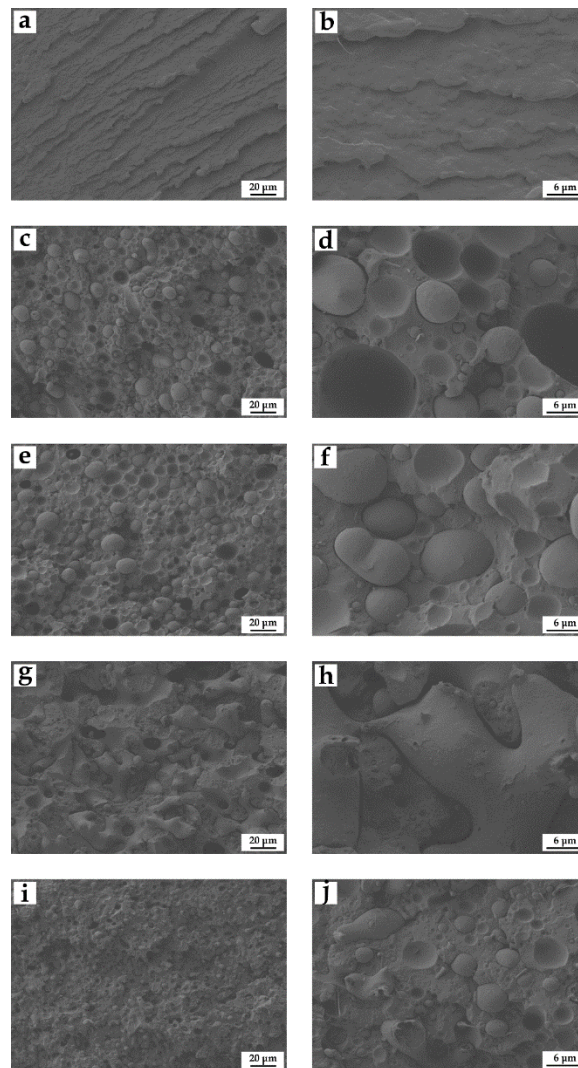
Figure III.4.4.2. Field emission scanning electron microscopy (FESEM) images of fractured surfaces from impacts tests, taken at 500x and 2500x (left and right, respectively) corresponding to polyamide 1010 (PA1010)/bio-based high-density polyethylene (bio-HDPE) blends processed with gallic acid (GA), maleinized linseed oil (MLO), and poly(ethylene-co-acrylic acid) copolymer (PE-*co*-AA): a, b) PA1010; c, d) PA1010/bio-HDPE; e, f) PA1010/bio-HDPE/GA; g, h) PA1010/bio-HDPE/MLO ; i, j) PA1010/bio-HDPE/GA/PE-*co*-AA.

With respect to the effect of the two compatibilizers, one can observe that both MLO and PE-*co*-AA modified the morphology of the biopolymer blends. **Figure III.4.4.2e-f** show the morphology of the fracture surfaces of the blend processed with MLO as compatibilizer. It should be noted that the droplets lost their spherical shape, forming stretched domains along the PA1010 matrix. It is also possible to observe a slight improvement in the miscibility in the mixture since the gaps were noticeably reduced. In this sense, the incorporation of the MLO generates a clear plasticization effect in the bio-HDPE. In a previous work, this plasticization phenomenon has already been observed in bio-HDPE/PLA blends with the typical droplet-like structure related to phase separation. In this study, the addition of the modified vegetable oil shows in a clear way a change in the droplet shape from spherical shapes to elliptical (stretched) shapes which give evidences of plasticization [50]. Other authors have reported the good plasticizing capacity of multi-functionalized vegetable oils in polymers [29, 51, 52]. Garcia-Campos *et al.* [53] also reported that the addition of acrylated and epoxidized vegetable oils offered quite good phase continuity as well as important evidences of plastic deformation after the impact test. Although the effect of MLO was clear and it provided the highest impact strength of all the developed materials, as observed during the mechanical analysis, the addition of PE-*co*-AA as compatibilizer also showed a positive effect on the overall miscibility with the subsequent increase in both tensile strength and elongation at break. **Figure III.4.4.2i-j** gather the morphology of the PA1010/bio-HDPE blend compatibilized with PE-*co*-AA. As it can be seen, the mean droplet size was remarkably reduced down to values of 5 μm or even lower, which is representative for a good compatibilizing effect. In addition, the gap between the dispersed bio-HDPE droplets almost disappeared. The resultant improved matrix continuity supports the improvement on the mechanical properties related to material's cohesion, that is, tensile strength, elongation at break, and impact strength. Similar to the results reported here, Halldén *et al.* [46] demonstrated that an uncompatibilized blend of LDPE with PA6 at 70/30 (wt/wt) results in a droplet like morphology with a sphere size of 21 μm while the same blend, containing 4% PE-*co*-AA, produces a remarkably reduced size of 0.9 μm that were aggregated to larger structures. Therefore, the use of PE-*co*-AA compatibilizers is able to act as good interfacial adhesion enhancer between the highly immiscible LDPE/PA6 blends. In this regard, our recent research reported on biopolymer blends that the reduction of the gap along the biopolymer-biopolymer interface is an indicator of improved compatibility [50]. Therefore, the present result suggests that higher coalescence stabilization in the PA1010/bio-HDPE blend was successfully achieved due to the PE-co-AA multi-functionality. This phenomenon can then explain the improved impact strength observed during the impact tests. Similar results with other copolymers were previously reported by Wang *et al*. [54] where PE-*g*-MA was used as a compatibilizer between HDPE and poly(ethylene-*co*-vinyl alcohol) (EVOH). It was observed that the domain size of EVOH significantly decreased in the HDPE matrix.

Chemical characterization

FTIR was performed in order to ascertain the chemical changes produced in PA1010 after blending with bio-HDPE and the addition of GA and the MLO and (PE-*co*-AA) compatibilizers. **Figure III.4.4.3** shows the FTIR absorbance spectra of PA1010 and the PA1010/bio-HDPE blends with GA and the different compatibilizers. In the PA1010 spectra one can observe that the main absorption peak was located at 1635

cm⁻¹, which has been assigned to the C=O of Amide I in both α- and β-crystalline phases [38, 55, 56]. The other most intense peak was located at 1535 cm⁻¹, which belongs to the bending vibration of N–H in Amide II [55-57]. Moreover, the C–N stretching vibration of the amide groups [38] and C–H bending vibration in methylene groups appeared on the band 1462 cm⁻¹ [56]. The group of bands located in the range 1300–1200 cm⁻¹ can be attributed to the gauche nitrogen-methylene group, that is, the N–H and C–H twisting [58, 59]. Finally, the low-intense peaks centered at 1160 cm⁻¹ and 940 cm⁻¹ have been attributed to the skeletal motion and in-plane modes of CO–NH bonds, respectively, which are characteristic of amide groups in semi-crystalline polyamides [60]. After the addition of bio-HDPE, it was observed slight intensity increases of the peaks centered at 1460 cm⁻¹ and 725 cm⁻¹, being those assigned to symmetric stretching vibration of the methylene (CH₂) groups [61] and indicating the presence of the green polyolefin in the blend. The incorporation of GA into the blends slightly changed the bands arising around 1030 cm⁻¹. Additionally, the new bands formed between 1021 cm⁻¹ and 1037 cm⁻¹ may be ascribed to dimers or oligomers of GA that can result from the stretching vibration of C−C and C−O bonds [62, 63].
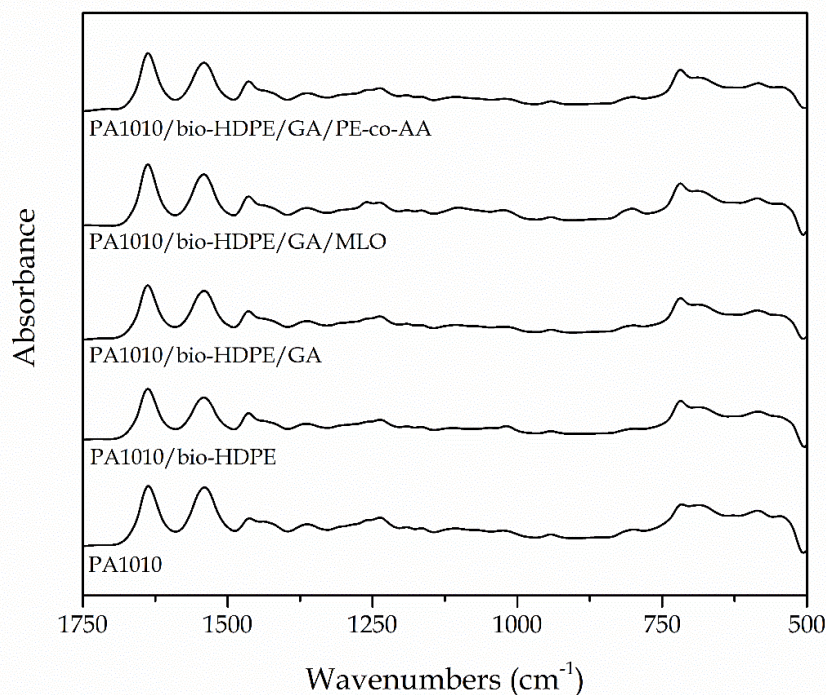
Figure III.4.4.3. Fourier transform infrared (FTIR) spectra, from bottom to top, of polyamide 1010 (PA1010), PA1010/ bio-based high-density polyethylene (bio-HDPE), PA1010/bio-HDPE/gallic acid (GA), PA1010/bio-HDPE/ maleinized linseed oil (MLO), and PA1010/bio-HDPE/GA/poly(ethylene-*co*-acrylic acid) copolymer (PE-*co*-AA).

In relation to the incorporation of the compatibilizers into the blend, one can observe the development of a shoulder in the carbonyl peak of PA1010 at approximately 1690 cm⁻¹. This chemical change was particularly more intense in the spectrum of the MLO-containing sample and it can be related to the C–O stretching group of hydrolyzed anhydride groups due to the reaction of the multiple functional groups of the compatibilizers with the terminal acid groups of PA1010 [64]. However,

the symmetric stretching of these newly formed functional groups, expected to appear close to 1350 cm^{-1}, were not explicitly visible to permit verification of this hypothesis due to the proximity of C–H band associated with PA1010. In any case, it is clear that the incorporation of both compatibilizers into the blend perturbed the band shape seen at ~1360 cm^{-1} and the formation of these delocalized carboxyl groups would readily explain this phenomenon [35].

Thermal properties

Figure III.4.4.4 shows the DSC curves during the second heating of the PA1010/bio-HDPE blends containing GA and the different compatibilizers. **Table III.4.4.3** gathers some of the most relevant thermal parameters obtained by DSC. Neat PA1010 showed a double melting peak with a low-intense melting point located at 185.2 °C whereas the main one was nearly at 203 °C. This phenomenon is related to a polymorphism effect on crystallites, showing multiple melting peaks of different intensities due to the presence of different crystalline forms of distinct lamellae and melting profile, that is, α, β, and γ [65]. One can observe that the addition of 30 wt% bio-HDPE to the blend did not generate any remarkable changes in the melting process of PA1010. In spite of this, more unstable crystals were present in PA1010/bio-HPPE sample due to the observed decrease in crystallinity. Alternatively, bio-HDPE was characterized by a melting temperature (T_m) of 133.4 °C whereas its onset of degradation temperature was 223.5 °C, which is relatively close to the Tm of PA1010. It can be observed that the addition of GA did not change in a remarkable way the melting process of both bio-HDPE and PA1010, although some PA1010 crystallites melted at lower temperatures. Interestingly, the main effect of GA on the thermal properties of the biopolymer blends was a delay in the onset degradation temperature from 223.5 °C up to 277.4 °C. This observation implies that the GA addition successfully improved the thermal stability of bio-HDPE, making it much more viable to be processed at higher temperatures without any degradation. Therefore, GA can successfully contribute to widen the processing temperature window of bio-HDPE, fitting these new conditions with the typical processing temperatures of PA1010. In this regard, Samper *et al*. [16] reported that the addition of different flavonoids, such as chrysin, quercetin, silibinin A, naringin, and hesperidin, delayed up to 25 °C the onset degradation process of PP providing, additionally, improved stability to UV radiation. With regard to the crystallinity of PA1010, the presence of the bio-HDPE phase potentially altered the nucleation rate of PA1010 by reducing its crystallinity [46]. With the addition of the different compatibilizers, some interesting changes in the thermal properties can be observed. While the melting profile of the blends remained almost constant with the addition of both MLO and PE-*co*-AA, the crystallinity of bio-HDPE increased to 58.6% and 62.9% for MLO and PE-*co*-AA, respectively. Therefore, the presence of MLO and, in particular, PE-*co*-AA, can favor the formation of more stable bio-HDPE crystals [35].

Table III.4.4.3. Main thermal parameters of polyamide 1010 (PA1010)/bio-based high-density polyethylene (bio-HDPE) blends processed with gallic acid (GA), maleinized linseed oil (MLO), and poly(ethylene-*co*-acrylic acid) copolymer (PE-*co*-AA) in terms of: melting temperature (T_m), normalized enthalpy of melting (ΔH_m), and degree of crystallinity (X_C) for the PA1010 and bio-HDPE phases and degradation temperature (T_{deg}) of bio-HDPE.

Sample	T_m (°C) PA1010	ΔH_m (J g^{-1}) PA1010	χ_c (%) PA1010	T_m (°C) Bio-HDPE	ΔH_m (J g^{-1}) Bio-HDPE	χ_c (%) Bio-HDPE	T_{deg} (°C) Bio-HDPE
PA1010	185.2/203.5 ± 1.1	86.6 ± 1.2	35.5 ± 1.1	-	-	-	-
Bio-HDPE	-	-	-	133.1 ± 0.6	159.3± 0.8	54.4 ± 0.7	224.9 ± 0.8
PA1010/bio-HDPE	183.2/203.8 ± 1.3	42.6 ± 1.1	24.9 ± 1.1	133.4 ± 0.7	45.3 ± 0.8	51.5 ± 0.7	223.5 ± 0.7
PA1010/bio-HDPE /GA	184.5/205.2 ± 0.9	43.1 ± 0.8	25.2 ± 0.8	135.5 ± 0.8	41.2 ± 0.6	46.9 ± 0.6	277.4 ± 0.9
PA1010/bio-HDPE/GA/MLO	183.3/203.8 ± 1.2	42.2 ± 1.0	24.7 ± 1.0	133.1 ± 0.4	51.5 ± 0.9	58.6 ± 0.9	275.5 ± 0.7
PA1010/bio-HDPE/GA/PE-*co*-AA	183.4/203.7 ± 1.1	40.2 ± 1.2	23.5 ± 1.1	133.5 ± 0.6	55.3 ± 0.5	62.9 ± 0.5	275.2 ± 0.8
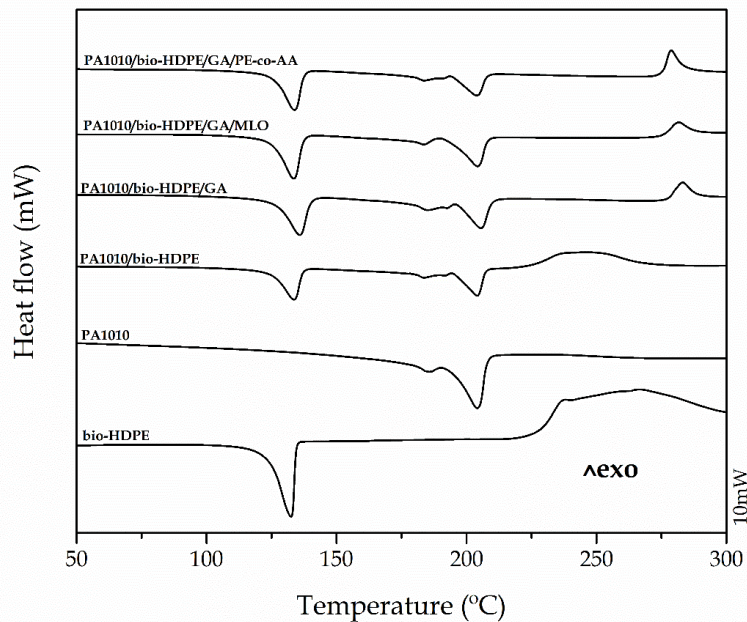
Figure III.4.4.4. Differential scanning calorimetry (DSC) curves corresponding to polyamide 1010 (PA1010)/bio-based high-density polyethylene (bio-HDPE) blends processed with gallic acid (GA), maleinized linseed oil (MLO), and poly(ethylene-*co*-acrylic acid) copolymer (PE-*co*-AA).

Regarding the analysis of thermal stability, **Figure III.4.4.5** shows the TGA curves of PA1010/bio-HDPE blends while **Table III.4.4.4** summarizes the main thermal degradation parameters obtained from the TGA curves. One can observe that neat PA1010 showed a relatively high thermal stability, showing a value of $T_{5\%}$ (temperature required for a 5 wt% loss) located at 422 °C, while the maximum degradation rate (T_{deg}) occurred at 461.6 °C. As it can be seen, PA1010 decomposed in a single step with a residual mass of nearly 1.5 wt%. According to this, Yang *et al.* [66] showed similar results for PA1010, observing that the onset thermal degradation was close to 414 °C. Bio-HDPE decomposition occurred at lower temperatures. After the addition of the green polyolefin, the values of $T_{5\%}$ and T_{deg} of the blend were reduced to 361 °C and 458 °C, respectively. Then, the most relevant change was observed in the $T_{5\%}$ value, which was reduced by 60 °C in comparison with the uncompatibilized and non-stabilized PA1010/bio-HDPE blend, mainly due thermal degradation of bio-HDPE during processing. As it has been described previously, the typical processing temperature for PA1010 overlaps with the initial stages of the thermo-oxidative degradation of bio-HDPE, thus leading to a blend with poor thermal stability. The incorporation of GA, interestingly, exerted an antioxidant effect on bio-HDPE, thus enlarging its onset degradation. Therefore, the GA addition provided an enlarged processing window of both polymers without thermal degradation. In particular, the stabilized blend with GA offered a $T_{5\%}$ value of 426 °C, slightly higher than neat PA1010, thus exerting a positive effect of GA on the overall thermal stability of the binary blend [67].

Table III.4.4.4. Main thermal degradation parameters of polyamide 1010 (PA1010)/bio-based high-density polyethylene (bio-HDPE) blends processed with gallic acid (GA), maleinized linseed oil (MLO), and poly(ethylene-*co*-acrylic acid) copolymer (PE-*co*-AA) in terms of: onset temperature for a mass loss of 5% ($T_{5\%}$), temperature for a mass loss of 10% ($T_{10\%}$), degradation temperature (T_{deg}), temperature for a mass loss of 90% ($T_{90\%}$), and residual mass at 700 °C.

Sample	$T_{5\%}$ (°C)	$T_{10\%}$ (°C)	T_{deg} (°C)	$T_{90\%}$ (°C)	Residual mass (%)
PA1010	422.0± 0.8	431.3 ± 0.8	461.6 ± 1.0	511.6 ± 0.9	1.5 ± 0.2
Bio-HDPE	304.2.± 0.8	331.0 ± 0.9	429.7 ± 0.8	480.2 ± 0.8	0.3 ± 0.1
PA1010/bio-HDPE	361.0 ± 0.9	424.2 ± 0.7	458.2 ± 1.1	492.4 ± 0.8	0.6 ± 0.1
PA1010/bio-HDPE /GA	426.0 ± 1.8	433.1 ± 0.8	457.8 ± 0.9	493.2 ± 0.7	1.2 ± 0.2
PA1010/bio-HDPE/GA/MLO	417.5 ± 1.2	429.3 ± 0.9	460.1 ± 0.8	494.3 ± 0.8	1.4 ± 0.3
PA1010/bio-HDPE/GA/PE-*co*-AA	431.0 ± 1.3	443.4 ± 0.7	469.5 ± 0.9	496.1 ± 1.0	1.1 ± 0.2
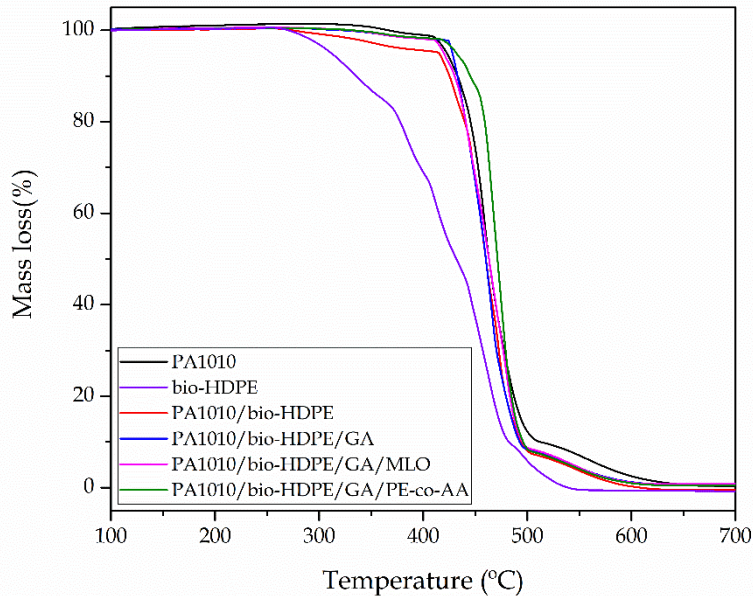
Figure III.4.4.5. Thermogravimetric analysis (TGA) curves corresponding to polyamide 1010 (PA1010)/bio-based high-density polyethylene (bio-HDPE) blends processed with gallic acid (GA), maleinized linseed oil (MLO), and poly(ethylene-*co*-acrylic acid) copolymer (PE-*co*-AA).

With the addition of MLO, the $T_{5\%}$ values were reduced by almost 10 °C compared to the GA-stabilized PA1010/bio-HDPE blend. This reduction can be related to the plasticizing effect generated by MLO in the blend and the lower thermal stability of the vegetable oil. Similarly, Ferri *et al.* [68] previously reported a decrease in the onset degradation temperature of PLA with the addition of bio-based epoxidized fatty acid esters (EFAEs). Regarding the maximum degradation temperature, one can observe that it remained almost constant. The addition of PE-*co*-AA produced an improvement in the thermal stability of the blend, as it improved both the $T_{5\%}$ and T_{deg} of PA1010 by more than 5 °C and 10 °C, respectively. This may be due to the improvement in miscibility between both materials discussed above. In any case, the most favorable result was the thermal stability increase of the blend attained after the incorporation of GA. According to these results, other authors have reported that the onset degradation temperature of bio-HDPE is approximately at 265 °C, ascribed to the start of thermo-oxidative processes, as corroborated by DSC. The presence of GA enhanced the thermal stability of the PA1010/bio-HDPE blend with a $T_{5\%}$ value of up to 420 °C. Finally, in relation to the residual mass, the incorporation of bio-HDPE into the blends slightly reduced the residual mass of PA1010.

Thermomechanical properties

Figure III.4.4.6a shows the evolution of the storage modulus (E′) of the PA1010/bio-HDPE blends in the temperature range comprised between -150 and 100 °C. The incorporation of bio-HDPE into the PA1010 matrix induced a slight increase in E′. In particular, at −100 °C, it increased from 1300 MPa, for neat PA1010, to 1400 MPa, for the uncompatibilized and non-stabilized PA1010/bio-HDPE blend. This increase

was observed up to temperatures close to 0 °C. Above this temperature, the stiffness of all materials decreased and it showed similar values at temperatures above 40 °C. The incorporation of GA and, in particular, the combination of GA and MLO, resulted in a slight increase in rigidity. In particular, E' reached a value 1500 MPa at -100 °C. Other authors have observed a similar behavior in PA1010/bio-HDPE blends compatibilized with MLO by reactive extrusion with dicumyl peroxide (DCP) [50]. In the case of PE-*co*-AA, one can observe that it did not provide any significant change in the E' values.
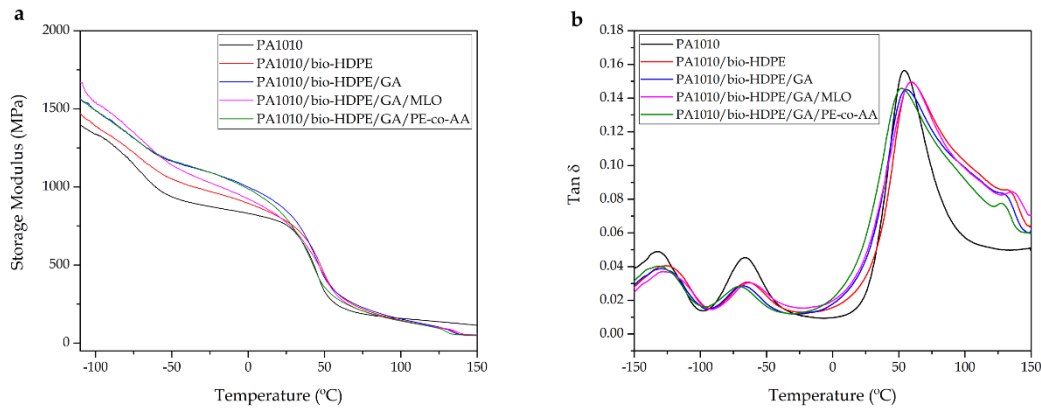
Figure III.4.4.6. Dynamic mechanical thermal analysis (DMTA) of polyamide 1010 (PA1010)/bio-based high-density polyethylene (bio-HDPE) blends processed with gallic acid (GA), maleinized linseed oil (MLO), and poly(ethylene-*co*-acrylic acid) copolymer (PE-*co*-AA): a) storage modulus (E') and b) dynamic damping factor (tan δ).

Figure III.4.4.6b shows the evolution of the dynamic damping factor (tan δ) with temperature of PA1010 and the PA1010/bio-HDPE blends. Regarding the neat PA1010, the typical relaxations are in total accordance to those reported by other authors. As indicated by Pagacz *et al.* [69], the peak around −130 °C is related to the γ-relaxation, which has been attributed to motions of methylene groups [70]. The peak located at around −80 °C corresponds to the β-relaxation, which is typically attributed to non-hydrogen-bonded amide group and, in some cases, to water molecules bonded on carbonyl groups [70]. Finally, the peak with the highest intensity, at nearly 50 °C, is attributed to the α-relaxation or glass transition temperature (T_g) of PA1010.[71, 72] With regard to the Tg of PA1010, the incorporation of MLO increased the T_g value from 54 °C to 59 °C. A similar behavior has been observed for MLO in different polymer systems. In particular, due to the molecular structure of MLO, different processes could occur simultaneously, that is, plasticization, chain extension, branching, compatibilization, cross-linking, etc. Therefore, despite the fact that the plasticizing effect was evident during the mechanical analysis, some cross-linking and compatibilization could also occur with a subsequent increase in Tg. Alternatively, the addition of PE-*co*-AA did not imply a remarkable change in Tg of PA1010. In accordance to this, Halldén *et al*. [73] reported that the addition of poly(ethylene-*graft*-ethylene oxide) (PE-*g*-PEO) did not produced any relevant change in the T_g of LDPE/PA6 blends.

The peak located between −112 °C and −116 °C corresponds to the α-relaxation of bio-HDPE, which is also related to its T_g. One can observe that this second order

transition temperature overlapped with the γ-relaxation process of PA1010. However, a slight increase of 3 °C was observed in the PA1010/bio-HDPE blend stabilized with GA and also compatibilized with MLO, which is in accordance to the above-mentioned potential effects of the multi-functionalized vegetable oil on the polymer blends. Indeed, T_g is a clear indicator of the level of miscibility in a polymer blend. Briefly, thermodynamically immiscible blends show different clearly distinguishable T_g values whereas in partially miscible blends a shift on T_g from the value of one component towards the other is typically attained and fully miscible blends are characterized by a single T_g [74].

In addition to the thermomechanical characterization carried out by DMTA, the dimensional stability was evaluated by thermomechanical analysis (TMA). In particular, the coefficient of linear thermal expansion (CLTE) was studied and the most relevant parameters are summarized in **Table III.4.4.5**. The CLTE values were measured below and above the T_g of PA1010. At temperatures below the T_g of PA1010, a slight increase in the CLTE values was seen for the uncompatibilized and non-stabilized PA1010/bio-HDPE blend. The incorporation of GA and the different compatibilizers, that is, MLO and PE-*co*-AA, did not provide any remarkable change in the CLTE values below the T_g of PA1010. As opposite, above the T_g of PA1010, changes in CLTE were much more noticeable. The addition of 30 wt% bio-HDPE resulted in an increase of more than 350 µm/m °C. This effect is mainly due to the large CLTE of bio-HDPE above 70 °C, which is around 465 µm/m °C as reported previously [50]. The only addition of GA provided slightly lower values, but with both compatibilizers, the CLTE increased in accordance to the above-reported results of elongation at break. In particular, it is worthy to note the high CLTE value observed for the blend compatibilized with PE-*co*-AA, which was 689 µm/m °C. This increase may be related to the plasticizing effect that both compatibilizers can provide to the blend, being particularly more intense in the case of PE-*co*-AA, as it was described in mechanical properties of the biopolymer blends. This increase in CLTE with the addition of MLO has been observed previously in PLA/ASF composites [35]. Moreover, the plasticization was much more pronounced at higher temperatures.

Table III.4.4.5. Values of the coefficients of linear thermal expansion (CLTE) of polyamide 1010 (PA1010)/bio-based high-density polyethylene (bio-HDPE) blends processed with gallic acid (GA), maleinized linseed oil (MLO), and poly(ethylene-*co*-acrylic acid) copolymer (PE-*co*-AA) below and above the glass transition temperature (T_g) of PA1010.

Sample	CLTE (µm/m°C)	
	Below T_g	**Above T_g**
PA1010	97.2 ± 1.9	206.0 ± 2.6
PA1010/bio-HDPE	107.2 ± 2.0	559.2 ± 3.8
PA1010/bio-HDPE/GA	104.0 ± 1.5	422.9 ± 2.9
PA1010/bio-HDPE/GA/MLO	105.9 ± 2.2	585.6 ± 3.1
PA1010/bio-HDPE/GA/PE-*co*-AA	111.3 ± 1.9	689.4 ± 7.6

CONCLUSIONS

This work shows the effectiveness of GA as a natural antioxidant in PA1010/bio-HDPE, both biopolymers being fully obtained from renewable resources but also highly immiscible as observed by FESEM. GA successfully enlarged the processing temperature window of the blend by increasing the thermal stability of bio-HDPE, thus allowing its better processability with PA1010. In addition, GA provided a clear plasticizing effect on the biopolymer blend, which resulted in a positive effect on the ductility of the PA1010/bio-HDPE blends. This binary blend, containing 70 wt% PA1010 and 30 wt% bio-HDPE, showed a droplet-like surface morphology with spherical bio-HDPE particles sizing 5–15 μm embedded in the PA1010 matrix. In addition to the improvement observed in the thermal stability by the addition GA, the two tested reactive compatibilizers showed a high efficiency to also provide partial compatibilization with a subsequent improvement in toughness. Addition of MLO provided certain plasticization and improved impact strength, whereas the addition of the petroleum-derived PE-*co*-AA compatibilizer induced improved elongation at break and tensile strength. This was representative for somewhat compatibilization, as corroborated by FESEM due to the size of the spherical bio-HDPE domains decreased to values lower than 5 μm and also by the chemical interactions described during FTIR analysis.

The results of this research work also overcome the main drawbacks related to the mechanical recycling of these two biopolymers. One the one hand, the processing temperature of the binary blend is improved by using GA. On the other, MLO compatibilizes both biopolymers resulting in a blend with improved toughness. Therefore, this approach could positively contribute to the development of high-performance blends based on immiscible biopolymers and also to the promotion of sustainable polymer technologies.

Acknowledgements

REFERENCES

1. Carole, T.M., J. Pellegrino and M.D. Paster. *Opportunities in the industrial biobased products industry*. in *Proceedings of the Twenty-Fifth Symposium on Biotechnology for Fuels and Chemicals Held May 4–7, 2003, in Breckenridge, CO*. 2004. Springer.
2. Ogunniyi, D.S., *Castor oil: a vital industrial raw material.* Bioresource technology, 2006. **97**(9): 1086-1091.
3. Kausar, A., *Polyamide 1010/polythioamide blend reinforced with graphene nanoplatelet for automotive part application.* Advances in Materials Science, 2017. **17**(3): 24-36.
4. Nishitani, Y., T. Kajiyama and T. Yamanaka, *Effect of silane coupling agent on tribological properties of hemp fiber-reinforced plant-derived polyamide 1010 biomass composites.* Materials, 2017. **10**(9): 1040.

5. Glasscock, D., W. Atolino, G. Kozielski and M. Martens, *High performance polyamides fulfill demanding requirements for automotive thermal management components.* DuPont Engineering Polymers, 2008.

6. Boros, R., P. Rajamani and J. Kovács, *Thermoplastic Overmolding onto Injection-Molded and In Situ Polymerization-Based Polyamides.* Materials, 2018. **11**(11): 2140.

7. Del Nobile, M., G. Buonocore, L. Palmieri, A. Aldi and D. Acierno, *Moisture transport properties of polyamides copolymers intended for food packaging applications.* Journal of food engineering, 2002. **53**(3): 287-293.

8. Nishida, H., *Development of materials and technologies for control of polymer recycling.* Polymer journal, 2011. **43**(5): 435.

9. Singh, R., R. Kumar, N. Ranjan, R. Penna and F. Fraternali, *On the recyclability of polyamide for sustainable composite structures in civil engineering.* Composite Structures, 2018. **184**: 704-713.

10. Laryea-Goldsmith, R., J. Oakey and N.J. Simms, *Gaseous emissions during concurrent combustion of biomass and non-recyclable municipal solid waste.* Chemistry Central Journal, 2011. **5**(1): 4.

11. Kumar, S., A.K. Panda and R. Singh, *A review on tertiary recycling of high-density polyethylene to fuel.* Resources, Conservation and Recycling, 2011. **55**(11): 893-910.

12. Araújo, J., W. Waldman and M. De Paoli, *Thermal properties of high density polyethylene composites with natural fibres: Coupling agent effect.* Polymer Degradation and stability, 2008. **93**(10): 1770-1775.

13. Sangroniz, L., et al., *The outstanding ability of nanosilica to stabilize dispersions of Nylon 6 droplets in a polypropylene matrix.* Journal of Polymer Science Part B: Polymer Physics, 2015. **53**(22): 1567-1579.

14. Sahnoune, M., A. Taguet, B. Otazaghine, M. Kaci and J.M. Lopez-Cuesta, *Inner surface modification of halloysite nanotubes and its influence on morphology and thermal properties of polystyrene/polyamide-11 blends.* Polymer International, 2017. **66**(2): 300-312.

15. Lim, M.-Y., J. Oh, H.J. Kim, K.Y. Kim, S.-S. Lee and J.-C. Lee, *Effect of antioxidant grafted graphene oxides on the mechanical and thermal properties of polyketone composites.* European Polymer Journal, 2015. **69**: 156-167.

16. Samper, M., E. Fages, O. Fenollar, T. Boronat and R. Balart, *The potential of flavonoids as natural antioxidants and UV light stabilizers for polypropylene.* Journal of Applied Polymer Science, 2013. **129**(4): 1707-1716.

17. Raspo, M.A., C.G. Gomez and A.E. Andreatta, *Optimization of antioxidant, mechanical and chemical physical properties of chitosan-sorbitol-gallic acid films by response surface methodology.* Polymer Testing, 2018. **70**: 180-187.

18. Graham, H.N., *Green tea composition, consumption, and polyphenol chemistry.* Preventive medicine, 1992. **21**(3): 334-350.

19. Yilmaz, Y. and R.T. Toledo, *Major flavonoids in grape seeds and skins: antioxidant capacity of catechin, epicatechin, and gallic acid.* Journal of agricultural and food chemistry, 2004. **52**(2): 255-260.

20. Vourdoubas, J. and V.K. Skoulou, *Possibilities of Upgrading Solid Underutilized Lingo-cellulosic Feedstock (Carob Pods) to Liquid Bio-fuel: Bio-ethanol Production and Electricity Generation in Fuel Cells-A Critical Appraisal of the Required Processes.* Studies in Engineering and Technology, 2017. **4**(1): 25-34.

21. Quiles-Carrillo, L., C. Mellinas, M. Garrigos, R. Balart and S. Torres-Giner, *Optimization of Microwave-Assisted Extraction of Phenolic Compounds with Antioxidant Activity from Carob Pods.* Food Analytical Methods, 2019: 1-11.

22. Macosko, C., P. Guegan, A.K. Khandpur, A. Nakayama, P. Marechal and T. Inoue, *Compatibilizers for melt blending: Premade block copolymers.* Macromolecules, 1996. **29**(17): 5590-5598.

23. Kumar, A., T.V. Rao, S.R. Chowdhury and S. Reddy. *Effect of electron beam irradiation on thermal and mechanical properties of poly (lactic acid)/poly (ethylene-co-glycidyl methacrylate) blend.* in *AIP Conference Proceedings.* 2017. AIP Publishing.

24.	Arostegui, A. and J. Nazabal, *Supertoughness and critical interparticle distance dependence in poly (butylene terephthalate) and poly (ethylene-co-glycidyl methacrylate) blends.* Journal of Polymer Science Part B: Polymer Physics, 2003. **41**(19): 2236-2247.

25.	Sheng, J., H. Ma, X.B. Yuan, X.Y. Yuan, N.X. Shen and D.C. Bian, *Relation of chain constitution with phase structure in blends: compatibility of two phases in blends of polyamide with low-density polyethylene and its ionomers.* Journal of applied polymer science, 2000. **76**(4): 488-494.

26.	Garcia-Garcia, D., J.M. Ferri, N. Montanes, J. Lopez-Martinez and R. Balart, *Plasticization effects of epoxidized vegetable oils on mechanical properties of poly (3-hydroxybutyrate).* Polymer International, 2016. **65**(10): 1157-1164.

27.	Mosiewicki, M.A. and M.I. Aranguren, *Recent developments in plant oil based functional materials.* Polymer International, 2016. **65**(1): 28-38.

28.	Quiles-Carrillo, L., S. Duart, N. Montanes, S. Torres-Giner and R. Balart, *Enhancement of the mechanical and thermal properties of injection-molded polylactide parts by the addition of acrylated epoxidized soybean oil.* Materials & Design, 2018. **140**: 54-63.

29.	Carbonell-Verdu, A., D. Garcia-Garcia, F. Dominici, L. Torre, L. Sanchez-Nacher and R. Balart, *PLA films with improved flexibility properties by using maleinized cottonseed oil.* European Polymer Journal, 2017. **91**: 248-259.

30.	Liu, K., S.A. Madbouly and M.R. Kessler, *Biorenewable thermosetting copolymer based on soybean oil and eugenol.* European Polymer Journal, 2015. **69**: 16-28.

31.	Quiles-Carrillo, L., M. Blanes-Martínez, N. Montanes, O. Fenollar, S. Torres-Giner and R. Balart, *Reactive toughening of injection-molded polylactide pieces using maleinized hemp seed oil.* European Polymer Journal, 2018. **98**: 402-410.

32.	Garcia-Campo, M.J., L. Quiles-Carrillo, J. Masia, M.J. Reig-Pérez, N. Montanes and R. Balart, *Environmentally friendly compatibilizers from soybean oil for ternary blends of poly (lactic acid)-PLA, poly (ε-caprolactone)-PCL and poly (3-hydroxybutyrate)-PHB.* Materials, 2017. **10**(11): 1339.

33.	Ferri, J., D. Garcia-Garcia, L. Sánchez-Nacher, O. Fenollar and R. Balart, *The effect of maleinized linseed oil (MLO) on mechanical performance of poly (lactic acid)-thermoplastic starch (PLA-TPS) blends.* Carbohydrate polymers, 2016. **147**: 60-68.

34.	Ferri, J.M., D. Garcia-Garcia, N. Montanes, O. Fenollar and R. Balart, *The effect of maleinized linseed oil as biobased plasticizer in poly (lactic acid)-based formulations.* Polymer International, 2017. **66**(6): 882-891.

35.	Quiles-Carrillo, L., N. Montanes, C. Sammon, R. Balart and S. Torres-Giner, *Compatibilization of highly sustainable polylactide/almond shell flour composites by reactive extrusion with maleinized linseed oil.* Industrial Crops and Products, 2018. **111**: 878-888.

36.	Miao, S., P. Wang, Z. Su and S. Zhang, *Vegetable-oil-based polymers as future polymeric biomaterials.* Acta Biomaterialia, 2014. **10**(4): 1692-1704.

37.	Aguero, A., L. Quiles-Carrillo, A. Jorda-Vilaplana, O. Fenollar and N. Montanes, *Effect of different compatibilizers on environmentally friendly composites from poly (lactic acid) and diatomaceous earth.* Polymer International, 2019. **68**(5): 893-903.

38.	Yan, M. and H. Yang, *Improvement of polyamide 1010 with silica nanospheres via in situ melt polycondensation.* Polymer Composites, 2012. **33**(10): 1770-1776.

39.	Quiles-Carrillo, L., N. Montanes, J. Lagaron, R. Balart and S. Torres-Giner, *In situ compatibilization of biopolymer ternary blends by reactive extrusion with low-functionality epoxy-based styrene–acrylic oligomer.* Journal of Polymers and the Environment, 2019. **27**(1): 84-96.

40.	Scaffaro, R., M.C. Mistretta, F.P. La Mantia, M. Gleria, R. Bertani, F. Samperi and C. Puglisi, *On the preparation and characterization of polyethylene/polyamide blends by melt processing in the presence of an ethylene/acrylic acid copolymer and of new phosphazene compounds.* Macromolecular Chemistry and Physics, 2006. **207**(21): 1986-1997.

41.	Wu, J., S. Chen, S. Ge, J. Miao, J. Li and Q. Zhang, *Preparation, properties and antioxidant activity of an active film from silver carp (Hypophthalmichthys molitrix) skin gelatin incorporated with green tea extract.* Food Hydrocolloids, 2013. **32**(1): 42-51.

42. Ambrogi, V., P. Cerruti, C. Carfagna, M. Malinconico, V. Marturano, M. Perrotti and P. Persico, *Natural antioxidants for polypropylene stabilization.* Polymer degradation and stability, 2011. **96**(12): 2152-2158.

43. Jamshidian, M., E.A. Tehrany, M. Imran, M.J. Akhtar, F. Cleymand and S. Desobry, *Structural, mechanical and barrier properties of active PLA–antioxidant films.* Journal of Food Engineering, 2012. **110**(3): 380-389.

44. Ferri, J.M., D. Garcia-Garcia, L. Sanchez-Nacher, O. Fenollar and R. Balart, *The effect of maleinized linseed oil (MLO) on mechanical performance of poly(lactic acid)-thermoplastic starch (PLA-TPS) blends.* Carbohydrate Polymers, 2016. **147**: 60-68.

45. Liminana, P., D. Garcia-Sanoguera, L. Quiles-Carrillo, R. Balart and N. Montanes, *Development and characterization of environmentally friendly composites from poly(butylene succinate) (PBS) and almond shell flour with different compatibilizers.* Composites Part B-Engineering, 2018. **144**: 153-162.

46. Halldén, Å., B. Ohlsson and B. Wesslén, *Poly (ethylene-graft-ethylene oxide)(PE-PEO) and poly (ethylene-co-acrylic acid)(PEAA) as compatibilizers in blends of LDPE and polyamide-6.* Journal of applied polymer science, 2000. **78**(13): 2416-2424.

47. Balart, J., V. Fombuena, O. Fenollar, T. Boronat and L. Sánchez-Nacher, *Processing and characterization of high environmental efficiency composites based on PLA and hazelnut shell flour (HSF) with biobased plasticizers derived from epoxidized linseed oil (ELO).* Composites Part B: Engineering, 2016. **86**: 168-177.

48. Mistretta, M., P. Fontana, M. Ceraulo, M. Morreale and F. La Mantia, *Effect of compatibilization on the photo-oxidation behaviour of polyethylene/polyamide 6 blends and their nanocomposites.* Polymer Degradation and Stability, 2015. **112**: 192-197.

49. Utracki, L.A., *Compatibilization of Polymer Blends.* The Canadian Journal of Chemical Engineering, 2002. **80**(6): 1008-1016.

50. Quiles-Carrillo, L., N. Montanes, A. Jorda-Vilaplana, R. Balart and S. Torres-Giner, *A comparative study on the effect of different reactive compatibilizers on injection-molded pieces of bio-based high-density polyethylene/polylactide blends.* Journal of Applied Polymer Science, 2019. **136**(16): 47396.

51. Carbonell-Verdu, A., D. Garcia-Sanoguera, A. Jordá-Vilaplana, L. Sanchez-Nacher and R. Balart, *A new biobased plasticizer for poly (vinyl chloride) based on epoxidized cottonseed oil.* Journal of Applied Polymer Science, 2016. **133**(27).

52. Petrović, Z.S., M. Ionescu, J. Milić and J.R. Halladay, *Soybean oil plasticizers as replacement of petroleum oil in rubber.* Rubber chemistry and technology, 2013. **86**(2): 233-249.

53. Garcia-Campo, M., L. Quiles-Carrillo, J. Masia, M. Reig-Pérez, N. Montanes and R. Balart, *Environmentally friendly compatibilizers from soybean oil for ternary blends of poly (lactic acid)-PLA, poly (ε-caprolactone)-PCL and poly (3-hydroxybutyrate)-PHB.* Materials, 2017. **10**(11): 1339.

54. Wang, Q., R. Qi, Y. Shen, Q. Liu and C. Zhou, *Effect of high-density polyethylene-g-maleic anhydride on the morphology and properties of (high-density polyethylene)/(ethylene–vinyl alcohol) copolymer alloys.* Journal of applied polymer science, 2007. **106**(5): 3220-3226.

55. Li, H.P. and Z.M. Li, *The effect of reactive compatibilization of carboxylated polystyrene on morphology and toughness of polyamide-1010/polystyrene blends.* Polymer International, 1999. **48**(2): 124-128.

56. Porubska, M., O. Szoellos, A. Konova, I. Janigova, M. Jaskova, K. Jomova and I. Chodak, *FTIR spectroscopy study of polyamide-6 irradiated by electron and proton beams.* Polymer Degradation and Stability, 2012. **97**(4): 523-531.

57. Pai, F.-C., S.-M. Lai and H.-H. Chu, *Characterization and Properties of Reactive Poly(lactic acid)/Polyamide 610 Biomass Blends.* Journal of Applied Polymer Science, 2013. **130**(4): 2563-2571.

58. Elzein, T., M. Brogly and J. Schultz, *Crystallinity measurements of polyamides adsorbed as thin films.* Polymer, 2002. **43**(17): 4811-4822.

59. Rhee, S. and J.L. White, *Investigation of structure development in polyamide 11 and polyamide 12 tubular film extrusion.* Polymer Engineering and Science, 2002. **42**(1): 134-145.

60. Vasanthan, N. and D.R. Salem, *FTIR spectroscopic characterization of structural changes in polyamide-6 fibers during annealing and drawing.* Journal of Polymer Science Part B-Polymer Physics, 2001. **39**(5): 536-547.

61. Barbeş, L., C. Rădulescu and C. Stihi, *ATR-FTIR spectrometry characterisation of polymeric materials.* Romanian Reports in Physics, 2014. **66**(3): 765-777.

62. Neo, Y.P., S. Ray, J. Jin, M. Gizdavic-Nikolaidis, M.K. Nieuwoudt, D. Liu and S.Y. Quek, *Encapsulation of food grade antioxidant in natural biopolymer by electrospinning technique: A physicochemical study based on zein–gallic acid system.* Food chemistry, 2013. **136**(2): 1013-1021.

63. Markarian, S.A., A.L. Zatikyan, S. Bonora and C. Fagnano, *Raman and FT IR ATR study of diethylsulfoxide/water mixtures.* Journal of molecular structure, 2003. **655**(2): 285-292.

64. Wu, C.H. and A.C. Su, *FUNCTIONALIZATION OF ETHYLENE-PROPYLENE RUBBER VIA MELT MIXING.* Polymer Engineering and Science, 1991. **31**(23): 1629-1636.

65. Logakis, E., C. Pandis, V. Peoglos, P. Pissis, C. Stergiou, J. Pionteck, P. Pötschke, M. Mičušík and M. Omastová, *Structure–property relationships in polyamide 6/multi-walled carbon nanotubes nanocomposites.* Journal of Polymer Science Part B: Polymer Physics, 2009. **47**(8): 764-774.

66. Yang, J., W. Dong, Y. Luan, J. Liu, S. Liu, X. Guo, X. Zhao and W. Su, *Crystallization and crosslinking of polyamide-1010 under elevated pressure.* Journal of applied polymer science, 2002. **83**(12): 2522-2527.

67. Pasanphan, W., G.R. Buettner and S. Chirachanchai, *Chitosan conjugated with deoxycholic acid and gallic acid: A novel biopolymer-based additive antioxidant for polyethylene.* Journal of applied polymer science, 2008. **109**(1): 38-46.

68. Ferri, J., M. Samper, D. García-Sanoguera, M. Reig, O. Fenollar and R. Balart, *Plasticizing effect of biobased epoxidized fatty acid esters on mechanical and thermal properties of poly (lactic acid).* Journal of materials science, 2016. **51**(11): 5356-5366.

69. Pagacz, J., K.N. Raftopoulos, A. Leszczyńska and K. Pielichowski, *Bio-polyamides based on renewable raw materials.* Journal of Thermal Analysis and Calorimetry, 2016. **123**(2): 1225-1237.

70. Prevorsek, D., R. Butler and H. Reimschuessel, *Mechanical relaxations in polyamides.* Journal of Polymer Science Part A-2: Polymer Physics, 1971. **9**(5): 867-886.

71. Zhao, C., G. Hu, R. Justice, D.W. Schaefer, S. Zhang, M. Yang and C.C. Han, *Synthesis and characterization of multi-walled carbon nanotubes reinforced polyamide 6 via in situ polymerization.* Polymer, 2005. **46**(14): 5125-5132.

72. Urman, K. and J. Otaigbe, *Novel phosphate glass/polyamide 6 hybrids: miscibility, crystallization kinetics, and mechanical properties.* Journal of Polymer Science Part B: Polymer Physics, 2006. **44**(2): 441-450.

73. Halldén, Å., M.J. Deriss and B. Wesslén, *Morphology of LDPE/PA-6 blends compatibilised with poly (ethylene-graft-ethylene oxide) s.* Polymer, 2001. **42**(21): 8743-8751.

74. Muthuraj, R., M. Misra and A.K. Mohanty, *Biodegradable biocomposites from poly (butylene adipate-co-terephthalate) and miscanthus: Preparation, compatibilization, and performance evaluation.* Journal of Applied Polymer Science, 2017. **134**(43): 45448.

CONCLUSIONES

IV. CONCLUSIONES

CONCLUSIONES

IV.1. CONCLUSIONES PARCIALES.

Una vez analizados los resultados obtenidos y teniendo en cuenta los objetivos específicos que se han planteado desde el inicio, se pueden definir las conclusiones parciales de cada uno de los bloques desarrollados a lo largo de la presente tesis doctoral. Las conclusiones parciales se muestran a continuación:

IV.1.1. Con relación a poliésteres con impacto mejorado a través de mezclas y extrusión reactiva.

Los resultados obtenidos de las mezcla binarias y ternarias basadas en PLA mediante extrusión reactiva con diferentes contenidos de PCL y TPS se presentan como novedosos plásticos sostenibles con mayor ductilidad y resistencia. En los ensayos de tracción y flexión realizados, se observó que la adición de PCL y TPS tuvo un efecto positivo en la flexibilidad y la resistencia al impacto, pero también una ligera reducción de las propiedades de resistencia mecánica. Aunque ambos biopolímeros produjeron individualmente un efecto positivo en las propiedades dúctiles del PLA, los mejores resultados se obtuvieron en las mezclas ternarias que combinaban altos contenidos de PCL con bajas cantidades de TPS. Por otro lado, la mezcla con agentes de acoplamiento altamente reactivos puede considerarse una herramienta novedosa para desarrollar nanocompuestos poliméricos de alto rendimiento. En particular, el incorporación durante la fusión de las nanopartículas, como la sepiolita, favorece potencialmente el rendimiento térmico y mecánico de los biopolímeros. Esto puede promover y revolucionar su accesibilidad a sectores industriales como el del envase y el embalaje.

La incorporación del ESAO en los films de mezclas ternarias de biopolímeros hechos de PHBV, PLA y PBAT, aumentó con éxito la miscibilidad de los biopolímeros mezclados, actuando como un compatibilizante reactivo durante el proceso de extrusión. En particular, las mezclas ternarias con alto contenido de PHBV comparten algunas similitudes con los polímeros rígidos tradicionales como el PET, el PS y el PC, lo que las hace atractivas como alternativa sostenible en el campo del envasado de alimentos para artículos desechables y compostables. Estos materiales pueden encontrar posibles usos como materiales de envasado que requieren un rendimiento de barrera moderado, como las bandejas y tapas de los alimentos.

Para aumentar la miscibilidad entre las mezclas de bio-HDPE y PLA, y, por tanto, el rendimiento mecánico y térmico de las piezas, se probaron diferentes compatibilizantes reactivos. En particular, se exploró el uso de un polímero injertado (PE-g-MA), un copolímero (PE-co-GMA) y un aceite vegetal multifuncional (MLO+DCP). Tras la incorporación de PE-g-MA o PE-co-GMA se observó una baja mejora en el rendimiento físico de las piezas, pero en relación con el MLO, se observó que el aceite vegetal multifuncional se solubilizaba principalmente en la fase dispersa del PLA, que se plastificaba mucho, de modo que inducía una mejora general de las propiedades dúctiles de la mezcla binaria. Por tanto, las piezas moldeadas por inyección obtenidas aquí, hechas de bio-HDPE con hasta un 20% de peso de PLA, presentan una resistencia mecánica más alta y una resistencia al impacto similar a la del bio-HDPE puro. Estas piezas, que son totalmente biobasadas, pueden considerarse entonces como grandes candidatas para ser utilizadas en envases rígidos sostenibles.

IV.1.2. Con relación a las formulaciones de ácido poliláctico con aditivos y cargas naturales.

La utilización de ciertos aditivos y cargas naturales, favorecieron la viabilidad del PLA en aplicaciones que hasta la fecha no tenían cabida. En particular, la incorporación del AESO genera un efecto positivo en la elongación a la rotura y logra que la resistencia mecánica de las piezas de PLA reforzadas con AESO, se posicionen en el mismo rango que la de las piezas de PLA puro. Por otro lado, a diferencia de los plastificantes típicos, el MHO generó piezas de PLA no sólo con una mayor ductilidad mecánica, sino también con una mayor resistencia mecánica. En este contexto, las piezas de PLA con AESO y MHO pueden ser especialmente interesantes para aplicaciones de embalaje rígido, automoción o construcción, en las que se exigen materiales elásticos, pero con mayor ductilidad y suficiente resistencia al impacto.

La incorporación de cargas provenientes de residuos naturales como la cáscara de naranja (OPF) o de almendra (ASF) se pueden utilizar para reforzar matrices de PLA cuando se combinan con compatibilizantes adecuados. En este sentido, la OPF puede incorporarse con éxito hasta un 10 % en peso al PLA mediante el procesamiento por extrusión reactiva en presencia de AESO, sin comprometer las propiedades físicas y la compostabilidad del biopolímero. La incorporación de la ASF, junto con bajas cantidades de MLO, da como resultado compuestos verdes altamente sostenibles debido a sus características completamente biodegradables y renovables. Se pueden aplicar en materiales de embalaje de base biológica, como bandejas y tapas, o incluso como sustitutos de tableros de madera.

En términos generales, el MLO y otros aceites vegetales multifuncionales pueden considerarse aditivos atractivos para mejorar la compatibilidad en compuestos verdes inmiscibles o poco miscibles basados en biopoliésteres y rellenos con grupos polares. Además, debido a sus orígenes naturales, representan una solución ecológica para mejorar las formulaciones industriales y puede contribuir positivamente al desarrollo de tecnologías de polímeros sostenibles.

IV.1.3. Con relación a los usos y aplicaciones de nuevas poliamidas de alto rendimiento medioambiental procedentes de recursos renovables.

Los resultados obtenidos en este bloque permiten seleccionar a una poliamida totalmente biobasada como la PA1010, en un material altamente eficiente, que se puede combinar con diferentes refuerzos y polímeros para ampliar en gran medida sus aplicaciones.

En este contexto, tras la incorporación de fibras de pizarra en la poliamida 1010, el compuesto presentó un aumento del triple en el módulo de tracción, mientras que la resistencia a la tracción se duplicó en comparación con la PA1010 virgen. Este enfoque fue mejorado aún más debido al pretratamiento de las fibras inorgánicas con agentes de acoplamiento de la familia del silano. La incorporación del SF pretratado con

silanos, dio como resultado un aumento adicional de la resistencia mecánica y la dureza, sin perjudicar la ductilidad y la resistencia del compuesto. El uso de PA1010 y SF puede contribuir positivamente al desarrollo de tecnologías de polímeros sostenibles al desvincular las materias primas del petróleo y promover también la valorización de los desechos industriales.

Por otro lado, la incorporación de fibras totalmente naturales como la fibra de coco (CF) en la PA1010, reveló el notable efecto que tienen las fibras en la reducción de la elongación a la rotura. La incorporación de compatibilizantes multifuncionales derivados de aceites vegetales, como el MLO y el ELO, dio lugar a una notable mejora de todas las propiedades mecánicas, incluida la resistencia. Otros compatibilizantes comerciales derivados del petróleo, también proporcionaron cierta mejora del rendimiento del compuesto. Este tipo de refuerzos supone una ventaja para de la fabricación de compuestos WPC muy respetuosos con el medio ambiente y de alto rendimiento, basados en una matriz totalmente biobasada y con un refuerzo completamente natural.

Finalmente se ha estudiado el potencial de la extrusión reactiva para compatibilizar las mezclas binarias completamente biobasadas de PA1010 y PLA. Con un 20 % de PLA constante en las formulaciones, los compatibilizadores derivados de aceites vegetales proporcionan un notable aumento de la elongación y la resistencia. Además, la adición de ELO genera películas de alta transparencia, algo de vital importancia en ciertas aplicaciones del sector del envase y embalaje. En cuanto al uso de aditivos basados en la GMA, así como en el MLO, dio lugar a películas con una mejor resistencia a la tracción, pero con un ligero aumento de la opacidad que podría ser útil para proteger los alimentos contra la luz ultravioleta. Finalmente, los cuatro compatibilizantes disminuyeron los valores de OTR en comparación con el PA1010 puro y la mezcla de PA1010/PLA no estabilizada, lo que demuestra la utilidad de los cuatro compatibilizantes para fabricar películas muy respetuosas con el medio ambiente para la industria del envase y embalaje.

IV.1.4. Con respecto a la utilidad del ácido gálico como aditivo funcional en formulaciones de polímeros y de mezclas.

Los resultados que se han obtenido de este apartado dan gran información sobre las ventajas de utilizar elementos antioxidantes como el ácido gálico para mejorar la aplicación de ciertos polímeros renovables en la industria del envase y embalaje.

La extracción asistida por microondas (MAE) es un proceso eficiente para la extracción de compuestos fenólicos con actividad antioxidante, en particular el ácido gálico (GA), del algarrobo europeo Ceratonia Silicua de la variedad "ramillete". Los resultados obtenidos del algarrobo han contribuido a la revalorización de este tipo de residuos agroalimentarios para diferentes aplicaciones en el sector de la industria alimentaria, como el encapsulado de compuestos fenólicos para alimentos funcionales o el desarrollo de películas activas.

Tras la utilización de GA para la creación de films con capacidad antioxidante mediante electrospinning, se observó como las películas de PLA bicapa pueden

proporcionar una rápida liberación de antioxidante en un simulador de alimentos salinos, lo cual puede ser de interés para los alimentos funcionales envasados con ciclos de vida relativamente cortos (1-2 semanas). Por otro lado, los sistemas multicapa pueden ser interesantes desde el punto de vista de los productos alimenticios almacenados en medios acuosos con una vida útil mucho más larga. Los resultados también mostraron que la incorporación del GA retrasó positivamente la degradación térmica del PLA hasta 10 °C y todas las películas fueron térmicamente estables hasta 345 °C.

La incorporación del ácido gálico también supuso un deterioro de la elasticidad mecánica y la ductilidad y también una reducción de la cristalinidad de films bio-HDPE debido a su limitada solubilidad con el biopolímero. No obstante, genera una mejora en más de 44 °C en la degradación térmica del bio-HDPE con la incorporación de un 0,8% de GA y aporta gran estabilidad a la luz ultravioleta del bio-HDPE. El GA puede considerarse un antioxidante natural y estabilizador de la luz UV que puede sustituir potencialmente a los aditivos sintéticos en las formulaciones de biopolímeros para aplicaciones de envasado de alimentos.

Finalmente, el GA amplió con éxito la ventana de procesado de la mezcla de bio-HDPE/PA1010, al aumentar la estabilidad térmica del bio-HDPE, permitiendo así su mejor procesabilidad con la PA1010. Además, el GA proporcionó un claro efecto plastificante en la mezcla de biopolímeros, lo que dio lugar a un efecto positivo en la ductilidad de las mezclas. Además de la mejora observada en la estabilidad térmica por la adición GA, los dos compatibilizantes reactivos probados mostraron una alta eficiencia para proporcionar también una compatibilidad parcial con una mejora subsiguiente en la resistencia. La adición de MLO proporcionó cierta plastificación y mejoró la resistencia al impacto, mientras que la adición del compatibilizante PE-*co*-AA derivado del petróleo indujo una mejor elongación a la rotura. Este enfoque podría contribuir positivamente al desarrollo de mezclas de alto rendimiento basadas en biopolímeros inmiscibles y también a la promoción de tecnologías de polímeros sostenibles.

IV.2. CONCLUSIONES GENERALES.

Como conclusión final de la presente tesis doctoral, se puede resaltar que la utilización de polímeros obtenidos a partir de recursos renovables, juntamente con la utilización de aditivos, cargas y refuerzos naturales, ha dado como resultado la creación de mezclas y formulaciones con un alto rendimiento medioambiental. Este tipo de combinaciones han dado a luz nuevas formulaciones altamente eficientes y respetuosas con el medio ambiente y en muchos casos biodegradables. Este tipo de formulaciones a partir de poliésteres y poliamidas renovables, y aditivos basado en aceites vegetales, cargas lignocelulósicas derivadas de residuos agroalimentarios o refuerzos y nanocargas renovables, representan una solución ecológica para mejorar las formulaciones industriales y puede contribuir positivamente al desarrollo de tecnologías de polímeros sostenibles.

Las formulaciones creadas a partir de este trabajo, pueden considerarse entonces como grandes candidatas para ser utilizadas en embalajes rígidos sostenibles,

envases activos, o de manera general, en la industria del envase y embalaje, reduciendo la huella de carbono, los elementos derivados del petróleo y la problemática actual con los plásticos desechables.

REFE**R**ENCIAS

VI. REFERENCIAS
REFERENCIAS

REFERENCIAS

1. Moore, C.J., *Synthetic polymers in the marine environment: a rapidly increasing, long-term threat.* Environmental research, 2008. **108**(2): 131-139.
2. Van der Ploeg, F., *Natural resources: curse or blessing?* Journal of Economic Literature, 2011. **49**(2): 366-420.
3. Creata, M.-L. and A.-M. Marinescu, *Directive (EU) 2019/790 of the European Parliament and of the Council of 17 April 2019 on Copyright and Related Rights in the Digital Single Market and Amending Directives 96/9/EC and 2001/29/EC.* Rom. J. Intell. Prop. L., 2019: 40.
4. Tschan, M.J.-L., E. Brulé, P. Haquette and C.M. Thomas, *Synthesis of biodegradable polymers from renewable resources.* Polymer Chemistry, 2012. **3**(4): 836-851.
5. Robert, C., F. De Montigny and C.M. Thomas, *Tandem synthesis of alternating polyesters from renewable resources.* Nature communications, 2011. **2**: 586.
6. Hong, M. and E.Y.-X. Chen, *Chemically recyclable polymers: a circular economy approach to sustainability.* Green Chemistry, 2017. **19**(16): 3692-3706.
7. Manson, J.A., *Polymer blends and composites.* 2012: Springer Science & Business Media.
8. Ozcalik, O. and F. Tihminlioglu, *Barrier properties of corn zein nanocomposite coated polypropylene films for food packaging applications.* Journal of Food Engineering, 2013. **114**(4): 505-513.
9. Jo, Y., C.V. Garcia, S. Ko, W. Lee, G.H. Shin, J.C. Choi, S.-J. Park and J.T. Kim, *Characterization and antibacterial properties of nanosilver-applied polyethylene and polypropylene composite films for food packaging applications.* Food bioscience, 2018. **23**: 83-90.
10. Karian, H., *Handbook of polypropylene and polypropylene composites, revised and expanded.* 2003: CRC press.
11. Al-Oqla, F.M., S. Sapuan, M. Ishak and A. Nuraini, *A decision-making model for selecting the most appropriate natural fiber–Polypropylene-based composites for automotive applications.* Journal of Composite Materials, 2016. **50**(4): 543-556.
12. Bouma, K. and D. Schakel, *Migration of phthalates from PVC toys into saliva simulant by dynamic extraction.* Food Additives & Contaminants, 2002. **19**(6): 602-610.
13. Kasirajan, S. and M. Ngouajio, *Polyethylene and biodegradable mulches for agricultural applications: a review.* Agronomy for Sustainable Development, 2012. **32**(2): 501-529.
14. Karaman, A.I., N. Kir and S. Belli, *Four applications of reinforced polyethylene fiber material in orthodontic practice.* American Journal of Orthodontics and Dentofacial Orthopedics, 2002. **121**(6): 650-654.
15. Donati, M., G. Brancato, G. Grosso, G.L. Volti, G. La Camera, F. Cardì, F. Basile and A. Donati, *Immunological reaction and oxidative stress after light or heavy polypropylene mesh implantation in inguinal hernioplasty: a CONSORT-prospective, randomized, clinical trial.* Medicine, 2016. **95**(24).
16. Siracusa, V., P. Rocculi, S. Romani and M. Dalla Rosa, *Biodegradable polymers for food packaging: a review.* Trends in Food Science & Technology, 2008. **19**(12): 634-643.
17. Kirwan, M.J. and J.W. Strawbridge, *Plastics in food packaging.* Food packaging technology, 2003. **1**: 174-240.
18. Javidi, Z., Z. Tarashi, A. Rostami and H. Nazockdast, *Role of nanosilica localization on morphology development of HDPE/PS/PMMA immiscible ternary blends.* eXPRESS Polymer Letters, 2017. **11**(5).
19. Lebreton, L., et al., *Evidence that the Great Pacific Garbage Patch is rapidly accumulating plastic.* Scientific reports, 2018. **8**(1): 4666.
20. Pervaiz, M., M. Faruq, M. Jawaid and M. Sain, *Polyamides: developments and applications towards next-generation engineered plastics.* Current Organic Synthesis, 2017. **14**(2): 146-155.

21.   Schmauder, T., K.-D. Nauenburg, K. Kruse and G. Ickes, *Hard coatings by plasma CVD on polycarbonate for automotive and optical applications.* Thin Solid Films, 2006. **502**(1-2): 270-274.

22.   Alexakou, E., M. Damanaki, P. Zoidis, E. Bakiri, N. Mouzis, G. Smidt and S. Kourtis, *PEEK High Performance Polymers: A Review of Properties and Clinical Applications in Prosthodontics and Restorative Dentistry.* The European journal of prosthodontics and restorative dentistry, 2019. **27**(3): 113-121.

23.   Panayotov, I.V., V. Orti, F. Cuisinier and J. Yachouh, *Polyetheretherketone (PEEK) for medical applications.* Journal of Materials Science: Materials in Medicine, 2016. **27**(7): 118.

24.   Karimzadeh, I., M. Aghazadeh, T. Doroudi, M.R. Ganjali and P.H. Kolivand, *Superparamagnetic iron oxide (Fe3O4) nanoparticles coated with PEG/PEI for biomedical applications: A facile and scalable preparation route based on the cathodic electrochemical deposition method.* Advances in Physical Chemistry, 2017. **2017**.

25.   Hamad, K., M. Kaseem, H. Yang, F. Deri and Y. Ko, *Properties and medical applications of polylactic acid: A review.* Express Polymer Letters, 2015. **9**(5).

26.   Miclaus, R., A. Repanovici and N. Roman, *Biomaterials: polylactic acid and 3D printing processes for orthosis and prosthesis.* Materiale Plastice, 2017. **54**: 98-102.

27.   Williams, J.M., A. Adewunmi, R.M. Schek, C.L. Flanagan, P.H. Krebsbach, S.E. Feinberg, S.J. Hollister and S. Das, *Bone tissue engineering using polycaprolactone scaffolds fabricated via selective laser sintering.* Biomaterials, 2005. **26**(23): 4817-4827.

28.   Lopes, M.S., A. Jardini and R. Maciel Filho, *Poly (lactic acid) production for tissue engineering applications.* Procedia Engineering, 2012. **42**: 1402-1413.

29.   de Valence, S., J.-C. Tille, D. Mugnai, W. Mrowczynski, R. Gurny, M. Möller and B.H. Walpoth, *Long term performance of polycaprolactone vascular grafts in a rat abdominal aorta replacement model.* Biomaterials, 2012. **33**(1): 38-47.

30.   Lam, C.X., D.W. Hutmacher, J.T. Schantz, M.A. Woodruff and S.H. Teoh, *Evaluation of polycaprolactone scaffold degradation for 6 months in vitro and in vivo.* Journal of Biomedical Materials Research Part A: An Official Journal of The Society for Biomaterials, The Japanese Society for Biomaterials, and The Australian Society for Biomaterials and the Korean Society for Biomaterials, 2009. **90**(3): 906-919.

31.   Audic, J.L. and B. Chaufer, *Properties of biodegradable poly(butylene adipate-co-terephtalate) and sodium caseinate blends.* Journal of Applied Polymer Science, 2012. **125**: E459-E467.

32.   Van Wouwe, P., M. Dusselier, E. Vanleeuw and B. Sels, *Lactide Synthesis and Chirality Control for Polylactic acid Production.* Chemsuschem, 2016. **9**(9): 907-921.

33.   Chikh, A., A. Benhamida, M. Kaci, I. Pillin and S. Bruzaud, *Synergistic effect of compatibilizer and sepiolite on the morphology of poly(3-hydroxybutyrate-co-3-hydroxyvalerate)/poly(butylene succinate) blends.* Polymer Testing, 2016. **53**: 19-28.

34.   Gigli, M., M. Fabbri, N. Lotti, R. Gamberini, B. Rimini and A. Munari, *Poly(butylene succinate)-based polyesters for biomedical applications: A review.* European Polymer Journal, 2016. **75**: 431-460.

35.   Meng, L.H., C.C. Gao, L. Yu, G.P. Simon, H.S. Liu and L. Chen, *Biodegradable composites of poly(butylene succinate-co-butylene adipate) reinforced by poly(lactic acid) fibers.* Journal of Applied Polymer Science, 2016. **133**(25): 6.

36.   van Velthoven, J.L.J., L. Gootjes, B.A.J. Noordover and J. Meuldijk, *Bio-based, amorphous polyamides with tunable thermal properties.* European Polymer Journal, 2015. **66**: 57-66.

37.   More, A.S., D.V. Palaskar, E. Cloutet, B. Gadenne, C. Alfos and H. Cramail, *Aliphatic polycarbonates and poly(ester carbonate)s from fatty acid derived monomers.* Polymer Chemistry, 2011. **2**(12): 2796-2803.

38.   Nakayama, A., *Development of Biobased Polyamides.* Sen-I Gakkaishi, 2010. **66**(11): P368-P372.

39.   Noordover, B.A.J., D. Haveman, R. Duchateau, R. van Benthem and C.E. Koning, *Chemistry, Functionality, and Coating Performance of Biobased Copolycarbonates from 1,4:3,6-Dianhydrohexitols.* Journal of Applied Polymer Science, 2011. **121**(3): 1450-1463.

40.   Simkovic, I., *What could be greener than composites made from polysaccharides?* Carbohydrate Polymers, 2008. **74**(4): 759-762.

41.   Williams, C.K. and M.A. Hillmyer, *Polymers from renewable resources: a perspective for a special issue of polymer reviews.* Polymer reviews, 2008. **48**(1): 1-10.

42.   Arrieta, M.P., J. López, D. López, J.M. Kenny and L. Peponi, *Biodegradable electrospun bionanocomposite fibers based on plasticized PLA–PHB blends reinforced with cellulose nanocrystals.* Industrial Crops and Products, 2016. **93**: 290-301.

43.   Carbonell-Verdu, A., D. Garcia-Garcia, F. Dominici, L. Torre, L. Sanchez-Nacher and R. Balart, *PLA films with improved flexibility properties by using maleinized cottonseed oil.* European Polymer Journal, 2017. **91**: 248-259.

44.   Reddy, N., Q. Jiang, E. Jin, Z. Shi, X. Hou and Y. Yang, *Bio-thermoplastics from grafted chicken feathers for potential biomedical applications.* Colloids and Surfaces B: Biointerfaces, 2013. **110**: 51-58.

45.   Tematio, C., M. Bassas-Galia, N. Fosso, V. Gaillard, M. Mathieu, M. Zinn, E.M. Staderini and S. Schintke. *Design and characterization of conductive biopolymer nanocomposite electrodes for medical applications*. in *Materials Science Forum*. 2017. Trans Tech Publ.

46.   Bhawani, S.A., H. Hussain, O. Bojo and S.S. Fong, *Proteins as agricultural polymers for packaging production*, in *Bionanocomposites for packaging applications*. 2018, Springer. p. 243-267.

47.   Samsudin, H., R. Auras, D. Mishra, K. Dolan, G. Burgess, M. Rubino, S. Selke and H. Soto-Valdez, *Migration of antioxidants from polylactic acid films: a parameter estimation approach and an overview of the current mass transfer models.* Food Research International, 2018. **103**: 515-528.

48.   Nagarajan, V., A.K. Mohanty and M. Misra, *Perspective on polylactic acid (PLA) based sustainable materials for durable applications: Focus on toughness and heat resistance.* ACS Sustainable Chemistry & Engineering, 2016. **4**(6): 2899-2916.

49.   Sousa, A.F., C. Vilela, A.C. Fonseca, M. Matos, C.S.R. Freire, G.J.M. Gruter, J.F.J. Coelhob and A.J.D. Silvestre, *Biobased polyesters and other polymers from 2,5-furandicarboxylic acid: a tribute to furan excellency.* Polymer Chemistry, 2015. **6**(33): 5961-5983.

50.   Altaee, N., G.A. El-Hiti, A. Fahdil, K. Sudesh and E. Yousif, *Biodegradation of different formulations of polyhydroxybutyrate films in soil.* Springerplus, 2016. **5**: 12.

51.   Ding, Y.P., W. Li, T. Muller, D.W. Schubert, A.R. Boccaccini, Q.Q. Yao and J.A. Roether, *Electrospun Polyhydroxybutyrate/Poly(epsilon-caprolactone)/58S Sol-Gel Bioactive Glass Hybrid Scaffolds with Highly Improved Osteogenic Potential for Bone Tissue Engineering.* Acs Applied Materials & Interfaces, 2016. **8**(27): 17098-17108.

52.   Vanovcanova, Z., et al., *Effect of PHB on the properties of biodegradable PLA blends.* Chemical Papers, 2016. **70**(10): 1408-1415.

53.   Yeo, J.C.C., J.K. Muiruri, W. Thitsartarn, Z. Li and C. He, *Recent advances in the development of biodegradable PHB-based toughening materials: Approaches, advantages and applications.* Materials Science and Engineering: C, 2018. **92**: 1092-1116.

54.   Modi, S.J., K. Cornish, K. Koelling and Y. Vodovotz, *Fabrication and improved performance of poly(3-hydroxybutyrate-co-3-hydroxyvalerate) for packaging by addition of high molecular weight natural rubber.* Journal of Applied Polymer Science, 2016. **133**(37): 9.

55.   Oner, M. and B. Ilhan, *Fabrication of poly(3-hydroxybutyrate-co-3-hydroxyvalerate) biocomposites with reinforcement by hydroxyapatite using extrusion processing.* Materials Science & Engineering C-Materials for Biological Applications, 2016. **65**: 19-26.

56.   Al-Sabagh, A., F. Yehia, G. Eshaq, A. Rabie and A. ElMetwally, *Greener routes for recycling of polyethylene terephthalate.* Egyptian Journal of Petroleum, 2016. **25**(1): 53-64.

57.   Cheng, Y., S. Deng, P. Chen and R. Ruan, *Polylactic acid (PLA) synthesis and modifications: a review.* Frontiers of chemistry in China, 2009. **4**(3): 259-264.

58.   Tokiwa, Y. and T. Suzuki, *Hydrolysis of copolyesters containing aromatic and aliphatic ester blocks by lipase.* Journal of Applied Polymer Science, 1981. **26**(2): 441-448.

59. Khalil, F., S. Galland, A. Cottaz, C. Joly and P. Degraeve, *Polybutylene succinate adipate/starch blends: A morphological study for the design of controlled release films.* Carbohydrate polymers, 2014. **108**: 272-280.

60. Janczak, K., K. Hrynkiewicz, Z. Znajewska and G. Dąbrowska, *Use of rhizosphere microorganisms in the biodegradation of PLA and PET polymers in compost soil.* International Biodeterioration & Biodegradation, 2018. **130**: 65-75.

61. Puchalski, M., G. Szparaga, T. Biela, A. Gutowska, S. Sztajnowski and I. Krucińska, *Molecular and supramolecular changes in polybutylene succinate (PBS) and polybutylene succinate adipate (PBSA) copolymer during degradation in various environmental conditions.* Polymers, 2018. **10**(3): 251.

62. Castilla-Cortázar, I., A. Vidaurre, B. Marí and A.J. Campillo-Fernández, *Morphology, Crystallinity, and Molecular Weight of Poly (ε-caprolactone)/Graphene Oxide Hybrids.* Polymers, 2019. **11**(7): 1099.

63. Wang, Y., M. Xian, X. Feng, M. Liu and G. Zhao, *Biosynthesis of ethylene glycol from d-xylose in recombinant Escherichia coli.* Bioengineered, 2018. **9**(1): 233-241.

64. Imaseki, H., *The biochemistry of ethylene biosynthesis*, in *The plant hormone ethylene*. 2018, CRC Press. p. 1-20.

65. Jorda, M., S. Montava-Jorda, R. Balart, D. Lascano, N. Montanes and L. Quiles-Carrillo, *Functionalization of Partially Bio-Based Poly (Ethylene Terephthalate) by Blending with Fully Bio-Based Poly (Amide) 10, 10 and a Glycidyl Methacrylate-Based Compatibilizer.* Polymers, 2019. **11**(8): 1331.

66. Neațu, F., G. Culică, M. Florea, V.I. Parvulescu and F. Cavani, *Synthesis of Terephthalic Acid by p-Cymene Oxidation using Oxygen: Toward a More Sustainable Production of Bio-Polyethylene Terephthalate.* ChemSusChem, 2016. **9**(21): 3102-3112.

67. Tachibana, Y., S. Kimura and K.-i. Kasuya, *Synthesis and verification of biobased terephthalic acid from furfural.* Scientific reports, 2015. **5**: 8249.

68. Hillmyer, M.A. and W.B. Tolman, *Aliphatic polyester block polymers: renewable, degradable, and sustainable.* Accounts of chemical research, 2014. **47**(8): 2390-2396.

69. Marra, A., C. Silvestre, D. Duraccio and S. Cimmino, *Polylactic acid/zinc oxide biocomposite films for food packaging application.* International journal of biological macromolecules, 2016. **88**: 254-262.

70. Cacciotti, I., S. Mori, V. Cherubini and F. Nanni, *Eco-sustainable systems based on poly (lactic acid), diatomite and coffee grounds extract for food packaging.* International journal of biological macromolecules, 2018. **112**: 567-575.

71. Silva, T.F.d., F. Menezes, L.S. Montagna, A.P. Lemes and F.R. Passador, *Preparation and characterization of antistatic packaging for electronic components based on poly (lactic acid)/carbon black composites.* Journal of Applied Polymer Science, 2019. **136**(13): 47273.

72. Rabnawaz, M., I. Wyman, R. Auras and S. Cheng, *A roadmap towards green packaging: The current status and future outlook for polyesters in the packaging industry.* Green Chemistry, 2017. **19**(20): 4737-4753.

73. Marcos, B., C. Bueno-Ferrer and A. Fernández, *Innovations in packaging of fermented food products*, in *Novel food fermentation technologies*. 2016, Springer. p. 311-333.

74. Emadian, S.M., T.T. Onay and B. Demirel, *Biodegradation of bioplastics in natural environments.* Waste management, 2017. **59**: 526-536.

75. Altaee, N., G.A. El-Hiti, A. Fahdil, K. Sudesh and E. Yousif, *Biodegradation of different formulations of polyhydroxybutyrate films in soil.* SpringerPlus, 2016. **5**(1): 762.

76. Dulnik, J., P. Denis, P. Sajkiewicz, D. Kołbuk and E. Choińska, *Biodegradation of bicomponent PCL/gelatin and PCL/collagen nanofibers electrospun from alternative solvent system.* Polymer Degradation and Stability, 2016. **130**: 10-21.

77. Stloukal, P., A. Kalendova, H. Mattausch, S. Laske, C. Holzer and M. Koutny, *The influence of a hydrolysis-inhibiting additive on the degradation and biodegradation of PLA and its nanocomposites.* Polymer Testing, 2015. **41**: 124-132.

78. Souza, V.G.L. and A.L. Fernando, *Nanoparticles in food packaging: Biodegradability and potential migration to food – A review.* Food Packaging and Shelf Life, 2016. **8**: 63-70.

79. Mueller, R.-J., *Biological degradation of synthetic polyesters – Enzymes as potential catalysts for polyester recycling.* Process Biochemistry, 2006. **41**(10): 2124-2128.

80. Tokiwa, Y. and T. Suzuki, *HYDROLYSIS OF POLYESTERS BY RHIZOPUS-DELEMAR LIPASE.* Agricultural and Biological Chemistry, 1978. **42**(5): 1071-1072.

81. Elsawy, M.A., K.-H. Kim, J.-W. Park and A. Deep, *Hydrolytic degradation of polylactic acid (PLA) and its composites.* Renewable and Sustainable Energy Reviews, 2017. **79**: 1346-1352.

82. ISO, U., *UNE-EN ISO 20200 Determinación del grado de desintegración de materiales plásticos bajo condiciones de compostaje simuladas en un laboratorio.* 2006.

83. Kale, G., R. Auras, S.P. Singh and R. Narayan, *Biodegradability of polylactide bottles in real and simulated composting conditions.* Polymer Testing, 2007. **26**(8): 1049-1061.

84. Gan, Z., K. Kuwabara, M. Yamamoto, H. Abe and Y. Doi, *Solid-state structures and thermal properties of aliphatic–aromatic poly (butylene adipate-co-butylene terephthalate) copolyesters.* Polymer Degradation and Stability, 2004. **83**(2): 289-300.

85. Muthuraj, R., M. Misra and A. Mohanty, *Hydrolytic degradation of biodegradable polyesters under simulated environmental conditions.* Journal of Applied Polymer Science, 2015. **132**(27).

86. Evandri, M.G., P. Tucci and P. Bolle, *Toxicological evaluation of commercial mineral water bottled in polyethylene terephthalate: a cytogenetic approach with Allium cepa.* Food Additives & Contaminants, 2000. **17**(12): 1037-1045.

87. Lu, Z., L. Ma, J. Tan, H. Wang and X. Ding, *Transparent multi-layer graphene/polyethylene terephthalate structures with excellent microwave absorption and electromagnetic interference shielding performance.* Nanoscale, 2016. **8**(37): 16684-16693.

88. Emamian, S., B.B. Narakathu, A.A. Chlaihawi, B.J. Bazuin and M.Z. Atashbar, *Screen printing of flexible piezoelectric based device on polyethylene terephthalate (PET) and paper for touch and force sensing applications.* Sensors and Actuators A: Physical, 2017. **263**: 639-647.

89. Fernández, S., J. Santos, C. Munuera, M. García-Hernández and F. Naranjo, *Effect of argon plasma-treated polyethylene terepthalate on ZnO: Al properties for flexible thin film silicon solar cells applications.* Solar Energy Materials and Solar Cells, 2015. **133**: 170-179.

90. Bheemaneni, G. and R. Kandaswamy, *Melt processing and characterization of tricalcium phosphate filled polybutylene adipate-co-terephthalate/polymethyl methacrylate composites for biomedical applications.* International Journal of Polymeric Materials and Polymeric Biomaterials, 2019. **68**(1-3): 119-125.

91. Bheemaneni, G., S. Saravana and R. Kandaswamy, *Processing and Characterization of Poly (butylene adipate-co-terephthalate)/Wollastonite Biocomposites for Medical Applications.* Materials Today: Proceedings, 2018. **5**(1): 1807-1816.

92. Malikmammadov, E., T.E. Tanir, A. Kiziltay, V. Hasirci and N. Hasirci, *PCL and PCL-based materials in biomedical applications.* Journal of Biomaterials science, Polymer edition, 2018. **29**(7-9): 863-893.

93. Augustine, R., N. Kalarikkal and S. Thomas, *Electrospun PCL membranes incorporated with biosynthesized silver nanoparticles as antibacterial wound dressings.* Applied Nanoscience, 2016. **6**(3): 337-344.

94. Bergstroem, J.S. and D. Hayman, *An overview of mechanical properties and material modeling of polylactide (PLA) for medical applications.* Annals of biomedical engineering, 2016. **44**(2): 330-340.

95. Tian, X., T. Liu, C. Yang, Q. Wang and D. Li, *Interface and performance of 3D printed continuous carbon fiber reinforced PLA composites.* Composites Part A: Applied Science and Manufacturing, 2016. **88**: 198-205.

96. Koronis, G., A. Silva and M. Fontul, *Green composites: A review of adequate materials for automotive applications.* Composites Part B: Engineering, 2013. **44**(1): 120-127.

97. Carbonell-Verdu, A., J. Ferri, F. Dominici, T. Boronat, L. Sanchez-Nacher, R. Balart and L. Torre, *Manufacturing and compatibilization of PLA/PBAT binary blends by cottonseed oil-based derivatives.* Express Polymer Letters, 2018. **12**(9): 808-823.

98.   Shibata, M., Y. Inoue and M. Miyoshi, *Mechanical properties, morphology, and crystallization behavior of blends of poly (L-lactide) with poly (butylene succinate-co-L-lactate) and poly (butylene succinate).* Polymer, 2006. **47**(10): 3557-3564.

99.   Torres, E., V. Fombuena, A. Vallés-Lluch and T. Ellingham, *Improvement of mechanical and biological properties of polycaprolactone loaded with hydroxyapatite and halloysite nanotubes.* Materials Science and Engineering: C, 2017. **75**: 418-424.

100.   Arruda, L.C., M. Magaton, R.E.S. Bretas and M.M. Ueki, *Influence of chain extender on mechanical, thermal and morphological properties of blown films of PLA/PBAT blends.* Polymer Testing, 2015. **43**: 27-37.

101.   Arrieta, M., M. Samper, M. Aldas and J. López, *On the use of PLA-PHB blends for sustainable food packaging applications.* Materials, 2017. **10**(9): 1008.

102.   Gerometta, M., J.R. Rocca-Smith, S. Domenek and T. Karbowiak, *Physical and Chemical Stability of PLA in Food Packaging*. 2019.

103.   Musioł, M., W. Sikorska, G. Adamus, H. Janeczek, M. Kowalczuk and J. Rydz, *(Bio) degradable polymers as a potential material for food packaging: studies on the (bio) degradation process of PLA/(R, S)-PHB rigid foils under industrial composting conditions.* European Food Research and Technology, 2016. **242**(6): 815-823.

104.   Petchwattana, N., S. Covavisaruch, S. Wibooranawong and P. Naknaen, *Antimicrobial food packaging prepared from poly (butylene succinate) and zinc oxide.* Measurement, 2016. **93**: 442-448.

105.   Nassar, S.F., A. Guinault, N. Delpouve, V. Divry, V. Ducruet, C. Sollogoub and S. Domenek, *Multi-scale analysis of the impact of polylactide morphology on gas barrier properties.* Polymer, 2017. **108**: 163-172.

106.   Li, X., X. Ai, H. Pan, J. Yang, G. Gao, H. Zhang, H. Yang and L. Dong, *The morphological, mechanical, rheological, and thermal properties of PLA/PBAT blown films with chain extender.* Polymers for Advanced Technologies, 2018. **29**(6): 1706-1717.

107.   Lizundia, E., J.L. Vilas, A. Sangroniz and A. Etxeberria, *Light and gas barrier properties of PLLA/metallic nanoparticles composite films.* European Polymer Journal, 2017. **91**: 10-20.

108.   Jamshidian, M., E.A. Tehrany, M. Imran, M. Jacquot and S. Desobry, *Poly-Lactic Acid: production, applications, nanocomposites, and release studies.* Comprehensive reviews in food science and food safety, 2010. **9**(5): 552-571.

109.   Castro-Aguirre, E., F. Iñiguez-Franco, H. Samsudin, X. Fang and R. Auras, *Poly (lactic acid)—Mass production, processing, industrial applications, and end of life.* Advanced Drug Delivery Reviews, 2016. **107**: 333-366.

110.   Kwan, T.H., Y. Hu and C.S.K. Lin, *Techno-economic analysis of a food waste valorisation process for lactic acid, lactide and poly (lactic acid) production.* Journal of cleaner production, 2018. **181**: 72-87.

111.   de Oliveira, R.A., A. Komesu, C.E.V. Rossell, M.R.W. Maciel and R. Maciel Filho, *A study of the residual fermentation sugars influence on an alternative downstream process for first and second-generation lactic acid.* Sustainable Chemistry and Pharmacy, 2020. **15**: 100206.

112.   Brodin, M., M. Vallejos, M.T. Opedal, M.C. Area and G. Chinga-Carrasco, *Lignocellulosics as sustainable resources for production of bioplastics–A review.* Journal of cleaner production, 2017. **162**: 646-664.

113.   Tripathi, A.D. and S. Srivastava, *Kinetic study of biopolymer (PHB) synthesis in Alcaligenes sp. in submerged fermentation process using TEM.* Journal of Polymers and the Environment, 2011. **19**(3): 732.

114.   Vink, E.T., K.R. Rabago, D.A. Glassner and P.R. Gruber, *Applications of life cycle assessment to NatureWorks™ polylactide (PLA) production.* Polymer Degradation and stability, 2003. **80**(3): 403-419.

115.   Singh, S. and S.S. Ray, *Polylactide based nanostructured biomaterials and their applications.* Journal of Nanoscience and Nanotechnology, 2007. **7**(8): 2596-2615.

116.   Auras, R., B. Harte and S. Selke, *An overview of polylactides as packaging materials.* Macromolecular bioscience, 2004. **4**(9): 835-864.

117. Hu, Y., W. Daoud, K. Cheuk and C. Lin, *Newly developed techniques on polycondensation, ring-opening polymerization and polymer modification: Focus on poly (lactic acid)*. Materials, 2016. **9**(3): 133.

118. Shaikh, T. and H. Kaur, *Synthesis and characterization of nanosized polylactic acid/TiO 2 particle brushes by azeotropic dehydration polycondensation of lactic acid*. Journal of Polymer Research, 2018. **25**(1): 22.

119. Ingrao, C., M. Gigli and V. Siracusa, *An attributional Life Cycle Assessment application experience to highlight environmental hotspots in the production of foamy polylactic acid trays for fresh-food packaging usage*. Journal of Cleaner Production, 2017. **150**: 93-103.

120. Briassoulis, D. and A. Giannoulis, *Evaluation of the functionality of bio-based food packaging films*. Polymer Testing, 2018. **69**: 39-51.

121. Vink, E.T. and S. Davies, *Life cycle inventory and impact assessment data for 2014 Ingeo™ polylactide production*. Industrial Biotechnology, 2015. **11**(3): 167-180.

122. Keshavarz, T. and I. Roy, *Polyhydroxyalkanoates: bioplastics with a green agenda*. Current opinion in microbiology, 2010. **13**(3): 321-326.

123. Urtuvia, V., P. Villegas, M. González and M. Seeger, *Bacterial production of the biodegradable plastics polyhydroxyalkanoates*. International journal of biological macromolecules, 2014. **70**: 208-213.

124. Philip, S., T. Keshavarz and I. Roy, *Polyhydroxyalkanoates: biodegradable polymers with a range of applications*. Journal of Chemical Technology & Biotechnology: International Research in Process, Environmental & Clean Technology, 2007. **82**(3): 233-247.

125. Khanna, S. and A.K. Srivastava, *Recent advances in microbial polyhydroxyalkanoates*. Process biochemistry, 2005. **40**(2): 607-619.

126. Leong, Y.K., P.L. Show, C.W. Ooi, T.C. Ling and J.C.-W. Lan, *Current trends in polyhydroxyalkanoates (PHAs) biosynthesis: insights from the recombinant Escherichia coli*. Journal of biotechnology, 2014. **180**: 52-65.

127. Rodriguez-Perez, S., A. Serrano, A.A. Pantión and B. Alonso-Fariñas, *Challenges of scaling-up PHA production from waste streams. A review*. Journal of environmental management, 2018. **205**: 215-230.

128. Colombo, B., M.V. Calvo, T.P. Sciarria, B. Scaglia, S.S. Kizito, G. D'Imporzano and F. Adani, *Biohydrogen and polyhydroxyalkanoates (PHA) as products of a two-steps bioprocess from deproteinized dairy wastes*. Waste Management, 2019. **95**: 22-31.

129. Du, G., J. Chen, J. Yu and S. Lun, *Continuous production of poly-3-hydroxybutyrate by Ralstonia eutropha in a two-stage culture system*. Journal of biotechnology, 2001. **88**(1): 59-65.

130. Pan, W., J.A. Perrotta, A.J. Stipanovic, C.T. Nomura and J.P. Nakas, *Production of polyhydroxyalkanoates by Burkholderia cepacia ATCC 17759 using a detoxified sugar maple hemicellulosic hydrolysate*. Journal of industrial microbiology & biotechnology, 2012. **39**(3): 459-469.

131. Jacquel, N., C.-W. Lo, Y.-H. Wei, H.-S. Wu and S.S. Wang, *Isolation and purification of bacterial poly (3-hydroxyalkanoates)*. Biochemical Engineering Journal, 2008. **39**(1): 15-27.

132. Modi, S., K. Koelling and Y. Vodovotz, *Assessment of PHB with varying hydroxyvalerate content for potential packaging applications*. European Polymer Journal, 2011. **47**(2): 179-186.

133. Marchildon, K., *Polyamides–still strong after seventy years*. Macromolecular reaction engineering, 2011. **5**(1): 22-54.

134. Carothers, W.H., *Studies on polymerization and ring formation. I. An introduction to the general theory of condensation polymers*. Journal of the American Chemical Society, 1929. **51**(8): 2548-2559.

135. Sato, Y., A. Ito, S. Maeda and M. Yamaguchi, *Structure and optical properties of transparent polyamide 6 containing lithium bromide*. Journal of Polymer Science Part B: Polymer Physics, 2018. **56**(22): 1513-1520.

136. Xu, S., L. Sun, J. He, H. Han, H. Wang, Y. Fang and Q. Wang, *Effects of LiCl on crystallization, thermal, and mechanical properties of polyamide 6/wood fiber composites.* Polymer Composites, 2018. **39**(S3): E1574-E1580.

137. Pant, H.R., M.P. Bajgai, K.T. Nam, Y.A. Seo, D.R. Pandeya, S.T. Hong and H.Y. Kim, *Electrospun nylon-6 spider-net like nanofiber mat containing TiO2 nanoparticles: a multifunctional nanocomposite textile material.* Journal of hazardous materials, 2011. **185**(1): 124-130.

138. Li, M., Y. Zhong, Z. Wang, A. Fischer, F. Ranft, D. Drummer and W. Wu, *Flame retarding mechanism of Polyamide 6 with phosphorus-nitrogen flame retardant and DOPO derivatives.* Journal of Applied Polymer Science, 2016. **133**(6).

139. Han, D., S. Sherman, S. Filocamo and A.J. Steckl, *Long-term antimicrobial effect of nisin released from electrospun triaxial fiber membranes.* Acta biomaterialia, 2017. **53**: 242-249.

140. Shi, Y., *Phase behavior of polyamide 6/612 blends.* SPE ANTEC™ Indianapolis, 2016. **1**: 76-80.

141. van den Broek, L.A., R.J. Knoop, F.H. Kappen and C.G. Boeriu, *Chitosan films and blends for packaging material.* Carbohydrate polymers, 2015. **116**: 237-242.

142. Naskar, A.K., J.K. Keum and R.G. Boeman, *Polymer matrix nanocomposites for automotive structural components.* Nature nanotechnology, 2016. **11**(12): 1026.

143. Patil, A., A. Patel and R. Purohit, *An overview of polymeric materials for automotive applications.* Materials Today: Proceedings, 2017. **4**(2): 3807-3815.

144. Garrett, D.W. and G.R. Owens, *Polyphthalamide resins for use as automotive engine coolant components.* 1995, SAE Technical Paper.

145. Ficici, F., Z. Ayparcasi and H. Unal, *Influence of cutting tool and conditions on machinability aspects of polyphthalamide (PPA) matrix composite materials with 30% glass fiber reinforced.* The International Journal of Advanced Manufacturing Technology, 2017. **90**(9-12): 3067-3073.

146. Ferrito, S.J. *An analytical approach toward monitoring degradation in engineering thermoplastic materials used for electrical applications.* in *Proceedings of Conference on Electrical Insulation and Dielectric Phenomena-CEIDP'96.* 1996. IEEE.

147. Wilfong, R.E. and J. Zimmerman, *Future organic tire fibers.* Journal of Applied Polymer Science, 1973. **17**(7): 2039-2051.

148. García, J.M., F.C. García, F. Serna and L. José, *High-performance aromatic polyamides.* Progress in polymer science, 2010. **35**(5): 623-686.

149. Carole, T.M., J. Pellegrino and M.D. Paster. *Opportunities in the industrial biobased products industry.* in *Proceedings of the Twenty-Fifth Symposium on Biotechnology for Fuels and Chemicals Held May 4–7, 2003, in Breckenridge, CO.* 2004. Springer.

150. Kind, S., S. Neubauer, J. Becker, M. Yamamoto, M. Völkert, G. von Abendroth, O. Zelder and C. Wittmann, *From zero to hero–production of bio-based nylon from renewable resources using engineered Corynebacterium glutamicum.* Metabolic engineering, 2014. **25**: 113-123.

151. Nguyen, A., J. Schneider, G. Reddy and V. Wendisch, *Fermentative production of the diamine putrescine: system metabolic engineering of Corynebacterium glutamicum.* Metabolites, 2015. **5**(2): 211-231.

152. Desroches, M., M. Escouvois, R. Auvergne, S. Caillol and B. Boutevin, *From vegetable oils to polyurethanes: synthetic routes to polyols and main industrial products.* Polymer Reviews, 2012. **52**(1): 38-79.

153. Severino, L.S., et al., *A review on the challenges for increased production of castor.* Agronomy journal, 2012. **104**(4): 853-880.

154. Jiang, Y. and K. Loos, *Enzymatic synthesis of biobased polyesters and polyamides.* Polymers, 2016. **8**(7): 243.

155. Yasuda, M. and A. Miyabo, *Polyamide derived from castor oil.* SEN-I GAKKAISHI, 2010. **66**(4): P137-P142.

156. Winnacker, M. and B. Rieger, *Biobased Polyamides: Recent Advances in Basic and Applied Research.* Macromolecular Rapid Communications, 2016. **37**(17): 1391-1413.

157. Ogunsona, E.O., M. Misra and A.K. Mohanty, *Sustainable biocomposites from biobased polyamide 6, 10 and biocarbon from pyrolyzed miscanthus fibers.* Journal of Applied Polymer Science, 2017. **134**(4).

158. Paterson, M. and J. White, *Effect of water absorption on residual stresses in injection-moulded nylon 6, 6.* Journal of materials science, 1992. **27**(22): 6229-6240.

159. Wang, M.-S. and J.-C. Huang, *Nylon 1010 properties and applications.* Journal of polymer engineering, 1994. **13**(2): 155-174.

160. Kakroodi, A.R., Y. Kazemi, M. Nofar and C.B. Park, *Tailoring poly (lactic acid) for packaging applications via the production of fully bio-based in situ microfibrillar composite films.* Chemical Engineering Journal, 2017. **308**: 772-782.

161. Kausar, A., *Polyamide 1010/polythioamide blend reinforced with graphene nanoplatelet for automotive part application.* Advances in Materials Science, 2017. **17**(3): 24-36.

162. *Bio-Polyamide Market Expected to Reach USD 220.6 Million by 2022*, in *Bio-Based Neww*. 2015, nova-Institut GmbH

163. González-Ausejo, J., J. Gámez-Pérez, R. Balart, J.M. Lagarón and L. Cabedo, *Effect of the addition of sepiolite on the morphology and properties of melt compounded PHBV/PLA blends.* Polymer Composites, 2019. **40**(S1): E156-E168.

164. Liu, Y. and J. Feng, *An attempt towards fabricating reduced graphene oxide composites with traditional polymer processing techniques by adding chemical reduction agents.* Composites Science and Technology, 2017. **140**: 16-22.

165. Huang, Z.-X., C. Meng, G. Zhang and J.-P. Qu, *Manufacturing polymer/clay nanocomposites through elongational flow technique.* Materials and Manufacturing Processes, 2017. **32**(12): 1409-1415.

166. Ferri, J.M., O. Fenollar, A. Jorda-Vilaplana, D. García-Sanoguera and R. Balart, *Effect of miscibility on mechanical and thermal properties of poly (lactic acid)/polycaprolactone blends.* Polymer International, 2016. **65**(4): 453-463.

167. Michaeli, W., A. Grefenstein and U. Berghaus, *Twin-screw extruders for reactive extrusion.* Polymer Engineering and Science, 1995. **35**(19): 1485-1504.

168. Raquez, J.M., R. Narayan and P. Dubois, *Recent advances in reactive extrusion processing of biodegradable polymer-based compositions.* Macromolecular Materials and Engineering, 2008. **293**(6): 447-470.

169. Yang, L., J. Huang, X. Lu, S. Jia, H. Zhang, G. Jin and J. Qu, *Influences of dicumyl peroxide on morphology and mechanical properties of polypropylene/poly (styrene-b-butadiene-b-styrene) blends via vane-extruder.* Journal of Applied Polymer Science, 2015. **132**(9).

170. Wu, F., M. Misra and A.K. Mohanty, *Novel tunable super-tough materials from biodegradable polymer blends: nano-structuring through reactive extrusion.* RSC advances, 2019. **9**(5): 2836-2847.

171. Spinella, S., M. Ganesh, G.L. Re, S. Zhang, J.-M. Raquez, P. Dubois and R. Gross, *Enzymatic reactive extrusion: moving towards continuous enzyme-catalysed polyester polymerisation and processing.* Green Chemistry, 2015. **17**(8): 4146-4150.

172. Zhang, S., Z. Lin, G. Jiang, J. Wang and D.-Y. Wang, *Construction of chelation structure between Ca2+ and starch via reactive extrusion for improving the performances of thermoplastic starch.* Composites Science and Technology, 2018. **159**: 59-69.

173. Torres-Giner, S., N. Montanes, T. Boronat, L. Quiles-Carrillo and R. Balart, *Melt grafting of sepiolite nanoclay onto poly (3-hydroxybutyrate-co-4-hydroxybutyrate) by reactive extrusion with multi-functional epoxy-based styrene-acrylic oligomer.* European Polymer Journal, 2016. **84**: 693-707.

174. Li, H. and M.A. Huneault, *Effect of chain extension on the properties of PLA/TPS blends.* Journal of Applied Polymer Science, 2011. **122**(1): 134-141.

175. Choi, K.-M., S.-W. Lim, M.-C. Choi, Y.-M. Kim, D.-H. Han and C.-S. Ha, *Thermal and mechanical properties of poly (lactic acid) modified by poly (ethylene glycol) acrylate through reactive blending.* Polymer bulletin, 2014. **71**(12): 3305-3321.

176. Villalobos, M., A. Awojulu, T. Greeley, G. Turco and G. Deeter, *Oligomeric chain extenders for economic reprocessing and recycling of condensation plastics.* Energy, 2006. **31**(15): 3227-3234.

177. Yang, L.-T., C.-S. Zhao, C.-L. Dai, L.-Y. Fu and S.-Q. Lin, *Thermal and mechanical properties of polyurethane rigid foam based on epoxidized soybean oil.* Journal of Polymers and the Environment, 2012. **20**(1): 230-236.

178. Pawar, M.S., A.S. Kadam, B.S. Dawane and O.S. Yemul, *Synthesis and characterization of rigid polyurethane foams from algae oil using biobased chain extenders.* Polymer Bulletin, 2016. **73**(3): 727-741.

179. Fonseca, L.R., J.A. Bergman, M.R. Kessler, S.A. Madbouly and B.S. Lima-Neto. *Self-Metathesis of 10-Undecen-1-Ol with Ru-Amine-Based Complex for Preparing the Soft Segment and Chain Extender of Novel Castor Oil-Based Polyurethanes.* in *Macromolecular Symposia.* 2016. Wiley Online Library.

180. Österle, W., A. Dmitriev, B. Wetzel, G. Zhang, I. Häusler and B. Jim, *The role of carbon fibers and silica nanoparticles on friction and wear reduction of an advanced polymer matrix composite.* Materials & Design, 2016. **93**: 474-484.

181. Loureiro, L., V.H. Carvalho and S.H.P. Bettini, *Reuse of p-aramid from industrial waste as reinforcement fiber in polyamide 6.6.* Polymer Testing, 2016. **56**: 124-130.

182. Fu, S.-Y., B. Lauke, E. Mäder, C.-Y. Yue and X. Hu, *Tensile properties of short-glass-fiber- and short-carbon-fiber-reinforced polypropylene composites.* Composites Part A: Applied Science and Manufacturing, 2000. **31**(10): 1117-1125.

183. Ferrero, B., T. Boronat, R. Moriana, O. Fenollar and R. Balart, *Green composites based on wheat gluten matrix and posidonia oceanica waste fibers as reinforcements.* Polymer Composites, 2013. **34**(10): 1663-1669.

184. Kim, S.-J., J.-B. Moon, G.-H. Kim and C.-S. Ha, *Mechanical properties of polypropylene/natural fiber composites: Comparison of wood fiber and cotton fiber.* Polymer testing, 2008. **27**(7): 801-806.

185. Avella, M., G. Bogoeva-Gaceva, A. Bužarovska, M.E. Errico, G. Gentile and A. Grozdanov, *Poly (lactic acid)-based biocomposites reinforced with kenaf fibers.* Journal of Applied Polymer Science, 2008. **108**(6): 3542-3551.

186. Balart, J., V. Fombuena, O. Fenollar, T. Boronat and L. Sánchez-Nacher, *Processing and characterization of high environmental efficiency composites based on PLA and hazelnut shell flour (HSF) with biobased plasticizers derived from epoxidized linseed oil (ELO).* Composites Part B: Engineering, 2016. **86**: 168-177.

187. Părpăriță, E., R.N. Darie, C.-M. Popescu, M.A. Uddin and C. Vasile, *Structure–morphology–mechanical properties relationship of some polypropylene/lignocellulosic composites.* Materials & Design (1980-2015), 2014. **56**: 763-772.

188. Balart, J., D. García-Sanoguera, R. Balart, T. Boronat and L. Sánchez-Nacher, *Manufacturing and properties of biobased thermoplastic composites from poly (lactid acid) and hazelnut shell wastes.* Polymer Composites, 2018. **39**(3): 848-857.

189. Nourbakhsh, A. and A. Ashori, *Wood plastic composites from agro-waste materials: Analysis of mechanical properties.* Bioresource technology, 2010. **101**(7): 2525-2528.

190. La Mantia, F. and M. Morreale, *Green composites: A brief review.* Composites Part A: Applied Science and Manufacturing, 2011. **42**(6): 579-588.

191. Zini, E. and M. Scandola, *Green composites: an overview.* Polymer composites, 2011. **32**(12): 1905-1915.

192. Dicker, M.P., P.F. Duckworth, A.B. Baker, G. Francois, M.K. Hazzard and P.M. Weaver, *Green composites: A review of material attributes and complementary applications.* Composites part A: applied science and manufacturing, 2014. **56**: 280-289.

193. Salatin, S., S. Maleki Dizaj and A. Yari Khosroushahi, *Effect of the surface modification, size, and shape on cellular uptake of nanoparticles.* Cell biology international, 2015. **39**(8): 881-890.

194. Angellier-Coussy, H., S. Torres-Giner, M.H. Morel, N. Gontard and E. Gastaldi, *Functional properties of thermoformed wheat gluten/montmorillonite materials with respect to*

formulation and processing conditions. Journal of applied polymer science, 2008. **107**(1): 487-496.

195. Chiou, B.-S., E. Yee, G.M. Glenn and W.J. Orts, *Rheology of starch–clay nanocomposites.* Carbohydrate Polymers, 2005. **59**(4): 467-475.

196. Lvov, Y.M., M.M. DeVilliers and R.F. Fakhrullin, *The application of halloysite tubule nanoclay in drug delivery.* Expert opinion on drug delivery, 2016. **13**(7): 977-986.

197. Hanif, M., F. Jabbar, S. Sharif, G. Abbas, A. Farooq and M. Aziz, *Halloysite nanotubes as a new drug-delivery system: a review.* Clay Minerals, 2016. **51**(3): 469-477.

198. García-Villén, F., E. Carazo, A. Borrego-Sánchez, R. Sánchez-Espejo, P. Cerezo, C. Viseras and C. Aguzzi, *Clay minerals in drug delivery systems*, in *Modified Clay and Zeolite Nanocomposite Materials.* 2019, Elsevier. p. 129-166.

199. Song, K., M.F. Rubner, R.E. Cohen and K.A. Askar, *Polymer/Halloysite Nanotubes Composites: Mechanical Robustness and Optical Transmittance.* MRS Advances, 2017. **2**(1): 27-32.

200. Goda, E.S., K.R. Yoon, S.H. El-sayed and S.E. Hong, *Halloysite nanotubes as smart flame retardants: a review.* Thermochimica acta, 2018.

201. Liu, M., Z. Jia, D. Jia and C. Zhou, *Recent advance in research on halloysite nanotubes-polymer nanocomposite.* Progress in polymer science, 2014. **39**(8): 1498-1525.

202. Chivrac, F., E. Pollet, M. Schmutz and L. Avérous, *Starch nano-biocomposites based on needle-like sepiolite clays.* Carbohydrate Polymers, 2010. **80**(1): 145-153.

203. Darder, M., M. López-Blanco, P. Aranda, A.J. Aznar, J. Bravo and E. Ruiz-Hitzky, *Microfibrous chitosan− sepiolite nanocomposites.* Chemistry of Materials, 2006. **18**(6): 1602-1610.

204. Benlikaya, R., M. Alkan and İ. Kaya, *Preparation and characterization of sepiolite-poly (ethyl methacrylate) and poly (2-hydroxyethyl methacrylate) nanocomposites.* Polymer Composites, 2009. **30**(11): 1585-1594.

205. Tartaglione, G., D. Tabuani, G. Camino and M. Moisio, *PP and PBT composites filled with sepiolite: morphology and thermal behaviour.* Composites science and technology, 2008. **68**(2): 451-460.

206. Singh, V.P., G. Kapur and V. Choudhary, *High-density polyethylene/needle-like sepiolite clay nanocomposites: effect of functionalized polymers on the dispersion of nanofiller, melt extensional and mechanical properties.* RSC Advances, 2016. **6**(64): 59762-59774.

207. Moazeni, N., Z. Mohamad and N. Dehbari, *Study of silane treatment on poly-lactic acid (PLA)/sepiolite nanocomposite thin films.* Journal of Applied Polymer Science, 2015. **132**(6).

208. Rai, S., P. Dutta and G. Mehrotra, *Agrowaste derived phenolic compounds as additives to chitosan film for food packaging applications: antibacterial and antioxidant study.* J. Indian Chem. Soc, 2016. **93**: 1-8.

209. Rai, S., P. Dutta and G. Mehrotra, *Natural Antioxidant and Antimicrobial Agents from Agrowastes: An Emergent Need to Food Packaging.* Waste and Biomass Valorization, 2018: 1-12.

210. Fritsch, C., et al., *Processing, valorization and application of bio-waste derived compounds from potato, tomato, olive and cereals: A review.* Sustainability, 2017. **9**(8): 1492.

211. Escarpa, A. and M. Gonzalez, *An overview of analytical chemistry of phenolic compounds in foods.* Critical Reviews in Analytical Chemistry, 2001. **31**(2): 57-139.

212. Garcia-Salas, P., A. Morales-Soto, A. Segura-Carretero and A. Fernández-Gutiérrez, *Phenolic-compound-extraction systems for fruit and vegetable samples.* Molecules, 2010. **15**(12): 8813-8826.

213. Lizárraga-Velázquez, C.E., C. Hernández, G.A. González-Aguilar and J. Basilio-Heredia, *Propiedades antioxidantes e inmunoestimulantes de polifenoles en peces carnívoros de cultivo.* CienciaUAT, 2018. **12**(2): 127-136.

214. Ralph, J., C. Lapierre and W. Boerjan, *Lignin structure and its engineering.* Current opinion in biotechnology, 2019. **56**: 240-249.

215. Naczk, M. and F. Shahidi, *Phenolics in cereals, fruits and vegetables: Occurrence, extraction and analysis.* Journal of pharmaceutical and biomedical analysis, 2006. **41**(5): 1523-1542.

216.   Radusin, T., S. Torres-Giner, A. Stupar, I. Ristic, A. Miletic, A. Novakovic and J.M. Lagaron, *Preparation, characterization and antimicrobial properties of electrospun polylactide films containing Allium ursinum L. extract.* Food Packaging and Shelf Life, 2019. **21**: 100357.

217.   Altan, A., Z. Aytac and T. Uyar, *Carvacrol loaded electrospun fibrous films from zein and poly (lactic acid) for active food packaging.* Food hydrocolloids, 2018. **81**: 48-59.

218.   Arcan, I. and A. Yemenicioğlu, *Incorporating phenolic compounds opens a new perspective to use zein films as flexible bioactive packaging materials.* Food Research International, 2011. **44**(2): 550-556.

219.   Gómez Caravaca, A.M., A. Carrasco Pancorbo, B. Cañabate Díaz, A. Segura Carretero and A. Fernández Gutiérrez, *Electrophoretic identification and quantitation of compounds in the polyphenolic fraction of extra-virgin olive oil.* Electrophoresis, 2005. **26**(18): 3538-3551.

220.   Castro-Vargas, H.I., L.I. Rodríguez-Varela, S.R. Ferreira and F. Parada-Alfonso, *Extraction of phenolic fraction from guava seeds (Psidium guajava L.) using supercritical carbon dioxide and co-solvents.* The Journal of Supercritical Fluids, 2010. **51**(3): 319-324.

221.   Vilkhu, K., R. Mawson, L. Simons and D. Bates, *Applications and opportunities for ultrasound assisted extraction in the food industry – A review.* Innovative Food Science & Emerging Technologies, 2008. **9**(2): 161-169.

222.   Şahin, S., R. Samli, A.S.B. Tan, F.J. Barba, F. Chemat, G. Cravotto and J.M. Lorenzo, *Solvent-free microwave-assisted extraction of polyphenols from olive tree leaves: Antioxidant and antimicrobial properties.* Molecules, 2017. **22**(7): 1056.

223.   Hayat, K., S. Hussain, S. Abbas, U. Farooq, B. Ding, S. Xia, C. Jia, X. Zhang and W. Xia, *Optimized microwave-assisted extraction of phenolic acids from citrus mandarin peels and evaluation of antioxidant activity in vitro.* Separation and Purification Technology, 2009. **70**(1): 63-70.

224.   Nayak, B., F. Dahmoune, K. Moussi, H. Remini, S. Dairi, O. Aoun and M. Khodir, *Comparison of microwave, ultrasound and accelerated-assisted solvent extraction for recovery of polyphenols from Citrus sinensis peels.* Food chemistry, 2015. **187**: 507-516.

225.   Pinela, J., M. Prieto, A.M. Carvalho, M.F. Barreiro, M.B.P. Oliveira, L. Barros and I.C. Ferreira, *Microwave-assisted extraction of phenolic acids and flavonoids and production of antioxidant ingredients from tomato: A nutraceutical-oriented optimization study.* Separation and Purification Technology, 2016. **164**: 114-124.

226.   Moreira, M.M., M.F. Barroso, A. Boeykens, H. Withouck, S. Morais and C. Delerue-Matos, *Valorization of apple tree wood residues by polyphenols extraction: Comparison between conventional and microwave-assisted extraction.* Industrial Crops and Products, 2017. **104**: 210-220.

227.   Ferreres, F., C. Grosso, A. Gil-Izquierdo, P. Valentão, A.T. Mota and P.B. Andrade, *Optimization of the recovery of high-value compounds from pitaya fruit by-products using microwave-assisted extraction.* Food Chemistry, 2017. **230**: 463-474.

228.   Desobry, S.A., F.M. Netto and T.P. Labuza, *Comparison of spray-drying, drum-drying and freeze-drying for β-carotene encapsulation and preservation.* Journal of Food Science, 1997. **62**(6): 1158-1162.

229.   Coneac, G., et al., *Propolis extract/β-cyclodextrin nanoparticles: synthesis, physico-chemical, and multivariate analyses.* Journal of Agroalimentary Processes and Technologies, 2008. **14**(1): 58-70.

230.   Vandamme, T.F., D. Poncelet and P. Subra-Paternault, *Microencapsulation: des sciences aux technologies.* 2007: Editions Tec & Doc.

231.   Leven, L. and A. Schnürer, *Effects of temperature on biological degradation of phenols, benzoates and phthalates under methanogenic conditions.* International Biodeterioration & Biodegradation, 2005. **55**(2): 153-160.

232.   Chaaban, H., I. Ioannou, L. Chebil, M. Slimane, C. Gérardin, C. Paris, C. Charbonnel, L. Chekir and M. Ghoul, *Effect of heat processing on thermal stability and antioxidant activity of six flavonoids.* Journal of food processing and preservation, 2017. **41**(5): e13203.

233. Torres-Giner, S., R. Pérez-Masiá and J.M. Lagaron, *A review on electrospun polymer nanostructures as advanced bioactive platforms.* Polymer Engineering & Science, 2016. **56**(5): 500-527.

234. Torres-Giner, S., S. Wilkanowicz, B. Melendez-Rodriguez and J.M. Lagaron, *Nanoencapsulation of aloe vera in synthetic and naturally occurring polymers by electrohydrodynamic processing of interest in food technology and bioactive packaging.* Journal of agricultural and food chemistry, 2017. **65**(22): 4439-4448.

235. Busolo, M., S. Torres-Giner, C. Prieto and J. Lagaron, *Electrospraying assisted by pressurized gas as an innovative high-throughput process for the microencapsulation and stabilization of docosahexaenoic acid-enriched fish oil in zein prolamine.* Innovative Food Science & Emerging Technologies, 2019. **51**: 12-19.

236. Torres-Giner, S., A. Martinez-Abad and J.M. Lagaron, *Zein-based ultrathin fibers containing ceramic nanofillers obtained by electrospinning. II. Mechanical properties, gas barrier, and sustained release capacity of biocide thymol in multilayer polylactide films.* Journal of Applied Polymer Science, 2014. **131**(18).

237. Alehosseini, A., L.G. Gómez-Mascaraque, M. Martínez-Sanz and A. López-Rubio, *Electrospun curcumin-loaded protein nanofiber mats as active/bioactive coatings for food packaging applications.* Food hydrocolloids, 2019. **87**: 758-771.

238. Aydogdu, A., G. Sumnu and S. Sahin, *Fabrication of gallic acid loaded hydroxypropyl methylcellulose nanofibers by electrospinning technique as active packaging material.* Carbohydrate polymers, 2019. **208**: 241-250.

239. Samarth, N.B. and P.A. Mahanwar, *Modified vegetable oil based additives as a future polymeric material.* Open Journal of Organic Polymer Materials, 2015. **5**(01): 1.

240. Espana, J., L. Sánchez-Nacher, T. Boronat, V. Fombuena and R. Balart, *Properties of biobased epoxy resins from epoxidized soybean oil (ESBO) cured with maleic anhydride (MA).* Journal of the American Oil Chemists' Society, 2012. **89**(11): 2067-2075.

241. Santacesaria, E., R. Tesser, M. Di Serio, R. Turco, V. Russo and D. Verde, *A biphasic model describing soybean oil epoxidation with H2O2 in a fed-batch reactor.* Chemical Engineering Journal, 2011. **173**(1): 198-209.

242. Mauck, S.C., S. Wang, W. Ding, B.J. Rohde, C.K. Fortune, G. Yang, S.-K. Ahn and M.L. Robertson, *Biorenewable tough blends of polylactide and acrylated epoxidized soybean oil compatibilized by a polylactide star polymer.* Macromolecules, 2016. **49**(5): 1605-1615.

243. Quiles-Carrillo, L., M. Blanes-Martínez, N. Montanes, O. Fenollar, S. Torres-Giner and R. Balart, *Reactive toughening of injection-molded polylactide pieces using maleinized hemp seed oil.* European Polymer Journal, 2018. **98**: 402-410.

244. Chieng, B., N. Ibrahim, Y. Then and Y. Loo, *Epoxidized vegetable oils plasticized poly (lactic acid) biocomposites: mechanical, thermal and morphology properties.* Molecules, 2014. **19**(10): 16024-16038.

245. Xu, Y.Q. and J.P. Qu, *Mechanical and rheological properties of epoxidized soybean oil plasticized poly (lactic acid).* Journal of applied polymer science, 2009. **112**(6): 3185-3191.

246. Seydibeyoğlu, M.Ö., M. Misra and A. Mohanty, *Synergistic improvements in the impact strength and% elongation of polyhydroxybutyrate-co-valerate copolymers with functionalized soybean oils and POSS.* International Journal of Plastics Technology, 2010. **14**(1): 1-16.

247. Ferri, J.M., D. Garcia-Garcia, N. Montanes, O. Fenollar and R. Balart, *The effect of maleinized linseed oil as biobased plasticizer in poly (lactic acid)-based formulations.* Polymer International, 2017. **66**(6): 882-891.

248. Garcia-Garcia, D., O. Fenollar, V. Fombuena, J. Lopez-Martinez and R. Balart, *Improvement of Mechanical Ductile Properties of Poly (3-hydroxybutyrate) by Using Vegetable Oil Derivatives.* Macromolecular Materials and Engineering, 2017. **302**(2): 1600330.

249. Muthuraj, R., M. Misra and A.K. Mohanty, *Biodegradable compatibilized polymer blends for packaging applications: A literature review.* Journal of Applied Polymer Science, 2018. **135**(24): 45726.

250. Aversa, C., M. Barletta, M. Puopolo and S. Vesco, *Cast extrusion of low gas permeability bioplastic sheets in PLA/PBS and PLA/PHB binary blends.* Polymer-Plastics Technology and Materials, 2019: 1-10.

251. Wu, N. and H. Zhang, *Mechanical properties and phase morphology of super-tough PLA/PBAT/EMA-GMA multicomponent blends.* Materials Letters, 2017. **192**: 17-20.

252. Al-Itry, R., K. Lamnawar and A. Maazouz, *Improvement of thermal stability, rheological and mechanical properties of PLA, PBAT and their blends by reactive extrusion with functionalized epoxy.* Polymer Degradation and Stability, 2012. **97**(10): 1898-1914.

253. Raj, A., K. Prashantha and C. Samuel, *Compatibility in biobased poly (L-lactide)/polyamide binary blends: From melt-state interfacial tensions to (thermo) mechanical properties.* Journal of Applied Polymer Science, 2019: 48440.

254. Gug, J.-I., B. Tan, J. Soule, M. Downie, J. Barrington and M. Sobkowicz, *Analysis of models predicting morphology transitions in reactive twin-screw extrusion of bio-based polyester/polyamide blends.* International Polymer Processing, 2017. **32**(3): 363-377.

255. Akrami, M., I. Ghasemi, H. Azizi, M. Karrabi and M. Seyedabadi, *A new approach in compatibilization of the poly (lactic acid)/thermoplastic starch (PLA/TPS) blends.* Carbohydrate polymers, 2016. **144**: 254-262.

256. Luyt, A. and S. Gasmi, *Influence of blending and blend morphology on the thermal properties and crystallization behaviour of PLA and PCL in PLA/PCL blends.* Journal of materials science, 2016. **51**(9): 4670-4681.

257. Wu, D., D. Lin, J. Zhang, W. Zhou, M. Zhang, Y. Zhang, D. Wang and B. Lin, *Selective localization of nanofillers: effect on morphology and crystallization of PLA/PCL blends.* Macromolecular Chemistry and Physics, 2011. **212**(6): 613-626.

258. Fenni, S.E., J. Wang, N. Haddaoui, B.D. Favis, A.J. Müller and D. Cavallo, *Crystallization and self-nucleation of PLA, PBS and PCL in their immiscible binary and ternary blends.* Thermochimica Acta, 2019. **677**: 117-130.

259. Arrieta, M.P., J. López, A. Hernández and E. Rayón, *Ternary PLA–PHB–Limonene blends intended for biodegradable food packaging applications.* European Polymer Journal, 2014. **50**: 255-270.

260. Arrieta, M.P., E. Fortunati, F. Dominici, J. López and J.M. Kenny, *Bionanocomposite films based on plasticized PLA–PHB/cellulose nanocrystal blends.* Carbohydrate polymers, 2015. **121**: 265-275.

261. Souza Junior, O.F., L.H. Staffa, L.C. Costa and M.A. Chinelatto. *Thermal and Rheological Behavior of Binary Blends of Poly (hydroxybutyrate-co-hydroxyvalerate) and Poly (ethylene-co-vinyl acetate) with Different Vinyl Acetate Content*. in *Macromolecular Symposia*. 2019. Wiley Online Library.

262. Ma, P., X. Cai, W. Wang, F. Duan, D. Shi and P.J. Lemstra, *Crystallization behavior of partially crosslinked poly (β-hydroxyalkonates)/poly (butylene succinate) blends.* Journal of Applied Polymer Science, 2014. **131**(21).

263. Garcia-Garcia, D., J. Ferri, T. Boronat, J. López-Martínez and R. Balart, *Processing and characterization of binary poly (hydroxybutyrate)(PHB) and poly (caprolactone)(PCL) blends with improved impact properties.* Polymer Bulletin, 2016. **73**(12): 3333-3350.

264. Kam, C., *Morphology and mechanical properties of poly (β-hydroxybutyrate)/poly (ε-caprolactone) blends controlled with cellulosic particles.* Carbohydrate polymers, 2017.

265. Mittal, V., T. Akhtar, G. Luckachan and N. Matsko, *PLA, TPS and PCL binary and ternary blends: structural characterization and time-dependent morphological changes.* Colloid and Polymer Science, 2015. **293**(2): 573-585.

266. Zhang, K., A.K. Mohanty and M. Misra, *Fully biodegradable and biorenewable ternary blends from polylactide, poly (3-hydroxybutyrate-co-hydroxyvalerate) and poly (butylene succinate) with balanced properties.* ACS applied materials & interfaces, 2012. **4**(6): 3091-3101.

267. García-Campo, M.J., T. Boronat, L. Quiles-Carrillo, R. Balart and N. Montanes, *Manufacturing and characterization of toughened poly (lactic acid)(PLA) formulations by ternary blends with biopolyesters.* Polymers, 2018. **10**(1): 3.

268. Wu, D., Y. Zhang, L. Yuan, M. Zhang and W. Zhou, *Viscoelastic interfacial properties of compatibilized poly (ε-caprolactone)/polylactide blend.* Journal of Polymer Science Part B: Polymer Physics, 2010. **48**(7): 756-765.

269. Supthanyakul, R., N. Kaabbuathong and S. Chirachanchai, *Random poly (butylene succinate-co-lactic acid) as a multi-functional additive for miscibility, toughness, and clarity of PLA/PBS blends.* Polymer, 2016. **105**: 1-9.

270. Zeng, J.-B., K.-A. Li and A.-K. Du, *Compatibilization strategies in poly (lactic acid)-based blends.* Rsc Advances, 2015. **5**(41): 32546-32565.

271. Islam, M.R., M.D.H. Beg and S.S. Jamari, *Development of vegetable-oil-based polymers.* Journal of applied polymer science, 2014. **131**(18).

272. Mosiewicki, M.A. and M.I. Aranguren, *Recent developments in plant oil based functional materials.* Polymer International, 2016. **65**(1): 28-38.

273. Garcia-Garcia, D., J.M. Ferri, N. Montanes, J. Lopez-Martinez and R. Balart, *Plasticization effects of epoxidized vegetable oils on mechanical properties of poly (3-hydroxybutyrate).* Polymer International, 2016. **65**(10): 1157-1164.

274. Garcia-Campo, M., L. Quiles-Carrillo, J. Masia, M. Reig-Pérez, N. Montanes and R. Balart, *Environmentally friendly compatibilizers from soybean oil for ternary blends of poly (lactic acid)-PLA, poly (ε-caprolactone)-PCL and poly (3-hydroxybutyrate)-PHB.* Materials, 2017. **10**(11): 1339.

APÉNDICES

APÉNDICES

VII.1. ÍNDICE DE TABLAS.

VII.2. ÍNDICE DE FIGURAS.